

(EXPERIMENTAL AND THEORETICAL TECHNIQUES FOR THE)
VIBRATION ANALYSIS OF DAMPED COMPLEX STRUCTURES

by

MICHAEL GEORGE SAINSBURY

M.Sc. (Eng), London

VOLUME I of a two-volume
Thesis presented for the degree of
Doctor of Philosophy of the University of London

Department of Mechanical Engineering
Imperial College of Science and Technology
London SW7

September 1976

ABSTRACT

With the development of reliable prediction techniques, it is now becoming possible to examine both the static and the dynamic behaviour of components and assemblies at the design stage, thereby leading to more efficient design. However, there are still some components which are not amenable to theoretical treatment, and if these are to be included in a full system analysis it is necessary to obtain the required data from impedance measurements on an existing component or model. The combined use of theoretical and experimental data comes under the general title of the "building block approach", and it offers the only means of solving the most complex vibration problems.

One such problem is that of multi-directional vibration isolation, and this has provided the impetus for most of the work described here. Faced initially with the task of analysing an existing heavily damped machinery foundation structure, it was necessary to develop a technique for measuring the multi-directional response properties of the most complex components, and to derive finite elements for the bending and torsion of multi-layer damped beams. Then, once the component data had been obtained, it was necessary to couple all the parts together to predict the system response. It was evident that a need existed for a general-purpose coupling program which would take either theoretical or experimental component data from virtually any source, thereby permitting the analysis of a wide variety of different systems, including the above-mentioned foundation structure. Accordingly, a suitable program was developed, along with a set of standard component routines, and this has subsequently been used for further, more general, studies of isolation systems.

The thesis is divided into four distinct parts, dealing respectively with isolation systems and frequency response analysis, multi-directional

measurements, multi-layer beams, and the analysis of the damped foundation structure (or "seating"). While the first three parts are virtually independent of one another, the final part draws on material from each of the preceding parts, thereby providing an excellent example of how advanced analytical and experimental techniques may be used together to solve complex vibration problems.

ACKNOWLEDGEMENTS

The Author is deeply grateful to Professor P. Grootenhuis for his encouragement and support during the six years in which this study was carried out. Thanks are also due to Dr. D.J. Ewins, who acted as joint supervisor with Professor Grootenhuis, and whose untiring efforts to set up a sophisticated impedance measuring facility have made possible much of the work described here. Their combined influence has been invaluable for encouraging a broad interest in dynamics, extending from measurement techniques to advanced analysis.

Many past and present members of the Dynamics Group have also given assistance: special thanks are due to Dr. E. Ioannides and to Messrs. P.T. Gleeson, J.L. Williams, and Júlio Montalvão e Silva for many hours of stimulating discussion on a wide range of topics; and to Mr. R.D. Gunn for all his help in the laboratory.

The Author is especially grateful to the Ministry of Defence (Admiralty Engineering Laboratory) for the opportunity of working on such a challenging project, and for the financial support given over a five-year period under two research contracts.

Useful technical assistance was also given by Solartron Ltd. (Dynamic Analysis Section), who at various times provided measuring equipment on free loan, thereby accelerating the early development of multi-directional measurement techniques.

Finally, the Author wishes to thank his parents for their encouragement over the years, and his wife Phi Đào for so carefully typing a large part of the thesis and for always displaying patience and understanding.

NOMENCLATURE

As this thesis embraces several different branches of dynamics, there is a certain amount of overlap between the symbols normally employed in the different branches. Therefore, most symbols are defined where they occur in the text, and only the most important of these are listed below.

Note that Mobility is represented by the letter Y, in preference to an M. Besides avoiding confusion with a couple or a mass, this preserves uniformity between the symbols used for mechanical and electrical admittance, just as one normally uses a Z for both mechanical and electrical impedance.

Also, note that the complex ratio $I = \frac{\text{acceleration}}{\text{force}}$ is here called "inertiance", whereas the more commonly used term is "inertance". It is the Author's contention that the former is more correct, since the ratio relates quite closely to inertia, while only gases are inert. However, since the present work was initiated, the term "inertance" has found more widespread use, so it is now the recommended term — but solely on the basis of usage.

Z	Impedance OR Dynamic stiffness
Y	Mobility (mechanical admittance) [see note above]
α	Receptance OR Rotational displacement [see α, β, θ]
I	Inertiance [see note above]
q_i	Generalised displacement on co-ordinate i
Q_i	Generalised exciting force on co-ordinate i (force or couple)
δ	Displacement
F	Force
M	Couple OR Mass
x,y,z	Cartesian co-ordinates OR Displacements in these co-ordinate directions
u,v,w	Displacements in x,y,z directions
α, β, θ	Rotations about x,y,z axes
m	Mass OR Metre
k,K	Stiffness
c	Viscous damping coefficient
I_G	Moment of inertia about centre of gravity

h	Hysteretic damping coefficient
η	Loss factor
Q	Q factor = $\frac{1}{\eta}$
ζ	Damping ratio $\approx \frac{1}{2}\eta$ for light damping
ω	Circular frequency (rad/s) = $2\pi \times$ Frequency(Hz)
ω_N	Undamped natural frequency (rad/s)
t	Time
.	Differentiation with respect to time (eg. $\dot{w} = \frac{dw}{dt}$)
'	Differentiation with respect to x (eg. $w' = \frac{dw}{dx}$)
i, j	$\sqrt{-1}$ (used in complex quantities) OR Subscript designating either co-ordinate or layer number
[]	Rectangular matrix
{ }	Column vector
V	Strain energy
T	Kinetic energy
L	Length of beam finite element
b	Width (breadth) of beam
t_i	Thickness of layer i of multi-layer beam
E	Elastic modulus (may be complex)
G	Shear modulus (may be complex)
ν	Poisson's ratio
ρ	Density
μ	Mass per unit length of beam
N	Number of finite elements into which beam is divided OR Normal force between two mating surfaces
μ_s, μ_d	Static and dynamic coefficients of friction
σ_x, σ_y	Direct stresses in x and y directions
τ_{xy}	Shear stress in x direction on y face
γ	Shear strain
θ, ϕ	Phase angle OR Rotational displacement [see α, β, θ]
v	Volts OR Velocity OR Displacement in y direction [see u, v, w]

CONTENTS

As the thesis is divided into four distinct parts, more detailed contents lists are given at the beginning of each part and at the beginning of each corresponding group of appendices.

Note that each part has its own reference list, with the numbers starting from 1 in each case, so the reader should take care to consult the correct list.

VOLUME I

<u>Chapter</u>		<u>Page</u>
	PART 1 - VIBRATION ISOLATION AND FREQUENCY RESPONSE ANALYSIS	10
1	General Introduction to Vibration Isolation	11
2	The Frequency Response Analysis of Damped Complex Structures	41
	References for Part 1	75
	PART 2 - MULTI-DIRECTIONAL MOBILITY MEASUREMENTS FOR THE VIBRATION ANALYSIS OF COUPLED STRUCTURES	82
3	Multi-directional Mobility Measurement	83
4	Multi-directional Measurements with a Single Shaker	94
5	Multi-directional Measurements with a Twin Shaker	147
6	Coupling of Beam to Spring-supported Block	160
7	Summary and Conclusions for Multi-directional Mobility Measurements	176
	References for Part 2	185
	PART 3 - THE FINITE ELEMENT VIBRATION ANALYSIS OF MULTI-LAYER DAMPED BEAMS IN FLEXURE AND TORSION	189
8	General Introduction to Multi-layer Damped Beams	191
9	Bending Finite Element for Symmetrical 5-layer Beam	199

10	Bending Finite Elements for Unsymmetrical 3- and 5-layer Beams	222
11	Torsional Finite Element for Symmetrical 5-layer Beam	238
12	Results and Conclusions for Multi-layer Damped Beams	257
	References for Part 3	283

VOLUME II

Chapter

	PART 4 - THE VIBRATION ANALYSIS OF A HEAVILY DAMPED V-BEAM SEATING	292
13	Details of Seating and its Analysis	293
14	Analysis of Seating Components	321
15	Results and Conclusions for the Seating	380
	References for Part 4	430

Appendix

	APPENDICES FOR PART 1	433
I	Flow Chart for the Computer Program COUPLE1	434
II	The Addition of a Single Friction Damper to a Linear Damped System	445
	APPENDICES FOR PART 2	460
III	Derivation of Matrices used in Multi- directional Measurements	461
IV	Some Multi-directional Mobility Measurements on a Large Mass	474
	APPENDICES FOR PART 3	501
V	The Convergence Rate of Energy Integrals in the Finite Element Method	502
VI	"Standard" Matrices arising in the Finite Element Analysis of Sandwich Beams	505

VII	Extensional and Bending Strain Energies in a Thin Plate	507
VIII	The Formation of a Tip Dynamic Stiffness Matrix for a Multi-element Beam	510
	APPENDICES FOR PART 4	517
IX	Derivation of Dynamic Stiffness Matrix for Spring-mass Model of Rubber V-block (RB)	518
X	Derivation of Dynamic Stiffness Matrix for Male V-piece (VB)	530
XI	Derivation of Dynamic Stiffness Matrix for Female V-support (VS)	537
<hr/>		
	PUBLICATIONS	547
1	Mobility Measurements for the Vibration Analysis of Connected Structures	
2	Vibration Analysis of a Damped Machinery Foundation Structure using the Dynamic Stiffness Coupling Technique	

PART 1VIBRATION ISOLATION AND FREQUENCY RESPONSE ANALYSISCONTENTS

<u>Chapter</u>		<u>Page</u>
1	GENERAL INTRODUCTION TO VIBRATION ISOLATION	
	1.1 Basic Aspects and Classical Theory	11
	1.2 Single-stage Isolation Systems	15
	1.3 Two-stage Isolation Systems	28
	1.4 Summary	39
2	THE FREQUENCY RESPONSE ANALYSIS OF DAMPED COMPLEX STRUCTURES	
	2.1 Introduction to the Building Block Approach	41
	2.2 The Dynamic Stiffness Coupling Program COUPLE1	45
	2.3 Ways of including Damping in the Analysis	57
	REFERENCES FOR CHAPTERS 1 AND 2	75

Appendices to Part 1 start on Page 433

CHAPTER 1

GENERAL INTRODUCTION TO VIBRATION ISOLATION

1.1 BASIC ASPECTS AND CLASSICAL THEORY

Any modern industrial society thrives on "bigger-and-better" machines for increased production, faster travel, labour-saving in the home, and for its own protection against outside aggression. An inevitable consequence of this has been a gradual increase in pollution of the environment, not only from chemicals and gases but also from noise and vibration. In the latter field, the situation has been aggravated by the recent steep rise in the cost of raw materials, since this has resulted in a more economical use of all materials, and hence lighter equipment that is more prone to vibration. With the growing public reaction against all form of pollution, it is becoming necessary to adopt a more scientific approach to its control by using all the practical and theoretical means at our disposal to effect solutions to the various problems.

In addition to polluting both the leisure and the working environment, vibration and noise often give rise to equipment failure — sometimes with disastrous consequences — and they may also reduce the effectiveness of those vessels that protect our shores and vital sea lanes by making them more easily detectable by an enemy. Besides all the man-made sources of vibration, nature is always a potential source and it has demonstrated its power just recently with a number of quite devastating earthquakes. Although the source is different, the problem of protecting a building from an earthquake is essentially no different from that of isolating it from the more continuous rumble of traffic (1)(2)*; it is simply a problem of VIBRATION ISOLATION.

The problem is best illustrated by the two systems shown in Fig. 1.1a. That on the left represents a machine (SOURCE) which is to be mounted in such a way that the force transmission to the supporting structure (RECEIVER) is kept down to an acceptable level (bearing in mind that the transmitted force

* Note that References for Chapters 1 and 2 are listed on Page 75.

FIG. 1.1a THE TWO BASIC TYPES OF ISOLATION PROBLEM

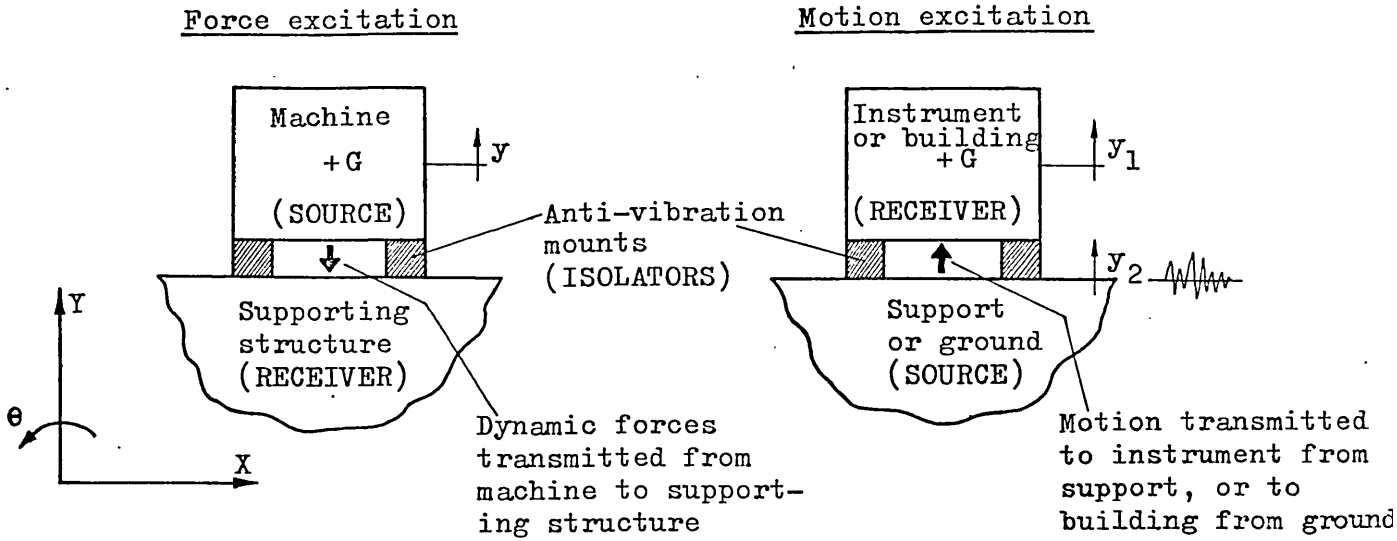


FIG. 1.1b CLASSICAL MODELS FOR THE TWO SYSTEMS GIVEN ABOVE

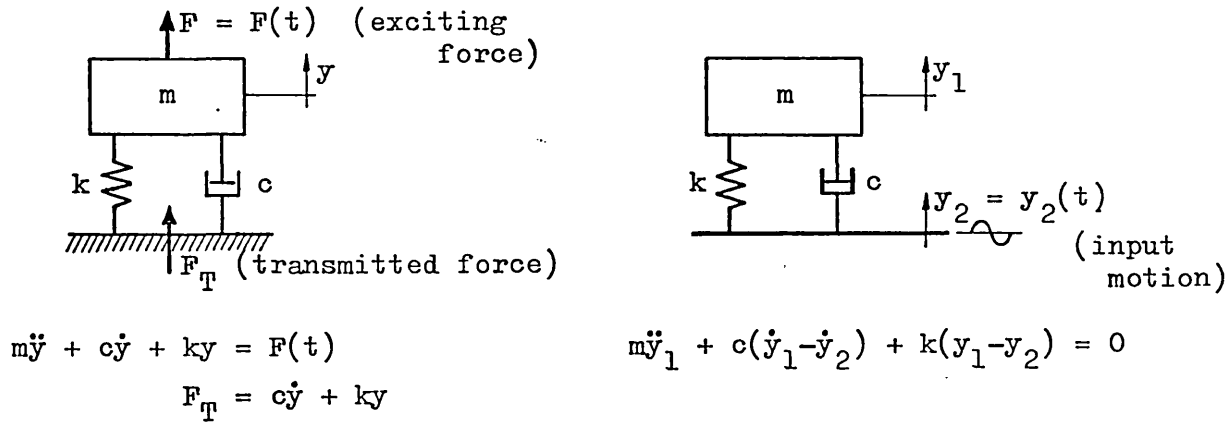
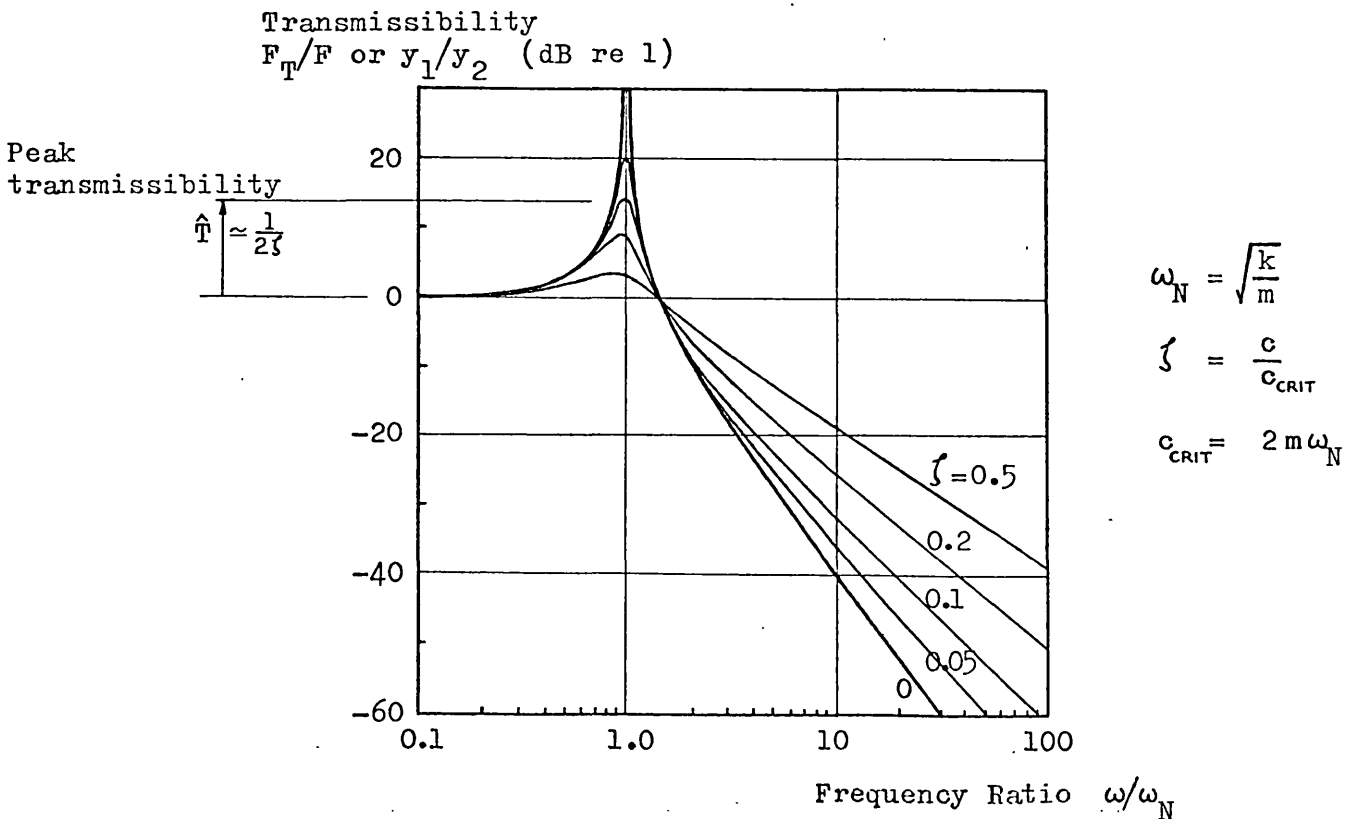


FIG. 1.1c TRANSMISSIBILITY YIELDED BY CLASSICAL MODELS



gives rise to noise and vibration at points remote from the machine). The mounting or isolation system normally takes the form of a number of fairly soft springs (ISOLATORS), but it must be carefully designed so that it does in fact have a beneficial effect at all frequencies in the excitation spectrum. It is especially important to bear in mind the multi-directional nature of the system, since practically every machine is a multi-directional vibration source and what is a good design for attenuating transmission in the vertical direction is not necessarily so good for attenuating transmission in either the horizontal or rotational directions. Exactly the same considerations apply for the system on the right, which may represent either a sensitive instrument that is to be isolated from a vibrating support or a building that is to be isolated from ground motion.

These two systems have long been represented by the simple "classical" models shown in Fig. 1.1b, where m is a rigid mass, k is a massless spring, and c is a massless VISCOUS DAMPER*. In the case of the force-excited system, the lower end of the spring and damper are assumed to be connected to a rigid supporting structure, or ground, so the system is said to be "grounded" and it has only a single degree of freedom y . With the support-excited system, both ends of the spring and damper are free to move, so the system is said to be "free" and it has two degrees of freedom y_1 and y_2 . The equations of motion given in the figure are valid for any sort of input variation with time, but the classical theory of vibration isolation is based upon the response to steady-state harmonic excitation⁺, and all the work described herein is confined to such steady-state vibrations. The solution of these equations is trivial and is dealt with in numerous texts on vibration⁽³⁾⁽⁴⁾, so the details will not be given here. It may be shown that the force ratio $\left| \frac{F_T}{F} \right|$ for the

* Viscous and other dampers are discussed in detail in Chapter 2, Section 2.3

+ This is no limitation, since any input may be broken down into a set of Fourier components and the total response is then obtained by summing the responses to these various input components.

force-excited system is identical to the motion ratio $\left| \frac{y_1}{y_2} \right|$ for the support-excited system, and we call both these ratios the TRANSMISSIBILITY: this is shown plotted against frequency in Fig 1.1c for various values of the damping ratio ζ ($\approx 1/2\hat{T}$ for light damping)*. Logarithmic scales are used for both axes, and the transmissibility is given in dB (deci-Bels), where $T(\text{dB}) = 20 \text{ Log}_{10} T$. This is useful because the log-log plot yields a clearer picture of high frequency behaviour than a linear plot, and in particular it shows constant rates of "drop-off" in transmissibility which are easily expressible in dB/octave or dB/decade[†]. Although the response is seen to be very small in this region, it cannot be ignored, since even supposedly rigid ^{Supporting} structures "break up"^X dynamically at high frequencies and are easily excited into resonant vibration by any very small forces or motions that may be transmitted.

These classical models are very simple and they were adequate in the days when all machines were solidly built and ran at low speeds. However, with the current trend towards lighter construction and higher speeds, they must be used with some caution, since they often fail to describe observed system behaviour, particularly at high frequencies ($> 100 \text{ Hz}$). Nevertheless, they do illustrate some important points that should be borne in mind before we proceed to more complex models. Referring once more to Fig. 1.1c, we see that the exciting force or motion is amplified at all frequencies below $1.414\omega_N$, so any real system should be designed to have a natural frequency ω_N that is well below the lowest excitation frequency (ω_N is typically about 4 to 10 Hz). We also see that an increase in the amount of viscous damping only has a beneficial

- * The term "damping ratio" only has significance in the case of viscous damping. A more general measure of damping is given by the LOSS FACTOR γ , which is equal to 2ζ when the damping is light. It is defined in Section 2.3.
- + When the frequency is increased by a factor of $\left\{ \begin{matrix} 2 \\ 10 \end{matrix} \right\}$, it is said to be increased by one $\left\{ \begin{matrix} \text{octave} \\ \text{decade} \end{matrix} \right\}$.
- X "Break-up" signifies a changeover from a more or less rigid state to a more flexible state as the frequency becomes high enough to excite structural resonances.

effect at the resonance, and it can have a very detrimental effect on the high-frequency attenuation. Whereas the transmissibility of the undamped system drops off at a rate of 12 dB/octave (=40 dB/decade), that of a viscously damped system drops off initially at a rate somewhere between 12 and 6 dB/octave (= 20 dB/decade), and eventually approaches 6 dB/octave, whatever the damping.

1.2 SINGLE-STAGE ISOLATION SYSTEMS

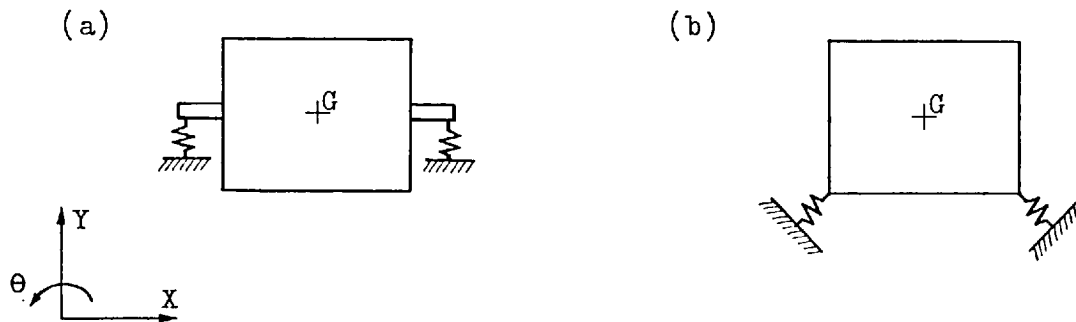
From this point onwards we shall confine our attention to the problem of force transmission between a vibrating machine and a receiver structure, and in this Section we shall look at various aspects of the design and analysis of single-stage isolation systems. As we are particularly interested in the accurate prediction of system performance, it is important that we be aware of the different factors that impair the performance of real systems, so that we can allow for these in our model. Hence, we shall start by considering the limitations of the classical model given in Section 1.1, which are as follows:

- (1) Most machines are multi-directional vibration sources, so one should also consider the vibration transmission in the horizontal and rotational directions.
- (2) The mount damping is not adequately described by the viscous damper. Also, internal wave effects (ie. resonances or "surges") are ignored.
- (3) Any real machine ceases to be a solid mass at high frequencies and starts to exhibit resonant behaviour. Similarly, an apparently rigid supporting structure ceases to be rigid.

The high-frequency limitations have been discussed by Ungar and Dietrich⁽⁵⁾ in a fairly general manner, and Ruzicka⁽⁶⁾ has pointed out inconsistencies between the elementary predictions and observed behaviour for support-excited systems and has modified the basic model by elastically mounting the damper. We shall now proceed to examine each of the limitations in detail, solely from the point of view of machine isolation systems.

Starting with multi-directional behaviour, we may return to consider the basic physical system shown in Fig. 1.1a. This might represent a reciprocating engine or some rotary machine, and in each of these cases the out-of-balance forces will excite the machine in both the vertical and the horizontal directions (Y and X). Also, since the horizontal and rotary motions X and θ are coupled, the machine will be forced to vibrate in the X, Y and θ directions. Hence, the system should be designed to provide isolation in all three directions.

From the simple theory, we know that isolation is only obtained at frequencies greater than 1.414 times the natural frequency, so the system will only be effective in all directions when the frequency has risen well beyond the highest of the three basic natural frequencies. For the configuration shown in the figure, the three modes will generally be well spaced, and a good example of this is given in Part 2, Chapter 4, where a resiliently mounted 135 Kg mass has been found to have natural frequencies of 7, 18.5 and 25.5 Hz for the X, Y and θ modes. Since the rotational mode has a higher frequency than the vertical mode, the system will not work so effectively as is predicted by the classical theory. In addition, the very low horizontal natural frequency may make the system sway too much, so it is obviously better if the modes can be grouped closer together, around the vertical frequency. This may be achieved if the X and θ motions are uncoupled, either by raising the mounts up to the same level as the machine's centre of gravity, or by inclining the isolators (7)(8)(9)(11);



Configuration (a) above is more suitable for heavy machinery, since most mounts are not designed to take the large static shear loads that are inevitable with the inclined mounting system (b). However, the cantilever feet necessitated by this arrangement may give rise to unwanted resonances, which will be discussed in detail at a later stage. The problems encountered with the 3-directional or plane motion are far less than with the more general case of 6-directional motion⁽¹⁰⁾, for which one may expect an even greater spread of natural frequencies.

The multi-directional motion of the machine produces force transmission to the supporting structure in various directions, and if we wish to predict the resulting motion at some distant point due to these forces, we should not forget to include the phase information when we sum the effects of the different forces. Although we have so far only considered a rigid support, it may be necessary to mount a machine on a structure that is more flexible, and in such a case it is necessary to include in the analysis the dynamic characteristics of the structure in all the principal directions of force transmission — both linear and rotational. Such information may only be obtainable from measurements (see Part 2).

We shall next examine the limitations of our isolator model in greater detail, but before we do this, it is useful to familiarise ourselves with the physical form of some typical machine mounts, four of which are shown in

Fig. 1.2a: (A) A rubber compression mount, (B) a rubber shear mount, (C) a rubber isolator pad, and (D) a double-U leaf spring isolator. Types A, B and C are designed primarily for steady-state vibration isolation, while type D allows larger deformations for absorbing shock loads in addition to providing steady-state isolation. The shear mount (B) is generally less stiff than the other types, so it is more suitable for light equipment. The isolation pad (D) is both cheap and effective and is suitable for isolating workshop machines, etc., while the other types are better in those applications where the isolator is to be bolted firmly in position, as in a ship for instance. The rubber mounts (A), (B) and (C) rely on hysteresis within the rubber to provide damping, while the leaf-spring (D) may either rely on dry friction between the leaves, or on some visco-elastic compound or wire-wool material packed in between.

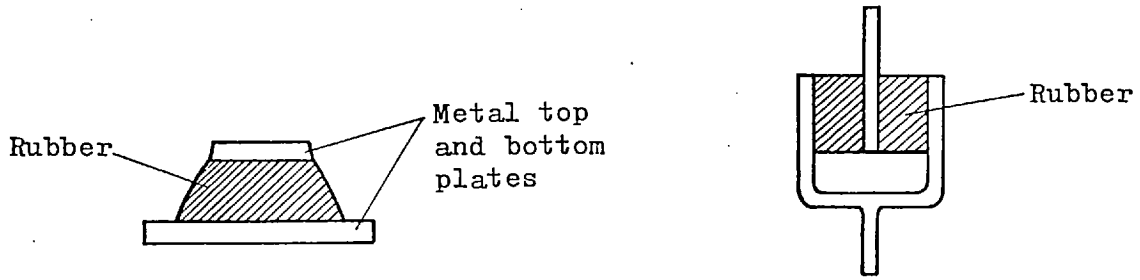
Except when viscous dashpots are purposely introduced, the only damping in the isolation system comes from within the mounts themselves. In the case of most rubbers, this damping increases only very slowly with frequency, so it is best represented by a HYSTERETIC DAMPER^{(12)(13)*}, which applies a damping force that is proportional to displacement, rather than velocity.[†] When used in place of a viscous damper, this gives a high-frequency transmissibility drop-off of 12 dB/octave, which is closer to observed behaviour.

At high frequencies the mounts cease to behave as pure massless springs, and they start to exhibit their own resonances, thereby giving rise to increased force transmission. This occurs at frequencies for which the mount dimensions become comparable with multiples of the half wavelength of the elastic wave travelling through: typical machine mounts may be expected to exhibit wave effects at something over 200 Hz, though steel springs and large rubber blocks may resonate at less than 100 Hz. As a very rough guide, it is unlikely that these wave effects will manifest themselves at frequencies below 20 times the natural frequency of the mounted mass⁽¹⁴⁾. Although their nature is well under-

† However, this force is still in anti-phase with the velocity.

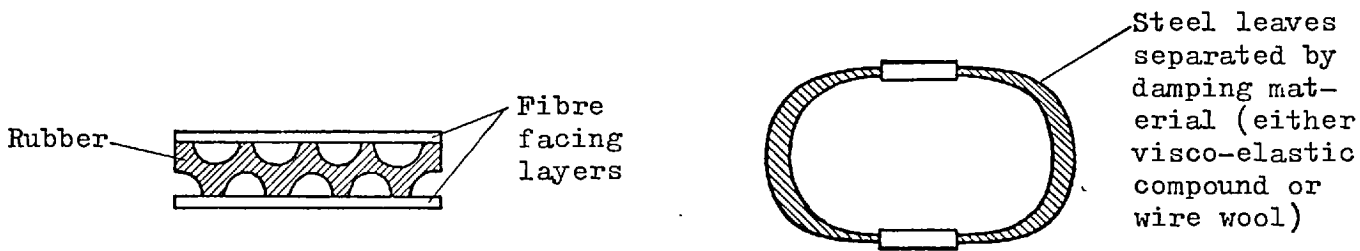
* See Chapter 2, Section 2.3

FIG. 1.2a SOME TYPICAL ANTI-VIBRATION MOUNTS



(A) Rubber mount (compression type)

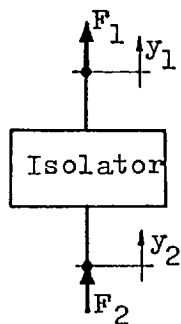
(B) Rubber mount (shear type)



(C) Rubber isolation pad

(D) Double-U leaf spring isolator (for vibration and SHOCK)

FIG. 1.2b THE AXIAL DYNAMIC STIFFNESS RELATION FOR AN ISOLATOR



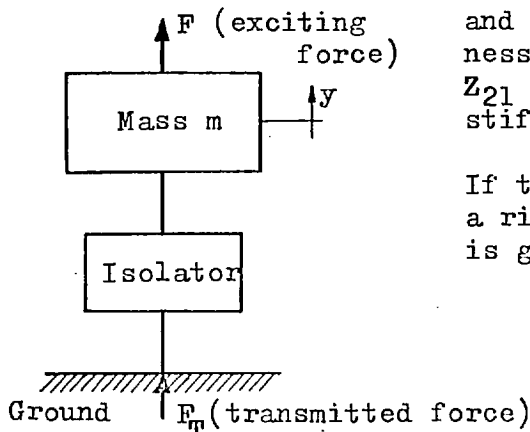
Considering the isolator as a two-terminal component with generalised properties, the forces applied to its two ends are related to the corresponding displacements by a 2 x 2 dynamic stiffness matrix:

$$\begin{pmatrix} F_1 \\ F_2 \end{pmatrix} = \begin{bmatrix} Z_{11} & Z_{12} \\ Z_{21} & Z_{22} \end{bmatrix} \begin{pmatrix} y_1 \\ y_2 \end{pmatrix}$$

where the coefficients Z_{ij} are in general complex and frequency dependent, to take account of stiffness, damping and mass. Also, due to reciprocity, $Z_{21} = Z_{12}$. For the special case of a PURE SPRING of stiffness k , $Z_{11} = Z_{22} = -Z_{12} = k$.

If this isolator is interposed between a mass m and a rigid support (ground), the FORCE TRANSMISSIBILITY is given by the following expression:

$$T = \left| \frac{F_T}{F} \right| = \left| \frac{-Z_{21}}{(Z_{11} - \omega^2 m)} \right|$$



stood, they may not in general be predicted from first principles with any great accuracy. The classical theory of longitudinal wave transmission in "long" rods yields only approximate answers, since most anti-vibration mounts have comparable longitudinal and lateral dimensions and are of complex shape. Improved results are yielded by the Love theory⁽¹⁵⁾, but this still cannot take account of complex shapes, and the finite element method probably offers the only hope of reliable predictions*. Snowdon has produced transmissibility curves using both of the approximate theories⁽¹⁷⁾.

If high-frequency transmissibility predictions are important, better results may be obtained by using measured frequency response data for the isolator. Referring to Fig. 1.2b, the generalised stiffness characteristics of any isolator may be expressed in terms of a 2×2 dynamic stiffness matrix⁽¹⁸⁾, where each element Z_{ij} is complex (to allow for phase differences between force and displacement) and frequency-dependent. This takes account of distributed mass, stiffness and damping and it may be obtained from "impedance" measurements⁺ on an existing isolator. By digitising this measured information at every frequency of interest, it is possible to then compute the force transmissibility from the expression given in the figure.

This exercise has been carried out by the Author in the case of a double-U leaf spring isolator called an X mount, for which the measured dynamic stiffness data are given in Fig. 1.3. It is clearly seen that this particular isolator has a stiffness which almost doubles between 10 and 100 Hz, after which some very heavily damped resonances of the steel leaves completely transform the behaviour, and by 500 Hz it looks like a fairly constant mass to whatever it supports. At low frequencies, the phase angle gives a direct measure of the damping in the spring, since the LOSS FACTOR is equal to the tangent

* Reference (16) shows some interesting finite element predictions of the response of a short cylindrical mass obtained using axi-symmetric elements. Good agreement has been obtained with measurements, and although this mass was made of steel, one may expect comparable accuracy when using rubber.

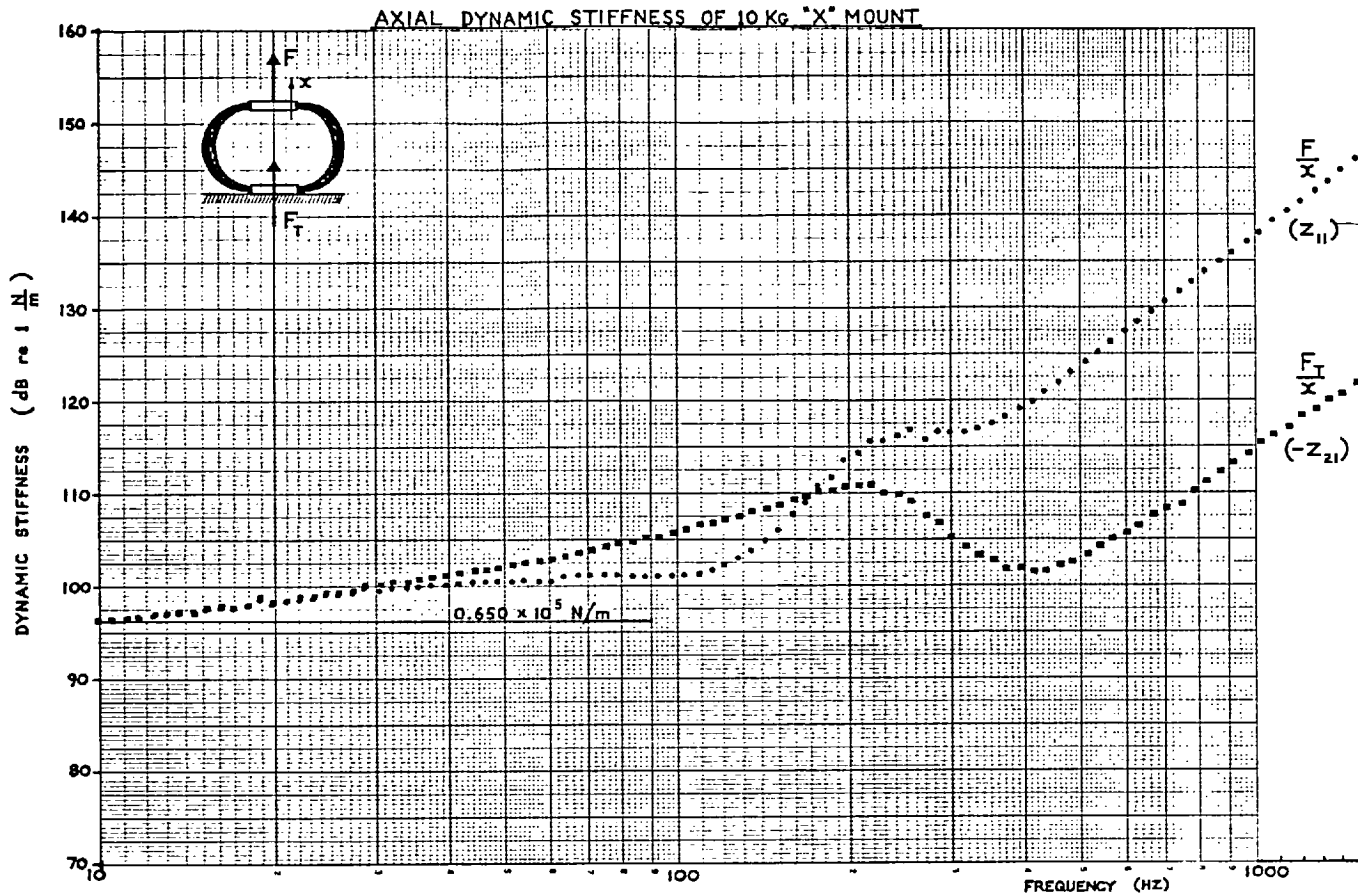
+ See Part 2, Chapter 3 for more information on the measurement of mobility and impedance.

FIG 1.3

CHART
WELL

Graph Data Ref. 5521

Log 2 Cycles 2 mm, 1 and 1 cm



WELL

Graph Data Ref. 5521

Log 2 Cycles 2 mm, 1 and 1 cm

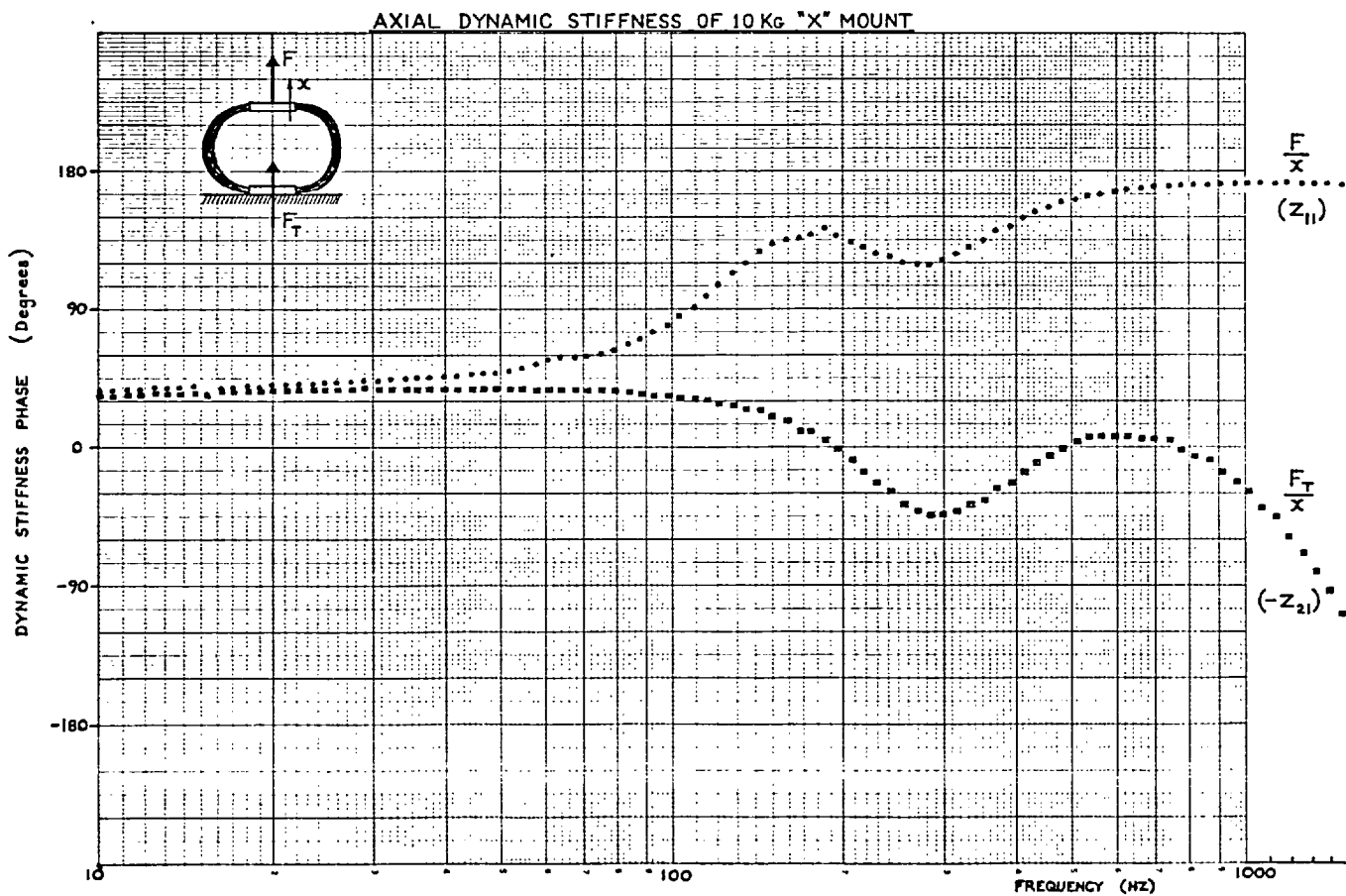
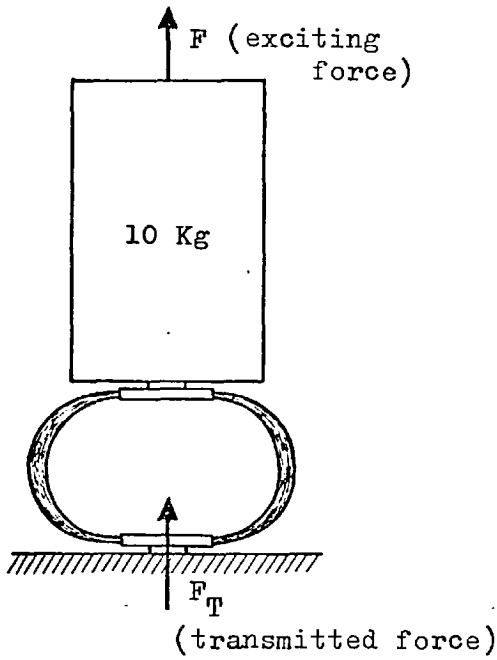
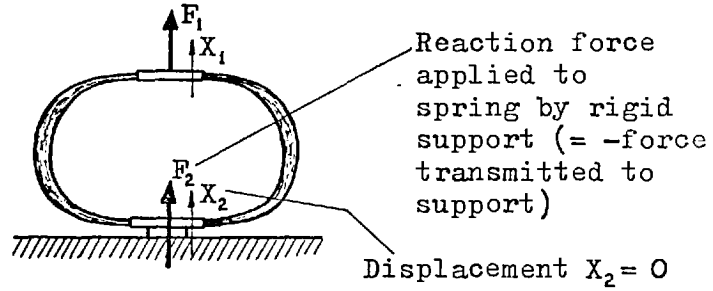


FIG. 1.4 FORCE TRANSMISSIBILITY FOR 10 KG MASS ON X MOUNT



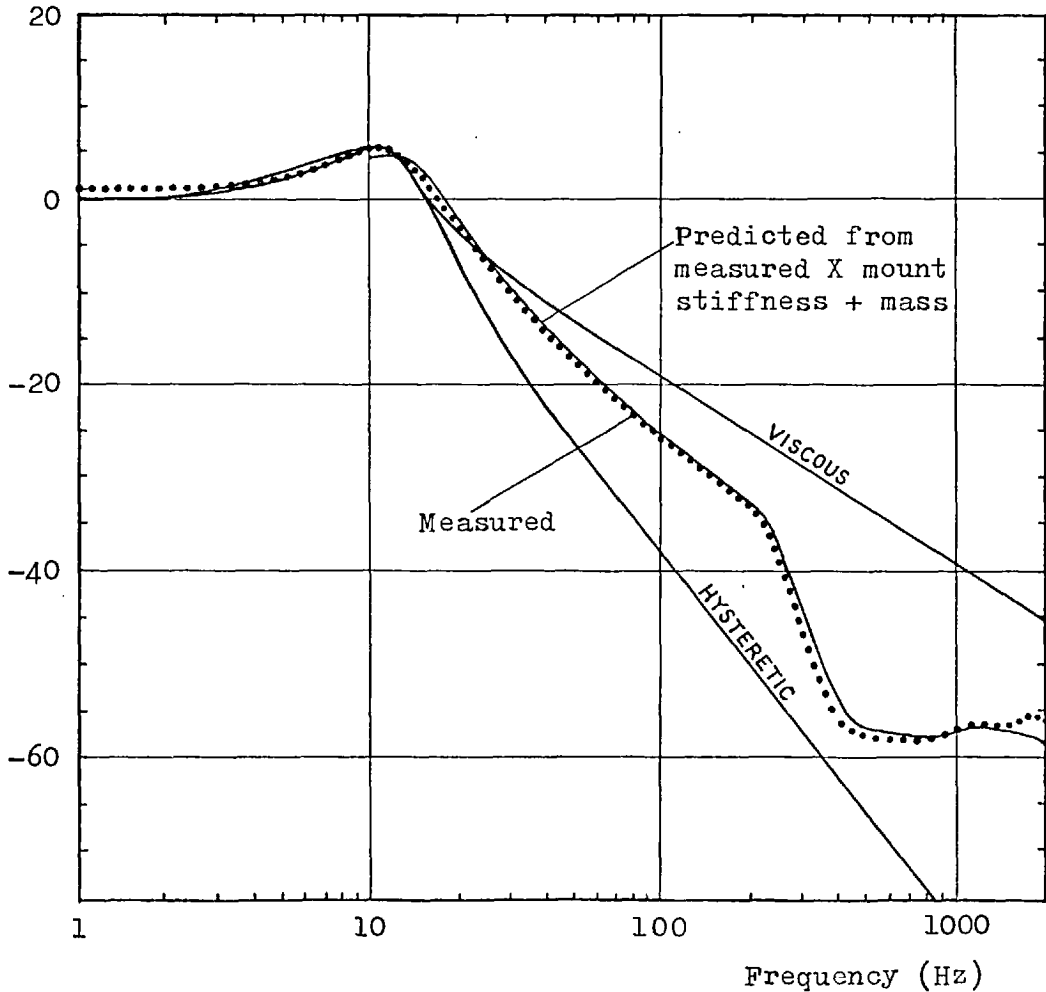
The dynamic stiffness of the X mount was measured with one side to ground:



For the isolator in a "free-free" state, the dynamic stiffness is given by the following 2 x 2 matrix:

$$\begin{bmatrix} Z_{11} & Z_{12} \\ Z_{21} & Z_{22} \end{bmatrix} = \begin{bmatrix} \left. \frac{F_1}{X_1} \right|_{x_2=0} & \left. \frac{F_2}{X_1} \right|_{x_2=0} \\ \left. \frac{F_2}{X_1} \right|_{x_2=0} & \left. \frac{F_1}{X_1} \right|_{x_2=0} \end{bmatrix}$$

Force Transmissibility
 F_T/F (dB re 1)

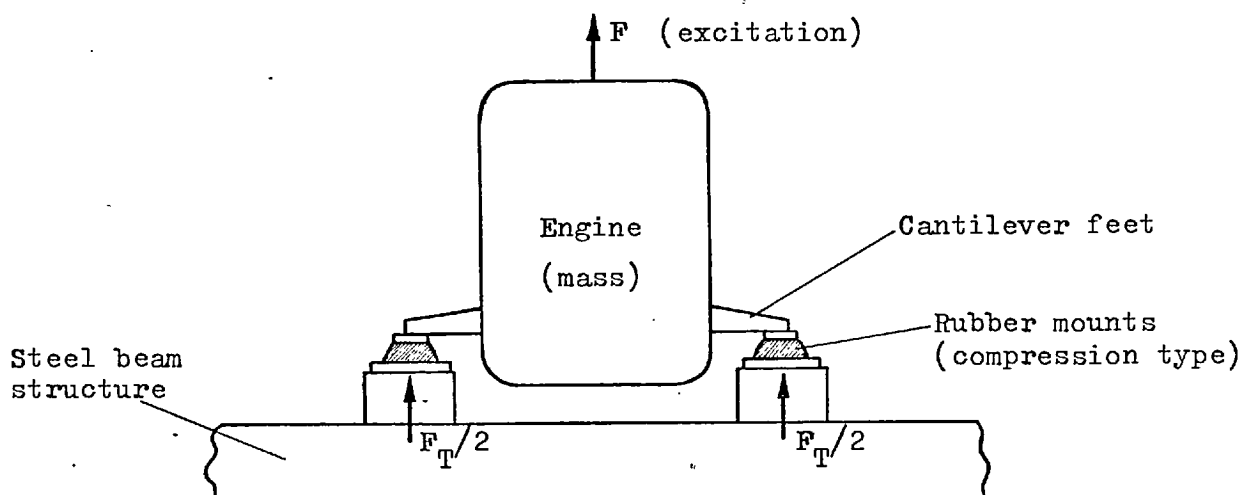


of this angle ($\tan 35^\circ = 0.7$). These data were obtained by mounting the isolator on top of a large steel mass (135 Kg, and therefore an effectively rigid support) and measuring the forces F_1 and $-F_2 (= F_T)$ together with the displacement y_1 , as shown in Fig. 1.4. Since a digital measuring system was used, the required information was punched out automatically onto paper tape ready for predicting the transmissibility. A 10 Kg steel mass was then attached to the top of the isolator, and the transmissibility was measured over the frequency range 1 to 2000 Hz. These measurements are shown in Fig. 1.4, together with the transmissibility predicted by theoretically combining the mass with the measured isolator properties, and it is seen that very good agreement has been obtained. In addition to demonstrating the feasibility of using measured mount data to improve predictions, this particular example shows that certain types of isolator obey neither a viscous nor a hysteretic damping law (though a similar exercise carried out with a rubber mount would undoubtedly yield closer agreement with the hysteretic model).

In the same way that a real isolator ceases to be a pure spring at high frequencies, the machine and the receiver structure also "break up" and exhibit resonant behaviour. To put this in perspective, a stiff steel structure comprising beams and plates may be expected to break up around 50 to 100 Hz, while an engine will probably remain masslike up to several hundred Hz, and a small block of steel (eg. 10 cm cube) up to several thousand Hz. This break-up will generally impair the performance of the isolation system, though it can sometimes have a beneficial effect at higher frequencies. A good example of this is provided in Fig. 1.5. This is based on the study of a real engine which was mounted on a stiff steel structure using conventional rubber mounts. (Type A in Fig. 1.2). An important feature of this design is the engine feet, which were bolted onto the body of the engine and were necessary to give a stable mounting configuration. Running tests on this machine showed a strong vibration transmission to the receiver structure at around 200 Hz. This was known to be

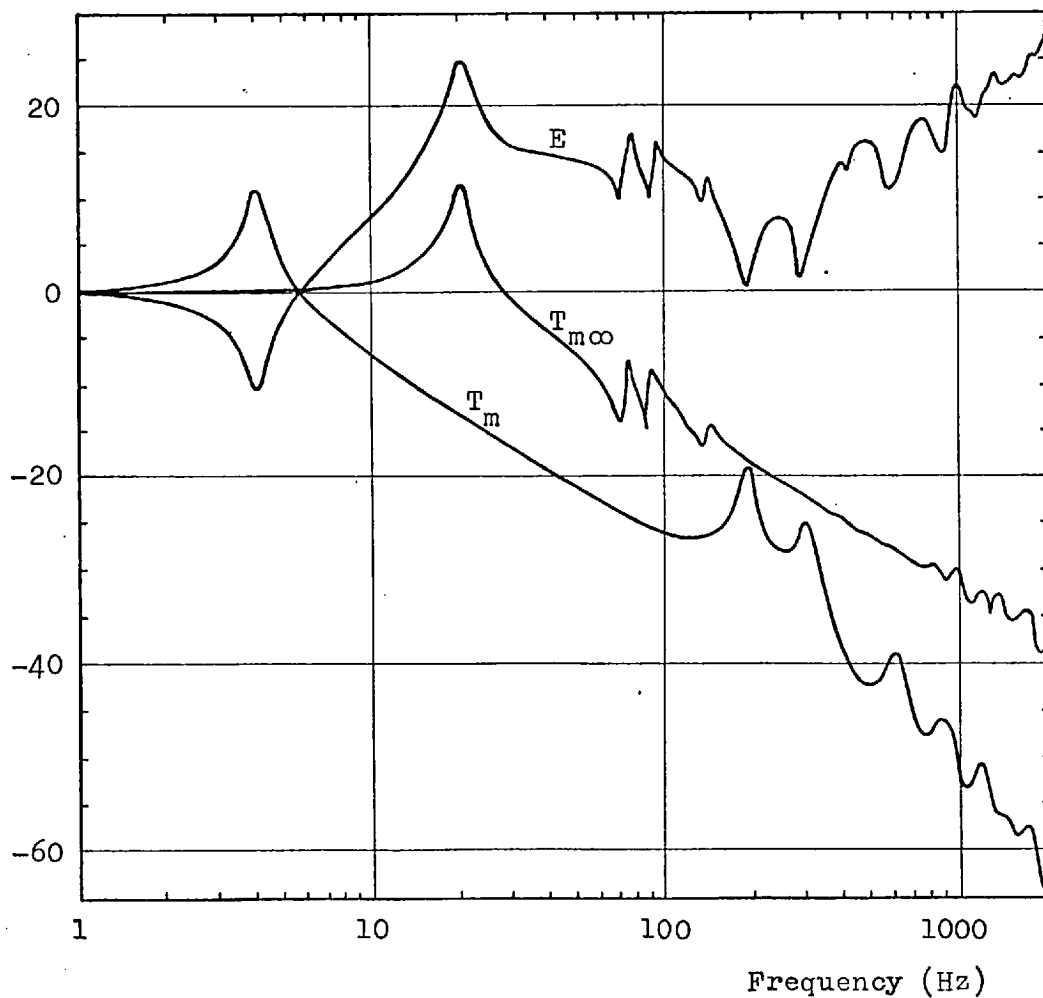
FIG. 1.5

EFFECTIVENESS OF RUBBER MOUNTS UNDER A REAL MACHINE



Force
Transmissibility F_T/F
and
Effectiveness (dB re 1)

T_m = Transmissibility with mounts
 $T_{m\infty}$ = Transmissibility without mounts
 E = Effectiveness of mounts = $T_{m\infty}/T_m$



somewhere near one of the principal excitation frequencies resulting from out-of-balance, but it was not clear whether system resonances were also contributing towards this strong transmission, so it was decided to model the system in order to examine its transmissibility properties.

Attention was first focused on the machine, and impedance measurements on one foot soon revealed a flapping resonance at 269 Hz, followed by approximately spring-like behaviour up to 5000 Hz. Although other resonances were observed, they were very heavily damped (possibly due to friction in the bolted joint), so they were quite insignificant and could be ignored. Thus, the machine could be modelled as a mass-spring-mass system, with the lower spring and mass representing the foot. Next, it was necessary to examine the mount, and it was particularly important to recognise that this comprised upper and lower metal plates in addition to the rubber spring element. Thus, it was represented initially as a mass-spring-mass system, and the rubber element was subsequently sub-divided into a series of masses and springs in order to allow approximately for wave effects. The steel receiver structure was very stiff, even up in *its* resonant region (1st resonance around 70 Hz), so it could probably have been assumed rigid. Nevertheless, its measured dynamic stiffness properties were digitised in small frequency steps over the full range of interest (just as for the X mount considered previously).

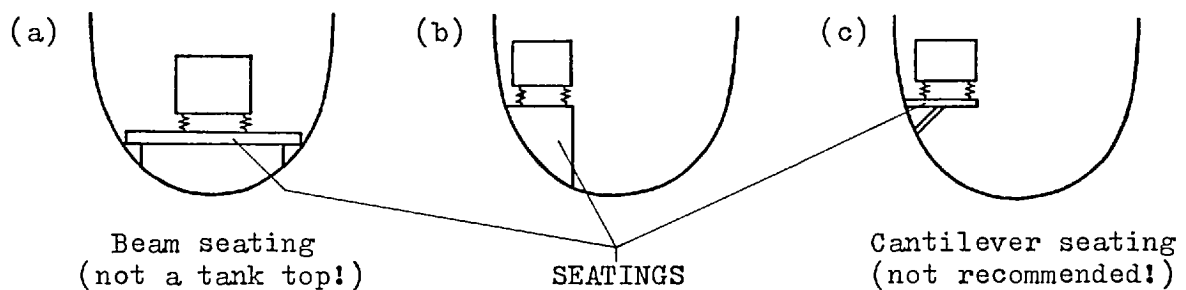
The machine, isolator and foundation were then coupled together theoretically to obtain the transmissibility curve T_m shown in Fig. 1.5. This clearly shows the basic bouncing resonance of the machine on its mounts at 4 Hz, followed by the characteristic drop-off at 12 dB/octave. Then at 190 Hz we find a fairly strong resonance which is associated with flapping of the engine foot, the frequency having been reduced from the original 269 Hz by the loading effect of the upper plate of the mount. This obviously combined with the nearby excitation component to yield the strong vibration transmission observed in the engine-running tests, but an improvement could be obtained by adding extra mass at the tip of the foot in order to further reduce its resonant frequency. The remaining resonances result from wave effects in the mounts, and if it were not for

these the transmissibility would drop off much more rapidly after the foot resonance. This curve is fairly typical of most single-stage isolation systems, in that break-up of the components normally starts to show itself at a frequency somewhere between 10 and 100 times the fundamental bouncing resonance. However, after its initially detrimental effect, the single resonance of the engine foot has proved very beneficial, since it has led to reduced high-frequency transmissibility; but this benefit would not have been obtained if the foot had exhibited significant higher resonances⁽¹⁴⁾.

Although the transmissibility T_m shows the attenuation in force through the complete system, it gives no information on the improvement that has been obtained by introducing the mounts beneath the machine, so it is useful to also consider the transmissibility $T_{m\infty}$ obtained with a directly mounted machine (ie. mounts effectively set to infinite stiffness). If we now form the ratio $T_{m\infty}/T_m$ (by simple subtraction on the log-log plot), we obtain the ISOLATION EFFECTIVENESS⁽⁵⁾⁽⁸⁾⁽¹⁷⁾. It is clearly seen that the effectiveness of the isolator in the present system fluctuates very considerably with frequency, and around 200 Hz, it has so little effect that it could ^{be} removed. In contrast, the classical model of Fig. 1.1b predicts an isolator effectiveness which is the reciprocal of the transmissibility, so it increases steadily with frequency.

This example has demonstrated the important effect that engine feet can have on the response; in particular, if the feet can be designed to have only one major resonance, they may *be dynamically decoupled and thus introduce* an extra stage of isolation. However, the decoupling frequency must be fixed by the designer, and the feet should be suitably damped (so they should not be integral with the body of the engine, but should be bolted in place in order to obtain some damping contribution from the joint). If the foot is multi-resonant, like the mounts, then the performance will definitely be impaired⁽¹⁴⁾.

The receiver structure in this example was so stiff as to have very little effect on the transmissibility, but it is sometimes necessary to interpose a slightly more flexible FOUNDATION STRUCTURE or SEATING between the mounts and the receiver structure. This is often only necessary because the mount positions on the machine do not line up with suitable attachment points on the receiver, and it is quite common in the case of shipboard machinery. Three possible examples are shown below:



One may be tempted to make use of existing support structures, such as a fuel tank, but this should be avoided if at all possible, since they are generally fairly flexible and lightly damped, with many natural frequencies even at moderately low frequencies (< 50 Hz). Hence, it is very likely that resonances will be excited, and large plates make perfect sound radiators in addition to transmitting vibration to the receiver structure. Therefore, seating structures should be carefully designed and should preferably be constructed from beams rather than plates, since beams possess a far smaller sound radiating surface and they do not generally resonate at such low frequencies. Also, from a purely analytical point of view, it is far easier to predict the high-frequency response of beam-like structures, so it is feasible to design such structures for optimum vibration isolation.

A complete analysis which takes into account the resonant behaviour of the machine, isolators and foundation structure is necessarily fairly complex, but it can yield much more realistic results than the classical model, and it can take into account multi-directional vibration transmission. Snowdon⁽¹⁴⁾⁽¹⁹⁾

has analysed a number of systems taking these factors into account, but he has treated each system separately, and he has not employed directly measured data for any of the components. Lachlan⁽²⁰⁾ has analysed a model system using a modal energy approach, but this is only approximate, and the use of modal parameters tends to cloud the basic physical aspects of the system. What is obviously required is a more general analysis procedure, which can be readily used by the designer to suit his own requirements, and this is provided by the "Building Block Approach"⁽²¹⁾⁽²²⁾. This permits one to break one's system down into a number of subsystems or building blocks, and then to obtain the dynamic characteristics of each by whichever method is most convenient (ie. "exact" theory, approximate theory, or measurements), so it is possible to combine data from various sources. The frequency response analysis of structures using this approach is discussed in Chapter 2, where details are also given of a general-purpose computer program developed by the Author to permit the solution of a wide variety of problems.

1.3 TWO-STAGE ISOLATION SYSTEMS

We have so far confined our attention to the theoretical analysis and the observed behaviour of single-stage mounting systems, and we have not yet looked at the basic physical aspects of vibration isolation. These are best explained by looking at the flow of force through the system:

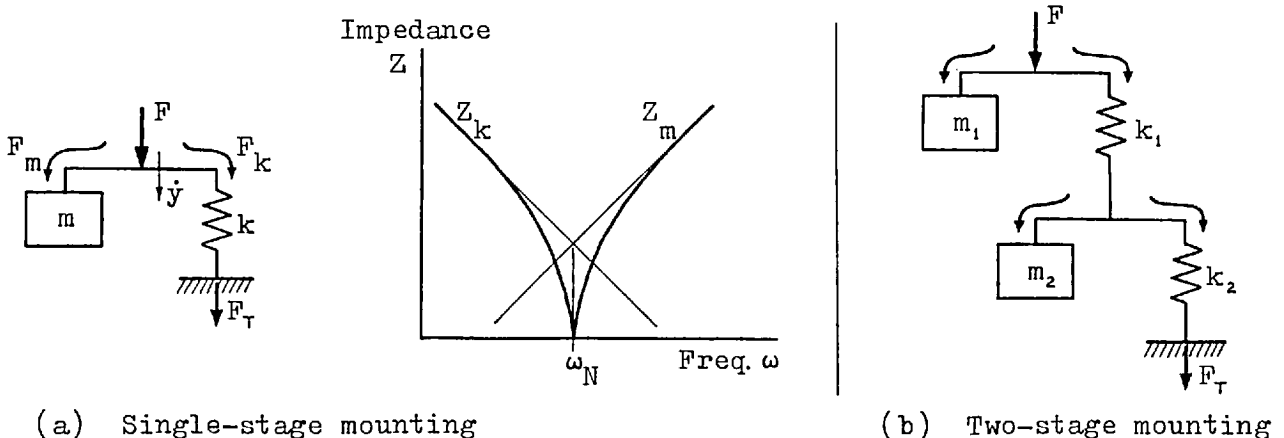


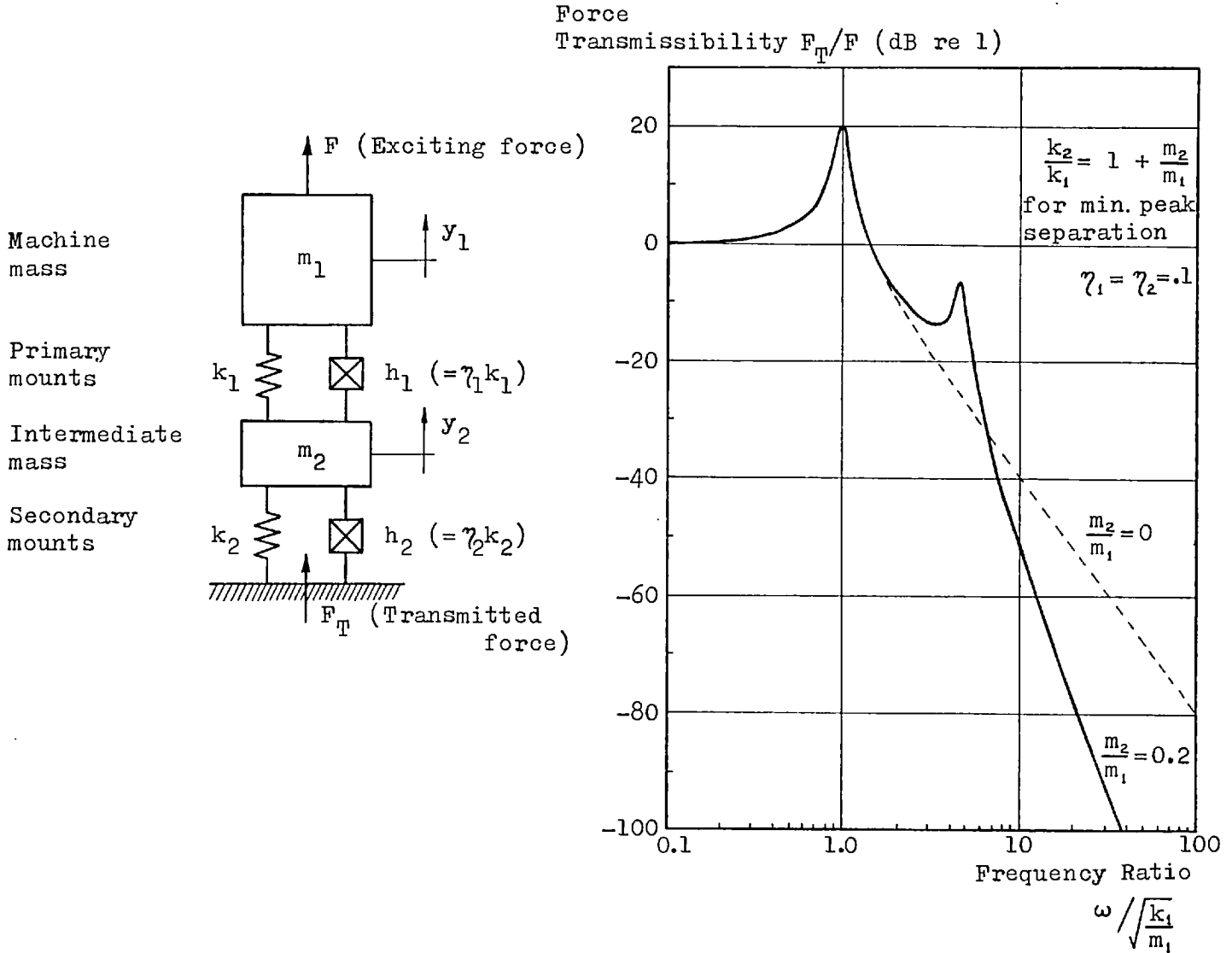
Diagram (a) above shows the basic single-stage isolation system (without damping) and it gives a much clearer picture of the force flow than does the classical diagram in Fig.1.1b. It is seen that the input force F divides between the mass m and the spring k , and the proportion taken by each depends upon their IMPEDANCES*, $Z_m = j\omega m$ and $Z_k = \frac{k}{j\omega}$, which are shown plotted against the circular frequency ω . At frequencies below ω_N , the impedance of the spring is dominant, so this takes most of the force and transmits it straight to ground; above ω_N the impedance of the mass becomes dominant, so this absorbs more and more of the force as the frequency is increased, thereby leaving less to go through the spring. Obviously, if more mass elements can be introduced into a system, then even less force will get through at high frequencies, so a logical next step is the two-stage system shown in diagram (b). The force flow through this system may also be examined graphically, and the details are given by Salter⁽²³⁾. This procedure is very useful for gaining a clear physical insight into the effect of various parameters on the isolation.

Thus, if high-frequency vibrations are of particular importance, it is better to use a two-stage mounting system, which is shown in its more classical form in Fig. 1.6a. Although this introduces a second vertical resonance at fairly low frequencies, it gives very much improved high-frequency attenuation due to the action of the intermediate mass, so the high-frequency drop-off in transmissibility becomes 24 dB/octave (= 80dB/decade). This system has been

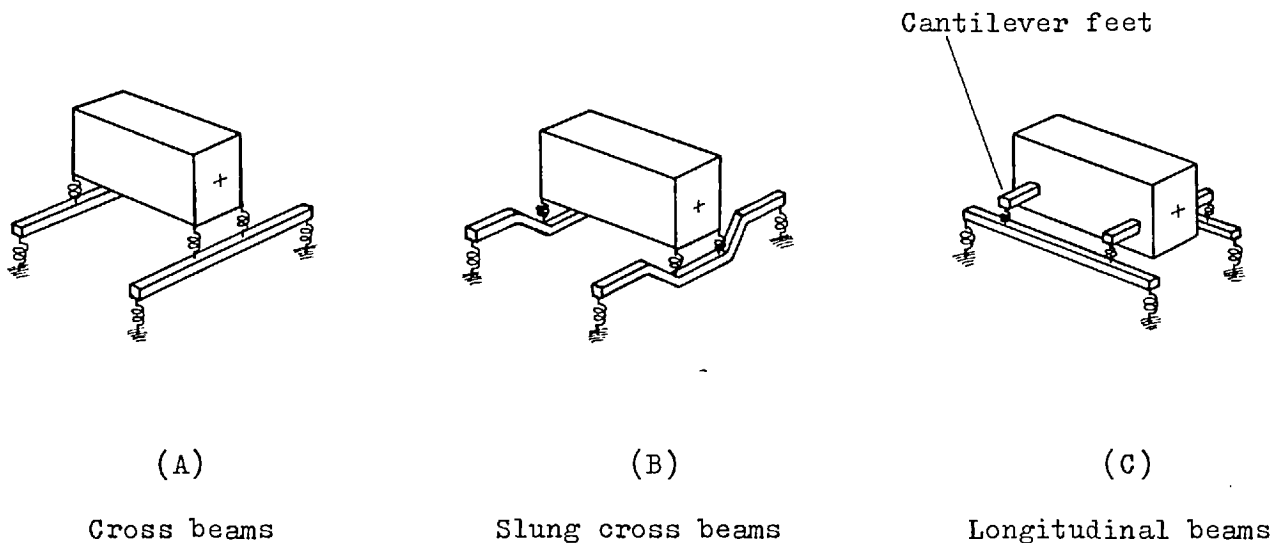
* Note that one could equally well employ DYNAMIC STIFFNESS ($-\omega^2 m$ for mass and k for spring). Dynamic stiffness is the complex ratio of force to displacement, and its reciprocal is RECEPTANCE: These are generally more convenient for calculation purposes, since the complex operator j (or i) is only introduced when damping is considered, besides which displacement is normally better understood by mechanical engineers. IMPEDANCE is the complex ratio of force to velocity, and its reciprocal is MOBILITY: These are normally more convenient when considering log-log frequency response plots, since they yield clearly identifiable stiffness and mass-like behaviour (lines with slopes of -1 and $+1$ respectively) and symmetric resonance curves. In addition, for complex structures the impedance and mobility curves fluctuate about an approximately horizontal mean line, so the overall dynamic range is less than for dynamic stiffness or receptance and it is possible to use larger dB divisions on the graph paper (thereby retaining more detail on the curve).

FIG. 1.6 TWO-STAGE ISOLATION SYSTEM

(a) "Classical" model (with Hysteretic damping)



(b) Possible configurations using beams for the intermediate mass



examined in detail by Snowdon⁽¹⁷⁾, and some practical examples of its use are given in References (8) and (24): the second of these relates to the mounting of shipboard diesel generators on an extensive intermediate mass, or RAFT.

Unfortunately, the ideal high-frequency drop-off of 24 dB/octave can rarely be obtained in practice, since the intermediate mass used in machine mounting systems is usually of such dimensions that its first resonance invariably occurs somewhere between 50 and 200 Hz. This is unavoidable, but these resonances can be controlled by the application of a suitable damping treatment.

The resiliently-mounted intermediate mass is called a foundation structure or seating, like the directly-mounted intermediate structure discussed in Section 1.2, and just as before, the use of a plate construction should be avoided if at all possible. The use of beams is recommended, and these should preferably be of either box or I section in order to obtain as high a stiffness/weight ratio as possible, thereby delaying the onset of break-up.

Three possible beam configurations are shown Fig. 1.6b. System A is the simplest, but there may be a tendency for the machine to sway at quite low frequencies, since its centre of gravity is so much above that of the cross beams. Systems B and C are to be preferred, since they give better low frequency stability, and obviously, C is easier to construct since it still uses straight beams. The two beams may be kept completely separate or they may be tied together using other beams at right angles, but it should be remembered that the introduction of these other beams must introduce other resonances, and most especially a low frequency torsional mode of the resulting frame. These resonances may be controlled using constrained layer damping, as will be demonstrated further below.

When designing such a system, the second vertical natural frequency should be carefully chosen so as to avoid the running speed of the machine. At the same time, even though it may be theoretically desirable to reduce this frequency as much as possible, one should take care not to make the system laterally

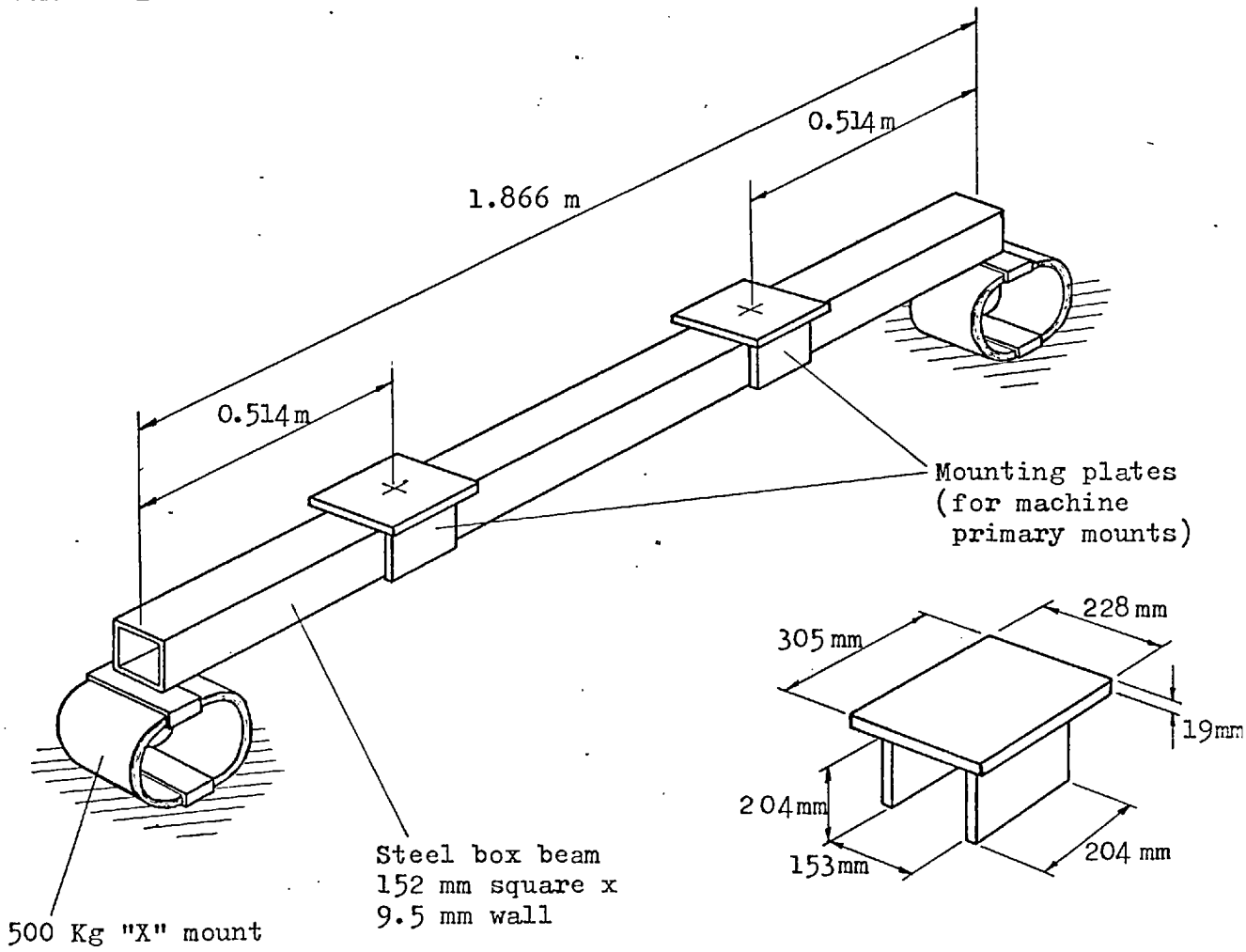
unstable. Typically, this second frequency will be somewhere between 4 and 10 times that of the machine on its primary mounts, and with this sort of separation, the frequencies of the compound system differ very little from $\sqrt{\frac{k_1}{m_1}}$ and $\sqrt{\frac{k_2}{m_2}}$ respectively. This implies that the intermediate mass looks almost like a rigid support for the primary mounts at low frequencies[†]; and this may very well continue to be the case when the seating breaks up, provided that the seating impedance is still considerably greater than the mount impedance (say 10 times or 20 dB greater). If this is so, it is possible to analyse the seating separately from the machine, and the total transmissibility is then given by the product of the seating transmissibility and the machine/primary-mount transmissibility, where the latter is obtained assuming a rigid support.

The analysis of this type of floating seating is relatively straightforward with the general-purpose computer program described in Chapter 2, so a detailed study was made of one particular system in order to formulate some general design rules⁽²⁵⁾. This is shown in Fig. 1.7, and it comprises a stiff undamped box-section beam^{*} (to give a high fundamental bending frequency) on heavily damped flexible supports. Sitting over the top of the beam are some mounting plates to which the primary mounts may be attached, so these add some mass loading. The mounting plate mass and moment of inertia are 22.508 Kg and 0.23277 Kg-m² respectively, and the beam is a 152 mm square box with 9.5 mm walls. As the X mount considered in Section 1.2 is a commercially available unit incorporating high damping, it was decided to use the existing measured data in order to introduce this type of mount under the beam tips. However, the existing data were for a 10 Kg mount, whilst the present seating was to be capable of supporting 1000 Kg per beam, so the measured data were scaled up by a factor of 50 in order to obtain approximate data for a 500 Kg mount.

* This was represented using a Timoshenko beam model, which includes the effects of shear stiffness and rotary inertia and is therefore more suitable for the present stiff beam.

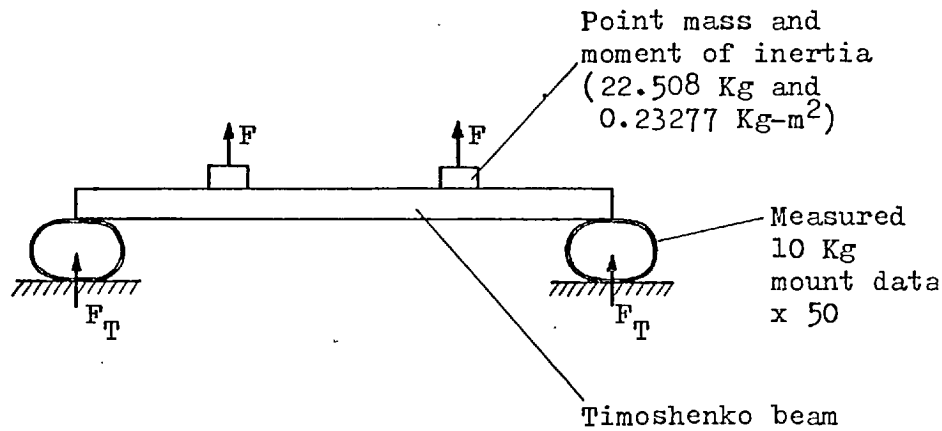
† Except near the resonance of the intermediate mass on the secondary mounts.

FIG. 1.7 FLOATING BEAM SEATING (Box section beam on X mounts)

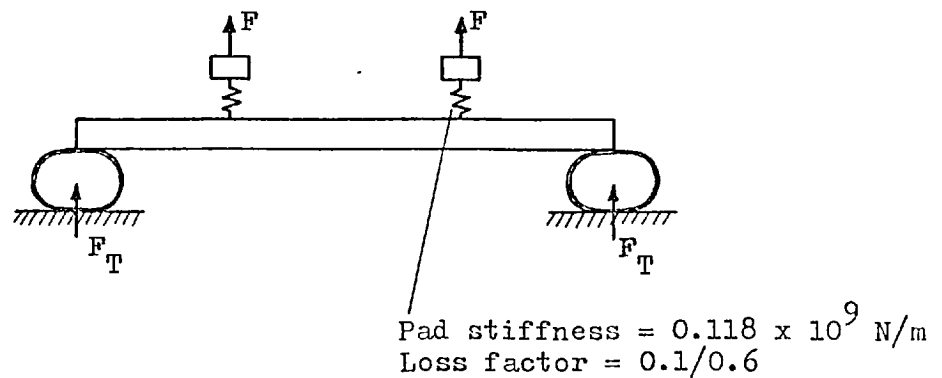


Model:

(a) Mounting plates connected directly to beam



(b) Mounting plates on decoupling pads



This floating beam might represent one of the cross or longitudinal beams in one of the systems shown in Fig. 1.6b, and it could be analysed independently of any machine due to its high input impedance relative to that of the primary mounts. The beam length and mounting plate positions were chosen to be the same as those used in an existing engine mounting system, but it is now instructive to look at Fig. 1.8, which shows the force transmissibility obtained with the mounting plate in various positions. It is seen that, quite by chance, the standard configuration gives an almost optimum response, since it yields a deep trough at 420 Hz due to a cancellation effect between the first and second symmetric modes of the beam. This phenomenon has been examined by Snowdon⁽¹⁷⁾⁽²⁶⁾ who has shown that it can be particularly effective in the case of a long machine with four mounts per side, that is supported by a floating foundation, since the forces then act together to completely eliminate all traces of the second beam mode⁽¹⁹⁾. As the present system is symmetric, one may consider just half the beam as a sprung-sliding beam with a single force input: then, the cancellation results from the beam tip response in mode 1 being equal and opposite to that in mode 2 (so that there is no compression of the secondary mount). By considering a two-term receptance series, it may be shown that cancellation is possible at any frequency ω_c between the two resonances Ω_1 , and Ω_2 provided that the excitation is applied at such a position that $\phi_F^{(1)} / \phi_F^{(2)} = (\omega_c^2 - \Omega_1^2) / (\Omega_2^2 - \omega_c^2)^*$, where $\phi_F^{(i)}$ represents the value of the beam characteristic function for mode i at position F . Thus, using either standard tables (as have been compiled by Bishop and Johnson⁽¹³⁾ for Bernoulli-Euler beams) or specially computed mode shapes, it is possible to determine the excitation position for cancellation at a specific frequency.

The heavy damping in the X mounts is seen to be very effective in controlling both the bouncing resonance and the 1st flexural resonance of the beam, but it has less effect on the 2nd beam resonance. Since this has a very

* Note that this ratio must be positive.

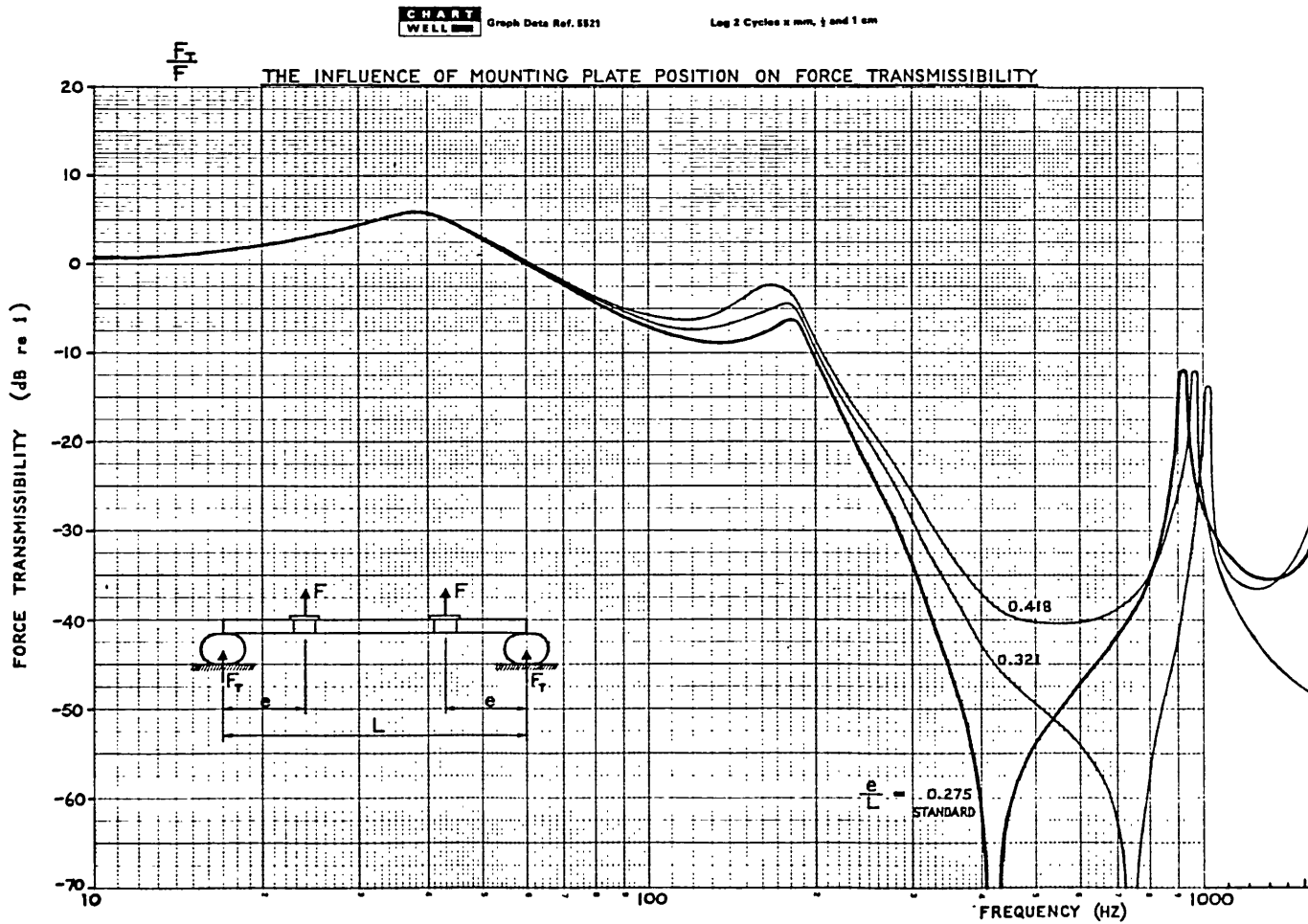
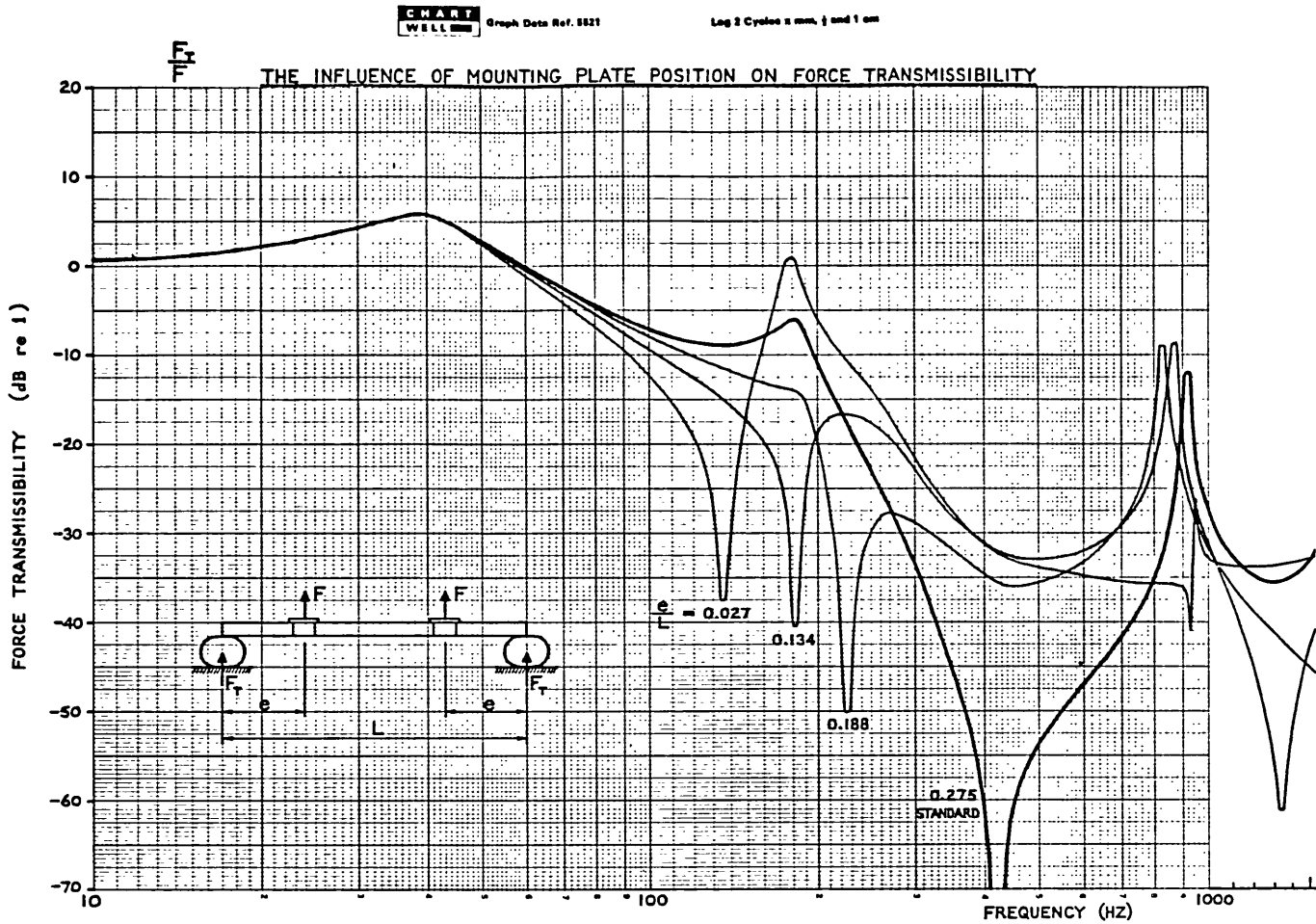
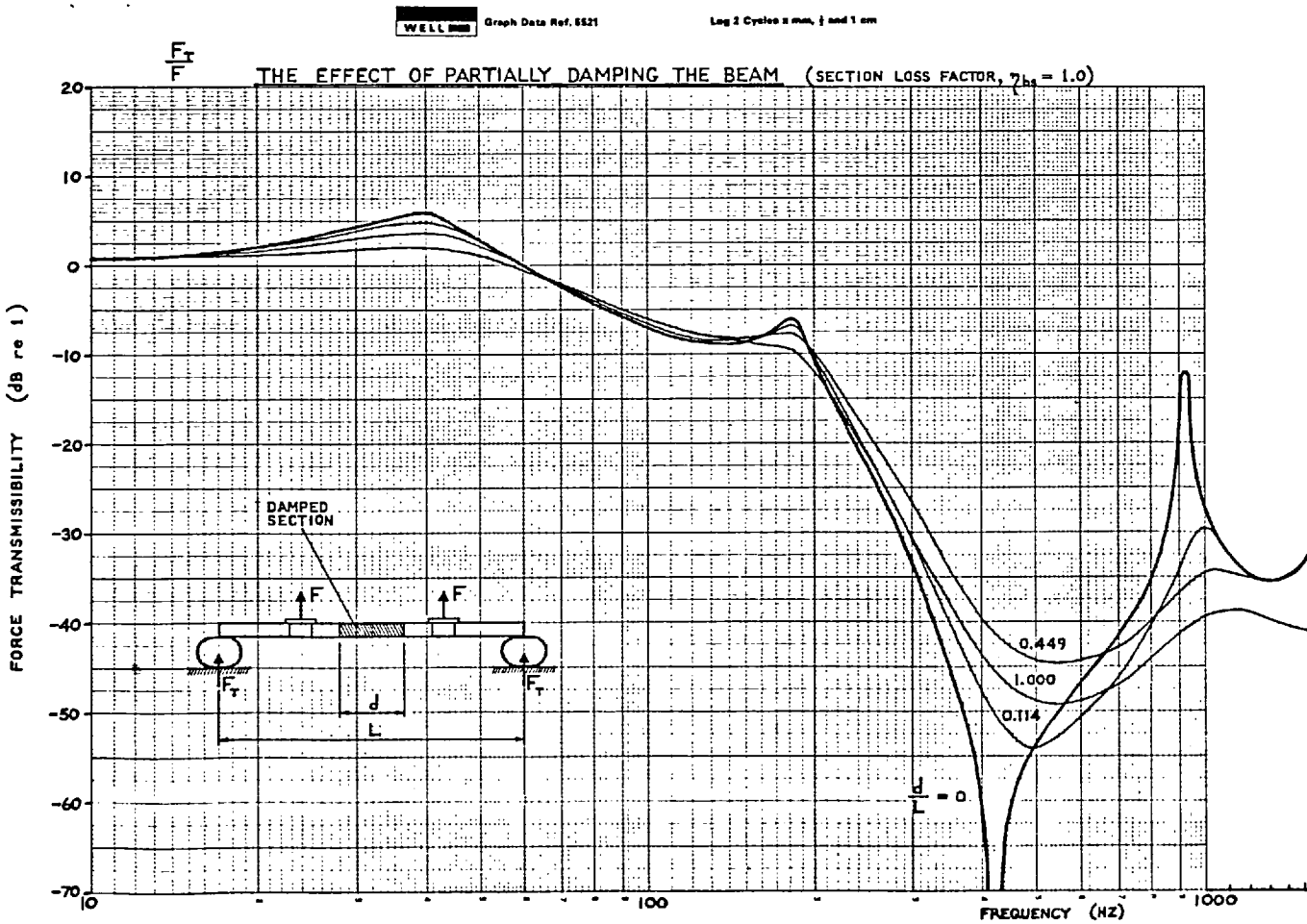
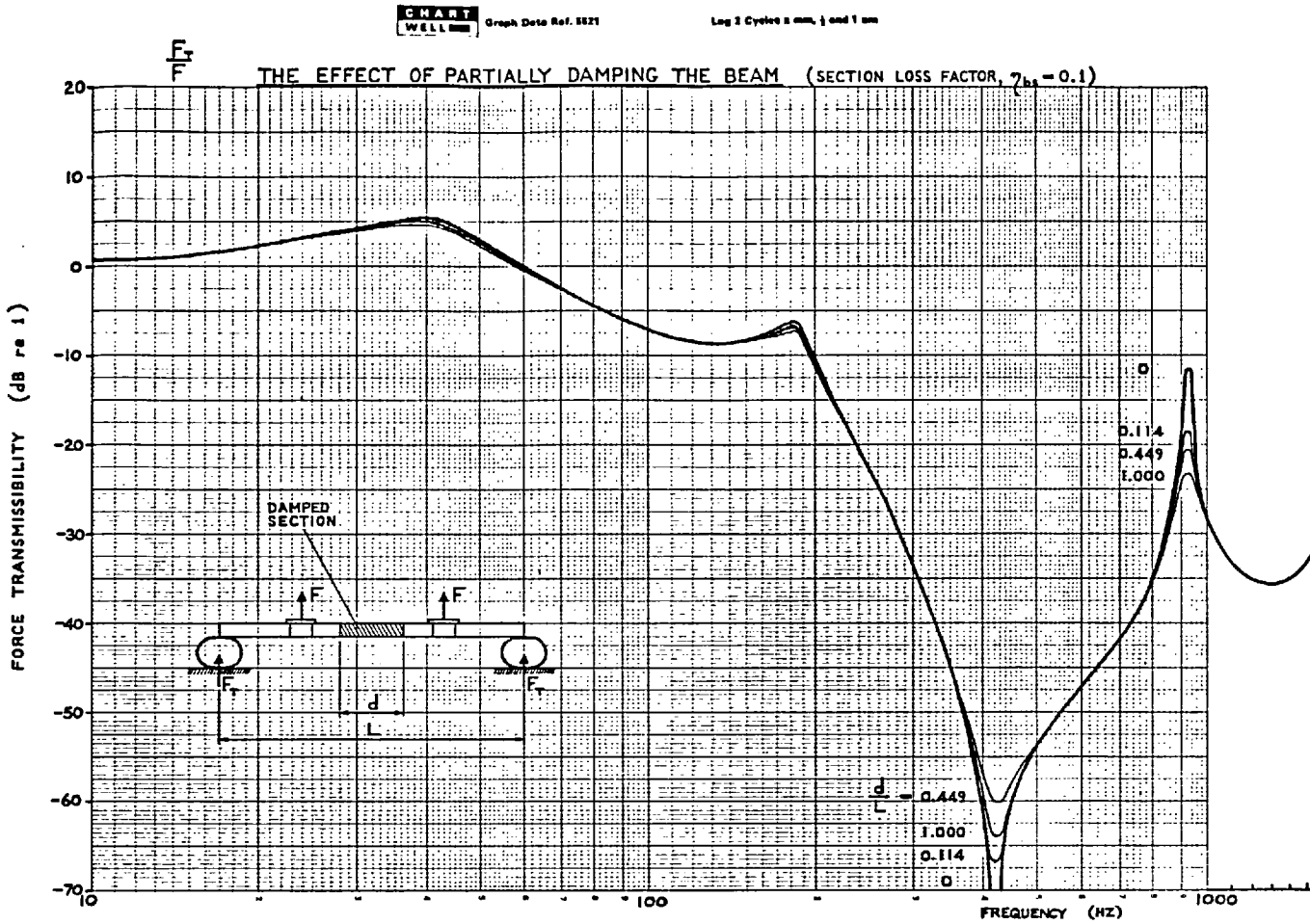
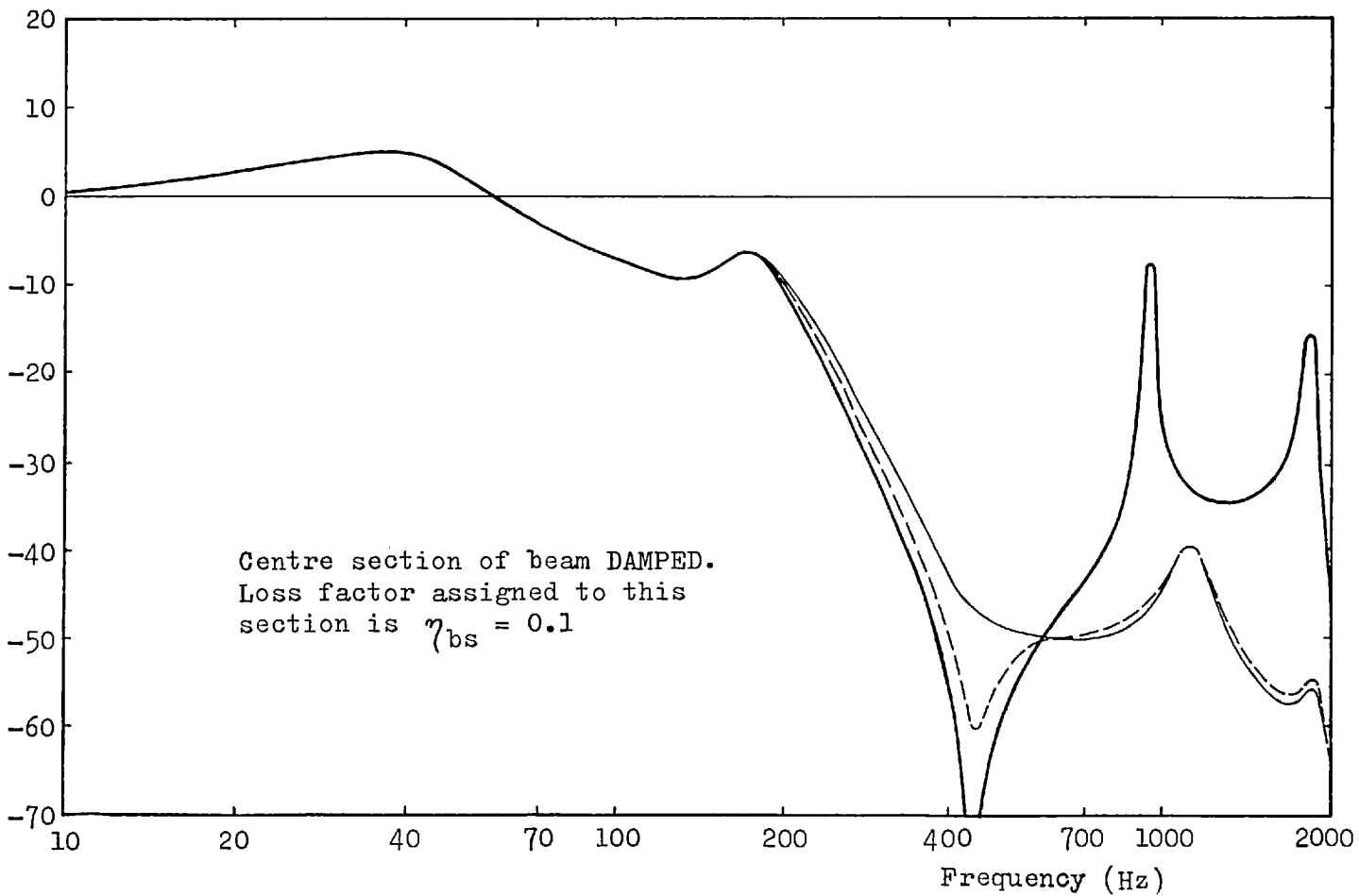
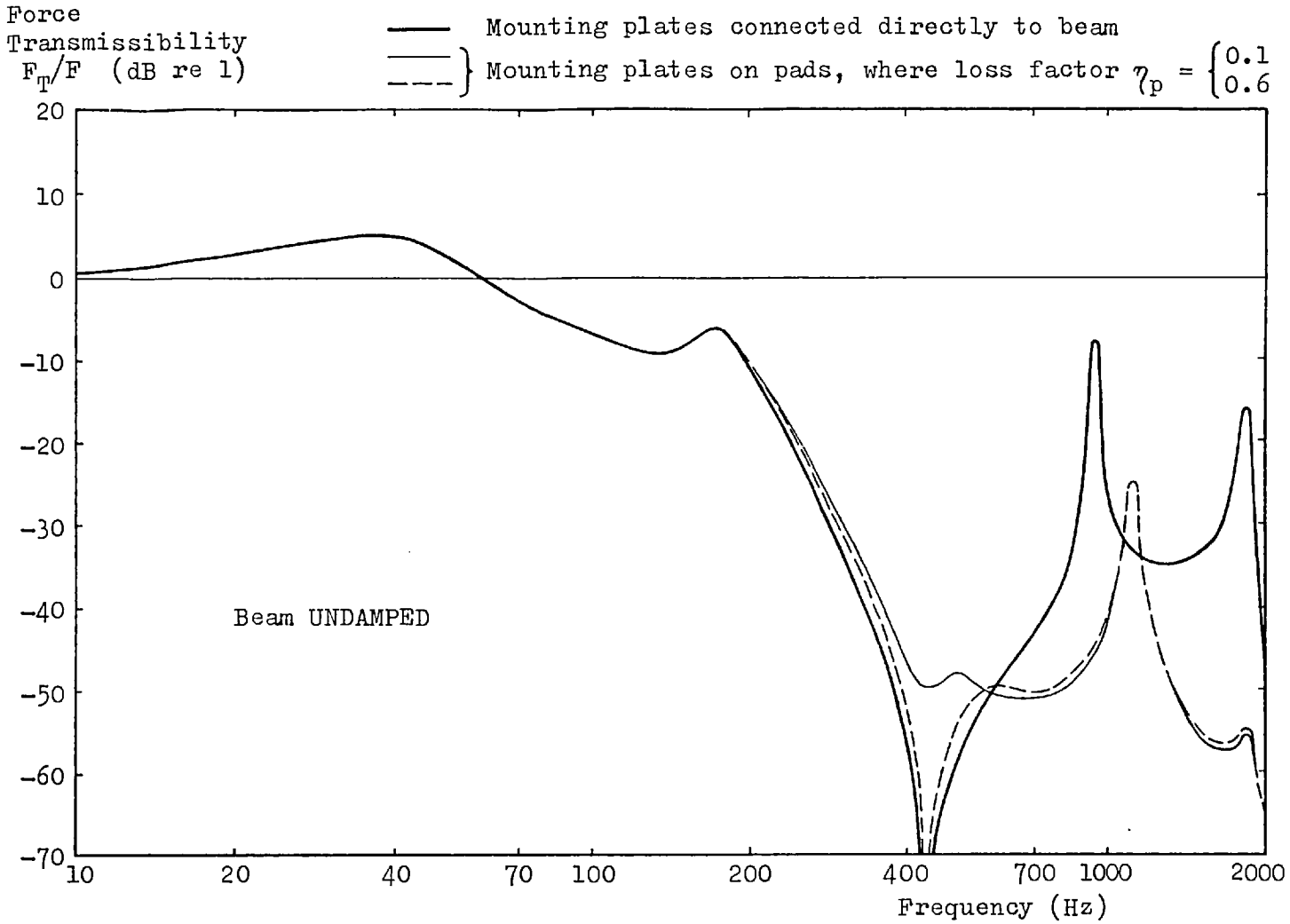


FIG 1.9



Symmetric excitation of steel box beam on 500 Kg X mounts.
 Each mounting plate resonates on its pads at 450 Hz.



detrimental effect on the high-frequency transmissibility, it would be helpful if it could be suppressed, so it was decided to investigate the possibility of achieving this by applying damping to the beam. The results are shown in Fig. 1.9, and it should be noted that the beam has been damped over sections of varying length, rather than only over the complete length. The damping has been assumed uniform in the section and has been introduced by using a Timoshenko beam with complex elastic and shear moduli. The results for a section loss factor of 0.1 clearly show that very little improvement is obtained, and only with a loss factor of 1.0 is the peak really cut down. Further calculations⁽²⁵⁾ were carried out using multi-layer beam finite elements to apply a constrained damping layer to the existing beam, and these have shown that no add-on treatment (as opposed to an integrally damped sandwich) can give much better results than the 0.1 section loss factor. Another important point to note from these results is that it is not always cost-effective to damp a beam or plate over its entire surface; in the present case, the drop in the resonant peak due to the application of damping over only 10 % of the length has not been matched by a similar drop when the treatment was applied to the remaining 90 %. This concurs with some results obtained by Plunkett⁽²⁷⁾: he has found that for a beam with damped supports, very little improvement is obtained by extending the beam damping beyond the centre section. Nokes and Nelson⁽²⁸⁾ and Grootenhuis⁽²⁹⁾ have also observed an optimum coverage for beams with other end conditions, whereby full coverage does not yield the highest damping.

As the application of damping to the beam was ineffective in controlling the troublesome resonance, it was necessary to try another remedy. This was to effectively introduce another stage at high frequencies by placing stiff pads under the mounting plates so that they would uncouple at a pre-determined frequency. However, since this would introduce a bouncing resonance of the mounting plates, it was decided to fix this resonance at the same frequency

as the transmissibility trough^{*}. The results are shown in Fig. 1.10, and a tremendous improvement is immediately seen, especially when damping is also applied over the centre section of the beam, between the mounting plates (0.449 coverage). The damping in the decoupling pads affects the depth of the trough, but even a loss factor of 0.1 is sufficient to prevent any significant peak from showing, and a higher loss factor is easily obtainable in practice. The required stiffness and damping could be obtained from four pads of Velbex PVC⁺, each approximately 25 x 25 x 4.5 mm (Loss factor = 0.66), so this provides a very practicable and cheap solution to the problem.

The decoupling of a fairly compact mass in this way is a very effective means of improving high-frequency transmissibility, and it is similar to the very fortuitous decoupling of the engine foot in the example given in Fig. 1.5. As a small mass does not break up until the frequency reaches several thousand Hz, it can remain effective long after the basic intermediate mass of the seating has broken up. Thus, the inclusion of thin stiff pads in all joints can prove very beneficial in applications where high frequencies are involved.

1.4 SUMMARY

We have examined the theoretical and practical aspects of single- and two-stage mounting systems, and have seen that classical vibration isolation theory has many limitations, especially at high frequencies. It has been shown that multi-directional vibration transmission should not be ignored, and that all the elements of any isolation system cease to behave as originally intended as soon as the frequency rises much above 100 Hz. The resulting resonances must be controlled by the application of damping, and this may often be quite effective when only applied to small areas of the structure. At the

* The chosen decoupling frequency corresponds to the 450 Hz trough yielded by the undamped system, rather than to the 420 Hz trough of the damped system.

+ See Part 3, Chapter 12

same time, efforts should be made to introduce further stages of isolation at high frequencies, to counteract the break-up of the major structural elements. This is possible by introducing stiff resilient elements underneath the more compact "massive" elements of the system.

The analysis may be carried out using general-purpose computer programs which permit one to "build" and "test" a system at the design stage. It has also been shown that more accurate theoretical predictions are possible if measured impedance data can be used to describe those elements of the system that are not amenable to reliable theoretical treatment.

We are now in a position to proceed to Chapter 2, where we shall examine the aforementioned programs which permit the frequency response analysis of a wide variety of damped complex structures; particular emphasis being given to efficient methods of introducing both linear damping and non-linear Coulomb friction damping. Then in Part 2 we shall look at the problem of measuring multi-directional mobility data, since this enables us ultimately to determine the full multi-directional vibration transmission into receiver structures and components which cannot at present be analysed. In Part 3 we shall consider the finite element analysis of multi-layer damped beams, thereby enabling us to include realistic distributed damping in the components of the isolation system. Finally, in Part 4 we shall look at the full analysis of a heavily damped machinery seating which was designed to provide efficient multi-directional isolation up to high frequencies. The design and analysis of this system takes account of all the factors discussed in this Introduction and gives some idea of the present analytical capabilities with regard to isolation system design.

Two publications based on this work are included at the end of Volume II. These relate to multi-directional measurements and the seating analysis, and they provide a useful summary of much of the work described in Parts 2 and 4.

CHAPTER 2

THE FREQUENCY RESPONSE ANALYSIS OF DAMPED COMPLEX STRUCTURES

2.1 INTRODUCTION TO THE BUILDING BLOCK APPROACH

The rapid development of the digital computer during the last few years has permitted the solution of many hitherto insoluble problems. However, a study of the resulting literature soon reveals that a large number of people have analysed many similar and highly idealised systems by a wide variety of different methods.

Many papers exist on the vibration of multi-degree of freedom systems of the spring-mass type, or more often its torsional equivalent. In addition, considerable emphasis has been placed on the flexural vibration of beams; generally of the Bernoulli-Euler type, with standard boundary conditions such as pinned-pinned, clamped-free, etc. Problems examined include the response of non-uniform beams continuous over one or more supports, two and three dimensional frames built up from beams, and beams with attached masses, springs and dampers. Other papers have dealt with the vibration of plates and shells, and the application of constrained layer damping to these, as well as to beams.

Many of these problems have been solved from first principles, by deriving the governing differential equation(s) and imposing the required boundary conditions, and the computer has only been used at the final stage to solve the resulting algebraic or transcendental equation(s) for the natural frequencies or the forced response. This approach is much too restricted, since individual problems are solved in isolation from one another. What is required is a more general approach, which is readily applicable to the analysis of any system built up from different types of component. A very important step in this direction has been the development of the "finite element" method^{(30)(31)*}, which has facilitated the analysis of some extremely complex structures, involving plates, shells, beams, etc. However, there are still some components which defy accurate analysis

* Note that References for Chapters 1 and 2 are listed on page 75.

and others for which this method does not give the most direct solution. A more general approach is to divide the structure or system into a number of subsystems which may be individually analysed for their frequency response properties by whichever method is most convenient, and whenever analysis is impossible, the data may be measured on an actual subsystem or on a scaled-down model. These subsystem data may then be combined to give the response properties of the assembled system. This technique is known as the "building block" approach⁽²¹⁾⁽²²⁾⁽³²⁾ to structural dynamics, and it is particularly attractive since it parallels the design process where major structural components, or substructures, are often designed by different engineering groups and then built up into an assembly.

There are basically two ways of determining total system behaviour from subsystem dynamic properties. The first of these is a direct coupling procedure which takes the subsystem frequency response data and builds a set of linear equations describing the total system response. With this approach the building process and the solution of the equations for the system response is carried out afresh at each frequency. The "dynamic stiffness coupling" technique⁽¹⁸⁾⁽³³⁾⁽³⁴⁾ falls into this category, since the subsystem data are set up as dynamic stiffness matrices and these are then combined to form a system dynamic stiffness relation which one solves for the forced response. Alternative techniques are "receptance coupling"⁽³⁵⁾⁽³⁶⁾ and the "general impedance method" used by Klosterman⁽²¹⁾⁽³²⁾⁽³⁷⁾⁽³⁸⁾. The latter is slightly more general in that one may mix receptance and dynamic stiffness data when building the system matrix. However, it does have the disadvantage that the system matrix is larger than that arising with the dynamic stiffness method.

The second approach to determining system response is that of "component mode synthesis"⁽²²⁾⁽³²⁾⁽³⁷⁾⁽³⁹⁾, in which one starts either with subsystem modal data or with the equivalent mass and stiffness matrices and combines

these in such a way as to obtain the natural frequencies and mode shapes of the full assembly. The forced response is then obtained by summing the responses in the various modes. This is a very powerful approach, but it is slightly less general than any of the direct coupling techniques, since one cannot utilise directly any response data obtained from an "exact" analysis or from measurements (eg. as for anti-vibration mounts with frequency-dependent stiffness and damping).

Bearing in mind the need to combine data from various sources, it was decided to make use of a direct coupling procedure in the present work. Also, in view of its inherent simplicity and the saving in computer time associated with a smaller system matrix it was decided to use the "dynamic stiffness coupling" technique*. Accordingly, a Fortran computer program called COUPLE1 was developed to provide the means for applying the building block approach to small-scale problems, where the number of coupling co-ordinates does not exceed 25 for damped systems, or 50 for undamped systems. The storage requirements of this program are small and it will run on the Instant Turnround computing facility at Imperial College (Batch mode self-service facility using CDC 6400 or Cyber 7314 computer, Core storage $\approx 24576_{10}$ words, Central processor time ≈ 16 secs). An enlarged version of the program (COUPLE1/100) was also produced to cope with the analysis of the 50 co-ordinate damped machinery foundation structure described in Part 4, but at the present time this is not so highly developed as the "standard" version (COUPLE1/50).

The complete program is retained on file (magnetic disc), and it consists of a main block of routines which perform the coupling, and of a library of special routines which generate the response data for certain standard types of component. The existing library of special routines caters for spring-mass

* All the work described in this report is based either on dynamic stiffness or impedance coupling (depending on whether the response is displacement or velocity), but one example is given in Chapter 6 (Part 2) in which straightforward impedance coupling is compared with the general impedance method.

systems, Timoshenko and Bernoulli-Euler beams (both damped and undamped, and including torsional and axial stiffness for frame analysis), symmetrical 3- and 5-layer sandwich beams, and response data stored on file from a previous analysis of a sub-assembly (or from impedance measurements on an existing component). However, it is also possible for the user to incorporate his own subsystem routines, so the program is very general in that it can take subsystem data from virtually any source. Once the user has loaded those routines which are relevant to his problem, the main program couples together the subsystems and calculates the forced response* of the assembly.

The details of how the program works are given in Section 2.2, and full user instructions may be found in a comprehensive manual⁽⁴⁰⁾⁺. The latter is in three parts, which deal respectively with the main coupling program, the special subsystem routines, and a selection of worked examples.

* The frequency is incremented either linearly or logarithmically and both motions and transmitted forces are computed. The program does not determine natural frequencies and mode shapes, but this facility could easily be introduced by using a systematic search procedure to detect the zeroes of the determinant of the system matrix.

+ Note that the manual dated May 1975 does not contain the instructions for running the program completely from file, since at that time it was still necessary to retain certain routines on cards. However, the instructions given in the manual are not invalidated by the later modifications.

2.2 THE DYNAMIC STIFFNESS COUPLING PROGRAM "COUPLE1"

In the Introduction we briefly considered the very powerful technique of system vibration analysis known as the "building block" approach. Now, we shall look in detail at the way in which it is applied using the computer program COUPLE1*.

The first step in applying the building block approach is to divide the system into a number of subsystems which may be individually analysed for their frequency response properties. The specific information sought from each subsystem analysis is the frequency response data⁺ relating to all points of interest on the subsystem, and especially to the points where it is coupled to other subsystems. Depending upon the complexity of the component, these data may be obtained either by exact analysis, or by an approximate technique such as the finite element method, or by measurement. The second step is to combine the subsystem response data in such a way as to obtain the response of the assembled system. This coupling may be carried out in various ways, but the method employed in the program COUPLE1 is the "dynamic stiffness coupling" technique⁽¹⁸⁾⁽³³⁾.

The term "stiffness" is well understood as expressing the relationship between force and deflection under static loading conditions, and the term "dynamic stiffness" is a simple extension of this idea, expressing the relationship between a harmonic loading and the corresponding vibratory displacement at any specified frequency. In the case of components which are acted upon by a number of forces, the dynamic stiffness is expressed in terms of a matrix which relates the vector of applied forces to the corresponding vector of displacements.

* The program structure and a detailed flow chart are given in Appendix I. Note that this flow chart corresponds to the program as it was when the manual (40) was written, and it does not include the recent modifications for running the complete program from file. These modifications affect subroutine SUBSYS, which calls up the routines for generating the subsystem data. Also note that the program has provision for up to 12 subsystems.

+ The frequency response data may be in any one of a number of forms, which are all quite simply related. These are: Dynamic stiffness, Receptance, Impedance, Mobility, Apparent mass, and Inertance. They are defined in Chapter 3, Section 3.2.

The dynamic stiffness coupling technique consists of collecting the dynamic stiffness matrices for the subsystems at some specified frequency, and combining these in such a way as to form the dynamic stiffness matrix for the assembled system. One may then obtain the response of the system to any applied forces by solving a set of equations.

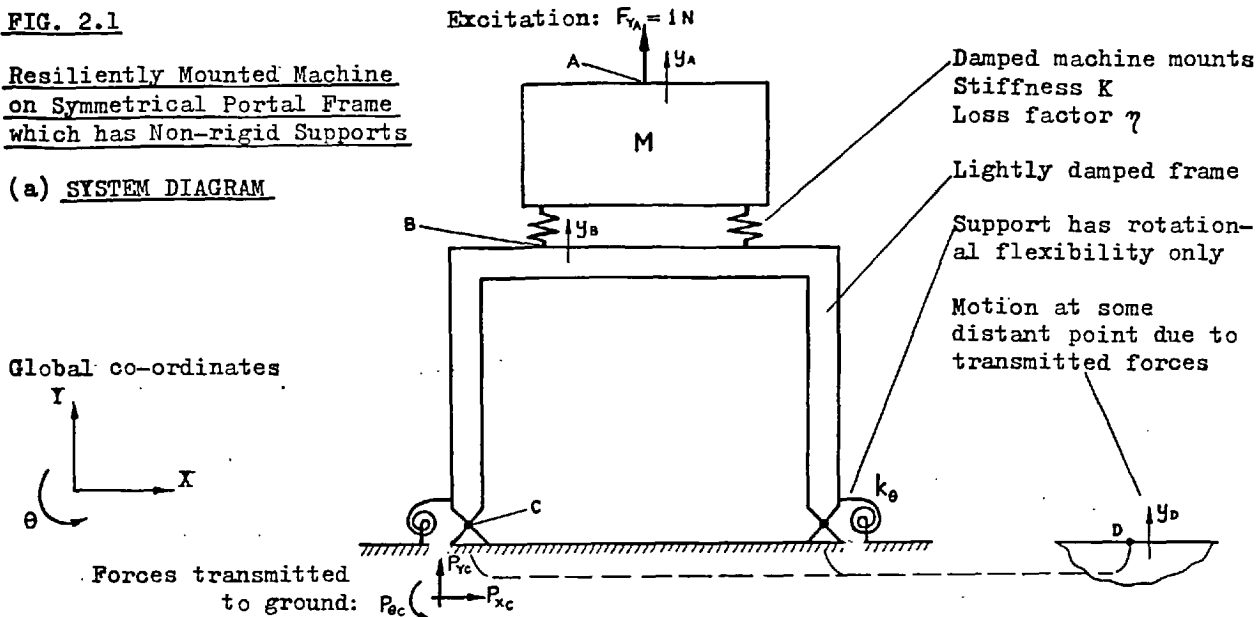
It was decided to use dynamic stiffness rather than one of the other forms of frequency response because stiffness and displacement are well understood and widely used in engineering analysis, and especially in the matrix analysis of vibration. Whether one is dealing with simple spring-mass systems, or the finite element analysis of large structures, one almost invariably uses, the "matrix displacement" approach (ie. a stiffness matrix relating force and displacement). If the system is at all complex, it certainly provides the most direct means of coupling the components together⁽⁴¹⁾. However, certain data will almost invariably be in receptance or mobility form, and these must first be converted to dynamic stiffness before the coupling is carried out.

The capabilities of the program and the way in which it works are best illustrated with reference to an example, so we shall consider the system shown in Fig. 2.1a. This comprises a resiliently mounted machine which is sitting on top of a foundation structure in the form of a symmetrical portal frame. The pillars of the frame are only quasi-encasté, (ie. partially built-in) there being some rotational flexibility at the support. When the machine is running, forces are transmitted through the frame to the ground, thereby giving rise to a disturbance at some point D which is remote from the machine. This might be a mounting point for some sensitive instrument, or it might be a point on the wall or floor of a room where people are working. Alternatively, it could very well be the sound pressure level within a room or in the water outside a ship.

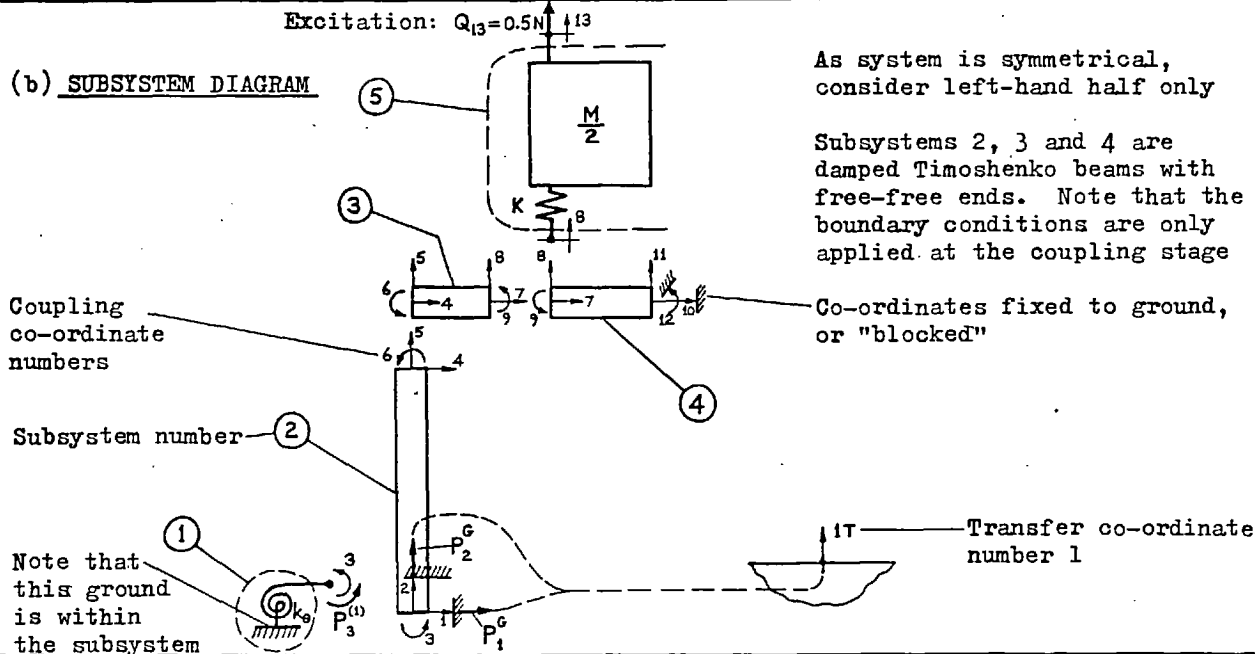
FIG. 2.1

Resiliently Mounted Machine on Symmetrical Portal Frame which has Non-rigid Supports

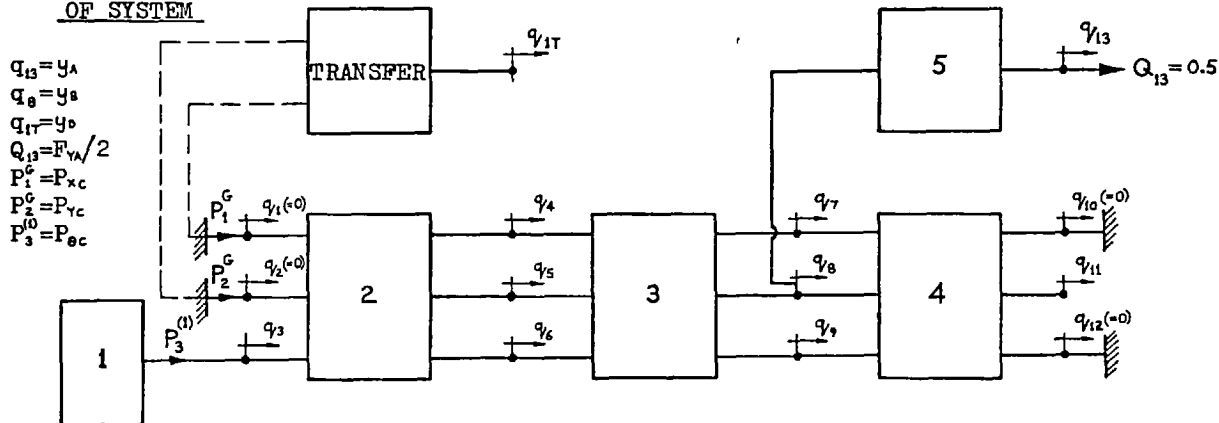
(a) SYSTEM DIAGRAM



(b) SUBSYSTEM DIAGRAM



(c) BLOCK DIAGRAM OF SYSTEM



q_i = Displacement at coupling co-ordinate i
 q_{iT} = Displacement at transfer co-ordinate iT
 Q_i = Externally applied force at coupling co-ordinate i
 P_i^G = Force transmitted to ground via fixed co-ordinate i
 $P_i^{(j)}$ = Force transmitted to subsystem j via coupling co-ordinate i

The very first stage in the analysis is to look for any symmetry in the system, as this can considerably reduce the amount of work involved in preparing the data, besides saving valuable computer time. However, care must be taken to apply the correct boundary conditions to any part of the system which is cut by the line of symmetry, so that the half-system which is being analysed behaves just as if the other half were still in position. As is seen from Fig. 2.1b, the present system may be cut down the middle and analysed in terms of 5 subsystems. These are a grounded spring, 3 free-free Timoshenko beams, and a free-free sprung mass. The reason why the beams are all considered in a free-free state is that this preserves generality, since it is only necessary to consider one type of beam. The boundary conditions may easily be applied once all the subsystems have been coupled together, by making use of the co-ordinate fixing* facility incorporated in the program. Thus, the pinned joint at the foot of the pillar is introduced by setting the displacements q_1 and q_2 to zero, and the sliding end⁺ condition imposed on the cross beam by the symmetry is obtained by making the displacements q_{10} and q_{12} zero.

The block diagram in Fig.2.1c represents the system as the coupling program sees it. The dynamic stiffness properties of the "black boxes" representing the 5 subsystems must be supplied by the user. The same thing applies for the transfer admittance data which relate the response at the remote point D to the forces transmitted to ground via the pin joint at C. For each subsystem one may either use one of the standard subroutines such as exist for spring-mass systems, beams, etc., or one may write a special set of Fortran instructions for generating the dynamic stiffness data. The standard routines must be loaded from file as and when they are required, while any user-inserted instructions must be formed into a subsystem routine called SUBSI, where I is the subsystem number (this routine may either be left on

* This "blocks" the required co-ordinates by setting their displacements to zero.

+ Note that this must be changed to a pinned end if the machine is excited by a couple, instead of a vertical force. The effective mass of the machine will also be different.

cards or it may be put on file). Such an arrangement is very flexible, since it is possible to incorporate virtually any type of subsystem data. The coupling program is simply given a letter code for each subsystem, to indicate whether it should call one of the standard routines (eg. A for a spring-mass system, C for a damped Timoshenko beam, etc.), or whether it should call SUBSI (indicated by a blank for the letter code). Thus, at each frequency the program proceeds through the set of subsystems, collecting the dynamic stiffness data from the various sources and building the system matrix. The resulting equations are then solved for motion responses and transmitted forces, and the transfer response routine SUBTRAN is called to generate the transfer admittance data from which the response at the remote point is computed. At the present time this routine must be built around a set of user-inserted instructions, in a similar manner to the subsystem routine SUBSI.

In the present example, the required subsystem response data are the 5 dynamic stiffness matrices given in Fig. 2.2. These are frequency-dependent matrices which relate the forces acting on the subsystem to the corresponding displacements, and in the case of subsystems 2 to 5 they are complex in order to take account of the damping^{*}. While the matrices for the grounded spring and the sprung mass may be formed quite simply from the relevant mass, stiffness and damping coefficients, those for the three beam sections are much more complicated. Using the "exact" solution for the flexural and axial vibrations of a Timoshenko beam, the elements of the dynamic stiffness matrix are given by complicated expressions containing both trigonometric and

* See Section 2.3 for a full discussion of damping, including how it may be incorporated in an analysis. Also note that the dynamic stiffness matrix for any passive linear subsystem is always symmetric, even if there is damping present. However, if a subsystem contains a rotor which is turning at a constant angular velocity the gyroscopic effect may cause the dynamic stiffness matrix to be non-symmetric (38)(42)(43). This is no problem as far as COUPLE1 is concerned, since the solution procedure does not require symmetric matrices.

FIG. 2.2 SUBSYSTEM DYNAMIC STIFFNESS MATRICES FOR MACHINE ON PORTAL FRAME

Subsystem 1 - Grounded spring

$$Q_3^{(1)} = Z_{33}^{(1)} q_3 = k_\theta q_3$$

Subsystem 2 - Damped Timoshenko beam (Pillar)

$$\begin{bmatrix} Q_1^{(2)} \\ Q_2^{(2)} \\ Q_3^{(2)} \\ Q_4^{(2)} \\ Q_5^{(2)} \\ Q_6^{(2)} \end{bmatrix} = \begin{bmatrix} Z_{11}^{(2)} & Z_{12}^{(2)} & Z_{13}^{(2)} & Z_{14}^{(2)} & Z_{15}^{(2)} & Z_{16}^{(2)} \\ Z_{21}^{(2)} & Z_{22}^{(2)} & Z_{23}^{(2)} & Z_{24}^{(2)} & Z_{25}^{(2)} & Z_{26}^{(2)} \\ Z_{31}^{(2)} & Z_{32}^{(2)} & Z_{33}^{(2)} & Z_{34}^{(2)} & Z_{35}^{(2)} & Z_{36}^{(2)} \\ Z_{41}^{(2)} & Z_{42}^{(2)} & Z_{43}^{(2)} & Z_{44}^{(2)} & Z_{45}^{(2)} & Z_{46}^{(2)} \\ Z_{51}^{(2)} & Z_{52}^{(2)} & Z_{53}^{(2)} & Z_{54}^{(2)} & Z_{55}^{(2)} & Z_{56}^{(2)} \\ Z_{61}^{(2)} & Z_{62}^{(2)} & Z_{63}^{(2)} & Z_{64}^{(2)} & Z_{65}^{(2)} & Z_{66}^{(2)} \end{bmatrix} \begin{bmatrix} q_1 \\ q_2 \\ q_3 \\ q_4 \\ q_5 \\ q_6 \end{bmatrix}$$

For beam dynamic stiffness, see Refs. 44 and 45

Subsystem 3 - Damped Timoshenko beam (Left hand section of cross beam)

$$\begin{bmatrix} Q_4^{(3)} \\ Q_5^{(3)} \\ Q_6^{(3)} \\ Q_7^{(3)} \\ Q_8^{(3)} \\ Q_9^{(3)} \end{bmatrix} = \begin{bmatrix} Z_{44}^{(3)} & Z_{45}^{(3)} & Z_{46}^{(3)} & Z_{47}^{(3)} & Z_{48}^{(3)} & Z_{49}^{(3)} \\ Z_{54}^{(3)} & Z_{55}^{(3)} & Z_{56}^{(3)} & Z_{57}^{(3)} & Z_{58}^{(3)} & Z_{59}^{(3)} \\ Z_{64}^{(3)} & Z_{65}^{(3)} & Z_{66}^{(3)} & Z_{67}^{(3)} & Z_{68}^{(3)} & Z_{69}^{(3)} \\ Z_{74}^{(3)} & Z_{75}^{(3)} & Z_{76}^{(3)} & Z_{77}^{(3)} & Z_{78}^{(3)} & Z_{79}^{(3)} \\ Z_{84}^{(3)} & Z_{85}^{(3)} & Z_{86}^{(3)} & Z_{87}^{(3)} & Z_{88}^{(3)} & Z_{89}^{(3)} \\ Z_{94}^{(3)} & Z_{95}^{(3)} & Z_{96}^{(3)} & Z_{97}^{(3)} & Z_{98}^{(3)} & Z_{99}^{(3)} \end{bmatrix} \begin{bmatrix} q_4 \\ q_5 \\ q_6 \\ q_7 \\ q_8 \\ q_9 \end{bmatrix}$$

Subsystem 4 - Damped Timoshenko beam (Right hand section of cross beam)

$$\begin{bmatrix} Q_7^{(4)} \\ Q_8^{(4)} \\ Q_9^{(4)} \\ Q_{10}^{(4)} \\ Q_{11}^{(4)} \\ Q_{12}^{(4)} \end{bmatrix} = \begin{bmatrix} Z_{77}^{(4)} & Z_{78}^{(4)} & Z_{79}^{(4)} & Z_{7,10}^{(4)} & Z_{7,11}^{(4)} & Z_{7,12}^{(4)} \\ Z_{87}^{(4)} & Z_{88}^{(4)} & Z_{89}^{(4)} & Z_{8,10}^{(4)} & Z_{8,11}^{(4)} & Z_{8,12}^{(4)} \\ Z_{97}^{(4)} & Z_{98}^{(4)} & Z_{99}^{(4)} & Z_{9,10}^{(4)} & Z_{9,11}^{(4)} & Z_{9,12}^{(4)} \\ Z_{10,7}^{(4)} & Z_{10,8}^{(4)} & Z_{10,9}^{(4)} & Z_{10,10}^{(4)} & Z_{10,11}^{(4)} & Z_{10,12}^{(4)} \\ Z_{11,7}^{(4)} & Z_{11,8}^{(4)} & Z_{11,9}^{(4)} & Z_{11,10}^{(4)} & Z_{11,11}^{(4)} & Z_{11,12}^{(4)} \\ Z_{12,7}^{(4)} & Z_{12,8}^{(4)} & Z_{12,9}^{(4)} & Z_{12,10}^{(4)} & Z_{12,11}^{(4)} & Z_{12,12}^{(4)} \end{bmatrix} \begin{bmatrix} q_7 \\ q_8 \\ q_9 \\ q_{10} \\ q_{11} \\ q_{12} \end{bmatrix}$$

Subsystem 5 - Sprung mass (free-free)

$$\begin{bmatrix} Q_8^{(5)} \\ Q_{13}^{(5)} \end{bmatrix} = \begin{bmatrix} Z_{88}^{(5)} & Z_{8,13}^{(5)} \\ Z_{13,8}^{(5)} & Z_{13,13}^{(5)} \end{bmatrix} \begin{bmatrix} q_8 \\ q_{13} \end{bmatrix} = \begin{bmatrix} K^* & -K^* \\ -K^* & K^* - \omega^2 M/2 \end{bmatrix} \begin{bmatrix} q_8 \\ q_{13} \end{bmatrix}$$

where $K^* = K(1 + i\eta)$
and $i = \sqrt{-1}$

hyperbolic functions^{(44)(45)⁺}. A standard subroutine called ZFLAX2D^x is available for setting up the exact dynamic stiffness matrix for a damped Timoshenko beam, and similarly, a subroutine called ZMAK2^x is available for dealing with spring-mass systems. Hence, the user need only load these two routines from file and introduce the letter codes A,C,C,C,A on the relevant data card, besides punching a few cards giving the beam parameters, spring stiffnesses, etc.

The coupling program increments the frequency in either linear or logarithmic steps over a specified range, and at each frequency it calls up the relevant subroutines to obtain the subsystem dynamic stiffness matrices for that particular frequency. These subsystem matrices are added together in such a way as to satisfy the laws of force equilibrium and displacement compatibility at the coupling co-ordinates, and the result is the system dynamic stiffness matrix shown in Fig. 2.3. At this stage the co-ordinates 1, 2, 10 and 12 are still free, so the matrix $[Z_{\text{sys}}]$ and the vector of applied forces $\{Q\}$ are both modified as shown in Fig. 2.4a in order to set the displacements q_1, q_2, q_{10} and q_{12} to zero. The forces Q_3 to Q_{11} listed in the force vector are only retained to preserve generality, and in fact the only non-zero force in the present problem is $Q_{13} = 0.5 \text{ N}$ *.

+ Both papers give the dynamic stiffness matrix for a Timoshenko beam, and each contains a different error.⁽⁴⁰⁾ Reference (45) is particularly recommended, since it gives an extremely good introduction to the analysis of beam systems.

x Details of the special subroutines ZFLAX2D and ZMAK2 are given in Part 2 of Reference (40).

* Although we are here restricting our attention to a force input, it should be mentioned that it is also possible to apply a motion input. This is not incorporated as a special feature, but it is easily arranged by connecting a very large impedance to each excitation point and then applying a correspondingly large force. As long as this "source impedance" is much greater than the system impedance at the same point, the response is governed by the former. Therefore, for constant displacement one must attach a large grounded spring, while for velocity or acceleration one must use a damper or a mass. This technique has been used for applying a base excitation to two frictionally damped systems analysed in Appendix II.

FIG. 2.3

SYSTEM DYNAMIC STIFFNESS MATRIX FOR MACHINE ON PORTAL FRAME

(Co-ordinates 1, 2, 10 and 12 still free)

Q_1	$Z_{11}^{(2)}$	$Z_{12}^{(2)}$	$Z_{13}^{(2)}$	$Z_{14}^{(2)}$	$Z_{15}^{(2)}$	$Z_{16}^{(2)}$	0	0	0	0	0	0	0	q_1
Q_2	$Z_{21}^{(2)}$	$Z_{22}^{(2)}$	$Z_{23}^{(2)}$	$Z_{24}^{(2)}$	$Z_{25}^{(2)}$	$Z_{26}^{(2)}$	0	0	0	0	0	0	0	q_2
Q_3	$Z_{31}^{(2)}$	$Z_{32}^{(2)}$	$Z_{33}^{(1)} + Z_{33}^{(2)}$	$Z_{34}^{(2)}$	$Z_{35}^{(2)}$	$Z_{36}^{(2)}$	0	0	0	0	0	0	0	q_3
Q_4	$Z_{41}^{(2)}$	$Z_{42}^{(2)}$	$Z_{43}^{(2)}$	$Z_{44}^{(2)} + Z_{44}^{(3)}$	$Z_{45}^{(2)} + Z_{45}^{(3)}$	$Z_{46}^{(2)} + Z_{46}^{(3)}$	$Z_{47}^{(3)}$	$Z_{48}^{(3)}$	$Z_{49}^{(3)}$	0	0	0	0	q_4
Q_5	$Z_{51}^{(2)}$	$Z_{52}^{(2)}$	$Z_{53}^{(2)}$	$Z_{54}^{(2)} + Z_{54}^{(3)}$	$Z_{55}^{(2)} + Z_{55}^{(3)}$	$Z_{56}^{(2)} + Z_{56}^{(3)}$	$Z_{57}^{(3)}$	$Z_{58}^{(3)}$	$Z_{59}^{(3)}$	0	0	0	0	q_5
Q_6	$Z_{61}^{(2)}$	$Z_{62}^{(2)}$	$Z_{63}^{(2)}$	$Z_{64}^{(2)} + Z_{64}^{(3)}$	$Z_{65}^{(2)} + Z_{65}^{(3)}$	$Z_{66}^{(2)} + Z_{66}^{(3)}$	$Z_{67}^{(3)}$	$Z_{68}^{(3)}$	$Z_{69}^{(3)}$	0	0	0	0	q_6
Q_7	0	0	0	$Z_{74}^{(3)}$	$Z_{75}^{(3)}$	$Z_{76}^{(3)}$	$Z_{77}^{(3)} + Z_{77}^{(4)}$	$Z_{78}^{(3)} + Z_{78}^{(4)}$	$Z_{79}^{(3)} + Z_{79}^{(4)}$	$Z_{7,10}^{(4)}$	$Z_{7,11}^{(4)}$	$Z_{7,12}^{(4)}$	0	q_7
Q_8	0	0	0	$Z_{84}^{(3)}$	$Z_{85}^{(3)}$	$Z_{86}^{(3)}$	$Z_{87}^{(3)} + Z_{87}^{(4)}$	$Z_{88}^{(3)} + Z_{88}^{(4)} + Z_{88}^{(5)}$	$Z_{89}^{(3)} + Z_{89}^{(4)}$	$Z_{8,10}^{(4)}$	$Z_{8,11}^{(4)}$	$Z_{8,12}^{(4)}$	$Z_{8,13}^{(5)}$	q_8
Q_9	0	0	0	$Z_{94}^{(3)}$	$Z_{95}^{(3)}$	$Z_{96}^{(3)}$	$Z_{97}^{(3)} + Z_{97}^{(4)}$	$Z_{98}^{(3)} + Z_{98}^{(4)}$	$Z_{99}^{(3)} + Z_{99}^{(4)}$	$Z_{9,10}^{(4)}$	$Z_{9,11}^{(4)}$	$Z_{9,12}^{(4)}$	0	q_9
Q_{10}	0	0	0	0	0	0	$Z_{10,7}^{(4)}$	$Z_{10,8}^{(4)}$	$Z_{10,9}^{(4)}$	$Z_{10,10}^{(4)}$	$Z_{10,11}^{(4)}$	$Z_{10,12}^{(4)}$	0	q_{10}
Q_{11}	0	0	0	0	0	0	$Z_{11,7}^{(4)}$	$Z_{11,8}^{(4)}$	$Z_{11,9}^{(4)}$	$Z_{11,10}^{(4)}$	$Z_{11,11}^{(4)}$	$Z_{11,12}^{(4)}$	0	q_{11}
Q_{12}	0	0	0	0	0	0	$Z_{12,7}^{(4)}$	$Z_{12,8}^{(4)}$	$Z_{12,9}^{(4)}$	$Z_{12,10}^{(4)}$	$Z_{12,11}^{(4)}$	$Z_{12,12}^{(4)}$	0	q_{12}
Q_{13}	0	0	0	0	0	0	0	$Z_{13,8}^{(5)}$	0	0	0	0	$Z_{13,13}^{(5)}$	q_{13}

FIG. 2.4

(a) DYNAMIC STIFFNESS MATRIX MODIFIED TO FIX CO-ORDINATES 1, 2, 10 AND 12 TO GROUND

		1	2							10		12			
1	0	1	0	0	0	0	0	0	0	0	0	0	0	$\begin{pmatrix} q_1 \\ q_2 \\ q_3 \\ q_4 \\ q_5 \\ q_6 \\ q_7 \\ q_8 \\ q_9 \\ q_{10} \\ q_{11} \\ q_{12} \\ q_{13} \end{pmatrix}$	
2	0	0	1	0	0	0	0	0	0	0	0	0	0		
	q_3	0	0	Z_{33}	Z_{34}	Z_{35}	Z_{36}	0	0	0	0	0	0		
	q_4	0	0	Z_{43}	Z_{44}	Z_{45}	Z_{46}	Z_{47}	Z_{48}	Z_{49}	0	0	0		
	q_5	0	0	Z_{53}	Z_{54}	Z_{55}	Z_{56}	Z_{57}	Z_{58}	Z_{59}	0	0	0		
	q_6	0	0	Z_{63}	Z_{64}	Z_{65}	Z_{66}	Z_{67}	Z_{68}	Z_{69}	0	0	0		
	q_7	0	0	0	Z_{74}	Z_{75}	Z_{76}	Z_{77}	Z_{78}	Z_{79}	0	Z_{711}	0		
	q_8	0	0	0	Z_{84}	Z_{85}	Z_{86}	Z_{87}	Z_{88}	Z_{89}	0	Z_{811}	0		Z_{813}
	q_9	0	0	0	Z_{94}	Z_{95}	Z_{96}	Z_{97}	Z_{98}	Z_{99}	0	Z_{911}	0		0
10	0	0	0	0	0	0	0	0	0	1	0	0	0		
	q_{11}	0	0	0	0	0	0	Z_{117}	Z_{118}	Z_{119}	0	Z_{1111}	0		0
12	0	0	0	0	0	0	0	0	0	0	0	1	0		
	q_{13}	0	0	0	0	0	0	0	Z_{138}	0	0	0	0		Z_{1313}

(b) SOLUTION OF EQUATIONS

The 13 complex equations above may be re-written as 26 real equations, which may be solved using any standard method such as Gaussian elimination, Jordan's method, etc.

$$\begin{pmatrix} Q \\ \vdots \\ Q \end{pmatrix}_{13 \times 1} = \begin{bmatrix} Z_{sys} \end{bmatrix}_{13 \times 13} \begin{pmatrix} q \\ \vdots \\ q \end{pmatrix}_{13 \times 1} \longrightarrow \begin{pmatrix} \text{Real } Q \\ \text{Imag } Q \end{pmatrix}_{26 \times 1} = \begin{bmatrix} \text{Real } Z_{sys} & -\text{Imag } Z_{sys} \\ \text{Imag } Z_{sys} & \text{Real } Z_{sys} \end{bmatrix}_{26 \times 26} \begin{pmatrix} \text{Real } q \\ \text{Imag } q \end{pmatrix}_{26 \times 1}$$

(c) TRANSMITTED FORCES

Forces transmitted directly to ground via co-ordinates 1 and 2:

$$\begin{pmatrix} P_1^G \\ P_2^G \end{pmatrix} = \begin{bmatrix} Z_{11} & Z_{12} & Z_{13} & Z_{14} & Z_{15} & Z_{16} & 0 & 0 & 0 & 0 & 0 & 0 & 0 \\ Z_{21} & Z_{22} & Z_{23} & Z_{24} & Z_{25} & Z_{26} & 0 & 0 & 0 & 0 & 0 & 0 & 0 \end{bmatrix} \begin{pmatrix} q \\ \vdots \\ q \end{pmatrix}_{13 \times 1}$$

Original rows 1 and 2 removed from Z_{sys} above

Force transmitted to subsystem 1 via co-ordinate 3:

$$P_3^{(1)} = Z_{33}^{(1)} q_3 \quad \text{where } Z_{33} = k_\theta = \text{subsystem dynamic stiffness}$$

(d) TRANSFER RESPONSE

$$q_{1T} = \begin{bmatrix} Y_{1T,1} & Y_{1T,2} \end{bmatrix} \begin{pmatrix} P_1^G \\ P_2^G \end{pmatrix}$$

1 x 2 transfer admittance matrix Y_{tran}

The 13 complex equations are actually set up as 26 real equations, as shown in Fig. 2.4b, and these are solved for the displacement response using a standard routine*. Besides being able to use a standard equation solver written for real arithmetic, there is the added advantage that when one is dealing with an undamped system the number of equations to be solved is only half what it would be if the system were damped, so the solution is much quicker. In addition, with the 50 x 60 main working array used in COUPLE1, one is able to analyse undamped systems with up to 50 co-ordinates, while damped systems are restricted to 25 co-ordinates†.

The program permits the calculation of forces transmitted to ground via blocked co-ordinates, so the next stage in the solution is to calculate the forces P_1^G and P_2^G transmitted to ground via co-ordinates 1 and 2. For this, a copy is taken of rows 1 and 2 of the original dynamic stiffness matrix before it is modified to fix these co-ordinates to ground. As is seen from Fig. 2.4c, the product of these rows and the displacement vector yields the required forces.

In addition to finding forces transmitted to ground, the program can obtain the forces transmitted internally to a specified subsystem, so this facility may be used to find the couple transmitted to the rotational spring, and hence to ground. For this, a copy is taken of the subsystem dynamic stiffness, and this is multiplied by the rotational displacement q_3 to give the "force" $P_3^{(1)}$ (ie. the couple).

We are now in a position to consider the transfer response, which may either be a function of the forces transmitted to ground or of the forces transmitted to a subsystem. In the present case, it is assumed to be related

* Cern Library routine MATIN1: uses Jordan's method, which simultaneously yields the inverse matrix and the solution of a set of equations. The COUPLE1 program provides a check on the solution accuracy by forming the product of the inverse and the original matrix and comparing this with the unit matrix.

† These figures relate to the "standard" version of the program (COUPLE1/50). The enlarged version (COUPLE1/100) used for the seating analysis described in Part 4 has a 100 x 110 main working array and is suitable for undamped systems with up to 100 co-ordinates and damped systems with up to 50.

to the forces transmitted to ground via the pin joint at C (ie. P_1^G and P_2^G obtained above). Of course, to be strictly correct, the forces transmitted to a rigid ground do not produce any motion anywhere. However, in assuming the ground to be rigid we are really assuming that it is sufficiently stiff in comparison with the attached structure that its exact behaviour is not important when calculating the response of that structure. It is seen from Fig. 2.4d that the transfer response is given by the product of a 1×2 transfer admittance matrix and the two forces transmitted to ground. These transfer admittance data might be obtainable by calculation, but in general they are more likely to be measured quantities, which must be set up in the subroutine SUBTRAN according to instructions inserted by the user.

The transfer response could equally well have been expressed in terms of internally transmitted forces, by finding the forces applied to subsystem 2 via co-ordinates 1, 2 and 3. The forces acting on co-ordinates 1 and 2 are just equal and opposite to the forces transmitted to ground, and that acting on co-ordinate 3 is equal and opposite to the couple applied to the spring. Although in this problem the transfer response has been assumed to relate to some remote point, it may equally well relate to a point somewhere on the structure itself. For example, if one wished to know the deflection at one or more points up the pillar, one could set up as transfer admittance data the receptance expressions relating the motion at any point to the tip forces and couples (on co-ordinates 1, 3, 4 and 6)*. As there is provision for up to 6 transfer responses, one should be able to obtain the mode shape for this subsystem in considerable detail.

* The relevant transfer receptance expressions for a Timoshenko beam have recently been derived by Silva (46). The corresponding receptances for a Bernoulli-Euler beam are given by Bishop and Johnson (13).

The final stage in the solution is the computation of any motion transmissibilities, such as y_B/y_A , which is given by the ratio q_8/q_{13} . All the responses are then converted to the required form for output and they are printed out. Provision also exists for saving specified data on a permanent file, so that it may be accessed later for plotting or other use. This facility is particularly useful when analysing complex systems, as it is possible to start by analysing the individual sub-assemblies, saving the response data for each of them on file. These data may then be read back from the files and used to form the complete assembly*.

* A standard subroutine called ZFILE is available for reading existing sub-assembly response data from a file and incorporating these into the analysis of a complete assembly. Details of this special subroutine are given in Part 2 of Reference (40).

2.3 WAYS OF INCLUDING DAMPING IN THE ANALYSIS

The Mathematical Representation of Damping

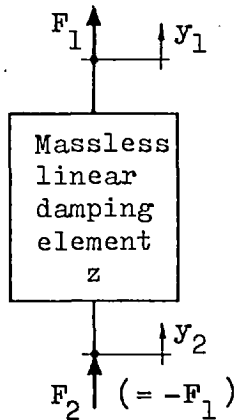
Damping often provides the only means of controlling resonant vibrations, so it is of great practical importance and it must be included in any analysis that is concerned with predicting either structural vibration levels or isolation system effectiveness. However, whereas in electrical systems damping is generally concentrated in discrete linear elements (resistors), in mechanical systems it is very often distributed non-uniformly over an area and it may be related in various ways to either velocity or displacement. Hence, it can be difficult to realistically represent this damping in an analytical model.

The simplest damping element from a theoretical point of view is the viscous damper (see Fig. 2.5). This is a linear device which opposes the relative velocity between its ends with a force which is proportional to that velocity. It is the mechanical equivalent of the electrical resistor^{*}, and is the only strictly linear damper, in the sense that the equations of motion of a system incorporating this damping may be solved for any type of input, whether it be steady-state or shock. Since it is so amenable to mathematical analysis it has received undue emphasis in most books and papers on vibration. In actual fact, it often bears little resemblance to damping mechanisms encountered in practice. In the field of steady-state vibration its use is only justified when it represents an actual source of viscous damping, such as an oil-filled dashpot or the oil film between the slides on a machine, or alternatively, when it represents an equivalent electro-mechanical device such as an eddy-current damper.

Before we consider other types of damping we shall look at the way in which a simple two-terminal element such as the viscous damper may be

* In the cgs system of units, the viscous damping coefficient c is in fact measured in "mechanical ohms" (= 1 dyne per cm/s). However, no special term has been adopted in either the in-lb-s or the SI system.

incorporated in a general system analysis. Supposing that the element is massless and in a free-free state, its complete dynamic stiffness properties are given by a 2 x 2 matrix:



$$\begin{bmatrix} F_1 \\ F_2 \end{bmatrix} = \begin{bmatrix} z & -z \\ -z & z \end{bmatrix} \begin{bmatrix} y_1 \\ y_2 \end{bmatrix}$$

where $z = \text{dynamic stiffness}$

(2.1)

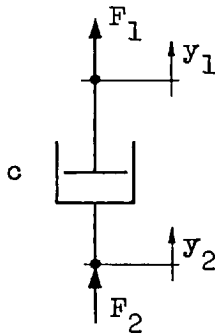
Thus, the damping element may be connected between any two co-ordinates of a system simply by including it as a subsystem and setting up a dynamic stiffness matrix of the type shown here. For the special case of a grounded damper, $y_2 = 0$ and we then have a single terminal element for which $F_1 = z y_1$. The dynamic stiffness z is real for a pure spring and imaginary for a pure damper, so in the general case of a damped elastic element it is a complex number. For the particular case of a viscous damper, $z = i\omega c$ (see Fig. 2.5)*, and the dynamic stiffness matrix is easily set up using the standard module ZMAK2⁽⁴⁰⁾.

Having looked at viscous damping from a purely mathematical point of view, we shall now consider how it differs from the type of damping that is generally encountered in mechanical structures. A good starting point is the damping inherent in all materials, and it is instructive to consider Fig. 2.6a, which shows typical dynamic load/deflection curves for a metal. The anti-symmetric curve passing through the origin corresponds to static loading, and it forms a "backbone" for the hysteresis loop produced by cyclic loading. The small loop (a) corresponds to loading within the linearly elastic region of the material, while the larger loop (b) corresponds to loading beyond the

* $i = \sqrt{-1}$, and it signifies that the force applied to the damper leads the relative displacement across it by 90° .

FIG. 2.5 THE BASIC LINEAR DAMPING ELEMENTS

VISCOUS DAMPER



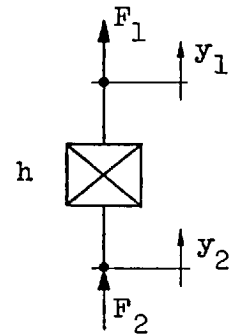
c = Viscous damping
coefficient

Transmitted force

$$F = F_1 = -F_2 = c(\dot{y}_1 - \dot{y}_2) \\ = i\omega c(y_1 - y_2)$$

Dynamic stiffness, $z = i\omega c$

HYSTERETIC DAMPER



h = Hysteretic damping
coefficient

Transmitted force

$$F = F_1 = -F_2 = ih(y_1 - y_2)$$

Dynamic stiffness, $z = ih$

where

F = Force

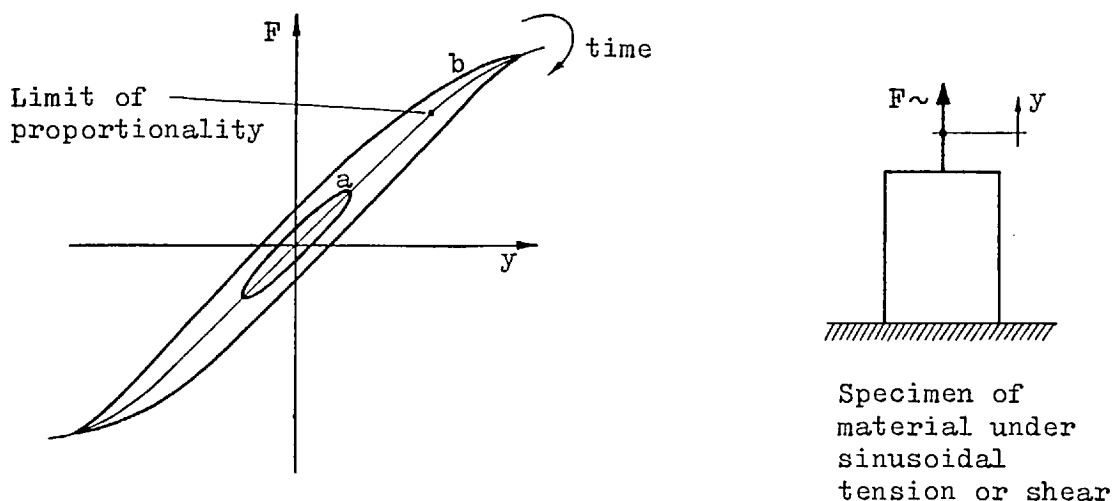
y = Displacement

$\dot{}$ = $\frac{d}{dt}$

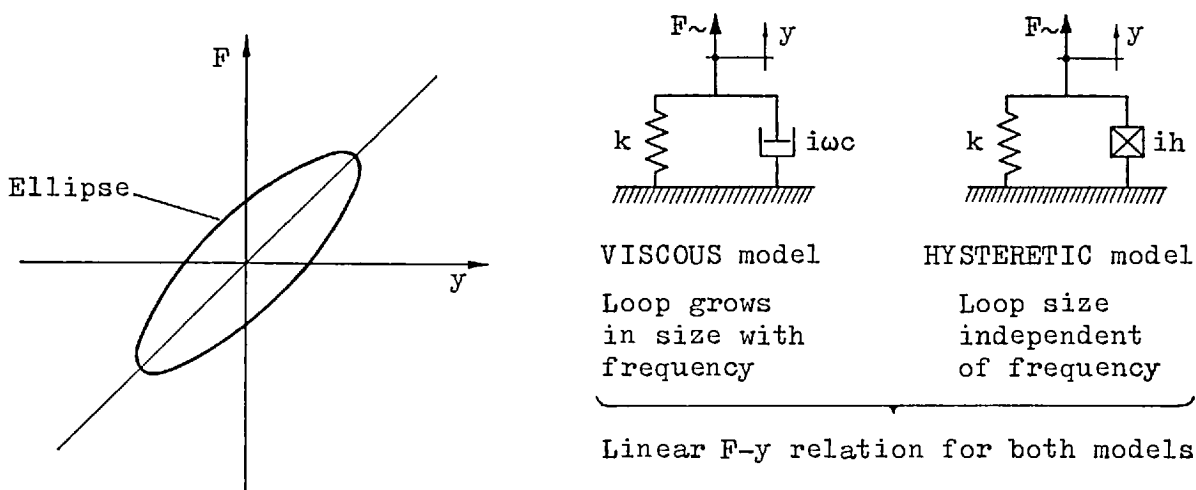
ω = 2π x frequency(Hz)

$i = \sqrt{-1}$

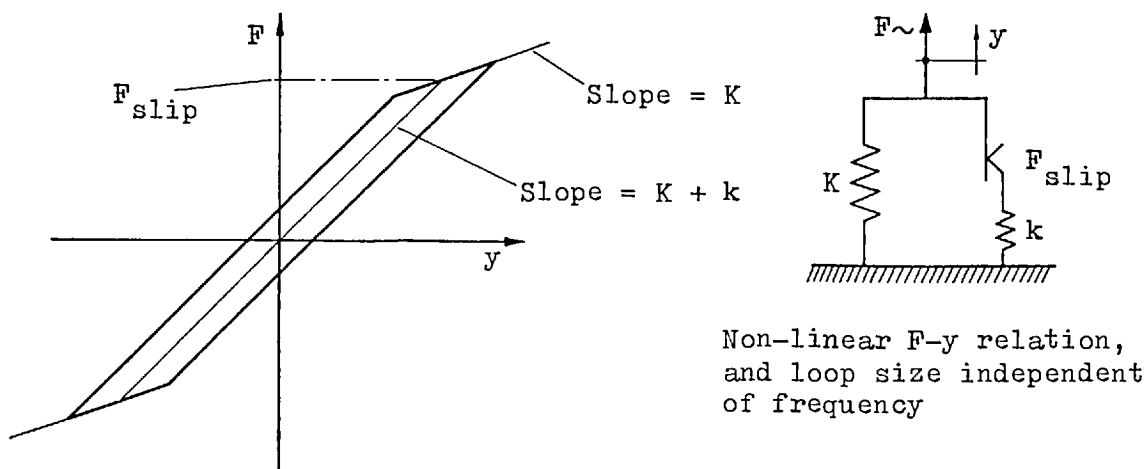
FIG. 2.6 HYSTERESIS LOOPS YIELDED BY COMMON MATERIALS AND MODELS



(a) Typical engineering material



(b) Simple models with either viscous or hysteretic damping



(c) Bi-linear model with Coulomb friction damping

linear region and possibly even into the plastic region. The area enclosed by each loop represents the energy loss D per cycle, and it is generally proportional to y^n (47)(8). Under normal low-amplitude stressing, as represented by loop (a), the value of n for most metals lies somewhere between 2 and 3, while for most rubbers it is almost exactly 2. For loop (b) it is much larger and it varies according to the peak stress.

For the moment we shall confine our attention to loop (a), since loop (b) is associated with non-linear behaviour, and any discussion of this is best postponed until we have examined all aspects of linear damping. In the case of loop (a) the energy loss is due to anelasticity or internal friction, and once the cyclic loading stops, the material returns to its original virgin state. For many metals it has been observed that this loop is essentially invariant with frequency, and that it is approximately elliptical in form. This elliptical shape corresponds to $n = 2$ and it is also characteristic of a spring in parallel with a viscous damper (see Fig. 2.6b). However, the viscous model differs from the observed material behaviour in that it yields a loop which grows in size with frequency. Hence, a more realistic model is obtained if the viscous damping element is replaced by one having a constant dynamic stiffness $z = ih$. This is known as a hysteretic damper⁽¹²⁾⁽¹³⁾ and the parameter h is called the "hysteretic damping coefficient". It is normally represented as in Fig. 2.5, and it is incorporated into a system analysis in just the same way as the viscous damper, by setting up the 2×2 dynamic stiffness matrix (2.1), either for the damper on its own ($z = ih$) or for the damper in parallel with a spring ($z = k + ih$).

It must be stressed that the hysteretic damper is only a linear device in the sense that it is described by a linear dynamic stiffness relation. Its use is restricted to steady-state vibration, and it cannot be employed when studying either free vibration or shock response. In such cases there is little option but to return to the viscous damper, however inadequate this may be.

Since the damping in a piece of material is associated with the stiffness, it is common to re-write the dynamic stiffness $z = (k + ih)$ as a complex stiffness $k^* = k(1 + i\eta)$, where $\eta = \frac{h}{k}$. This parameter η is called the loss factor and it is basically a material property⁺. Since the in-phase stiffness k is a function of either the elastic modulus E or the shear modulus G , it is also common to use the complex moduli $E^* = E(1 + i\eta)$ and $G^* = G(1 + i\eta)$, so that any undamped analysis may be extended to include damping simply by replacing the real modulus by a complex one. This is the usual way of introducing damping into a beam analysis⁽¹⁷⁾⁽⁴⁸⁾⁽⁴⁵⁾, and it has been utilised in the standard routine ZFLAX2D for a damped Timoshenko beam.

Rubbers and other visco-elastic materials normally yield elliptical hysteresis loops⁽⁴⁹⁾⁽²⁹⁾, and they only differ from metals in generally having larger loss factors and in exhibiting frequency and temperature dependence^{(17)x}. For ordinary natural rubber one may expect a loss factor of the order of 0.025, but many filled rubbers and similar synthetic materials exhibit far greater damping than this, with the loss factor sometimes exceeding 1. In comparison, metals such as steel and aluminium have loss factors of the order of 0.001, and woods have loss factors around 0.006⁽⁵⁰⁾. Although visco-elastic materials exhibit frequency dependence, it is far less pronounced than that associated with a viscous damping model, and over a limited frequency range the properties may often be assumed constant. However, frequency dependence presents no problems when the system is built afresh at each frequency, since one may simply employ the properties corresponding to the exciting frequency. To facilitate this, data for 4 typical visco-elastic materials are currently available on file for direct use with the COUPLE1 program⁽⁴⁰⁾.

+ To be strictly correct, the measured loss factor of a solid metal component varies slightly according to its shape and the way in which it is loaded (8). However, it is normally considered as a material property in the same way as the elastic and shear moduli.

x See Part 4, page 324 for shear modulus and loss factor of high-damping PVC.

So far we have only looked at the damping in a homogeneous piece of material or component, but most built-up structures often exhibit far greater damping than one might predict from material damping alone. This normally results from losses in the joints, but it is far from being well understood; particularly when the joint area is large and the mating surfaces are not uniformly clamped together, as is often the case with bolted or riveted joints. However, on the basis of observations, one may reasonably expect a typical overall loss factor of about 0.01 for a normal metal structure with no other significant source of damping⁽⁵¹⁾. This is not a material loss factor as defined above, but an overall structural loss factor resulting from the non-uniformly distributed joint damping. A more general definition of the loss factor is obviously called for, and this is given in terms of energies:

$$\text{Loss Factor, } \eta = \frac{\text{Energy dissipated per cycle}}{\text{Maximum strain energy per cycle}}$$

Although the damping is actually concentrated at the joints, its exact form is seldom known and it is generally easier to distribute it uniformly throughout the model of the structure. For instance, in a frame analysis one may assign to each member a loss factor equal to the expected overall loss factor, or one may even perform an undamped analysis and then determine the heights of the resonant peaks afterwards (this is discussed further below).

Obviously, when the concentrated sources of damping are simple rubber springs and pads there is no problem, since these may each be described as subsystems with complex stiffness. However, heavy damping may also be applied to parts of a beam or plate structure by adding a constrained damping layer. This comprises a layer of high-damping visco-elastic material which is attached to the surface of the structure, and a metal constraining layer. As the visco-elastic material shares its damping with the metal structure, the overall loss factor is usually considerably less than the material loss factor, but even so, it is possible to achieve loss factors as high as 0.1 with a thin add-on

treatment; and if the damping material is built into the structure so as to form a "sandwich", the loss factor may even reach 0.3 to 0.5. This form of damping is discussed fully in Part 3 (Chapters 8 to 12), where finite elements are derived for various types of multi-layer beam. These finite elements may be used to form a complex dynamic stiffness matrix which fully describes the damping distribution through the beam, so it is possible to incorporate one or more sandwich beams into a general structural analysis, along with uniform undamped beams. This is particularly useful for studying the effect of partial damping⁽²⁸⁾⁽⁵²⁾, where the treatment is restricted to a limited area of the structure. A standard routine called ZSAM1⁽⁴⁰⁾ is available on file for dealing with symmetrical 3- and 5-layer beams, and this may be used in conjunction with the visco-elastic material properties routines mentioned above. Any other multi-layer configuration must be specially programmed, but in the case of a light add-on treatment it is possible to use a uniformly damped Timoshenko or Bernoulli-Euler beam, provided one is able to assign to it the correct loss factor⁽⁵³⁾⁽⁵⁴⁾.

Up to this stage we have confined our attention to linear damping, but many damping mechanisms are in fact non-linear and they may not be adequately described by a linear model. Probably the most important of these is dry friction or Coulomb damping⁽⁵⁵⁾⁽⁵⁶⁾, which arises wherever there is relative slip between two mating surfaces. In our theoretical model we assume that the mating surfaces are pressed together with a force N , and that the static coefficient of friction between the two surfaces is μ_s . As long as the shear force transmitted between the two parts is less than $\mu_s N$, the damper remains locked and acts as a rigid link, but if it reaches this level slip commences, and under steady-state conditions a constant friction force opposes the relative velocity across the damper. As it is non-linear, its characteristics cannot be described in terms of a dynamic stiffness, so it cannot be incorporated in a system analysis in the same way as linear damping elements.

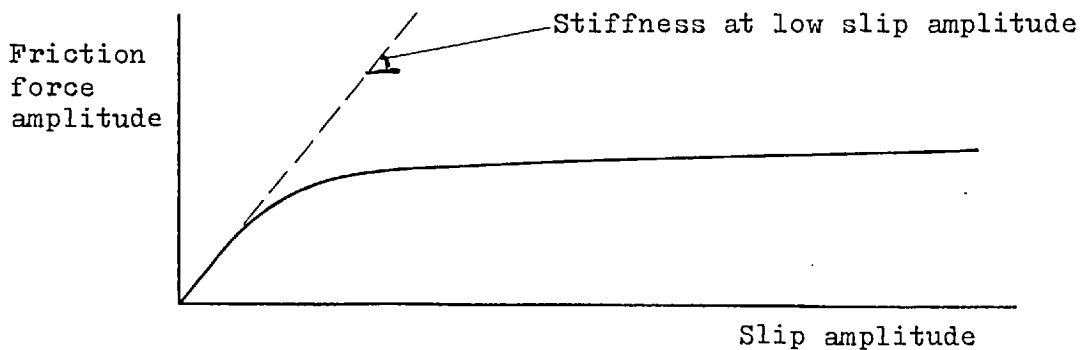
However, it can be added to a linear system as an insert once the main system has been analysed. This is discussed in general terms a little further on, and full details are given in Appendix II (including a thorough discussion of the slipping friction force).

In practice, friction damping may arise either from specially designed damping units or from joints in a structure. Various commercially produced units are available, and these either employ fibre pads rubbing on steel or a stack of metal plates clamped together using bolts and compression springs and loaded axially⁽⁸⁾. Friction damping is also incorporated in certain isolator units, such as the larger types employing coil springs, since it is both simple and cheap to introduce. In isolation systems it may often supplement other forms of damping, such as the hysteretic damping inherent in rubber springs, whilst in metal structures it may be the predominant source of damping. Therefore, any general purpose program should be capable of dealing with a combination of friction and linear damping, and the theory developed in Appendix II allows for this. A special subroutine called FRIC1 has been developed on the basis of this theory, so it is possible to add a single friction damper (either linear or rotational) to an otherwise linear system which already incorporates either viscous or hysteretic damping.

In the case of isolation systems, the simple isolator consisting of a grounded spring in parallel with a grounded damper (either friction or viscous) has often failed to predict observed behaviour. Ruzicka⁽⁶⁾ has found that a more realistic isolator model is one in which the damper is elastically supported, as shown in Fig. 2.6c. It is interesting now to compare the hysteresis loop yielded by this bi-linear model with the loop (b) in Fig. 2.6a. It is clearly seen that they exhibit similar characteristics, so the bi-linear model represents a first approximation to material hysteresis at high stress levels. Whereas the model only "yields" once under static loading, the actual material yields very gradually, and this plastic deformation even takes place

within the elastic region on a microscopic scale, as local inhomogeneities within the material give rise to local stresses which are high enough to cause local slipping. Obviously, if one increased the number of elastically-supported dampers in parallel with the spring it would be possible to allow for gradual yielding; and if the spring itself were replaced by an elastically-supported damper this would allow for the possibility of fracture. Although the bi-linear model may easily be set up using COUPLE1 (by building the linear two-spring system and then inserting the damper between the springs), the extension to a multi-linear model is not possible at present, as the necessary theory has yet to be developed. However, Iwan⁽⁵⁷⁾ has performed such an analysis for the limiting case of an infinite number of dampers and he has obtained good agreement with experimental response data.

When incorporating friction in a structural analysis, it is normal to interpose the damper between the two co-ordinates of interest without including any associated stiffness (unlike a visco-elastic pad, which introduces both damping and stiffness)⁽⁵⁶⁾⁽⁵⁸⁾⁽⁵⁹⁾. This results in a very sudden transition from a fully locked to a slipping condition and is inconsistent with the observed behaviour of metal structures under conditions of small amplitude vibration. To illustrate this, we may consider a typical curve of friction force versus slip as measured by Earles and Mott⁽⁶⁰⁾:



It is clearly seen that for small slip amplitudes the behaviour is spring-like, and this suggests initial elastic deformation of the contacting asperities on

the mating surfaces. This is followed by an intermediate condition where the more rigidly clamped asperities continue to behave elastically, while others slip; and finally there is complete slip — though the friction force amplitude is still not absolutely constant. Comparing this with the force/deflection curve in Fig. 2.6c, it would appear that a bi-linear damping element would more closely describe the actual behaviour at the friction joint, provided one could estimate the relevant stiffnesses. It would also permit the inclusion of a small amount of hysteretic damping in the springs, to describe the essentially linear "friction" damping associated with low-amplitude "slip", before the joint actually unlocks.

Regardless of whether the damper forms part of an isolation system or is incorporated within a structure, the friction force is rarely the "square" wave assumed in most text books and papers. This is because a perfect square wave can only be obtained if the damper is connected to a rigid support, and an elastic support such as that considered above gives rise to a more nearly sinusoidal wave. The analysis given in Appendix II is linearised, in the sense of only considering the fundamental component of the friction force and the fundamental component of the response. However, as the force is often very nearly sinusoidal, the error involved in neglecting the harmonics is generally quite small.

Other types of non-linear damping, such as velocity-squared⁽⁶¹⁾⁽⁹⁾, could be introduced in a similar manner. It is only necessary to determine the fundamental component of the damping force wave and then apply this as an excitation to the linear system. Although the force is no longer constant, one may utilise the same procedure as for the friction case and just adjust the force amplitude iteratively to take account of the displacement dependence.

In summary, the three most important types of damping are viscous, hysteretic, and friction, where the first two are linear and the third is non-linear. Although constrained layer damping is a very important form,

it can be treated mathematically using linear theory and it falls into the category of hysteretic damping. For general material and structural damping one should use the hysteretic model, and viscous damping should only be used to represent actual viscous behaviour. Despite its non-linear nature, a single friction damper may be introduced into an isolation system or structure as an insert, once the main linear analysis has been carried out.

Special Techniques for the More Efficient Computation of Damped Response

The dynamic stiffness coupling technique described in Section 2.2 is both straightforward and very general, since one may easily mix component data from various sources, and some components may be damped while others remain undamped. However, as the system dynamic stiffness matrix must be built from scratch and inverted at each frequency, this approach can become expensive on computer time if the number of co-ordinates n is large. Although damping is easily introduced by using complex material properties, the resulting real matrix for the damped system is twice the size of that for the undamped system. Two problems arise as a consequence of this: (a) If the computer storage space is limited to n_{\max} equations (50 for standard version of COUPLE1), one is unable to analyse damped systems having more than $n_{\max}/2$ co-ordinates, and (b) when n is large the damped solution takes considerably longer than the undamped solution*. For systems with up to about 12 co-ordinates one may proceed quite happily with a full damped analysis, but when the number increases beyond this one should begin to consider whether other more economical means exist for computing the required responses.

If the damping is light ($\eta < 0.02$) and is fairly evenly distributed through the structure, the damped and undamped solutions only differ around the resonant peaks and are practically identical everywhere else. Hence, one

* This is illustrated by the following examples: The total time required for building a 15 co-ordinate undamped system from 4 Timoshenko beams and then solving the resulting equations was 0.210 second per frequency. The corresponding time for a similar damped system having 13 co-ordinates was 0.450 second per frequency. In each case the times relate to a CDC 6400 computer, and for a CDC 6600 they should be divided by 3.

may perform an undamped analysis over the complete frequency range and then do a damped analysis at one or two spot frequencies around each resonant peak. Alternatively, if one is able to estimate the damping associated with each mode it is possible to determine the resonant peak amplitude using a simple technique devised by Ewins⁽⁶²⁾. Using this latter approach it is only necessary to compute the undamped response at two frequencies ω_1 and ω_2 , where ω_1 is slightly below and ω_2 is slightly above the resonant frequency ω_0 . If these responses are q_{ω_1} and q_{ω_2} respectively, and the estimated modal loss factor is η , the resonant peak amplitude is given approximately by the formula:

$$|\bar{q}_{\omega_0}| = \frac{\omega_2 - \omega_1}{\eta \omega_0} \left[\frac{1}{0.5 \left(\frac{1}{|q_{\omega_1}|} + \frac{1}{|q_{\omega_2}|} \right)} \right]$$

This is the most general of several formulae derived in Reference (62), and it will yield a peak amplitude estimate that is within a few percent of the exact value (unless the modes are closely spaced). The only apparent problem with this approach is that one must be able to assign a value to the modal loss factor. In the case of uniformly damped structures (eg. machined components, with no joints) there is no real problem since the modal loss factor is equal to the material loss factor, but when the damping is non-uniform (eg. any structure with non-rigid joints), the modal loss factor is always less than the localised damping, and it can only be estimated approximately. Since the level of damping in any real structure can rarely be specified to an accuracy of more than 10 %, the approximate nature of the formula is of little consequence.

If the damping is heavy and is distributed through the structure (either uniformly or non-uniformly) one must perform a full analysis, taking into account the different amounts of damping in the various components. However, if the damping is concentrated in one area of the structure or in a small number of discrete damping inserts (eg. rubber pads or gaskets) it is better

to perform the analysis in two parts. One starts by analysing the undamped section of the structure for its receptance properties at those co-ordinates to which the damped section is to be connected, and at any other co-ordinates at which excitation is to be applied or response is to be computed. One then combines the damped section with this in one of two ways:

(1) The Sub-Assembly Method

The computed receptance matrix for the undamped section of the structure is written onto permanent file frequency-by-frequency, so that it is available for later use. A new system is then set up, in which the undamped structure is just one sub-assembly which is to be connected to the various damped sub-systems. Since the damping is concentrated at only one or two points, the total number of coupling co-ordinates is small and the damped part of the solution is quickly and efficiently carried out. This is particularly useful when one wishes to experiment with the damping, since one can use the existing data for the undamped structure instead of re-building the complete structure every time.

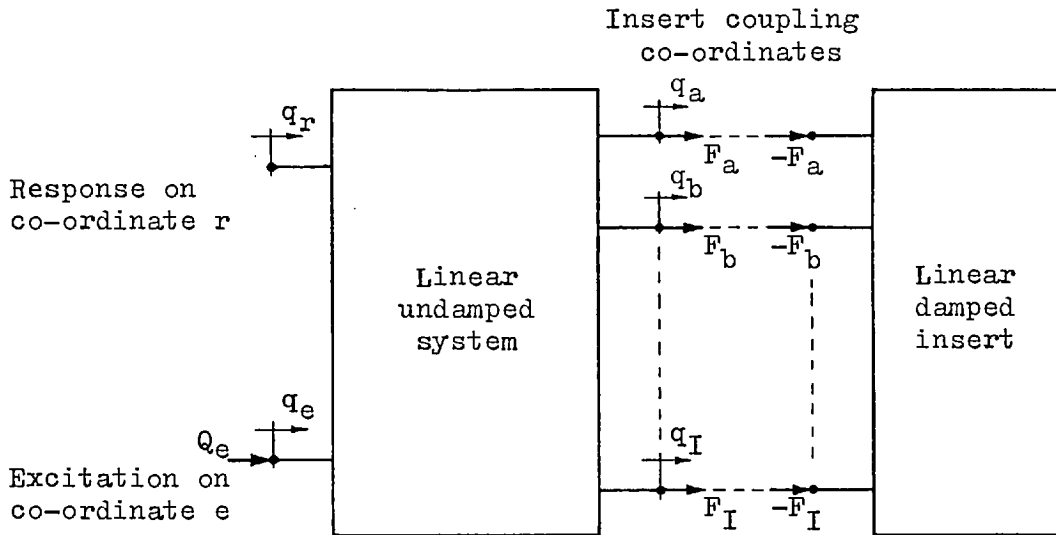
This sort of analysis in terms of sub-assemblies is easily carried out using COUPLE1, and it illustrates the great power of the building block approach, since it is possible to tackle problems which would otherwise be beyond the capacity of the program. The writing of the receptance data onto file is a standard feature incorporated in the main program, and the reverse process of reading back the data and setting up the subsystem dynamic stiffness may be carried out using the special subroutine ZFILE⁽⁴⁰⁾.

(2) The Insert Method

As before, one computes the receptance properties of the undamped section of the structure, but these data need not be saved for later use in a further coupling exercise. Instead, one uses the properties of the undamped structure and of the inserts in order to calculate the reaction forces that the inserts

apply to the structure. Since these are external forces acting on the undamped structure, it is then a simple matter to compute the combined response resulting from the excitation and the inserts.

The procedure will be illustrated in terms of the system shown below:



In the most general case there may be a total of E excitation forces and R responses of interest, so the force Q_e represents a typical excitation and the displacement q_r is a typical response. The damped section is connected to the undamped structure via co-ordinates q_a to q_I , and in the most general case it may represent a damped sub-assembly which incorporates mass, stiffness and damping, and which includes internal coupling between the various co-ordinates. However, it may equally well represent a set of massless damped springs which are only associated with pairs of co-ordinates. Thus, the insert which we shall consider is a general linear damped system which may represent either one or a number of actual physical inserts.

Before the insert is added, the response on any co-ordinate r is

$q_{rf} = \sum_{e=1}^E \alpha_{re} Q_e$, where α_{re} is the receptance coefficient relating the response on co-ordinate r to the force on co-ordinate e . The subscript f indicates that this is a "free" response, in the sense that the structure is still a free undamped system, not yet connected to the damping insert.

When the insert is added, a set of supplementary excitation forces F_a to F_I is applied to the undamped structure, thereby modifying its response. Therefore, it is only necessary to determine these transmitted forces in order to obtain the response of the complete damped system. We may start by considering the modified responses on co-ordinates a to I due to the presence of the insert:

$$\begin{Bmatrix} q_a \\ q_b \\ \vdots \\ q_I \end{Bmatrix} = \begin{Bmatrix} q_{af} \\ q_{bf} \\ \vdots \\ q_{If} \end{Bmatrix} + \begin{bmatrix} \alpha_{aa} & \alpha_{ab} & \cdots & \alpha_{aI} \\ \alpha_{ba} & \alpha_{bb} & \cdots & \alpha_{bI} \\ \vdots & \vdots & & \vdots \\ \alpha_{Ia} & \alpha_{Ib} & \cdots & \alpha_{II} \end{bmatrix} \begin{Bmatrix} F_a \\ F_b \\ \vdots \\ F_I \end{Bmatrix}$$

$$\{q\} = \{q_f\} + [\alpha]\{F\} \quad (2.2)$$

Remembering that the forces exerted on the insert are in the opposite direction to those exerted on the structure, the dynamic stiffness relation for the insert takes the form

$$\begin{Bmatrix} F_a \\ F_b \\ \vdots \\ F_I \end{Bmatrix} = - \begin{bmatrix} D_{aa} & D_{ab} & \cdots & D_{aI} \\ D_{ba} & D_{bb} & \cdots & D_{bI} \\ \vdots & \vdots & & \vdots \\ D_{Ia} & D_{Ib} & \cdots & D_{II} \end{bmatrix} \begin{Bmatrix} q_a \\ q_b \\ \vdots \\ q_I \end{Bmatrix}$$

$$\{F\} = -[D]\{q\} \quad (2.3)$$

where the dynamic stiffness elements D_{ab} , etc., are complex numbers.

If we pre-multiply (2.2) by $-[D]$, we obtain

$$\{F\} = -[D]\{q_f\} - [D][\alpha]\{F\}$$

$$\text{whence} \quad \{F\} = -([I] + [D][\alpha])^{-1}[D]\{q_f\} \quad (2.4)$$

Thus, the transmitted forces are a function of the insert dynamic stiffness, and of the receptance properties and free response of the undamped structure.

The response of the damped structure on any co-ordinate r is now given by

$$q_r = q_{rf} + \sum_{i=1}^I \alpha_{ri} F_i \quad (2.5)$$

where F_i is the force transmitted to the structure via coupling co-ordinate i .

This procedure is similar to that used by Hammill and Andrew⁽⁶³⁾, except that they confined their attention to a number of discrete massless inserts. In such a case, each insert is connected between a pair of co-ordinates such as a and b , and since it is massless $F_b = -F_a$. Thus, it is only necessary to determine half the number of forces, thereby leading to a more rapid solution. Obviously, the present very general solution could be simplified to cover this specific case.

The advantage of the general procedure is that the insert may equally well be a number of simple rubber pads or a complicated sub-assembly. One possible application is the addition of a "thin" add-on damping treatment to one beam in an otherwise undamped frame (instead of using a multi-layer finite element). Although this has not yet been investigated, it might be possible to represent a constrained damping layer as a 4 co-ordinate damped insert to be connected between the tips of the beam.

One advantage that the insert method has over the sub-assembly method is that it is not restricted to linear damping elements. The only requirement is that one should be able to determine the forces transmitted by the inserts, and it is then a simple matter to apply these forces to the linear structure in order to obtain the damped response. In the procedure outlined above, the transmitted forces were expressed in terms of the linear response properties of the insert and of the structure, and the insert could take virtually any form. However, if the insert is non-linear there is no general procedure available, and it is necessary to examine each case separately and to determine

the forces by whatever method is most convenient. As this may involve some sort of iterative solution, it is difficult to progress beyond a single damper.

Since any non-linear device gives rise to non-sinusoidal forces, the linear structure is actually excited by a fundamental component plus a number of harmonics; but very often these harmonics are only small and they may be neglected. Any analysis based only on the fundamental component is said to be "linearised" and it may often be relatively straightforward.

At present COUPLE1 does not incorporate a general purpose insert facility, but the previously mentioned subroutine FRIC1 does allow a non-linear friction damper to be added to a linear system. The latter is analysed in the normal way, and once the equations have been solved, the receptance matrix and the free response columns are immediately available from the arrays ZSYS and X via a blank common block. Referring to the flow chart given in Appendix I, it is only necessary to introduce a call to the insert subroutine immediately before the call to CALFOR in the main program COUPLE1. This is explained in detail in Appendix II, and based upon the experience gained from this it should not be difficult to extend the theory to include other non-linear inserts, such as a velocity-squared damper or an undamped spring with a linear-plus-cubic characteristic*.

As described here, the insert method replaces the actual insert by a force excitation source. However, Mahalingam has recently proposed an alternative technique which uses a displacement excitation source instead⁽⁶⁵⁾. This is based on the concept of "internal receptances"⁽⁶⁶⁾, and he has shown how it may be used for adding both linear and friction damping inserts to a linear undamped system.

* Paslay and Gurtin⁽⁶⁴⁾ have analysed a linear undamped system resting on a non-linear spring. They used a similar approach to that adopted here, in that they considered the spring force as an external excitation acting on the linear system.

REFERENCES FOR CHAPTERS 1 AND 2 (PART 1)

1. Grootenhuis, P., "Control of the noise and vibration environment", Inaugural lecture, Imperial College of Science and Technology, University of London, 12 November 1974
2. Derham, C. J., Wootton, L. R. and Learoyd, S. B. B., "Vibration isolation and earthquake protection of buildings by natural rubber mountings", Natural Rubber Technology (published by the Malaysian Rubber Producers' Research Association), Vol. 6, Part 2, 1975
3. Den Hartog, J. P., "Mechanical vibrations", McGraw-Hill (New York), 4th edition, 1956
4. Timoshenko, S. and Young, D. H., "Vibration problems in engineering", Van Nostrand, Princeton, 3rd edition, 1955
5. Ungar, E. E. and Dietrich, C. W., "High-frequency vibration isolation", Journal of Sound and Vibration, Vol. 4, No. 2, 1966, pp 224-241
6. Ruzicka, J. E., "Resonance characteristics of uni-directional viscous and coulomb-damped vibration isolation systems", Trans. ASME, Journal of Engineering for Industry, November 1967, pp 729-740
7. Crede, C. E., "Vibration and shock isolation", Wiley, New York, 1951
8. Harris, C. M. and Crede C. E., "Shock and vibration handbook", McGraw-Hill, 1961
9. Crede, C. E., "Shock and vibration concepts in engineering design", Prentice-Hall, 1965
10. Grootenhuis, P. and Ewins, D. J., "Vibration of a spring-supported body", Journal of Mechanical Engineering Science, Vol. 7, No. 2, 1965, pp 185-192
11. Gupta, K. M., "Force transmissibility provided by inclined isolators", Journal of the Institution of Engineers of India, Vol. 47, No. 11, 1967, pp 507-522
12. Bishop, R. E. D., "The general theory of hysteretic damping", Aeronautical Quarterly, February 1956

13. Bishop, R. E. D. and Johnson, D. C., "The mechanics of vibration", Cambridge University Press, 1960
14. Snowdon, J. C., "Isolation and absorption of machinery vibration", *Acustica*, Vol. 28, No. 6, 1973, pp 307-317
15. Love, A. E. H., "A treatise on the mathematical theory of elasticity", Dover Publications, New York, 4th edition, 1944
16. Silva, J. M. M., "On the influence of the push-rod in mechanical impedance testing", Imperial College Dynamics Group report, October 1975
17. Snowdon, J. C., "Vibration and shock in damped mechanical systems", Wiley, 1968
18. McCallion, H., "Vibration of linear mechanical systems", Longmans, 1973
19. Snowdon, J. C., "Isolation of machinery vibration from non-rigid sub-structures using multiple anti-vibration mountings", reprinted from *Isolation of Mechanical Vibration, Impact, and Noise* (published by ASME)
20. Lachlan, B., "The reduction of vibrational energy in complex structures", Imperial College Dynamics Group report - Final report on MOD Contract No. N/CP 95/62313/65, December 1969
21. Klosterman, A. L. and Lemon, J. R., "Building block approach to structural dynamics", ASME publication VIBR-30, 1969
22. Klosterman, A. L. and Lemon, J. R., "Dynamic design analysis via the building block approach", *Shock and Vibration Bulletin*, 42, Part 1, 1972
23. Salter, J. P., "Steady-state vibration", Kenneth Mason Publishers, 1969
24. Gorman, R. M., "Design and advantages of a two-stage mounting system for major machines in ship's engine room", *Shock and Vibration Bulletin*, 35, Part 5, 1966, p 227
25. Grootenhuis, P., Ewins, D. J. and Sainsbury, M. G., "Rules and procedures for the design of machinery vibration isolation systems", Design manual prepared by the Imperial College Dynamics Group for the Admiralty Engineering Laboratory, June 1975

26. Snowdon, J. C. and Kerlin, R. L. "Vibration attenuation with beams - Theory and reciprocal experiment", Journal of the Acoustical Society of America, Vol. 51, No. 1 (Part 2), 1972, pp 249-264
27. Plunkett, R., "Optimum damping distribution for structural vibration", Shock and Vibration Bulletin, 1970 (?)
28. Nokes, D. S. and Nelson, F. C., "Constrained layer damping with partial coverage", Shock and Vibration Bulletin, No. 38, Part 3, November 1968
29. Grootenhuis, P., "Damping mechanisms in structures and some applications of the latest techniques", Paper presented at the Symposium on Applications of Experimental and Theoretical Structural Dynamics, Institute of Sound and Vibration Research, Southampton University, April 1972
30. Zienkiewicz, O. C., "The finite element method in engineering science", McGraw-Hill (London), 1971
31. Fenner, R. T., "Finite element methods for engineers", Macmillan, London, 1975
32. Klosterman, A. L., "A combined experimental and analytical procedure for improving automotive system dynamics", SAE publication 720093, 1972
33. Sainsbury, M. G. and Ewins, D. J., "Vibration analysis of a damped machinery foundation structure using the dynamic stiffness coupling technique", Trans ASME, Journal of Engineering for Industry, Aug 1974
34. Laursen, H. I., Shubinski, R. P. and Clough, R. S., "Dynamic matrix analysis of framed structures", Proc. 4th US National Congress on Applied Mechanics, 1, 1962, pp 99-105
35. Heer, E., "Coupled systems subjected to determinate and random input", International Journal of Solids and Structures, Vol. 3, 1967, pp 155-166
36. Lutes, L. D. and Heer, E., "Receptance coupling of structural components near a component resonance frequency", Technical Memorandum 33-411, Jet Propulsion Laboratory, California Institute of Technology, Oct 1968

37. Klosterman, A. L., "On the experimental determination and use of modal representations of dynamic characteristics", Ph.D. thesis, University of Cincinnati, 1971
38. Klosterman, A. L., et al., "Complete design analysis and simulation of a 1750 horsepower AC electric motor", Report on joint Project No. 9097 carried out by US Steel Corp., Westinghouse LRA Division, and Structural Dynamics Research Corporation, April 1971
39. Hurty, W., "Dynamic analysis of structural systems using component modes", AIAA Journal, Vol. 3, No. 4, April 1965
40. Sainsbury, M. G., "Users' guide for the structural dynamic analysis computer program COUPLE1", Manual in 3 parts, Dynamics Group, Imperial College, May 1975
41. Uhrig, R., "The transfer matrix method seen as one method of structural analysis among others", Jnl. of Sound and Vibration, Vol. 4 (2), 1966, pp 136-148
42. Dimentberg, F. M., "Flexural vibrations of rotating shafts", Butterworths, London, 1961
43. Ten Wolde, T., "Reciprocity experiments on the transmission of sound in ships", Doctorate thesis, Technische Hogeschool, Delft, Holland, 1973
44. Henshell, R. D., Bennett, P. J., McCallion, H. and Milner, M., "Natural frequencies and mode shapes of vibration of transformer cores", Proc. IEE, Vol. 112, No. 11, Nov 1965
45. Henshell, R. D. and Warburton, G. B., "Transmission of vibration in beam systems", International Journal of Numerical Methods in Engineering, Vol. 1, 1969, pp 47-66
46. Silva, J. M. M., "The influence of the joint on the vibration response of a cross-beam assembly", M.Sc. thesis, Imperial College, University of London, December 1974

47. Lazan, B. J., "Damping of materials and members in structural mechanics"
Pergamon Press, 1968
48. Snowdon, J. C., "Transverse vibration of beams with internal damping,
rotary inertia and shear", JASA, Vol, 35, No. 12, Dec. 1963
49. Grootenhuis, P., "The control of vibrations with viscoelastic materials"
Journal of Sound and Vibration, Vol. 11 (4), 1970, pp 421-433
50. Yeh, C. T., Hartz, B. J. and Brown, C. B., "Damping sources in wood
structures", Journal of Sound and Vibration, Vol. 19(4), 1971, pp 411-419
51. Ungar, E. E., "The status of engineering knowledge concerning the damping
of built-up structures", Journal of Sound and Vibration, Vol. 26 (1),
1973, pp 141-154
52. Kolarik, J., "Partial constrained layer damping of beams", M.Sc. thesis,
Imperial College, University of London, October 1972
53. Berthier, P., Lalanne, M. and Martinat, J., "Dynamical behaviour of a
damped frame model of machinery seating", ASME paper 73-DET-74, presented
at the Design Engineering Technical Conference, Cincinnati, Sept. 1973
54. Ochs, J. B. and Snowdon, J. C., "Transmissibility across simply supported
thin plates: I - Rectangular and square plates with and without damping
layers", JASA, Vol. 58, No. 4, October 1975
55. Den Hartog, J. P., "Forced vibrations with combined coulomb and viscous
friction", Trans. ASME, APM-107, Vol. 53, 1931, pp 107-115
56. Earles, S. W. E. and Williams, E. J., "A linearized analysis for fric-
tionally damped systems", Journal of Sound and Vibration, Vol. 24 (4),
1972, pp 445-458
57. Iwan, W. D., "A distributed-element model for hysteresis and its steady-
state dynamic response", Trans. ASME, Journal of Applied Mechanics,
December 1966, pp 893-900

58. Earles, S. W. E. and Mansoori, F. S., "Frictional damping applied to a cantilever-beam structure: A theoretical and experimental response comparison", International Journal of Machine Tool Design and Research, Vol. 14, 1974, pp 11-124
59. Williams, E. J. and Earles, S. W. E., "Optimization of the response of frictionally damped beam type structures with reference to gas turbine compressor blading", Trans. ASME, Journal of Engineering for Industry, May 1974, pp 471-476
60. Earles, S. W. E. and Mott, N., "A response prediction and optimisation of a frictionally damped structure", 13th International Machine Tool Design and Research Conference, Birmingham, September 1972
61. Jacobsen, L. S., "Steady forced vibration as influenced by damping", Trans. ASME, APM-52-15, Vol. 52, 1930, pp 169-181
62. Ewins, D. J., "Estimation of resonant peak amplitudes", Journal of Sound and Vibration, Vol. 43 (4), 1975, pp 595-605
63. Hammill, W. J. and Andrew, C., "Receptances of lumped-parameter systems containing discrete damping sources", Journal of Mechanical Engineering Science, Vol. 13, No. 4, 1971, pp 296-301
64. Paslay, P. R. and Gurtin, M. E., "The vibration response of a linear undamped system resting on a nonlinear spring", Trans. ASME, Journal of Applied Mechanics, June 1960, pp 272- 274
65. Mahalingam, S., "The response of vibrating systems with coulomb and linear damping inserts", Journal of Sound and Vibration, Vol. 41 (3), 1975, pp 311-320
66. Mahalingam, S., "The synthesis of vibrating systems by use of internal harmonic receptances", Journal of Sound and Vibration, Vol. 40, 1975, pp 337-350

67. Levitan, E. S., "Forced oscillation of a spring-mass system having combined coulomb and viscous damping", *Journal of the Acoustical Society of America*, Vol. 32, No. 10, October 1960, pp 1265-1269
68. Den Hartog, J. P. and Ormondroyd, J., "Torsional-vibration dampers", *Trans. ASME*, APM-52-13, 1930, pp 133-152
69. Williams, J. L., "An investigation into the effects of frictional damping on the frequency response of a fabricated steel framework structure", M.Sc. thesis, Imperial College, University of London, September 1975
70. Yeh, G. C. K., "Forced vibrations of a two-degree-of-freedom system with combined coulomb and viscous damping", *Journal of the Acoustical Society of America*, Vol. 39, 1966, pp 14-24
71. Den Hartog, J. P., "Forced vibrations with combined viscous and coulomb damping", *Philosophical Magazine*, Vol. 9, 1930, pp 801-817

PART 2MULTI-DIRECTIONAL MOBILITY MEASUREMENTS FOR
THE VIBRATION ANALYSIS OF COUPLED STRUCTURESCONTENTS

<u>Chapter</u>		<u>Page</u>
3	MULTI-DIRECTIONAL MOBILITY MEASUREMENT	
	3.1 Introduction	83
	3.2 Terminology	89
4	MULTI-DIRECTIONAL MEASUREMENTS WITH A SINGLE SHAKER	
	4.1 Three-directional Point Mobility Measurement — The Basic Principles of a Single Shaker Method	94
	4.2 Measurement and Processing of the Data	99
	4.3 The Initial Exciting Block (Mk 1)	102
	4.4 An Improved Exciting Block (Mk 2)	104
	4.5 Two-directional Point Mobility Measurement using a Computer-controlled Measuring System	132
5	MULTI-DIRECTIONAL MEASUREMENTS WITH A TWIN SHAKER	147
6	COUPLING OF BEAM TO SPRING-SUPPORTED BLOCK	160
7	SUMMARY AND CONCLUSIONS FOR MULTI-DIRECTIONAL MOBILITY MEASUREMENTS	
	7.1 General Discussion and Summary	176
	7.2 Conclusions	184
	REFERENCES FOR CHAPTERS 3 TO 7	185

Appendices to Part 2 start on Page 460

CHAPTER 3

MULTI-DIRECTIONAL MOBILITY MEASUREMENT

3.1 INTRODUCTION

In Part 1 we have considered how any complex structure may be analysed in terms of the mobility or impedance properties of its constituent components. Although it would be nice to determine all these component data by theoretical means, this is not always feasible in practice, and if we are to proceed with the analysis we must resort to experiments in order to determine the properties of the more complex components. Hence, the predicted response for the complete structure must be obtained using a combination of theory and measurement.

At each coupling point between two components, as many as six motions are possible, these being translational motion in the x, y and z directions and rotations about these axes. Although it is seldom necessary to consider all six of these co-ordinates, it is usually the case that one must consider more than a single co-ordinate. This has long been recognised in the purely theoretical analysis of structures, but in the case of predictions made from measured data it has generally been ignored. As suggested by Noiseux and Meyer^{(1)(2)*}, the limitations imposed by the available measurement techniques have for several years impeded the application of mobility concepts and distorted the applications by requiring the use of what can be measured, rather than what ought to be measured. Although great advances have been made recently in the field of electronic equipment for measuring the transducer signals, comparatively little attention appears to have been given to what one should be measuring with this sophisticated equipment.

* Note that References for Chapters 3 to 7 are listed on Page 185.

In consequence, many equipment users have remained blissfully ignorant of anything other than uni-axial measurements with a conventional impedance head.* Even these measurements may on occasions have been erroneous, either due to limitations imposed by the impedance head or to restraints applied to the structure in directions other than that of the intended excitation. For instance, in the case of very low mobility structures errors may arise due to any of the following:

- (1) An impedance head end stiffness comparable with the dynamic stiffness of the structure under test.
- (2) Non overall contact between the face of the head and the surface of the structure, giving rise to contact resonances in the higher frequency regions (e.g. around 1000 Hz or above).
- (3) Electrical crosstalk between the force and acceleration channels in the head, so that for very low acceleration levels the crosstalk from the force channel may even swamp the true acceleration signal.

At the other extreme, in the case of fairly mobile structures an excitation in one direction can cause a quite significant response in several co-ordinate directions, and errors can be caused by:

- (a) Secondary excitation due to the inertia loading of the structure in various directions by the head. Note that conventional mass cancellation only corrects for inertia loading in the direction of the head axis.
- (b) Secondary excitation due to restraints imposed on the free motion of the head by a stiff connection to the shaker, coupled with a laterally stiff shaker suspension.

* An impedance head comprises a force gauge and an accelerometer mounted in a single housing. Readers unfamiliar with the more basic aspects of "impedance testing" should consult references (3) to (8). The last three are particularly recommended, since they form a three-part article dealing with both the measurement and application of mechanical impedance data.

To illustrate (b) some measurements were made on the spring-supported steel block shown in Fig. 3.1, using a Wilcoxon impedance head and three different sizes of push rod between the head and the shaker. The second resonance of this system corresponds to a rocking mode and the results clearly demonstrate the quite severe effect of the lateral restraint imposed by a stiff push rod used in conjunction with a laterally stiff shaker suspension. Kerlin and Snowdon⁽⁹⁾ have also examined these effects, by carrying out carefully controlled tests on a cantilever beam, and Silva⁽¹⁰⁾ has made a fairly detailed study using various rods and testpieces.

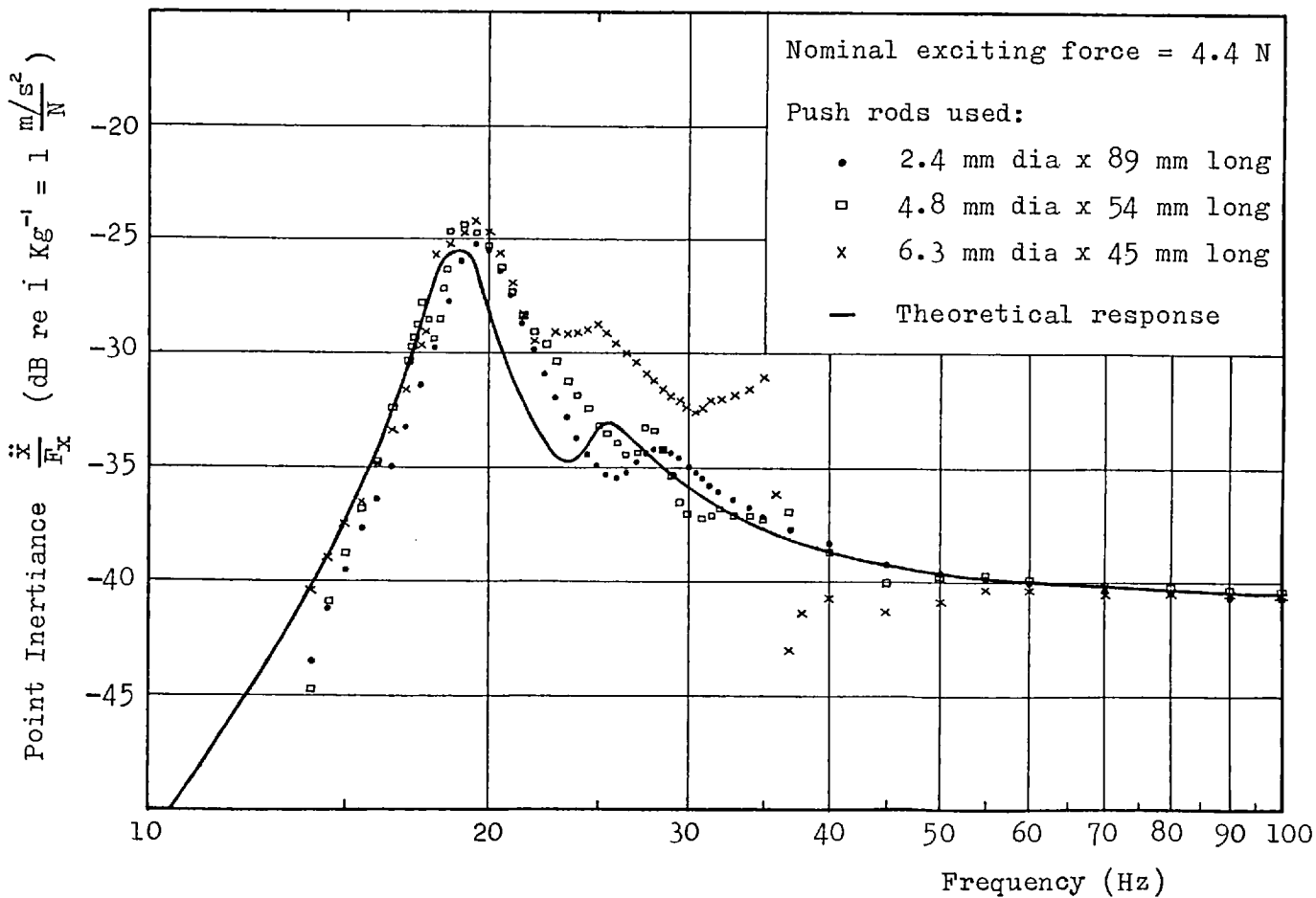
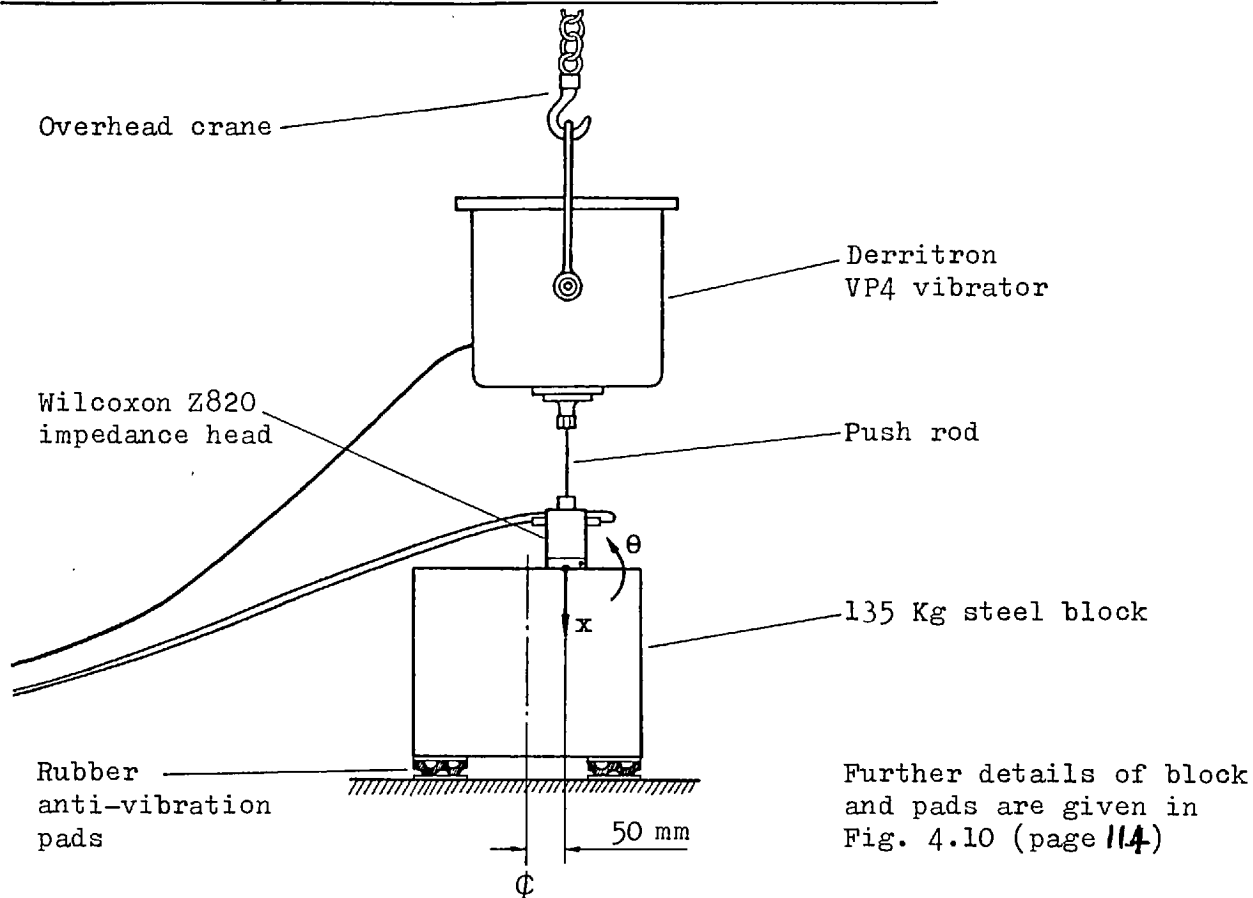
Even when mobility measurements have been made in more than one direction, they have almost universally been confined to the linear co-ordinate directions, simply because suitable rotational accelerometers, impedance heads, and electrodynamic shakers have not been commercially available*. In spite of this, complete mobility data have been measured by Smith⁽¹¹⁾, who uses two linear shakers vibrating in antiphase in order to produce a couple, whilst Lemon⁽¹²⁾ either uses a hydraulic rotational shaker or he avoids the problem of applying couples by taking purely linear point and transfer mobility measurements at points on either side of the coupling point.

It should be mentioned that it is possible to deduce the rotation couple response of resonant systems from a knowledge of the translation and rotation force responses⁽¹³⁾, thereby obviating the need for applying and measuring couples. However, it is first necessary to mathematically model the measured data, and this is not easy in the case of heavily damped structures.

* A rotational accelerometer suitable for high frequency use has recently been introduced by the Endevco Corporation, but at present it is very much more expensive than conventional linear accelerometers. A rotational shaker developed at Imperial College is now produced by Derritron Ltd., but its large size precludes its use for the majority of impedance measurement applications.

FIG. 3.1

THE EFFECT OF THE VIBRATOR/IMPEDANCE-HEAD CONNECTION ON THE MEASURED RESPONSE OF A 135 KG STEEL BLOCK MOUNTED ON RUBBER PADS



In addition, the known relationship between these mobilities no longer applies in the case of very large structures such as buildings, ships, etc., which exhibit both resonant and dispersive characteristics, and do not obey classical vibration theory when subjected to small excitation forces. Hence there still exists a need for measuring multi-directional mobility data directly.

Faced with the limitations imposed by the existing measurement techniques and the lack of suitable hardware, it was decided to conduct a fairly detailed investigation into mobility or impedance* testing. The primary aims of this work were to develop a method for measuring multi-directional mobility data, and to assess the feasibility of using such measured data for the vibration analysis of coupled structures.

In view of the symmetry inherent in many engineering structures, it is often possible to restrict one's attention to motion in a single plane, and even if the structure is only quasi-symmetrical the errors incurred by assuming plane motion may not be great. The motion of a point in a plane is described by just three co-ordinates — two translational and one rotational — so both the measurements and the analysis are greatly simplified. In those cases where the two translational motions are uncoupled (e.g. flexure of beams and plates) one may even confine one's attention to just two co-ordinates — translation and rotation.

So as to keep the problem within manageable bounds during the initial stages, it was decided to consider only these simplified cases of two- and three-directional motion in a plane. Accordingly, a multi-directional measurement technique has been developed and applied to measurements in a single plane on a free-free steel beam and on the large steel block already shown in Fig. 3.1. These data have then been

* The term "impedance" should be avoided, for reasons given on Page 91.

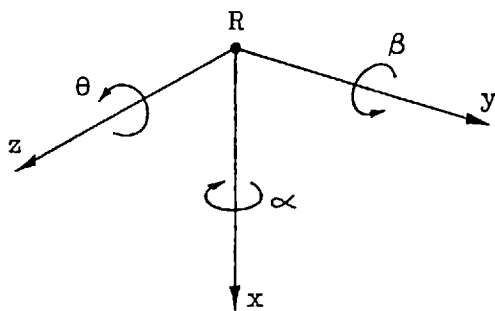
used to predict the response of the beam coupled to the block, in order to investigate the feasibility of using measured information in the coupling process.

The basic measurement technique requires the use of only a single shaker and standard measuring equipment, but the raw data from the test does have to be processed subsequently in a digital computer. However, this problem has been overcome by using a computer-controlled measuring system, which facilitates on-line processing of the data during the test.

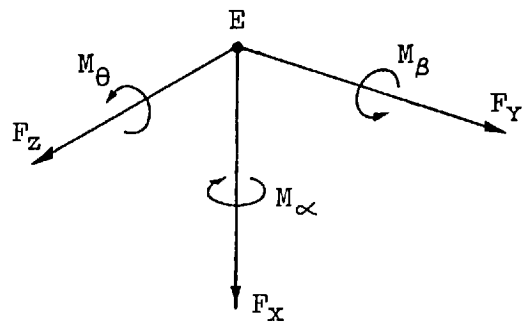
An extension of the basic techniques is to use a pair of shakers, and results are presented for comparison with the single-shaker measurements.

3.2 TERMINOLOGY

The motion at any point on a structure is described completely by six generalised co-ordinates, of which three are translational and three are rotational. The co-ordinates are most conveniently chosen so as to form an orthogonal set. Similarly, any arbitrary excitation at a point may be resolved into six generalised forces acting along the chosen co-ordinate directions. Hence the force system comprises three linear forces and three couples. We shall employ the co-ordinate system shown below.



Displacements at point R



Forces at point E

For our purposes all motions and forces vary harmonically with time, so that $x = \bar{x}.e^{j\omega t}$, $F = \bar{F}.e^{j\omega t}$, etc., where \bar{x} and \bar{F} are complex numbers to take account of phase differences.

Considering the general case, the velocity response at point R is related to an excitation at point E by a 6×6 mobility matrix:

$$\begin{array}{c}
 \left[\begin{array}{c} \dot{x} \\ \dot{y} \\ \dot{z} \\ \dot{\alpha} \\ \dot{\beta} \\ \dot{\theta} \end{array} \right] \\
 \text{R}
 \end{array}
 =
 \begin{array}{c}
 \left[\begin{array}{cccccc}
 Y_{11} & Y_{12} & Y_{13} & Y_{14} & Y_{15} & Y_{16} \\
 Y_{21} & Y_{22} & Y_{23} & Y_{24} & Y_{25} & Y_{26} \\
 Y_{31} & Y_{32} & Y_{33} & Y_{34} & Y_{35} & Y_{36} \\
 Y_{41} & Y_{42} & Y_{43} & Y_{44} & Y_{45} & Y_{46} \\
 Y_{51} & Y_{52} & Y_{53} & Y_{54} & Y_{55} & Y_{56} \\
 Y_{61} & Y_{62} & Y_{63} & Y_{64} & Y_{65} & Y_{66}
 \end{array} \right] \\
 \text{E}
 \end{array}
 \begin{array}{c}
 \left[\begin{array}{c} F_x \\ F_y \\ F_z \\ M_\alpha \\ M_\beta \\ M_\theta \end{array} \right] \\
 \text{E}
 \end{array}
 \quad (3.1)$$

where the elements Y_{ij} are complex numbers, to allow for the phase difference between the response and the excitation*.

If $R = E$, we define the matrix as being a point mobility matrix.

If $R \neq E$, we define the matrix as being a transfer mobility matrix.

In addition we define the terms on the leading diagonal of the matrix to be direct mobilities, whilst the off-diagonal terms are cross mobilities. This complies with the terminology used by Bishop and Johnson⁽¹⁴⁾.

The distinction between transfer and cross mobilities should be noted, since it has been common practice in the measurement field to refer to any mobility Y_{ij} as a transfer mobility whenever $i \neq j$. As most mobility measurements in the past have been confined to a single direction at each point, there has been no confusion. However, now that we are considering up to six directions at a point, it would obviously be confusing to refer to the off-diagonal terms in the point mobility matrix as transfer mobilities.

Although we have chosen the response quantity to be velocity, we may equally well use either acceleration or displacement. The corresponding generalised mobility matrices are then "inertance" and "receptance" matrices respectively. The three forms are simply related:

* Note that the mobility matrix is symmetric, so $Y_{ji} = Y_{ij}$. This is a consequence of the well-known reciprocity principle.

$$\text{Inertance} = j\omega \text{ Mobility}$$

$$\text{Receptance} = \frac{-j}{\omega} \text{ Mobility}$$

When dealing with multi-directional measurements it is advisable to avoid the term "impedance" wherever possible. This equally well applies to the associated terms "apparent mass" and "dynamic stiffness", which are related to impedance in the following manner:

$$\text{Apparent Mass} = \frac{-j}{\omega} \text{ Impedance}$$

$$\text{Dynamic Stiffness} = j\omega \text{ Impedance}$$

The reason for this is that there exist two types of impedance, namely true impedance and pseudo impedance.

True impedance is a matrix quantity, and is the inverse of the mobility matrix, so that

$$\begin{array}{c} \left[\begin{array}{c} F_x \\ F_y \\ F_z \\ M_\alpha \\ M_\beta \\ M_\theta \end{array} \right] \\ E \end{array} = \begin{array}{c} \left[\begin{array}{cccccc} Z_{11} & Z_{12} & Z_{13} & Z_{14} & Z_{15} & Z_{16} \\ Z_{21} & Z_{22} & Z_{23} & Z_{24} & Z_{25} & Z_{26} \\ Z_{31} & Z_{32} & Z_{33} & Z_{34} & Z_{35} & Z_{36} \\ Z_{41} & Z_{42} & Z_{43} & Z_{44} & Z_{45} & Z_{46} \\ Z_{51} & Z_{52} & Z_{53} & Z_{54} & Z_{55} & Z_{56} \\ Z_{61} & Z_{62} & Z_{63} & Z_{64} & Z_{65} & Z_{66} \end{array} \right] \\ R \end{array} \begin{array}{c} \left[\begin{array}{c} \dot{x} \\ \dot{y} \\ \dot{z} \\ \dot{\alpha} \\ \dot{\beta} \\ \dot{\theta} \end{array} \right] \end{array}$$

(3.2)

When using the impedance or dynamic stiffness coupling technique* for analysing built-up structures, the component data must be presented in terms of true impedance matrices. However, the elements of the true impedance matrix cannot usually be measured directly.† To illustrate

* See Part 1 of this report (Chapter 2).

† A "direct measurement" here means one in which the required matrix, or a transformed version of it, is obtained directly.

this, let us consider the situation when the only excitation is that in the x direction:

$$F_x = Z_{11}\dot{x} + Z_{12}\dot{y} + Z_{13}\dot{z} + Z_{14}\dot{\alpha} + Z_{15}\dot{\beta} + Z_{16}\dot{\theta} \quad (3.3)$$

In order to measure any element Z_{ij} directly one would have to prevent motion in the other five directions, thereby leaving only one non-zero term on the right hand side of (3.3). When all the co-ordinates refer to a single point this is obviously impossible from a practical point of view. Even if each co-ordinate refers to a different point on the structure this is still very difficult to achieve. Direct measurement of the mobility matrix poses no such problem, as constraints are not applied to the system. Hence the impedance matrix must almost invariably be obtained by inverting the mobility matrix.

Pseudo-impedance is the type of impedance which is generally measured in so-called "impedance tests". It is not a true matrix quantity, in that it cannot be post-multiplied by a velocity vector to yield a force vector. Accepting this, we may define the pseudo-impedance matrix corresponding to (3.1) as a matrix whose elements $Z_{ij}^{\text{pseudo}} = \frac{1}{Y_{ij}}$. It should be noted that this is not the inverse of the mobility matrix. However, if the measured data are required for any coupling procedure, it is the inverse mobility matrix that is needed, and the use of pseudo impedance is quite pointless and can lead to confusion. These basic mobility and impedance concepts are discussed in more detail in references (15) and (16).

The matrix of (3.1) will additionally be called a six-directional mobility matrix, since it describes the mobility properties in all six of the possible co-ordinate directions, thereby describing any motion in

space due to any conceivable point excitation.

Since most of the work described in this report is limited to the case of motion in a single plane, it is convenient to consider the following simplified mobility relations, which describe respectively the $x-\theta$ and $x-y-\theta$ motions in a plane:

$$\begin{array}{c} \left[\begin{array}{c} \dot{x} \\ \dot{\theta} \end{array} \right] \\ R \end{array} = \begin{array}{c} \left[\begin{array}{cc} Y_{11} & Y_{12} \\ Y_{21} & Y_{22} \end{array} \right] \\ E \end{array} \begin{array}{c} \left[\begin{array}{c} F_x \\ M_\theta \end{array} \right] \\ E \end{array} \quad (3.4)$$

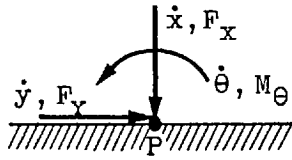
$$\begin{array}{c} \left[\begin{array}{c} \dot{x} \\ \dot{y} \\ \dot{\theta} \end{array} \right] \\ R \end{array} = \begin{array}{c} \left[\begin{array}{ccc} Y_{11} & Y_{12} & Y_{13} \\ Y_{21} & Y_{22} & Y_{23} \\ Y_{31} & Y_{32} & Y_{33} \end{array} \right] \\ E \end{array} \begin{array}{c} \left[\begin{array}{c} F_x \\ F_y \\ M_\theta \end{array} \right] \\ E \end{array} \quad (3.5)$$

where the subscripts of the θ mobility terms no longer correspond to those used in (3.1). These simpler matrices will be called two-directional and three-directional plane mobility matrices.

CHAPTER 4

MULTI-DIRECTIONAL MEASUREMENTS WITH A SINGLE SHAKER4.1 THREE-DIRECTIONAL POINT MOBILITY MEASUREMENTThe Basic Principles of a Single Shaker Method

We wish to measure the mobility matrix relating the three velocities \dot{x} , \dot{y} and $\dot{\theta}$ to the three forces F_x , F_y and M_θ acting at the same point. As the elements of this matrix are frequency-dependent, the complete matrix must be measured at all frequencies of interest.



The diagram shows a point P on a hatched surface. A vertical force F_x acts downwards from P, and a horizontal force F_y acts to the right from P. A curved arrow indicates a counter-clockwise moment M_θ about P. Above the point, the corresponding velocities are shown: \dot{x} (vertical), \dot{y} (horizontal), and $\dot{\theta}$ (rotational).

$$\begin{matrix} \left[\begin{array}{c} \dot{x} \\ \dot{y} \\ \dot{\theta} \end{array} \right] \\ R=P \end{matrix} = \begin{bmatrix} Y_{11} & Y_{12} & Y_{13} \\ Y_{21} & Y_{22} & Y_{23} \\ Y_{31} & Y_{32} & Y_{33} \end{bmatrix} \begin{matrix} \left[\begin{array}{c} F_x \\ F_y \\ M_\theta \end{array} \right] \\ E=P \end{matrix} \quad (4.1)$$

Only \dot{x} and F_x can be measured directly. Hence, of all the nine elements in the matrix, only Y_{11} can be measured with a conventional impedance head and linear shaker.

The velocity \dot{y} cannot in general be measured directly, since it is physically impossible to bring the axis of a finite-size accelerometer or impedance head down to the surface of the test structure.

The rotational velocity θ could until recently only be measured by using two linear accelerometers and taking the difference of their signals. When the present work was carried out, the only rotational accelerometers in existence had an upper frequency limit somewhere in the range 10 to 100 Hz, and it is only with the recent introduction of a high-frequency rotational accelerometer by the Endevco Corporation that the situation has changed. However, in view of its high cost and the fact that we also need to measure linear accelerations,

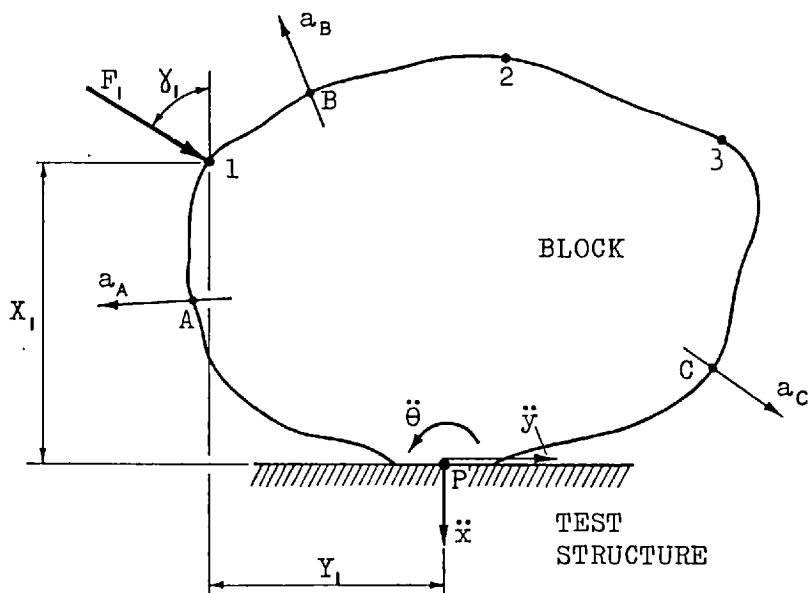
there is still good reason for using a pair of linear accelerometers.

The force F_Y cannot in general be applied directly, owing to the finite size of the force gauge or impedance head.

The couple M_Θ can be applied using a rotational hydraulic shaker, but at the present time there is no small rotational electro-dynamic shaker commercially available. Even given the necessary means of excitation, there is still not available a rotational force gauge or impedance head.

As we are unable to measure the required matrix directly we must instead measure a related mobility matrix. Then, knowing the relationship between the matrices, we may transform the measured matrix into the required point mobility matrix.

Suppose that we attach a massless, non-deformable block to the surface of the test structure at point P, as shown below.



Attached to the block at points A, B and C are three massless accelerometers. As the block does not deform, the accelerations \ddot{x} , \ddot{y} and $\ddot{\theta}$ at point P are related to the measured accelerations a_A , a_B and a_C by a simple

transformation matrix $[C_P]$, which is a function of the block geometry only. Hence the velocities at P are given by

$$\begin{Bmatrix} \dot{x} \\ \dot{y} \\ \dot{\theta} \end{Bmatrix} = \frac{1}{j\omega} [C_P] \begin{Bmatrix} a_A \\ a_B \\ a_C \end{Bmatrix} \quad (4.2)$$

We apply a force to the block at either 1, 2 or 3 via a massless force gauge, and as the block also has no mass all the force is transmitted through to P. For a force applied at point i ($i = 1, 2, 3$) the resultant force system acting on the structure is

$$\begin{Bmatrix} F_x \\ F_y \\ M_\theta \end{Bmatrix} = \begin{Bmatrix} \cos \gamma_i \\ \sin \gamma_i \\ (Y_i \cos \gamma_i - X_i \sin \gamma_i) \end{Bmatrix} F_i \quad (4.3)$$

Now substitute expressions (4.2) and (4.3) for the velocity and force vectors in (4.1), at the same time dividing through by F_i :

$$\frac{1}{j\omega} [C_P] \begin{Bmatrix} \left(\frac{a_A}{F}\right)_i \\ \left(\frac{a_B}{F}\right)_i \\ \left(\frac{a_C}{F}\right)_i \end{Bmatrix} = \begin{bmatrix} Y_{11} & Y_{12} & Y_{13} \\ Y_{21} & Y_{22} & Y_{23} \\ Y_{31} & Y_{32} & Y_{33} \end{bmatrix} \begin{Bmatrix} \cos \gamma_i \\ \sin \gamma_i \\ (Y_i \cos \gamma_i - X_i \sin \gamma_i) \end{Bmatrix} \quad (4.4)$$

Considering the three excitation cases together we obtain

$$\frac{1}{j\omega} \left[C_p \right] \begin{bmatrix} \left(\frac{a_A}{F} \right)_1 & \left(\frac{a_A}{F} \right)_2 & \left(\frac{a_A}{F} \right)_3 \\ \left(\frac{a_B}{F} \right)_1 & \left(\frac{a_B}{F} \right)_2 & \left(\frac{a_B}{F} \right)_3 \\ \left(\frac{a_C}{F} \right)_1 & \left(\frac{a_C}{F} \right)_2 & \left(\frac{a_C}{F} \right)_3 \end{bmatrix} = \begin{bmatrix} Y_{11} & Y_{12} & Y_{13} \\ Y_{21} & Y_{22} & Y_{23} \\ Y_{31} & Y_{32} & Y_{33} \end{bmatrix} \begin{bmatrix} \cos \gamma_1 & \cos \gamma_2 & \cos \gamma_3 \\ \sin \gamma_1 & \sin \gamma_2 & \sin \gamma_3 \\ (Y_1 \cos \gamma_1, -X_1 \sin \gamma_1) & (Y_2 \cos \gamma_2, -X_2 \sin \gamma_2) & (Y_3 \cos \gamma_3, -X_3 \sin \gamma_3) \end{bmatrix}$$

$$\frac{1}{j\omega} \left[C_p \right] \left[I_m \right] = \left[Y \right] \left[\Gamma \right] \quad (4.5)$$

Post-multiply (4.5) by $\left[\Gamma \right]^{-1}$ to obtain the required point mobility matrix in terms of the measured inertiance matrix:

$$\left[Y \right] = \frac{1}{j\omega} \left[C_p \right] \left[I_m \right] \left[\Gamma \right]^{-1} \quad (4.6)$$

where $\left[I_m \right]$ and hence $\left[Y \right]$ are complex matrices.

Thus equation (4.6) gives the required point mobility matrix in terms of mobility measurements on the block attached to the structure. The block will henceforth be called an exciting block, since it provides the means whereby different known excitations may be applied to a point on the structure.

The above theory has been derived on the assumption that the exciting block is both non-deformable and massless. The first assumption can be satisfied sufficiently well with a suitable choice of block shape and accelerometer positions, the main requirement being that any relative motion across the block should be small in comparison with the motion of the structure underneath the block. Problems only arise in the case of very low mobility structures. In contrast, the assumption of a massless block produces no noticeable error

in the case of a low mobility structure, since motions are then small, resulting in negligible inertia loading. However, when the structure mobility is high, the loading effect of the block may cause the resonant frequencies to be lowered by around 5 to 10%. Hence it is desirable to introduce into (4.6) a correction for the block inertia. The resulting inertia-corrected mobility equation is then

$$[Y] = \frac{1}{j\omega} [C_p] [I_m] \left([\Gamma] - [M] [C_p] [I_m] \right)^{-1} \quad (4.7)$$

where the inertia matrix $[M]$ is a function of the block mass, moment of inertia and geometry. The various matrices are derived in detail in Appendix III.

Four different exciting blocks have been made and tried out, and the various results are presented in this and the following chapter, and in Appendix IV.

4.2 MEASUREMENT AND PROCESSING OF THE DATA

Any measurement technique is only as good as the equipment used to acquire the data. Therefore, before we consider the details of the exciting block we should be sure that the measuring equipment is capable of giving us reliable data, in a form suited to our requirements.

The technique described in section 4.1 requires three different excitations and subsequent processing of the measured data, so one cannot employ a continuous sweep and obtain an immediate response plot. As the processing must be carried out with a digital computer, the measured data should preferably be output or displayed directly in digital form, and it must obviously be acquired at discrete frequencies. Since mobility is a frequency-dependent quantity, all the elements of the matrix must be obtained at the same frequency, so for each of the three excitations one must be capable of returning to precisely the same frequency. In addition to digital data and good frequency repeatability, we also require accurate measurements of the modulus and phase of the force and acceleration signals. Thus, filtering of the signals is an absolute necessity.

In the case of the experiments described in this report, the above requirements have been met with a Solartron digital transfer function analyser (Type JM1600A). This instrument provides a digital display of either in-phase and quadrature response or modulus and phase angle, without the need to continually read meters or to take readings off a graph. It has very good frequency accuracy ($\pm 0.05\%$), a typical measuring accuracy per channel of ± 0.1 dB and 0.5° , and a very effective constant percentage bandwidth filter*. The basic unit has a upper frequency limit of 480 Hz, but this may be extended

* The filtering process is simple Fourier Analysis, carried out digitally over a number of cycles to yield the fundamental component of the incoming signal.

to 160 KHz with the addition of a high-frequency extension unit (Type JX1639).

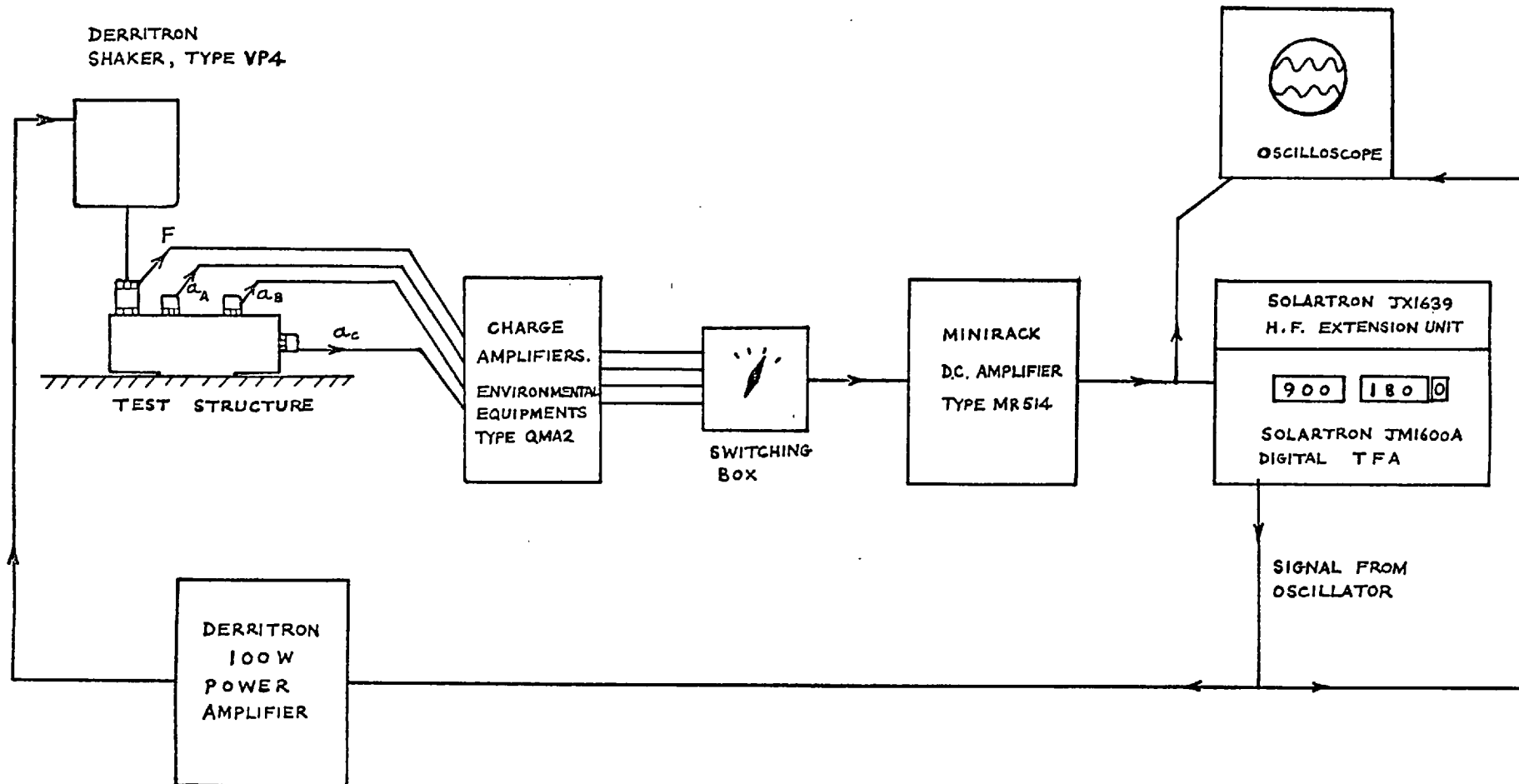
The complete measuring system used for the initial experiments is shown in Fig. 4.1. The force gauge and accelerometers were standard piezo-electric types, and the latter had quoted maximum cross sensitivities of 5 %. After amplification in standard charge amplifiers the signals were fed into a switching box, the output of which went through an extra amplifier before reaching the analyser.

The digital information was written down and later punched onto cards. Then, using a Fortran IV computer program based on equation (4.7), the data were processed to yield the required mobility matrix. The whole process was naturally rather time consuming, but this disadvantage has subsequently been overcome by utilising a computer-controlled measuring system. This has facilitated automation of the measurements and processing of the data on-line in the laboratory, thereby speeding up the whole process (see Section 4.5).

The computer-controlled system currently in use within the Dynamics Group is the Solartron Programmable Frequency Response Analyser, Type 3381^{(17)(18)*}. This consists of the above-mentioned JM1600A TFA and the JX1639 HF unit, interfaced with a Digital Equipment PDP 8E mini-computer⁺. The latter is used to control the measurements and to process the measured response data, and it is programmed via a tele-typewriter using a simple conversational language called FOCAL. Data may either be punched out on paper tape, printed, or plotted on an X-Y plotter. Similarly, the controlling programs may be kept on paper tape, ready for loading when required.

* Note that References for Chapters 3 to 7 are listed on Page 185.

+ It should be noted that a more modern system is now available from the same manufacturers. This comprises the more sophisticated Type 1172 TFA and a PDP 11 computer, and the BASIC language is used instead of FOCAL.



APPARATUS USED FOR EXPERIMENTS

4.3 THE INITIAL EXCITING BLOCK (MK 1)

Introduction

The first exciting block to be tried is shown in Fig. 4.2. This block was made a rather strange shape in order to try and satisfy the following requirements:

- (1) The excitation points 1, 2 and 3 should be such that the shaker is always well clear of the test structure.
- (2) The block should be as compact as possible, so as to compare favourably with the average impedance head as regards size and inertia.

Tests with Mk 1 Block

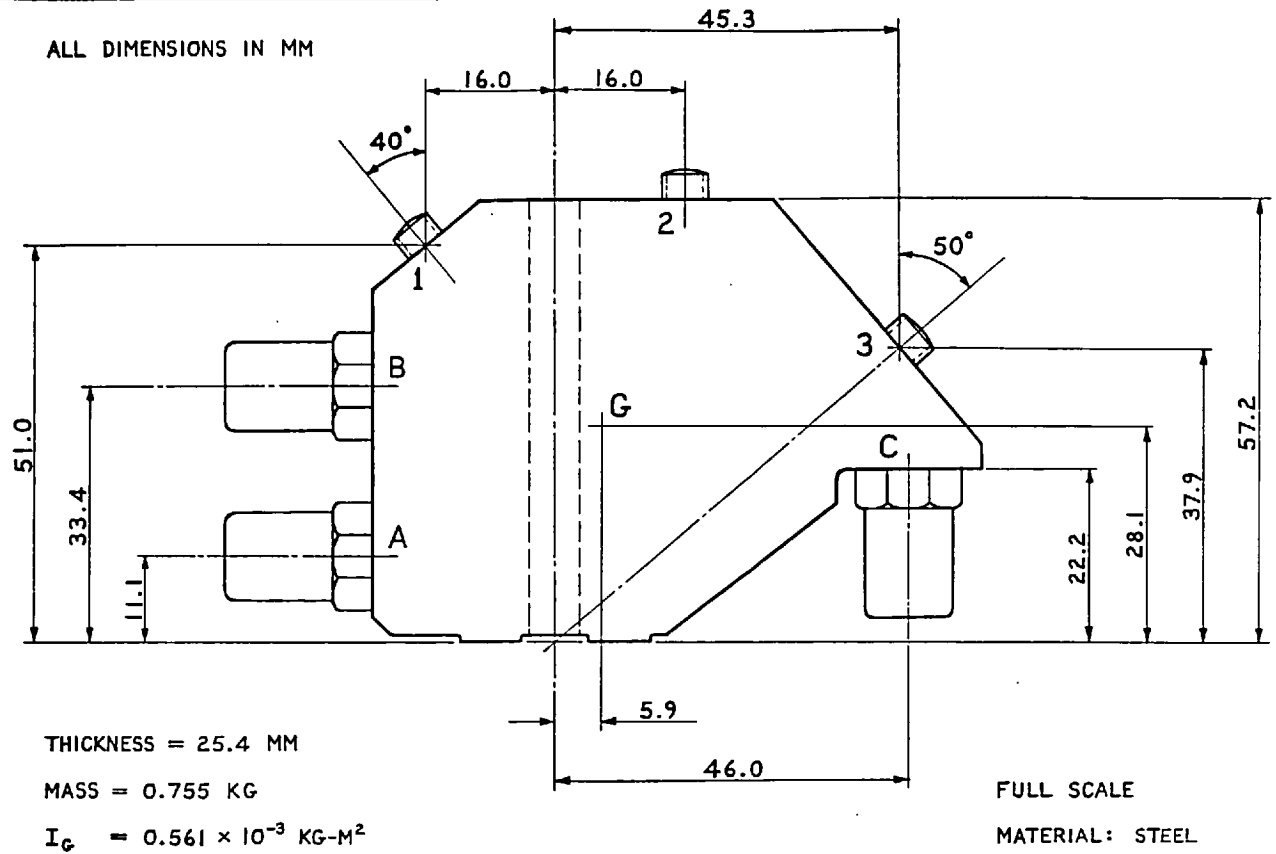
The exciting block was mounted near the tip of the 1.83 m steel beam shown in Fig. 4.10 (page 114), and the beam was suspended on ropes at the nodes of the first free-free mode. The block was attached with a $\frac{1}{2}$ UNF Allen screw.

Measurements were made at a few frequencies around the fundamental resonance of the beam. The first set of readings was taken with the exciter at position 1. The exciter was then moved to positions 2 and 3 respectively for the second and third sets of readings.

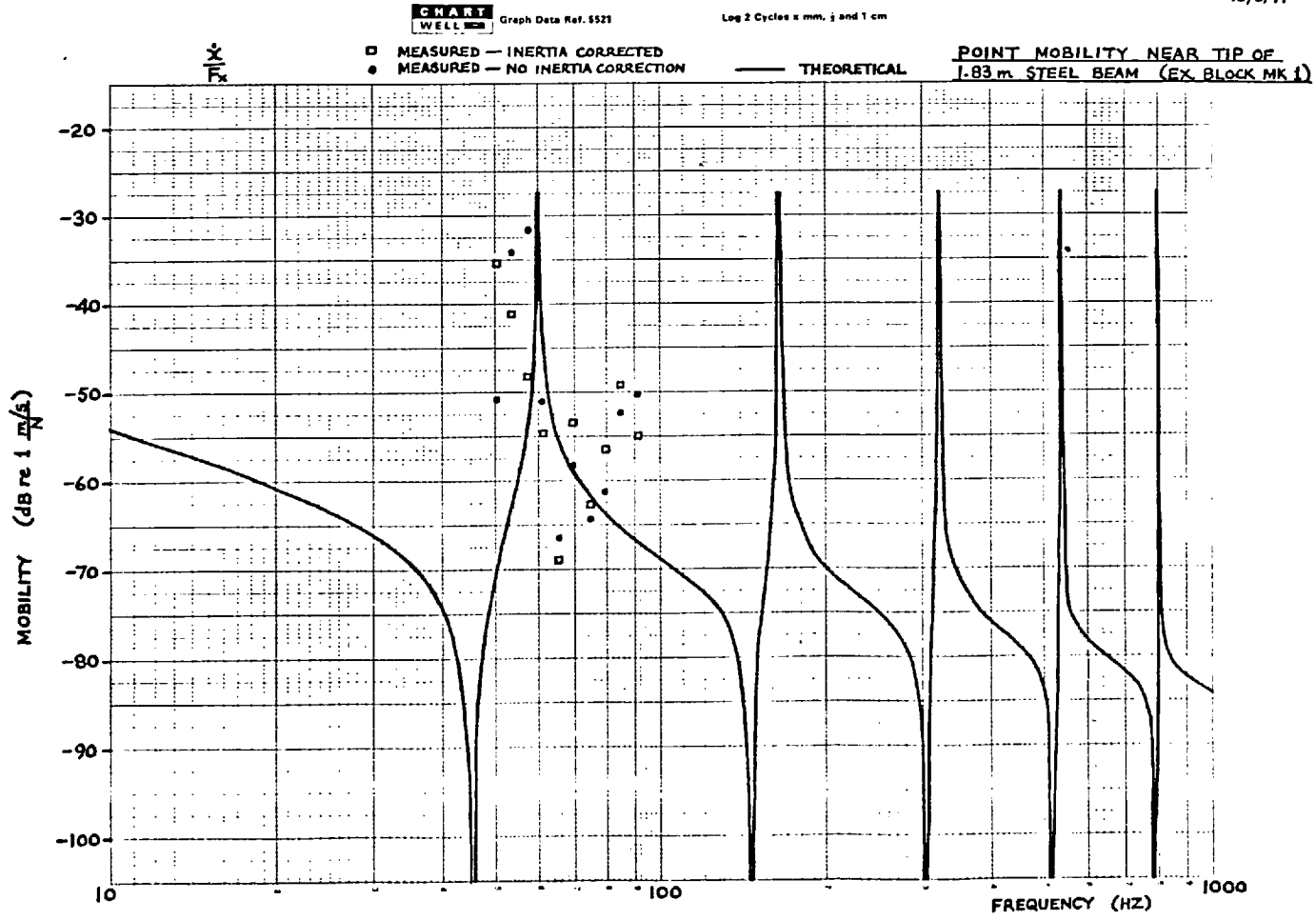
Using equation (4.6) the point mobility matrix was derived from the measured data at each frequency. Equation (4.7) was also used in order to obtain the inertia-corrected mobility matrix. The results for the transverse mobility $\frac{\dot{x}}{F_x}$ are shown in modulus only in Fig. 4.2, and they are seen to exhibit considerable scatter, with large deviations from the theory. Though the results for the other eight mobility elements are not shown, they are in fact at least as bad. It is particularly interesting that the introduction of the block inertia cancellation produces such large changes in the results over all ten frequencies, since the block mass is only 0.752 Kg, as compared to a beam mass of 28.9 Kg. This tends to indicate a mathematically ill-conditioned system.

FIG 4.2

EXCITING BLOCK MK 1



13/8/71



4.4 AN IMPROVED EXCITING BLOCK (MK 2)

Introduction

The tests with the Mk 1 block have shown the impracticability of unscrambling the measured data when each of the forces applied to the test structure is of a comparable size. If we are to measure the mobility to an acceptable degree of accuracy we must therefore try to produce a predominant excitation in each of the three measurement runs. This conclusion led to the consideration of the simple rectangular shaped block shown in Fig.4.3. Ignoring the inertia of the block, it is seen that excitation at position 1 yields the response to F_x directly. Excitation at position 2 produces both a force $F_y = F_2$ and a couple $M_\theta = F_2 \cdot e$ at P, but if e is sufficiently large the couple excitation should be predominant. Excitation at position 3 produces a force $F_x = F_3$ and a couple $M_\theta = -F_3 \cdot h_E$, but if h_E is kept small the force excitation should this time be predominant.

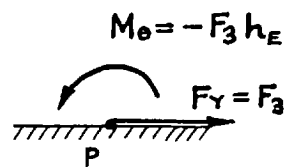
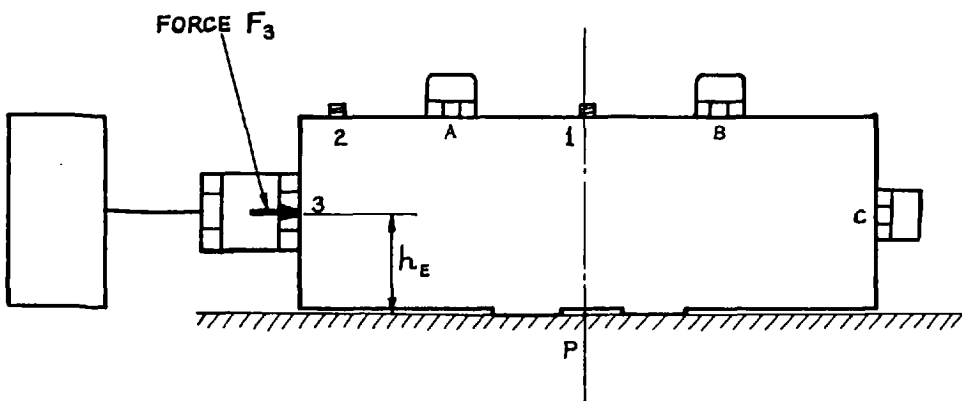
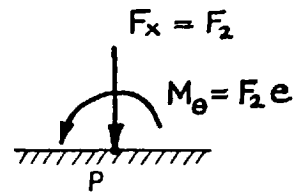
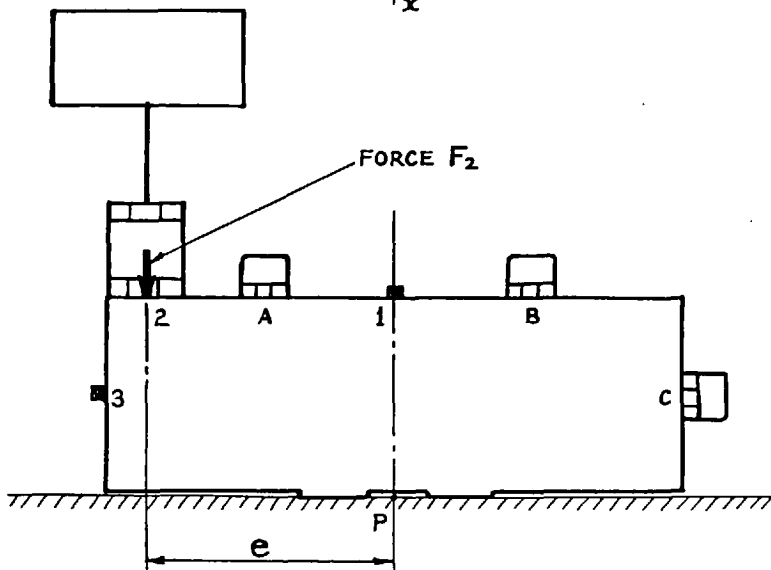
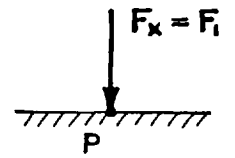
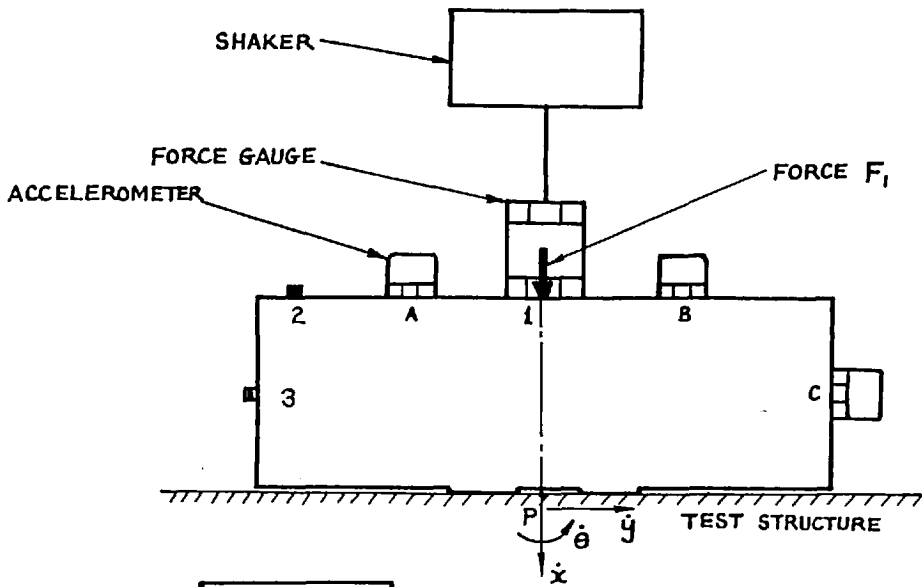
This excitation sequence lends itself to a systematic elimination solution for the required mobilities, since the results of run 1 may be used to remove the effect of the force in run 2, thereby yielding the couple response. Similarly the results of run 2 may be used to remove the effect of the couple in run 3. This is useful if facilities exist for processing the measured data on-line, but it cannot be used if a full correction is to be made for the inertia of the block.

For a rigid, massless block the results must obviously improve as e , and hence the block length, is increased. However, the largest practical length is of the order of 250mm (≈ 10 inch). If its length is large in relation to the length in contact with the structure the block may bend sufficiently during excitation 2 to have an effect upon the results. In addition, an increase in size causes a corresponding increase in mass. Although theoretically it is possible to cancel any mass, it is a practical fact that if the mobility of the exciting block as a free rigid body is small

FIG 4.3

FORCES APPLIED TO TEST
STRUCTURE WITH EXCITING
BLOCK MK 2,3

(IGNORING BLOCK INERTIA)



in comparison with the mobility of the structure, then accurate measurement of the latter is impossible. This is because the small part of the measured data pertaining to the structure is of the same order of magnitude as typical measuring errors, and may be completely lost.

It was decided to examine the feasibility of a 250mm block. However, before having one made a computer simulation was carried out for a block/test-structure system, and systematic errors were injected into the "measured" data. This should show the typical sensitivity to data errors, and hence give an indication of the sort of accuracy required from the measurements.

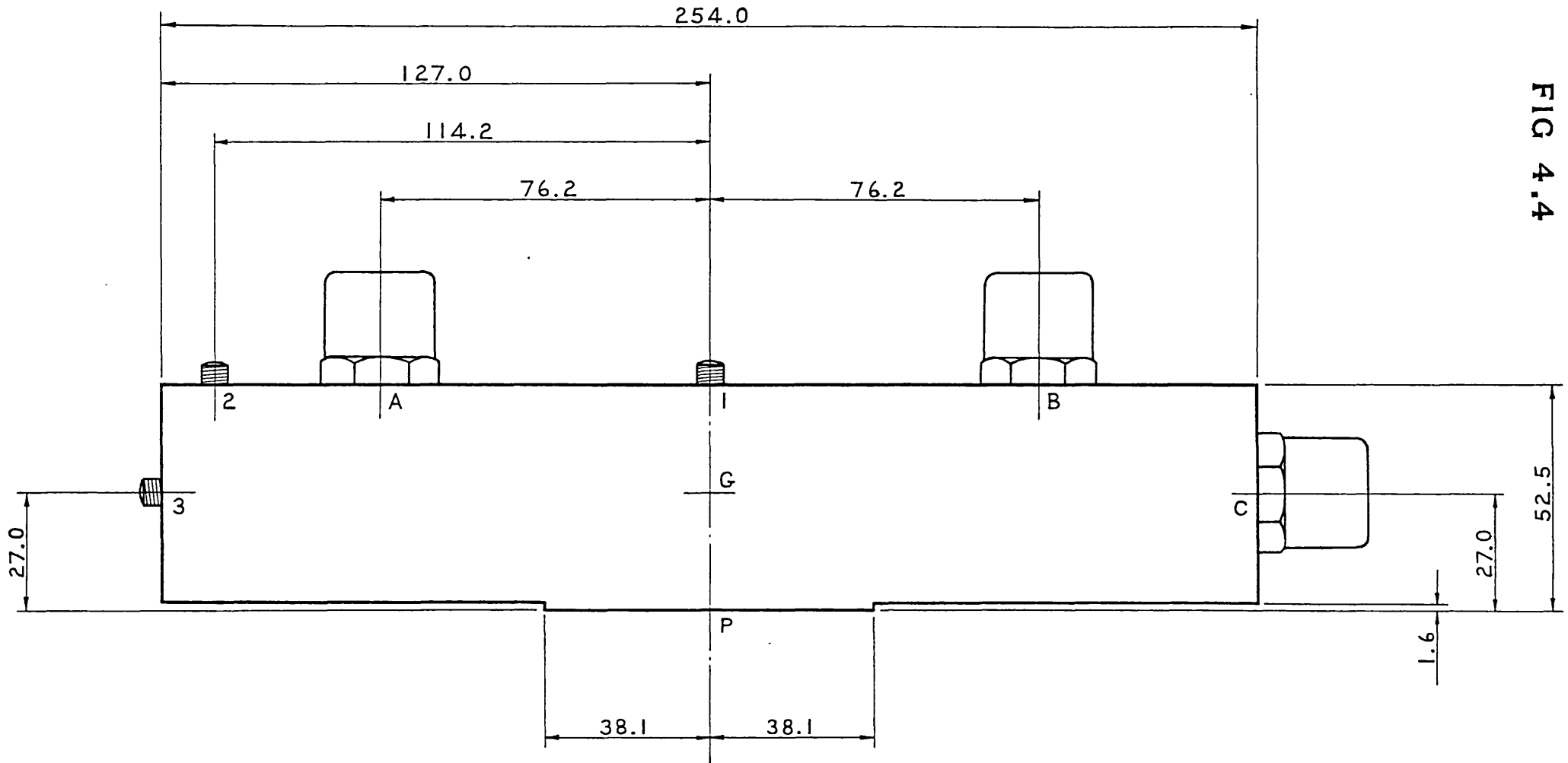
Computer Simulation

The theoretical exciting block Mk 2B and the theoretical test structure are shown in Figs. 4.4 and 4.5 respectively. Also given in Fig.4.5 are two sets of error matrices, which show the way in which the exact inertiances on top of the exciting block were polluted in order to give a more realistic "measured" inertiance matrix $[I_m]$. The point mobility matrix for the test structure has been calculated from these "measured" data using equation 4.7. The results of this simulation are presented in Figs. 4.6 to 4.8, only the lower triangle of the matrix being given here. In the legend on the graphs, Mk 2B signifies a steel block and Mk 2B/Al an aluminium block (masses are 5.1 and 1.8 Kg respectively). The full line represents the true mobility of the structure.

The results clearly indicate that quite acceptable results can be obtained if the inertiance data can be measured to within $\pm 5\%$ (± 0.4 dB) on the modulus and $\pm 3^\circ$ on the phase. These estimates of the required accuracy are necessarily only approximate, as the true nature of the errors is not known. However, the results do indicate that this system is not unduly sensitive to errors in the measured data.

It may also be observed that the lighter aluminium block gives slightly better results than the steel block.

FIG 4.4



BLOCK THICKNESS = 50.8 MM

MASS (STEEL) = 5 KG

MASS (ALUMINIUM) = 1.81 KG

$\frac{3}{4}$ SCALE

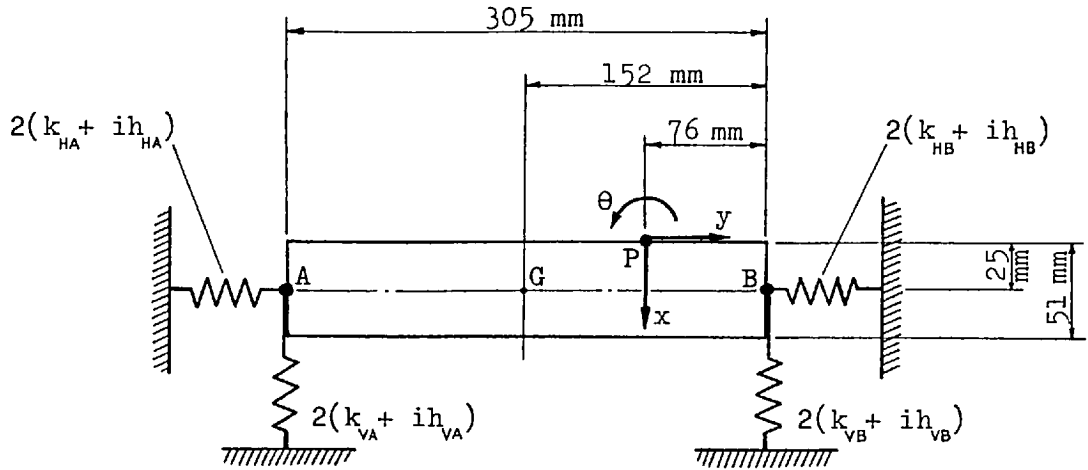
ALL DIMENSIONS IN MM

EXCITING BLOCK MK 2B

(USED IN THEORETICAL STUDY ONLY)

FIG. 4.5

DYNAMIC SYSTEM AND ERROR MATRICES USED IN
THEORETICAL TEST WITH EXCITING BLOCK MK 2B



Natural frequencies:

- 50 Hz (x)
- 150 Hz (θ)
- 400 Hz (y)

- Mass = 18.12 Kg (40 lb)
 - $I_G = 0.0468 \text{ Kg-m}^2$
 - $k_{VA} = k_{VB} = 4.46 \times 10^5 \text{ N/m}$
 - $k_{HA} = k_{HB} = 2.85 \times 10^7 \text{ N/m}$
 - $h_{VA} = h_{VB} = 2.22 \times 10^4 \text{ N/m}$
 - $h_{HA} = h_{HB} = 1.43 \times 10^6 \text{ N/m}$
- } $\eta = 0.050$

ERRORS ADDED TO "MEASURED" INERTIANCE DATA PRIOR TO PROCESSING:

	Modulus	Phase
1	$\begin{bmatrix} +2\% & +2\% & -2\% \\ -2\% & +2\% & +2\% \\ +2\% & -2\% & -2\% \end{bmatrix}$	$\begin{bmatrix} -2^\circ & +2^\circ & -2^\circ \\ -2^\circ & -2^\circ & +2^\circ \\ +2^\circ & +2^\circ & -2^\circ \end{bmatrix}$
2	$\begin{bmatrix} +5\% & +5\% & -5\% \\ -5\% & +5\% & +5\% \\ +5\% & -5\% & -5\% \end{bmatrix}$	$\begin{bmatrix} -3^\circ & +3^\circ & -3^\circ \\ -3^\circ & -3^\circ & +3^\circ \\ +3^\circ & +3^\circ & -3^\circ \end{bmatrix}$

CHART
WELL

Graph Data Ref. 6525

Log 2 Cycles x 10th inch (Multipurpose)

**EFFECT OF SYSTEMATIC INPUT DATA ERRORS ON THE
COMPUTED MOBILITY $\frac{X}{F_A}$ FOR EXCITING BLOCK MK 2 B**

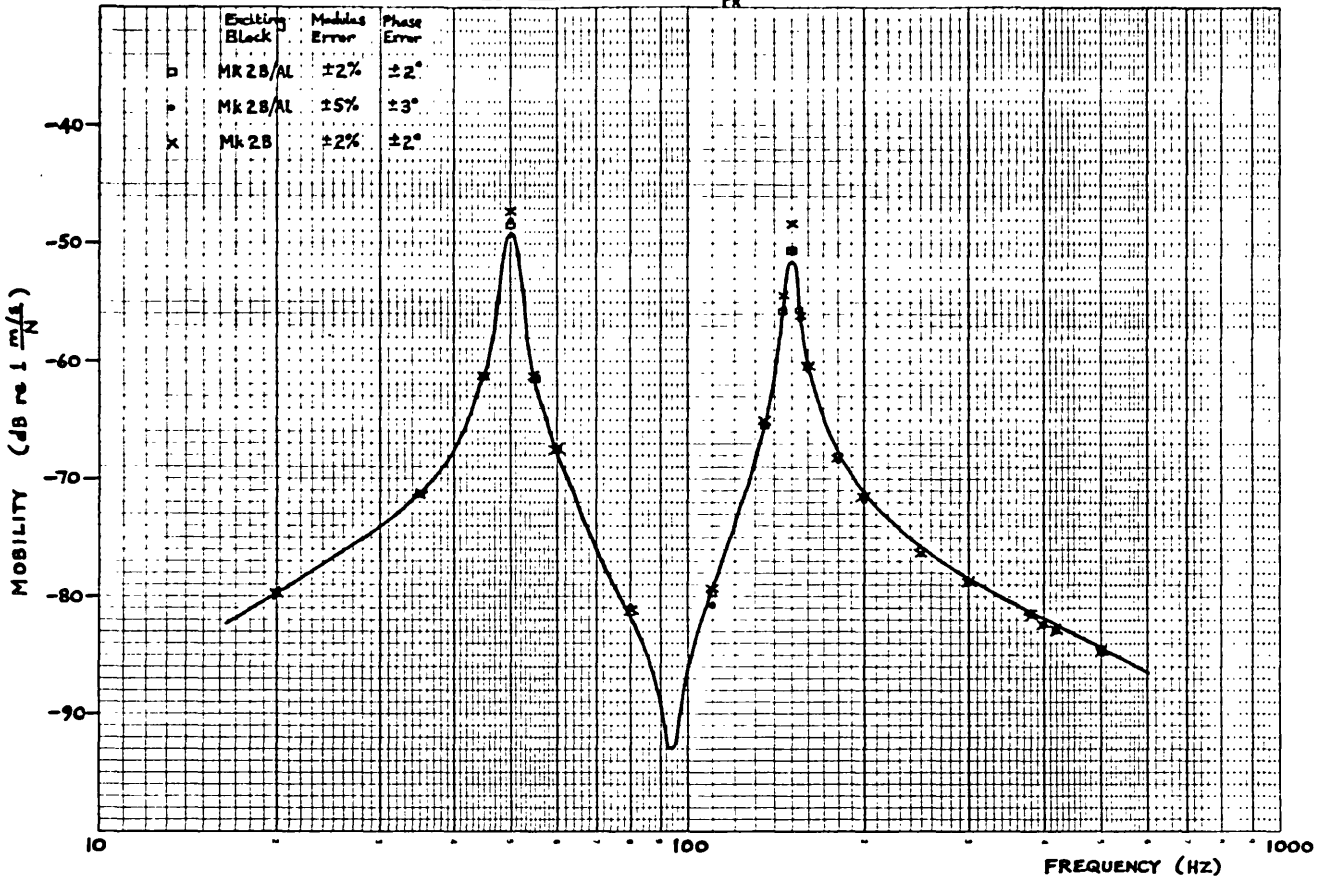


CHART
WELL

Graph Data Ref. 6525

Log 2 Cycles x 10th inch (Multipurpose)

**EFFECT OF SYSTEMATIC INPUT DATA ERRORS ON THE
COMPUTED MOBILITY $\frac{Y}{F_A}$ FOR EXCITING BLOCK MK 2 B**

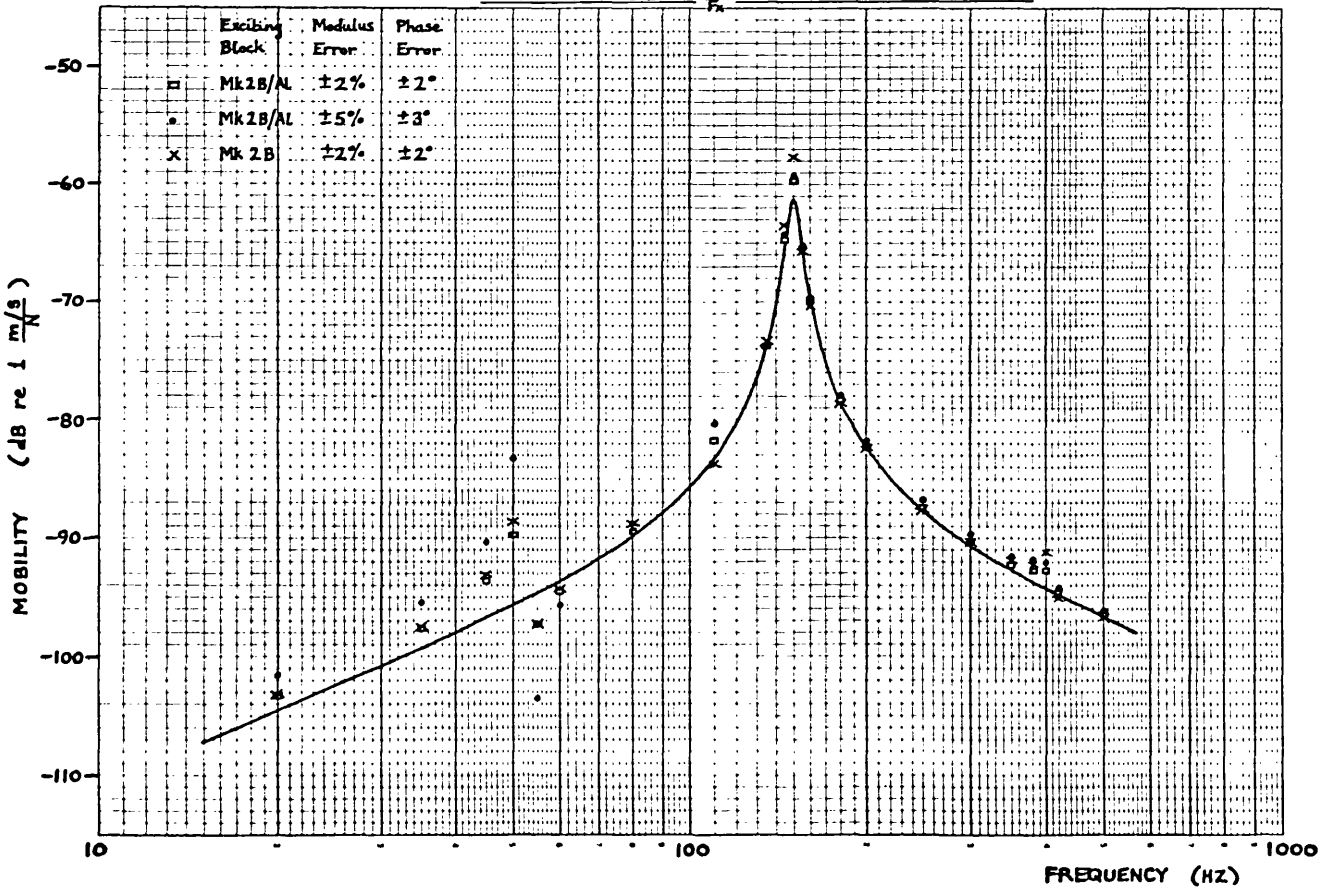


FIG 4.7

CHART WELL Graph Data Ref. 6525 Log 2 Cycles x 10th inch (Multipurpose)

EFFECT OF SYSTEMATIC INPUT DATA ERRORS ON THE COMPUTED MOBILITY $\frac{S}{F_1}$ FOR EXCITING BLOCK MK 2 B

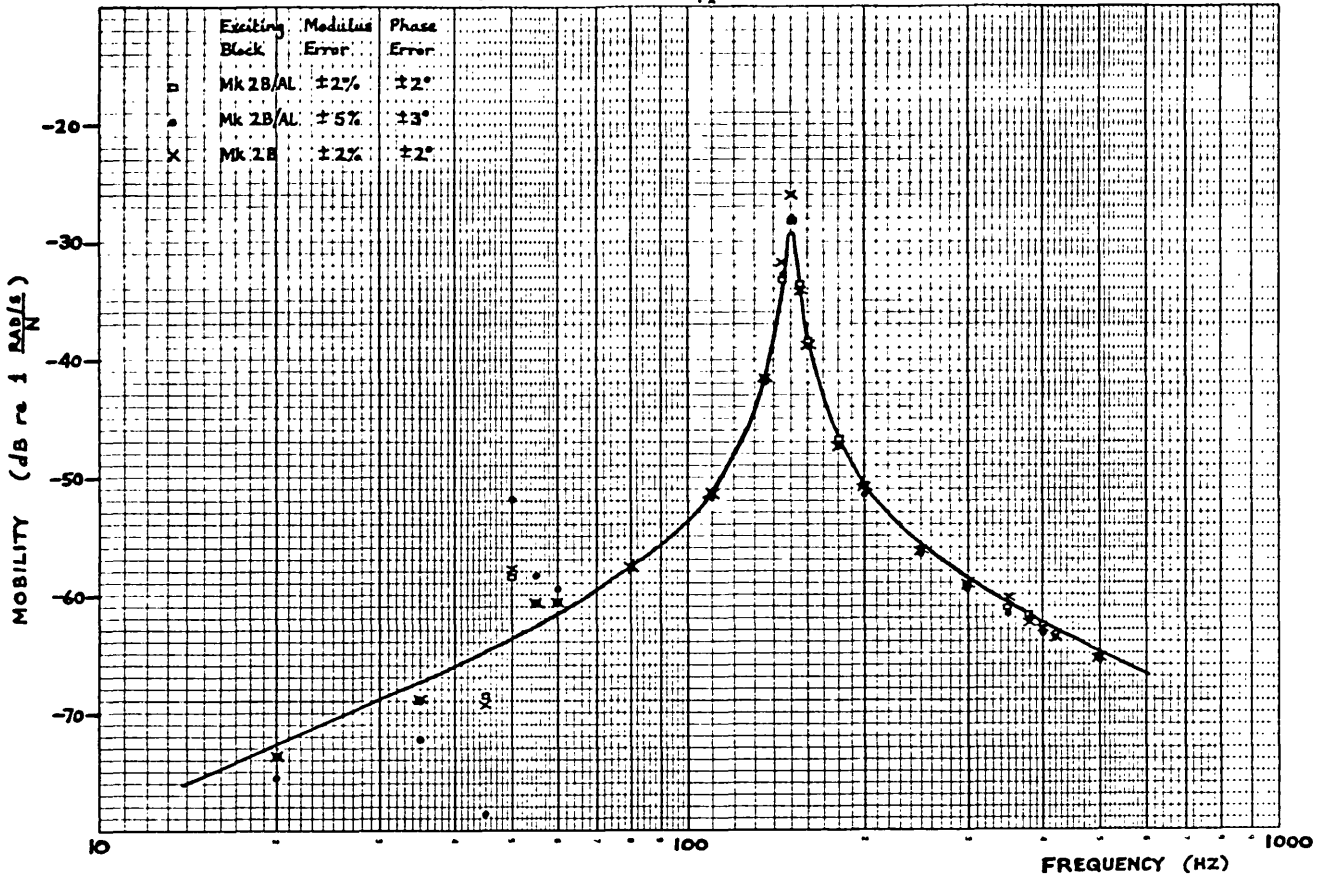


CHART WELL Graph Data Ref. 6525 Log 2 Cycles x 10th inch (Multipurpose)

EFFECT OF SYSTEMATIC INPUT DATA ERRORS ON THE COMPUTED MOBILITY $\frac{S}{F_2}$ FOR EXCITING BLOCK MK 2 B

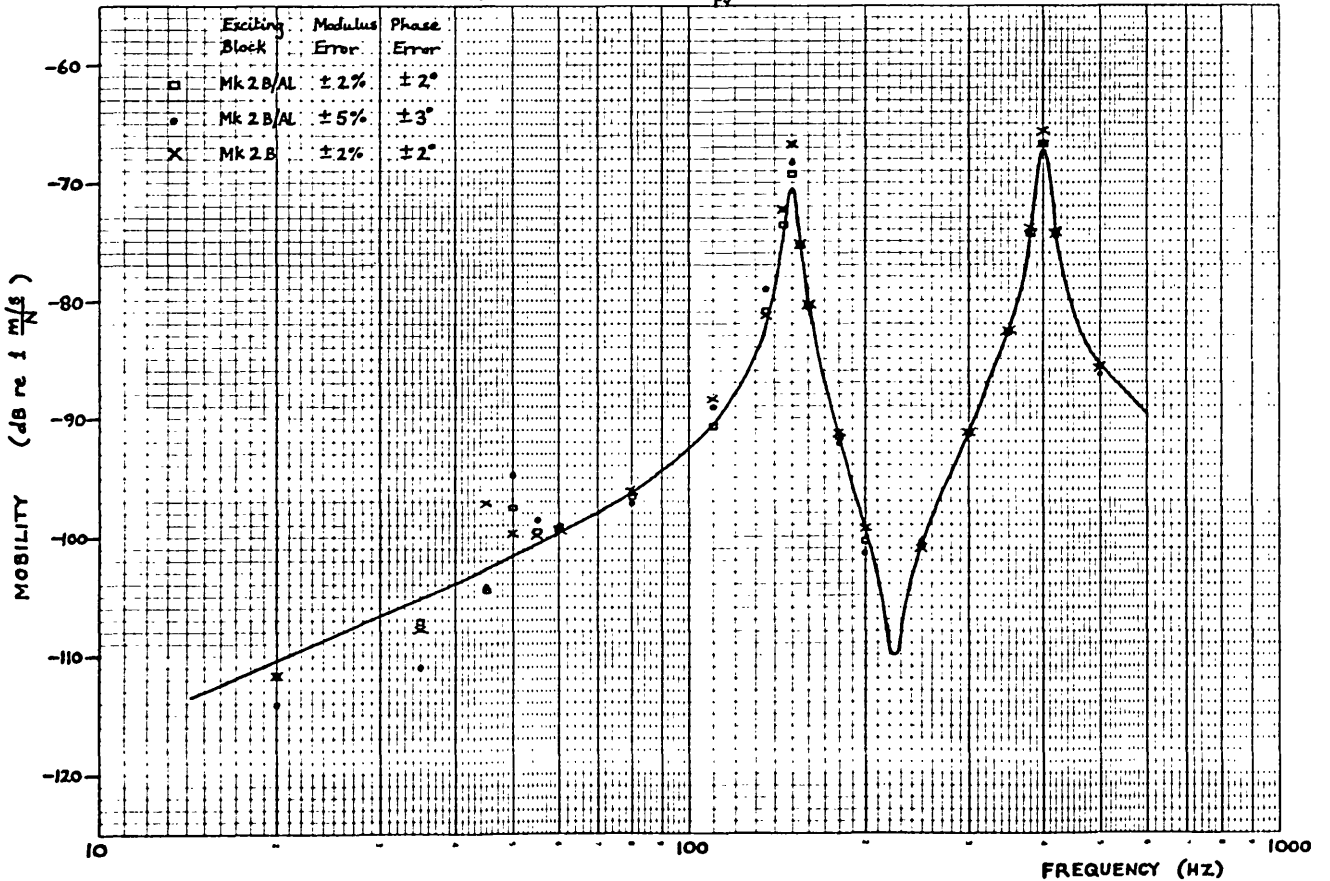


FIG 4.8

CHART WELL Graph Data Ref. 6525 Log 2 Cycles x 10th inch (Multipurpose)

EFFECT OF SYSTEMATIC INPUT DATA ERRORS ON THE COMPUTED MOBILITY $\frac{g}{s}$ FOR EXCITING BLOCK MK 2B

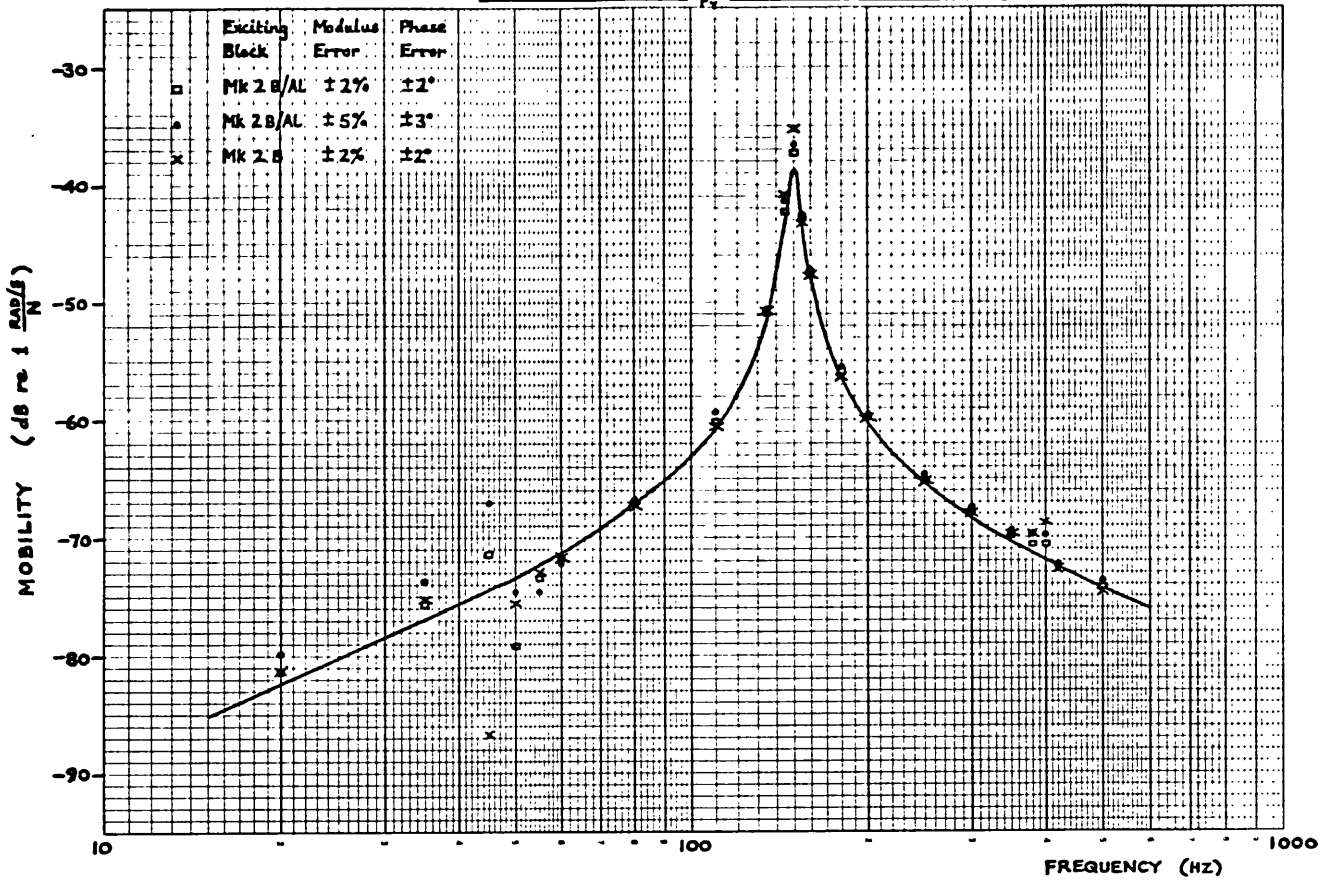
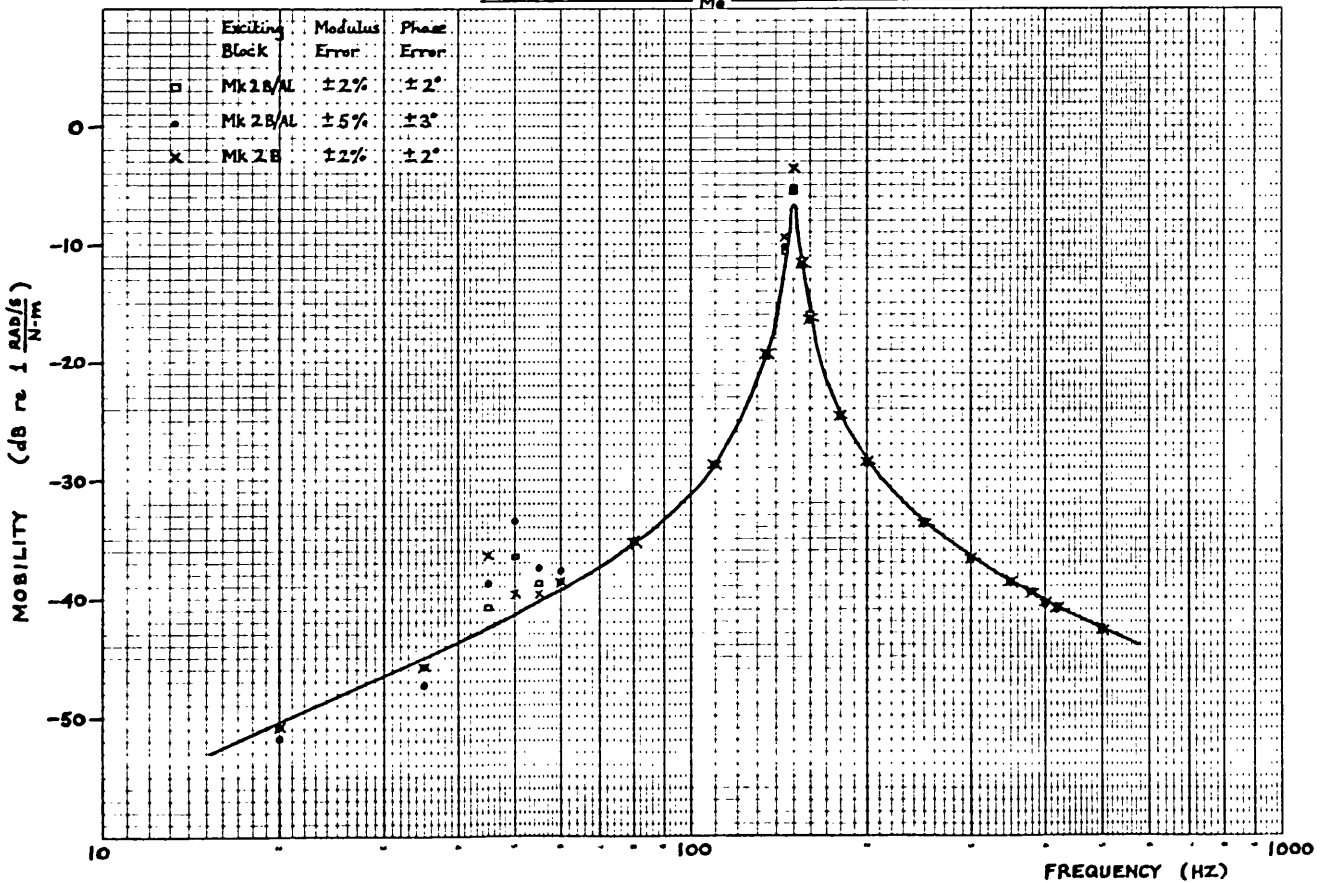


CHART WELL Graph Data Ref. 6525 Log 2 Cycles x 10th inch (Multipurpose)

EFFECT OF SYSTEMATIC INPUT DATA ERRORS ON THE COMPUTED MOBILITY $\frac{g}{N \cdot m}$ FOR EXCITING BLOCK MK 2B



Tests with Mk 2 Block

As the simulation yielded quite reasonable results, it was decided to manufacture the Mk 2 exciting block shown in Fig. 4.9. Measurements were then made on the steel beam and on the spring-supported mass shown in Fig. 4.10, the block being attached in both cases by means of two $\frac{3}{8}$ UNC Allen screws.

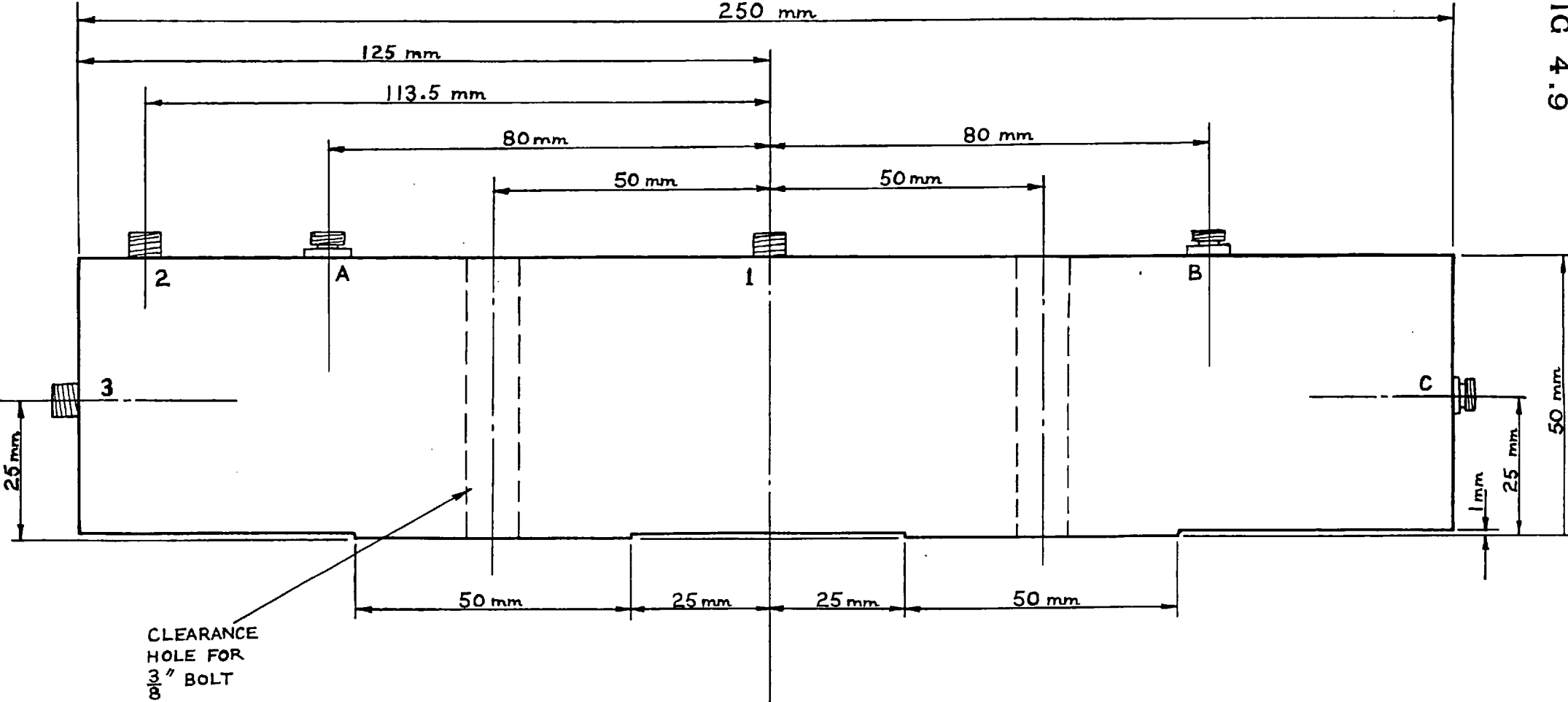
The uniform steel beam was suspended on ropes at the nodes of the first free-free mode. The first test was performed in the vertical plane, with the exciting block mounted on top of the beam, near one end. However, a further test was subsequently carried out with the beam on its side, in order to ascertain whether the stiffness of the ropes was affecting the results. Measurements were made of the three-directional point mobility near one end and of the transfer to the transverse co-ordinate ξ at the other end. The measured data were processed using the standard equation (4.7), modified to include the transfer co-ordinate, and the resulting mobility moduli are presented in Figs. 4.11 to 4.18. The results have been fully corrected for the effects of exciting block and accelerometer inertia. The theoretical curves were obtained using the closed-form beam receptances listed by Bishop and Johnson⁽¹⁴⁾. The analysis was performed by considering the beam in three sections, whose tip receptance properties could be calculated using standard expressions. The sections were then coupled together to yield the response properties at points 1 and 2 (76 mm from each tip)*.

In the case of the heavy mass on the rubber pads, measurements were made of the three-directional mobility at point P, 50 mm off the centre of the top face. These results are presented in Figs. 4.19 to 4.23. The theoretical response was obtained using a known value of mass, together with a calculated value of moment of inertia and tabulated stiffness data for the rubber pads⁽²⁰⁾.

* Instead of using receptances, one may work directly with the "exact" dynamic stiffnesses; or alternatively one may use finite elements. These two approaches are compared in reference (19). If using the computer program COUPLE1 described in Chapter 2 (Part 1), the dynamic stiffness matrices for the three sections of beam may be set up using one of the standard modules: either ZFLAX1 for a Bernoulli-Euler beam, or ZFLAX2 for a Timoshenko beam.

BLOCK THICKNESS = 51 mm

FIG 4.9



STUDS

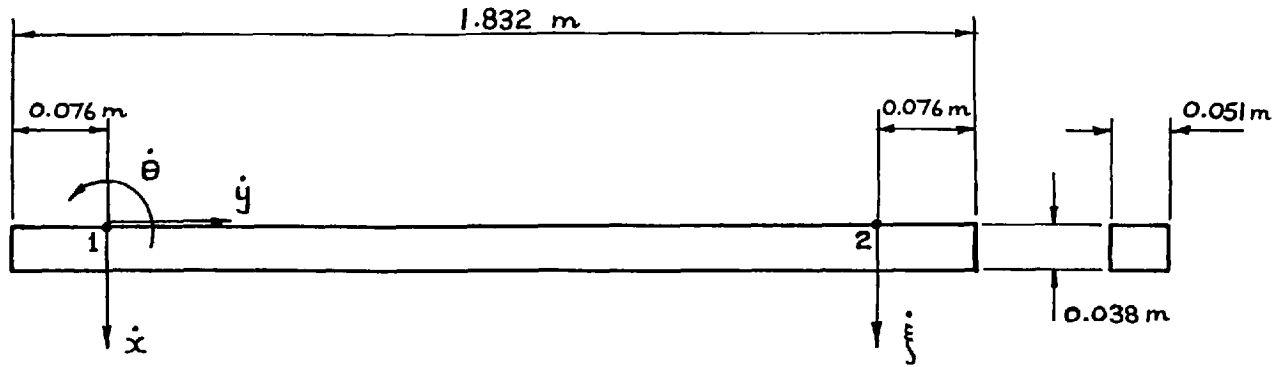
- A, B, C $\frac{1}{4}$ UNF INSULATING FOR BIRCHALL A/OI ACCELEROMETER
- 1, 2, 3 $\frac{1}{4}$ UNF FOR ENDEVCO FORCE GAUGE TYPE 2103-100

MATERIAL: ALUMINIUM ALLOY

EXCITING BLOCK MK 2

FULL SCALE

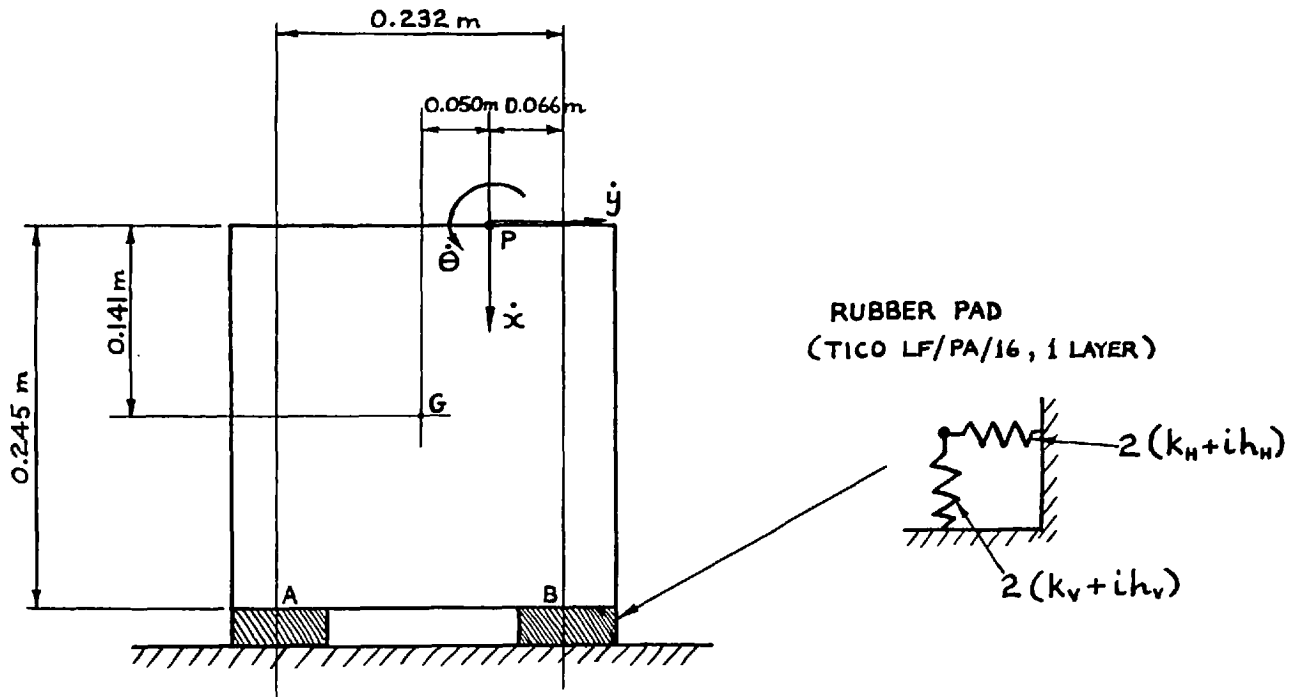
FIG 4.10



UNIFORM STEEL BEAM

DENSITY, $\rho = 7740 \text{ Kg/m}^3$

MODULUS OF ELASTICITY, $E = 20.6 \times 10^{10} \text{ N/m}^2$



STEEL BLOCK ON RUBBER PADS

MASS OF BLOCK, $m = 135 \text{ Kg}$

MOMENT OF INERTIA, $I_G = 1.70 \text{ Kg m}^2$

$k_{VA} = k_{VB} = 460\,000 \text{ N/m}$

$k_{HA} = k_{HB} = 200\,000 \text{ N/m}$

$h_{VA} = h_{VB} = 64\,000 \text{ N/m}$

$h_{HA} = h_{HB} = 28\,000 \text{ N/m}$

FIG 4.11

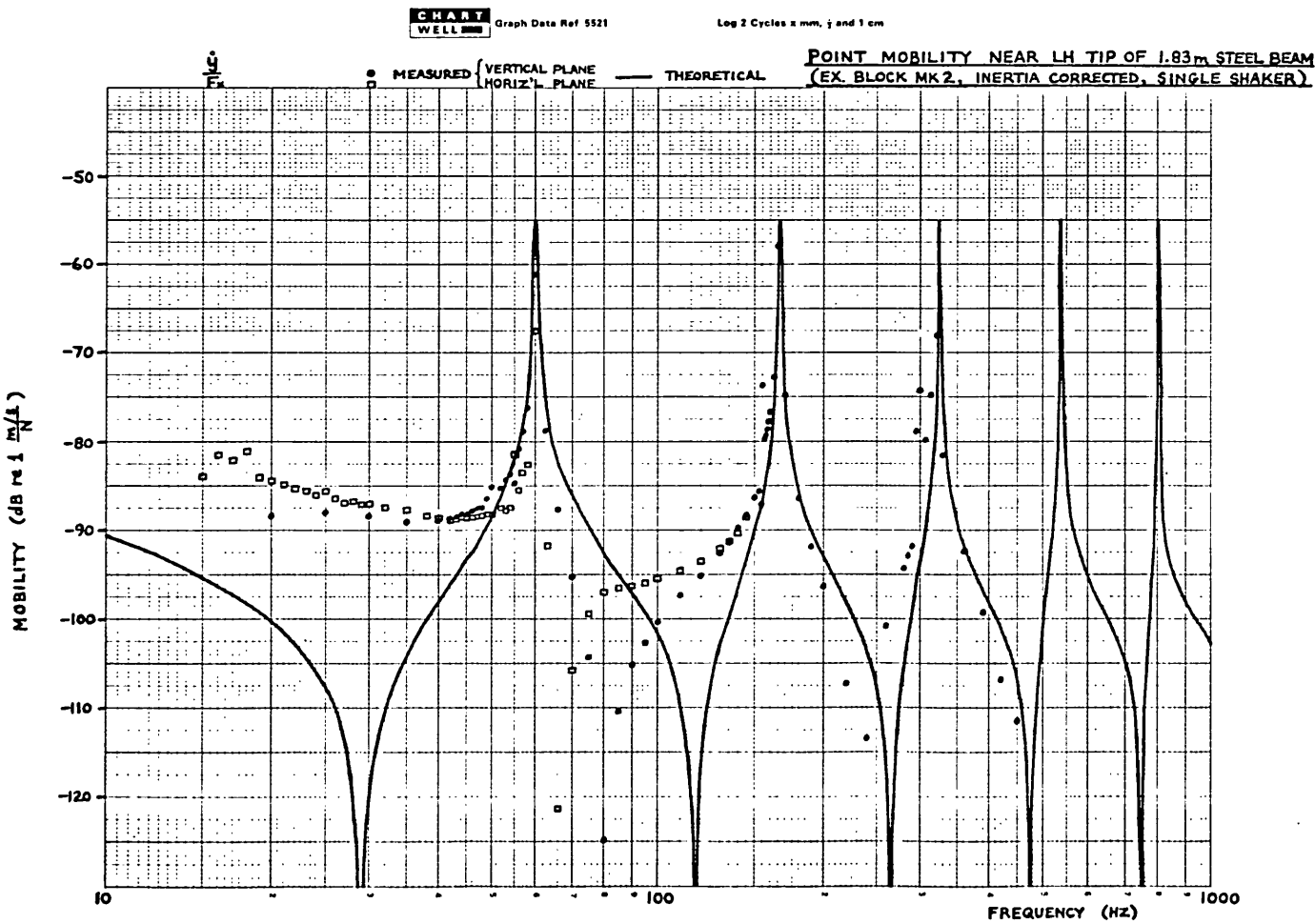
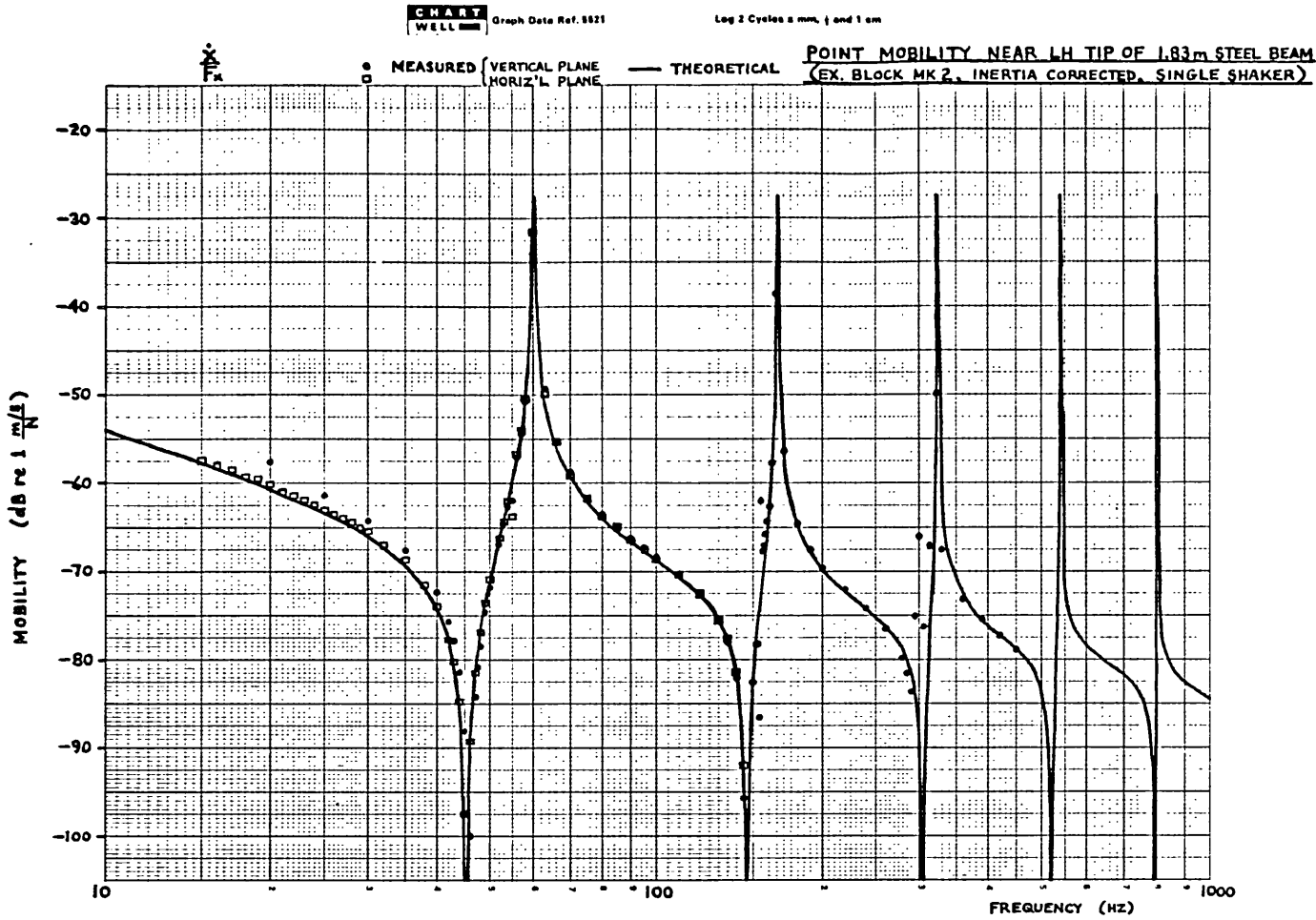


FIG 4.12

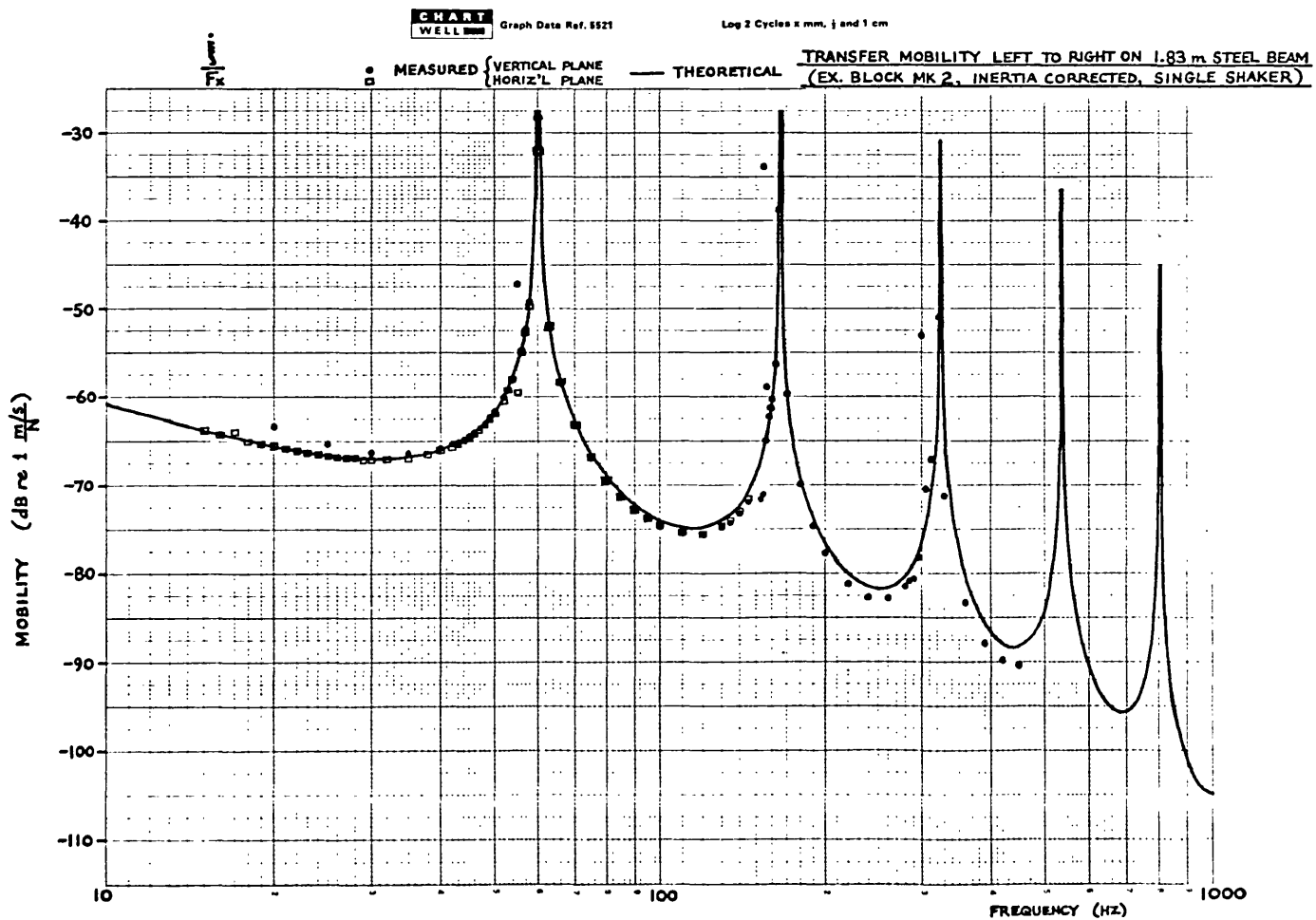
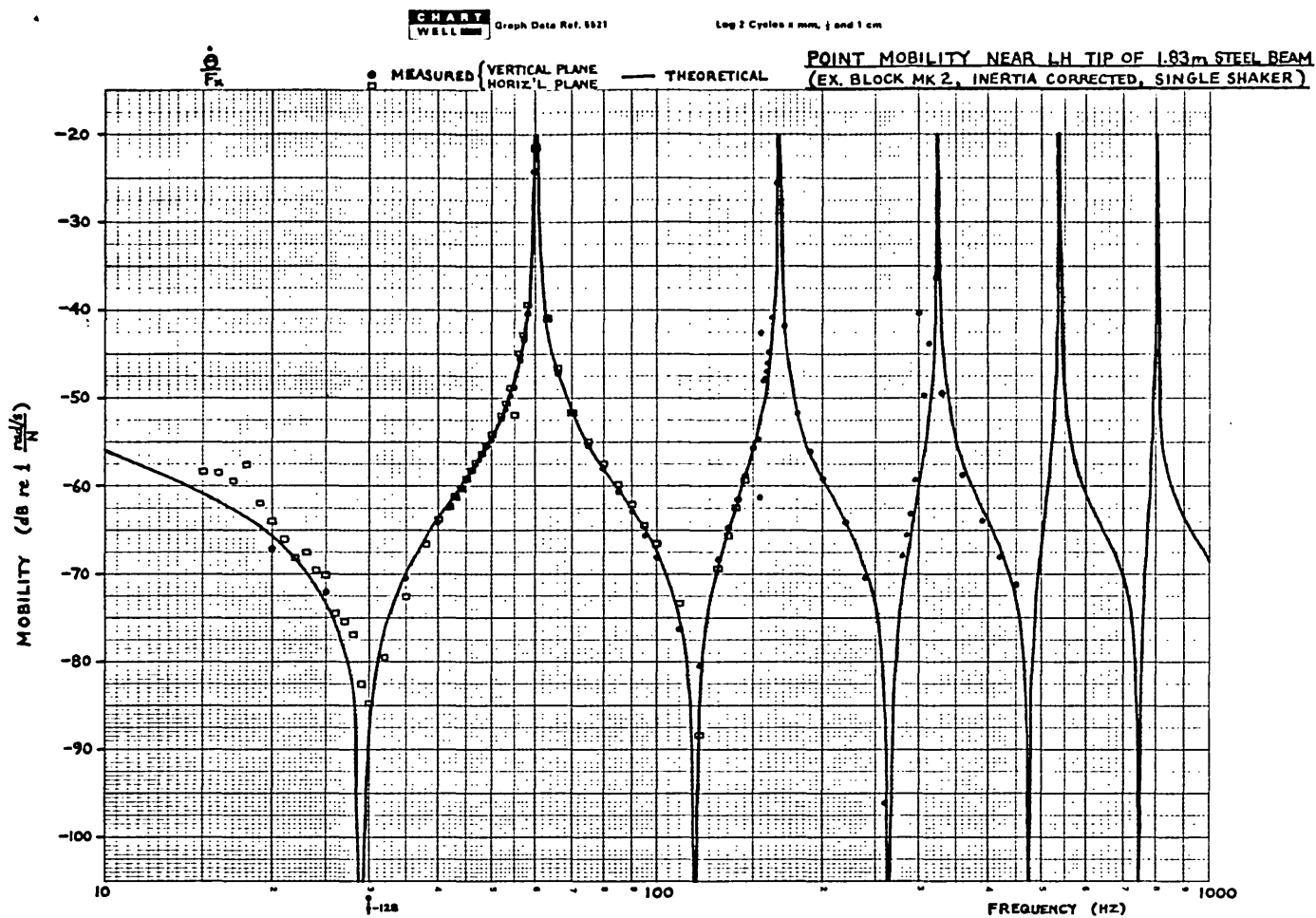


FIG 4.13

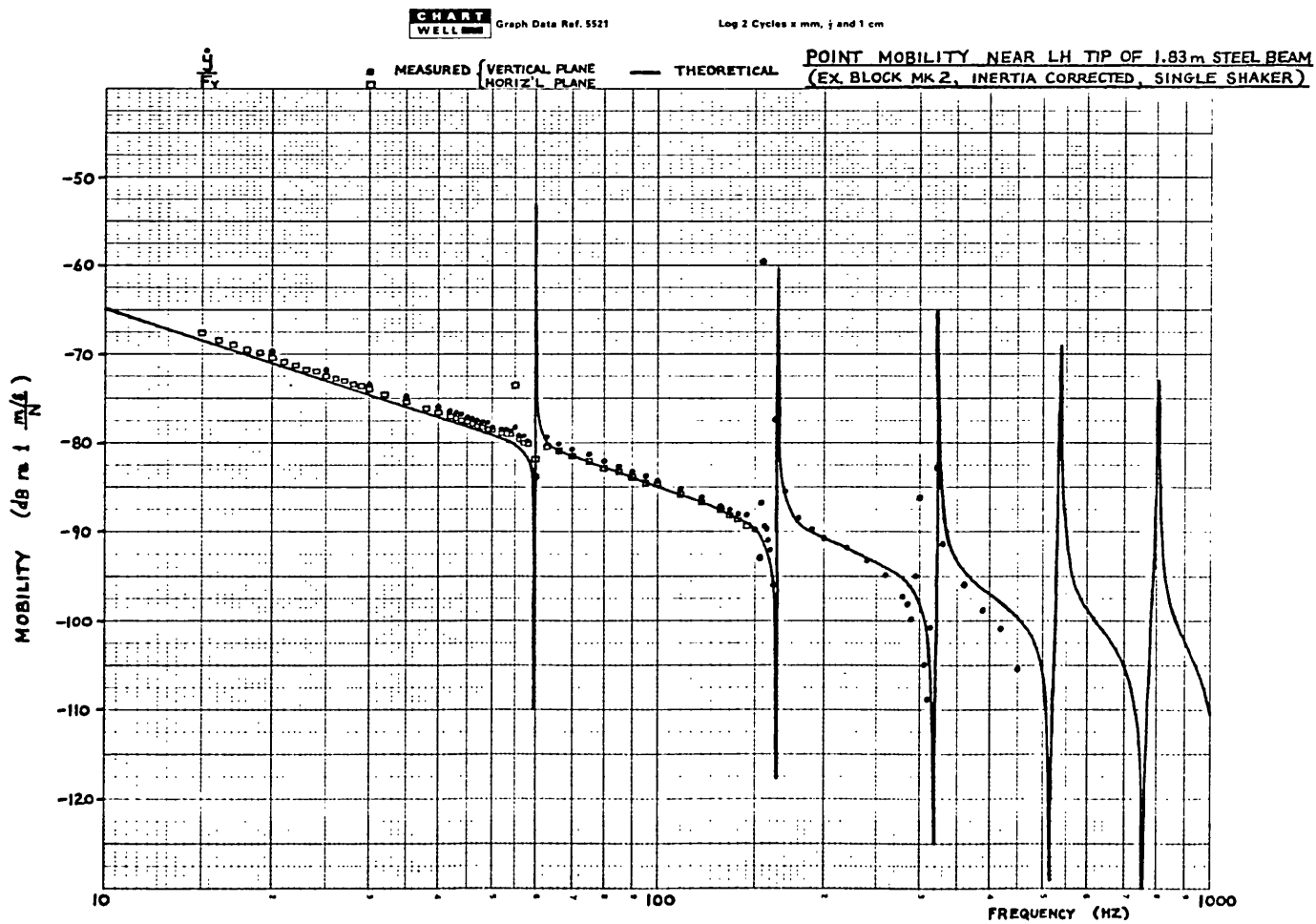
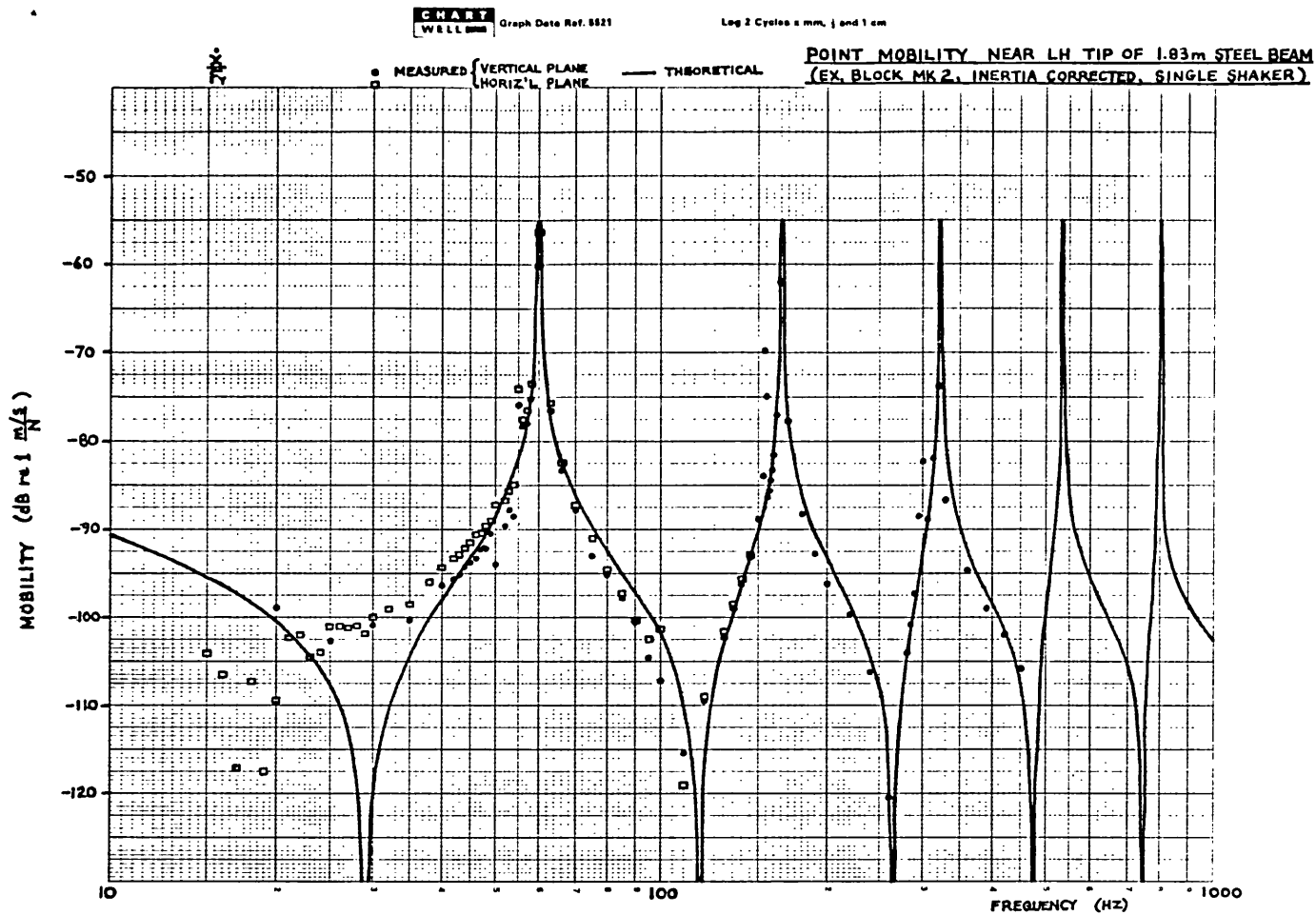


FIG 4.14

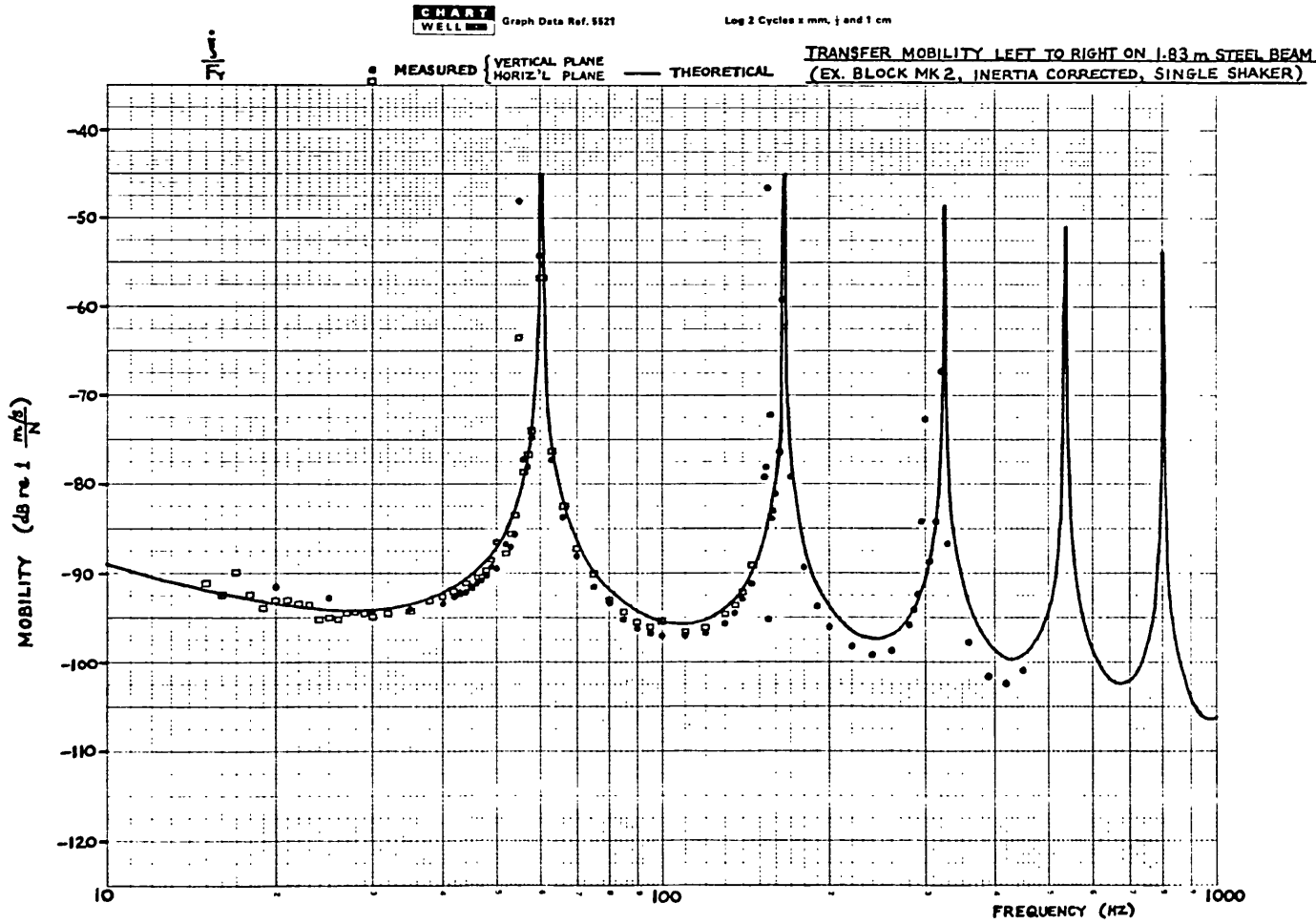
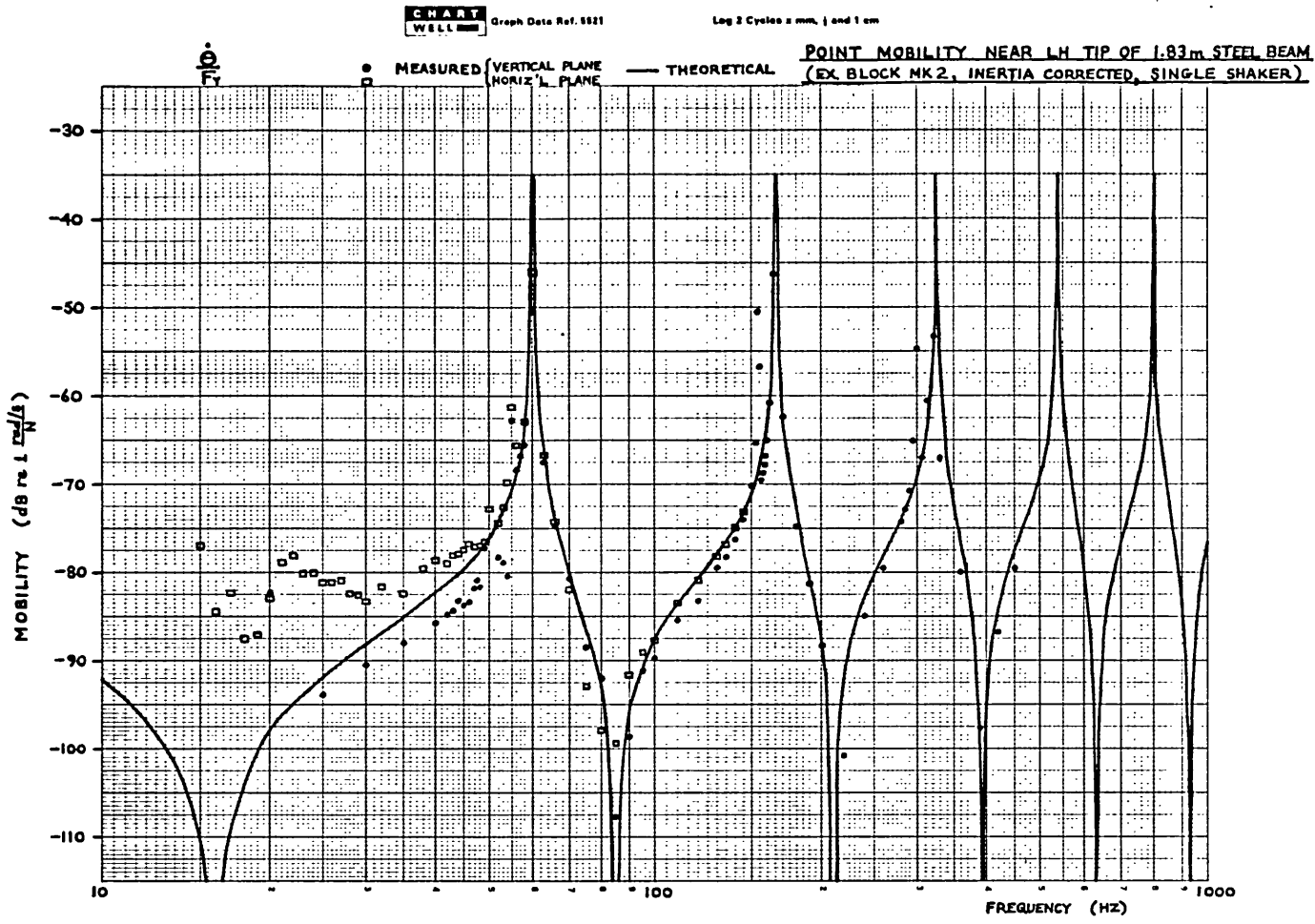


FIG 4.15

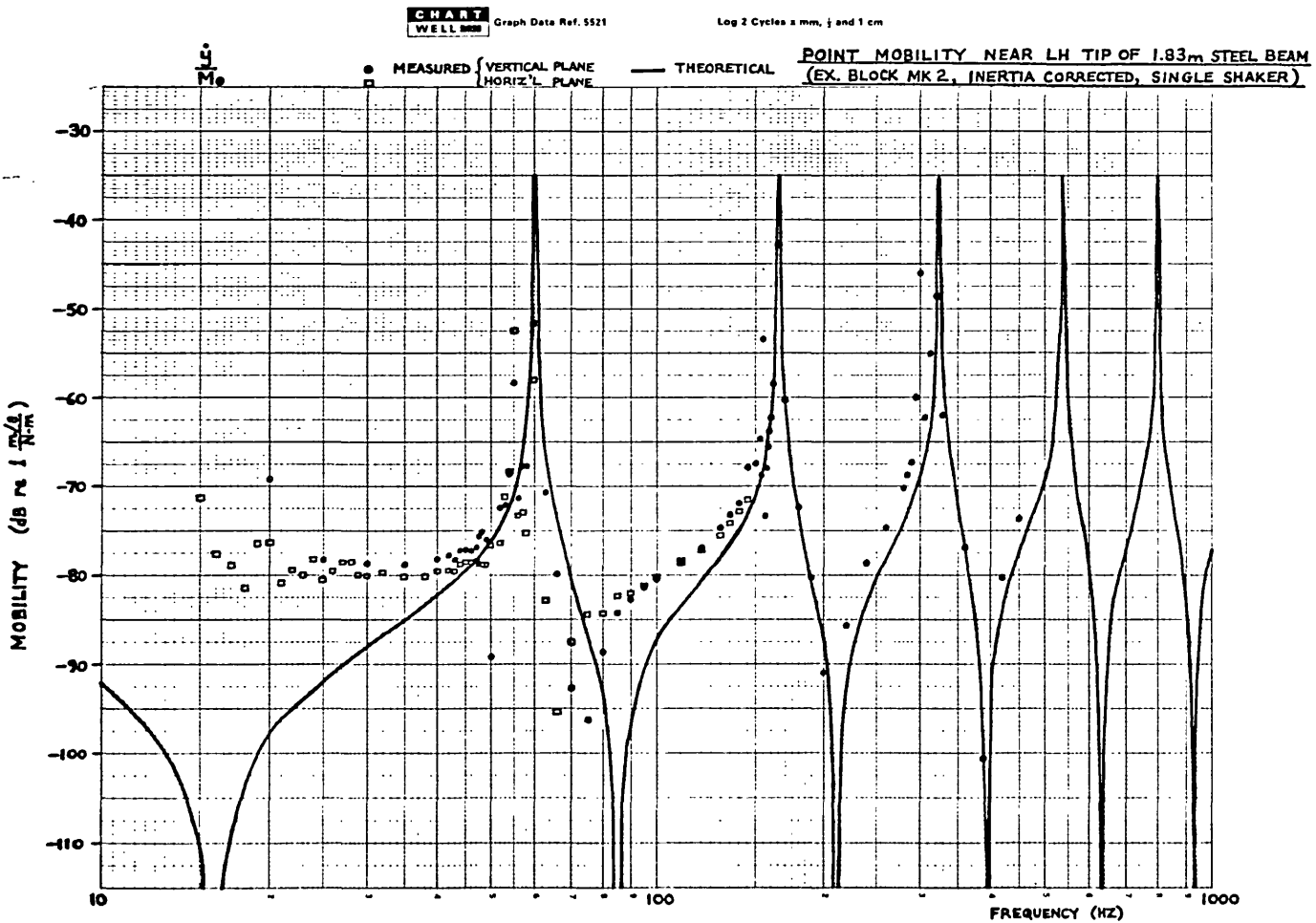
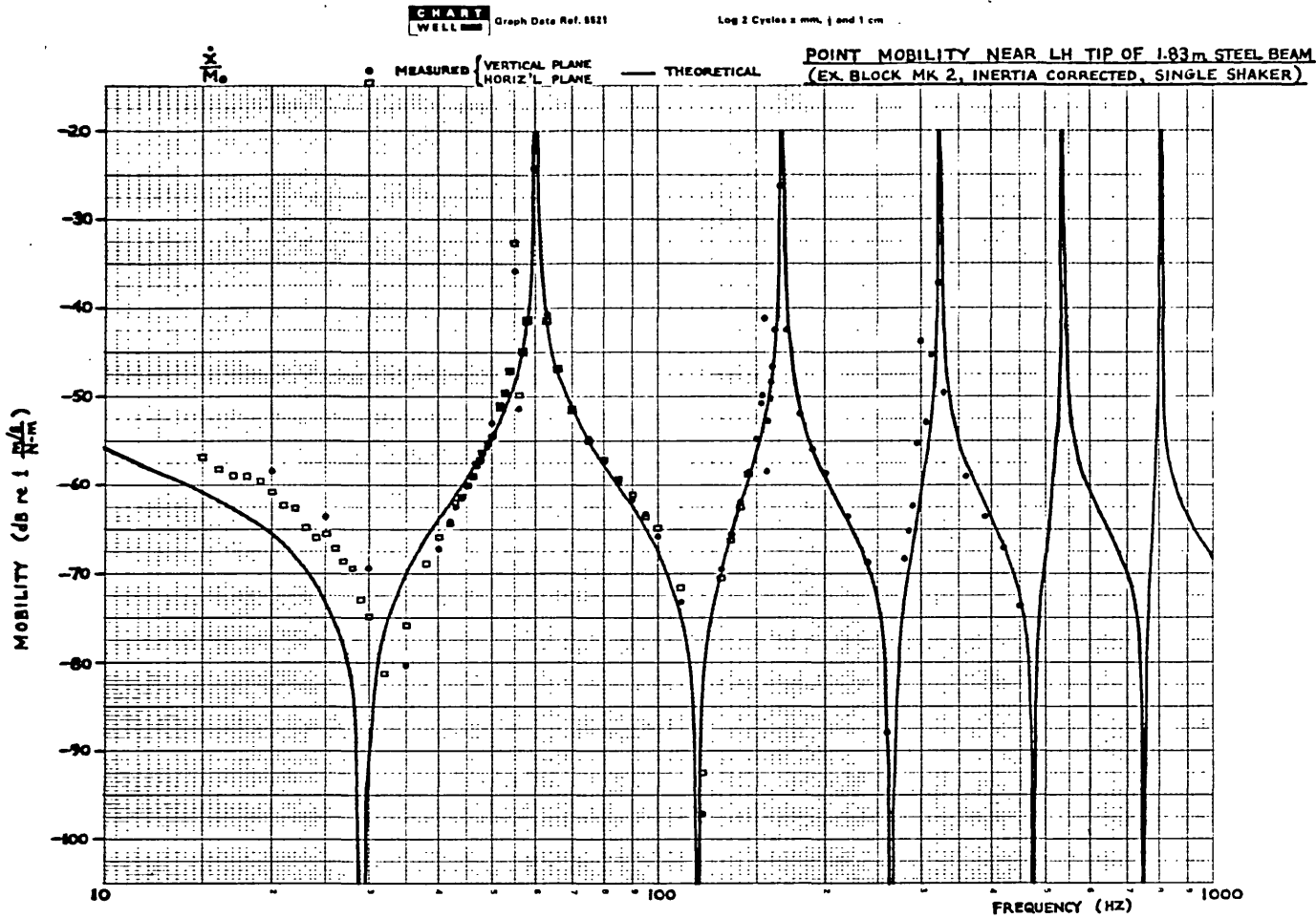


FIG 4.16

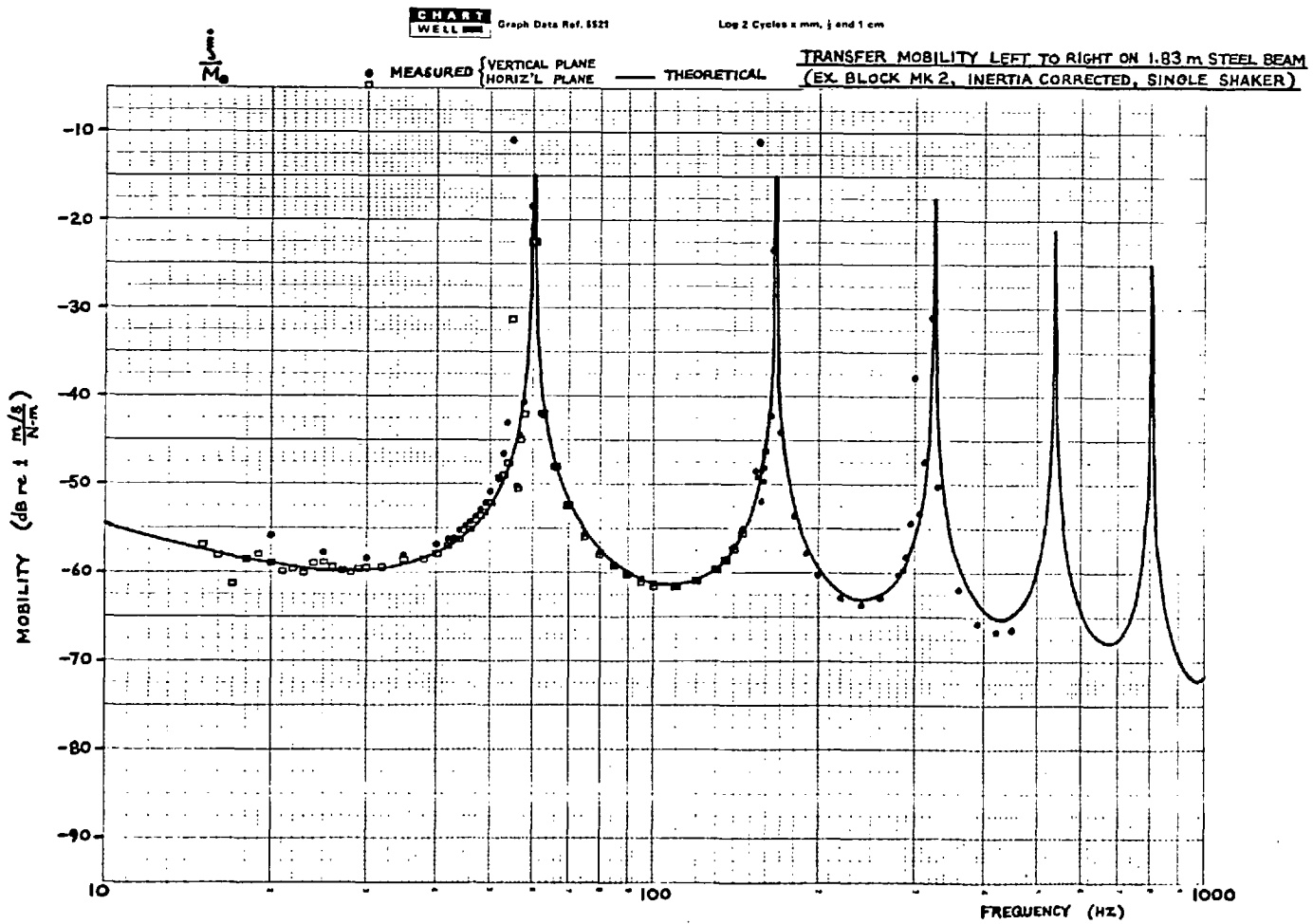
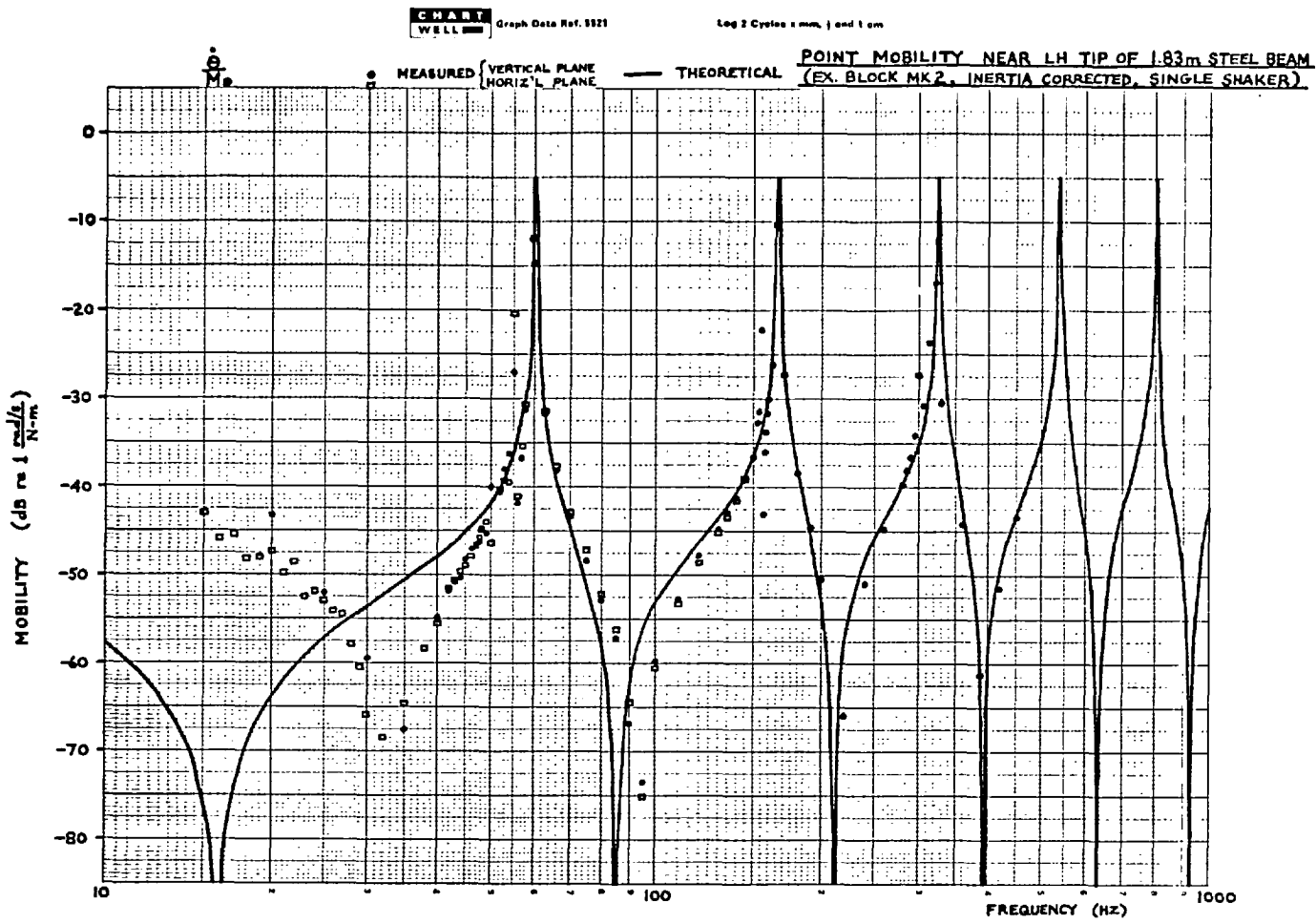


FIG 4.17

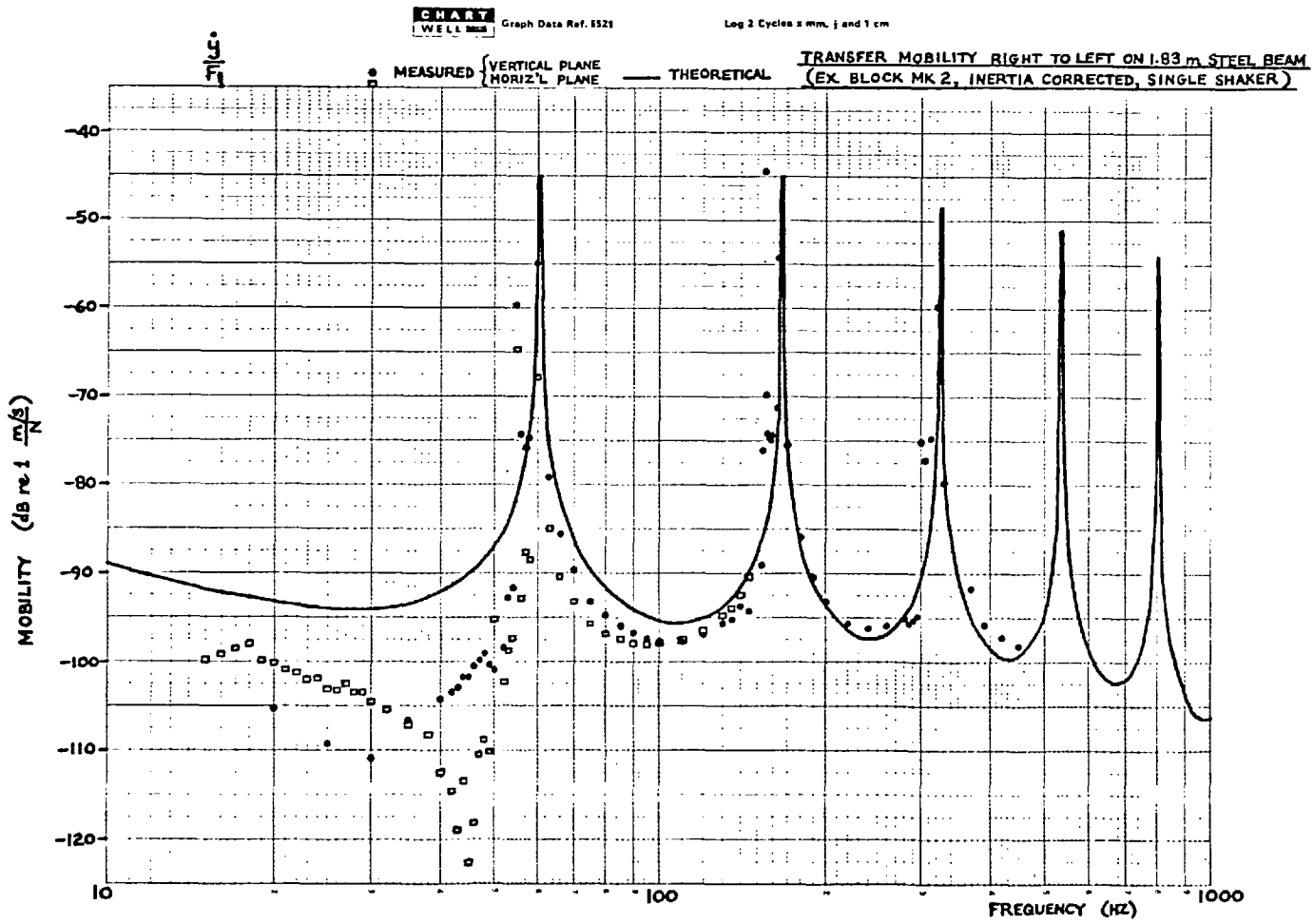
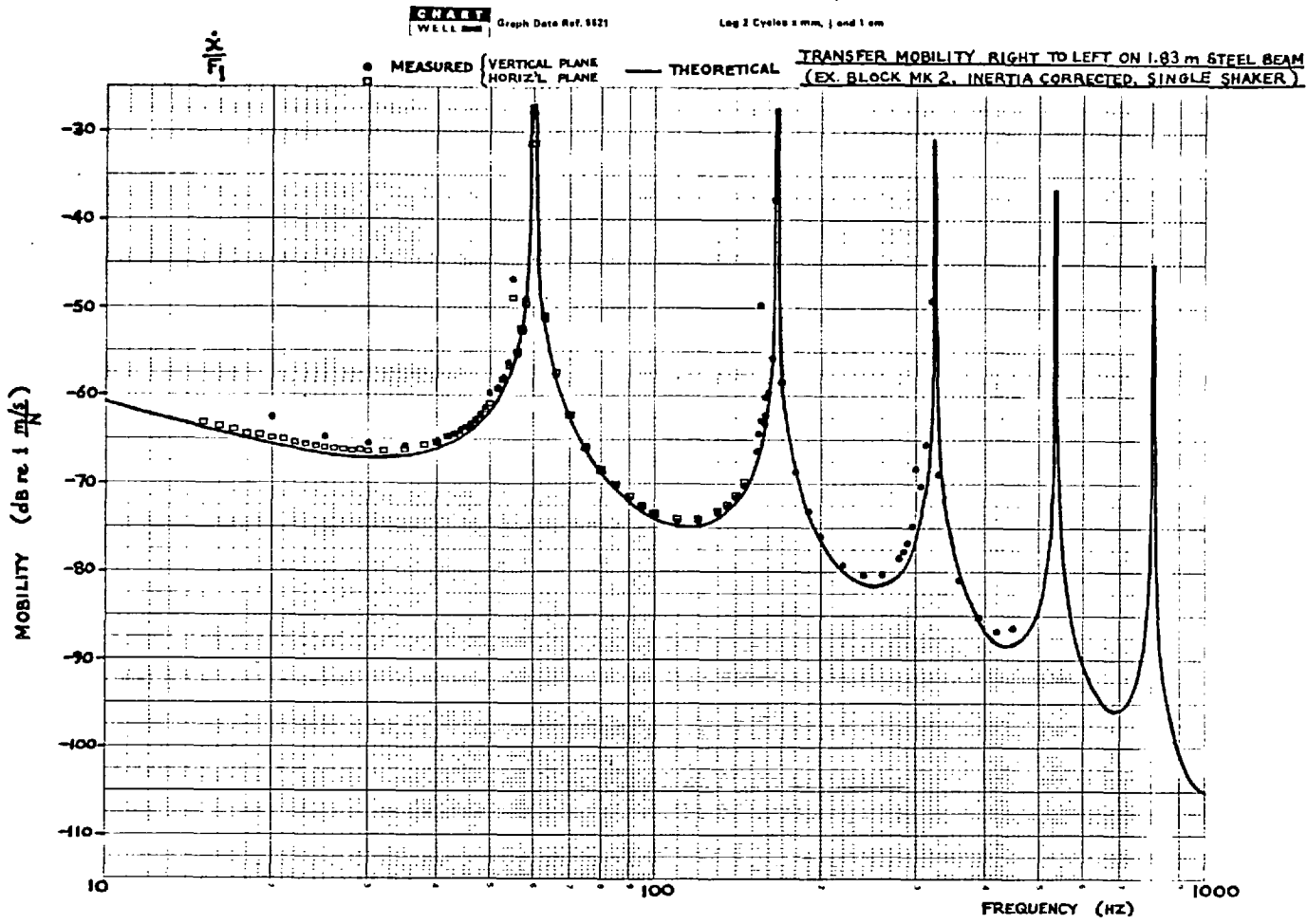
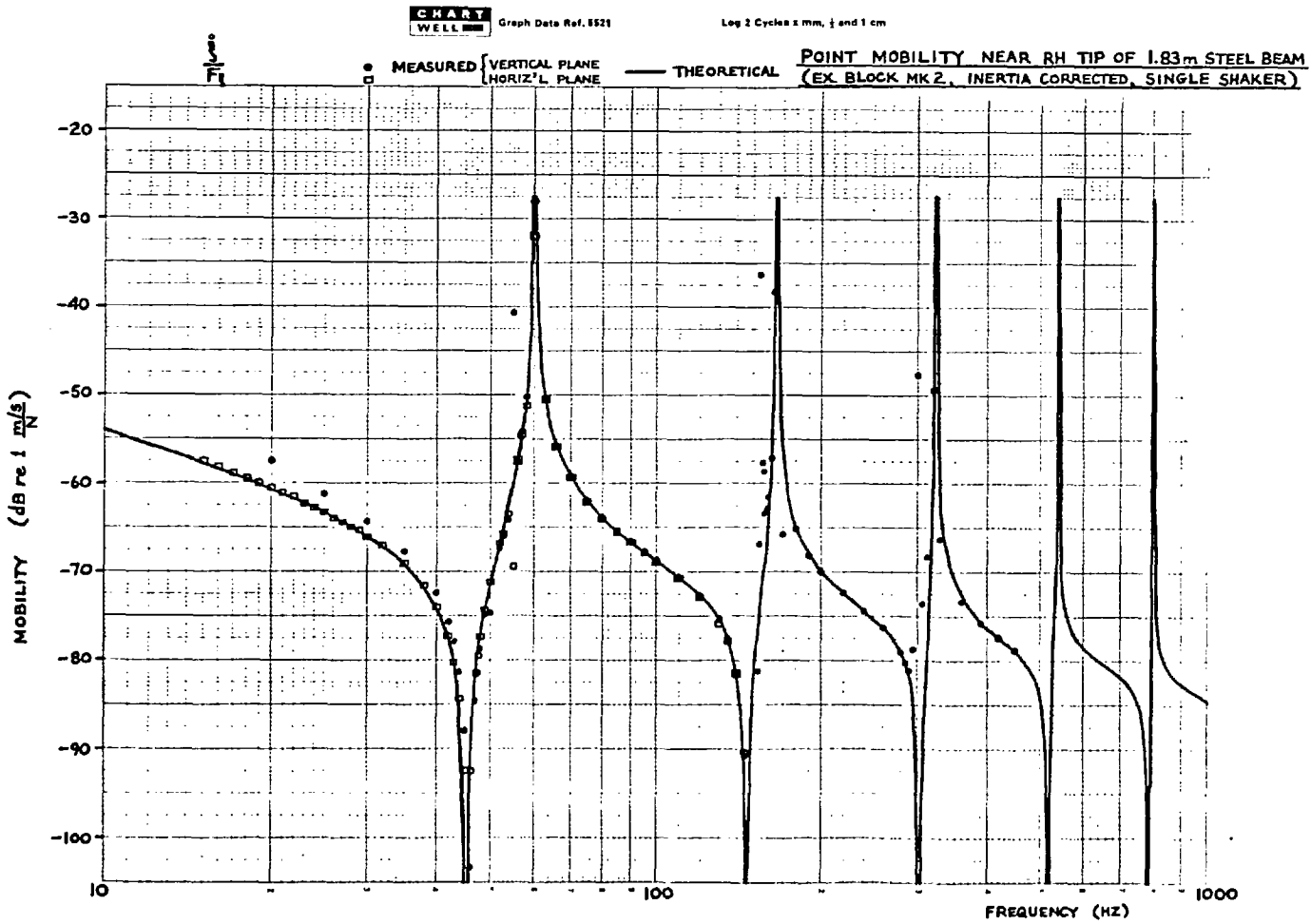
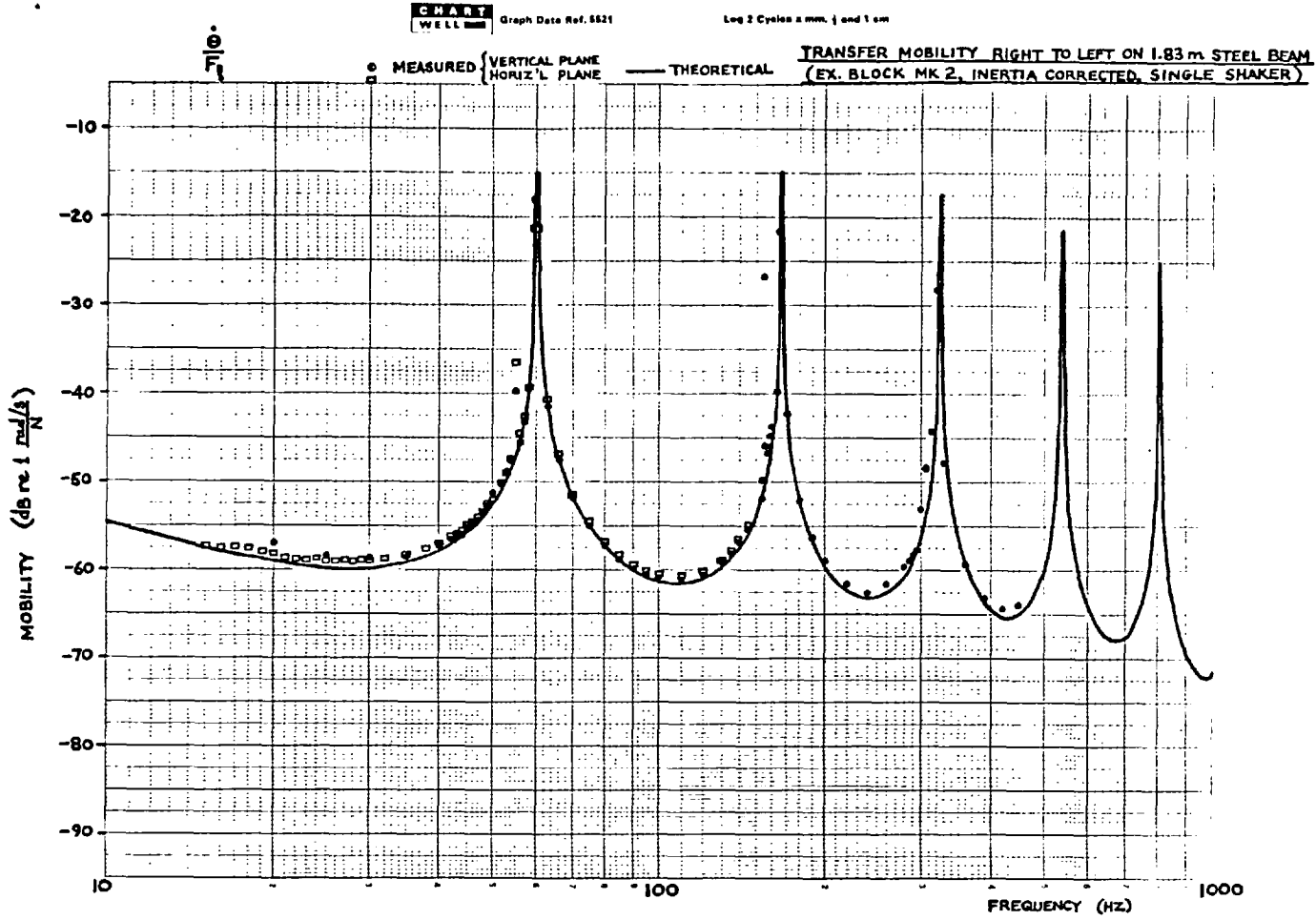
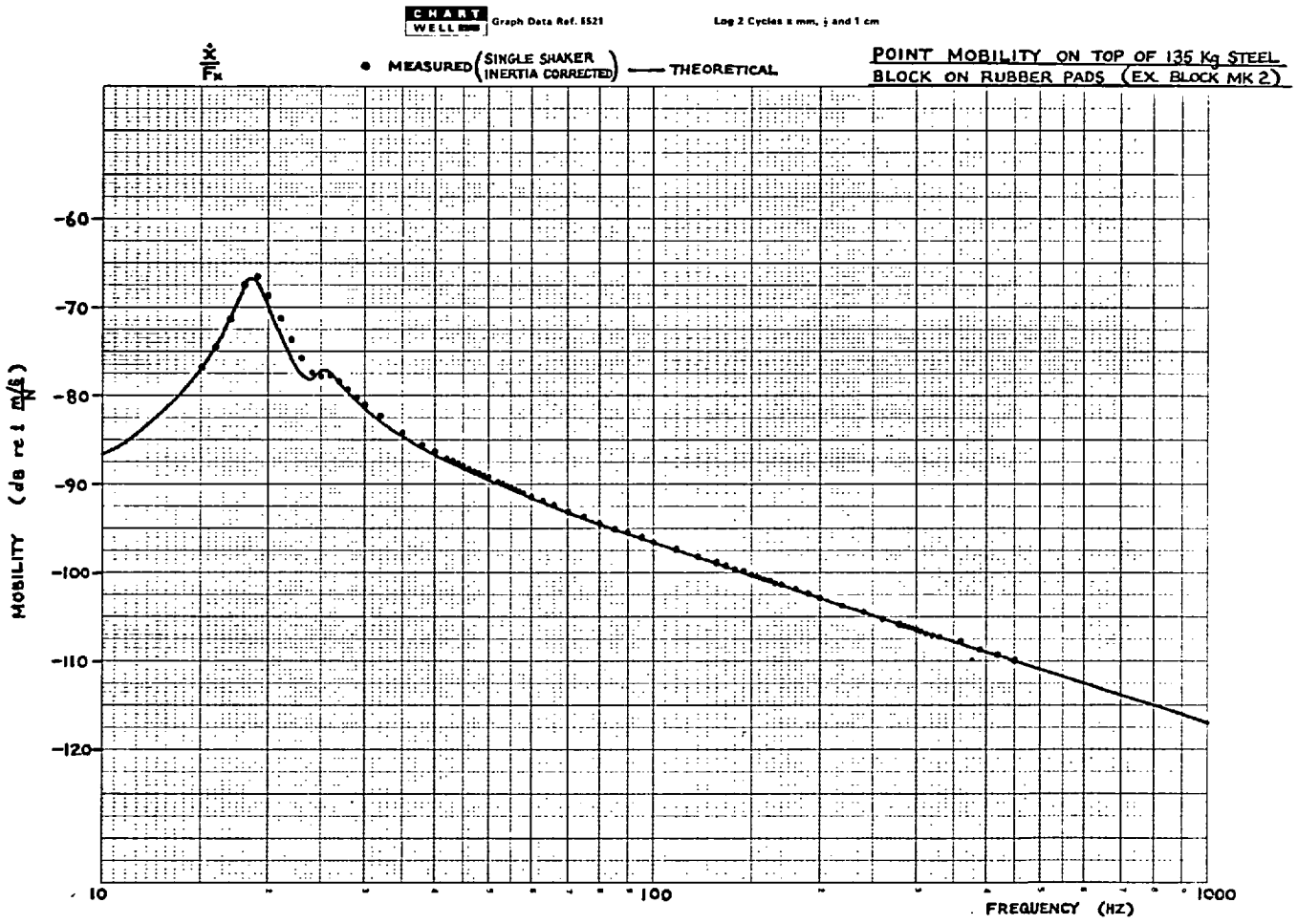


FIG 4.18





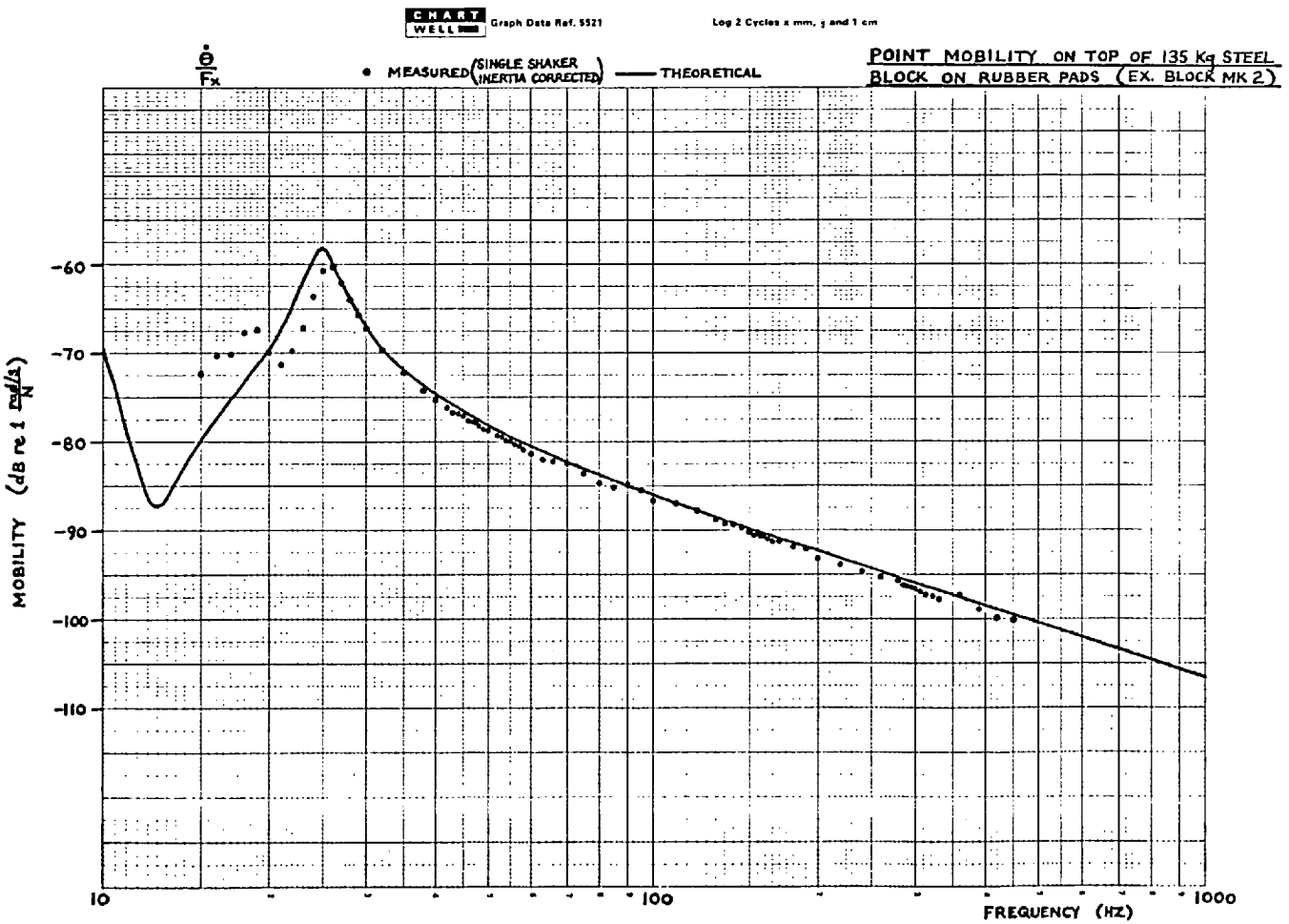
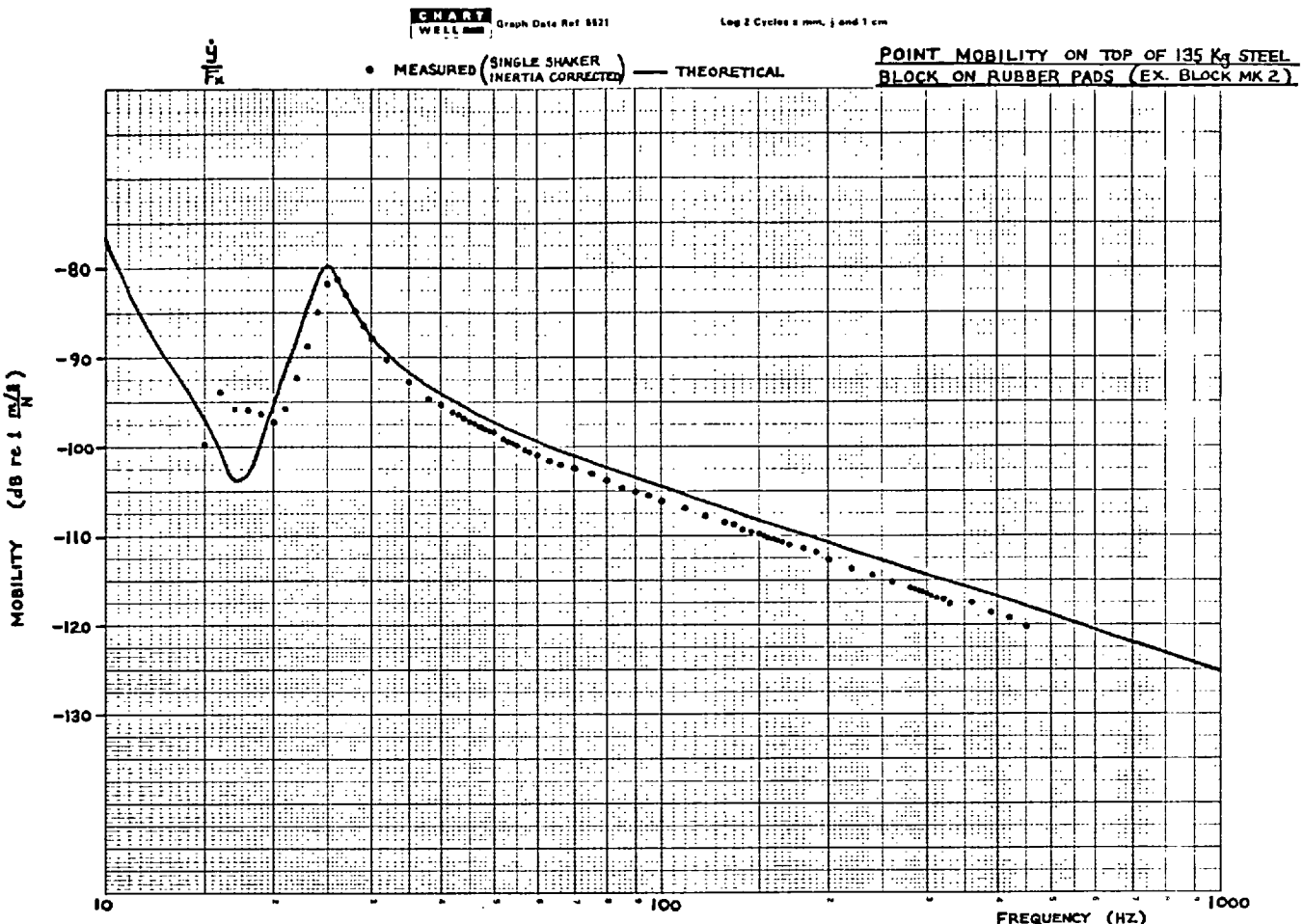


FIG 4.21

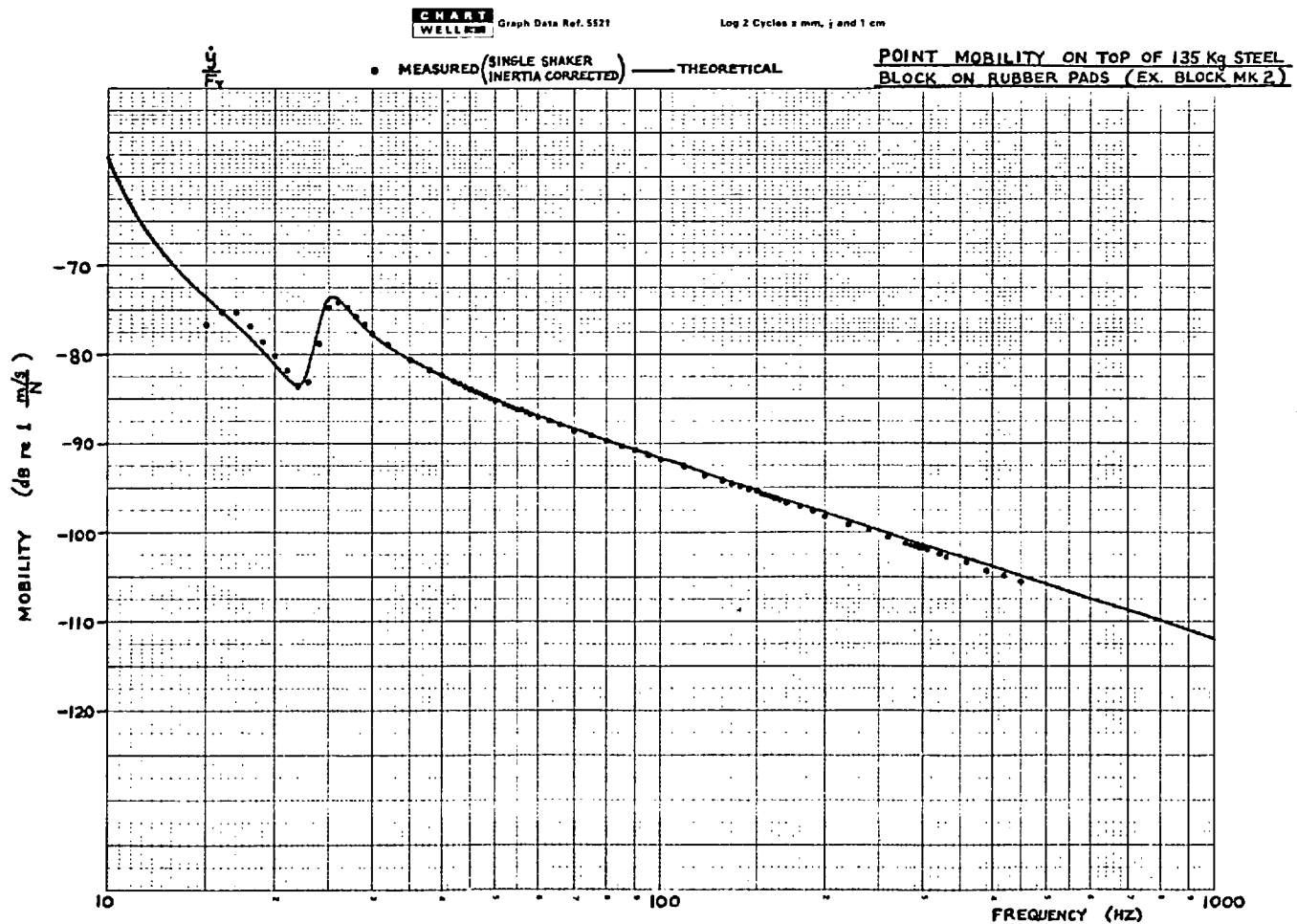
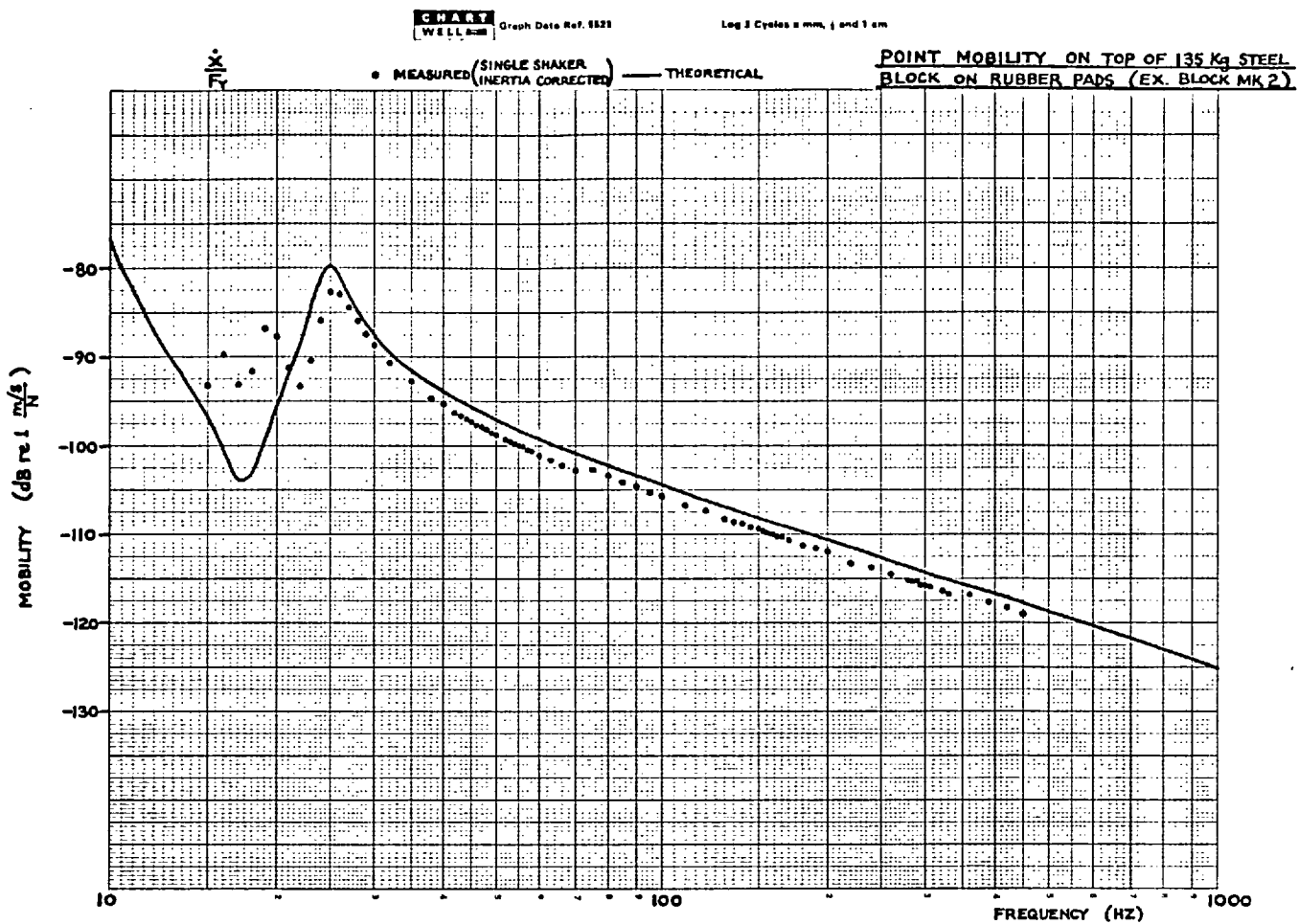
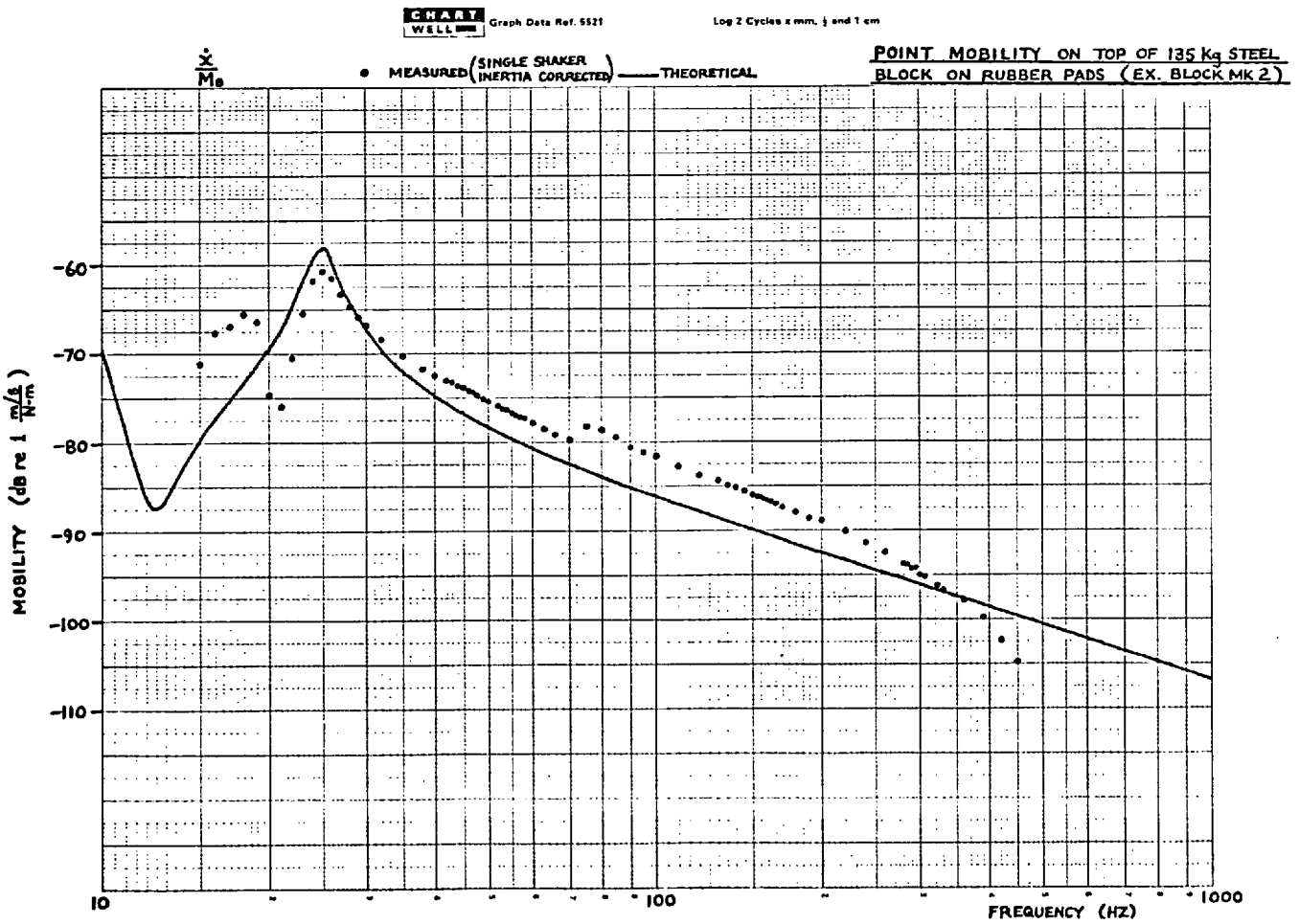
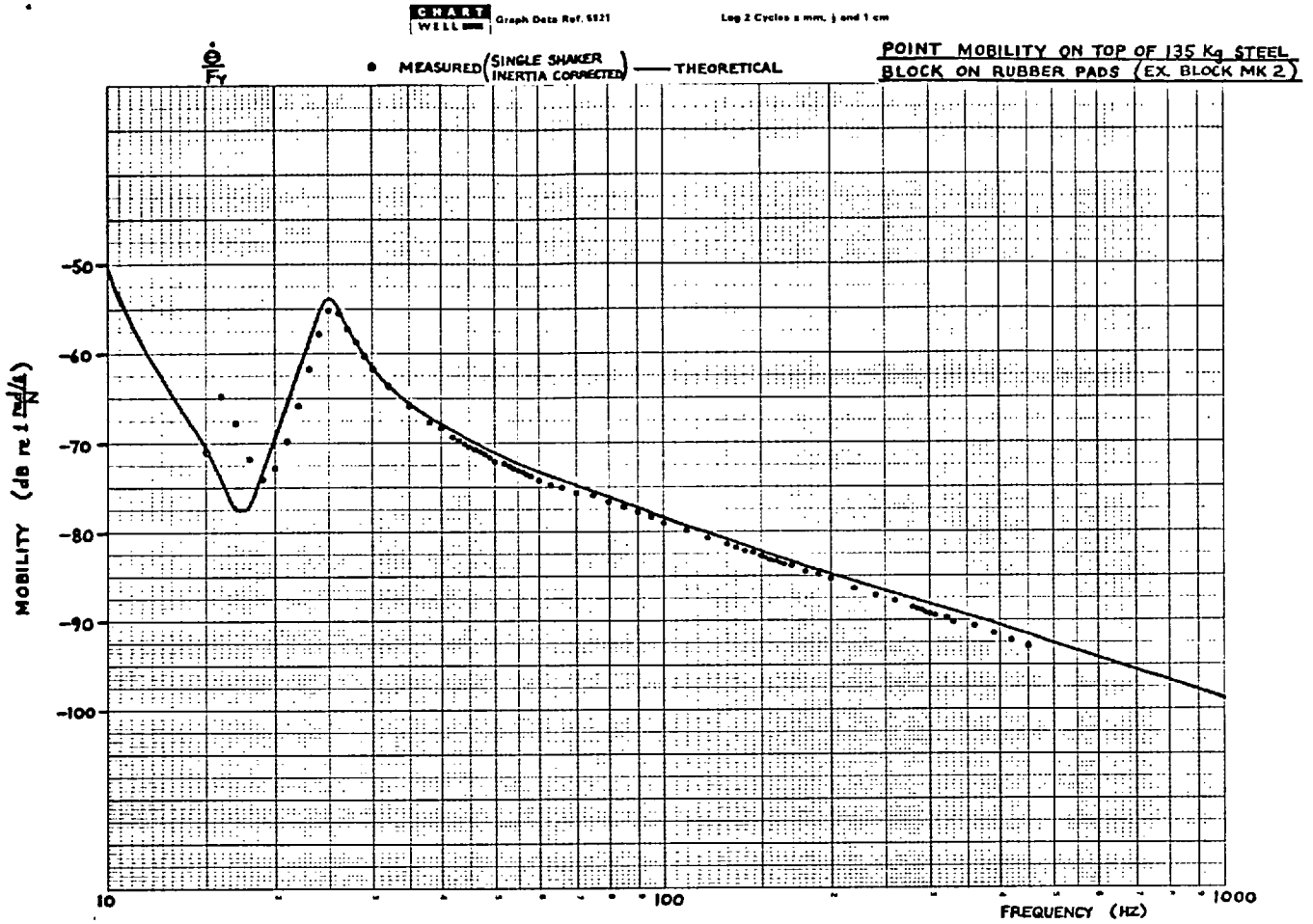
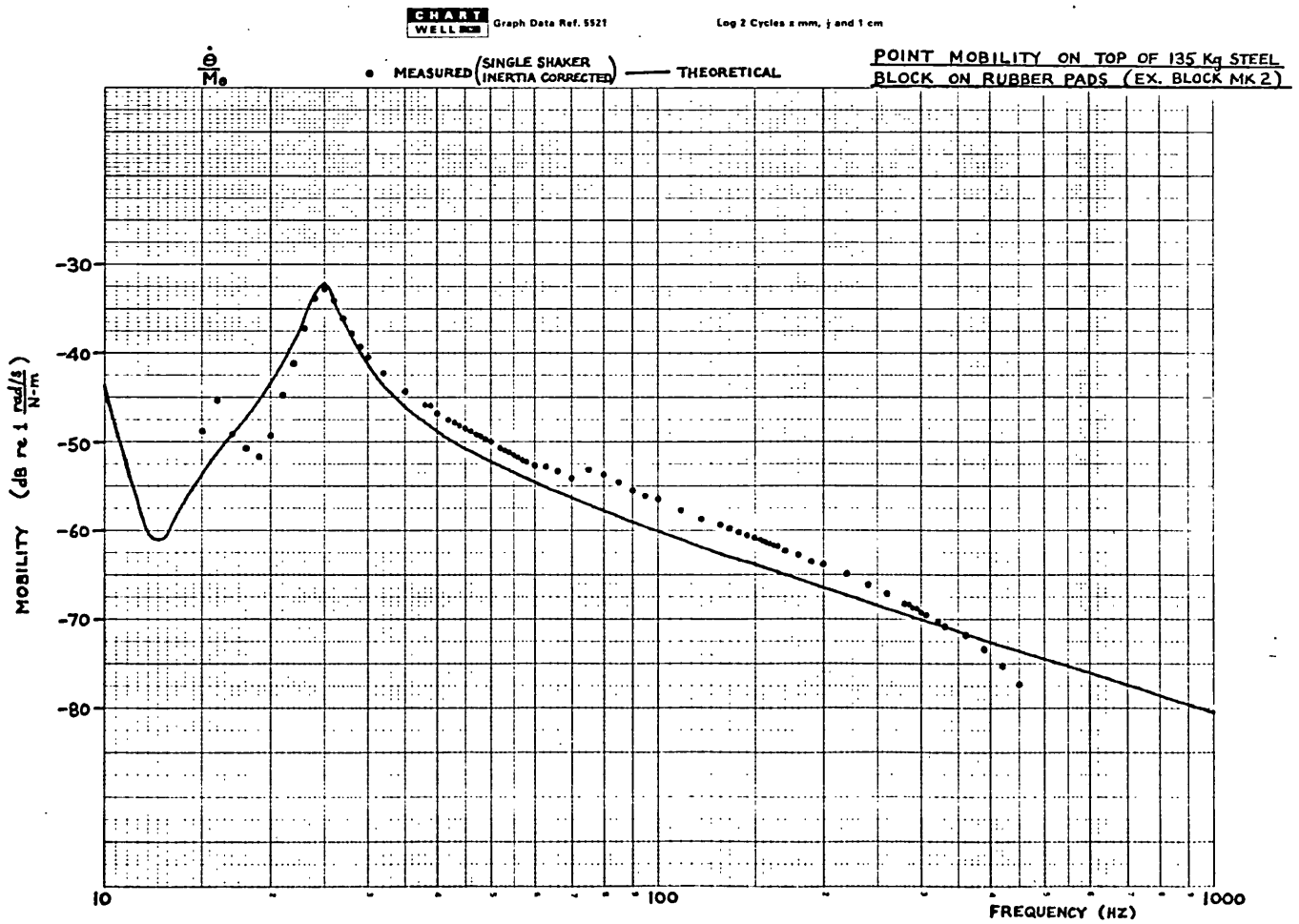
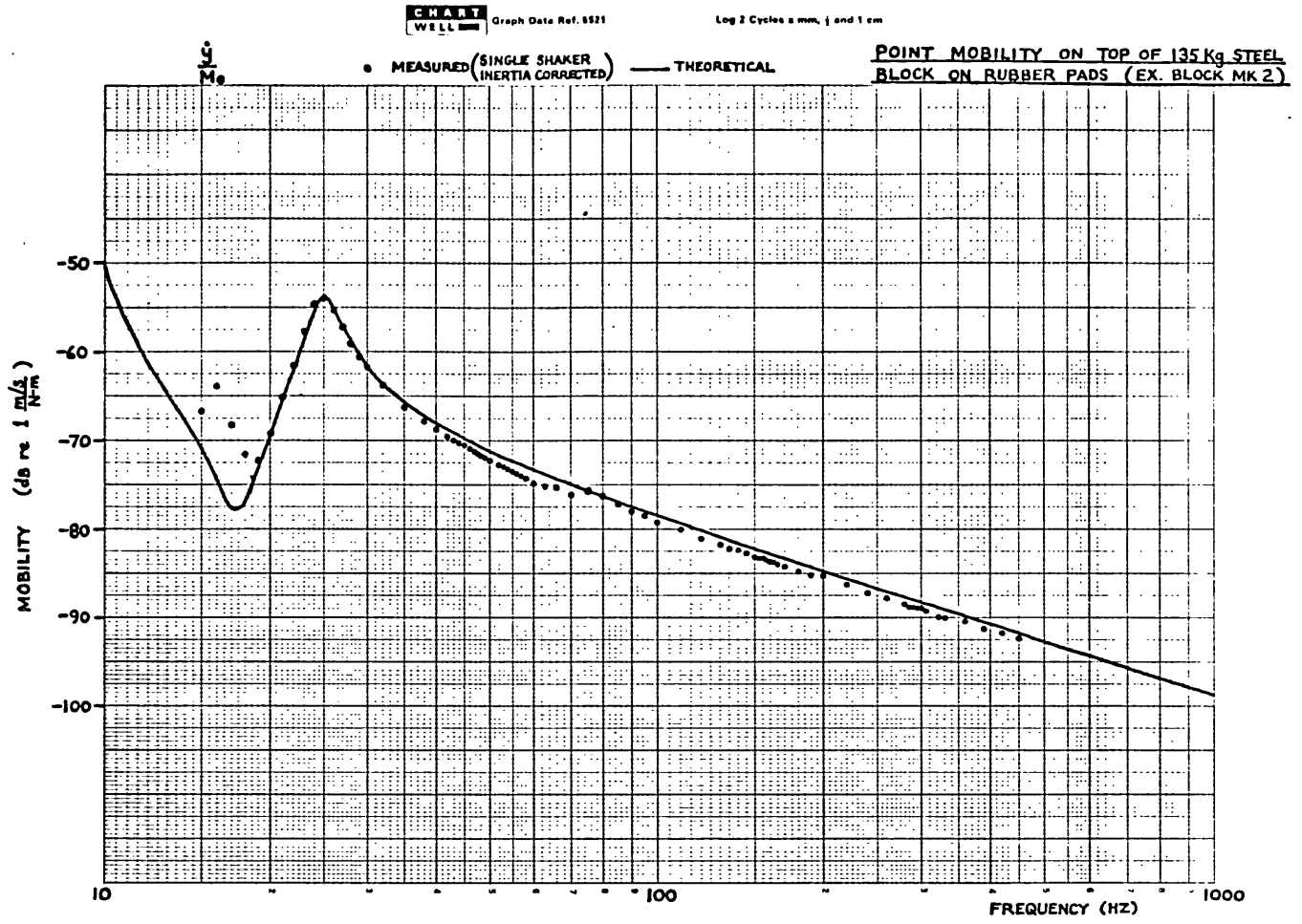


FIG 4.22





Discussion of Results for Tests on 1.83 m Steel Beam

The x , θ and ξ direct and cross mobilities show very good agreement with the theoretical response, the only appreciable differences occurring below about 50 Hz. The direct y mobility is also quite accurate up to about 350 Hz where it begins to descend to a premature anti-resonance. The greatest errors are apparent in the cross mobilities containing the y coordinate, but this is not surprising in view of the fact that the coupling between y and the other directions is here very small.

The errors below about 50 Hz have probably been caused by a combination of the effects of small accelerometer signals, electrical noise, accelerometer cross-sensitivity, and the constraining effect of the suspension ropes, but the last two are thought to be the most significant effects.

The test was first performed in the vertical plane, but because of the errors apparent in the lower part of the frequency range it was decided to repeat all the readings up to 145 Hz with the beam turned onto its side and excited in the horizontal plane. It was thought that the beam would be constrained less in this configuration and that the results would be improved, but the reverse seems to have been the case. It is possible that this unexpected deterioration in the results may have been caused by rocking of the beam in the plane perpendicular to its axis, since the supporting ropes were only in contact with its low side. A small rocking motion was in fact observed *visually* at the very low frequencies.

The accelerometers used in this and in all the other experiments were piezo-electric, and of the compression type. Those used on the Mk 2 block had a high axial sensitivity, and a quoted maximum cross sensitivity of 5%*. The sensitivity of an accelerometer to cross-axis motion in a given direction

* Birchall accelerometers, Type A/01. Charge sensitivity = 250 pC/g
Voltage sensitivity = 170 mV/g

may be varied by rotating the accelerometer about its axis, and the quoted figure of 5 % for the present accelerometers is only the maximum value. In addition, this figure does not include the effect of possible misalignment when attaching the accelerometer to the item under test. However, if we assume that the mounted y accelerometer has a cross sensitivity of 5%, we may expect that it won't generally give a signal which is more than 26 dB below the x acceleration. If we look at Fig. 4.11, which shows the x and y responses to a force F_x , we see that at 20 Hz the y motion should theoretically be 40 dB less than the x motion, whilst in fact it is only 25 dB. Although the difference does vary with frequency, it is certainly of the same order as that expected on the basis of accelerometer cross sensitivity, so it seems clear that this is one of the prime causes of inaccuracy in the measurements. One may arrive at the same conclusion by considering Fig. 4.13, which shows the x and y responses to a force F_y . For instance, at 30 Hz the measured x motion is 26 dB less than the corresponding y motion. The effect of the cross sensitivity may be minimised if the directional properties of the accelerometer are known, but it is preferable to use specially selected accelerometers which typically have a cross sensitivity of less than 1%. If the directional properties are known accurately, it should also be possible to apply a correction to the measured results, either by analogue means or digitally when the data are processed. The necessary correction is included in the response transformation $[C_p]$ derived in Appendix III, but it has not been applied to the present data. The effect of cross sensitivity upon multi-directional measurements is discussed further in Appendix IV and in reference (21).

Apart from the more readily apparent errors, it may be seen that on practically every graph there are a number of erroneous points very slightly below each resonance. As the measurements are not continuous it is difficult to see the exact behaviour, but there appears to be a very sharp pseudo-

resonance, followed by a corresponding pseudo-anti-resonance. This effect is due to numerical difficulties in the digital correction for the inertia of the exciting block. These pseudo-resonances in the corrected data coincide with the resonant frequencies of the combined beam/exciting-block system. The difficulty is caused by the fact that data measured on or near to a resonance is ill-conditioned, so that any subsequent numerical operations with these data may propagate large numerical errors. The same problem is discussed in Chapter 6 in connection with mobility coupling using measured data.

Considering the size of the block, together with the large contact area and two-bolt fixing, the measured results are certainly very encouraging.

Discussion of Results for Test on 135 Kg Spring-supported Mass

Except at low frequencies in the region of 25 Hz and below, the responses to both F_x and F_y have been measured to a reasonable degree of accuracy, with the largest error occurring in $\frac{\dot{y}}{F_x}$ and being about 2 dB. The disagreement between measurement and theory at the low frequencies is probably a combination of the effects of small accelerometer signals, accelerometer cross-sensitivity, and inaccuracies in the theoretical response due to an imprecise knowledge of the properties of the rubber pads.

Still discounting the low frequencies, far larger errors are apparent in the measurement of the response to M_θ , as might be expected from the fact that this is neither a direct nor a quasi-direct measurement. The largest error occurs in $\frac{\dot{x}}{M_\theta}$, and is about 5 dB, and even $\frac{\dot{\theta}}{M_\theta}$ shows as much as 4 dB error. In contrast, $\frac{\dot{y}}{M_\theta}$ is very good, with the largest error being about 1.5 dB. The reason for the mysterious jump in the response at 75 Hz is not known for certain. As the test was performed manually, with occasional breaks in the measurements, it was initially thought that this might correspond to such a break; however, it was soon found that this was not the case. Since the x and θ responses above

this frequency appear to have been shifted upwards by about 2.5 dB, it is just possible that the gains of the two acceleration channels might have increased, but this is thought to be unlikely. A more reasonable explanation is a purely mechanical one: namely a steel mounting bracket screwed into the underside of the block. This was left in position after some other experiment, and it was at the time discounted as being insignificant in comparison with the mass of the steel block. In fact, since the mobility $\frac{\dot{x}}{F_x}$ shows no jump, this assumption was probably justified. However, as the bracket was mounted a considerable distance from the centre of the block, it is very probable that its effect on the moment of inertia was far more significant. If this was the case, then the jump probably corresponds to the decoupling of the bracket from the block, as the former ceased to remain a pure mass.

The other deviation from the theory occurs from about 300 Hz upwards, where both $\frac{\dot{x}}{M_\theta}$ and $\frac{\dot{\theta}}{M_\theta}$ begin to gradually drop off, probably to an anti-resonance at around 550 Hz. This is thought to be caused by the bending flexibility of the exciting block, and it is probable that if the measurements had been continued up to 1000 Hz they would have shown this spring acting against the almost stationary inertia of the steel mass. If we take the theoretical moment of inertia of the mass, which is 1.7 Kg-m^2 , and assume that there is an anti-resonance at 550 Hz, we obtain an effective rotational stiffness of $2 \times 10^7 \text{ N-m/rad}$ for the exciting block*.

* For a fuller discussion of exciting-block flexibility, see Appendix IV
(Page 493)

4.5 TWO-DIRECTIONAL POINT MOBILITY MEASUREMENT USING A COMPUTER-CONTROLLED MEASURING SYSTEM

Introduction

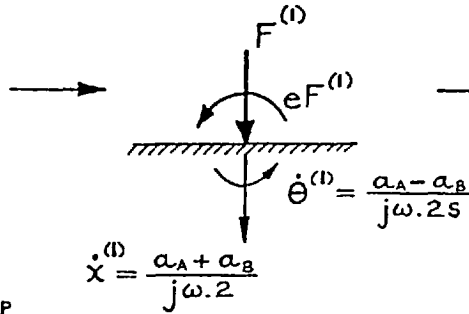
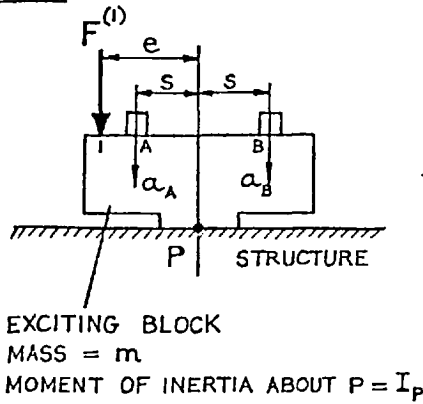
Following the successful measurements with exciting block Mk 2, it was decided to look into the possibility of automating the procedure: this was necessitated by the large amount of data to be measured, stored, and ultimately processed during each test, and it was the only way that such tests could ever become fairly routine. What was required was some sort of computer-controlled frequency response analysis system, in which the computer would control the frequency sweep and measurements and then subsequently process these data to yield the required multi-directional mobilities. A large central computer could obviously be used for this purpose, but this was not permitted by the Imperial College Computer Centre, so it was necessary to think in terms of a mini-computer in the laboratory. Quite fortuitously it was discovered that Solartron Ltd. were at that time* developing a computer-controlled system around their JMI600A transfer function analyser (see Section 4.2). This used a PDP 8E mini-computer (8 K store) which was accessed via a tele-typewriter, and it incorporated all the required features for automating the multi-directional tests. Therefore, Solartron Ltd. made available the prototype system for some tests to be carried out, and such a system was later acquired by the Dynamics Group.

The computer system has so far only been used for two-directional point mobility measurements, and the measurement and processing procedure will be explained with reference to Fig. 4.24. The two motions with which we are concerned are the linear velocity \dot{x} , in a direction normal to the surface, and the rotational velocity $\dot{\theta}$: as the accelerometers A and B are symmetrically disposed relative to point P, these velocities are yielded by simple sum and difference relations. The excitation points 1 and 2 are also

* 1971

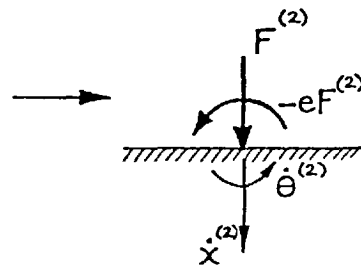
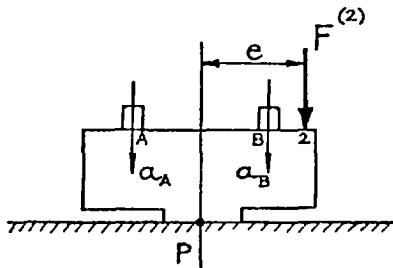
THE MEASUREMENT OF THE X-θ POINT MOBILITY MATRIX USING A SINGLE SHAKER

RUN 1



$$\begin{Bmatrix} \dot{x}^{(1)} \\ \dot{\theta}^{(1)} \end{Bmatrix} = \begin{bmatrix} Y_{xx} & Y_{xe} \\ Y_{ex} & Y_{\theta\theta} \end{bmatrix} \begin{Bmatrix} F^{(1)} \\ eF^{(1)} \end{Bmatrix}$$

RUN 2



$$\begin{Bmatrix} \dot{x}^{(2)} \\ \dot{\theta}^{(2)} \end{Bmatrix} = \begin{bmatrix} Y_{xx} & Y_{xe} \\ Y_{ex} & Y_{\theta\theta} \end{bmatrix} \begin{Bmatrix} F^{(2)} \\ -eF^{(2)} \end{Bmatrix}$$

COMBINE THE TWO SETS OF DATA TO OBTAIN THE X-θ POINT MOBILITY MATRIX :

$$\begin{bmatrix} \dot{x}^{(1)} & \dot{x}^{(2)} \\ \dot{\theta}^{(1)} & \dot{\theta}^{(2)} \end{bmatrix} = \begin{bmatrix} Y_{xx} & Y_{xe} \\ Y_{ex} & Y_{\theta\theta} \end{bmatrix} \begin{bmatrix} F^{(1)} & F^{(2)} \\ eF^{(1)} & -eF^{(2)} \end{bmatrix} \rightarrow \begin{bmatrix} Y_{xx} & Y_{xe} \\ Y_{ex} & Y_{\theta\theta} \end{bmatrix} = \begin{bmatrix} \left(\frac{\dot{x}}{F}\right)^{(1)} & \left(\frac{\dot{x}}{F}\right)^{(2)} \\ \left(\frac{\dot{\theta}}{F}\right)^{(1)} & \left(\frac{\dot{\theta}}{F}\right)^{(2)} \end{bmatrix} \begin{bmatrix} 1 & 1 \\ e & -e \end{bmatrix}^{-1}$$

THE FOLLOWING MORE COMPLETE EXPRESSION ALSO CORRECTS FOR EXCITING BLOCK INERTIA :

$$\begin{bmatrix} Y_{xx} & Y_{xe} \\ Y_{ex} & Y_{\theta\theta} \end{bmatrix} = \begin{bmatrix} \left(\frac{\dot{x}}{F}\right)^{(1)} & \left(\frac{\dot{x}}{F}\right)^{(2)} \\ \left(\frac{\dot{\theta}}{F}\right)^{(1)} & \left(\frac{\dot{\theta}}{F}\right)^{(2)} \end{bmatrix} \left(\begin{bmatrix} 1 & 1 \\ e & -e \end{bmatrix} - \begin{bmatrix} m & 0 \\ 0 & I_p \end{bmatrix} \begin{bmatrix} \left(\frac{\ddot{x}}{F}\right)^{(1)} & \left(\frac{\ddot{x}}{F}\right)^{(2)} \\ \left(\frac{\ddot{\theta}}{F}\right)^{(1)} & \left(\frac{\ddot{\theta}}{F}\right)^{(2)} \end{bmatrix} \right)^{-1}$$

symmetrically disposed relative to P, unlike in the earlier tests with block Mk 2: this yields more "information" on the response to a couple than does the single off-centre excitation employed previously, so it leads to improved rotational results. In addition, the required mobilities are obtained by simply superposing the responses to the separate excitations: the response to a force F_x is yielded by the sum of the run 1 and run 2 results, while the response to a couple M_θ is obtained by taking their difference.

During run 1 the mobilities $\left(\frac{\dot{x}}{F}\right)^{(1)}$ and $\left(\frac{\dot{\theta}}{F}\right)^{(1)}$ are measured and punched onto paper tape at each frequency. The tape is then rewound and threaded into the tape reader before starting the next run. During run 2 the mobilities $\left(\frac{\dot{x}}{F}\right)^{(2)}$ and $\left(\frac{\dot{\theta}}{F}\right)^{(2)}$ are measured using exactly the same frequency sweep as before, and at each frequency the corresponding data from run 1 are read in from the tape and are combined with the run 2 data to yield the required 2×2 point mobility matrix (which may be corrected for exciting block inertia if necessary). This is then punched out on tape before proceeding to the next frequency. Thus, the processing is carried out on-line during run 2, so the full set of response data is immediately available in the laboratory.

The test is controlled by a standard program, which was written by the Author in a conversational language called FOCAL. This program is available on paper tape, and is accompanied by a set of user instructions, so that it may be loaded and used as required.

Tests using Computer-controlled System

A number of multi-directional mobility measurements have been made using this system, and we shall now consider two examples*. The first relates to a heavily damped multi-layer beam used in the machinery seating that is analysed in Part 4: this beam is designated UT, and it is shown in Fig. 4.25. It was

* Other examples may be found in Chapter 12 (Figs. 12.12 and 12.13) and in Chapter 15 (Figs. 15.2 to 15.4)

suspended on two 6 mm diameter ropes, which were sufficiently elastic to provide essentially free-free boundary conditions except at very low frequencies. In order to minimise their constraining effect, these ropes were positioned at the nodes of the first free-free bending mode, and in addition the beam was mounted on its side and excited in the horizontal plane. The $x-\theta$ mobility matrix was measured at a point near the end of the beam using exciting block Mk 3, which is shown in Fig. 4.26. This block is much smaller than Mk 2 and had already been successfully employed for some three-directional measurements on the 1.83 m steel beam⁽²⁴⁾. With its single-bolt fixing, smaller contact area and lower mass (0.880 Kg including bolt and accelerometers), it is not much larger than a Wilcoxon Z820 impedance head and is more suitable for measurements on medium-size components and structures than the rather bulky Mk 2 block. It was attached to the sandwich beam solely by

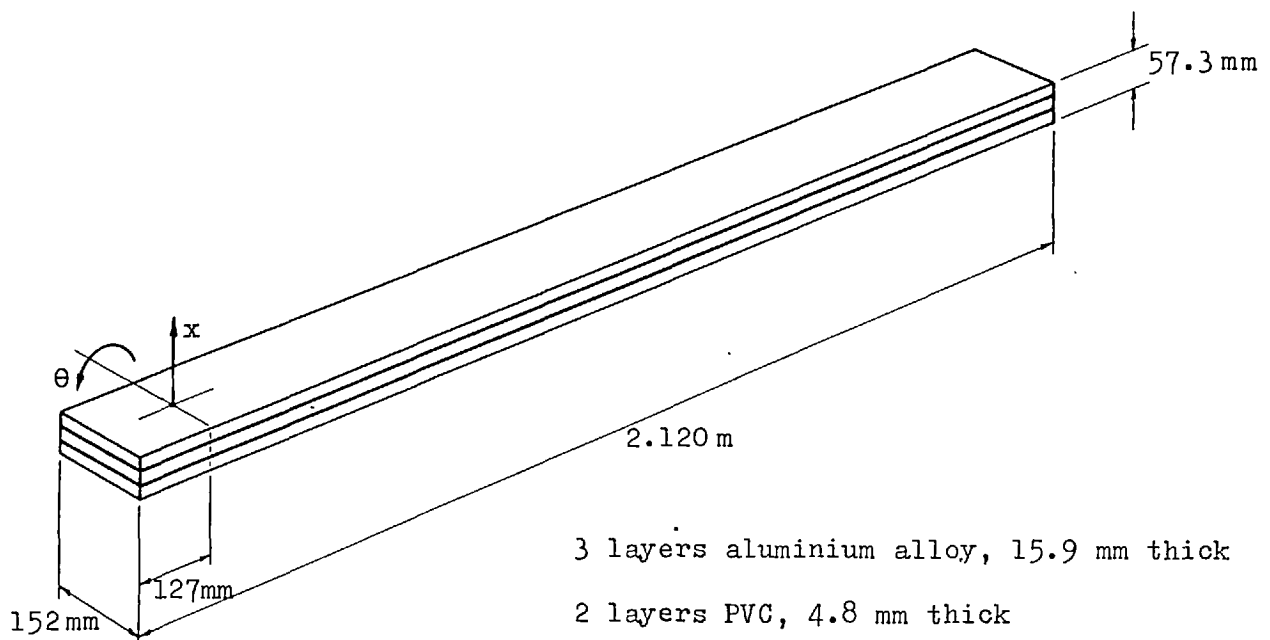


FIG. 4.25 BEAM UT — Symmetrical 5-layer beam used in V-beam seating

means of the fixing bolt, which was screwed into a hole tapped in the outer layer, and only a very thin film of grease was interposed between the contacting surfaces. In the case of the three-directional measurements described in Reference (24), the excitations during the three runs were applied at points 1S, 2 and 3 respectively, but in the present two-directional test the excitations were applied at points 1T and 2 respectively.

The measured response data representing the four elements of the 2×2 matrix are presented in Figs. 4.27 to 4.30 as curves of mobility modulus and phase. These results have been corrected for exciting block inertia in both the x and θ directions. Also shown on each graph is the theoretical response predicted using the 5-layer beam finite element derived in Chapter 9 (Part 3)*. The material properties and constructional details for this beam are given in Section 14.1 (Part 4, Chapter 14), and the analysis is discussed both there and in Chapter 12 (Part 3).

The second example that we shall consider relates to the two-stage beam shown in Fig. 4.31. This was used by Cottney⁽²²⁾ as a simple but readily analysable model for a turbine blade, and although it differs considerably from the real thing, it does possess similar dynamic characteristics. It was suspended on light elastics to simulate a free-free condition, and measurements were made of the transverse and torsional mobilities at point P, which was effectively at the tip of the beam. No exciting block was used in this case: instead, the accelerometers and the force gauge were attached directly to the beam using small studs which were stuck in place with Plastic Padding.

The measured responses are shown in Fig. 4.32, together with theoretical predictions obtained by Cottney. Only direct mobilities are given, since there is no coupling between the x and θ responses, and the measurements have not been corrected for either accelerometer or force gauge inertia.

* Note that the present displacements x and θ correspond to w and ψ in the element derivation.

BLOCK THICKNESS = 51 mm

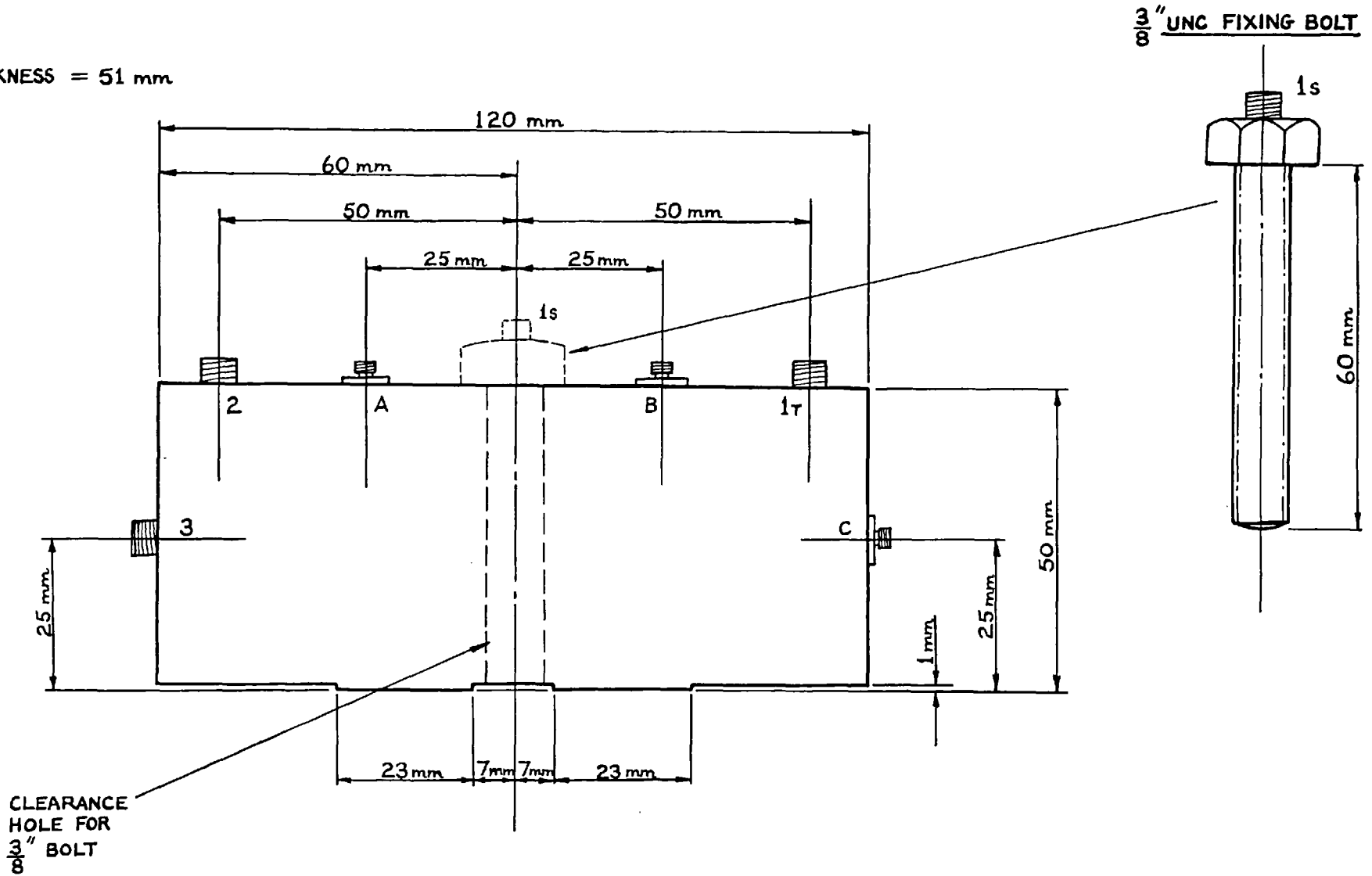


FIG 4.26

STUDS

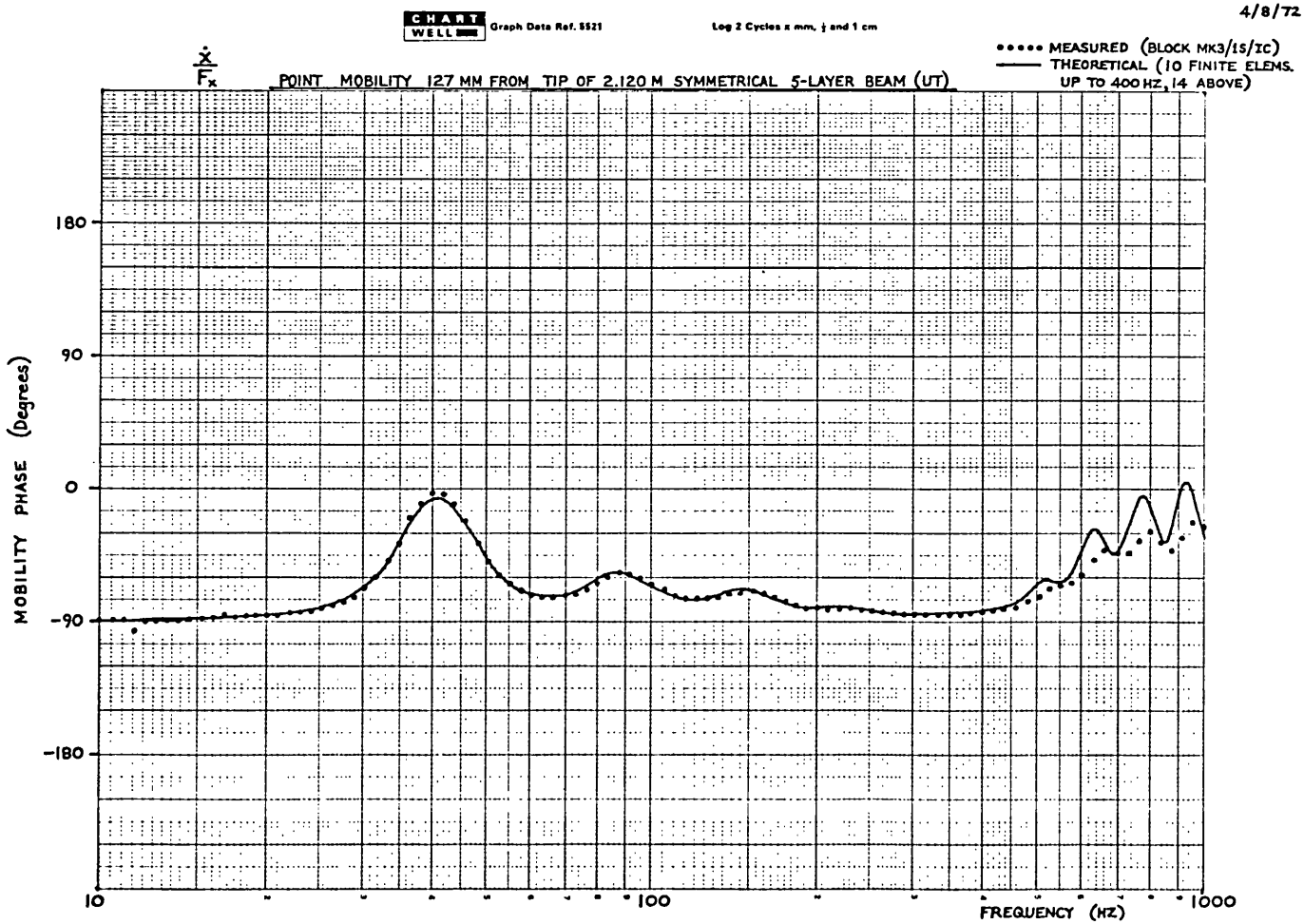
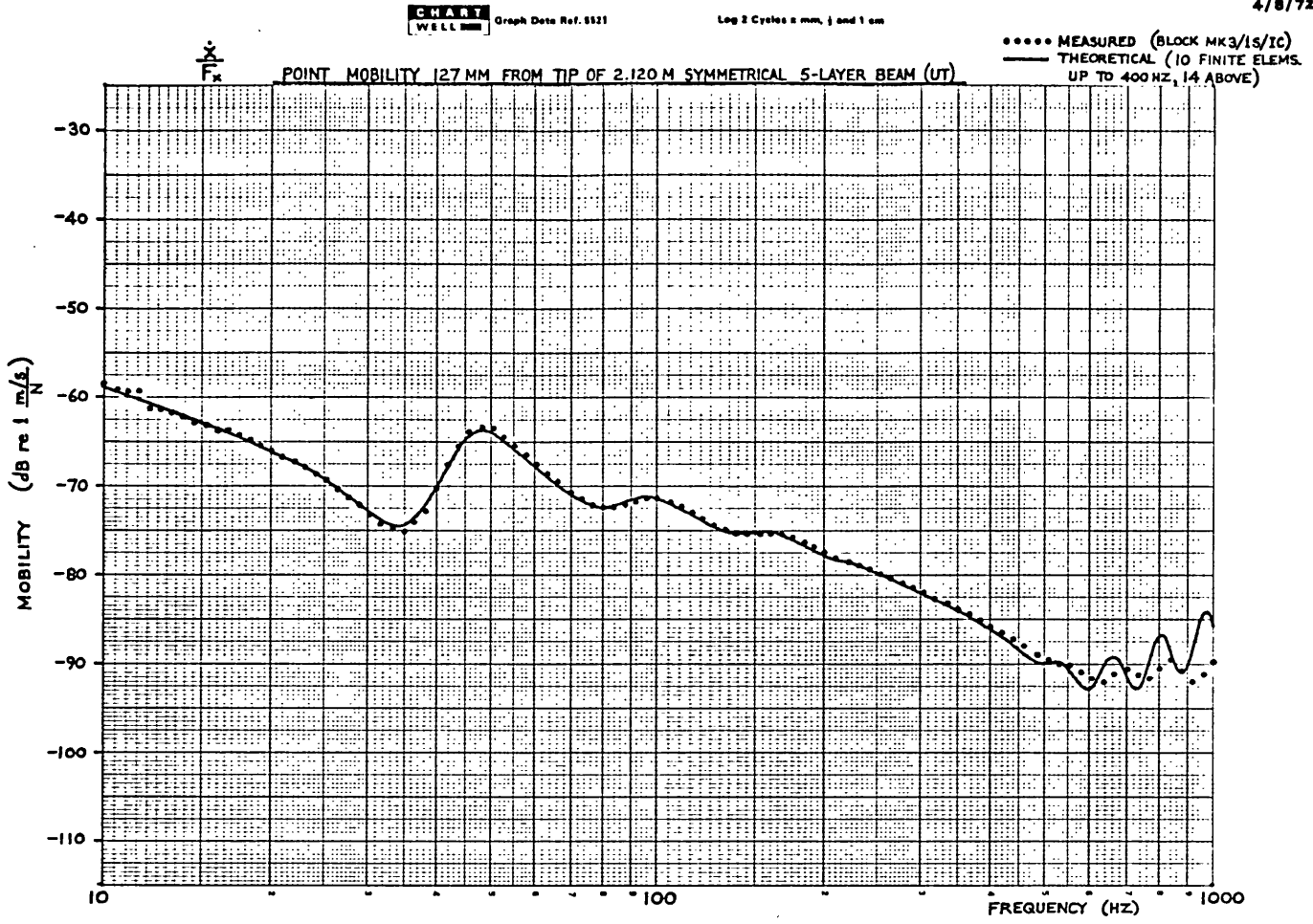
- A, B, C 10-32 UNF INSULATING FOR BIRCHALL A/O2 ACCELEROMETER
- 1s, 1T, 2, 3 1/4 UNF FOR ENDEVCO FORCE GAUGE TYPE 2103-100

MATERIAL: ALUMINIUM ALLOY

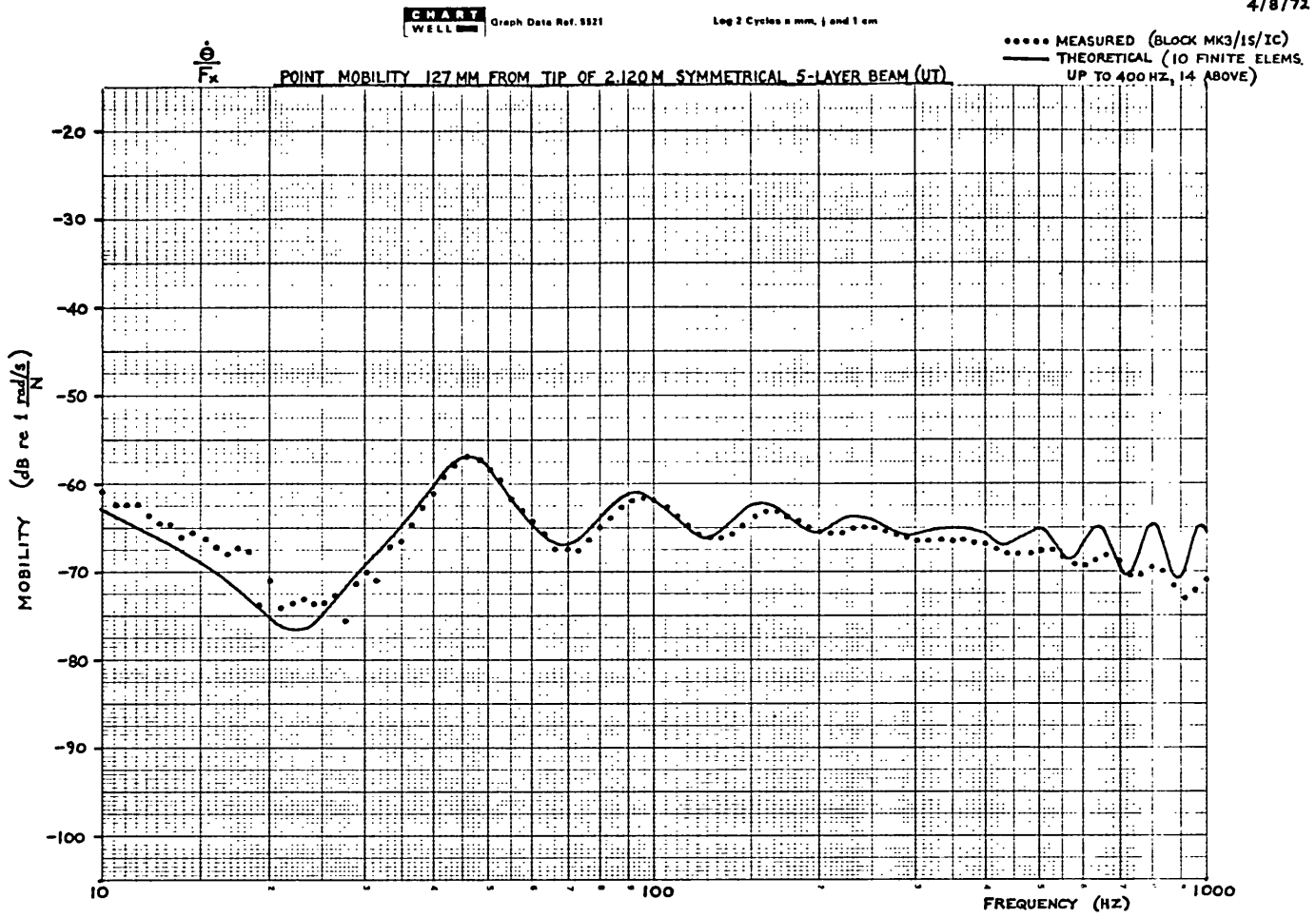
FULL SCALE

EXCITING BLOCK MK 3
(WITH FIXING BOLT)

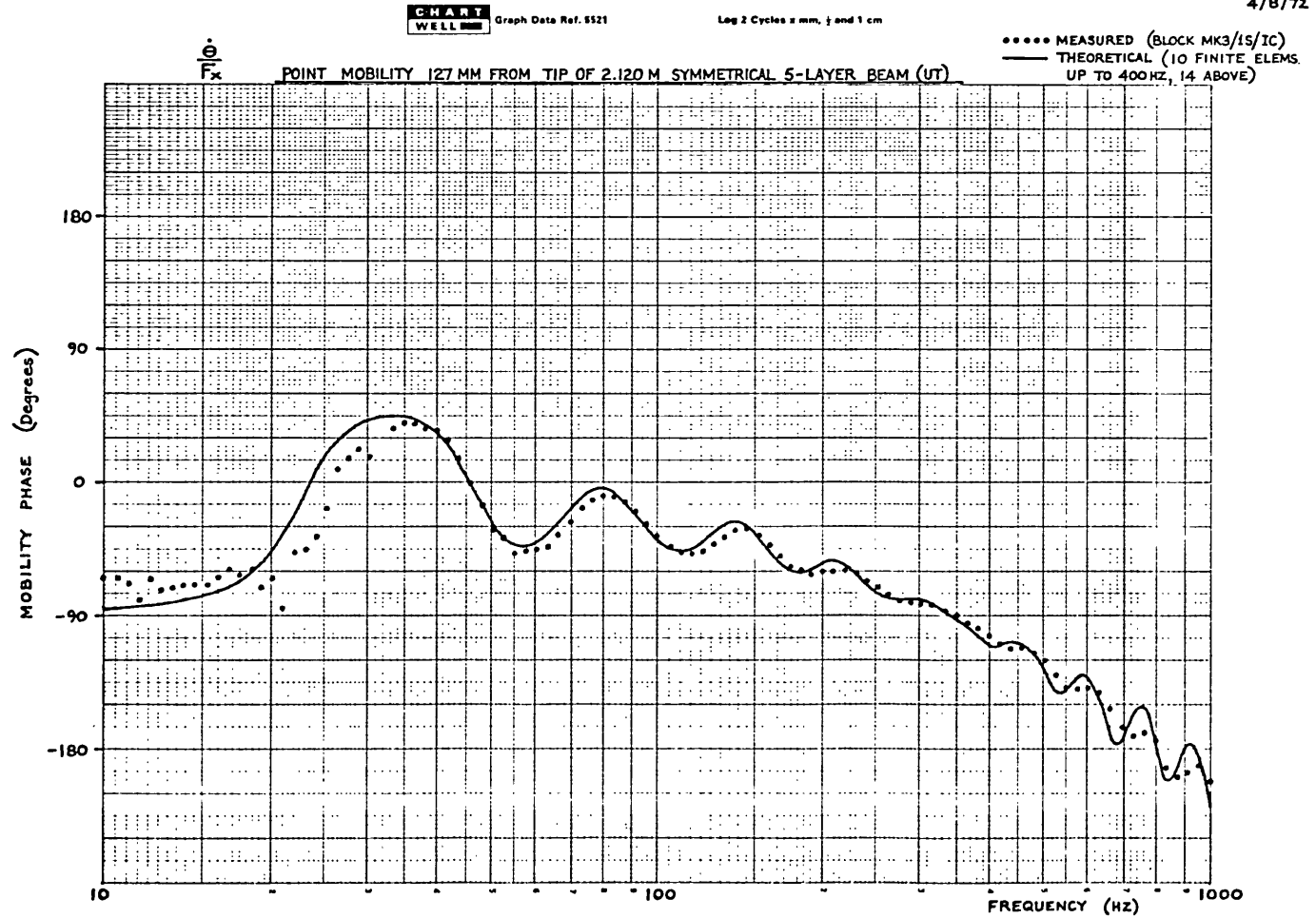
4/8/72



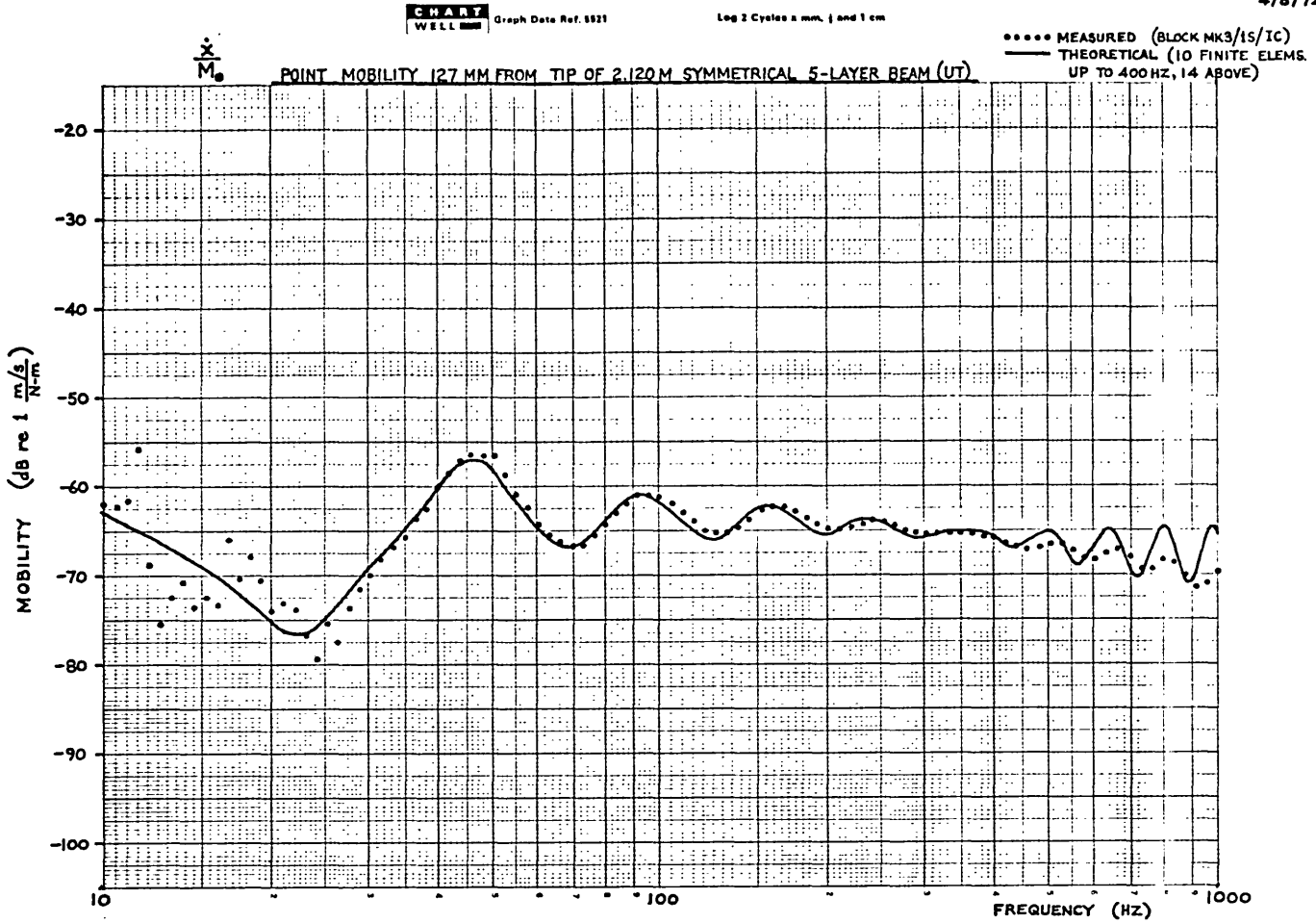
4/8/72



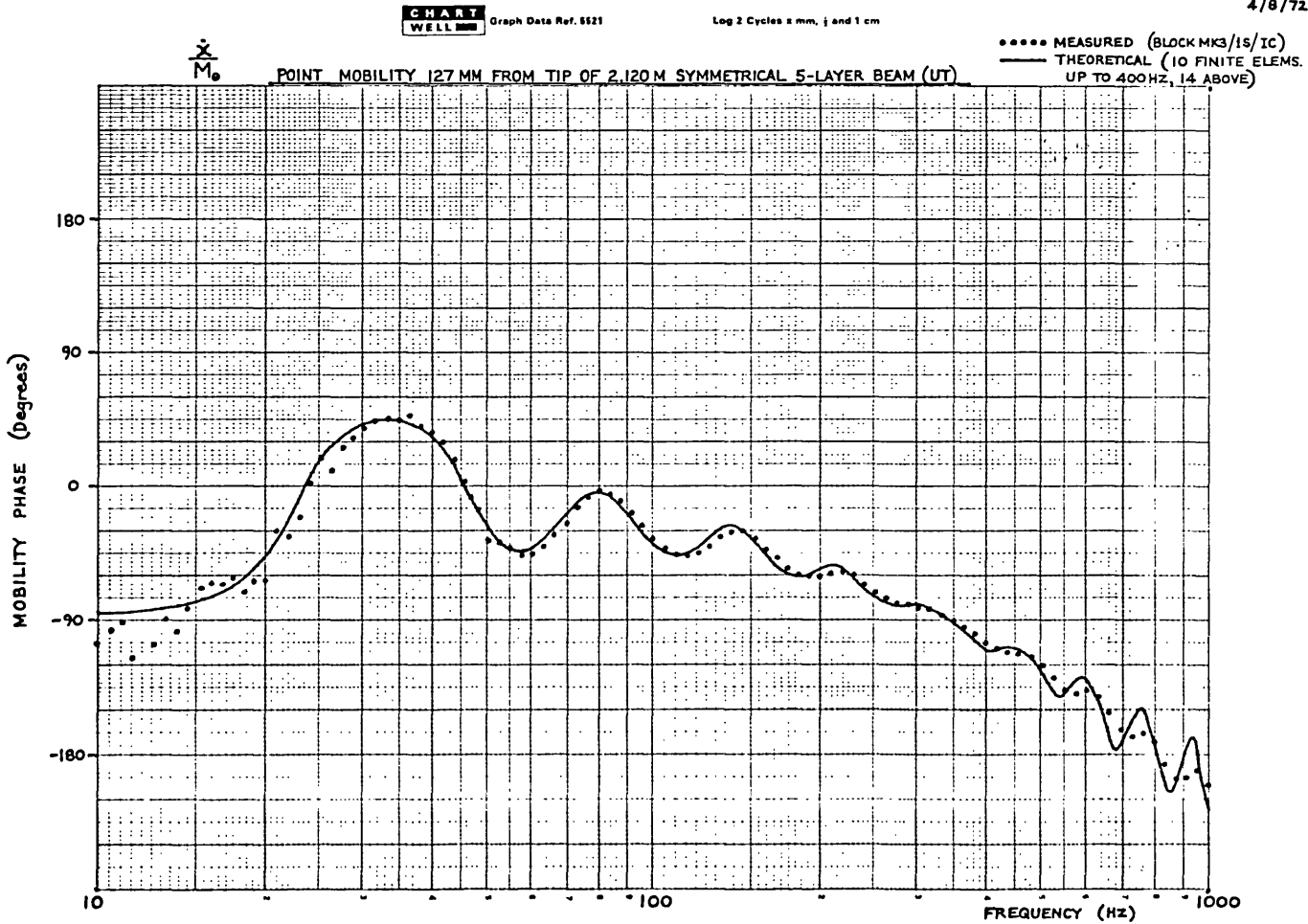
4/8/72



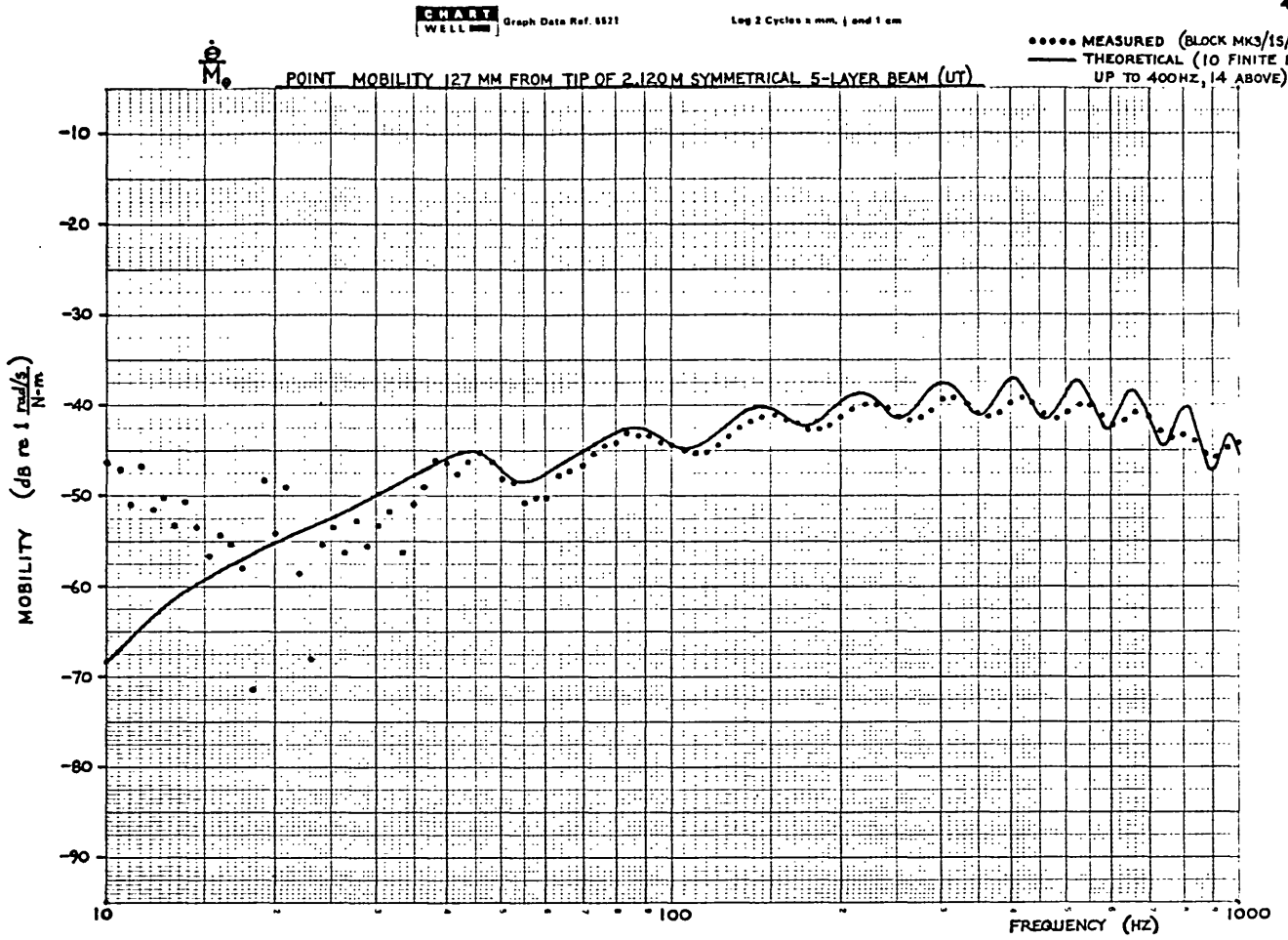
4/8/72



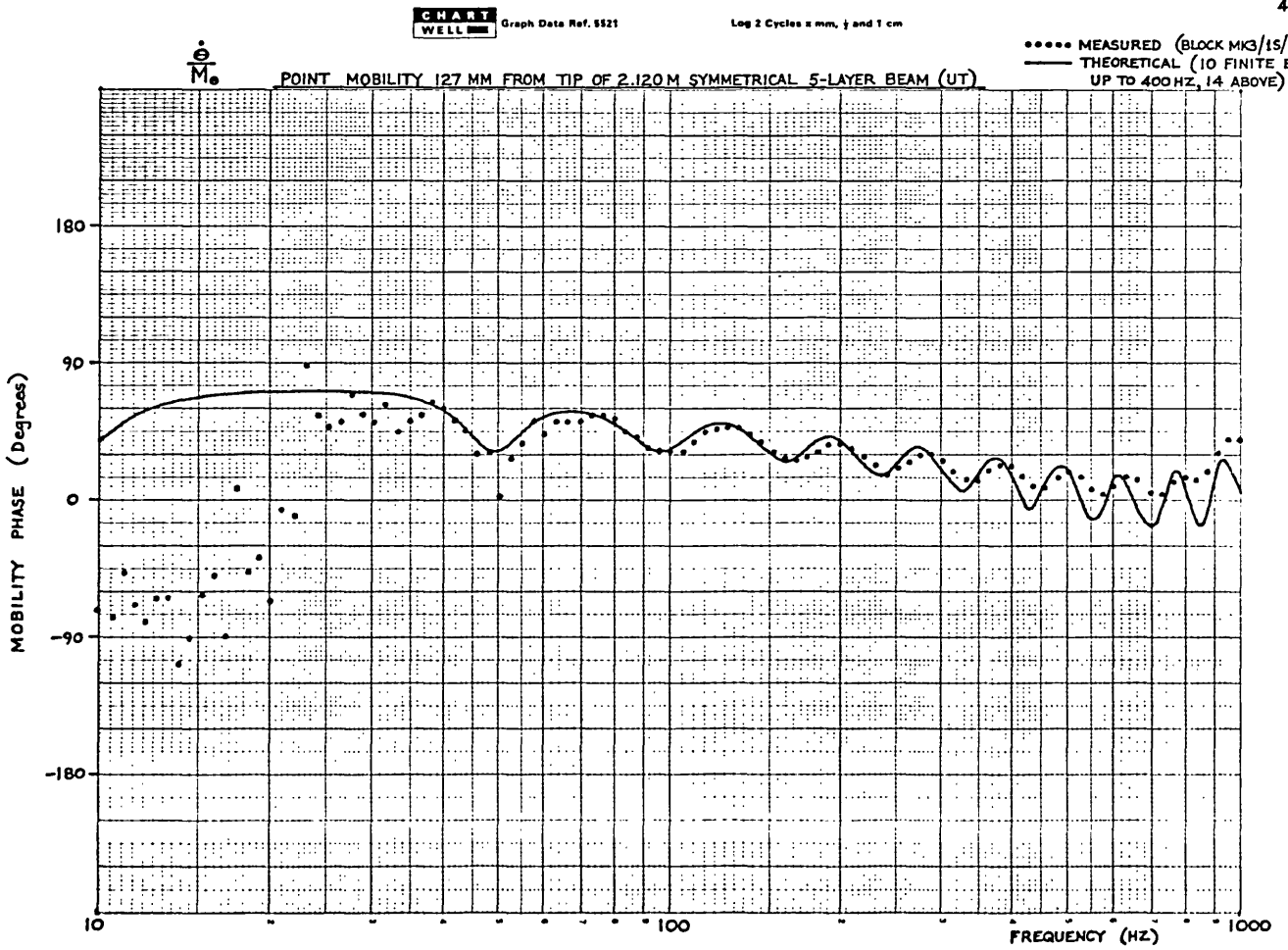
4/8/72



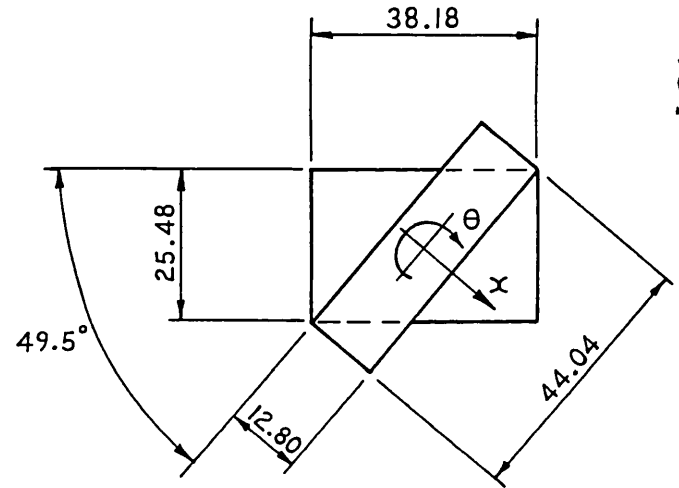
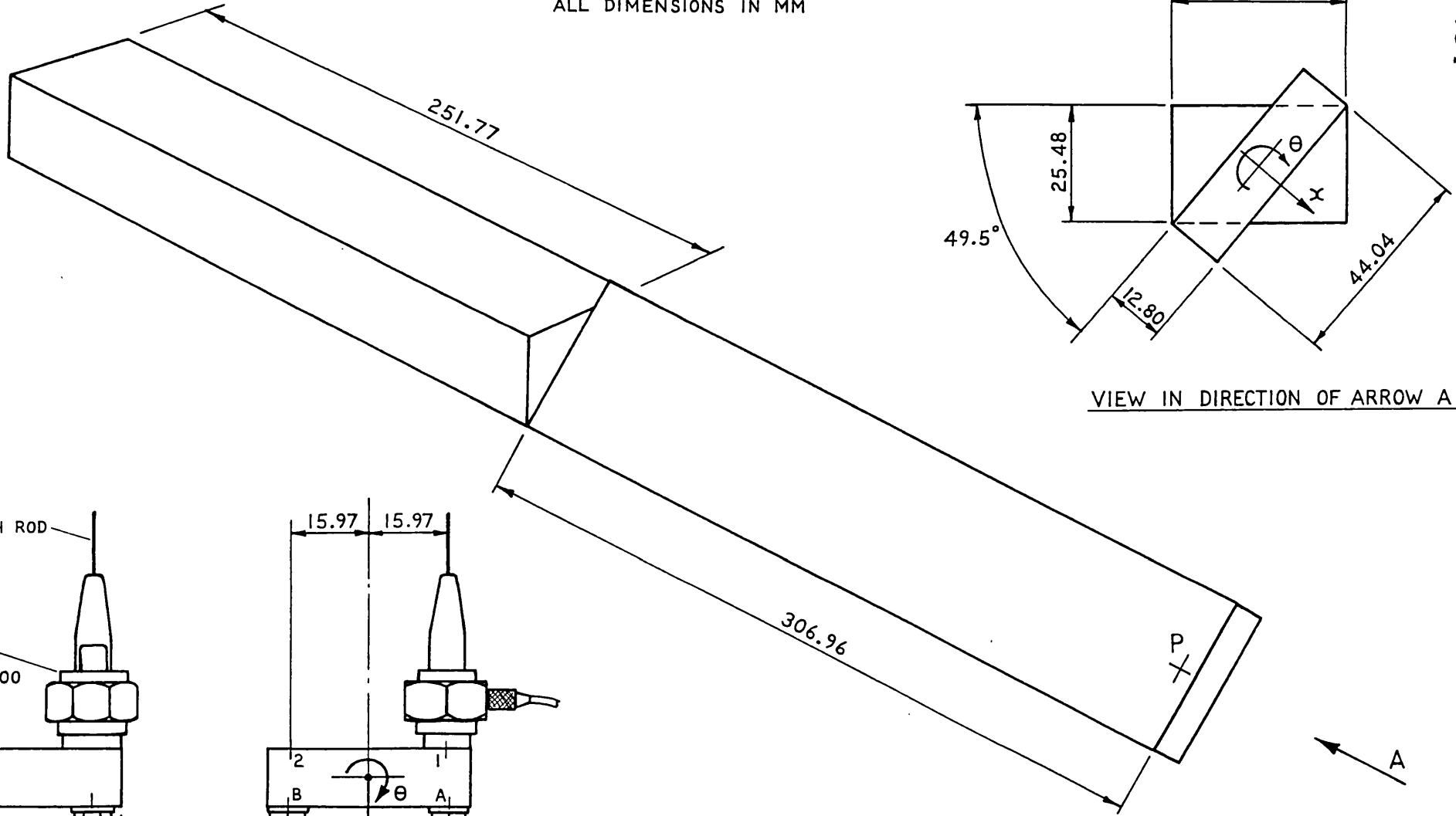
4/8/72



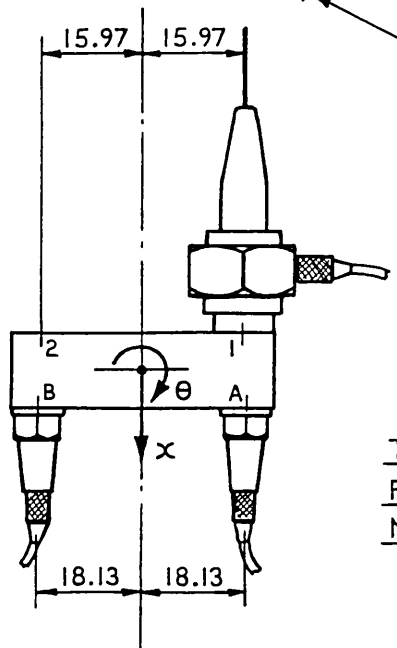
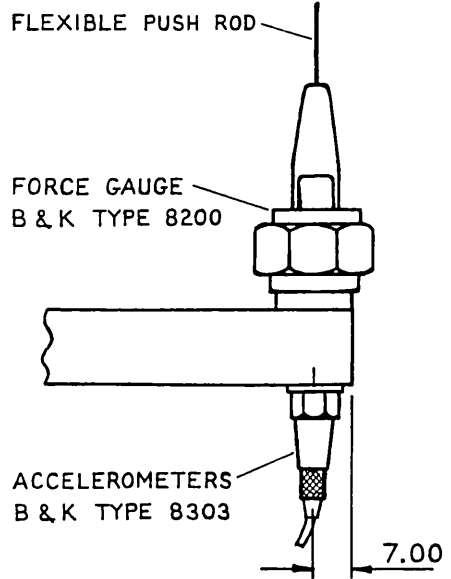
4/8/72



MATERIAL: MILD STEEL
ALL DIMENSIONS IN MM



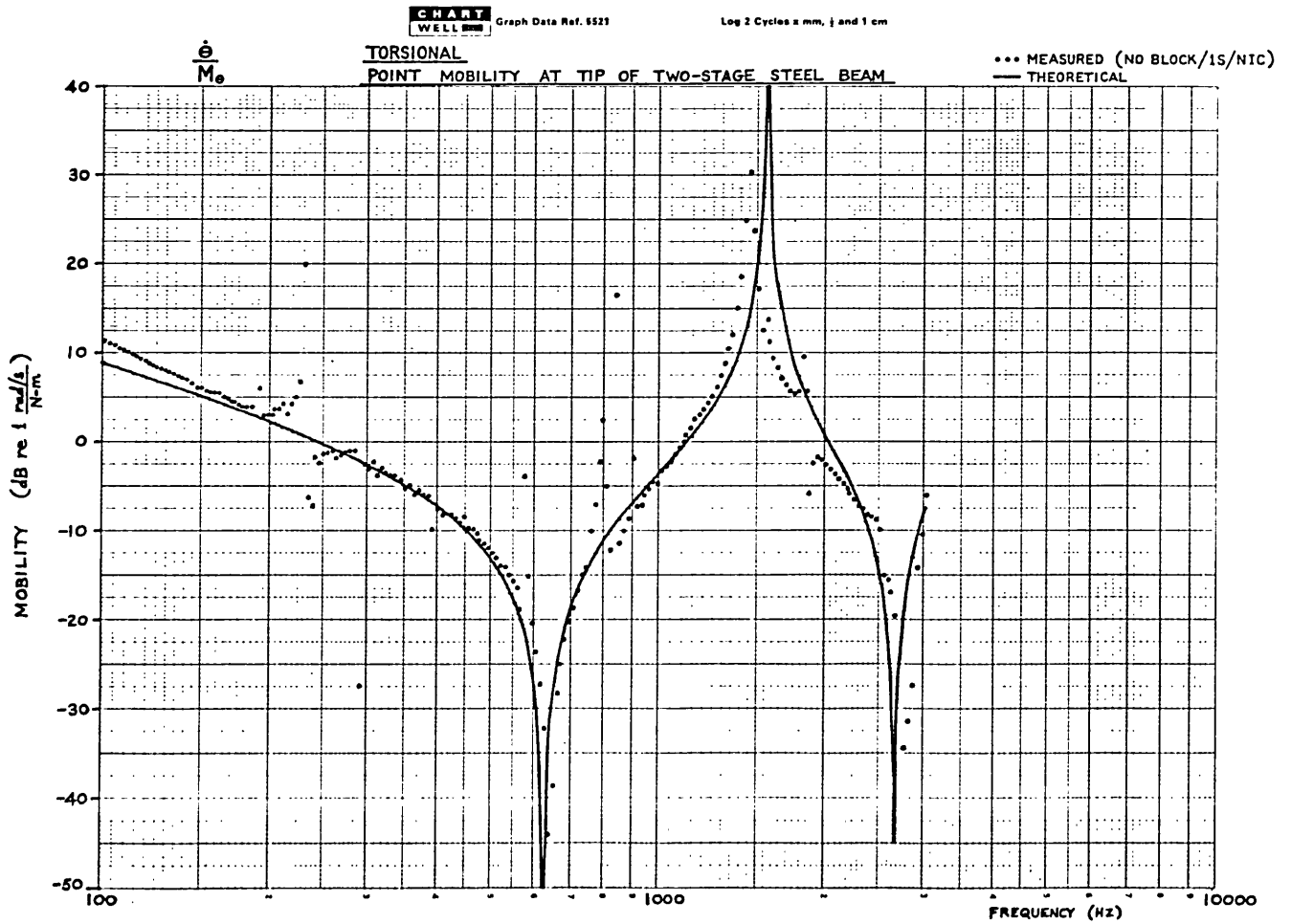
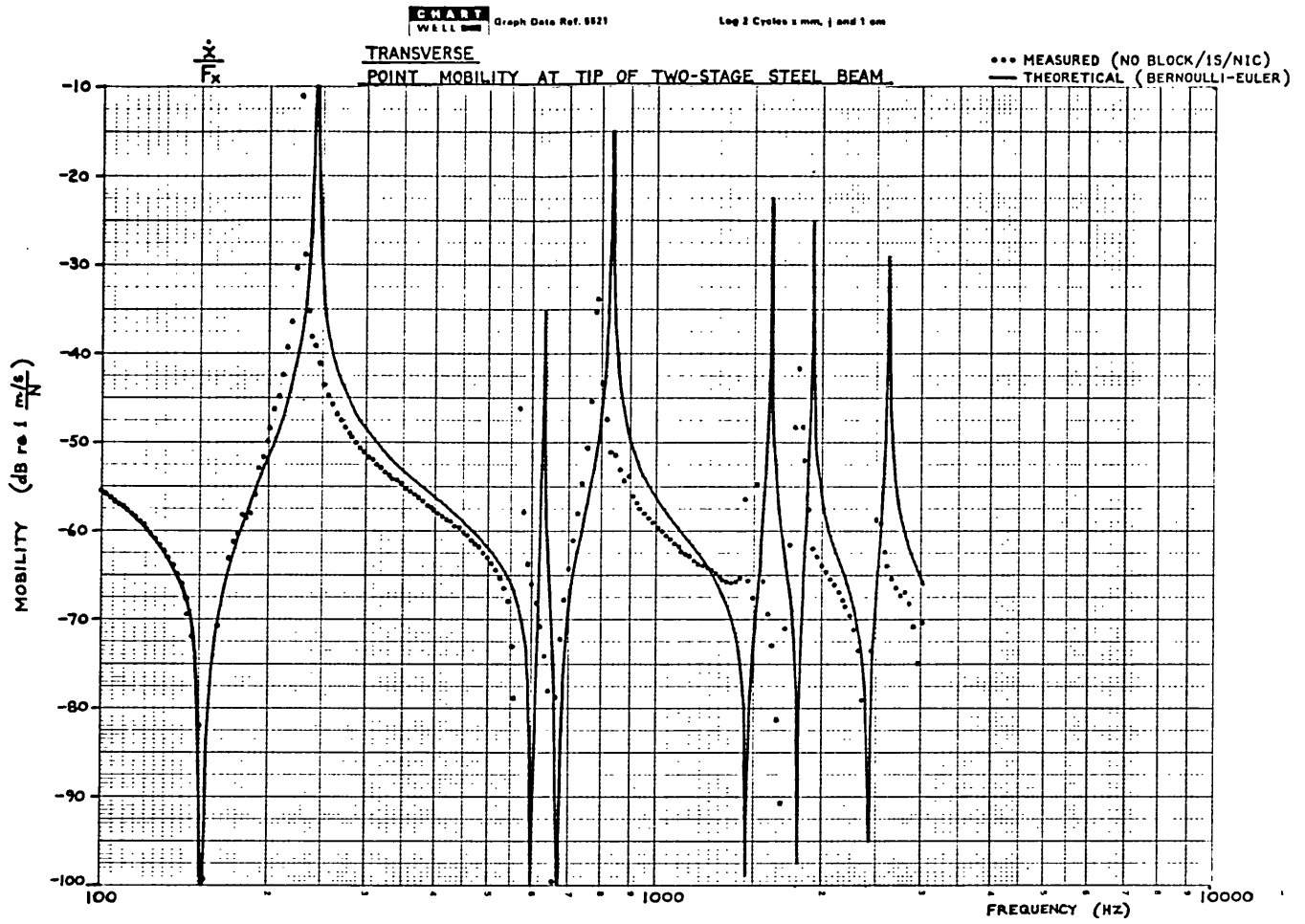
VIEW IN DIRECTION OF ARROW A



TRANSDUCERS USED
FOR MEASURING $x-\theta$
MOBILITY AT POINT P

TWO-STAGE BEAM

FIG 4.32



Discussion of Results for Tests using Computer-controlled System

The excellent set of results obtained for the sandwich beam UT justifies the use of the smaller Mk 3 exciting block. Comparing the size of the block with that of the beam, it is in fact quite remarkable that such good agreement could be obtained for both the modulus and the phase over so many modes. The only significant errors occur below the first bending resonance, and these are restricted to those mobilities which include either rotational response or excitation. This is because points 1, 2, A and B on the block are a long way from the centre of gravity of the beam, and are at the same time grouped quite closely together, so the rigid-body response at either A or B due to a force at either 1 or 2 is large and changes very little with position. Since all rotational information is obtained from differences of these nearly equal response data, it is hardly surprising that errors arise. The worst case is the rotational mobility $\frac{\dot{\theta}}{M_{\theta}}$, since this involves two differences, but although there is considerable scatter, the points still follow a discernable trend: the mobility starts off as the moment of inertia of the rigid beam, and it then displays an anti-resonance at about 20 Hz before going on to the first bending resonance around 45 Hz. This only differs from the theoretical prediction because of the effect of the suspension ropes. Above this region of rigid-body behaviour, all the responses have been measured with comparable accuracy, and the differences between experimental and theoretical results are attributable as much to errors in the finite element model as to errors in the measurement. However, it should be noted that this two-directional measurement does not include any correction for exciting block inertia along the surface of the beam parallel to its axis, so the extra couple applied by this force must obviously have some effect on the higher modes.

The results for the two-stage beam are not so good, as often seems to be the case with mobility measurements on small items. However, in the case of the transverse mobility $\frac{\dot{x}}{F_x}$ it is almost certainly the theoretical model which

is primarily at fault, since the beam is fairly short, yet it was analysed using Bernoulli-Euler theory. The extra flexibility of the Timoshenko model would pull all the theoretical resonances down in frequency, bringing them closer to the measured values. At the same time, if a correction were made for the mass of the force and acceleration transducers, this would raise the measured resonances very slightly. On the whole, the torsional mobility $\frac{\dot{\theta}}{M_{\theta}}$ shows closer agreement between the measurements and the theory, although there is more scatter of the measured points. This scatter represents breakthrough from the bending resonances, which are ^{theoretically} completely uncoupled from the torsion, and it arises because the numerical calculation that yields the mobility matrix is ill-conditioned around any resonance, so that small errors in the measured data are greatly magnified. The fact that the measured torsional resonant frequency is slightly lower than the theoretical one is almost certainly due to the inertia loading applied to the beam tip by the transducers — particularly the force gauge.

It should be noted that it is not in fact necessary in this particular case to perform two measurement runs. As the x and θ motions are uncoupled, the two runs should yield responses which are equal in magnitude but opposite in sign, and it is the small experimental differences which have led to the breakthrough of the bending resonances into the torsional mobility, and vice versa. Thus, whenever the motions are known to be uncoupled, it is both quicker and more accurate to only perform a single measurement run.

Conclusions

The tests with the computer-controlled system have demonstrated the feasibility of the single-shaker multi-directional measurement technique developed here. As the measuring system, the shaker, and the transducers are all standard pieces of equipment, it is only necessary to have a range of exciting blocks to suit different structures or components.

Although only the two-directional measurements have been fully automated in this way, there is no reason why the system should not be programmed to deal with the three-directional case. This would entail saving the results from two previous runs before performing the processing during run 3. Even if there were only a single tape reader available, one could still read in the run 1 data during run 2, and then produce a new tape containing both the run 1 and the run 2 data, ready for use in run 3.

Further discussion and conclusions relating to multi-directional measurements and their use in structural analysis are given in Chapter 7.

CHAPTER 5MULTI-DIRECTIONAL MEASUREMENTS WITH A TWIN SHAKERIntroduction

The multi-directional measurement technique outlined in the previous chapter makes use of a single shaker to provide either two or three different conditions of excitation, and the responses to these separate excitations are then combined to give the required point mobility matrix. In the case of the $x-\theta$ measurements described in Section 4.5, a force F was first applied to one end of the exciting block, and then to the other end. Ignoring the effect of block inertia, the response of the structure to a force $F_x = 2F$ or to a couple $M_\theta = 2Fe$ was obtained by suitably superposing the responses to the separate inputs. A logical alternative to this numerical superposition is to actually apply the two forces simultaneously using a twin-shaker unit: this comprises a matched pair of small shakers mounted in a frame and connected electrically in series, so that each takes the same current and hence gives nominally the same force. The two shakers are used to drive opposite ends of the block, and they may run in phase to apply a force F_x or in anti-phase to apply a couple M_θ . The purity of the force or couple depends upon the matching of the shakers, and it is also affected by the dynamics of the system under test.

The measurement technique currently used by Smith^{(11)*} also employs a twin shaker, but differs from that described here in that he takes no force measurements explicitly. Instead, he considers the complete shaker/exciting-block system as a multi-directional vibration source, which in accordance with Thévenin's theorem⁽²³⁾ must comprise a force generator in parallel with an internal impedance⁺. The latter is effectively the rigid-body impedance of the exciting block, which is known either from theory or from simple tests, and the properties of the force generator may be determined by measuring the response of the free

* Note that References for Chapters 3 to 7 are listed on Page 185.

+ Smith actually develops his theory in terms of a Norton source, which comprises a velocity generator in series with an internal mobility. However, these two source models are closely related.

exciting block when excited by the pair of shakers. Provided that this free velocity measurement can be made in all directions with sufficient accuracy, one obtains the full multi-directional properties of the force generator. However, in the subsequent development of the technique Smith makes various assumptions to simplify the calibration and the analysis, and in the process he assumes a diagonal free velocity matrix. This is the equivalent of assuming a pure excitation in each of the translational and rotational directions, so the initial generality of the method seems to be sacrificed. Nevertheless, he has obtained some quite reasonable results.

Provided that the structure under test is far less mobile than the exciting block, and that the shakers are fairly well matched, twin-shaker excitation does have the advantage of yielding the mobility data for the x and θ excitations directly, without the need to unscramble the results obtained for excitation in several directions. With the addition of a simple sum/difference unit one is able to plot the required mobilities directly using standard analogue impedance measuring equipment.

However, these directly measured responses do not always represent the true mobility of the structure, and it is sometimes necessary to analyse the results on a computer, just as with the single-shaker method. For instance, if there is strong coupling between the x and θ motions, any impurity in the excitation due to slight mismatching of the shakers may significantly affect the results. As an example, consider a couple excitation with the shaker axes 100 mm apart ($= 2e$) and with 10 % mismatching. If the true $\frac{\dot{\theta}}{F_x}$ and $\frac{\dot{\theta}}{M_\theta}$ mobilities are numerically equal in magnitude, the θ response to the net force $F_x = (F_1 + F_2)$ is as great as the response to the couple $M_\theta = (F_1 - F_2).e$ *. Depending upon their relative phases these may either add together or cancel each other out, so that the measured value of $\frac{\dot{\theta}}{M_\theta}$ may either be 6 dB too high or many dB too low.

* Note that for a couple excitation the force F_2 is 180° out of phase with F_1 . This is why a positive sign is associated with F_2 in the expression for F_x and a negative sign in the expression for M_θ .

When testing quite mobile items the exciting block inertia may have a significant effect upon the measurements, and a full inertia correction may be necessary. This is especially the case with small items, such as a short beam or turbine blade whose length may only be 30 cm or even less. Another problem with such items is that it is not feasible to bring the shaker axes closer than about 75 mm (without constructing special miniature shakers), so the block size cannot be reduced as much as might be desirable. This difficulty does not arise with the single-shaker method.

The measurement of the mobility in a direction along the surface of the test structure is in no way facilitated by the use of a twin shaker, since one can still only apply the excitation to the block at some finite distance above the surface. For full accuracy, the results so obtained must be transformed down to the surface.

Thus, if the full inertia cancellation and response transformation are to be carried out there appears to be only a limited advantage in using the twin shaker, since the measured data still require processing in a computer. The only real advantage lies in the application of quasi-pure forces and couples, which may lead to better results; at least if both force inputs are measured and the data are fully processed.

The twin-shaker technique is therefore presented as an alternative, and not as a replacement for the single-shaker technique. Future experience with these two methods will indicate the applications for which each is preferred.

Tests with Twin Shaker

The shaker unit is shown in Fig. 5.1, and it comprises two Derritron VP2 shakers mounted in an aluminium frame. As the shakers must push on each end of the block, the distance between their centres has been made 100 mm. Owing to their necessarily small size, they are each limited in their force output to about 11 Newtons.

A test has been carried out on the previously considered 1.83 m steel beam using this twin-shaker unit in conjunction with the Mk 3 exciting block. As before, the beam was turned on its side and excited in the horizontal plane. The results are presented in Figs. 5.2 to 5.6.

The x and θ excitations were carried out with the twin shaker, but the y excitation was performed with a single shaker. In the case of the x and θ excitations both the force inputs to the block were measured, and the ratio of these forces is shown plotted against frequency in the upper graph of Fig. 5.2.

The measured data have not been fully corrected, either for impure x or θ excitation, or for the block inertia. Thus in the case of the x excitation the force F_x is taken to be $(F_1 + F_2)$, whilst for the θ excitation the couple M_θ is taken as $(F_1 - F_2) \cdot e = \left(\frac{F_1 - F_2}{2}\right) \cdot 2e^*$. The force for the y excitation is just $F_y = F_1$, but a couple correction is applied using the results of the θ excitation.

On the response graphs, the points marked with the symbol (\bullet) correspond to no block inertia correction. Those marked with a (x) were obtained on the assumption of a constant force ratio, such that $F_2 = \pm k F_1$, the factor k being obtained from the force ratio graph. These points have only been marked in cases where they differ from the first set. The final set of points, marked with the symbol (\square), corresponds to partially inertia-corrected results. Hence for x excitation the inertia correction has been applied in the x direction only, whilst for θ excitation there is only a correction in the θ direction. For y excitation the correction is in both the y and θ directions.

The various assumptions and the partial correction of the results have been made in order to ascertain the sort of accuracy obtainable from direct x and θ tests, such as might be carried out using analogue equipment.

In addition to these tests on the beam, a comprehensive series of measurements has been carried out on the 135 Kg mass considered in the previous chapter, and these are completely described in Appendix IV (Page 474). The same twin-

* Note that for a force excitation the force F_2 is in phase with F_1 , and for a couple excitation it is in anti-phase with F_1 .

FIG 5.1

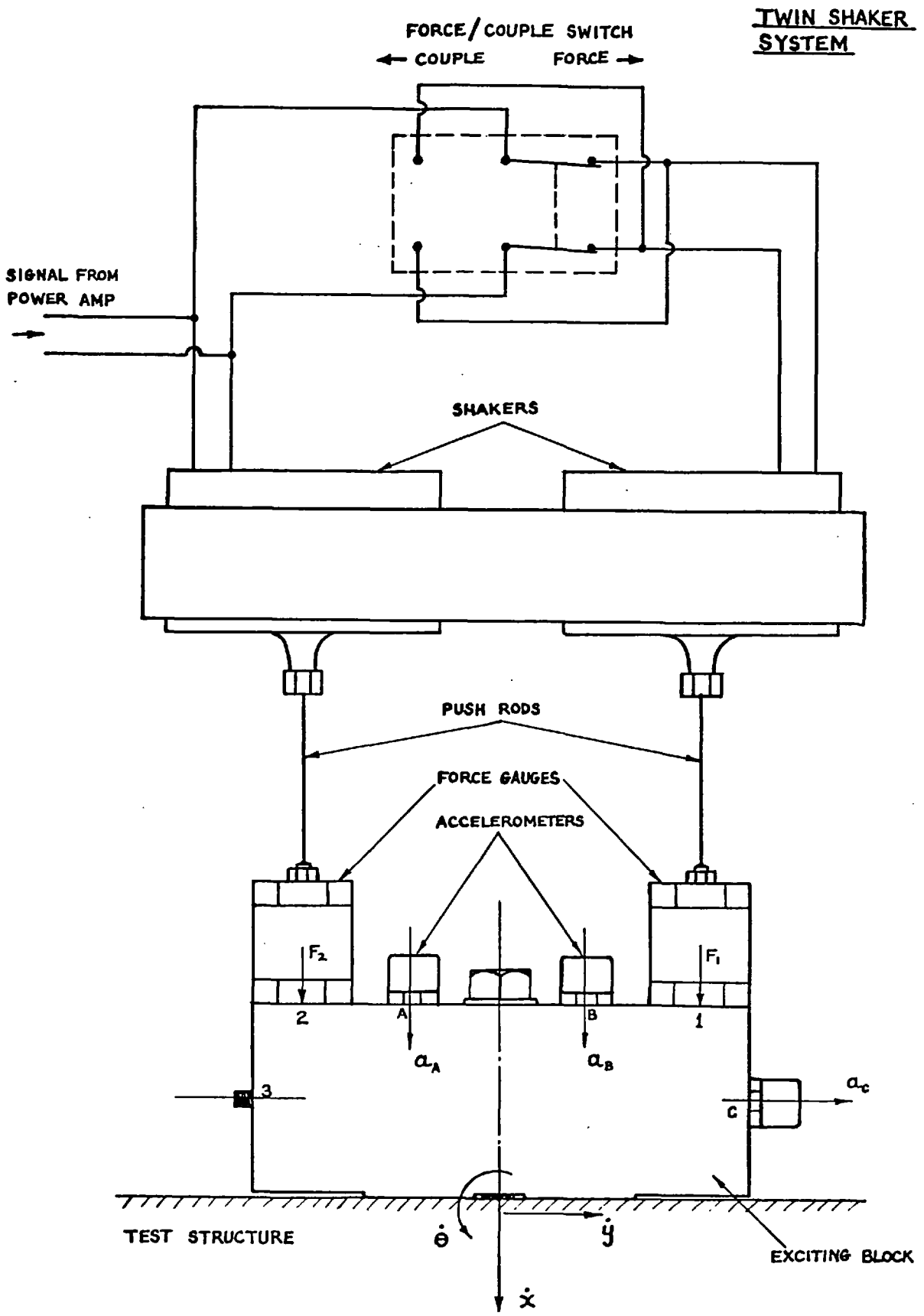
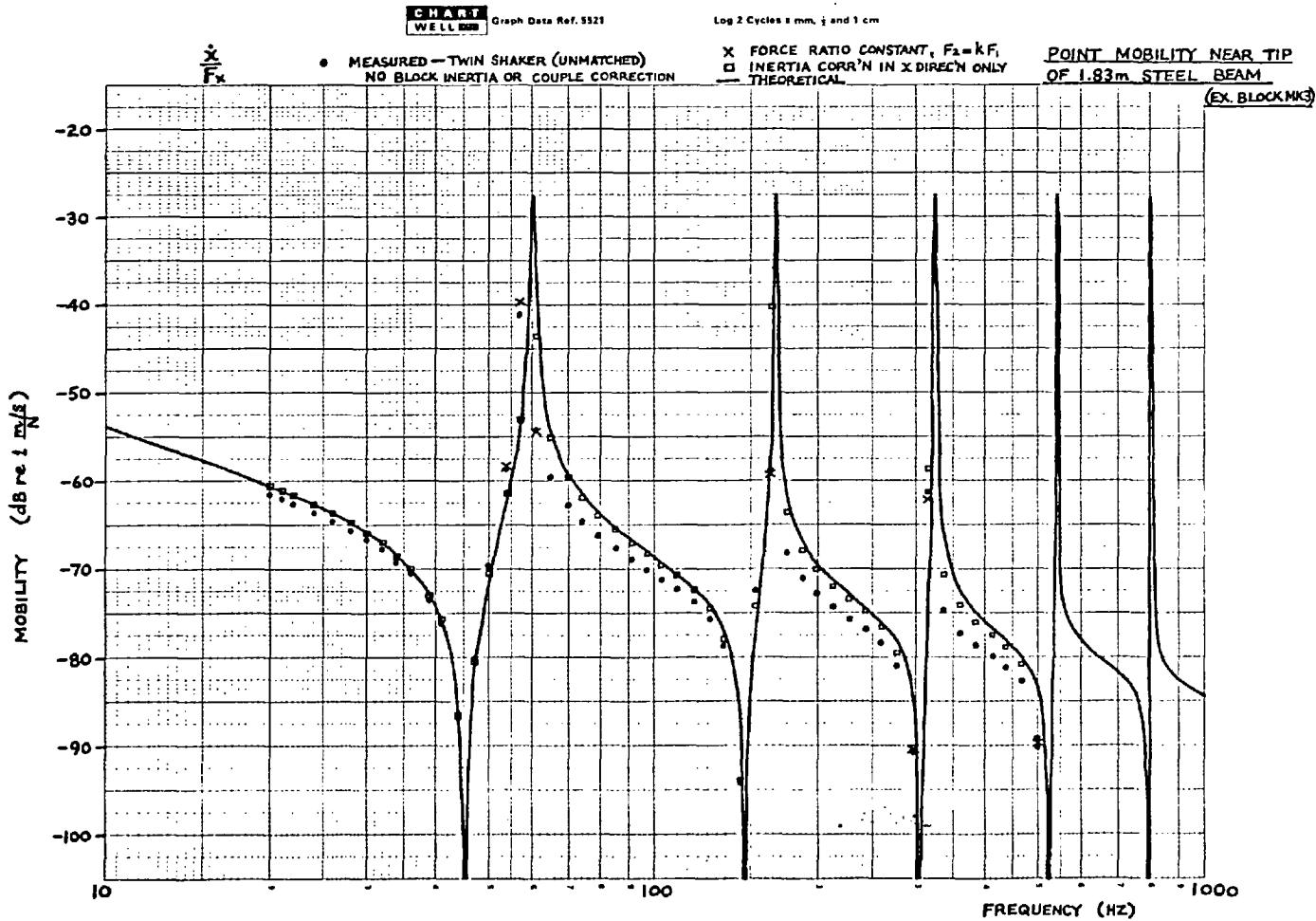
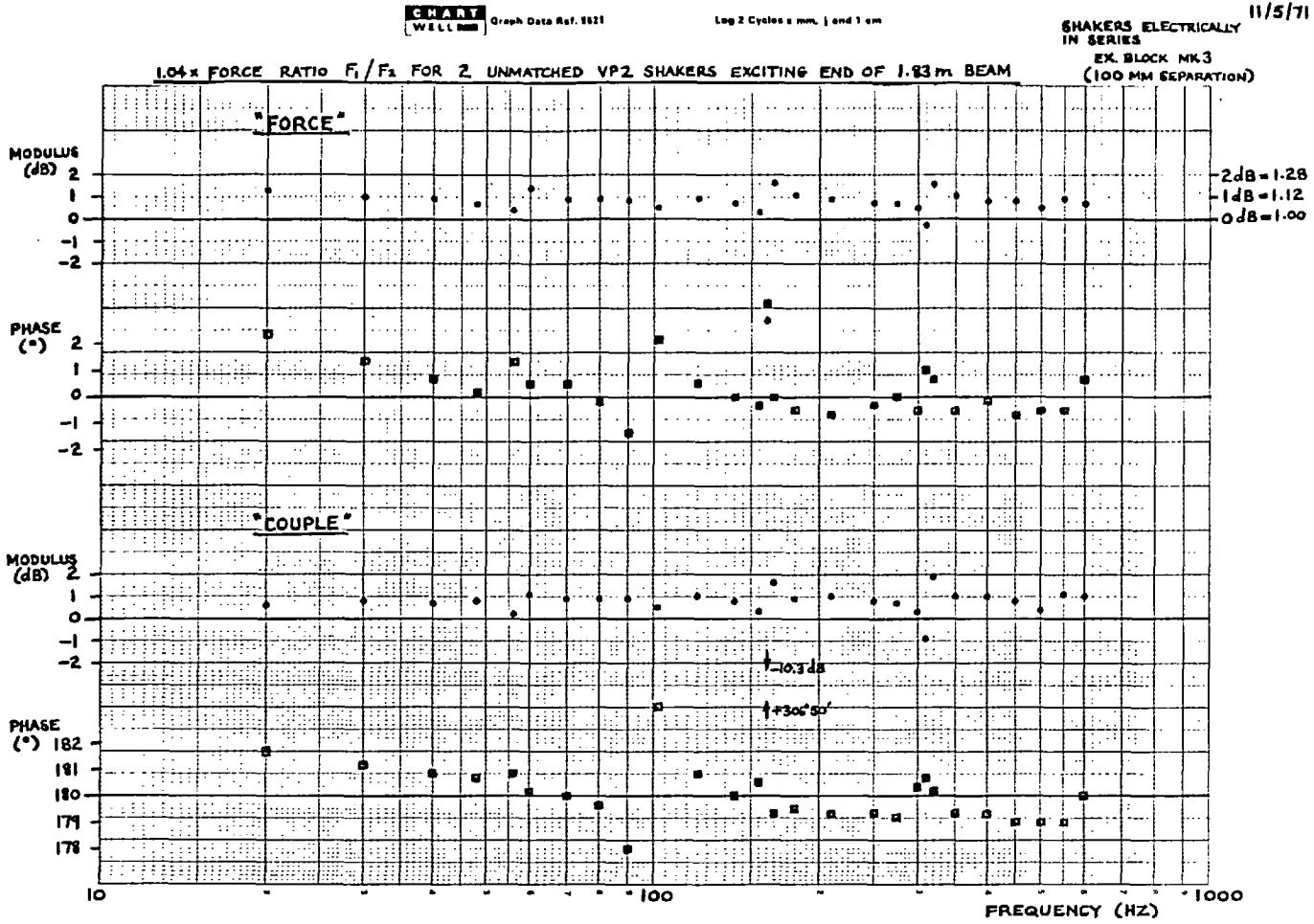


FIG 5.2



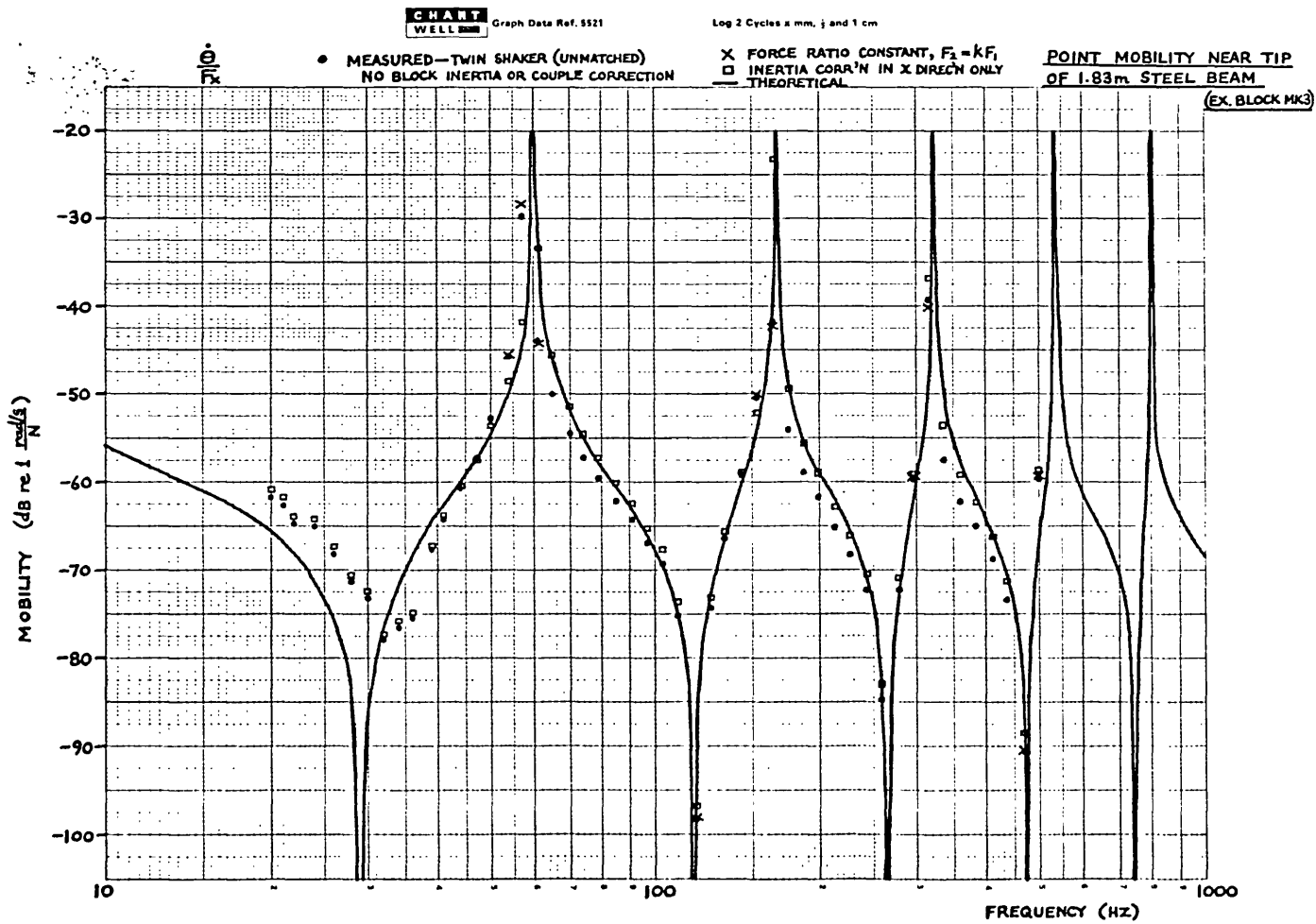
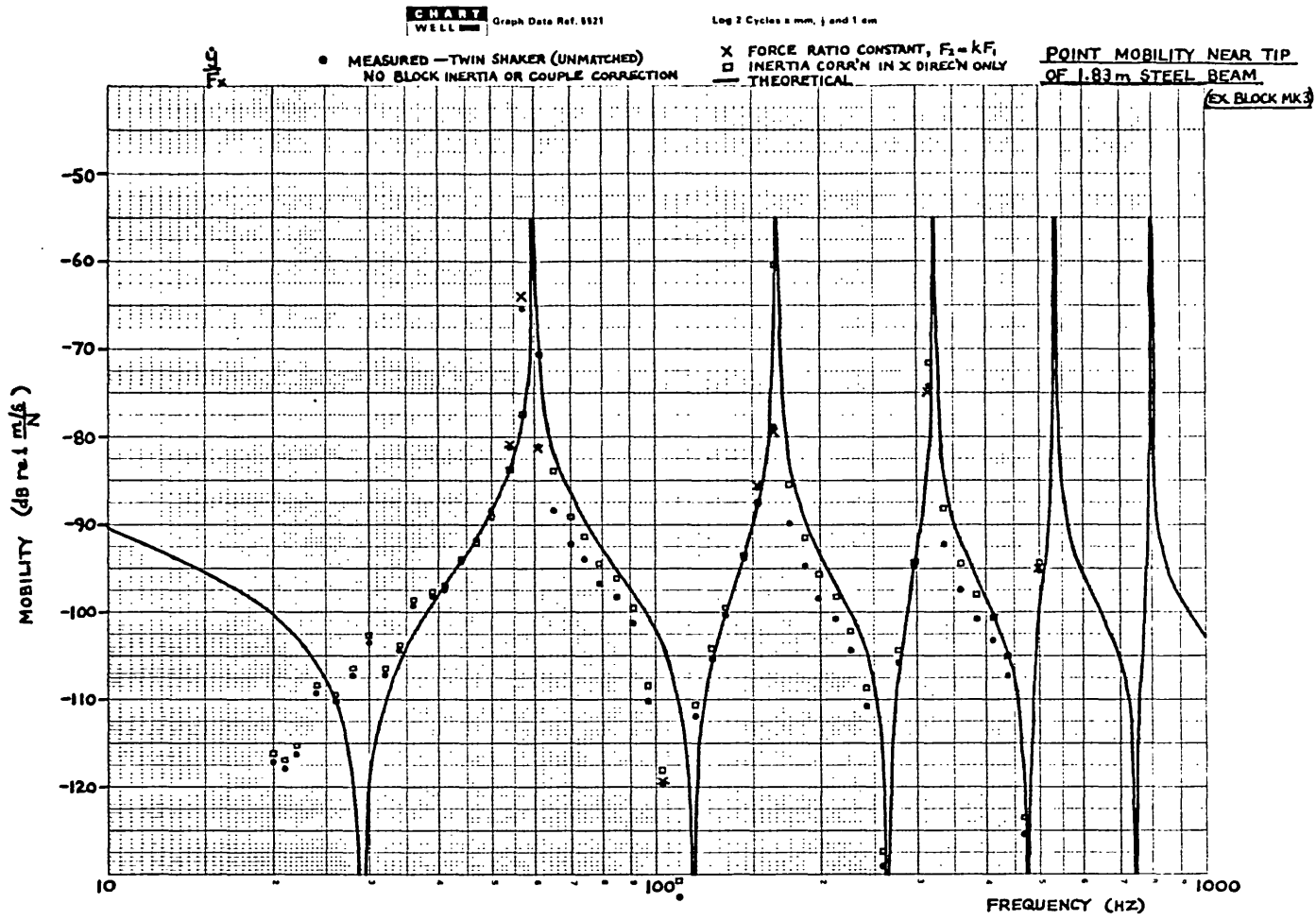


FIG 5.4

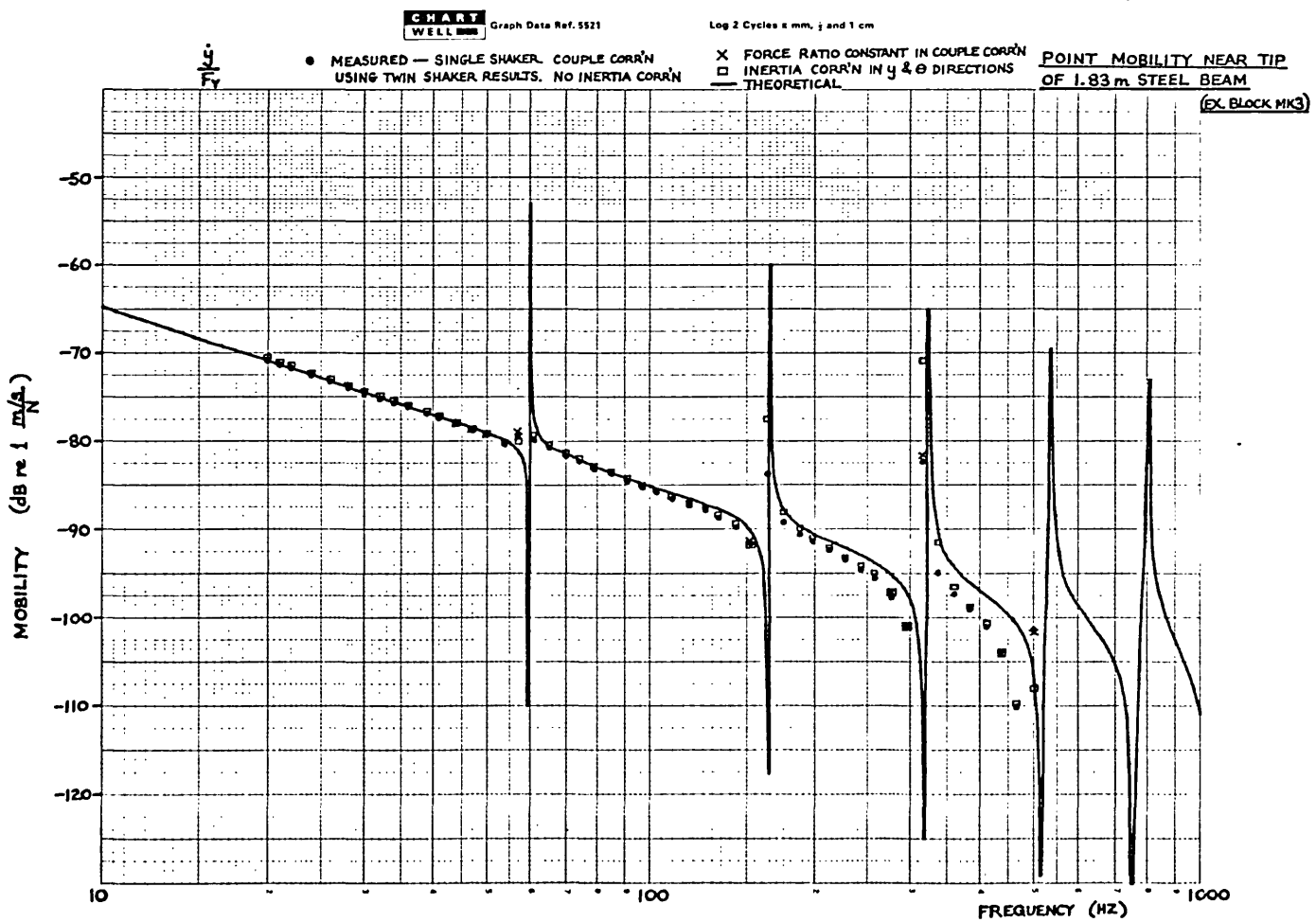
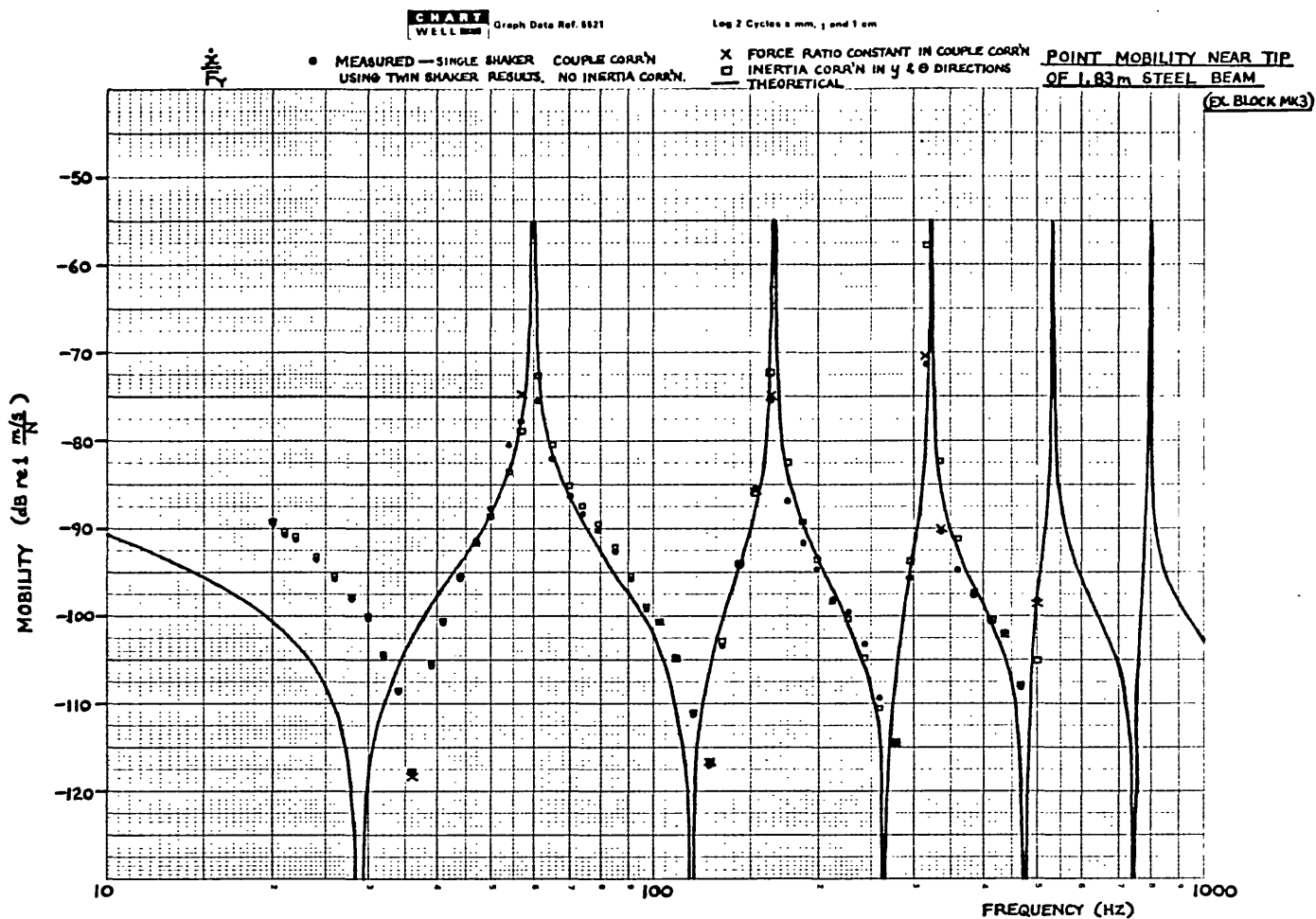


FIG 5.5

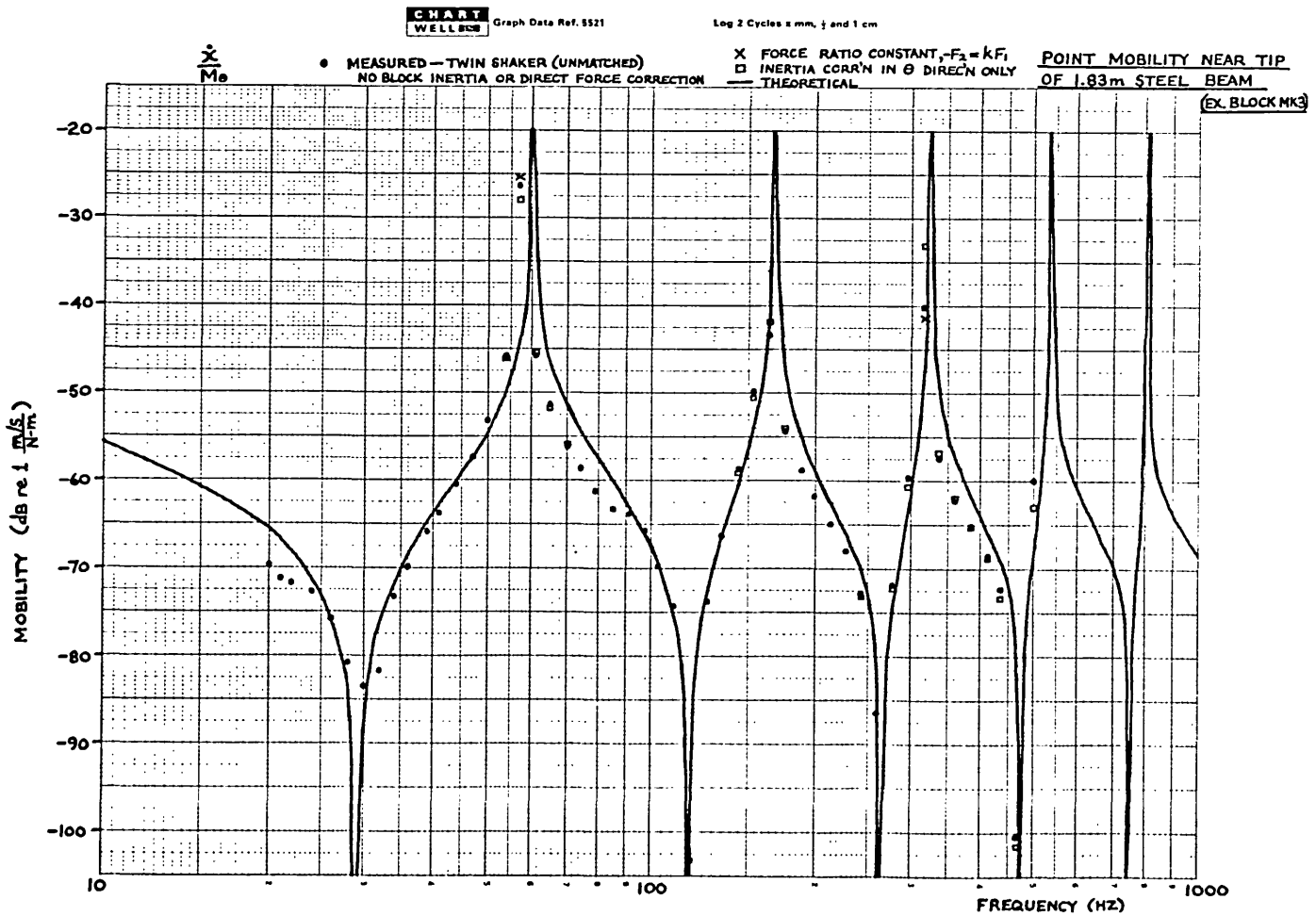
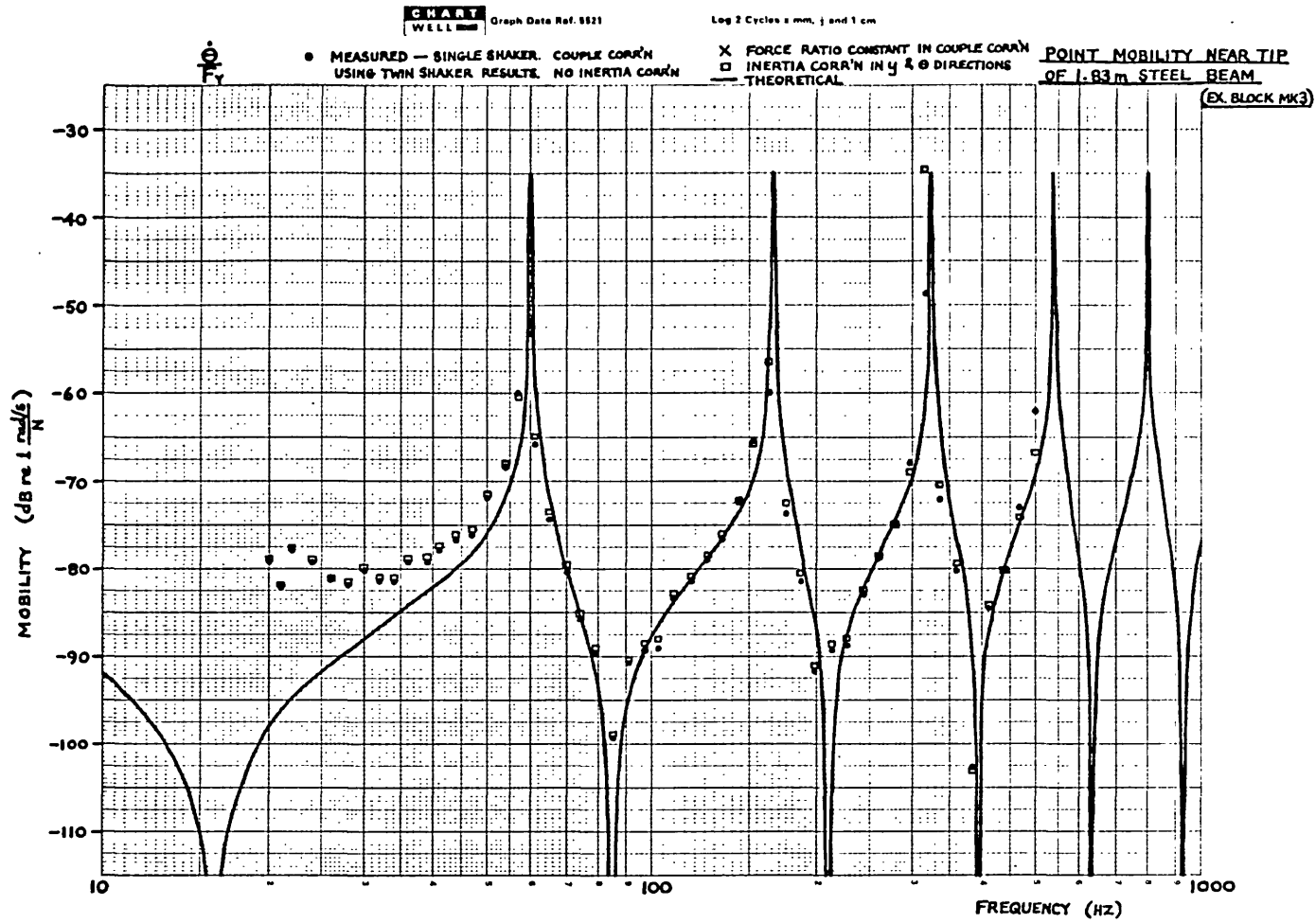
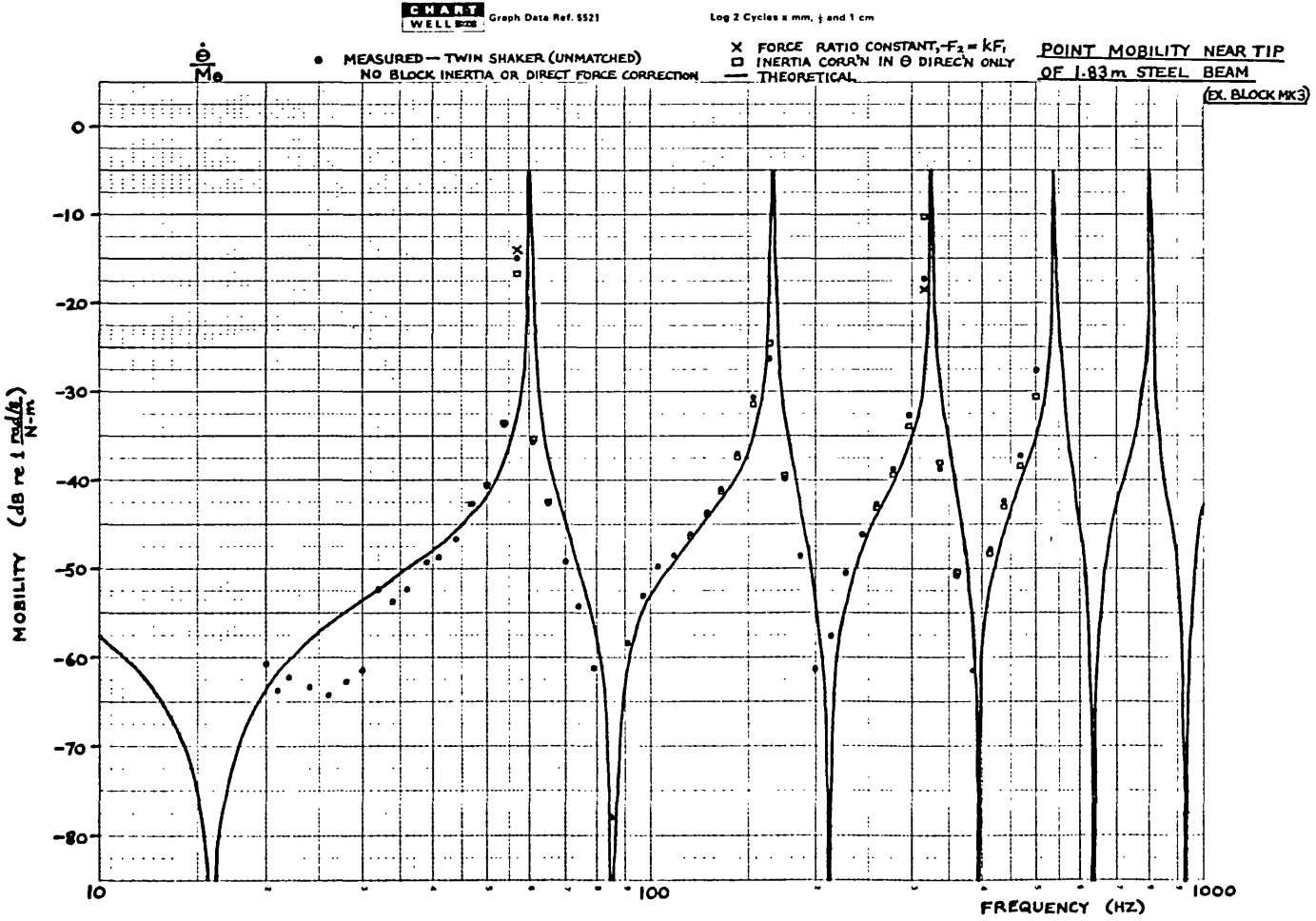
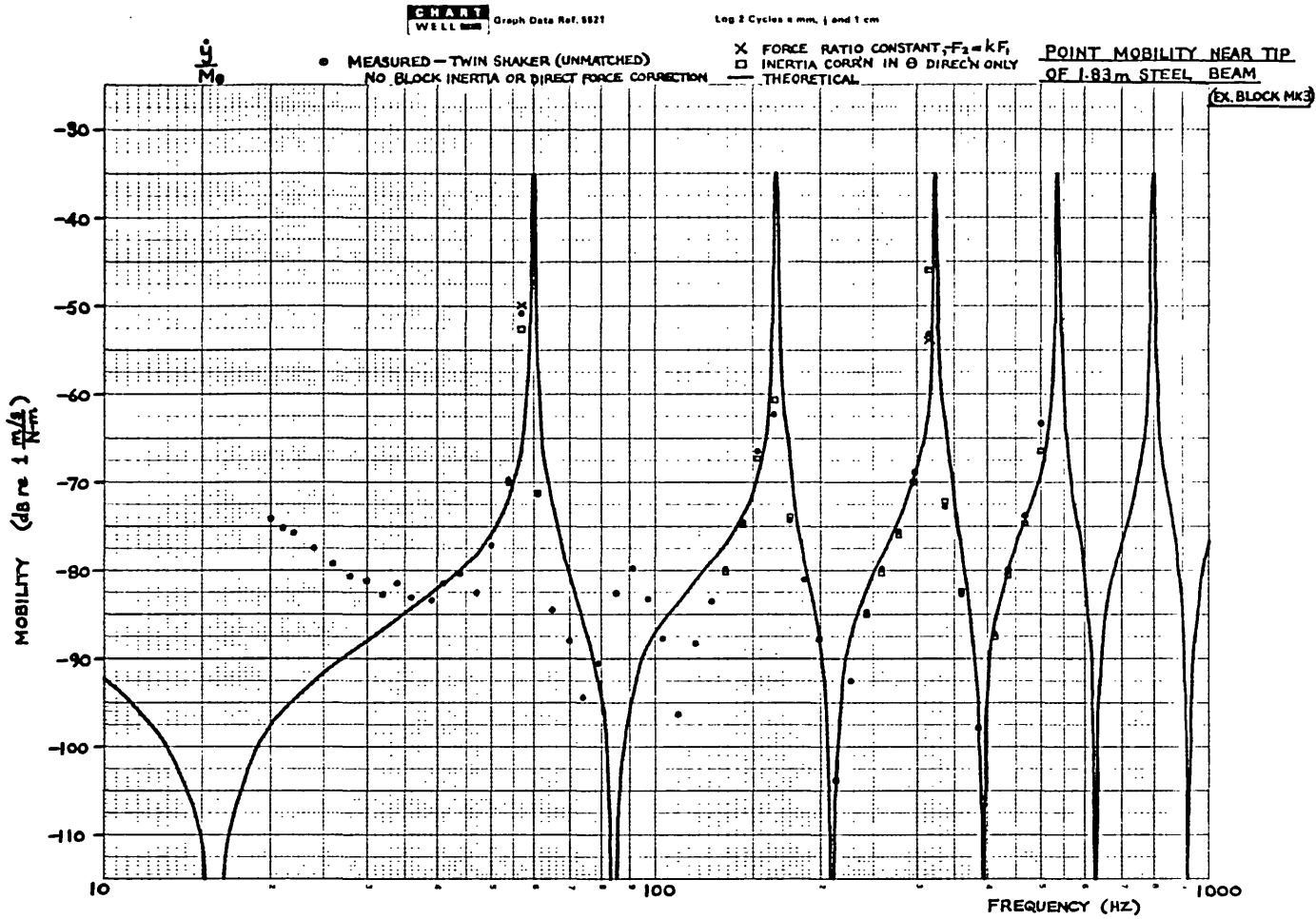


FIG 5.6



shaker unit has been employed in conjunction with a slightly larger exciting block, designated Mk 4, in order to measure 12 selected elements of the full 6×6 inertiance matrix for a point on top of the mass (not the same point as before). The results have not been processed, so they indicate the sort of accuracy one may expect to achieve with direct measurements on a low mobility structure, besides yielding useful information on the effective stiffness of the exciting block and on the effect of accelerometer cross sensitivity. These measurements were carried out in order to assess the validity of some measurements made on a stiff receiver structure (See Part 4, Chapter 14, Section 14.5).

Discussion of Results for Test with Twin Shaker on 1.83 m Steel Beam

It is seen from the upper graph of Fig. 5.2 that with the twin shaker operating either in the force or in the couple mode the ratio of the two input forces to the block is fairly constant. Taking account of the factor 1.04, which is the gain ratio between the two force channels, the resulting mean force ratio is 1.05 for both modes of operation. The scatter about the mean is mostly within ± 0.5 dB, with a phase scatter within $\pm 2^\circ$. The quite large error apparent at 160 Hz is caused by the resonance of the beam influencing the individual force inputs, and if the plot were continuous this sort of behaviour would probably be apparent at each beam resonance. It can be concluded from this graph that even with the unmatched pair of shakers chosen for the experiment the force and couple excitations so produced were almost pure.

There is quite good agreement between the measured results and the theory. However, apart from certain low frequency errors, the single-shaker measurements with exciting block Mk 2 yielded equally good agreement; and even better results have been obtained using a single shaker with the Mk 3 block (These latter results have not been included in Chapter 4, but they may be found in Reference 24). To be strictly correct, the comparison is not perfectly fair, since the twin-shaker results have not been fully corrected either for the block inertia

or for impurity of the excitation. The former is probably the greatest cause of error, and it produces the downward shift in all the resonant frequencies. Associated with the shift in the peaks is a slight distortion of the curves, and this causes errors as large as 3 or 4 dB over quite a wide frequency band above each resonance. It is interesting to note the effects of the partial inertia correction: A correction in the x direction when exciting in the x direction causes a large improvement in the results, and gives very good agreement with theory, whilst corrections in the θ or y directions only, when exciting in these directions, produce hardly any improvement over the uncorrected results. Thus, for this particular system it is apparent that the principal inertia effect is due to motion of the exciting block in the x direction. Whilst this can be corrected directly when exciting in this direction, the same is not true when exciting in the other directions. For instance, when exciting in the θ direction the total effective excitation is the couple input from the shakers, plus the x force due to the block inertia. The response to this combined input cannot be unscrambled on-line, so the results must be recorded and processed by computer after completion of the test.

The results obtained by using the measured value of F_1 and assuming a constant force ratio only differ slightly from those obtained by measuring and using both the forces. Hence it is evidently sufficient to measure only one of the forces and to determine the mean force ratio from a subsidiary test. If the shakers are well matched the ratio may be taken as ± 1 .

Where disagreement between measurement and theory occurs below about 40 Hz, the causes are probably the effects of the suspension ropes, accelerometer cross-sensitivity, and the rather weak and very noisy acceleration signals. These signals were particularly noisy for the case of a couple input, the useful signal being as much as 20 dB down behind the noise.

The only other noteworthy disagreement occurs at around 90 Hz on the $\frac{\dot{y}}{M_\theta}$ curve, where a trough in the response has been replaced by a small peak. This

was observe to be caused by a lateral resonance of one of the push rods on a rather "sloppy" vibrator suspension. Although this resonance was also noted in the case of force excitation, it appears only to have a noticeable effect on the results for the couple.

Conclusions

The results given in this chapter and in Appendix IV show that it is possible to make reasonable direct measurements of both linear and rotational mobilities using a twin-shaker unit, even on very low mobility structures where the small forces generated by the shakers can produce very little motion.

Further discussion and conclusions relating to multi-directional measurements and their use in structural analysis are given in Chapter 7.

CHAPTER 6

COUPLING OF BEAM TO SPRING-SUPPORTED BLOCK

Introduction

The work of the previous two chapters has demonstrated the feasibility of measuring the multi-directional response properties of components, and we now wish to assess whether such measured data may be used directly for predicting the response of an assembly of components. We shall therefore take the mobility data obtained with exciting block Mk 2 (250 mm block) for the beam and the spring-supported block individually, and we shall use these data to predict the mobility of the system formed by bolting the end of the beam to the block (see Fig. 6.1). The component data are combined according to the rules of mobility or impedance coupling, and the procedure for this simple case is illustrated below.

Coupling Procedure and Results

For the beam and the block individually we have the mobility relations

$$\begin{array}{l}
 \text{Beam} \\
 \text{Mobility}
 \end{array}
 \begin{Bmatrix} \dot{x}^a \\ \dot{y}^a \\ \dot{\theta}^a \\ \dot{\xi}^a \end{Bmatrix} = \begin{bmatrix} Y_{11}^a & Y_{12}^a & Y_{13}^a & Y_{14}^a \\ Y_{21}^a & Y_{22}^a & Y_{23}^a & Y_{24}^a \\ Y_{31}^a & Y_{32}^a & Y_{33}^a & Y_{34}^a \\ Y_{41}^a & Y_{42}^a & Y_{43}^a & Y_{44}^a \end{bmatrix} \begin{Bmatrix} F_x^a \\ F_y^a \\ M_\theta^a \\ F_\xi^a \end{Bmatrix}$$

$$\begin{array}{l}
 \text{Block} \\
 \text{Mobility}
 \end{array}
 \begin{Bmatrix} \dot{x}^b \\ \dot{y}^b \\ \dot{\theta}^b \end{Bmatrix} = \begin{bmatrix} Y_{11}^b & Y_{12}^b & Y_{13}^b \\ Y_{21}^b & Y_{22}^b & Y_{23}^b \\ Y_{31}^b & Y_{32}^b & Y_{33}^b \end{bmatrix} \begin{Bmatrix} F_x^b \\ F_y^b \\ M_\theta^b \end{Bmatrix} \quad (6.1)$$

where all the matrix elements are complex numbers, to take account of both modulus and phase.

By inverting the mobility matrices we obtain the impedance relations

$$\begin{array}{l} \text{Beam} \\ \text{Impedance} \end{array} \begin{bmatrix} F_x^a \\ F_Y^a \\ M_\theta^a \\ F_\xi^a \end{bmatrix} = \begin{bmatrix} Z_{11}^a & Z_{12}^a & Z_{13}^a & Z_{14}^a \\ Z_{21}^a & Z_{22}^a & Z_{23}^a & Z_{24}^a \\ Z_{31}^a & Z_{32}^a & Z_{33}^a & Z_{34}^a \\ Z_{41}^a & Z_{42}^a & Z_{43}^a & Z_{44}^a \end{bmatrix} \begin{bmatrix} \dot{x}^a \\ \dot{y}^a \\ \dot{\theta}^a \\ \dot{\xi}^a \end{bmatrix} \\ \\ \begin{array}{l} \text{Block} \\ \text{Impedance} \end{array} \begin{bmatrix} F_x^b \\ F_Y^b \\ M_\theta^b \end{bmatrix} = \begin{bmatrix} Z_{11}^b & Z_{12}^b & Z_{13}^b \\ Z_{21}^b & Z_{22}^b & Z_{23}^b \\ Z_{31}^b & Z_{32}^b & Z_{33}^b \end{bmatrix} \begin{bmatrix} \dot{x}^b \\ \dot{y}^b \\ \dot{\theta}^b \end{bmatrix} \quad (6.2)$$

The components may now be joined together by combining these impedance data in such a way as to satisfy the rules of force equilibrium and displacement compatibility at the coupling point. This results in the following matrix equation for the response of the coupled system:

$$\begin{bmatrix} \dot{x} \\ \dot{y} \\ \dot{\theta} \\ \dot{\xi} \end{bmatrix} = \begin{bmatrix} Z_{11}^a + Z_{11}^b & Z_{12}^a + Z_{12}^b & Z_{13}^a + Z_{13}^b & Z_{14}^a \\ Z_{21}^a + Z_{21}^b & Z_{22}^a + Z_{22}^b & Z_{23}^a + Z_{23}^b & Z_{24}^a \\ Z_{31}^a + Z_{31}^b & Z_{32}^a + Z_{32}^b & Z_{33}^a + Z_{33}^b & Z_{34}^a \\ Z_{41}^a & Z_{42}^a & Z_{43}^a & Z_{44}^a \end{bmatrix}^{-1} \begin{bmatrix} F_x \\ F_Y \\ M_\theta \\ F_\xi \end{bmatrix} \quad (6.3)$$

where $\dot{x} = \dot{x}^a = \dot{x}^b$, $\dot{y} = \dot{y}^a = \dot{y}^b$, $\dot{\theta} = \dot{\theta}^a = \dot{\theta}^b$ and F_x , F_Y , M_θ and F_ξ are externally applied forces.

Apart from the fact that we are here working with velocities rather than displacements, this impedance coupling technique is exactly the same as the dynamic stiffness coupling explained in Chapter 2 (Part 1). In fact, the computer program COUPLE1 could be used for this problem.

As an alternative to the above, one may employ the "General Impedance Method" used by Klosterman^{(25)(26)(27)*}. This permits the formation of a system dynamic matrix directly in terms of subsystem data which are either in mobility or impedance form. Hence, in the present case we may form the system matrix directly in terms of the mobility matrices (6.1), without the need for an initial inversion to obtain impedances. Using this method, the response of the coupled system is given by the following matrix equation:

$$\begin{bmatrix} \dot{x} \\ \dot{y} \\ \dot{\theta} \\ \dot{\xi} \\ F_x^b \\ F_y^b \\ M_\theta^b \end{bmatrix} = \begin{bmatrix} 1 & 0 & 0 & 0 & Y_{11}^a & Y_{12}^a & Y_{13}^a \\ 0 & 1 & 0 & 0 & Y_{21}^a & Y_{22}^a & Y_{23}^a \\ 0 & 0 & 1 & 0 & Y_{31}^a & Y_{32}^a & Y_{33}^a \\ 0 & 0 & 0 & 1 & Y_{41}^a & Y_{42}^a & Y_{43}^a \\ 1 & 0 & 0 & 0 & -Y_{11}^b & -Y_{12}^b & -Y_{13}^b \\ 0 & 1 & 0 & 0 & -Y_{21}^b & -Y_{22}^b & -Y_{23}^b \\ 0 & 0 & 1 & 0 & -Y_{31}^b & -Y_{32}^b & -Y_{33}^b \end{bmatrix}^{-1} \begin{bmatrix} Y_{11}^a & Y_{12}^a & Y_{13}^a & Y_{14}^a \\ Y_{21}^a & Y_{22}^a & Y_{23}^a & Y_{24}^a \\ Y_{31}^a & Y_{32}^a & Y_{33}^a & Y_{34}^a \\ Y_{41}^a & Y_{42}^a & Y_{43}^a & Y_{44}^a \\ 0 & 0 & 0 & 0 \\ 0 & 0 & 0 & 0 \\ 0 & 0 & 0 & 0 \end{bmatrix} \begin{bmatrix} F_x \\ F_y \\ M_\theta \\ F_\xi \end{bmatrix} \quad (6.4)$$

Although it is not necessary to invert the subsystem mobility matrices, the complex system matrix is now 7 x 7 instead of 4 x 4, since the internally transmitted forces F_x^b , F_y^b and M_θ^b are also included in the response vector. This increase in matrix size is unimportant in the present small problem, but it may significantly lengthen the solution time when a large number of co-ordinates are involved.

The choice of technique is largely a matter of personal preference, since they both yield the same results. However, the first approach has been used here. The results of the coupling procedure are shown in Figs. 6.2 to 6.9, where they are compared with both the directly measured and the theoretically predicted responses. In addition to the full coupling procedure using co-ordinates x , y and θ , the process has been repeated using less co-ordinates in order to assess the effect of using incomplete data, such as might be obtained from a standard uni-directional mobility test at a single coupling point.

* Note that References for Chapters 3 to 7 are listed on Page 185.

FIG 6.1

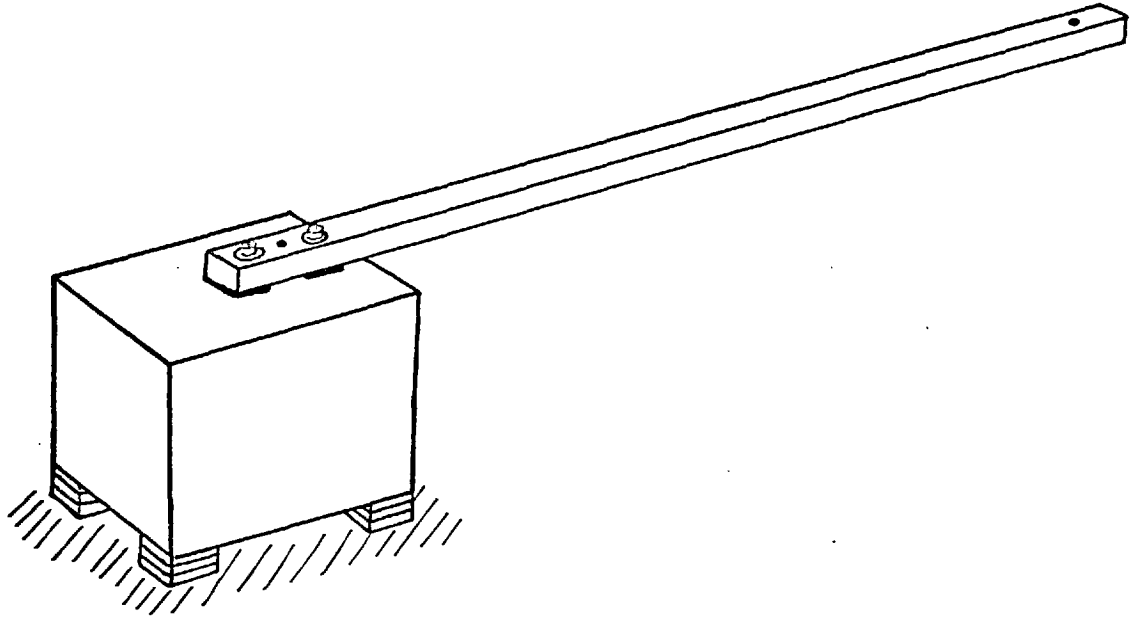
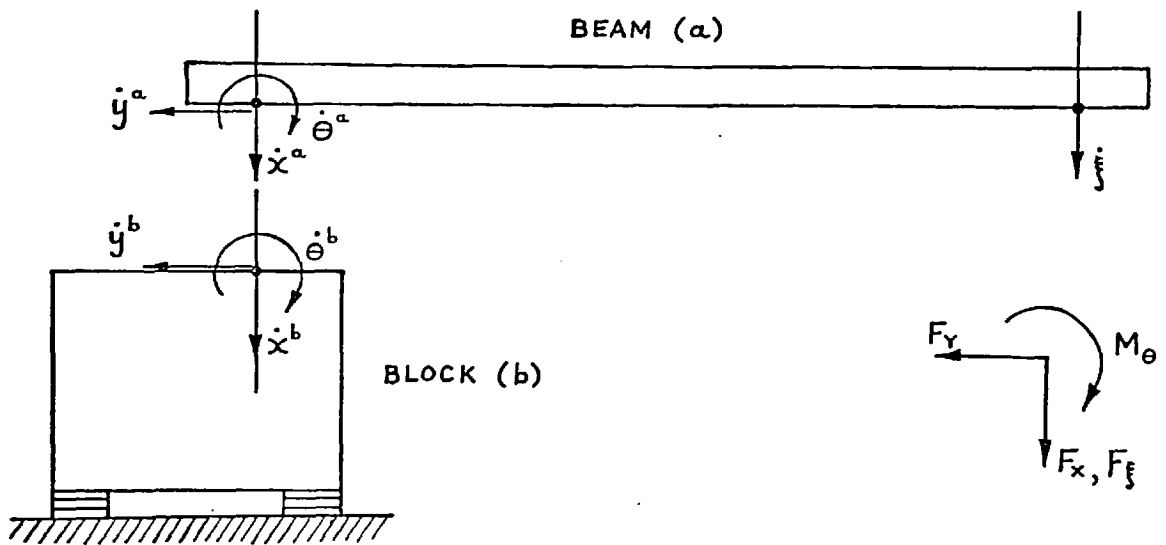
BLOCK AND BEAM ASSEMBLYCO-ORDINATES FOR COUPLING BEAM TO BLOCK

FIG 6.2

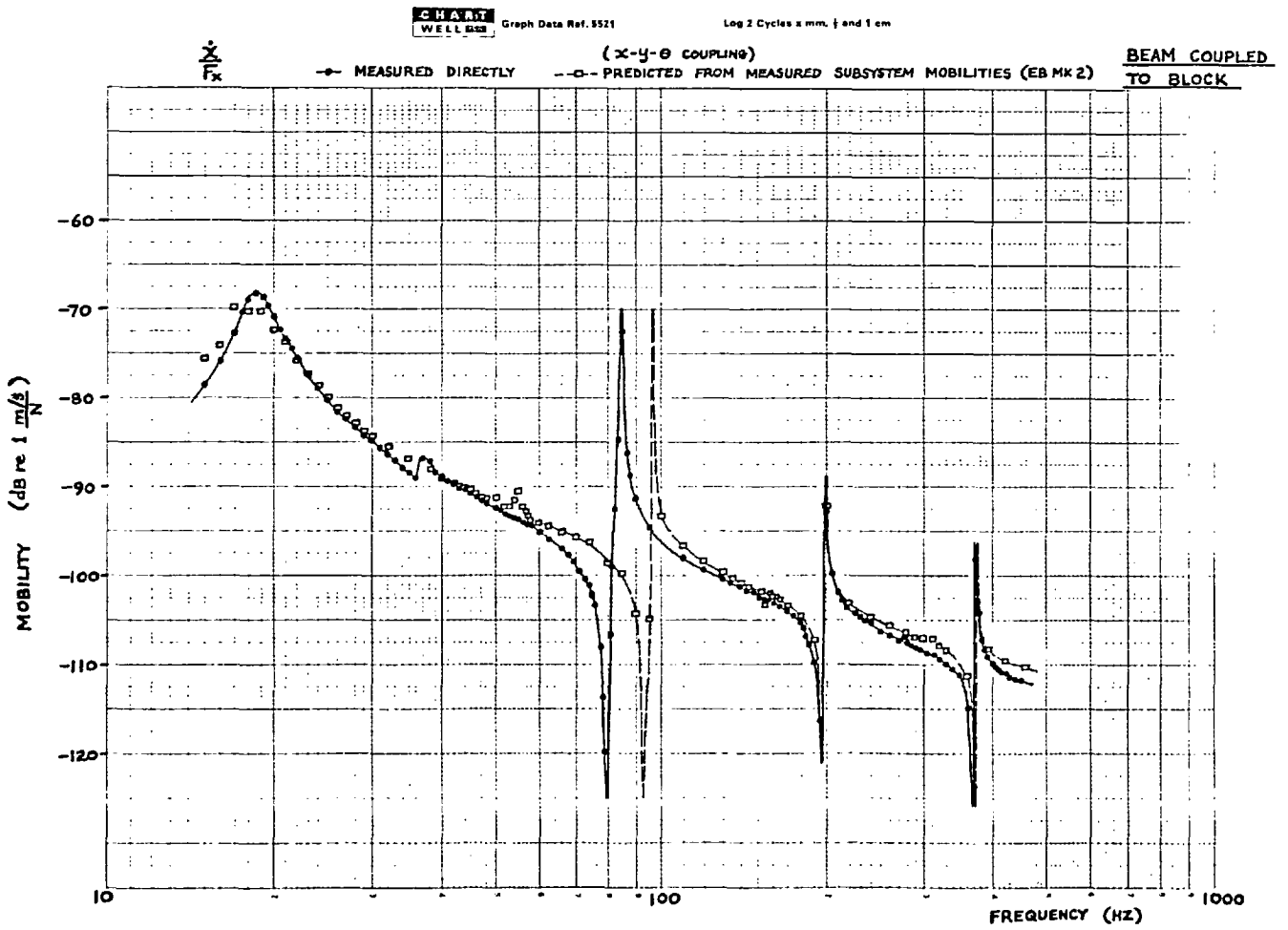
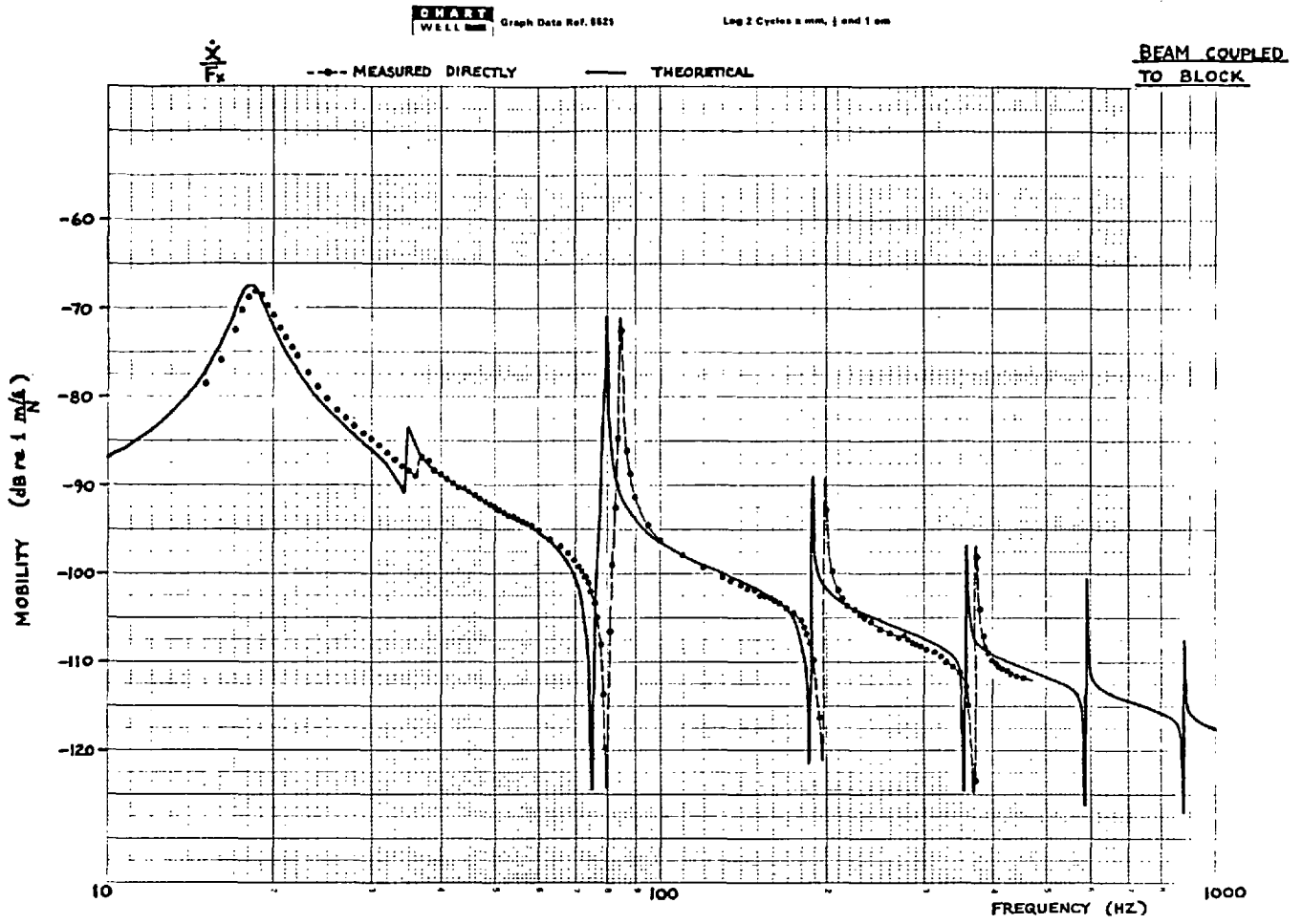


FIG 6.3

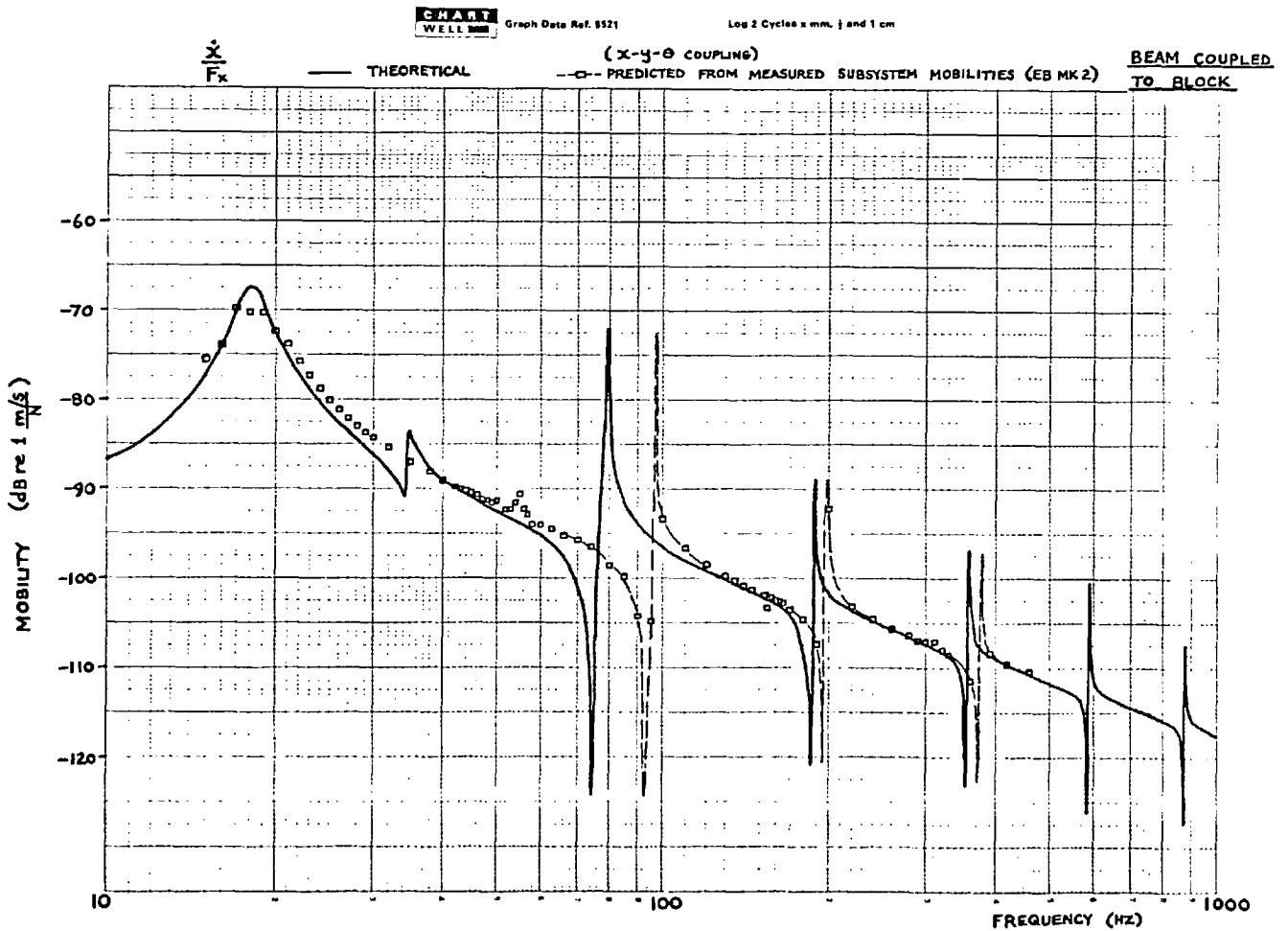
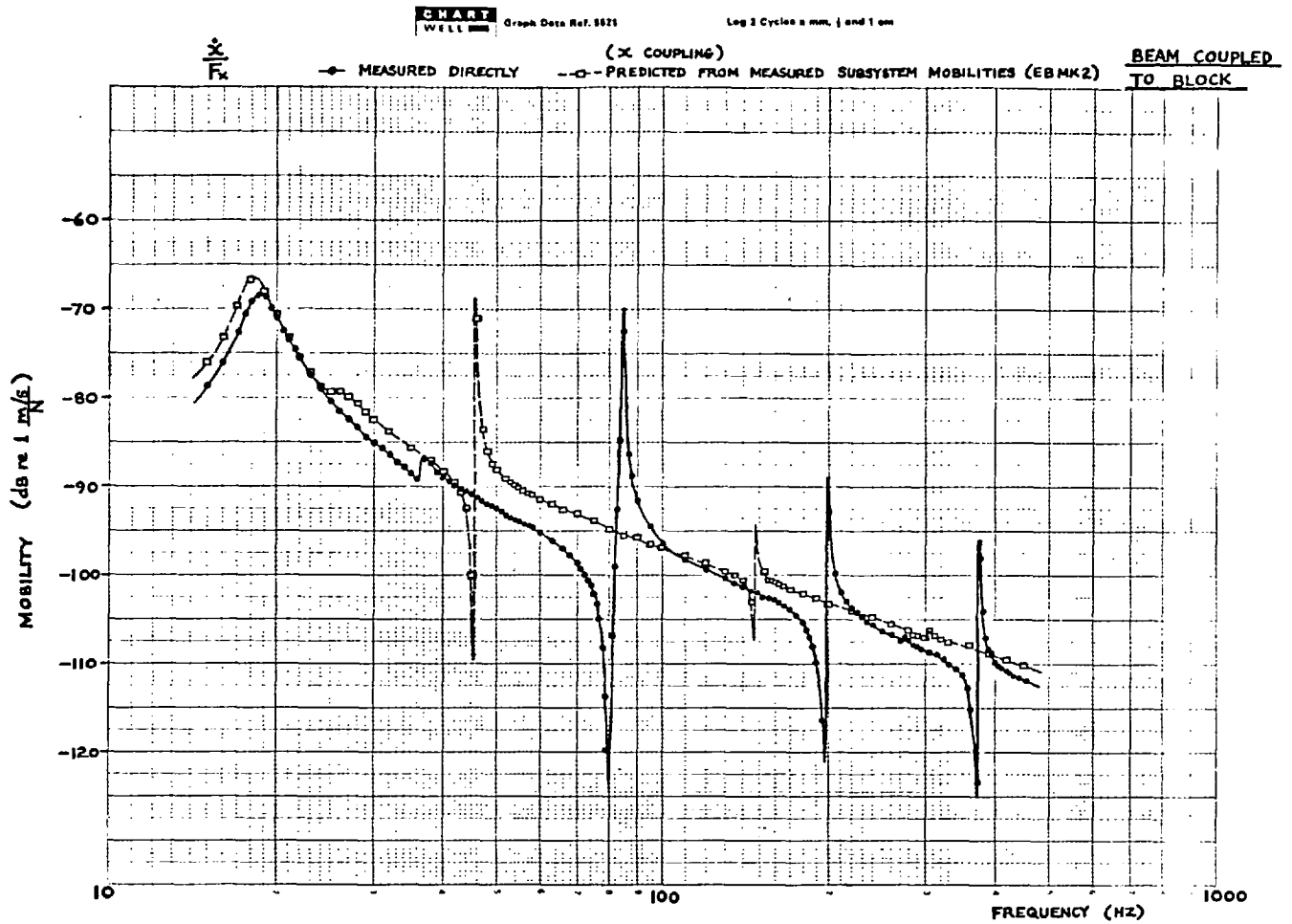


FIG 6.4

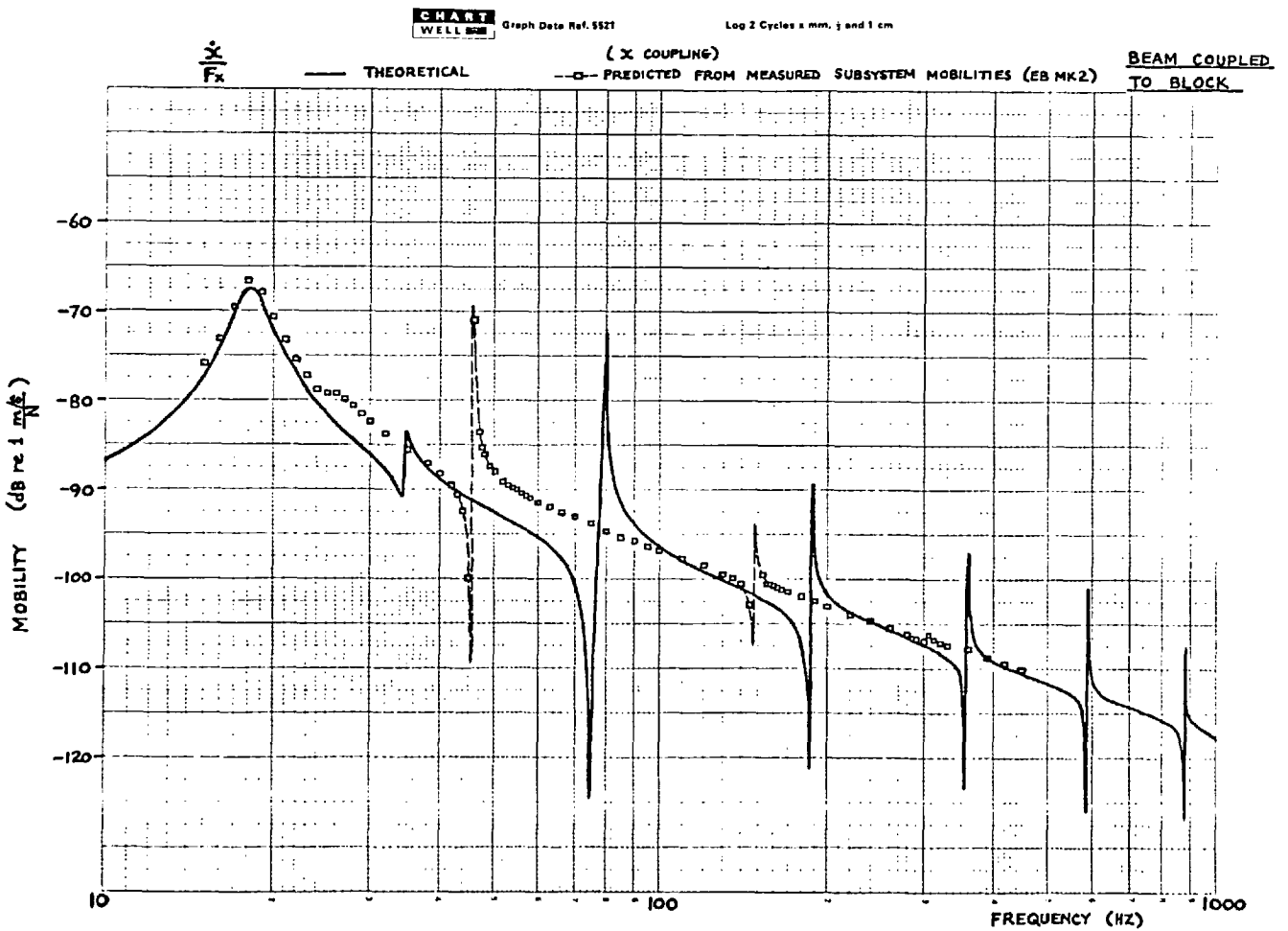
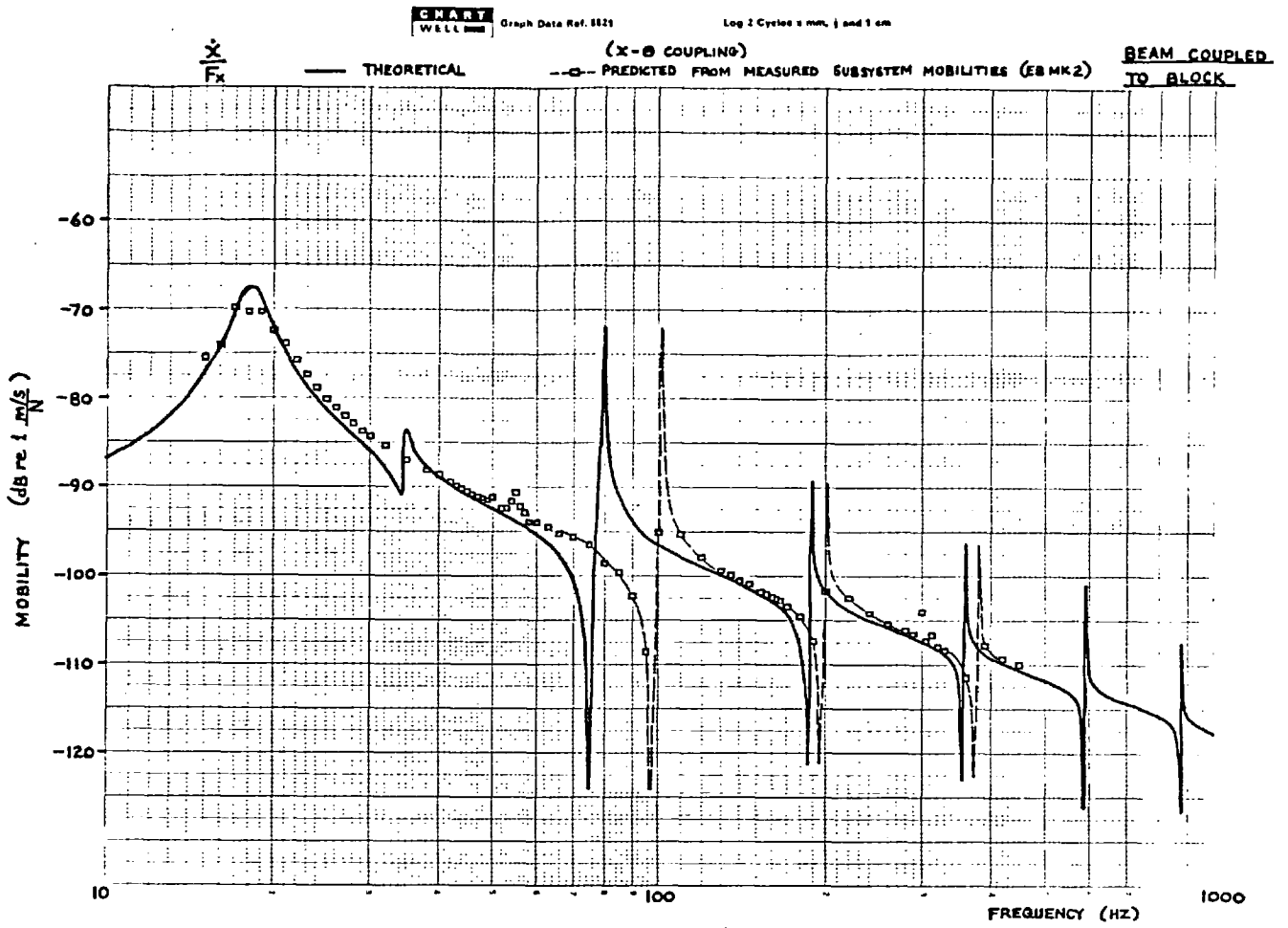
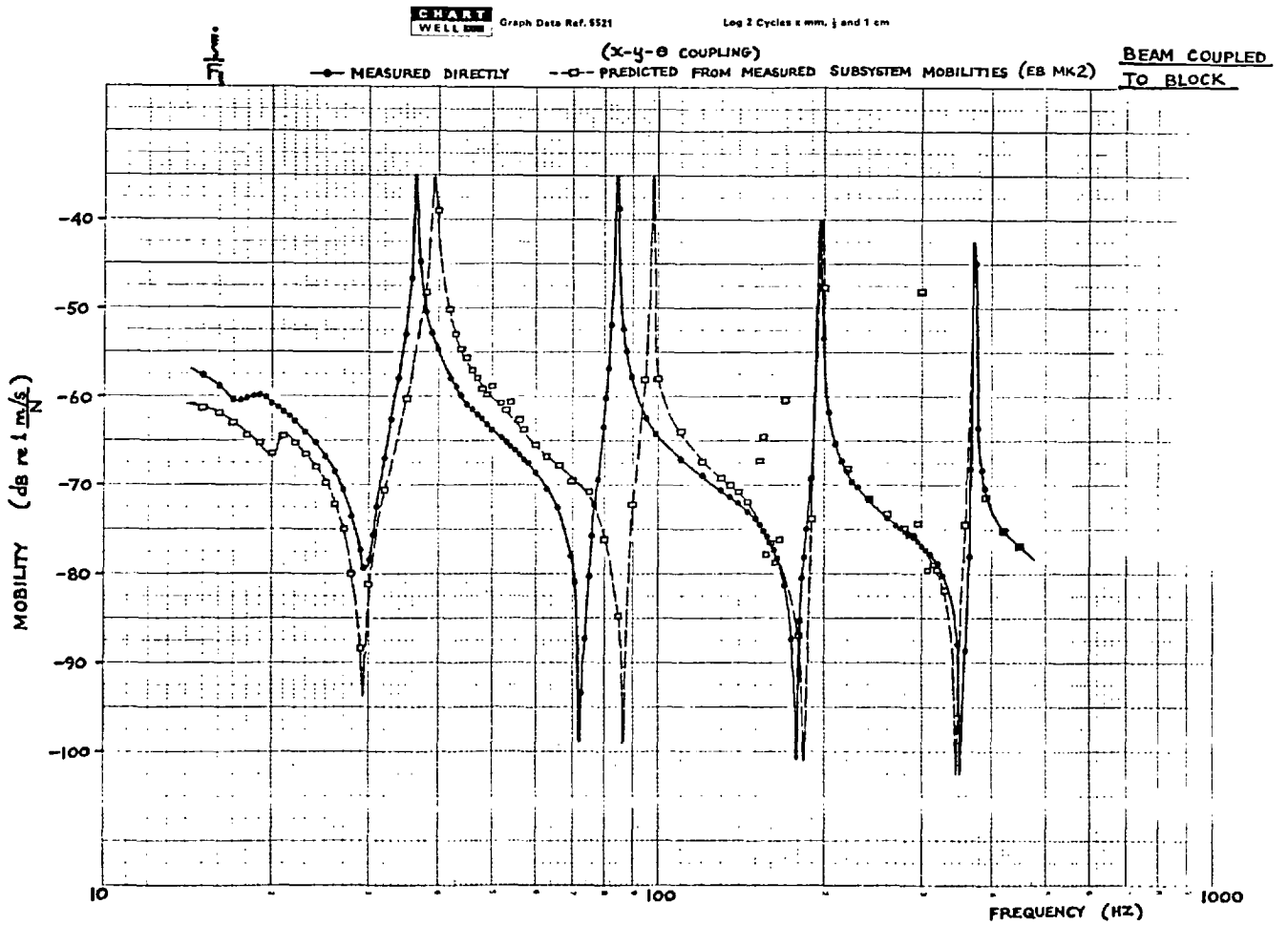
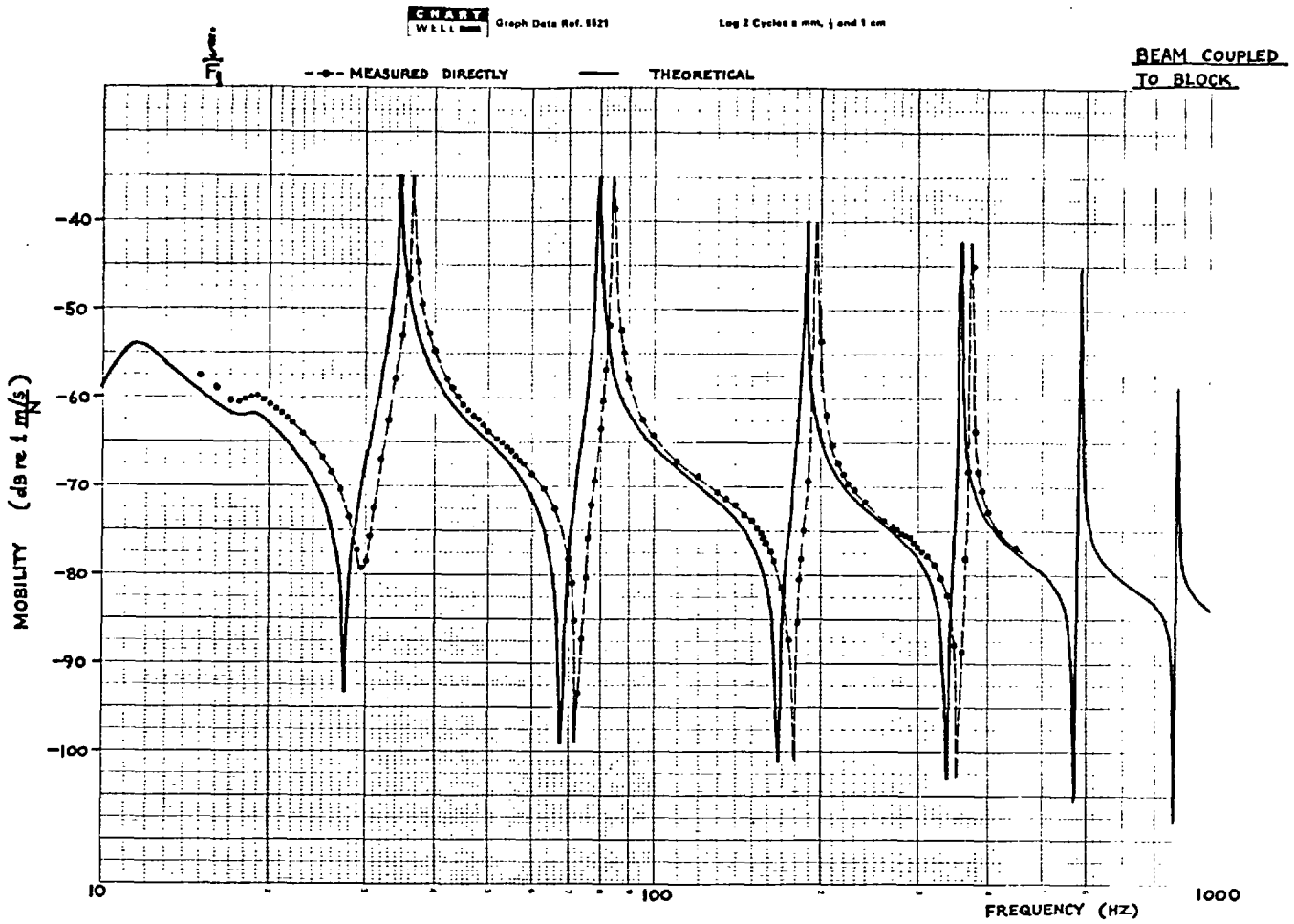


FIG 6.5



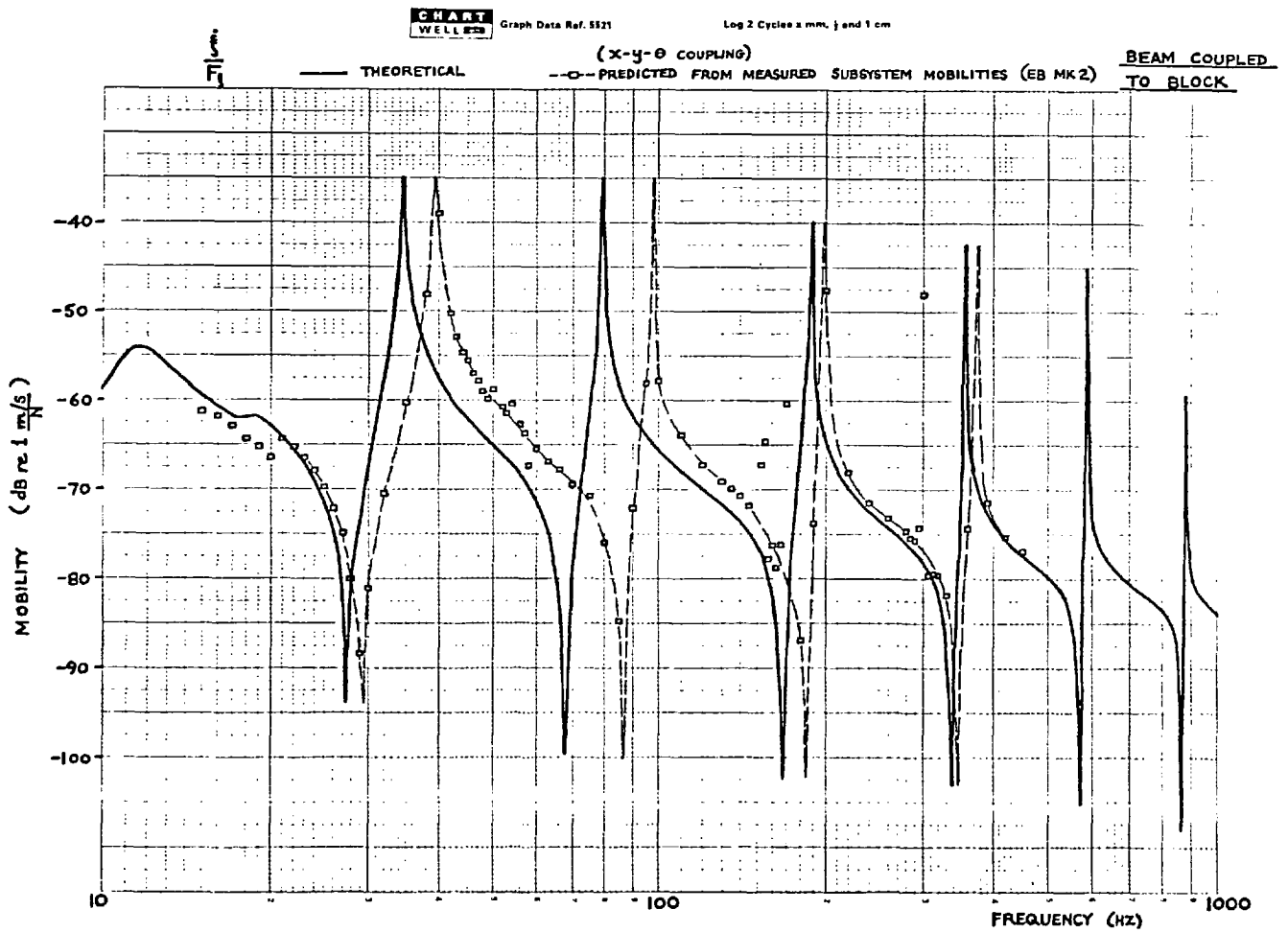
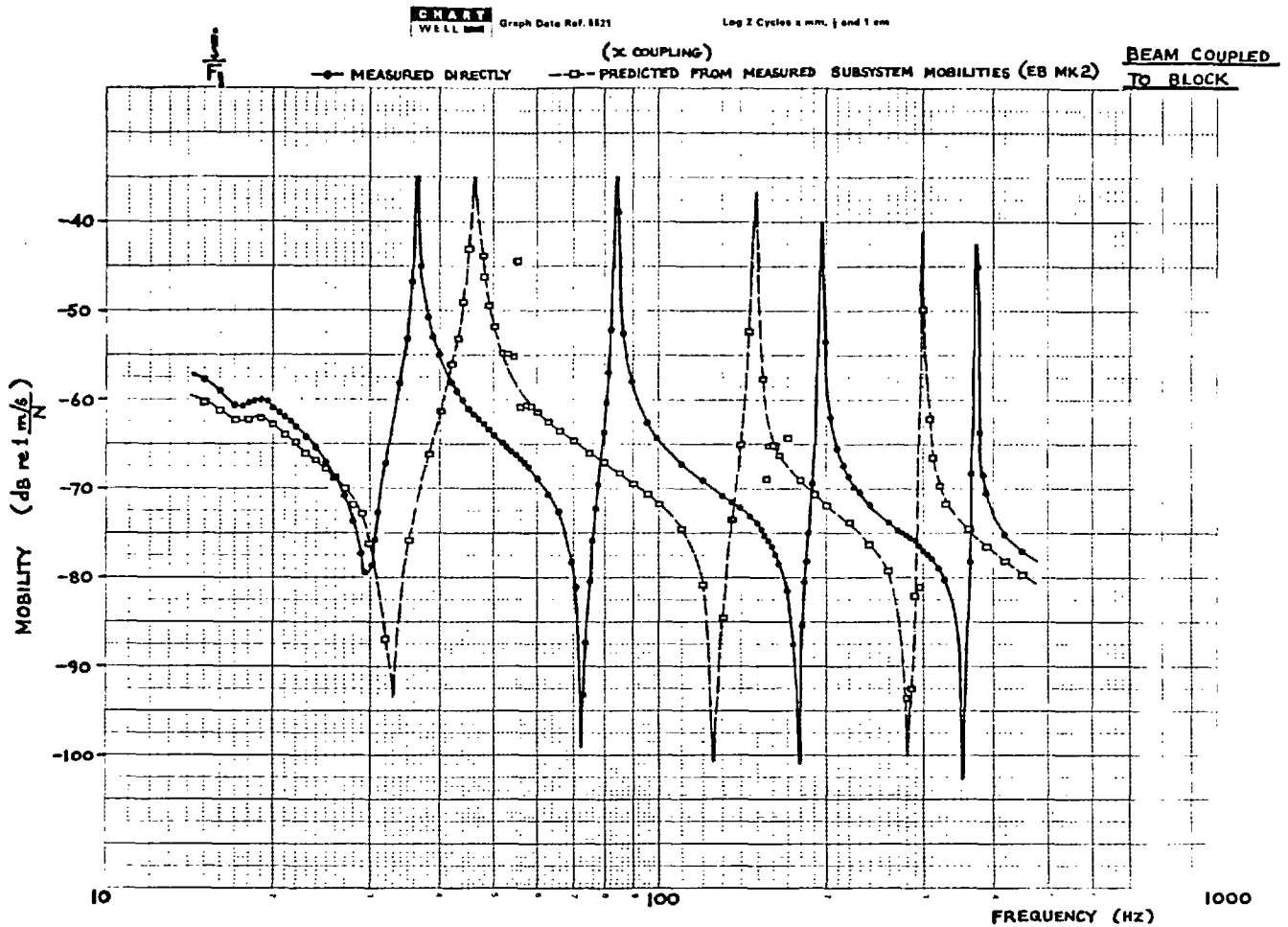


FIG 6.7

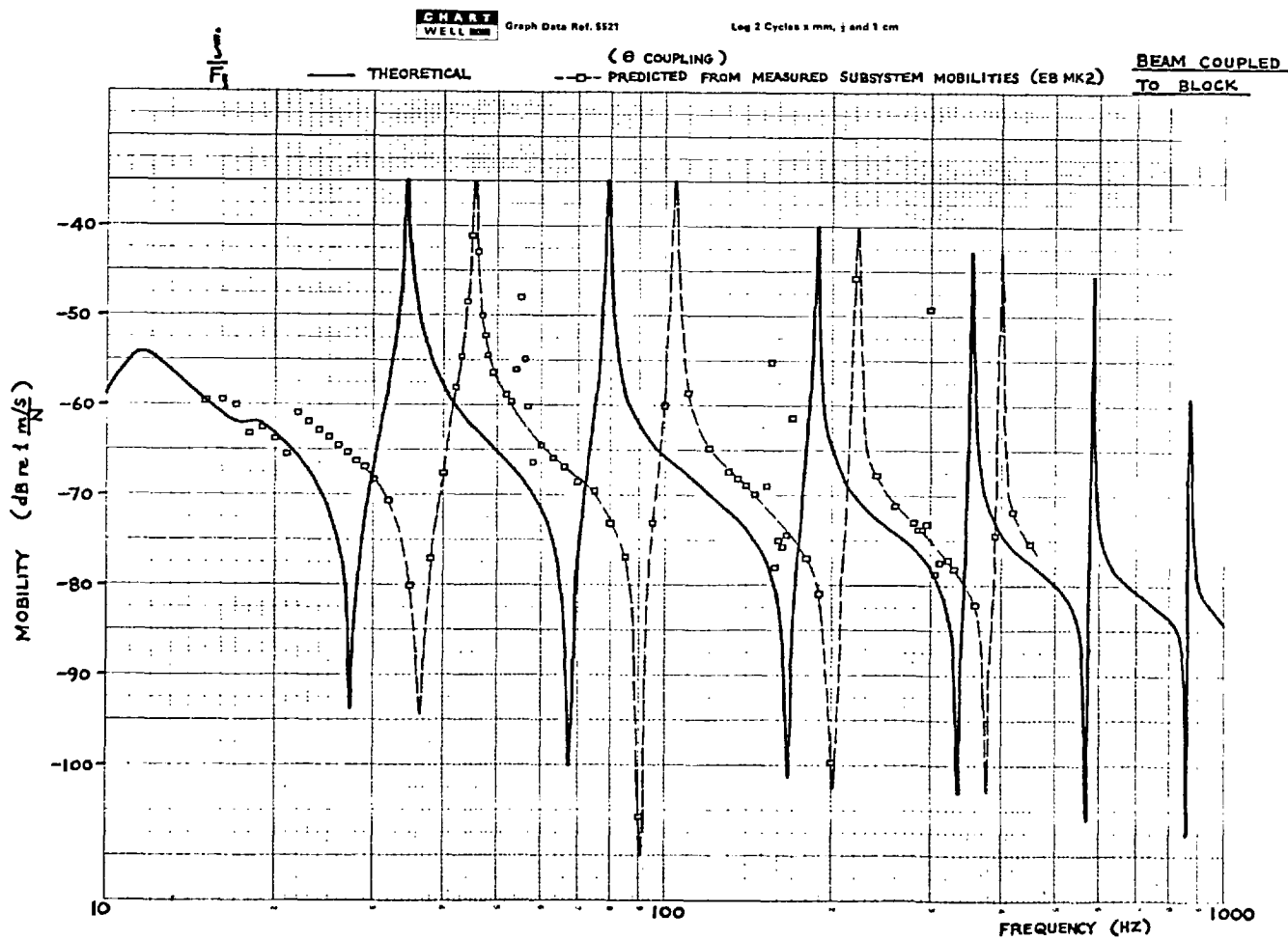
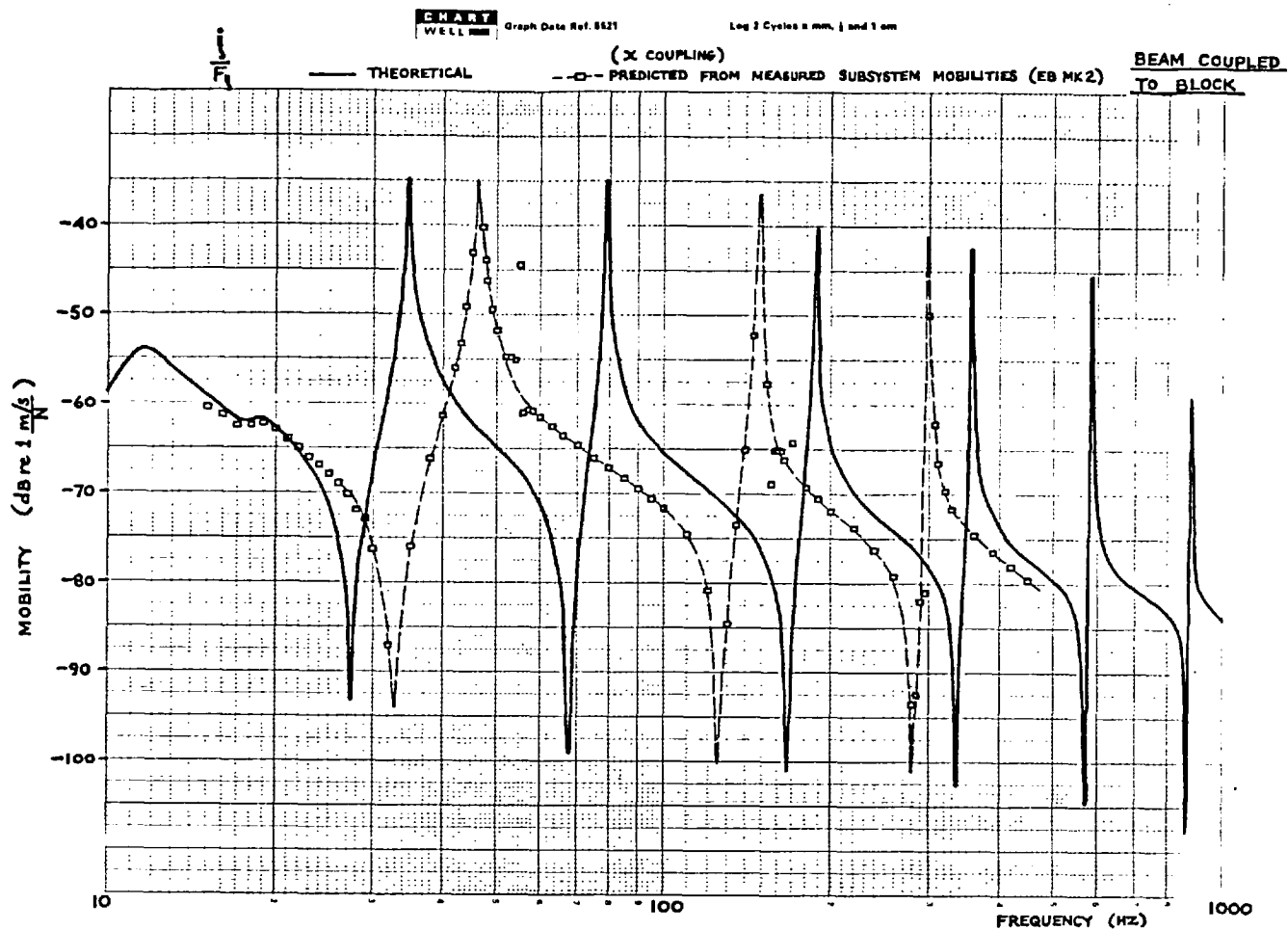
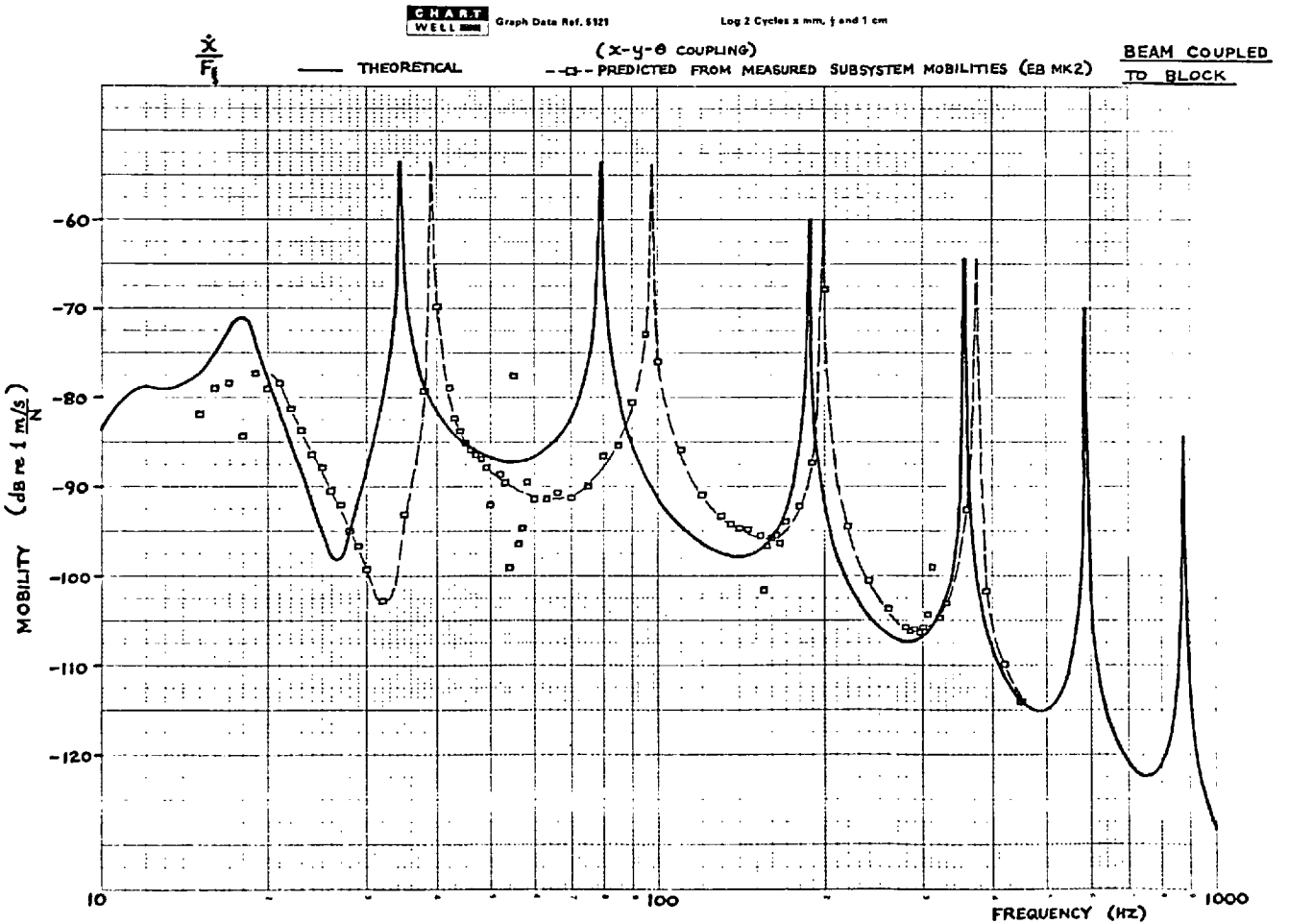
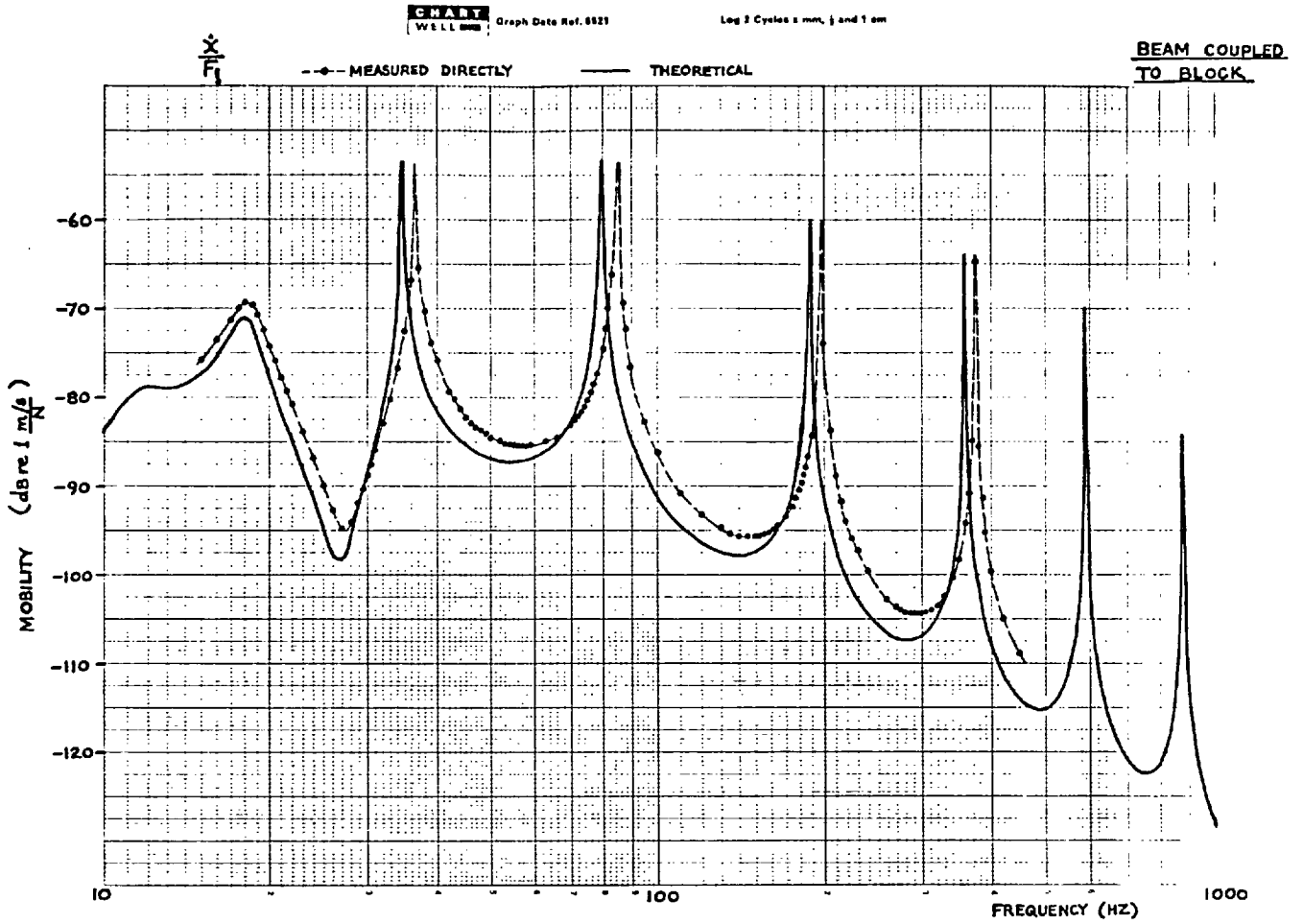
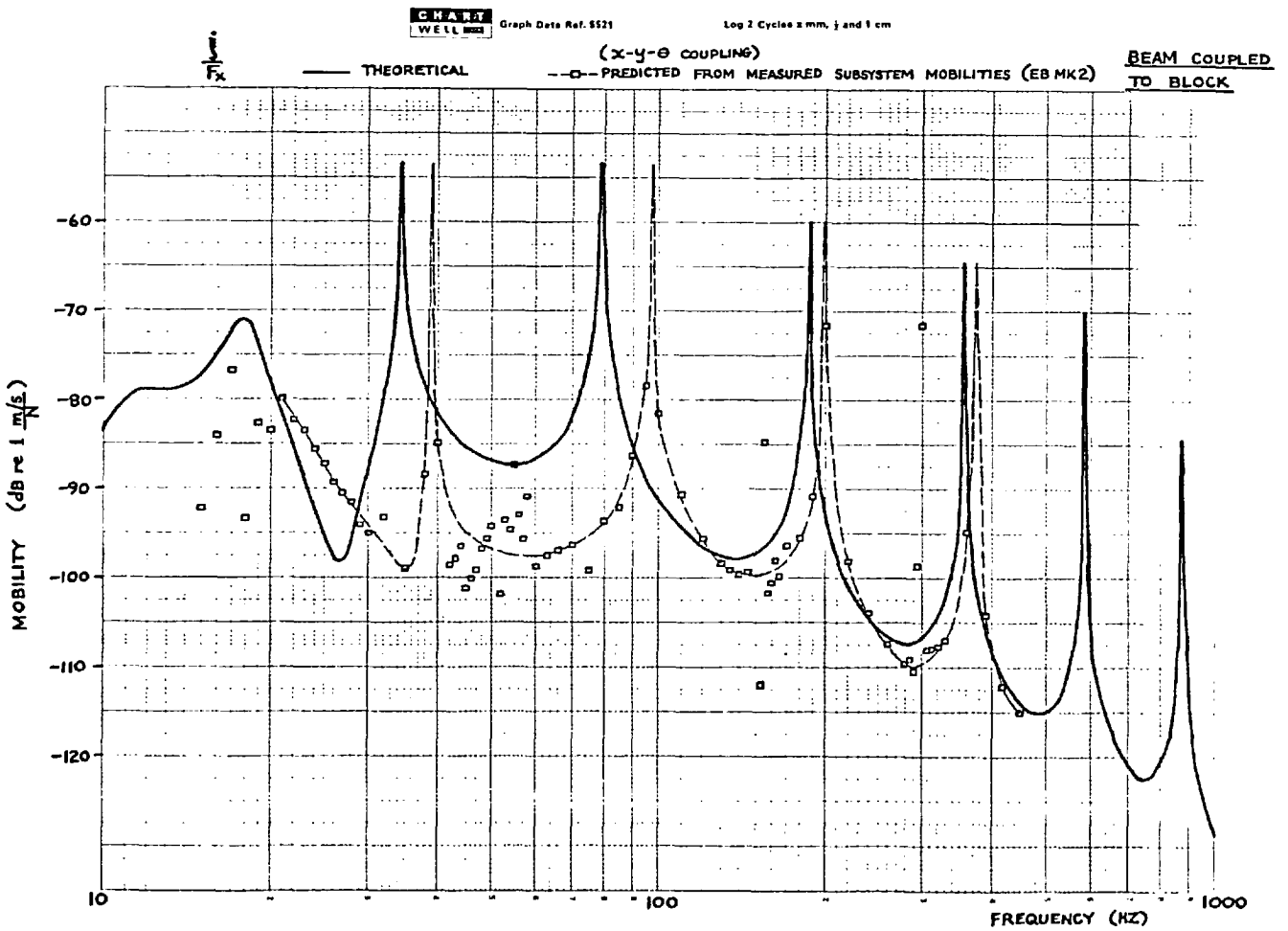
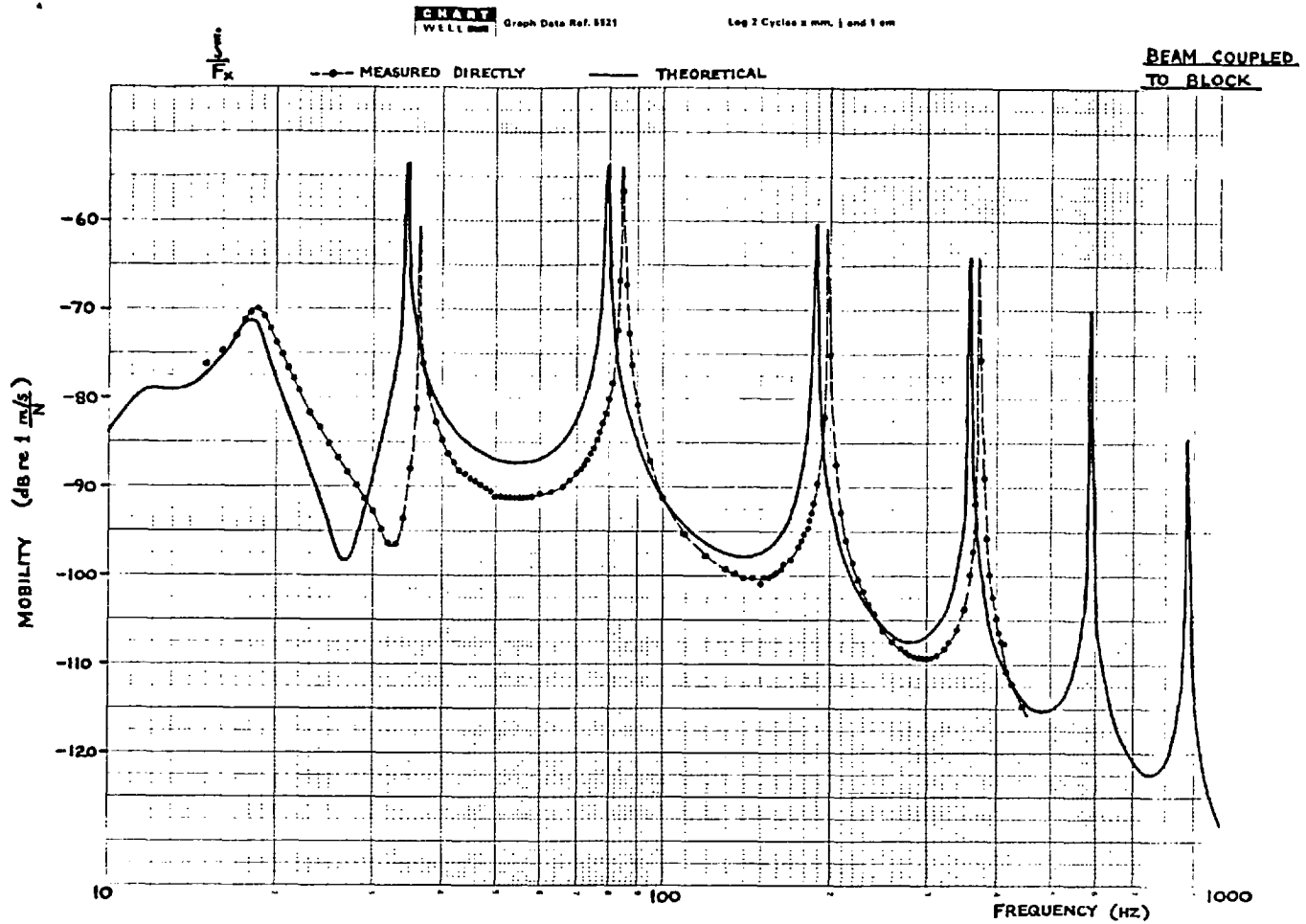


FIG 6.8





Discussion of Results for Coupling of Beam to Spring-Supported Block

We shall first compare the directly measured response of the coupled system with that obtained from theory. Only the x and ξ responses were measured and the results are given in the upper graphs of Figs. 6.2, 6.5, 6.8 and 6.9. The agreement is quite reasonable, although the bodily shift of the theoretical curves to the left is a little puzzling. It would tend to indicate a mis-estimate of the inertia properties of the block, since the accuracy of the theoretical beam data has been proved by the various multi-directional tests. The difference may also be partly attributable to the fact that the point measurements were made with separate force and acceleration transducers, mounted side by side. Although the distance between the force gauge and the accelerometer was only 27 mm, this could have a noticeable effect upon the anti-resonant frequencies, and it might be a possible reason for the differences of up to 5 dB between the two transfer responses, which should of course be identical in accordance with the reciprocal theorem.

We shall next compare the response predicted* from the component measurements with that measured directly on the coupled system. Referring to the lower graphs of Figs. 6.2 and 6.5, it is seen that for frequencies above about 120 Hz the full x - y - θ coupling gives very good agreement, both as regards the general level of the mobility and the positions of the resonances. The slight disagreement at the lower frequencies is probably almost entirely due to errors in the measured component data. It is unlikely that it might be due to imperfect coupling between the components, since both the beam and the exciting block were attached to the steel mass in the same way, using the same fixing bolts. Also, imperfect coupling would probably affect the results more at the high frequencies than at the low. The 14 % upward shift in the 84 Hz resonance may be due primarily to the jump in the measured $\frac{\dot{x}}{M_\theta}$ and $\frac{\dot{\theta}}{M_\theta}$ data for the mass at around 75 Hz. From the lower graph of Fig. 6.5 it is seen that the 36.5 Hz

* In the present discussion, the term "predicted response" is used for the response predicted from measured component data, and not for the theoretical response.

resonance has suffered an 8 % upward shift, but this is less surprising, in view of the low frequency errors in the measured beam data.

It is interesting to look now at the upper graphs of Figs. 6.3 and 6.6, which show the effect of using only a single coupling co-ordinate. These are the results that one would obtain by performing single-point coupling of the beam to the mass using standard uni-directional mobility data measured in the x direction on the two components^{*}. This single co-ordinate coupling can lead to predictions which are nowhere near the truth, and to allow for the transmission of couples between components it is necessary either to include rotational co-ordinates or to consider two-point coupling, with a translational co-ordinate at each point. To see the effect of introducing the rotational co-ordinate, let us now consider the upper graph of Fig. 6.4, which shows the response predicted assuming x- θ coupling. The predicted results are given with the theoretical results, rather than with the directly measured response, but if we also consider the corresponding graph for x-y- θ coupling (lower graph of Fig. 6.3) we can see quite clearly that there is hardly any distinguishable difference between the two sets of results. The general conclusion to be drawn from this observation is that whereas it is usually necessary to consider more than just a single co-ordinate when applying the mobility coupling procedure, it is rarely necessary to go to the other extreme and consider every possible co-ordinate.

Regarding this use of limited data for coupling, it is also interesting to consider Fig. 6.7, which shows the $\frac{\dot{x}}{F_x}$ responses predicted using x coupling and θ coupling respectively. Comparing these results with those obtained using x-y- θ coupling (lower graph of Fig. 6.6), it is readily seen that the θ coupling yields results which are much closer to the x-y- θ results than those predicted using x coupling. Hence, in this case the θ co-ordinate is predominant, the x co-ordinate is secondary, but must still be included, and the y co-ordinate is quasi-redundant and may safely be neglected — unless one needs to know the y response.

* ie. Linear mobility data measured with a conventional impedance head or with separate force and acceleration transducers.

The transfer mobilities relating forces and responses in the x and ξ directions are shown in Figs. 6.8 and 6.9, where the upper graphs give the directly measured results and the lower graphs give the results predicted from the measured component data. These are each compared with the theory. As with the point response data, the results predicted from the coupling procedure compare very well with the directly measured results above about 120 Hz. It is interesting to note that these predicted results do not follow the theoretical curve between the resonances, and that they disobey symmetry in the same way as the directly measured results. The agreement at frequencies below about 120 Hz is not so good, even discounting the resonant frequency shifts previously mentioned, and this is primarily due to errors in the component mobility measurements.

On all the predicted mobility graphs it is seen that there are a number of erroneous points around each of the resonant frequencies of the original free beam, or more specifically, around the resonant frequencies of the beam/exciting-block system*. The scatter of these points is a result of the numerical ill-conditioning of the beam data in the neighbourhood of these resonances, and in the present type of problem, where the modes of the assembly are well separated, the erroneous points may safely be ignored since their origin is clear.

In the case of the point mobility $\frac{\dot{x}}{F_x}$ (Fig. 6.2) at the junction between the beam and the mass, the scatter is far less pronounced, and this is probably due to the fact that the mobility of the mass is predominant at this point, thereby drowning the effect of the ill-conditioned beam data. The very subdued peak at 55 Hz also tends to indicate that the damping associated with the rubber pads beneath the mass has helped to damp out the pseudo-resonances associated with inaccuracies in the data. This is also apparent from the $\frac{\dot{\xi}}{F_{\xi}}$ graph (Fig. 6.5) which exhibits very little scatter around 55 Hz, but quite significant scatter around 155 and 300 Hz. The decrease in the effect of the damping at the higher

* Resonant frequencies (Hz). Beam + exciting-block: 55, 155, 300
 Beam alone: 60, 166, 322

frequencies is to be expected, since the boundary conditions have a diminishing influence on the behaviour of a beam as the frequency is increased*.

Conclusions

The results show that it is feasible to use measured component data directly in order to predict the response of an assembly. However, there are some obvious limitations, and these will be discussed further in Chapter 7.

* See lower graph on page 401 (Part 4, Chapter 15, Fig. 15.19). Curve $\frac{\dot{q}_8}{Q_8}$ relates to an effectively undamped beam supported at each end by a damped rubber block ($\gamma=0.1$). The flexural resonances of the beam occur at 175, 455 and 850 Hz, and although the first peak is heavily damped, the second and third peaks become progressively much sharper.

CHAPTER 7

SUMMARY AND CONCLUSIONS FOR MULTI-DIRECTIONAL MOBILITY MEASUREMENTS

7.1 GENERAL DISCUSSION AND SUMMARY

The work described in Chapters 3 to 6 has shown that the measurement of multi-directional mobility data is feasible, and that such data can be measured with sufficient accuracy for their use in predicting the response of a simple assembly. We shall now consider the main findings of this study and look at the developments that have taken place during the four years since most of this work was carried out.

The single-shaker multi-directional measurement technique has yielded fairly accurate results, even using an exciting block only 120 mm in length (block Mk 3). This contrasts with the findings of Smith^{(28)*}, who abandoned his attempt at using a single shaker after experiencing the same numerical difficulties as were encountered with the Mk 1 block. An advantage of this method is that only a conventional shaker is required, so there is no restriction on the level of the force input, and also alignment is easier. The biggest disadvantage is that the data must be processed in order to obtain the required mobilities, but the same is true of the twin-shaker approach when the results are to be fully corrected for exciting block inertia and impure excitation, and if one uses a computer-controlled measuring system this processing is easily carried out in the laboratory anyway.

The twin-shaker technique has also given quite good accuracy and has the advantage of yielding linear and rotational mobilities directly, provided one is able to neglect the inertia of the exciting block. It is particularly suitable if one only has conventional analogue impedance measuring equipment with graphical output. A disadvantage is the need for a special shaker unit, which is necessarily restricted in its force output due to size limitations. Also, the use of two force inputs to the block means that shaker/push-rod stiffnesses and resonances may have a greater effect than with a single input.

* Note that References for Chapters 3 to 7 are listed on Page 185.

The mobility coupling exercise with the beam and the spring-supported mass has shown the need for accurate and sufficiently complete measured data for the components. A knowledge of the uni-directional dynamic characteristics as given by conventional "impedance testing" techniques, is rarely sufficient for this purpose, since most joints transmit both forces and couples. However, the exact number of co-ordinates to be used in the coupling process is a personal choice, based upon an assessment of the importance of each co-ordinate in a given problem. One should always remember that the measurement of multi-directional mobility data is relatively time consuming, and it leaves one with large quantities of information, so it is advisable to use only as many coupling co-ordinates as are absolutely necessary for acceptable accuracy when performing the coupling. When using measured data directly, it should be borne in mind that any small errors in the component data will inevitably be magnified by the numerical coupling process, so one must balance the loss of accuracy caused by restricting the number of co-ordinates against the larger numerical errors associated with using more co-ordinates.

These encouraging results provided the incentive for further studies in this area, and this next phase of the work has been carried out by P.T. Gleeson, also of the Imperial College Dynamics Group. He started with the single-shaker measurement technique, as presented in Section 4.5, and has taken measurements on a number of steel beams⁽²⁹⁾. As these were smaller than the 1.83 m beam considered here, it was necessary to reduce the size of the exciting block, and this led to a number of difficulties. Three blocks have been developed* in working towards the "ideal" design, and various investigations have been carried out into the effects of accelerometer cross sensitivity⁽²¹⁾, the inter-action between force and acceleration transducers, etc. The measured

* Blocks Mk 4, 5 and 6. Owing to a lack of communication, Gleeson's initial block was given the same designation (Mk 4) as the large block used for the twin-shaker tests described in Appendix IV.

beam mobilities were subsequently used to predict the response of a two-beam assembly, both in the form of an L and in the form of a long straight beam⁽¹³⁾, but the results were not encouraging, and were particularly sensitive to errors in the $\frac{\dot{\theta}}{M_{\theta}}$ mobilities of the two component beams. Bagley⁽³⁰⁾ has performed a similar coupling exercise with beams, utilising just transverse mobilities and two coupling points, and he has been reasonably successful in predicting natural frequencies and mode shapes, but he does conclude that one cannot expect good results if the assembly has natural frequencies which are either closely spaced or are near those of any of the components. Even when using purely theoretical component data, errors sometimes arise at frequencies around the component resonant frequencies. Lutes and Heer⁽³¹⁾ have developed a special coupling algorithm which overcomes this problem of ill-conditioning, and this might conceivably improve predictions from measured data as well. However, it would appear that multi co-ordinate coupling using raw measured data can only be expected to yield reliable results when the various components are not all highly resonant*.

The much better results obtained here for the beam and the mass are probably a consequence of the fairly docile nature of the mass, and one might expect similar agreement for any assembly of damped components.

Klosterman⁽²⁷⁾ has looked at this problem of errors in the component data, and has concluded that the only way of obtaining reliable response predictions from measured data is to determine the modal characteristics of the components. From this modal information one is able to generate suitably smoothed component mobility data. It is important to note that the elements of any mobility matrix are related to one another in a special way, so it is only necessary to measure one column of the matrix in order to deduce all the other elements. If the inter-relationship constraint imposed by the modal representation is violated by even one or two per cent, this leads to signi-

* There is no problem in the case of single co-ordinate coupling. A good example of this given by Silva⁽³²⁾, who has predicted the response of a symmetrical cross-beam assembly from the transverse point mobilities measured at the centres of the two beams.

ficant errors in the response prediction for the assembly of components, so it is perhaps hardly surprising that difficulties have been experienced when using the raw data for two highly resonant beams.

Faced with this problem, Gleeson developed an alternative two-directional measurement technique⁽¹³⁾ which takes account of the special relationship between the elements of the point mobility matrix: he measures $\frac{\dot{x}}{F_x}$ and either $\frac{\dot{\theta}}{F_x}$ or $\frac{\dot{x}}{M_\theta}$ and then derives the other two elements of the matrix from these. This has yielded very much improved results, both for the individual component mobilities and for the predicted response of an assembly. The modal identification process yields receptance (or mobility) series for the measured matrix elements, and is suitable for undamped and lightly damped components⁽¹³⁾⁽³³⁾⁽³⁴⁾. A fairly general identification program has recently been developed by Gleeson for use on the PDP 8E mini computer. This is written in FOCAL and is described in detail in Reference (35). Although no attempt has so far been made to extend this multi-directional measurement technique to more heavily damped systems, a suitable identification program based on polar response plots has been developed by Silva^{(36)*} and this has been used successfully for identifying a complex helicopter structure⁽³⁸⁾. However, the sandwich beam example in Section 4.5 shows that the direct measurement technique can yield good results for a damped system, so it may not be necessary to go through the lengthy process of identifying a large number of damped modes. The other type of system for which the direct measurement is appropriate is any large dispersive system which does not obey resonant vibration theory (eg. buildings, ships, or an elastic half space).

If the measured component data are to be used in the analysis of an assembly, these data are obviously required in a digital form, so one should either use a digital measuring system or an analogue system incorporating an analogue-to-digital converter. An analogue system with purely graphical

* See also References (27) and (37)

output is not to be recommended, since one loses accuracy in the plotting and it is still necessary to digitise the data afterwards, either manually or using a digitising table (which measures the X and Y co-ordinates of points on a graph and punches these onto either cards or paper tape). Whatever the system, it should incorporate automatic frequency sweep and data output facilities. A digital system is more accurate, and it can sweep the frequency incrementally through an exactly repeatable range of frequencies, so it is certainly to be preferred. Such systems are nowadays being developed very rapidly, and when they incorporate a mini computer they offer a versatility not available with analogue equipment, since the operator is able to program the system to measure and process the data in exactly the way he wishes.

The 1172 digital transfer function analyser currently marketed by Solartron Ltd. is a fairly compact unit which incorporates a built-in slow sweep facility, and the data may be output directly onto punched tape via a suitable interface. This analyser may be coupled to a mini computer in order to form a completely integrated system or one may take the punched tape from the analyser and feed this into a separate computer. It is obviously desirable that a computing capability should be available in the laboratory, either in the form of a mini computer or in the form of a link with a large central computer. This permits the processing of direct measurements or the identification of measured response on the spot, while the test items are still available, so it allows the final results to be checked and measurements to be immediately repeated if necessary. An alternative to this purpose-built analyser is a more general type of frequency response analysis system, such as is now available from both Hewlett Packard and General Radio. Whereas the Solartron analyser incorporates digital hardware to perform a slow incremental sweep and filter and measure the signals, these general-purpose systems use a mini computer to do everything, so they

rely completely on software. This offers the possibility of either performing a slow sweep for steady-state tests, or of using the digital fast sweep testing technique⁽³⁹⁾⁽⁴⁰⁾⁽⁴¹⁾, which considerably reduces the testing time — though at the cost of reduced accuracy.

With the improvements in electronic equipment for measuring the signals, it is now the transducers and the mechanical connections to the test item that are the most significant sources of error. For instance, the use of a fairly flexible interconnection between the shaker and the force gauge (or impedance head) is very important when testing most grounded and lightly suspended items, especially if the shaker has a high lateral stiffness. However, in trying to reduce restraints imposed by the connection to the shaker, one must be careful not to employ push rods which are too flexible and resonate nicely in the working frequency range. Since the rod resonates laterally and is a high Q system, a relatively large lateral force may be transmitted through to the structure under test, at the same time possibly affecting the force gauge signal*. The result is a "spurious resonance" in the measured lateral response, and very often also in the response along the excitation direction⁽¹⁰⁾. Therefore, push rods must be carefully designed, and if necessary one may wrap an elastic band around the rod so as to apply damping. Although they are very necessary when the test item responds in several directions, they should be avoided in favour of a stiffer connection whenever the test item is known to respond only in the direction of application of the force (eg. calibration test using axially excited cylindrical mass, or central excitation of a symmetrical beam).

When making any multi-directional response measurements one should be aware of the cross-sensitivity limitations of the accelerometers. This is particularly important when one is trying to measure the response in a direction at right angles to the principal direction of motion. If the accelera-

* Note that a force gauge which is designed to measure an axially transmitted force is generally also sensitive to any lateral force or couple which tries to rock it.

tion to be measured is more than about 25 to 30 dB below that in the principal direction, the majority of the accelerometer signal derives from the cross-axis motion, and the motion along the accelerometer axis cannot normally be measured. The exact limit depends upon the cross sensitivity of the accelerometer, and also upon the squareness of the mounting surface relative to the principal direction⁽²¹⁾, but even with the very best accelerometers, which typically have a cross sensitivity around 1 %, one still cannot hope to measure accelerations which are more than about 35 to 40 dB below the principal acceleration. If very low measurements are obtained, they are probably caused by cancellation of the cross-axis signal by the real signal and are therefore suspect. Rotational response measurements are also affected by cross sensitivity, and it has been shown in Appendix IV that errors of 2 or 3 dB are quite possible.

Another source of error with accelerometers is the effect of base strain. Gleeson has recently discovered that this can be particularly significant in the case of multi-directional measurements with an exciting block, since the forces transmitted through the block to the test structure give rise to surface strain at the accelerometer attachment points, and this has been found to lead to errors of several dB in the low frequency acceleration measurements. The accelerometers used in this test were of the compression type and they were screwed directly down onto the block surface. Very much better results were subsequently yielded by the latest Bruel and Kjaer shear-type accelerometers, which are far less sensitive to base strain. However, when the compression-type accelerometers were mounted on shouldered studs (which kept the accelerometer base off the block surface), the results improved significantly and were more or less the same as were obtained with the directly-mounted shear accelerometers. In the case of the multi-directional measurements described in this report, special shouldered insulating studs were used for the accelerometers (though solely as a precaution against

earth loops!), so it is unlikely that the results were much affected by base strain). A similar strain effect was encountered by Gleeson when he mounted a force gauge and an accelerometer on the two ends of a common stud, so one should avoid this practice when measuring the uni-directional point mobility on a beam or plate: it is far better to use completely separate studs, either stuck or screwed in position.

The other important sources of error in multi-directional measurements are the flexibility and the inertia of the exciting block. The flexibility only becomes significant when one is testing very low-mobility structures, and the results given in Appendix IV suggest that it is associated primarily with the foot of the block and the interface with the structure. In the case of exciting block Mk 4, the compressive stiffness is relatively high and is comparable with that of a conventional impedance head. However, it has been found that the effective rotational stiffness is low enough to seriously limit the capability for measuring low rotational mobilities. This limitation was immediately apparent when measurements were carried out on a very stiff steel structure*, since the rotational mobility measurements yielded the stiffness of the block, instead of that of the structure. The block inertia only becomes significant in the case of high-mobility structures, and it can be corrected for when processing the measured data. When using the twin-shaker technique, it is possible to apply a partial correction when performing the measurement, by cancelling the inertia force or couple only. However, the full correction can only be applied afterwards, once all the multi-directional data have been collected.

This discussion has covered the most important aspects of "impedance testing", with particular emphasis on the multi-directional measurement techniques developed in the preceding chapters. However, useful supplementary reading on the measurement and use of mechanical impedance (or mobility) is provided by Ewins in References (6), (7) and (8). A very comprehensive bibliography on the subject has also been compiled, and this may be found either in Reference (42) or in the above three references.

* See Part 4, Chapter 14, Section 14.5

7.2 CONCLUSIONS

From the work presented here and from the resumé of subsequent developments, it is seen that the capability now exists for measuring multi-directional mobility data. The main significance of this is that it now becomes possible to predict the vibration response of complex assemblies, even though the component parts may not be amenable to theoretical treatment. Despite recent advances in finite element analysis, certain large structures, rubber components, castings and internally-stressed parts still cannot be analysed with any precision, especially at relatively high frequencies, but the possibility of measuring the relevant multi-directional characteristics enables one to bypass the component analysis problem and to proceed with the more important analysis of the assembly.

Multi-directional measurements are necessarily more involved than the conventional uni-directional variety, but the use of a computer-controlled system with standard testing programs has made such measurements fairly routine. It now appears that P.T. Gleeson's derived measurement technique is preferable for highly resonant components, but there is still a place for the Author's direct measurement techniques in the case of damped components and large dispersive structures. Derived multi-directional data should be used when analysing undamped assemblies, but directly measured data may still be used for components which are not highly resonant.

REFERENCES FOR CHAPTERS 3 TO 7 (PART 2)

1. Noiseux, D. U. and Meyer, E. B., "Application of impedance theory and measurements to structural vibration", Bolt, Beranek and Newman Inc., Report 1562, Aug. 1968 (Alternatively, see Tech. Report AFFDL-TR-67-182)
2. Noiseux, D.U. and Meyer, E.B., "Applicability of mechanical admittance techniques", Shock and Vibration Bulletin, No. 38, 1968
3. Ewins, D. J., "The whys and wherefores of mechanical impedance measurement", Solartron Electronic Group publication, 1973
4. Ewins, D. J. "A short guide to mechanical impedance testing", Solartron Electronic Group publication, 1974
5. Ewins, D. J. "Some whys and wherefores of mechanical impedance testing", SEE Symposium on Dynamic Testing, Imperial College, London, Jan. 1971
6. Ewins, D. J., "Measurement and application of mechanical impedance data: Part 1 - Introduction and ground rules", Jnl. of Society of Environmental Engineers, Vol. 14-4, Dec. 1975
7. Ewins, D. J., "Measurement and application of mechanical impedance data: Part 2 - Measurement techniques", Jnl. of SEE, Vol. 15-1, March 1976
8. Ewins, D. J., "Measurement and application of mechanical impedance data: Part 3 - Interpretation and application of measured impedance data", Jnl. of SEE, Vol. 15-2, June 1976
9. Kerlin, R.L. and Snowdon, J.C., "Driving-point impedance of cantilever beams - Comparison of measurement and theory", JASA, Vol. 47, No. 1 (Part 2), 1970
10. Silva, J. M. M., "On the influence of the push-rod in mechanical impedance testing", Imperial Collegue Dynamics Group report, Oct. 1975
11. Smith, J. E., "Measurement of the total structural mobility matrix", Shock and Vibration Bulletin, No. 40, 1970
12. Lemon, J. R. (of Structural Dynamics Research Corporation), Private communication.

13. Ewins, D. J. and Gleeson, P. T., "Experimental determination of multi-directional mobility data for beams", Shock and Vibration Bulletin, No. 45, Part 5, June 1975
14. Bishop, R. E. D. and Johnson, D. C., "The mechanics of vibration", Cambridge University Press, 1960
15. O'Hara, G. J., "Mechanical impedance and mobility concepts", JASA, Vol. 41, No. 5, May 1967
16. O'Hara, G. J. and Remmers, G. M., "Shipboard shock fundamentals (Some thoughts on mobility and impedance)", Report on NRL Progress, June 1965, pp 24-25
17. Martin, A. and Ashley, C., "A computer-controlled digital transfer function analyser and its application in automobile testing", SEE Symposium on Dynamic Testing, Imperial College, London, Jan. 1971
18. Ewins, D. J. and Gleeson, P. T., "A computer-controlled mechanical impedance facility for vibration teaching and research", 1st British Conference on Vibration Teaching and Research, Sheffield Polytechnic, July 1975
19. Henshell, R. D. and Warburton, G. B., "Transmission of vibration in beam systems", Intl. Jnl. of Numerical Methods in Engineering, Vol. 1, 1969, pp 47-66
20. "Tico LF pad materials: Technical data on dynamic and static properties", Booklet issued by the James Walker Organisation, 1968
21. Gleeson, P. T., "Limitations of accelerometers in the measurement of rotational mobilities", Imperial College Dynamics Group Report No. SRC/DA/1, Feb 1973
22. Cottney, D. J., "The receptance analysis of disc, blade and shroud vibration", Ph.D. thesis, University of London, April 1975
23. Harris, C. M. and Crede, C. E., "Shock and vibration handbook", Vol. 1, Chapter 10, McGraw-Hill, 1961

24. Sainsbury, M. G., "Mobility measurements for the vibration analysis of coupled structures", Imperial College Dynamics Group Report No. 3 on MOD Contract No. DC 20(1)/55384/69, December 1971
25. Klosterman, A. L. and Lemon, J. R., "Building block approach to structural dynamics", ASME publication VIBR-30, 1969
26. Klosterman, A. L., "A combined experimental and analytical procedure for improving automotive system dynamics", SAE publication 720093, 1972
27. Klosterman, A. L., "On the experimental determination and use of modal representations of dynamic characteristics", Ph.D. thesis, University of Cincinnati, 1971
28. Smith, J. E., "Measurement of the total structural mobility matrix", Phase I, US Navy Marine Engineering Laboratory Report 360/66, Dec. 1966
29. Gleeson, P. T., "Multidirectional mobility measurements on beams", Imperial College Dynamics Group Report, November 1973
30. Bagley, R. L., "The analysis of two simple composite structures using mechanical admittance methods", Technical Note 1971-40 (M.Sc. thesis), Lincoln Laboratory, Massachusetts Institute of Technology, September 1971
31. Lutes, L. D. and Heer, E., "Receptance coupling of structural components near a component resonance frequency", Technical Memorandum 33-411, Jet Propulsion Laboratory, California Institute of Technology, Oct. 1968
32. Silva, J. M. M., "The influence of the joint on the vibration response of a cross-beam assembly", M.Sc. thesis, Imperial College, University of London, December 1974
33. Gleeson, P. T., "Factors affecting the accuracy of the modal identification process", Imperial College Dynamics Group Report, March 1976
34. Gleeson, P. T., "Modal identification in a limited range of frequencies", Imperial College Dynamics Group Report, March 1976
35. Gleeson, P. T., "Modal identification of lightly damped systems — User's guide to program IDENT", Imperial College Dynamics Group, June 1976

36. Silva, J. M. M., "Analysis of vector response loci — User's guide for program POLAR-1", Imperial College Dynamics Group, March 1975
37. Gaukroger, D. R., Skingle, C. W. and Heron, K. H., "Numerical analysis of vector response loci", Journal of Sound and Vibration, Vol. 29, No. 3, 1973, pp 341-353
38. Silva, J. M. M., "Experimental determination of the mechanical impedance of an airframe", Imperial College Dynamics Group report in 2 parts, on Research Contract K/A12/1068, 1976. Part 1: "Experimental procedure and presentation of results". Part 2: (a) "Analysis and interpretation of results", and (b) "System identification and modelling"
39. White, R. G., "Measurement of structural frequency response by transient excitation", Technical Report No. 12, Institute of Sound and Vibration Research, University of Southampton, 1969
40. White, R. G., "Evaluation of the dynamic characteristics of structures by transient testing", Journal of Sound and Vibration, Vol. 15, No. 1, 1971
41. Holmes, P. J., "Mechanical impedance measurement by the transient loading technique", Technical Report No. 53, Institute of Sound and Vibration Research, University of Southampton, 1972
42. Ewins, D. J., "A classified bibliography of mechanical impedance", Solartron Electronic Group publication.

PART 3THE FINITE ELEMENT VIBRATION ANALYSIS OF MULTI-LAYER DAMPED BEAMS IN FLEXURE AND TORSIONCONTENTS

<u>Chapter</u>		<u>Page</u>
8	GENERAL INTRODUCTION TO MULTI-LAYER DAMPED BEAMS	191
9	BENDING FINITE ELEMENT FOR SYMMETRICAL 5-LAYER BEAM	
	9.1 Introduction	199
	9.2 Nodal Co-ordinates and Displacement Functions	201
	9.3 Strain and Kinetic Energies	208
	9.4 Formulation of Energy Expressions in terms of Assumed Displacement Functions	212
	9.5 Stiffness and Inertia Matrices for the Element	215
	9.6 Reduction of Stiffness Matrix from 7 to 6 Degrees of Freedom	217
	9.7 Summary	219
10	BENDING FINITE ELEMENTS FOR UNSYMMETRICAL 3- AND 5-LAYER BEAMS	
	10.1 Introduction	222
	10.2 Nodal Co-ordinates and Displacement Functions	222
	10.3 Strain and Kinetic Energies	225
	10.4 Formulation of Energy Expressions in terms of Assumed Displacement Functions	230
	10.5 Stiffness and Inertia Matrices for the Element	231
	10.6 Reduction of Order of Stiffness Matrix	233
	10.7 Summary	234

11	TORSIONAL FINITE ELEMENT FOR SYMMETRICAL 5-LAYER BEAM	
	11.1 Introduction	238
	11.2 Nodal Co-ordinates and Displacement Functions	242
	11.3 Strain and Kinetic Energies	243
	11.4 Formulation of Energy Expressions in terms of Assumed Displacement Functions	250
	11.5 Stiffness and Inertia Matrices for the Element	252
	11.6 Summary	253
12	RESULTS AND CONCLUSIONS FOR MULTI-LAYER DAMPED BEAMS	
	12.1 Introduction	257
	12.2 Results for Flexural Vibration of Symmetrical 3- and 5-layer Beams	257
	12.3 Results for Flexural Vibration of Unsymmetrical 3- and 5-layer Beams	271
	12.4 Results for Torsional Vibration of Symmetrical 3- and 5-layer Beams	277
	12.5 Conclusions	281
	REFERENCES FOR CHAPTERS 8 TO 12	283

Appendices to Part 3 start on Page 501

CHAPTER 8GENERAL INTRODUCTION TO MULTI-LAYER DAMPED BEAMS

Most beams plates and other engineering components are constructed from metals which have high strength but very little inherent damping. A typical solid metal component might have a loss factor of the order of 0.001, whilst a fabricated component would certainly be a little better, possibly with a loss factor of 0.01.^{(1)*} However, many components which are excited either by wide band noise or at a large number of discrete frequencies must be more heavily damped than this if high amplitude resonant vibrations are to be avoided. A more desirable loss factor would be 0.1 or even higher.

Whereas metals are stiff with very little damping, certain visco-elastic materials⁺ possess high damping but are not very stiff. Using the two materials together, one should therefore be able to obtain both high stiffness and high damping. The initial work in this direction was carried out around 1951-2 by Oberst⁽²⁾ and Lienard⁽³⁾, who examined the effect of applying a layer of visco-elastic damping material to the surface of a metal plate. This 2-layer configuration is shown in Fig. 8.1a, and is known as an unconstrained or extensional damping treatment, since the damping is due to direct strains induced in the visco-elastic layer as the plate bends. Further experimental and theoretical work is presented in reference (4), and a general review of the topic is given in (5). However, the most important conclusion was that very high damping could not be obtained at low frequencies, due to the relatively small direct strains induced in the visco-elastic layer.

A much more effective means of introducing damping was found to be the addition of a constrained damping layer to the surface of the metal, thereby forming a 3-layer sandwich, as shown in Fig. 8.1c. In this configuration, the

* Note that References for Chapters 8 to 12 are listed on Page 283.

+ ie. Rubber-like materials.

visco-elastic core undergoes considerable shearing as the beam bends, and it is this shearing action which gives rise to the high damping. With this discovery, various damping tapes became commercially available. These tapes comprise a thin layer of damping material on a foil backing strip, and they are simply stuck down onto the surface to be damped.

In 1959, Kerwin⁽⁶⁾ presented an approximate analysis of a 3-layer beam, the results being applicable to cases where the loss factor of the core material is small, and the bending stiffness of one of the faces is small relative to that of the other face. He and his co-workers at Bolt, Beranek and Newman later gave a more general analysis, which was extended to include plates⁽⁷⁾⁽⁸⁾⁽⁹⁾.

Most of the early work on constrained layer damping was based on Kerwin's approximate analysis, and it was not until 1965 that a more exact theory appeared, when DiTaranto⁽¹⁰⁾ derived the general sixth-order differential equation of motion for an arbitrary unsymmetrical 3-layer beam. The equation was derived in terms of the longitudinal displacement of layer 1, rather than in terms of the transverse displacement. He used a complex shear modulus for the core, and proceeded to solve the equation for the complex eigen-frequencies of the system. Although he wrongly attributed this eigen-solution to a decaying free vibration, the analysis and the conclusions drawn from it are in no way invalidated. A later paper⁽¹¹⁾ extended the solution, to include the complex eigen-modes.

Mead and Markus⁽¹²⁾ derived the sixth-order equation of motion in terms of the transverse displacement, and explained the complex eigen-solution as corresponding to a special type of resonant forced vibration. In the same way that the forced response of an undamped system may be expressed in terms of its real eigen-modes, the response of a hysteretically damped system may be expressed in terms of its complex eigen-modes⁽¹³⁾. Markus and Valášková⁽¹⁴⁾ have performed a detailed eigen-solution for a sandwich cantilever, and Mead and DiTaranto⁽¹⁵⁾ have derived various damping effectiveness criteria for beams, based upon the uncoupled modal responses.

The first really comprehensive analysis of multi-layer beam vibration was presented by Agbasiere⁽¹⁶⁾ in 1966, and this work is summarised in reference (17). Although he restricted his attention to symmetrical-section beams, he examined both 3- and 5-layer configurations (see Figs. 8.1b and 8.1d), and considered the effects of direct stresses in the visco-elastic layers, the strain dependence of visco-elastic properties, the effect of longitudinal and rotary inertia, etc. Using the finite difference method, he has solved the equations of motion for the forced response of 3- and 5-layer cantilevers, and the results have been verified experimentally. The properties of the visco-elastic materials were determined in shear tests, and take into account the effects of frequency, temperature and strain level. A design study has also been reported on the above mentioned sandwich configurations.

Nakra⁽¹⁸⁾ has analysed unsymmetrical 3-, 4-, 5- and 7-layer beams (see Figs. 8.1c, 8.1f, 8.1e). The equations of motion were set up by first obtaining expressions for the total strain and kinetic energies, then applying Hamilton's Principle. Although a cantilever beam has been examined using both the Rayleigh-Ritz and Lagrangian Multiplier methods, most of the work is concentrated on simply-supported beams, for which the mode shapes are pure sinusoids, and in consequence an exact solution is possible. It is shown that whereas 3-layer beams have an optimum loss factor over a relatively restricted frequency range, the unsymmetrical beams with a higher number of layers can possess optimum damping over a very much wider frequency range. The analysis of the 4-layer dual core beam is also given in reference (19), whilst the various types of multi-layer configuration are discussed by Grootenhuis⁽²⁰⁾.

Ahmed⁽²¹⁾⁽²²⁾ has applied the finite element displacement method to the dynamic analysis of curved sandwich beams of the symmetrical 3-layer type, and Leone and Perlman⁽²³⁾ have used the same method to examine straight unsymmetrical 3-layer beams. Whereas other investigators have been interested in the damping effect of a visco-elastic core, Ahmed's interest lies in all-elastic honeycomb

sandwich beams, which comprise thin metal face plates separated by a thick aluminium or glass fibre honeycomb core. However, the analysis is identical for the two problems, and damping may be introduced in the normal way by using a complex shear modulus for the core.

The work described in the following pages extends the finite element approach to all the most common types of multi-layer beam: types (a) to (f) in Fig. 8.1. Although this work was initiated prior to the publication of reference (21), the basic approach is very similar. The main differences lie in the choice of nodal co-ordinates and the corresponding displacement functions, and in the fact that only straight beams will be considered here. In addition to the bending vibration analyses, the finite element method will also be applied to the torsional vibration of a symmetrical 5-layer beam, this being a problem which appears to have received no attention whatsoever in the literature.

The initial motivation for this work was the need to be able to predict the dynamic behaviour of the sandwich beams used in an existing machinery foundation structure*. These beams are of the symmetrical 5-layer type, and due to the three-dimensional nature of the structure, they are subjected not only to bending in two planes, but also to torsion. In addition, simple boundary conditions such as simply-supported, etc., no longer prevail, since the beams are attached to other non-rigid components. It was soon realised that none of the existing work could be applied directly to this problem, since practically all the standard references given above deal only with the 3-layer type of beam, with the usual textbook boundary conditions, and certainly no mention is ever made of bending in the plane of the layers, or of torsion about the beam axis. Only Agbasiere and Nakra have dealt with 5-layer beams, and their solution techniques are not really suitable for use in a general structural analysis. It was obvious that the finite element displacement method would provide the most general approach to the problem,

* See Part 4 of this report.

FIG. 8.1 THE MOST COMMON CONFIGURATIONS FOR MULTI-LAYER DAMPED BEAMS

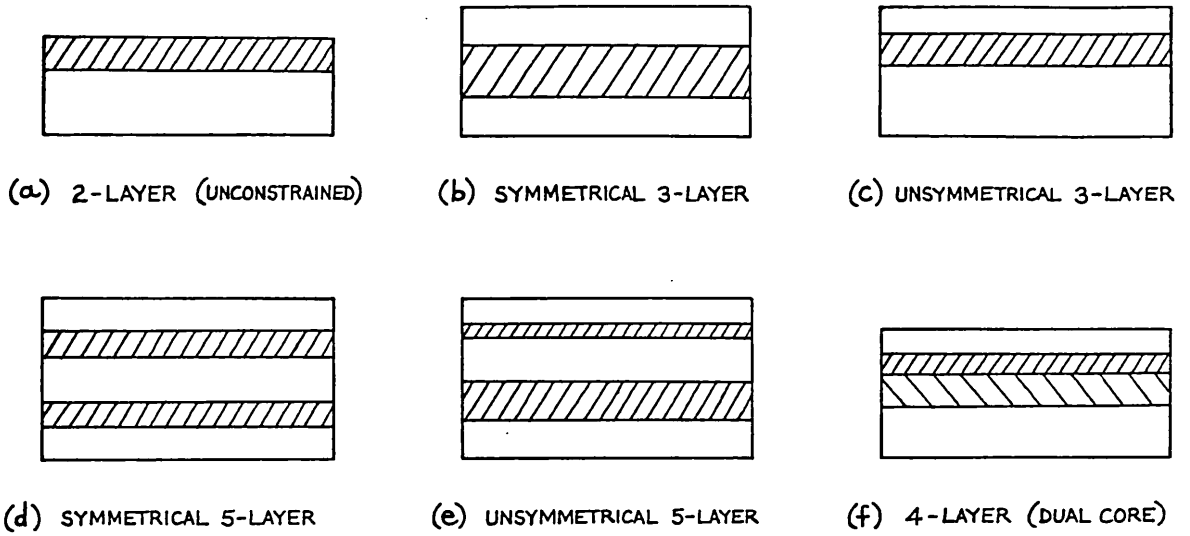


FIG. 8.2 FREE-FREE BEAM DIVIDED INTO A NUMBER OF FINITE ELEMENTS

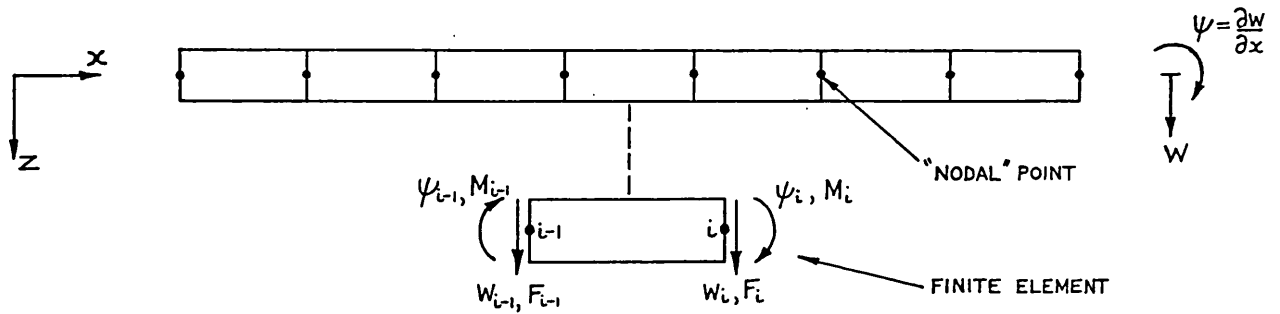
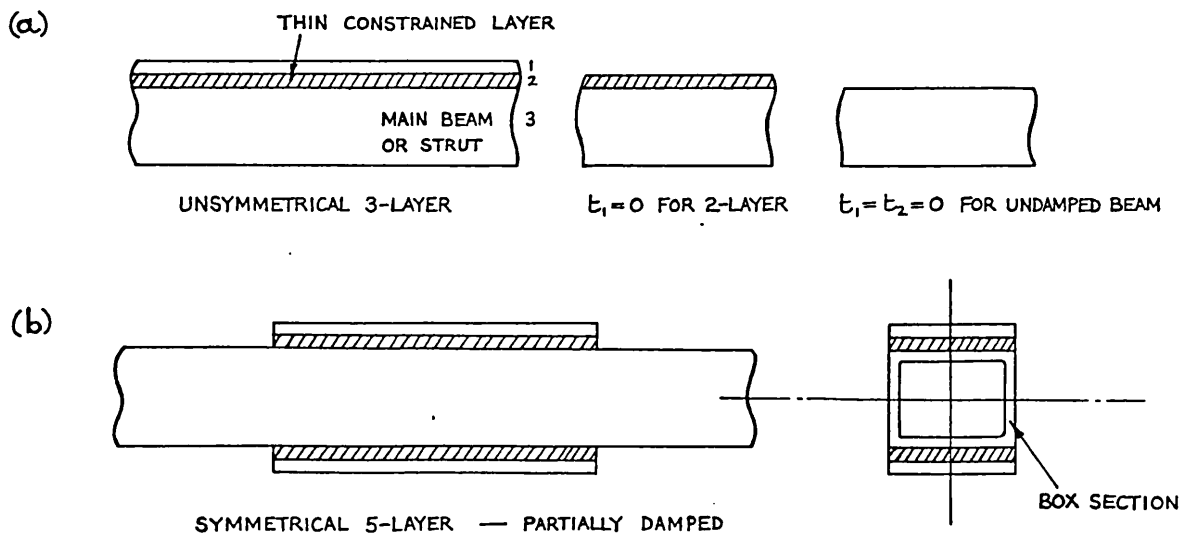


FIG. 8.3 APPLICATIONS FOR SANDWICH BEAM FINITE ELEMENTS



especially since it would yield stiffness matrices which could be utilised directly by the general purpose dynamic stiffness coupling programme described in Chapter 2 (Part 1).

References (24) and (25) provide a good introduction to the very powerful finite element method. They start from first principles, and go on to deal with the solution of a large number of practical problems covering many branches of engineering. The basic work on the finite element analysis of beam vibration was carried out by Leckie and Lindberg⁽²⁶⁾ and by Archer⁽²⁷⁾, who independently derived the stiffness and inertia matrices for a uniform Bernoulli-Euler beam element in 1963. Other beam elements of interest are those for a Timoshenko beam⁽²⁸⁾⁽²⁹⁾, for a uniform twisted beam⁽³⁰⁾, and for a beam with non-uniform taper⁽³¹⁾, besides the previously mentioned element for a curved sandwich beam. Henshell and Warburton⁽³²⁾ give an excellent introduction to the dynamic analysis of beam systems, and they compare the conventional finite element solution with lumped mass and "exact" dynamic stiffness.

To briefly illustrate the finite element method as applied to beam vibration let us consider Fig. 8.2, which shows a free-free beam which has been divided up into a number of sections of finite length. These sections are finite elements of the beam, and the coupling points at the two ends of each element are called "nodal" points. The bending stiffness of an element can be expressed as a matrix which relates the shear forces and bending moments at the two nodes to the corresponding displacements at these nodes. Applying the laws of equilibrium and displacement compatibility at each node, the stiffness matrix for the complete beam may be built up from the element stiffnesses, and the solution obtained for specified force or displacement inputs. If the response or stiffness are not required at intermediate points along the beam, then a more compact coupling procedure such as the Transfer Matrix method may be used. At the heart of the finite element method is the derivation of an approximate element stiffness matrix. This matrix may be obtained using a procedure similar to that used in the Rayleigh-Ritz

method: one assumes an approximate "displacement function"^{*}, in the form of a series which is capable of describing the rigid body motion and the flexing of the element. This series contains unknown constants which may be expressed in terms of the displacements at nodes of the element, and the number of constants is obviously limited to the number of nodal co-ordinates. Strain and kinetic energy expressions are formulated, and upon substituting the approximate displacement function, the energies are obtained in terms of the nodal displacements. The element stiffness and inertia matrices are then obtained from the energies by using the Lagrange equation. This procedure is not unique, but it is the one which will be employed in this report.

In the case of the foundation structure cited above, the heavily damped beams were purposely incorporated in the initial design. However, it is often the case that one wishes to ascertain the effect of adding damping to an existing undamped structure. As an example of the utility of the various finite elements, let us consider two practical cases to which they may be applied:

- (1) Fig. 8.3a shows a beam or strut to which a thin constrained layer has been added, on one face only. This gives an unsymmetrical 3-layer configuration. When analysing this system, any of the three layers may be given zero thickness, thereby facilitating a comparison of the behaviour for the three cases of zero damping, extensional damping, and constrained layer damping.
- (2) Fig. 8.3b shows a box-section beam with constrained damping layers on both faces, these layers only covering part of the length of the beam. This gives a 5-layer configuration, which in most practical cases would probably be symmetrical. Although only solid layers have been considered in the analyses, the box-section could obviously be replaced by an equivalent solid layer. The partial coverage may be taken account of quite easily, either by using 5-layer elements for the damped section and simple undamped uniform elements for the remainder, or by using 5-layer elements for the whole beam, and giving zero thickness to layers 1, 2, 4 and 5 of the undamped section.

* More than one displacement function may be required.

It is hoped that this Introduction has served to provide a thorough background to the subject of sandwich beam vibration, in addition to presenting the rudiments of the finite element method, and demonstrating its applicability. We shall now proceed to consider the individual elements in detail. Chapters 9, 10 and 11 contain the element analyses, whilst all results and comparisons with experimental data are grouped together in Chapter 12.

CHAPTER 9

BENDING FINITE ELEMENT FOR SYMMETRICAL 5-LAYER BEAM

9.1 INTRODUCTION

As was explained in the General Introduction, the type of finite element which we shall be considering is a section of beam, and the elements are joined end-to-end in order to form a complete beam. It must be emphasised that, in spite of the heterogeneous nature of the multi-layer beam, it is not necessary to sub-divide the section of beam into separate elements for the different layers. The multi-layer element is considered as a whole, and expressions are formulated for the total strain and kinetic energies in terms of the nodal co-ordinates. The element stiffness and inertia matrices are then obtained using the Lagrange equation, which simply minimises the total energy with respect to the nodal co-ordinates.

The symmetrical 5-layer beam element is shown in Fig 9.1. The elastic layers 1 and 5 are identical to one another, as are the two visco-elastic layers 2 and 4. Because of this symmetry, the centre-line of layer 3 is the neutral axis of the beam.

Before proceeding further with the element, we shall consider the various assumptions used in the analysis. These are basically the same as those used by Nakra^{(18)*}, and are as follows:

- (1) The elastic layers 1, 3 and 5 bend according to Bernoulli-Euler theory.
- (2) The visco-elastic layers 2 and 4 act primarily in shear, and the normals to the longitudinal fibres rotate through a total angle α . Stretching and bending effects are included, but are of secondary importance.
- (3) All layers are homogeneous and isotropic.
- (4) All displacements are small, as in linear elasticity theory.
- (5) There is perfect continuity at all interfaces between layers, and no slip occurs there when the sandwich bends.

* Note that References for Chapters 8 to 12 are listed on Page 283.

- (6) At any section, the transverse displacement w remains constant throughout the thickness of the laminated beam, there being no compression of the layers in the z direction.
- (7) The longitudinal displacements at an initially plane section vary linearly across the thickness of each layer, though with different slopes. The middle of layer 3 is a neutral axis and suffers no longitudinal displacement.
- (8) The strain dependence of the visco-elastic material properties is not sufficiently significant to warrant its inclusion in the analysis.
- (9) The most significant inertia terms are due to transverse motion, and rotary and longitudinal inertia are therefore ignored.

Assumption (1) is valid provided that the elastic layers are not thick. While it is highly unlikely that the constraining layers 1 and 5 would ever be thick, the centre layer might be part of an existing structure of deep cross section, to which damping layers had been added. In such a case, the exclusion of shear might introduce significant errors.

Assumption (6) is certainly valid in the case of rubber-like damping layers; which are surprisingly stiff in compression. Since rubber is virtually incompressible, and the metal layers prevent significant lateral bulging, the compressive stiffness of a typical layer might be 10 to 100 times greater than one would expect from simple elasticity theory⁽³³⁾. Experimental verification of the assumption is provided in Chapter 12, for a 5-layer beam with PVC damping layers. However, it is probable that in the case of softer, more viscous damping compounds, the damping layer would not be so effectively restrained in the lateral direction by the metal layer, and the compressive stiffness would be relatively low. The combination of a soft damping layer with a thick constraining layer would almost certainly invalidate the assumption.

Assumption (8) is valid as long as the strain levels are small, since most

visco-elastic materials possess strain-independent properties at low strain levels. The level at which the properties begin to be significantly affected varies inversely as the stiffness and frequency. Nakra⁽¹⁸⁾ has measured the properties of several common damping materials, and his results show that at 30 Hz and at the maximum strain level used in the shear test, the greatest change in the shear modulus and loss factor is only of the order of 10%. At higher frequencies the change is more significant, but at such frequencies the vibration amplitude is almost invariably much less, giving rise to correspondingly smaller strains in the visco-elastic layers. Thus, the effect is not great, and in those cases for which strain dependence is considered important, one may use an iterative procedure, starting with properties corresponding to an arbitrary strain level.

Assumption (9) is valid if the frequency is not too high. As will be shown below, it also permits a very significant improvement in the accuracy of the element stiffness representation, without any increase in the size of the final matrices.

9.2 NODAL CO-ORDINATES AND DISPLACEMENT FUNCTIONS

The accuracy of a finite element solution depends upon (a) the number of elements, (b) the chosen nodal co-ordinates, and (c) the assumed displacement function(s). Provided that (b) and (c) are correctly chosen, the solution will converge to the right answers as the number of elements is increased. In the present problem, convergence is assured if the end faces of adjacent elements remain in intimate contact with one another during bending of the beam, and if the displacement functions are capable of describing rigid body translation and rotation of the element, in addition to its flexure. The first of these two criteria may be expressed more precisely in terms of the derivatives in the total strain energy expression, but this will be postponed until we have looked at the problem from a physical point of view.

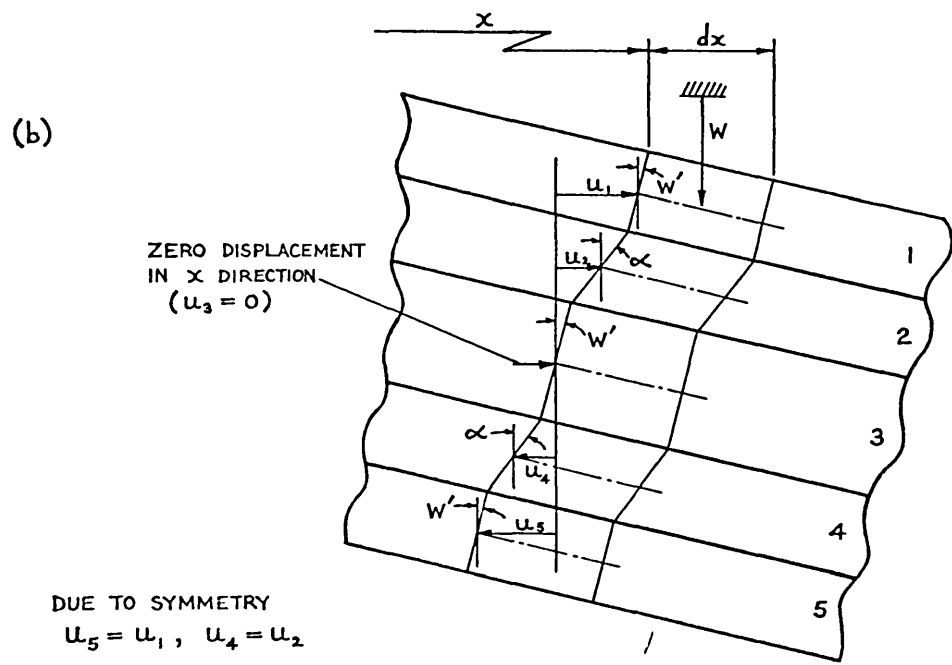
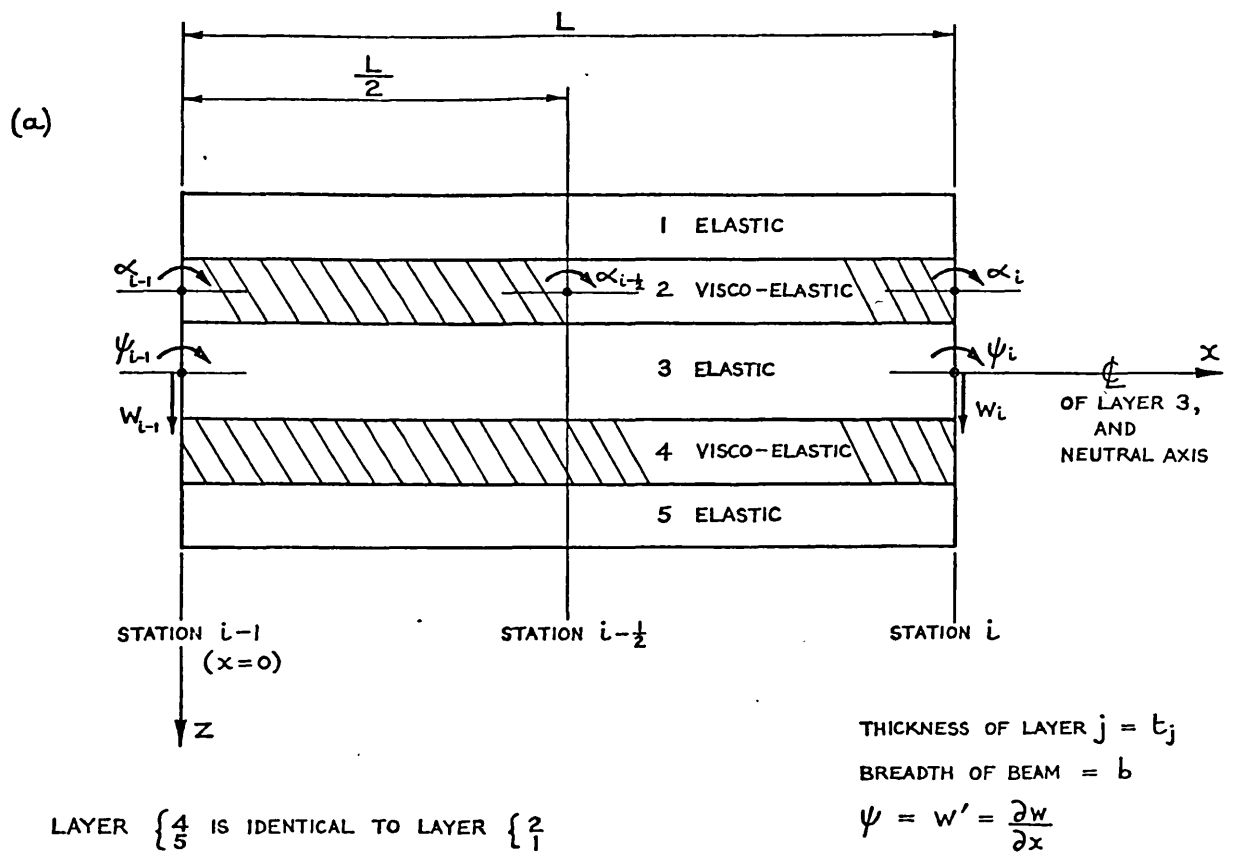


FIG. 9.1

BENDING FINITE ELEMENT FOR SYMMETRICAL 5-LAYER BEAM

The requirement that adjacent elements mate together intimately under all conditions is justified by the obvious fact that no gaps or holes appear in an actual physical beam when it is subjected to normal loads. If gaps appear with the finite element model, this implies that certain internal forces which should be acting on the end faces of each element are in fact missing. Since the strain distribution within the element is a function of all the forces applied to the end faces, a missing force gives rise to an incorrect strain distribution, which in turn affects the total strain energy and the stiffness matrix obtained from it. Obviously, the effect of a missing force upon the strain energy could be very small, in which case the solution might still converge, but there is no guarantee.

We are now in a position to consider once again the finite element shown in Fig. 9.1a. When this element is subjected to bending, any initially plane section distorts to the shape illustrated in Fig. 9.1b. In order to ensure intimate mating together of adjacent elements, one must choose nodal co-ordinates which will allow a complete description of the displacement of any point on the two end faces. By matching together the nodal displacements of adjacent elements at their coupling points, the mating faces will then distort in an identical manner, thereby ensuring perfect physical continuity between the elements. The choice of nodal co-ordinates is fairly arbitrary, in that any set which completely describes the face displacement is acceptable. In line with uniform beam theory, we shall take two of the co-ordinates to be the translation w and the rotation $\frac{\partial w}{\partial x}$ ($=\psi$) of the centre elastic layer. Since this layer does not move longitudinally when the beam bends, these two co-ordinates are sufficient to describe the displacement of any point on its end face*. As a consequence of assumption (6), layers 1 and 5 also translate and rotate by amounts w and $\frac{\partial w}{\partial x}$, in addition

* Note that the total rotation ψ of the elastic layers is equal to $\frac{\partial w}{\partial x}$ since we are neglecting the effect of shear stresses in these layers. In actual fact, there is a small amount of shearing associated with (a) the bending stresses, as in the uniform Timoshenko beam, and (b) the shear stresses transmitted from the adjacent visco-elastic layers.

to moving longitudinally through equal and opposite distances u_1 and u_5 . The longitudinal displacement u_1 is a possible third and final co-ordinate for completely describing the face displacement of the element, since the three co-ordinates w , $\frac{\partial w}{\partial x}$ and u_1 fix the displacement of any point on the end face of the outer layer, and the longitudinal displacement across the visco-elastic layer is assumed to vary linearly. The longitudinal displacement of the face layer has been used as a nodal co-ordinate by Ahmed⁽²¹⁾ in the case of his first 3-layer beam element. As an alternative, one may use either the shear γ or the total rotation α ($= \gamma + \frac{\partial w}{\partial x}$) of the visco-elastic layer. The latter was used by Ahmed⁽²²⁾ in a later 3-layer beam analysis, and it will also be used in the present case. This choice was largely due to the influence of Nakra⁽¹⁸⁾⁽¹⁹⁾ during the early stages of the work. However, it has been found that there is a definite advantage in using either γ or α rather than u_1 when one progresses to the analysis of plane frames built from sandwich members, since difficulties can arise in matching the nodal displacements of two beams meeting at an angle.

As was mentioned above, a more precise mathematical criterion exists for ensuring physical continuity between the beam elements. This is that all displacements and their derivatives, up to the second highest derivative appearing in the strain energy expression, should be continuous across the nodes^{(24)(25)*}. Obviously, in order to apply the criterion one must first choose sufficient co-ordinates to completely describe the strain in the element. In the present problem, the total strain energy comprises contributions from the shearing of the visco-elastic layers and from the bending and stretching of all the layers. The shear energy is a function of the shear strain ($\alpha - \frac{\partial w}{\partial x}$), whilst the other energies are a function of the longitudinal strains in the fibres of all the layers. Since the variation of longitudinal displacement across any section is expressible in terms of $\frac{\partial w}{\partial x}$ and α , the corresponding longitudinal strain distribution is obviously a function of the derivatives of these co-ordinates (ie. $\frac{\partial^2 w}{\partial x^2}$ and $\frac{\partial \alpha}{\partial x}$). Hence, the criterion tells us what we already concluded from

* eg. If $\frac{\partial^2 w}{\partial x^2}$ is the highest derivative of w in the strain energy expression, then w and $\frac{\partial w}{\partial x}$ must be continuous across the nodes.

physical reasoning; namely that w , $\frac{\partial w}{\partial x}$ and α must be continuous across the nodes, and must therefore be taken as nodal co-ordinates. Whilst the physical and mathematical convergence criteria lead to the same conclusion in the case of beams, it should be pointed out that this is not the case with plates. A plate element which satisfies the mathematical criterion will yield results which converge to the correct solution, even though the elements may not mate intimately together. In such a case, the strain energy associated with the missing edge forces is obviously very small in comparison with the total strain energy, so the stiffness is little affected and convergence is still obtained. In fact, such "non-conforming" elements may even give ^{accurate} ~~more~~ results than the perfectly mated or "conforming" elements⁽²⁴⁾⁽³⁴⁾. This is because the stiffness of a plate built from conforming elements is always slightly above the true value, so any reduction in stiffness brought about by allowing imperfect mating of the elements may sometimes bring this stiffness closer to the true value (even if it drops slightly below the latter). Thus, it is seen that whereas the mathematical criterion is a necessary condition for convergence, the physical criterion is a sufficient condition, which need not always be satisfied.

It has been shown that a minimum of 6 nodal co-ordinates are required in order to ensure physical continuity between elements, and these co-ordinates will be w , $\frac{\partial w}{\partial x}$ and α at the two nodes $i-1$ and i . The displacements w and α must therefore be expressed in terms of series which adequately describe the variation in these quantities over the length of the element, including the particular case of rigid body motion, and which only contain a total of 6 unknown constants. As in the case of the uniform beam element⁽²⁶⁾, a cubic polynomial will be used for w , leaving α to be represented by a linear expression:

$$\begin{aligned}
 w &= a_0 + a_1x + a_2x^2 + a_3x^3 \quad * \\
 &\quad \left(\text{whence } \psi = \frac{\partial w}{\partial x} = a_1 + 2a_2x + 3a_3x^2 \right) \\
 \alpha &= b_0 + b_1x
 \end{aligned}$$

* Note that $a_0 + a_1x$ describes rigid body translation and rotation, whilst $a_2x^2 + a_3x^3$ describes flexure.

It is seen that the rotations ψ and α of the elastic and visco-elastic layers are represented by quadratic and linear expressions respectively. However, from physical considerations these two quantities must obviously vary in a similar manner; especially in the extreme case where the two visco-elastic layers alone are used to represent a uniform solid beam⁺, since then $\alpha \approx \psi$. In consequence, the overall accuracy of the element is limited by the linear representation of α , and for uniform accuracy the cubic expression for w should be paired with a quadratic expression for α . This conclusion is indirectly confirmed by Cowper, Lindberg and Olson⁽³⁵⁾, who have stated that for higher accuracy the membrane and normal representation of shell structures should lead to equal rates of strain energy convergence. Following the procedure indicated in their paper, it may be shown that the use of cubic and quadratic expressions for w and α respectively leads to a convergence rate of $1/N^4$, where N is the number of elements into which the beam is divided. In the same way, it may be shown that if α is linear the convergence rate drops very dramatically to $1/N^2$. The procedure for examining the convergence rate is explained fully in Appendix V of this report.

The use of a higher degree polynomial for α introduces extra unknown constants, thereby necessitating the use of extra nodal displacements. However, these need not be actual physical displacements, and may equally well be higher derivatives of the basic nodal displacements. For instance, in the present case one could specify $\frac{d\alpha}{dx}$ at each of the nodes. The disadvantage of this approach is that one cannot introduce the higher derivative at one node and not at the other, so in the present case one is forced to make α cubic, rather than quadratic, thereby once more upsetting the uniformity of accuracy of the bending and stretching energy expressions. Ahmed has used this approach to improve the accuracy of his sandwich element, but he wrongly claims that the two cubic displacement functions give uniform strain energy convergence. Further disadvantages of using higher

+ See Section 9.3, pages 208 and 209, for further information on using this sandwich element to represent a uniform solid beam in which the effect of shear stiffness is included.

derivatives are that the resulting matrices are larger, and that the "forces" corresponding to these extra "displacements" have no physical significance.

An alternative approach to providing extra nodal displacements is to introduce one or more "internal nodes"⁽³⁶⁾. These differ from the "external nodes" at the two ends of the element, in that they are not connected to adjacent elements. In the present case we require one extra nodal displacement associated with the upper visco-elastic layer, to enable us to use a quadratic expression for α . Referring to Fig. 9.1a, the obvious choice is the rotation $\alpha_{i-\frac{1}{2}}$ at a position half way along the element. Although the resulting model has 7 degrees of freedom, the size of the stiffness matrix may be reduced to 6 x 6 by removing the co-ordinate $\alpha_{i-\frac{1}{2}}$. This is achieved quite simply, by specifying that the couple acting on this co-ordinate is zero, and eliminating the corresponding equation. In the general case, such an elimination can only be carried out on the dynamic stiffness matrix, obtained from the individual stiffness and inertia matrices at each frequency. However, as a consequence of assumption (9), the inertia matrix in the present case contains zero rows and columns corresponding to the displacements α_{i-1} , α_i and $\alpha_{i-\frac{1}{2}}$, thereby permitting the elimination to be carried out on the original stiffness matrix at the formation stage. Thus, it is possible to significantly increase the accuracy of the sandwich element without increasing the size of the element stiffness and inertia matrices.

In view of the above, the following displacement functions will be used for this symmetrical 5-layer element:

$$\begin{aligned} \frac{w}{L} &= a_0 + a_1 \xi + a_2 \xi^2 + a_3 \xi^3 \\ \alpha &= b_0 + b_1 \xi + b_2 \xi^2 \end{aligned} \quad (9.1)$$

where $a_j = a_j(t)$, etc.

The dimensionless distance $\xi = \frac{x}{L}$ is used in order to simplify the algebra by keeping the element length L outside the matrices when setting up the quadratic forms (9.15) and (9.16) corresponding to the various energy integrals. The use

of the dimensionless displacement $\frac{w}{L}$ permits the setting up of these energy quadratic forms in terms of non-dimensional displacement vectors, thereby facilitating the formation of non-dimensional stiffness and mass matrices suitable for use in parameter studies. This has been done in the case of uniform beams⁽²⁶⁾ and plates⁽³⁷⁾, where only a single frequency parameter is involved, and it is equally feasible in the case of the present sandwich beam. However, it should be noted that this will not be pursued here, so the present use of dimensionless displacements only facilitates further study in this direction at some later stage. Hence, one might equally well work in terms of the actual displacements w and α right from the start, and in general this is to be recommended.

Using these functions, the 7 x 7 stiffness and inertia matrices will be derived in the manner previously indicated. The number of degrees of freedom will then be reduced to 6 by eliminating the co-ordinate $\alpha_{l-\frac{1}{2}}$ associated with the node half way along the element.

We start by considering the strain and kinetic energies in the beam element.

9.3 STRAIN AND KINETIC ENERGIES

The total strain energy comprises contributions due to shearing of the visco-elastic layers, and to bending and stretching of all the layers. Although bending and stretching energies associated with the visco-elastic layers are generally very small, these energy terms are retained in the present analysis so that the sandwich element may also be used to represent uniform beams of deep cross section, in which the shear effect is important. This is done by giving layers 1, 3 and 5 zero thickness and treating layers 2 and 4 as the upper and lower halves of the uniform beam.

Shear Strain Energy in Visco-elastic Layers

Due to symmetry, both the visco-elastic layers shear by an equal amount $(\alpha - w')$, where the $'$ signifies $\frac{d}{dx}$. The corresponding shear strain energy in the two layers is given by

$$V_{\text{shear}} = 2 \times \frac{1}{2} b k_2 G_2 t_2 \int_0^L (\alpha - w')^2 dx \quad (9.2)$$

Where k_2 is the shear constant for layer 2.

The shear constant is defined as follows:

$$k = \frac{\text{Average shear stress in layer}}{\text{Shear modulus} \times \text{Angle of shear at middle of layer}}$$

$$= \frac{\text{Average shear stress in layer}}{\text{Shear stress at middle of layer}}$$

It is actually a correction factor to allow for an approximation made in the theory. When the beam bends, any section through a visco-elastic layer is assumed to remain plane and to rotate through an angle α (which varies along the length of the layer). However, this assumption is only strictly correct if the layer has a shear stiffness, but no bending stiffness. When there is bending stiffness, the pure shearing of the layer between the adjacent elastic layers is supplemented by a small amount of shearing associated with the bending stresses in the layer, so the section no longer remains plane (though it is very nearly so). In the theory, the shear strain energy in the layer is calculated assuming pure shearing, and the result is multiplied by a correction factor (the shear constant) in order to give the energy associated with the actual stress distribution.

In practice, the elastic modulus E_2^* of the visco-elastic layers is so much smaller than that of the elastic layers that the bending stresses and their associated shear contribution are fairly insignificant. Nakra⁽¹⁸⁾ has computed the shear constant for the core of a 3-layer beam, and for G_2 as high as

* For most soft visco-elastic materials, Poisson's ratio $\nu = 0.5$ and $E \approx 3G$. However, for the harder varieties of filled rubber E is closer to $4G$ (33).

$0.69 \times 10^8 \text{ N/m}^2$ (10^4 lbf/in^2) has still obtained a figure of 0.9977. Hence, k_2 may generally be set to unity, and it is only retained here so that the sandwich element may also be used to represent a uniform beam, in the manner described above. It should be noted that the correct value for the shear constant of a uniform beam of rectangular cross section with a Poisson's ratio of 0.3 is about 0.85⁽²⁸⁾⁽³⁸⁾⁽³⁹⁾, and this differs significantly from the value of 0.66 calculated by Timoshenko⁽⁴⁰⁾ using the definition given above.

Bending Strain Energy in All Layers

The total bending strain energy in all the layers of this symmetrical beam is given by

$$\begin{aligned}
 V_{\text{bend}} = & 2 \times \frac{b E_1 t_1^3}{2 \times 12} \int_0^L w''^2 dx + 2 \times \frac{b E_2 t_2^3}{2 \times 12} \int_0^L \alpha'^2 dx \\
 & + \frac{b E_3 t_3^3}{2 \times 12} \int_0^L w''^2 dx
 \end{aligned} \tag{9.3}$$

Extensional Strain Energy in All layers

The total extensional or stretching energy in all the layers is given by

$$V_{\text{ext}} = \frac{b}{2} \sum_{j=1 \text{ to } 5} E_j t_j \int_0^L \left(\frac{\partial u_j}{\partial x} \right)^2 dx \tag{9.4}$$

Referring to Fig. 9.1b, it is readily seen that the longitudinal displacements of the layers are as follows:

$$\begin{aligned}
 u_1 &= u_5 = t_2 \alpha + \frac{(t_1 + t_3)}{2} w' \\
 u_2 &= u_4 = \frac{t_2}{2} \alpha + \frac{t_3}{2} w' \\
 u_3 &= 0
 \end{aligned} \tag{9.5}$$

Substituting the displacements (9.5) into (9.4), we obtain

$$\begin{aligned}
 V_{\text{ext}} = & 2 \times \frac{1}{2} b E_1 t_1 \int_0^L \left[t_2 \alpha' + \frac{(t_1 + t_3)}{2} w'' \right]^2 dx \\
 & + 2 \times \frac{1}{2} b E_2 t_2 \int_0^L \left[\frac{t_2}{2} \alpha' + \frac{t_3}{2} w'' \right]^2 dx \quad (9.6)
 \end{aligned}$$

Total Strain Energy

The total strain energy in the finite element is

$$V = V_{\text{shear}} + V_{\text{bend}} + V_{\text{ext}}$$

Summing the energy expressions (9.2), (9.3) and (9.6), we obtain

$$\begin{aligned}
 V = & 2 q_2 \int_0^L (\alpha - w')^2 dx \\
 & + 2 r_1 \int_0^L \left[t_2 \alpha' + \frac{(t_1 + t_3)}{2} w'' \right]^2 + \frac{t_1^2}{12} w''^2 dx \\
 & + 2 r_2 \int_0^L \left[\frac{t_2}{2} \alpha' + \frac{t_3}{2} w'' \right]^2 + \frac{t_2^2}{12} \alpha'^2 dx \\
 & + r_3 \int_0^L \frac{t_3^2}{12} w''^2 dx \quad (9.7)
 \end{aligned}$$

$$\text{where } q_2 = \frac{b k_2 G_2 t_2}{2} \quad \text{and} \quad r_j = \frac{b E_j t_j}{2} \quad (j = 1 \text{ to } 3)$$

Expression (9.7) may be expanded into the sum of 6 integrals:

$$\begin{aligned}
 V = & V_1 \int_0^L \alpha^2 dx + V_2 \int_0^L w'^2 dx \\
 & + V_3 \int_0^L \alpha w' dx + V_4 \int_0^L \alpha'^2 dx \\
 & + V_5 \int_0^L w''^2 dx + V_6 \int_0^L \alpha' w'' dx \quad (9.8)
 \end{aligned}$$

The constants V_1 to V_6 are listed in Fig. 9.2 (Page 220).

Kinetic Energy

The kinetic energy due to transverse motion of the symmetrical section beam is given by

$$\begin{aligned}
 T &= \frac{b}{2} \sum_{j=1 \text{ to } 5} \rho_j t_j \int_0^L \dot{w}^2 dx \\
 &= \frac{b}{2} \underbrace{\left[2(\rho_1 t_1 + \rho_2 t_2) + \rho_3 t_3 \right]}_{\frac{\mu}{2}} \int_0^L \dot{w}^2 dx \quad (9.9)
 \end{aligned}$$

where $\dot{} = \frac{\partial}{\partial t}$

Rotary and axial kinetic energies will not be considered.

9.4 FORMULATION OF ENERGY EXPRESSIONS IN TERMS OF ASSUMED DISPLACEMENT

FUNCTIONS

The displacement functions (9.1) and their derivatives may be expressed in matrix form:

$$\begin{aligned}
 w &= L \left[1 \quad \xi \quad \xi^2 \quad \xi^3 \right] \{ a_0 \quad a_1 \quad a_2 \quad a_3 \}^* = L [X] \{ a \} \\
 w' &= \left[0 \quad 1 \quad 2\xi \quad 3\xi^2 \right] \{ a_0 \quad a_1 \quad a_2 \quad a_3 \} = [X'] \{ a \} + \\
 w'' &= \frac{1}{L} \left[0 \quad 0 \quad 2 \quad 6\xi \right] \{ a_0 \quad a_1 \quad a_2 \quad a_3 \} = \frac{1}{L} [X''] \{ a \} \\
 \alpha &= \left[1 \quad \xi \quad \xi^2 \right] \{ b_0 \quad b_1 \quad b_2 \} = [\bar{X}] \{ b \} \\
 \alpha' &= \frac{1}{L} \left[0 \quad 1 \quad 2\xi \right] \{ b_0 \quad b_1 \quad b_2 \} = \frac{1}{L} [\bar{X}'] \{ b \}
 \end{aligned} \tag{9.10}$$

* The braces $\{ \}$ denote a column matrix.

+ Note that $\xi = \frac{x}{L}$ and $\frac{\partial}{\partial x} = \frac{1}{L} \frac{\partial}{\partial \xi}$.

We may now obtain the relationship between the dimensionless nodal displacements and the sets of "constants" a and b :

$$\begin{Bmatrix} \frac{w_{i-1}}{L} \\ \psi_{i-1} \\ \frac{w_i}{L} \\ \psi_i \end{Bmatrix} = \begin{bmatrix} 1 & 0 & 0 & 0 \\ 0 & 1 & 0 & 0 \\ 1 & 1 & 1 & 1 \\ 0 & 1 & 2 & 3 \end{bmatrix} \begin{Bmatrix} a_0 \\ a_1 \\ a_2 \\ a_3 \end{Bmatrix}$$

$$\{\delta_w\} = [C_1] \{a\} \quad (9.11)$$

$$\begin{Bmatrix} \alpha_{i-1} \\ \alpha_i \\ \alpha_{i-\frac{1}{2}} \end{Bmatrix} = \begin{bmatrix} 1 & 0 & 0 \\ 1 & 1 & 1 \\ 1 & \frac{1}{2} & \frac{1}{4} \end{bmatrix} \begin{Bmatrix} b_0 \\ b_1 \\ b_2 \end{Bmatrix}$$

$$\{\delta_\alpha\} = [C_2] \{b\} \quad (9.12)$$

The inverse transformations are

$$\begin{aligned} \{a\} &= [C_1]^{-1} \{\delta_w\} = [T_1] \{\delta_w\} \quad * \\ \{b\} &= [C_2]^{-1} \{\delta_\alpha\} = [T_2] \{\delta_\alpha\} \end{aligned} \quad (9.13)$$

Using these inverse transformations, the displacements functions and their derivatives may be expressed directly in terms of the nodal displacements:

$$\begin{aligned} w &= L [X] [T_1] \{\delta_w\} \\ w' &= [X'] [T_1] \{\delta_w\} \\ w'' &= \frac{1}{L} [X''] [T_1] \{\delta_w\} \\ \alpha &= [\bar{X}] [T_2] \{\delta_\alpha\} \\ \alpha' &= \frac{1}{L} [\bar{X}'] [T_2] \{\delta_\alpha\} \end{aligned} \quad (9.14)$$

Substituting these displacement functions into the six strain energy integrals (9.8), we obtain the following quadratic forms:

* These transformation matrices are listed in Appendix VI.

$$\begin{aligned}
\int_0^L \alpha^2 dx &= \int_0^L \left([\bar{x}] [T_2] \{ \delta_\alpha \} \right)^T [\bar{x}] [T_2] \{ \delta_\alpha \} dx \\
&= L \{ \delta_\alpha \}^T \left([T_2]^T \int_0^1 [\bar{x}]^T [\bar{x}] d\xi [T_2] \right) \{ \delta_\alpha \} \quad * \\
&= \frac{L}{60} \{ \delta_\alpha \}^T [A_1] \{ \delta_\alpha \} + \\
\int_0^L w'^2 dx &= L \{ \delta_w \}^T \left([T_1]^T \int_0^1 [x']^T [x'] d\xi [T_1] \right) \{ \delta_w \} \\
&= \frac{L}{30} \{ \delta_w \}^T [A_2] \{ \delta_w \} \\
\int_0^L \alpha w' dx &= L \{ \delta_\alpha \}^T \left([T_2]^T \int_0^1 [\bar{x}]^T [x'] d\xi [T_1] \right) \{ \delta_w \} \\
&= \frac{L}{60} \{ \delta_\alpha \}^T [A_3] \{ \delta_w \} \\
\int_0^L \alpha'^2 dx &= \frac{1}{L} \{ \delta_\alpha \}^T \left([T_2]^T \int_0^1 [\bar{x}]^T [\bar{x}] d\xi [T_2] \right) \{ \delta_\alpha \} \\
&= \frac{1}{3L} \{ \delta_\alpha \}^T [A_4] \{ \delta_\alpha \} \\
\int_0^L w''^2 dx &= \frac{1}{L} \{ \delta_w \}^T \left([T_1]^T \int_0^1 [x'']^T [x''] d\xi [T_1] \right) \{ \delta_w \} \\
&= \frac{1}{L} \{ \delta_w \}^T [A_5] \{ \delta_w \} \\
\int_0^L \alpha' w'' dx &= \frac{1}{L} \{ \delta_\alpha \}^T \left([T_2]^T \int_0^1 [\bar{x}]^T [x''] d\xi [T_1] \right) \{ \delta_w \} \\
&= \frac{1}{L} \{ \delta_\alpha \}^T [A_6] \{ \delta_w \} \quad (9.15)
\end{aligned}$$

Similarly, the kinetic energy integral (9.9) yields

$$\begin{aligned}
\int_0^L \dot{w}^2 dx &= L^3 \{ \dot{\delta}_w \}^T \left([T_1]^T \int_0^1 [x]^T [x] d\xi [T_1] \right) \{ \dot{\delta}_w \} \\
&= \frac{L^3}{420} \{ \dot{\delta}_w \}^T [A_7] \{ \dot{\delta}_w \} \quad (9.16)
\end{aligned}$$

Substituting these quadratic forms into the strain and kinetic energy expressions (9.8) and (9.9), we obtain the final matrix expressions for the energies:

* Note the matrix operation $([A][B])^T = [B]^T[A]^T$

+ The matrices $[A_1]$ to $[A_7]$ in the quadratic forms are listed in Appendix VI.

$$\begin{aligned}
 V = & \frac{V_1 L}{60} \{ \delta_\alpha \}^T [A_1] \{ \delta_\alpha \} + \frac{V_2 L}{30} \{ \delta_w \}^T [A_2] \{ \delta_w \} + \frac{V_3 L}{60} \{ \delta_\alpha \}^T [A_3] \{ \delta_w \} \\
 & + \frac{V_4}{3L} \{ \delta_\alpha \}^T [A_4] \{ \delta_\alpha \} + \frac{V_5}{L} \{ \delta_w \}^T [A_5] \{ \delta_w \} + \frac{V_6}{L} \{ \delta_\alpha \}^T [A_6] \{ \delta_w \}
 \end{aligned} \tag{9.17}$$

$$T = \frac{\mu L^3}{2 \times 420} \{ \dot{\delta}_w \}^T [A_7] \{ \dot{\delta}_w \} \tag{9.18}$$

9.5 STIFFNESS AND INERTIA MATRICES FOR THE ELEMENT

The stiffness and inertia matrices may be obtained from the strain and kinetic energy expressions (9.17) and (9.18) by using the Lagrange equation:

$$\frac{d}{dt} \left(\frac{\partial T}{\partial \dot{q}_i} \right) - \frac{\partial T}{\partial q_i} + \frac{\partial V}{\partial q_i} = Q_i \tag{9.19}$$

Where q_i and Q_i are the i 'th generalised co-ordinate and force respectively. In the present case the generalised co-ordinates are the dimensionless nodal displacements, so the corresponding "forces" all have the dimensions of a couple:

Forces	Displacements
$ \{ F_w \} = \begin{Bmatrix} F_{w_{i-1}} L \\ M_{\psi_{i-1}} \\ F_{w_i} L \\ M_{\psi_i} \end{Bmatrix} $	$ \{ \delta_w \} = \begin{Bmatrix} \frac{w_{i-1}}{L} \\ \psi_{i-1} \\ \frac{w_i}{L} \\ \psi_i \end{Bmatrix} $
$ \{ F_\alpha \} = \begin{Bmatrix} M_{\alpha_{i-1}} \\ M_{\alpha_i} \\ M_{\alpha_{i-\frac{1}{2}}} \end{Bmatrix} $	$ \{ \delta_\alpha \} = \begin{Bmatrix} \alpha_{i-1} \\ \alpha_i \\ \alpha_{i-\frac{1}{2}} \end{Bmatrix} $

(9.20)

If we confine our attention to simple harmonic motion, the damping in the visco-elastic layers may be described quite simply by making the shear and extensional moduli G_2 and E_2 complex. Applying (9.19), we then obtain a matrix equation of the form

$$\left(\begin{array}{c} [K] \\ \hline \omega^2 [M] \end{array} \right) \begin{array}{c} \left\{ \begin{array}{c} \delta_w \\ \delta_\alpha \end{array} \right\} \\ \hline \end{array} = \begin{array}{c} \left\{ \begin{array}{c} F_w \\ F_\alpha \end{array} \right\} \\ \hline \end{array} \quad (9.21)$$

7×7 7×1 7×1

where the stiffness matrix $[K]$ is complex and the inertia matrix $[M]$ is real. The differentiation of the energy terms is carried out using the product rule*, and the matrices of (9.21) may be written directly in terms of the submatrices $[A_1]$ to $[A_7]$:

$$\left[\begin{array}{c|c} \left(S_2[A_2] + S_5[A_5] \right) - \omega^2 C_0[A_7] & S_3[A_3]^T + S_6[A_6]^T \\ \hline S_3[A_3] + S_6[A_6] & S_1[A_1] + S_4[A_4] \end{array} \right] \begin{array}{c} \left\{ \begin{array}{c} \delta_w \\ \delta_\alpha \end{array} \right\} \\ \hline \end{array} = \begin{array}{c} \left\{ \begin{array}{c} F_w \\ F_\alpha \end{array} \right\} \\ \hline \end{array} \quad (9.22)$$

where the stiffness coefficients S_1 to S_6 and the inertia coefficient C_0 are listed in Fig. 9.2. It should be noted that although there are six strain energy terms, these are not all associated with the same nodal displacements, so any individual element in $[K]$ contains contributions from only two of the six terms.

Whilst the energy expressions and the stiffness and inertia matrices are most easily formulated in terms of the individual displacement vectors $\{\delta_w\}$ and $\{\delta_\alpha\}$, the resulting co-ordinate order in (9.22) is not very convenient from a practical point of view. A better arrangement is to group together all the co-ordinates corresponding to each node. The re-arranged stiffness and inertia matrices are shown in Fig. 9.3, and these are for use with the following force and displacement vectors:

$$* \quad \frac{d}{dq_i} (u^T A v) = \frac{d v^T}{dq_i} \cdot A u + \frac{d u^T}{dq_i} \cdot A v$$

Force	Displacement	
$\begin{Bmatrix} F_{w_{i-1}} \\ M_{\psi_{i-1}} \\ M_{\alpha_{i-1}} \\ F_{w_i} \\ M_{\psi_i} \\ M_{\alpha_i} \\ M_{\alpha_{i-\frac{1}{2}}} \end{Bmatrix}$	$\begin{Bmatrix} w_{i-1} \\ \psi_{i-1} \\ \alpha_{i-1} \\ w_i \\ \psi_i \\ \alpha_i \\ \alpha_{i-\frac{1}{2}} \end{Bmatrix}$	(9.23)

Note that the dimensionless form has now been dispensed with, and the element length L has been introduced into the matrices of Fig. 9.3 in the form of the constants $C_1 = 1/L$ and $C_2 = 1/L^2$.

It should be emphasised that the dimensionless displacements were only used so that the resulting dynamic stiffness relation (9.22) could readily be converted to non-dimensional form if the need arose. By suitably combining the various constants in the matrix, it should be possible to form non-dimensional stiffness and inertia matrices in terms of the shear, thickness and frequency parameters⁽²⁰⁾ of the beam. This would facilitate a study of the effect of the individual parameters on the overall damping. However, this will not be pursued here, since the present work is directed towards predicting the forced response of specified beams, rather than carrying out detailed parameter surveys.

The stiffness and inertia matrices in Fig. 9.3 may now be reduced in size, as is shown below.

9.6 REDUCTION OF STIFFNESS MATRIX FROM 7 TO 6 DEGREES OF FREEDOM

As was explained on page 207, the 7×7 element stiffness matrix may be reduced to 6×6 by removing the co-ordinate $\alpha_{i-\frac{1}{2}}$ associated with the internal node. The reduction procedure is quite simple, and is as follows:

Consider the stiffness matrix partitioned into submatrices A, B, and C:

$$\begin{bmatrix} K \end{bmatrix}_{7 \times 7} = \begin{array}{|c|c|} \hline A & B \\ \hline B^T & C \\ \hline \end{array} \begin{array}{l} 1 \text{ --- } w_{i-1} \\ \\ \\ 6 \text{ --- } \alpha_i \\ 7 \text{ --- } \alpha_{i-\frac{1}{2}} \end{array}$$

We may then write

$$\begin{bmatrix} F_{i-1,i} \\ F_{i-\frac{1}{2}} \end{bmatrix}_{7 \times 1} = \begin{array}{|c|c|} \hline A & B \\ \hline B^T & C \\ \hline \end{array} \begin{bmatrix} \delta_{i-1,i} \\ \delta_{i-\frac{1}{2}} \end{bmatrix}_{7 \times 1} \quad (9.24)$$

where the upper parts of the force and displacement vectors contain the six forces and displacements at the nodes $i-1$ and i . These equations may be expanded in terms of the submatrices, and since no external forces are applied at node $i-\frac{1}{2}$, the force $F_{i-\frac{1}{2}} = 0$.

$$\begin{Bmatrix} F_{i-1,i} \end{Bmatrix} = \begin{bmatrix} A \end{bmatrix} \begin{Bmatrix} \delta_{i-1,i} \end{Bmatrix} + \begin{bmatrix} B \end{bmatrix} \begin{Bmatrix} \delta_{i-\frac{1}{2}} \end{Bmatrix} \quad (9.25)$$

$$\begin{Bmatrix} 0 \end{Bmatrix} = \begin{bmatrix} B \end{bmatrix}^T \begin{Bmatrix} \delta_{i-1,i} \end{Bmatrix} + \begin{bmatrix} C \end{bmatrix} \begin{Bmatrix} \delta_{i-\frac{1}{2}} \end{Bmatrix} \quad (9.26)$$

From (9.26),

$$\begin{Bmatrix} \delta_{i-\frac{1}{2}} \end{Bmatrix} = - \begin{bmatrix} C \end{bmatrix}^{-1} \begin{bmatrix} B \end{bmatrix}^T \begin{Bmatrix} \delta_{i-1,i} \end{Bmatrix} \quad (9.27)$$

Substitute (9.27) into (9.25) :

$$\begin{Bmatrix} F_{i-1,i} \end{Bmatrix} = \left(\begin{bmatrix} A \end{bmatrix} - \begin{bmatrix} B \end{bmatrix} \begin{bmatrix} C \end{bmatrix}^{-1} \begin{bmatrix} B \end{bmatrix}^T \right) \begin{Bmatrix} \delta_{i-1,i} \end{Bmatrix} \quad (9.28)$$

In the present case, $\begin{bmatrix} B \end{bmatrix}$ and $\begin{bmatrix} C \end{bmatrix}$ are respectively a vector and a scalar, so (9.28) simplifies to

$$\begin{Bmatrix} F_{i-1,i} \end{Bmatrix}_{6 \times 1} = \left(\begin{bmatrix} A \end{bmatrix} - \frac{1}{C} \begin{Bmatrix} B \end{Bmatrix} \begin{Bmatrix} B \end{Bmatrix}^T \right) \begin{Bmatrix} \delta_{i-1,i} \end{Bmatrix}_{6 \times 1} \quad (9.29)$$

This reduction is best performed numerically, and is a trivial operation once the 7 x 7 stiffness matrix of Fig. 9.3 has been set up. The inertia matrix is not included in the above, since there are no transverse inertia terms associated with the co-ordinate $\alpha_{i-\frac{1}{2}}$. However, the 6 x 6 inertia matrix is simply obtained by deleting the null row and column corresponding to this co-ordinate.

9.7 SUMMARY

Stiffness and inertia matrices have been derived for a 7 degree-of-freedom bending finite element of a symmetrical 5-layer beam. Uniform accuracy of strain representation has been assured by the introduction of an internal node, which may subsequently be eliminated, thereby reducing the matrix size to 6 x 6.

Results obtained with this element may be found in Chapter 12, and in addition to comparisons with measured data, a comparison is also made with an element derived using the inferior linear representation for α .

FIG. 9.2 STRAIN ENERGY AND STIFFNESS COEFFICIENTS

For bending finite element of symmetrical 5-layer beam

Strain energy coefficients

$$V_1 = 2q_2$$

$$V_2 = 2q_2$$

$$V_3 = -4q_2$$

$$V_4 = \frac{2}{3} t_2^2 (3r_1 + r_2)$$

$$V_5 = \frac{1}{12} \left[2r_1 (3\bar{a}_1^2 + t_1^2) + (6r_2 + r_3) t_3^2 \right]$$

$$V_6 = t_2 (2r_1 \bar{a}_1 + r_2 t_3)$$

$$q_2 = \frac{1}{2} b k_2 G_2 t_2$$

$$r_j = \frac{1}{2} b E_j t_j \quad (j = 1 \text{ to } 3)$$

$$\bar{a}_1 = t_1 + t_3$$

Note that the moduli E_2 and G_2 are complex in order to take account of the damping properties of the visco-elastic material

Stiffness coefficients (Used in stiffness matrix given in Fig. 9.3)

$$S_1 = 2 V_1 \frac{L}{60}$$

$$S_2 = 2 V_2 \frac{L}{30}$$

$$S_3 = V_3 \frac{L}{60}$$

$$S_4 = 2 V_4 \frac{1}{3L}$$

$$S_5 = 2 V_5 \frac{1}{L}$$

$$S_6 = V_6 \frac{1}{L}$$

Also note the constants

$$C_0 = \frac{\mu L^3}{420}, \quad C_1 = \frac{1}{L} \quad \text{and} \quad C_2 = \frac{1}{L^2}$$

where μ is the mass per unit length of the sandwich beam

FIG. 9.3

STIFFNESS AND INERTIA MATRICES FOR 7 DEGREE OF FREEDOM
BENDING FINITE ELEMENT OF SYMMETRICAL 5-LAYER BEAM

STIFFNESS MATRIX

1	$(36S_2+12S_3) \times C_2$	$(3S_2+6S_5) \times C_1$	$(-6S_3+4S_6) \times C_1$	$(-36S_2-12S_3) \times C_2$	$(3S_2+6S_5) \times C_1$	$(-6S_3+4S_6) \times C_1$	$(-48S_3-8S_6) \times C_1$	W_{i-1}
2		$(4S_2+4S_5)$	$(7S_3+3S_6)$	$(-3S_2-6S_5) \times C_1$	$(-S_2+2S_5)$	$(-3S_3+S_6)$	$(-4S_3-4S_6)$	ψ_{i-1}
3			$(8S_1+7S_4)$	$(6S_3-4S_6) \times C_1$	$(-3S_3+S_6)$	$(-2S_1+S_4)$	$(4S_1-8S_4)$	α_{i-1}
4				$(36S_2+12S_3) \times C_2$	$(-3S_2-6S_5) \times C_1$	$(6S_3-4S_6) \times C_1$	$(48S_3+8S_6) \times C_1$	W_i
5	S Y M M E T R I C				$(4S_2+4S_5)$	$(7S_3+3S_6)$	$(-4S_3-4S_6)$	ψ_i
6						$(8S_1+7S_4)$	$(4S_1-8S_4)$	α_i
7							$(32S_1+16S_4)$	$\alpha_{i-\frac{1}{2}}$
	1	2	3	4	5	6	7	

INERTIA MATRIX

1	$156C_0C_2$	$22C_0C_1$	0	$54C_0C_2$	$-13C_0C_1$	0	0	W_{i-1}
2		$4C_0$	0	$13C_0C_1$	$-3C_0$	0	0	ψ_{i-1}
3			0	0	0	0	0	α_{i-1}
4				$156C_0C_2$	$-22C_0C_1$	0	0	W_i
5	S Y M M E T R I C				$4C_0$	0	0	ψ_i
6						0	0	α_i
7							0	$\alpha_{i-\frac{1}{2}}$
	1	2	3	4	5	6	7	

CHAPTER 10BENDING FINITE ELEMENTS FOR UNSYMMETRICAL 3- AND 5-LAYER BEAMS10.1 INTRODUCTION

We shall immediately proceed to consider the unsymmetrical 5-layer beam. Since the asymmetry necessitates a completely general analysis, the 3-layer beam may be considered as the special case when layers 4 and 5 are of zero thickness. In consequence, a stiffness matrix will first be derived for the 5-layer beam, and the matrix for the 3-layer beam will subsequently be obtained from this by deleting all those terms which pertain to layers 4 and 5.

The unsymmetrical 5-layer element is shown in Fig. 10.1. Due to the asymmetry, the normals to the longitudinal fibres in layers 2 and 4 now rotate through different angles α and β . In addition, the middle of layer 3 is no longer the neutral axis of the beam, and it now suffers a longitudinal displacement u . In fact, the neutral axis is neither co-incident with the middle of layer 3 nor with the geometric centre-line of the beam, and for different end conditions its position can vary along the length of the beam. Apart from these two differences, all the assumptions made in the symmetrical beam analysis still apply.

10.2 NODAL CO-ORDINATES AND DISPLACEMENT FUNCTIONS

The nodal co-ordinates and the displacement functions are chosen in the same manner as before. Referring to Fig. 10.1b, it is seen that the displacement of any point on an initially plane section may be described in terms of the co-ordinates w , ψ , α , β and u . By using these 5 co-ordinates at the two external nodes $i-1$ and i , plus the α , β and u co-ordinates at the internal node $i-\frac{1}{2}$, we are able to employ the following displacement functions:

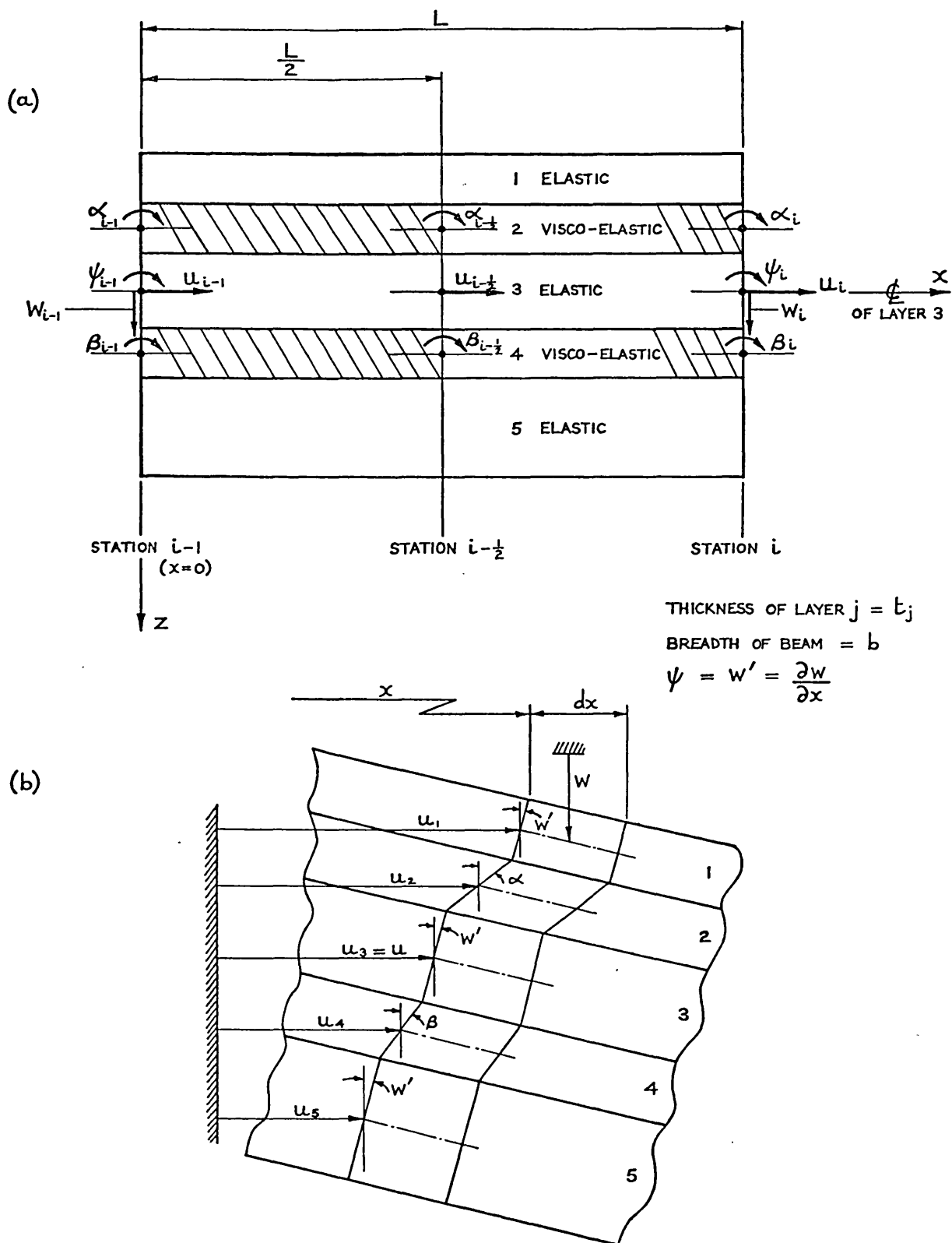


FIG. 10.1

BENDING FINITE ELEMENT FOR UNSYMMETRICAL 5-LAYER BEAM

$$\begin{aligned}
 \frac{w}{L} &= a_0 + a_1 \xi + a_2 \xi^2 + a_3 \xi^3 \\
 \alpha &= b_0 + b_1 \xi + b_2 \xi^2 \\
 \beta &= c_0 + c_1 \xi + c_2 \xi^2 \\
 \frac{u}{L} &= d_0 + d_1 \xi + d_2 \xi^2
 \end{aligned} \tag{10.1}$$

where $\xi = \frac{x}{L}$ and $a_j = a_j(t)$, etc.

Using these functions a 13 x 13 stiffness matrix will be derived for the 5-layer element, and a 10 x 10 matrix will subsequently be obtained for the 3-layer element. By eliminating the co-ordinates associated with the internal node, the numbers of degrees of freedom will be reduced to 10 and 8 respectively.

The present choice of nodal co-ordinates and displacement functions may be compared with that of Leone and Perlman^{(23)*}, who have derived a finite element for the unsymmetrical 3-layer beam. They have introduced nodes only at the ends of the element, and they make the four co-ordinates w , $\frac{\partial w}{\partial x}$, u_3 and $\frac{\partial u_3}{\partial x}$ continuous at these nodes ($u_3 = u$ in the present analysis). They then employ cubic displacement functions for w and for the core shear strain γ (rather than for u_3), so the resulting finite element has 8 degrees of freedom, just like the reduced version of the element which will be derived in this report. A slight limitation of their element for general structural analysis is the fact that it is derived on the assumption that the net axial force on a section is zero, so its use is limited to flexural vibration, and it cannot be used to

* Note that References for Chapters 8 to 12 are listed on Page 283.

describe axial vibration. Although only transverse motion and inertia are considered in the present work, the basic 10 x 10 stiffness matrix describes both bending and stretching of the beam element. The subsequent reduction to an 8 x 8 stiffness matrix is possible if axial inertia is ignored, but this simplification is only introduced at the final stage.

10.3 STRAIN AND KINETIC ENERGIES

Shear Strain Energy in Visco-elastic Layers

The shear strain energy in the two visco-elastic layers is given by

$$\begin{aligned}
 V_{\text{shear}} = & \frac{1}{2} b k_2 G_2 t_2 \int_0^L (\alpha - w')^2 dx \\
 & + \frac{1}{2} b k_4 G_4 t_4 \int_0^L (\beta - w')^2 dx
 \end{aligned} \tag{10.2}$$

where k_2 and k_4 are the shear constants for the visco-elastic layers, and $(\alpha - w')$ and $(\beta - w')$ are the shear strains.

Bending Strain Energy in All Layers

The total bending strain energy in all the layers is given by

$$\begin{aligned}
 V_{\text{bend}} = & \frac{b E_1 t_1^3}{2 \times 12} \int_0^L w''^2 dx & + & \frac{b E_2 t_2^3}{2 \times 12} \int_0^L \alpha'^2 dx \\
 & + \frac{b E_3 t_3^3}{2 \times 12} \int_0^L w''^2 dx & + & \frac{b E_4 t_4^3}{2 \times 12} \int_0^L \beta'^2 dx \\
 & + \frac{b E_5 t_5^3}{2 \times 12} \int_0^L w''^2 dx
 \end{aligned} \tag{10.3}$$

Extensional Strain Energy in All Layers

The total extensional or stretching energy in all the layers is given by

$$V_{\text{ext}} = \frac{b}{2} \sum_{j=1 \text{ to } 5} E_j t_j \int_0^L \left(\frac{\partial u_j}{\partial x} \right)^2 dx \quad (10.4)$$

Referring to Fig. 10.1b, it is readily seen that the longitudinal displacements of the layers are as follows:

$$\begin{aligned} u_1 &= u + t_2 \alpha + \frac{(t_1 + t_3)}{2} w' \\ u_2 &= u + \frac{t_2}{2} \alpha + \frac{t_3}{2} w' \\ u_3 &= u \\ u_4 &= u - \frac{t_4}{2} \beta - \frac{t_3}{2} w' \\ u_5 &= u - t_4 \beta - \frac{(t_3 + t_5)}{2} w' \end{aligned} \quad (10.5)$$

Substituting the displacements (10.5) into (10.4), we obtain

$$\begin{aligned} V_{\text{ext}} &= \frac{1}{2} b E_1 t_1 \int_0^L \left[u' + t_2 \alpha' + \frac{(t_1 + t_3)}{2} w'' \right]^2 dx \\ &+ \frac{1}{2} b E_2 t_2 \int_0^L \left[u' + \frac{t_2}{2} \alpha' + \frac{t_3}{2} w'' \right]^2 dx \\ &+ \frac{1}{2} b E_3 t_3 \int_0^L u'^2 dx \\ &+ \frac{1}{2} b E_4 t_4 \int_0^L \left[u' - \frac{t_4}{2} \beta' - \frac{t_3}{2} w'' \right]^2 dx \\ &+ \frac{1}{2} b E_5 t_5 \int_0^L \left[u' - t_4 \beta' - \frac{(t_3 + t_5)}{2} w'' \right]^2 dx \end{aligned} \quad (10.6)$$

Total Strain Energy

The total strain energy in the finite element is

$$V = V_{\text{shear}} + V_{\text{bend}} + V_{\text{ext}}$$

Summing the energy expressions (10.2), (10.3) and (10.6), we obtain

$$\begin{aligned}
 V = & q_{v_2} \int_0^L (\alpha - w')^2 dx \\
 & + q_{v_4} \int_0^L (\beta - w')^2 dx \\
 & + r_1 \int_0^L \left[u' + t_2 \alpha' + \frac{(t_1 + t_3)}{2} w'' \right]^2 + \frac{t_1^2}{12} w'''^2 dx \\
 & + r_2 \int_0^L \left[u' + \frac{t_2}{2} \alpha' + \frac{t_3}{2} w'' \right]^2 + \frac{t_2^2}{12} \alpha'^2 dx \\
 & + r_3 \int_0^L u'^2 + \frac{t_3^2}{12} w'''^2 dx \\
 & + r_4 \int_0^L \left[u' - \frac{t_4}{2} \beta' - \frac{t_3}{2} w'' \right]^2 + \frac{t_4^2}{12} \beta'^2 dx \\
 & + r_5 \int_0^L \left[u' - t_4 \beta' - \frac{(t_3 + t_5)}{2} w'' \right]^2 + \frac{t_5^2}{12} w'''^2 dx
 \end{aligned}
 \tag{10.7}$$

where $q_{v_j} = \frac{b k_j G_j t_j}{2}$ ($j = 2$ and 4)

$r_j = \frac{b E_j t_j}{2}$ ($j = 1$ to 5)

Expression (10.7) may now be expanded into the sum of 14 integrals:

$$\begin{aligned}
 V = & V_1 \int_0^L \alpha^2 dx & + & V_2 \int_0^L \beta^2 dx \\
 & + V_3 \int_0^L w'^2 dx & + & V_4 \int_0^L \alpha w' dx \\
 & + V_5 \int_0^L \beta w' dx & + & V_6 \int_0^L \alpha'^2 dx \\
 & + V_7 \int_0^L \beta'^2 dx & + & V_8 \int_0^L u'^2 dx \\
 & + V_9 \int_0^L u' \alpha' dx & + & V_{10} \int_0^L u' \beta' dx \\
 & + V_{11} \int_0^L w''^2 dx & + & V_{12} \int_0^L \alpha' w'' dx \\
 & + V_{13} \int_0^L \beta' w'' dx & + & V_{14} \int_0^L u' w'' dx
 \end{aligned} \tag{10.8}$$

The constants V_1 to V_{14} are listed in Fig. 10.2.

Kinetic Energy

The kinetic energy due to transverse motion is given by

$$\begin{aligned}
 T &= \frac{b}{2} \sum_{j=1 \text{ to } 5} \rho_j t_j \int_0^L \dot{w}^2 dx \\
 &= \frac{b}{2} \underbrace{[\rho_1 t_1 + \rho_2 t_2 + \rho_3 t_3 + \rho_4 t_4 + \rho_5 t_5]}_{\frac{\mu}{2}} \int_0^L \dot{w}^2 dx
 \end{aligned} \tag{10.9}$$

where $\dot{} = \frac{\partial}{\partial t}$

Rotary and axial kinetic energies will not be considered.

FIG. 10.2 STRAIN ENERGY COEFFICIENTS

For bending of unsymmetrical 3- and 5-layer beams

$$V_1 = q_2$$

$$V_2 = q_4$$

$$V_3 = (q_2 + q_4)$$

$$V_4 = -2q_2$$

$$V_5 = -2q_4$$

$$V_6 = \frac{1}{3} t_2^2 (3r_1 + r_2)$$

$$V_7 = \frac{1}{3} t_4^2 (r_4 + 3r_5)$$

$$V_8 = (r_1 + r_2 + r_3 + r_4 + r_5)$$

$$V_9 = t_2(2r_1 + r_2)$$

$$V_{10} = -t_4(r_4 + 2r_5)$$

$$V_{11} = \frac{1}{12} \left[r_1(3\bar{a}_1^2 + t_1^2) + (3r_2 + r_3 + 3r_4)t_3^2 + r_5(3\bar{a}_2^2 + t_5^2) \right]$$

$$V_{12} = \frac{1}{2} t_2(2r_1\bar{a}_1 + r_2t_3)$$

$$V_{13} = \frac{1}{2} t_4(r_4t_3 + 2r_5\bar{a}_2)$$

$$V_{14} = \left[r_1\bar{a}_1 + (r_2 - r_4)t_3 - r_5\bar{a}_2 \right]$$

$$q_j = \frac{1}{2} b k_j G_j t_j \quad (j = 2 \text{ and } 4)$$

$$r_j = \frac{1}{2} b E_j t_j \quad (j = 1 \text{ to } 5)$$

$$\bar{a}_1 = t_1 + t_3$$

$$\bar{a}_2 = t_3 + t_5$$

Note that the moduli E and G for the visco-elastic layers 2 and 4 are complex in order to take account of the damping properties

10.4 FORMULATION OF ENERGY EXPRESSIONS IN TERMS OF ASSUMED DISPLACEMENT FUNCTIONS

The procedure is the same as for the symmetrical 5-layer beam considered previously. In consequence, only the essential details will be given here, and the displacement functions and their derivatives will be written directly in terms of the nodal displacements:

$$\begin{aligned}
 w &= L [X] [T_1] \{ \delta_w \} \\
 w' &= [X'] [T_1] \{ \delta_w \} \\
 w'' &= \frac{1}{L} [X''] [T_1] \{ \delta_w \} \\
 \alpha &= [\bar{X}] [T_2] \{ \delta_\alpha \} \\
 \alpha' &= \frac{1}{L} [\bar{X}'] [T_2] \{ \delta_\alpha \} \\
 \beta &= [\bar{X}] [T_2] \{ \delta_\beta \} \\
 \beta' &= \frac{1}{L} [\bar{X}'] [T_2] \{ \delta_\beta \} \\
 u &= L [\bar{X}] [T_2] \{ \delta_u \} \\
 u' &= [\bar{X}'] [T_2] \{ \delta_u \}
 \end{aligned} \tag{10.10}$$

where the matrices $[X]$, $[\bar{X}]$, $[T_1]$, etc. are exactly the same as in the previous analysis, and the dimensionless nodal displacement vectors are the following:

$$\left\{ \delta_w \right\} = \begin{Bmatrix} \frac{w_{i-1}}{L} \\ \psi_{i-1} \\ \frac{w_i}{L} \\ \psi_i \end{Bmatrix} \quad \left\{ \delta_\alpha \right\} = \begin{Bmatrix} \alpha_{i-1} \\ \alpha_i \\ \alpha_{i-\frac{1}{2}} \end{Bmatrix} \quad \left\{ \delta_\beta \right\} = \begin{Bmatrix} \beta_{i-1} \\ \beta_i \\ \beta_{i-\frac{1}{2}} \end{Bmatrix} \quad \left\{ \delta_u \right\} = \begin{Bmatrix} \frac{u_{i-1}}{L} \\ \frac{u_i}{L} \\ \frac{u_{i-\frac{1}{2}}}{L} \end{Bmatrix} \tag{10.11}$$

Substituting the functions (10.10) into the fourteen strain energy integrals (10.8), we obtain the total strain energy in matrix form:

$$\begin{aligned}
V = & \frac{V_1 L}{60} \{ \delta_\alpha \}^T [A_1] \{ \delta_\alpha \} + \frac{V_2 L}{60} \{ \delta_\beta \}^T [A_1] \{ \delta_\beta \} + \frac{V_3 L}{30} \{ \delta_w \}^T [A_2] \{ \delta_w \} \\
& + \frac{V_4 L}{60} \{ \delta_\alpha \}^T [A_3] \{ \delta_w \} + \frac{V_5 L}{60} \{ \delta_\beta \}^T [A_3] \{ \delta_w \} + \frac{V_6}{3L} \{ \delta_\alpha \}^T [A_4] \{ \delta_\alpha \} \\
& + \frac{V_7}{3L} \{ \delta_\beta \}^T [A_4] \{ \delta_\beta \} + \frac{V_8}{3L} \{ \delta_u \}^T [A_4] \{ \delta_u \} + \frac{V_9}{3L} \{ \delta_u \}^T [A_4] \{ \delta_\alpha \} \\
& + \frac{V_{10}}{3L} \{ \delta_u \}^T [A_4] \{ \delta_\beta \} + \frac{V_{11}}{L} \{ \delta_w \}^T [A_5] \{ \delta_w \} + \frac{V_{12}}{L} \{ \delta_\alpha \}^T [A_6] \{ \delta_w \} \\
& + \frac{V_{13}}{L} \{ \delta_\beta \}^T [A_6] \{ \delta_w \} + \frac{V_{14}}{L} \{ \delta_u \}^T [A_6] \{ \delta_w \}
\end{aligned} \tag{10.12}$$

where the six matrices $[A_1]$ to $[A_6]$ are the same as before, due to the use of quadratic expressions for α , β and u .

The kinetic energy does not change at all, and is given by

$$T = \frac{\mu L^3}{2 \times 420} \{ \dot{\delta}_w \}^T [A_7] \{ \dot{\delta}_w \} \tag{10.13}$$

10.5 STIFFNESS AND INERTIA MATRICES FOR THE ELEMENT

The stiffness and inertia matrices are obtained from the energy expressions (10.12) and (10.13) by using the Lagrange equation. Since the procedure has been explained in the previous chapter with reference to the symmetrical 5-layer element, it is not necessary to consider the details here.

The stiffness matrices for the 5- and 3-layer elements respectively are shown in Figs. 10.4 and 10.5, and are for use with the following force and displacement vectors:

<u>Unsymmetrical 5-layer (13 d.f.)</u>		<u>Unsymmetrical 3-layer (10 d.f.)</u>	
Force	Displacement	Force	Displacement
$\begin{Bmatrix} F_{w_{i-1}} \\ M_{\psi_{i-1}} \\ M_{\alpha_{i-1}} \\ M_{\beta_{i-1}} \\ F_{u_{i-1}} \\ F_{w_i} \\ M_{\psi_i} \\ M_{\alpha_i} \\ M_{\beta_i} \\ F_{u_i} \\ M_{\alpha_{i-\frac{1}{2}}} \\ M_{\beta_{i-\frac{1}{2}}} \\ F_{u_{i-\frac{1}{2}}} \end{Bmatrix}$	$\begin{Bmatrix} w_{i-1} \\ \psi_{i-1} \\ \alpha_{i-1} \\ \beta_{i-1} \\ u_{i-1} \\ w_i \\ \psi_i \\ \alpha_i \\ \beta_i \\ u_i \\ \alpha_{i-\frac{1}{2}} \\ \beta_{i-\frac{1}{2}} \\ u_{i-\frac{1}{2}} \end{Bmatrix}$	$\begin{Bmatrix} F_{w_{i-1}} \\ M_{\psi_{i-1}} \\ M_{\alpha_{i-1}} \\ F_{u_{i-1}} \\ F_{w_i} \\ M_{\psi_i} \\ M_{\alpha_i} \\ F_{u_i} \\ M_{\alpha_{i-\frac{1}{2}}} \\ F_{u_{i-\frac{1}{2}}} \end{Bmatrix}$	$\begin{Bmatrix} w_{i-1} \\ \psi_{i-1} \\ \alpha_{i-1} \\ u_{i-1} \\ w_i \\ \psi_i \\ \alpha_i \\ u_i \\ \alpha_{i-\frac{1}{2}} \\ u_{i-\frac{1}{2}} \end{Bmatrix}$

(10.14)

The stiffness coefficients S_1 to S_{14} are listed in Fig. 10.3. As before, the element length has been introduced into the stiffness matrices in the form of the constants $C_1 = \frac{1}{L}$ and $C_2 = \frac{1}{L^2}$. The matrix for the 3-layer element has been obtained from that for the 5-layer element simply by deleting all those terms which become zero when $t_4 = t_5 = 0$. The removal of the rows and columns corresponding to the β co-ordinates reduces the matrix size from 13 x 13 to 10 x 10.

The inertia matrix is basically the same as for the symmetrical element and will not be given here. The order of the stiffness matrix may now be reduced by removing the node $i - \frac{1}{2}$.

10.6 REDUCTION OF ORDER OF STIFFNESS MATRIX

The procedure has been fully explained with reference to the symmetrical 5-layer element (see page 217), and will only be briefly summarised here.

The stiffness matrices for the 5- and 3-layer elements respectively may be partitioned as follows:

$$\text{Unsymmetrical 5-Layer } \begin{bmatrix} K \\ 13 \times 13 \end{bmatrix} = \begin{array}{|c|c|} \hline A & B \\ \hline B^T & C \\ \hline \end{array} \begin{array}{l} 1 \text{ --- } w_{i-1} \\ \\ 10 \text{ --- } u_i \\ 11 \text{ --- } \alpha_{i-\frac{1}{2}} \\ 13 \text{ --- } u_{i-\frac{1}{2}} \end{array}$$

$$\text{Unsymmetrical 3-Layer } \begin{bmatrix} K \\ 10 \times 10 \end{bmatrix} = \begin{array}{|c|c|} \hline A & B \\ \hline B^T & C \\ \hline \end{array} \begin{array}{l} 1 \text{ --- } w_{i-1} \\ \\ 8 \text{ --- } u_i \\ 9 \text{ --- } \alpha_{i-\frac{1}{2}} \\ 10 \text{ --- } u_{i-\frac{1}{2}} \end{array}$$

By eliminating the co-ordinates corresponding to the node $i - \frac{1}{2}$, one obtains a reduced order stiffness matrix:

$$\begin{bmatrix} K \\ 5 \text{ Layer --- } 10 \times 10 \\ 3 \text{ Layer --- } 8 \times 8 \end{bmatrix} = \begin{bmatrix} A \\ 10 \times 10 \end{bmatrix} - \begin{bmatrix} B \\ 10 \times 2 \end{bmatrix} \begin{bmatrix} C \\ 2 \times 2 \end{bmatrix}^{-1} \begin{bmatrix} B^T \\ 2 \times 10 \end{bmatrix} \quad (10.15)$$

which is referred to the end nodes $i-1$ and i only.

10.7 SUMMARY

Stiffness matrices have been derived for unsymmetrical 5- and 3-layer beam elements, these having 13 and 10 degrees of freedom respectively. As with the symmetrical beam element, uniform accuracy of strain representation has been assured by the introduction of an internal node, which may subsequently be eliminated, thereby reducing the matrix sizes to 10×10 and 8×8 respectively.

Results obtained with these elements may be found in Chapter 12.

FIG. 10.3 STIFFNESS COEFFICIENTS

Used in stiffness matrices for bending finite elements of unsymmetrical 3- and 5-layer beams (See Figs. 10.4 and 10.5)

$$S_1 = 2 V_1 \frac{L}{60}$$

$$S_2 = 2 V_2 \frac{L}{60}$$

$$S_3 = 2 V_3 \frac{L}{30}$$

$$S_4 = V_4 \frac{L}{60}$$

$$S_5 = V_5 \frac{L}{60}$$

$$S_6 = 2 V_6 \frac{1}{3L}$$

$$S_7 = 2 V_7 \frac{1}{3L}$$

$$S_8 = 2 V_8 \frac{L}{3}$$

$$S_9 = V_9 \frac{1}{3}$$

$$S_{10} = V_{10} \frac{1}{3}$$

$$S_{11} = 2 V_{11} \frac{1}{L}$$

$$S_{12} = V_{12} \frac{1}{L}$$

$$S_{13} = V_{13} \frac{1}{L}$$

$$S_{14} = V_{14}$$

The strain energy coefficients V_j are listed in Fig. 10.2

Also note the constants

$$C_1 = \frac{1}{L} \quad \text{and} \quad C_2 = \frac{1}{L^2}$$

FIG. 10.4

STIFFNESS MATRIX FOR 13 DEGREE OF FREEDOM FINITE ELEMENT OF UNSYMMETRICAL 5-LAYER BEAM

1	$(36S_3+12S_{11}) \times C_2$	$(3S_3+6S_{11}) \times C_1$	$(-6S_4+4S_{12}) \times C_1$	$(-6S_5+4S_{13}) \times C_1$	$4S_{14}C_2$	$(-36S_3-12S_{11}) \times C_2$	$(3S_3+6S_{11}) \times C_1$	$(-6S_4+4S_{12}) \times C_1$	$(-6S_5+4S_{13}) \times C_1$	$4S_{14}C_2$	$(-48S_4-8S_{12}) \times C_1$	$(-48S_5-8S_{13}) \times C_1$	$-8S_{14}C_2$	W_{i-1}
2		$(4S_3+4S_{11})$	$(7S_4+3S_{12})$	$(7S_5+3S_{13})$	$3S_{14}C_1$	$(-3S_3-6S_{11}) \times C_1$	$(-S_3+2S_{11})$	$(-3S_4+S_{12})$	$(-3S_5+S_{13})$	$S_{14}C_1$	$(-4S_4-4S_{12})$	$(-4S_5-4S_{13})$	$-4S_{14}C_1$	ψ_{i-1}
3			$(8S_1+7S_6)$	0	$7S_9C_1$	$(6S_4-4S_{12}) \times C_1$	$(-3S_4+S_{12})$	$(-2S_1+S_6)$	0	S_9C_1	$(4S_1-8S_6)$	0	$-8S_9C_1$	α_{i-1}
4				$(8S_2+7S_7)$	$7S_{10}C_1$	$(6S_5-4S_{13}) \times C_1$	$(-3S_5+S_{13})$	0	$(-2S_2+S_7)$	$S_{10}C_1$	0	$(4S_2-8S_7)$	$-8S_{10}C_1$	β_{i-1}
5					$7S_8C_2$	$-4S_{14}C_2$	$S_{14}C_1$	S_9C_1	$S_{10}C_1$	S_8C_2	$-8S_9C_1$	$-8S_{10}C_1$	$-8S_8C_2$	u_{i-1}
6						$(36S_3+12S_{11}) \times C_2$	$(-3S_3-6S_{11}) \times C_1$	$(6S_4-4S_{12}) \times C_1$	$(6S_5-4S_{13}) \times C_1$	$-4S_{14}C_2$	$(48S_4+8S_{12}) \times C_1$	$(48S_5+8S_{13}) \times C_1$	$8S_{14}C_2$	W_i
7							$(4S_3+4S_{11})$	$(7S_4+3S_{12})$	$(7S_5+3S_{13})$	$3S_{14}C_1$	$(-4S_4-4S_{12})$	$(-4S_5-4S_{13})$	$-4S_{14}C_1$	ψ_i
8								$(8S_1+7S_6)$	0	$7S_9C_1$	$(4S_1-8S_6)$	0	$-8S_9C_1$	α_i
9									$(8S_2+7S_7)$	$7S_{10}C_1$	0	$(4S_2-8S_7)$	$-8S_{10}C_1$	β_i
10										$7S_8C_2$	$-8S_9C_1$	$-8S_{10}C_1$	$-8S_8C_2$	u_i
11											$(32S_1+16S_6)$	0	$16S_9C_1$	$\alpha_{i-\frac{1}{2}}$
12												$(32S_2+16S_7)$	$16S_{10}C_1$	$\beta_{i-\frac{1}{2}}$
13													$16S_8C_2$	$u_{i-\frac{1}{2}}$
	1	2	3	4	5	6	7	8	9	10	11	12	13	

FIG. 10.5

STIFFNESS MATRIX FOR 10 DEGREE OF FREEDOM FINITE ELEMENT OF UNSYMMETRICAL 3-LAYER BEAM

1	$(36S_3+12S_{11}) \times C_2$	$(3S_3+6S_{11}) \times C_1$	$(-6S_4+4S_{12}) \times C_1$	$4S_{14}C_2$	$(-36S_3-12S_{11}) \times C_2$	$(3S_3+6S_{11}) \times C_1$	$(-6S_4+4S_{12}) \times C_1$	$4S_{14}C_2$	$(-48S_4-8S_{12}) \times C_1$	$-8S_{14}C_2$	W_{i-1}
2		$(4S_3+4S_{11})$	$(7S_4+3S_{12})$	$3S_{14}C_1$	$(-3S_3-6S_{11}) \times C_1$	$(-S_3+2S_{11})$	$(-3S_4+S_{12})$	$S_{14}C_1$	$(-4S_4-4S_{12})$	$-4S_{14}C_1$	ψ_{i-1}
3			$(8S_1+7S_6)$	$7S_9C_1$	$(6S_4-4S_{12}) \times C_1$	$(-3S_4+S_{12})$	$(-2S_1+S_6)$	S_9C_1	$(4S_1-8S_6)$	$-8S_9C_1$	α_{i-1}
4				$7S_8C_2$	$-4S_{14}C_2$	$S_{14}C_1$	S_9C_1	S_8C_2	$-8S_9C_1$	$-8S_8C_2$	u_{i-1}
5					$(36S_3+12S_{11}) \times C_2$	$(-3S_3-6S_{11}) \times C_1$	$(6S_4-4S_{12}) \times C_1$	$-4S_{14}C_2$	$(48S_4+8S_{12}) \times C_1$	$8S_{14}C_2$	W_i
6						$(4S_3+4S_{11})$	$(7S_4+3S_{12})$	$3S_{14}C_1$	$(-4S_4-4S_{12})$	$-4S_{14}C_1$	ψ_i
7							$(8S_1+7S_6)$	$7S_9C_1$	$(4S_1-8S_6)$	$-8S_9C_1$	α_i
8		S	Y	M	M	E	T	R	I	C	u_i
9									$(32S_1+16S_6)$	$16S_9C_1$	$\alpha_{i-\frac{1}{2}}$
10										$16S_8C_2$	$u_{i-\frac{1}{2}}$
	1	2	3	4	5	6	7	8	9	10	

CHAPTER 11

TORSIONAL FINITE ELEMENT FOR SYMMETRICAL 5-LAYER BEAM

11.1 INTRODUCTION

The analysis of the torsional vibration of a multi-layer beam is more complex than the corresponding bending analysis. No longer are we confronted with a simple plane stress problem; since an element of any layer is now able to stretch, bend and twist in any plane. In view of the greater complexity, it is necessary to start with the general strain energy expressions for a multi-layer plate. By making certain assumptions regarding the behaviour of the layers during torsion, these energy expressions may later be simplified slightly.

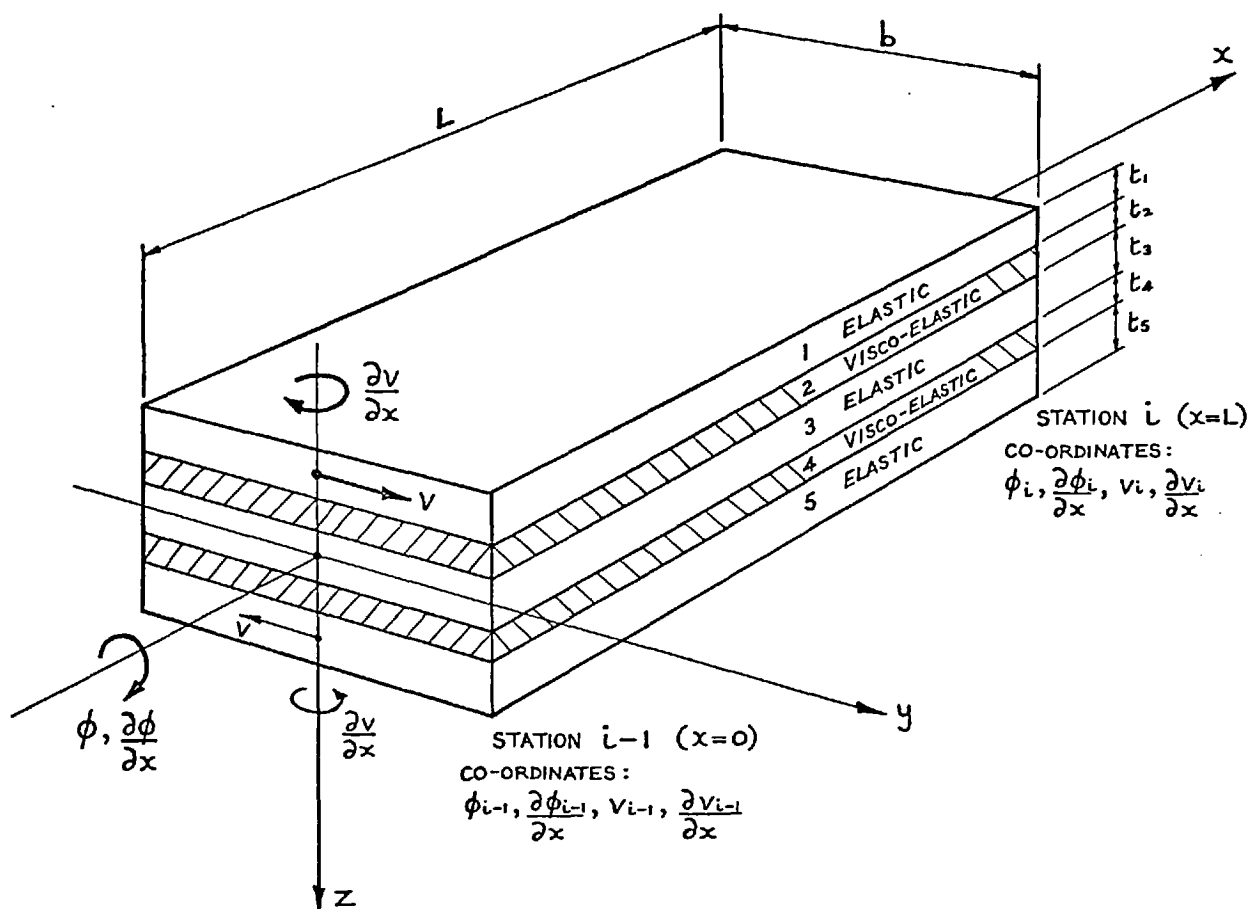
Fig. 11.1 shows the finite element of beam. The distortion with which we are concerned is the pure twist ϕ about the x axis, under the action of opposing couples at stations $i-1$ and i of the element. Due to the symmetry of the beam section about the y and z axes, layer 3 just twists about the x axis, whilst layers 1 and 5 not only twist in the same manner as layer 3, but they also translate and bend laterally in their respective planes. The lateral displacement v of layer 1 is equal and opposite to that of layer 5, and it obviously varies along the length of the element. The relatively complex motion of the centre and outer layers causes the visco-elastic layers to shear in both the x-z and y-z planes, thereby dissipating energy.

Before proceeding further we shall consider the various assumptions used in the analysis. Since the torsion problem differs considerably from the bending problems dealt with in the last two chapters, a new list of assumptions will be given:

- (1) The elastic layers 1, 3 and 5 bend according to standard thin plate theory, and the effect of shear is therefore ignored.

- (2) The visco-elastic layers 2 and 4 shear in both the $x-z$ and $y-z$ planes, and in both cases the in-plane displacement in the direction of shear is assumed to vary linearly across the thickness of the layer. Due to symmetry, the two layers shear by equal amounts. Stretching and bending effects are also included.
- (3) All layers are homogeneous and *isotropic*.
- (4) All displacements are small, as in linear elasticity theory.
- (5) There is perfect continuity at all interfaces between layers, and no slip occurs when the sandwich twists.
- (6) The layers do not compress in the z direction (i.e. $\frac{\partial w}{\partial z} = 0$)*
- (7) The layers do not bend or stretch in the $y-z$ plane (i.e. across their width). Thus $\frac{\partial^2 w}{\partial y^2} = \frac{\partial v}{\partial y} = 0$
- (8) On any line parallel to the y axis, the longitudinal displacement u varies linearly across the width of the beam, and is zero wherever the line cuts the $x-z$ plane or is co-incident with the $x-y$ plane. In consequence, $u=0$ for any point on the $x-z$ or $x-y$ plane.
- (9) The x axis forms the centre line of layer 3, and due to symmetry it is also the axis of twist of the sandwich.
- (10) The strain dependence of the visco-elastic material properties is not sufficiently significant to warrant its inclusion in the analysis.
- (11) The only significant inertia terms are those pertaining to motion in the $y-z$ plane (translations in y and z directions, and rotation about x axis). The effects of longitudinal motion and of rotation about the y axis will be ignored.

* Note that u , v and w refer to displacements in the x , y and z directions.



LAYER $\left\{ \begin{matrix} 4 \\ 5 \end{matrix} \right\}$ IS IDENTICAL TO LAYER $\left\{ \begin{matrix} 2 \\ 1 \end{matrix} \right\}$

ASSUMED DISPLACEMENT FUNCTIONS:

$$\phi = \phi(x, t) = a_0 + a_1 \xi + a_2 \xi^2 + a_3 \xi^3$$

$$\frac{v}{L} = \frac{v(x, t)}{L} = b_0 + b_1 \xi + b_2 \xi^2 + b_3 \xi^3$$

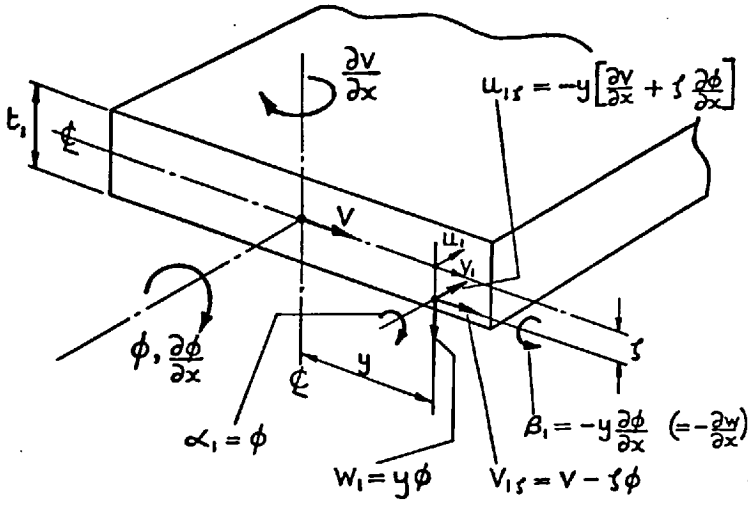
WHERE $\xi = \frac{x}{L}$

$$a_j = a_j(t), \quad b_j = b_j(t), \quad j=0,3$$

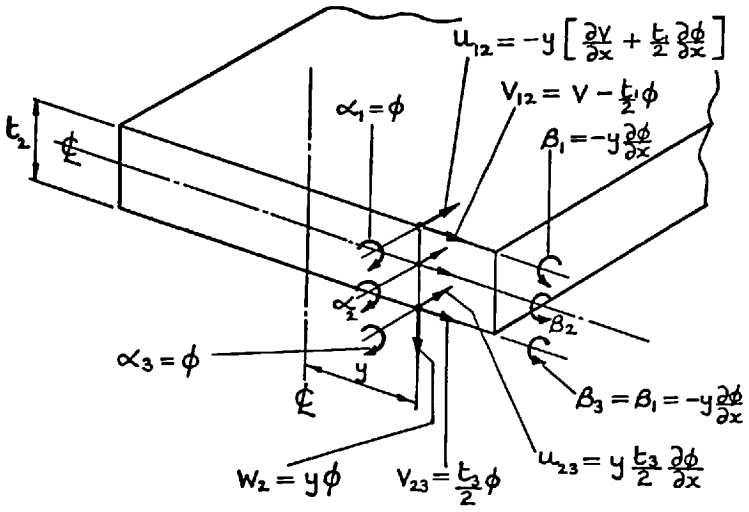
FIG. 11.1

TORSIONAL FINITE ELEMENT FOR SYMMETRICAL 5-LAYER BEAM

LAYER 1



LAYER 2



LAYER 3

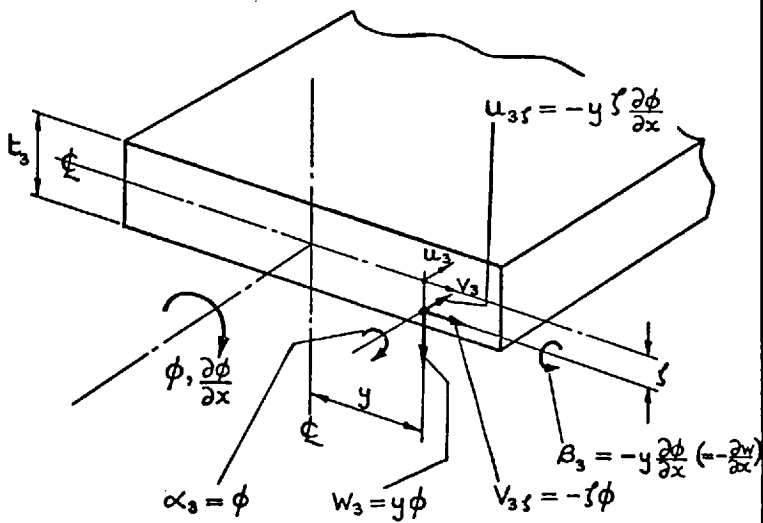
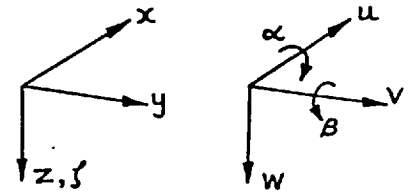


FIG. 11.2

DISPLACEMENTS OF LAYERS,
IN TERMS OF $\phi, \frac{\partial \phi}{\partial x}, v, \frac{\partial v}{\partial x}$



CO-ORDINATES

DISPLACEMENTS

$$u_1 = -y \frac{\partial v}{\partial x}$$

$$v_1 = v$$

$$w_1 = y\phi$$

$$\alpha_1 = \phi$$

$$\beta_1 = -y \frac{\partial \phi}{\partial x}$$

$$u_2 = -\frac{y}{2} \left[\frac{\partial v}{\partial x} + \frac{(t_1 - t_3)}{2} \frac{\partial \phi}{\partial x} \right]$$

$$v_2 = \frac{1}{2} \left[v - \frac{(t_1 - t_3)}{2} \phi \right]$$

$$w_2 = y\phi$$

$$\alpha_2 = \frac{1}{t_2} \left[v - \frac{(t_1 + t_3)}{2} \phi \right]$$

$$\beta_2 = \frac{y}{t_2} \left[\frac{\partial v}{\partial x} + \frac{(t_1 + t_3)}{2} \frac{\partial \phi}{\partial x} \right]$$

SHEAR $\gamma_{yz} = \alpha_2 - \alpha_1$
 $= \frac{1}{t_2} \left[v - \frac{(t_1 + 2t_2 + t_3)}{2} \phi \right]$

SHEAR $\gamma_{xz} = \beta_2 - \beta_1$
 $= \frac{y}{t_2} \left[\frac{\partial v}{\partial x} + \frac{(t_1 + 2t_2 + t_3)}{2} \frac{\partial \phi}{\partial x} \right]$

$$u_3 = 0$$

$$v_3 = 0$$

$$w_3 = y\phi$$

$$\alpha_3 = \phi$$

$$\beta_3 = -y \frac{\partial \phi}{\partial x}$$

Assumption (1) is valid provided that the elastic layers are not thick. Assumption (6) is possibly less valid in the torsion case than in the bending case considered previously. Assumption (7) follows from the fact that we are considering a beam, and not a plate. It is obviously valid as long as the beam is not too wide.

11.2 NODAL CO-ORDINATES AND DISPLACEMENT FUNCTIONS

Co-ordinates must be chosen which will completely describe the distortion of any initially plane section when the sandwich is twisted. Referring to Fig. 11.2, and bearing in mind the assumptions listed above, it is seen that the four co-ordinates ϕ , $\frac{\partial\phi}{\partial x}$, v and $\frac{\partial v}{\partial x}$ are sufficient to describe the three displacement components u , v and w at any point on the section. Therefore, subject to the choice of correct displacement functions, the solution must converge if these co-ordinates are made continuous at the nodes $i-1$ and i of the element. Although the rate of twist $\frac{\partial\phi}{\partial x}$ is not a displacement in the conventional sense, it must be included as a nodal co-ordinate in order to ensure continuity of the layer end rotations β_1 to β_5 across the interface between adjacent elements (i.e. It ensures slope continuity. Note that $\beta_1 = \beta_3 = \beta_5 = -\frac{\partial w}{\partial x} = -y \frac{\partial\phi}{\partial x}$).

Thus, a minimum of 8 nodal co-ordinates may be used. This enables us to represent both ϕ and v by cubic polynomials:

$$\begin{aligned}\phi &= a_0 + a_1 \xi + a_2 \xi^2 + a_3 \xi^3 \\ \frac{v}{L} &= b_0 + b_1 \xi + b_2 \xi^2 + b_3 \xi^3\end{aligned}\tag{11.1}$$

where $\xi = \frac{x}{L}$ and $a_j = a_j(t)$, etc.

Once again the dimensionless forms are used to simplify the algebraic analysis. Using the procedure outlined in Appendix V, it may be shown that the use of these functions gives a uniform convergence rate of $\frac{1}{N^4}$

for the twisting and in-plane bending strain energies, so it is not necessary to introduce an internal node. The uniformity of convergence rate between this torsional element and the previously considered bending element is very convenient, since a given division of the beam into elements will yield bending and torsional response data of the same order of accuracy, in those cases where there are a similar number of bending and torsional modes within a given frequency range.

Using the above functions, 8×8 stiffness and inertia matrices will be derived for the torsional beam element. In contrast to the bending element, no reduction is possible in the number of degrees of freedom, since 8 is the minimum permissible number of nodal co-ordinates for convergence.

We now proceed to consider the strain and kinetic energies associated with twisting of the beam element.

11.3 STRAIN AND KINETIC ENERGIES

The total strain energy is the sum of the energies due to shearing of the visco-elastic layers, and to bending and stretching of all the layers. Whilst in the flexural problem considerable proof exists that the bending and extensional effects in the visco-elastic layers are negligible, far less is known about the torsional problem, so one must include these effects at the present stage. From physical considerations, it seems reasonable to expect each visco-elastic layer to be relatively stiff in bending in its own plane, so it is possible that these effects are far more important than in the flexural problem. Besides this, the inclusion of these extra energy terms is quite straightforward, and it does facilitate the use of the sandwich element for representing the torsion of uniform beams, by using layers 2 and 4 and setting the other

layers to zero thickness.

Shear Strain Energy in Visco-elastic Layers

The shear strain energy in the two visco-elastic layers is given by

$$V_{\text{shear}} = \frac{1}{2} \sum_{j=2 \& 4} G_j t_j \int_{x=0}^{x=L} \int_{y=-\frac{b}{2}}^{y=\frac{b}{2}} \left[\gamma_{yzj}^2 + \gamma_{xzj}^2 \right] dy dx \quad (11.2)$$

This expression includes only the shear in the $y-z$ and $x-z$ planes, and any shear in the plane of the layers is taken account of in the extensional energy expression (11.6) below.

The shear strains are given in Fig. 11.2. Substituting these in (11.2), we obtain for the symmetrical section beam

$$V_{\text{shear}} = 2 \times \frac{1}{2} \frac{G_2}{t_2} \int_0^L \int_{-\frac{b}{2}}^{\frac{b}{2}} \left[v - \bar{a}_1 \cdot \phi \right]^2 + y^2 \left[\frac{\partial v}{\partial x} + \bar{a}_1 \cdot \frac{\partial \phi}{\partial x} \right]^2 dy dx$$

where $\bar{a}_1 = \frac{t_1 + 2t_2 + t_3}{2}$

Following integration with respect to y , this may be expanded into the sum of 6 integrals:

$$\begin{aligned} V_{\text{shear}} = & V_{s1} \int_0^L v^2 dx & + & V_{s2} \int_0^L \phi^2 dx \\ & + V_{s3} \int_0^L v \cdot \phi dx & + & V_{s4} \int_0^L \left(\frac{\partial v}{\partial x} \right)^2 dx \\ & + V_{s5} \int_0^L \left(\frac{\partial \phi}{\partial x} \right)^2 dx & + & V_{s6} \int_0^L \frac{\partial v}{\partial x} \cdot \frac{\partial \phi}{\partial x} dx \end{aligned} \quad (11.3)$$

The constants V_{s1} to V_{s6} are listed in Fig. 11.3 (Page 249).

Bending Strain Energy in All Layers

The total bending strain energy in all the layers is given by

$$V_{\text{bend}} = \frac{1}{2} \sum_{j=1}^5 \frac{E_j t_j^3}{12(1-\nu_j^2)} \int_{x=0}^{x=L} \int_{y=-\frac{b}{2}}^{y=\frac{b}{2}} \left[\left(\frac{\partial^2 w_j}{\partial x^2} \right)^2 + \left(\frac{\partial^2 w_j}{\partial y^2} \right)^2 + 2\nu_j \frac{\partial^2 w_j}{\partial x^2} \cdot \frac{\partial^2 w_j}{\partial y^2} + 2(1-\nu_j) \left(\frac{\partial^2 w_j}{\partial x \partial y} \right)^2 \right] dy dx \quad (11.4)$$

This expression is well-known from thin plate theory, and gives the energy associated with the combined bending and twisting of the layers, assuming no stretching of their middle planes. Although it is derived in fundamental texts such as reference (41)*, an alternative derivation is presented in Appendix VII, this being based on the two-dimensional theory of elasticity. The first three terms relate to bending, whilst the fourth relates to twist. Since it has been assumed that no bending takes place in the y - z plane (i.e. across the width of the beam), the second and third terms disappear. In addition, since the layers have been assumed incompressible in the z direction, $w_1 = w_2 = w_3 = w_4 = w_5 = w$

The elemental transverse displacement w is given in Fig. 11.2. On differentiating and substituting in (11.4), we obtain for the symmetrical section beam

$$\begin{aligned} V_{\text{bend}} = & 2 \times \frac{1}{2} \frac{E_1 t_1^3}{12(1-\nu_1^2)} \int_0^L \int_{-\frac{b}{2}}^{\frac{b}{2}} \left[y^2 \left(\frac{\partial^2 \phi}{\partial x^2} \right)^2 + 2(1-\nu_1) \left(\frac{\partial \phi}{\partial x} \right)^2 \right] dy dx \\ & + 2 \times \frac{1}{2} \frac{E_2 t_2^3}{12(1-\nu_2^2)} \int_0^L \int_{-\frac{b}{2}}^{\frac{b}{2}} \left[y^2 \left(\frac{\partial^2 \phi}{\partial x^2} \right)^2 + 2(1-\nu_2) \left(\frac{\partial \phi}{\partial x} \right)^2 \right] dy dx \\ & + \frac{1}{2} \frac{E_3 t_3^3}{12(1-\nu_3^2)} \int_0^L \int_{-\frac{b}{2}}^{\frac{b}{2}} \left[y^2 \left(\frac{\partial^2 \phi}{\partial x^2} \right)^2 + 2(1-\nu_3) \left(\frac{\partial \phi}{\partial x} \right)^2 \right] dy dx \end{aligned}$$

Following integration with respect to y , this may be expanded into the sum of 2 integrals:

* Note that References for Chapters 8 to 12 are listed on Page 283.

$$V_{\text{bend}} = V_{B1} \int_0^L \left(\frac{\partial \phi}{\partial x} \right)^2 dx + V_{B2} \int_0^L \left(\frac{\partial^2 \phi}{\partial x^2} \right)^2 dx \quad (11.5)$$

The constants V_{B1} and V_{B2} are listed in Fig. 11.3.

Extensional Strain Energy in All Layers

The total extensional or stretching energy in all the layers is given by

$$V_{\text{ext}} = \frac{1}{2} \sum_{j=1 \text{ to } 5} \frac{E_j t_j}{(1-\nu_j^2)} \int_{x=0}^{x=L} \int_{y=-\frac{b}{2}}^{y=\frac{b}{2}} \left[\left(\frac{\partial u_j}{\partial x} \right)^2 + \left(\frac{\partial v_j}{\partial y} \right)^2 + 2\nu_j \frac{\partial u_j}{\partial x} \frac{\partial v_j}{\partial y} + \frac{(1-\nu_j)}{2} \left(\frac{\partial u_j}{\partial y} + \frac{\partial v_j}{\partial x} \right)^2 \right] dy dx \quad (11.6)$$

This expression is derived from first principles in Appendix VII, and is associated with the plane stress system in the plane of each layer. The first three terms relate to pure stretching in the x and y directions, whilst the fourth term relates to shearing in the x-y plane. In the present problem, this energy arises from in-plane bending of layers 1, 2, 4 and 5. One might argue on the basis of simple bending theory for beams that the term $(1-\nu_j^2)$ should be deleted from the denominator. However, its retention is consistent with the assumption that the in-plane displacement v of layers 1 and 5 is independent of y . It simply implies that any elemental strip along the length of a layer is incompressible in the y direction, and is therefore in a state of uni-directional strain, in the x direction.

The required elemental displacements are given in Fig. 11.2. On differentiating and substituting these in (11.6), we obtain for the symmetrical section beam

$$\begin{aligned}
 V_{\text{ext}} = & 2 \times \frac{1}{2} \frac{E_1 t_1}{(1-\nu_1^2)} \int_0^L \int_{-\frac{b}{2}}^{\frac{b}{2}} \left[y^2 \left(\frac{\partial^2 v}{\partial x^2} \right)^2 \right] dy dx \\
 & + 2 \times \frac{1}{2} \frac{E_2 t_2}{(1-\nu_2^2)} \int_0^L \int_{-\frac{b}{2}}^{\frac{b}{2}} \left[\frac{y^2}{4} \left(\frac{\partial^2 v}{\partial x^2} \right)^2 + \bar{a}_2 \cdot \left(\frac{\partial^2 \phi}{\partial x^2} \right)^2 + \frac{(1-\nu_2)}{2} \left(\bar{a}_2 \cdot \frac{\partial \phi}{\partial x} \right)^2 \right] dy dx \\
 & \text{where } \bar{a}_2 = \frac{t_1 - t_3}{2}
 \end{aligned}$$

Following integration with respect to y , this may be expanded into the sum of 4 integrals:

$$\begin{aligned}
 V_{\text{ext}} = & V_{E1} \int_0^L \left(\frac{\partial \phi}{\partial x} \right)^2 dx + V_{E2} \int_0^L \left(\frac{\partial^2 v}{\partial x^2} \right)^2 dx \\
 & + V_{E3} \int_0^L \left(\frac{\partial^2 \phi}{\partial x^2} \right)^2 dx + V_{E4} \int_0^L \frac{\partial^2 v}{\partial x^2} \cdot \frac{\partial^2 \phi}{\partial x^2} dx \quad (11.7)
 \end{aligned}$$

The constants V_{E1} to V_{E4} are listed in Fig. 11.3.

Total Strain Energy

The total strain energy in the finite element is

$$V = V_{\text{shear}} + V_{\text{bend}} + V_{\text{ext}}$$

Summing the energy expressions (11.3), (11.5) and (11.7), we obtain a final total of 9 integrals:

$$\begin{aligned}
 V = & V_{S1} \int_0^L v^2 dx + V_{S2} \int_0^L \phi^2 dx \\
 & + V_{S3} \int_0^L v \cdot \phi dx + V_{S4} \int_0^L \left(\frac{\partial v}{\partial x} \right)^2 dx \\
 & + (V_{S5} + V_{B1} + V_{E1}) \int_0^L \left(\frac{\partial \phi}{\partial x} \right)^2 dx + V_{S6} \int_0^L \frac{\partial v}{\partial x} \cdot \frac{\partial \phi}{\partial x} dx \\
 & + V_{E2} \int_0^L \left(\frac{\partial^2 v}{\partial x^2} \right)^2 dx + (V_{B2} + V_{E3}) \int_0^L \left(\frac{\partial^2 \phi}{\partial x^2} \right)^2 dx \\
 & + V_{E4} \int_0^L \frac{\partial^2 v}{\partial x^2} \cdot \frac{\partial^2 \phi}{\partial x^2} dx \quad (11.8)
 \end{aligned}$$

Total Kinetic Energy

The total significant kinetic energy in all the layers is given by

$$T = \frac{1}{2} \sum_{j=1 \text{ to } 5} \rho_j t_j \int_{x=0}^{x=L} \int_{y=-\frac{b}{2}}^{y=\frac{b}{2}} \left[\dot{w}_j^2 + \dot{v}_j^2 + \frac{t_j^2}{12} \dot{\alpha}_j^2 \right] dy dx \quad (11.9)$$

where $\dot{} = \frac{\partial}{\partial t}$

This expression includes all motions in the plane of twist (y - z plane). The energy associated with motions in the other directions is obviously of second order importance and will be ignored here (Assumption 11).

The elemental displacements are given in Fig. 11.2. On differentiating and substituting these in (11.9), we obtain for the symmetrical section beam

$$\begin{aligned} T = & 2 \times \frac{1}{2} \rho_1 t_1 \int_0^L \int_{-\frac{b}{2}}^{\frac{b}{2}} \left[y^2 \dot{\phi}^2 + \dot{v}^2 + \frac{t_1^2}{12} \dot{\phi}^2 \right] dy dx \\ & + 2 \times \frac{1}{2} \rho_2 t_2 \int_0^L \int_{-\frac{b}{2}}^{\frac{b}{2}} \left[y^2 \dot{\phi}^2 + \frac{1}{4} (\dot{v} - \bar{\alpha}_2 \dot{\phi})^2 + \frac{t_2^2}{12} \left(\dot{\phi} + \frac{1}{t_2} \dot{v} - \frac{\bar{\alpha}_3}{t_2} \dot{\phi} \right)^2 \right] dy dx \\ & + \frac{1}{2} \rho_3 t_3 \int_0^L \int_{-\frac{b}{2}}^{\frac{b}{2}} \left[y^2 \dot{\phi}^2 + \frac{t_3^2}{12} \dot{\phi}^2 \right] dy dx \end{aligned}$$

where $\bar{\alpha}_2 = \frac{t_1 - t_3}{2}$, $\bar{\alpha}_3 = \frac{t_1 + t_3}{2}$

Following integration with respect to y , this may be expanded into the sum of 3 integrals:

$$T = T_1 \int_0^L \dot{v}^2 dx + T_2 \int_0^L \dot{\phi}^2 dx + T_3 \int_0^L \dot{v} \dot{\phi} dx \quad (11.10)$$

The constants T_1 to T_3 are listed in Fig. 11.3.

FIG. 11.3 STRAIN AND KINETIC ENERGY COEFFICIENTS

For torsion of symmetrical 5-layer beam

Shear

$$V_{S1} = b G_2 / t_2$$

$$V_{S2} = \bar{a}_1^2 V_{S1}$$

$$V_{S3} = -2\bar{a}_1 V_{S1}$$

$$V_{S4} = \frac{1}{12} b^2 V_{S1}$$

$$V_{S5} = \bar{a}_1^2 V_{S4}$$

$$V_{S6} = 2\bar{a}_1 V_{S4}$$

$$D_j = \frac{E_j t_j^3}{12(1 - \nu_j^2)} \quad (j = 1 \text{ to } 3)$$

$$\mu_j = b \rho_j t_j \quad (j = 1 \text{ to } 3)$$

$$\bar{a}_1 = \frac{1}{2} (t_1 + 2t_2 + t_3)$$

$$\bar{a}_2 = \frac{1}{2} (t_1 - t_3)$$

$$\bar{a}_3 = \frac{1}{2} (t_1 + t_3)$$

Note that $E_2 = 2(1 + \nu_2) G_2$

where the shear modulus G_2 is complex in order to take account of the damping properties of the visco-elastic layers

Bending

$$V_{B1} = 2b \left[D_1(1 - \nu_1) + D_2(1 - \nu_2) + \frac{1}{2} D_3(1 - \nu_3) \right]$$

$$V_{B2} = \frac{1}{12} b^3 (D_1 + D_2 + \frac{1}{2} D_3)$$

Extension

$$V_{E1} = 6b D_2(1 - \nu_2) \bar{a}_2^2 / t_2^2$$

$$V_{E2} = b^3 (D_1 / t_1^2 + D_2 / 4t_2^2)$$

$$V_{E3} = \frac{1}{4} b^3 D_2 \bar{a}_2^2 / t_2^2$$

$$V_{E4} = \frac{1}{2} b^3 D_2 \bar{a}_2 / t_2^2$$

Kinetic

$$T_1 = \mu_1 + \frac{1}{3} \mu_2$$

$$T_2 = \frac{1}{12} \left[\mu_1 (b^2 + t_1^2) + \mu_2 (b^2 + 3\bar{a}_2^2 + \bar{a}_3^2) + \frac{1}{2} \mu_3 (b^2 + t_3^2) \right]$$

$$T_3 = -\frac{1}{6} \mu_2 (3\bar{a}_2 + \bar{a}_3)$$

11.4 FORMULATION OF ENERGY EXPRESSIONS IN TERMS OF ASSUMED DISPLACEMENT FUNCTIONS

The displacement functions (11.1) and their derivatives may be expressed in matrix form:

$$\begin{aligned}
 \phi &= [1 \quad \xi \quad \xi^2 \quad \xi^3] \{ a_0 \quad a_1 \quad a_2 \quad a_3 \} = [X] \{ a \} \\
 \frac{\partial \phi}{\partial x} &= \frac{1}{L} [0 \quad 1 \quad 2\xi \quad 3\xi^2] \{ a_0 \quad a_1 \quad a_2 \quad a_3 \} = \frac{1}{L} [X'] \{ a \} \\
 \frac{\partial^2 \phi}{\partial x^2} &= \frac{1}{L^2} [0 \quad 0 \quad 2 \quad 6\xi] \{ a_0 \quad a_1 \quad a_2 \quad a_3 \} = \frac{1}{L^2} [X''] \{ a \} \\
 v &= L [1 \quad \xi \quad \xi^2 \quad \xi^3] \{ b_0 \quad b_1 \quad b_2 \quad b_3 \} = L [X] \{ b \} \\
 \frac{\partial v}{\partial x} &= [0 \quad 1 \quad 2\xi \quad 3\xi^2] \{ b_0 \quad b_1 \quad b_2 \quad b_3 \} = [X'] \{ b \} \\
 \frac{\partial^2 v}{\partial x^2} &= \frac{1}{L} [0 \quad 0 \quad 2 \quad 6\xi] \{ b_0 \quad b_1 \quad b_2 \quad b_3 \} = \frac{1}{L} [X''] \{ b \}
 \end{aligned} \tag{11.11}$$

The sets of constants a and b are each related to the corresponding nodal displacements by the transformation matrix $[T_i]$, which was derived in the bending analysis and is listed in Appendix VI.

$$\begin{aligned}
 \{ a \} &= [T_i] \{ \delta_\phi \} \\
 \{ b \} &= [T_i] \{ \delta_v \}
 \end{aligned} \tag{11.12}$$

where the non-dimensional displacement vectors are

$$\begin{aligned}
 \{ \delta_\phi \} &= \begin{Bmatrix} \phi_{i-1} \\ L \frac{\partial \phi_{i-1}}{\partial x} \\ \phi_i \\ L \frac{\partial \phi_i}{\partial x} \end{Bmatrix} & \{ \delta_v \} &= \begin{Bmatrix} \frac{v_{i-1}}{L} \\ \frac{\partial v_{i-1}}{\partial x} \\ \frac{v_i}{L} \\ \frac{\partial v_i}{\partial x} \end{Bmatrix}
 \end{aligned} \tag{11.13}$$

Using the transformations (11.12), the displacement functions and their derivatives may be expressed directly in terms of the nodal displacements:

$$\begin{aligned}
\phi &= [X][T_1]\{\delta_\phi\} \\
\frac{\partial\phi}{\partial x} &= \frac{1}{L}[X'] [T_1]\{\delta_\phi\} \\
\frac{\partial^2\phi}{\partial x^2} &= \frac{1}{L^2}[X''] [T_1]\{\delta_\phi\} \\
v &= L[X][T_1]\{\delta_v\} \\
\frac{\partial v}{\partial x} &= [X'] [T_1]\{\delta_v\} \\
\frac{\partial^2 v}{\partial x^2} &= \frac{1}{L}[X''] [T_1]\{\delta_v\}
\end{aligned} \tag{11.14}$$

Substituting the functions (11.14) into the nine strain energy integrals (11.8), we obtain the total strain energy in matrix form:

$$\begin{aligned}
V &= \frac{V_{S1}L^3}{420}\{\delta_v\}^T[A_7]\{\delta_v\} + \frac{V_{S2}L}{420}\{\delta_\phi\}^T[A_7]\{\delta_\phi\} + \frac{V_{S3}L^2}{420}\{\delta_v\}^T[A_7]\{\delta_\phi\} \\
&+ \frac{V_{S4}L}{30}\{\delta_v\}^T[A_2]\{\delta_v\} + \frac{(V_{S5} + V_{B1} + V_{E1})}{30L}\{\delta_\phi\}^T[A_2]\{\delta_\phi\} \\
&+ \frac{V_{S6}}{30}\{\delta_v\}^T[A_2]\{\delta_\phi\} + \frac{V_{E2}}{L}\{\delta_v\}^T[A_5]\{\delta_v\} \\
&+ \frac{(V_{B2} + V_{E3})}{L^3}\{\delta_\phi\}^T[A_5]\{\delta_\phi\} + \frac{V_{E4}}{L^2}\{\delta_v\}^T[A_5]\{\delta_\phi\}
\end{aligned} \tag{11.15}$$

Similarly, the three kinetic energy integrals (11.10) yield the following matrix expression:

$$T = \frac{T_1L^3}{420}\{\dot{\delta}_v\}^T[A_7]\{\dot{\delta}_v\} + \frac{T_2L}{420}\{\dot{\delta}_\phi\}^T[A_7]\{\dot{\delta}_\phi\} + \frac{T_3L^2}{420}\{\dot{\delta}_v\}^T[A_7]\{\dot{\delta}_\phi\} \tag{11.16}$$

The matrices $[A_2]$, $[A_5]$ and $[A_7]$ are exactly the same as those derived in the bending analysis, and are listed in Appendix VI.

11.5 STIFFNESS AND INERTIA MATRICES FOR THE ELEMENT

The stiffness and inertia matrices are obtained from the strain and kinetic energy expressions (11.15) and 11.16) by using the Lagrange equation. For simple harmonic motion we obtain the following matrix equation:

$$\begin{bmatrix} (S_2[A_7] + S_5[A_2] + S_8[A_5]) - \omega^2 m_2[A_7] & (S_3[A_7] + S_6[A_2] + S_9[A_5]) - \omega^2 m_3[A_7] \\ (S_3[A_7] + S_6[A_2] + S_9[A_5]) - \omega^2 m_3[A_7] & (S_1[A_7] + S_4[A_2] + S_7[A_5]) - \omega^2 m_1[A_7] \end{bmatrix} \begin{Bmatrix} \delta_\phi \\ \delta_v \end{Bmatrix} = \begin{Bmatrix} F_\phi \\ F_v \end{Bmatrix} \tag{11.17}$$

where the stiffness coefficients S_1 to S_9 , and the inertia coefficients m_1 to m_3 are listed in Fig. 11.4. Since the displacement sub-vectors $\{\delta_\phi\}$ and $\{\delta_v\}$ are dimensionless, the corresponding force vectors have the dimensions of a couple:

Force	Displacement	Force	Displacement
$\{F_\phi\} = \begin{Bmatrix} M_{\phi_{i-1}} \\ \frac{1}{L} M_{\phi'_{i-1}} \\ M_{\phi_i} \\ \frac{1}{L} M_{\phi'_i} \end{Bmatrix}$	$\{\delta_\phi\} = \begin{Bmatrix} \phi_{i-1} \\ L \frac{\partial \phi_{i-1}}{\partial x} \\ \phi_i \\ L \frac{\partial \phi_i}{\partial x} \end{Bmatrix}$	$\{F_v\} = \begin{Bmatrix} V_{i-1} L \\ M_{v'_{i-1}} \\ V_i L \\ M_{v'_i} \end{Bmatrix}$	$\{\delta_v\} = \begin{Bmatrix} \frac{v_{i-1}}{L} \\ \frac{\partial v_{i-1}}{\partial x} \\ \frac{v_i}{L} \\ \frac{\partial v_i}{\partial x} \end{Bmatrix}$

(11.18)

The "force" M_ϕ , corresponding to the rate of twist $\frac{\partial \phi}{\partial x}$ has the dimensions Force x Length² and is therefore not a physically recognisable force or couple. However, it must be transmitted between elements in the same way as the other forces if the beam model is to behave correctly.

The equations (11.17) are better re-arranged so as to group together all the co-ordinates corresponding to each node. The final re-arranged stiffness and inertia matrices are shown in Figs. 11.5 and 11.6 respectively, and are for use with the following force and displacement vectors:

Force

Displacement

$$\begin{array}{c}
 \left[\begin{array}{c}
 M_{\phi_{i-1}} \\
 M'_{\phi_{i-1}} \\
 V_{i-1} \\
 M_{v_{i-1}} \\
 M_{\phi_i} \\
 M'_{\phi_i} \\
 V_i \\
 M_{v_i}
 \end{array} \right]
 \end{array}
 \qquad
 \begin{array}{c}
 \left[\begin{array}{c}
 \phi_{i-1} \\
 \frac{\partial \phi_{i-1}}{\partial x} \\
 v_{i-1} \\
 \frac{\partial v_{i-1}}{\partial x} \\
 \phi_i \\
 \frac{\partial \phi_i}{\partial x} \\
 v_i \\
 \frac{\partial v_i}{\partial x}
 \end{array} \right]
 \end{array}
 \qquad
 (11.19)$$

The dimensionless form has now been dispensed with, and the element length L has been introduced into the stiffness and inertia matrices either directly or in the form of the constants $C_1 = \frac{1}{L}$ and $C_2 = \frac{1}{L^2}$

The matrices in Figs. 11.5 and 11.6 are ready for immediate use, since no reduction in order is possible in the present problem.

11.6 SUMMARY

Stiffness and inertia matrices have been derived for an 8 degree of freedom torsional finite element of a symmetrical 5-layer beam. Uniform accuracy of strain representation has been obtained without the need to introduce an internal node.

Results obtained with this element may be found in Chapter 12.

FIG. 11.4 STIFFNESS AND INERTIA COEFFICIENTS

Used in stiffness and inertia matrices for torsional finite element of symmetrical 5-layer beam (See Figs. 11.5 and 11.6)

Stiffness coefficients

$$S_1 = 2 V_{S1} \frac{L^3}{420}$$

$$S_2 = 2 V_{S2} \frac{L}{420}$$

$$S_3 = V_{S3} \frac{L^2}{420}$$

$$S_4 = 2 V_{S4} \frac{L}{30}$$

$$S_5 = 2 (V_{S5} + V_{B1} + V_{E1}) \frac{1}{30L}$$

$$S_6 = V_{S6} \frac{1}{30}$$

$$S_7 = 2 V_{E2} \frac{1}{L}$$

$$S_8 = 2 (V_{B2} + V_{E3}) \frac{1}{L^3}$$

$$S_9 = V_{E4} \frac{1}{L^2}$$

The coefficients V_{Sj} , V_{Bj} , V_{Ej} and T_j are listed in Fig. 11.3

Also note the constants

$$C_1 = \frac{1}{L} \quad \text{and} \quad C_2 = \frac{1}{L^2}$$

Inertia coefficients

$$m_1 = 2 T_1 \frac{L^3}{420}$$

$$m_2 = 2 T_2 \frac{L}{420}$$

$$m_3 = T_3 \frac{L^2}{420}$$

FIG. 11.5

STIFFNESS MATRIX FOR 8 DEGREE OF FREEDOM TORSIONAL FINITE ELEMENT OF SYMMETRICAL 5-LAYER BEAM

1	$(156S_2+36S_3+12S_8)$	$(22S_2+3S_3+6S_8)$ $\times L$	$(156S_3+36S_6+12S_7)$ $\times C_1$	$(22S_3+3S_6+6S_7)$	$(54S_2-36S_3-12S_8)$	$(-13S_2+3S_3+6S_8)$ $\times L$	$(54S_3-36S_6-12S_7)$ $\times C_1$	$(-13S_3+3S_6+6S_7)$	ϕ_{i-1}
2		$(4S_2+4S_3+4S_8)$ $\times L^2$	$(22S_3+3S_6+6S_7)$	$(4S_3+4S_6+4S_7)$ $\times L$	$(13S_2-3S_3-6S_8)$ $\times L$	$(-3S_2-S_3+2S_8)$ $\times L^2$	$(13S_3-3S_6-6S_7)$	$(-3S_3-S_6+2S_7)$ $\times L$	$\frac{\partial \phi_{i-1}}{\partial x}$
3			$(156S_1+36S_4+12S_5)$ $\times C_2$	$(22S_1+3S_4+6S_5)$ $\times C_1$	$(54S_3-36S_6-12S_7)$ $\times C_1$	$(-13S_3+3S_6+6S_7)$	$(54S_1-36S_4-12S_5)$ $\times C_2$	$(-13S_1+3S_4+6S_5)$ $\times C_1$	V_{i-1}
4				$(4S_1+4S_4+4S_5)$	$(13S_3-3S_6-6S_7)$	$(-3S_3-S_6+2S_7)$ $\times L$	$(13S_1-3S_4-6S_5)$ $\times C_1$	$(-3S_1-S_4+2S_5)$	$\frac{\partial V_{i-1}}{\partial x}$
5					$(156S_2+36S_3+12S_8)$	$(-22S_2-3S_3-6S_8)$ $\times L$	$(156S_3+36S_6+12S_7)$ $\times C_1$	$(-22S_3-3S_6-6S_7)$	ϕ_i
6		S Y M M E T R I C				$(4S_2+4S_3+4S_8)$ $\times L^2$	$(-22S_3-3S_6-6S_7)$	$(4S_3+4S_6+4S_7)$ $\times L$	$\frac{\partial \phi_i}{\partial x}$
7							$(156S_1+36S_4+12S_5)$ $\times C_2$	$(-22S_1-3S_4-6S_5)$ $\times C_1$	V_i
8								$(4S_1+4S_4+4S_5)$	$\frac{\partial V_i}{\partial x}$
	1	2	3	4	5	6	7	8	

FIG. 11.6

INERTIA MATRIX FOR 8 DEGREE OF FREEDOM TORSIONAL FINITE ELEMENT OF SYMMETRICAL 5-LAYER BEAM

1	$156 m_2$	$22 m_2 L$	$156 m_3 C_1$	$22 m_3$	$54 m_2$	$-13 m_2 L$	$54 m_3 C_1$	$-13 m_3$	ϕ_{i-1}
2		$4 m_2 L^2$	$22 m_3$	$4 m_3 L$	$13 m_2 L$	$-3 m_2 L^2$	$13 m_3$	$-3 m_3 L$	$\frac{\partial \phi_{i-1}}{\partial x}$
3			$156 m_1 C_2$	$22 m_1 C_1$	$54 m_3 C_1$	$-13 m_3$	$54 m_1 C_2$	$-13 m_1 C_1$	V_{i-1}
4				$4 m_1$	$13 m_3$	$-3 m_3 L$	$13 m_1 C_1$	$-3 m_1$	$\frac{\partial V_{i-1}}{\partial x}$
5					$156 m_2$	$-22 m_2 L$	$156 m_3 C_1$	$-22 m_3$	ϕ_i
6		S Y M	M E T	R I C		$4 m_2 L^2$	$-22 m_3$	$4 m_3 L$	$\frac{\partial \phi_i}{\partial x}$
7							$156 m_1 C_2$	$-22 m_1 C_1$	V_i
8								$4 m_1$	$\frac{\partial V_i}{\partial x}$
	1	2	3	4	5	6	7	8	

CHAPTER 12

RESULTS AND CONCLUSIONS FOR MULTI-LAYER DAMPED BEAMS

12.1 INTRODUCTION

The results given in this chapter relate to the beam finite elements derived in Chapters 9 to 11. Only a limited selection of results is given for each element, but this is sufficient to illustrate the sort of accuracy that is obtainable. As the initial motivation for this work was the need to analyse the symmetrical 5-layer beams used in a machinery seating, we shall use the results obtained with one of these beams to justify certain assumptions made in the analysis, and in particular to demonstrate the superiority of a bending finite element having an "internal node". All the theoretical results are compared with measured frequency response data, obtained either by the Author or by earlier researchers in this field.

12.2 RESULTS FOR FLEXURAL VIBRATION OF SYMMETRICAL 3- AND 5-LAYER BEAMS

We shall start by considering the symmetrical 5-layer beam UT, shown in Fig. 12.1. This is one of the beams in the machinery seating analysed in Part 4, and as it constitutes part of the intermediate mass in a two-stage mounting system, it is both heavy (43.7 Kg) and highly damped. The design and the finite element representation are discussed in detail in Sections 13.2 and 14.1 (of Chapters 13 and 14 respectively), and consideration is given to bending in both planes, as well as to torsional and axial behaviour. Some particularly interesting experimental results are presented which show that whereas the beam is very heavily damped when bending in the plane at right angles to the layers, it behaves as an essentially undamped uniform beam when bending in the plane of the layers. The bending in both planes may be described using the symmetrical 5-layer finite element, but in this chapter we shall confine our attention to bending in the heavily damped

plane, since the in-plane vibration is dealt with in sufficient detail in Section 14.1. The torsional response of this same beam is considered in Section 12.4.

Beam UT comprises 3 identical aluminium layers and 2 layers of Velbex PVC Type 629/0900^{*}. The latter is a high-damping visco-elastic material, with a loss factor around 0.6, and its dynamic properties are given in Section 14.1, together with those of the metal layers. The PVC shear modulus formula given in Fig. 14.1 was obtained by Agbasiere⁽¹⁶⁾^x from measurements on a sheet A of the material, and it includes frequency-, temperature- and strain-dependence. The graph in Fig. 14.3 shows the variation of modulus and loss factor with frequency, but it corresponds to a fixed temperature and strain (22.8°C and 5.27×10^{-3} respectively). Also included on this graph are some results obtained by Nakra⁽¹⁸⁾ for a nominally identical sheet B, and it is seen that the shear moduli for the two sheets differ by as much as 30%. As no tests were carried out on the sheet of PVC used in this beam, it was decided to use the properties corresponding to sheet A, though the loss factor was not allowed to vary and was kept constant at 0.66. The temperature and strain were assumed to correspond to those in Fig. 14.3.

Referring to Fig. 12.1, measurements have been made of the point mobility $\frac{\dot{x}}{F_x}$ ⁺ at the two points B and A, and the results are given in Figs. 12.2 and 12.5 respectively. The beam was suspended on two ropes and was therefore in an effectively free-free state, except at low frequencies. The measured data were obtained using an electrodynamic shaker and separate force and acceleration transducers, in conjunction with the Solartron Programmable Frequency Response Analyser described in Section 4.2 (Part 2, Chapter 4).

* Black industrial grade Polyvinylchloride with 35-40 % phthalate plasticizer. It is supplied in sheets of various thickness and is manufactured by British Industrial Plastics Ltd., Manningtree, Essex.

The layers of the sandwich are bonded together using Araldite epoxy resin.

⁺ The transverse displacement x used here corresponds to w in the element analysis.

^x Note that References for Chapters 8 to 12 are listed on Page 283.

The theoretical response was obtained by building the beam from a string of symmetrical 5-layer elements. These elements were joined together using the dynamic stiffness coupling program COUPLE1 in conjunction with some specially developed routines*. Just as if it were a uniform solid beam, the present sandwich beam may be divided into 3 sections: LH tip — A, A — B, B — RH tip. The tip dynamic stiffness properties of each section are set up using special routines and these sections or subsystems are then joined together using the general-purpose coupling program, in order to obtain the forced response of the complete beam at points A and B. Since the beam is built afresh at each frequency, it is a simple matter to change both the visco-elastic properties and the number of elements with the frequency. At anything other than very low frequencies, it is necessary to sub-divide each section into a number of elements, but it is quite a simple matter to join elements end-to-end and to eliminate the inter-element coupling co-ordinates as one progresses, so that one is just left with a dynamic stiffness matrix relating to the co-ordinates at the two tips of the multi-element section. This may be accomplished using the well-known Transfer Matrix method, or alternatively, using a procedure based upon Gaussian elimination. The latter has been employed in the present work, as it is less prone to numerical difficulties. The two techniques are discussed in detail in Appendix VIII.

The mobility modulus and phase curves in Fig. 12.2 relate to point B, which is at the centre of the beam, so only symmetric modes are excited and the beam is effectively a root-excited double cantilever. These curves are particularly interesting in that they illustrate the high level of damping that is obtainable with a carefully designed sandwich construction.

* See both Part 1, Chapter 2 and Reference (49) for further information on COUPLE1. A standard module called ZSAM1 has been developed from the present sandwich beam studies to facilitate the inclusion of symmetrical 3- and 5-layer beams in any general structural analysis. Standard routines are also available for visco-elastic material properties, and these include one called GPVCA which yields the properties of PVC sheet A.

In addition, they illustrate the frequency-dependence of the damping, since the loss factor gradually drops from about 0.25 at the 1st mode to approximately half this value by the 5th symmetric mode. Both response plots show quite good agreement between measurements and theory, except at frequencies below 40 Hz, where the effect of the suspension ropes became more significant. In assessing these results one should remember that the properties of the sheet of PVC used in this beam were not measured; and in addition, both the assumed temperature and the strain were probably slightly in error. Since the mobility was measured directly as a ratio, the input force was not obtained explicitly; so it was not possible to apply the true input force to the finite element model in order to determine the actual strain, and ultimately the correct properties.

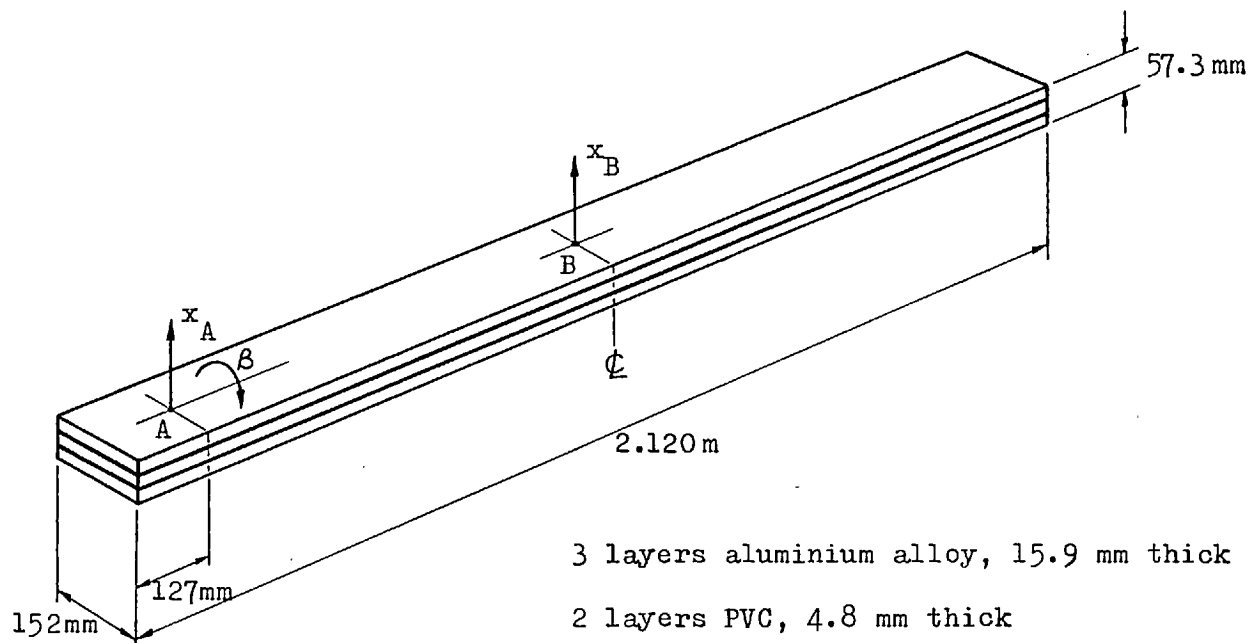
As the results in Fig. 12.2 prove the validity of the model, we may now look at the number of elements that are required for accurately representing a given mode of vibration. At the same time, we shall examine the practical effect of not correctly matching the displacement function for the visco-elastic rotation α with that for the transverse displacement w . This was discussed in Section 9.2 of Chapter 9, where it was concluded that a cubic polynomial for w required a quadratic polynomial for α . In order to achieve this it was necessary to introduce an "internal node" half way along the element, and to consider the visco-elastic rotation at this node as an extra degree of freedom: this resulted in a 7 degree-of-freedom element, but as transverse inertia was not included it was possible to immediately eliminate this extra freedom and still obtain a 6 x 6 element stiffness matrix. Without the internal node one is restricted to using only a linear polynomial for α , resulting in a 6 degree-of-freedom element with vastly inferior convergence properties. The difference is immediately apparent when one studies the computed response curves in Figs. 12.3 and 12.4. These correspond to the point mobility shown in Fig. 12.2, and they allow one to compare the 6 and

7 degree-of-freedom finite elements for different numbers of elements along the length of the beam. The full line represents the "exact" solution and was obtained using 18 elements. It is quite clear from these curves that the use of a quadratic polynomial for α gives greatly improved results, as one might expect from the discussion in Section 9.2. This improvement is best measured by comparing the proportion of a bending wavelength that can be adequately described by the different elements. If we take the 10-element beam as an example, it is evident that the 7 degree-of-freedom element adequately describes all modes up to the 4th symmetric, which is the 7th mode when one also counts the anti-symmetric ones. When the beam vibrates in this mode the beam length corresponds to 3.5 wave-lengths, so each element is describing 0.35 wave-length. If we now turn to the 6 degree-of-freedom element, we see that the 2nd symmetric is the highest mode that is adequately described, and for this mode each element represents only 0.15 wavelength. Thus, one must use around twice as many of the 6 degree-of-freedom elements in order to achieve the same sort of accuracy! As this astounding improvement has been obtained without any effective increase in the size of the element stiffness matrix, the use of an internal node with no associated inertia is obviously an extremely worthwhile means of refining sandwich elements. Similar figures are obtained if one considers the 2-, 6- and 14-element beams, and as a very rough guide one may assume that the standard 7 degree-of-freedom element is capable of describing anything up to about $\frac{3}{8}$ wavelength with acceptable engineering accuracy.

We shall now proceed to consider the upper graph in Fig. 12.5. This shows the mobility at point A, which is not far from the tip of the beam, and the agreement between measurements and theory is generally better than in Fig. 12.2. The reader may also care to consult either Section 4.5 in Part 2 or Section 14.1 in Part 4, where he will find the same response quantity measured using a multi-directional measurement technique. Despite

FIG. 12.1 SYMMETRICAL MULTI-LAYER BEAMS

BEAM UT Symmetrical 5-layer beam used in V-beam seating



BEAM 3B Symmetrical 3-layer beam used by Agbasiere

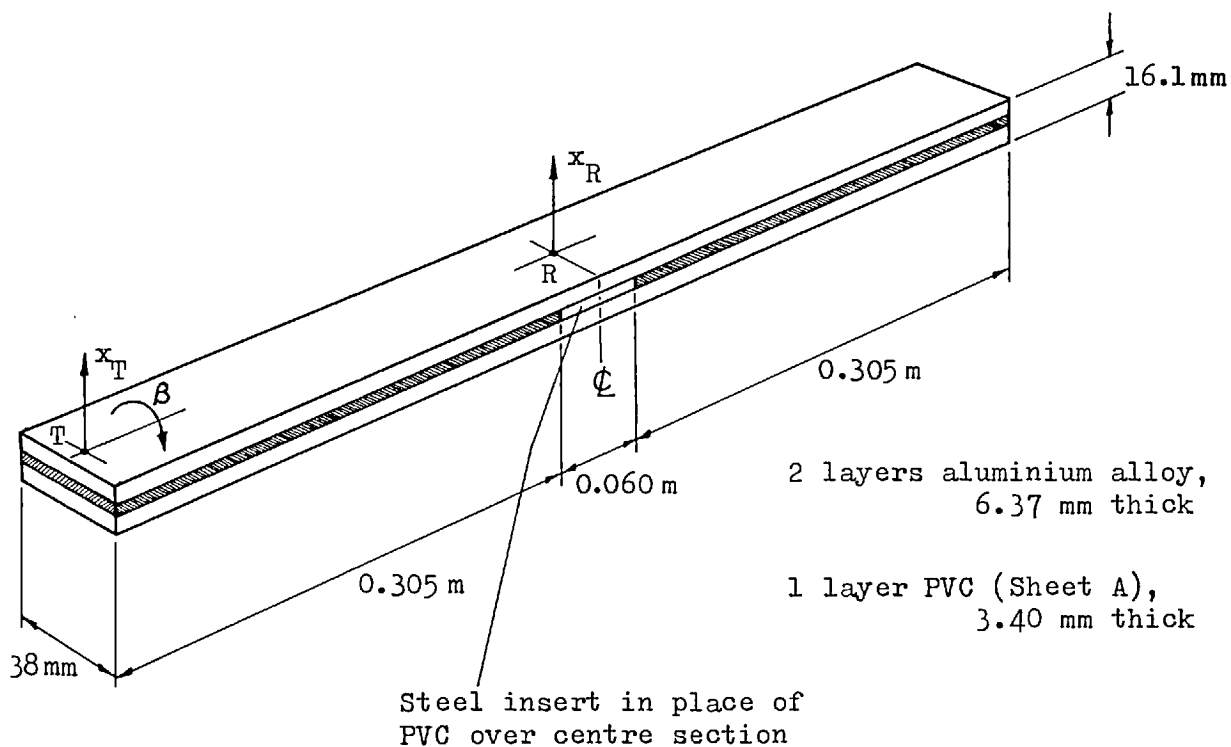


FIG. 12.2

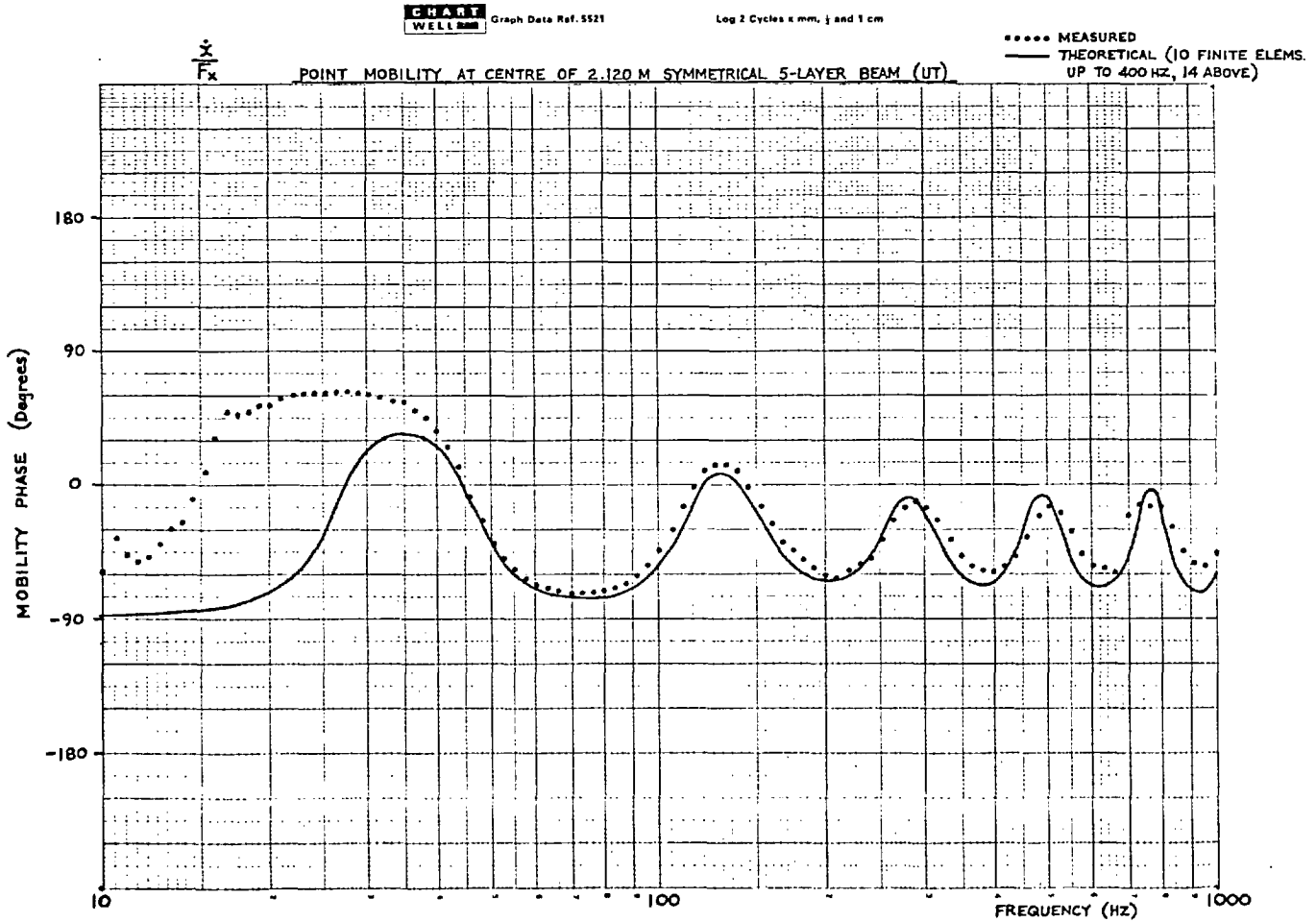
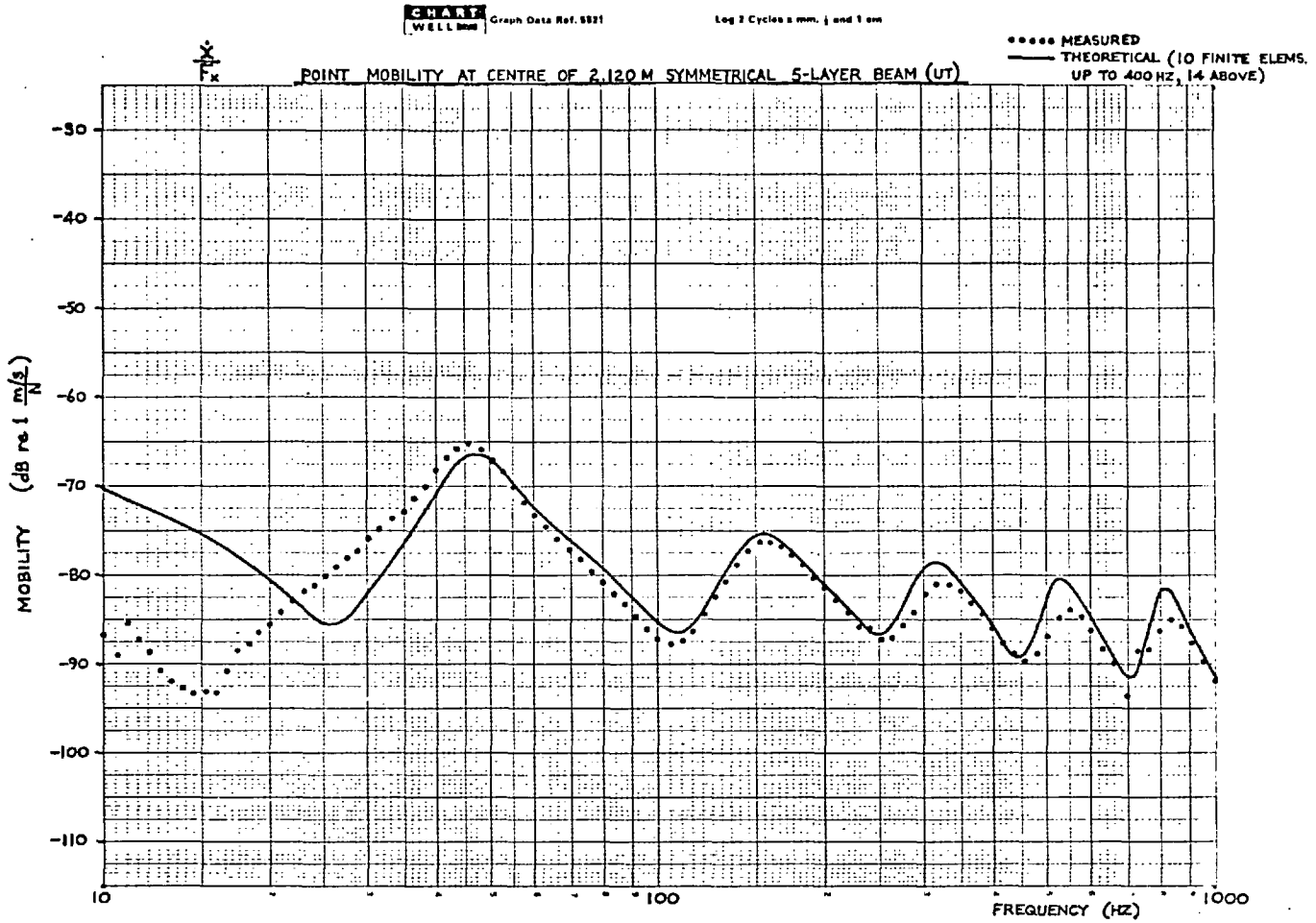


FIG. 12.3

CHART
WELL Graph Data Ref. 5521

Log 2 Cycles x mm, j and 1 cm

COMPARISON OF 6 AND 7 DEGREE OF FREEDOM FINITE ELEMENTS FOR SYMMETRICAL 5-LAYER BEAM — 2.120 M FREE-FREE, DRIVEN AT CENTRE

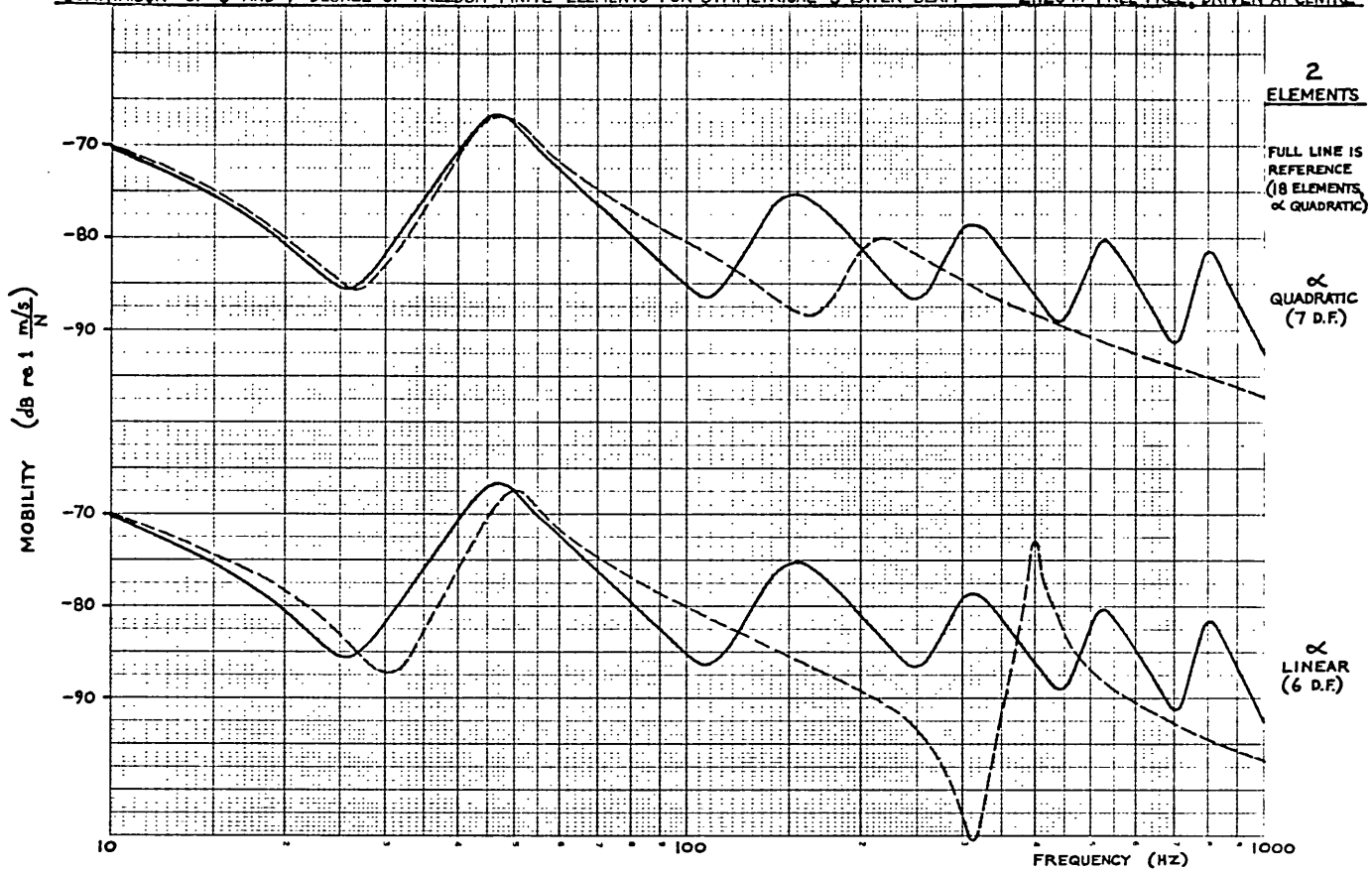


CHART
WELL Graph Data Ref. 5521

Log 2 Cycles x mm, j and 1 cm

COMPARISON OF 6 AND 7 DEGREE OF FREEDOM FINITE ELEMENTS FOR SYMMETRICAL 5-LAYER BEAM — 2.120 M FREE-FREE, DRIVEN AT CENTRE

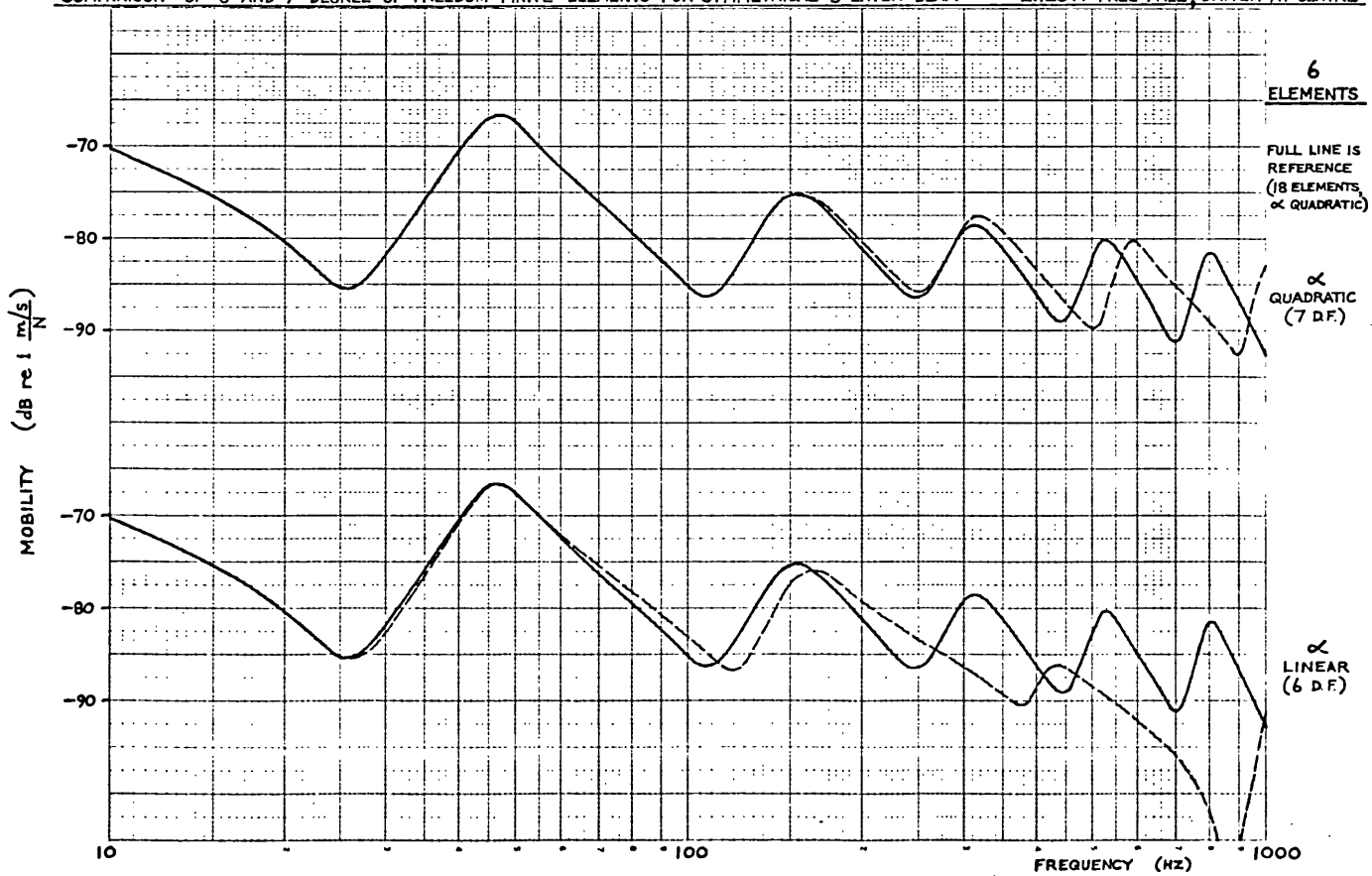


FIG. 12.A

CHART WELL Graph Data Ref. 5521

Log 3 Cycles x mm, y and 1 cm

COMPARISON OF 6 AND 7 DEGREE OF FREEDOM FINITE ELEMENTS FOR SYMMETRICAL 5-LAYER BEAM — 2.120 M FREE-FREE, DRIVEN AT CENTRE

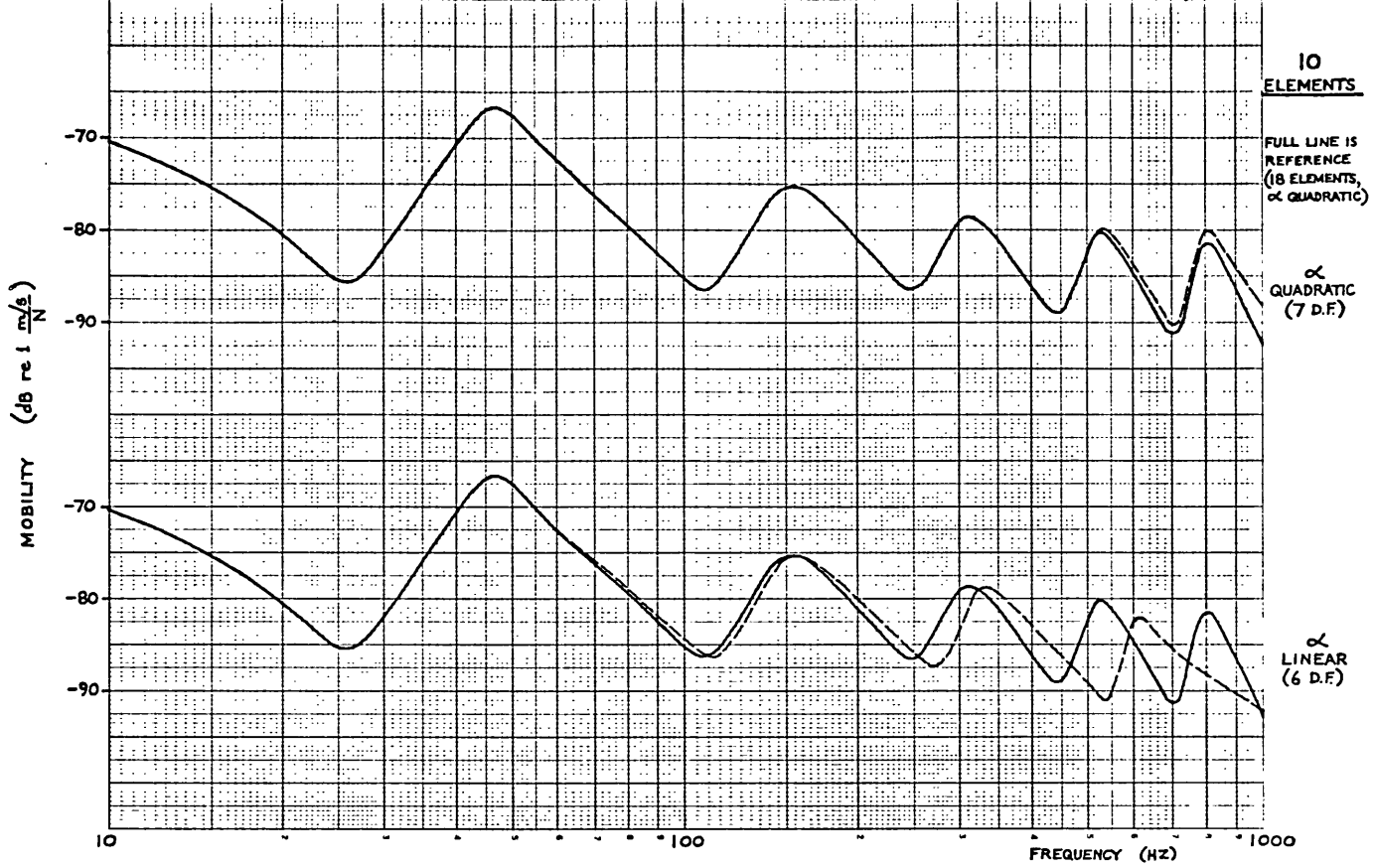


CHART WELL Graph Data Ref. 5521

Log 2 Cycles x mm, y and 1 cm

COMPARISON OF 6 AND 7 DEGREE OF FREEDOM FINITE ELEMENTS FOR SYMMETRICAL 5-LAYER BEAM — 2.120 M FREE-FREE, DRIVEN AT CENTRE

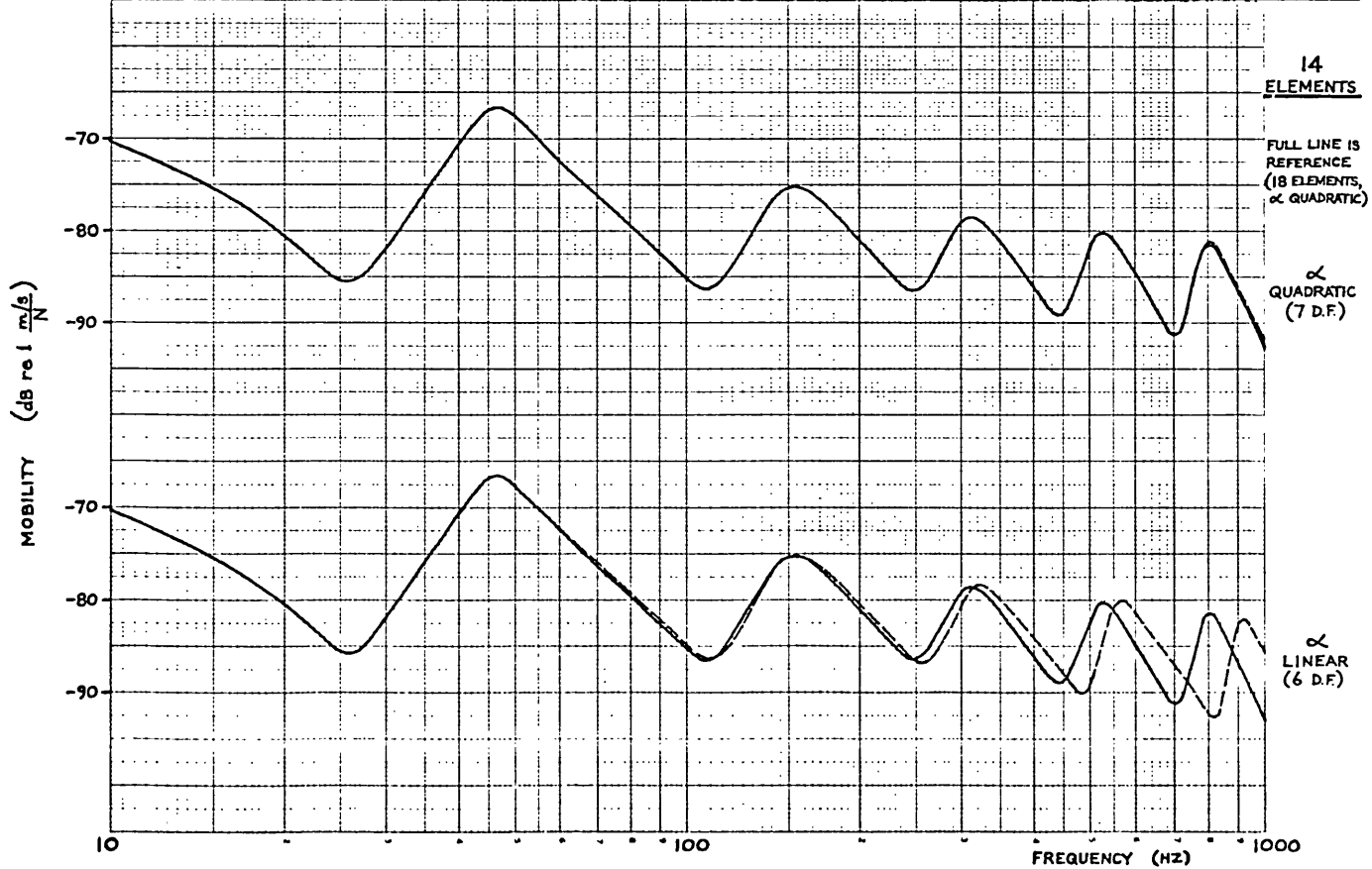
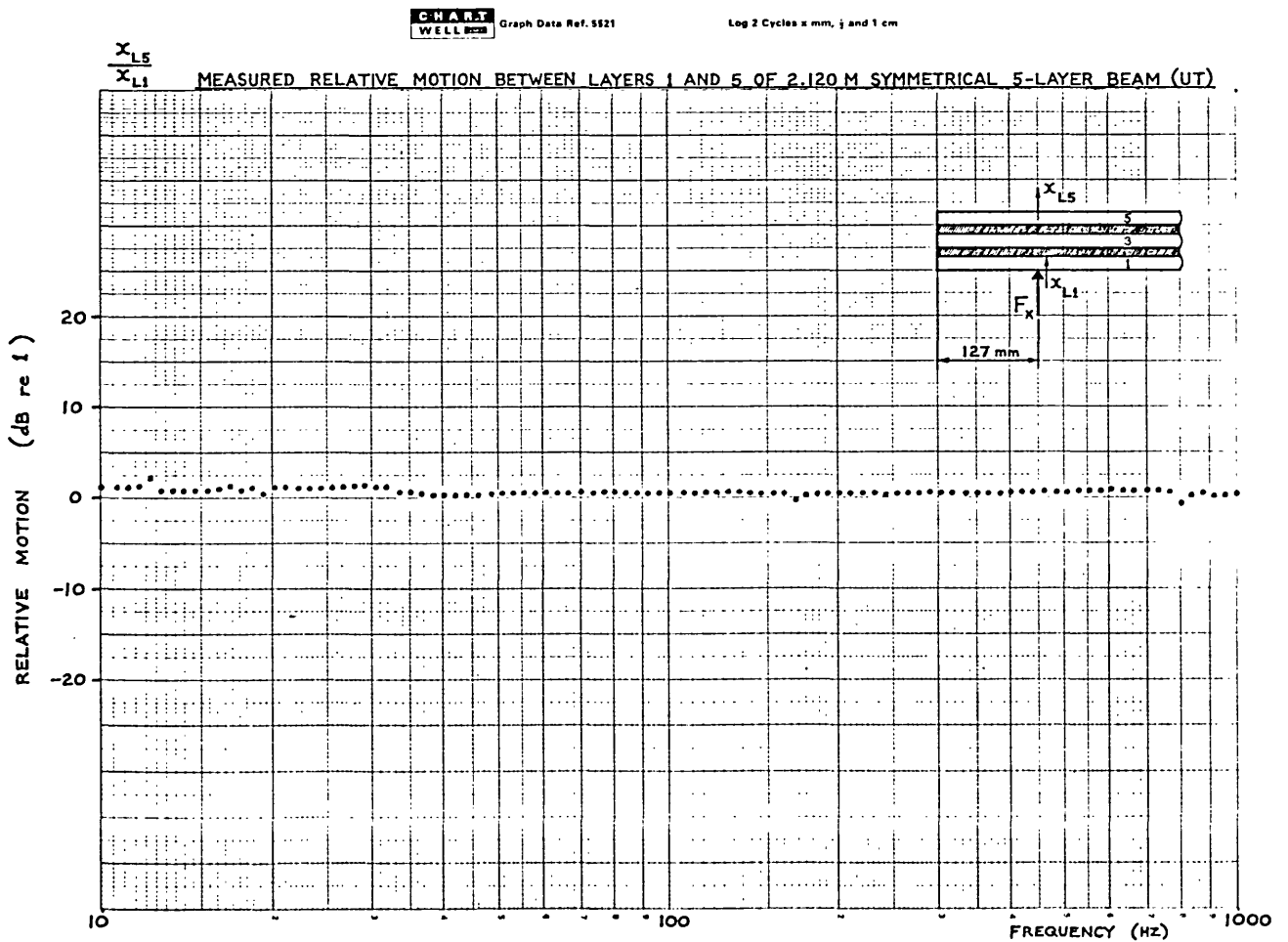
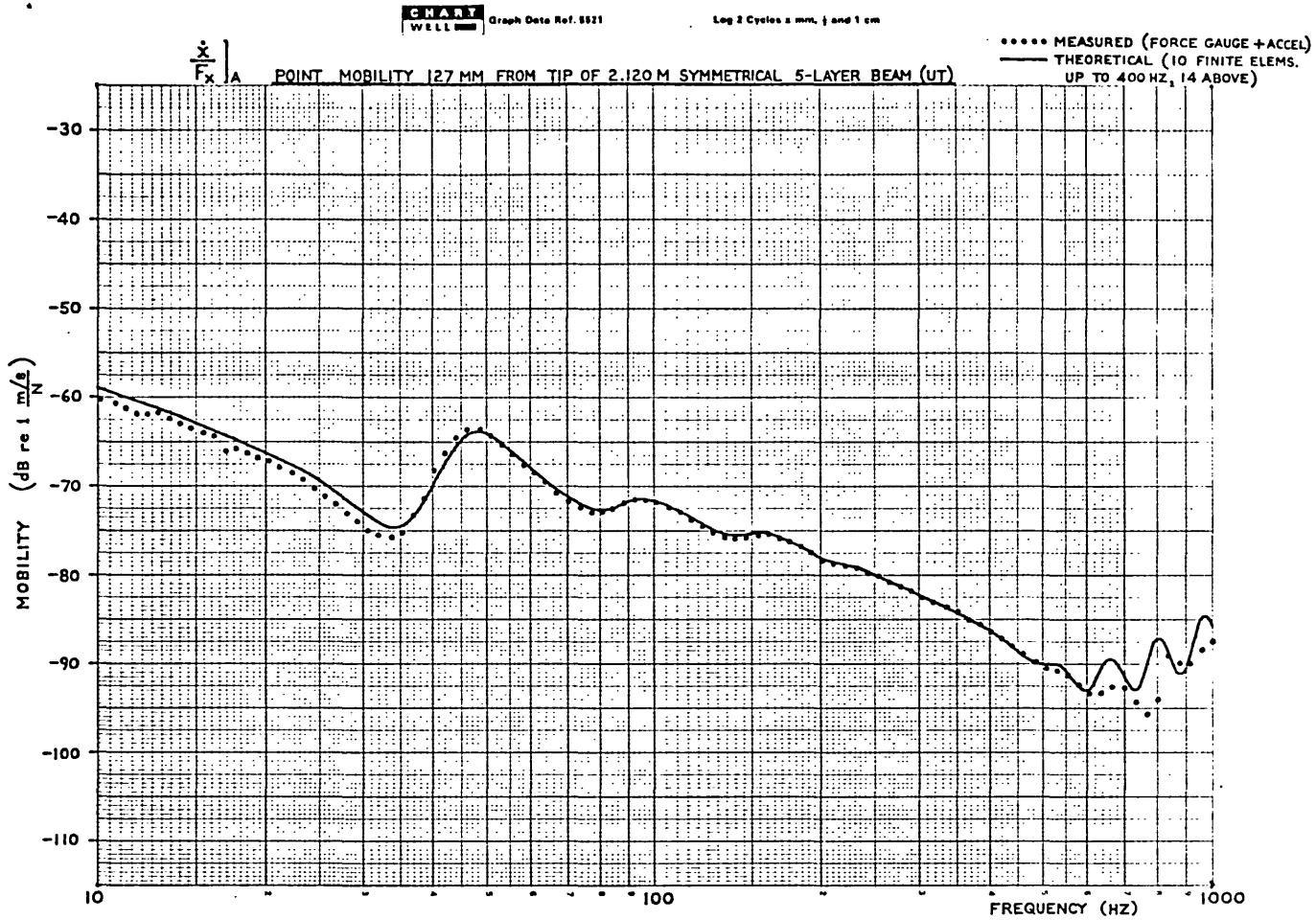
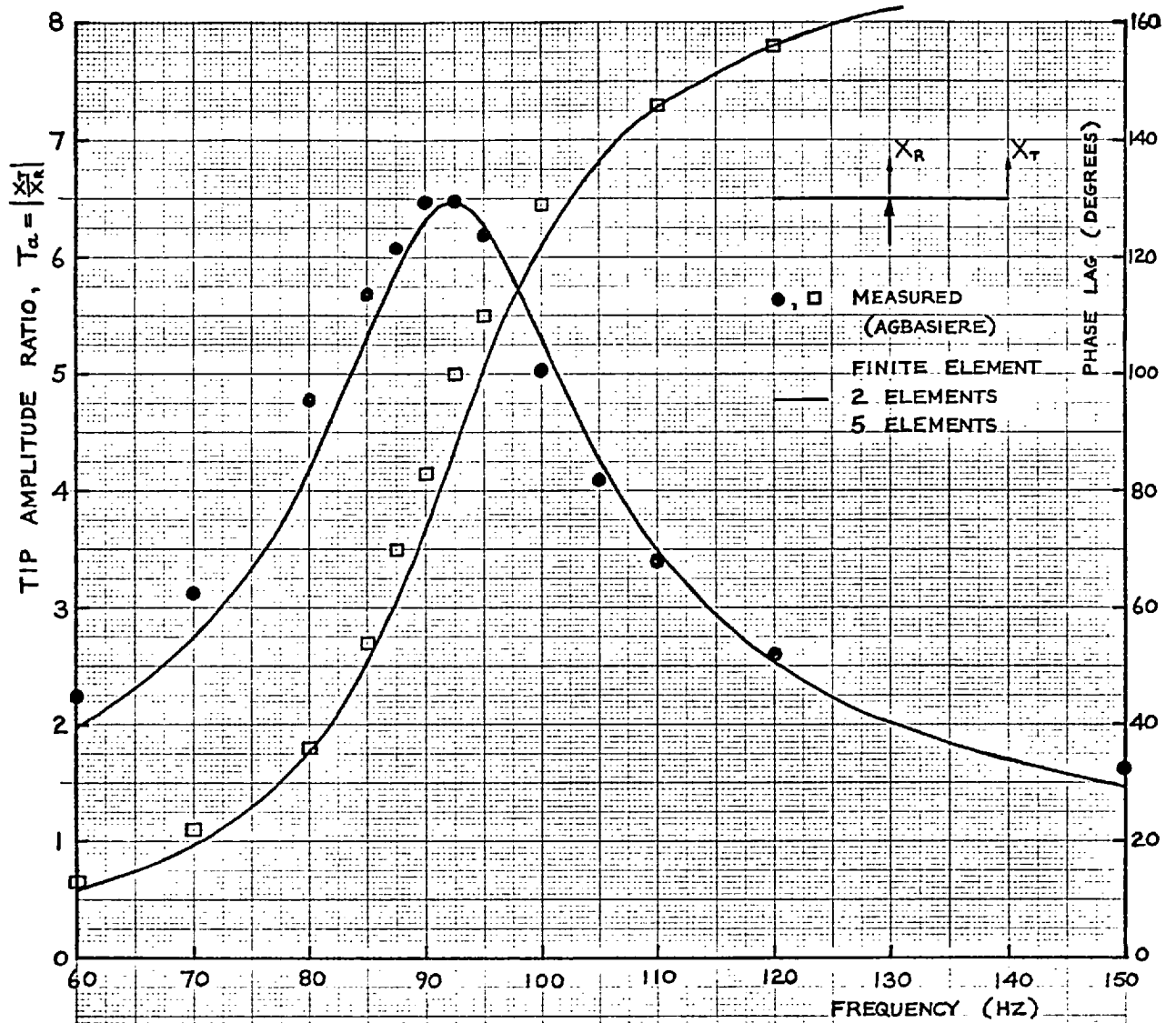
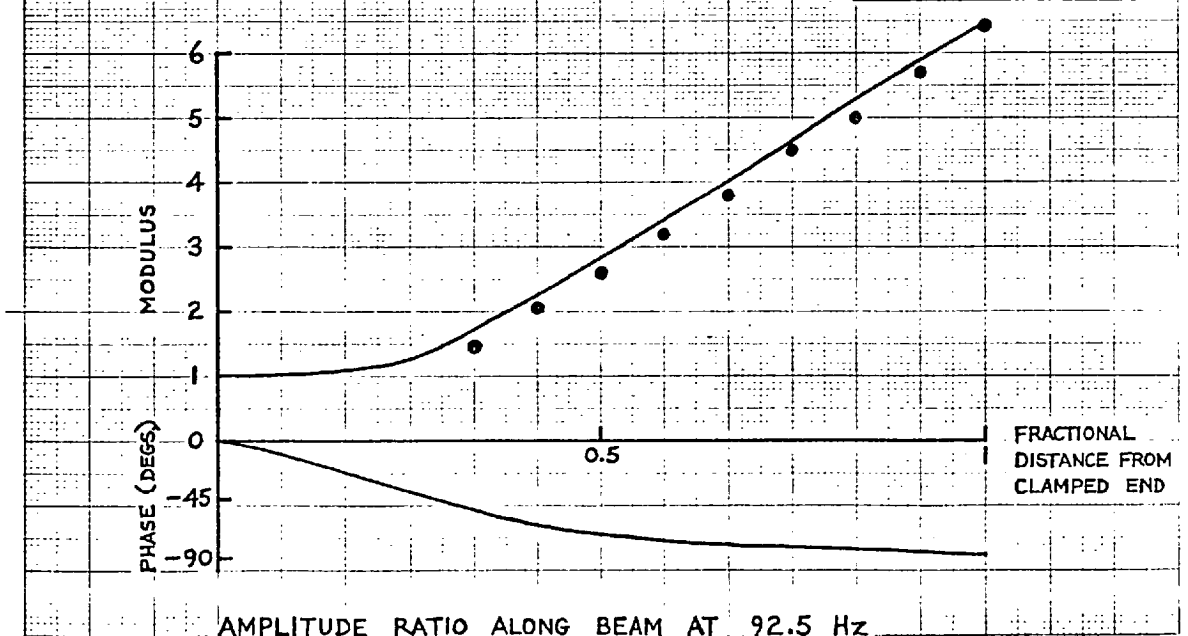


FIG. 12.5



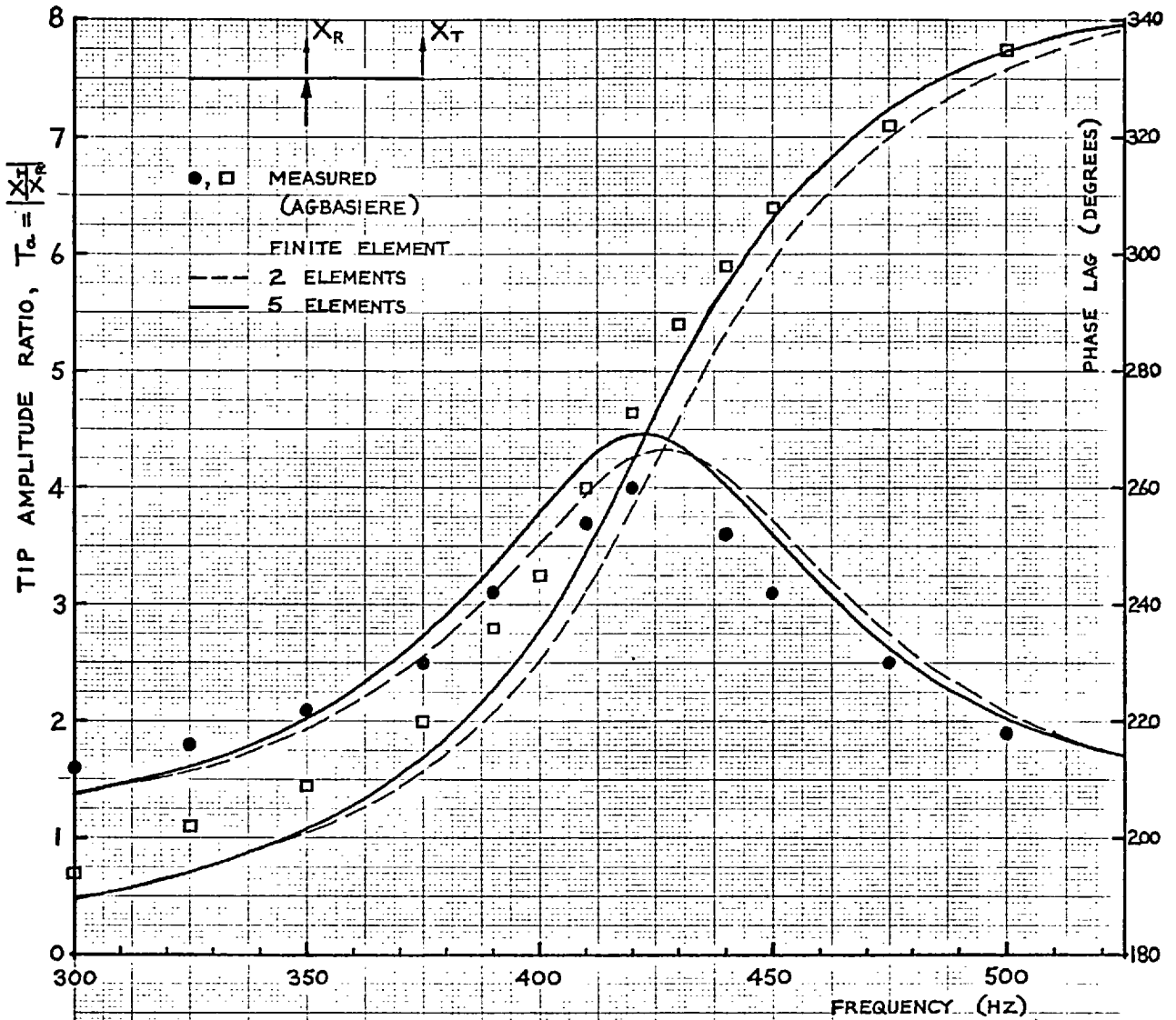


1st MODE RESONANCE CURVE FOR ROOT-EXCITED SYMMETRICAL 3 LAYER CANTILEVER (AGBASIERE BEAM 3 B)

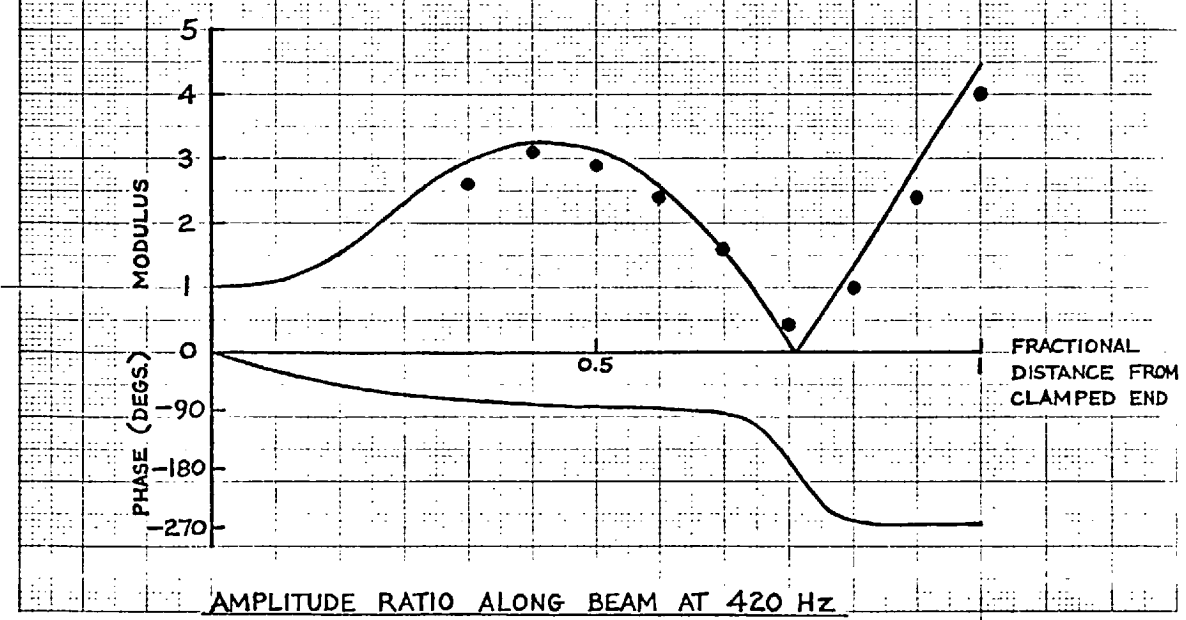


AMPLITUDE RATIO ALONG BEAM AT 92.5 Hz

FIG. 12.7



2ND MODE RESONANCE CURVE FOR ROOT-EXCITED SYMMETRICAL 3 LAYER CANTILEVER (AGBASIERE BEAM 3 B)



AMPLITUDE RATIO ALONG BEAM AT 420 Hz

the greater complexity of the multi-directional measurement, it has in fact yielded results which are closer to the theoretical predictions, especially at the low frequencies. Thus, the straightforward measurements with the force gauge and accelerometer may have been very slightly in error: this was probably due to the fact that the accelerometer was not on the same axis as the force gauge, but was mounted just beside it.

The lower graph in Fig. 12.5 also corresponds to excitation near the tip of the beam, and it shows the measured relative motion between the two outer faces of the 5-layer sandwich. The lack of relative motion clearly justifies the assumption that the layers are incompressible in the transverse direction. It was in fact necessary to proceed beyond 2000 Hz before any relative motion occurred.

The response curves here and in the other sections clearly show that the element is capable of adequately describing the vibrational behaviour of a symmetrical 5-layer beam over a wide frequency range, encompassing a large number of modes: beam UT possesses 10 bending modes (symmetric + anti-symmetric) in the range 0 to 1000 Hz, and even among the highest of these the peak mobility is rarely in error by more than 4 dB. These results also justify the omission of rotary and axial inertia terms when deriving the element mass matrix. As was explained before, it is this which permits one to introduce an internal node without effectively increasing the size of the element stiffness matrix. Since the predicted resonant frequencies already tend to be slightly below the measured ones, the inclusion of extra inertia terms would in fact only accentuate the error!

Having examined the 5-layer beam UT in considerable detail, we shall now look briefly at a symmetrical 3-layer beam used by Agbasiere⁽¹⁶⁾. This is beam 3B in Fig. 12.1, and it consists of a layer of PVC (sheet A), sandwiched between two layers of aluminium alloy Si C $\frac{1}{2}$ H (composition specified in BS 1470). The properties of the PVC are exactly the same as for the

previous beam, but the elastic modulus of the aluminium is very slightly lower than before, with a value of $0.689 \times 10^{11} \text{ N/m}^2$. This beam was tested by Agbasiere as a double-cantilever, and as he clamped the centre section directly onto an exciter, a steel insert was used in place of the PVC over this section. The root and tip displacements X_R and X_T were measured using capacitance-type displacement transducers, and Figs. 12.6 and 12.7 show the variation of amplitude ratio $\frac{X_T}{X_R}$ with frequency for the first and second cantilever resonances*. Below each frequency response curve is the forced "mode shape" corresponding to the resonant frequency, where the latter is here defined as being the frequency at which the tip amplitude ratio is a maximum. The shape was measured by moving the tip displacement transducer towards the root in small steps.

The theoretical frequency response curve was obtained by setting up the complete 0.305 m cantilever beam as a single multi-element subsystem, with only the tip co-ordinates retained. The root was excited by a constant force of 1 N and the amplitude ratio was computed. As the element was developed for a 5-layer beam, this 3-layer case was dealt with by setting the centre layer to zero thickness, while each of the visco-elastic layers was set to half the core thickness. For the mode shape, the beam was divided up into nine single-element subsystems, so that the coupling program would yield the transverse response at sufficient points for the mode to be plotted. As COUPLE1 does not take account of banding in the stiffness matrix, this calculation was somewhat inefficient and was only carried out at the two resonant frequencies. The graphs show quite good agreement between experiment and theory, especially for the 1st mode, and the errors are almost certainly due to the use of an incorrect temperature and/or strain when computing the PVC properties, since neither this information nor the root

* Note that these cantilever resonant frequencies correspond to the anti-resonant frequencies associated with the point mobility at R.

displacement were specified by Agbasiere. In the case of the 2nd mode resonance curve, it will be observed that the response obtained with only 2 elements differs very little from that yielded by 5 elements. Remembering that a single element can describe up to $\frac{3}{8}$ wavelength, and noting that for the 2nd mode the cantilever length corresponds to about $\frac{3}{4}$ wavelength, we immediately see that 2 is the minimum number of elements that will give acceptable results and the "error" incurred by using this minimum number is seen to be very small. Hence, the rule has been substantiated using a completely separate example.

12.3 RESULTS FOR FLEXURAL VIBRATION OF UNSYMMETRICAL 3- AND 5-LAYER BEAMS

As no unsymmetrical section beams were tested by the Author, the unsymmetrical 3- and 5-layer elements will be checked against measurements and theoretical predictions obtained by Nakra⁽¹⁸⁾. He tested a number of simply-supported beams, applying an equal displacement excitation X_T at each support and measuring the displacement response X_C at the centre span. His analysis followed an energy approach, just as with the finite elements derived here, but he proceeded from the energy expressions to the differential equations of motion by using Hamilton's Principle, and he then solved these equations exactly. This exact solution is only possible when the beam is simply-supported, since the mode shape for this particular case is known to be a sinusoid, but for any other boundary conditions it is necessary to solve the equations by some approximate technique.

We shall consider the three beams shown in Fig. 12.8. These comprise various combinations of steel, aluminium and PVC layers, bonded together with Araldite epoxy resin. The aluminium alloy is Si C $\frac{1}{2}$ H, while the steel is ordinary commercial grade bright mild steel strip: Nakra measured the elastic moduli of both these materials and obtained figures of 0.6828×10^{11}

and $0.2066 \times 10^{12} \text{ N/m}^2$ for the aluminium and the steel respectively. Although all the PVC layers are nominally the same, it was found that the properties of sheet B differed considerably from those of sheet A. As was explained in Section 12.2, sheet A was tested by Agbasiere⁽¹⁶⁾ and its properties were subsequently expressed in terms of the formula given in Fig. 14.1. Sheet B was tested by Nakra and its full properties are only available in graphical form in Reference (18). However, Fig. 14.3 shows the variation in properties with frequency for one particular value of temperature and strain, and it is clearly seen that the shear moduli of the two sheets differ by as much as 30 %.

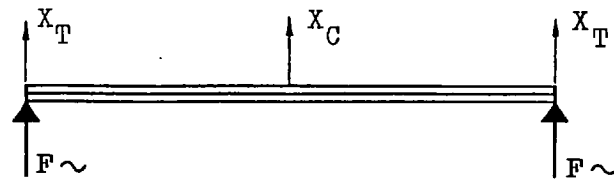
Because of symmetry, the finite element calculation was carried out using just half the beam, and this was set up in COUPLE1 as a single 3-element section (so the beam length from tip to tip corresponds to 6 elements). Figs. 12.9 to 12.11 show the frequency response plots corresponding to the first two modes of each beam. Although there is reasonable agreement between measurements and theory, it is immediately apparent that Nakra's theoretical predictions are generally closer to the measured data points than the present finite element predictions. This is almost certainly due to the fact that the finite element model was excited by equal forces of 1 N at the two supports, whereas Nakra's model was excited by a displacement input equal to that measured on the experimental setup*. Although both models are linear, the properties of the PVC vary with strain, and since this has been allowed for in both calculations it is inevitable that the results should be slightly different.

In addition to these comparisons with Nakra's results, the unsymmetrical 5-layer element has been used to predict the response of the symmetrical 5-layer beam UT considered in Section 12.2, and it has yielded identical results to the symmetrical 5-layer element.

* At the time that the finite element calculations were carried out, the Author had not yet investigated the possibility of applying a "constant" displacement excitation using COUPLE1. Only subsequently was it realised that this could be achieved by using very stiff elastic supports K in conjunction with a large exciting force F, such that Displacement = F/K. This is illustrated in an example given in Appendix II (to Part 1).

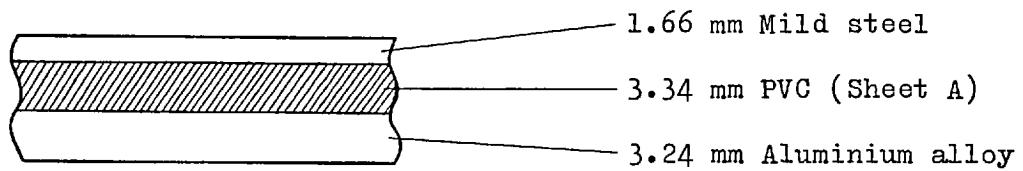
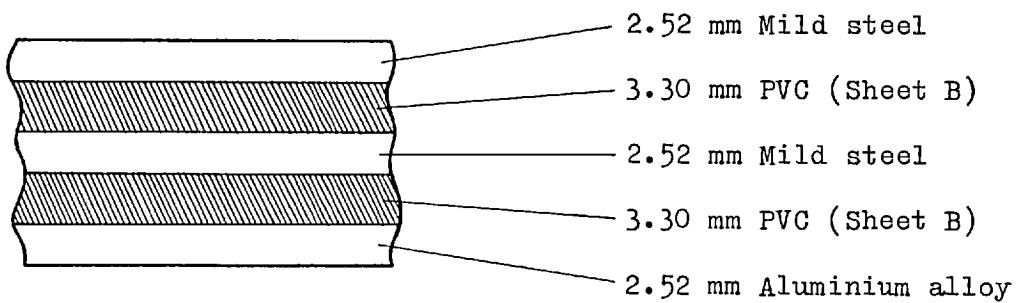
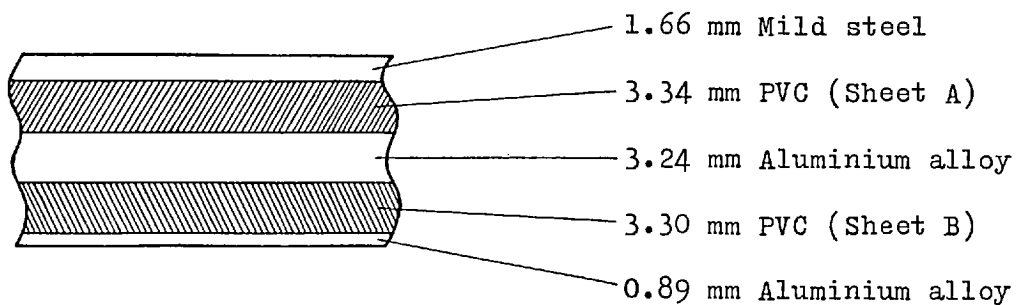
In case the reader should wish to try this for beam S2, the support excitations used by Nakra were 0.0378 and 0.0182 mm for modes 1 and 2 respectively and the corresponding temperatures in the visco-elastic core were 21.1 and 22.9°C. For beams M1 and M2, it is necessary to consult Reference (18) to obtain the properties of PVC sheet B and the necessary excitation data.

FIG. 12.8

UNSYMMETRICAL MULTI-LAYER BEAMS USED BY NAKRA

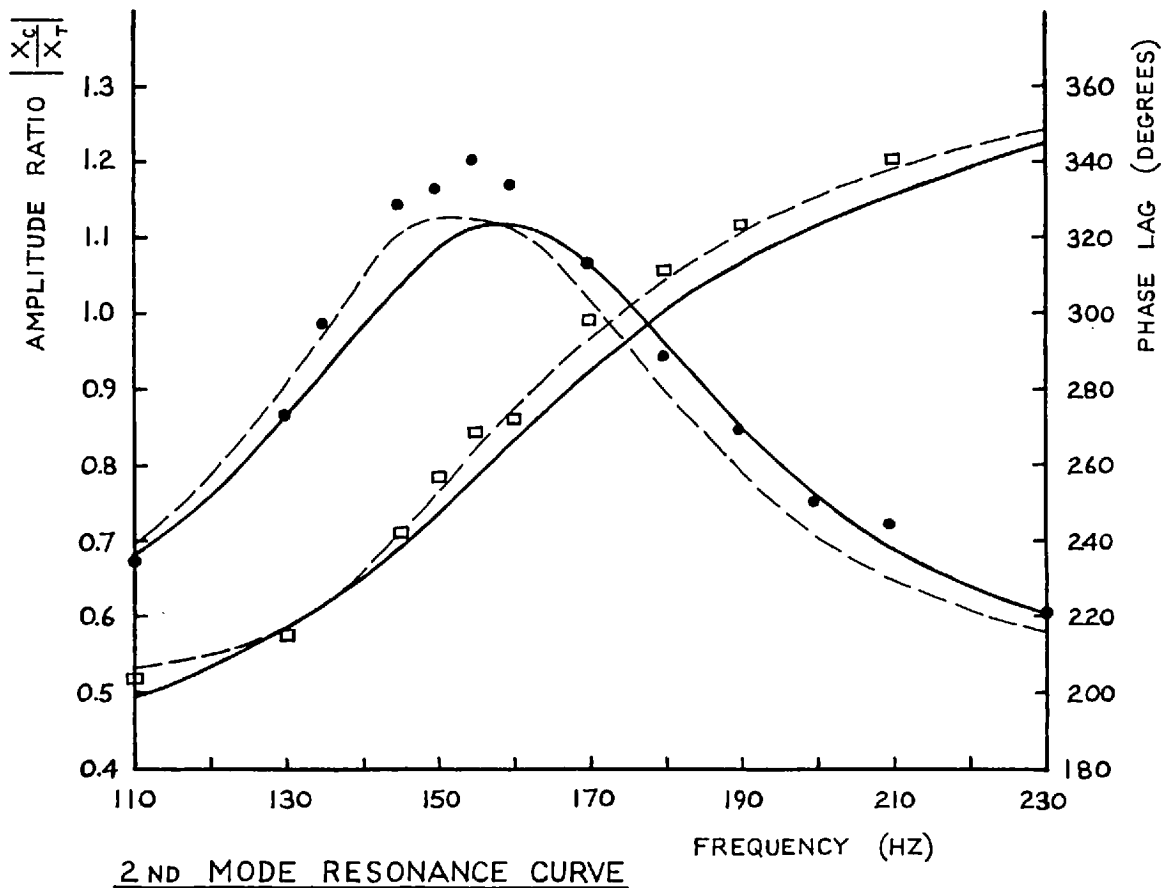
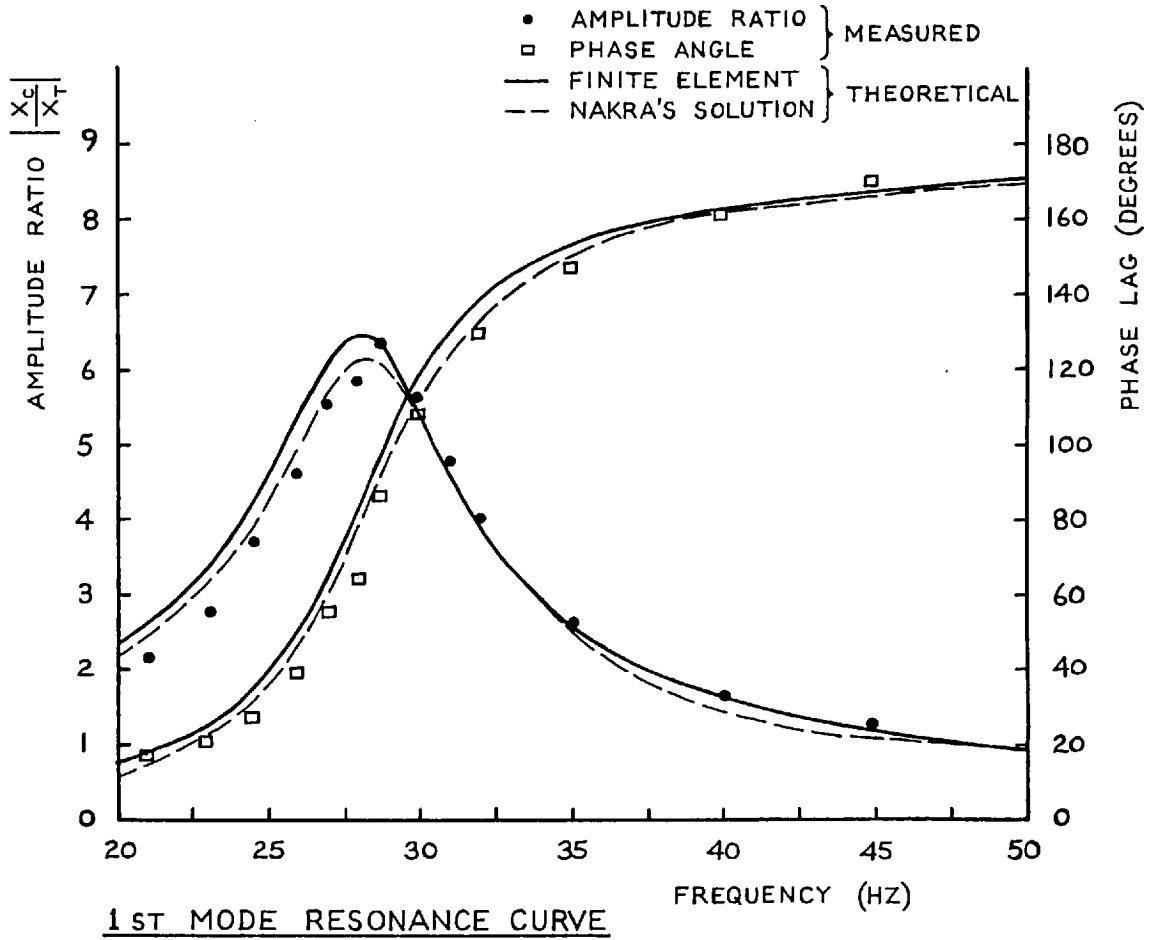
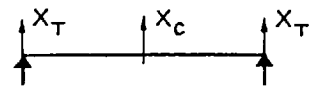
Length = 0.762 m

Width = 38.1 mm

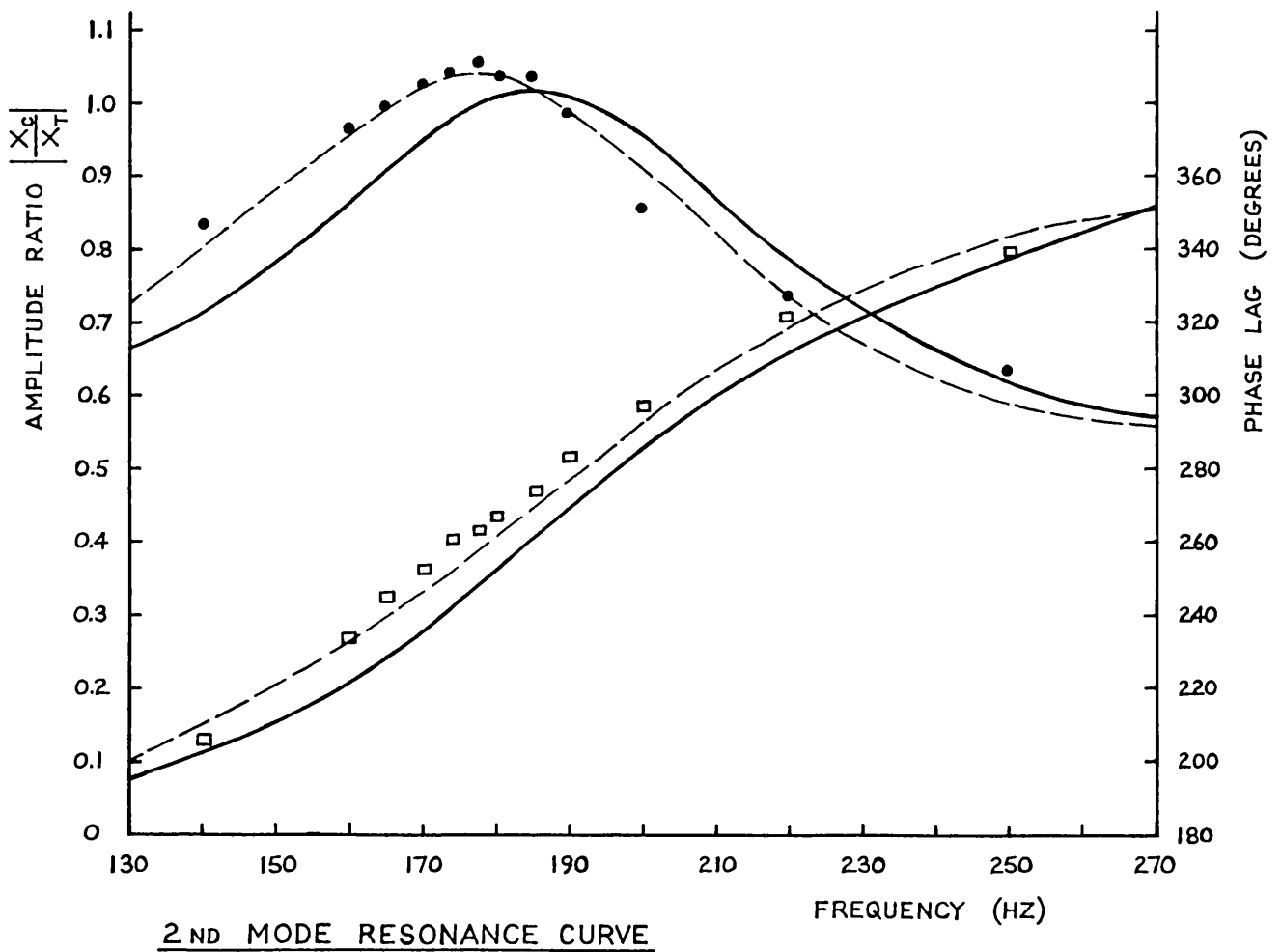
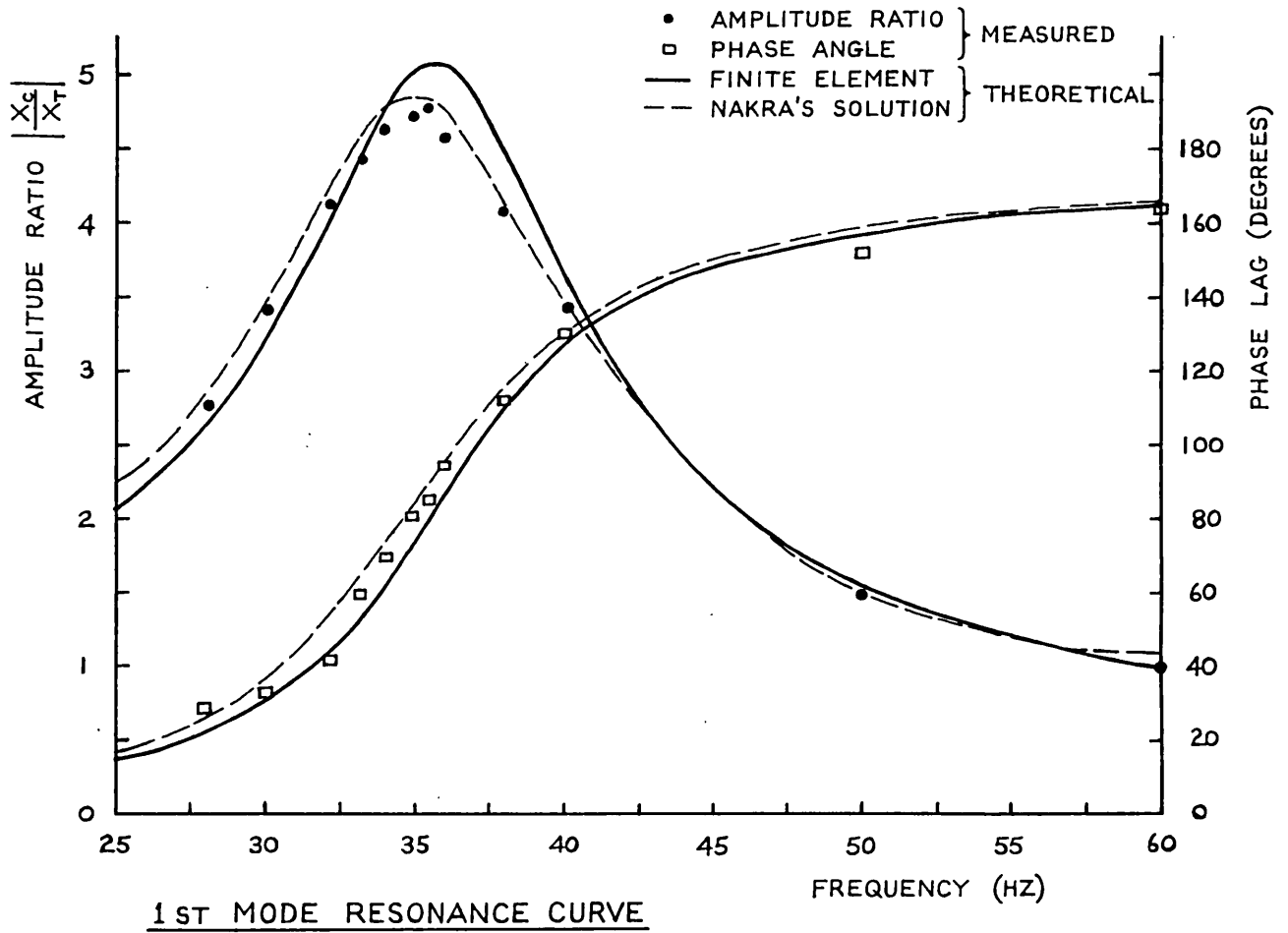
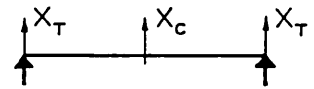
BEAM S2 Unsymmetrical 3 layerBEAM M1 Unsymmetrical 5 layerBEAM M2 Unsymmetrical 5 layer

NAKRA BEAM S2 FIG 12.9

SIMPLY-SUPPORTED UNSYMMETRICAL 3-LAYER BEAM WITH SUPPORT EXCITATION

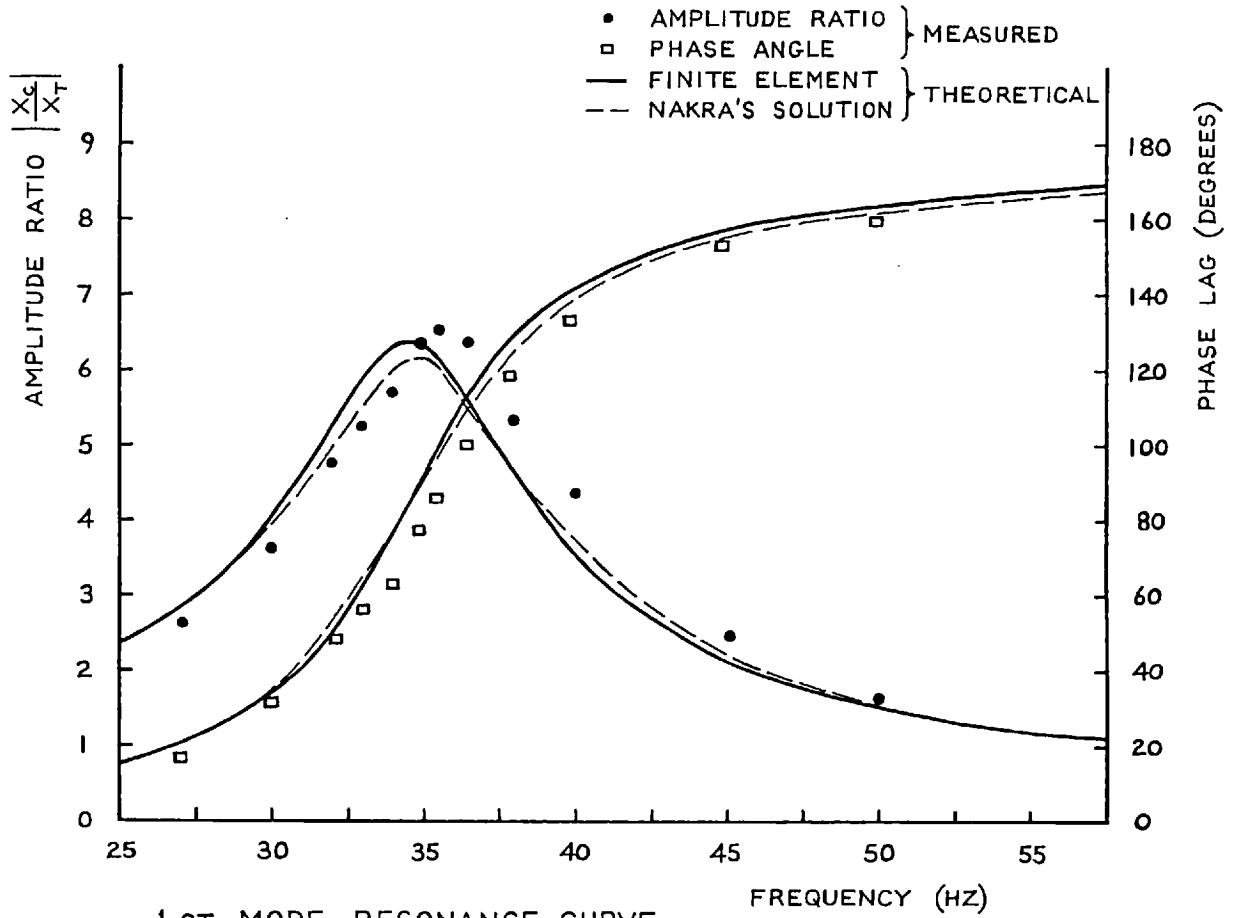
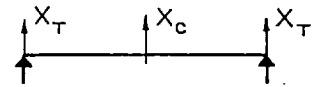


SIMPLY-SUPPORTED UNSYMMETRICAL 5-LAYER BEAM WITH SUPPORT EXCITATION

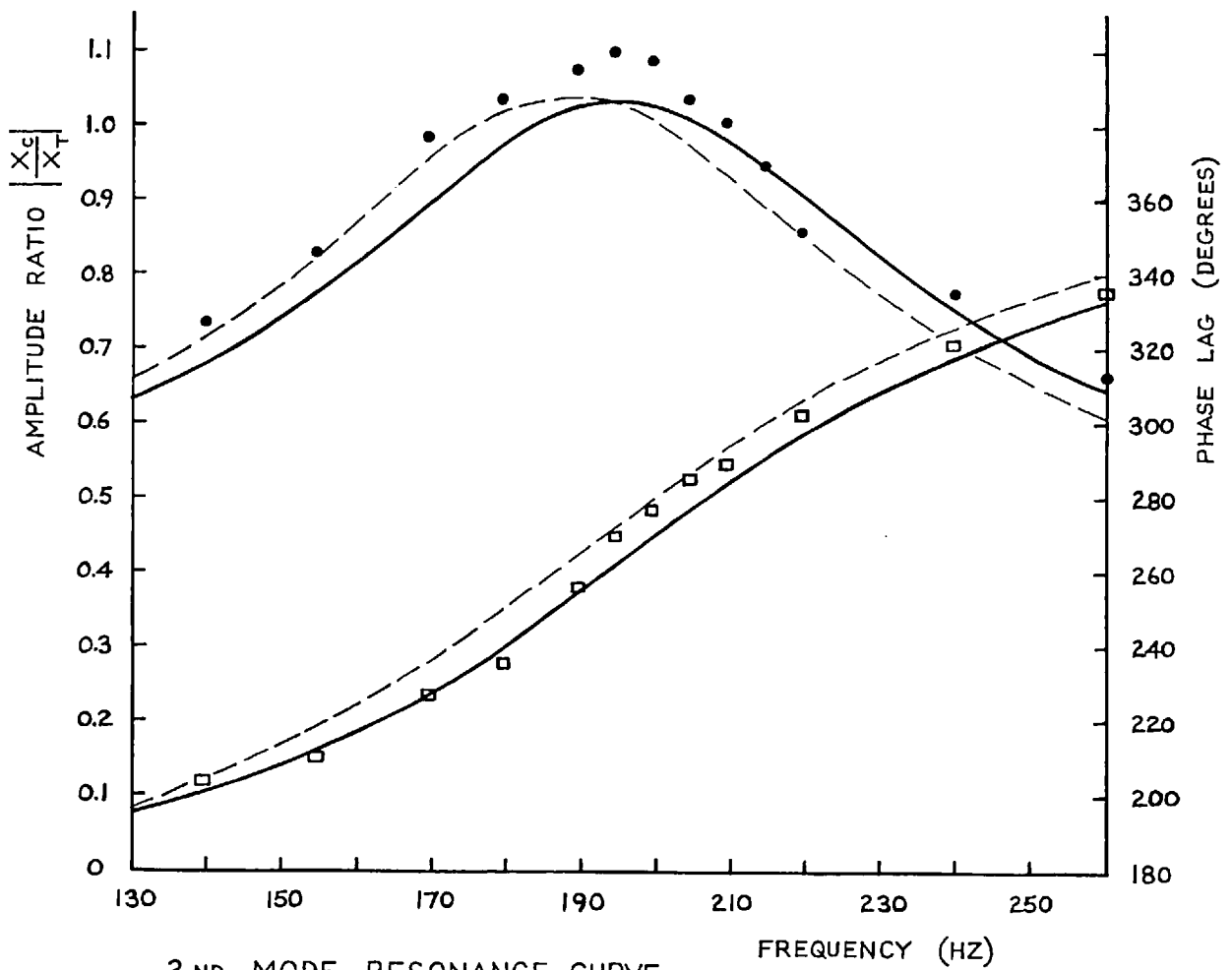


NAKRA BEAM M2 FIG 12.11

SIMPLY-SUPPORTED UNSYMMETRICAL 5-LAYER BEAM WITH SUPPORT EXCITATION



1st MODE RESONANCE CURVE



2nd MODE RESONANCE CURVE

12.4 RESULTS FOR TORSIONAL VIBRATION OF SYMMETRICAL 3- AND 5-LAYER BEAMS

As the torsional vibration of sandwich beams has not received any attention in the literature, the torsional finite element can only be checked against measurements made by the Author. The two beams in Fig. 12.1 have been used for this purpose, and torsional point mobility measurements have been made using the single-shaker multi-directional measurement technique developed in Part 2 (see Chapter 4, Section 4.5). In each case the beam was suspended on fairly resilient supports in order to simulate a free-free condition.

In the case of the symmetrical 5-layer beam UT, the torque was applied at point A and the resulting mobility curve is shown in Fig. 12.12. The measured data were obtained from a multi-directional test using exciting block Mk 3, where the latter was bolted to the upper face of the beam with its axis at right angles to the beam axis. The block was first excited at one end, then at the other end, and the two sets of response data were subsequently combined to yield the transverse and torsional mobilities. This test included a correction for the exciting block inertia in the x and β directions, but there was no correction for transverse loading in the plane of the layers.

As point A is inboard from the tip, it was necessary in the analysis to divide the beam into two multi-element sections which were subsequently coupled together to yield the response at A. Just as for the bending analysis considered in Section 12.2, it was decided to use 10 elements up to 400 Hz, and 14 at higher frequencies; but these numbers could undoubtedly have been reduced without adversely affecting the results. All the beam data are the same as before, except that Poisson's ratio must now be included: 0.33 for the aluminium and 0.5 for the PVC.

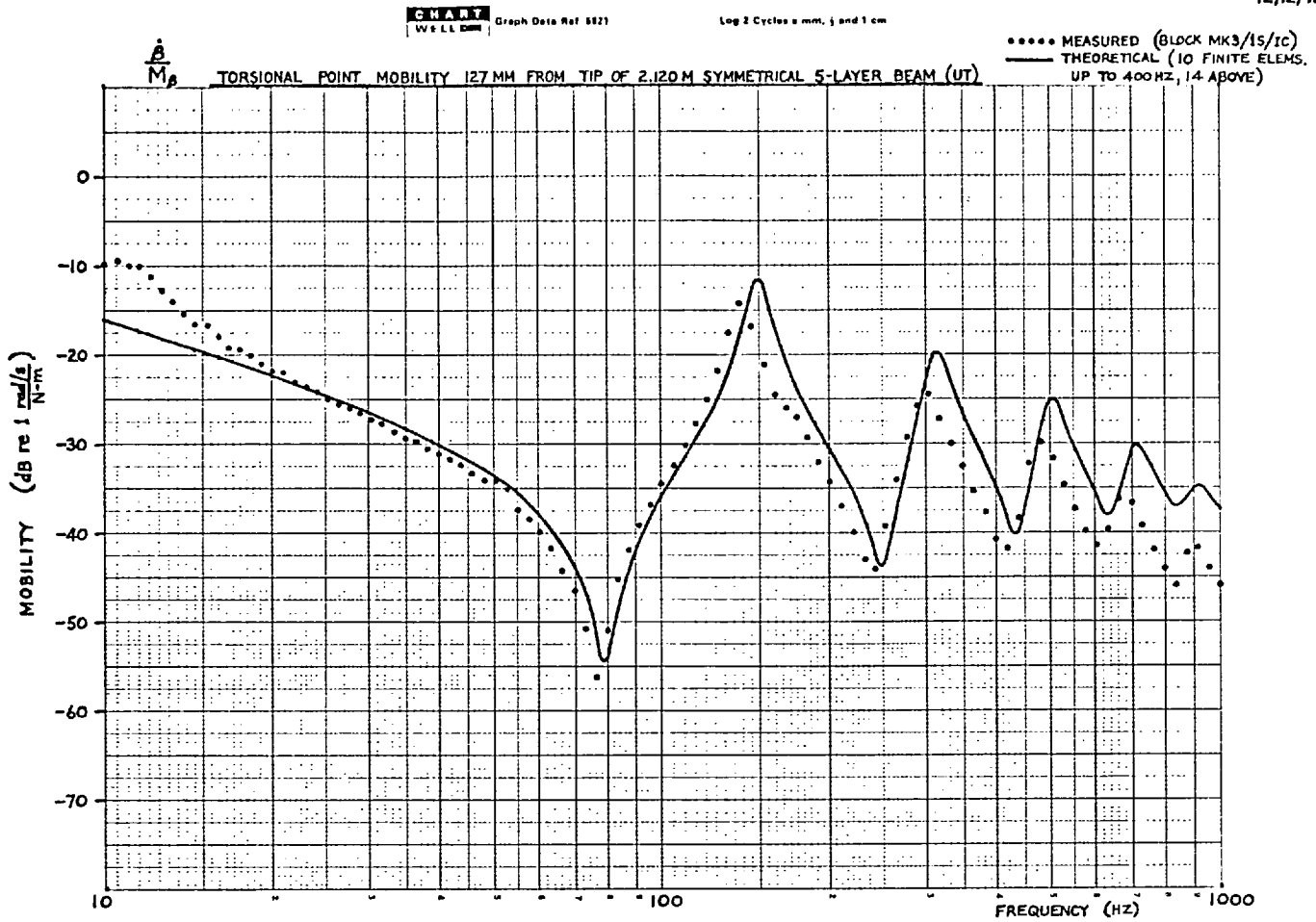
It will be observed that this beam exhibits less damping in torsion than in bending, with a loss factor of approximately 0.1 for the 1st torsional

mode, in comparison with a figure of about 0.25 for the 1st bending mode. The measured and theoretical responses agree reasonably well, especially around the first resonance, although the overall agreement is not quite so good as for the bending analysis. This is probably due to a combination of three factors: (a) The assumption of incompressible visco-elastic layers, (b) the neglect of shear stiffness when analysing the in-plane bending of the outer layers, and (c) the transverse inertia loading applied to the beam by the exciting block along the surface of the outer layer. The second of these may be quite significant in the present case, since the ratio of beam length to width is only 13.9, and it would have the effect of stiffening the beam, thereby raising its resonant frequencies. However, it is likely that the loading effect of the block is the most significant source of error, since this would cause the measured resonant frequencies to be reduced, and at the same time it would pull the response curve down towards a line representing the effective block inertia.

This beam has also been analysed by E. Ioannides⁽⁴²⁾ using a finite element program developed for unsymmetrical 5-layer sandwich plates. The beam was divided into a large number of triangular elements, and the couple was applied as equal and opposite forces at two of the nodes. His results are very similar to those yielded by the present beam element, and if anything they are marginally better, but the solution time per frequency is very much higher.

In the case of the symmetrical 3-layer beam 3B, the torque was applied at point T and the resulting mobility curve is shown in Fig. 12.13. Once again the measured data were obtained from a multi-directional test, but in this case no exciting block was used. Instead, the force and acceleration transducers were attached to the beam using studs, in just the same way as for the torsion test on the two-stage beam in Section 4.5. This minimised the extra inertia attached to the tip of the beam, but the force gauge inertia was still present.

12/12/72



12/12/72

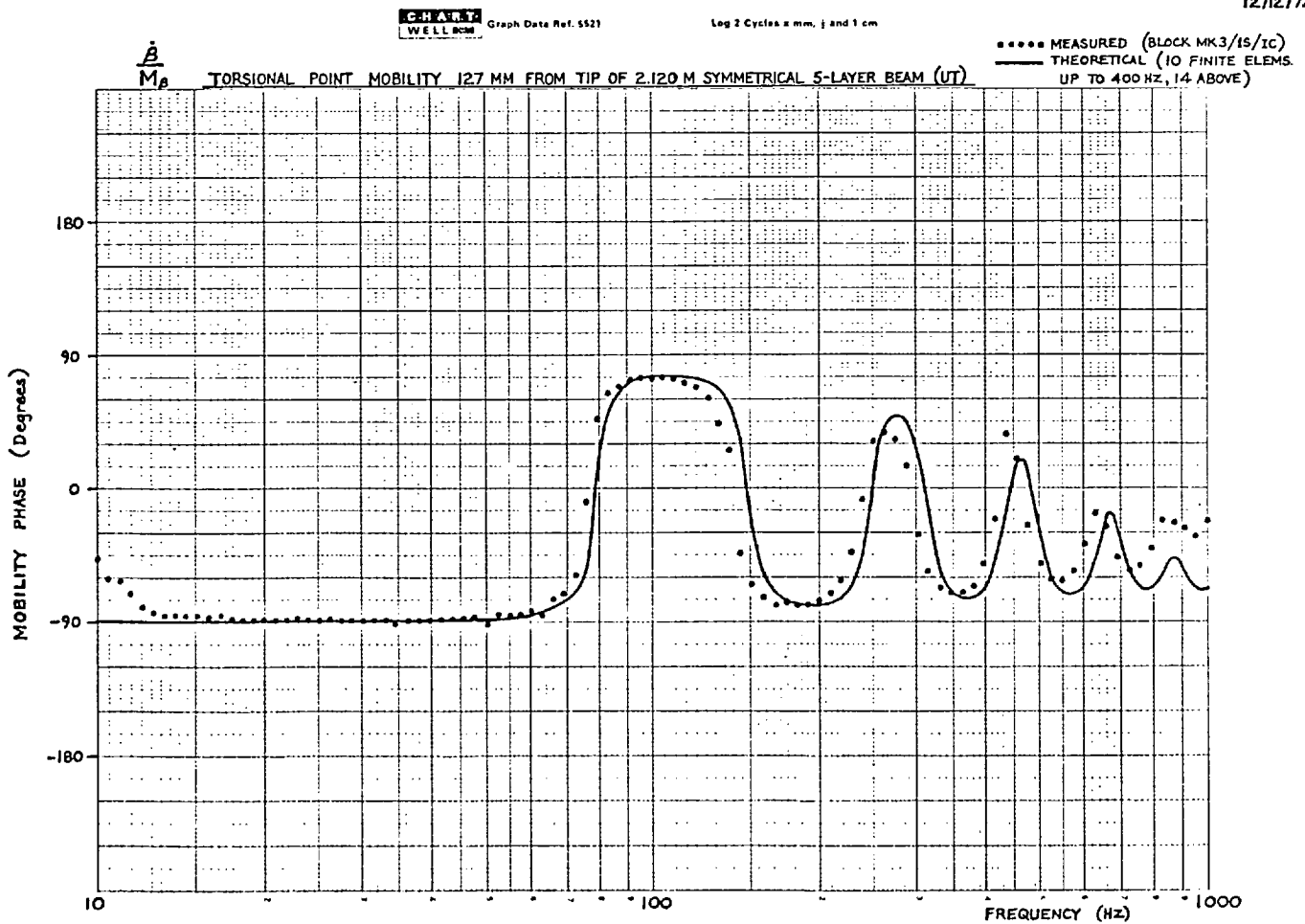
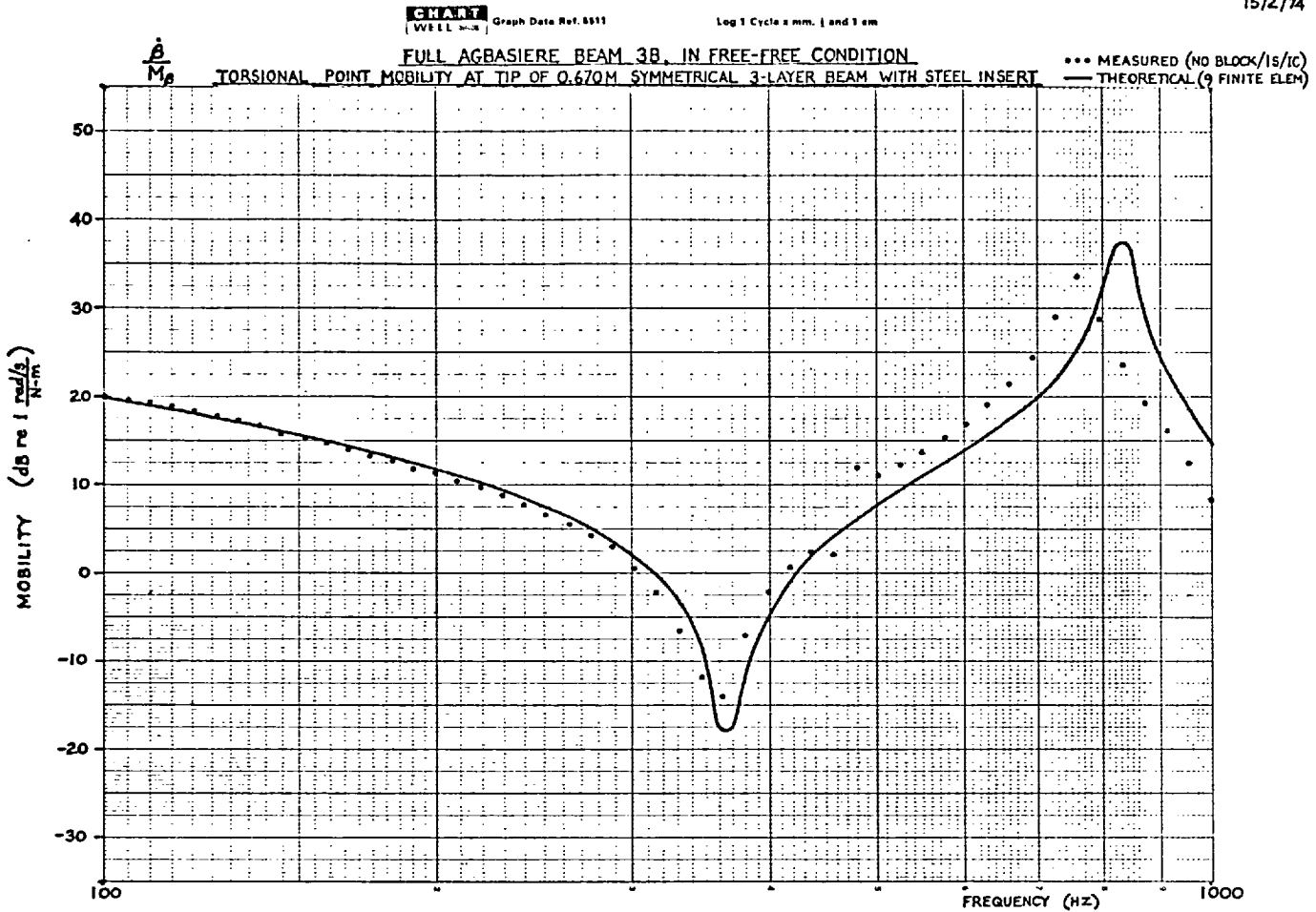
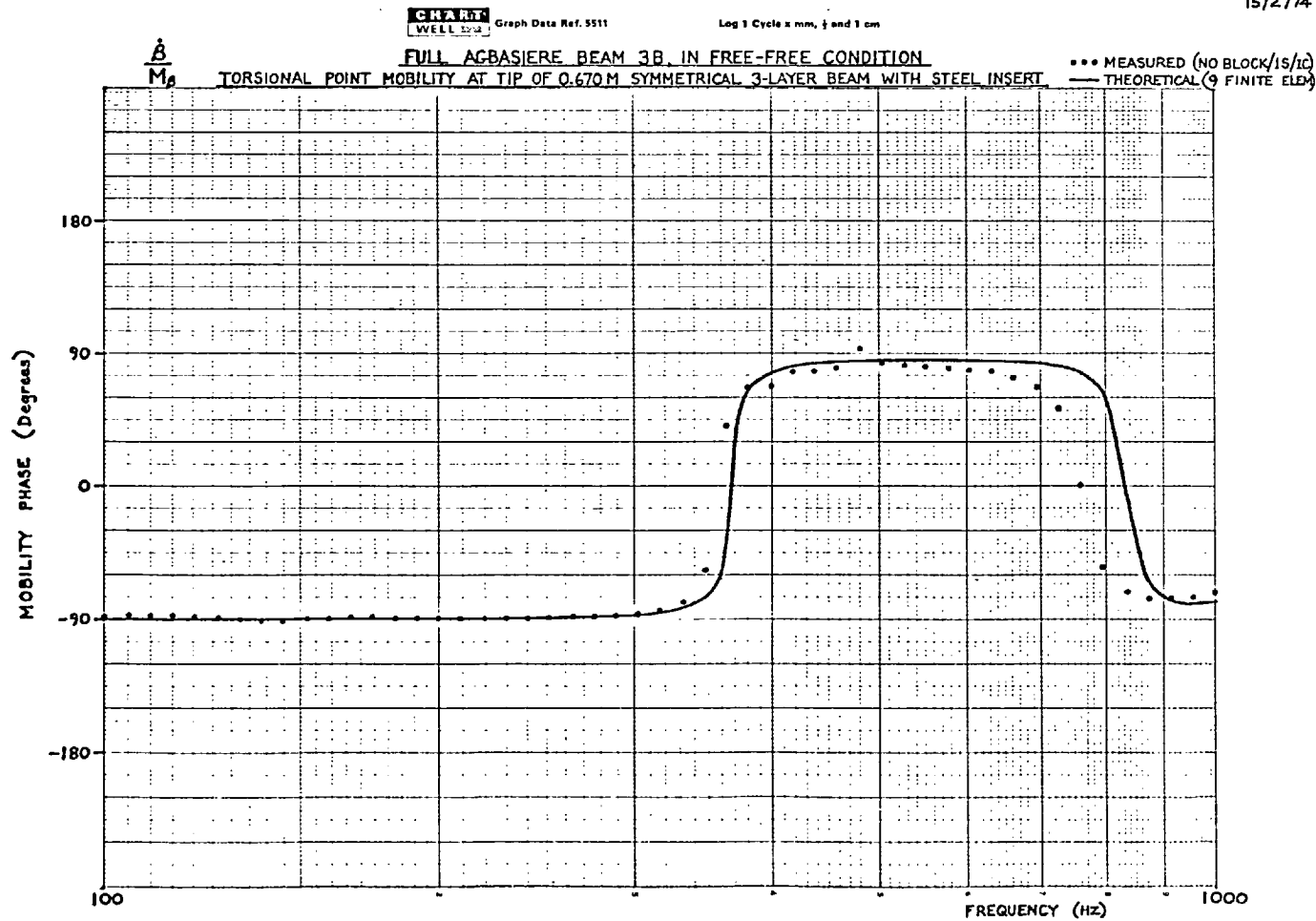


FIG. 12.13.

15/2/74



15/2/74



As the centre section of the beam contains a steel insert in place of the PVC, it was necessary to analyse the beam as three sections or subsystems. Each damped section was divided into 4 elements, while a single element was used for the stiff centre section. All the beam data are the same as before, except that Poisson's ratio must now be included.

The beam only has a single resonance below 1000 Hz, so it does not provide such a good check as the previous beam. Nevertheless, the anti-resonance is fairly well described; and although the predicted resonance is a little high, the peak mobility is only about 3 dB greater than the measured value. As with beam UT, it is probable that the measured resonance is lower than it should be, since the force gauge applied quite a significant loading to the beam.

12.5 CONCLUSIONS

The results presented here prove the validity of the various multi-layer beam elements developed in Chapters 9 to 11. The errors in the predicted response are thought to be mainly due to the use of slightly incorrect visco-elastic material properties or to difficulties in correctly measuring the dynamic response, rather than to failings in the elements themselves.

It has been shown that the introduction of an "internal node" mid-way along a multi-layer bending element can very greatly improve its accuracy, since it allows one to match together the different displacement functions. In the case of the symmetrical 5-layer element derived here, the introduction of just one co-ordinate at this internal node has halved the number of elements that are needed to build a beam, and each element is capable of describing anything up to $\frac{3}{8}$ wavelength. It has also been shown that an element with only transverse inertia can adequately describe the vibrational behaviour up to quite high frequencies, so it is not necessary to associate any inertia

with the internal node. This allows one to obtain the improved accuracy associated with an internal node, without the disadvantage of having extra unwanted degrees of freedom, since it is possible to reduce the (static) stiffness matrix immediately after it has been formed, thereby eliminating these extra freedoms, while still retaining the improved accuracy.

With the development of the torsional finite element for a symmetrical 5-layer beam, it now becomes possible to analyse more general 3-dimensional beam-type structures incorporating constrained layer damping. However, when designing such structures it is important to bear in mind that the damping associated with in-plane bending and with torsion will always be less than that associated with bending in the plane at right angles to the layers.

REFERENCES FOR CHAPTERS 8 TO 12 (PART 3)

1. Ungar, E. E., "The status of engineering knowledge concerning the damping of built-up structures", *Jnl. of Sound and Vibration*, Vol. 26 (1), 1973, pp 141-154
2. Oberst, H., "Über die dämpfung der biegeschwingungen dünner bleche, durch fest haftende beläge", Part I: *Acustica*, Vol. 2, 1952. Part II: *Acustica*, Vol. 4, 1954
3. Lienard, P., "Étude d'une méthode de mesure du frottement intérieur de revêtements plastiques travaillant en flexion", *La Recherche Aéronautique*, Vol. 20, 1951, p 11
4. Mead, D. J., "The effect of a damping compound on jet efflux excited vibrations", Part I: *Aircraft Engineering*, Vol. 32, March 1960. Part II: *Aircraft Engineering*, Vol. 32, April 1960
5. Ruzicka, J. E., (Ed.), "Structural Damping". Papers presented at the Colloquium on Structural Damping, ASME, Dec. 1959
6. Kerwin, E. M., "Damping of flexural waves by a constrained visco-elastic layer", *JASA*, Vol. 31, July 1959
7. Ross, D., Kerwin, E.M. and Dyer, I., "Flexural vibration damping of multi-layer plates", BBN Report 564, June 1958
8. Ross, D. and Kerwin, E. M., "Damping of flexural vibrations in plates by free and constrained visco-elastic layers", BBN Report 632, May 1959
9. Ross D., Ungar, E. E. and Kerwin, E. M., "Damping of plate flexural vibrations by means of visco-elastic laminae", section 3 of "Structural Damping" (Reference 5)
10. DiTaranto, R. A., "Theory of vibratory bending for elastic and visco-elastic layered finite-length beams", *Jnl. of Applied Mechanics*, Vol. 32, No. 4, Dec. 1965

11. DiTaranto, R. A. and Blasingame, W., "Composite damping of vibrating sandwich beams", Jnl. of Engineering for Industry (Trans ASME 633), 1967
12. Mead, D. J. and Markus, S., "The forced vibration of a three-layer damped sandwich beam with arbitrary boundary conditions", Jnl. of Sound and Vibration, Vol. 10, 1969, pp 163-175
13. Mead, D. J., "The existence of normal modes of linear systems with arbitrary damping", Paper C5 at Symposium on Structural Dynamics, Univ. of Loughborough, 1970
14. Markus, S. and Valášková, O. "On eigenvalue boundary problems of transversely vibrating sandwich beams", Jnl. of Sound and Vibration, Vol. 23, 1972, pp 423-432
15. Mead, D. J. and DiTaranto, R. A., "Resonance response criteria of a damped three-layered beam", Jnl. of Engineering for Industry, Feb. 1972, pp 174-180
16. Agbasiere, J., "Flexural Vibrations of multi-layered beams with visco-elastic damping", Ph.D. thesis, Univ. of London, 1966
17. Agbasiere, J. and Grootenhuis, P., "Flexural vibration of symmetrical multi-layer beams with visco-elastic damping", Jnl. of Mech. Eng. Science, Vol. 10 (3), 1968, p 269
18. Nakra, B. C., "Vibrations of visco-elastically damped laminated structures", Ph.D. thesis, Univ. of London, 1966
19. Nakra, B. C. and Grootenhuis, P. "Structural damping using a four layer sandwich", Jnl. of Engineering for Industry, Feb. 1972
20. Grootenhuis, P. "The control of vibrations with visco-elastic materials", Jnl. of Sound and Vibration, Vol. 11 (4), 1970, pp 421-433
21. Ahmed, K. M., "Free vibration of curved sandwich beams by the method of finite elements", Jnl. of Sound and Vibration, Vol. 18 (1), 1971, pp 61-74
22. Ahmed, K. M., "Dynamic analysis of sandwich beams", Jnl. of Sound and Vibration, Vol. 21 (3), 1972, pp 263-276

23. Leone, S. G., and Perlman, A. B., "A numerical study of damping in visco-elastic sandwich beams", ASME paper No. 73-DET-73 at Design Eng. Technical Conf., Cincinnati, Sept. 1973.
24. Zienkiewicz, O. C., "The finite element method in engineering science", McGraw-Hill (London), 1971
25. Tottenham, H. and Brebbia, C. A., (Eds.), "Finite element techniques in structural mechanics", Univ. of Southampton Publications.
26. Leckie, F. A. and Lindberg, G. M., "The effect of lumped parameters on beam frequencies", Aeronautical Quarterly, Vol. 14, 1963, pp 224-240
27. Archer, J. S., "Consistent mass matrix for distributed systems", Proc. ASME, Vol. 89, ST4, 1963, p 161
28. Davis, R., Henshell, R. D. and Warburton, G. B., "A Timoshenko beam element", Jnl. of Sound and Vibration, Vol. 22 (4), 1972, pp 475-487
29. Thomas, D. L., Wilson, J. M. and Wilson, R. R., "Timoshenko beam finite elements", Jnl. of Sound and Vibration, Vol. 31 (3), 1973, pp 315-330
30. Dokumaci, E., Thomas, J. and Carnegie, W., "Matrix displacement analysis of coupled bending-bending vibrations of pretwisted blading", Jnl. of Mech. Eng. Science, Vol. 9 (4), 1967, pp 247-254
31. Gallagher, R. M. and Lee, C. H., "Matrix dynamic and instability analysis with non-uniform elements", Intl. Jnl. for Numerical Methods in Engineering, Vol. 2, 1970, pp 265-275
32. Henshell, R. D. and Warburton, G. B., "Transmission of vibration in beam systems", Intl. Jnl. for Numerical Methods in Engineering, Vol. 1 (1), 1969, pp 47-66
33. Lindley, P. B., "Engineering design with natural rubber", Malaysian Rubber Producers' Research Association, Tech. Bulletin No. 8, 1964
34. McCallion, H., "Vibration of linear mechanical systems", Longmans, 1973

35. Cowper, G. R., Lindberg, G. M. and Olson, M. D., "A shallow shell finite element of triangular shape", Intl. Jnl. of Solids and Structures, Vol. 6, 1970, p 1133
36. Carnegie, W., Thomas, J. and Dokumaci, E., "An improved method of matrix displacement analysis in vibration problems", Aeronautical Quarterly, Vol. 20, 1960, pp 321-332
37. Dawe, D. J., "A finite element approach to plate vibration problems", Jnl. of Mechanical Engineering Science, Vol. 7, No. 1, 1965, pp 28-32
38. Cowper, G. R., "The shear coefficient in Timoshenko's beam theory", Jnl. of Applied Mechanics, Vol. 33, 1966, pp 335-340
39. Goodman, L. E. and Sutherland, J. G., Discussion of paper "Natural frequencies of continuous beams of uniform span length" by Ayre and Jacobsen, Jnl. of Applied Mechanics, Vol. 18, 1951, pp 217-218
40. Timoshenko, S. P., "Strength of materials - Part 1", Second edition, D. Van Nostrand Co. Inc., New York, N.Y., pp 170-171
41. Timoshenko, S. P. and Woinowsky-Krieger, S., "Theory of plates and shells", McGraw-Hill, Second edition, 1959
42. Ioannides, E., "The harmonic response of structural elements with visco-elastic layers", Ph.D. thesis, Imperial College, University of London, 1974
43. Holzer, H., "Die berechnung der drehschwingungen", Springer (Berlin), 1921
44. Myklestad, N. O., "New method of calculating natural modes of uncoupled bending vibrations of airplane wings and other types of beams", Jnl. of Aeronautical Science, Vol. 6, 1944, p 153
45. Uhrig, R., "The transfer matrix method seen as one method of structural analysis among others", Jnl. of Sound and Vibration, Vol. 4 (2), 1966, pp 136-148

46. Dokainish, M. A., "A new approach to plate vibrations: combination of transfer matrix and finite element technique", Jnl. of Engineering for Industry (Trans ASME), May 1972
47. Pestel, E. C. and Leckie, F. A., "Matrix methods in elastomechanics", McGraw-Hill (New York), 1963
48. Falk, S., "Eine variante des verfahrens der ubertragungsmatrizen", Lecture given on 13/7/61 at Technische Hochschule, Darmstadt.
(See also Reference 45)
49. Sainsbury, M. G., "Users' guide for the structural dynamic analysis computer program COUPLE1", Manual in 3 parts, Dynamics Group, Imperial College, May 1975

EXPERIMENTAL AND THEORETICAL TECHNIQUES FOR THE
VIBRATION ANALYSIS OF DAMPED COMPLEX STRUCTURES

by

MICHAEL GEORGE SAINSBURY

M.Sc. (Eng), London

VOLUME II of a two-volume

Thesis presented for the degree of

Doctor of Philosophy of the University of London

Department of Mechanical Engineering
Imperial College of Science and Technology
London SW7

September 1976

CONTENTS

As the thesis is divided into four distinct parts, more detailed contents lists are given at the beginning of each part and at the beginning of each corresponding group of appendices.

Note that each part has its own reference list, with the numbers starting from 1 in each case, so the reader should take care to consult the correct list.

VOLUME I

<u>Chapter</u>		<u>Page</u>
	PART 1 - VIBRATION ISOLATION AND FREQUENCY RESPONSE ANALYSIS	10
1	General Introduction to Vibration Isolation	11
2	The Frequency Response Analysis of Damped Complex Structures	41
	References for Part 1	75
	PART 2 - MULTI-DIRECTIONAL MOBILITY MEASUREMENTS FOR THE VIBRATION ANALYSIS OF COUPLED STRUCTURES	82
3	Multi-directional Mobility Measurement	83
4	Multi-directional Measurements with a Single Shaker	94
5	Multi-directional Measurements with a Twin Shaker	147
6	Coupling of Beam to Spring-supported Block	160
7	Summary and Conclusions for Multi-directional Mobility Measurements	176
	References for Part 2	185
	PART 3 - THE FINITE ELEMENT VIBRATION ANALYSIS OF MULTI-LAYER DAMPED BEAMS IN FLEXURE AND TORSION	189
8	General Introduction to Multi-layer Damped Beams	191
9	Bending Finite Element for Symmetrical 5-layer Beam	199

10	Bending Finite Elements for Unsymmetrical 3- and 5-layer Beams	222
11	Torsional Finite Element for Symmetrical 5-layer Beam	238
12	Results and Conclusions for Multi-layer Damped Beams	257
	References for Part 3	283

VOLUME II

Chapter

	PART 4 - THE VIBRATION ANALYSIS OF A HEAVILY DAMPED V-BEAM SEATING	292
13	Details of Seating and its Analysis	293
14	Analysis of Seating Components	321
15	Results and Conclusions for the Seating	380
	References for Part 4	430

Appendix

	APPENDICES FOR PART 1	433
I	Flow Chart for the Computer Program COUPLE1	434
II	The Addition of a Single Friction Damper to a Linear Damped System	445
	APPENDICES FOR PART 2	460
III	Derivation of Matrices used in Multi- directional Measurements	461
IV	Some Multi-directional Mobility Measurements on a Large Mass	474
	APPENDICES FOR PART 3	501
V	The Convergence Rate of Energy Integrals in the Finite Element Method	502
VI	"Standard" Matrices arising in the Finite Element Analysis of Sandwich Beams	505

VII	Extensional and Bending Strain Energies in a Thin Plate	507
VIII	The Formation of a Tip Dynamic Stiffness Matrix for a Multi-element Beam	510
	APPENDICES FOR PART 4	517
IX	Derivation of Dynamic Stiffness Matrix for Spring-mass Model of Rubber V-block (RB)	518
X	Derivation of Dynamic Stiffness Matrix for Male V-piece (VB)	530
XI	Derivation of Dynamic Stiffness Matrix for Female V-support (VS)	537
<hr/>		
	PUBLICATIONS	547
1	Mobility Measurements for the Vibration Analysis of Connected Structures	
2	Vibration Analysis of a Damped Machinery Foundation Structure using the Dynamic Stiffness Coupling Technique	

PART 4THE VIBRATION ANALYSIS OF A HEAVILY DAMPED V-BEAM SEATINGCONTENTS

<u>Chapter</u>		<u>Page</u>
13	DETAILS OF SEATING AND ITS ANALYSIS	
	13.1 Introduction	293
	13.2 Discussion and Details of the V-beam Assembly	299
	13.3 Details of the Analysis	306
14	ANALYSIS OF SEATING COMPONENTS	
	14.1 Transverse and Longitudinal Sandwich Beams	321
	14.2 Rubber V-Block	335
	14.3 Male V-Piece	352
	14.4 Female V-Support	356
	14.5 Cruciform	359
	14.6 Stiffness of the V-Support/Cruciform Interface	368
15	RESULTS AND CONCLUSIONS FOR THE SEATING	
	15.1 Results for the Assembled Structure	380
	15.2 Discussion of Results	403
	15.3 General Discussion and Summary	423
	15.4 Conclusions	429
	REFERENCES FOR CHAPTERS 13 TO 15	430

Appendices to Part 4 start on Page 517

CHAPTER 13

DETAILS OF SEATING AND ITS ANALYSIS

13.1 INTRODUCTION

The measurement and analysis techniques introduced in Parts 1, 2 and 3 will now be applied to the analysis of an existing highly damped machinery foundation structure or "seating". This structure was conceived and designed prior to the development of the necessary analytical capability, and is based on simple isolation concepts and intuitive reasoning, rather than on mathematical analysis. Although it has been found to work fairly effectively, the lack of any analysis makes optimisation virtually impossible, and one cannot say how much better or worse the performance might be with a few minor modifications. However, if it is possible to compute the performance with sufficient accuracy, the effect of modifications may be examined quite simply. In addition, if the adequacy of the measurement and analysis techniques can be proven on this fairly complex system, then any structure of comparable complexity may in future be designed, analysed and modified to have the required characteristics, before a prototype is built.

Fig. 13.1 shows the complete seating with an engine in position on top of it. The bottom of the seating is bolted down onto four steel cruciforms, which form part of the receiver structure, and we require that the dynamic forces transmitted to these cruciforms should be as small as possible. The lower part of the seating comprises two longitudinal beam assemblies, which are attached to the cruciforms by means of steel V-supports, and which each consist of a pair of highly damped sandwich beams arranged so as to form a "V". The upper part of the seating comprises two transverse beam assemblies, again highly damped and arranged as a "V", and supported by complex-shaped rubber blocks which sit in the "V" formed by the lower beams. Each transverse beam assembly includes two steel V-pieces which sit in the "V" between the beams, and to which are attached the soft rubber mounts which support the engine. All these components are connected together with steel bolts, but

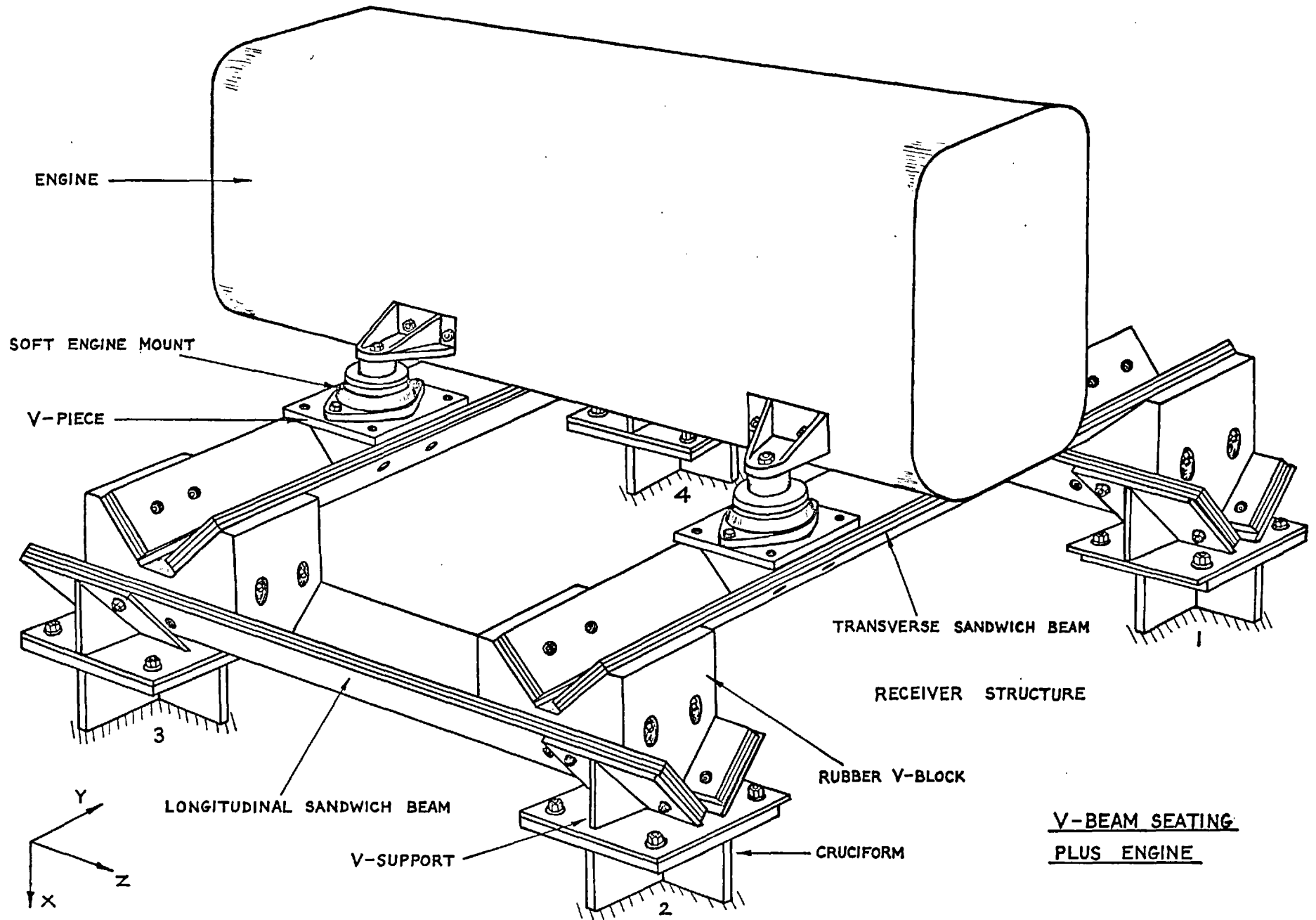


FIG 13.1

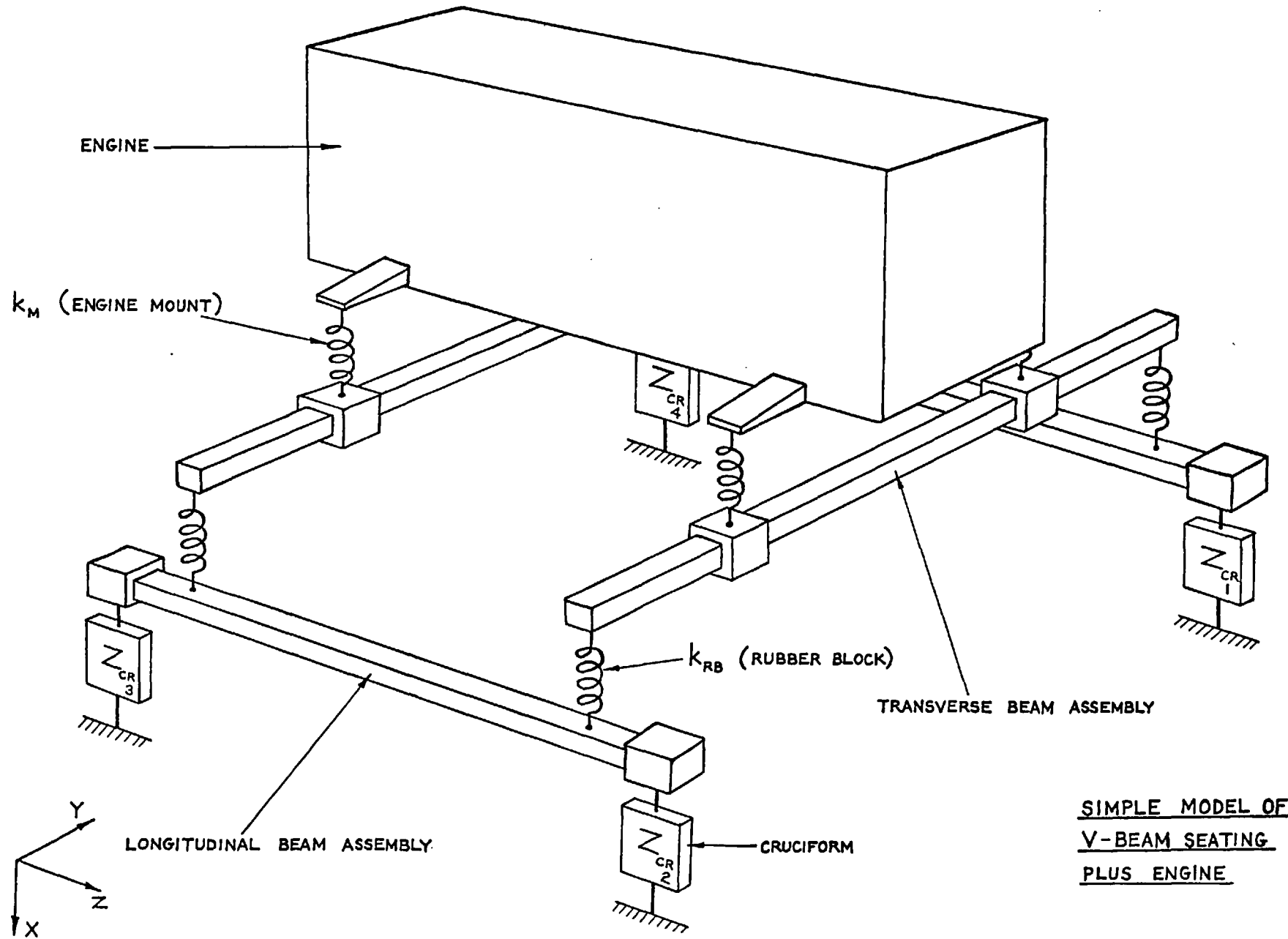


FIG 13.2

a very important feature of the design is the avoidance of any metal-to-metal contact between one component and another. This has been achieved by interposing rubber pads between the metal components* and by using rubber sleeves and washers on the connecting bolts.

It is because of the "V" arrangement of the beams that this foundation structure has been given the name "V-Beam Seating". This arrangement was decided upon in order to try and achieve good isolation in more than just the vertical direction. The requirement for multi-directional isolation was necessitated by the fact that the multi-cylinder diesel engine for which the seating was designed generates a complex mixture of forces and couples, acting in various directions, and each of these must be attenuated within the seating. Since the normal running speed of the engine is 1800 revs/min., the seating should be effective at all frequencies from 30 Hz upwards.

Before we proceed to consider the V-beam arrangement and other aspects of the system in great detail, let us first obtain a clear picture of the complete system by considering the simplified model shown in Fig.13.2. In this model, the beam assemblies have been represented by rigid beams, with attached concentrated masses for the V-supports and V-pieces. The springs k_M and k_{RB} represent the stiffnesses of the engine mounts and of the rubber blocks respectively, and the four nominally identical cruciforms are represented by the impedances Z_{CR1-4} , it being assumed that no coupling exists between the cruciforms through the receiver structure⁺. As the cruciform impedances are very high relative to the impedances of the springs k_{RB} , the motion of the lower end of any of these springs is extremely small, and the force transmitted by the spring is

* 3.5 mm PVC pads between the V-pieces and the transverse beams, and between the V-supports and the longitudinal beams.

+ Measurements in the vertical direction have shown that the transfer mobility between cruciforms 1 and 2 is at least 20 dB less than the point mobility on cruciform 1⁽¹⁾.

virtually independent of the exact behaviour of the lower part of the seating. Hence, the engine plus the upper part of the seating form a two-stage mounting system. The longitudinal beam assemblies are not an essential part of the isolation system, but were necessary in the present case because the longitudinal distance between the engine feet is not the same as the distance between the fore and aft cruciforms, and this is something over which the seating designer has little or no control! However, the lower beams probably have a beneficial effect, in that they stiffen the cruciforms in the relatively flexible rotational directions about the X and Y axes.

Although the complete engine-seating system has been presented above, it is not proposed to include the engine and its mounts in the present analysis, and our attention will be confined to the seating mounted on the cruciforms. If required, the engine may be added at a later stage, once the input characteristics of the seating have been obtained. However, if one is to predict the absolute levels of the forces which will be transmitted when the engine is running on the seating, one does need to know the multi-directional mobility properties and force spectra of the engine, and such data are not easily obtained. Hence, it seems wiser at the present stage to concentrate on the seating structure, and to endeavour to obtain good force attenuation through the seating for all possible inputs from the engine mounts.

Regarding the analysis, the reader should not be misled into thinking that all the work described in the following pages is based on the simple model shown in Fig. 13.2. This model has only been introduced at the present stage because it clearly shows the isolation system in an easily recognisable form. It should not be construed from this that the V-beam arrangement is an irrelevance, since it does have a definite purpose, as is explained in the following section.

In order to predict the response of the seating to all possible

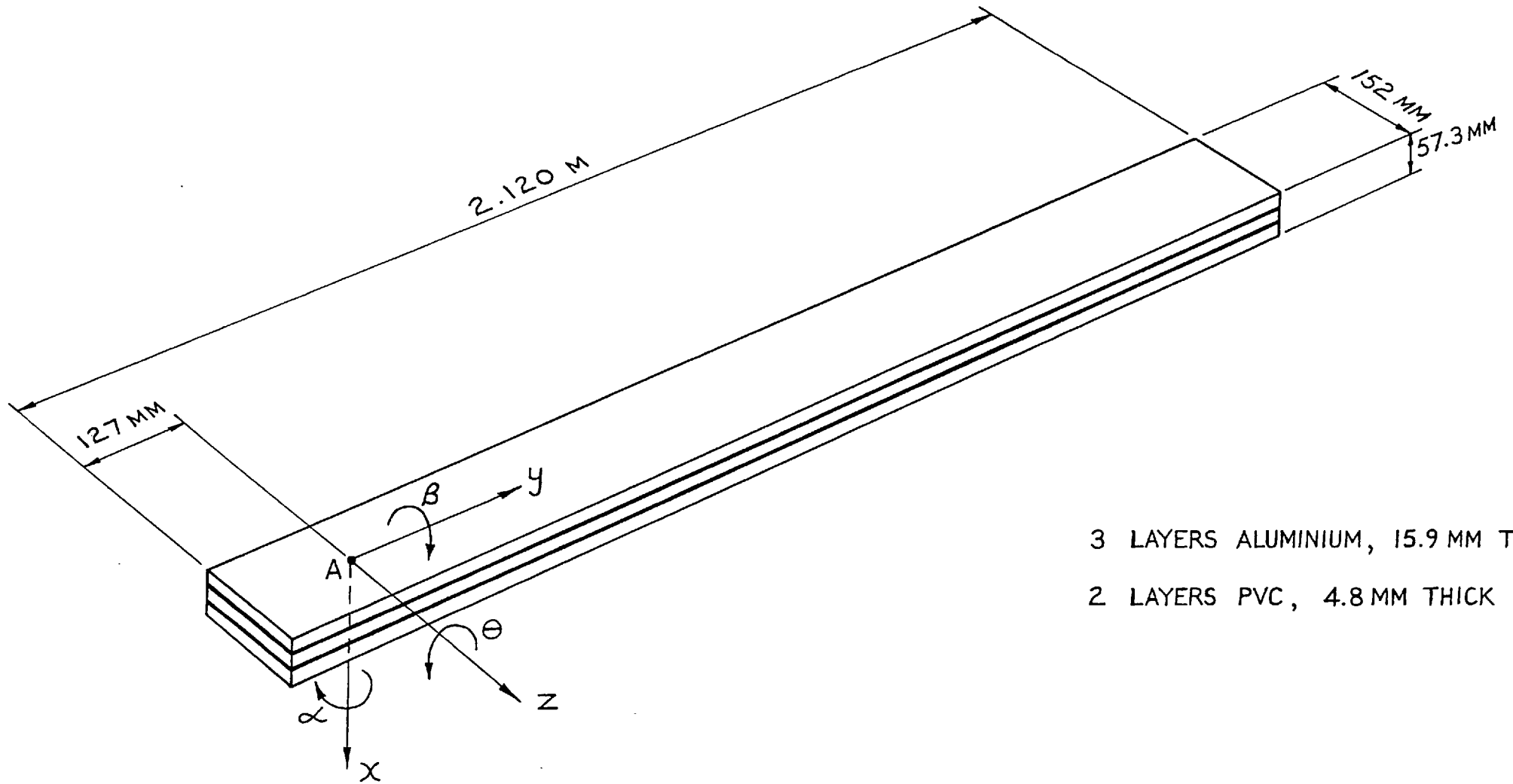
force inputs and to examine the effect of changing various parameters (e.g. damping in beams, PVC pad stiffness, rubber block stiffness, etc), it is necessary to resort to a more detailed analysis which is capable of describing the multi-directional dynamic behaviour of each component. No longer do we idealise the components as pure masses and springs, but instead we consider them as the complex dynamic elements that they are, each with its own distributed mass and stiffness, and in consequence its own resonant behaviour. As was explained in Part 1 of this report, one may consider each of the components or "building blocks" in turn, obtaining their dynamic properties by the most convenient means, and then one can mathematically couple them together in order to predict the dynamic behaviour of the built-up structure. For given force inputs on the V-pieces, one may then examine in detail not only the motions and transmitted forces at the cruciforms, but also the response at various intermediate points, thereby gaining a clearer insight into the way in which the system works. The analysis will be checked against measurements on the assembled seating, but because it is not easy to physically apply a carefully controlled mixture of forces, we must rely on straightforward point and transfer mobility measurements. All forces will be applied to the V-piece nearest to cruciform 2, and since the majority of the force is obviously transmitted to this cruciform, most attention will be given to this one corner of the seating. The results of the full multi-directional analysis will also be compared with results obtained using the simple model already described.

Since the excitation forces from the engine are known to be most severe in the frequency range 30 to 500 Hz, the seating performance will be examined over the slightly wider range of 10 to 1000 Hz. This range encompasses most of the main seating resonances, and the chosen upper frequency limit of 1000 Hz probably extends the analysis to somewhere near its limit, given the assumptions made in the present work.

Before proceeding to consider the analysis, we shall now examine the V-beam system in more detail.

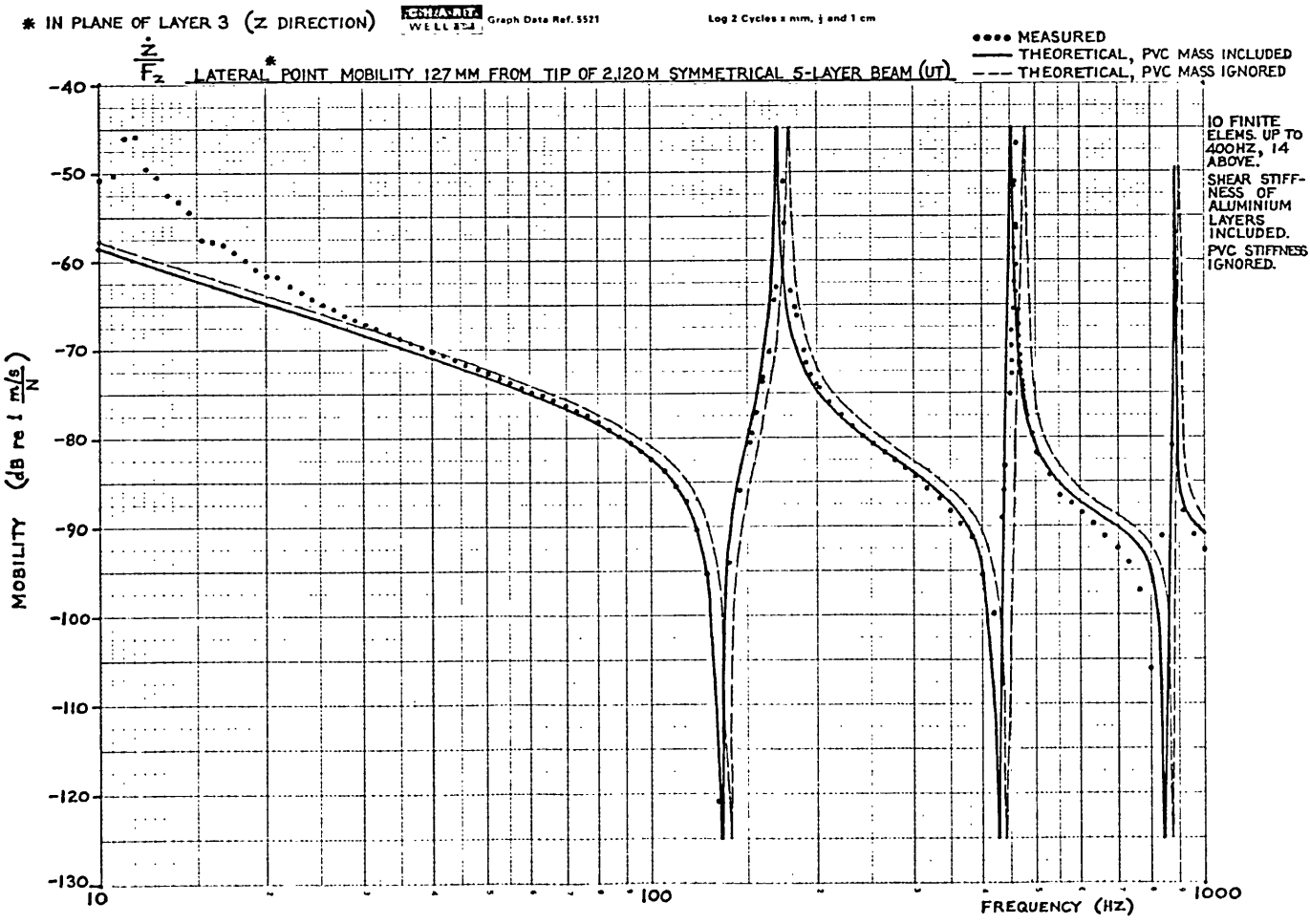
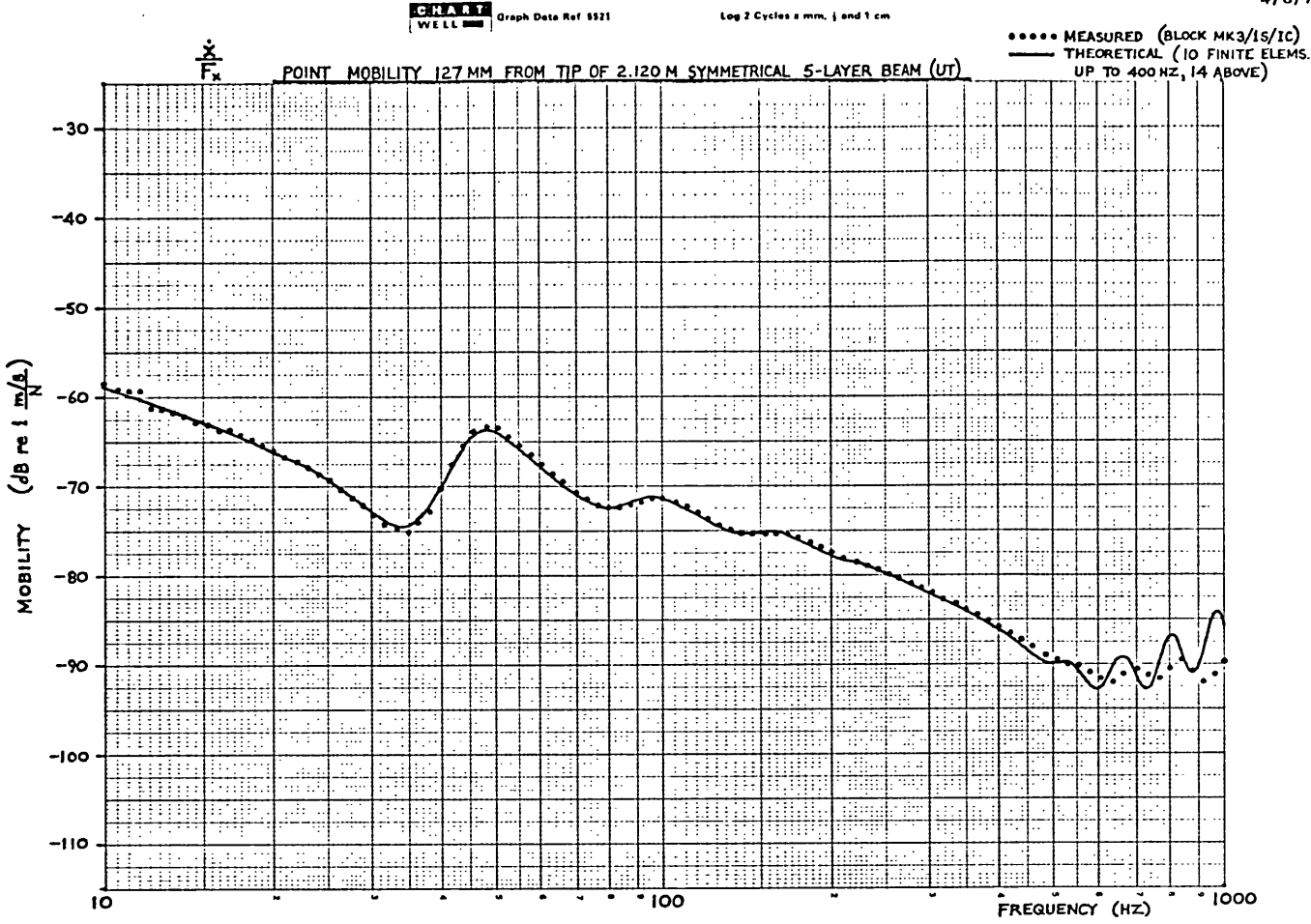
13.2 DISCUSSION AND DETAILS OF THE V-BEAM ASSEMBLY

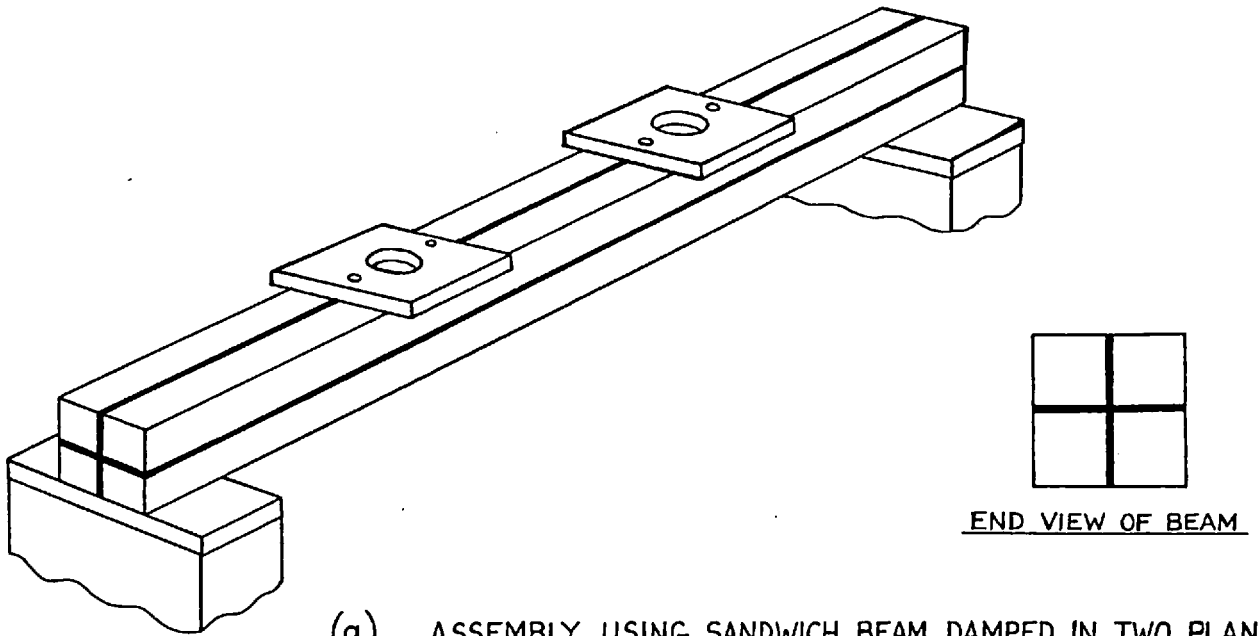
In the simple model presented in the Introduction, the transverse and longitudinal beam assemblies have been represented by rigid beams. As they introduce considerable mass loading between the flexible elements of the mounting system, the rigid beams are able to shunt a large part of the input force to ground, thereby allowing only a small proportion of this force to reach the cruciforms. Unfortunately, no beam of sensible proportions remains a purely rigid mass up to our chosen upper frequency limit of 1000 Hz. In fact, other than in the axial direction, one is lucky if it is still behaving as a pure mass at even 100 Hz! To illustrate the point, let us consider one of the transverse sandwich beams UT on its own and in a free-free condition. Figs. 13.3 and 13.4 show the beam and the two point mobility curves corresponding to transverse excitation normal to and in the plane of the layers. It is clearly seen that even in the plane of the layers, in which direction the beam is very stiff, the limiting frequency is only of the order of 100 Hz. A fairly deep box section beam might have a slightly higher limiting frequency in flexure, but the torsional limiting frequency would probably be lower, so no dramatic improvement could be expected. The conclusion to be drawn from this is that the textbook idealisation of a perfectly rigid intermediate mass is only achievable in practice at relatively low frequencies. One is therefore faced with the fact that the beam assemblies in the seating cannot possibly be made rigid over the complete frequency range 10 to 1000 Hz. However, the "break-up" and consequent resonant behaviour can be controlled by the introduction of damping. Whilst the high-frequency behaviour can never be that of the ideal pure mass or inertia, the damping does at least ensure that the assembly will not resonate severely, with consequent amplification of the transmitted force.



3 LAYERS ALUMINIUM, 15.9 MM THICK
 2 LAYERS PVC, 4.8 MM THICK

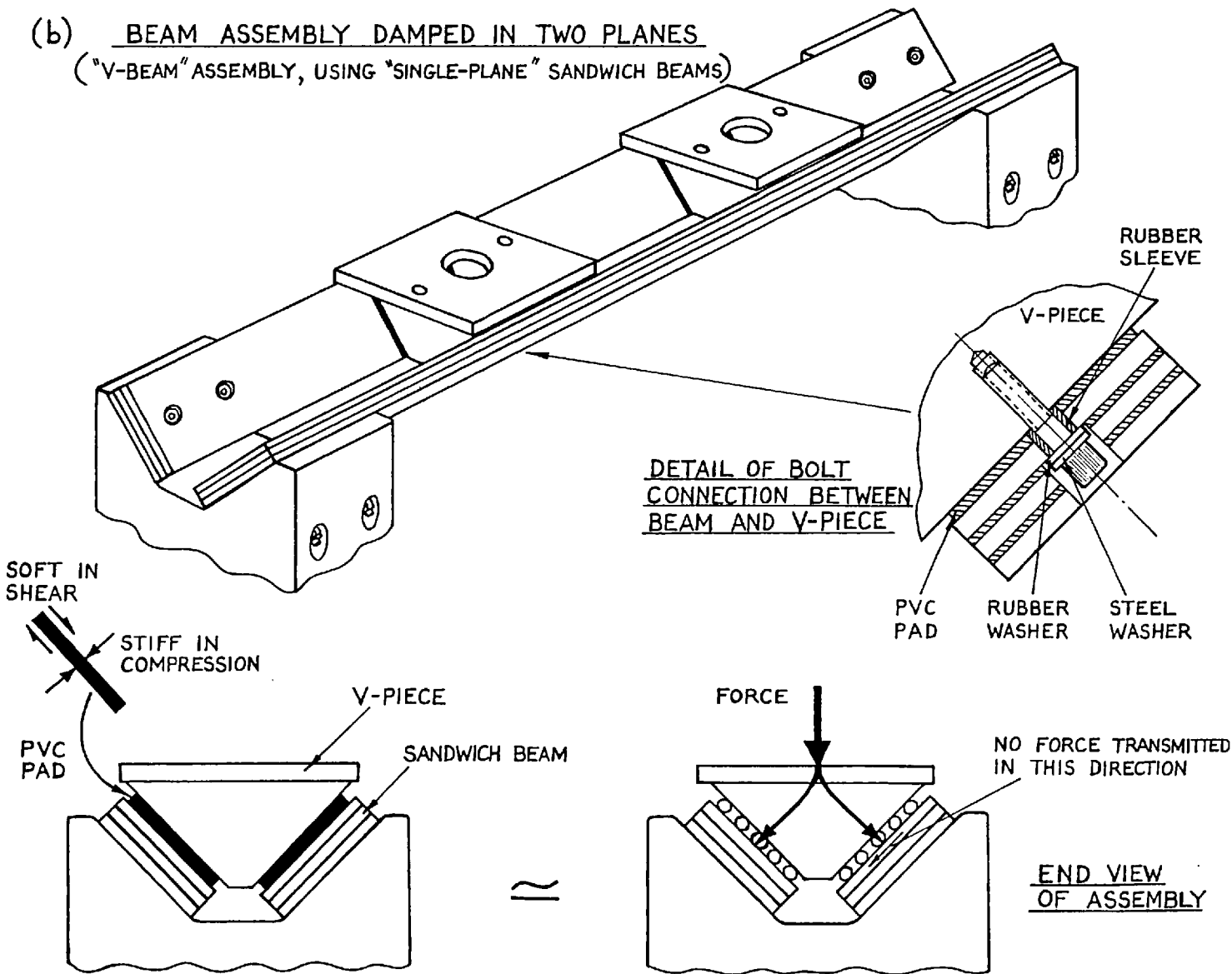
FIG. 13.3 SYMMETRICAL 5-LAYER SANDWICH BEAM "UT" (TRANSVERSE BEAM IN V-BEAM SEATING)





(a) ASSEMBLY USING SANDWICH BEAM DAMPED IN TWO PLANES
("DUAL-PLANE" SANDWICH BEAM)

(b) BEAM ASSEMBLY DAMPED IN TWO PLANES
("V-BEAM" ASSEMBLY, USING "SINGLE-PLANE" SANDWICH BEAMS)



Since multi-layer or "sandwich" beams are known to possess high damping in flexure, one might suppose that the solid beams need only be replaced by simple 3- or 5-layer beams in order to introduce the required damping. This would be the case if one were only concerned with isolation in the vertical direction, but experience with a flat beam seating* has shown that this is inadequate if multi-directional isolation is to be achieved. Referring once again to Fig.13.4, it is clearly seen that the sandwich beam UT is extremely heavily damped in the direction normal to the layers (x direction), whilst it is virtually undamped laterally in the plane of the layers (z direction). It will be shown later that the torsional damping lies somewhere between these two extremes. Thus, a simple multi-layer beam does not possess omnidirectional damping properties, and is clearly inadequate on its own. Obviously, what is required is a beam or beam assembly which does have such properties, and two possibilities are shown in Fig.13.5.

The first is a "dual-plane" 3-layer beam, which simply consists of a 3-layer construction in the two planes of flexure. The flexural behaviour in each plane is the same as for the corresponding simple or "single-plane" 3-layer beam bending in its damped plane. A dual-plane sandwich beam is obviously more difficult to manufacture than the single-plane type, and for this reason must almost certainly be restricted to 3 layers. In addition, one must be extra careful regarding attachments to the beam so as not to "short out" the layers, since this results in reduced flexibility and damping.

* The AEL highly damped flat beam seating (1)(2)

An alternative to the dual-plane sandwich beam is the V-beam arrangement used in the present seating. This comprises a pair of simple sandwich beams arranged in the form of a "V", and the input forces are transmitted to these beams by means of a metal V-piece and rubber pads. This V-piece has been fabricated from thick steel plate and is essentially rigid, and the pads have been made from 3.5mm thick PVC sheet. The idea behind this arrangement is that the rubber pads should be sufficiently flexible in shear to approximate to sets of rollers between the V-piece and the beams, thereby ensuring that forces are only transmitted to the beams in the axial direction and in the direction normal to the layers (i.e. the heavily damped direction), and not laterally in the plane of the layers (i.e. the undamped flexural direction). The effectiveness of this arrangement depends upon the softness of the rubber pads in shear, and this will be examined in greater detail when we look at the measured and computed response data for the seating. Of course, the pads will not work effectively if they are "shorted out" by the connecting bolts which pass through from the beams to the V-pieces, so another important feature of the assembly is the use of rubber sleeves and washers on all the bolts (see Fig. 13.5b). The longitudinal beam assembly works in a similar manner to the transverse assembly, but the PVC pads are this time interposed between the beams and the steel V-supports. Again, the connecting bolts are suitably sleeved, etc.

The V-beam seating evolved from the previously mentioned flat beam seating, and utilises very similar multi-layer beams. As has been seen from Fig. 13.3, these are of the symmetrical 5-layer type, comprising 3 layers of aluminium and 2 of PVC, the latter material being chosen because of its high damping capacity (Loss Factor, $\eta = \frac{1}{Q} \approx 0.6$). The dual-plane sandwich beam was not seriously considered at the time, mainly because of the associated manufacturing difficulties, but it probably merits greater consideration in any future design, in view of the alignment and assembly difficulties encountered with the V-beam assemblies. 5-layer beams were

chosen in preference to the more common 3-layer type because it was desired to have a relatively high beam-assembly mass, combined with heavy damping in the beams. The mass requirement dictates the beam thickness, and it is known that for a given thickness the damping increases with the number of layers, whilst the stiffness decreases. Hence, the 5-layer beam possesses higher damping at the expense of stiffness, and is simply a good compromise. The uniformity of damping over the frequency range could have been improved by using an unsymmetrical 5-layer construction, but it is doubtful whether this would have been worthwhile, in view of the very high damping already achieved (see upper graph of Fig.13.4).

The chosen beams give a total intermediate mass of 250 Kg for the two transverse beam assemblies, and since the engine is approximately 2000 Kg, the mass ratio is 8. Such a figure is quite normal for a two-stage mounting system, though it could usefully be lower in the present case.

13.3 DETAILS OF THE ANALYSIS

It was explained in the Introduction that the analysis of the seating for its full multi-directional response properties must be carried out using the building block approach. To apply this, the system is first divided into its basic components, and these are then examined in detail for their multi-directional response properties, the required information being obtained either from theory or experiment. The components are then coupled together mathematically to predict the overall system response, in the form of motions and transmitted forces.

In the present work, the dynamic stiffness coupling technique has been used throughout, the complete building and solution procedure being repeated at each frequency. This method was chosen in preference to other more sophisticated modelling methods for a number of reasons. First, the properties of the seating components have been obtained from a number of sources - direct analysis, finite element modelling and experimental measurement - all of which could readily be adapted to provide the data as dynamic stiffness. Second, it was considered likely that it would be necessary to allow for material property variations in the frequency range of interest (10 to 1000 Hz), especially for the visco-elastic layers in the sandwich beams. This could not be so easily achieved with a mathematical procedure which required the component data as separate inertia and stiffness matrices, and which solved for the forced response by summing modal responses.

Our primary interest in performing this analysis is to predict the force transmission to cruciform 2 when input forces are applied to the V-piece nearest to this cruciform. In consequence, it is not necessary to analyse the complete seating system, and in fact it is sufficient to consider just the forward transverse beam assembly with its rubber blocks, together with the starboard longitudinal beam assembly on cruciforms 2 and 3 of the receiver structure. Henceforth, these two parts will be referred to as the upper and lower parts of the seating.

Due to the considerable complexity of the problem, the analysis is best carried out in two parts. This is most clearly explained in terms of the simple seating model, as shown in Fig.13.6. Since each rubber block has a very much lower stiffness than the structure which supports it, the motion of the transverse beam assembly and the forces which are transmitted via the blocks are virtually independent of the exact behaviour of the lower part of the seating. Thus, one may analyse the upper part, assuming the blocks to be grounded, and one may then use the transmitted forces obtained from this analysis as the input forces for calculating the response of the lower part. This is just a special case of a more general procedure in which the upper part is considered as a Thévenin type force source ⁽³⁾, which comprises a force generator \bar{P} in parallel with the internal impedance Z_1 . Hence, it would still be quite feasible to perform the analysis in two parts even if the rubber blocks were very much stiffer. It is readily seen that the transmitted force P equals the blocked force \bar{P} when $Z_2 \gg Z_1$. Since Z_1 is the mass impedance of half the upper beam assembly at very low frequencies, and the stiffness impedance of the rubber block at higher frequencies, its value should always be small - except possibly at the resonant frequencies of the upper system, and at the frequencies of wave resonances in the rubber blocks.

In the present analysis, point coupling is assumed between all components in each half of the seating. Hence, the transverse beams are considered to be connected to the upper faces of the rubber V-blocks only at the centre of each face. Similarly, the actual fairly large area of contact between the bottom plate of the V-support and the top plate of the cruciform is also represented by a single point connection. The implications of this assumption will be discussed further at a later stage. At each coupling point, all six possible motions are considered.

To avoid confusion at a later stage, it should be made clear that two systems of co-ordinates will be referred to in the following pages.

DIVISION OF SEATING INTO
TWO PARTS FOR ANALYSIS

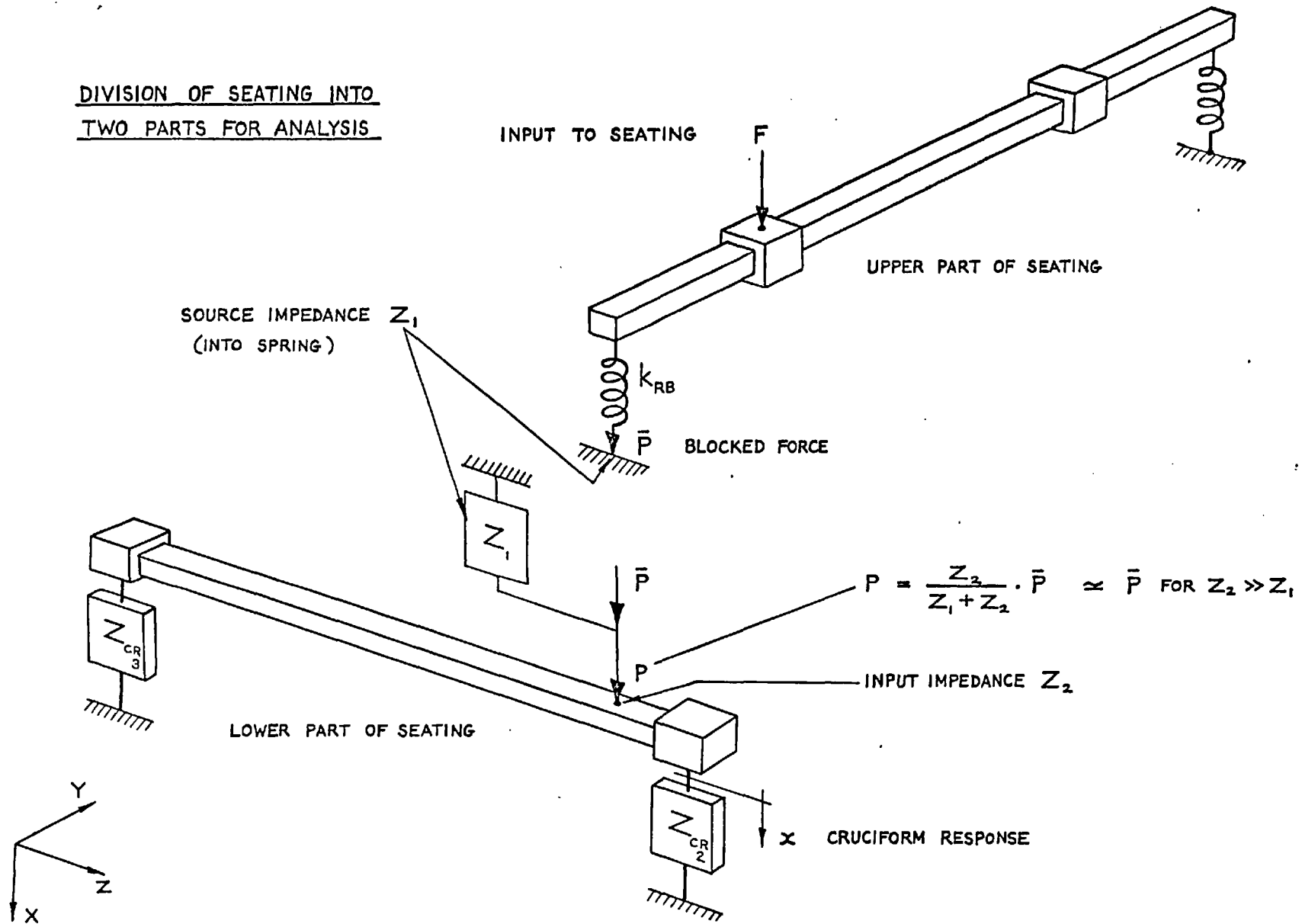
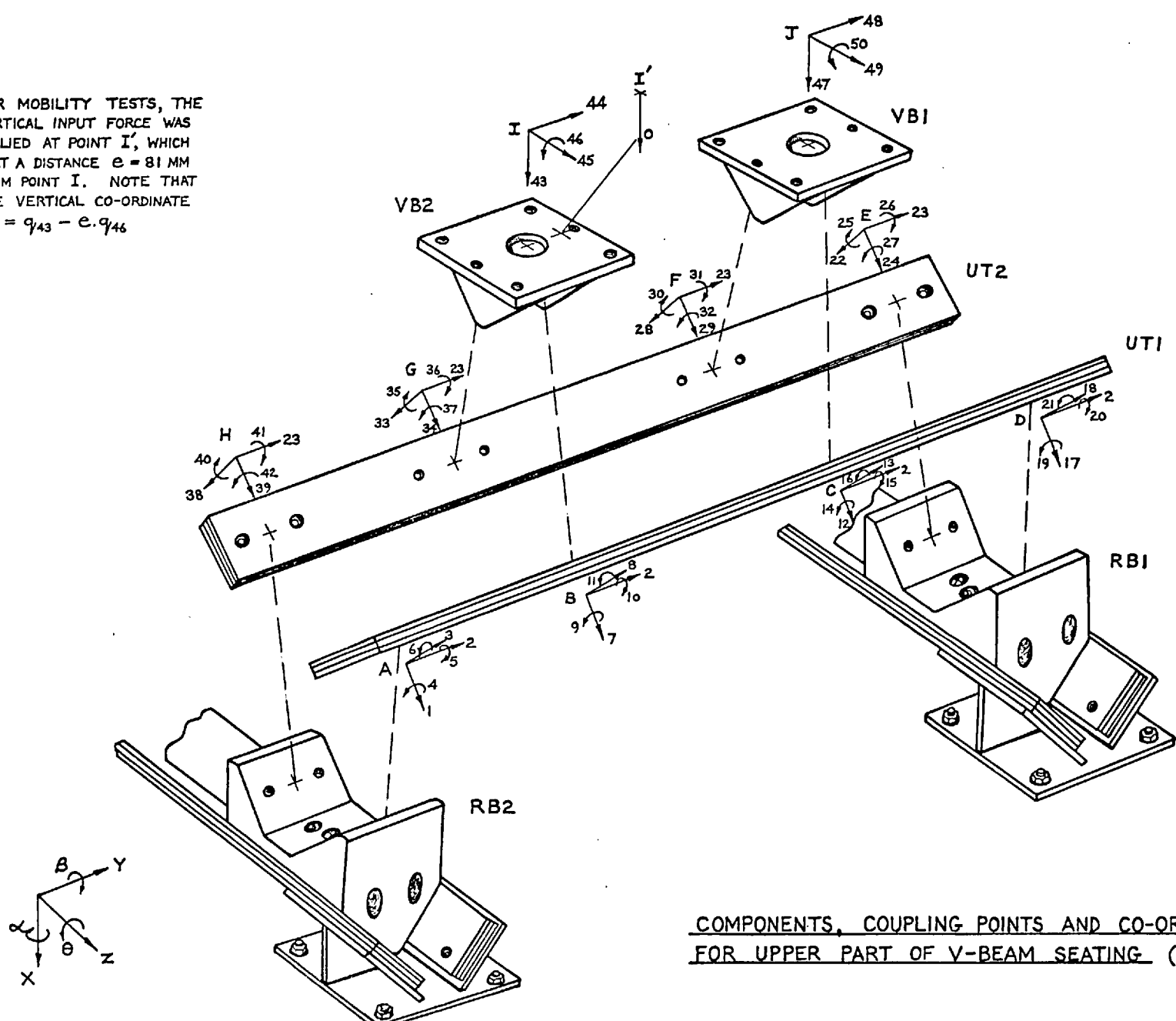


FIG 13,6

FOR MOBILITY TESTS, THE VERTICAL INPUT FORCE WAS APPLIED AT POINT I', WHICH IS AT A DISTANCE $e = 81$ MM FROM POINT I. NOTE THAT THE VERTICAL CO-ORDINATE $q_0 = q_{43} - e \cdot q_{46}$



COMPONENTS, COUPLING POINTS AND CO-ORDINATES
FOR UPPER PART OF V-BEAM SEATING (FORWARD HALF)

FIG. 13.8 FORMATION OF DYNAMIC STIFFNESS MATRIX FOR UPPER PART OF V-BEAM SEATING

(a) DYNAMIC STIFFNESS MATRICES FOR COMPONENTS

1 - UT1

$$\begin{Bmatrix} F_A^1 \\ F_B^1 \\ F_C^1 \\ F_D^1 \end{Bmatrix} = \begin{bmatrix} Z_{AA}^1 & Z_{AB}^1 & Z_{AC}^1 & Z_{AD}^1 \\ Z_{BA}^1 & Z_{BB}^1 & Z_{BC}^1 & Z_{BD}^1 \\ Z_{CA}^1 & Z_{CB}^1 & Z_{CC}^1 & Z_{CD}^1 \\ Z_{DA}^1 & Z_{DB}^1 & Z_{DC}^1 & Z_{DD}^1 \end{bmatrix} \begin{Bmatrix} \delta_A \\ \delta_B \\ \delta_C \\ \delta_D \end{Bmatrix}$$

2 - UT2

$$\begin{Bmatrix} F_E^2 \\ F_F^2 \\ F_G^2 \\ F_H^2 \end{Bmatrix} = \begin{bmatrix} Z_{EE}^2 & Z_{EF}^2 & Z_{EG}^2 & Z_{EH}^2 \\ Z_{FE}^2 & Z_{FF}^2 & Z_{FG}^2 & Z_{FH}^2 \\ Z_{GE}^2 & Z_{GF}^2 & Z_{GG}^2 & Z_{GH}^2 \\ Z_{HE}^2 & Z_{HF}^2 & Z_{HG}^2 & Z_{HH}^2 \end{bmatrix} \begin{Bmatrix} \delta_E \\ \delta_F \\ \delta_G \\ \delta_H \end{Bmatrix}$$

3 - RBI

$$\begin{Bmatrix} F_D^3 \\ F_E^3 \end{Bmatrix} = \begin{bmatrix} Z_{DD}^3 & Z_{DE}^3 \\ Z_{ED}^3 & Z_{EE}^3 \end{bmatrix} \begin{Bmatrix} \delta_D \\ \delta_E \end{Bmatrix}$$

4 - RB2

$$\begin{Bmatrix} F_A^4 \\ F_H^4 \end{Bmatrix} = \begin{bmatrix} Z_{AA}^4 & Z_{AH}^4 \\ Z_{HA}^4 & Z_{HH}^4 \end{bmatrix} \begin{Bmatrix} \delta_A \\ \delta_H \end{Bmatrix}$$

5 - VBI

$$\begin{Bmatrix} F_J^5 \\ F_F^5 \\ F_C^5 \end{Bmatrix} = \begin{bmatrix} Z_{JJ}^5 & Z_{JF}^5 & Z_{JC}^5 \\ Z_{FJ}^5 & Z_{FF}^5 & Z_{FC}^5 \\ Z_{CJ}^5 & Z_{CF}^5 & Z_{CC}^5 \end{bmatrix} \begin{Bmatrix} \delta_J \\ \delta_F \\ \delta_C \end{Bmatrix}$$

6 - VB2

$$\begin{Bmatrix} F_I^6 \\ F_G^6 \\ F_B^6 \end{Bmatrix} = \begin{bmatrix} Z_{II}^6 & Z_{IG}^6 & Z_{IB}^6 \\ Z_{GI}^6 & Z_{GG}^6 & Z_{GB}^6 \\ Z_{BI}^6 & Z_{BG}^6 & Z_{BB}^6 \end{bmatrix} \begin{Bmatrix} \delta_I \\ \delta_G \\ \delta_B \end{Bmatrix}$$

(b) DYNAMIC STIFFNESS MATRIX FOR SYSTEM

$$\begin{Bmatrix} F_A \\ F_B \\ F_C \\ F_D \\ F_E \\ F_F \\ F_G \\ F_H \\ F_I \\ F_J \end{Bmatrix} = \begin{bmatrix} Z_{AA}^1 + Z_{AA}^4 & Z_{AB}^1 & Z_{AC}^1 & Z_{AD}^1 & - & - & - & Z_{AH}^4 & - & - \\ Z_{BA}^1 & Z_{BB}^1 + Z_{BB}^6 & Z_{BC}^1 & Z_{BD}^1 & - & - & Z_{BG}^6 & - & Z_{BI}^6 & - \\ Z_{CA}^1 & Z_{CB}^1 & Z_{CC}^1 + Z_{CC}^5 & Z_{CD}^1 & - & - & - & - & - & Z_{CJ}^5 \\ Z_{DA}^1 & Z_{DB}^1 & Z_{DC}^1 & Z_{DD}^1 + Z_{DD}^3 & Z_{DE}^3 & - & - & - & - & - \\ - & - & - & Z_{ED}^3 & Z_{EE}^2 + Z_{EE}^3 & Z_{EF}^2 & Z_{EG}^2 & Z_{EH}^2 & - & - \\ - & - & - & - & Z_{FE}^2 & Z_{FF}^2 + Z_{FF}^5 & Z_{FG}^2 & Z_{FH}^2 & - & Z_{FJ}^5 \\ - & Z_{GB}^6 & - & - & Z_{GE}^2 & Z_{GF}^2 & Z_{GG}^2 + Z_{GG}^6 & Z_{GH}^2 & Z_{GI}^6 & - \\ Z_{HA}^4 & - & - & - & Z_{HE}^2 & Z_{HF}^2 & Z_{HG}^2 & Z_{HH}^2 + Z_{HH}^4 & - & - \\ - & Z_{IB}^6 & - & - & - & - & Z_{IG}^6 & - & Z_{II}^6 & - \\ - & - & Z_{JC}^5 & - & - & Z_{JF}^5 & - & - & - & Z_{JJ}^5 \end{bmatrix} \begin{Bmatrix} \delta_A \\ \delta_B \\ \delta_C \\ \delta_D \\ \delta_E \\ \delta_F \\ \delta_G \\ \delta_H \\ \delta_I \\ \delta_J \end{Bmatrix}$$

The first is the GLOBAL system X-Y-Z, as given in Fig.13.1, where the three co-ordinates correspond to vertical, transverse and longitudinal directions, and are invariant. The second is the LOCAL system x-y-z, which is used in component analysis, and which may or may not correspond to the global system. Having clarified this point, we may now proceed to consider the two halves of the seating in detail.

The forward transverse beam assembly and its rubber blocks are shown in detail in Fig.13.7, and it is seen that the complete system comprises six components: A pair of sandwich beams, a pair of rubber blocks, and a pair of male V-pieces. There are thus three basic items which are designated UT, RB and VB, respectively. Six coupling co-ordinates have been used at each of the inter-component connection points A to H, but the beams are assumed to behave as rigid masses in the axial direction, so the total number of co-ordinates associated with each beam is only 21. As four co-ordinates have been used at each of the force input points I and J on top of the seating, the complete assembly has a total of 50 degrees of freedom. However, it should be noted that this is only the number of degrees of freedom retained at the system assembly stage. If one includes all the internal co-ordinates used in the finite element analysis of the beams, the total number of degrees of freedom is actually between two and three hundred. It will be observed that in addition to co-ordinates 1 to 50, a co-ordinate 0 is also shown, corresponding to the X direction at point I'. Since a large hole prevented the application of a vertical force at the centre of the V-piece top plate, it was necessary to use point I' as the vertical excitation point for mobility measurements on the seating. However, it is assumed in the analysis that the V-piece behaves as a rigid inertia, so co-ordinate 0 is simply related to co-ordinates 43 and 46, in the manner indicated in the figure.

The 3.5mm PVC pads which are interposed between the V-pieces and the beams have not been shown as separate components, since they are best considered in conjunction with the V-pieces. Hence, unless otherwise stated, it will in future be understood that the term "V-piece" refers to the

assembly comprising the steel V-piece and the PVC facing pads. If these parts were not considered together as a single component, it would be necessary to use 6 co-ordinates at each V-piece/pad interface and a further 6 co-ordinates at each pad/beam interface. Since there are four connection points B,C, F and G, the total number of degrees of freedom would then be increased by 24, with a corresponding threefold increase in solution time for the system response!

The response properties of the components have been obtained as dynamic stiffness matrices, which relate the forces at the component connection points to the displacements at these points. These matrices are frequency-dependent and complex, and each has been obtained by the method most suited to the particular component. For instance, the beam UT has been analysed using the finite elements derived in Part 3 of this report, and the V-piece VB has been considered as a rigid inertia to which are attached hysteretically damped springs, which represent the PVC pads, and have easily calculable stiffness. On the other hand, the rubber block RB was not amenable to theoretical treatment, so it has been represented by a multi-directional spring model, whose parameters were obtained from measurements on one of the actual blocks. This model also incorporates a number of lumped masses, which allow it to describe wave effects within the rubber. Since the analysis of the components is considered in great detail in the following chapter, it is not proposed to go into any further detail at the present stage.

The resulting dynamic stiffness matrices for the six components are shown diagrammatically in Fig.13.8a,* and the sub-matrices and vectors relate to the various connection points, and are of order 6 or less.

* Note that as given in the figure, the matrices for RB1 and 2 are identical, as are those for VB1 and 2. However, the co-ordinate order for UT2 must be changed to H, G, F, E if UT1 and 2 are to have identical matrices. The rearrangement in the figure has no significance.

At each frequency, these dynamic stiffness data are first derived; then, using force equilibrium and displacement compatibility relations, the component stiffnesses are combined to form the overall system dynamic stiffness matrix shown in Fig.13.8b. This matrix relates the externally applied forces at each of the connection points to the corresponding displacements, and for the present system is 50 x 50 and complex. The required displacement responses are obtained by inverting this matrix and multiplying by various force vectors.

This complete building and solution process has been carried out using the dynamic stiffness coupling programme COUPLE 1, which was described in Part 1 of this report. In that programme, the complex system matrix is converted into a double-size real matrix, which is inverted using a very efficient real matrix inversion routine (Cern library routine MATIN 1: Uses Jordan's method with partial pivoting). In the present problem this matrix is 100 x 100, and it has been found that it can be inverted in approximately 4 seconds* on a CDC 6600 computer. Taking into account the known solution time per frequency (5 seconds for present system), and the relatively heavy damping in the structure, it was decided to compute the response at just 51 frequencies in the range 10 to 1000 Hz.

It should be mentioned that the upper part of the seating could have been analysed more economically by making use of its symmetry with respect to the X-Y plane that passes through the apex of the "V" formed by the two beams. One need then only consider half of each rubber block, one transverse beam, and half of each V-piece, thereby reducing the total number of degrees of freedom to less than 30. Since the inversion time for a 30 x 30 stiffness matrix would be between 20 and 30% of that required for the 50 x 50 matrix considerable savings could be made in computing time. If one were

* Time taken by COMPASS (Assembler language) version of routine. FORTRAN IV version takes 5 secs.

restricting one's attention to excitation in either the X or Y directions, the procedure would be quite straightforward, since the half V-pieces need only have their motions blocked in the Z, α and β directions in order to satisfy the conditions of symmetry. However, for excitation in the Z direction one would first need to calculate the input mobility properties of one half of the system, as seen by the other half,* and then one would use these data to couple together the two halves and predict the forced response. Matters are further complicated by the need to calculate the displacements at point A, for the purpose of calculating the force transmission through the block. In view of these difficulties, it was decided that the straightforward coupling together of all six complete components would provide a much simpler and more direct solution to the problem. The increased computation time associated with this direct approach only becomes significant if one wishes to repeat the calculation a large number of times.

We shall now proceed to consider the force transmission through the rubber blocks to the lower part of the seating. Referring to Fig.13.7, it is seen that the lower faces of the rubber V-block are in contact with the longitudinal beams over quite a large area, so the transmitted forces cannot be considered as acting at a single point. To take account of this, the spring model used to represent the rubber block has been set up in such a way that it divides the forces between six points, and at each of these points, three linear forces are assumed to be transmitted in the local x, y and z directions. Since the axial co-ordinate is assumed to be common for

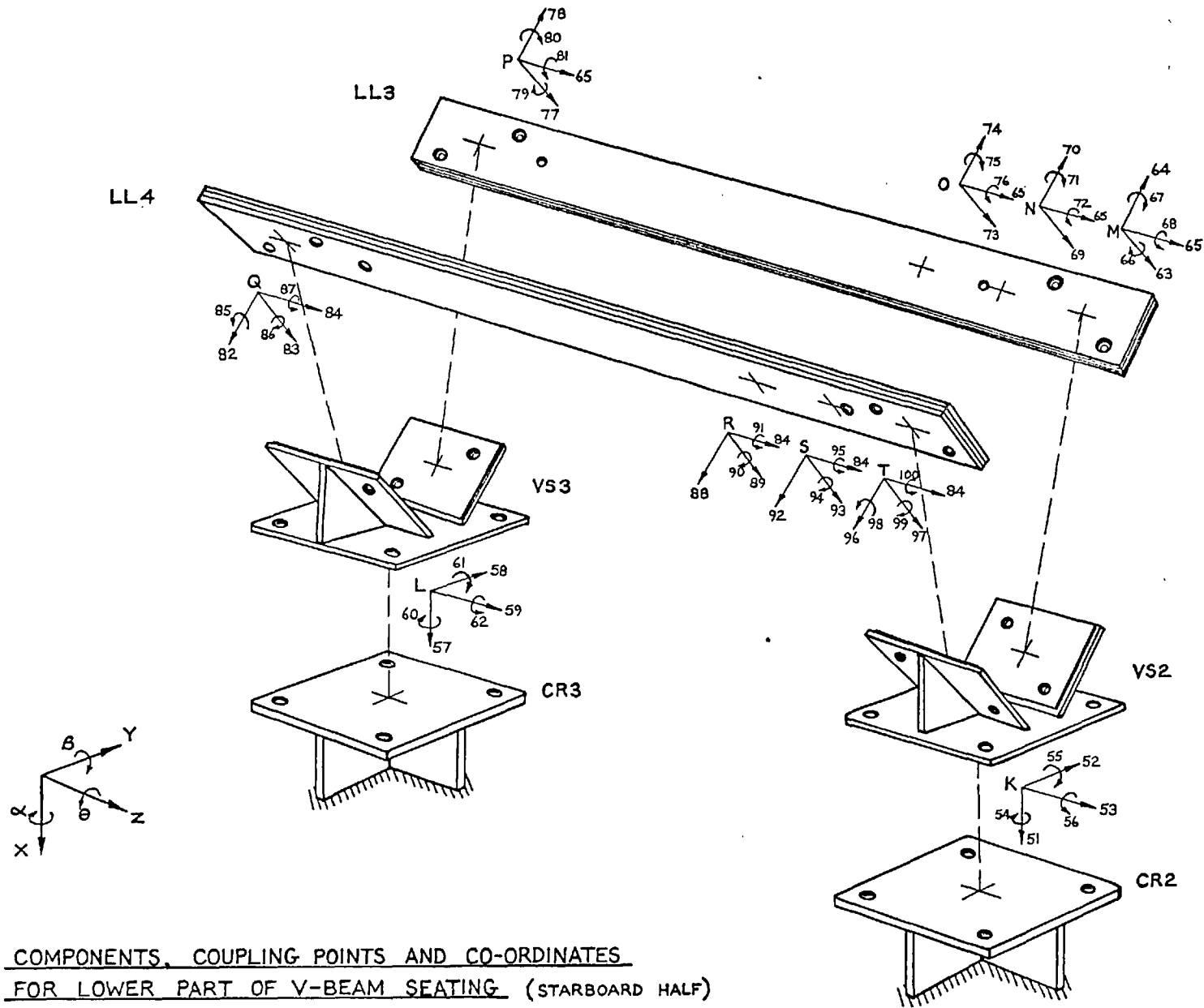
* i.e. Looking into the half V-pieces, at the imaginary interfaces where the two halves of the system are joined together.

all points along each of the lower beams, the total number of forces transmitted to the lower part of the seating by any one block is 14.

The forces transmitted via rubber block RB2 were not obtained directly from the analysis described above, since it was only possible to compute the displacements and forces on the top faces of the block (i.e. at coupling points A and H). However, one can calculate the force transmission if one knows the transfer characteristics of the rubber block, given either in terms of the input displacements or forces. Hence, it was decided to write the displacement data onto a magnetic disc,* where it could be stored for subsequent use by a subsidiary programme, specially written to compute the force transmission. This special programme proceeds frequency by frequency, first setting up the transfer dynamic stiffness matrix for the block, then reading the 12 complex displacements, and finally obtaining the transmitted forces from the product of the stiffness matrix and the displacements. At each frequency, these 14 complex forces are written onto another magnetic disc, so that they can be used later as input forces in the analysis of the lower part of the seating. In addition to obtaining the complete set of forces, it was also decided to calculate the net force transmission in the global X, Y and Z directions. Since the rubber blocks are so close to the cruciforms, the net forces in the X and Y directions at RB2 may be expected to differ only slightly from the corresponding forces transmitted to cruciform CR2.

We shall now consider the lower part of the seating; or more specifically, the starboard longitudinal beam assembly and the cruciforms to which it is attached. It is seen from Fig.13.9 that there are once again six components: A pair of sandwich beams (LL), a pair of V-supports (VS), and the two cruciforms (CR) which form part of the receiver structure. However, in spite

* A "permanent file" in this case.



M, N, O, R, S, T ARE ASSUMED POINTS OF FORCE INPUT FROM RUBBER BLOCK RB2.

COMPONENTS, COUPLING POINTS AND CO-ORDINATES FOR LOWER PART OF V-BEAM SEATING (STARBOARD HALF)

FIG. 13.10 FORMATION OF DYNAMIC STIFFNESS MATRIX FOR LOWER PART OF V-BEAM SEATING

(a) DYNAMIC STIFFNESS MATRICES FOR COMPONENTS

1 - LL3

$$\begin{Bmatrix} F_M^1 \\ F_N^1 \\ F_O^1 \\ F_P^1 \end{Bmatrix} = \begin{bmatrix} Z_{MM}^1 & Z_{MN}^1 & Z_{MO}^1 & Z_{MP}^1 \\ Z_{NM}^1 & Z_{NN}^1 & Z_{NO}^1 & Z_{NP}^1 \\ Z_{OM}^1 & Z_{ON}^1 & Z_{OO}^1 & Z_{OP}^1 \\ Z_{PM}^1 & Z_{PN}^1 & Z_{PO}^1 & Z_{PP}^1 \end{bmatrix} \begin{Bmatrix} \delta_M \\ \delta_N \\ \delta_O \\ \delta_P \end{Bmatrix}$$

2 - LL4

$$\begin{Bmatrix} F_Q^2 \\ F_R^2 \\ F_S^2 \\ F_T^2 \end{Bmatrix} = \begin{bmatrix} Z_{QQ}^2 & Z_{QR}^2 & Z_{QS}^2 & Z_{QT}^2 \\ Z_{RQ}^2 & Z_{RR}^2 & Z_{RS}^2 & Z_{RT}^2 \\ Z_{SQ}^2 & Z_{SR}^2 & Z_{SS}^2 & Z_{ST}^2 \\ Z_{TQ}^2 & Z_{TR}^2 & Z_{TS}^2 & Z_{TT}^2 \end{bmatrix} \begin{Bmatrix} \delta_Q \\ \delta_R \\ \delta_S \\ \delta_T \end{Bmatrix}$$

3 - VS2

$$\begin{Bmatrix} F_M^3 \\ F_T^3 \\ F_K^3 \end{Bmatrix} = \begin{bmatrix} Z_{MM}^3 & Z_{MT}^3 & Z_{MK}^3 \\ Z_{TM}^3 & Z_{TT}^3 & Z_{TK}^3 \\ Z_{KM}^3 & Z_{KT}^3 & Z_{KK}^3 \end{bmatrix} \begin{Bmatrix} \delta_M \\ \delta_T \\ \delta_K \end{Bmatrix}$$

4 - VS3

$$\begin{Bmatrix} F_P^4 \\ F_Q^4 \\ F_L^4 \end{Bmatrix} = \begin{bmatrix} Z_{PP}^4 & Z_{PQ}^4 & Z_{PL}^4 \\ Z_{QP}^4 & Z_{QQ}^4 & Z_{QL}^4 \\ Z_{LP}^4 & Z_{LQ}^4 & Z_{LL}^4 \end{bmatrix} \begin{Bmatrix} \delta_P \\ \delta_Q \\ \delta_L \end{Bmatrix}$$

5 - CR

$$\begin{Bmatrix} F_K^5 \\ F_L^5 \end{Bmatrix} = \begin{bmatrix} Z_{KK}^5 & Z_{KL}^5 \\ Z_{LK}^5 & Z_{LL}^5 \end{bmatrix} \begin{Bmatrix} \delta_K \\ \delta_L \end{Bmatrix}$$

(b) DYNAMIC STIFFNESS MATRIX FOR SYSTEM

$$\begin{Bmatrix} F_K \\ F_L \\ F_M \\ F_N \\ F_O \\ F_P \\ F_Q \\ F_R \\ F_S \\ F_T \end{Bmatrix} = \begin{bmatrix} Z_{KK}^3 + Z_{KK}^5 & Z_{KL}^5 & Z_{KM}^3 & - & - & - & - & - & - & - & Z_{KT}^3 \\ Z_{LK}^5 & Z_{LL}^4 + Z_{LL}^5 & - & - & - & Z_{LP}^4 & Z_{LQ}^4 & - & - & - & - \\ Z_{MK}^3 & - & Z_{MM}^1 + Z_{PM}^3 & Z_{MN}^1 & Z_{MO}^1 & Z_{MP}^1 & - & - & - & - & Z_{MT}^3 \\ - & - & Z_{NM}^1 & Z_{NN}^1 & Z_{NO}^1 & Z_{NP}^1 & - & - & - & - & - \\ - & - & Z_{OM}^1 & Z_{ON}^1 & Z_{OO}^1 & Z_{OP}^1 & - & - & - & - & - \\ - & Z_{PL}^4 & Z_{PM}^1 & Z_{PN}^1 & Z_{PO}^1 & Z_{PP}^1 + Z_{PP}^4 & Z_{PQ}^4 & - & - & - & - \\ - & Z_{QL}^4 & - & - & - & Z_{QP}^4 & Z_{QQ}^2 + Z_{QQ}^4 & Z_{QR}^2 & Z_{QS}^2 & Z_{QT}^2 & - \\ - & - & - & - & - & - & Z_{RQ}^2 & Z_{RR}^2 & Z_{RS}^2 & Z_{RT}^2 & - \\ - & - & - & - & - & - & - & Z_{SQ}^2 & Z_{SR}^2 & Z_{SS}^2 & Z_{ST}^2 \\ Z_{TK}^3 & - & Z_{TM}^3 & - & - & - & - & Z_{TQ}^2 & Z_{TR}^2 & Z_{TS}^2 & Z_{TT}^2 + Z_{TT}^3 \end{bmatrix} \begin{Bmatrix} \delta_K \\ \delta_L \\ \delta_M \\ \delta_N \\ \delta_O \\ \delta_P \\ \delta_Q \\ \delta_R \\ \delta_S \\ \delta_T \end{Bmatrix}$$

of the fact that the two cruciforms are assumed to be uncoupled, it is more convenient to consider the complete receiver structure as a single component. Therefore, the present analysis is carried out in terms of five components.

The PVC pads which are interposed between the lower beams and the steel V-supports have been considered in conjunction with the V-supports, in just the same way as the pads beneath the V-pieces were considered as forming part of a V-piece assembly. Hence, unless otherwise stated, it will in future be understood that the term "V-support" refers to the assembly comprising the steel V-support and the PVC facing pads.

Six co-ordinates have been used at each of the inter-component connection points K, L, M, P, Q and T, and when one includes the co-ordinates introduced at points N, O, R and S, this complete assembly also has 50 degrees of freedom. The six points of force input from the rubber block RB2 are M, N, O, R, S and T, and the 14 forces applied at these points act in the following co-ordinate directions: 96, 97, 84, 92, 93, 88, 89, 63, 64, 65, 69, 70, 73 and 74. The co-ordinate order given corresponds to that used in the analysis of the rubber block. The rotational co-ordinates corresponding to points N, O, R and S could have been omitted from the analysis, and were only included in order to obtain further response data which might be compared with future mobility measurements on the lower part of the seating.

As before, the response properties of each component have been obtained by the method most suited to the particular component. The longitudinal beam LL has been analysed in precisely the same way as the transverse beam UT, using the finite element method. Since the cross-sectional properties and the number of connection points are the same for these two beams, it has been possible to use the same computer subroutines for both. The V-support VS has been considered as an essentially rigid inertia, whose response properties could be obtained exactly. However, the torsional stiffness of its inclined face plates has been calculated approximately using plate finite elements, and this stiffness has been lumped with the calculated stiffness of the attached PVC pads. As it was not considered possible to

theoretically predict the response properties of the receiver structure, it was necessary to measure the complete 6-directional mobility matrix for the cruciform CR. This data has subsequently been modelled in such a way that it can easily be reproduced at any specified frequency in the range 10 to 1000 Hz. After modelling all the components in the manner described, it was found that the actual connection between the cruciform and the V-support was far from being a rigid joint. To allow for this, an "interface stiffness" has been added between the two components, and since all response measurements were made on the upper side of the interface (i.e. on the bottom plate of the V-support VS2), this stiffness has been combined with the cruciform dynamic stiffness in order to yield a modified cruciform model. Full details of these three basic components are given in the next chapter, together with the results of an investigation into the interface behaviour (see Section 14.6).

The resulting dynamic stiffness matrices are shown diagrammatically in Fig.13.10a*, and as before, the sub-matrices and vectors refer to the various connection points and are of order 6 or less. In the case of component 5, the cruciform point stiffness matrices $[Z_{KK}^5]$ and $[Z_{LL}^5]$ are identical to one another, whilst the transfer stiffnesses $[Z_{KL}^5]$ and $[Z_{LK}^5]$ are assumed to be zero. Upon combining the various component data, one obtains the overall system dynamic stiffness matrix shown in Fig.13.10b. The required displacement responses are obtained by inverting this 50 x 50 complex matrix and multiplying by various force vectors.

* In the same way as before, the matrices given for VS2 and 3 are identical, whilst the co-ordinate order for LL4 must be changed to T, S, R, Q, if LL3 and 4 are to have identical matrices. Once again, the rearrangement in the figure has no significance.

It should be noted that the lower part of the seating does not possess the same inherent symmetry as the upper part, since the X and Y motions of the cruciforms are coupled. In addition, the forces transmitted by the rubber block are not equally distributed between the two lower beams. Hence, it is not possible to economise on solution time by only considering a single beam with half V-supports and half cruciforms.

The cruciform response due to a given input on top of the seating has been obtained by first reading from the magnetic disc the stored values of the 14 forces transmitted by rubber block RB2, and then applying them at points M, N, O, R, S and T. As the basic COUPLE 1 programme contains no provision for changing the force vectors at each frequency, it was necessary to write a special subsidiary routine which is called at each frequency, and which reads the force data from the disc and forms the required complex force vector.

The results of this full analysis are presented in Chapter 15, in the form of a large number of frequency response curves. The majority of these are point and transfer mobility curves, which show the velocity responses at various points on the seating due to different force inputs on V-piece VB2. All such predictions are compared with measurements made either in the laboratory or with the seating mounted on the actual receiver structure, the primary purpose being to fully check the adequacy of the analysis technique for predicting the multi-directional behaviour of the seating structure. In addition to these mobility data, curves are also given of force transmission to the lower part of the seating and to the cruciforms. Since the prime requirement of the seating is that it should reduce the force input to the receiver structure by as much as possible, the force transmission curves are obviously more useful for assessing the effectiveness of the isolation system. However, since the measurement of internal forces is in general either impossible or extremely difficult, only limited experimental data are available for checking the predicted forces.

CHAPTER 14

ANALYSIS OF SEATING COMPONENTS

14.1 TRANSVERSE AND LONGITUDINAL SANDWICH BEAMS (Components UT and LL)

The transverse and longitudinal beams are shown in detail in Fig.14.1. The two types of beam have the same symmetrical 5-layer construction, but they differ in length and in the arrangement of the fixing holes, and they weigh 43.7 and 34.7 Kg respectively. The sandwich comprises 3 layers of aluminium alloy and 2 of PVC, all bonded together with Araldite epoxy resin, and full details of the dimensions and of the material properties are given in the figure. An important practical feature of the design is the use of counterbored holes for the connection bolts, so that the heads of these bolts only clamp down onto the bottom layer of the sandwich and do not "short out" the damping layers. Thus, when the beams are built into the seating system, there is no metal transmission path between their top and bottom layers.

Since the beams form part of a relatively complex 3 dimensional structure, they are subjected to both bending and torsion, and it is necessary to consider all 6 motions at each connection point. Although this is not uncommon in analyses using uniform beams ^{(4) (5) (6)*}, the author is not aware of any such analysis having been carried out with highly damped sandwich beams. Practically all the standard references on sandwich beam vibration deal with the 3-layer type, with the usual textbook boundary conditions such as simply-supported, etc., and certainly no mention is ever made of bending in the plane of the layers or of torsion about the beam axis. In view of the lack of any suitable solution for the bending and torsional characteristics of the beams, it was necessary to examine sandwich beams in some depth, and to derive a solution in a form suitable for inclusion in the dynamic stiffness coupling procedure. The obvious

* Note that References for Chapters 13 to 15 are listed on Page 430.

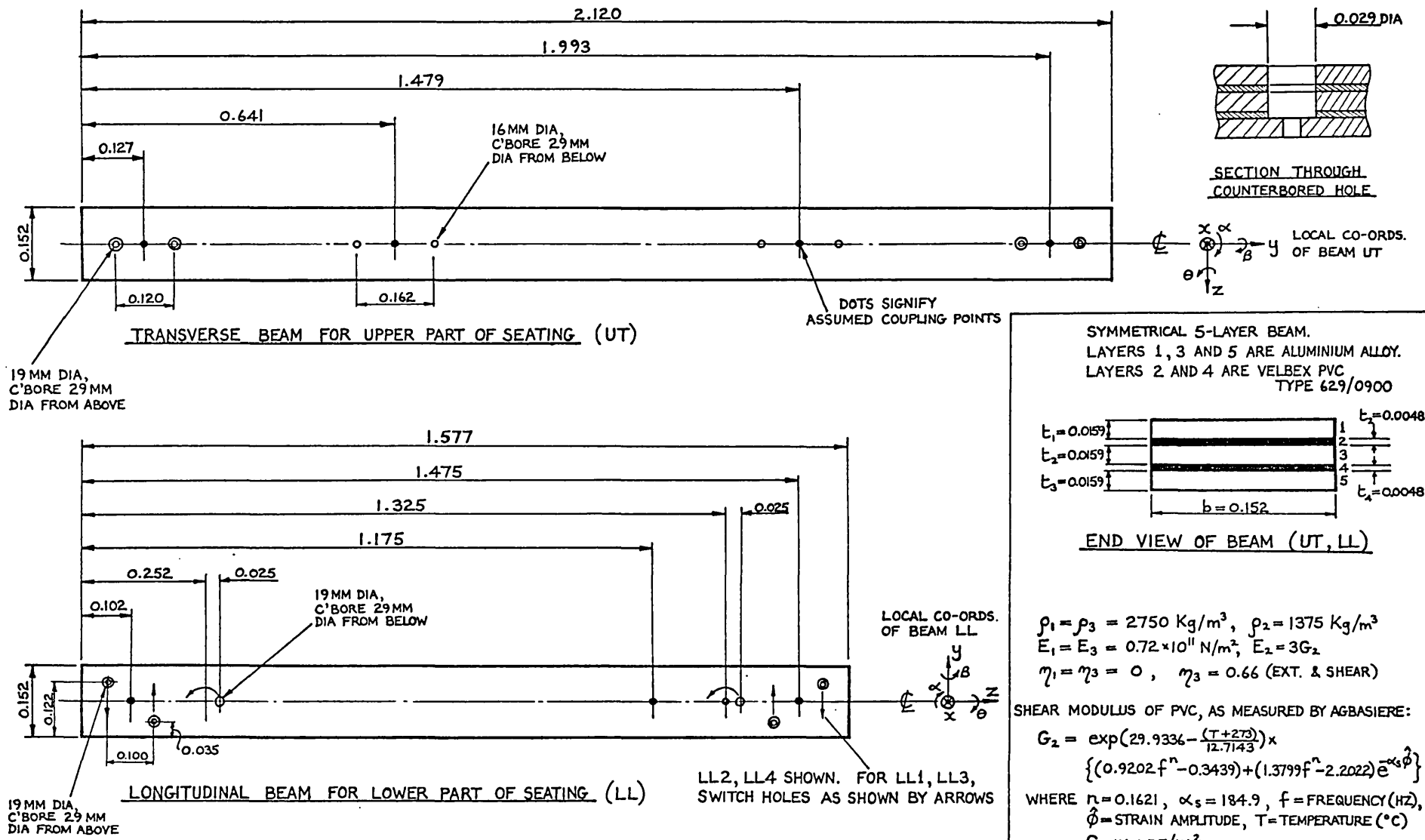
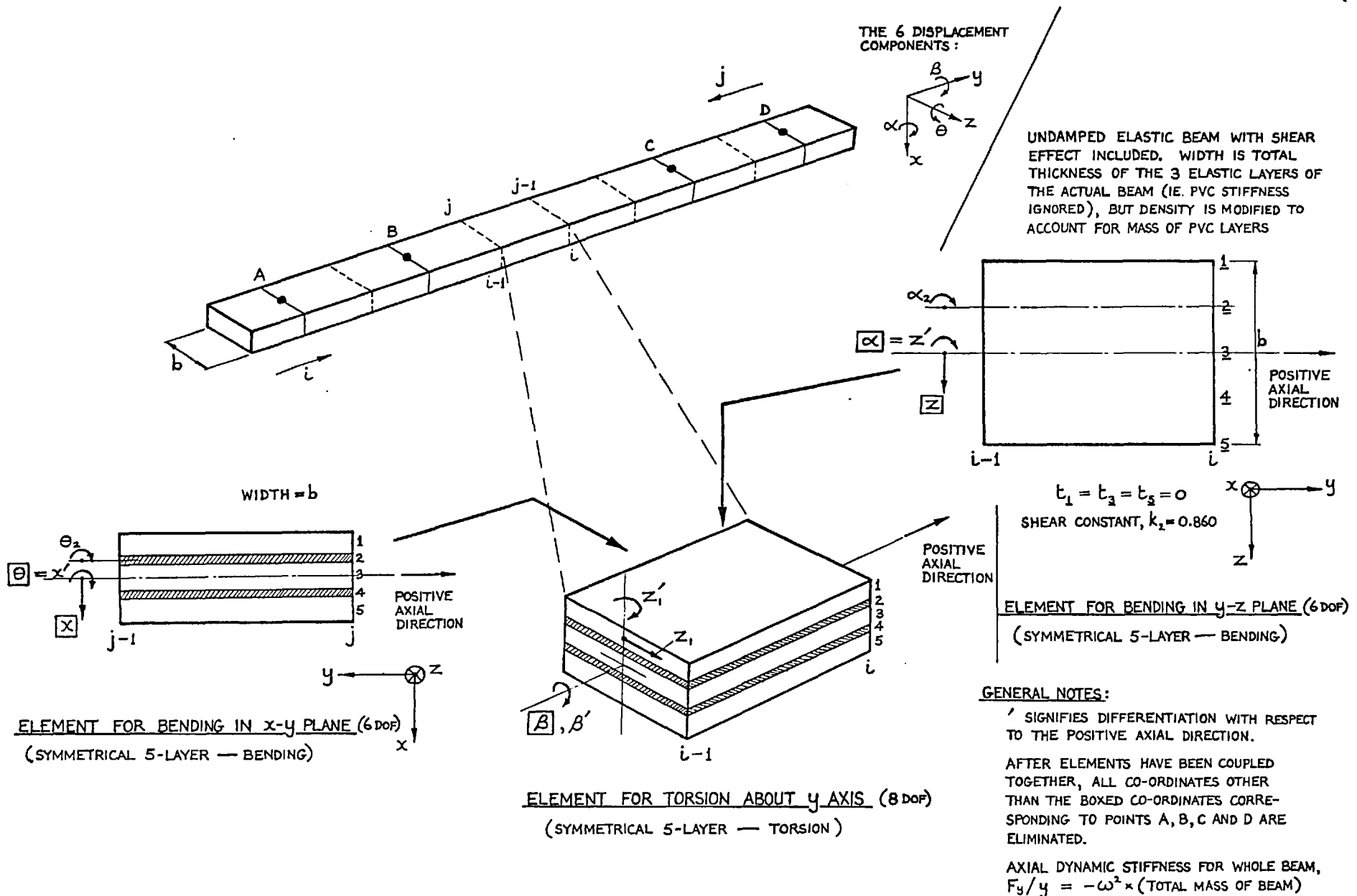
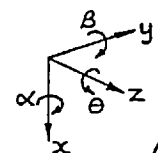


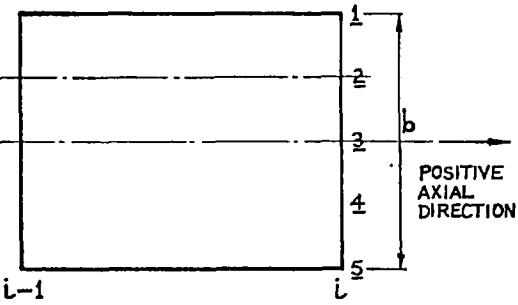
FIG. 14.1 SANDWICH BEAMS USED IN V-BEAM SEATING (SYMMETRICAL 5-LAYER)



THE 6 DISPLACEMENT COMPONENTS:



UNDAMPED ELASTIC BEAM WITH SHEAR EFFECT INCLUDED. WIDTH IS TOTAL THICKNESS OF THE 3 ELASTIC LAYERS OF THE ACTUAL BEAM (IE. PVC STIFFNESS IGNORED), BUT DENSITY IS MODIFIED TO ACCOUNT FOR MASS OF PVC LAYERS



$t_1 = t_3 = t_5 = 0$
SHEAR CONSTANT, $k_s = 0.860$

ELEMENT FOR BENDING IN y-z PLANE (6 DOF)
(SYMMETRICAL 5-LAYER - BENDING)

ELEMENT FOR BENDING IN x-y PLANE (6 DOF)
(SYMMETRICAL 5-LAYER - BENDING)

ELEMENT FOR TORSION ABOUT y AXIS (8 DOF)
(SYMMETRICAL 5-LAYER - TORSION)

GENERAL NOTES:

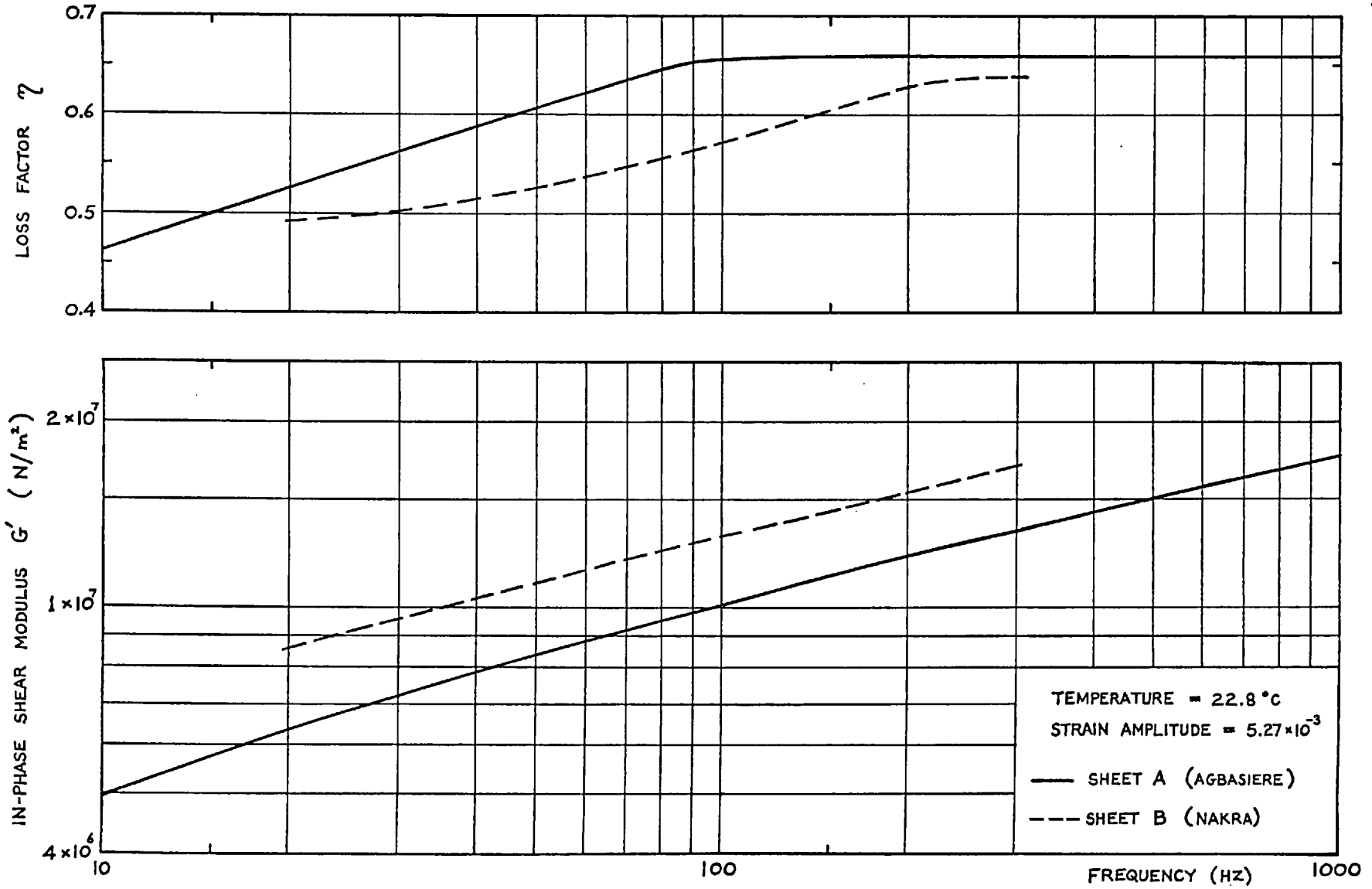
' SIGNIFIES DIFFERENTIATION WITH RESPECT TO THE POSITIVE AXIAL DIRECTION.
AFTER ELEMENTS HAVE BEEN COUPLED TOGETHER, ALL CO-ORDINATES OTHER THAN THE BOXED CO-ORDINATES CORRESPONDING TO POINTS A, B, C AND D ARE ELIMINATED.

AXIAL DYNAMIC STIFFNESS FOR WHOLE BEAM,
 $F_y/y = -\omega^2 \times (\text{TOTAL MASS OF BEAM})$

FIG. 14.2 AN ELEMENT OF BEAM UT1 CONSIDERED IN TERMS OF THE "STANDARD" BENDING AND TORSIONAL BEAM FINITE ELEMENTS

FIG. 14.3

DYNAMIC PROPERTIES OF VELBEX PVC TYPE 629/0900 IN SHEAR (AT A SINGLE TEMPERATURE AND CONSTANT STRAIN)



choice was to use the finite element displacement method, since this approach yields stiffness matrices which may be utilised directly in the coupling process. Hence, elements have been specially derived for flexure and for torsion of the symmetrical 5-layer beam, these having 7 and 8 degrees of freedom respectively*. For full details of these finite elements, together with the resulting stiffness and inertia matrices, the reader should consult Part 3 of this report (Chapters 9 and 11). The finite element modelling of the beam response properties will now be discussed with reference to the transverse beam UT 1.

In Fig.14.2 this beam is shown divided into a number of finite elements, these being finite lengths of beam which are joined end to end. It should be emphasised that each element is a complete 5-layer slice, there being no subdivision of the beam through its thickness. Hence, the only "nodes"⁺ that we shall be considering here are at the ends of each element (e.g. nodes $i-1$ and i in Fig.14.2). Referring back to Fig.13.7 in the last chapter, we see that the connection points A and D are actually on the lower face of the beam, whilst the points B and C are on the upper face. Because of this, a force input in the local Z direction at any of the connection points gives rise not only to an in-plane motion but also to a small rotation β about the beam axis. However, for the purposes of the present analysis it is assumed that all connection points lie on the neutral axis of the beam, so the motions in the different planes are uncoupled, and they may consequently be considered separately using the above mentioned flexural and torsional finite elements. Returning to Fig.14.2 we shall now consider how these standard elements have been utilised in order to give the full 6-directional response properties of the beam.

* Bending element has 7 dof - 3 co-ordinates at each end of element, plus 1 at centre which is eliminated immediately stiffness matrix is formed, in order to leave 6 x 6 matrix. Torsional element has 8 dof - 4 co-ordinates at each end of element.

+ In finite element analysis, the term "node" refers to a point where two or more elements are connected together.

Bending in the x-y plane has been described using the symmetrical 5-layer bending element, and as is seen from Fig.14.4, excellent correlation has been obtained between theoretical and experimental data, for the beam in a free-free condition. The two curves correspond to point A, near the tip of the beam, and the upper curve shows the transverse direct mobility $\frac{\dot{x}}{F_x}$, whilst the lower gives the rotational mobility $\frac{\dot{\theta}}{M_\theta}$. It is clearly seen that the beam is extremely heavily damped in this plane, the loss factor being of the order of 0.3. It is also interesting to observe how a transverse force at this position only weakly excites those modes in the frequency range 100 to 600 Hz, whilst a couple excites all the modes. The excellent results were obtained notwithstanding the use of measured data for the shear modulus of the PVC, which is frequency-, temperature - and strain-dependent (see Fig.14.3 for curves of shear properties of PVC at constant strain, and Fig.14.1 for shear modulus expression obtained by Agbasiere). Both the measured curves were obtained using the multi-directional measurement technique developed in Part 2 of this report*, and the errors in the low frequency rotational data were due to deficiencies in the measurement technique and to the effect of the suspension ropes.

The flexure of a sandwich beam in the plane of its layers has not been accorded the same detailed theoretical examination as the heavily damped flexural motion in the plane at right angles to the layers. Hence, it was necessary to experiment a little before arriving at a suitable representation of bending in the y-z plane, and a point mobility test was therefore carried out at point A, exciting the beam in the z direction on the centre layer (i.e. layer 3). The results of the test are shown in Fig.14.5, and it is clearly seen that the beam is virtually undamped in this plane. Consequently, it was decided to represent the in-plane behaviour by a solid undamped beam model; though still using symmetrical 5-layer elements, rather than simple uniform beam elements. The sandwich element has been

* See Part 2, Chapter 4, Page 132. Exciting block Mk 3 was used (Aluminium, 120 x 50 x 50mm, Weight 0.950 Kg with accels)

used in the manner indicated in Fig.14.2, layers 2 and 4 representing the upper and lower halves of the beam, and being assigned real elastic and shear moduli, whilst layers 1, 3 and 5 are set to zero thickness. The use of this element has permitted the same computer subroutines to be used for bending in both planes, and it has also facilitated the inclusion of shear stiffness* in the analysis. The effect of shear is certainly not insignificant in the present case, since the ratio of beam length to width is only 13.9 for the transverse beams, and even less for the longitudinal beams. The Timoshenko shear constant k_2 has been set to 0.860, this figure having been obtained from reference (7). In view of the very high in-plane bending stiffness of the aluminium layers, it was decided to ignore the PVC stiffness. However, it was necessary to experiment a little with the PVC mass, and as is seen from the two theoretical curves for $\frac{\dot{z}}{F_z}$ in Fig.14.5, far better agreement is obtained between experiment and theory if the mass of the PVC layers is included. Thus, the beam model for in-plane behaviour has been given a width equal to the total thickness of the 3 aluminium layers of the actual beam, and the material density has been modified slightly to account for the mass of the PVC layers. In spite of the fact that a solid beam model has yielded results which agree quite closely with measured point mobility data, one might still expect the overall behaviour of the model to differ slightly from that of the actual beam, since it cannot describe relative motion between the layers due to shearing of the PVC. It is therefore instructive to consider the lower graph in Fig.14.5, which shows the relative motion between layers 1 and 3, as measured during the above mentioned point mobility test. This clearly shows that the two motions are essentially equal at all frequencies other than those in the neighbourhood of the antiresonances in the point mobility response.

* Note that in deriving the stiffness properties of this 5-layer element, bending, stretching and shear effects were included for layers 2 and 4.

Torsion about the y axis has been described using the symmetrical 5-layer torsional element. The upper graph in Fig.14.6 shows both the measured and the theoretical direct mobilities corresponding to the β direction at point A, and the agreement between the two is seen to be quite adequate, although not so good as for the bending motions considered above. However, bearing in mind the greater complexity of the torsional problem, this is not surprising. The principal causes of disagreement are thought to be the assumption of incompressible visco-elastic layers, and the neglect of shear stiffness when considering the in-plane bending of the outer layers (due to twisting of the beam about its neutral axis), but without these assumptions the derivation of the finite element would have been greatly complicated. The measured results were obtained using the multi-directional measurement technique, with the exciting block bolted to the upper face of the beam. Since no correction was made for block inertia in the z direction, it is possible that the slight shift of all the measured peaks relative to the theoretical ones is due to the mass loading effect of the block.

The axial response has been assumed to be masslike, thereby precluding the possibility of longitudinal wave motion. The tip-to-tip transfer mobility curve in Fig.14.6 shows this assumption to be sufficiently accurate, even though the measured results do begin to deviate gradually from a mass line at around 300 Hz. As a result of this assumption, each of the connection points A, B, C and D has the same motion in the y direction, so a single axial co-ordinate may be used for all four points. In consequence, the full 6-directional response properties at the four connection points may be expressed in terms of 21 co-ordinates, instead of 24. Fig.14.7a shows the 21 seating co-ordinates associated with beam UT 1, co-ordinate 2 being the common axial co-ordinate.

We shall now consider the number of elements that are needed, and the way in which they are coupled together to yield the required response

4/8/72

CHART
WELL

Graph Data Ref. 5521

Log 2 Cycles x mm, $\frac{1}{2}$ and 1 cm

MEASURED (BLOCK MK3/15/1C)
THEORETICAL (10 FINITE ELEMS.
UP TO 400HZ, 14 ABOVE)

$\frac{\dot{x}}{F_x}$

POINT MOBILITY 127 MM FROM TIP OF 2.120 M SYMMETRICAL 5-LAYER BEAM (UT)

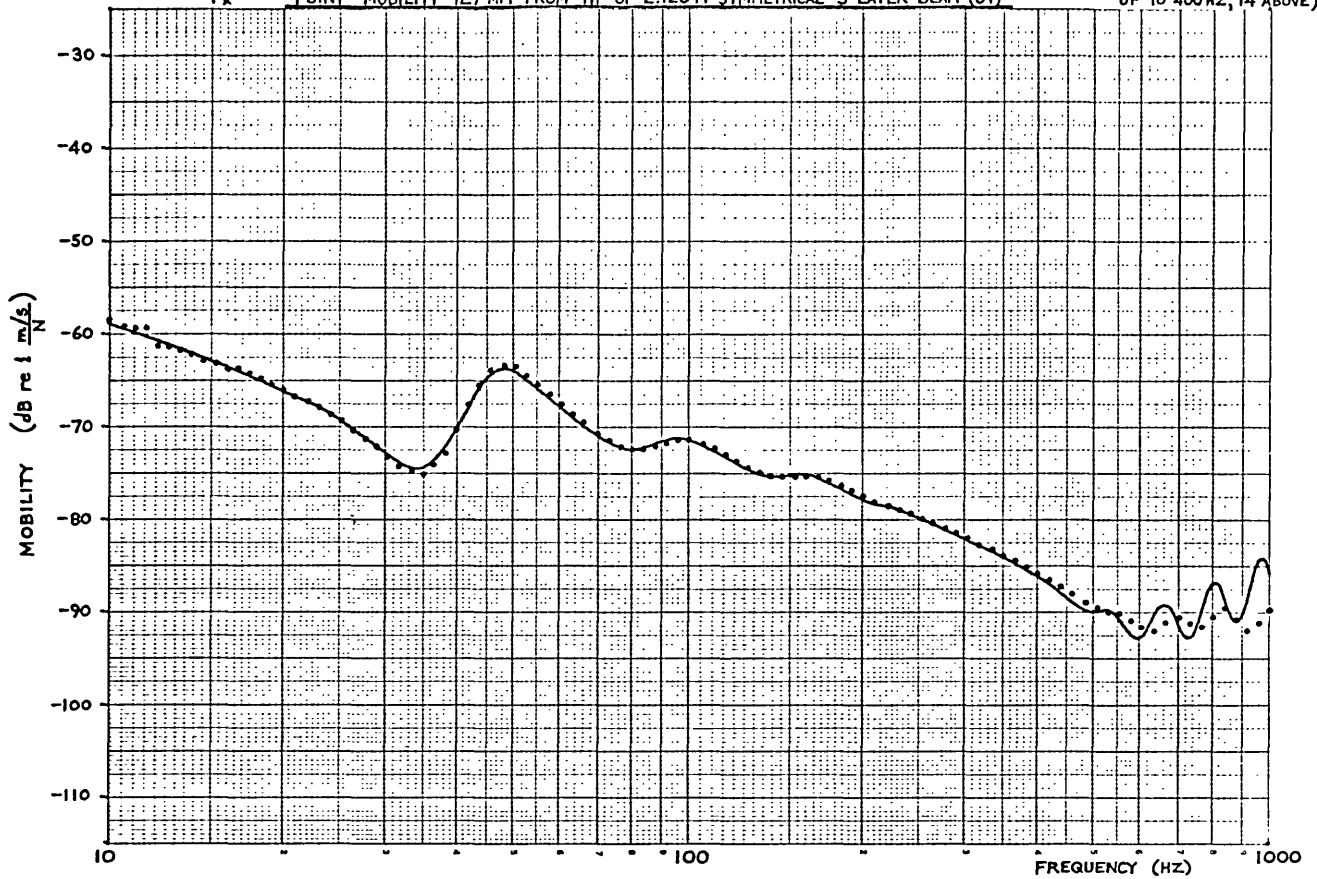


CHART
WELL

Graph Data Ref. 5521

Log 2 Cycles x mm, $\frac{1}{2}$ and 1 cm

4/8/72

MEASURED (BLOCK MK3/15/1C)
THEORETICAL (10 FINITE ELEMS.
UP TO 400HZ, 14 ABOVE)

$\frac{\dot{\theta}}{M_0}$

POINT MOBILITY 127 MM FROM TIP OF 2.120 M SYMMETRICAL 5-LAYER BEAM (UT)

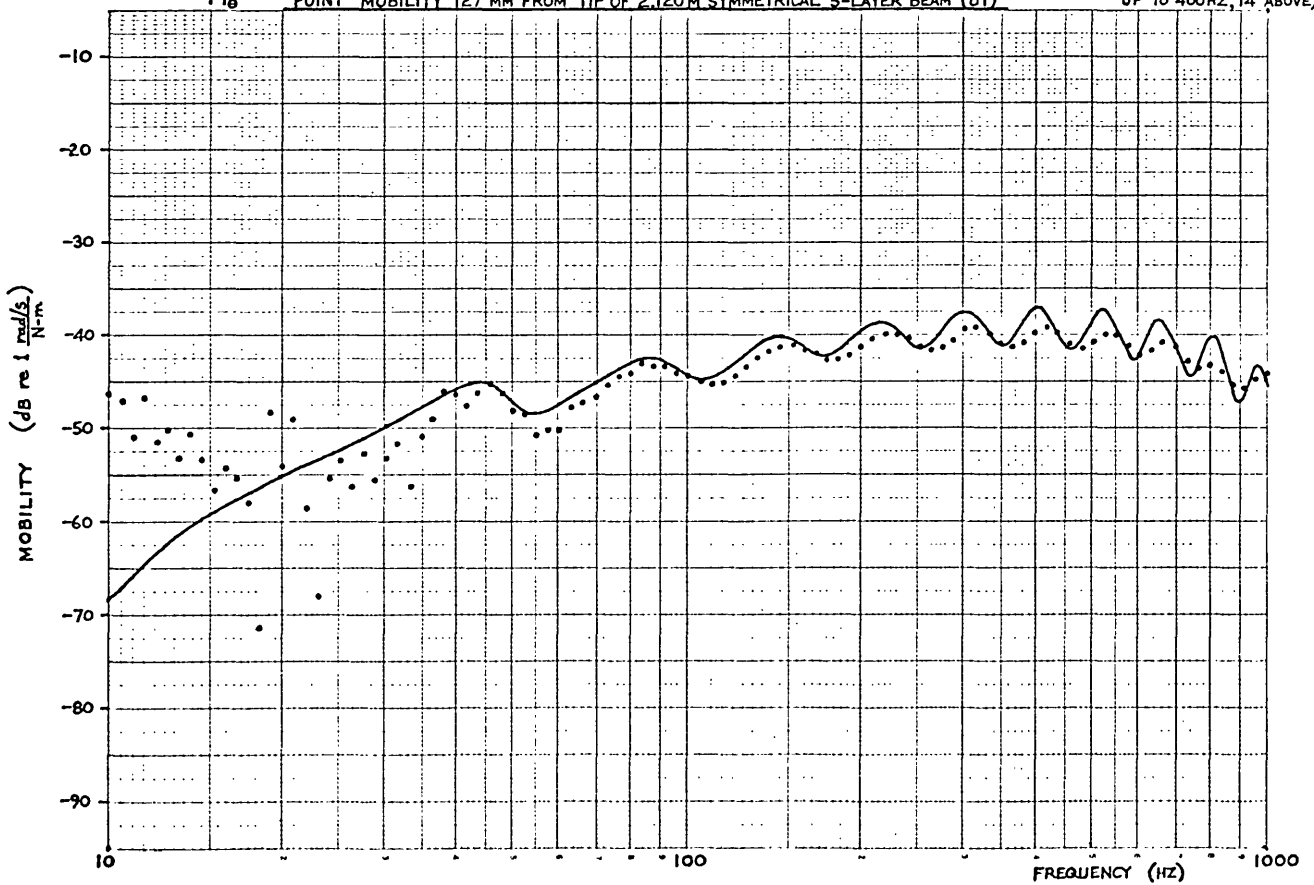
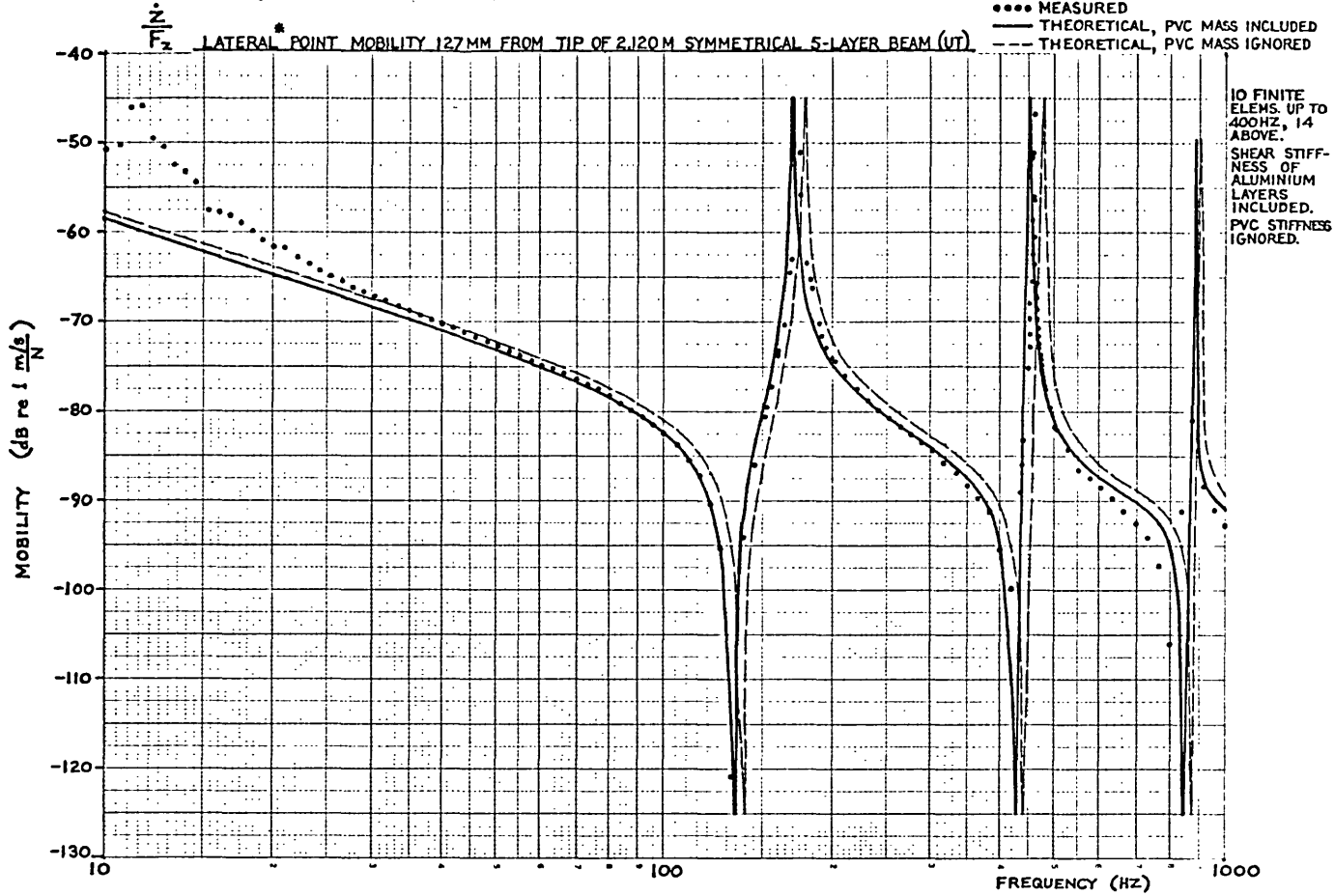


FIG 14.5

* IN PLANE OF LAYER 3 (Z DIRECTION)

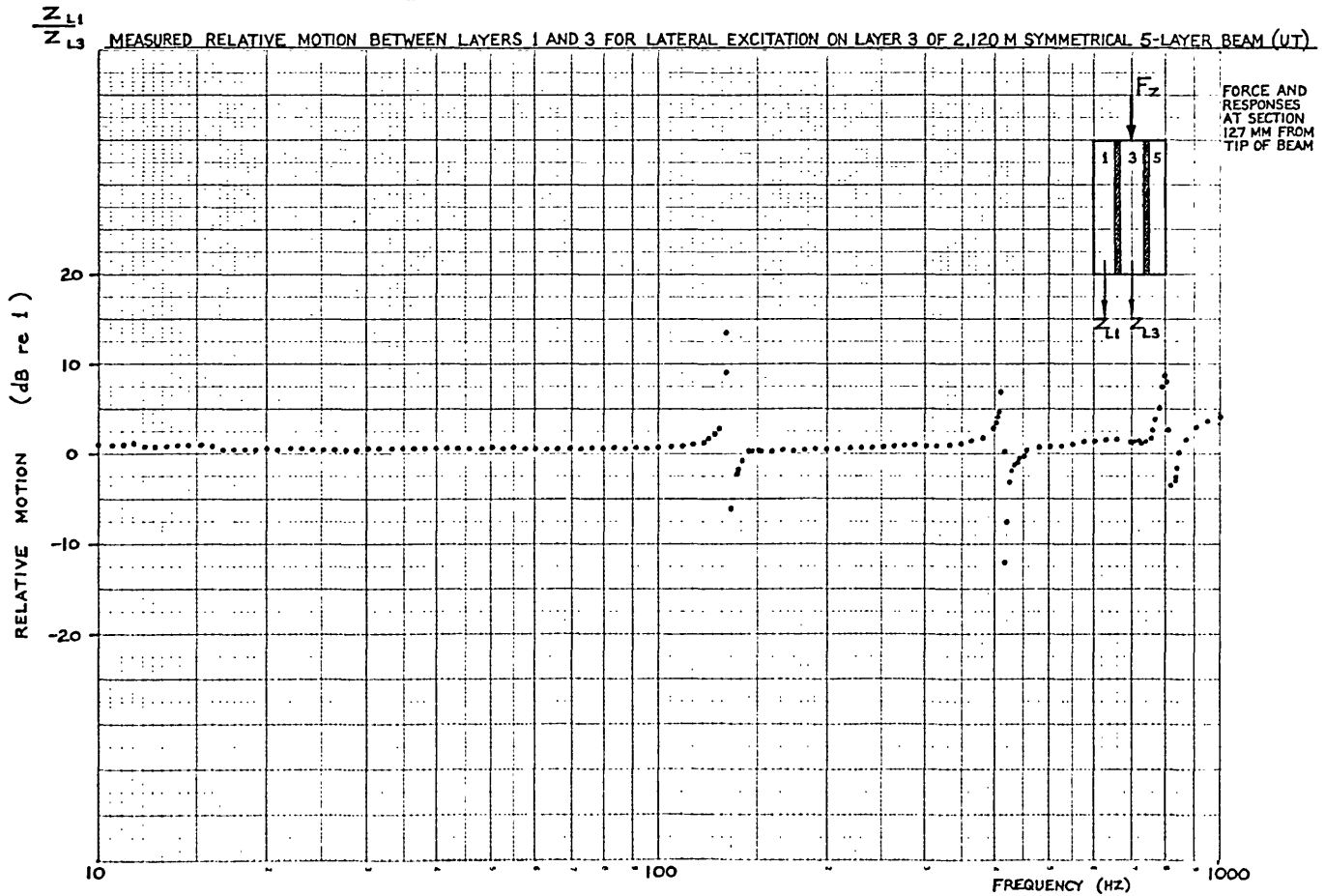
GRAPHICS WELLFORD Graph Data Ref. 5521

Log 2 Cycles a mm, j and 1 cm



GRAPHICS WELLFORD Graph Data Ref. 5521

Log 2 Cycles a mm, j and 1 cm



12/12/72

CHART WELLBORN Graph Data Ref. 5521

Log 2 Cycles x mm, j and 1 cm

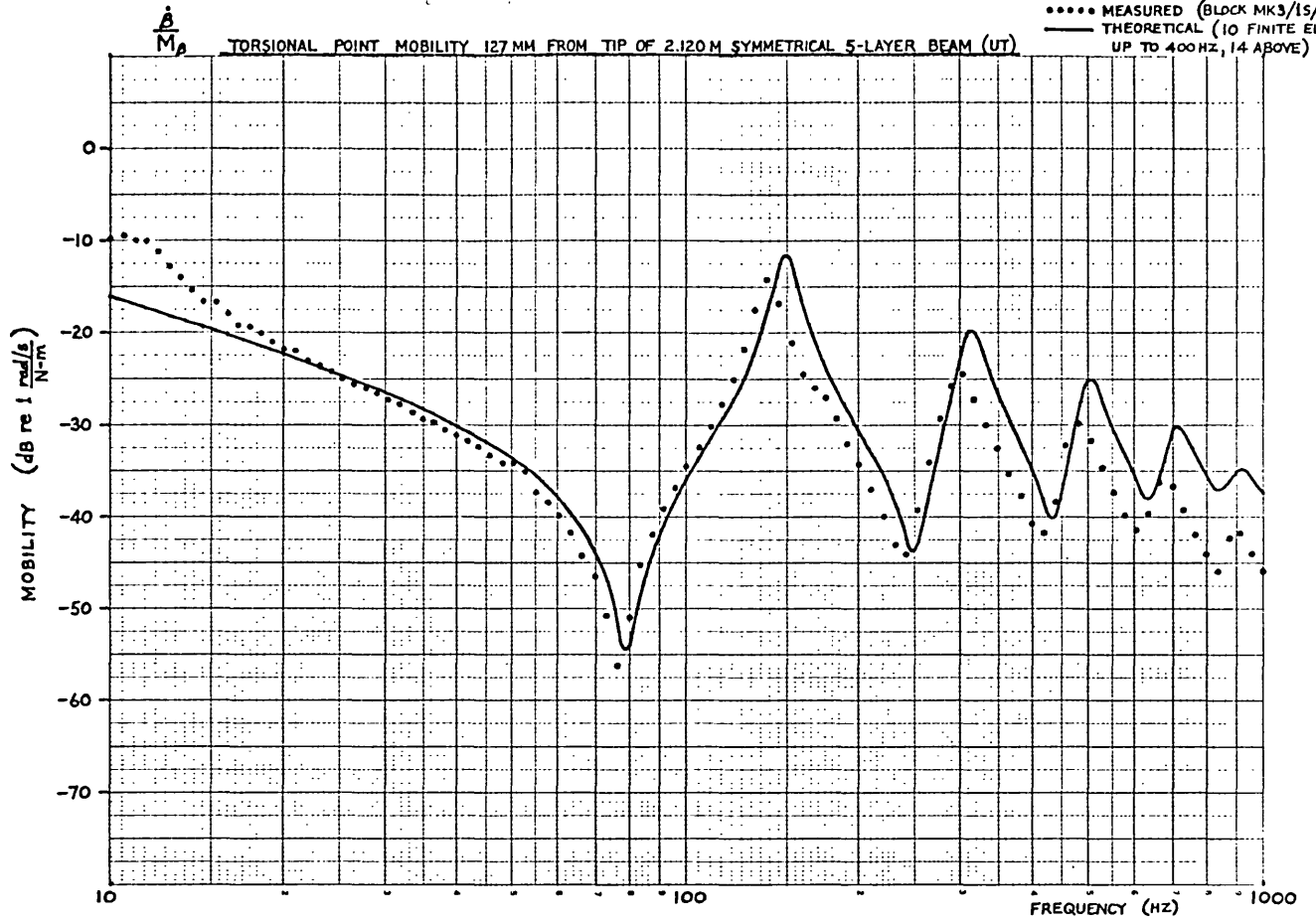
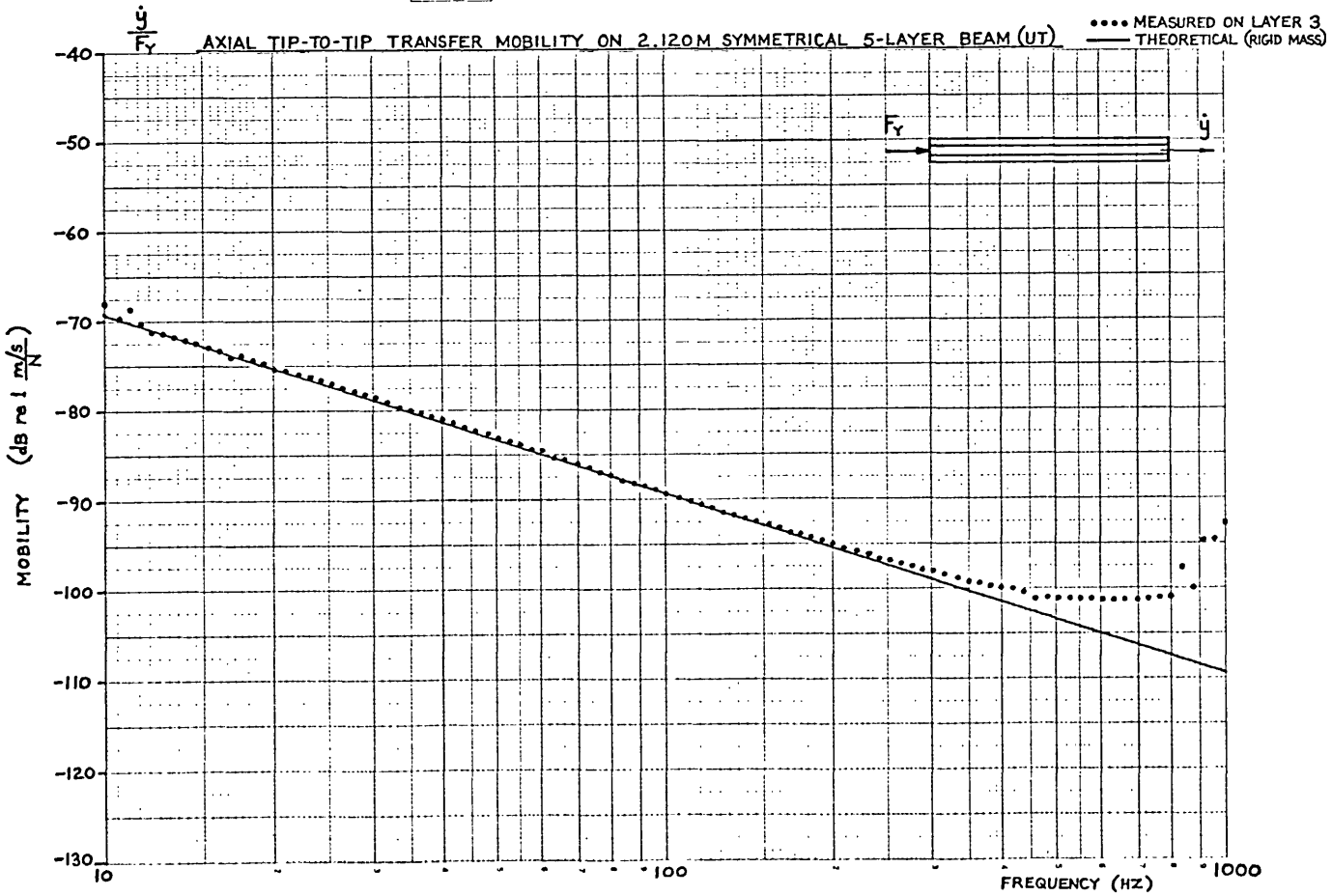


CHART WELLBORN Graph Data Ref. 5521

Log 2 Cycles x mm, j and 1 cm



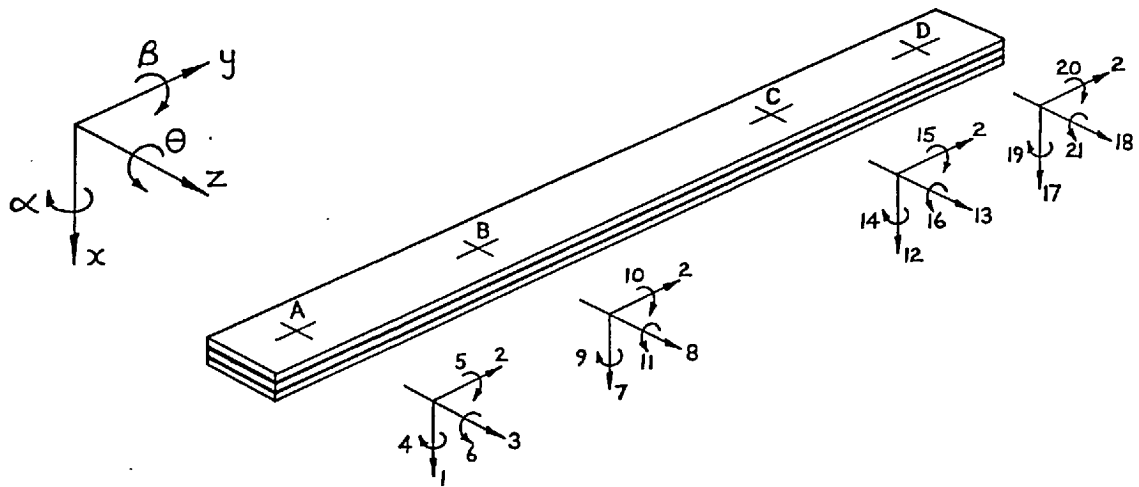
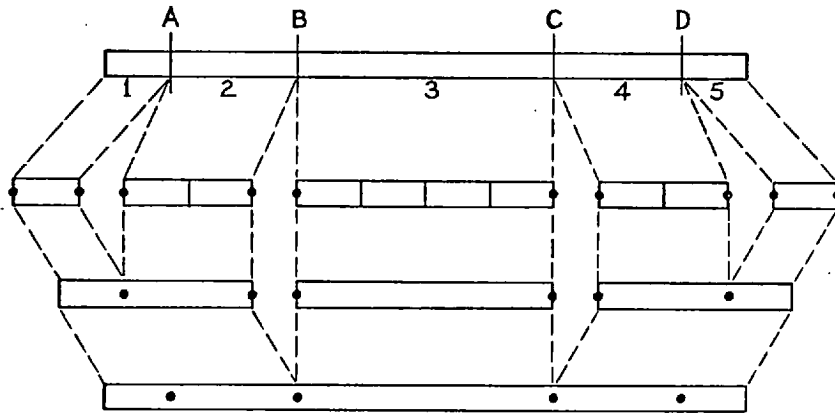


FIG. 14.7a SYSTEM CO-ORDINATES ASSOCIATED WITH COUPLING POINTS A,B,C,D ON BEAM UT1



DIVIDE BEAM INTO 5 SECTIONS. THE SECTIONS ARE NUMBERED $S=1$ TO 5 AND EACH IS BUILT UP FROM N_s FINITE ELEMENTS. FORM DYNAMIC STIFFNESS MATRICES RELATING TO TIPS OF SECTIONS. CO-ORDINATES AT INTERMEDIATE ELEMENT CONNECTIONS ARE ELIMINATED

COUPLE TOGETHER SECTIONS 1 AND 2, AND ALSO 4 AND 5. ELIMINATE CO-ORDS. AT BEAM TIPS.

COUPLE TOGETHER THE THREE PARTS 1/2, 3, 4/5 TO FORM REQUIRED DYNAMIC STIFFNESS MATRIX FOR POINTS A,B,C,D

"•" SIGNIFIES A POINT AT WHICH THE CO-ORDINATES ARE RETAINED AT ANY STAGE OF THE BUILDING

FIG. 14.7b DIVISION OF BEAM INTO ELEMENTS AND SYSTEMATIC COUPLING OF SECTIONS

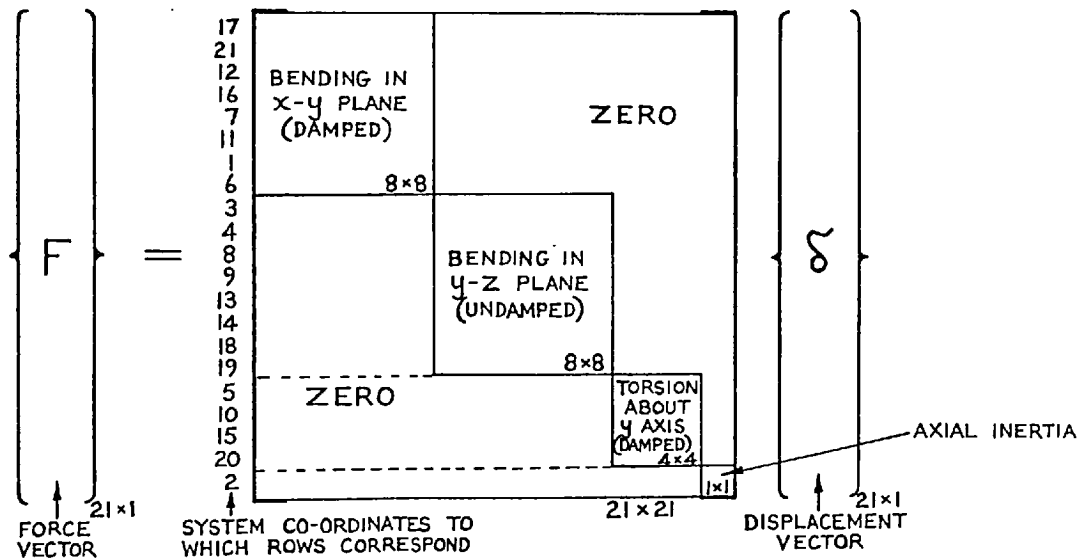


FIG. 14.7c THE 6 DIRECTIONAL DYNAMIC STIFFNESS MATRIX FOR POINTS A,B,C,D ON BEAM UT1

properties. Referring to Fig.14.4 the curve of $\frac{\dot{\theta}}{M_e}$ clearly shows that the beam possesses 10 damped flexural modes in the frequency range 10 to 1000 Hz. This means that at the upper frequency there are approximately 5 complete waves along the length of the beam, and even at 400 Hz there are still as many as 3. It has previously been shown* that the 7 degree of freedom bending element is capable of describing as much as $\frac{3}{8}$ of a wavelength of flexure with quite reasonable accuracy, so this leads to the requirement for at least 8 elements at 400 Hz and at least 13 at 1000 Hz. Due to the non-uniform division of the beam into elements, it was decided to increase these numbers slightly, and 10 elements have been used at all frequencies up to 400 Hz, whilst 14 have been used between 400 and 1000 Hz. With 14 elements, the model for bending in the x-y plane alone has 45 degrees of freedom, and when we also consider bending in the y-z plane and torsion about the y axis, the total number of degrees of freedom for a single beam is well over 100.

Whilst it is quite common in finite element analysis to work with very large systems of equations, this is neither necessary nor desirable in the present problem, especially since the beams form only part of a far more complex assembly. It is much better to eliminate all degrees of freedom other than those at the four connection points. This elimination is performed at the component stage, and in finite element analysis it is known as "substructuring". (8) The procedure is outlined diagrammatically in Fig.14.7b starting with the division of the beam into 5 sections and the subdivision of these sections into elements. The tip dynamic stiffness properties of a section comprising N_s elements are obtained by building up the section element by element, at the same time eliminating the co-ordinates

* See Part 3, Chapter 12, Page 260.

associated with the inter-element coupling points. This may be accomplished using a procedure based upon Gaussian elimination, or alternatively, using the Transfer Matrix method. The former procedure has been adopted in the present work, but for a fuller discussion of these two techniques the reader is referred to Appendix VIII (to Part 3). Once the tip dynamic stiffness matrices have been formed for the 5 sections, 1 and 2 are coupled together and the co-ordinates associated with the left hand beam tip are eliminated, again using Gaussian elimination. A similar procedure is then followed for sections 4 and 5, after which the dynamic stiffness matrices for the 3 parts are added together to yield the required dynamic stiffness properties for the four connection points A, B, C and D. The number of co-ordinates associated with each of these points may also be reduced at the same time.*

Since we are assuming that the bending in the two planes and the torsion about the beam axis are all dynamically uncoupled from one another, this complete building and elimination procedure must be carried out three times at each frequency.⁺ The resulting 21 x 21 complex dynamic stiffness matrix is banded, as is shown in Fig.14.7c, but the row order does not correspond to the co-ordinate number sequence used in the seating analysis. However, it is not necessary to re-arrange the rows and columns, since this is done automatically by the dynamic stiffness coupling programme when building up the system matrix from the component data.

* See Fig.14.2, which shows all the nodal co-ordinates used in the building process. Those co-ordinates which are retained at A, B, C and D are shown boxed.

+ Note that time required to form complete 21 x 21 complex matrix on CDC 6600 computer is only 280 mS for beam UT, and 315 mS for beam LL cf. 4s to solve the 50 complex equations for the system.

14.2 RUBBER V-BLOCK (Component RB)

The rubber block is shown in Fig.14.8. It is solid, weighs 15.4 Kg, and was moulded from an almost natural rubber. Besides being relatively difficult to manufacture, a block of such complex shape is not easily analysed, and it was apparent from the outset that the stiffness properties would have to be measured, whether this be for the purpose of modelling the block directly from measured data or for the purpose of checking an analysis. As a full analysis did not appear feasible at that time, it was decided to use measurements to model the block. However, this posed certain problems, since not only were the point dynamic stiffness properties to be obtained for the two upper faces of the block, but also required were the transfer stiffness properties relating the transmitted forces to the displacements of the upper faces. In view of the basically spring-like nature of this component, it is doubtful whether the necessary data could be obtained with sufficient accuracy by performing receptance* tests on the block in a freely suspended condition. In consequence, it was necessary to mount the block in an effectively rigid V-support and to measure its "grounded" receptance properties. Whilst the point receptances on the upper faces could be measured without undue difficulty, it was considered impracticable to even attempt to measure the force transmission to the support, since not only is it multi-directional, but it is also distributed non-uniformly over a very large area. Since it was not possible to obtain the required data exclusively by experimental means, it was necessary to resort to a compromise solution, whereby a physically realistic model was chosen to represent the block, and the parameters of the model were adjusted until it yielded receptance data which approximated to the available measurements.

* We shall consider receptance rather than mobility, because the block is a spring and therefore has constant receptances at low frequencies.

Before proceeding to consider the model, it should be emphasised that the rubber block is being considered throughout as an effectively "grounded" component*, both for the purpose of determining the stiffness which it presents to the transverse beam assembly, and also for determining the force transmission to the lower part of the seating. As has been discussed elsewhere, this is justified by the relatively high flexibility of the block in comparison with the supporting structure. The coupling points P_1 and P_2 on the two upper faces of the block are each allowed 6 degrees of freedom, and the force transmission to the lower sandwich beams is assumed concentrated at three points along each of the lower faces of the block, there being a total of 14 force transmission co-ordinates associated with these points (see Appendix IX). Thus, the resulting point and transfer dynamic stiffness matrices are of size 12 x 12 and 14 x 12 respectively.

The model is shown in Fig.14.8, and also in Fig.14.9, where it is superimposed upon a drawing of half the rubber block. It comprises a network of springs arranged in such a way as to adequately describe the behaviour of the actual block, especially with regard to the probable paths by which forces are transmitted through to the supporting structure. The assumption is made that the two halves of the block are uncoupled, and this is justified by the fact that the block is attached to the lower part of the seating by a pair of 12.7mm ($\frac{1}{2}$ in) bolts which pass through the centre section and thereby minimise elastic coupling between the two halves. The rigid massless plates on the two faces distribute the load and prevent deformation in the planes of the faces, thereby approximating to the conditions which prevail when the transverse beams are attached to the block. In view of the relatively large dimensions of the block, it was obvious that wave effects within the rubber could not be ignored, and in consequence it was decided to lump mass at the ends and at the mid-point of each spring, as shown in Fig.14.8.

* i.e. No motion is possible for points on the lower faces of the block.

The analysis of the spring-mass model for its point and transfer dynamic stiffness properties is a little involved, especially since the spring "framework" is an indeterminate structure. The details are therefore given in Appendix IX. Computer subroutines have been written which generate the necessary dynamic stiffness matrices, given the stiffness and mass data for the members of the framework. However, these basic data must be obtained from tests on an actual block, so we shall now consider the various experiments which were performed for this purpose.

Selected point receptance measurements were made at the centre of one face of the block, which was mounted as shown in Fig.14.15. The steel plate attached to the face served to distribute the load, and in addition it acted as an "exciting block" for obtaining rotational point receptance data*. However, the addition of this 3.6 Kg mass to the relatively flexible "ear" of the rubber block gave rise to a flapping resonance at around 30 Hz, so measurements were confined to the frequency range 5 to 20 Hz. Although mass cancellation was employed, this could not be expected to be very effective with such a large mass near to a resonance, and certainly not above it. Thus, only "static" stiffness and damping information were yielded by these tests. The nylon rope shown in Fig.14.15 was used to apply a small preload to the rubber block, so as to hold it down reasonably firmly even when the shaker was pulling on the face. It is not thought that this applied any significant constraints to the block, since the rope was only in contact with its corners and these were obviously far less stiff than the centre of the face.⁺

* See Part 2 of this report.

+ i.e. The combination of a stiff spring K_1 with a weak pre-loading spring K_2 in parallel still looks like K_1 .

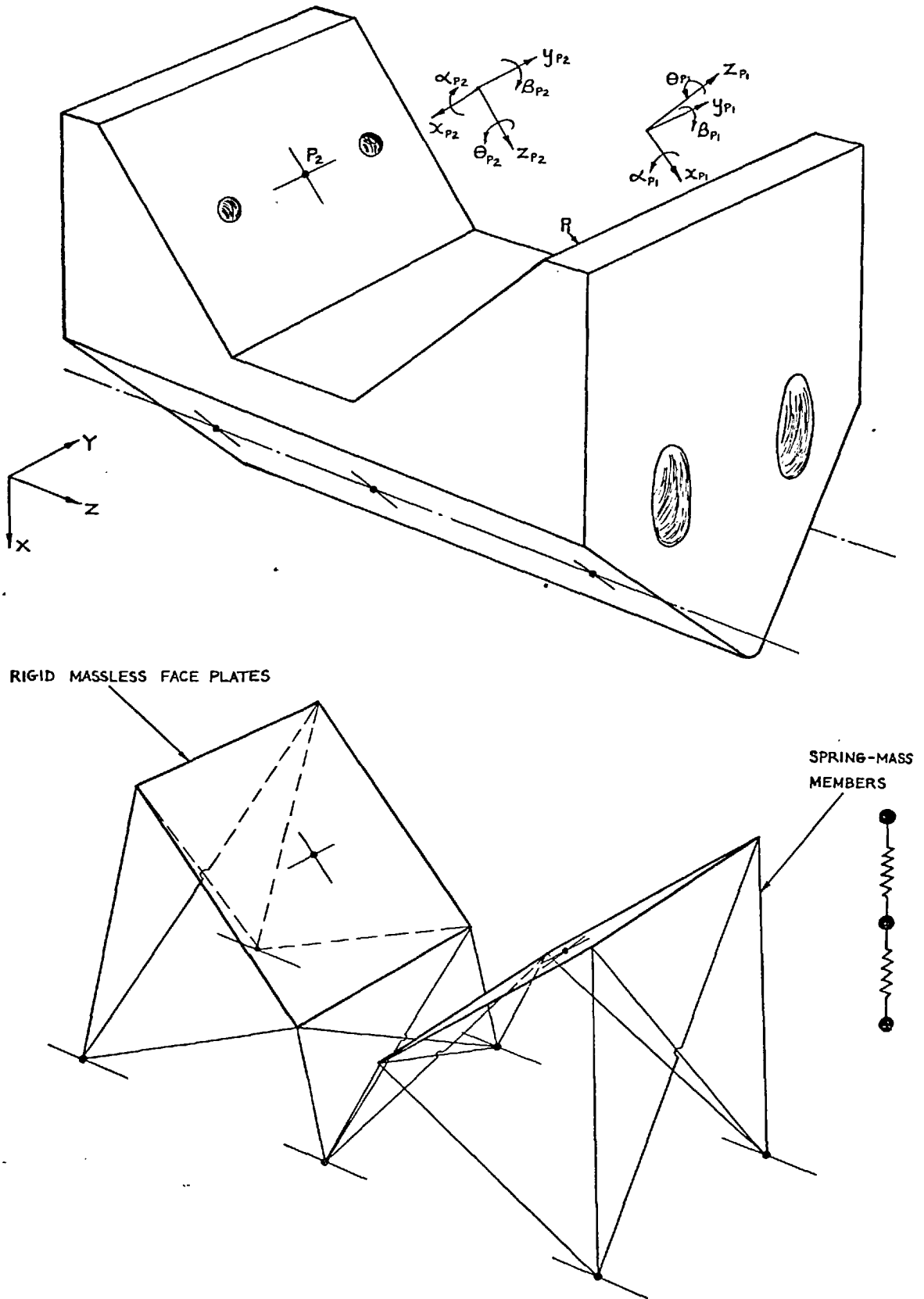
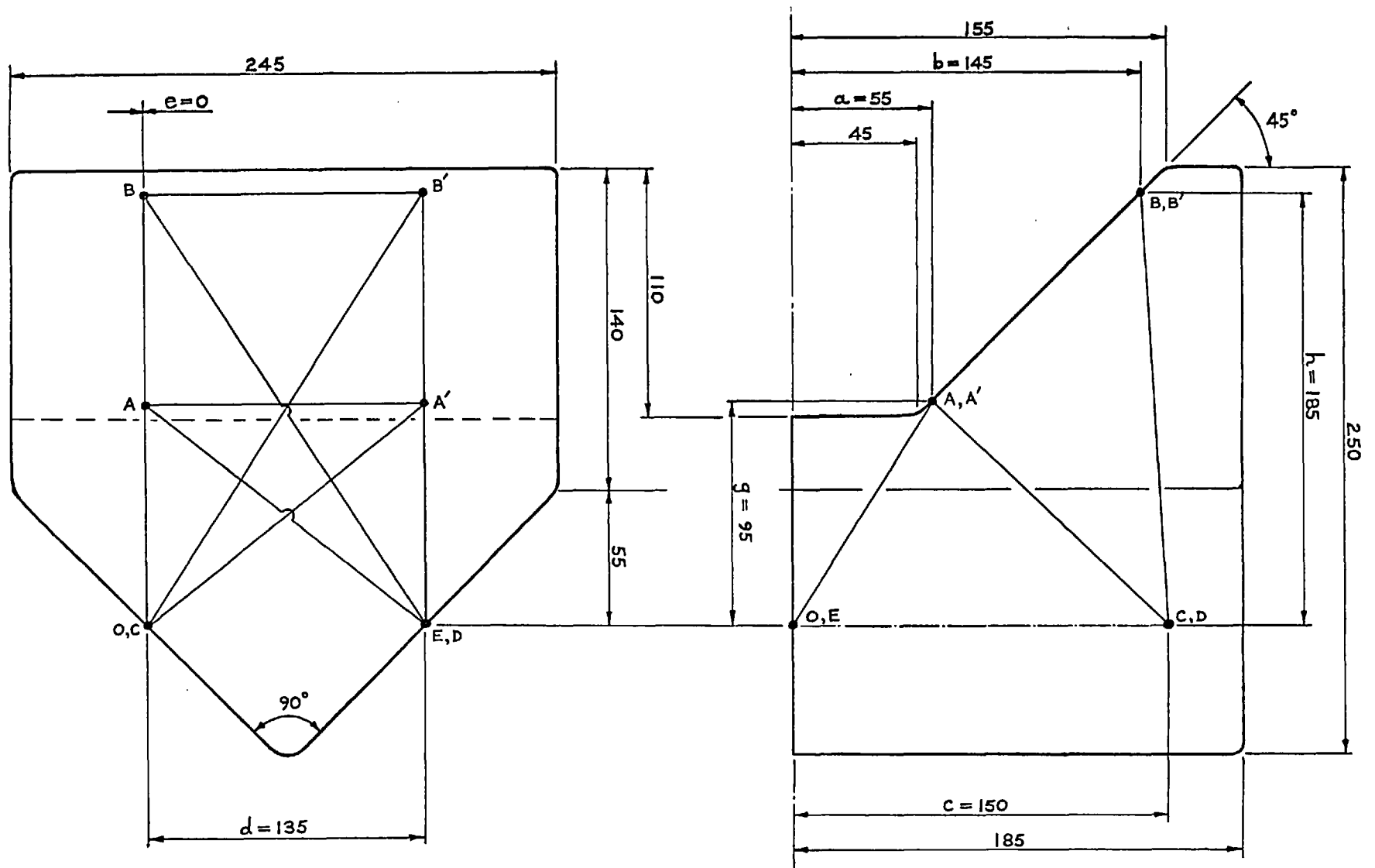


FIG. 14.8 THE RUBBER V-BLOCK AND THE SPRING MODEL USED TO REPRESENT IT



ALL DIMENSIONS IN MM
FIRST ANGLE PROJECTION
APPROX. HALF SIZE

FIG. 14.9 DIMENSIONS OF HALF RUBBER V-BLOCK AND OF THE CORRESPONDING SPRING MODEL

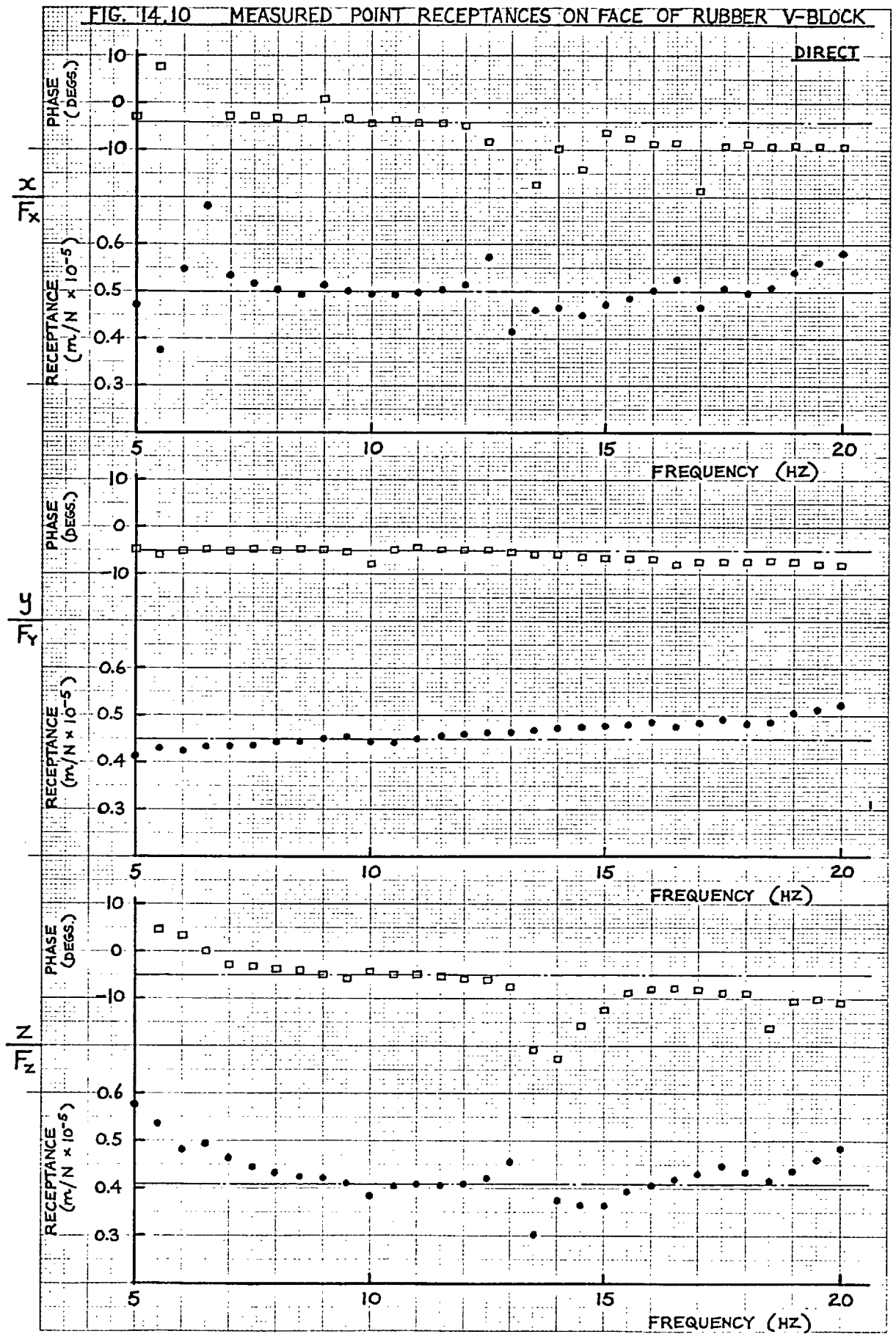
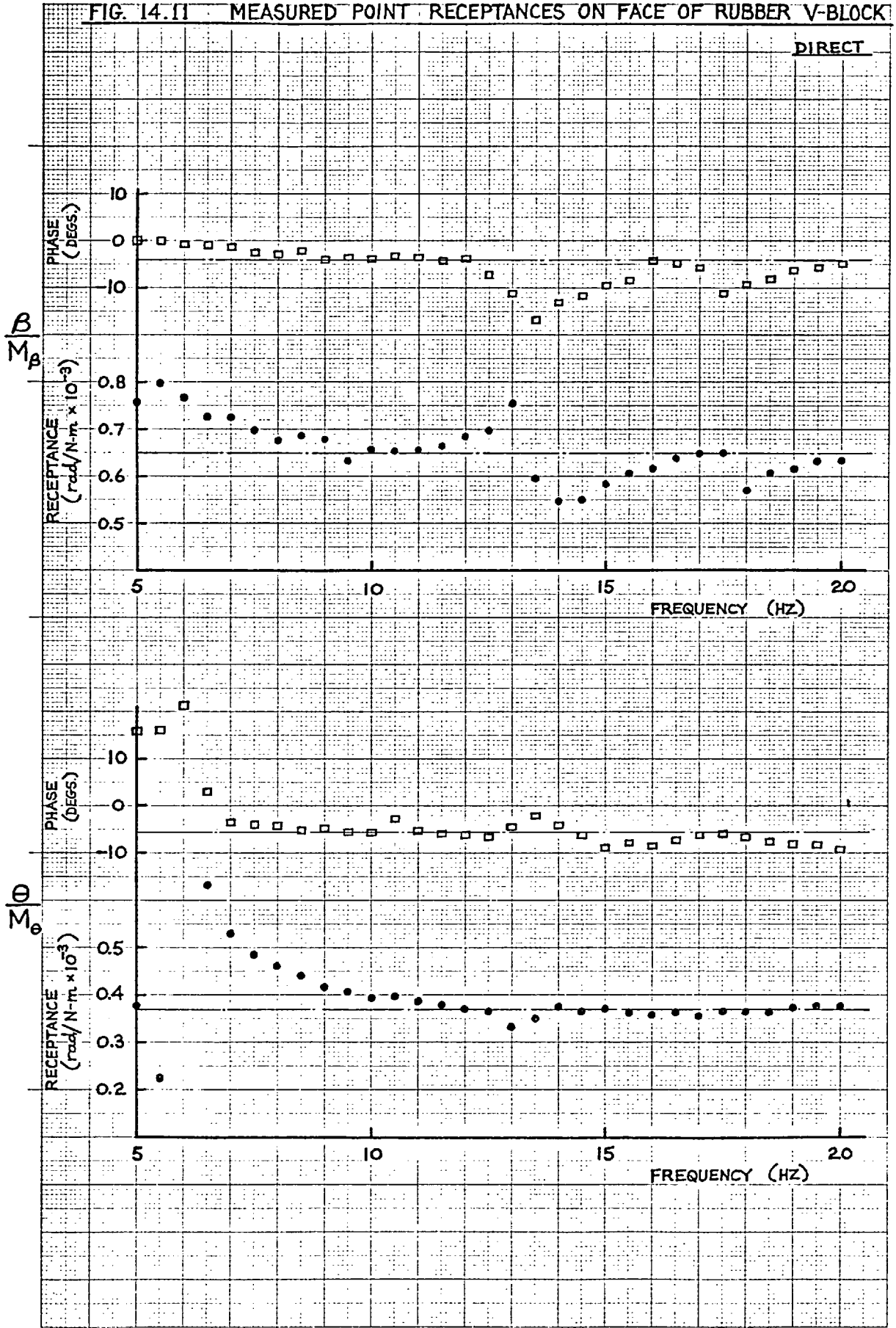


FIG. 14.11 MEASURED POINT RECEPTANCES ON FACE OF RUBBER V-BLOCK



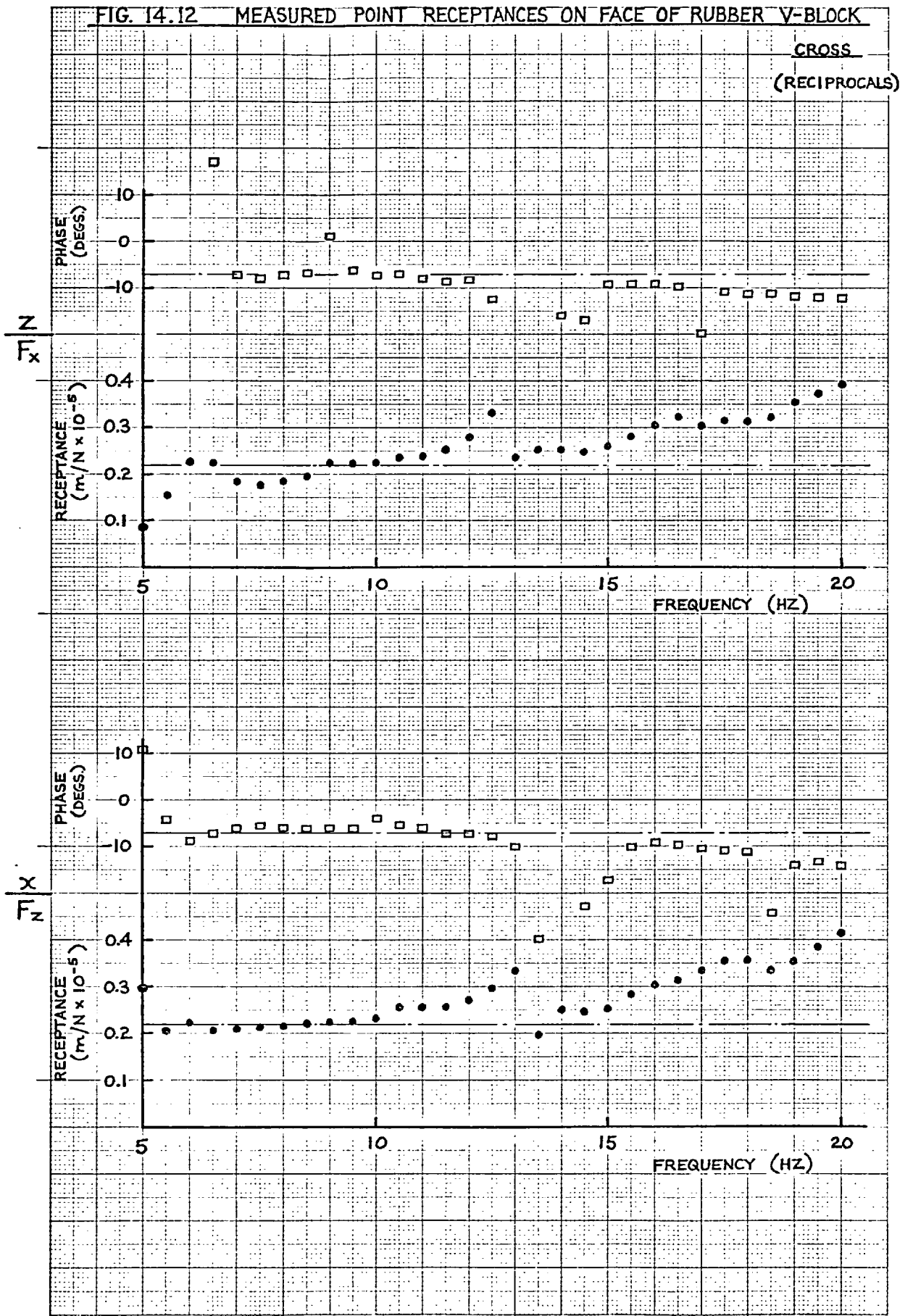
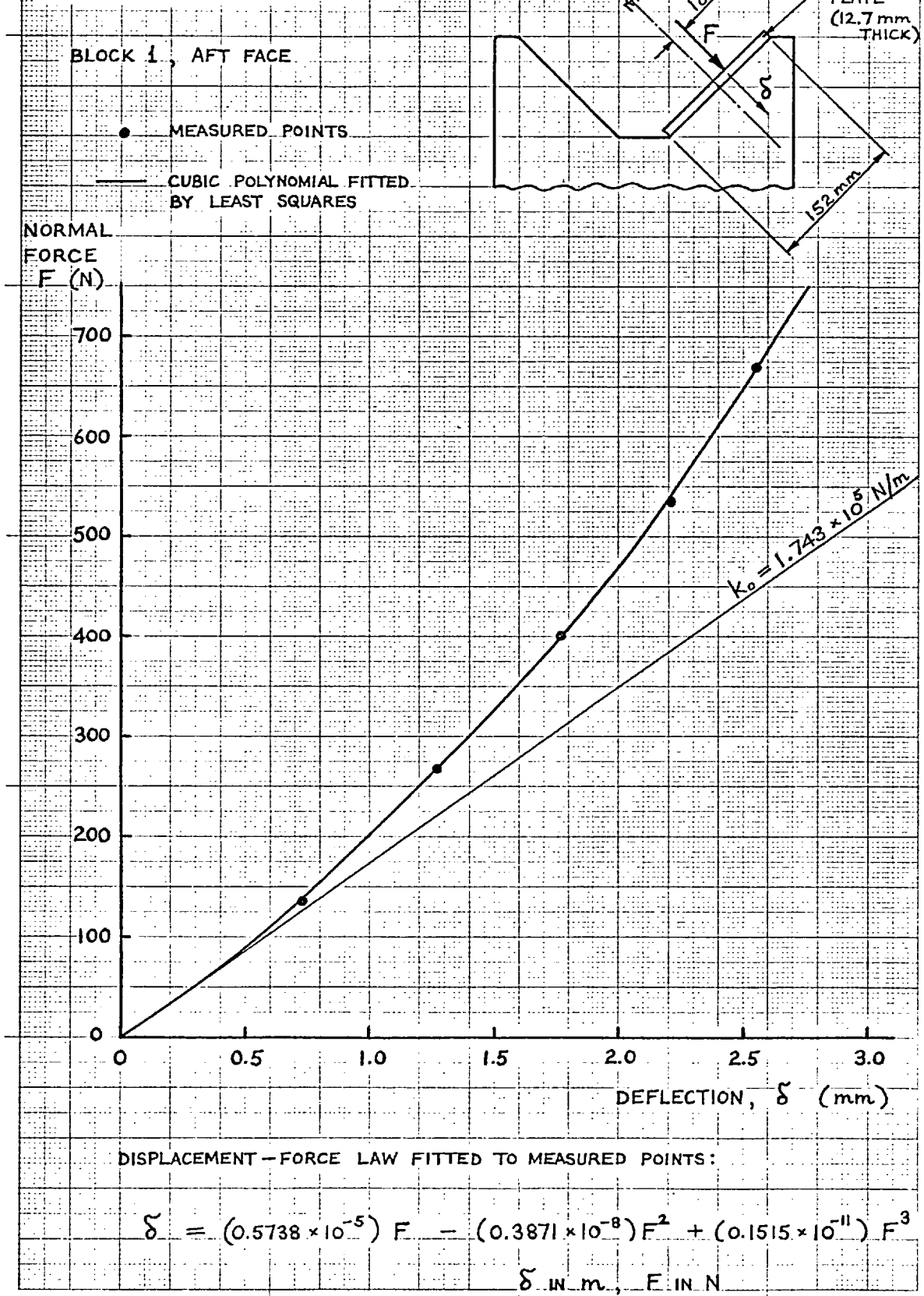


FIG. 14.13

STATIC LOAD/DEFLECTION CURVE
FOR LOADING NORMAL TO FACE
OF RUBBER V-BLOCK



The measured direct and cross receptance curves are shown in Figs. 14.10 to 14.12, and the average values of modulus and phase obtained from these curves have been listed in Fig. 14.15. These measured receptances are relatively constant, as one would expect for a spring, and are best in the range 10 to 15 Hz. The errors below 10 Hz were probably due to the small accelerometer signals and to changes in amplifier gain, whilst those above 15 Hz were due to the flapping resonance, and possibly also to accelerometer cross-sensitivity in the case of the cross receptance measurements. The bump at 13 Hz was caused by a resonance of the chain supporting the shaker.

These dynamic measurements were obtained using forces of the order of 50N, and the preload applied by the nylon rope was of the same order. To examine the behaviour under higher loads, a static test was carried out in which normal loads were applied simultaneously to the two faces of the rubber block using large steel discs which sat in the "V". The deflection was measured with dial gauges. The resulting load/deflection curve is given in Fig. 14.13, and it clearly shows that the block becomes stiffer with increasing normal load. Whilst the dynamic forces transmitted from the engine are probably less than 50N, the static load due to the weight of the engine is very much larger, so the effective stiffness of the loaded block may be at least twice that of the unloaded block. The dynamic tests should ideally have been performed with representative amounts of preload applied to the block, but the lack of a hydraulic shaker precluded this. However, since this report is concerned primarily with the response of the unloaded seating, the effect of preload need not be considered here. Admittedly, the blocks are subjected to a small preload due to the weight of the transverse beam assembly, but this is probably not much greater than that applied by the nylon rope during the dynamic tests. If the seating analysis were later extended to include the effect of the engine, the results of the static test could of course be used to increase the stiffness of the linearised V-block model.

The static test also provides a good check on the receptance measurements: From the displacement/force law which has been fitted to the measured data in Fig.14.13, it is seen that for small loads the ratio $\frac{\delta}{F} = 0.574 \times 10^{-5} \text{ m/N}$, which compares quite well with the figure of about $0.5 \times 10^{-5} \text{ m/n}$ obtained from the receptance test for $\frac{x}{F_x}$. The slightly higher figure obtained in the static test is a consequence of two factors; (a) The normal load was applied 18mm above the centreline of the face, and (b) The load was applied by means of a disc which sat in the "V", so a small force μF^* was also applied down the face.

Using the measured receptances as a guide, and taking physically realistic dimensions for the model, the stiffnesses of the six basic members were judiciously guessed. By a process of trial and error, the dimensions and the stiffnesses were then adjusted to give the best possible agreement between the measured receptances and those given by the model. The final dimensions and stiffnesses are given in Figs. 14.9 and 14.14. respectively, and the corresponding zero frequency receptances given by the model are listed in Fig.14.15, together with the measured values. With the exception of $\frac{y}{F_y}$ and $\frac{\theta}{M_\theta}$, which are both approximately twice the measured figures, the agreement is quite reasonable, especially bearing in mind the complexity of the problem. This agreement was obtained after only two or three tries, and could not be improved upon, since any attempt to improve $\frac{y}{F_y}$ and $\frac{\theta}{M_\theta}$ had a detrimental effect upon the other receptances.

Since the shear modulus of rubber is known to increase slightly with frequency, the member stiffnesses were increased by 20% in progressing from 10 to 1000 Hz. It is interesting to note that the measured phase angles were best described with a loss factor of 0.1, whilst natural rubber only possesses a loss factor of about 0.025⁽⁹⁾. This tends to suggest that

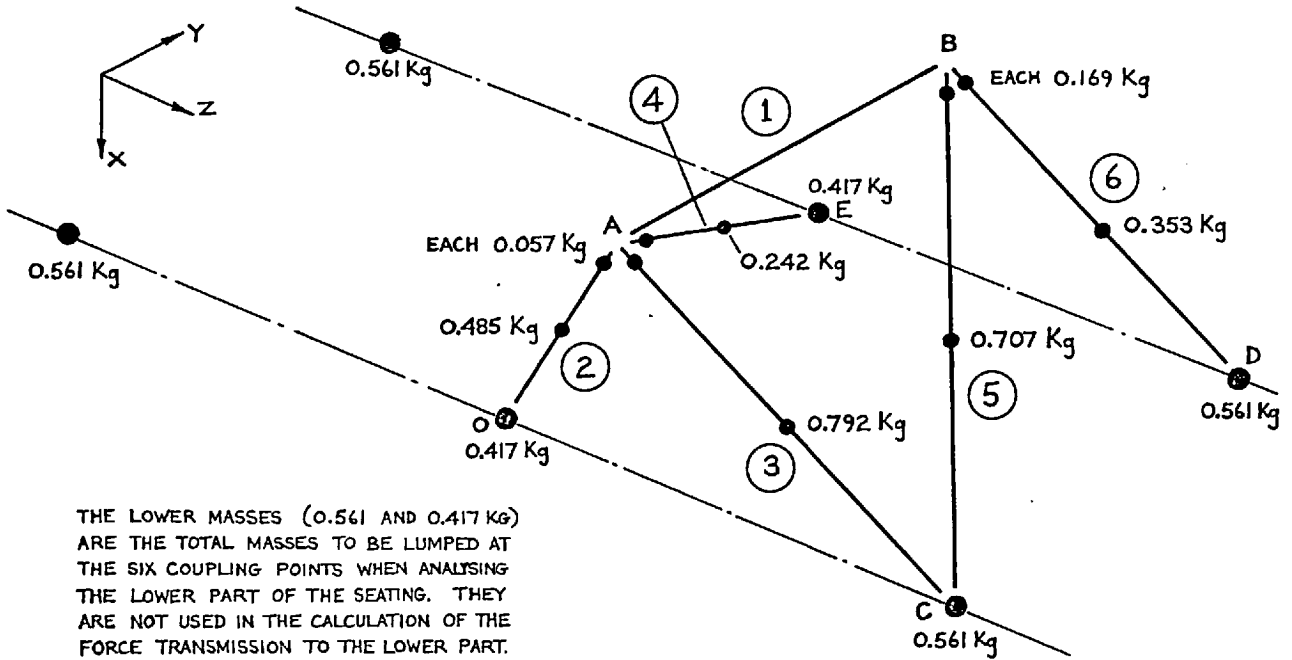
* μ = coefficient of friction between disc and plate on face of block.

MEMBER STIFFNESSES (N/m)

- $K_1 = 1.0 \times 10^6$
- $K_2 = 1.2 \times 10^5$
- $K_3 = 0.8 \times 10^5$
- $K_4 = 1.2 \times 10^5$
- $K_5 = 0.8 \times 10^5$
- $K_6 = 1.0 \times 10^5$

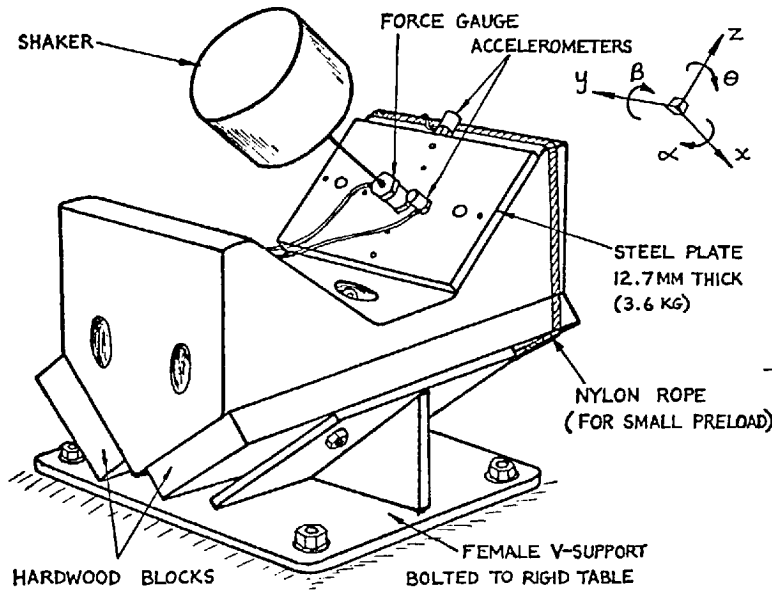
BALLOONED NUMBERS ARE REFERENCE NUMBERS OF THE BASIC MEMBERS OF THE RUBBER V-BLOCK MODEL

LOSS FACTOR, $\eta = 0.1$
FOR ALL SPRINGS



THE LOWER MASSES (0.561 AND 0.417 KG) ARE THE TOTAL MASSES TO BE LUMPED AT THE SIX COUPLING POINTS WHEN ANALYSING THE LOWER PART OF THE SEATING. THEY ARE NOT USED IN THE CALCULATION OF THE FORCE TRANSMISSION TO THE LOWER PART.

FIG. 14.14 LUMPED MASSES AND SPRING STIFFNESSES USED IN MODEL OF RUBBER V-BLOCK.



AVERAGE MEASURED RECEPTANCES

	MODULUS ($\frac{g}{UNITS}$)	PHASE ($^{\circ}$)
x/F_x	0.5×10^{-5}	-4
y/F_y	0.45×10^{-5}	-5
z/F_z	0.41×10^{-5}	-5
β/M_{β}	0.65×10^{-3}	-4
θ/M_{θ}	0.37×10^{-3}	-5.5
$z/F_x = x/F_z$	0.22×10^{-5}	-7

RECEPTANCES OF SPRING MODEL AT 0 HZ

x/F_x	0.48×10^{-5}	-5.7
y/F_y	0.80×10^{-5}	-5.7
z/F_z	0.36×10^{-5}	-5.7
β/M_{β}	0.79×10^{-3}	-5.7
θ/M_{θ}	0.79×10^{-3}	-5.7
$z/F_x = x/F_z$	0.25×10^{-5}	-5.7

FIG. 14.15 MEASUREMENT SETUP, MEASURED RECEPTANCES, AND RECEPTANCES GIVEN BY SPRING MODEL.

$$M_1 = M_A + \frac{1}{3}M_D$$

$$M_2 = M_B$$

$$M_3 = M_C + \frac{1}{2}M_F$$

$$M_4 = M_E$$

$$M_5 = M_I + \frac{1}{2}M_F$$

$$M_6 = M_H$$

$$M_7 = M_G + \frac{2}{3}M_D$$

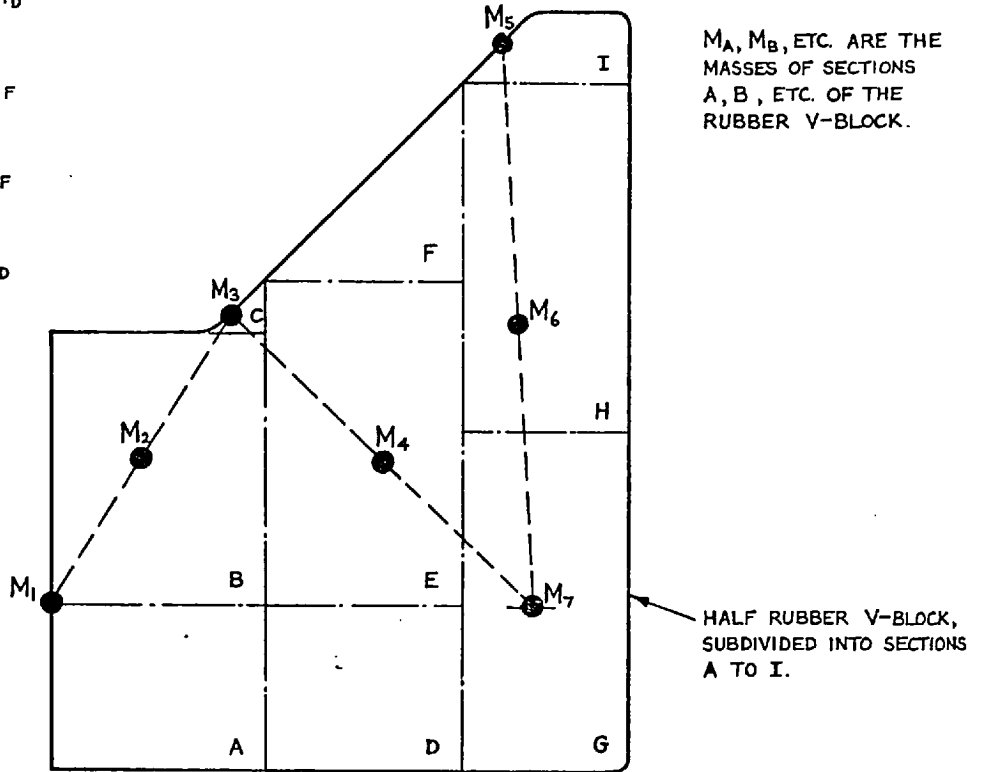


FIG. 14.16 INITIAL LUMPING OF MASS FOR RUBBER V-BLOCK MODEL

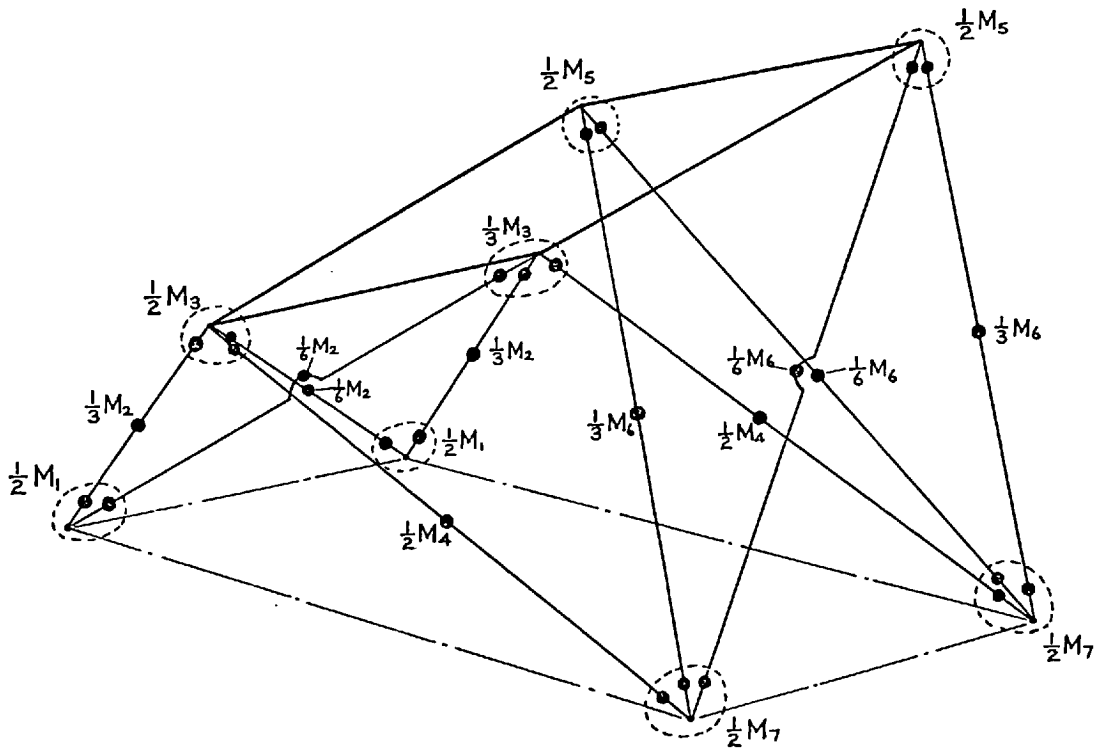


FIG. 14.17 LUMPING OF MASS AT NODES AND AT MID-POINTS OF MEMBERS

PREDICTED $\left(\frac{\text{NET TRANSMITTED FORCE IN X DIRECTION}}{\text{NET INPUT FORCE IN X DIRECTION}} \right)$ FOR RUBBER V-BLOCK RB2 WHEN INPUT TO SEATING IS $Q_0=1N$

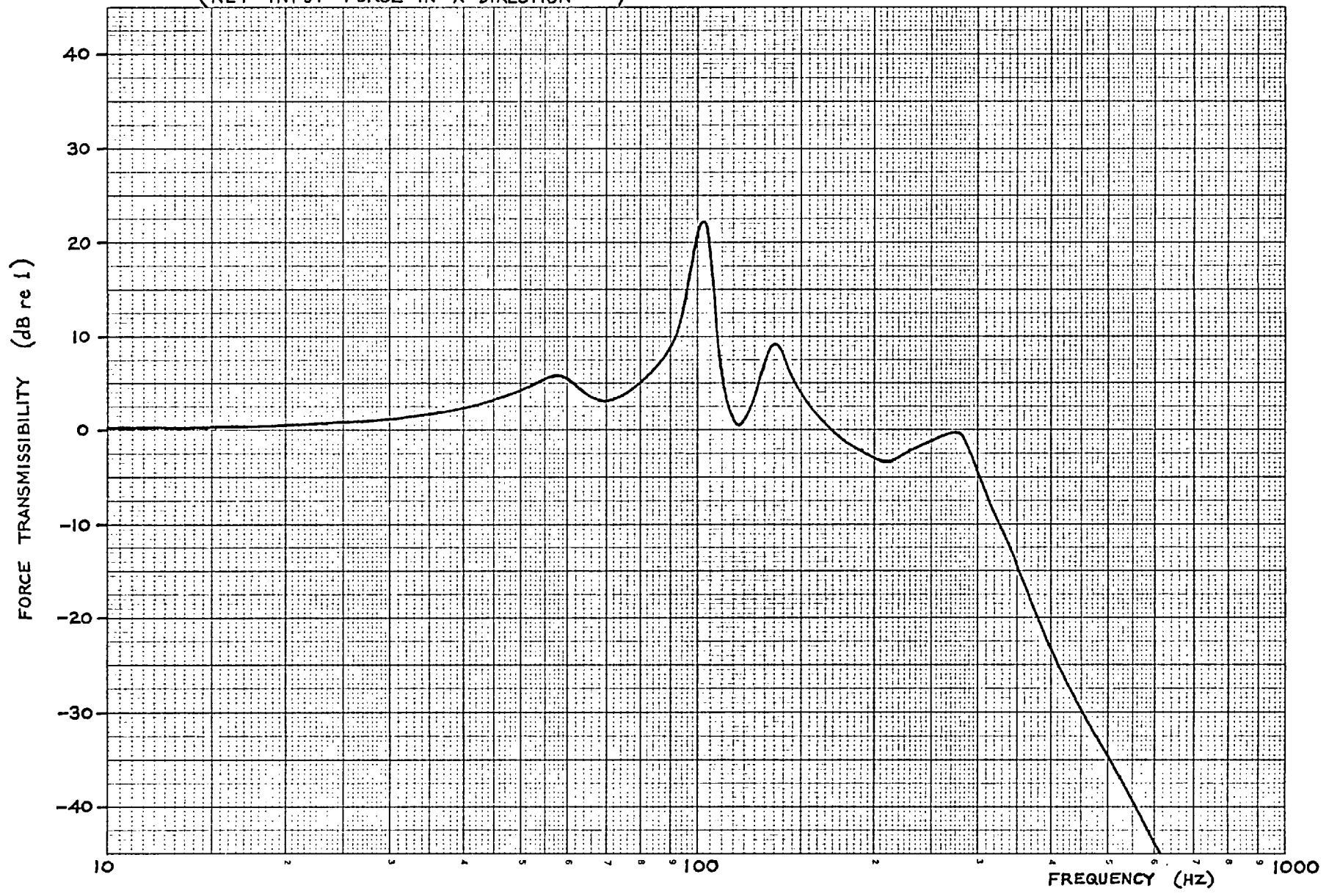


FIG 14.18

most of the damping arose from friction between the lower faces of the rubber block and the supporting surfaces, and not from within the block itself.

Having modelled the stiffness properties of the block, it was then necessary to consider the mass distribution and to lump suitable masses at the nodes of the spring model and at the mid-points of the members. Referring to Fig.14.16, the half block was first divided into nine sections A to I. The masses of these sections were calculated and proportions of these masses were then judiciously lumped at the seven points shown. The masses M_1 to M_7 were finally divided up across the width of the block, as shown in Fig.14.17. The resulting masses associated with the six basic members of the model are given in Fig.14.14. Following the procedure outlined in Appendix IX, the masses at the mid-points and upper ends of the members are combined with the member stiffnesses in order to form the point and transfer dynamic stiffness matrices for the block. Since it has been assumed that the six points of support for the model displace a negligible amount in comparison with the points on the upper faces, the six lower masses (0.561 and 0.417 Kg) are not used in the calculation of the dynamic stiffnesses. However, when analysing the lower part of the seating, these masses are concentrated at the six points of force input on the lower sandwich beams.

Although necessarily very approximate, and unsubstantiated by measurements, this fairly arbitrary lumping of mass does give block resonances at the right sort of frequencies, as will now be demonstrated by considering basic wave theory. It is well known that any elastic body exhibits wave effects when the excitation frequency is such that the resulting elastic waves passing through the body have half wavelengths, or multiples thereof, which are comparable with the dimensions of the body. If we consider the classical problem of a uniform long rod of length l , the natural frequencies of axial vibration are given by $f_n = \frac{nkC_0}{2l}$, where $n = 1, 2, \dots$, the factor $k = 1$, and the "long rod wave velocity" $C_0 = \sqrt{\frac{E}{\rho}}$. However, Davies (10)

has shown that if the cross sectional dimensions of the rod are comparable with its length, and Poisson's Ratio $\nu = 0.29$, then the factor $k \approx 0.58$. Since the wave velocity kC_0 is a function of the coupling between motion along the axis and motion at right angles to it, the virtual incompressibility of rubber may give rise to an even lower value of k . If we now consider Fig.14.9, we see that a typical path length l for the V-block is about 150 mm (e.g. centre of face down to region of point C). Assuming $k=0.58$, this gives a natural frequency of 95 Hz. We may next refer to Fig.14.13, which shows the computed vertical force transmissibility across the block when it is mounted in the seating and a vertical force is applied to the top of the seating. Due to the multi-directional nature of the seating, the transmitted force also comprises components due to inputs to the block in the horizontal directions Y and Z, but this is immaterial in the present discussion. The important thing is the prediction of internal resonances at relatively low frequencies, and in the same sort of frequency range as one would expect from basic wave theory. Another point of interest is the rather rapid drop-off in transmissibility above 300 Hz. This is a consequence of the limited number of masses into which the block has been divided, and it is unlikely that the actual block would exhibit such a marked decrease in transmissibility.

The combined use of measurement and theory has led to a successful representation of the rubber V-block in all its aspects. However, it now appears that the finite element method may be successfully applied to the analysis of such a block; at least for determining the stiffness under zero preload. Following the recent development of a suitable volume finite element computer programme by S. Ioannides of the Dynamics Group, a trial calculation has been performed on the rubber block, and using a 200 degree of freedom model for half of the block, the computed $\frac{x}{F_x}$ receptance was found to be about 30% of the measured value. The fact that the computed figure was low is not surprising, since it was observed that the actual block did not sit snugly in the supporting "V", and this was not allowed

for in the analysis. In addition, one cannot be absolutely sure of the material properties. It therefore appears that the finite element method may be considered in any future analysis of a complex-shaped rubber block, provided that preload is not important. However, the behaviour under large loads is very non-linear, and the analysis becomes far more complex⁽¹¹⁾. For other than very simple shapes the analysis should certainly be checked against measurements wherever possible.

14.3 MALE V-PIECE (Component VB)

The V-piece is shown in Figs.14.19 and 14.20. It is built up from thick steel plate, and comprises a top plate and two triangular plates which are welded to it. On the faces of the "V" are the 3.5mm PVC pads which separate it from the cross beams. The complete assembly weighs 16.7 Kg. To avoid further complicating the seating analysis, the steel V-piece plus the pads have been considered as a single component. These parts have been analysed separately and coupled together at the subsystem stage, in order to yield a 16 x 16 dynamic stiffness matrix for the component. This matrix relates the four forces at point P and the six forces at each of the assumed coupling points A and B to the corresponding displacements. The co-ordinates have been given in Fig.13.7, and they may also be found in Appendix X, along with full details of the analysis. It should be noted that points A and B are only fictitious coupling points, since they lie half-way between the actual physical coupling points on the inclined faces of the triangular plates (see Fig.14.20).

In view of its fairly stiff construction, and the way in which forces are applied to its top face, the steel V-piece has been idealised as a rigid body with six-directional inertial properties. Since the mobility measurements on the seating were carried out with a vertical force applied directly over the top of one of the triangular plates (see Fig.14.19), one can be fairly sure that the actual V-piece remained essentially rigid during the tests. Also, when an engine is mounted on the seating, the engine mount which is bolted to the V-piece should further stiffen it. As final proof of the rigid body behaviour, we may refer to Fig.14.21, which shows the results of a point mobility test on a freely suspended V-piece. These results also provide a check on the calculated figures for the mass and for the moment of inertia about the Z axis, since the theoretical response is a function of these two quantities.

The PVC pads on the two inclined faces have been represented as hysteretically damped springs (linear and rotational), concentrated at the assumed coupling points A and B, and the spring stiffnesses have been calculated using simple theory. However, the compressive stiffness of a firmly held rubber pad is also affected by the bulging restraint imposed by the metal surfaces between which it is sandwiched. This has been taken account of by replacing Young's Modulus E by a Compression Modulus E_c , which is a function of the Shape Factor ⁽¹²⁾ of the pad. The PVC properties are the same as those used in the sandwich beam analysis, and the damping has been introduced by making E and G complex.

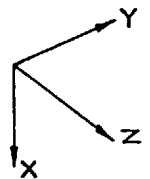
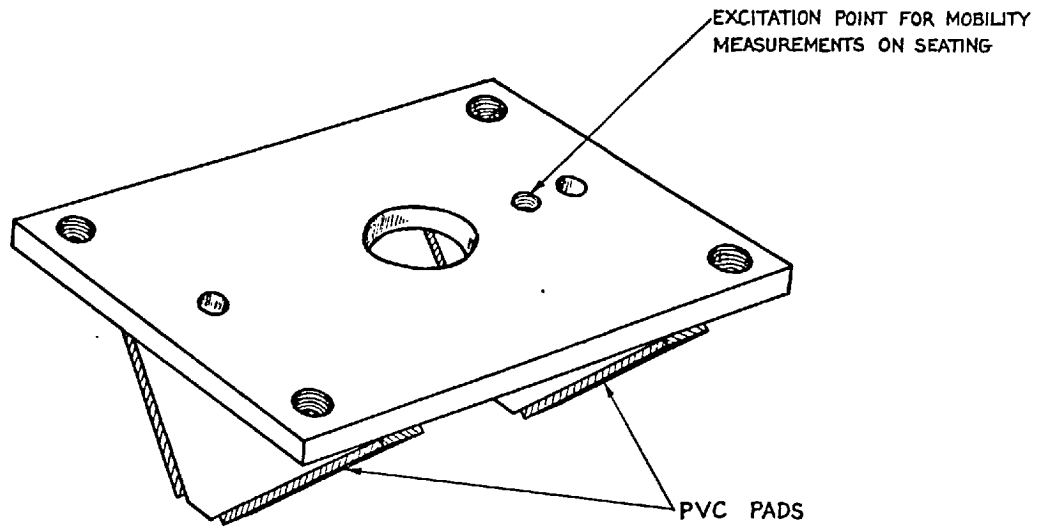
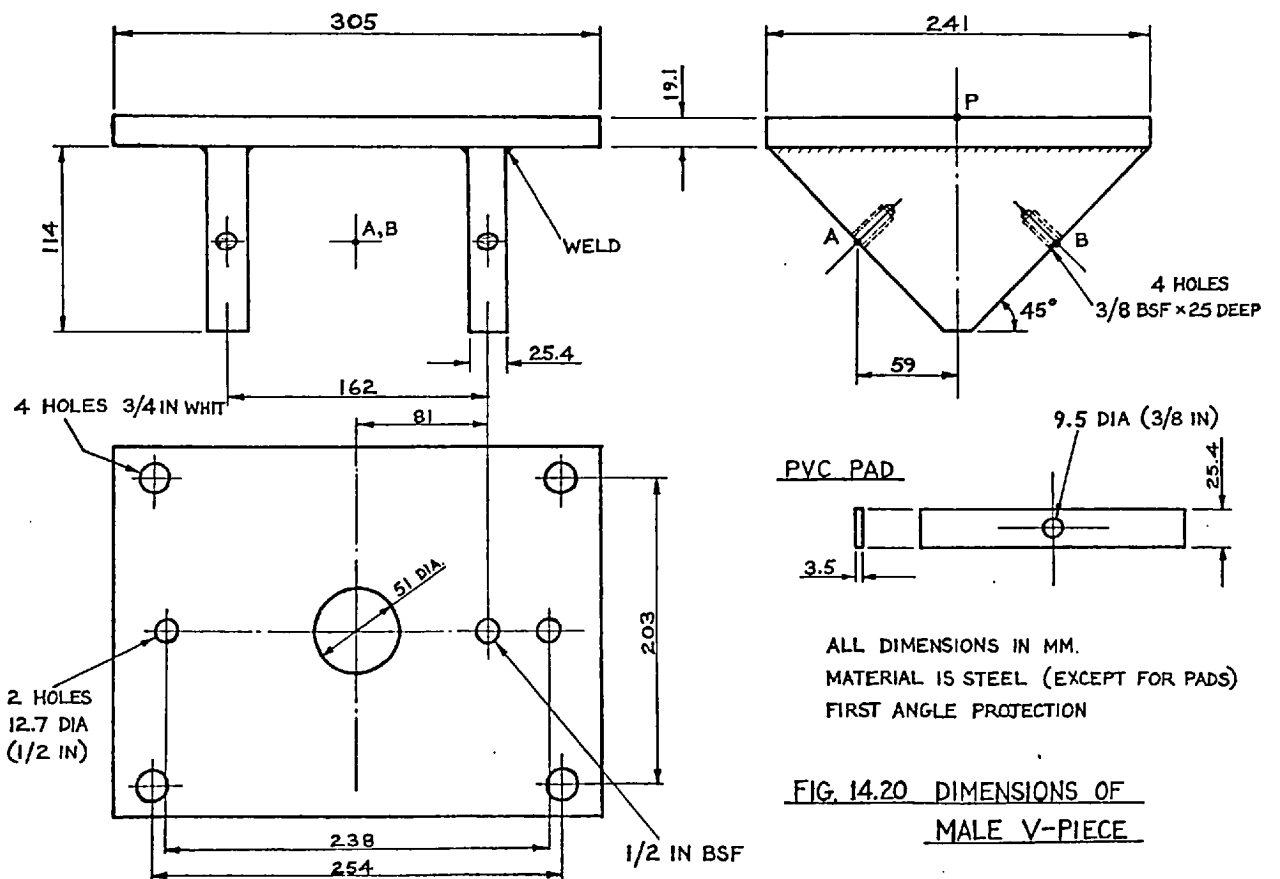


FIG. 14.19 MALE V-PIECE (VB)



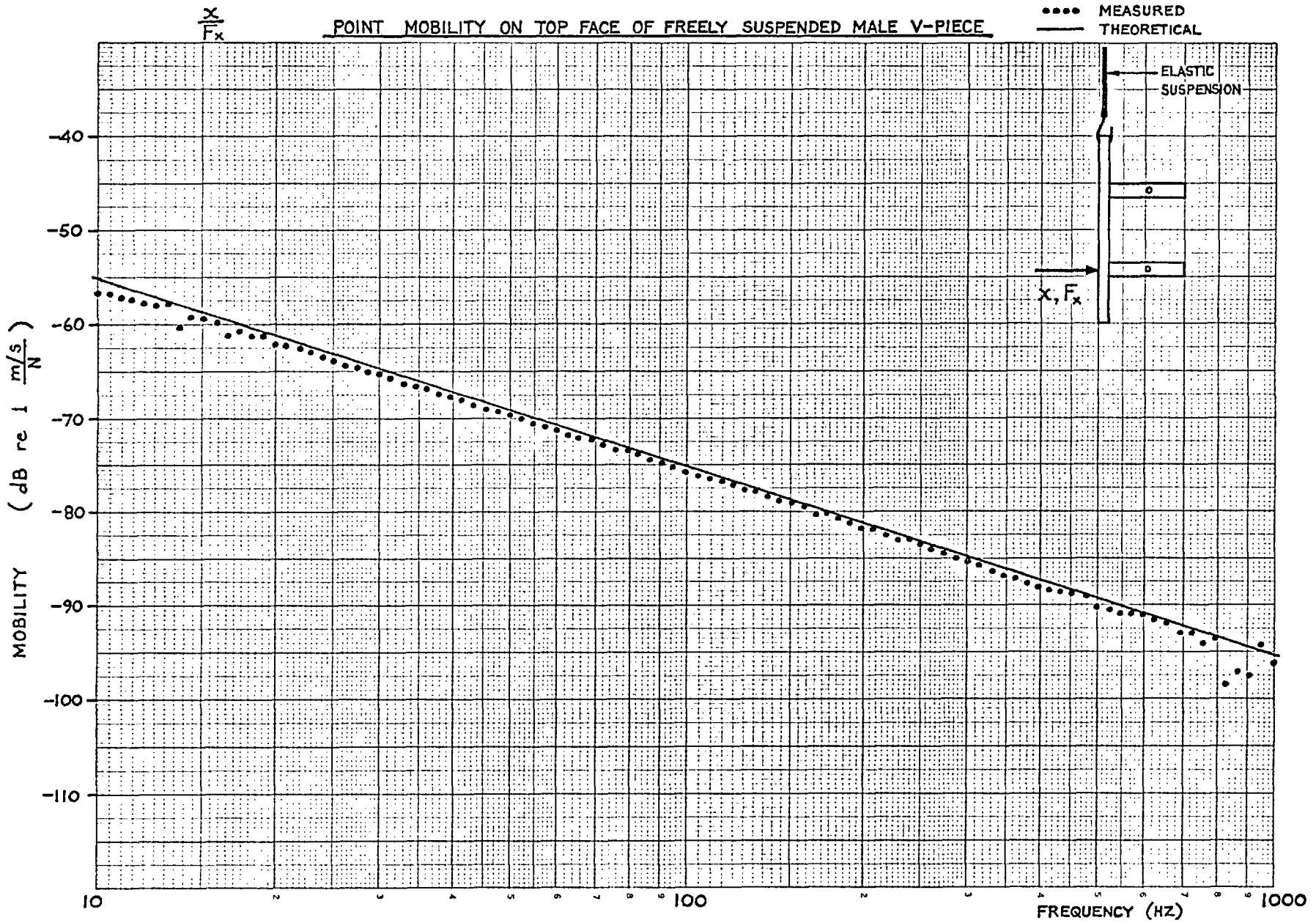


FIG 14.21

14.4 FEMALE V-SUPPORT (Component VS)

The V-support is shown in Figs. 14.22 and 14.23. It is fabricated from 9.5mm steel plate, and consists of five steel parts which are welded together, plus two 3.5mm PVC facing pads. The latter separate the upper faces of the steel support from the longitudinal beams which lie in the "V". The complete assembly weighs 13.5 Kg. In the same way as for the Male V-piece, the steel V-support plus the pads have been considered as a single component, and the analytical coupling together of these parts has been carried out at the subsystem stage. The resulting 18 x 18 dynamic stiffness matrix relates the six forces at each of the coupling points A, B and C to the corresponding displacements. Full details of the component analysis are given in Appendix XI.

Since the steel V-support appears relatively stiff, it has been idealised as a rigid body with six-directional inertial properties. When the longitudinal beams are bolted to the face plates, they effectively prevent any bending distortion, and the only obvious flexibility is in torsion of the faces about their supporting gusset plates. The torsional stiffness of a face has therefore been calculated approximately ($K_{\beta} \simeq 1.4 \times 10^6 \text{ N-m/rad.}$)
Face and this has been combined with the corresponding rotational stiffness of the attached PVC pad. As regards the base plate, since it is bolted down to the thick top plate of the cruciform by 19mm ($\frac{3}{4}$ in) bolts, its bending flexibility in situ would appear to be minimal, and it will be neglected for the present. However, it should be mentioned at this stage that the assumption of a rigid base plate has subsequently been found to be invalid, and this will be discussed in detail in section 14.6. For reasons there outlined, the base plate stiffness will be considered in conjunction with the cruciform stiffness, so it need not enter into the analysis of the V-support.

The PVC pads have been represented as hysteretically damped springs (linear and rotational), concentrated at the assumed coupling points at the centre of each of the face plates, and the spring stiffnesses have been calculated using simple elasticity theory. As a consequence of face plate

distortion caused by the welding, the pads are not sandwiched very tightly between the steel V-support and the longitudinal beams, so it seemed valid to ignore the effect of bulging restraint on the compressive stiffness of the pads (i.e. stiffness term which is a function of shape factor ⁽¹²⁾). The PVC properties are the same as those used in the sandwich beam analysis, and the damping has been introduced by making E and G complex.

PVC FACING PADS

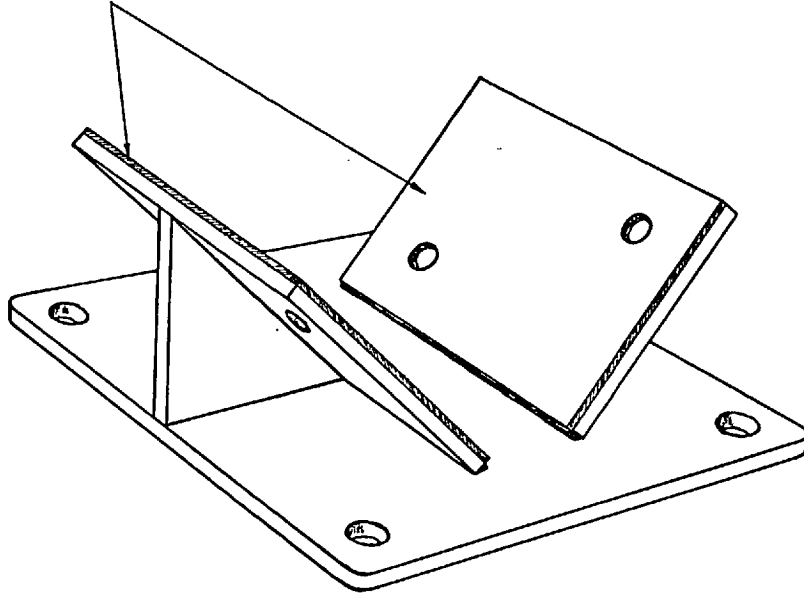
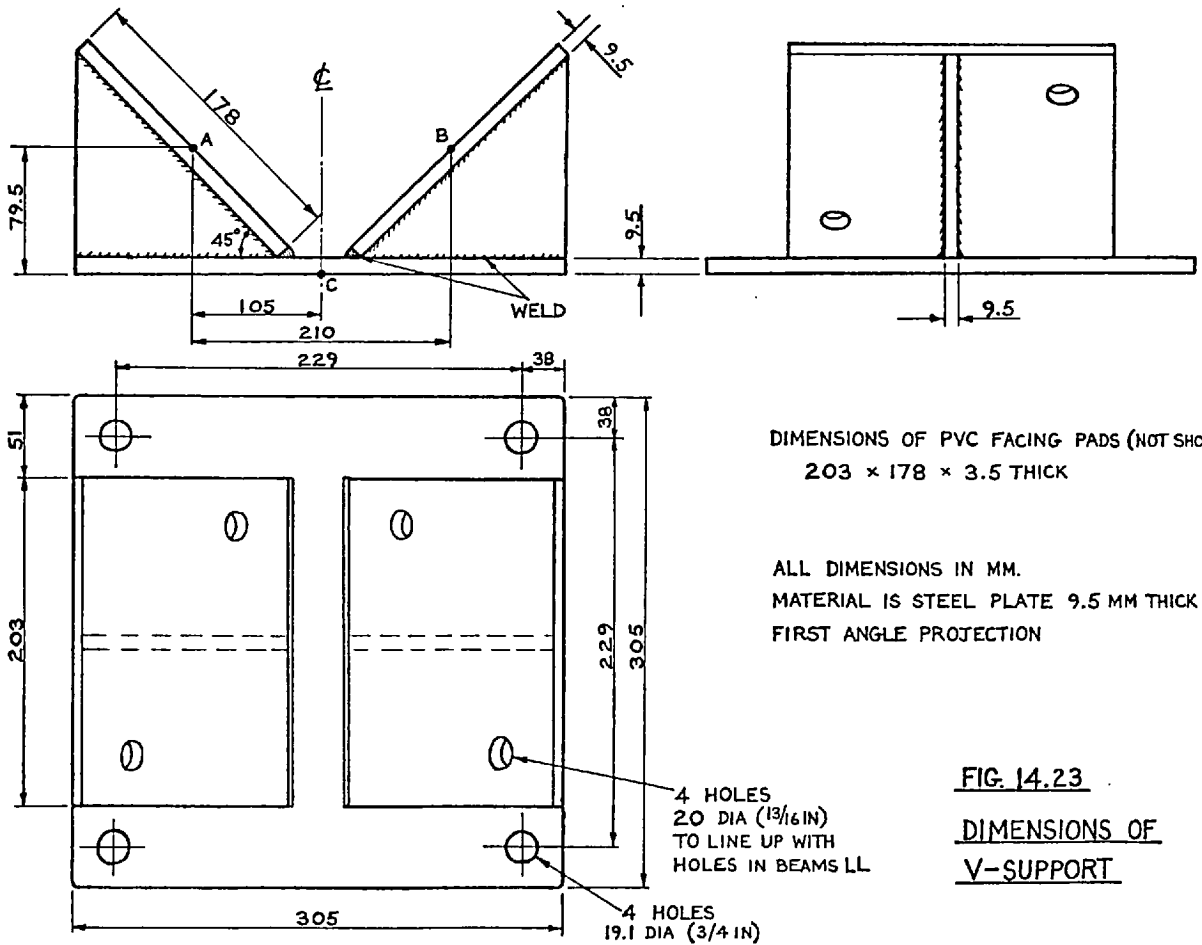


FIG. 14.22 V-SUPPORT (VS)



14.5 CRUCIFORM (Component CR)

The four nominally identical cruciforms were fabricated from 19mm steel plate, and as is seen from Fig.14.24, each comprises a 305mm square top plate which is welded to web plates arranged in the form of a cross. This assembly is welded to the steel supporting structure. As was stated in the Introduction, transfer mobility measurements between two cruciforms have shown that the dynamic coupling between them is relatively small, so we may justifiably assume the cruciforms to be uncoupled for the purposes of the present seating analysis. Therefore, we may now confine our attention to the dynamics of a single cruciform, which we shall choose to be cruciform 2.

Due to the complex nature of the cruciform and of the surrounding steel structure, no attempt has been made to predict its mobility properties theoretically. However, it is possible that if the mobility on the cruciform top plate is little influenced by the surrounding structure, then one might be able to obtain sufficiently accurate data from a finite element analysis of the cruciform alone, assuming it to be attached to a rigid supporting structure. As yet, this has not been investigated, and anyway it would require experimental verification. Hence it was decided to obtain the necessary data by measurement.

Since all the work described herein assumes single-point coupling between components, it was necessary to measure the complete multi-directional mobility matrix pertaining to the assumed coupling point P at the centre of the cruciform top plate. This 6 x 6 matrix relates the 3 translational and 3 rotational motions to the corresponding forces and couples, and may be measured using the special techniques developed in Part 2 of this report. Due to externally imposed limitations on testing time, it was decided to use a twin-shaker unit in conjunction with a conventional analogue impedance measuring system. This permitted the direct measurement of the elements of the mobility matrix, without the need for on-line processing of the data, and the slow frequency sweep only lasted about 4 minutes, so setting-up time

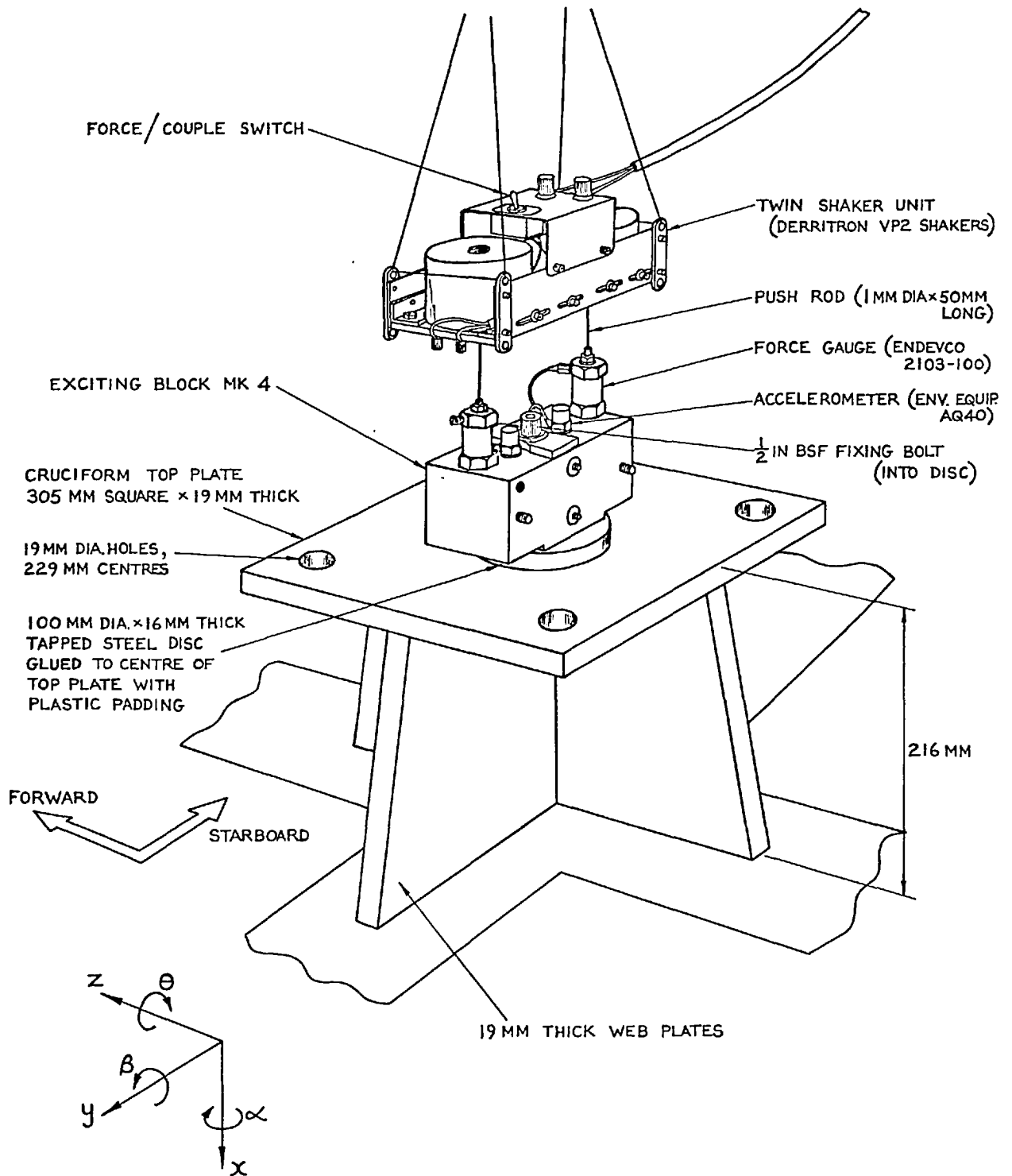


FIG. 14.24 FORWARD STARBOARD CRUCIFORM (2)

(WITH EXCITING BLOCK AND TWIN SHAKER IN POSITION FOR MOBILITY MEASUREMENTS)

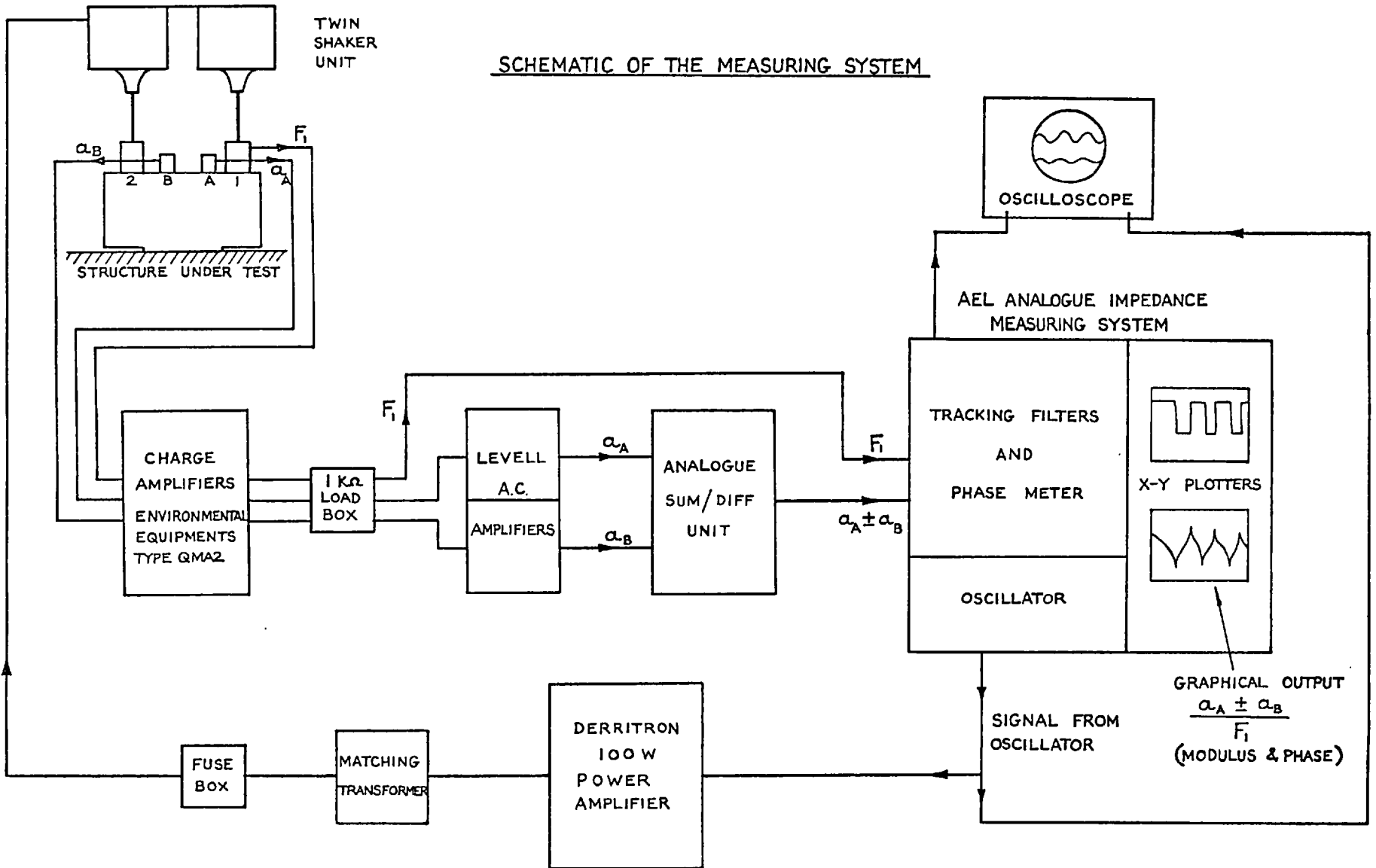


FIG 14.25

MEASURED INERTIANCE MATRIX RELATING TO CENTRE OF GRAVITY G OF EXCITING BLOCK ATTACHED TO CENTRE OF CRUCIFORM TOP PLATE

$$\begin{Bmatrix} \ddot{x} \\ \ddot{y} \\ \ddot{z} \\ \ddot{\alpha} \\ \ddot{\beta} \\ \ddot{\theta} \end{Bmatrix}_G = \begin{bmatrix} \frac{\ddot{x}}{F_x} & & & & & \\ & \frac{\ddot{y}}{F_y} & & & & \\ & & \frac{\ddot{z}}{F_z} & & & \\ & & & \frac{\ddot{\alpha}}{M_\alpha} & & \\ & & & & \frac{\ddot{\beta}}{M_\beta} & \\ & & & & & \frac{\ddot{\theta}}{M_\theta} \end{bmatrix} \begin{Bmatrix} F_x \\ F_y \\ F_z \\ M_\alpha \\ M_\beta \\ M_\theta \end{Bmatrix}_G$$

$\{ \ddot{\delta} \}_G = [I_m] \{ F \}_G$

ELEMENTS H, I, N, S, T NOT MEASURED, BUT SMALL. SET TO $-99 \text{ dB } / 0^\circ$

DISPLACEMENT TRANSFORMATION FROM G TO POINT P ON SURFACE OF CRUCIFORM

$$\begin{Bmatrix} x \\ y \\ z \\ \alpha \\ \beta \\ \theta \end{Bmatrix}_P = \begin{bmatrix} 1 & 0 & 0 & 0 & 0 & 0 \\ 0 & 1 & 0 & 0 & 0 & h \\ 0 & 0 & 1 & 0 & -h & 0 \\ 0 & 0 & 0 & 1 & 0 & 0 \\ 0 & 0 & 0 & 0 & 1 & 0 \\ 0 & 0 & 0 & 0 & 0 & 1 \end{bmatrix} \begin{Bmatrix} x \\ y \\ z \\ \alpha \\ \beta \\ \theta \end{Bmatrix}_G$$

$\{ \delta \}_P = [T_{PG}] \{ \delta \}_G$

POINT G IS A DISTANCE $h = 50 \text{ MM}$ ABOVE POINT P

DYNAMIC STIFFNESS RELATION FOR POINT P ON CRUCIFORM

$$\{ F \}_P = \left(-\frac{1}{\omega^2} [T_{PG}] [I_m] [T_{PG}]^T \right)^{-1} \{ \delta \}_P$$

NOTE THAT THE MATRIX WITHIN THE PARENTHESES () IS THE CRUCIFORM RECEPTANCE MATRIX

FIG. 14.26 THE 6 x 6 DYNAMIC STIFFNESS MATRIX FOR THE CRUCIFORM

usually exceeded actual measurement time. However, no digital output was available with this system, so the mobility data could only be collected as plots of modulus and phase angle versus frequency.

Referring once again to Fig.14.24, we see an aluminium exciting block attached to the centre of the cruciform top plate, and above this is the twin-shaker unit. This unit comprises a pair of small shakers connected electrically in series, and each capable of delivering up to about 10N thrust. Since the two shakers are nominally identical and the same current passes through both, they each deliver approximately the same force, and by reversing the direction of current flow through one of them, they will either run in phase to apply a pure force to the block, or out of phase to apply a couple. It is only necessary to measure the force input from one shaker, whilst the response is obtained as the sum or difference of the signals from two accelerometers, depending on whether translational or rotational response is being measured. A schematic diagram of the complete measuring system is shown in Fig.14.25. For more information on multi-directional measurements using a twin shaker, the reader is referred to Part 2 of this report, and particularly to Appendix IV, which describes in detail some test measurements made with precisely the same exciting block and transducers as were used for these cruciform tests.

It will be observed that the exciting block was not attached directly to the cruciform. Instead, a 100 mm dia. x 16 mm thick steel disc was first stuck down using Plastic Padding adhesive, and the block was then bolted down onto the ground upper face of the disc using a 12.7 mm high tensile steel bolt ($\frac{1}{2}$ inch BSF). A thin film of Plastic Padding was also interposed between the block and the disc, so as to ensure an absolutely solid joint. This arrangement obviated the need for attachment holes in the cruciform, and it also simplified re-orientation of the exciting block for measurements in another plane. When it was necessary to rotate the exciting block axis through 90° , the fixing bolt was removed and a sharp tap then separated the block from the disc (which remained attached to the cruciform). After gently scraping the mating surfaces

and applying a thin film of Plastic Padding, the block was bolted down in the new position.

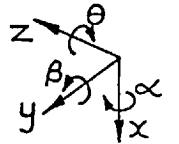
The matrix which was measured is shown in Fig.14.26. It will be observed that inertiances were obtained, rather than mobilities, but this was only due to limitations in the integrating amplifiers of the analogue measuring equipment. Due to symmetry, only 21 of the 36 elements are unique, and also 5 of the off-diagonal elements were obviously very small in the present case, so only 16 inertiances were actually measured. The complete sequence of tests for obtaining these data is shown in Fig.14.27. Each test gave either the acceleration sum or difference divided by the force measured by gauge 1, and the curves were subsequently scaled to give the required inertiance properties.

From the table it is clearly seen that the resultant of a horizontal pure force input acts through the exciting block centre of gravity G, and not along the surface of the cruciform. Similarly, horizontal acceleration measurements also correspond to the same point. Thus, the measured inertiance matrix relates to the block centre of gravity, and not to the point P immediately below it on the cruciform top plate. Since point G was only 50 mm above point P, the effect has been found to be relatively small. However, a correction may be applied using the transformation matrix $[T_{PG}]$ of Fig.14.26, provided that one is able to express the measured data in a numerical form. Since the data is ultimately required in such a form for inclusion in the seating analysis, it was decided to apply this correction after digitisation of the graphical data.

The curves pertaining to element A of the matrix are shown in Fig.14.28, but for the complete set of measured data the reader should consult reference (13). Studying both the modulus and phase plots, it is clearly seen that the vertical point inertiance is approximately spring-like over the frequency range 35 to 150 Hz, but outside this range it deviates considerably from a spring-like behaviour. Similarly, the other 15 measured responses fail to exhibit exclusively spring-, damper- or mass-like characteristics, especially in the

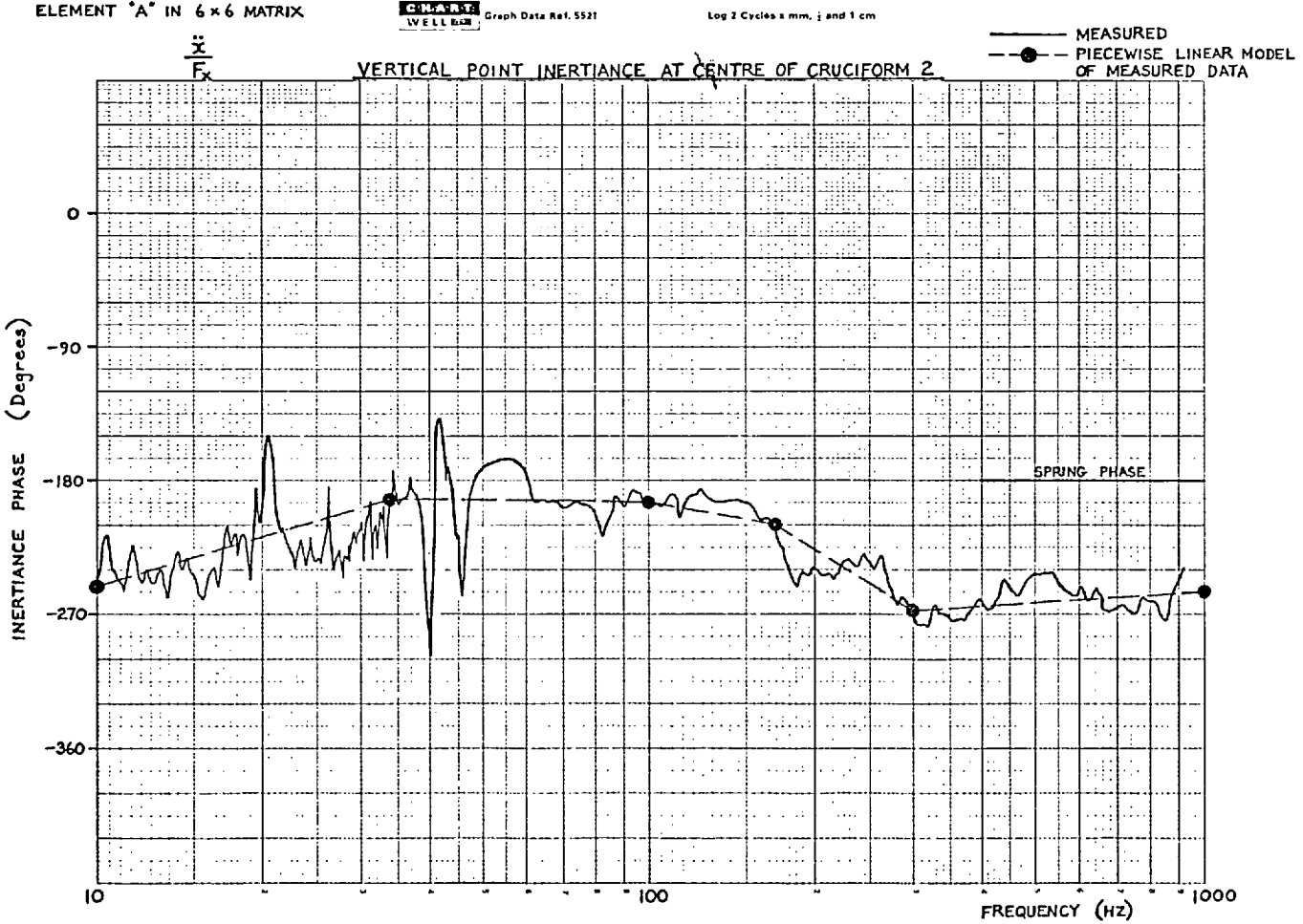
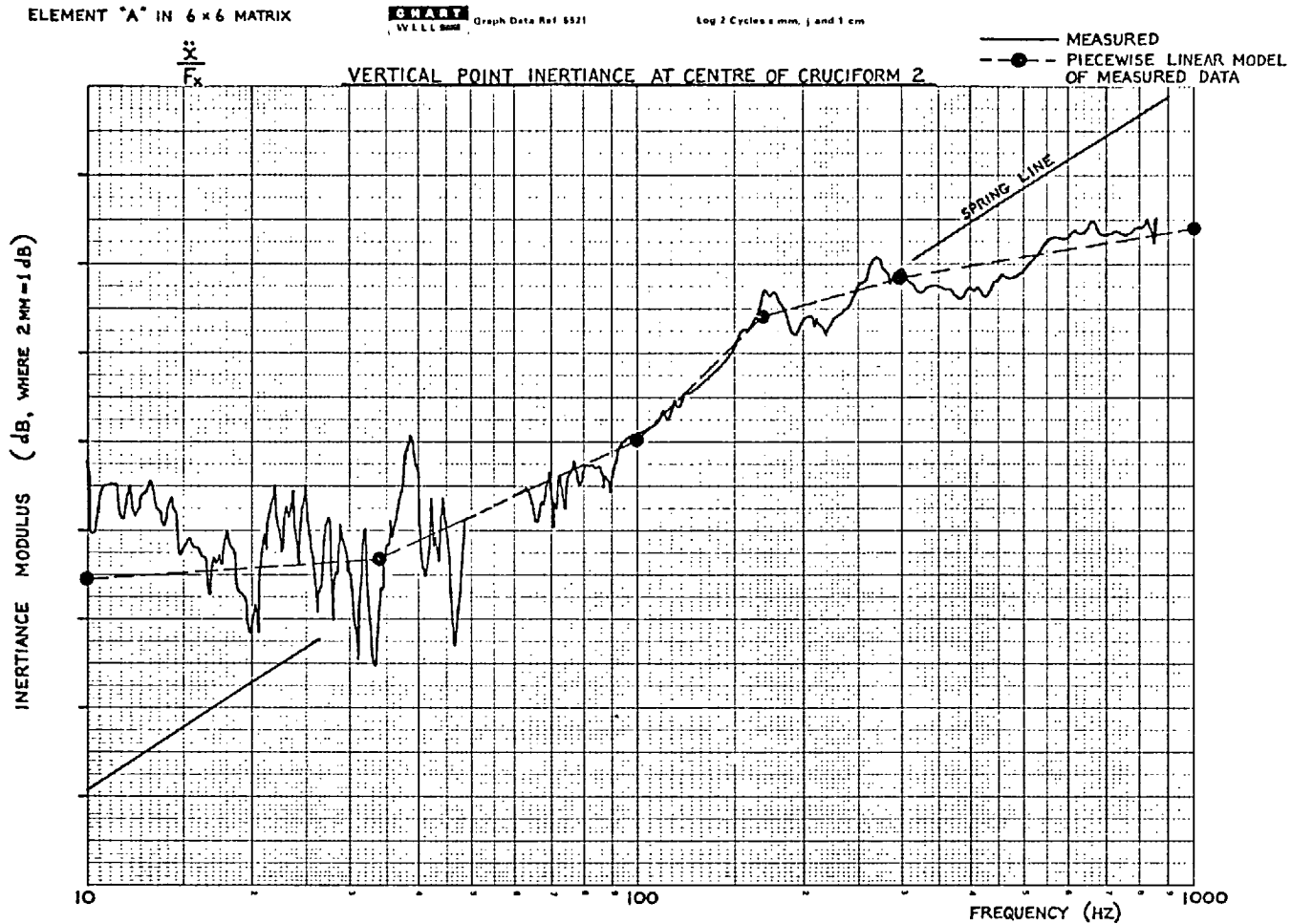
FIG. 14.27 EXCITATION ARRANGEMENTS AND RESPONSE MEASUREMENT POSITIONS USED FOR TWIN SHAKER TESTS ON CRUCIFORM

(TESTS CARRIED OUT IN ORDER SHOWN, LEFT TO RIGHT, TOP TO BOTTOM)



$\frac{\ddot{x}}{F_x}$ R=ACCEL. A (RED) B=ACCEL. B (BLUE) A FORCE ACCEL. SUM (R+B)	$\frac{\ddot{\theta}}{F_x}$ P FORCE ACCEL. DIFF.(R-B)	$\frac{\ddot{\theta}}{M_\theta}$ U COUPLE ACCEL. DIFF.	$\frac{\ddot{x}}{F_x}$ G FORCE ACCEL. DIFF.
$\frac{\ddot{y}}{F_x}$ B FORCE ACCEL. SUM	$\frac{\ddot{z}}{F_x}$ D FORCE ACCEL. SUM	$\frac{\ddot{\beta}}{F_x}$ K FORCE ACCEL. DIFF.	$\frac{\ddot{\theta}}{F_z}$ R FORCE ACCEL. DIFF.
$\frac{\ddot{z}}{F_z}$ F FORCE ACCEL. SUM	$\frac{\ddot{\beta}}{F_z}$ M FORCE ACCEL. DIFF.	$\frac{\ddot{y}}{F_y}$ C FORCE ACCEL. SUM	$\frac{\ddot{\theta}}{F_y}$ Q FORCE -ACCEL. DIFF.
$\frac{\ddot{z}}{F_y}$ E FORCE -ACCEL. SUM	$\frac{\ddot{\alpha}}{M_\alpha}$ J COUPLE ACCEL. DIFF.	$\frac{\ddot{\beta}}{F_y}$ L FORCE ACCEL. DIFF.	$\frac{\ddot{\theta}}{M_\beta}$ O COUPLE ACCEL. DIFF.

FIG 14.28



case of the cross inertiances. Another observation to be made from Fig.14.28 is the lack of any sharp resonances or anti-resonances. The same has been found to hold for the other curves, and as a consequence it was decided to mathematically model the measured data by representing each response curve by 5 straight line segments, in the manner indicated by the dashed line in Fig.14.28. This has permitted a more accurate representation of the data than could be obtained using single straight lines such as spring lines, whilst at the same time the amount of data to be stored is minimal in comparison with what would have been required if the curves had been digitised at small frequency intervals so as to describe every little detail. From the stored data at the 6 frequencies, one may easily compute the inertia modulus and phase corresponding to any intermediate frequency. All the measured responses have been modelled in this way, whilst the 5 unmeasured responses H, I, N, S and T have each been set to $-99 \text{ dB} / \underline{0}^\circ$, this being smaller than any of the measurements. With this numerical representation of the measured data, it is quite easy to set up the complete 6 x 6 inertia matrix $[I_m]$ at any frequency, and to transform from the exciting block centre of gravity G to the cruciform surface P using the transformation matrix $[T_{PG}]$. The 6 x 6 dynamic stiffness matrix $[Z_{CR2}]$ is obtained in terms of these two matrices in the manner indicated in Fig.14.26.

In the present analysis we are only concerned with cruciforms 2 and 3, which support the starboard longitudinal beam assembly. Since these are assumed to be identical and uncoupled, the required dynamic stiffness relation for the two cruciforms is

$$\begin{array}{c} \left[\begin{array}{c} F_{CR2} \\ F_{CR3} \end{array} \right] \\ 12 \times 1 \end{array} = \begin{array}{c} \left[\begin{array}{c|c} Z_{CR2} & 0 \\ \hline 0 & Z_{CR2} \end{array} \right] \\ 12 \times 12 \end{array} \begin{array}{c} \left[\begin{array}{c} \delta_{CR2} \\ \delta_{CR3} \end{array} \right] \\ 12 \times 1 \end{array}$$

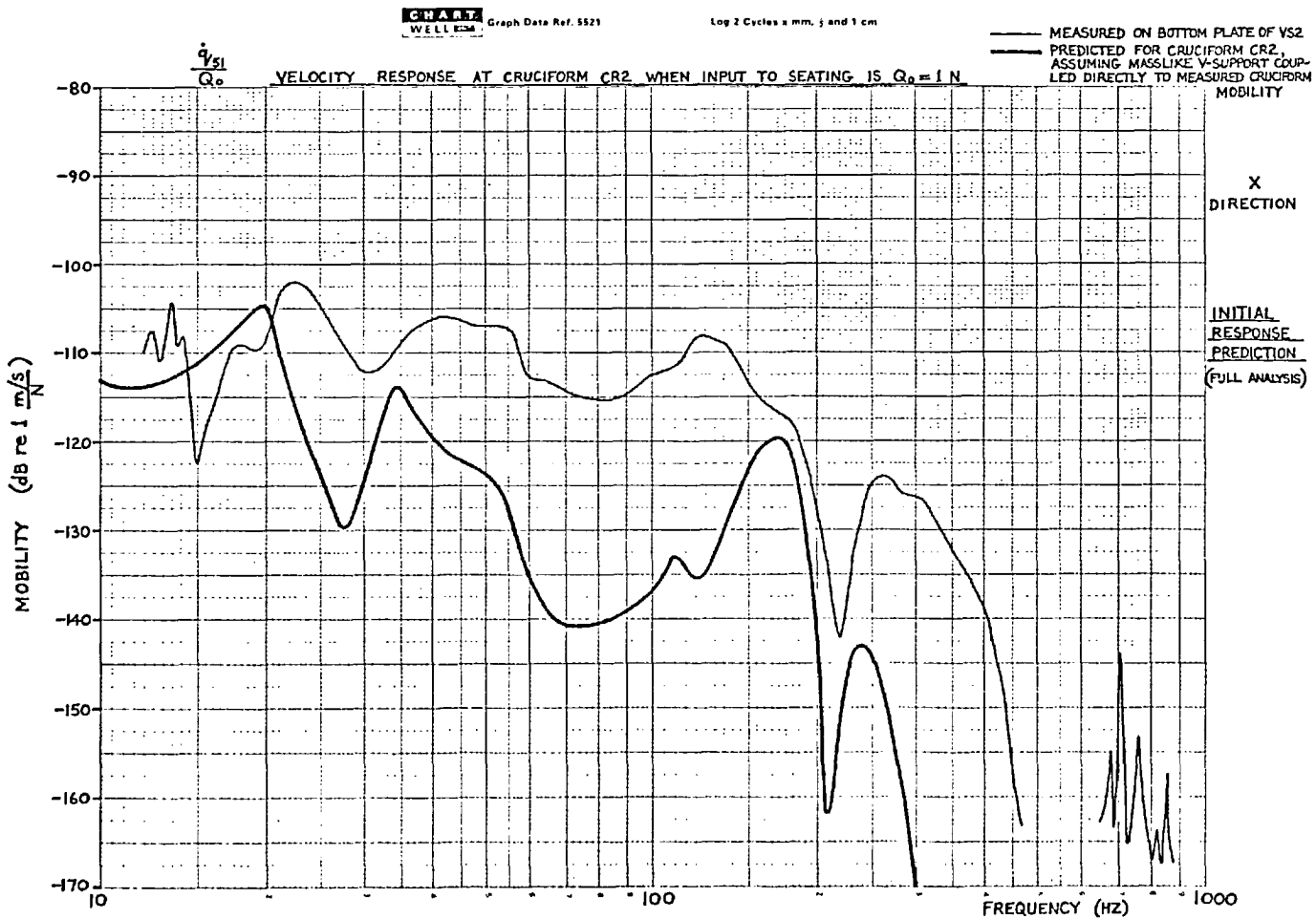
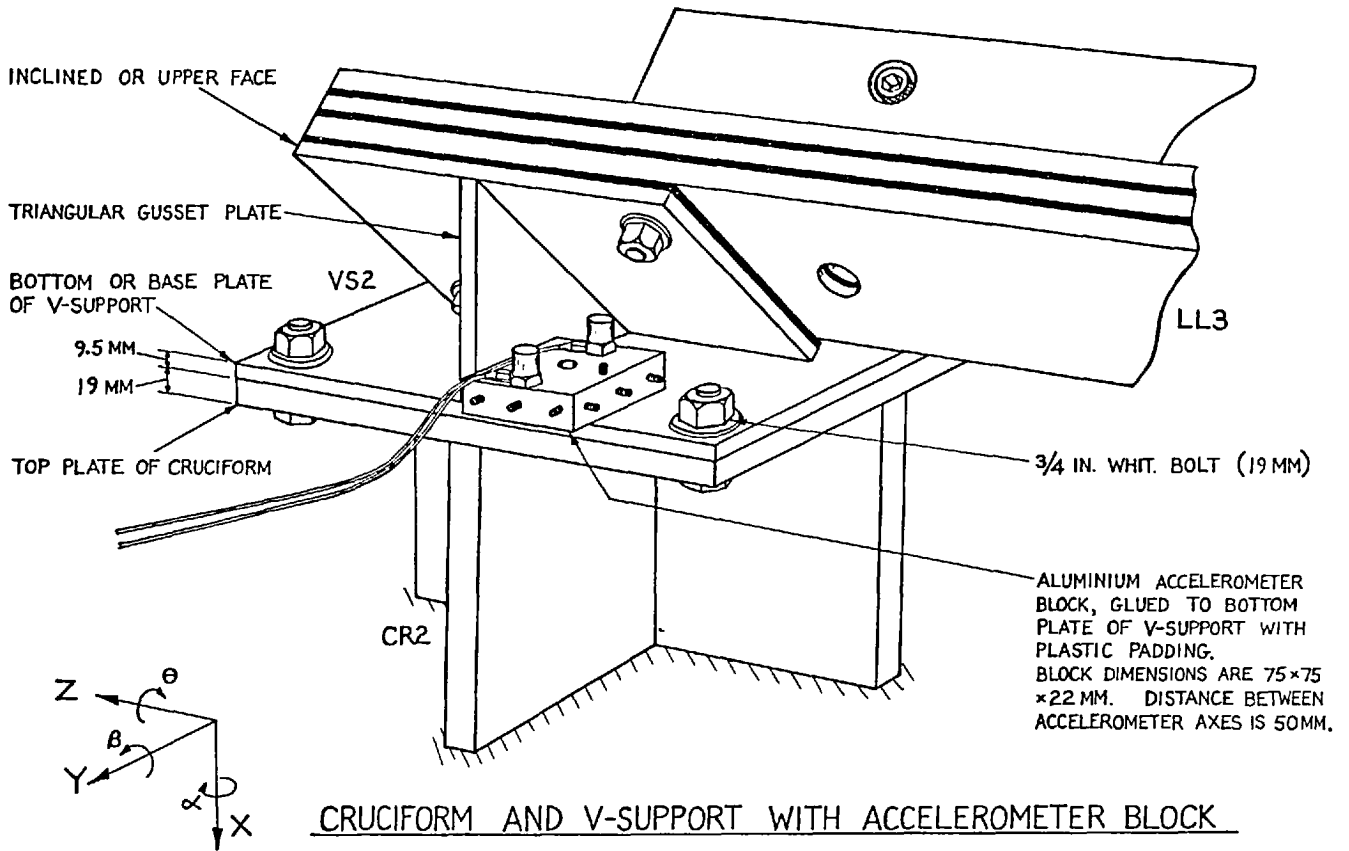
The computer subroutine for generating the dynamic stiffness matrix is listed in reference (13).

14.6 STIFFNESS OF THE V-SUPPORT/CRUCIFORM INTERFACE

In deriving the dynamic stiffness of the V-Support, it was assumed that this component was effectively a rigid mass, and that its steel base plate would not flex. Although this plate is only 9.5 mm thick, and is obviously quite flexible in a free condition, it was thought that when it was fixed to the stiff top plate of the cruciform it would be held down fairly rigidly. This seemed reasonable, in view of the 19 mm top plate thickness and the four 19 mm fixing bolts. Thus the V-support/cruciform assembly was initially modelled as a basically masslike V-support sitting on a basically springlike cruciform. Only after the lower part of the seating had been analysed did it become apparent that the V-support might not be so rigid as had been supposed. Fig.14.29 shows the measured and initially predicted vertical responses at cruciform CR2 for a vertical force input to the seating at V-piece VB2. The measurement was obtained by mounting accelerometers on the bottom plate of the V-support, and for the calculation, the masslike V-support was assumed to be connected directly to the measured cruciform mobility (corresponding to the centre of the cruciform). Upon discovering the difference of approximately 20 dB between these measured and predicted responses, a thorough check was carried out on the analysis. However, when no errors were discovered, it became obvious that the difference could only be attributed to the V-support/cruciform interface, so it was decided to examine this more closely. The results of this investigation will be seen to be very instructive, since they bring into question the assumption of point coupling between components when the actual coupling is over a relatively large area. In addition, they show how a bad choice of accelerometer mounting position can give a completely false impression of the seating performance.

We shall start by considering the accelerometer arrangement used for the measurements on the installed seating. It is seen from Fig.14.29 that an

THE RUBBER BLOCK AND UPPER BEAMS HAVE BEEN OMITTED FOR CLARITY



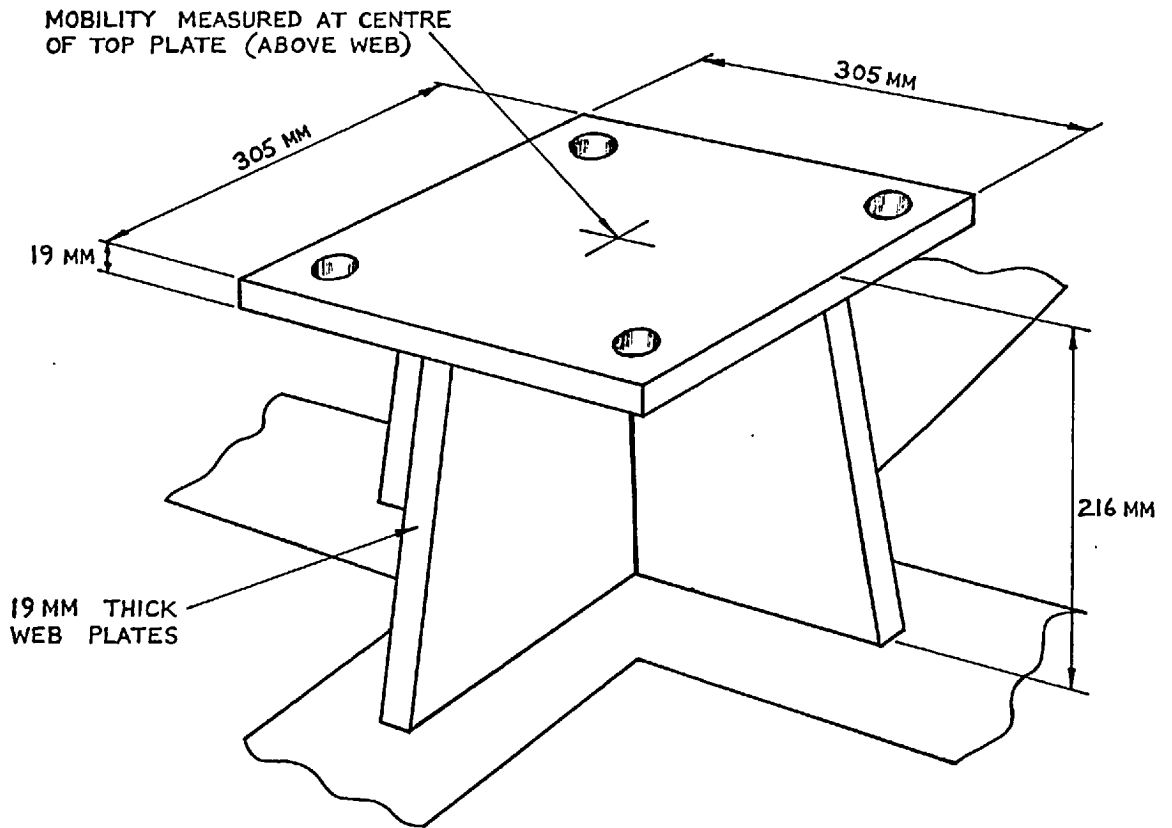


FIG. 14.30 ACTUAL CRUCIFORM

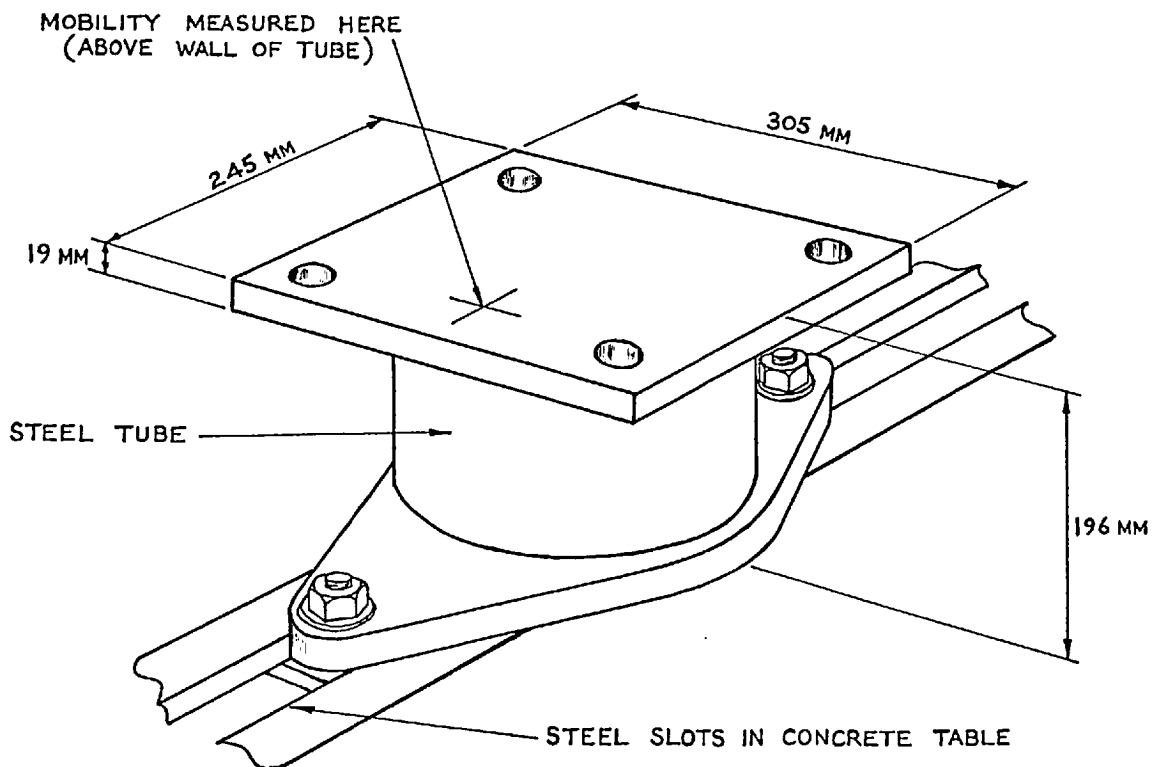


FIG. 14.31 IMITATION CRUCIFORM

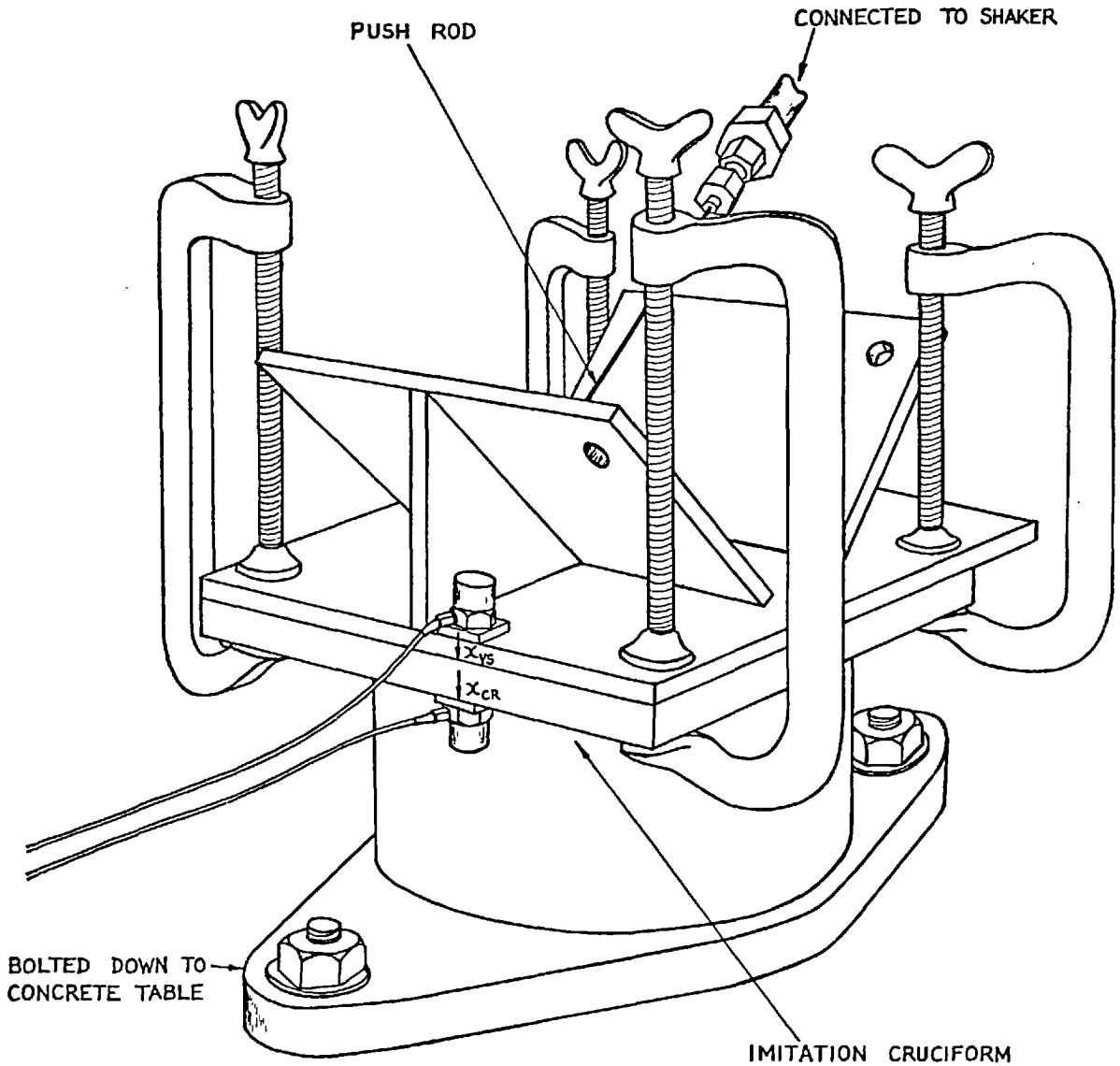


FIG. 14.32 V-SUPPORT CLAMPED TO IMITATION CRUCIFORM FOR LABORATORY TESTS

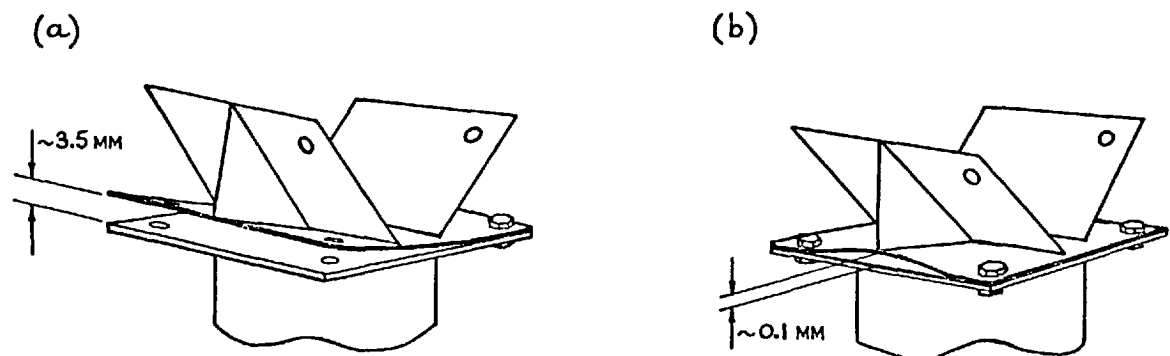


FIG. 14.33 OBSERVED DISTORTION OF V-SUPPORT AT DIFFERENT STAGES OF CLAMPING

aluminium block was glued to the bottom plate of the V-support, and two accelerometers were attached to the block by means of studs. By moving these accelerometers to various positions on the block, and by passing the signals through an analogue sum and difference unit, all six motions could be measured. When the accelerometer block was placed in this position it was mistakenly believed that there would be negligible relative motion between the bottom plate of the V-support and the top plate of the cruciform. However, as the measured response turned out to be greater than that predicted on the basis of a rigid coupling, it was decided to examine the relative motion across the interface. Unfortunately, by that stage it was no longer possible to return to the actual cruciform used in the main tests, but the cruciform could be simulated sufficiently accurately by using one of the four spacing pillars normally employed to raise the engine well clear of the seating structure*. The pillar was inverted and bolted down onto a large spring-mounted concrete table weighing several tons. The actual cruciform and this imitation are shown in Figs. 14.30 and 14.31 respectively. The former was constructed from 19 mm steel plate, and owes its name to the cross arrangement of the web plates to which the top plate was welded. The imitation "cruciform" does not strictly deserve this name, as it is simply a pillar made up from large diameter steel tube, with 19 mm steel plates welded to its two ends. However, it has similar dimensions to the actual cruciform, and was therefore considered to be an adequate imitation both as regards size and dynamic properties. As the top plate of the inverted pillar was slightly smaller than that of the actual cruciform, the bolt holes would not line up with those in the V-support, and rather than drill new holes it was decided to use large G-clamps to join the two components together (see Fig. 14.32). It should be mentioned that the V-support

* These pillars were necessary when the engine was clad, as the cladding otherwise fouled the seating.

used in these special tests was not one of the four used in the present seating assembly, but was one which had been manufactured earlier, during the initial development of the seating. It was of the same type, and was only used in preference to one of the others because the seating had already been assembled in the laboratory*, and it was not wished to disassemble part of it unless absolutely necessary.

Upon clamping down one side of the V-support, it was observed that the other side lifted off the top face of the cruciform by approximately 3.5 mm, as shown in Fig.14.33a. This resulted from distortion of the component during welding. When the other clamps were applied, they pulled down the bottom plate of the V-support in the manner indicated in Fig.14.33b. The drawing is slightly exaggerated, but there remained a gap of at least 0.1 mm (0.004 in) between the bottom plate and the surface of the cruciform in the region immediately beneath the triangular gusset plate. Consequently, the distorted bottom plate formed a relatively flexible bow spring underneath the gusset plate, and the total vertical stiffness presented by the V-support/cruciform assembly comprised the fairly low stiffness K_{VS} of this spring in series with the considerably higher stiffness K_{CR} of the cruciform. The measurements on the installed seating were made on the bottom plate of the V-support, and hence on top of the bow spring, whilst the prediction shown by the thick line in Fig.14.29 corresponds to the cruciform. It is easily shown that the relative motion between the two points is given by $1 + \frac{K_{CR}}{K_{VS}}$, so the 20 dB difference between the measured and predicted vertical responses suggests that the V-support is approximately $\frac{1}{10}$ the stiffness of the cruciform.

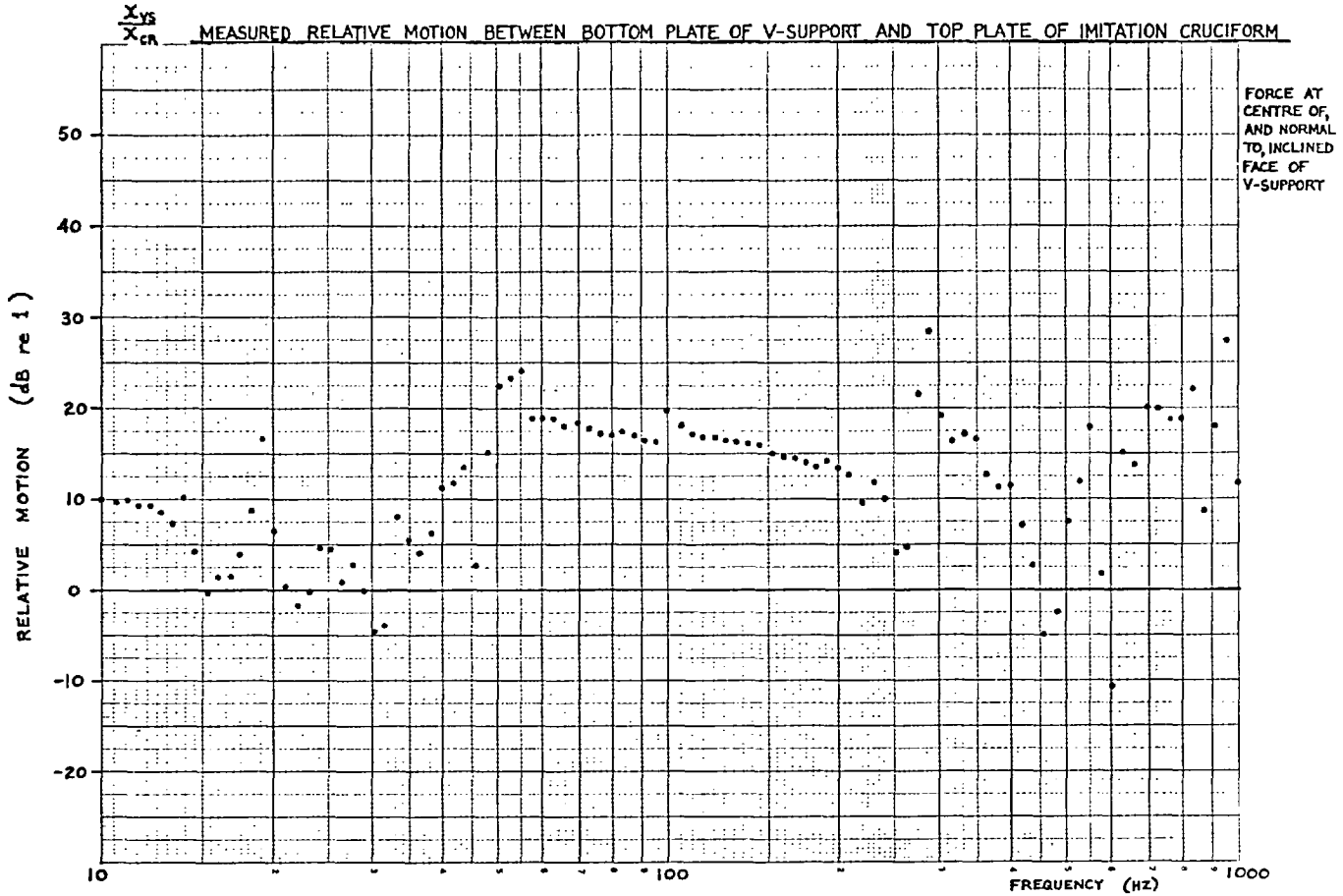
* The seating was assembled with the four V-supports bolted directly onto the concrete table.

In order to confirm the large relative motion across the interface, accelerometers were attached to the V-support and to the imitation cruciform, as shown in Fig.14.32, and a normal excitation was applied at the centre of the inclined face above the accelerometers. The upper graph of Fig.14.34 gives the measured relative motion between the upper and lower points, and clearly shows a difference of 15 to 20 dB over the frequency range 50 to 200 Hz. The results below 50 Hz may be ignored, since the concrete table no longer remains an effectively rigid termination for the springlike cruciform, and the combination of cruciform and table in series then has a mobility which is comparable with that of the attached V-support, leading to very little relative motion. The considerable variation above 200 Hz must be due to local plate resonances, and to resonances of the large G-clamps used to hold the assembly together.

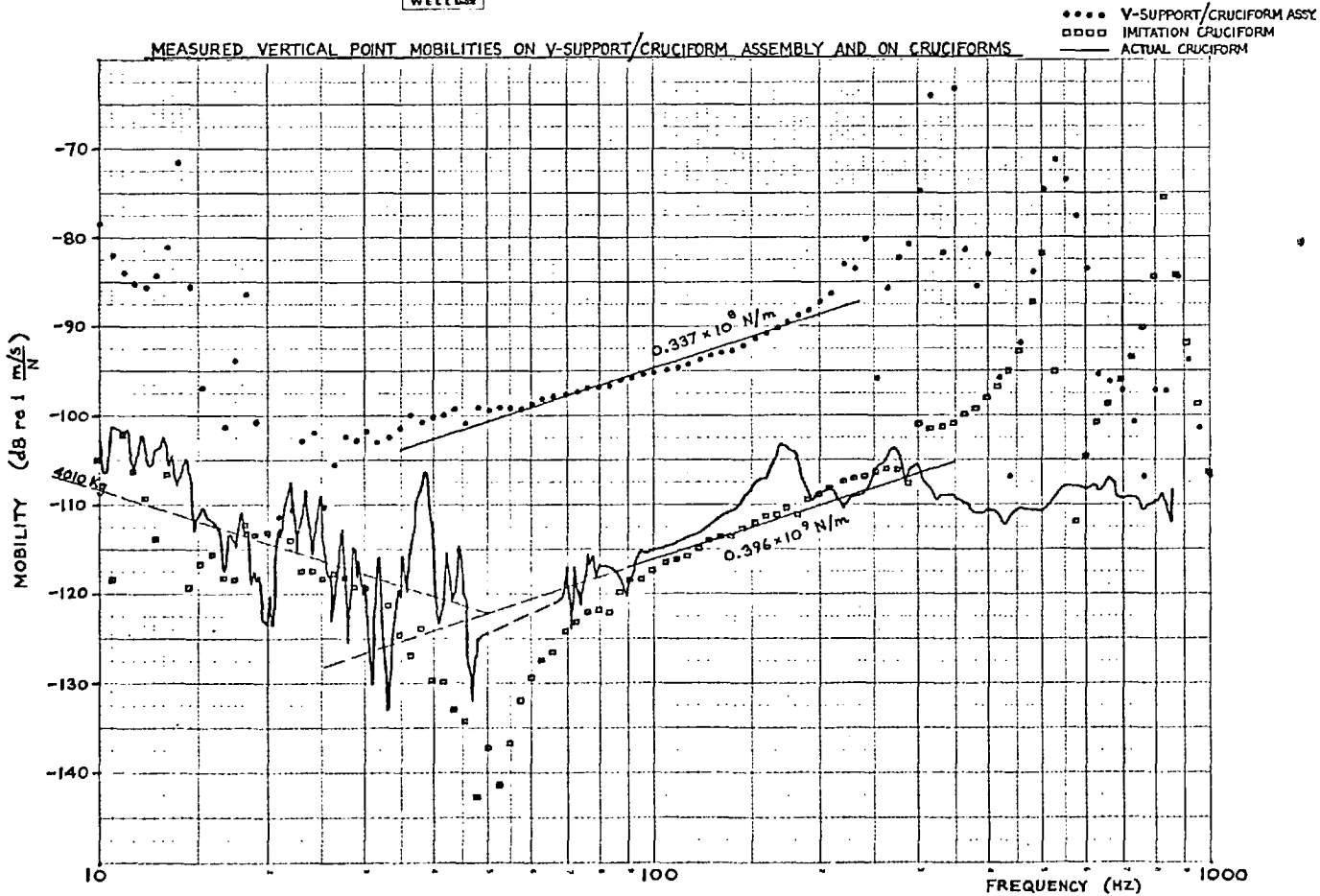
Having confirmed the large relative motion, it was decided to measure the vertical stiffness both of the assembly and of the cruciform, and to use this information to obtain the effective stiffness of the V-support. The stiffness of the assembly was obtained from mobility measurements on one of the upper faces of the V-support. However, due to the difficulty of applying a force at 45° to the inclined upper face, the vertical stiffness was not measured directly. Instead, direct and cross mobility measurements were made in the directions normal to and up the face. The resulting 2×2 mobility matrix was then subjected to a co-ordinate transformation, in order to yield the matrix relating to the vertical and horizontal directions. The procedure is outlined in Fig. 14.35, and all the measurements and the processing of the measured data were performed in the laboratory using the computer-controlled measuring system. The resulting vertical point mobility is shown in the lower graph of Fig.14.34, but it should be stressed that this is only the mobility one sees when looking into one of the inclined faces of the

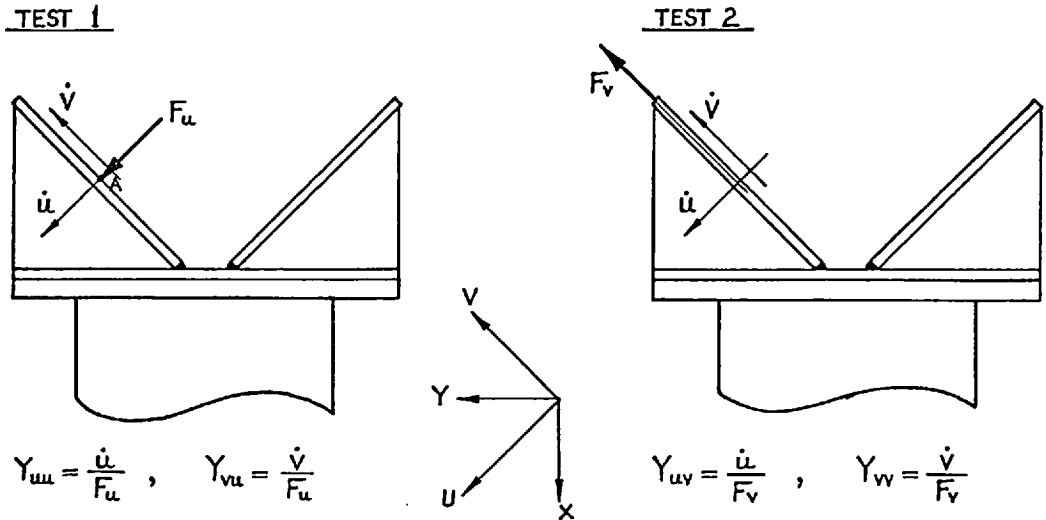
FIG 14.34

GRAPH Well 1 2-29 Graph Data Ref. 5521 Log 2 Cycles a mm, j and 1 cm



GRAPH Well 1 2-29 Graph Data Ref. 5521 Log 2 Cycles a mm, j and 1 cm





COMBINE THE RESULTS OF THE TWO TESTS:

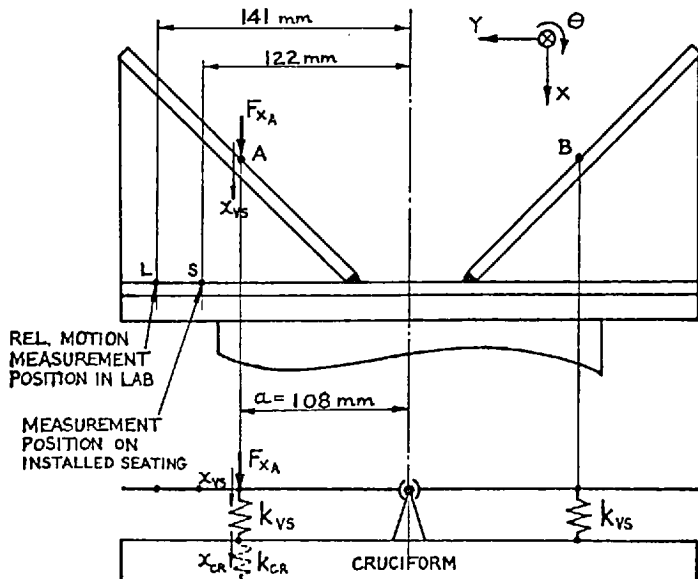
$$\begin{Bmatrix} \dot{u} \\ \dot{v} \end{Bmatrix} = \begin{bmatrix} Y_{uu} & Y_{uv} \\ Y_{vu} & Y_{vv} \end{bmatrix} \begin{Bmatrix} F_u \\ F_v \end{Bmatrix}$$

TRANSFORM TO X AND Y CO-ORDINATES:

$$\begin{Bmatrix} \dot{x} \\ \dot{y} \end{Bmatrix} = \begin{bmatrix} \frac{1}{\sqrt{2}} & -\frac{1}{\sqrt{2}} \\ \frac{1}{\sqrt{2}} & \frac{1}{\sqrt{2}} \end{bmatrix} \begin{bmatrix} Y_{uu} & Y_{uv} \\ Y_{vu} & Y_{vv} \end{bmatrix} \begin{bmatrix} \frac{1}{\sqrt{2}} & \frac{1}{\sqrt{2}} \\ -\frac{1}{\sqrt{2}} & \frac{1}{\sqrt{2}} \end{bmatrix} \begin{Bmatrix} F_x \\ F_y \end{Bmatrix}$$

$$\begin{bmatrix} Y_{xx} & Y_{xy} \\ Y_{yx} & Y_{yy} \end{bmatrix} = \frac{1}{2} \begin{bmatrix} (Y_{uu} - Y_{vu} - Y_{uv} + Y_{vv}) & (Y_{uu} - Y_{vu} + Y_{uv} - Y_{vv}) \\ (Y_{uu} + Y_{vu} - Y_{uv} - Y_{vv}) & (Y_{uu} + Y_{vu} + Y_{uv} + Y_{vv}) \end{bmatrix}$$

FIG. 14.35 MEASUREMENT OF X-Y MOBILITY OF V-SUPPORT/CRUCIFORM ASSEMBLY



FROM FIG. 14.34

MEASURED V-SUPPORT/CRUCIFORM STIFFNESS AT POINT A = $k_{vs/cr} = \frac{F_{xA}}{x_{vs}} = 0.337 \times 10^8 \text{ N/m}$

MEASURED CRUCIFORM STIFFNESS = $k_{cr} = \frac{F_{xA}}{x_{cr}} = 3.960 \times 10^8 \text{ N/m}$

WHENCE $k_{vs} = \frac{k_{cr} k_{vs/cr}}{k_{cr} - k_{vs/cr}} = 0.368 \times 10^8 \text{ N/m}$

LOOKING INTO POINTS A AND B SIMULTANEOUSLY, THE X AND θ INTERFACE FLEXIBILITIES ARE

$$\alpha_{x_{INT}} = 1/2 k_{vs} = 0.136 \times 10^{-7} \text{ m/N}$$

$$\alpha_{\theta_{INT}} = 1/2 k_{vs} a^2 = 0.116 \times 10^{-5} \text{ rad/N-m}$$

FIG. 14.36 V-SUPPORT/CRUCIFORM INTERFACE FLEXIBILITIES

assembly. Also shown in this figure are the vertical point mobilities measured on the imitation cruciform in the laboratory and on the actual cruciform attached to the receiver structure. The measurement on the imitation cruciform was at a point immediately above the wall of the tube which supports the top plate, whilst the measurement on the actual cruciform was at the centre of the top plate, immediately above one of the stiff webs (see Fig.14.30). Each of these measurements was made at a point of maximum stiffness for the particular cruciform, and due to the considerable variation in mobility over the surface of the top plate, the effective stiffness presented to the V-support must certainly be less than is indicated from the measurements shown. However, the flexibility of the cruciform top plate has been included with that of the V-support base plate in order to give an overall coupling flexibility which may be used in the seating model.

The mobility curves for the actual and imitation cruciforms are extremely interesting, since they are in very close agreement with one another over quite a wide frequency range. However, the apparently good agreement at the low frequencies is misleading, as below 50 Hz the measurements on the imitation cruciform show only the effective mass (4010 Kg) of the concrete table. The trough at 50 Hz is an anti-resonance of the table-cruciform system, and this is then followed by the springlike behaviour of the cruciform on the effectively rigid table. If we ignore the effect of the table, and extend the stiffness line down to the low frequencies, we see that the two cruciforms behave in a very similar manner between 30 and 300 Hz. Bearing in mind the similar top plate and web/wall thicknesses for the two cruciforms, and the dissimilar nature of the supporting structures, it seems probable that the cruciform behaviour up to 300 Hz at least is only a function of local deformation of that part of the cruciform in the immediate vicinity of the measurement point. The observed resonances of the imitation cruciform above 300 Hz

may have corresponded to rocking and bouncing resonances of the top plate on the springiness of the vertical tube, or alternatively they may just have been top plate resonances, if the exciting force were not exactly over the tube wall. The measurements are certainly thought to have been reliable, since the mobility of the imitation cruciform was measured using separate force and acceleration transducers, and the force gauge was attached by means of a stud screwed into the cruciform.

It is clearly seen that the measured cruciform stiffness is almost exactly 10 times greater than the stiffness measured on one of the inclined faces of the V-support. The large intermediate flexibility is obviously due to the combined effects of the flexibilities in the V-support bottom plate and in the cruciform top plate, but the proportions are unimportant. Referring to Fig.14.36, the measured stiffness of the assembly and of the cruciform have been used to calculate the stiffness K_{VS} of one half of the V-support. If it is assumed that the two upper faces are uncoupled, the two halves act as a pair of simple springs in parallel, and the total X stiffness of the support is then $2 K_{VS}^*$. Similarly, the total Θ stiffness is given by $2 K_{VS} a^2$. The corresponding flexibilities $\alpha_{X INT}$ and $\alpha_{\Theta INT}$ are the reciprocals of these stiffnesses, and because the springiness of the V-support bottom plate only affects the x and Θ motions of the accelerometer attachment point S, these two flexibilities are sufficient to correct the model.

Since the seating response measurements were made on the V-support bottom plate, above the flexible part of the assembly, the simplest way of correcting the analysis was to still consider the V-support to be masslike, and to combine the intermediate flexibility with the measured

* Note that this total stiffness is only about 5 times (i.e. 14dB) less than the cruciform stiffness.

cruciform data. In this way, the computed responses would correspond to the same point as the measurements - and no longer to the centre of the cruciform top plate. Hence, the two flexibilities $\alpha_{X INT}$ and $\alpha_{\theta INT}$ have been added to the corresponding diagonal terms of the cruciform receptance matrix. The corresponding re-computed response data for the lower part of the seating are given with all the other results in Chapter 15, and they will be seen to agree much more closely with the measurements.

The findings of this section clearly illustrate the danger of taking measurements at a single point and then assuming true point coupling, when the two components are in fact coupled rather imperfectly over a relatively large area. The initially predicted results might have been more accurate if the components had been either glued or welded together, but the seating performance in terms of force transmissibility would probably have been no different, and it is not the job of the dynamic analyst to modify the system solely to enable him to accurately compute its response!

The other important lesson to be learnt from these findings is the very startling effect that the accelerometer position can have on the measurements of seating performance. In this particular example, the accelerometers were only mounted on the V-support bottom plate because this was more accessible than the underside of the cruciform top plate, yet the two points were later found to have a very large relative motion. Thus, the true motion transmissibility from the top of the seating down to the cruciform is in fact about 20 dB better than was indicated by the measurements made on the installed system. It is believed that many seating response measurements in the past have been made with accelerometers mounted on the bottom part of the seating, rather than on the cruciform, and since the intermediate flexibility must vary considerably from one seating to another, comparisons of seating performance based upon these figures may not be very reliable.

CHAPTER 15RESULTS AND CONCLUSIONS FOR THE SEATING15.1 RESULTS FOR THE ASSEMBLED STRUCTURE

The results are presented as frequency response plots of mobility and force transmissibility, and in most cases both theoretical and measured responses are given. In every case but one, the excitation has been applied to the top of the seating on V-piece VB2, either at point I or at point I'* (See Fig.15.1). The results are grouped together in the following order:

<u>Upper Part of Seating</u> (shown in Fig.15.1)	<u>Figures</u>
(1) Point mobilities on V-piece VB2.	15.2 - 15.4
(2) Transfer mobilities on upper part of seating.	15.4 - 15.8
(3) Forces transmitted to lower part of seating via rubber blocks RB1 and RB2.	15.9 - 15.11
<u>Lower Part of Seating</u> (shown in Fig.15.12)	
(4) Velocities at cruciform CR2 due to excitation at VB2.(i.e. transfer mobility from top to bottom of seating).	15.13 - 15.15
(5) Forces transmitted to cruciform CR2 due to excitation at VB2 (i.e. overall force transmissibility across seating).	15.15 - 15.16
<u>Simple Analysis</u>	
(6) Comparison between results of full analysis and simple analysis.	15.17 - 15.18
<u>The Influence of Pad Shear Stiffness</u>	
(7) Force transmissibility and mobility data showing effect of shear stiffness of PVC Pads beneath the V-pieces.	15.19 - 15.20

* Horizontal forces F_y and F_z were applied on edge of top plate, and acted through I. Vertical force F_x and couple M_θ were applied directly at I.

All measurements in the laboratory were carried out with the Solartron computer-controlled frequency response analyser, which was described in Chapter 4 (Part 2). Other measurements have been made on the seating when it was mounted on the actual receiver structure, and these were performed with a slow-sweep analogue measuring system.

The laboratory measurements on the transverse beam assembly were made with the lower beams removed, the rubber blocks being mounted directly on the V-supports, just as for the block stiffness measurements described in Section 14.2. Since the blocks are quite soft in relation to the support impedance, this should not effect the response of the beam assembly.

A force gauge and separate accelerometers* were used for all point and transfer mobility measurements. In the case of the point measurements on VB2, the results for $\frac{\dot{x}}{F_x}$, $\frac{\dot{\theta}}{M_\theta}$ and $\frac{\dot{\theta}}{F_x}$ were obtained using the multi-directional measurement techniques developed in Part 2. Exciting block Mk4⁺ was used for this purpose, the block being securely bolted down at point I' with a 12.7 mm bolt ($\frac{1}{2}$ inch BSF). The laboratory measurements were performed using a single shaker, whilst the measurements on the installed seating were made with a twin shaker (see code at top of upper graph in Fig.15.2 - Block Mk4/1S/IC signifies exciting block Mk4 and single shaker, with results inertia-corrected for effect of block).

When measuring the responses on beam UT1 due to an excitation on VB2, the velocities \dot{q}_2 and \dot{q}_3 in the plane of the layers were obtained from accelerometers mounted on the centre and bottom layers respectively (i.e. layer 3 for \dot{q}_2 and layer 5 for \dot{q}_3).

* Force gauge: Endevco type. 2103-100
Accelerometers: Environmental Equipments AQ40 and Birchall A/02

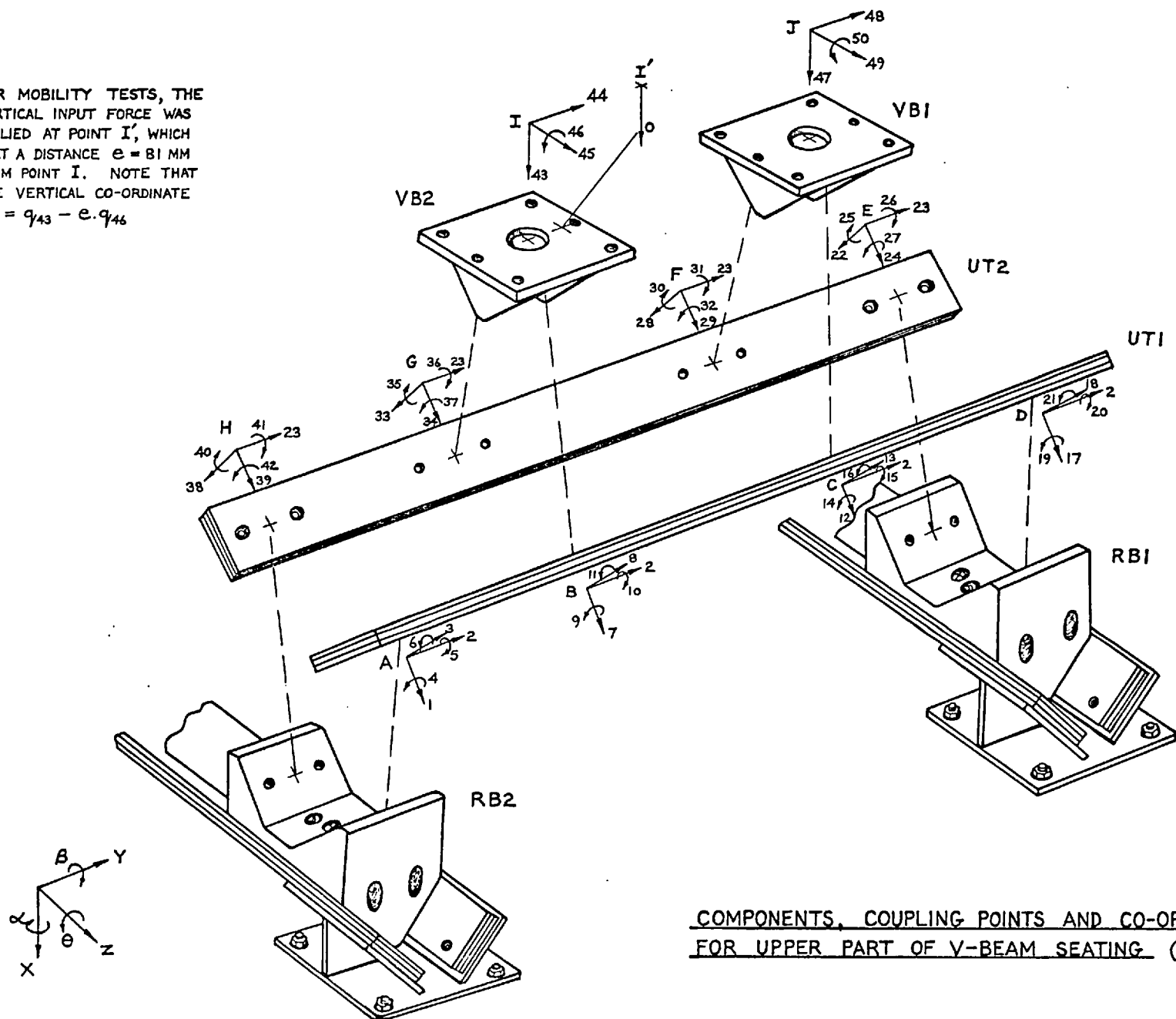
+ See Appendix IV for block data.

The force transmission to the lower part of the seating was measured in the laboratory, with the seating fully assembled. Due to the very large area of contact between the lower faces of the rubber block and the longitudinal beams, it was obviously impossible to measure the forces directly, so it was decided to measure the compression of the block in each direction and to multiply this by the relevant block stiffness. Thus, the net vertical force $P_x = K_x (X_{top} - X_{bottom})$, and the horizontal forces P_y and P_z are given by similar expressions. Whilst this does not take account of the reduction in effective stiffness due to wave effects, it does give a sensible estimate of the force at low frequencies. The block compressions in the X, Y and Z directions were measured by accelerometers mounted on triangular aluminium blocks which were glued to beams UT1 and LL4, and the forces were calculated on-line by the computer. The block stiffnesses were calculated from the multi-directional dynamic stiffness data generated by the spring model; and when obtaining the vertical stiffness K_x , the rotation β of the inclined upper face was "blocked", since it is not free to rotate when the V-beam assembly is in position. The stiffnesses obtained in this way are:

$$K_x = 1.240 \times 10^6 \text{ N/m}, K_y = 0.501 \times 10^6 \text{ N/m}, K_z = 0.297 \times 10^6 \text{ N/m}.$$

The velocity response at cruciform CR2 was measured with the seating attached to the actual receiver structure. The vertical input on VB2 was applied by a twin-shaker unit, with the two shakers running in phase. Both translational and rotational responses were measured using a pair of accelerometers on an aluminium block, which was glued to the bottom plate of V-support VS2. The exact arrangement and the implications of using this particular measurement position have already been discussed in considerable detail in Section 14.6.

FOR MOBILITY TESTS, THE VERTICAL INPUT FORCE WAS APPLIED AT POINT I', WHICH IS AT A DISTANCE $e = 81$ MM FROM POINT I. NOTE THAT THE VERTICAL CO-ORDINATE $q_0 = q_{43} - e \cdot q_{46}$



COMPONENTS, COUPLING POINTS AND CO-ORDINATES
FOR UPPER PART OF V-BEAM SEATING (FORWARD HALF)

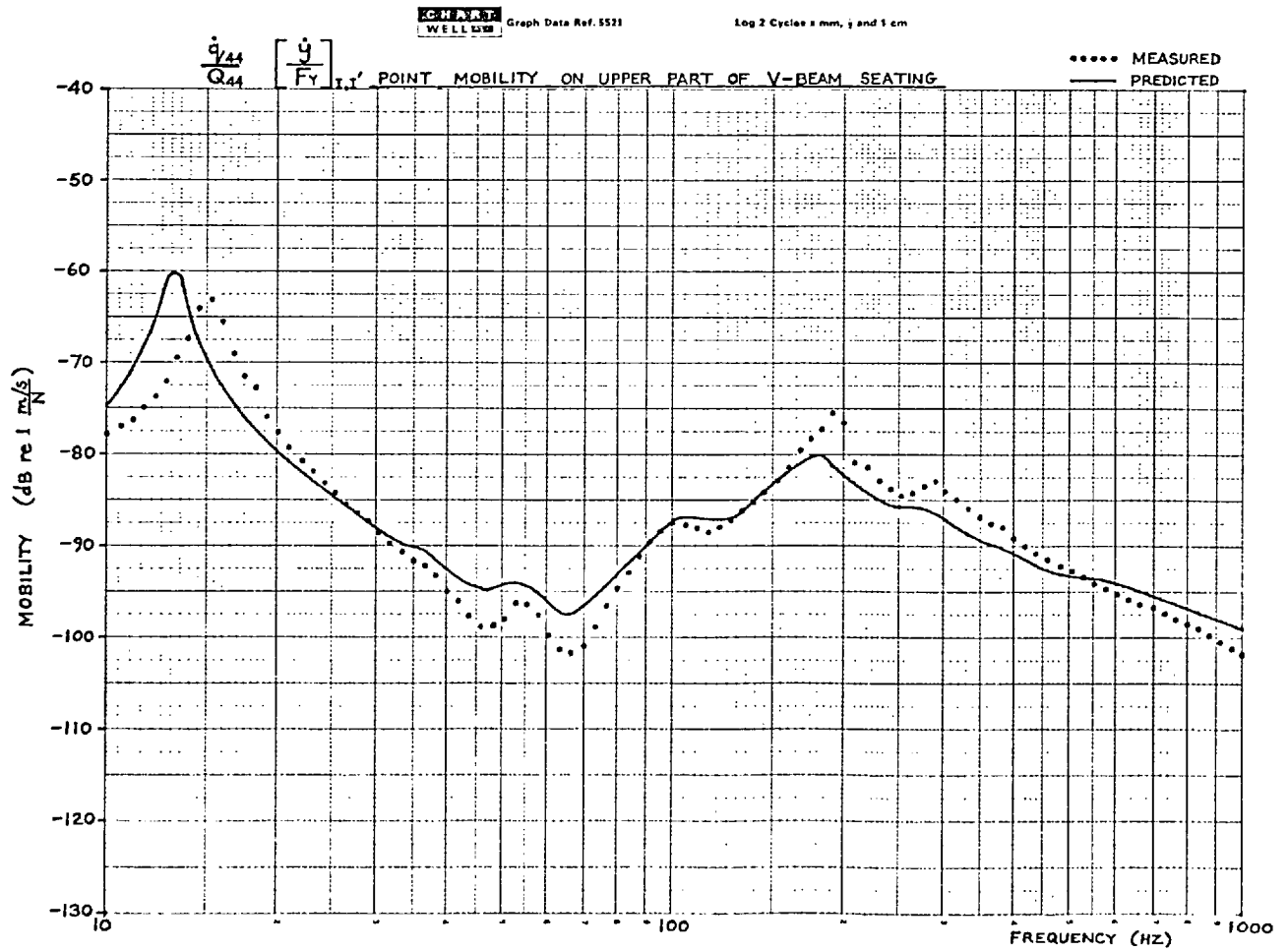
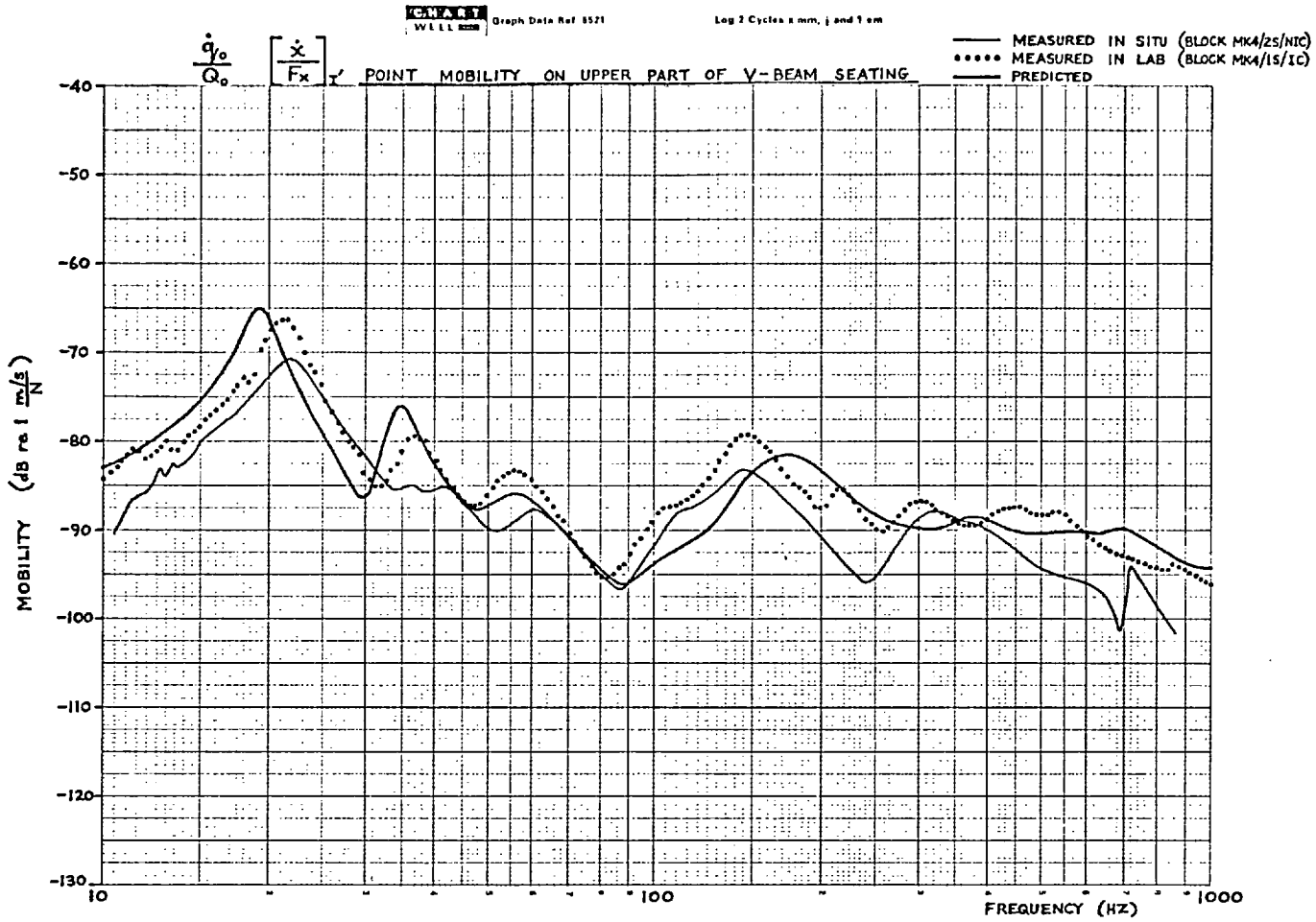


FIG 15.3

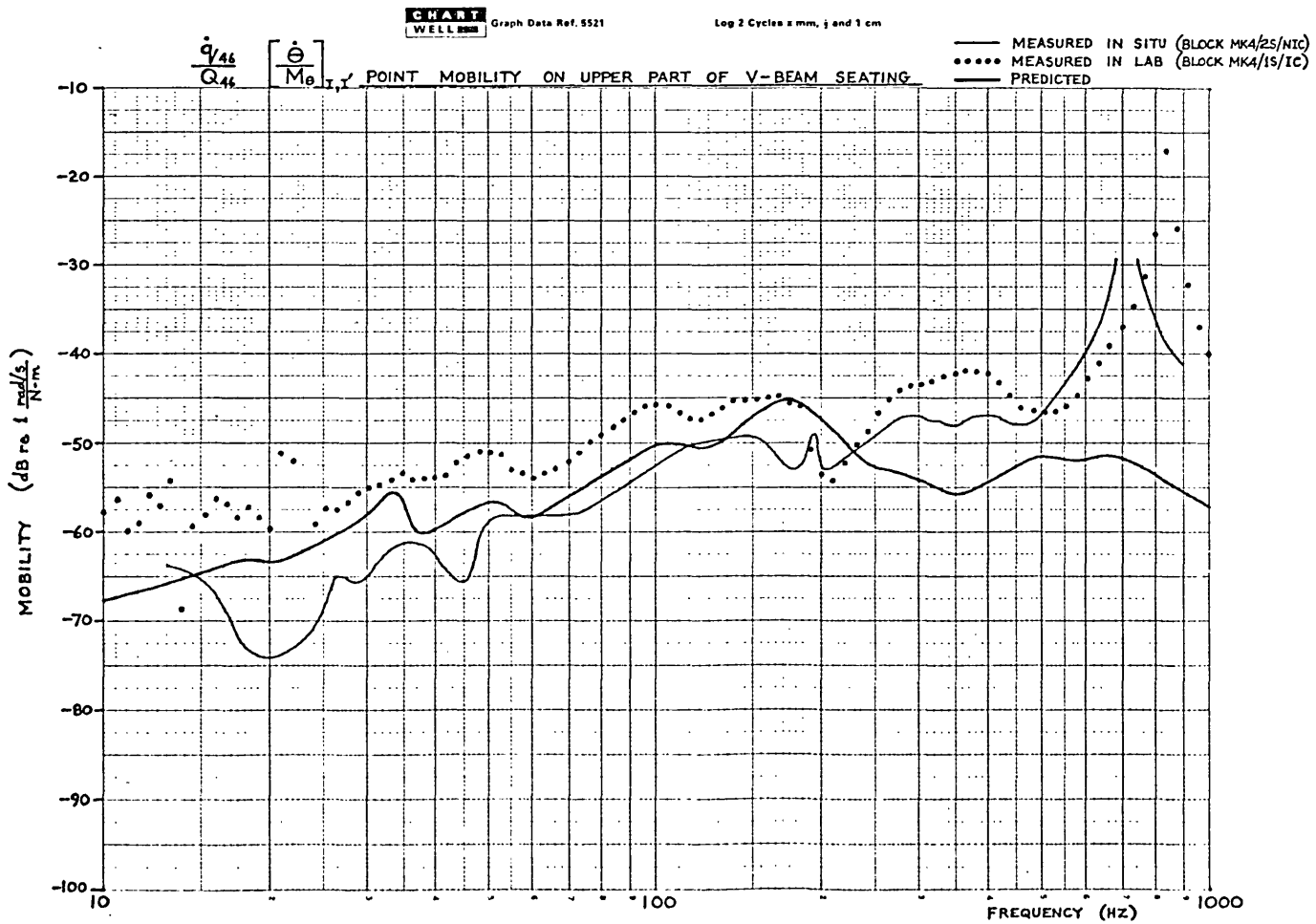
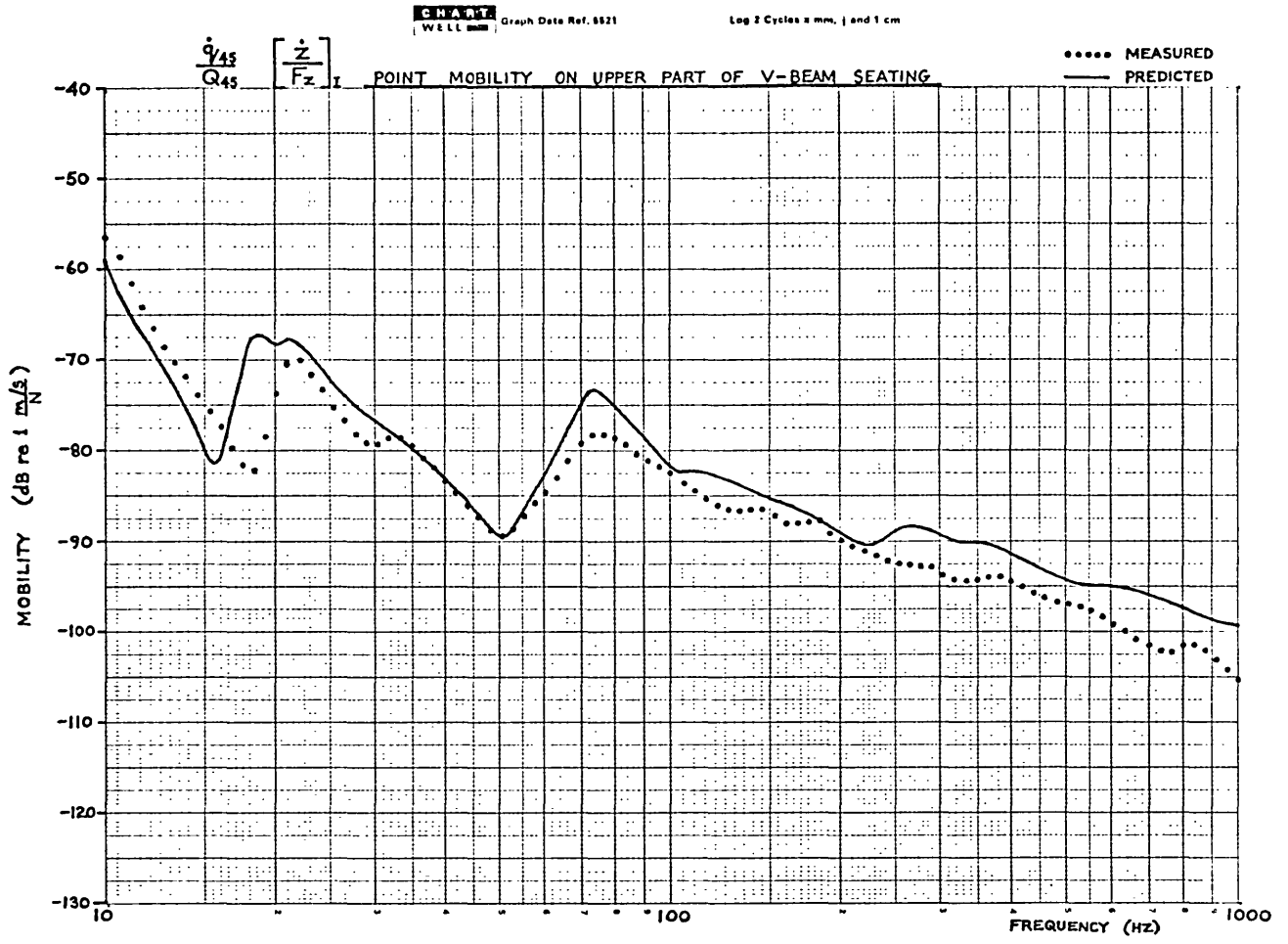
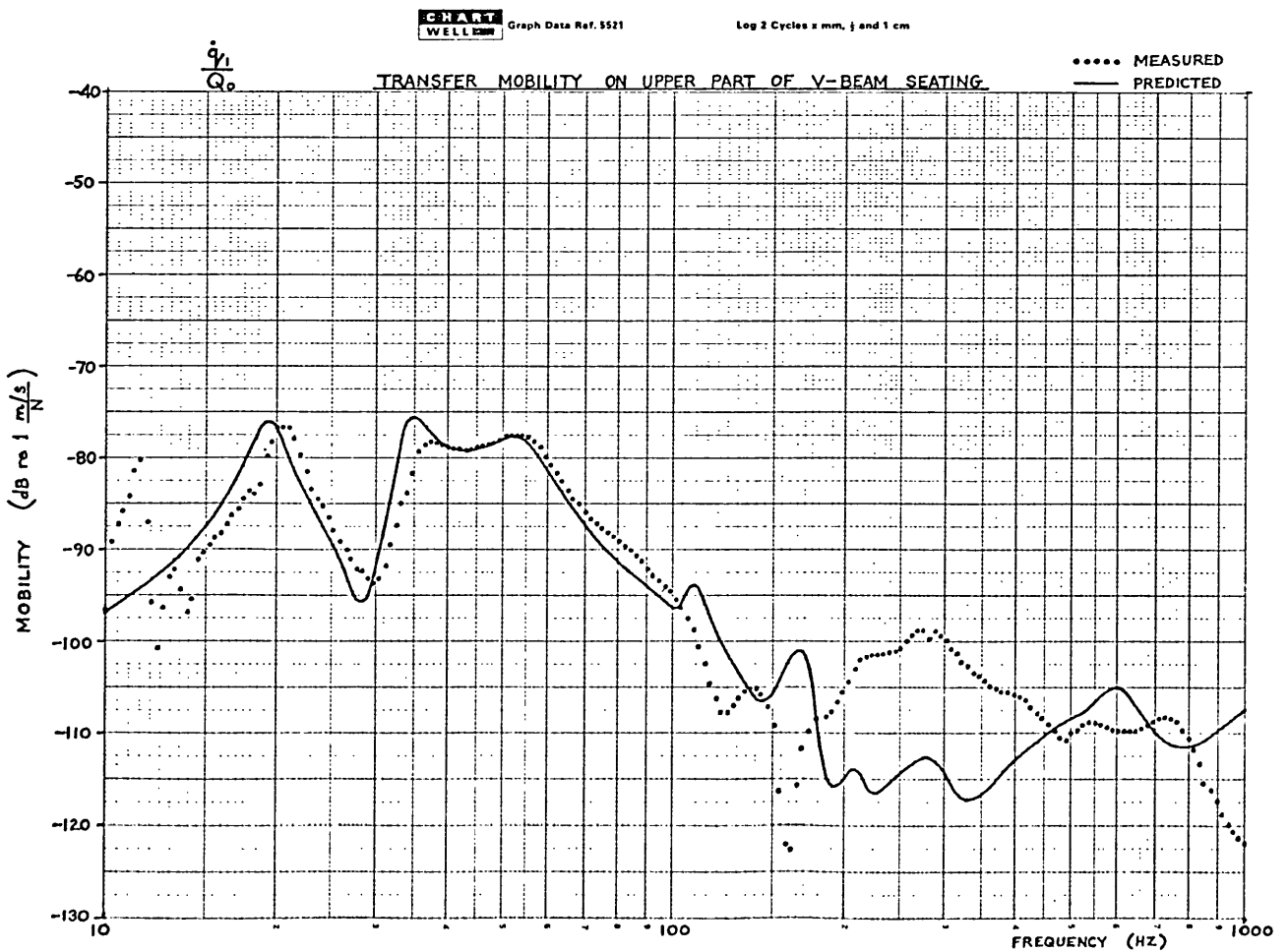
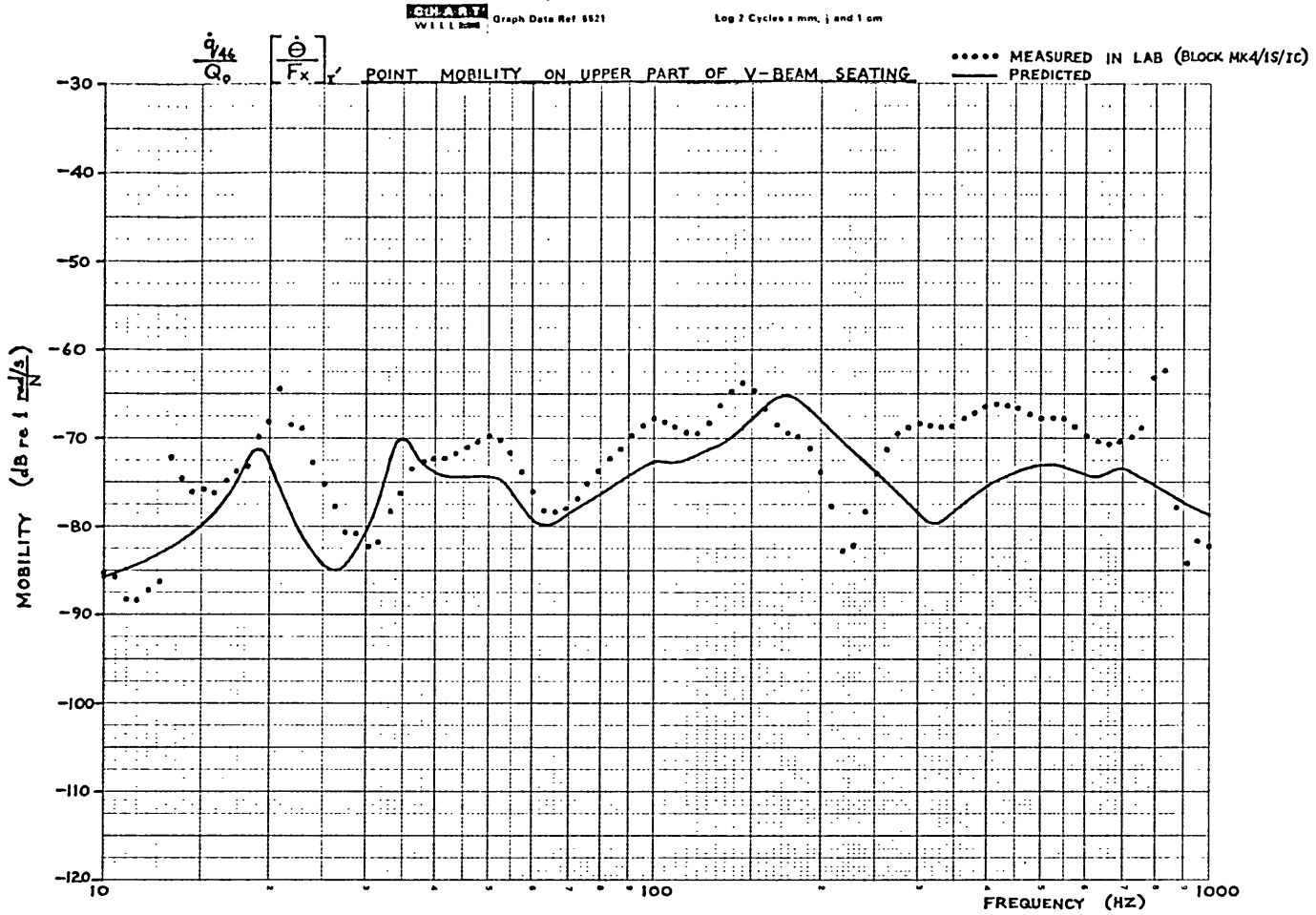


FIG 15.4



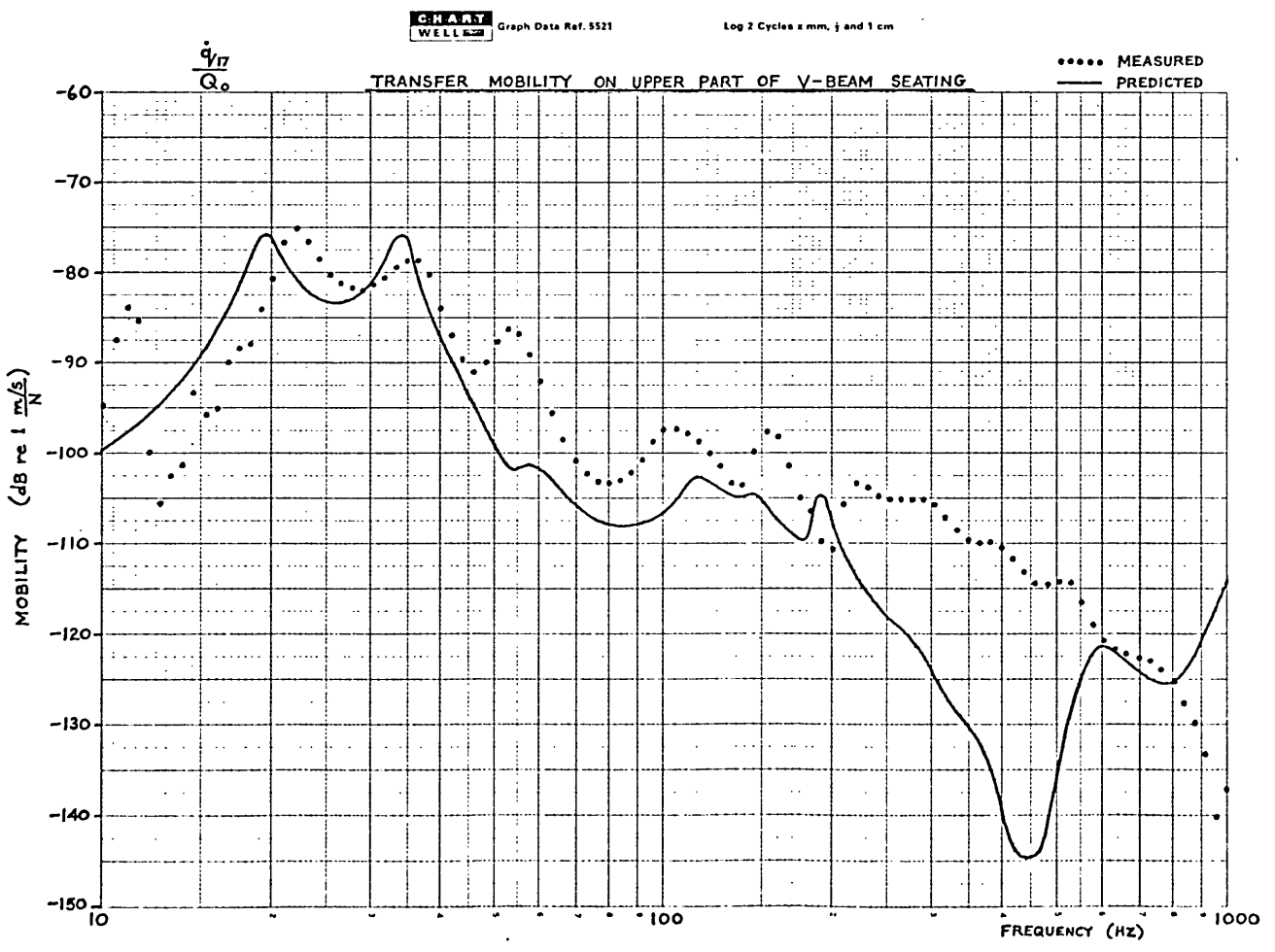
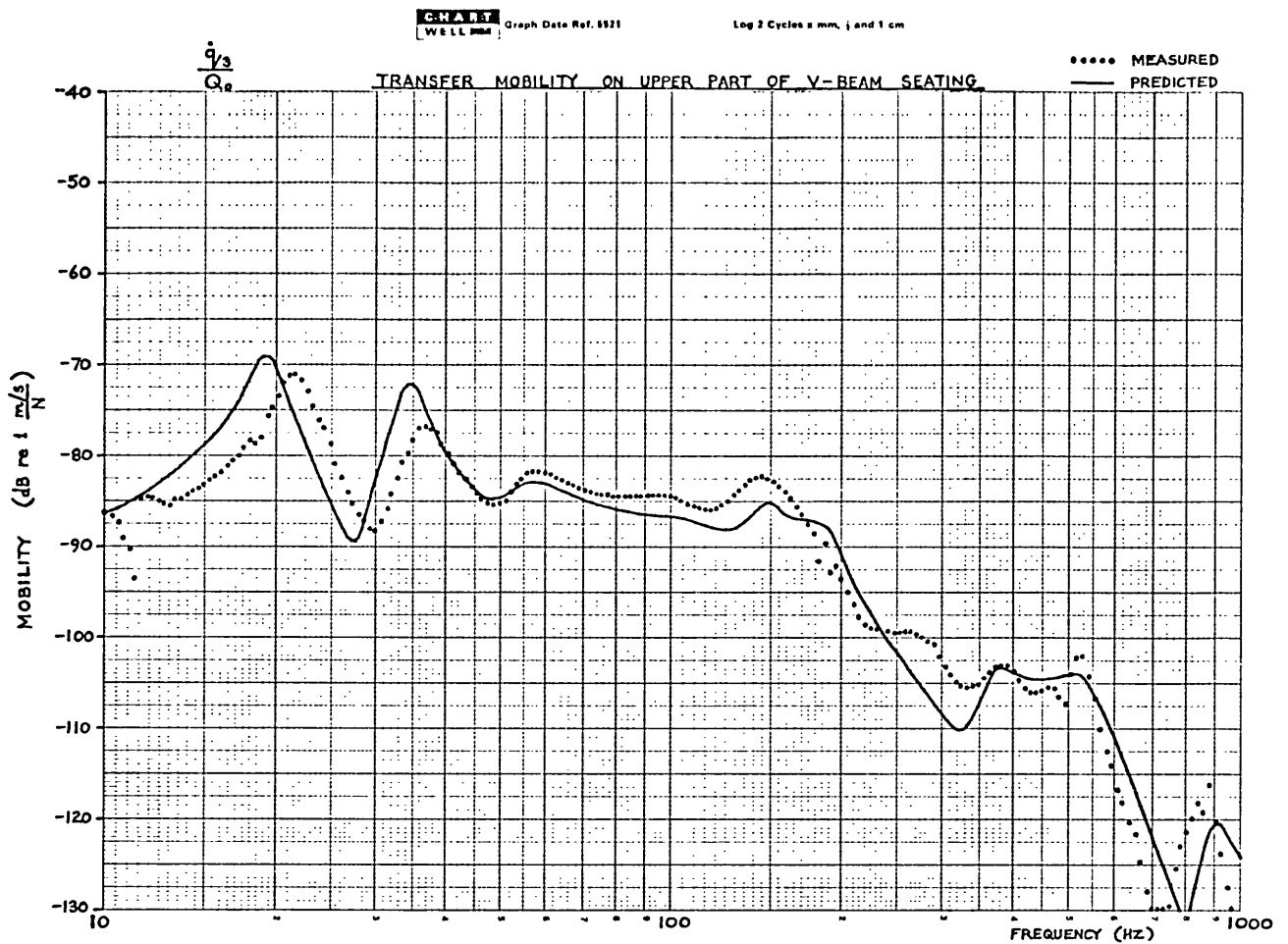


FIG 15.6

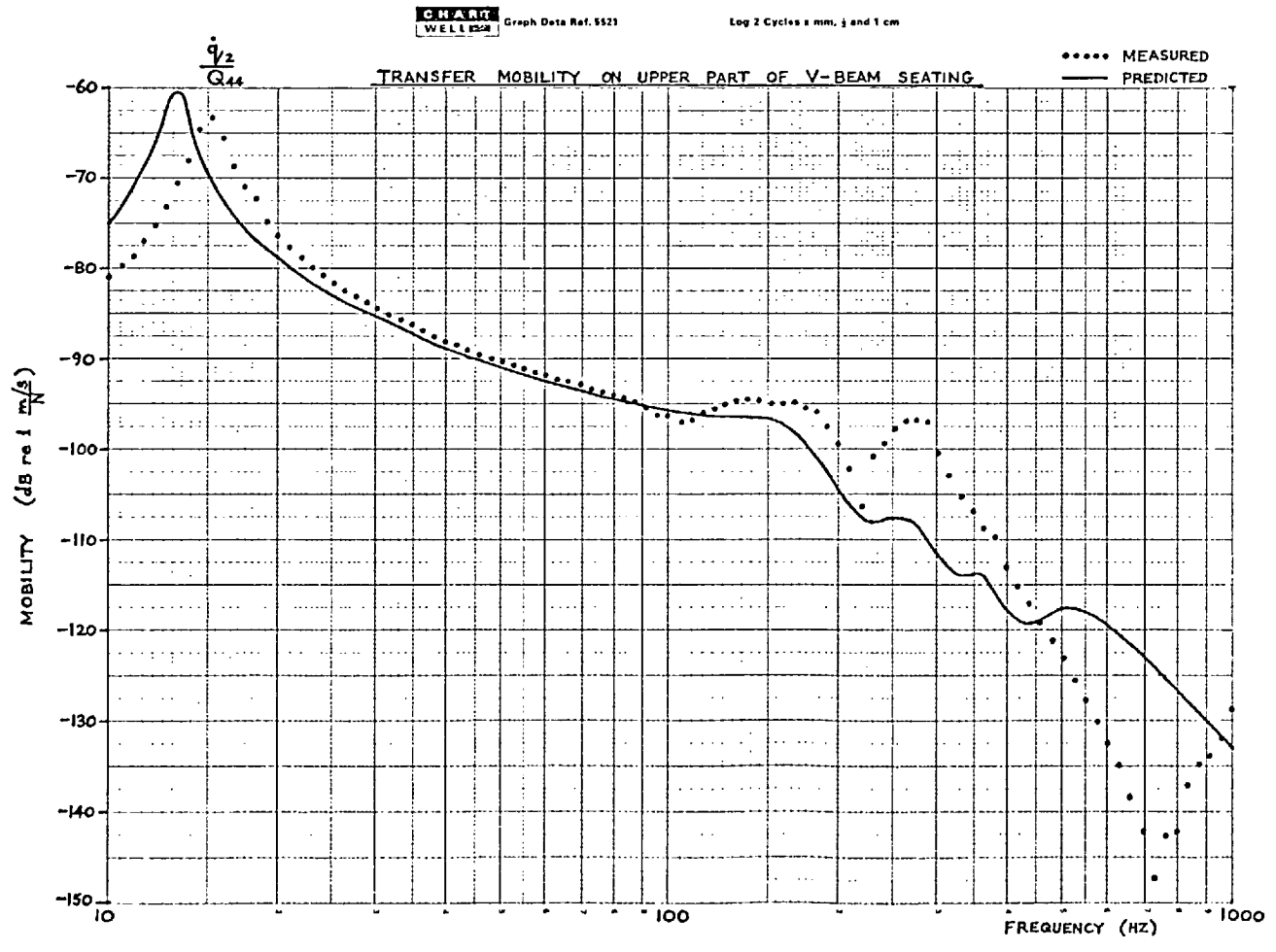
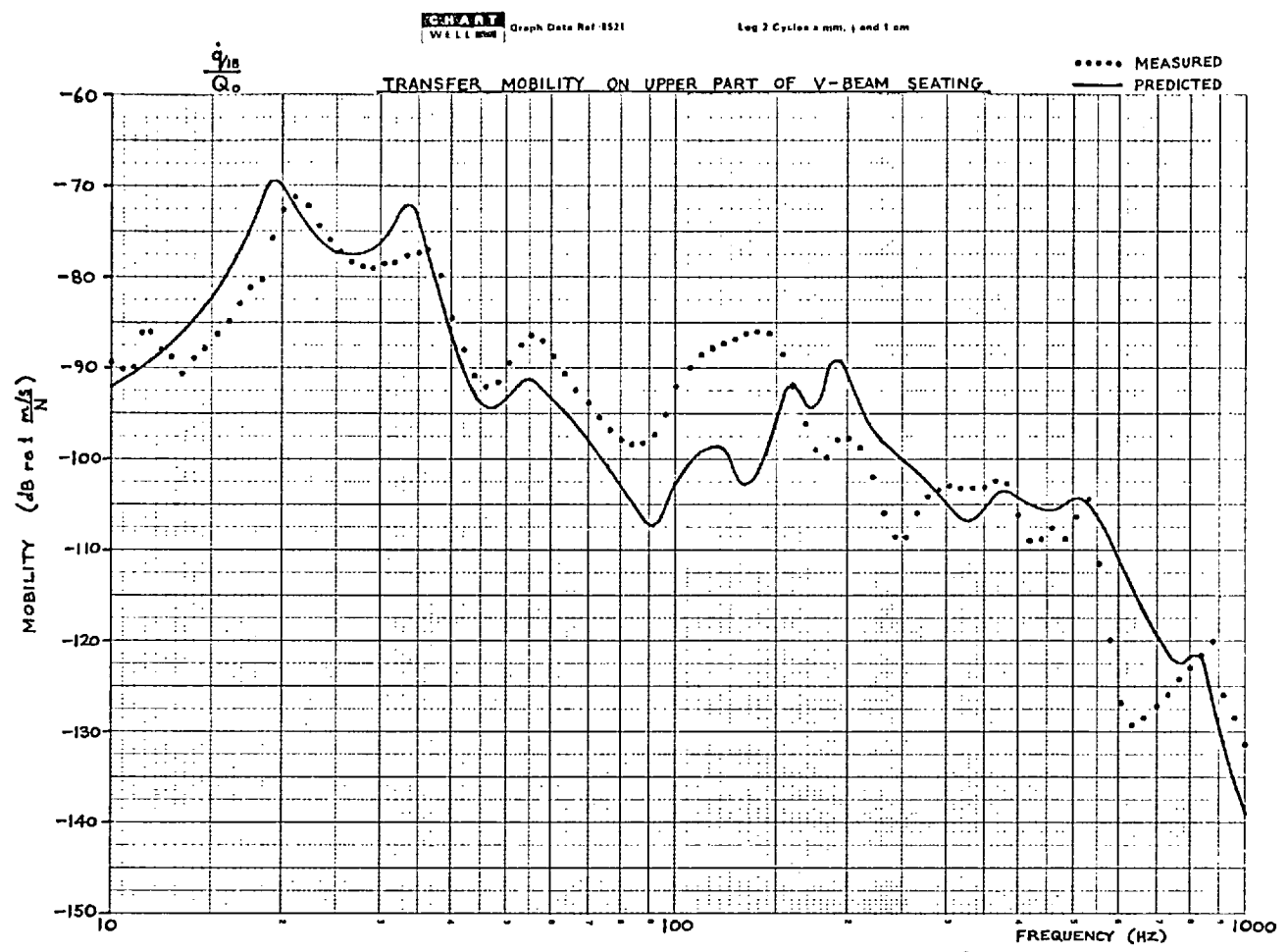


CHART WELL Graph Date Ref. 5521 Log 2 Cycles x mm, j and 1 cm

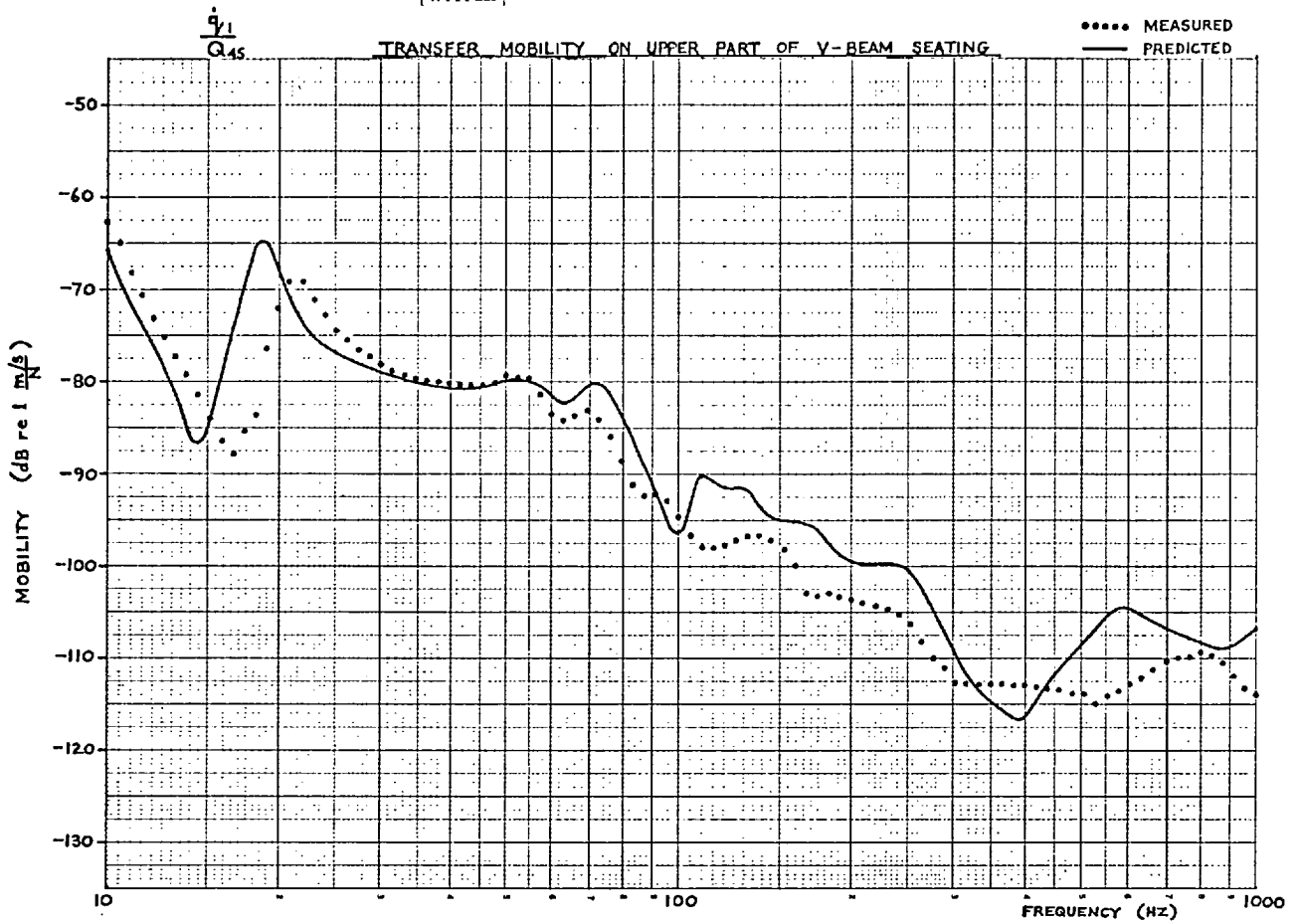


CHART WELL Graph Date Ref. 5521 Log 2 Cycles x mm, j and 1 cm



FIG 15.8

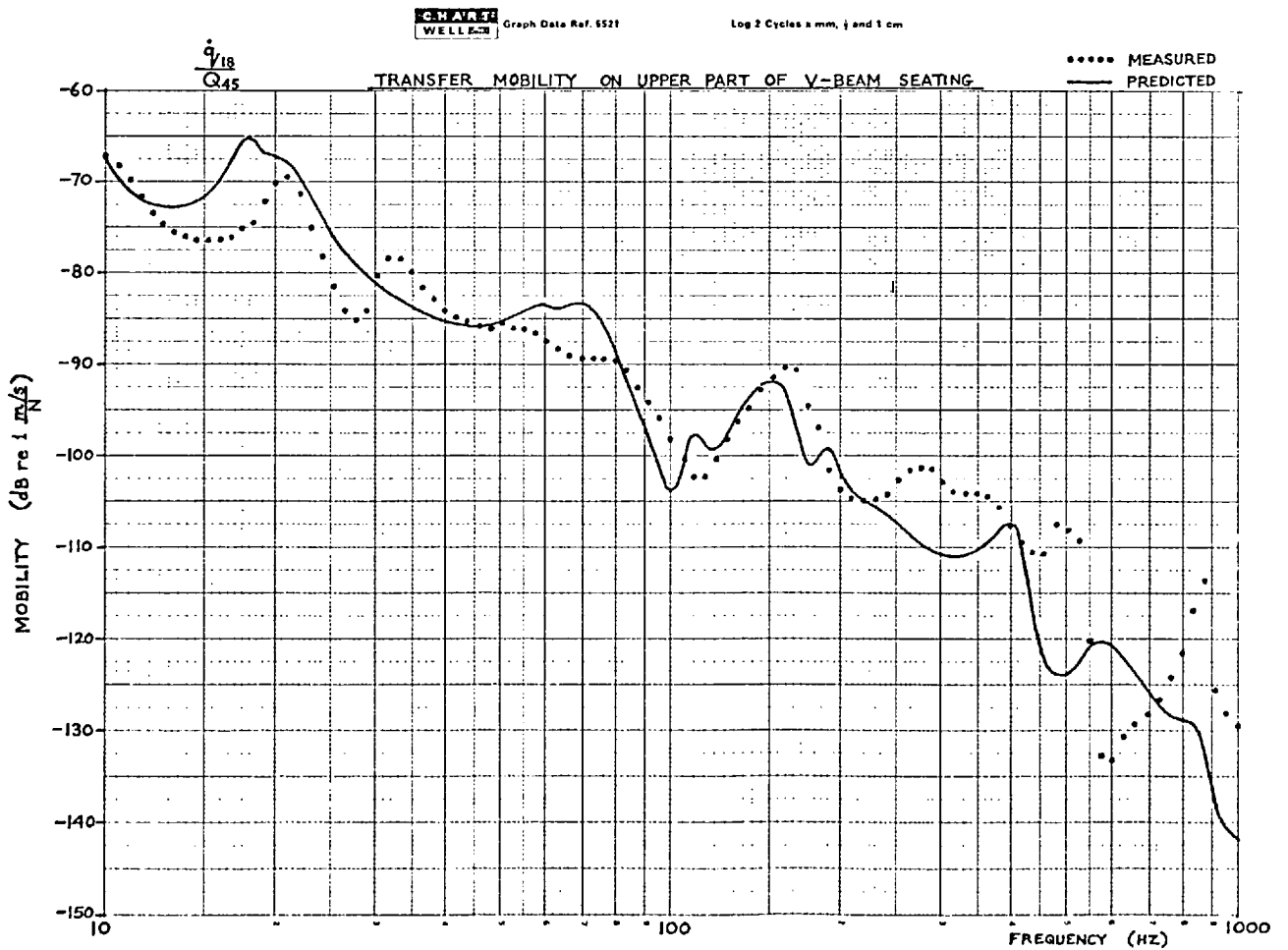
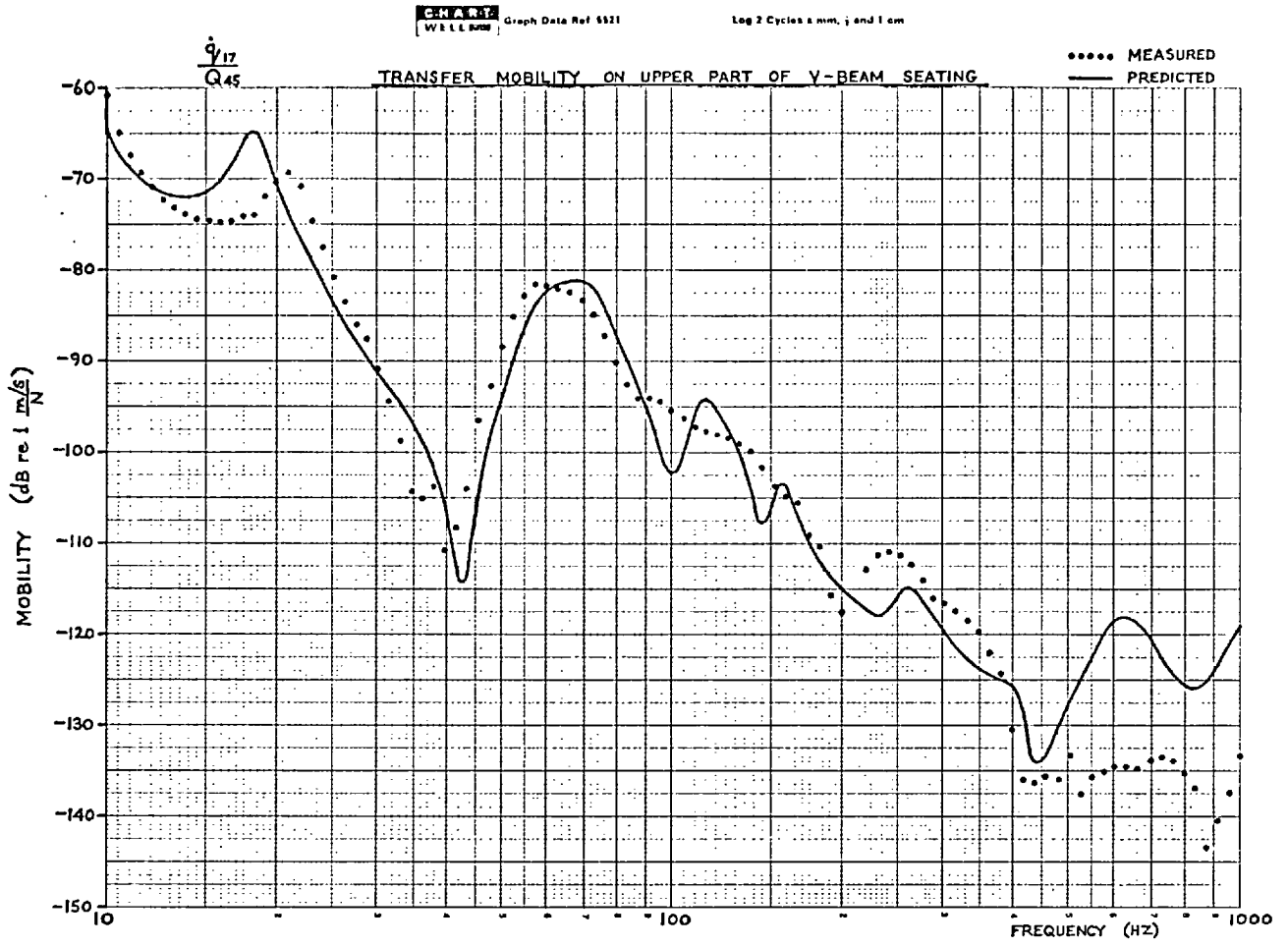


FIG 15.9

CHART
WELL 2232

Graph Data Ref 5521

Log 2 Cycles x mm, y and 1 cm

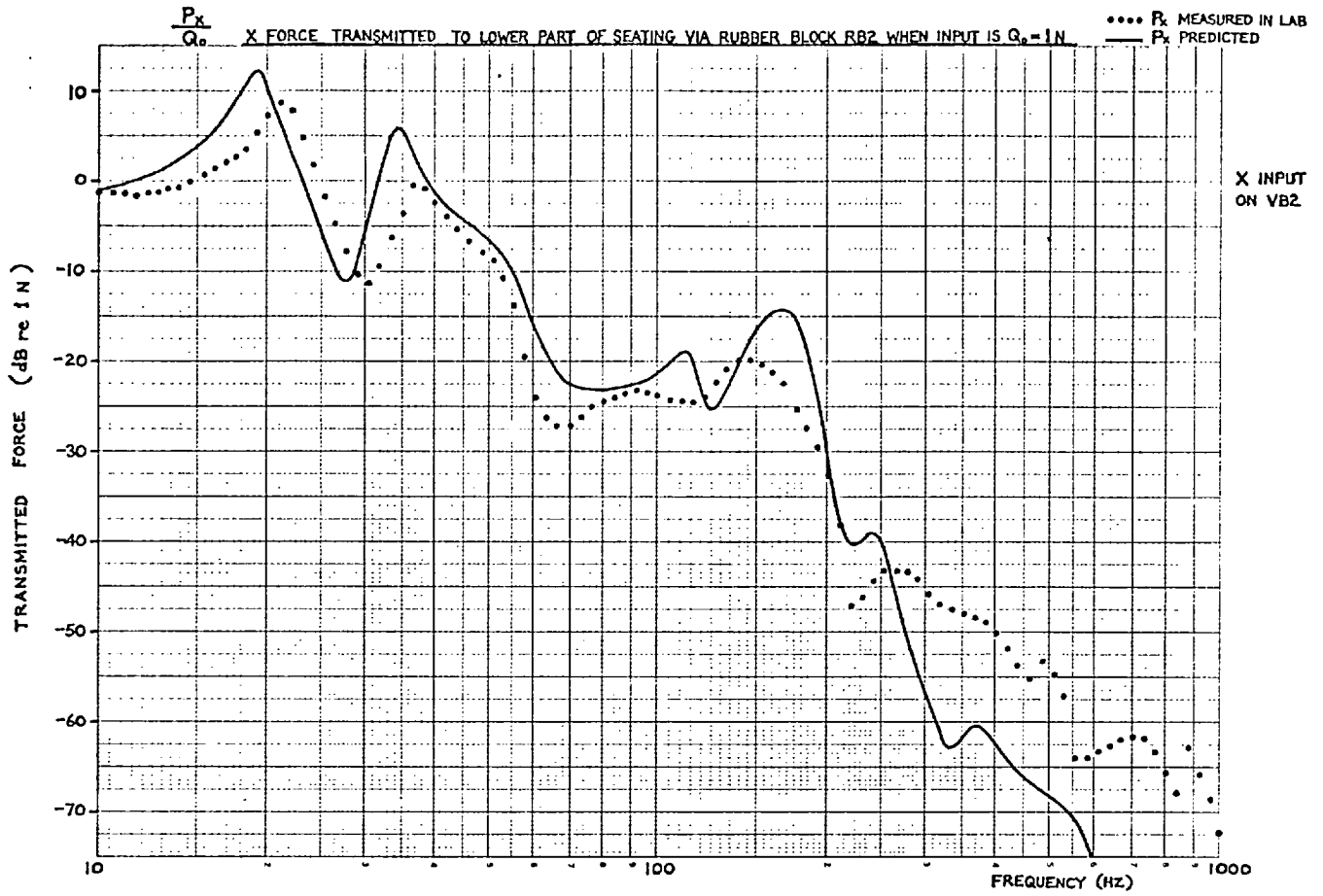
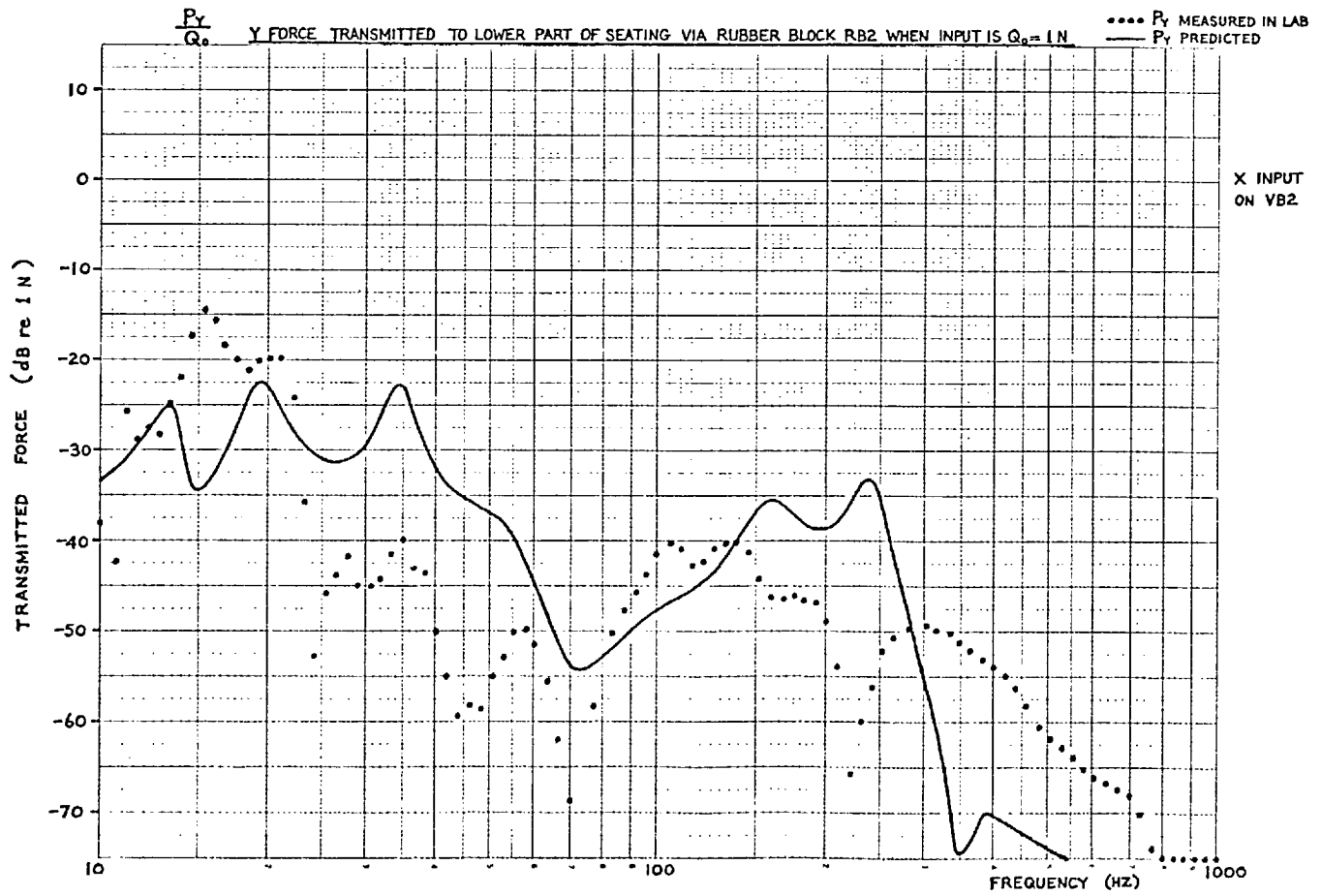


CHART
WELL 2232

Graph Data Ref 5521

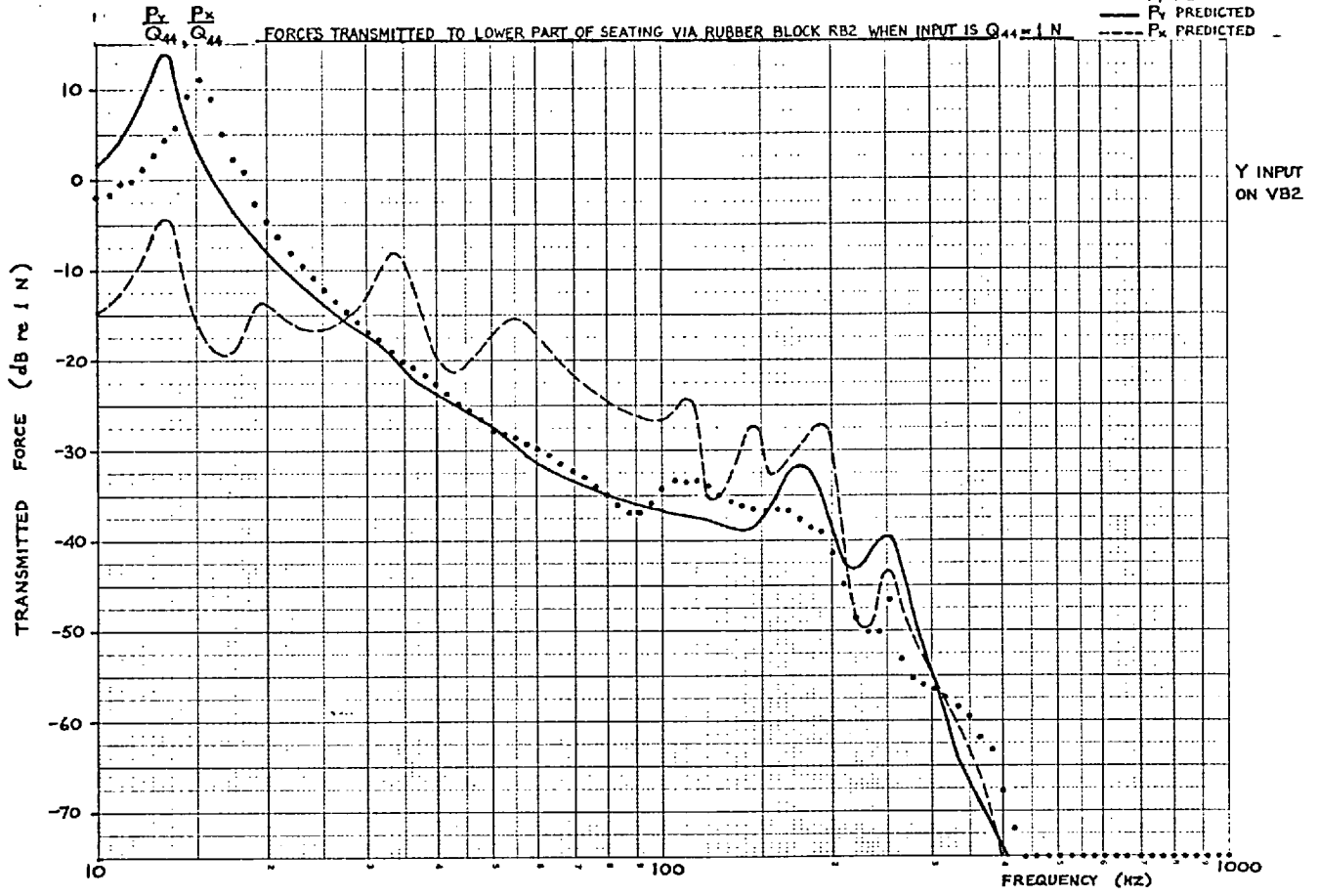
Log 2 Cycles x mm, y and 1 cm



CHARTE WELL 3021 Graph Data Ref. 5521

Log 2 Cycles a mm. j and 1 cm

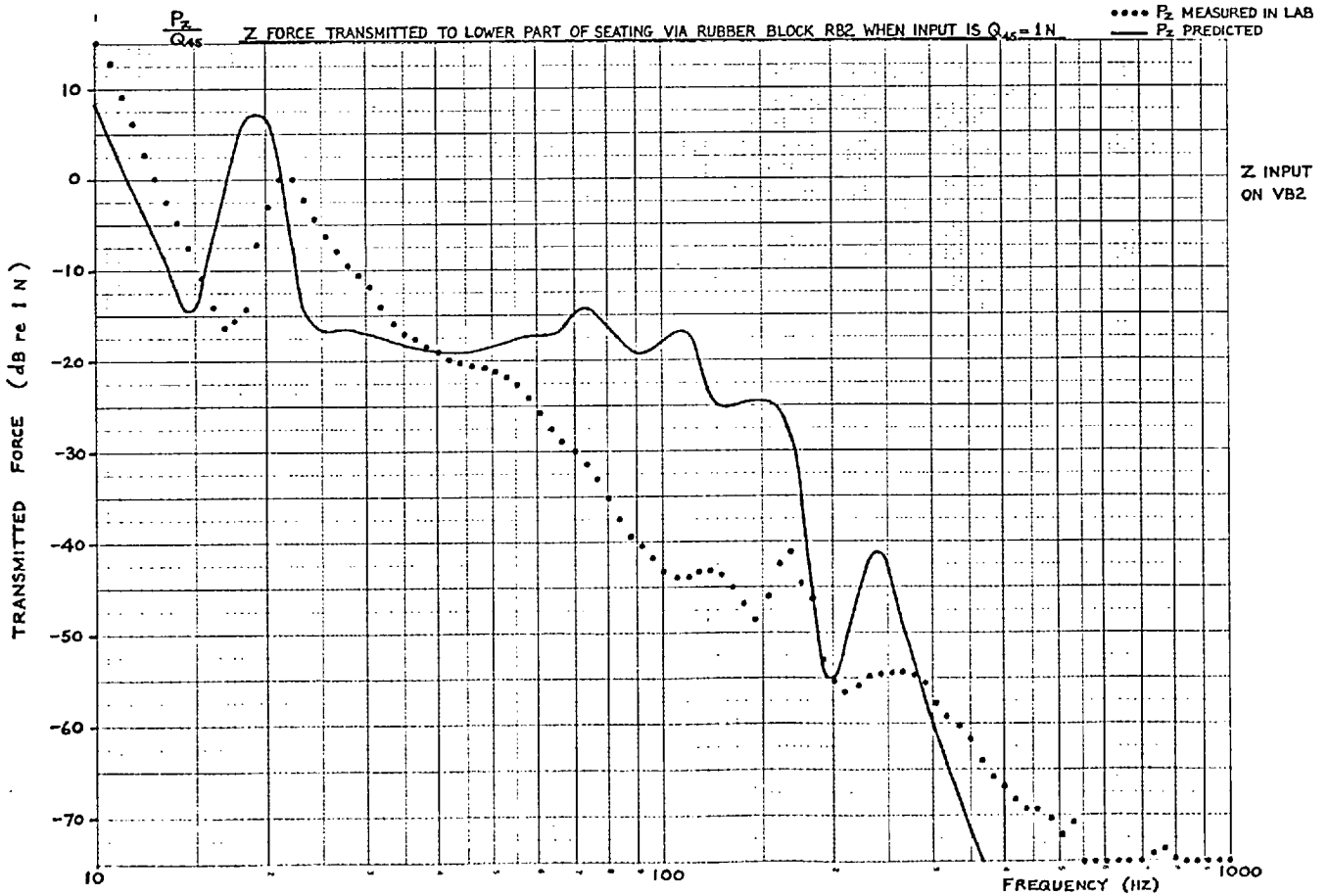
..... P_y MEASURED IN LAB
 ——— P_y PREDICTED
 - - - P_x PREDICTED

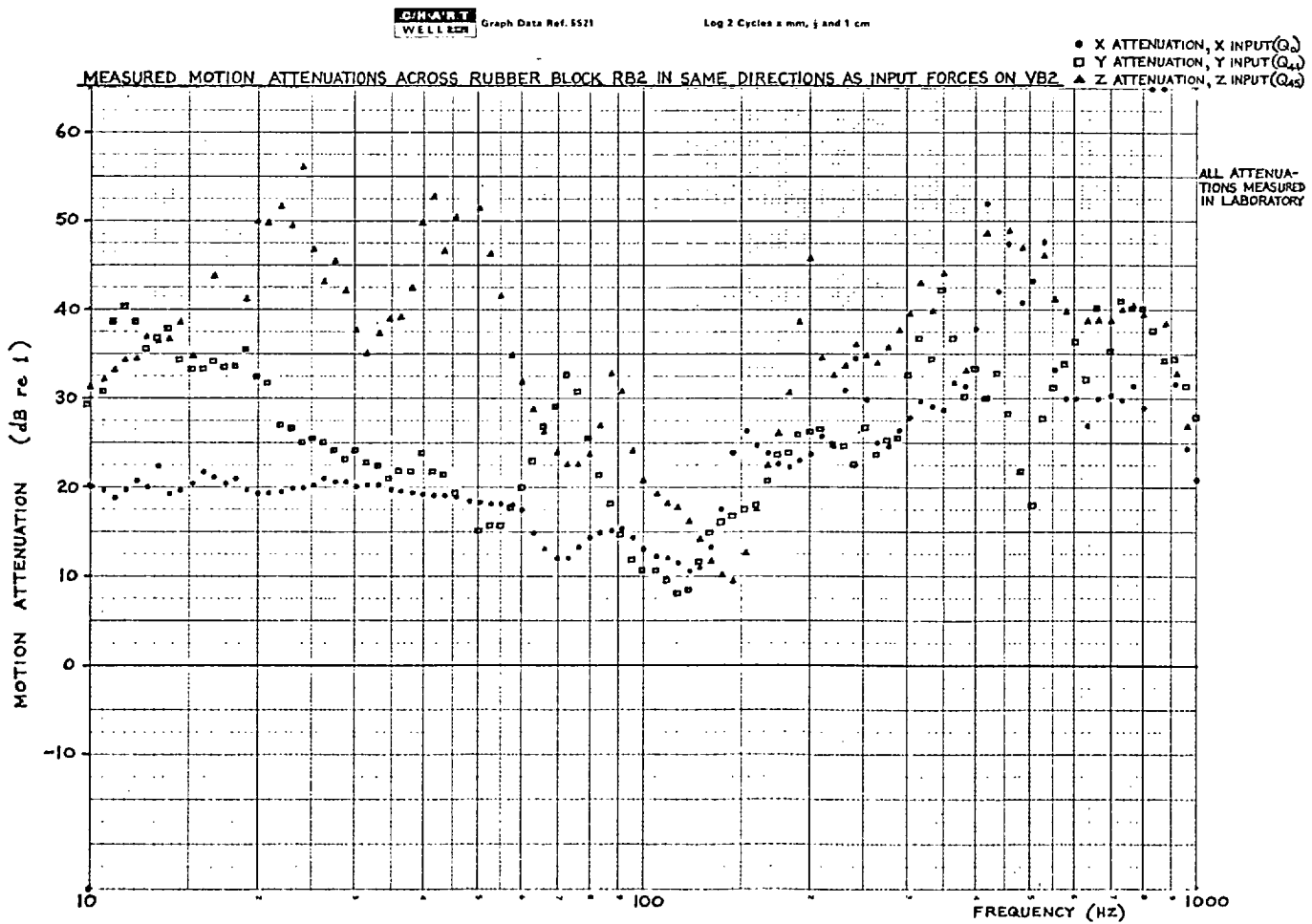
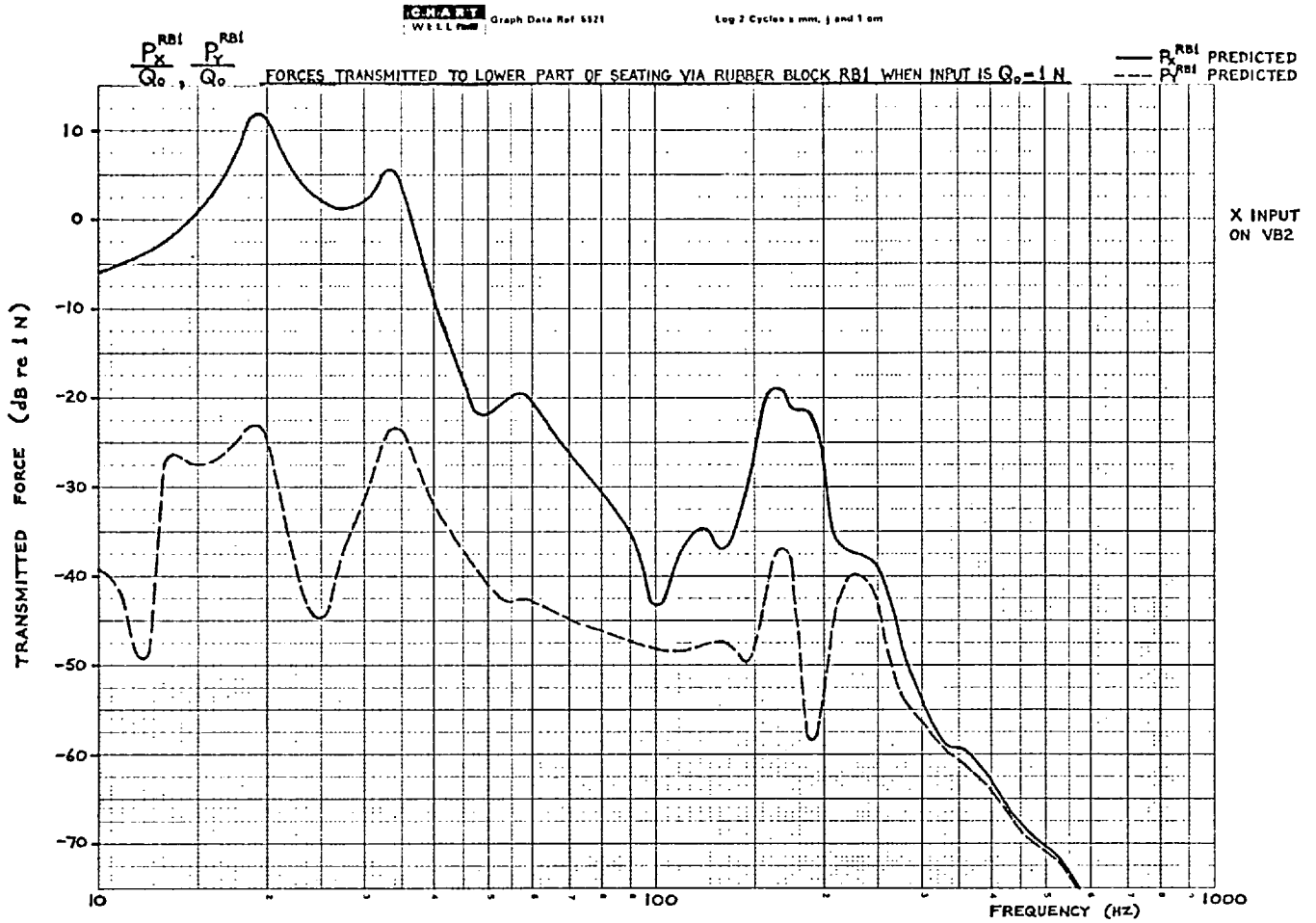


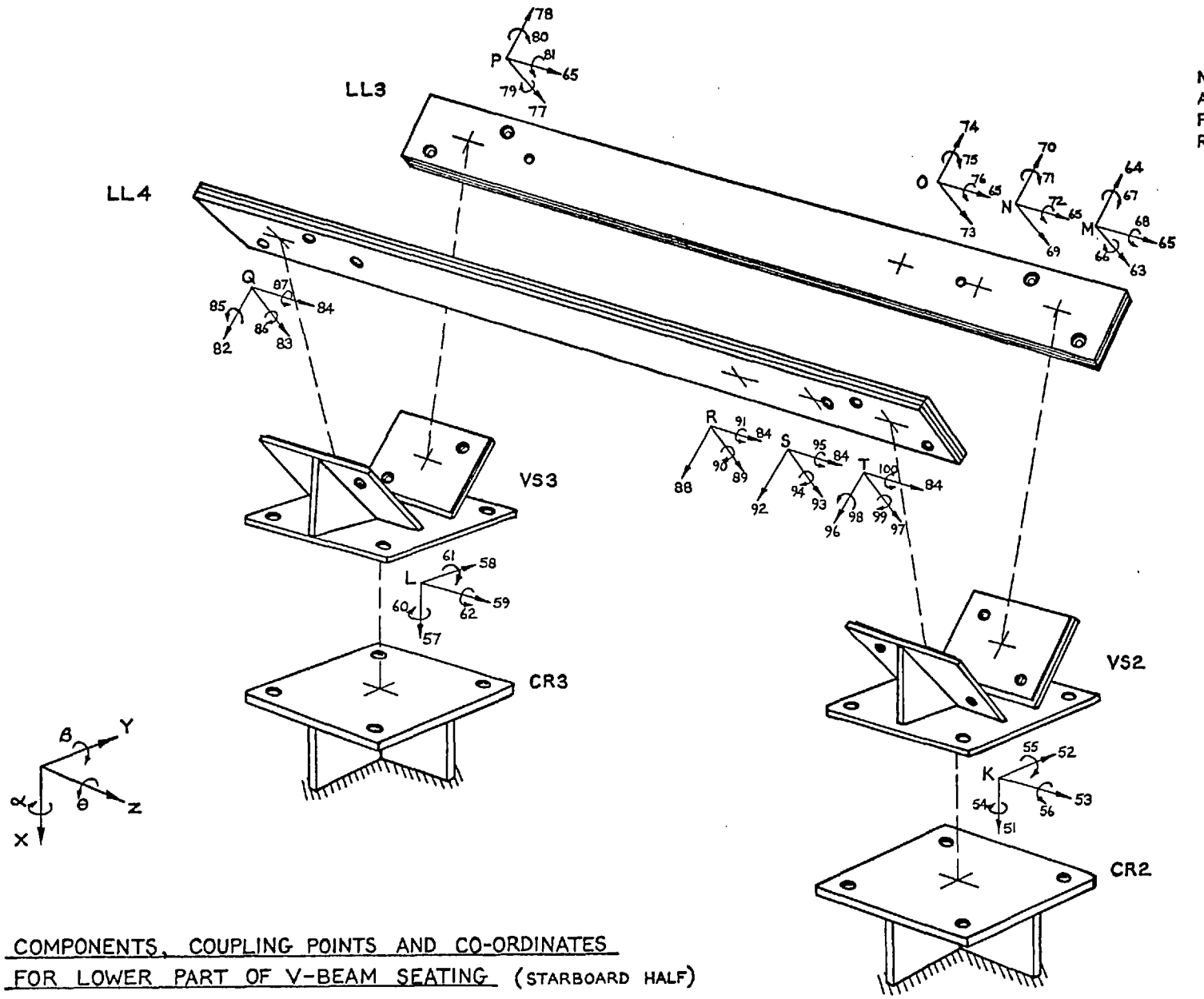
CHARTE WELL 3021 Graph Data Ref. 5521

Log 2 Cycles a mm. j and 1 cm

..... P_z MEASURED IN LAB
 ——— P_z PREDICTED







M, N, O, R, S, T ARE ASSUMED POINTS OF FORCE INPUT FROM RUBBER BLOCK RB2

COMPONENTS, COUPLING POINTS AND CO-ORDINATES
FOR LOWER PART OF V-BEAM SEATING (STARBOARD HALF)

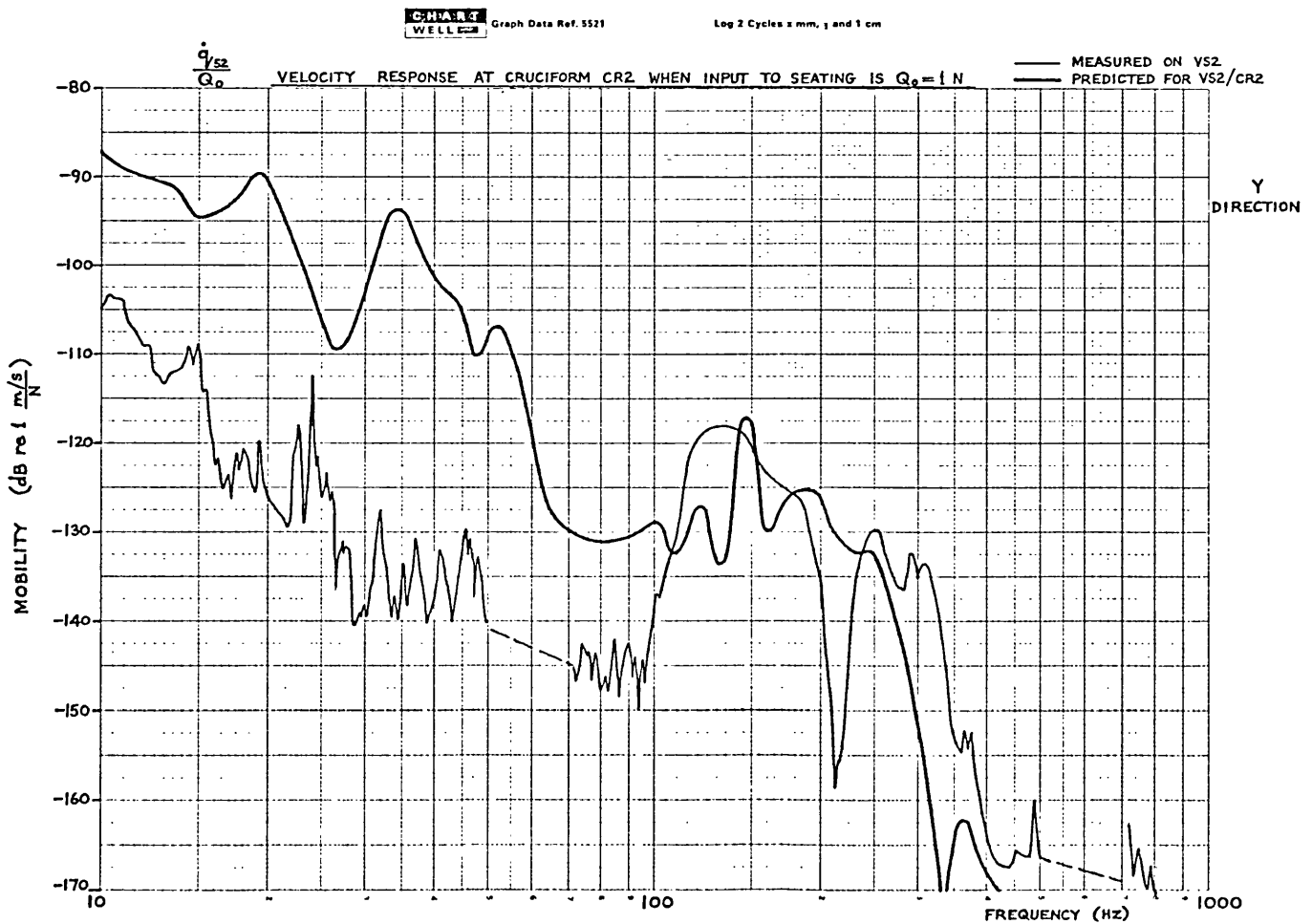
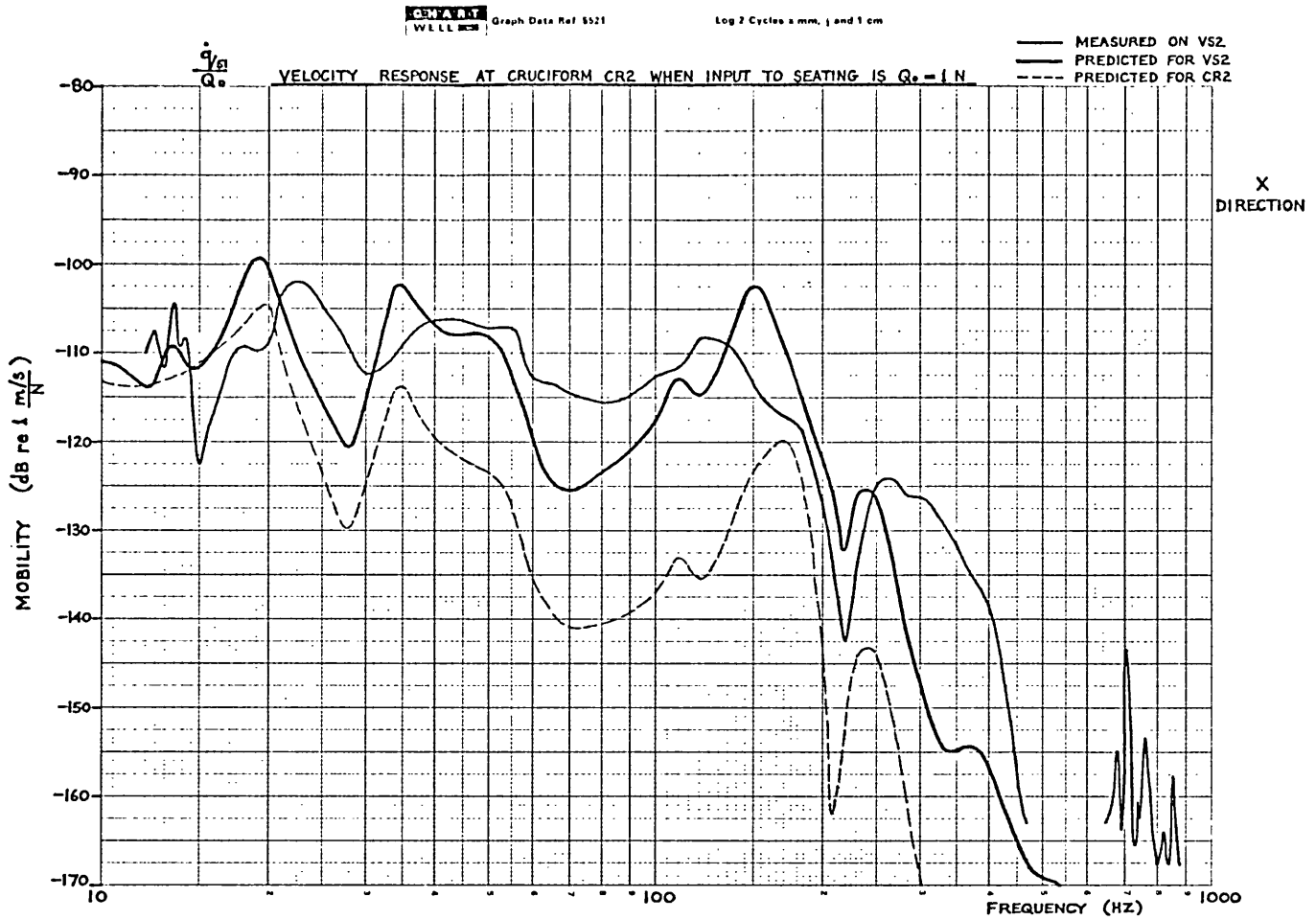
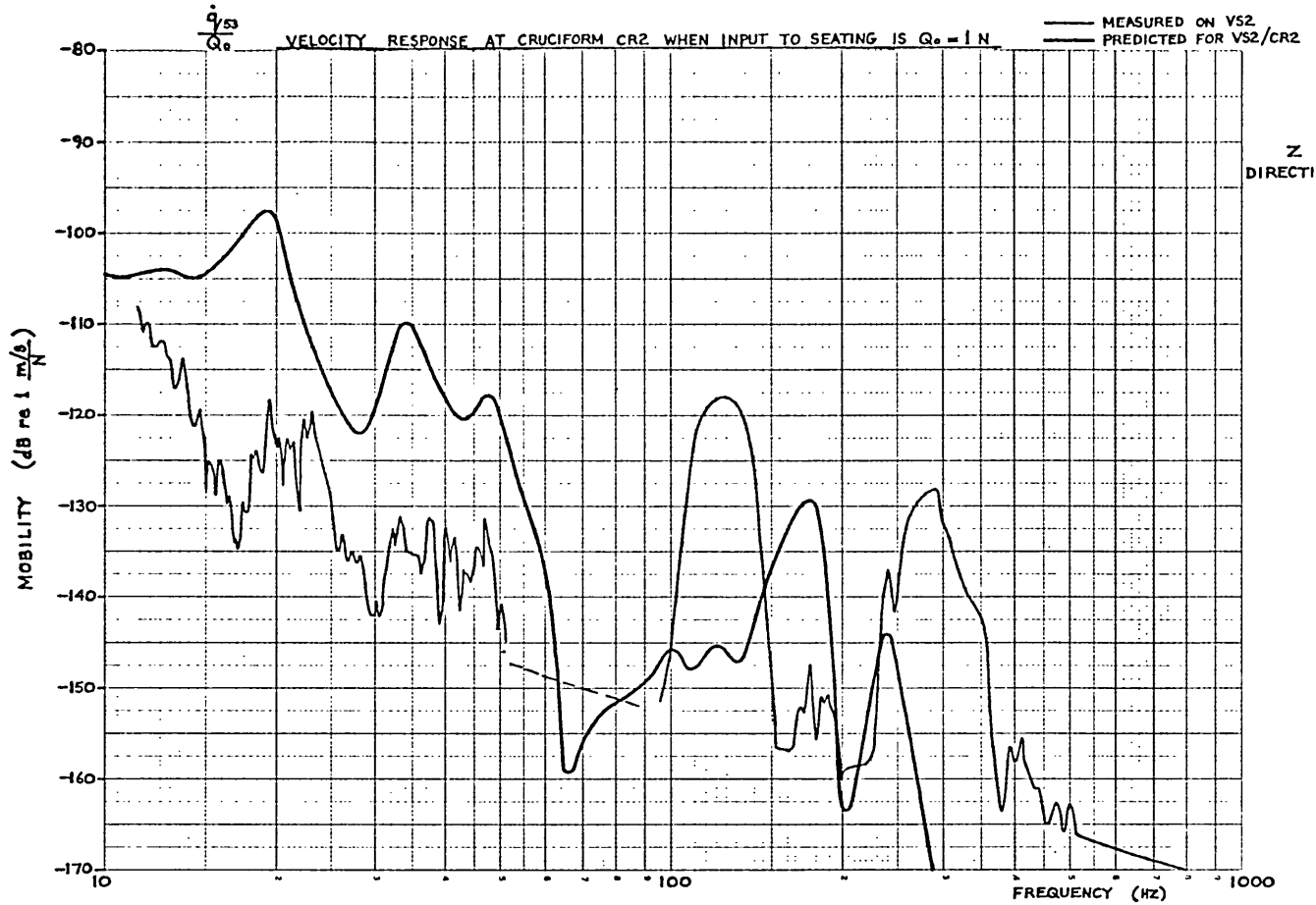


FIG 15.14

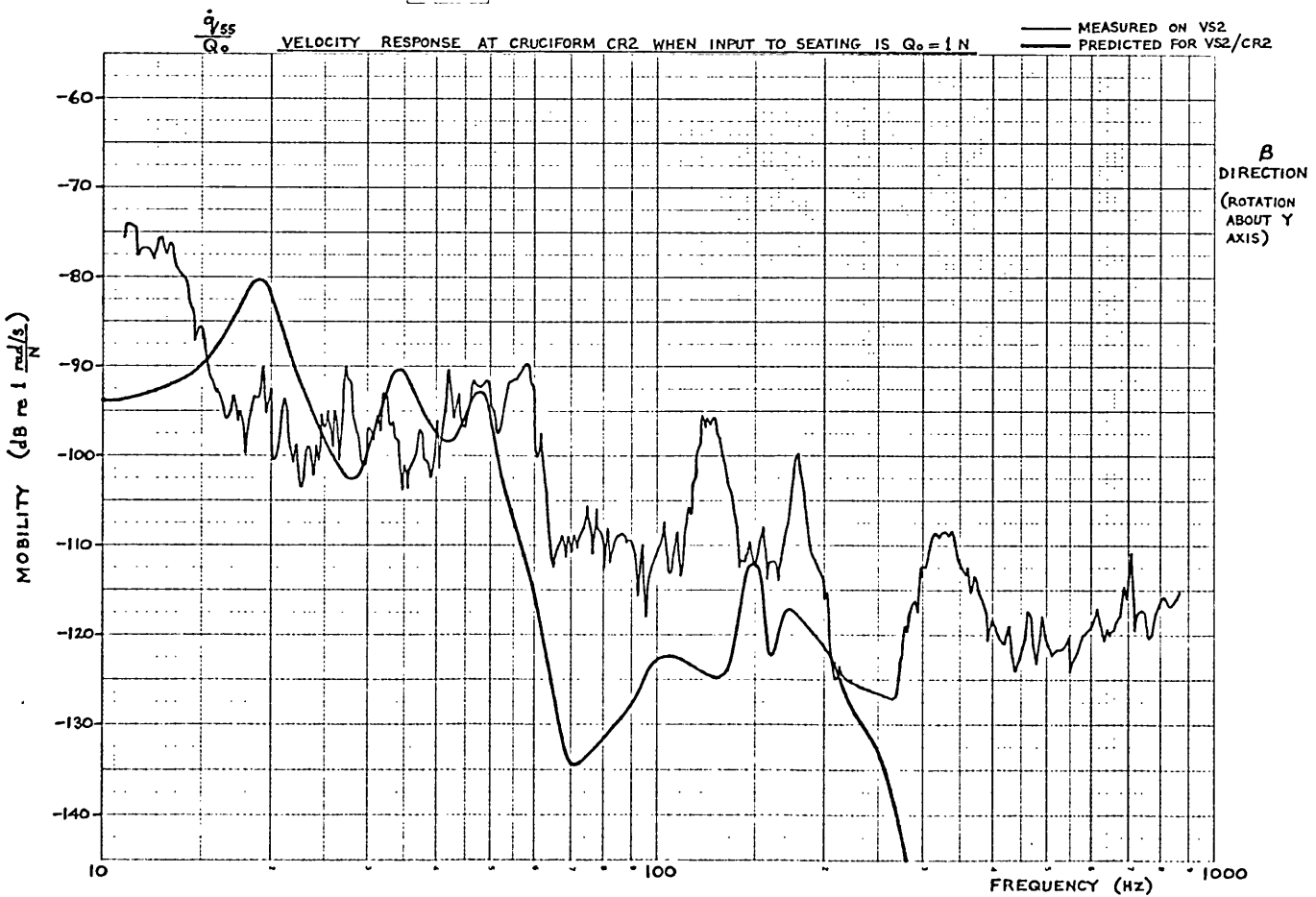
CHINA 27
WELL 8288
Graph Data Ref. 5521

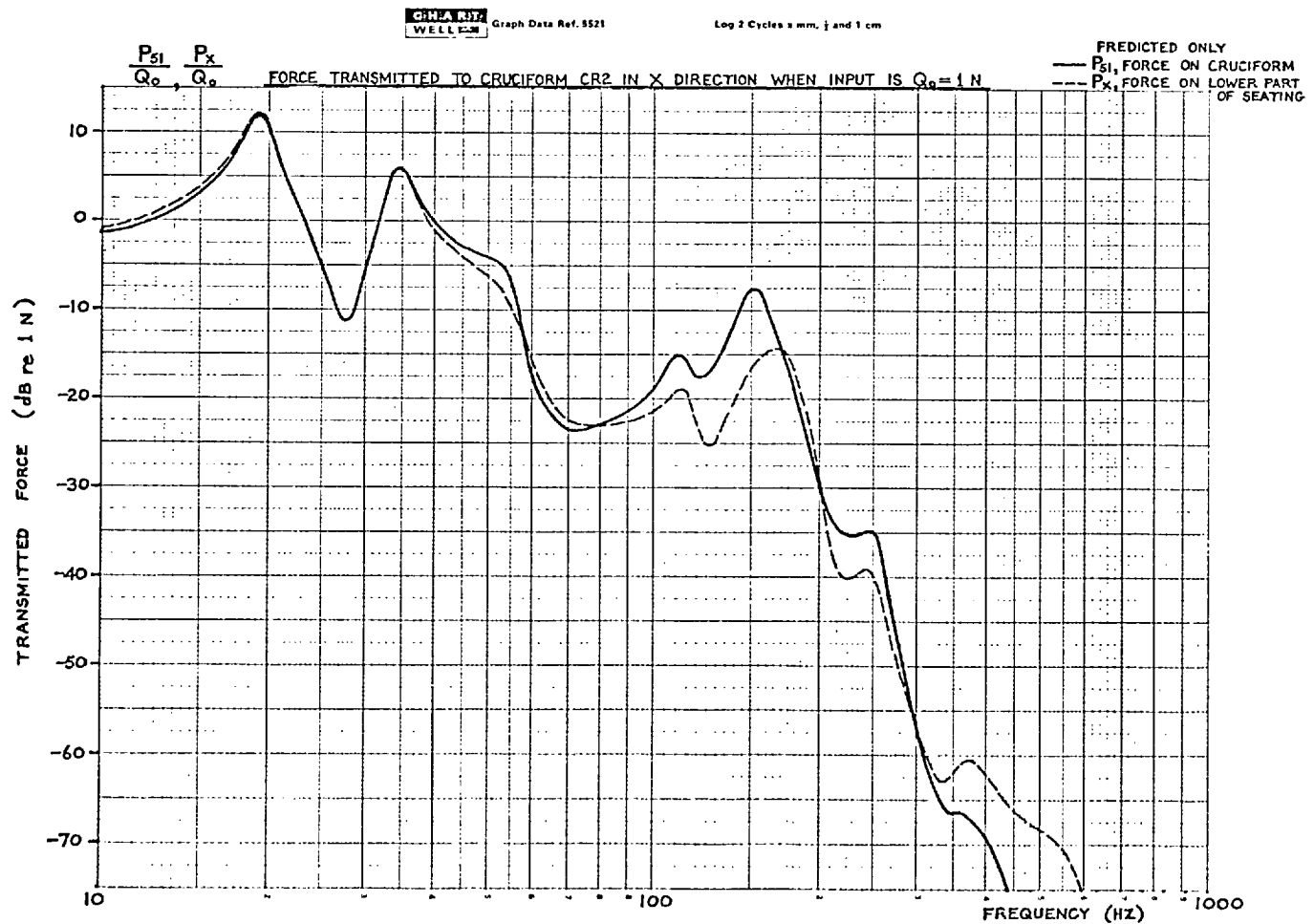
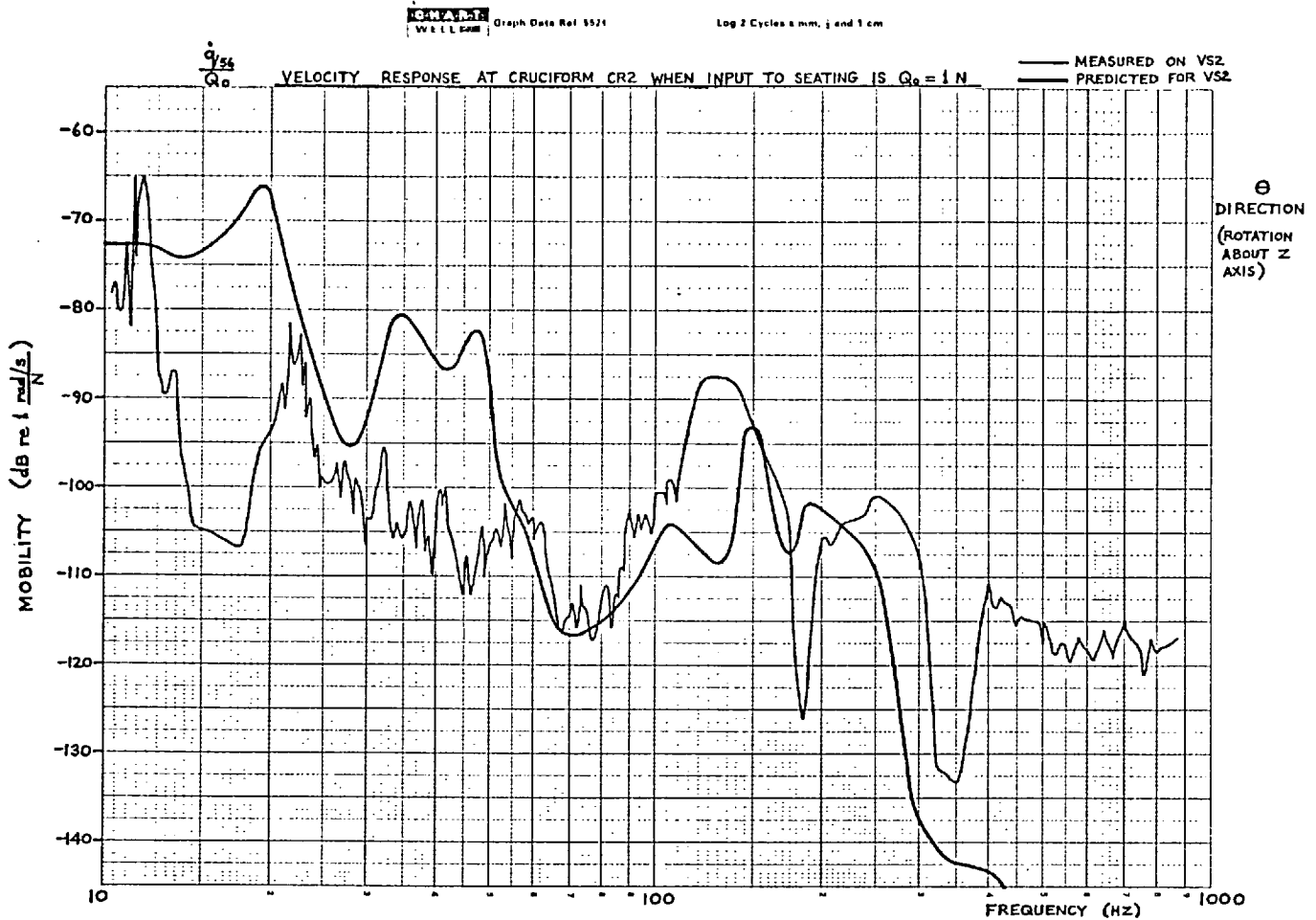
Log 2 Cycles x mm, j and 1 cm



CHINA 27
WELL 8288
Graph Data Ref. 5521

Log 2 Cycles x mm, j and 1 cm

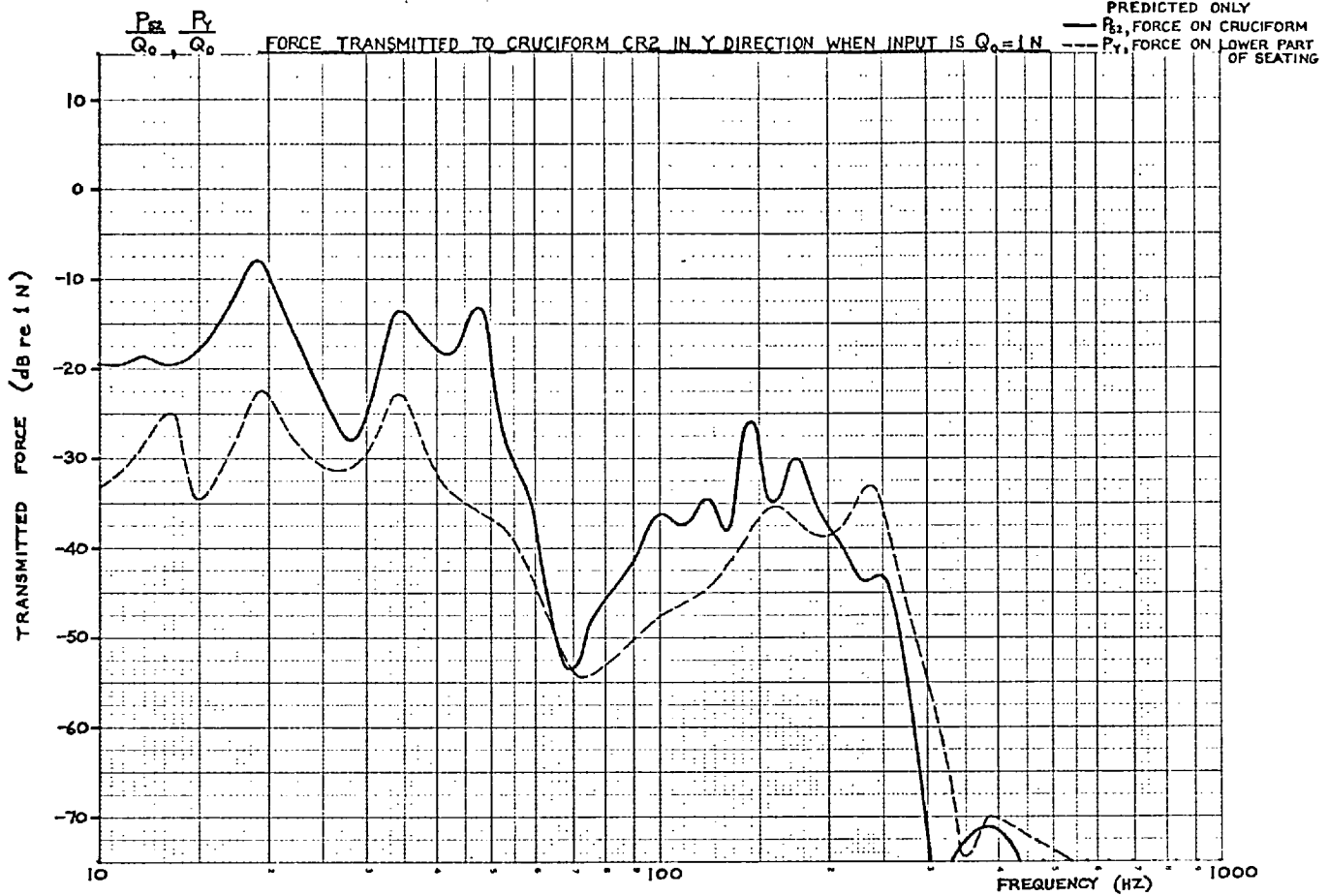




CRIVELLO
WELL 1 PC28

Graph Date Ref. 5521

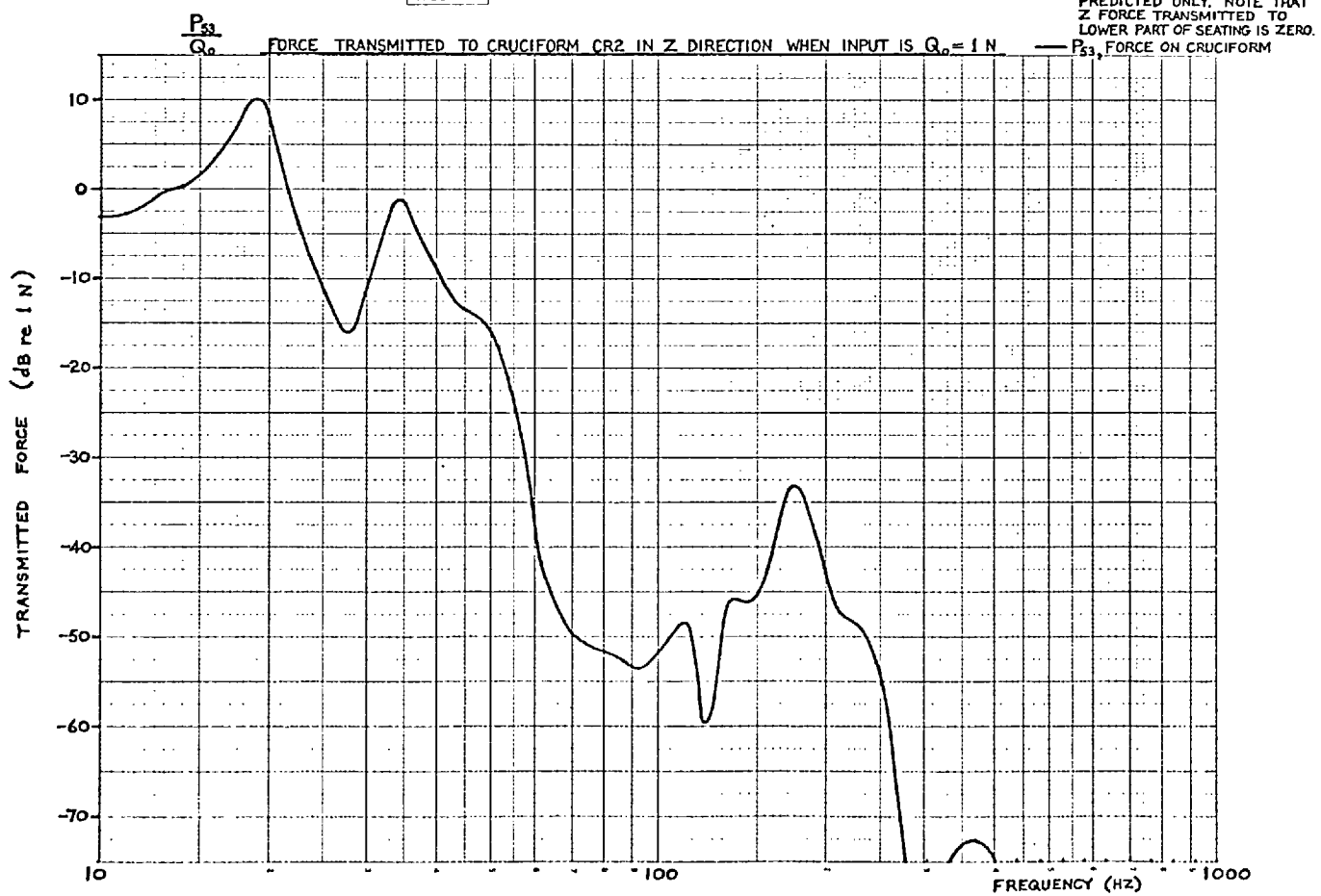
Log 2 Cycles x mm. j and 1 cm



CRIVELLO
WELL 1 PC28

Graph Date Ref. 5521

Log 2 Cycles x mm. j and 1 cm



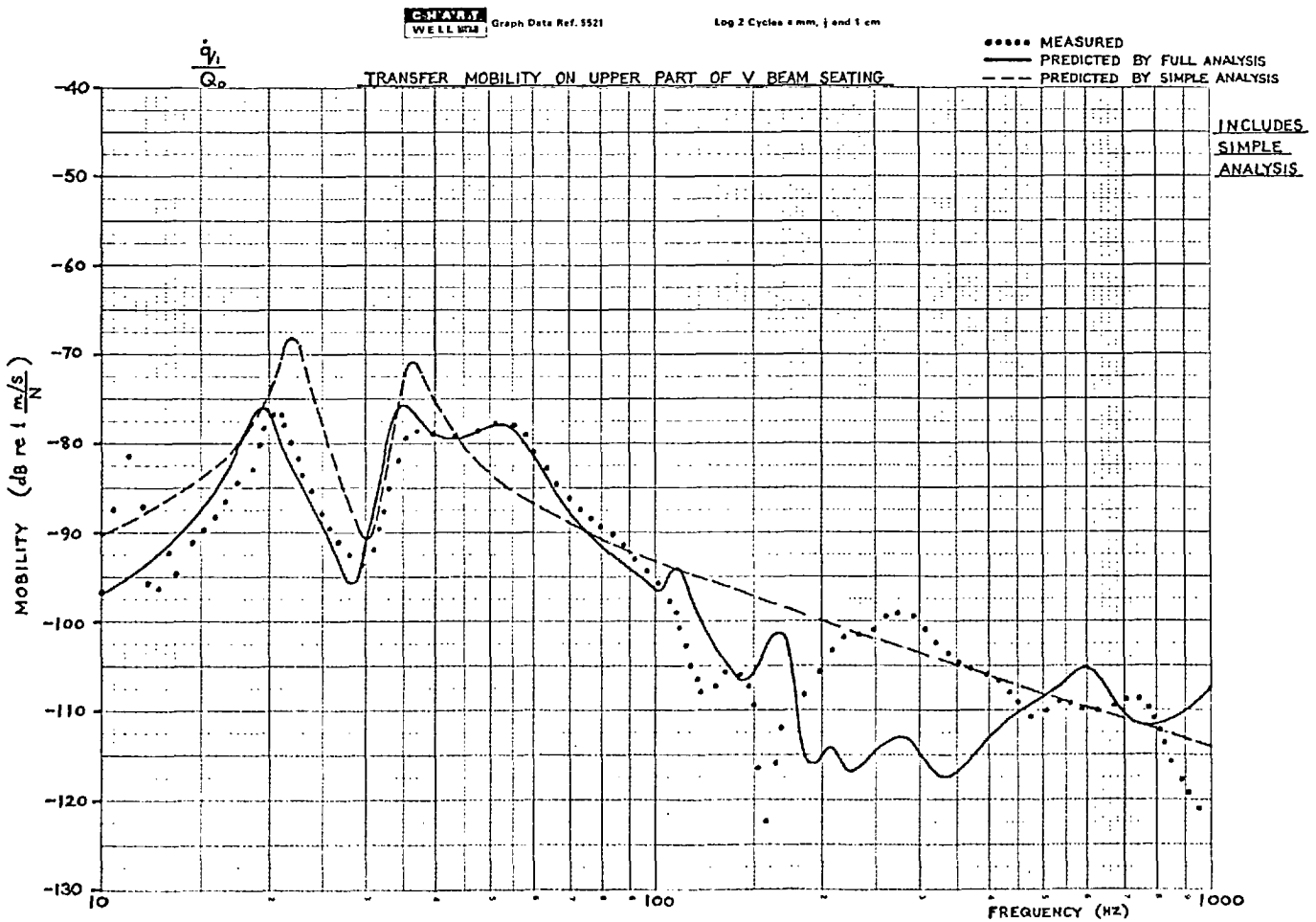
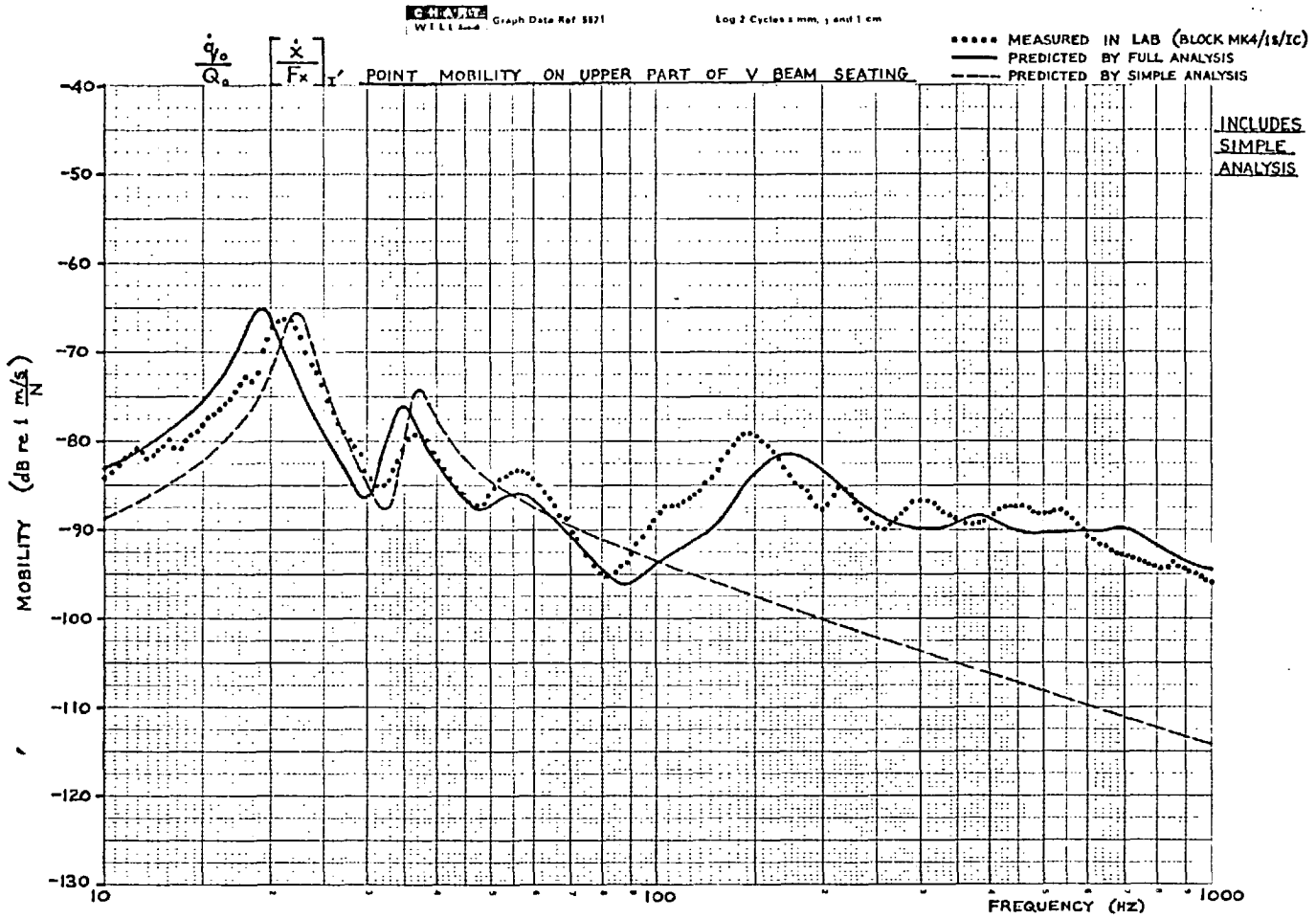
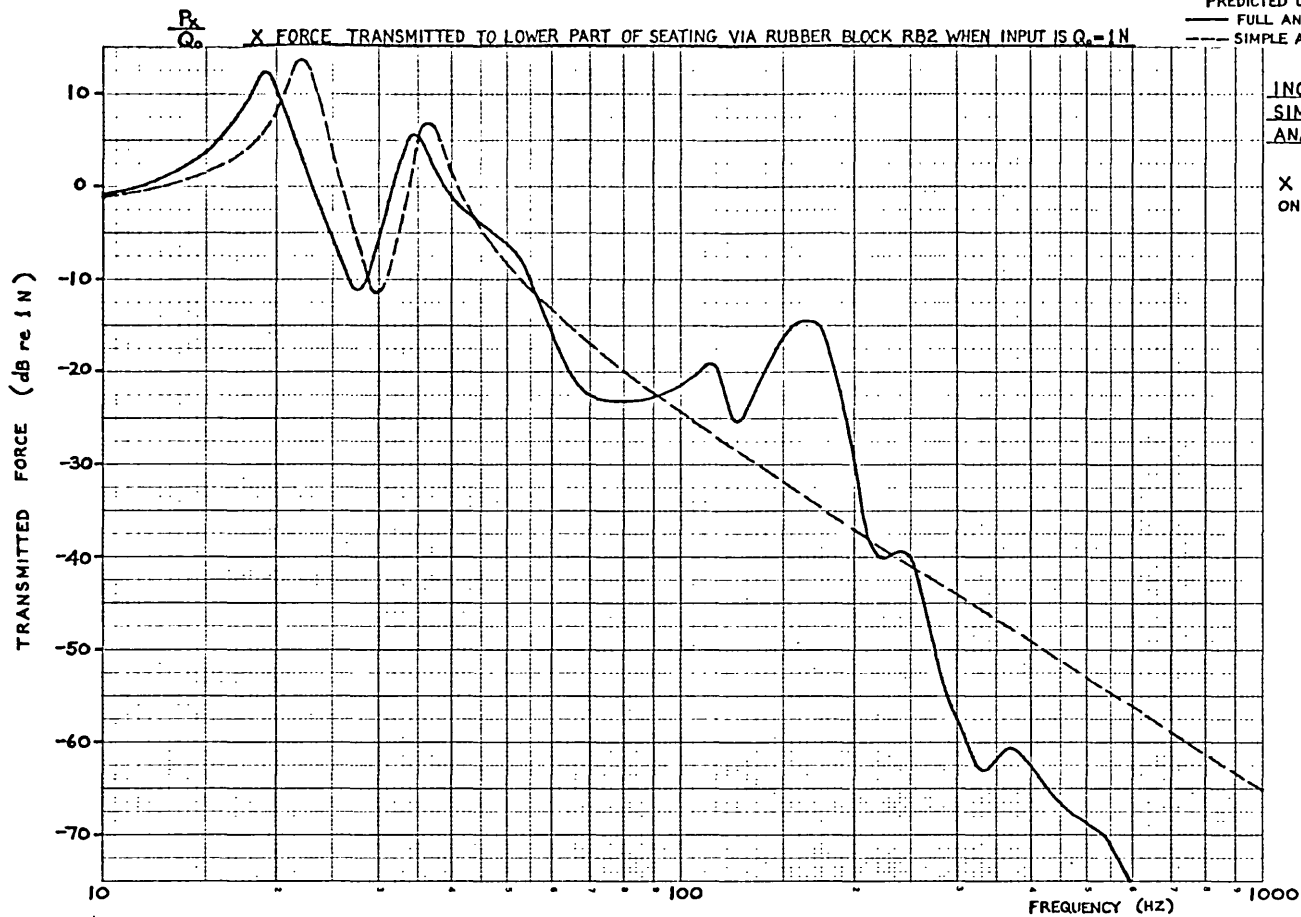


FIG 15.18

CHRYSLER
WELL LOG Graph Data Ref. 5521

Log 2 Cycles x mm, y and 1 cm

PREDICTED ONLY
— FULL ANALYSIS
- - - SIMPLE ANALYSIS



CHRYSLER
WELL LOG Graph Data Ref. 5521

Log 2 Cycles x mm, y and 1 cm

— MEASURED
— PREDICTED BY FULL ANALYSIS
- - - PREDICTED BY SIMPLE ANALYSIS

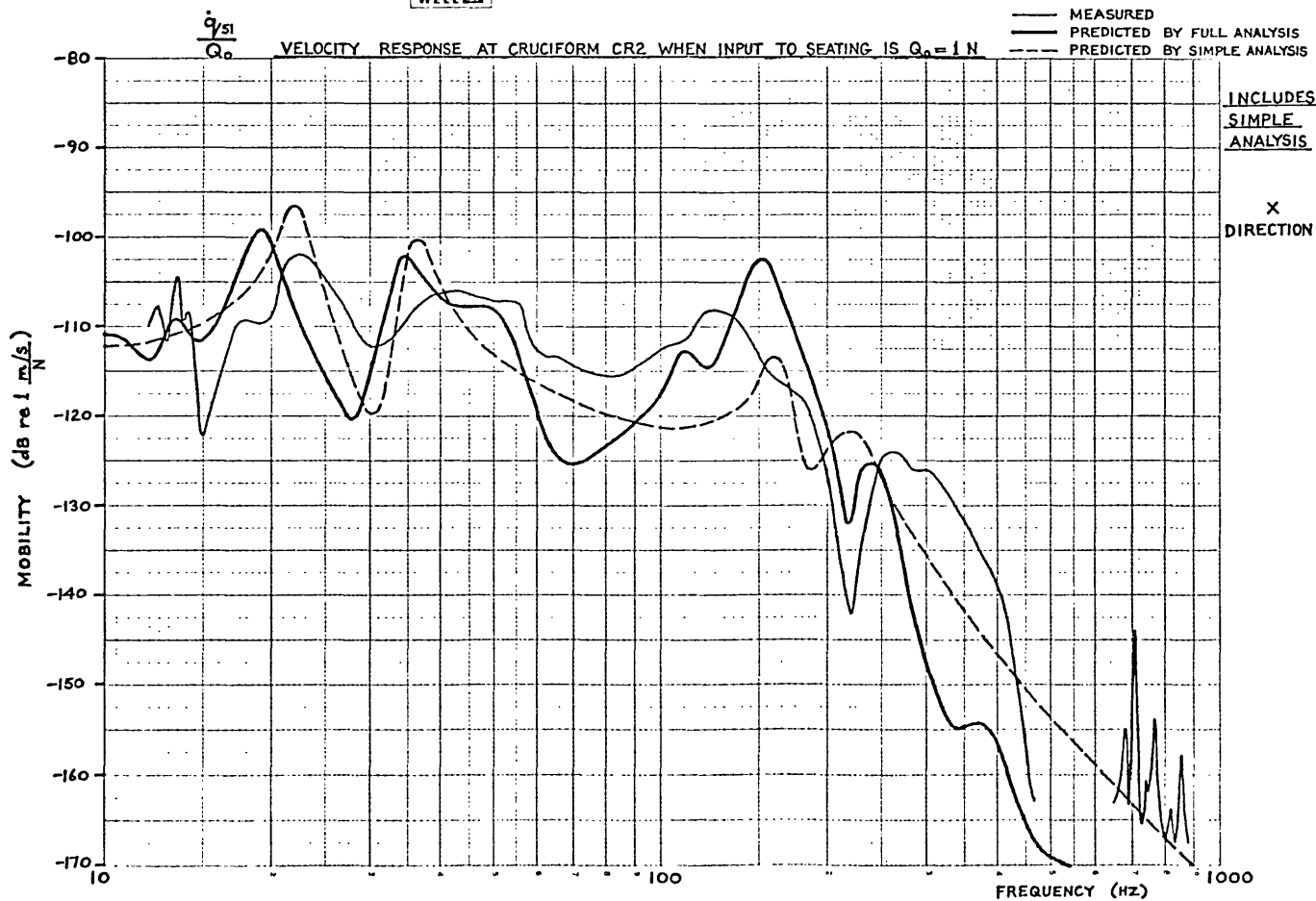


CHART Graph Data Ref 5521 Log 2 Cycles x mm, y and 1 cm

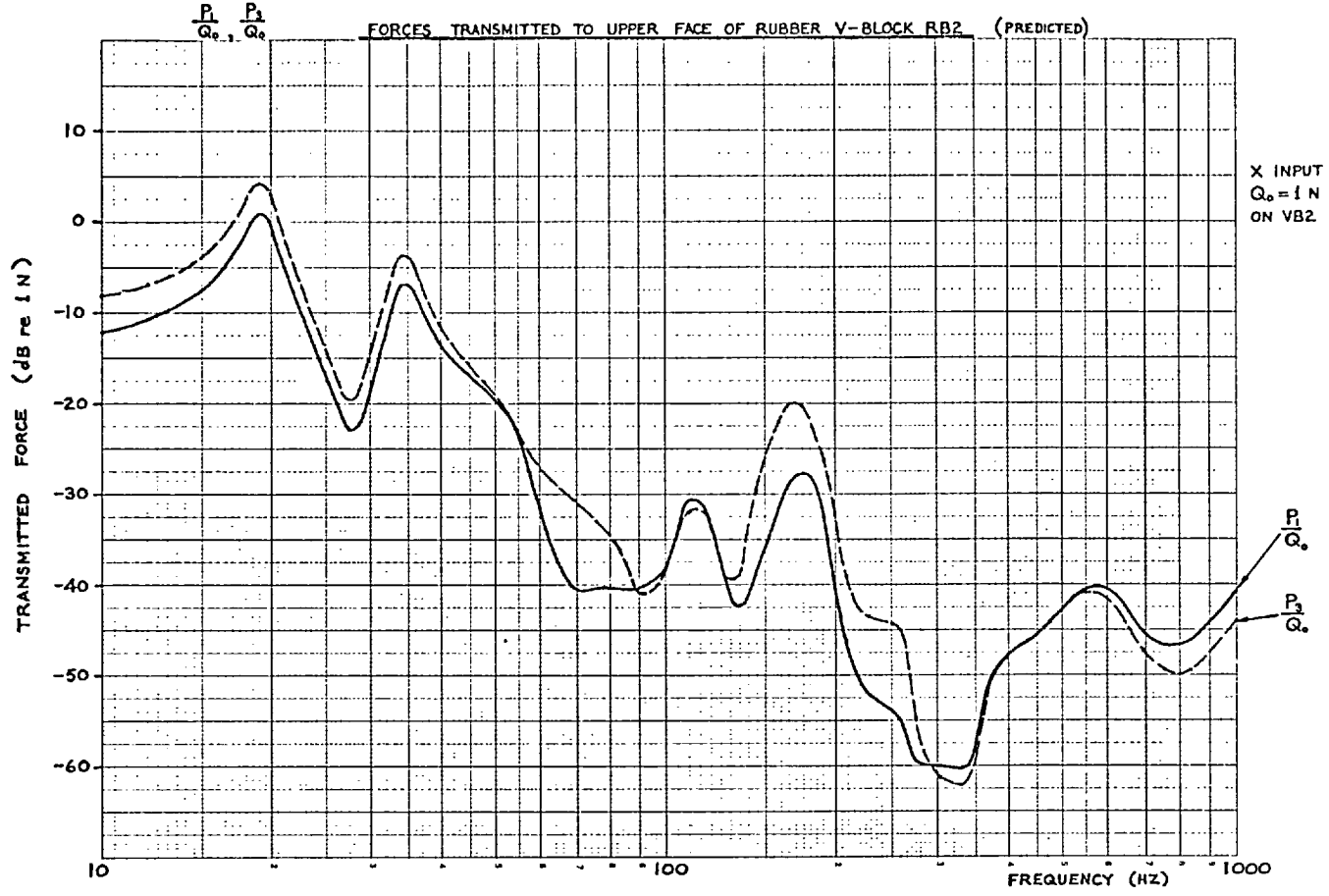


CHART Graph Data Ref 5521 Log 2 Cycles x mm, y and 1 cm

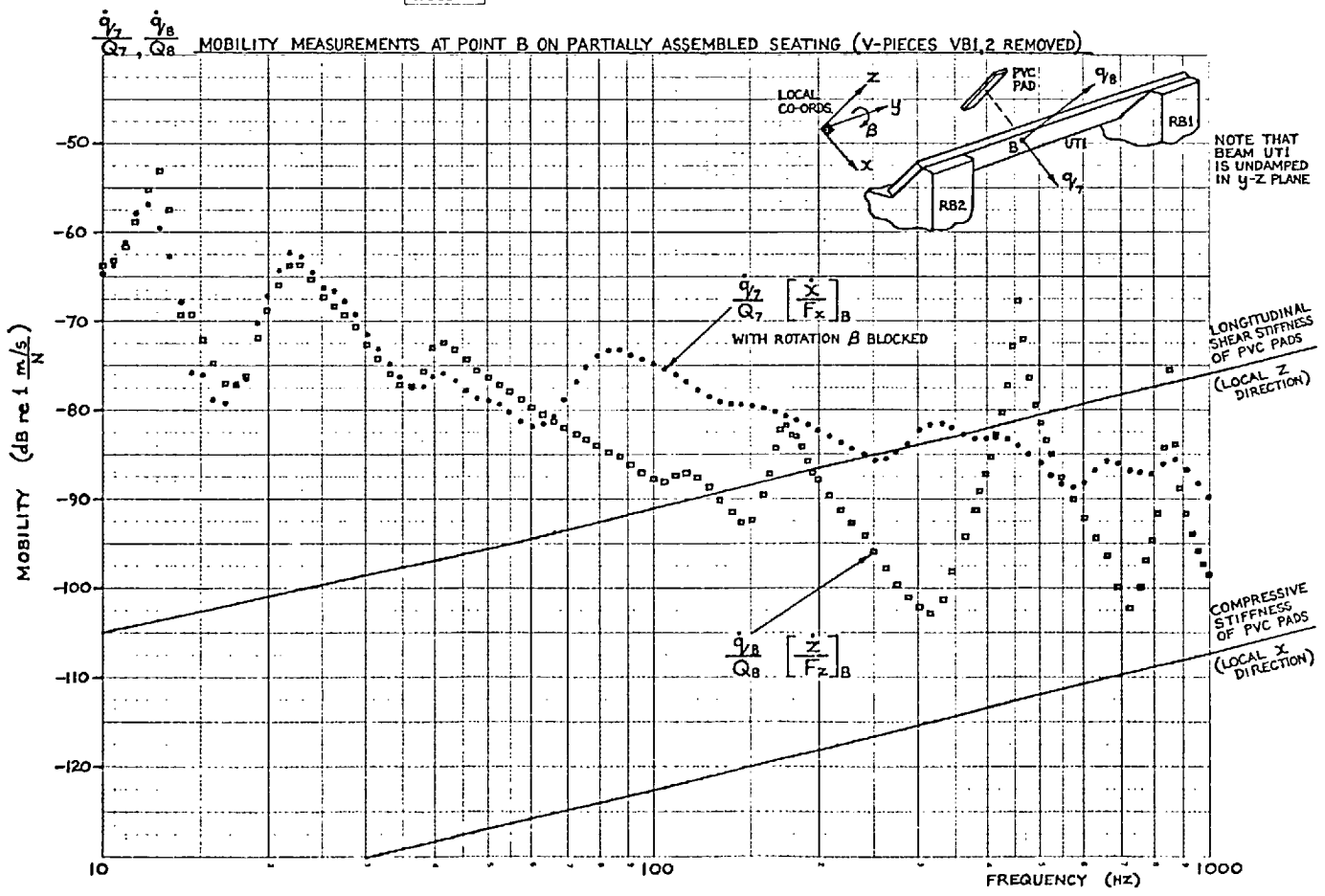
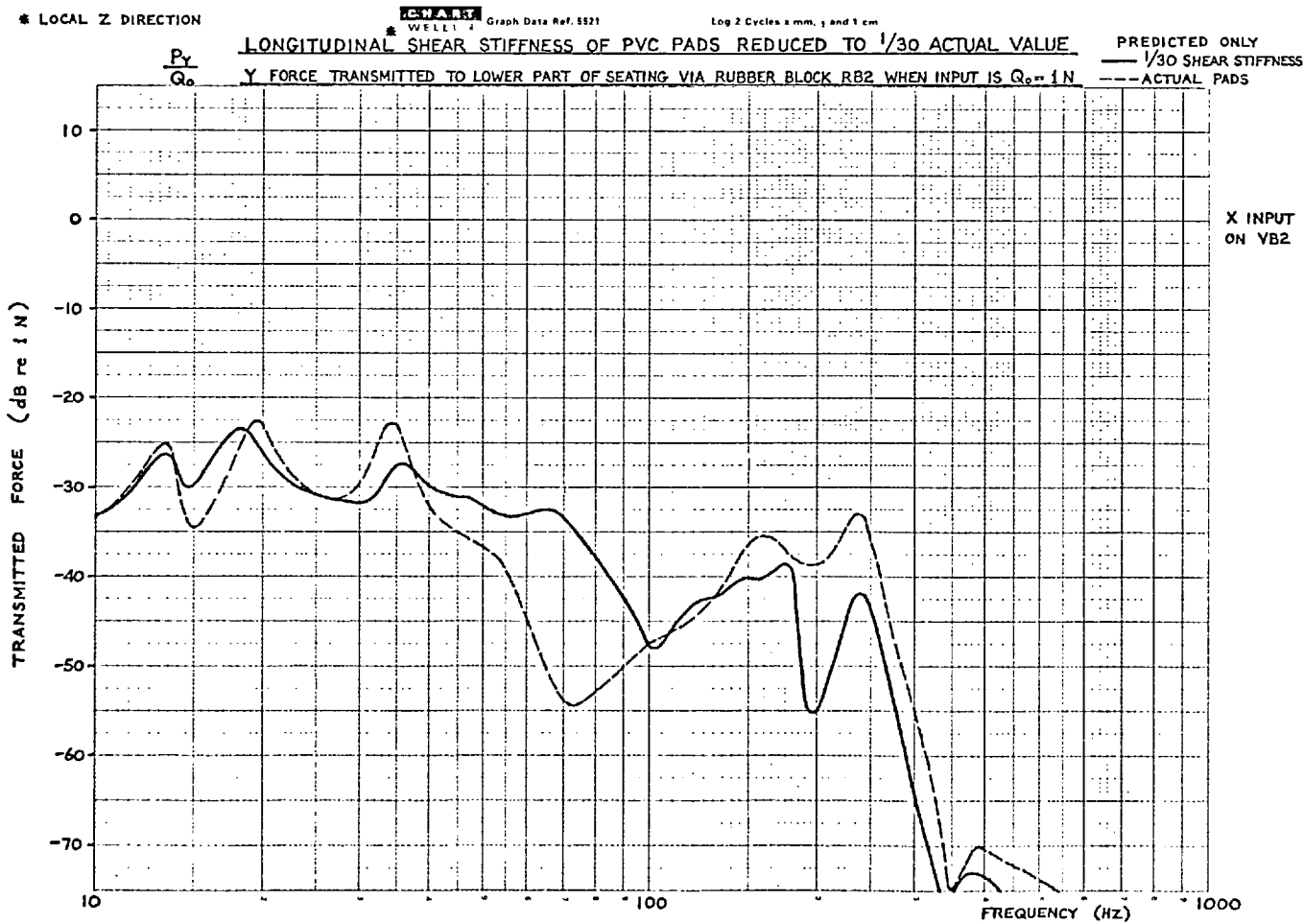
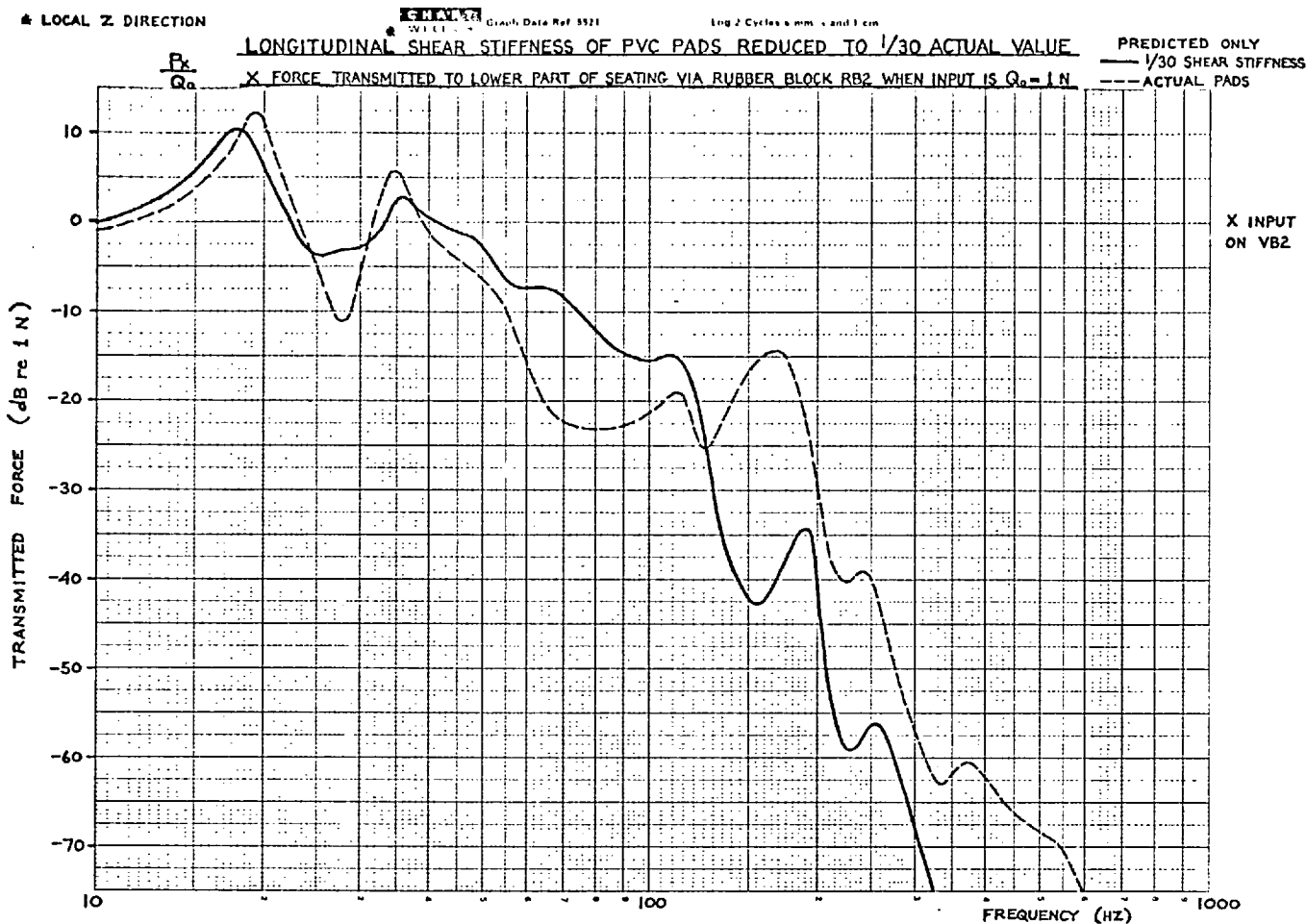


FIG 15.20



15.2 DISCUSSION OF RESULTS

Upper Part of the Seating (shown in Fig.15.1)

The various point mobility curves are given in Figs.15.2 to 15.4, and the transfer mobilities in Figs. 15.4 to 15.8. Before proceeding to consider these and the other results in more detail, it will be useful to list the major seating resonances, which are associated with the peaks in the point mobility curves. However, as a consequence of the heavy damping, some of these peaks are very much subdued, whilst on the transfer mobility and force transmissibility curves they show more strongly. The identification of the corresponding modes of vibration involves examination of many responses, both in magnitude and phase, so it is only proposed to list the modes, without going into the details of how they were identified. In order to see all the major resonances from point mobility data, it is necessary in the most general case to look at the mobilities in the X, Y, Z, α , β and θ directions. However, in the present case, all the major resonances show themselves to some degree in the X, Y and Z point mobility curves. This is because of the offset of the V-piece from the centre of the cross beams, together with the strong coupling between motions in the different directions. Nevertheless, one of the most important peaks, occurring at 175 Hz, is in fact a combination of two peaks.

The curve of vertical point mobility $\frac{\dot{y}_o}{Q_o} \left[= \frac{\dot{x}}{F_x} \right]_I$, shows five of the major seating resonances, which have been identified as corresponding to the following modes of vibration:

19 Hz Vertical bouncing of essentially rigid beam assembly on rubber blocks (X)*.

* The principal direction of motion in each mode is given in parentheses. The corresponding global co-ordinate system is shown in Fig. 15.1.

	35 Hz	Rocking of beam assembly on rubber blocks (Θ).	
	56 Hz	First flexural mode of beam assembly (flapping of sandwich beams in their plane of high flexibility and damping).	
Single peak at 175 Hz on graph	{	165 Hz	Rocking of steel V-piece on PVC pads (Θ).
		185 Hz	Vertical bouncing of V-piece on pads (X).

where the frequencies given are those predicted by the analysis, rather than the measured values.

The transverse point mobility $\frac{\dot{q}_{44}}{Q_{44}} \left[= \frac{\dot{y}}{F_y} \right]_I$ shows three other resonances:

	13 Hz	Transverse motion of rigid beam assembly on rubber blocks (Y).
	110 Hz	Principal resonance of rubber V-block in X-Z plane* (See Fig. 14.18).
	260 Hz	Transverse motion of V-piece on pads (Y).
		and the longitudinal mobility $\frac{\dot{q}_{45}}{Q_{45}} \left[= \frac{\dot{z}}{F_z} \right]_I$ shows five more:
	approx. 8 Hz	Fore and aft motion of beam assembly on rubber blocks (Z).
	19 Hz+	Rotational motion of beam assembly in horizontal plane on rubber blocks (α).
	21 Hz	Rotational motion of beam assembly about its own axis (β).
	74 Hz	Rotational motion of V-piece on pads (β).
	265 Hz	Fore and aft motion of V-piece on pads (Z).

From this list, it is seen that the 6 basic modes of the beam-assembly/rubber-block system are spread over the relatively wide frequency range of 8 to 35 Hz.

* Excited by rocking of beam assembly, since horizontal force causes rotation Θ in addition to translation Y.

+ This has been distinguished from the 19 Hz vertical resonance by the fact that the phase difference between q_{45} and q_{49} is 180° .

We shall now consider some of the mobility curves in a little more detail. Returning to the vertical point mobility $\frac{\dot{q}_o}{Q_o}$, it is seen that one of the major peaks occurs at 175 Hz. This rather broad peak is a combination of the 165 and 185 Hz peaks associated with the rocking and bouncing resonances of the V-piece on its pads (Θ and X resonances). It is rather pronounced because the offset vertical excitation at point I' is equivalent to a vertical force and a couple acting at point I (Centre of top plate of VB2). Although it is not shown here, the vertical mobility at point I is less than $\frac{\dot{q}_o}{Q_o}$ by between 2 and 7 dB over the range 100 to 1000 Hz, with the maximum difference occurring around 175 Hz. Hence, the chosen excitation position has given rise to a strong excitation of the Θ resonance of the V-piece on its pads, and this should be remembered when interpreting all subsequent results. In addition to the predicted curve, there are two measured curves, which correspond to tests performed in the laboratory and on the installed system. Bearing in mind the complexity of the system, the predicted results are very good, with a maximum deviation of only 5 dB from the laboratory measurements. One could hardly hope for better agreement, especially since the two sets of measurements differ by a similar amount. This latter difference was probably caused by the connecting bolts between the V-pieces and the beams having been tightened up different amounts in the two cases. It is certainly unlikely that it has anything to do with the different supporting structures, since the rubber block is sufficiently soft to completely mask the effect of the support impedance.

The point mobility $\frac{\dot{q}_{44}}{Q_{44}} \left[= \frac{\dot{y}}{F_Y} \right]_I$ together with the transfer mobility $\frac{\dot{q}_2}{Q_{44}}$ (Fig.15.6) show the effect of the resonances of the V-piece on its PVC pads. The pronounced peak in the point mobility curve at 180 Hz is again due to a combination of the Θ and X resonances of the V-piece on its pads, and in contrast, the Y resonance at 260 Hz is very much subdued.

The theoretical transfer mobility curve clearly shows an increase in drop-off rate from 6 to 12 dB per octave above the 165 Hz Θ resonance, thereby indicating that the V-piece is effectively decoupled from the beams at the higher frequencies. The measured results show a stronger Y resonance, which delays the increased drop-off rate till about 300 Hz, but both sets of results demonstrate that the transverse beam assembly on its rubber blocks is in fact a two-stage system, comprising V-piece mass, pad stiffness, beam mass, and rubber block stiffness. When we come to consider the force transmission to the lower part of the seating, it will be seen that this two-stage behaviour in the X, Y and Z directions has a very beneficial effect upon the high frequency attenuation.

The rotational point mobility $\frac{\dot{q}_{46}}{Q_{46}} \left[= \frac{\dot{\Theta}}{M_{\Theta}} \right]_{I'}$ clearly shows the same major peak as was observed on the vertical point mobility curve at 175 Hz. The width of the peak and its centre frequency suggest that there is strong coupling between the Θ and X motions, and this is borne out by the cross mobility $\frac{\dot{q}_{46}}{Q_0} \left[= \frac{\Theta}{F_x} \right]_{I'}$, shown in Fig.15.4. The coupling gives rise to a strong excitation of the V-piece in both its rocking and bouncing modes. It is also interesting to observe that once again there is a difference of several dB between the measurements made in the laboratory and those made on the installed system, with the predicted results generally lying somewhere between the two sets of measurements. Apart from minor differences in the system in the two cases, it is possible that the differences between the two sets of experimental results may be partly due to the fact that the laboratory tests were performed using the single-shaker measurement technique, whilst the measurements on the installed system were made using the twin-shaker technique. The only major deviation between the experimental and theoretical results occurs in the neighbourhood of 800 Hz, where both measured curves show a resonant peak. It is thought that the resonance corresponds to the bending mode of the 19 mm top plate of the V-piece, which was not allowed for in the analysis. Although the results are not perfect, the reasonable agreement

between prediction and experiments testifies to the adequacy of the analysis and of the multi-directional measurement techniques.

It is not proposed to discuss all the transfer mobility results for the upper part of the seating, since we are more interested in the force transmission to the lower part of the seating and to the cruciforms. However, it will be observed that very good agreement has been obtained between predictions and measurements. Although in some cases these differ by as much as 10 dB or more, the average difference is probably less than 5 dB. Bearing in mind the various unknowns associated with such a complex damped structure, this agreement is very gratifying.

Figs. 15.9 to 15.11. show the net force transmission to the lower part of the seating when various inputs are applied on V-piece VB2. $\frac{P_x}{Q_0}$ is the vertical transmissibility via rubber block RB2 and it is seen to exhibit three major peaks. The first two correspond to the basic bouncing and rocking modes of the beam assembly on the blocks, whilst the third is due to the resonances of the V-piece on its pads, and is in fact the combination of two close peaks. The fat peak associated with these V-piece/pad resonances is only kept down to a reasonable level by the very heavy damping in the pads ($\gamma = 0.66$). However, the 15 to 20 dB rise in transmissibility around 165 Hz is followed by a much more rapid drop-off* after 200 Hz, due to the partial decoupling of the V-piece from the beams in the X and Θ directions. Hence, the high frequency performance is even better than if the transverse beam assembly were rigid! The predicted and measured forces agree remarkably well, especially remembering that the measurements were obtained as the product of block static stiffness and measured block compression. The differences at the

* 24 dB/octave, as against 12 dB/octave before the resonance.

higher frequencies were to be expected, since the effective stiffness of the block decreases due to wave effects. In addition, the limited number of modes allowed for in the rubber block model undoubtedly causes its effective stiffness to decrease too rapidly with frequency. Thus, the actual force transmission above 250 Hz probably lies between the two curves.

The corresponding transmission in the Y direction is given by $\frac{P_Y}{Q_0}$ and it is very interesting to note that whereas P_x and P_Y differ by around 30 dB at the lower frequencies, they become practically equal around 200 Hz. The considerable scatter of the measured data was caused by two factors: (a) The very small accelerometer signals at low frequencies, and (b) the effect of cross-axis motion, due to the triangular accelerometer blocks not being mounted exactly in the vertical plane.

The upper graph in Fig.15.10 shows the forces which are transmitted in the X and Y directions when a horizontal input is applied in the Y direction (i.e. $\frac{P_x}{Q_{44}}$ and $\frac{P_Y}{Q_{44}}$). Once again it is seen that the two curves converge around 200 Hz, after which the drop-off is quite rapid, as a consequence of the decoupling of the V-piece from the beams.

The lower graph in the same figure shows the force transmissibility in the Z direction (i.e. $\frac{P_z}{Q_{45}}$). The fairly large difference between the predicted and measured results between 50 and 180 Hz may be the result of inadequate modelling of the force transmission characteristics of the rubber block in the Z direction.

It should be emphasised that the four graphs of Figs.15.9 and 15.10 only show the forces which are transmitted to the lower part of the seating via rubber block RB2. Of course, forces are also transmitted via RB1, and the upper graph in Fig.15.11 shows the transmission in the X and Y directions when a vertical input is applied to VB2. Comparing $\frac{P_x^{RB1}}{Q_0}$ with $\frac{P_x}{Q_0} \left[= \frac{P_x^{RB2}}{Q_0} \right]$, it is seen that over a large part of the frequency range the transmission via RB1 is a few dB less than that via RB2,

just as one would expect from the fact that the excitation point is closer to RB2. However, it is very interesting to observe that above about 250 Hz the four transmitted forces P_x , P_y , P_x^{RB1} and P_y^{RB1} differ only very slightly from one another.

Another point of interest is the existence of two close peaks in the $\frac{P_x}{Q_0}^{RB1}$ curve between 150 and 200 Hz, as compared with the single fat peak in the $\frac{P_x}{Q_0}$ curve. This clearly shows that there are two adjacent resonances, which in the latter case have merged together to form a single peak. These are the rocking and bouncing resonances of the V-piece on its pads. If the input had been applied to the V-piece at point I, instead of at the offset point I', the 165 Hz peak would probably have been considerably reduced in magnitude. However, the 185 Hz peak associated with the bouncing resonance would still be there - though in the case of $\frac{P_x}{Q_0}$ it might be as much as 5 to 10 dB lower than the present 165 Hz peak.

In the analysis it has been assumed that the motion of the structure supporting each rubber block is negligible in comparison with the motion of the top of the block. This has permitted the calculation of the transmitted forces from a knowledge just of the displacements on the upper faces of the block. The validity of this assumption is substantiated by the lower graph in Fig.15.11, which shows the measured relative motions across block RB2 in the same directions as the applied forces on VB2. These results clearly show that over most of the frequency range 10 to 1000 Hz the relative motion is at least 20 dB. The poorer results between 40 and 170 Hz may be a consequence of wave effects within the block. Although these measurements were made in the laboratory, there is no reason to suppose that the results would have been any different if the tests had been carried out in the actual operating environment, since the receiver structure has quite a high impedance.

In studying the transmissibility curves, it should always be borne in mind that one is only looking at the force transmission corresponding to a single input force in either the X, Y or Z direction. Whilst this is useful for assessing the seating performance, it does not give quantitative information regarding the overall force transmission to the lower part of the seating when the engine is running. If this were required, it would be necessary to know the various force inputs to the seating, and these are certainly not just in the vertical direction (as is often assumed in textbooks on vibration isolation). Tests carried out with the engine running on the seating have shown that the X, Y and Z motions of an engine foot are of comparable magnitude, as are the attenuations across the primary mount in these three directions. (14)

Since the mount has similar stiffnesses in the vertical and lateral directions, it is obvious that the X, Y and Z forces transmitted to the top of each V-piece are each of the same order of magnitude. The forces are also bound to differ somewhat in phase, so the engine is able to excite all the seating modes, and the overall force transmission can only be obtained from a knowledge of all the excitation forces and all the transmissibilities, both in magnitude and phase. It must therefore be stressed that even though the engine is symmetrically mounted on the seating, it does not apply a pure symmetrical excitation to the V-pieces.

Hence, although the symmetry of the system might lead one to expect that the 34 Hz rocking mode would not be excited, the existence of a significant horizontal input in the Y direction ensures that it will always be excited (see $\frac{P_x}{Q_{44}}$ in Fig.15.10), even if the vertical input is symmetrical. The same is also true of the 165 Hz rocking mode of the V-piece on its pads. The close proximity of the 34Hz resonance to the 30 Hz fundamental excitation frequency is obviously undesirable, and the situation is probably made even worse if spacing pillars are interposed between the mounts and the V-pieces, since the extra mass brings

the rocking frequency even closer to 30 Hz, besides permitting a stronger excitation of the mode.

We have so far only considered motions of various points on the upper part of the seating, together with the forces which are transmitted to the lower part via the rubber blocks. Since the whole purpose of the isolation system is to attenuate vibration transmission to the receiver structure, we shall now proceed to examine the motions at cruciform CR2, together with the forces transmitted to that cruciform.

Lower Part of the Seating (shown in Fig.15.12)

The dynamical behaviour of the lower part of the seating has not been examined in such detail as that of the upper part, so its modal characteristics are not so well understood. However, limited point and transfer data have been computed for the lower part on its own, and although no curves are given here, it is certainly worthwhile to consider the main results. Since we are interested in how the longitudinal beam assembly affects the force transmission to the cruciforms, it is instructive to consider the force transmissibilities $\frac{P_{51}}{Q_{69}}$ and $\frac{P_{51}}{Q_{70}}$, where P_{51} is the force transmitted to cruciform CR2 in the vertical direction. Since Q_{69} excites the beam in its plane of high flexibility and heavy damping, the transmissibility $\frac{P_{51}}{Q_{69}}$ exhibits a number of well damped resonant peaks in the range 10 to 1000 Hz, the first occurring at 138 Hz, with a peak value of -0.5 dB (or + 2.5 dB in terms of vertical component of input force, i.e. $\frac{P_{51}}{\frac{1}{\sqrt{2}}Q_{69}}$). Q_{70} is an excitation in the plane of the layers, and since the beam is very much stiffer in this plane, the transmissibility $\frac{P_{51}}{Q_{70}}$ only exhibits two resonant peaks in the same frequency range. These are at 180 and 570 Hz, with peak values of + 2.5 and - 0.5 dB respectively (or + 5.5 and + 2.5 dB in terms of vertical component of input force). Thus, the 180 Hz resonance is the major resonance of the system. The two peaks are thought to

correspond either to in-plane resonances of beam LL3 on its shear pads or to resonances of the complete beam assembly on the relatively flexible cruciform/V-support interfaces. An examination of the phase angles associated with forces P51 and P57 shows these to be in phase at 180 Hz, and approximately 180° out of phase at 570 Hz, so this suggests bouncing and rocking motions.

We shall now examine the predicted and measured velocities at cruciform CR2 due to a vertical input on V-piece VB2. These responses have been measured on the bottom plate of V-support VS2 in the X, Y, Z, β and Θ directions and they are shown in Figs. 15.13 to 15.15. It should be emphasised that only three of these five responses represent actual cruciform motions, since a detailed examination of the V-support/cruciform assembly has shown that there is a relative motion of approximately 20 dB across the interface in the vertical direction (see Section 14.6); and the flexibility which causes this also gives rise to relative motion in the Θ direction.

The vertical motion of the V-support bottom plate is shown in the upper graph of Fig.15.13, and it is seen that quite good agreement has been obtained between the predicted results and the measurements. Up to 250 Hz, the maximum difference does not exceed 10 dB, and the deviation above this frequency is only a consequence of the premature stiffening of the rubber block model, due to inadequate modelling of its higher modes. It may be observed that the predicted response exhibits all the same characteristics as the measured response, even though there may be slight differences in level and frequency. Hence, the model adequately describes all the principal modes of the seating.

The dashed line on the same graph is the initial response prediction, which corresponds to a rigid connection between the V-support and the cruciform. It also represents the motion at the centre of the cruciform top plate when the interface flexibility has been introduced,

since this flexibility has little effect upon the force transmission — at least at the low frequencies. This response is obviously the one which one should consider when assessing the overall motion attenuation across the seating. Upon comparing the transfer response $\frac{\dot{y}_{51}}{Q_0}$ with the point response $\frac{\dot{y}_0}{Q_0}$ (see Fig.15.2), it is seen that up to about 250 Hz the motion attenuation between the V-piece and the bottom plate of the V-support is only between 20 and 35 dB ; although there is a more rapid increase above this frequency, and by 500 Hz the attenuation is as much as 75 dB . However, when we include the 20 dB of attenuation across the V-support/cruciform interface we obtain much better figures: 40 to 55 dB up to 250 Hz, increasing to 95 dB at 500 Hz. These figures represent the attenuation of vertical motion between the V-piece and the centre of the cruciform top plate, and are thus the overall attenuations across the seating.

The above results show that it is possible to get as much attenuation across the bolted joint between the seating and the cruciform as across the seating itself! This clearly demonstrates the importance of carefully choosing accelerometer positions when performing comparative measurements on different seatings, since measured differences in motion attenuation may only be a function of joint flexibility, and may have nothing to do with differences in force attenuation. It is obviously best to measure the motion on the cruciform itself, rather than on the bottom of the seating.

The predicted velocities in the other directions do not show such good agreement with the measurements. The greatest disagreement occurs in the frequency range 10 to 100 Hz, where the predicted responses are seen to exceed the measurements by as much as 40 dB . In addition, the "measurements" are generally only noise, so the actual response may be even lower. However, between 100 and 300 Hz the agreement is much better, with the predicted responses having the right sort of level and

the same basic character as the measurements. This suggests that the measured cross mobilities of the cruciform may generally be a little high at the low frequencies, possibly due to the effects of noise and accelerometer transverse sensitivity. It is interesting to note that the measurements show the cruciform motion to be more strongly influenced by the V-piece, rubber block and lower beam resonances than by the low frequency resonances of the beam assembly on the blocks.

We shall now consider the forces transmitted to cruciform CR2 when the same vertical excitation is applied at V-piece VB2. These forces obviously cannot be measured, so only theoretical results are available. The vertical force is shown in the lower graph of Fig.15.15, whilst the horizontal forces in the Y and Z directions are given in Fig.15.16. Also shown for comparison are the forces transmitted to the lower part of the seating via rubber block RB2. As one might expect, the vertical force P51 does not differ very much from the input P_x to the lower part of the seating, though there is a magnification of up to 9 dB in the frequency range 100 to 170 Hz. From the previous discussion on the transmissibility characteristics of the lower part of the seating, it is obvious that this 9 dB magnification has been caused by the 138 and 180 Hz resonances of the system*. The Y force P52 shows the same magnification in this region, and the distinct peaks at 145 and 175 Hz are almost certainly these same two resonances. The increased low frequency transmission is probably due to the suspected errors in the cruciform mobility data. It is interesting to observe how a significant Z force P53 has been generated internally even though no force was transmitted in this direction by the rubber block. Whilst the low

* Note that these are theoretically predicted. The actual resonances may be lower, due to reduced stiffness of pads and face plates of V-support (caused by distortion of faces).

frequency results are almost certainly in error, the peak at 175 Hz is thought to be of the correct sort of magnitude, and it could even be a little higher. This is clearly seen from the Z velocity response graph shown in Fig.15.14: This shows a theoretical peak of -129.5 dB at 175 Hz, as compared with the corresponding measured peak of -118 dB at 125 Hz.

It will have been observed that all these results are less accurate than the predictions for the upper part of the seating. This is partly due to inadequate modelling of the force transmission characteristics of the rubber blocks, but the main source of inaccuracy is thought to be the measured cruciform data. Smith and Hanners (5)* have encountered the same problem in the analysis of a uniform beam seating, although they were using less complete data for the seating attachment points.

Probably the most important observation to be made regarding all the results is the fact that an uni-directional force input at the top of the seating gives rise to a multi-directional force transmission to the lower part of the seating, and hence to the cruciforms. Whilst the transmission in the direction of the applied force is usually dominant at low frequencies, the present results show that at high frequencies the forces transmitted in the various directions may each be of comparable magnitude. This will always be the case with any complex structure, so simple uni-directional isolation theory is clearly inadequate at high frequencies.

The foregoing results show that the seating gives very good isolation at the high frequencies, due to the two-stage behaviour of the transverse beam assembly on its rubber blocks. However, it should be mentioned that this was not intentionally incorporated in the design, and it has only arisen as a side effect of trying to minimise force transmission to the transverse beams in the plane of their layers.

* Note that References for Chapters 13 to 15 are listed on Page 430.

Unfortunately, the basic modes of the system give rise to troublesome peaks at 19 and 34 Hz, and the latter is uncomfortably close to the 30 Hz excitation from the engine. In addition, the rocking and bouncing resonances of the V-piece on its pads give rise to a significant peak in the $\frac{Px}{Q_0}$ curve* at 165 Hz, and this is further amplified in the lower part of the seating as a consequence of its own resonances, thereby forming a particularly high peak in the $\frac{P51}{Q_0}$ curve at 152 Hz. It is purely coincidental that all these resonances should be so close together, and the performance could probably be improved by spreading them over a wider frequency range.

Simple Analysis

Figs.15.17 and 15.18 show selected response plots on which are superimposed the results of the simple seating analysis⁺. This analysis was based upon the simple model shown in Figs.13.2 and 13.6, in which the transverse and longitudinal beam assemblies are represented by rigid beams, with concentrated masses for the V-pieces and V-supports. The rubber block is represented by a simple hysteretically damped spring, whose stiffness K_{RB} is the block stiffness K_x given on page 382, and the cruciform impedance Z_{CR} comprises the interface flexibility in series with the measured cruciform data in the vertical direction. The analysis has once again been carried out in two parts, in the manner indicated in Fig.13.6. An examination was also made of the effect of including the "source impedance" Z_1 when analysing the lower part of the seating, and this showed that it could quite safely be ignored (as has been assumed in the complex analysis).

* Dashed line on lower graph of Fig.15.15.

+ The results of the simple analysis are given by the dashed line in every case.

The point mobility graph $\frac{\dot{q}_0}{Q_0}$ shows a slight upward frequency shift in the basic bouncing and rocking resonances of the beam assembly on the blocks. This is because the stiffness associated with these modes is not solely that of the rubber blocks. The bending stiffness of the beams also has an effect, and this is ignored in the simple analysis. The large difference between the results of the simple and complex analyses above 100 Hz is due to the assumption of rigid coupling between the V-piece and the cross beams in the simple model. Obviously, a spring-mass subsystem could be used to represent the resonances of the V-piece on its pads, but there is no simple way of determining the correct spring stiffness, since the actual effective stiffness is a function of both the PVC pads and the beams underneath the pads.

The transfer mobility $\frac{\dot{q}_1}{Q_0}$ has been obtained as $\frac{1}{\sqrt{2}}$ of the vertical motion at the tip of the cross beam, and in the frequency range 200 to 400 Hz it shows slightly better agreement with the measurements than do the results of the complex analysis.

Since the resonances of the V-piece on its pads have not been allowed for, the force transmissibility curve $\frac{P_x}{Q_0}$ fails to describe the large peak at 165 Hz, followed by the rapid drop-off. Nevertheless, surprisingly good agreement has been obtained for the cruciform response $\frac{\dot{q}_{51}}{Q_0}$. This is mainly due to the fact that the bouncing resonance of the lower beam assembly has been predicted fairly accurately (160 Hz peak), thereby making up in part for the lack of the V-piece resonance at almost the same frequency. If the V-piece resonances were included, the existing 160 Hz peak would just be accentuated, without any change in the basic character of the curve. However, if the resonance of the lower part of the seating had been at a higher frequency, the agreement would not have been so good. The 220 Hz peak associated with rocking of the lower beam assembly does not concur with the results of the complex analysis.

Whilst this simple analysis has yielded quite satisfactory results in the present case, it is doubtful whether it could be extended to give sufficiently accurate multi-directional transmissibility data. In addition, the results would not be so good if the blocks were stiffer or if the damping were reduced, since the structural resonances which have been so conveniently ignored would then show as much sharper peaks.

The Influence of Pad Shear Stiffness on Seating Performance

The foregoing results show how the analysis has been able to predict multi-directional motions and forces with a fair degree of accuracy. It is now instructive to look at how this analytical capability can give us a clearer insight into what is happening within the system, thereby enabling us to propose sensible modifications which may improve its performance. The effect of such modifications may then be examined analytically using the model. This is a far quicker procedure than modifying the actual physical system and re-testing every time, and in addition, the analysis furnishes the engineer with far more information to assist him in his choice of modifications.

The aspect of the system which we shall examine in detail is the functioning of the transverse beam assembly. The reason for adopting this type of construction was the need for an assembly which would provide heavily damped transmission paths between the V-pieces and the rubber blocks, for any force input in the X-Z plane. As was explained in Chapter 13 (see page 304), a very important feature of the assembly is the PVC pads which are interposed between the steel V-pieces and the transverse beams, and it is a prime requirement that these should be as soft as possible in shear, so as to prevent force being transmitted into the beams in the plane of the layers. We shall now examine whether the system actually behaves as intended, and if not, we shall see what

happens when it is put right.

Let us start by considering the upper graph in Fig.15.19. This shows the forces transmitted into the face of the rubber V-block RB2 when a vertical input of 1N is applied on V-piece VB2. The force P_1 is normal to the face*, and is therefore associated with bending of the beam in its damped plane, whilst the force P_3 is up the face, and is associated with bending in the plane of the layers. It is immediately apparent that the system is not behaving as intended, since over most of the frequency range, P_3 is greater than P_1 . Although these forces are a function of the rubber block stiffness, it is known⁺ that the stiffnesses normal to and up the face are very nearly the same, so the cause must lie in the PVC pads. Since P_3 exceeds P_1 , the principal transmission path is via the undamped plane of the beam; which is the exact opposite of what was originally intended!

Before we proceed to rectify this, it is useful if we have some idea by how much the shear stiffness of the pads must be reduced. A useful guide is given by the lower graph of Fig.15.19, which shows the measured mobilities at point B on beam UT1, with the two V-pieces removed. The mobility $\frac{\dot{q}_8}{Q_8}$ was measured directly using an impedance head, whilst the mobility $\frac{\dot{q}_7}{Q_7}$ has been obtained from the results of a multi-directional mobility test, and corresponds to the case where rotation about the beam axis is "blocked" (since the beam is normally restrained from rotating by the attached V-piece). Obviously, these same responses could have been calculated, though this was not done. It is interesting to note in passing that the response $\frac{\dot{q}_8}{Q_8}$ does not exhibit such sharp peaks as one might expect from the results obtained

* For co-ordinate directions and numbering, see Fig.15.1.

+ See page 346, Fig.14.15, for direct and transfer receptances on inclined face of rubber block.

for the free-free beam (i.e. virtually undamped). This is due to the damping effect of the rubber blocks ($\eta = 0.1$), and is quite significant in the case of the first mode. The theoretical compressive and shear stiffnesses of the PVC pads are also shown*, and since these stiffnesses are frequency-dependent, the lines do not have the usual 6 dB/octave slope. The mobilities seen by the V-piece are obtained by adding together the beam and pad mobilities. Remembering that the graph is drawn to a logarithmic scale, it is seen that the mobility in the direction normal to the layers is just the beam mobility $\frac{\dot{q}_7}{Q_7}$, whilst that in the plane of the layers is equal to the beam mobility $\frac{\dot{q}_8}{Q_8}$ up to about 100 Hz, after which it approximately follows the pad shear stiffness line. Even allowing for the fact that $\frac{\dot{q}_7}{Q_7}$ will drop a little when the other V-piece is bolted in place, it is still quite apparent that the V-piece at point B sees a beam-pad assembly which has comparable mobilities in the local x and z directions. It is clearly seen that if the pads are to effectively eliminate force transmission to the beam in the local z direction over most of the frequency range, the shear mobility of these pads must be increased very considerably. Since a 30 dB increase appears to be adequate, we shall now see what happens when the longitudinal shear stiffness of the pads is decreased by 30 times. The loss factor will not be changed.

The computer programme has been re-run with this reduced value of pad shear stiffness, and the resulting force transmission to the lower part of the seating is shown in Fig.15.20. The change in seating performance is quite remarkable, since the attenuation at all frequencies above about 135 Hz has been improved by around 10 to 20 dB ; though at the expense of a slight degradation in performance between 40 and 120 Hz.

* Note that these stiffnesses refer to pairs of pads.

The great improvement in high frequency response has been achieved as a result of two factors: (a) The reduced force transmission to the beam in its undamped plane, and (b) the lowering of the resonant frequency of the V-piece on the pads. The resonant frequency has dropped from 170 to 110 Hz, and since the mean slope of the transmissibility curve changes at this frequency from -12 to -24 dB per octave, it does appear to be the prime cause of the improved high frequency performance. The shift of the 170 Hz peak to the lower frequency has uncovered the previously hidden 190 Hz resonance of the beam in its undamped plane. The reason for this resonance still being excited despite the decreased pad stiffness is probably the coupling* within the rubber block. This coupling causes the beam to be excited in its undamped plane via the rubber blocks, as well as via the PVC pads directly. Since both force inputs existed previously, the reduction or elimination of one of these must almost certainly effect some improvement; although this cannot be measured, due to the fact that the original peak was hidden.

The re-routing of forces via the damped transmission path has produced a 2 to 3 dB attenuation in the first two peaks, but the transmission in the intermediate frequency range is not so good. This is because the majority of the force was previously transmitted in the stiff undamped plane of the beam, and up to around 100 Hz the beam behaved as an ideal rigid mass in this plane. Now that the forces have been re-routed, they are transmitted in the flexible and highly damped plane, in which the beam no longer behaves as a rigid mass. Thus, the effective mass of the transverse beam assembly has been reduced, thereby resulting in a higher force transmission at these intermediate frequencies.

* Coupling between local x and z motions.

This detailed examination of a particular aspect of the seating has demonstrated the power of the analysis technique employed herein, since not only has it been possible to examine exactly what is happening within the system, but also it has been possible to see and understand the effect of making a modification. Besides this, it has shown that the transverse beam assembly was not behaving in the manner originally intended.

It is not proposed to consider any further parameter variations at the present stage, since these will be reported separately ⁽¹⁵⁾.

15.3 GENERAL DISCUSSION AND SUMMARY

Although the present mass-spring type of seating gives good isolation at the high frequencies, it does have the disadvantage of introducing six basic seating resonances at the low frequencies, and in the present case the fundamental excitation frequency of 30 Hz lies within the frequency range of these resonances. At the same time, the system has a very low natural frequency in the fore and aft direction, which tends to make it a little unstable when the engine is in position. These faults highlight the need for attempting to group the six basic frequencies in a narrower band, so as to ensure a fair amount of attenuation of the fundamental excitation, whilst at the same time not making the system unstable.

If it is not possible to satisfy these two objectives, it may be necessary to employ a more conventional frame or box type of seating, which is attached directly to the receiver structure, and has no troublesome low frequency modes. Although the high frequency isolation is not as good as that achieved with the mass-spring seating, the performance can be improved considerably by introducing high natural frequency mass-spring systems between the four engine mounts and the seating frame. This has been found to be very effective in the case of the V-beam seating, and the associated resonances need not be very severe if high damping material is used for the pads under the masses. The resonant frequencies can also be suitably adjusted to fall between known major excitation frequencies. With such an arrangement, one sacrifices low frequency performance for stability, since the complete engine-seating system only gives a single stage of isolation at the beginning of the frequency range. However, at a chosen intermediate frequency the performance improves dramatically, as the mass underneath the engine mounts decouples from the seating frame, thereby giving two-stage isolation.

It has been shown that the assumption of point coupling between components can lead to considerable errors when the components are coupled rather imperfectly over quite a large area. If the seating had been welded or stuck to the cruciform, it is probable that the measured cruciform mobilities would have represented the true foundation seen by the seating model. However, the rather imperfect coupling caused by the distortion of the V-support and by the widely spaced bolts has demonstrated the need for a closer examination of the dynamic characteristics of junctions between components. It is possible that in such cases as this cruciform, it would be better to measure the X, Y and Z mobility properties at four or more points over the surface, rather than obtain the linear and rotational properties at a single point. An alternative procedure might be to deduce the support mobility properties from measurements on a simple resonant structure which is attached to the support. For instance, one might use a uniform beam which was welded to an attachment plate. This plate could then be bolted to the support in the same way as the seating. By combining the known theoretical response properties of the beam with the measured data for the beam on the support, it should be possible to deduce the support properties. Such a procedure would have the advantage of giving an overall mobility which would also include the flexibility of the joint between the plate and the support.

However, the discovery of a significant "interface flexibility" between the V-support and the cruciform in the vertical direction leads one to suggest that it might even be beneficial to purposely insert a known 6-directional flexibility*, which is less than the cruciform flexibility. This would have the advantage of completely eliminating metal-to-metal contact between the seating and the cruciform, and it would

* e.g. Rubber pads.

provide a further stage of isolation at high frequencies. In addition, one could then calculate the force transmission to a cruciform without actually knowing its mobility properties, in the same way as the force transmission to the lower part of the seating was obtained without having to consider the impedance seen by the bottom faces of the rubber V-blocks.

Use of the dynamic stiffness coupling technique has permitted the use of component data from various sources, and in addition, the necessity for re-building the system dynamic stiffness matrix at each frequency makes it easy to take account of the frequency-dependence of material properties. An alternative procedure would have been to use the more general coupling technique employed by Klosterman ^{(16)*}, but this would have resulted in even larger matrices, and hence increased solution time.

The analysis has demonstrated how one may examine the behaviour of an isolation system in considerable detail, thereby leading to a clearer understanding of the way in which vibration is transmitted to the supporting structure. This then facilitates a study of the effect that various parameters have upon the response. These parameters are not obscure quantities such as modal mass, coupling stiffness, etc., ⁽¹⁾⁽¹⁷⁾ but are actual seating dimensions and material properties. This in turn opens up the possibility of optimising the isolation performance of the seating, either by a process of trial and error, or using mathematical optimisation techniques ⁽¹⁸⁾.

Whilst it has been shown that fairly complex structures can be analysed successfully up to high frequencies, there are still many practical seating structures which are too complex to permit accurate prediction of their performance, this being particularly the case with

* This technique permits the direct combination of receptance and dynamic stiffness data.

box type structures. Although it may not be possible to analyse such structures at the design stage, it is still possible to optimise their performance, provided that they can be represented by a mathematical model. Using recently developed System Identification techniques, it is possible to set up such a model from measured data (i.e. point and transfer mobility measurements on the structure), and this procedure has already been applied to practical systems.⁽¹⁶⁾⁽¹⁹⁾⁽²⁰⁾⁽²¹⁾

Obviously, the ideal is that one should be able to design and optimise the seating on paper, before it is ever built, for only in this way can one hope to obtain the very best performance possible. However, if this is to be done, the designer must accept the limitations of the currently used analytical techniques, and design his seating in such a way that its performance can be predicted. It has been shown that multi-layer beams can be treated analytically, and multi-layer plates can also be dealt with, but complex stiffened boxes can pose problems. This does not rule out the use of one or two components which defy accurate analysis (e.g. the rubber blocks in the V-beam seating), since their properties can be obtained from measurements on a specially built component. However, it is preferable that the majority of components should be analysable.

Regarding analysis techniques, there is a popular belief that finite element analysis must always lead to large systems of equations, and that even then it can only be used to predict the fundamental modes of a structure. This is certainly true if one couples together all the elements without eliminating any of the nodal co-ordinates. However, by combining the finite element method with a coupling and elimination procedure based upon either Gaussian elimination or the transfer matrix method, it is possible to obtain the required response properties of a complex component or structure without forming any large matrices. Although it is necessary to repeat the process at each frequency, this can be an advantage, since the material properties and the number of elements can be varied to suit

the frequency. Hence, one need only use a few elements to describe low frequency behaviour, whilst a large number may be used at high frequencies. The utility of such a procedure has been demonstrated quite effectively by the sandwich beam analysis, where a beam having well over 100 nodal co-ordinates has been "built" very rapidly in the computer, and only those co-ordinates relating to the four connection points have been retained. Such a procedure has also been applied to the analysis of rectangular plates,⁽²²⁾ where a strip across the width has first been divided into triangular elements and analysed for its dynamic stiffness properties, and then all the identical strips have been coupled together using the transfer matrix method. It is possible that the same technique might be used for analysing box structures which comprise a number of identical sections joined end to end.

The Seating analysis described in this report is certainly quite complex and the reader may well question the need for examining a system in such detail, especially in view of the reasonable results obtained using the simple model. Of course, it is unnecessary to go into such detail in many practical cases, and a simple analysis will often suffice - if any analysis is attempted at all! However, in those critical applications where optimum multi-directional isolation is essential, the use of this type of complex analysis can prove very beneficial.

In the present case, the simple model only gave such good results because of the relatively high stiffness of the beam assemblies in comparison with the rubber block stiffness. This is shown very clearly when one increases the block stiffness.⁽¹⁵⁾ Admittedly, the rigid cross beams in the model could be replaced by simple flexible beams, but there remains the problem of assigning the correct value of flexural rigidity to such a beam. In the same way, the resonances of the V-piece on its pads could be represented quite simply if the effective stiffness of the pad-beam assembly were known. Obviously, such information is only available

from a full analysis of the complete V-beam assembly. Hence, the simple model is severely limited in its applicability. On the other hand, the building block approach used for the full seating analysis is far more general, in that it can take account of the distributed mass and stiffness properties of every component in every direction. This is particularly important when analysing conventional stiff seatings, which are generally more highly resonant,⁽⁵⁾⁽²³⁾ with a large number of flexural and torsional modes.

Although this type of analysis is fairly complex, it will soon become more commonplace and quite straightforward, with the rapid development of computing facilities and the growth of dynamic analysis programme libraries. This is currently happening in the United States, where it is now possible to access an extensive dynamic analysis library via a telephone link, on a time-sharing basis.⁽²⁴⁾ Under such conditions, it is much cheaper and less time consuming to analyse and optimise a design with the aid of the computer than to build an expensive prototype and then modify and re-test it many times. In addition, one computer run lasting several minutes can yield as much response information as several hundred measured mobility plots, so it can lead to a better understanding of the system behaviour.

The present work has spurred the development of a general purpose coupling programme, plus various subroutines for generating the response characteristics of both uniform and multi-layer beams in flexure and torsion; and other developments will inevitably follow. Using such a programme library, the engineer does not need to know the details of how each component is analysed, and his work is reduced to deciding upon component dimensions and material properties, which are then used by the standard library routines for generating the component data. This opens the way for more creative design, and for system optimisation.

15.4. CONCLUSIONS

The highly successful vibration analysis of the V-beam seating has demonstrated the feasibility of analysing damped complex structures for their multi-directional response properties. Use of the "building block" approach has permitted each individual component to be analysed in detail by whichever method was most convenient. Thus, it has been possible to combine data obtained from exact theory, finite element modelling, and a model based upon measured data. The power of the analysis technique has been demonstrated by examining a particular aspect of the seating in detail, and from this it has been found that the system failed to behave precisely as intended. Nevertheless, the seating has been found to possess good multi-directional isolation properties over a wide frequency range.

An important result of the analysis has been to show the way in which a uni-directional force input on the top of the seating generates multi-directional response at the points of connection to the receiver structure. This is especially important at the high frequencies, since the responses in the different directions are of comparable magnitude; and it highlights the inadequacy of simple uni-directional analysis when dealing with high frequency vibration isolation. The combination of multi-directional excitation from the engine together with this coupling within the seating demonstrates the necessity of designing the system to give effective isolation in all directions.

REFERENCES FOR CHAPTERS 13 TO 15 (PART 4)

1. Lachlan, B., AEL Internal Memo No. NV.319. Dec. 1970 (Restricted)
2. Lachlan, B., AEL Internal Memo No. NV.320, Jan. 1971 (Restricted)
3. Harris, C. M. and Crede, C. E., "Shock and vibration handbook", McGraw-Hill, 1961. Page 24 of chapter 10.
4. Henshell, R. D. and Warburton, G. B., "Transmission of vibration in beam systems", Intl. Jnl. for Numerical Methods in Engineering, Vol.1(1), 1969, pp47-66
5. Smith, J. E. and Hanners, R. J., NSRDC Report C2707, Feb. 1969 (Confidential)
6. Lee, C. L. and Huang, T. C., "Dynamic response of three-dimensional framed structures", ASME paper No.73-DET-138 at Design Eng. Technical Conf., Cincinnati, Sept. 1973 (To be printed in Jnl. of Engineering for Industry)
7. Davis, R., Henshell, R. D and Warburton G. B., "A Timoshenko beam element", Jnl. of Sound and Vibration, Vol.22(4), 1972, pp 475-487
8. Zienkiewicz, O. C., "The finite element method in engineering science", McGraw-Hill (London) 1971
9. Snowdon, J. C., "Vibration and shock in damped mechanical systems", Wiley, 1968
10. Volterra, E. and Zachmanoglou, E. C., "Dynamics of vibrations", Merrill, 1965, Page 552.
11. Lindley, P. B., "Plane stress analysis of rubber at high strains using finite elements", Jnl. of Strain Analysis, Vol.6(1), 1971, pp 45-52
12. Lindley, P. B., "Engineering design with natural rubber", Natural Rubber Producers' Research Association, Tech. Bulletin No.8
13. Sainsbury, M. G., Imperial College Report No.4 on MOD Contract No. DC 20(1)/55384/69, Dec. 1973 (Restricted)

14. Hardenberg, J. F., AEL Internal Memo No. NV.376, March, 1972
(Restricted)
15. Ewins, D. J., Grootenhuis, P. and Sainsbury, M. G., "The effect of design parameter variations upon the performance of the Imperial College V-beam seating", IC report on MOD Contract AT/2037/0130 AEL, Feb. 1974
16. Klosterman, A. L., "A combined experimental and analytical procedure for improving automotive system dynamics", SAE paper No.720093 at Automotive Engineering Congress. Detroit, Jan.1972.
17. Lachlan, B., "The reduction of vibrational energy in complex structures", Imperial College Dynamics Group Report - Final Report on MOD Contract No. N/CP 95/62313/65, Dec. 1969
18. Haynor, D. R., "Minimisation of vibration transmission through uniform-beam foundation structures". NSRDC Technical Note, Feb.1969
19. Klosterman, A. L., "On the experimental determination and use of modal representations of dynamic characteristics", Ph.D. thesis, University of Cincinnati, 1971
20. Flannelly, W. G., McGarvey J. H., and Berman, A., "A theory of identification of equations of motion of a structure through dynamic testing", Structural Dynamics Symp., Loughborough, March 1970
21. Flannelly, W. G and Berman, A., "The state of the art of system indentification of aerospace structures", ASME, Winter meeting, Nov. 1972
22. Dokainish, M. A., "A new approach to plate vibrations: Combination of transfer matrix and finite element technique", Jnl. of Engineering for Industry, May 1972
23. Galpin, M., AEL Internal Memo No. NV.322, June 1971 (Restricted)
24. Henke, R. F., "The use of time sharing in engineering design analysis", SAE paper No.720014 at Automotive Engineering Congress, Detroit, Jan. 1972
25. Gent, A. N., and Lindley, P. B., "The compression of bonded rubber blocks", Proc. I.Mech.E., Vol.173, No.3, 1959, pp111 - 122

APPENDICES

Appendices	$\left\{ \begin{array}{c} \text{I} \\ \text{III} \\ \text{V} \\ \text{IX} \end{array} \right\}$	to	$\left\{ \begin{array}{c} \text{II} \\ \text{IV} \\ \text{VIII} \\ \text{XI} \end{array} \right\}$	relate to Part	$\left\{ \begin{array}{c} 1 \\ 2 \\ 3 \\ 4 \end{array} \right\}$	and start on page	$\left\{ \begin{array}{c} 433 \\ 460 \\ 501 \\ 517 \end{array} \right\}$
------------	---	----	--	----------------	--	-------------------	--

Note that separate reference lists are given for the four parts of the thesis, so any references quoted in a given appendix relate to the reference list for the corresponding part.

APPENDICES FOR PART 1

	<u>Page</u>
I FLOW CHART FOR THE COMPUTER PROGRAM COUPLE1	434
II THE ADDITION OF A SINGLE FRICTION DAMPER TO A LINEAR DAMPED SYSTEM	445

Note that all references quoted in these appendices are given in the reference list for Part 1, on Page 75

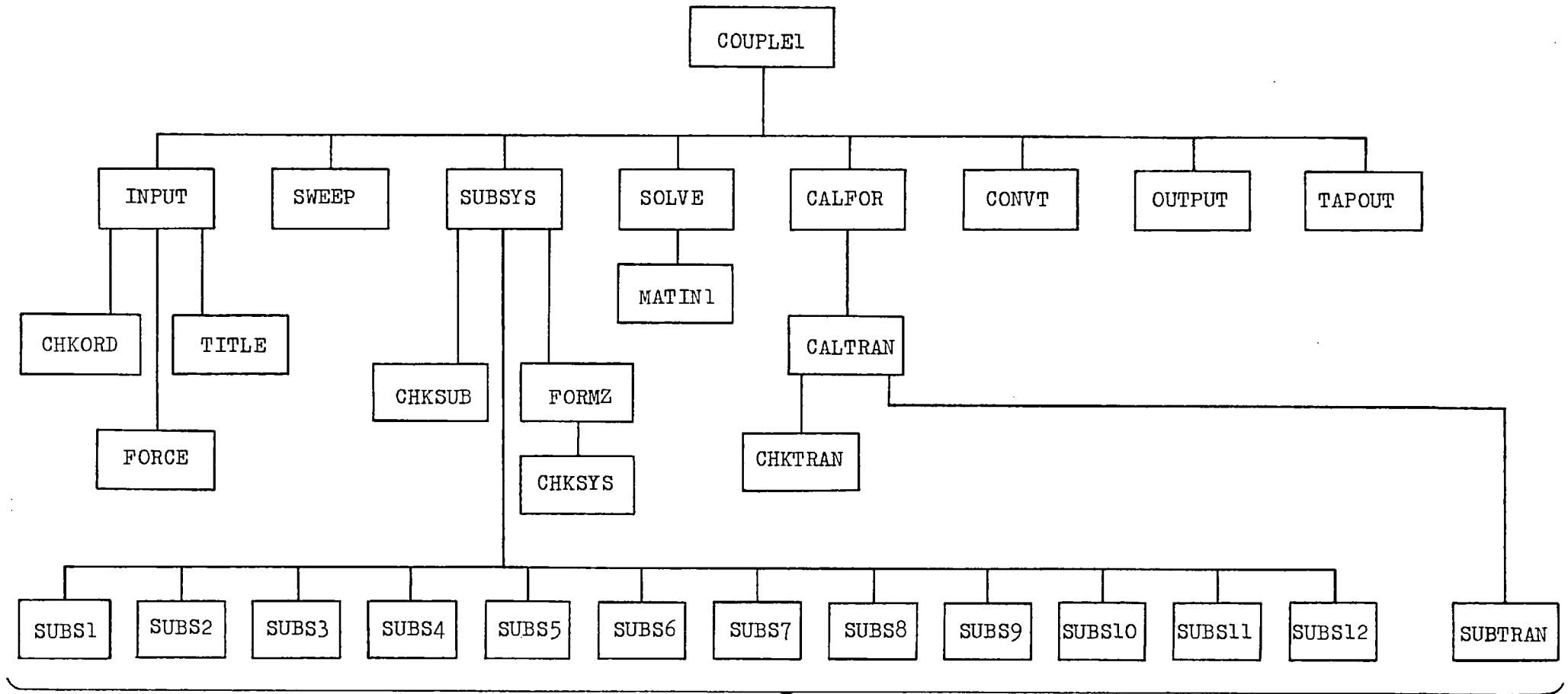
APPENDIX IFLOW CHART FOR THE COMPUTER PROGRAM COUPLE1

The program structure is shown in Fig. I.1, where each box represents a subroutine. Flow charts are then given for the following routines:

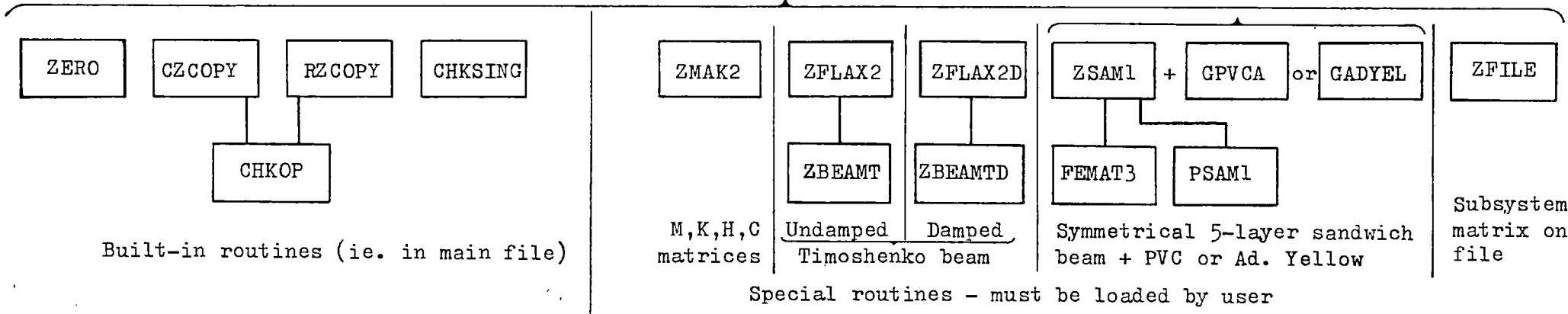
COUPLE1, INPUT, SUBSYS, SUBSi, FORMZ, SOLVE, CALFOR, CALTRAN, SUBTRAN

The variable names used in the flow chart are the same as those used in the Fortran program, and they are defined in the table below. The variables are listed in the order in which they occur in the flow charts.

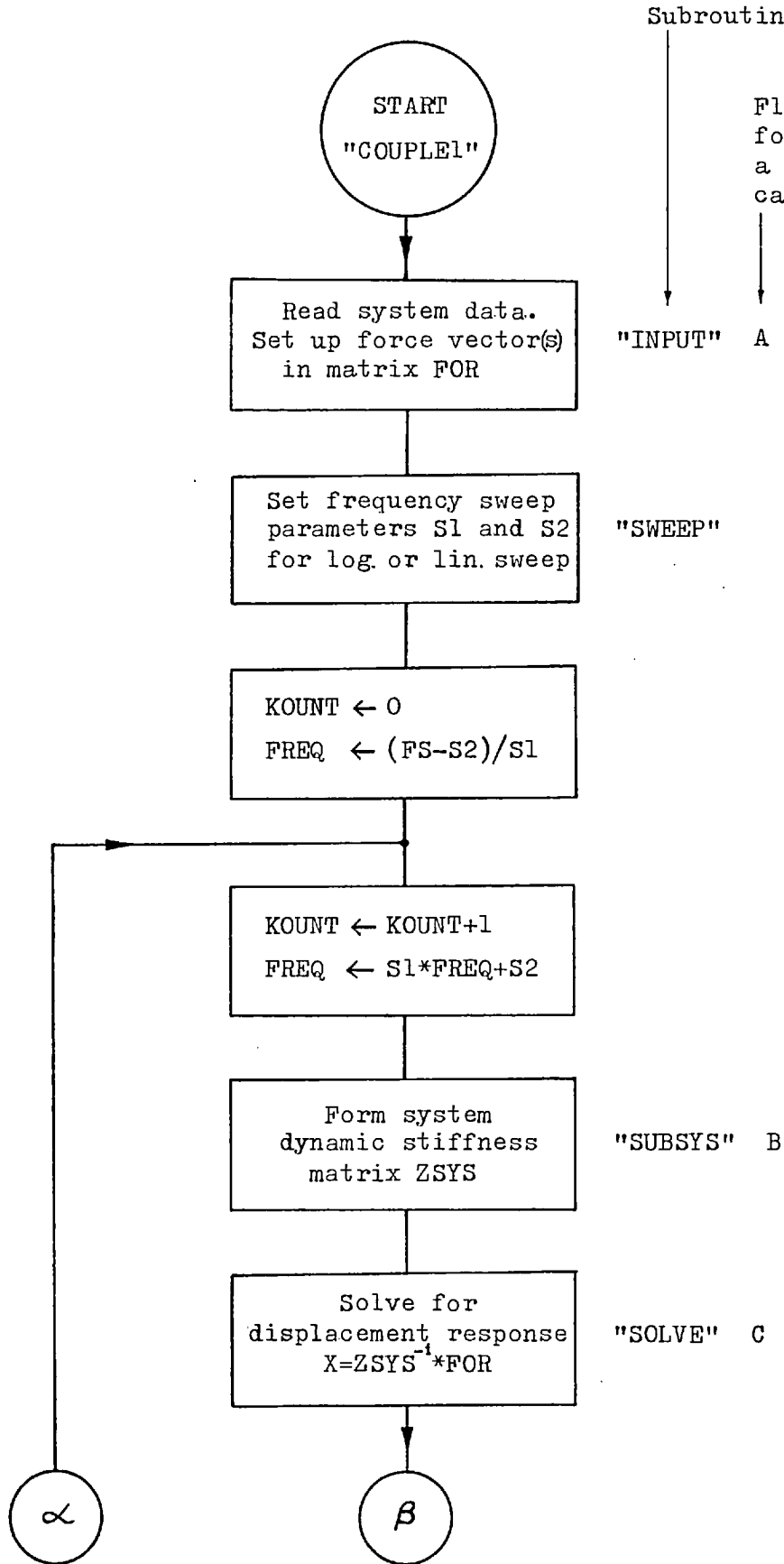
Program Symbol(s)	Definition and Notes
FOR	50 x 10 real array to hold force vectors
S1,S2	Frequency sweep parameters. For log sweep, $freq_{i+1} = S1 \times freq_i$ so $S2=0$. For linear sweep, $freq_{i+1} = freq_i + S2$, so $S1=1$.
KOUNT	Counter for number of the frequency
FREQ	Frequency in Hz
ZSYS	50 x 60 real array for system dynamic stiffness matrix (put in upper left hand corner).
X	50 x 10 real array to hold the computed displacement vectors.
KS	Number of subsystem for which internally transmitted forces are required.
NF	Total number of frequencies in sweep.
KSUBS	Current subsystem number.
N	Number of subsystems.
ZSUBS	12 x 12 complex array in which dynamic stiffness matrix for current subsystem is set up (put in upper left hand corner).
NFIX	Number of co-ordinates to be fixed to ground.
IFG	12 x 1 integer array for holding co-ordinate numbers which are to be fixed to ground.
F	12 x 50 complex array used for keeping original rows of ZSYS when co-ordinates are fixed to ground. Also holds transmitted forces following solution for displacements.
NFI	Number of forces transmitted to subsystem KS that are to be output.
NFG	Number of forces transmitted to ground via fixed co-ordinates that are to be output.
ITRAN	Transfer response code. ITRAN=0 for no transfer response.
YTRAN	6 x 12 complex array in which transfer admittance matrix is set up (put in upper left hand corner).
TRAN	6 x 10 complex array to hold computed transfer responses.
ZS	12 x 12 complex array to hold dynamic stiffness matrix for subsystem KS.

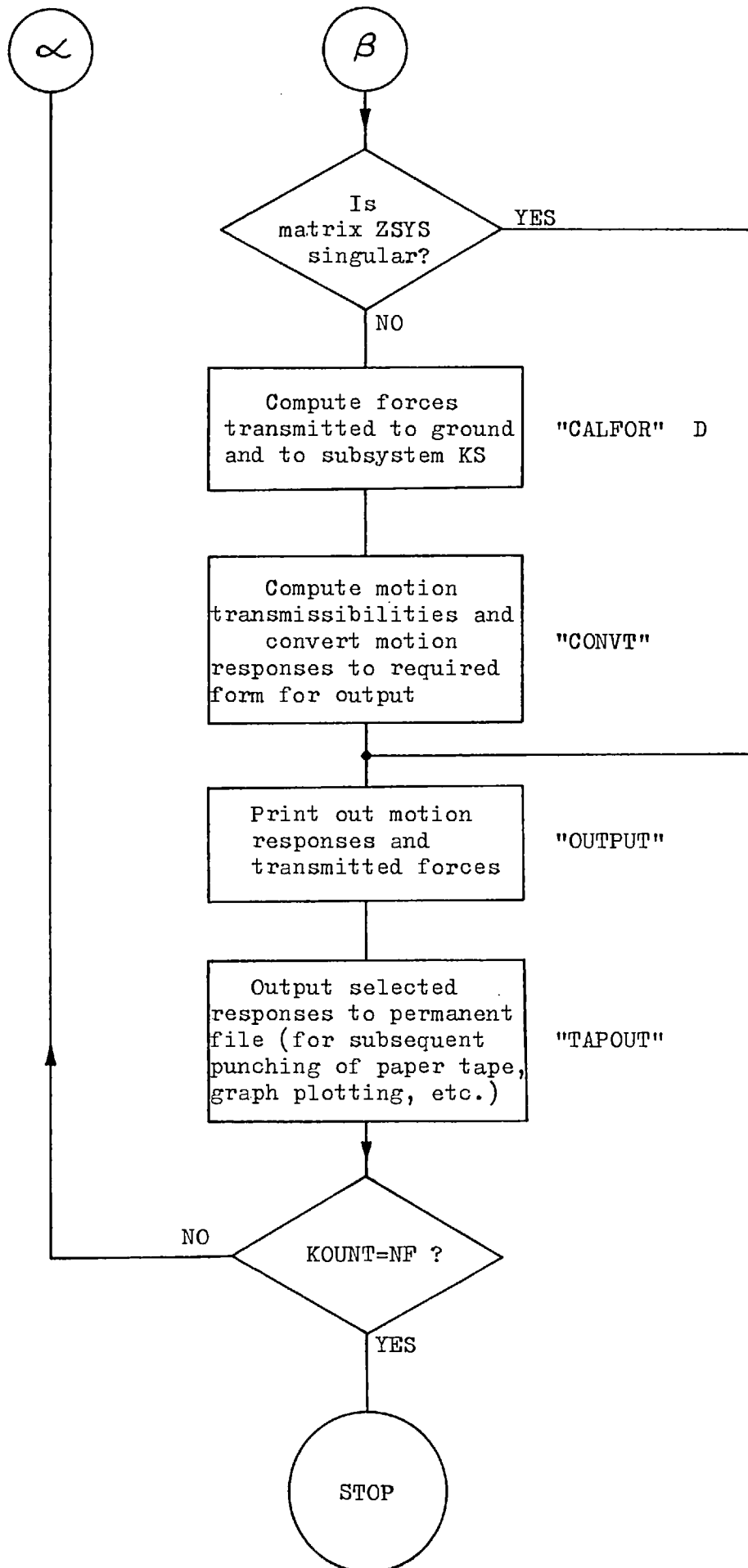


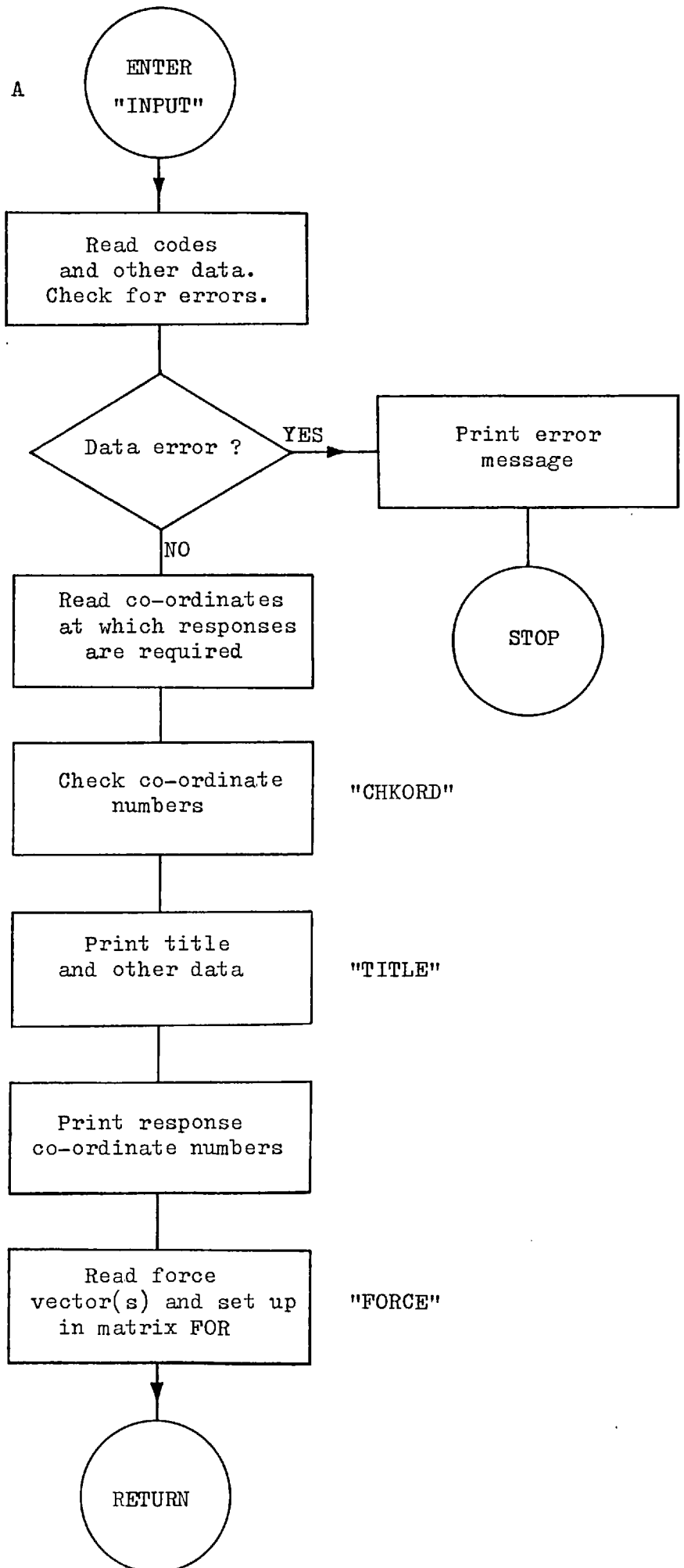
Standard routines which may be called from set routines in SUBS1 to SUBS12 and SUBTRAN



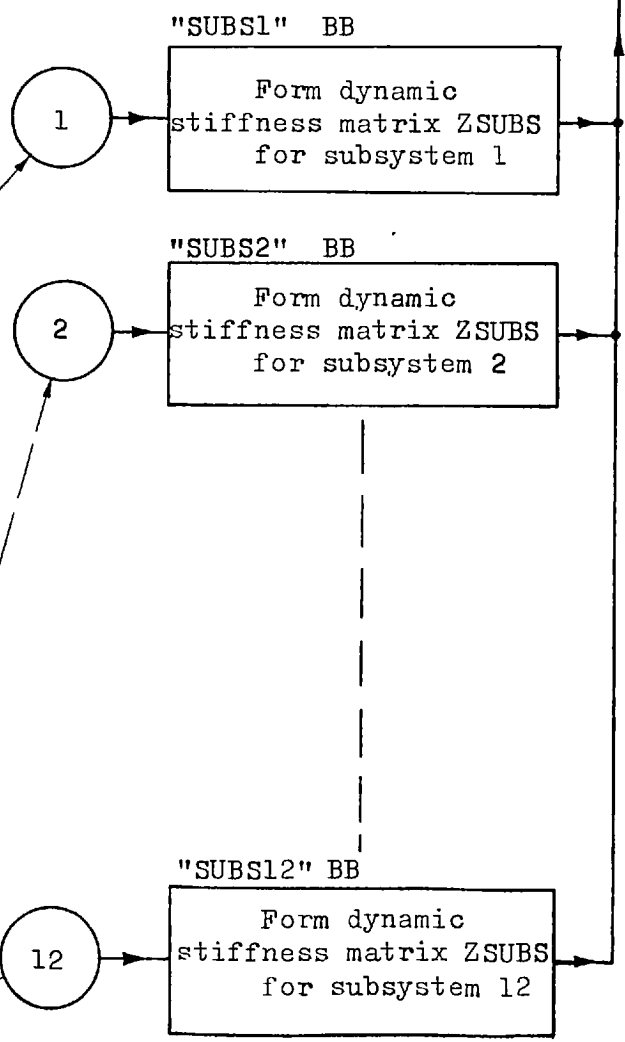
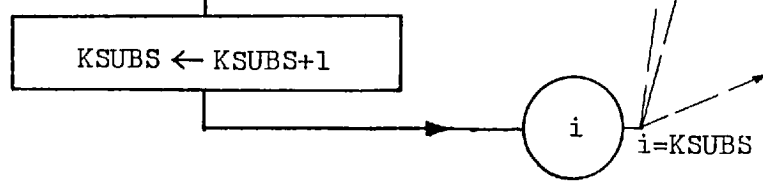
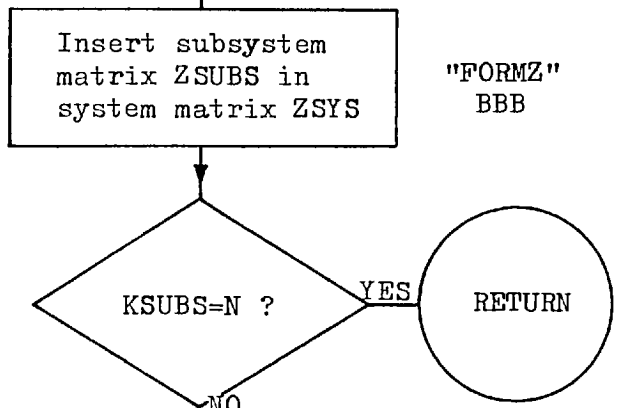
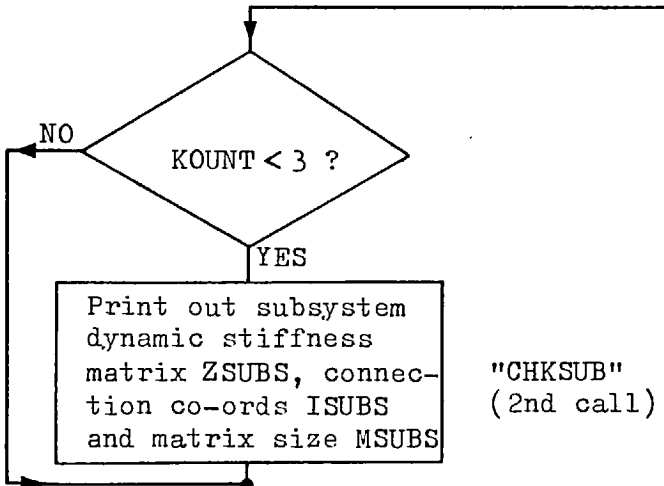
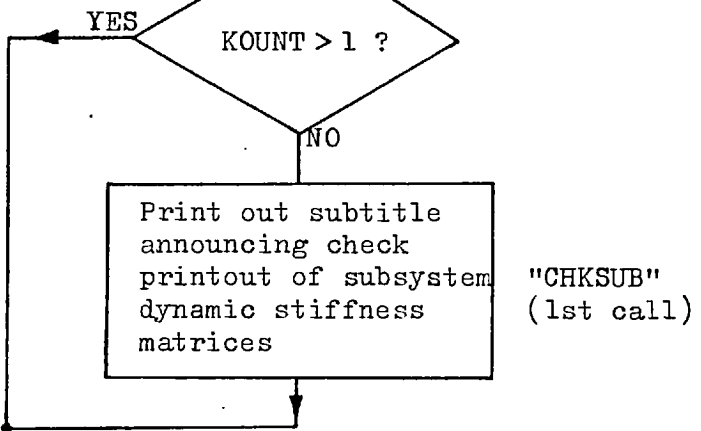
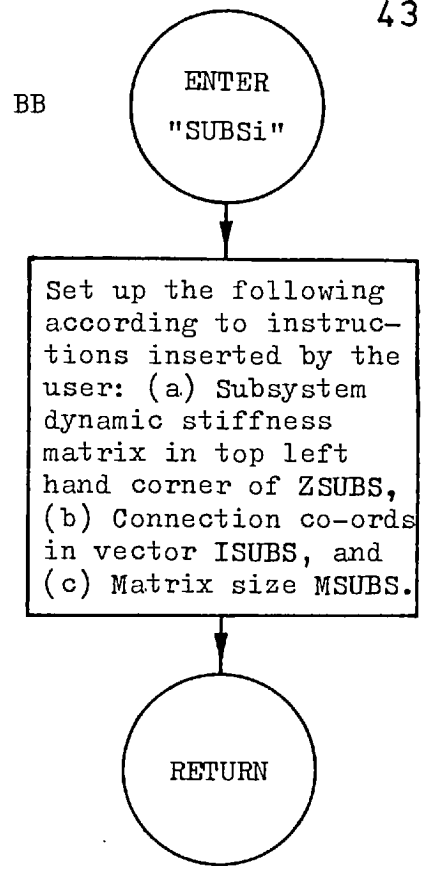
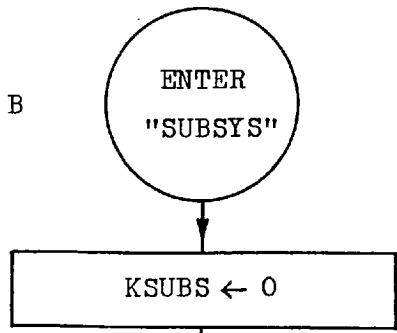
Main program COUPLE1

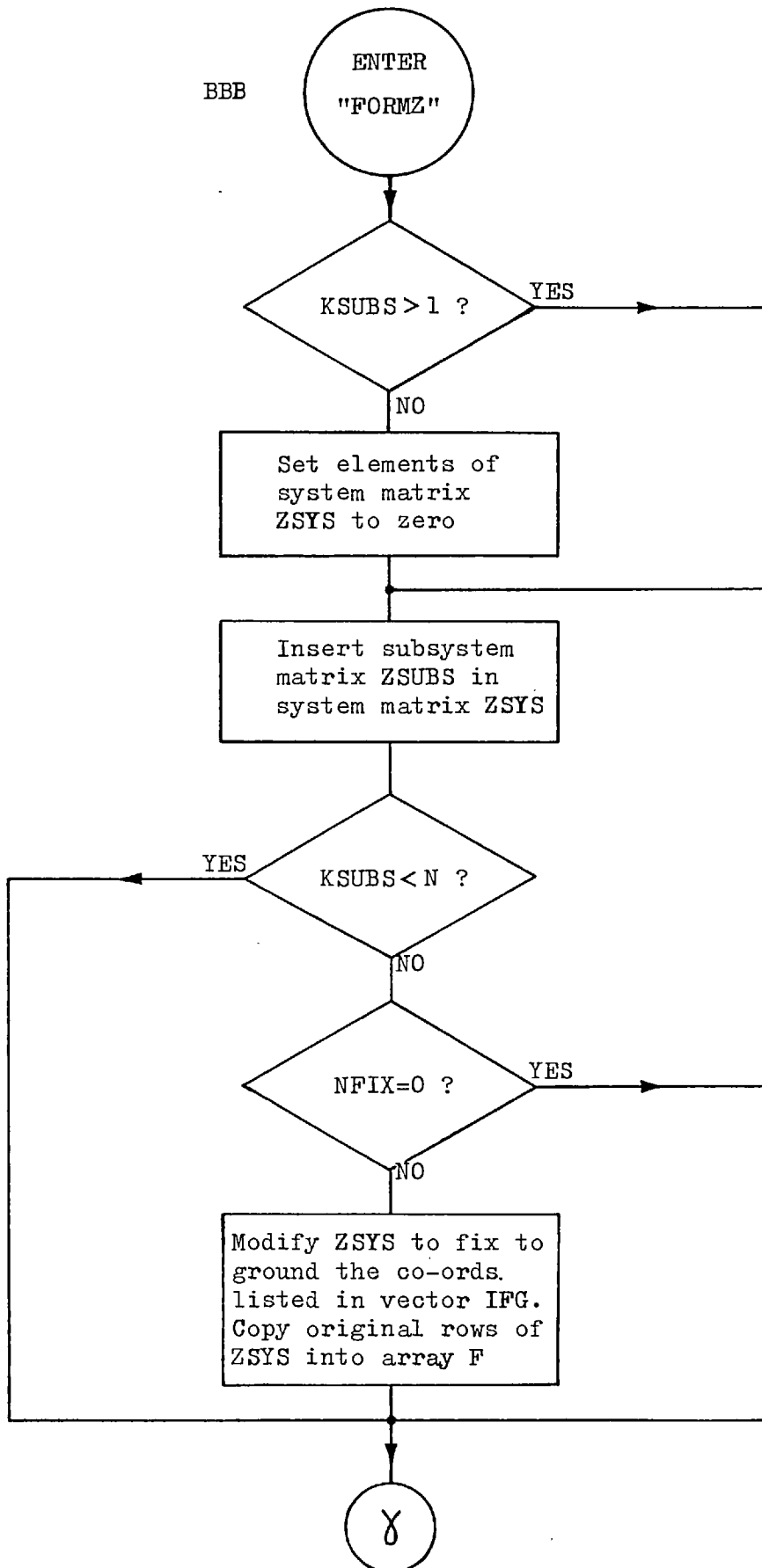


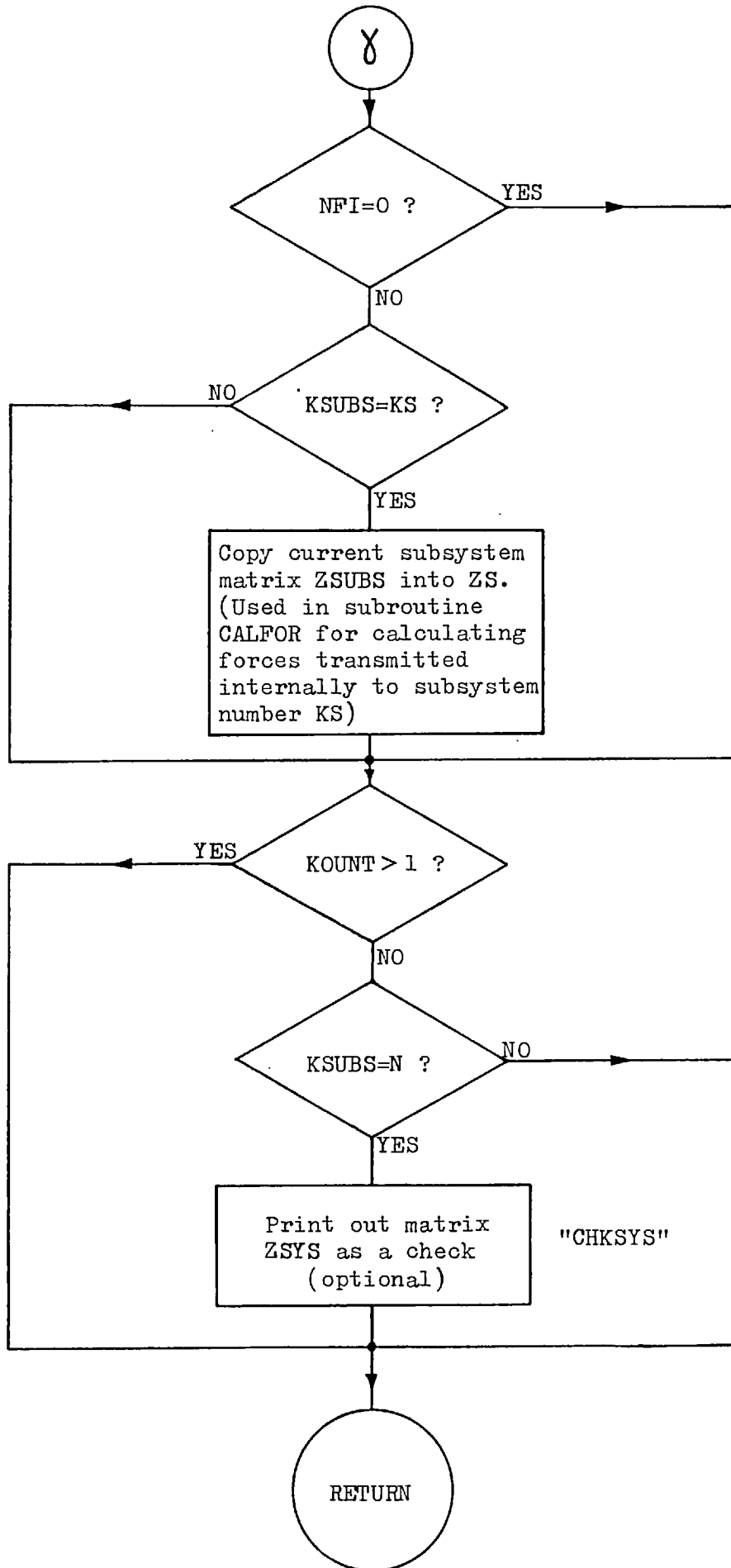


Subroutine INPUT

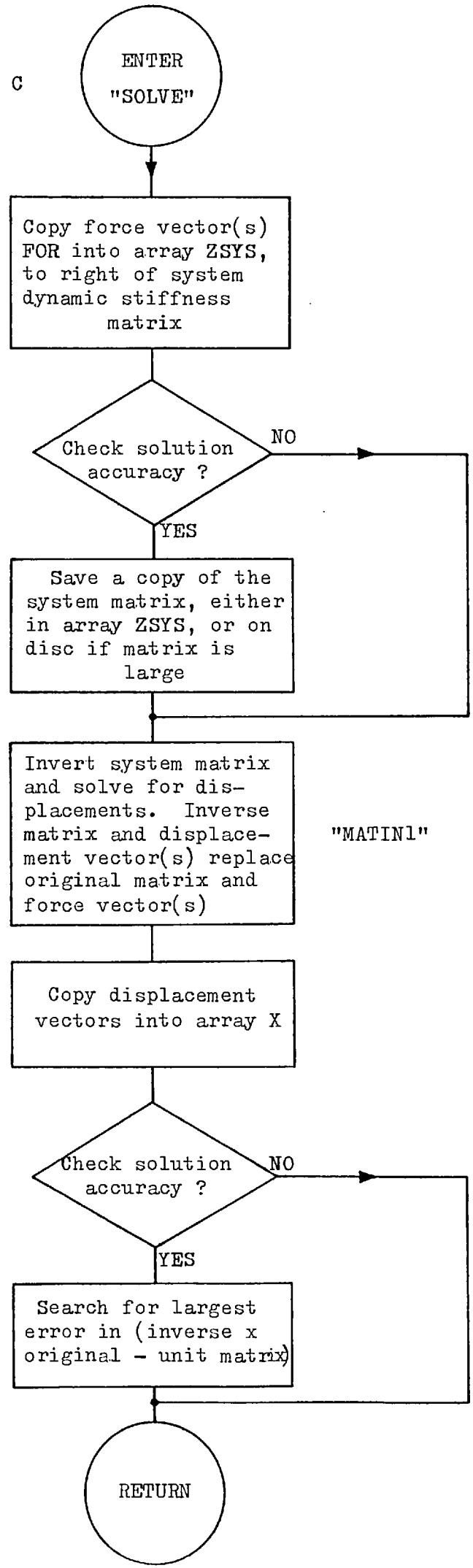
Subroutines SUBSYS and SUBSi (i=1,12)



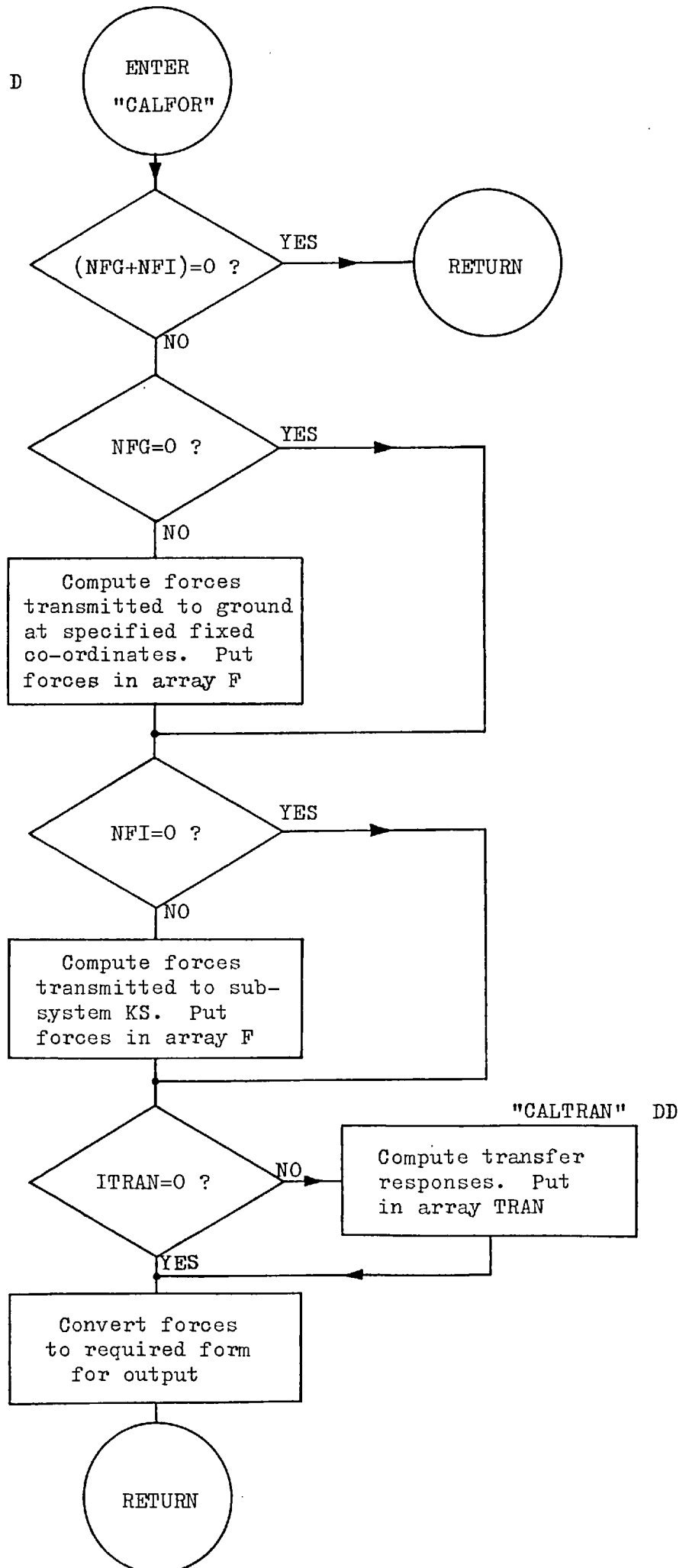
Subroutine FORMZ



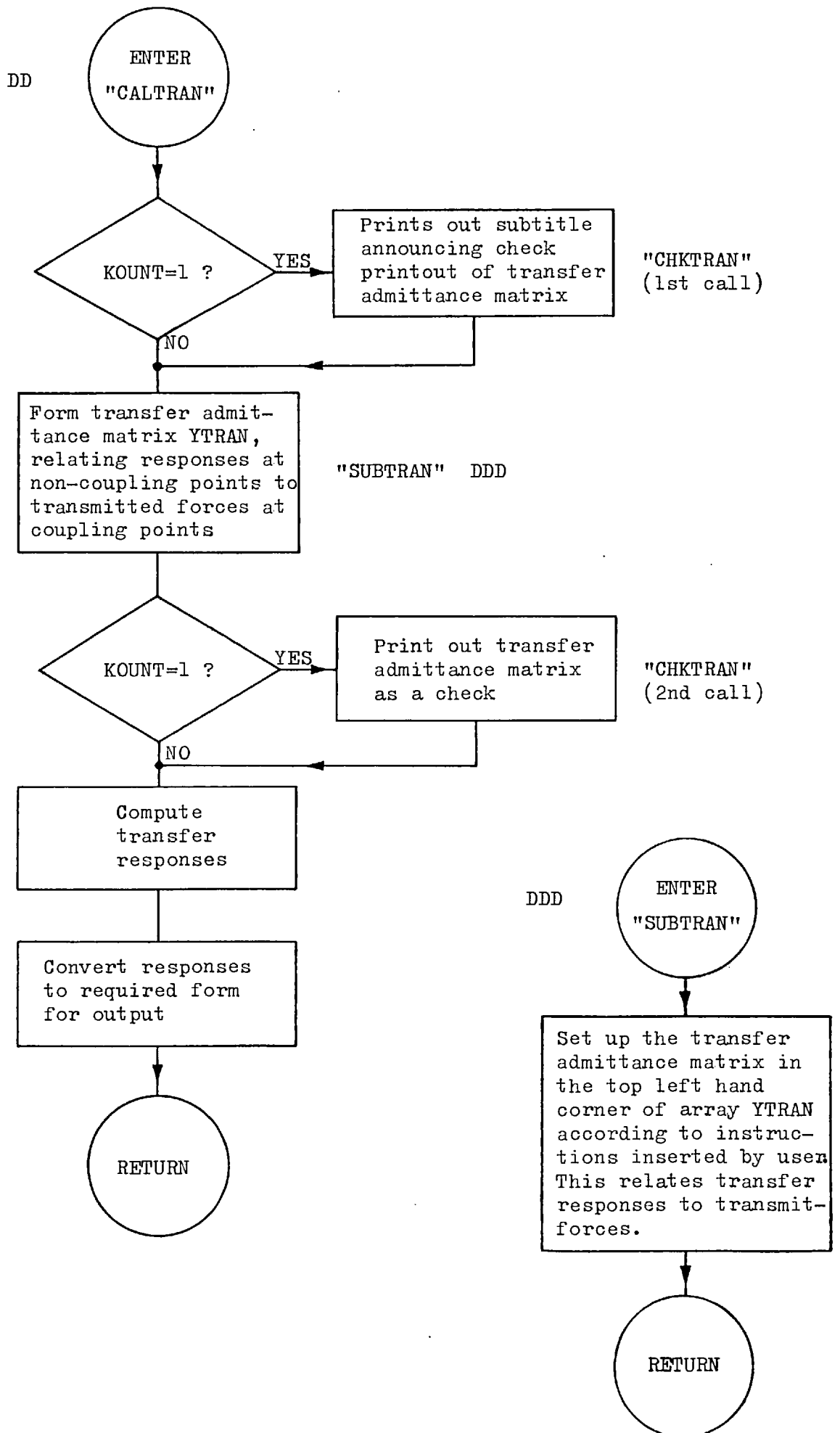
Subroutine SOLVE



Subroutine CALFOR



Subroutines CALTRAN and SUBTRAN



APPENDIX IITHE ADDITION OF A SINGLE FRICTION DAMPER TO A LINEAR DAMPED SYSTEMIntroduction

Linear damping of the hysteretic or viscous type is easily incorporated in a system analysis, simply by giving the damped subsystems a complex dynamic stiffness. However, if the system is large and the damping is just concentrated at one or two points, it is computationally more efficient to analyse the undamped part of the system for its receptance properties, and then to add the damping afterwards in the form of inserts*. As far as the undamped section is concerned, the reaction forces applied to it by each insert are just external forces; so once these are known it is a simple matter to modify the responses to include the effect of the inserts. The set of forces is easily determined by suitably combining the dynamic stiffness properties of the inserts, the receptance properties of the undamped system at the insert attachment points, and the "free" response of the system at the same points.

So far we have only considered the addition of linear damping inserts to an undamped system, and this approach simply provides an alternative and more efficient solution to the problem. However, it also opens up the possibility of introducing non-linear inserts, which cannot be incorporated in the general coupling procedure. One such insert which is of great practical importance is the Coulomb friction damper, since all built-up structures automatically incorporate a certain amount of friction in the joints, and if this can be understood and controlled it can provide a cheap and efficient source of damping. Hence, it is necessary to examine the properties of the damper and to use these to determine the reaction forces that it applies to the linear system.

* This is discussed more fully in Chapter 2, Section 2.3

The procedure given below is very similar to that developed by Earles et al. (56)(58)(60)*, and it yields an approximate "linearised" solution, since the actual non-sinusoidal friction force is replaced by an equivalent sinusoidal force of constant amplitude. The present work extends Earles's solution to include linear damping within the main system, but the extra complexity of the analysis makes it impossible to include any displacement dependence of the friction force, unless this is done numerically using an iterative procedure. The inclusion of linear damping facilitates the study of isolation systems which employ a combination of friction and viscous (or hysteretic) damping (67).

The Linear System and the Damper Characteristics

We shall consider a general linear multi degree-of-freedom system excited by E sinusoidally varying forces \bar{Q}^+ , as shown in Fig. II.1a. A single friction damper is to be introduced into this system between co-ordinates a and b , as shown in Fig. II.1b. The basic linear system may incorporate any type of linear damping, so it may equally well represent an essentially undamped structure or an isolation system with viscous and/or hysteretic damping elements.

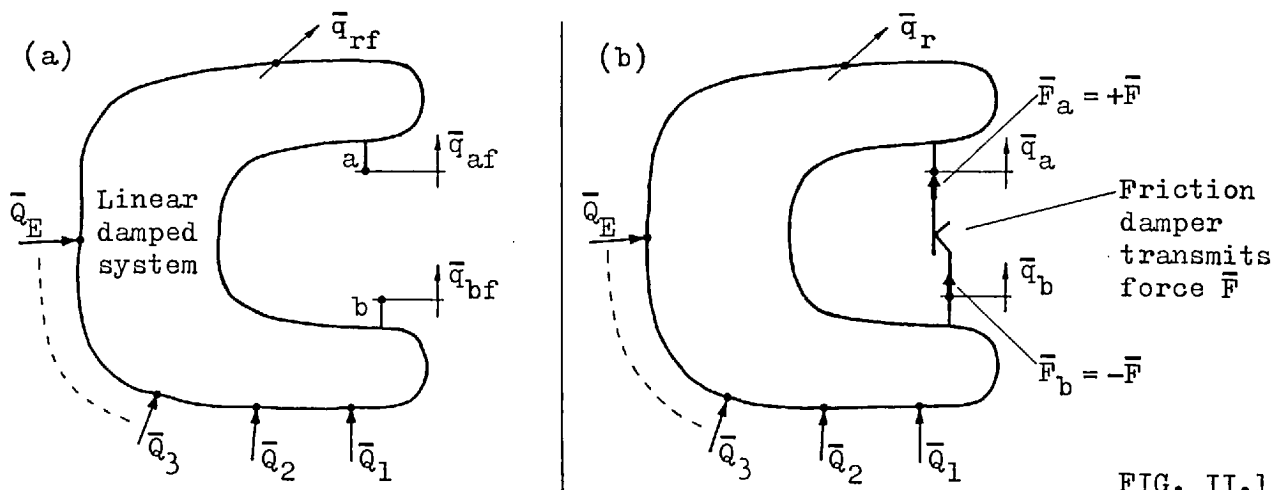


FIG. II.1

* References for Appendices I and II are given on page 75.

+ Note that a bar (-) over a variable signifies that it is a complex number. In the present analysis this prevents confusion between the complex number and its modulus. Thus $\bar{Q} = Q e^{i\theta}$ or $|\bar{Q}| e^{i\theta}$, where Q is the modulus and θ is the Phase angle.

Before the friction damper is added, the displacement response on any general co-ordinate r is given by $\bar{q}_{rf} = \sum_{e=1}^E \bar{\alpha}_{re} \bar{Q}_e$, where $\bar{\alpha}_{re}$ is the transfer receptance relating the displacement on co-ordinate r to the force applied on co-ordinate e . As co-ordinates a and b are left free, we shall define this as being the "free" response of the system, and this is indicated by the suffix f .

When the damper is fitted the linear system experiences two extra excitation forces $\bar{F}_a = +\bar{F}$ and $\bar{F}_b = -\bar{F}$, where \bar{F} is the complex force transmitted through the damper. If this force can be determined, the response \bar{q}_r of the modified system may be obtained by superposing the "free" response \bar{q}_{rf} and the response to the two extra forces.

Before we can determine the transmitted force \bar{F} ($= F e^{i\theta}$) we must look at the way in which the damper works. Basically, it consists of two parts which are clamped together by a normal force N . If the mating surfaces at the interface between the two parts have a static coefficient of friction μ_s , the damper will remain locked throughout the complete cycle as long as the transmitted force does not reach the level $\mu_s N$ at any time during the cycle. Once this level is reached slip commences and the magnitude and nature of the force change.

Under slip conditions, the damping force applied to the linear system is exactly 180° out-of-phase with the relative velocity between the ends of the damper. This is the same as with a viscous damper, and it means that the relative displacement $(\bar{q}_a - \bar{q}_b)$ leads the friction force by 90° . The force does not vary sinusoidally, but is a flat-topped or "clipped" wave as shown in Fig. II.2. The flat top corresponds to a level $\mu_d N$, where μ_d is the dynamic coefficient of friction for the damper surfaces and is typically about $\frac{\pi}{4} \mu_s$. The exact waveform depends upon the proportion of the cycle that is taken up with slipping. In case (b), for example, that part of the cycle during which

the force remains constant at a level $\mu_d N$ corresponds to slipping, while the part during which the force is changing from its maximum value in one direction to its maximum in the other direction corresponds to a locked condition.

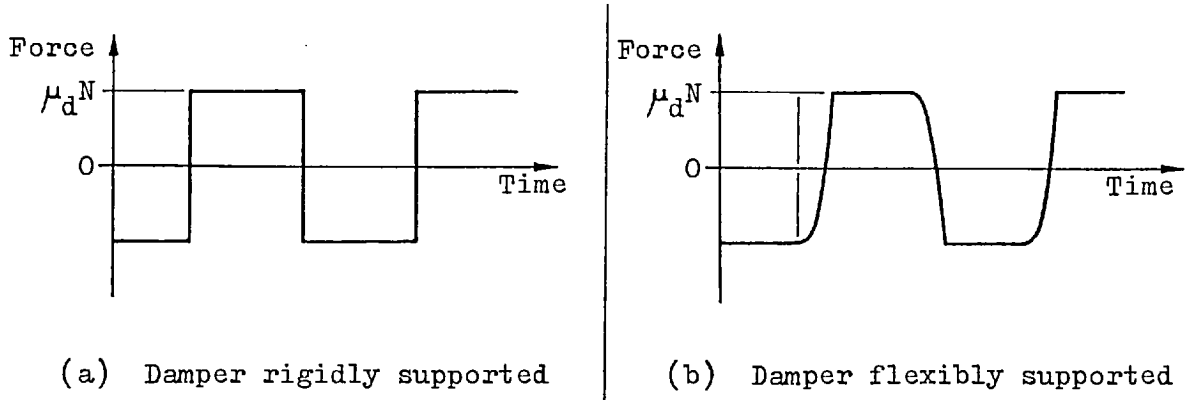


FIG. II.2 TYPICAL FRICTION FORCE WAVEFORMS

This alternate slipping and locking is characteristic of a damper which is either connected between two points on a flexible structure or to a grounded elastic support. The locked condition during part of the cycle is associated with elastic deformation of the structure or support as the friction force is reduced to zero then applied in the opposite direction. The pure "square" wave of case (a) corresponds to slipping throughout the cycle, and is only strictly obtainable if one side of the damper is connected directly to ground. However, it is possible to obtain an approximate square wave even when the damper is flexibly supported, provided that the slipping friction force $\mu_d N$ is small enough to cause negligible elastic deformation. Whatever the system to which the damper is attached, it is quite obvious that the limiting cases for the friction force waveform are a pure sine wave and a square wave, each with a peak value of $\mu_d N$.

In the linearised analysis we shall only consider the fundamental component of the wave, so the amplitude F of our sinusoidal friction force must lie somewhere between $\mu_d N$ and $\frac{4}{\pi} \mu_d N$ *. Remembering that for most materials $\mu_d \approx \frac{\pi}{4} \mu_s$,

* Note that the square wave only has odd components ($n = 1, 3, 5, \dots$) and that each component has an amplitude $\frac{1}{n} \left(\frac{4}{\pi} \mu_d N \right)$

these limits conveniently become $\mu_d N$ and $\mu_s N$. Since the force is restricted to a fairly narrow range it is reasonable to assume a constant value $F = F_{\text{slip}} = S \mu_s N$, where S is a suitable scale factor which depends upon the type of system. Thus, when the friction damper is connected to a rigid support or when it loosely couples two co-ordinates in a flexible structure, one may set $S = 1.000$, and under other conditions one may give it a lower value, approaching the bottom limit of $0.785 (= \frac{\pi}{4})$. Since the true value of the force depends upon a number of factors, it cannot be predicted with any precision, but this crude procedure gives the vibration analyst the possibility of using his experience to assign to it a realistic value.

Even Den Hartog's early experiments on a single degree-of-freedom system with a supposedly grounded damper yielded a friction force wave like that of case (b) in Fig. II.2, so his "exact" solution⁽⁵⁵⁾⁽⁶⁸⁾ assuming a square wave is in fact only an approximation to the truth, and the use of his "linearised" force⁽³⁾ $\frac{4}{\pi} \mu_d N$ is clearly incorrect when the damper is contained within a structure, as in the example in Reference (58). This is quite clear from a similar example in Reference (56), where the measured friction force was very nearly sinusoidal and certainly nothing like a square wave, since none of the harmonic components was more than 5.5% of the fundamental. Most of the measured data for dampers built into systems shows a variation of the force with frequency, and Earles and Williams⁽⁵⁶⁾⁽⁵⁹⁾ have established that this is due to a slight dependence on the relative slip amplitude. In consequence, they have used a force $F = \mu_d N + \delta U$, where U is the relative slip ($= \bar{q}_a - \bar{q}_b$) and δ is a parameter dependent on the system. Although this gives slightly improved results, there is no way of knowing the parameter δ without testing an actual system, and it varies considerably from one system to another. It is particularly interesting to observe the friction force and receptance curves shown in Reference (59) for a system with an elastically supported damper.

These show that for a moderate normal force N across the damper the receptance curve is basically that of the locked system, but with the resonance peak cut off, and the slipping friction force is essentially constant at around $\mu_d N$. Only in the case of the lowest normal force is there any significant variation of slipping force with frequency, but over the complete slip region the level lies somewhere between $\mu_d N$ and $\mu_s N$, thereby indicating the expected tendency towards a square wave as the normal force N is reduced. From the above observations it is clear that the use of a constant friction force with an approximate scale factor can adequately describe the slip behaviour in most cases, and only for more detailed studies need one consider including slip amplitude dependence.

Before proceeding with the analysis it is convenient to summarise the damper characteristics, and to outline the procedure for determining the complex transmitted force \bar{F} :

- (1) The damper will remain locked as long as the maximum transmitted force does not reach a level $\mu_s N$ at any time during the cycle. Therefore, lock the damper by setting $\bar{q}_a = \bar{q}_b$ and compute the complex transmitted force \bar{F} . If the modulus of this force, $F_{\text{lock}} \geq \mu_s N$, the damper will slip.
- (2) Once slip commences, the complex damping force \bar{F} applied to the surrounding system lags the relative displacement $(\bar{q}_a - \bar{q}_b)$ by 90° and has a constant magnitude $F_{\text{slip}} = S \mu_s N$, where the slipping friction factor S has a suitable value between 0.785 and 1.000. Therefore, set the magnitude of the force and determine its phase angle ϕ (relative to the reference) such that it lags the relative displacement by 90° .

The Linearised Analysis

Referring back to Fig. II.1, consider once more the linear system vibrating under the influence of one or more exciting forces. Before the friction damper is introduced between co-ordinates a and b, the "free" displacement responses are \bar{q}_{af} and \bar{q}_{bf} .

As soon as the damper is fitted, a complex friction force $\bar{F} = F e^{i\phi}$ is transmitted between these co-ordinates, so the responses are modified:

$$\bar{q}_a = \bar{q}_{af} + (\bar{\alpha}_{aa} - \bar{\alpha}_{ab}) \bar{F} \quad (\text{II.1})$$

$$\bar{q}_b = \bar{q}_{bf} + (\bar{\alpha}_{ba} - \bar{\alpha}_{bb}) \bar{F} \quad (\text{II.2})$$

In order to determine the correct force we must find out whether the damper remains locked or whether it slips. Both these conditions are conveniently examined if we combine equations (II.1) and (II.2) to obtain an expression for the ratio of the relative displacement to the friction force:

$$\left(\frac{\bar{q}_a - \bar{q}_b}{\bar{F}} \right) = \left(\frac{\bar{q}_{af} - \bar{q}_{bf}}{\bar{F}} \right) + \Delta \quad (\text{II.3})$$

where $\Delta = (\bar{\alpha}_{aa} - \bar{\alpha}_{ab} - \bar{\alpha}_{ba} + \bar{\alpha}_{bb})$

LOCKED Condition

Since $(\bar{q}_a - \bar{q}_b) = 0$, the force \bar{F} is given by

$$\bar{F} = \frac{-(\bar{q}_{af} - \bar{q}_{bf})}{\Delta} \quad (\text{II.4})$$

The force magnitude $F_{\text{lock}} = |\bar{F}|$. If $F_{\text{lock}} \geq \mu_s N$, the damper will slip.

SLIP Condition

The force magnitude is now constant and is given by $F_{\text{slip}} = S \mu_s N$, where S is a slipping friction factor whose value depends on the type of system ($0.785 \leq S \leq 1.000$). Thus, $\bar{F} = F_{\text{slip}} e^{i\phi}$, where the phase angle ϕ is to be determined.

Since $(\bar{q}_a - \bar{q}_b)$ leads \bar{F} by 90° , the ratio $\left(\frac{\bar{q}_a - \bar{q}_b}{\bar{F}}\right)$ is a purely imaginary number with positive sign. Hence the real part is zero:

$$\begin{aligned} \text{Real} \left(\frac{\bar{q}_a - \bar{q}_b}{\bar{F}} \right) &= \text{Real} \left(\frac{\bar{q}_{af} - \bar{q}_{bf}}{\bar{F}} \right) + \text{Real } \Delta = 0 \\ \text{Real} \left(\frac{|\bar{q}_{af} - \bar{q}_{bf}| e^{i\theta_f}}{F_{\text{slip}} e^{i\phi}} \right) + \text{Real } \Delta &= 0 \\ \text{Real} \left(\frac{|\bar{q}_{af} - \bar{q}_{bf}| e^{i(\theta_f - \phi)}}{F_{\text{slip}}} \right) + \text{Real } \Delta &= 0 \quad (\text{II.5}) \end{aligned}$$

Employing the identity $e^{i\theta} = \cos \theta + i \sin \theta$, equation (II.5) becomes

$$\frac{|\bar{q}_{af} - \bar{q}_{bf}|}{F_{\text{slip}}} \cos(\theta_f - \phi) + \text{Real } \Delta = 0$$

$$\text{whence} \quad \cos(\theta_f - \phi) = \frac{-\text{Real } \Delta}{|\bar{q}_{af} - \bar{q}_{bf}|} \cdot F_{\text{slip}} \quad (\text{II.6})^*$$

Upon taking the arc cosine of the right hand side of (II.6), we obtain two possible values for the angle $(\theta_f - \phi)$, and since we know the phase θ_f associated with the free relative displacement we get two values for ϕ . The correct value is determined by seeing which one makes the imaginary part of (II.3) positive:

$$\text{Imag} \left(\frac{\bar{q}_a - \bar{q}_b}{\bar{F}} \right) = \text{Imag} \left(\frac{\bar{q}_{af} - \bar{q}_{bf}}{\bar{F}} \right) + \text{Imag } \Delta > 0 \quad (\text{II.7})$$

$$\text{whence} \quad \frac{|\bar{q}_{af} - \bar{q}_{bf}|}{F_{\text{slip}}} \sin(\theta_f - \phi) > \text{Imag } \Delta$$

$$\sin(\theta_f - \phi) > \frac{\text{Imag } \Delta}{|\bar{q}_{af} - \bar{q}_{bf}|} \cdot F_{\text{slip}} \quad (\text{II.8})$$

Thus, one may either solve (II.6) for the two values of ϕ and then see which satisfies (II.7) or one may apply the test to $(\theta_f - \phi)$ directly using (II.8) and only afterwards obtain ϕ .

* When the linear system is undamped, this simplifies to $\cos \phi = \frac{F_{\text{slip}}}{F_{\text{lock}}}$ where F_{lock} is the real force (with sign) yielded by eqn. (II.4).

Response with Damper in Position

Once the transmitted force \bar{F} has been determined, the response on any co-ordinate r is given by:

$$\bar{q}_r = \bar{q}_{rf} + (\bar{\alpha}_{ra} - \bar{\alpha}_{rb}) \bar{F} \quad (\text{II.9})$$

Friction Force with Slip Amplitude Dependence

It is generally adequate to keep the friction force F_{slip} constant. However, the force may be allowed to vary slightly with slip amplitude by employing an iterative procedure*.

If the slip amplitude is $U = (\bar{q}_a - \bar{q}_b)$, the force is given by:

$$F_{\text{slip}} = \mu_d N + \delta U \approx 0.785 \mu_s N + \delta U \quad (\text{II.10})$$

Since F_{slip} must lie somewhere between $0.785 \mu_s N$ and $\mu_s N$, we may employ a constant force $F_{\text{slip}} = S \mu_s N$ and increment S in small steps up from 0.785. At each step, after computing the slip U we may calculate a new force $F_{\text{slip}U}$ using (II.10), and obtain a difference $d = F_{\text{slip}U} - F_{\text{slip}}$. By searching for the zero of the continuous function d we obtain the actual slip-dependent force.

* If the linear system is undamped, it is possible to obtain the slip-dependent force directly (56)(59).

Implementation of the Procedure

The computer program COUPLE1* already provides the means for analysing a wide variety of linear systems, both with and without damping. The introduction of an insert into such a system is fairly straightforward, even though the program does not at present incorporate this facility as a standard feature. Referring to Appendix I, and specifically to the flow chart for the main program COUPLE1, it is only necessary to insert a call to a special subroutine immediately before the call to CALFOR. By this stage the linear system has been built and the resulting equations have been solved, so the system receptance matrix and the "free" response columns are available from the top left-hand corners of arrays ZSYS and X respectively. These arrays form part of a blank common block and are readily accessible, so we have at our disposal everything that is required for adding an insert. Thus, for the single friction damper being considered here, it is only necessary to write a subroutine which will extract the relevant elements from the array and implement the procedure given above. Once the transmitted force has been determined, the responses are suitably modified and the new values \bar{q}_r are inserted into X in place of the original free responses \bar{q}_{rf} . The program then proceeds in the normal way.

A special subroutine called FRIC1 has been developed which will add a friction damper between any two system co-ordinates (linear or rotational) or between two points which are free to slip in a plane. It also includes provision for a slip-dependent friction force, although this still requires further refinement. Data input is via cards, which are placed immediately after the sub-system data cards. This routine is available from file and it is used in conjunction with a special version of the main program which incorporates the necessary call instruction.

A similar routine was developed by J.L. Williams for adding a torsional friction damper to an undamped linear system, but this is less general than FRIC1. Full information on his routine is given in Reference (69).

* See Chapter 2.

Results Obtained Using the Subroutine FRIC1 in Conjunction with COUPLE1

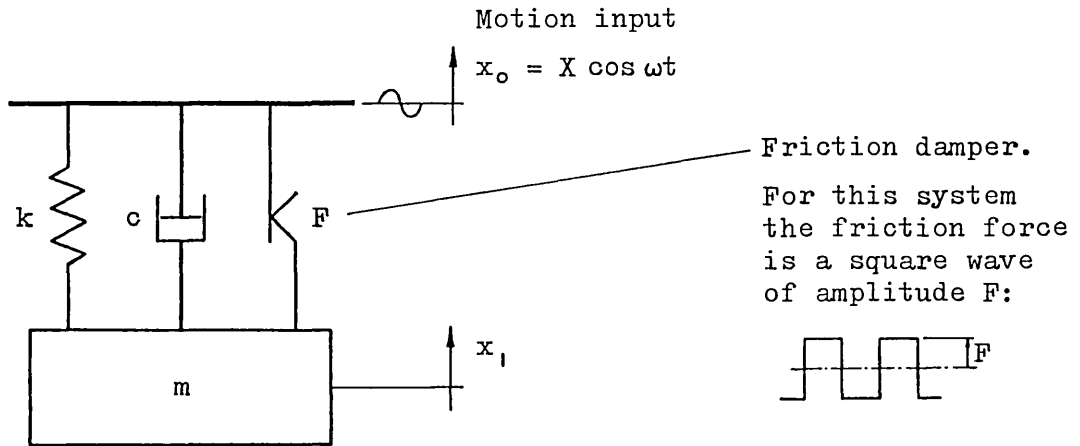
Several systems have been analysed, but only two examples will be considered in detail. The first of these is a base-excited spring-mass system which was examined by Levitan⁽⁶⁷⁾. This is shown in Fig. II.3 and it includes both a viscous and a friction damper in parallel with the spring. It is clearly seen that the addition of friction to the viscously damped linear system significantly reduces the transmissibility at resonance. In addition, as the friction is increased the transmissibility peak shifts upwards in frequency, instead of downwards, as would be the case with extra viscous damping. The approximate solution yielded by the linearised analysis is here compared with an "exact" solution obtained by breaking down the square-wave friction force into its harmonic components, and it is seen that the agreement is extremely good. It should be noted that the curves given here differ very slightly from those given in Reference (67), in that "breakaway" (unlocking of the damper) occurs here at higher frequencies. This is because Levitan did not take account of the different coefficients of friction associated with the locked and slip conditions. Thus, he assumed a locked condition as long as the transmitted force was less than F , and when slipping commenced he assumed a square-wave friction force with a peak value of F . In the present calculations it has been assumed that F is only associated with slipping, so that the maximum locked force is $\frac{4}{\pi} F$ (since $\mu_s \approx \frac{4}{\pi} \mu_d$), and the linearised slipping friction force has the same value.

As COUPLE1 does not at present have any built-in provision for including a "constant" displacement input, it was necessary to connect the base of the system to ground using a very stiff spring and then to apply a very large force to the base. Since the spring stiffness is very much greater than the dynamic stiffness of the attached spring-mass system, the base displacement remains constant throughout the frequency range. Similarly, if one required either a constant velocity or a constant acceleration input, one could employ either a large damper or a large mass as the "source impedance".

FIG. II.3

FORCED VIBRATION OF A SPRING-MASS SYSTEM HAVING COMBINED COULOMB AND VISCOUS DAMPING

(Exact solution given by E.S. Levitan in J.A.S.A., Vol. 32, 1960, page 1265)



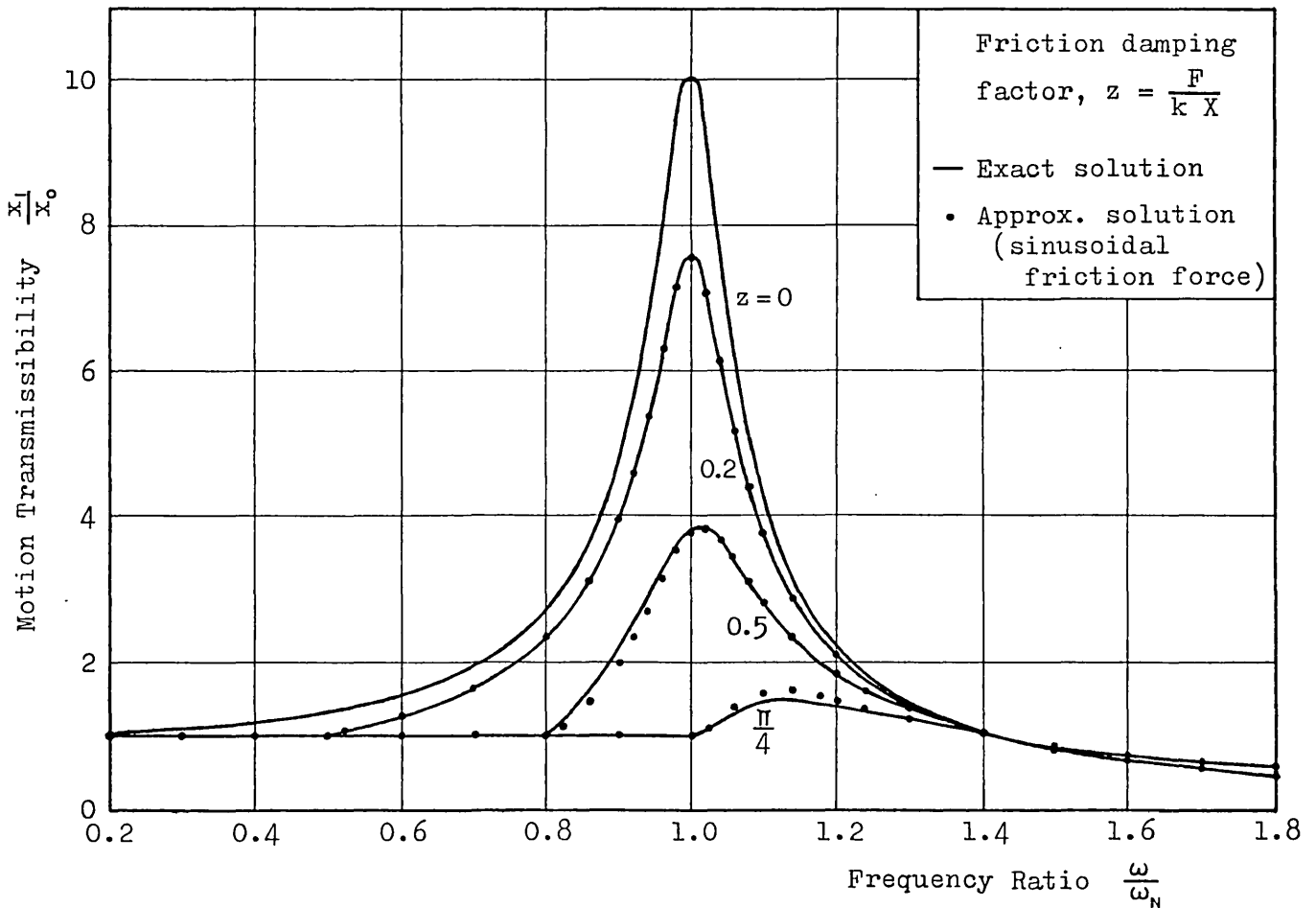
System parameters

Viscous damping ratio, $\zeta = \frac{c}{c_c} = 0.05$

where

Critical damping, $c_c = 2\sqrt{km} = 2m\omega_N$

Undamped natural frequency, $\omega_N = \sqrt{\frac{k}{m}}$ rad/s



This system was set up as two subsystems, representing the sprung mass and the source spring respectively, and the various elements were assigned the following values: $k = 1$, $m = 0.0253$, $c = 0.0159$, source spring stiffness = 1000, and linearised friction force = $\frac{4}{\pi} F$. A force input of 1000 was then applied to the base, to produce a base motion of unity. Using these values, the motion transmissibility, friction damping factor and frequency ratio were numerically equal to x_1 , F and $\frac{\omega}{2\pi}$ (= frequency in Hz) respectively.

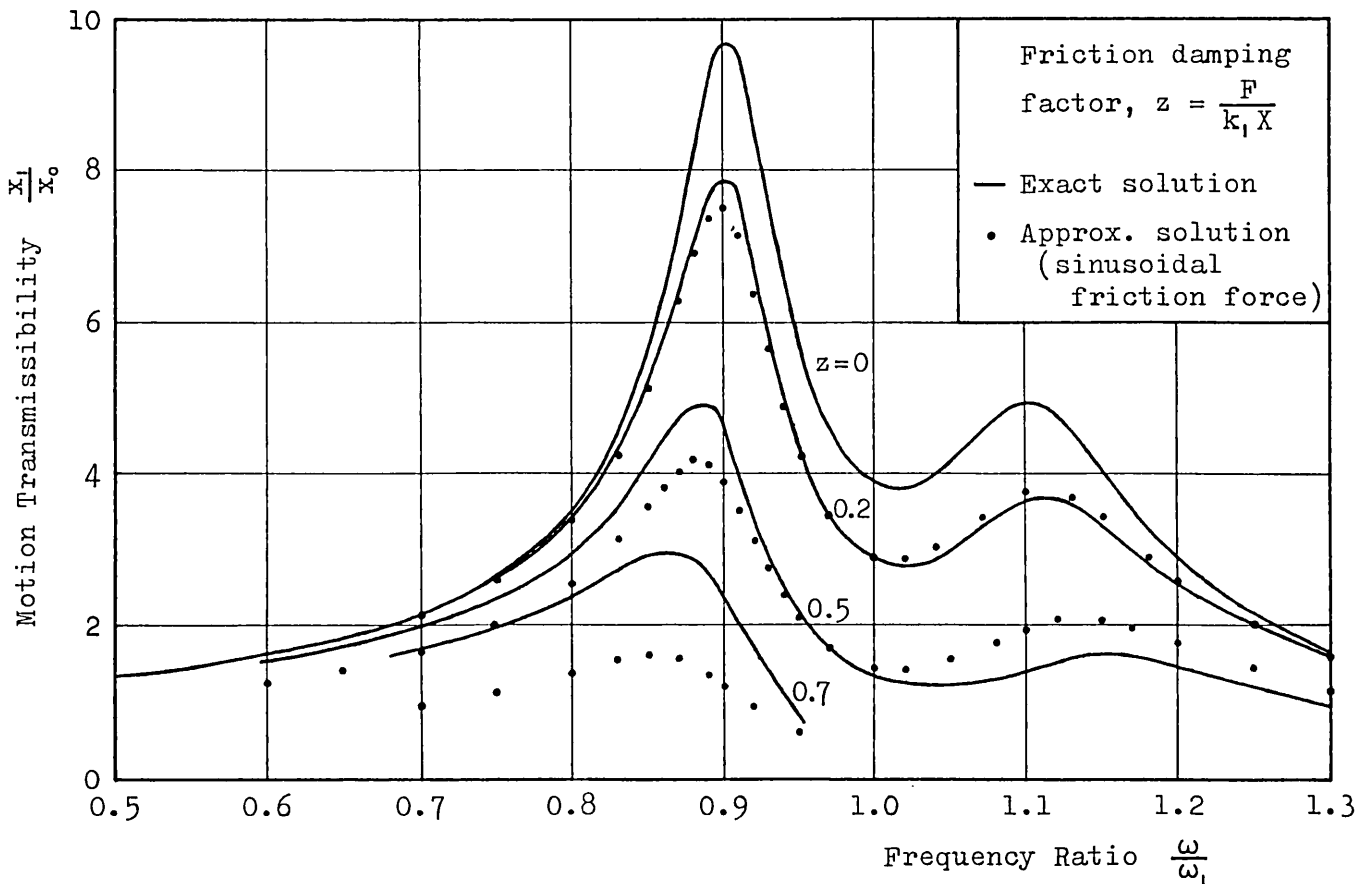
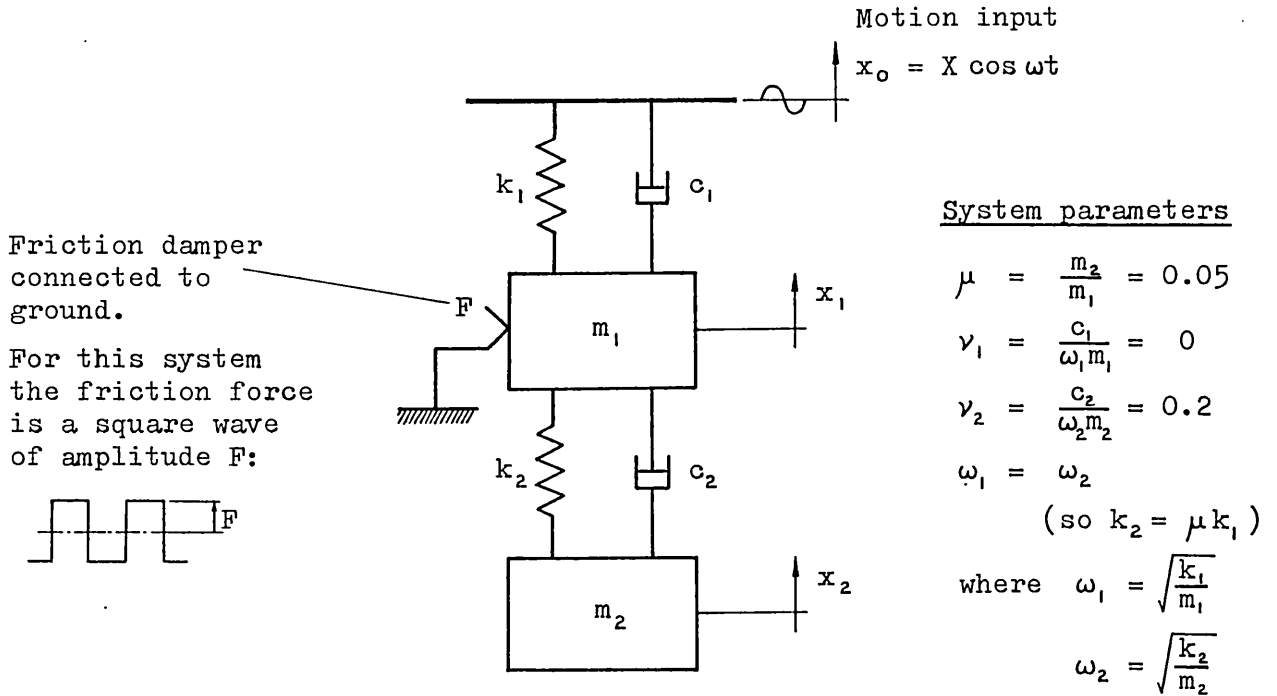
The other system that we shall consider is shown in Fig. II.4. This is a two-mass system with viscous damping and base excitation, but in this case the friction damper is attached between the main mass and a rigid support. The results of the linearised analysis are compared with an "exact" solution performed by Yeh⁽⁷⁰⁾, and it is seen that fairly good agreement is obtained for low friction forces, whereas the errors become considerable when the friction becomes large. These linearised results agree exactly with an approximate solution used as a check by Yeh, and they are adequate for most practical purposes. However, in a case such as this in which the friction force is an exact square wave, it would be very easy to improve the accuracy by also computing the response to higher harmonics of the friction force. These could then be added together to obtain the "exact" peak value of the response at any frequency.

Once again the system was broken into two subsystems, representing the two-mass system and the source spring respectively, and the following values were assigned to the various elements: $k_1 = 1$, $m_1 = 0.0253$, $c_1 = 0$, $k_2 = 0.050$, $m_2 = 0.00127$, $c_2 = 0.00159$, source spring stiffness = 1000, and linearised friction force = $\frac{4}{\pi} F$. As before, a force input of 1000 on the base produced unit displacement, so the transmissibility, friction factor and frequency ratio were given by x_1 , F and $\frac{\omega}{2\pi}$ respectively.

FIG. II.4

FORCED VIBRATION OF A TWO-MASS SYSTEM HAVING COMBINED COULOMB AND VISCOUS DAMPING

(Exact solution given by G.C.K. Yeh in J.A.S.A., Vol. 39, 1966, page 14)



COUPLE1 has also been used to analyse the idealised turbine blade considered by E. J. Williams⁽⁵⁹⁾. This provides a very good example of the use of the general purpose coupling program in conjunction with the friction damping routine, since the blade was built up from various undamped beam sections and spring supports, and then the damper was added (including slip-dependence of the friction force). Another good example is that of a rectangular frame with a single diagonal member which was loosely clamped at one corner. This system was analysed by J. L. Williams⁽⁶⁹⁾ using COUPLE1, and a single torsional damper was inserted at one end of the diagonal between it and the frame. The friction was introduced using a specially developed routine which was similar to FRIC1, though less general and only applicable to undamped systems. However, the system has also been analysed using FRIC1 and identical results have been obtained. The only other system to be examined was the very basic single-degree of freedom system with combined viscous and friction damping, as studied by Den Hartog⁽⁷¹⁾, and the results for this system agree exactly with an approximate solution given by Yeh⁽⁷⁰⁾.

APPENDICES FOR PART 2

	<u>Page</u>
III DERIVATION OF MATRICES USED IN MULTI- DIRECTIONAL MEASUREMENTS	461
IV SOME MULTI-DIRECTIONAL MOBILITY MEASUREMENTS ON A LARGE MASS	474

Note that all references quoted in these appendices are given in the reference list for Part 2, on Page 185

APPENDIX III

DERIVATION OF MATRICES USED IN MULTI-DIRECTIONAL MEASUREMENTS

In this appendix are derived the matrices associated with the multi-directional measurement method described in chapter 4. The matrices are given in a completely general form.

The response transformation $[C_p]$ includes the effect of accelerometer cross-sensitivity. Inertia correction terms are derived for the exciting block, accelerometers and force gauge. Both the accelerometer cross-sensitivity and force gauge inertia effects are known to be small, but are included in the analysis so as to preserve generality.

Each inertia term is considered separately, its effect being expressed as a system of forces acting at the point P, and given in terms of the accelerations at this point.

The completely corrected mobility matrix is given by:

$$[Y] = \frac{1}{j\omega} [C_p] [I_m] \left([\Gamma] - [M] [C_p] [I_m] - \underbrace{\left[[MF] \left\{ I_m \right\}_1, [MF] \left\{ I_m \right\}_2, [MF] \left\{ I_m \right\}_3 \right]}_{\text{FORCE GAUGE INERTIA CORRECTION}} \right)^{-1}$$

WHERE $[M] = [MB] + \underbrace{[MA]_A + [MA]_B + [MA]_C}_{\text{ACCELEROMETER INERTIA CORRECTION}}$ (III.1)

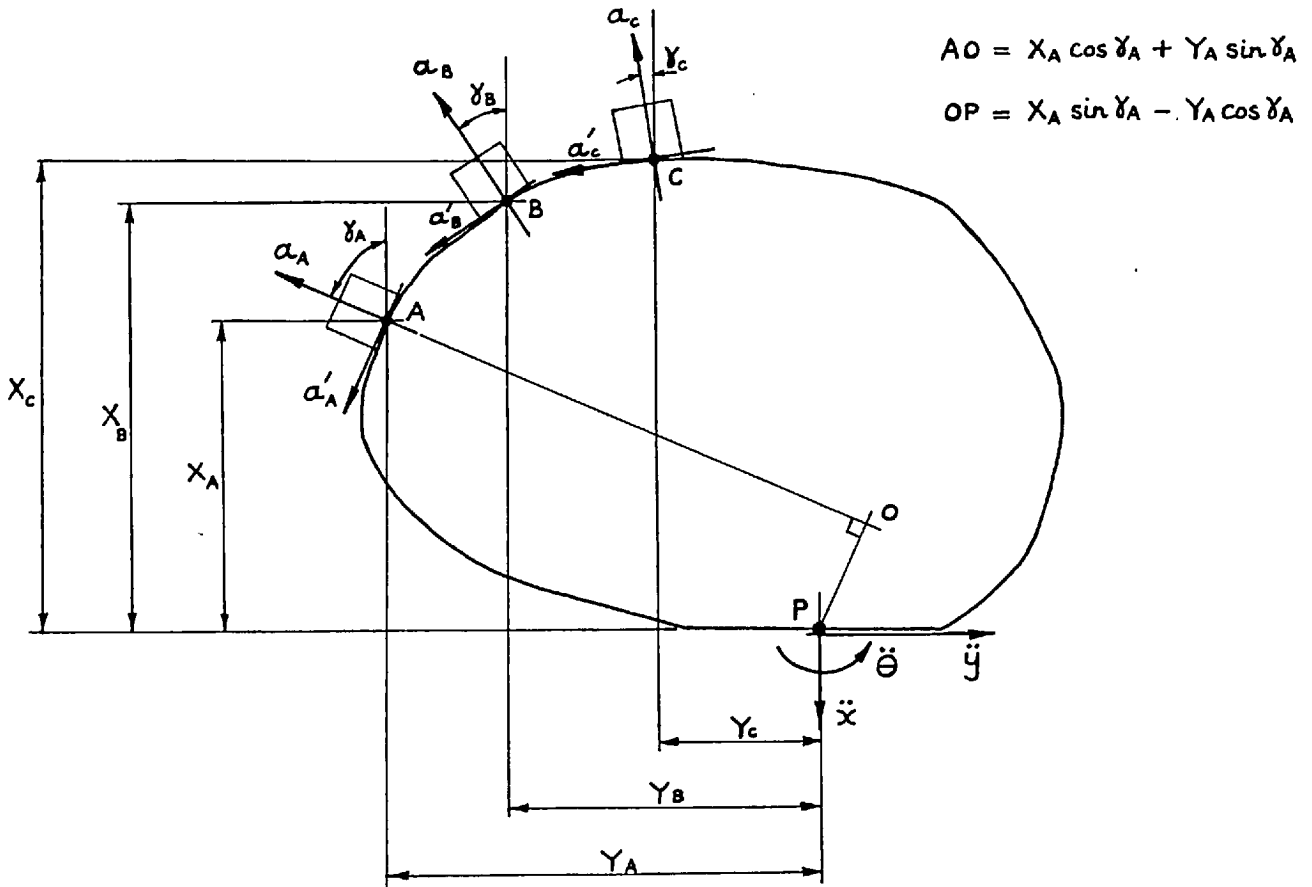
|
EXCITING BLOCK INERTIA

However, the force gauge inertia correction may usually be omitted, so that (III.1) reduces to the form (4.7)*.

* Equation (4.7) in Chapter 4.

TRANSFORMATION FROM MEASURED ACCELERATIONS TO THOSE AT P.

Consider the block shown below, where the three accelerometers are arbitrarily positioned at the points A, B and C.



When the block moves, each accelerometer produces a signal which is amplified and measured as a voltage e . If the acceleration scale factor is \bar{s} , then the measured acceleration $\bar{a} = \bar{s} \cdot e$. Because an accelerometer has a small cross-sensitivity ϵ , this acceleration differs slightly from the true axial acceleration a , so that $\bar{a} = \bar{s} \cdot e = a + \epsilon \cdot a'$, where a' is the acceleration at the accelerometer base in a direction perpendicular to the axis.

We require the transformation

$$\begin{Bmatrix} \ddot{x} \\ \ddot{y} \\ \ddot{\theta} \end{Bmatrix} = \begin{bmatrix} c_{11} & c_{12} & c_{13} \\ c_{21} & c_{22} & c_{23} \\ c_{31} & c_{32} & c_{33} \end{bmatrix} \begin{Bmatrix} \bar{a}_A \\ \bar{a}_B \\ \bar{a}_c \end{Bmatrix}$$

(III.2)

However (III.2) is most easily obtained via its inverse transformation:

$$\begin{Bmatrix} \bar{a}_A \\ \bar{a}_B \\ \bar{a}_c \end{Bmatrix} = \begin{Bmatrix} a_A \\ a_B \\ a_c \end{Bmatrix} + \begin{bmatrix} \epsilon_A & 0 & 0 \\ 0 & \epsilon_B & 0 \\ 0 & 0 & \epsilon_c \end{bmatrix} \begin{Bmatrix} a'_A \\ a'_B \\ a'_c \end{Bmatrix}$$

$$\begin{Bmatrix} \bar{a}_A \\ \bar{a}_B \\ \bar{a}_c \end{Bmatrix} = \left([P] + \begin{bmatrix} \epsilon_A & 0 & 0 \\ 0 & \epsilon_B & 0 \\ 0 & 0 & \epsilon_c \end{bmatrix} [Q] \right) \begin{Bmatrix} \ddot{x} \\ \ddot{y} \\ \ddot{\theta} \end{Bmatrix}_P$$

(III.3)

where $[P]$ and $[Q]$ relate respectively the axial and transverse accelerations to the accelerations at point P. By considering the accelerations at A, B and C due to accelerations \ddot{x} , \ddot{y} and $\ddot{\theta}$ in turn, we may obtain the columns of these matrices.

It is easily shown that

$$\left\{ \begin{array}{l} a_A \\ a_B \\ a_c \end{array} \right\} = \underbrace{\left[\begin{array}{c|c|c} -\cos \gamma_A & -\sin \gamma_A & (X_A \sin \gamma_A - Y_A \cos \gamma_A) \\ -\cos \gamma_B & -\sin \gamma_B & (X_B \sin \gamma_B - Y_B \cos \gamma_B) \\ -\cos \gamma_c & -\sin \gamma_c & (X_c \sin \gamma_c - Y_c \cos \gamma_c) \end{array} \right]}_{[P]} \left\{ \begin{array}{l} \ddot{x} \\ \ddot{y} \\ \ddot{\theta} \end{array} \right\}_P \quad (\text{III.4})$$

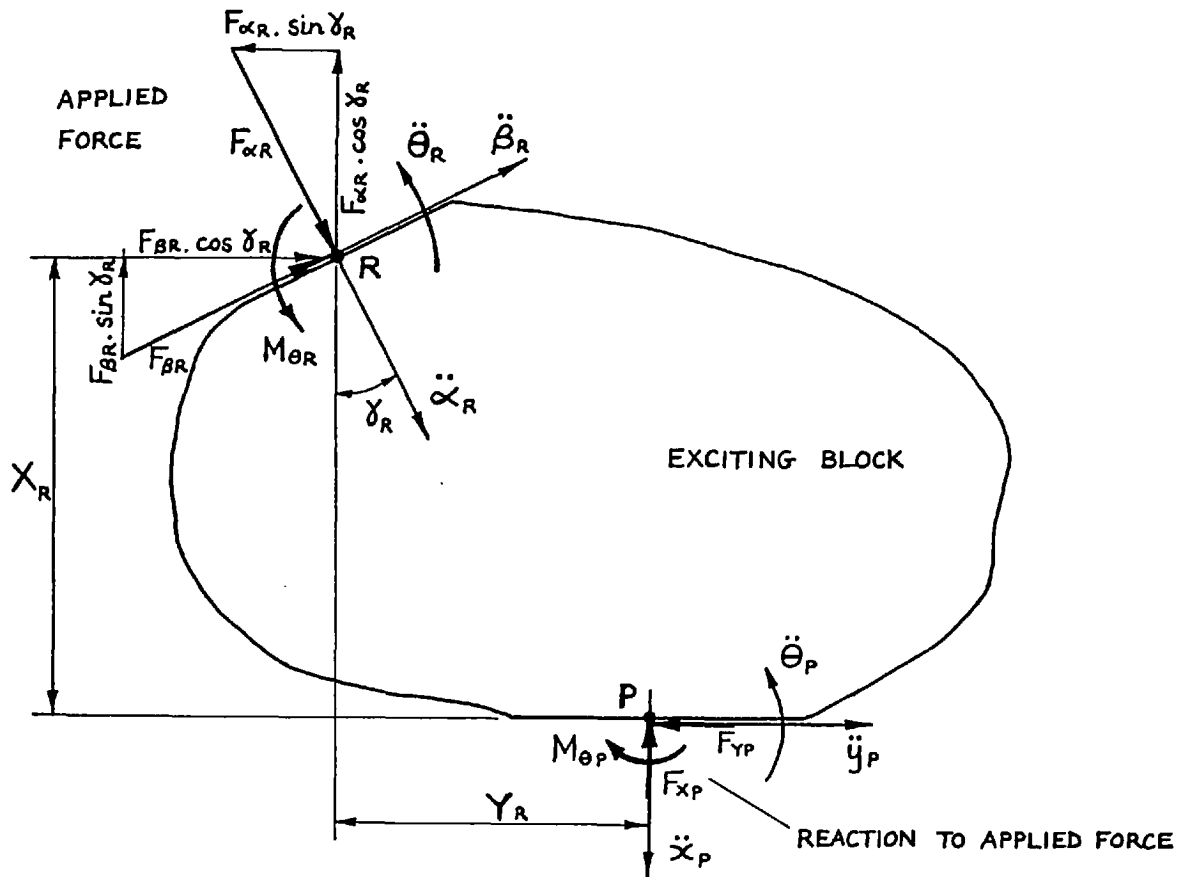
and

$$\left\{ \begin{array}{l} a'_A \\ a'_B \\ a'_c \end{array} \right\} = \underbrace{\left[\begin{array}{c|c|c} \sin \gamma_A & -\cos \gamma_A & (X_A \cos \gamma_A + Y_A \sin \gamma_A) \\ \sin \gamma_B & -\cos \gamma_B & (X_B \cos \gamma_B + Y_B \sin \gamma_B) \\ \sin \gamma_c & -\cos \gamma_c & (X_c \cos \gamma_c + Y_c \sin \gamma_c) \end{array} \right]}_{[Q]} \left\{ \begin{array}{l} \ddot{x} \\ \ddot{y} \\ \ddot{\theta} \end{array} \right\}_P \quad (\text{III.5})$$

Then the transformation (III.2) is given by

$$\left\{ \begin{array}{l} \ddot{x} \\ \ddot{y} \\ \ddot{\theta} \end{array} \right\}_P = \underbrace{\left([P] + \left[\begin{array}{ccc} \epsilon_A & 0 & 0 \\ 0 & \epsilon_B & 0 \\ 0 & 0 & \epsilon_c \end{array} \right] [Q] \right)^{-1}}_{[C_P]} \left\{ \begin{array}{l} \bar{a}_A \\ \bar{a}_B \\ \bar{a}_c \end{array} \right\} \quad (\text{III.6})$$

FORCE AND ACCELERATION TRANSFORMATIONS ACROSS THE EXCITING BLOCK



The application of forces $F_{\alpha R}$, $F_{\beta R}$ and $M_{\theta R}$ to the exciting block at point R causes forces F_{xP} , F_{yP} and $M_{\theta P}$ to be applied to the test structure at point P.

It is readily seen that the force transformation is

$$\begin{Bmatrix} F_x \\ F_y \\ M_{\theta} \end{Bmatrix}_P = \begin{bmatrix} 1 & 0 & 0 \\ 0 & 1 & 0 \\ Y & -X & 1 \end{bmatrix}_R \begin{bmatrix} \cos \gamma & -\sin \gamma & 0 \\ \sin \gamma & \cos \gamma & 0 \\ 0 & 0 & 1 \end{bmatrix} \begin{Bmatrix} F_{\alpha} \\ F_{\beta} \\ M_{\theta} \end{Bmatrix}_R$$

$$\begin{Bmatrix} F_x \\ F_y \\ M_{\theta} \end{Bmatrix}_P = \begin{bmatrix} \cos \gamma & -\sin \gamma & 0 \\ \sin \gamma & \cos \gamma & 0 \\ (Y \cos \gamma - X \sin \gamma) & -(Y \sin \gamma + X \cos \gamma) & 1 \end{bmatrix} \begin{Bmatrix} F_{\alpha} \\ F_{\beta} \\ M_{\theta} \end{Bmatrix}_R$$

$$\{F\}_P = [T_1]_R \{f\}_R$$

(III.7)

is Similarly, the inverse acceleration transformation

$$\left\{ \begin{array}{c} \ddot{\alpha} \\ \ddot{\beta} \\ \ddot{\theta} \end{array} \right\}_R = \left[\begin{array}{ccc} \cos \gamma & \sin \gamma & 0 \\ -\sin \gamma & \cos \gamma & 0 \\ 0 & 0 & 1 \end{array} \right]_R \left[\begin{array}{ccc} 1 & 0 & Y \\ 0 & 1 & -X \\ 0 & 0 & 1 \end{array} \right]_R \left\{ \begin{array}{c} \ddot{x} \\ \ddot{y} \\ \ddot{\theta} \end{array} \right\}_P$$

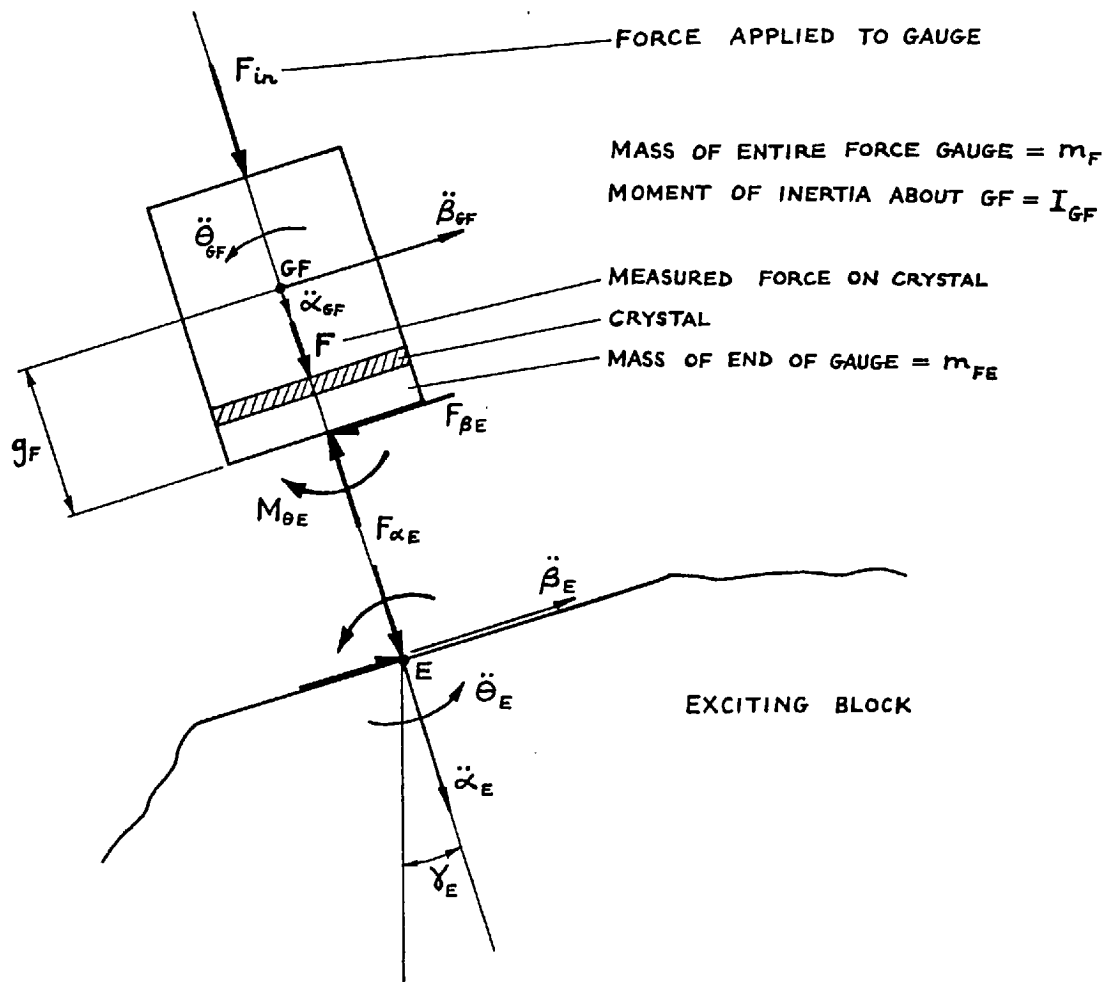
$$\left\{ \begin{array}{c} \ddot{\alpha} \\ \ddot{\beta} \\ \ddot{\theta} \end{array} \right\}_R = \left[\begin{array}{c|cc} \cos \gamma & \sin \gamma & (Y \cos \gamma - X \sin \gamma) \\ -\sin \gamma & \cos \gamma & -(Y \sin \gamma + X \cos \gamma) \\ 0 & 0 & 1 \end{array} \right]_R \left\{ \begin{array}{c} \ddot{x} \\ \ddot{y} \\ \ddot{\theta} \end{array} \right\}_P$$

$$\left\{ \ddot{\Delta} \right\}_R = \left[T_2 \right]_R \left\{ \ddot{\delta} \right\}_P$$

(III.8)

THE FORCE APPLIED BY THE FORCE GAUGE

The force gauge transmits through to the block an axial force from the shaker. However, due to its own motion the gauge also applies inertia forces to the block. These inertia forces are only a second order effect, but they will be included in the analysis in order to preserve generality.



By applying Newton's 2nd Law to the force gauge, and to the end of the gauge below the crystal, we obtain the matrix equation:

$$\begin{Bmatrix} F_\alpha \\ F_\beta \\ M_\theta \end{Bmatrix}_E = \begin{Bmatrix} F \\ 0 \\ 0 \end{Bmatrix}_E - \begin{bmatrix} m_{FE} & 0 & 0 \\ 0 & m_F & 0 \\ 0 & -m_F g_F & I_{GF} \end{bmatrix} \begin{Bmatrix} \ddot{x} \\ \ddot{\beta} \\ \ddot{\theta} \end{Bmatrix}_{GF}$$

Transform accelerations to point E on the block:

$$\begin{Bmatrix} F_\alpha \\ F_\beta \\ M_\theta \end{Bmatrix}_E = \begin{Bmatrix} F \\ 0 \\ 0 \end{Bmatrix}_E - \begin{bmatrix} m_{FE} & 0 & 0 \\ 0 & m_F & 0 \\ 0 & -m_F g_F & I_{GF} \end{bmatrix} \begin{bmatrix} 1 & 0 & 0 \\ 0 & 1 & -g_F \\ 0 & 0 & 1 \end{bmatrix} \begin{Bmatrix} \ddot{x} \\ \ddot{\beta} \\ \ddot{\theta} \end{Bmatrix}_E$$

Now transform both the forces and the accelerations to point P on the block, using the transformation (III.7) and (III.8):

$$\begin{Bmatrix} F_x \\ F_y \\ M_\theta \end{Bmatrix}_P = \begin{bmatrix} T_1 \\ T_1 \\ T_1 \end{bmatrix}_E \begin{Bmatrix} F \\ 0 \\ 0 \end{Bmatrix}_E - \left(\begin{bmatrix} T_1 \\ T_1 \\ T_1 \end{bmatrix}_E \begin{bmatrix} m_{FE} & 0 & 0 \\ 0 & m_F & 0 \\ 0 & -m_F g_F & I_{GF} \end{bmatrix} \begin{bmatrix} 1 & 0 & 0 \\ 0 & 1 & -g_F \\ 0 & 0 & 1 \end{bmatrix} \begin{bmatrix} T_2 \\ T_2 \\ T_2 \end{bmatrix}_E \right) \begin{Bmatrix} \ddot{x} \\ \ddot{y} \\ \ddot{\theta} \end{Bmatrix}_P$$

The expanded matrices are given on the following page.

$$\begin{Bmatrix} F_x \\ F_y \\ M_\theta \end{Bmatrix}_P = \begin{Bmatrix} F \cos \delta \\ F \sin \delta \\ F(Y \cos \delta - X \sin \delta) \end{Bmatrix}_E - \begin{bmatrix} m_{FE} \cos^2 \delta + m_F \sin^2 \delta & (m_{FE} - m_F) \cos \delta \cdot \sin \delta & m_{FE} \cos \delta (Y \cos \delta - X \sin \delta) + m_F \sin \delta \{(Y \sin \delta + X \cos \delta) + g_F\} \\ (m_{FE} - m_F) \cos \delta \cdot \sin \delta & m_{FE} \sin^2 \delta + m_F \cos^2 \delta & m_{FE} \sin \delta (Y \cos \delta - X \sin \delta) - m_F \cos \delta \{(Y \sin \delta + X \cos \delta) + g_F\} \\ m_{FE} \cos \delta (Y \cos \delta - X \sin \delta) + m_F \sin \delta \{(Y \sin \delta + X \cos \delta) + g_F\} & m_{FE} \sin \delta (Y \cos \delta - X \sin \delta) - m_F \cos \delta \{(Y \sin \delta + X \cos \delta) + g_F\} & m_{FE} (Y \cos \delta - X \sin \delta)^2 + m_F \{(Y \sin \delta + X \cos \delta) + g_F\}^2 + I_{GF} \end{bmatrix}_E \begin{Bmatrix} \ddot{x} \\ \ddot{y} \\ \ddot{\theta} \end{Bmatrix}_P$$

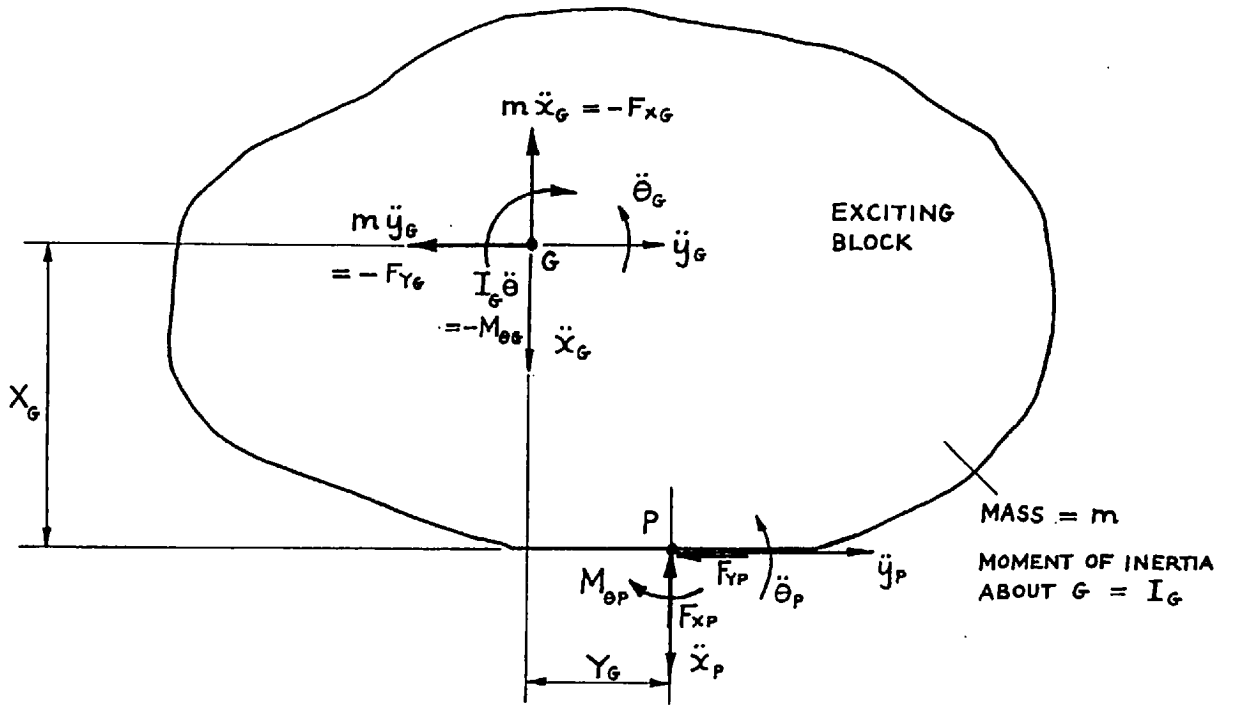
$$F \left\{ \Gamma \right\}_E$$

$$\left[MF \right]_E$$

(III.9)

THE EFFECT OF EXCITING BLOCK INERTIA

We shall consider the inertia effect by applying D'Alembert forces to the block at its centre of gravity G.




The D'Alembert or inertia forces applied at G are

$$\begin{Bmatrix} F_x \\ F_y \\ M_{\theta} \end{Bmatrix}_G = - \begin{bmatrix} m & 0 & 0 \\ 0 & m & 0 \\ 0 & 0 & I_G \end{bmatrix} \begin{Bmatrix} \ddot{x} \\ \ddot{y} \\ \ddot{\theta} \end{Bmatrix}_G$$

Transform both the forces and the accelerations to point P on the block, using the transformations (III.7) and (III.8):

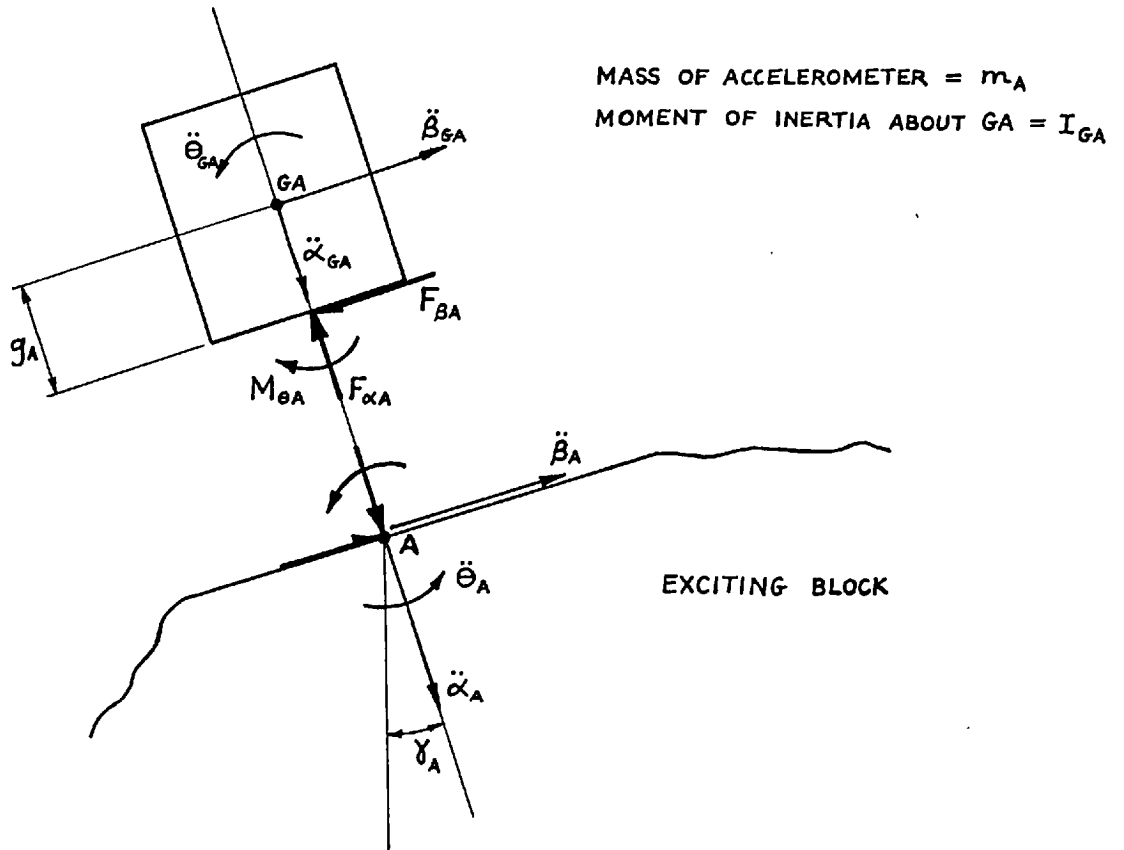
$$\begin{Bmatrix} F_x \\ F_y \\ M_\theta \end{Bmatrix}_P = - \begin{bmatrix} T_1 \\ T_1 \end{bmatrix}_G \begin{bmatrix} m & 0 & 0 \\ 0 & m & 0 \\ 0 & 0 & I_G \end{bmatrix} \begin{bmatrix} T_2 \\ T_2 \end{bmatrix}_G \begin{Bmatrix} \ddot{x} \\ \ddot{y} \\ \ddot{\theta} \end{Bmatrix}_P$$

$$\begin{Bmatrix} F_x \\ F_y \\ M_\theta \end{Bmatrix}_P = - \begin{bmatrix} m & 0 & mY_G \\ 0 & m & -mX_G \\ mY_G & -mX_G & I_G + m(X_G^2 + Y_G^2) \end{bmatrix} \begin{Bmatrix} \ddot{x} \\ \ddot{y} \\ \ddot{\theta} \end{Bmatrix}_P$$


[MB]

(III.10)

THE INERTIA EFFECT OF AN ACCELEROMETER



Apply Newton's 2nd Law to the accelerometer:

$$\begin{Bmatrix} F_\alpha \\ F_\beta \\ M_\theta \end{Bmatrix}_A = - \begin{bmatrix} m_A & 0 & 0 \\ 0 & m_A & 0 \\ 0 & -m_A g_A & I_{GA} \end{bmatrix} \begin{Bmatrix} \ddot{\alpha} \\ \ddot{\beta} \\ \ddot{\theta} \end{Bmatrix}_{GA}$$

Transform accelerations to point A on the block:

$$\begin{Bmatrix} F_\alpha \\ F_\beta \\ M_\theta \end{Bmatrix}_A = - \begin{bmatrix} m_A & 0 & 0 \\ 0 & m_A & 0 \\ 0 & -m_A g_A & I_{GA} \end{bmatrix} \begin{bmatrix} 1 & 0 & 0 \\ 0 & 1 & -g_A \\ 0 & 0 & 1 \end{bmatrix} \begin{Bmatrix} \ddot{x} \\ \ddot{y} \\ \ddot{\theta} \end{Bmatrix}_A$$

Now transform both the forces and the accelerations to point P on the block, using the transformations(III.7) and (III.8):

$$\begin{Bmatrix} F_x \\ F_y \\ M_\theta \end{Bmatrix}_P = \begin{bmatrix} T_1 \\ T_2 \end{bmatrix}_A \begin{bmatrix} m_A & 0 & 0 \\ 0 & m_A & 0 \\ 0 & -m_A g_A & I_{GA} \end{bmatrix} \begin{bmatrix} 1 & 0 & 0 \\ 0 & 1 & -g_A \\ 0 & 0 & 1 \end{bmatrix} \begin{bmatrix} T_1 \\ T_2 \end{bmatrix}_A \begin{Bmatrix} \ddot{x} \\ \ddot{y} \\ \ddot{\theta} \end{Bmatrix}_P$$

whence

$$\begin{Bmatrix} F_x \\ F_y \\ M_\theta \end{Bmatrix}_P = \begin{bmatrix} m_A & 0 & m_A(Y + g_A \sin \delta) \\ 0 & m_A & -m_A(X + g_A \cos \delta) \\ m_A(Y + g_A \sin \delta) & -m_A(X + g_A \cos \delta) & m_A\{X^2 + Y^2 + g_A^2 + 2g_A(X \cos \delta + Y \sin \delta)\} + I_{GA} \end{bmatrix} \begin{Bmatrix} \ddot{x} \\ \ddot{y} \\ \ddot{\theta} \end{Bmatrix}_P$$

$\underbrace{\hspace{10em}}_{\begin{bmatrix} MA \\ A \end{bmatrix}}$

(III.11)

APPENDIX IV

SOME MULTI-DIRECTIONAL MOBILITY MEASUREMENTS ON A LARGE MASS

Introduction

It has been shown in Chapters 4 and 5 that multi-directional mobility measurements may be made using a specially designed "exciting block" in conjunction with either a single or a twin shaker. For the test items considered in those chapters, quite good agreement was obtained between measured and theoretical results. However, if the measurement technique is to be applied to structures of unknown mobility it is essential that accuracy bounds be known, so that the results may be interpreted correctly.

The measurements described in this appendix were carried out on a large steel mass using exciting block Mk 4 and a twin shaker, the object being to determine the effective stiffness of the exciting block and to examine the effect of accelerometer cross-sensitivity. This information may be used to assess the validity of any other measurements made with the same block-shaker system, in addition to giving a qualitative guide to the limitations of the multi-directional measurement technique.

Instrumentation and experimental details

The exciting-block/twin-shaker system is shown in Fig. IV.1, and a detailed drawing of the Mk 4 block is given in Fig. IV.2. It will be observed that the block was not attached directly to the item under test. Instead, a 100 mm dia. x 16 mm thick steel disc was first stuck down using Plastic Padding, and the block was then bolted down onto the ground upper surface of the disc using a $\frac{1}{2}$ inch BSF high tensile steel bolt. A thin film of Plastic Padding was also interposed between the block and the disc, so as to ensure an absolutely solid joint. This arrangement had been used previously for some measurements on a large steel structure*, since it

* See Part 4, Chapter 14, Section 14.5.

FIG IV.1

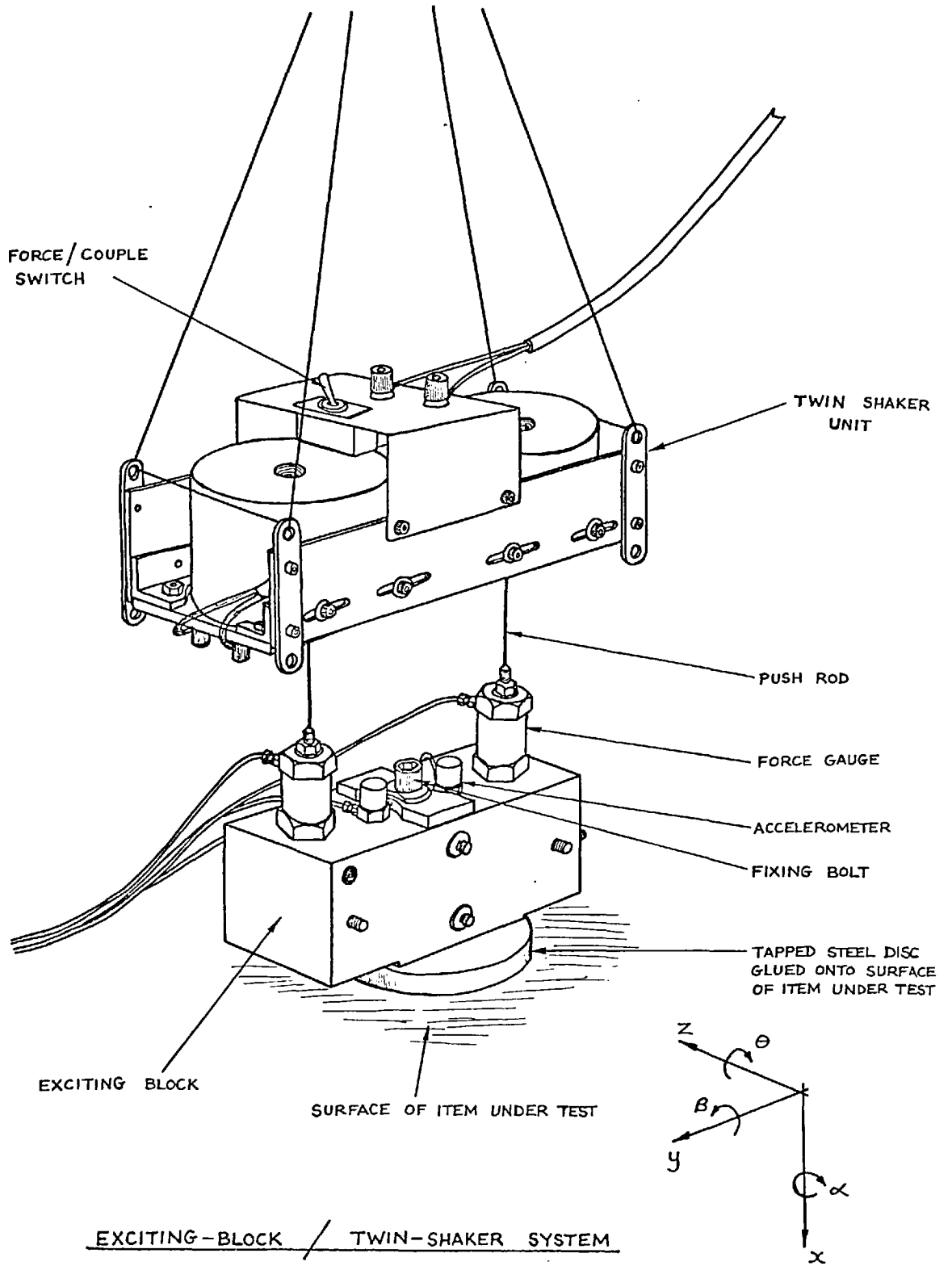
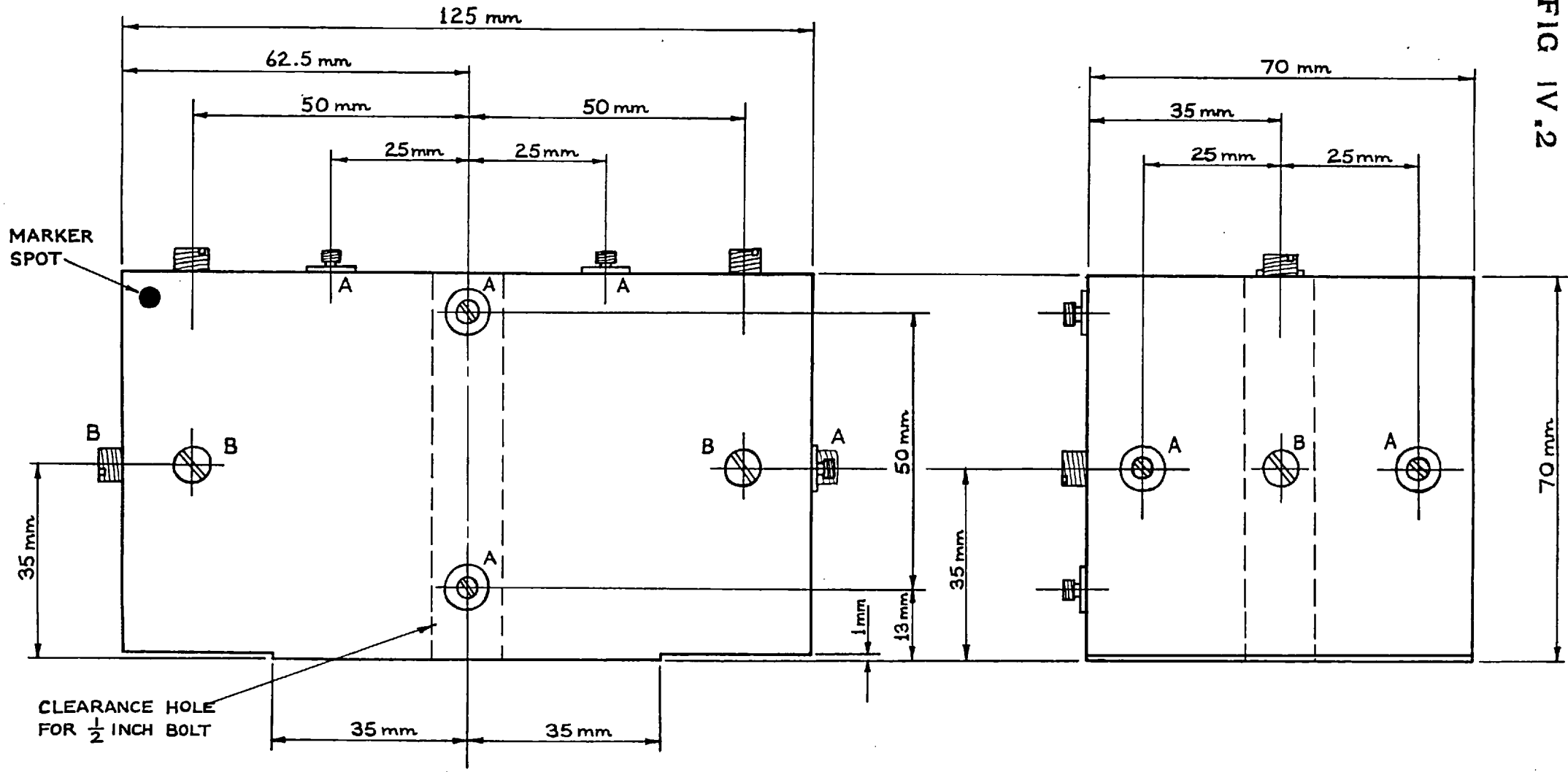


FIG IV.2



STUDS

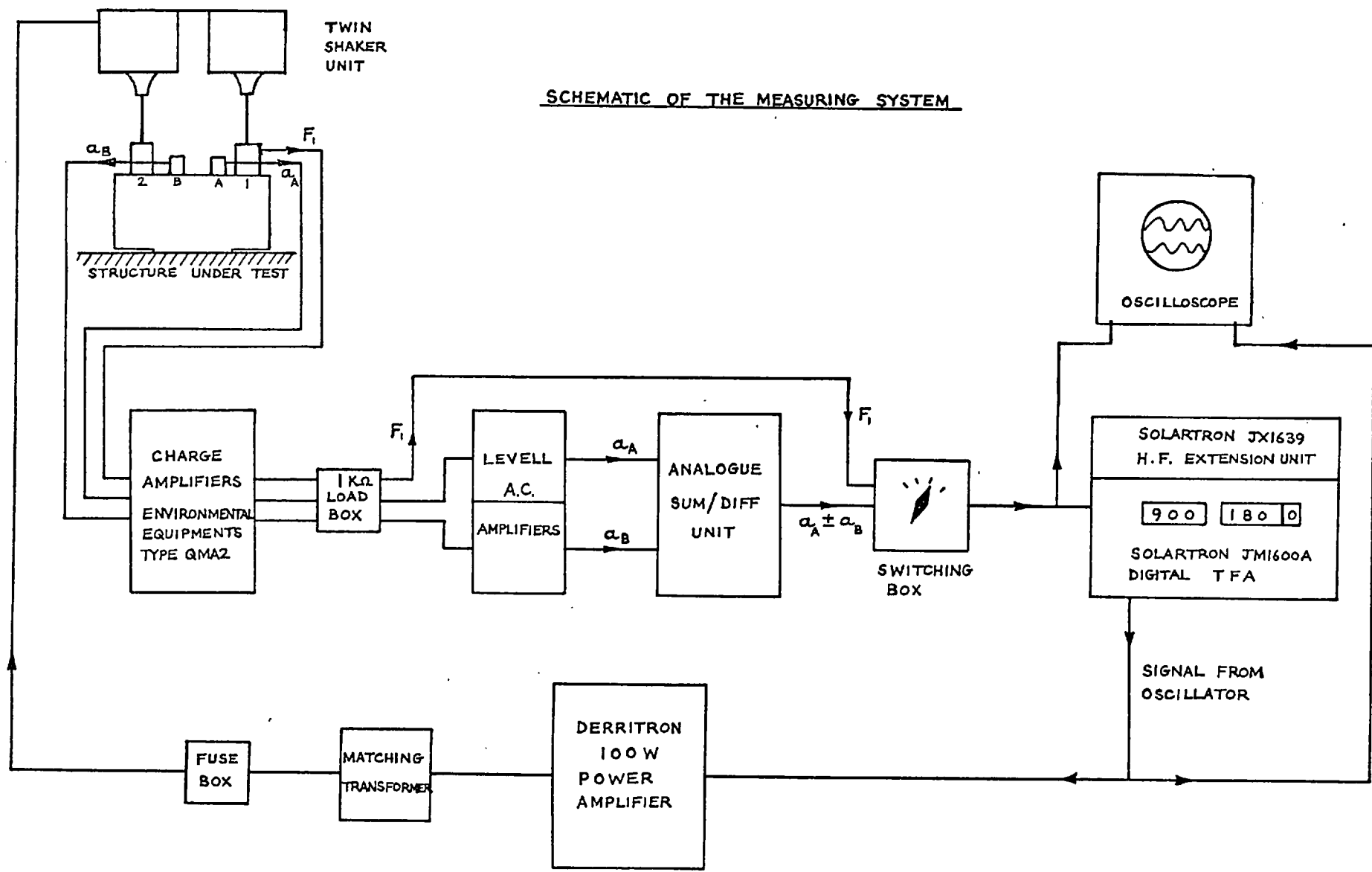
- A 10-32 UNF INSULATING FOR ACCELEROMETER
- B 1/4 UNF FOR FORCE GAUGE

MATERIAL: ALUMINIUM ALLOY

EXCITING BLOCK MK 4

FULL SCALE

THIRD ANGLE PROJECTION



SCHEMATIC OF THE MEASURING SYSTEM

FIG IV.3

obviated the need for attachment holes in the structure, and it also simplified re-orientation* of the exciting block for measurements in another plane.

As a precaution against earth loops, the accelerometers⁺ were attached to the block by means of insulating studs. Two force gauges[∕] were mounted on top of the block, but only one of these was actually used for measuring force, it being assumed that $F_2 = \pm F_1$. It has been shown in Chapter 5 that this assumption is not far from the truth, provided that the two shakers are fairly closely matched. The push rods were 1 mm dia. x 50 mm long, so they only introduced a minimal constraint on the six directional motion of the block.

The complete measuring system is shown in Fig. IV.3. Apart from the twin-shaker unit, the only important difference between this and the system shown in Chapter 4 is the inclusion of an analogue sum and difference unit. This permits the direct measurement of linear and rotational accelerations with the transfer function analyser (TFA). The twin shaker is switchable to give either a force or a couple, which may be measured with force gauge 1 : Force = $2F_1$; Couple = $2 eF_1$.^X

Using this system, measurements were made of 12 of the 36 elements of the 6 x 6 mobility matrix for a point on top of the large mass. These measurements were obtained directly, and were not subsequently processed. Hence, no correction has been made for the inertia of the exciting block or for impurity of excitation due to slight mismatching of the shakers. In

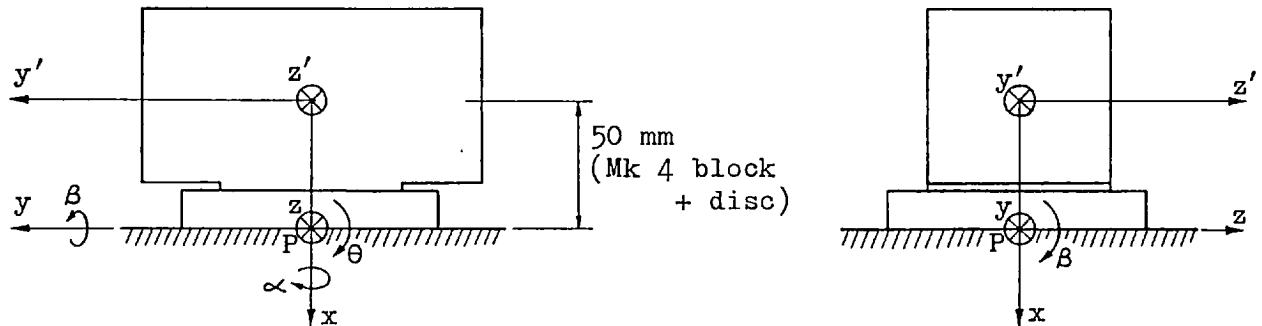
* After removing the fixing bolt the block could be released with a sharp tap, since the ground surface of the disc did not allow a rigid bond.

+ Environmental Equipments type AQ40 (3 and 5% max. cross sensitivity).

∕ Endevco type 2103-100

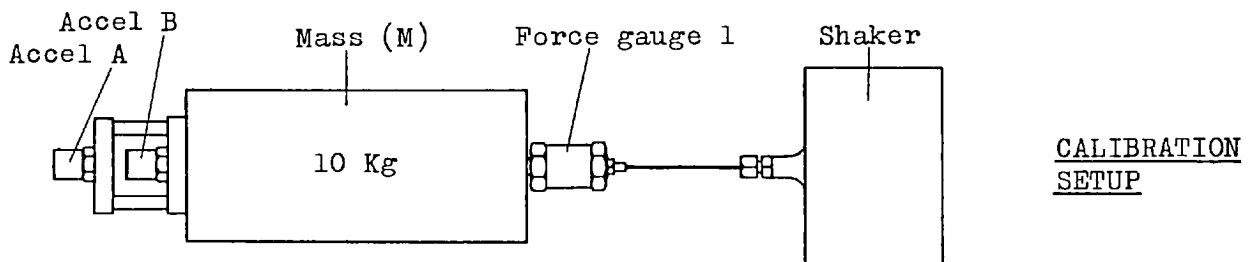
X $2e$ = distance between push rods.

addition, the measurements correspond to axes x , y' and z' through the centre of the exciting block, whilst the required mobility properties pertain to axes x , y and z through point P on the surface of the item under test. Although the two points are only 50 mm apart, it will be shown that this is



sufficient to introduce errors of several dB.

Prior to performing the tests on the large mass, it was necessary to set up the amplifier gains and to calibrate the system. For this purpose the two accelerometers and the force gauge were mounted co-axially on a cylindrical 10 Kg mass, as shown below. The mass was then vibrated at a fixed frequency and the gains of the two acceleration channels were adjusted



to give equal outputs. The two signals were measured independently using the TFA, although one could alternatively measure their difference and set this to zero. The setting was checked at various other frequencies and was found to remain constant. Then the inertance calibration factor \bar{S} was obtained by measuring acceleration A and force 1 in volts at a number of frequencies in the range of interest (60 to 1500 Hz). If the average value of $\frac{\text{accel. } A \text{ [v]}}{\text{force } 1 \text{ [v]}}$ is Δ and the calibration mass is M , then $\bar{S} = \frac{1}{\Delta \cdot M}$.

The various multi-directional inertance responses were then given by the following expressions:

$$\begin{aligned}
 \frac{\text{Translation}}{\text{Force}} &= \frac{\bar{S} (a_A [v] + a_B [v])}{4 F_1 [v]} \\
 \frac{\text{Rotation}}{\text{Force}} &= \frac{\bar{S} (a_A [v] - a_B [v])}{4s F_1 [v]} \\
 \frac{\text{Translation}}{\text{Couple}} &= \frac{\bar{S} (a_A [v] + a_B [v])}{4e F_1 [v]} \\
 \frac{\text{Rotation}}{\text{Couple}} &= \frac{\bar{S} (a_A [v] - a_B [v])}{4se F_1 [v]} \tag{IV.1}
 \end{aligned}$$

where $a_A [v]$, $a_B [v]$ and $F_1 [v]$ are the accelerations and the force in volts and $2s$ is the distance between the two accelerometer axes. These responses could easily have been converted to mobilities by dividing by $j\omega$, but it was not considered worthwhile in the present case, since the inertiance properties of a pure mass are independent of frequency and are therefore represented by horizontal lines on an inertiance frequency response plot.

Tests on the large mass

The mass was a 135 Kg block of steel, which was mounted on rubber pads (see Fig. IV.4). Since the six natural frequencies of this system were all less than 30 Hz, the response was purely masslike above about 80 Hz. The inertiance properties were to be measured at point P on top of the mass, and because only the masslike response was of interest, measurements were confined to the frequency range 60 to 1500 Hz. The complete 6 x 6 point inertiance matrix is shown below:

$\frac{\ddot{x}}{F_x}$	$\frac{\ddot{x}}{F_y}$	$\frac{\ddot{x}}{F_z}$	$\frac{\ddot{x}}{M_\alpha}$	$\frac{\ddot{x}}{M_\beta}$	$\frac{\ddot{x}}{M_\theta}$
$\frac{\ddot{y}}{F_x}$	$\frac{\ddot{y}}{F_y}$	$\frac{\ddot{y}}{F_z}$	$\frac{\ddot{y}}{M_\alpha}$	$\frac{\ddot{y}}{M_\beta}$	$\frac{\ddot{y}}{M_\theta}$
$\frac{\ddot{z}}{F_x}$	$\frac{\ddot{z}}{F_y}$	$\frac{\ddot{z}}{F_z}$	$\frac{\ddot{z}}{M_\alpha}$	$\frac{\ddot{z}}{M_\beta}$	$\frac{\ddot{z}}{M_\theta}$
$\frac{\ddot{\alpha}}{F_x}$	$\frac{\ddot{\alpha}}{F_y}$	$\frac{\ddot{\alpha}}{F_z}$	$\frac{\ddot{\alpha}}{M_\alpha}$	$\frac{\ddot{\alpha}}{M_\beta}$	$\frac{\ddot{\alpha}}{M_\theta}$
$\frac{\ddot{\beta}}{F_x}$	$\frac{\ddot{\beta}}{F_y}$	$\frac{\ddot{\beta}}{F_z}$	$\frac{\ddot{\beta}}{M_\alpha}$	$\frac{\ddot{\beta}}{M_\beta}$	$\frac{\ddot{\beta}}{M_\theta}$
$\frac{\ddot{\theta}}{F_x}$	$\frac{\ddot{\theta}}{F_y}$	$\frac{\ddot{\theta}}{F_z}$	$\frac{\ddot{\theta}}{M_\alpha}$	$\frac{\ddot{\theta}}{M_\beta}$	$\frac{\ddot{\theta}}{M_\theta}$

Point inertiance
matrix
(theoretically
symmetric)

(IV.2)

The 12 boxed elements have been measured in the manner described in the previous section.

The exciting block orientation and the force gauge and accelerometer positions are shown in Fig. IV.5. Since incorrect positioning of the transducers can lead to a 180° phase shift in the measured inertiance, it is important to observe the convention adopted: This is best illustrated by considering the $\frac{\ddot{\theta}}{M_\theta}$ case, and imagining the exciting block to be connected to a spring-like structure. Then the application of a positive couple must cause force gauge 1 (the measurement gauge) to push against the block, whilst gauge 2 pulls it. As the block rotates in a positive sense it must pull accelerometer A (Red) with it and push accelerometer B (Blue). This convention only gives the correct inertiance phase if the calibration test described in the previous section gives a 180° phase difference between the force and acceleration signals. If the calibration phase is 0° , then a 180° correction must be applied to the measured inertiance data. It should be noted that reversing the positions of the force gauges or accelerometers will not correct the phases of all the elements in the matrix.

The theoretical point inertiance matrix may be obtained in terms of the mass and the principal moments of inertia, in the manner indicated in

Fig. IV.6. The resulting matrix is given in Fig. IV.7, both in inertiance units and in dB with phase angle.

The 12 selected responses are given in Figs. IV.8 to IV.13, where the order corresponds to the rows of matrix (IV.2).

FIG IV.4

$$\text{MASS} = 135 \text{ Kg} = m$$

$$I_{Gx} = \frac{m}{12} (b^2 + c^2) = 1.630 \text{ Kg m}^2$$

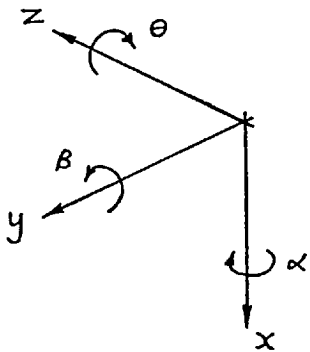
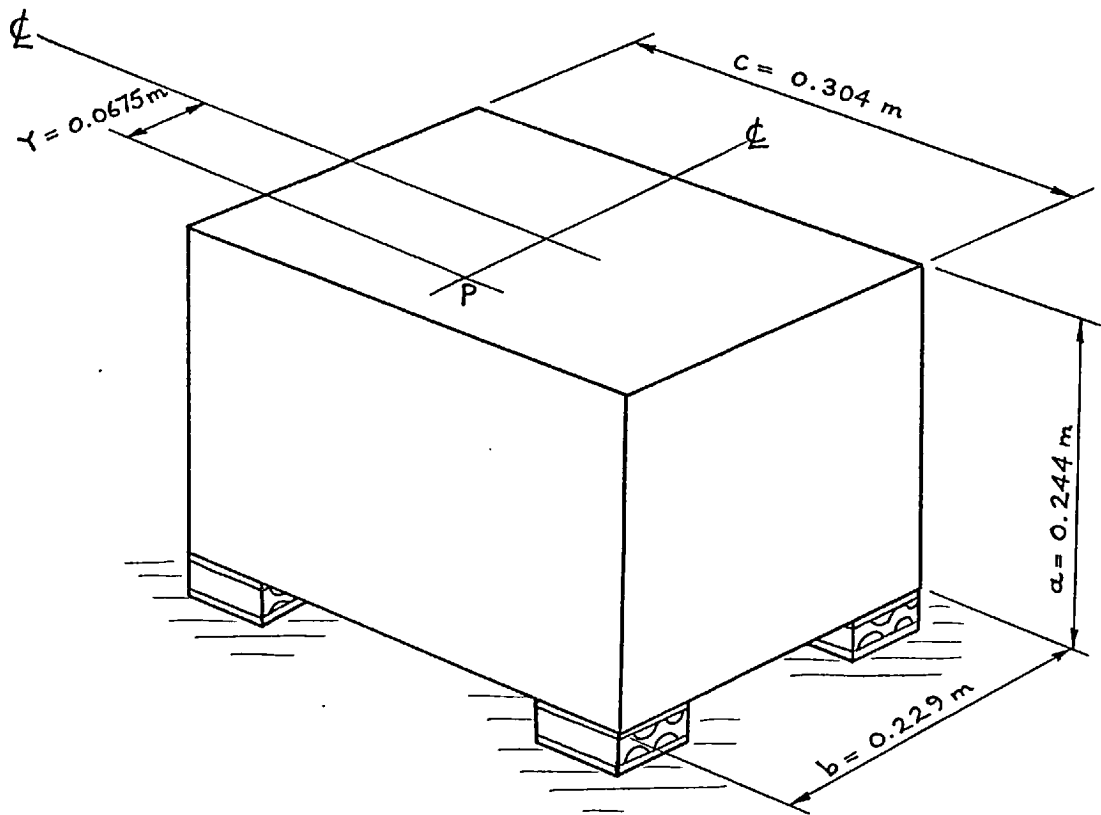
$$I_{Gy} = \frac{m}{12} (a^2 + c^2) = 1.709 \text{ Kg m}^2$$

$$I_{Gz} = \frac{m}{12} (a^2 + b^2) = 1.260 \text{ Kg m}^2$$

$$X = -0.122 \text{ m}$$

$$Y = 0.0675 \text{ m}$$

$$Z = 0$$



MASS ON RUBBER PADS

FIG. IV.5 EXCITATION ARRANGEMENTS AND RESPONSE MEASUREMENT
POSITIONS USED FOR TWIN SHAKER TESTS ON 135 KG MASS

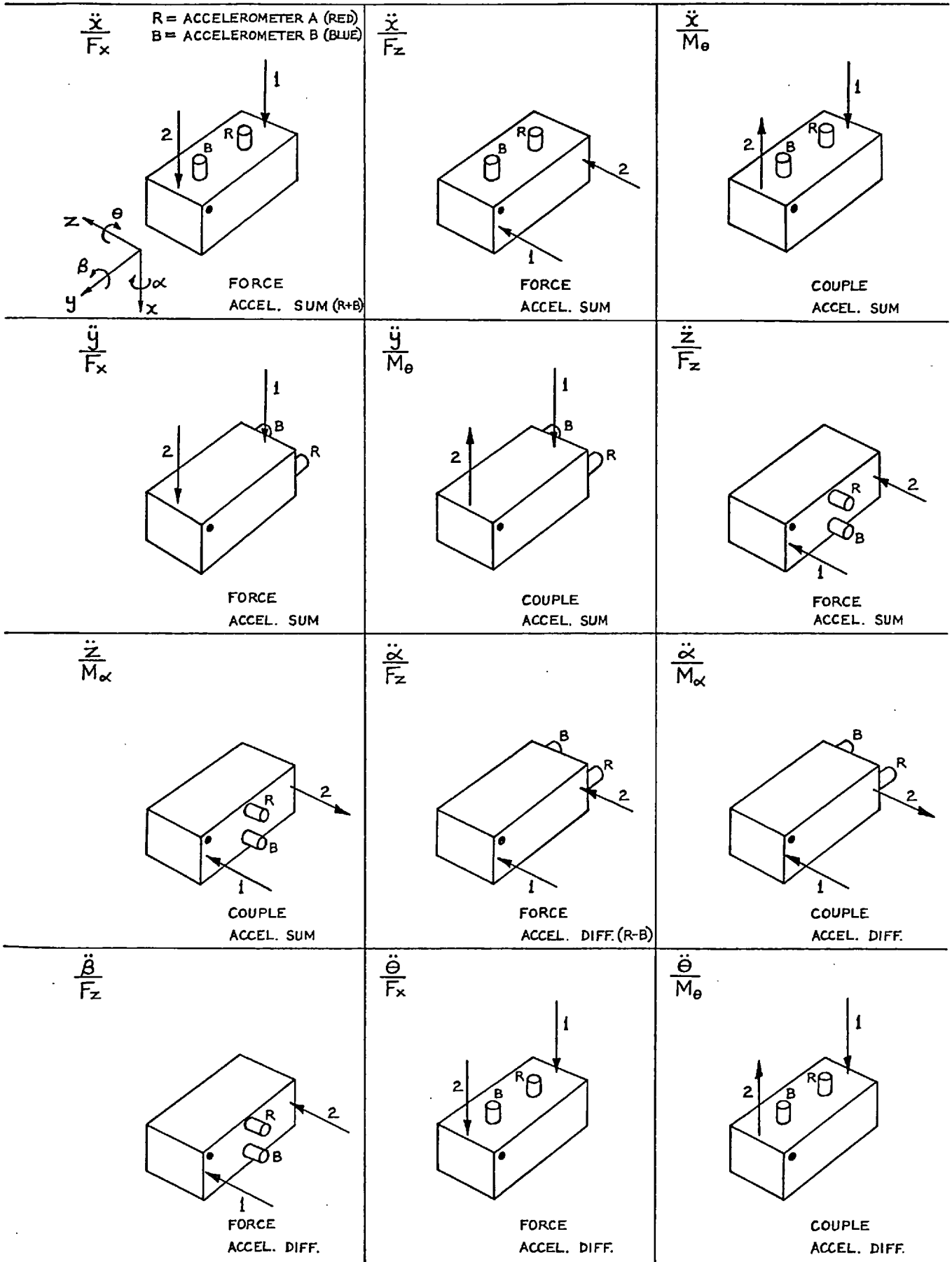


FIG IV.7

$$\begin{pmatrix} \ddot{x} \\ \ddot{y} \\ \ddot{z} \\ \ddot{\alpha} \\ \ddot{\beta} \\ \ddot{\theta} \end{pmatrix}_P = \begin{matrix} \begin{matrix} 0.1102 \times 10^{-1} & 0.6537 \times 10^{-2} & 0 & 0 & 0 & -0.5358 \times 10^{-1} \\ & 0.1922 \times 10^{-1} & 0 & 0 & 0 & -0.9684 \times 10^{-1} \\ & & 0.1891 \times 10^{-1} & 0.4142 \times 10^{-1} & 0.7137 \times 10^{-1} & 0 \\ & & & 0.6136 \times 10^0 & 0 & 0 \\ & & & & 0.5850 \times 10^0 & 0 \\ & & & & & 0.7938 \times 10^0 \end{matrix} \\ \text{SYMMETRICAL} \end{matrix} \begin{pmatrix} F_x \\ F_y \\ F_z \\ M_\alpha \\ M_\beta \\ M_\theta \end{pmatrix}_P$$

THEORETICAL POINT INERTIANCE MATRIX FOR POINT ON TOP OF 135 KG. MASS

S. I. UNITS: ACCELERATIONS IN m/s^2 AND rad/s^2 ,
 FORCES IN N, MOMENTS IN N-m

$$\begin{pmatrix} \ddot{x} \\ \ddot{y} \\ \ddot{z} \\ \ddot{\alpha} \\ \ddot{\beta} \\ \ddot{\theta} \end{pmatrix}_P = \begin{matrix} \begin{matrix} -39.15 / 0^\circ & -43.69 / 0^\circ & -\infty & -\infty & -\infty & -25.42 / 180^\circ \\ & -34.32 / 0^\circ & -\infty & -\infty & -\infty & -20.28 / 180^\circ \\ & & -34.47 / 0^\circ & -27.66 / 0^\circ & -22.93 / 0^\circ & -\infty \\ & & & -4.24 / 0^\circ & -\infty & -\infty \\ & & & & -4.66 / 0^\circ & -\infty \\ & & & & & -2.00 / 0^\circ \end{matrix} \\ \text{SYMMETRICAL} \end{matrix} \begin{pmatrix} F_x \\ F_y \\ F_z \\ M_\alpha \\ M_\beta \\ M_\theta \end{pmatrix}_P$$

INERTIANCE IN DB RE UNIT INERTIANCE, PHASE IN DEGREES

FIG IV.8

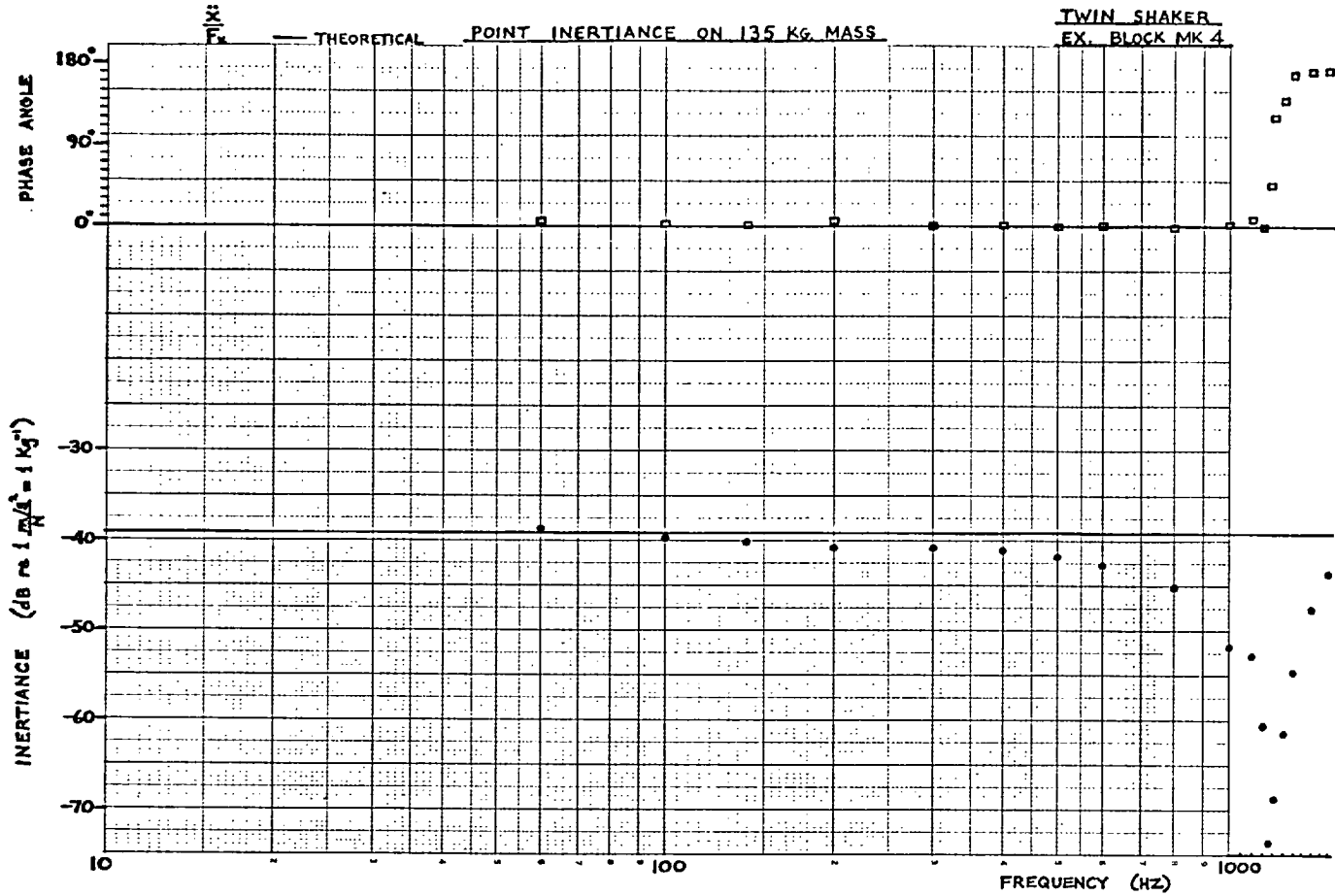
2/12/71

CHART
WELL 8021

Graph Data Ref. 5521

Log 2 Cycles x mm, y and 1 cm

TWIN SHAKER
EX. BLOCK MK 4



2/12/71

CHART
WELL 8021

Graph Data Ref. 5521

Log 2 Cycles x mm, y and 1 cm

TWIN SHAKER
EX. BLOCK MK 4

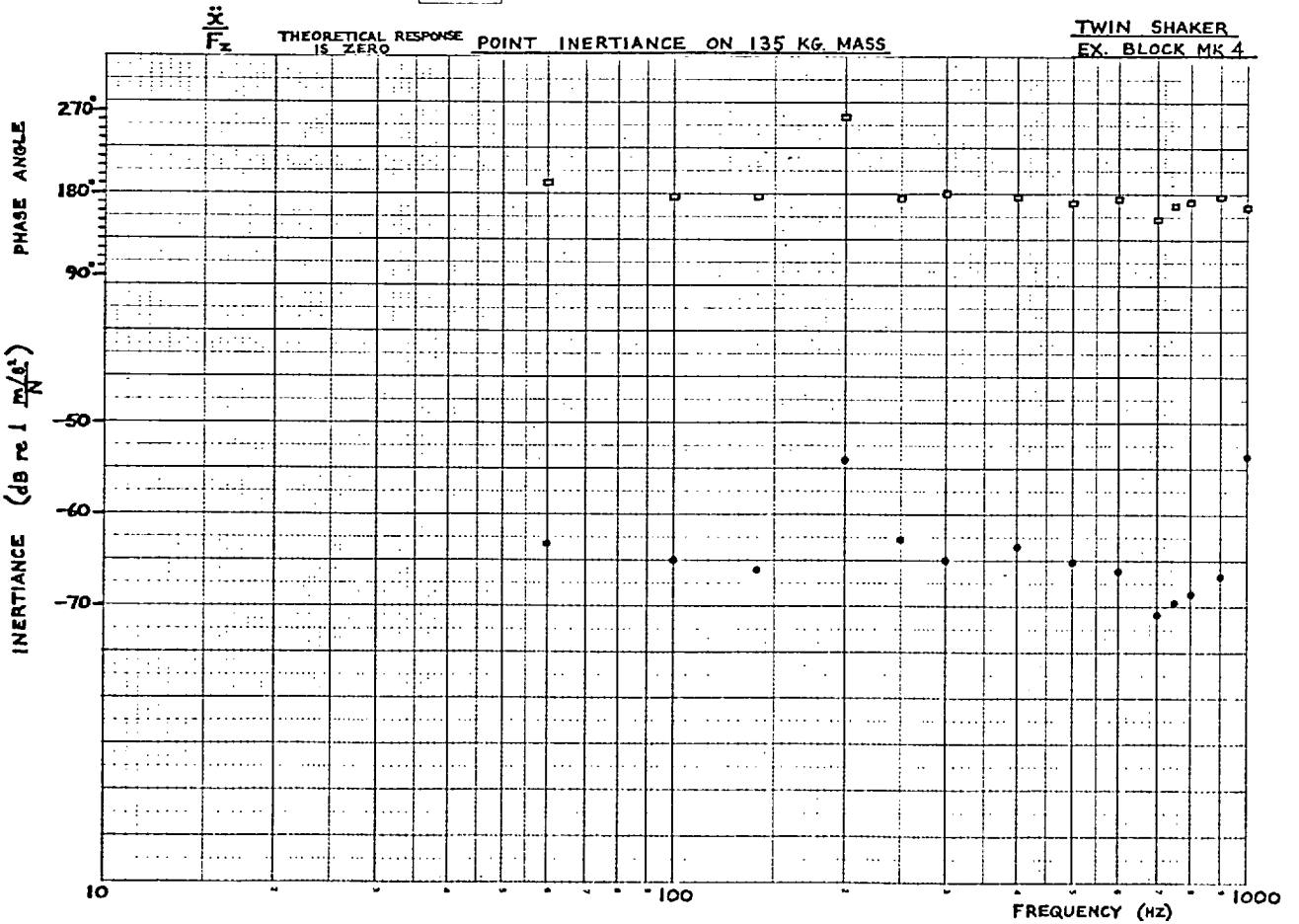
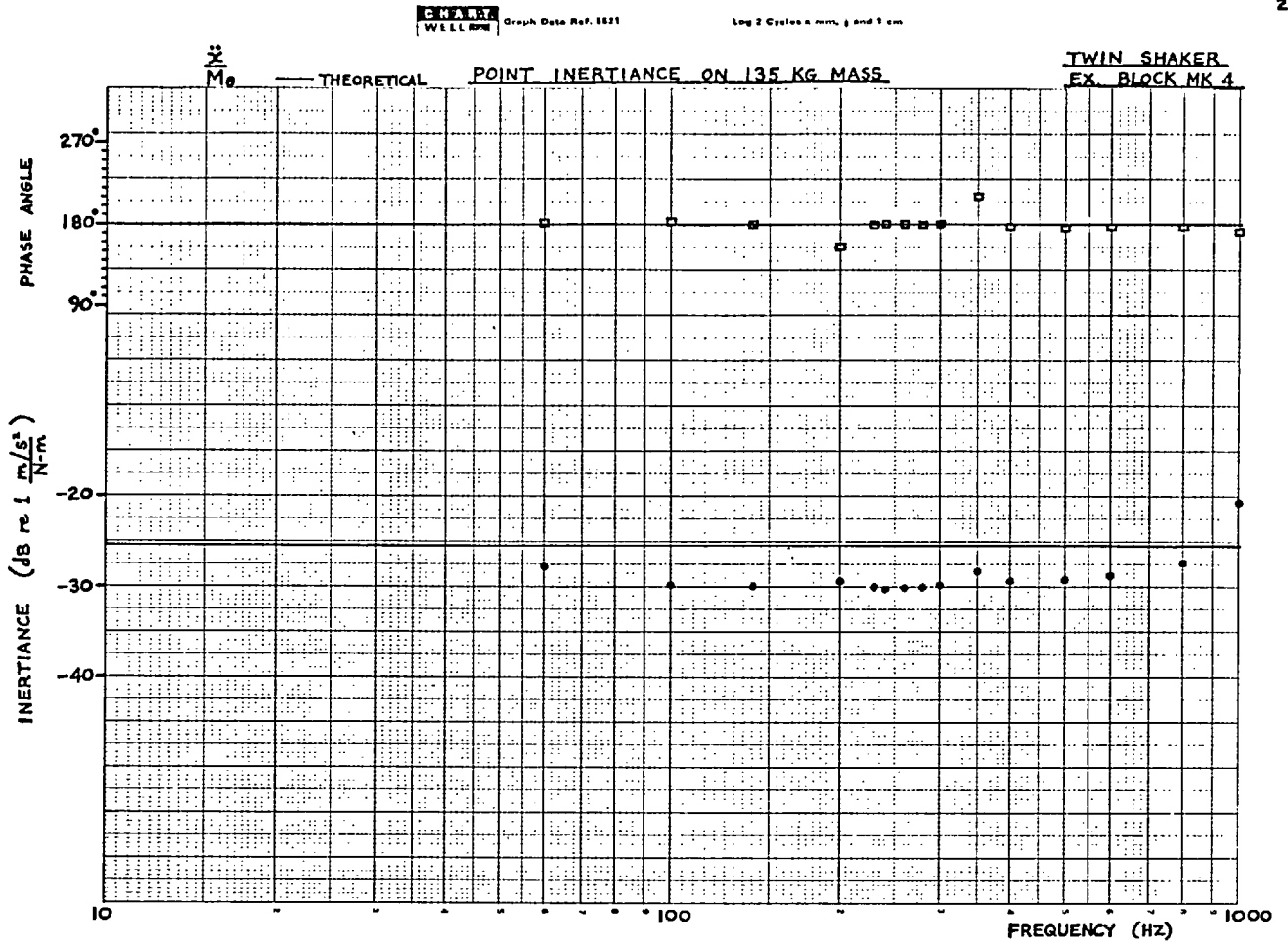
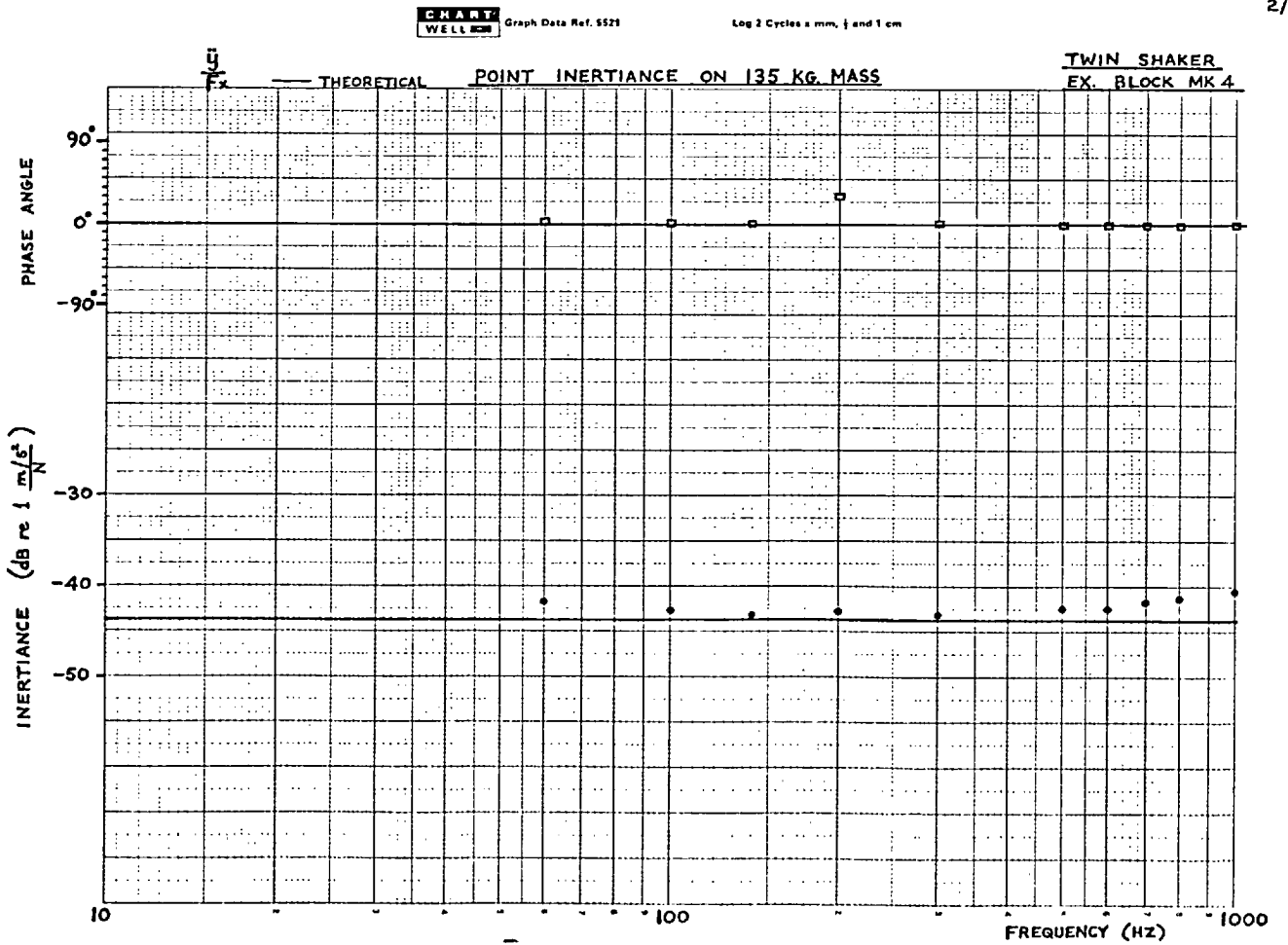


FIG IV.9

2/12/71

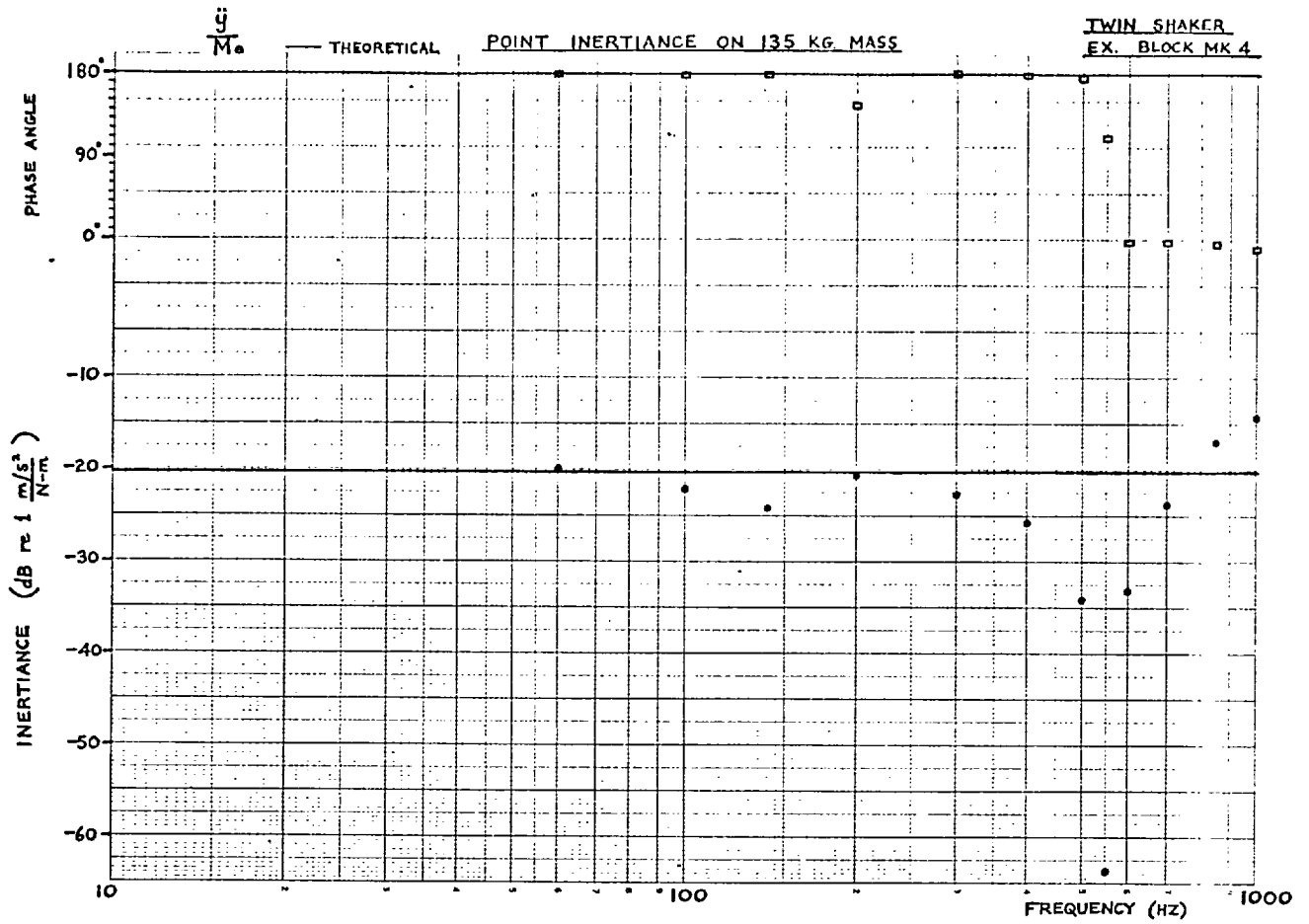


2/12/71



Graph Data Ref. 5521

Log 2 Cycles x mm, j and 1 cm



Graph Data Ref. 5521

Log 2 Cycles x mm, j and 1 cm

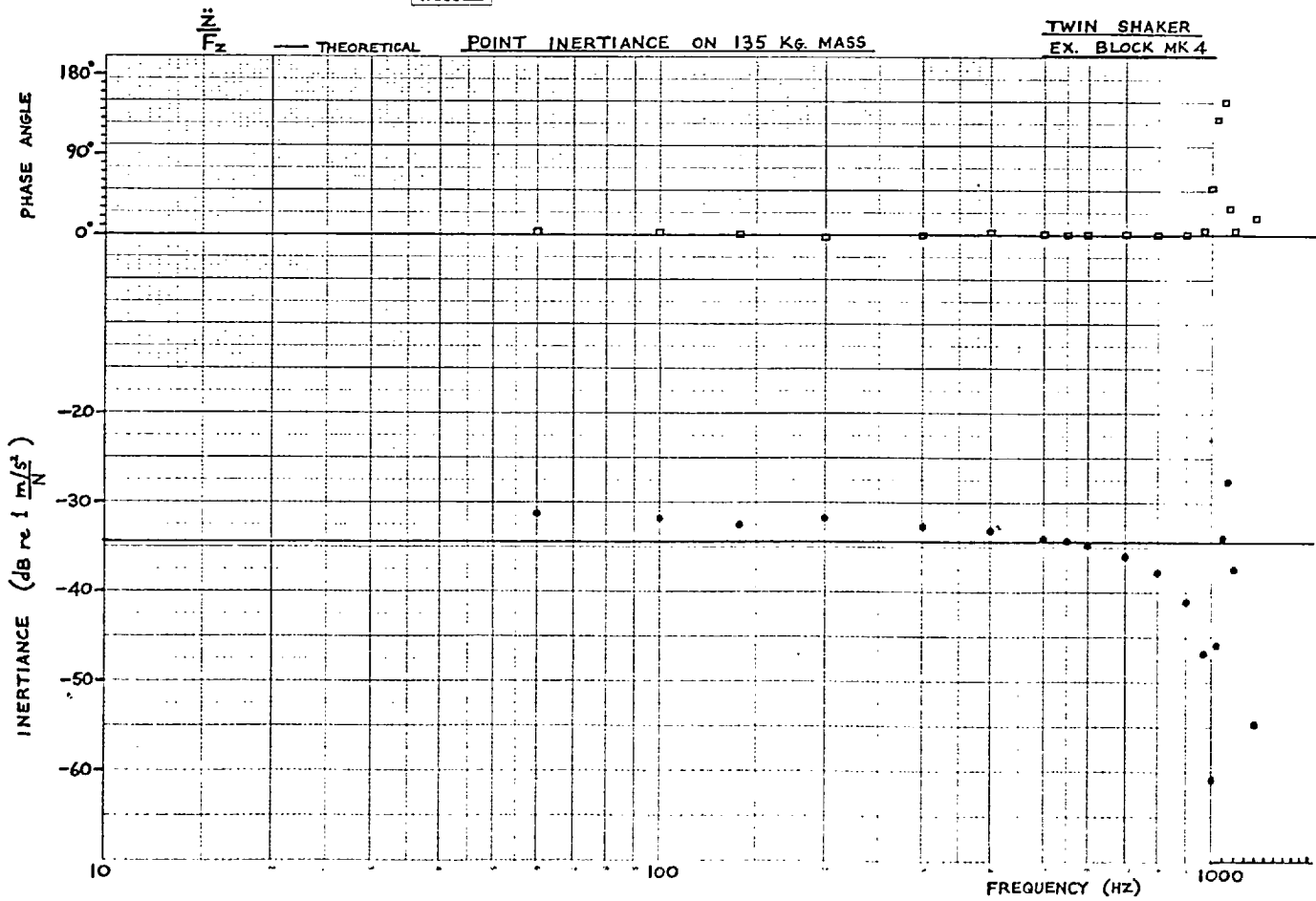
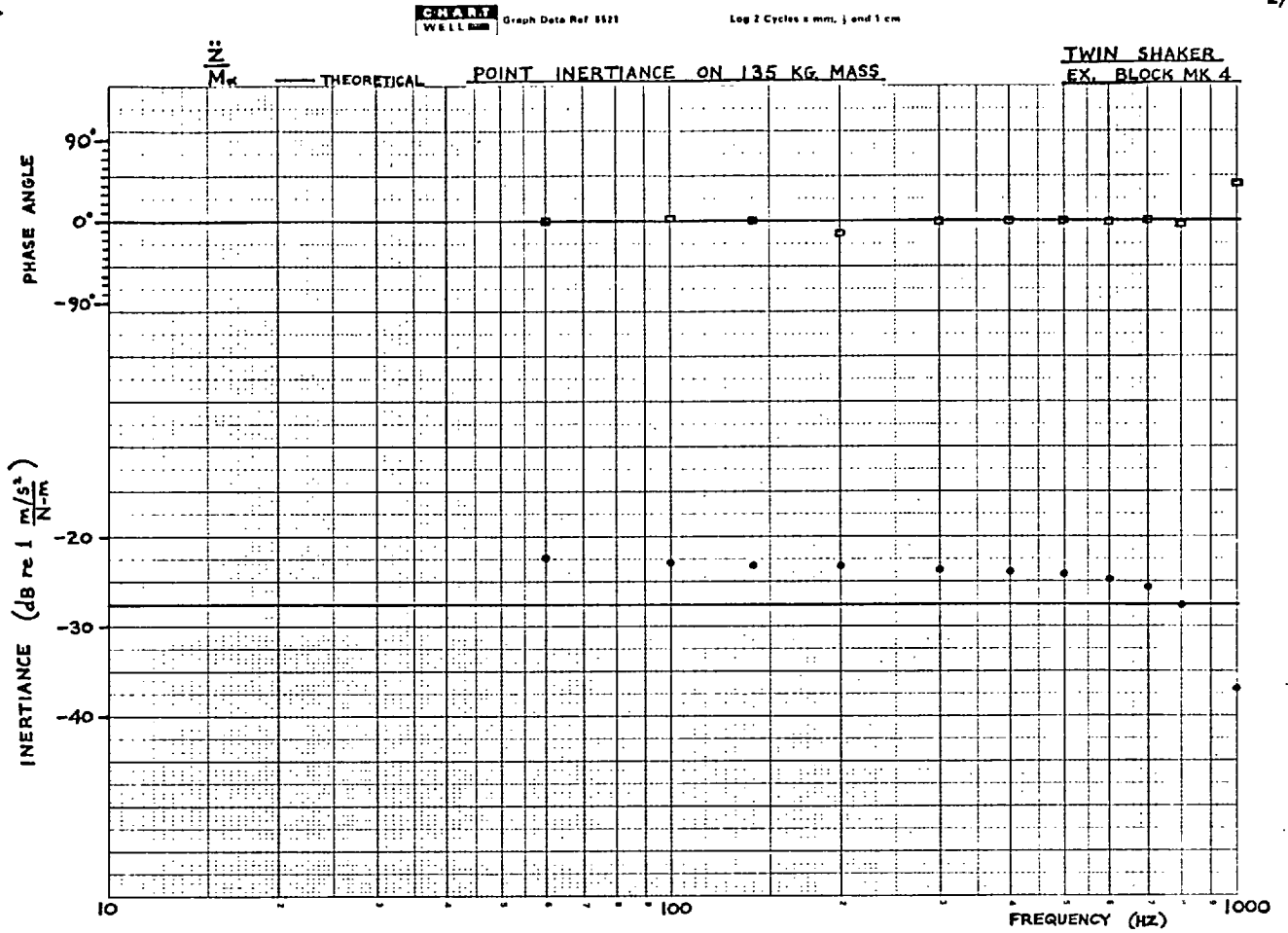


FIG IV.11

2/12/71



2/12/71

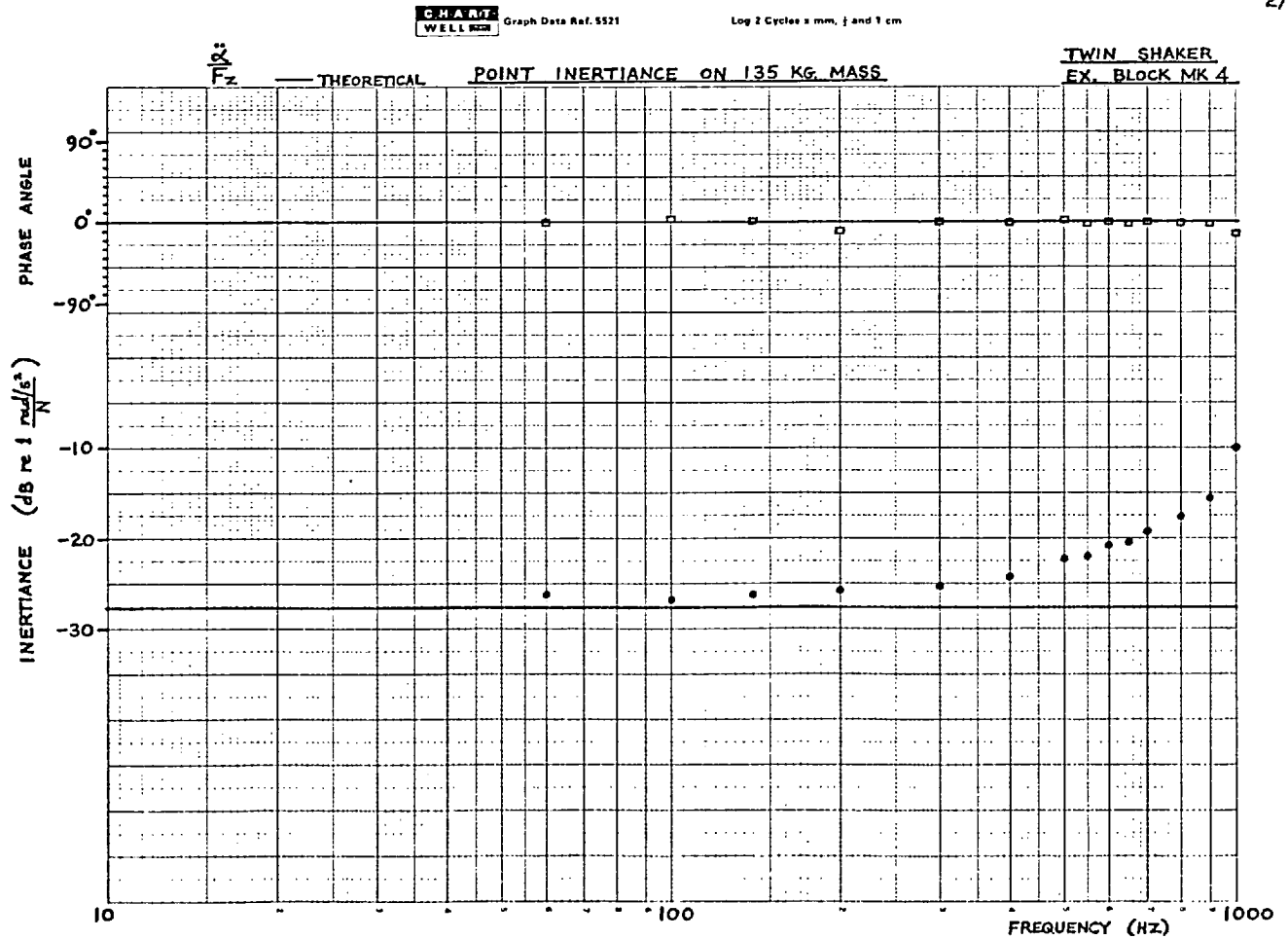
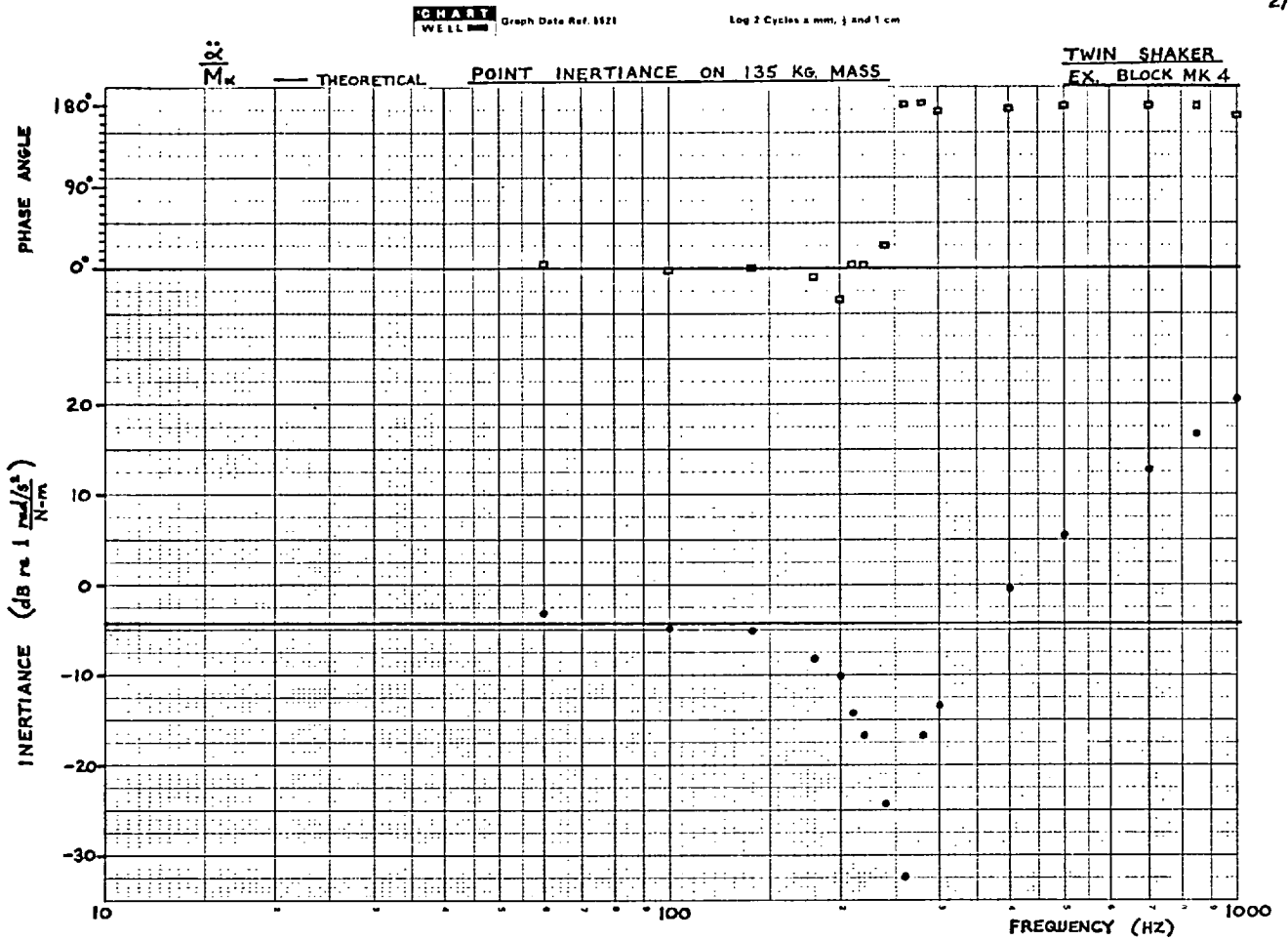


FIG IV.12

2/12/71



2/12/71

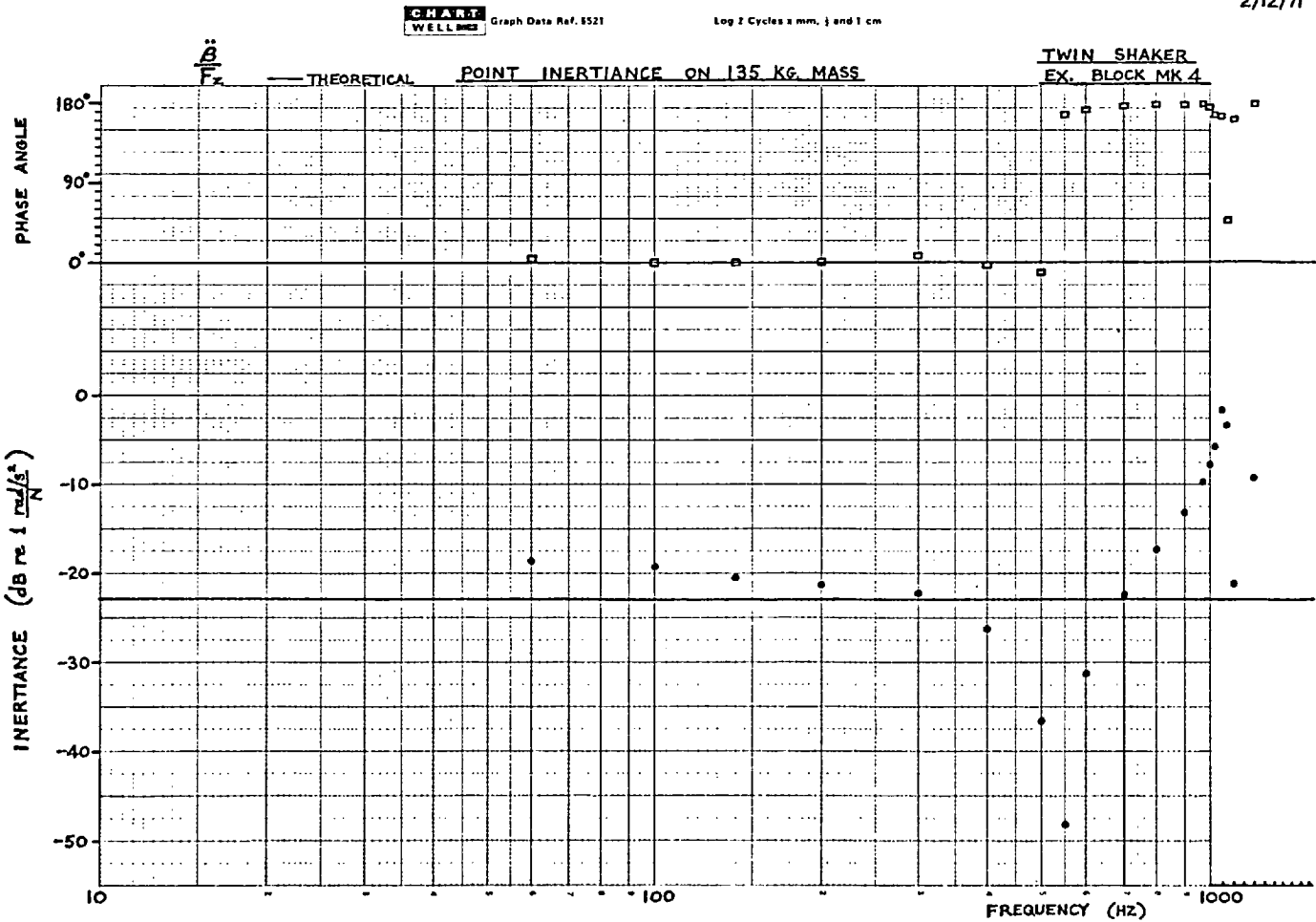
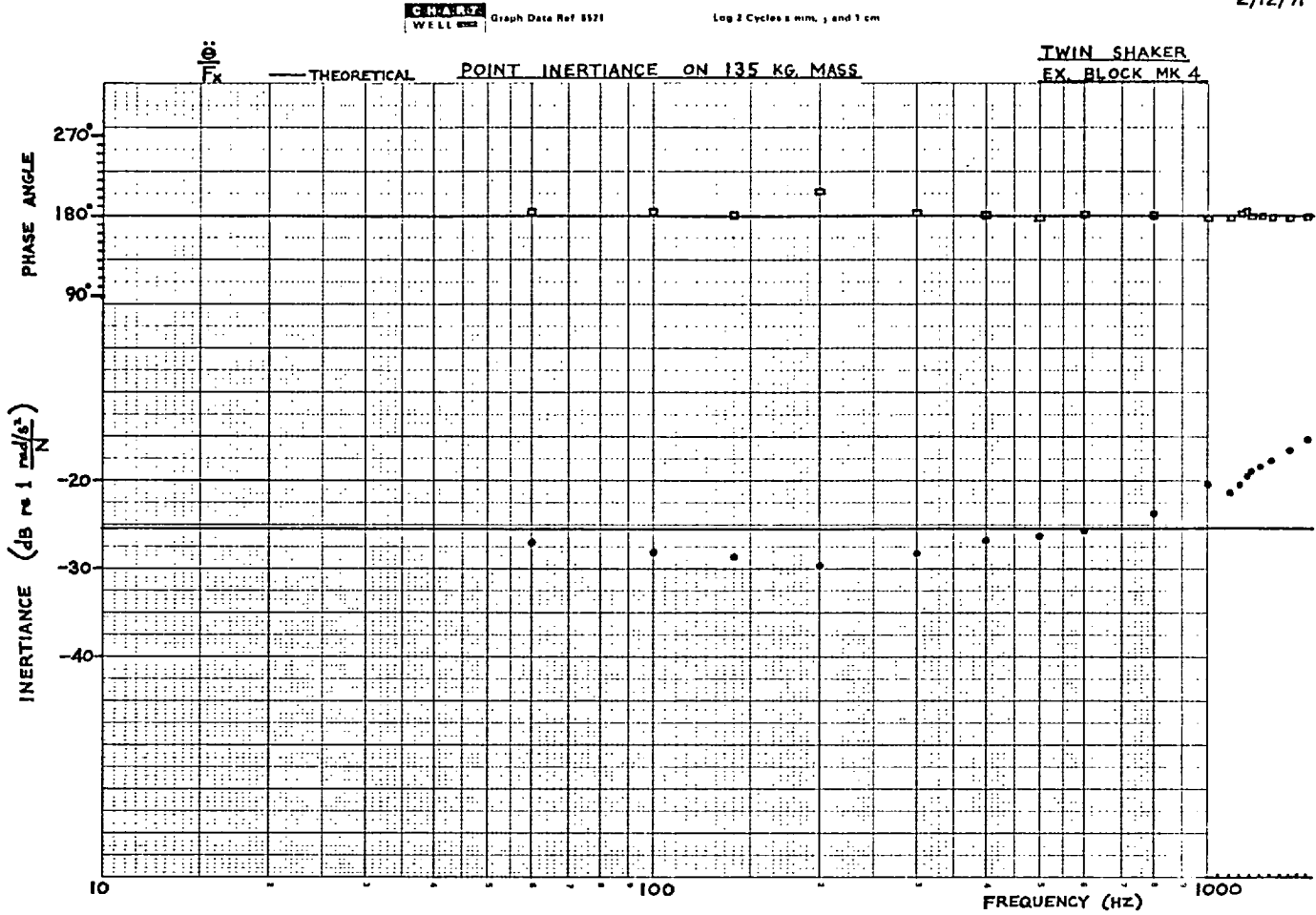
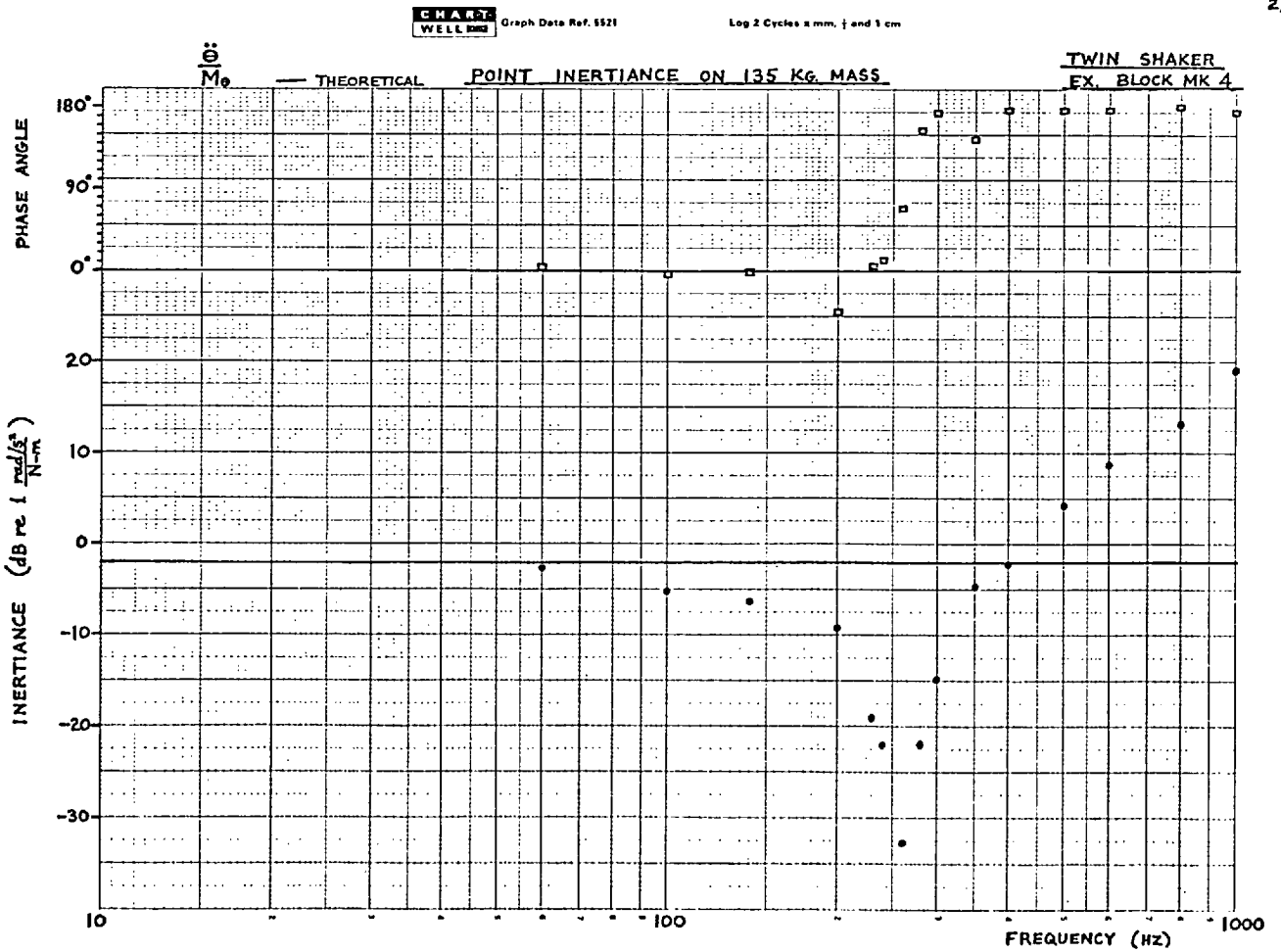


FIG IV.13

2/12/71

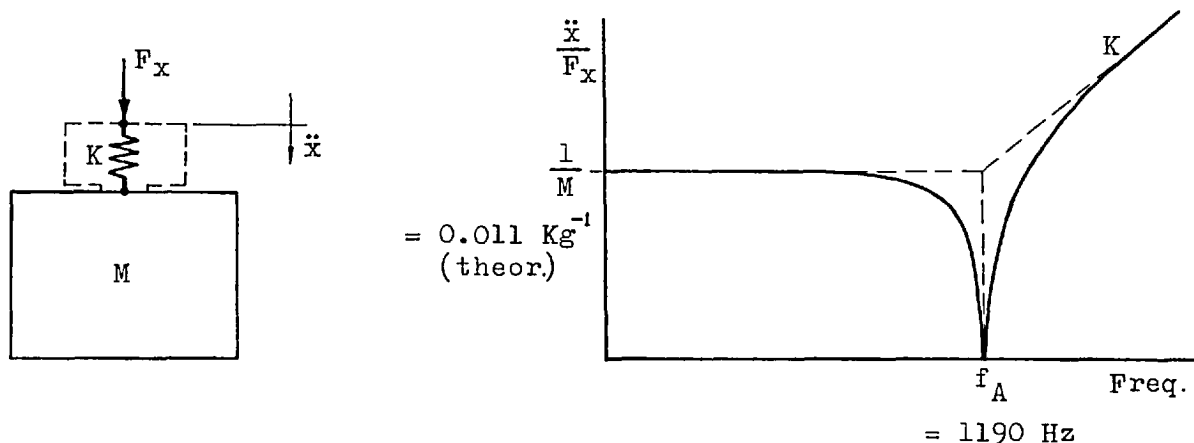


2/12/71



The effective stiffness of the exciting block in various directions

Fig. IV.8 shows the measured $\frac{\ddot{x}}{F_x}$ response to be almost constant up to 400 Hz, with a maximum error of 2dB. It then drops gradually to an antiresonant trough around 1190 Hz, after which it rises quickly and become spring-like. This behaviour is characteristic of an antiresonant oscillator, which comprises a spring in series with a mass, neither element being connected to ground:



In the present case, M is the effective mass at the point of excitation of the steel block, and K is the effective stiffness of the exciting block, given by $K = (2\pi f_A)^2 M$. It must be emphasised that M is not simply the total mass of the steel block. The effective stiffness in the x direction is therefore

$$K_x = (2\pi \times 1190)^2 \times \frac{1}{0.0110} = 5.08 \times 10^9 \text{ N/m}$$

In the same manner, we obtain the following stiffnesses for the z, α and θ directions:

$$K_z = 1.47 \times 10^9 \text{ N/m}$$

$$K_\alpha = 4.02 \times 10^6 \text{ N-m/rad}$$

$$K_\theta = 3.49 \times 10^6 \text{ N-m/rad}$$

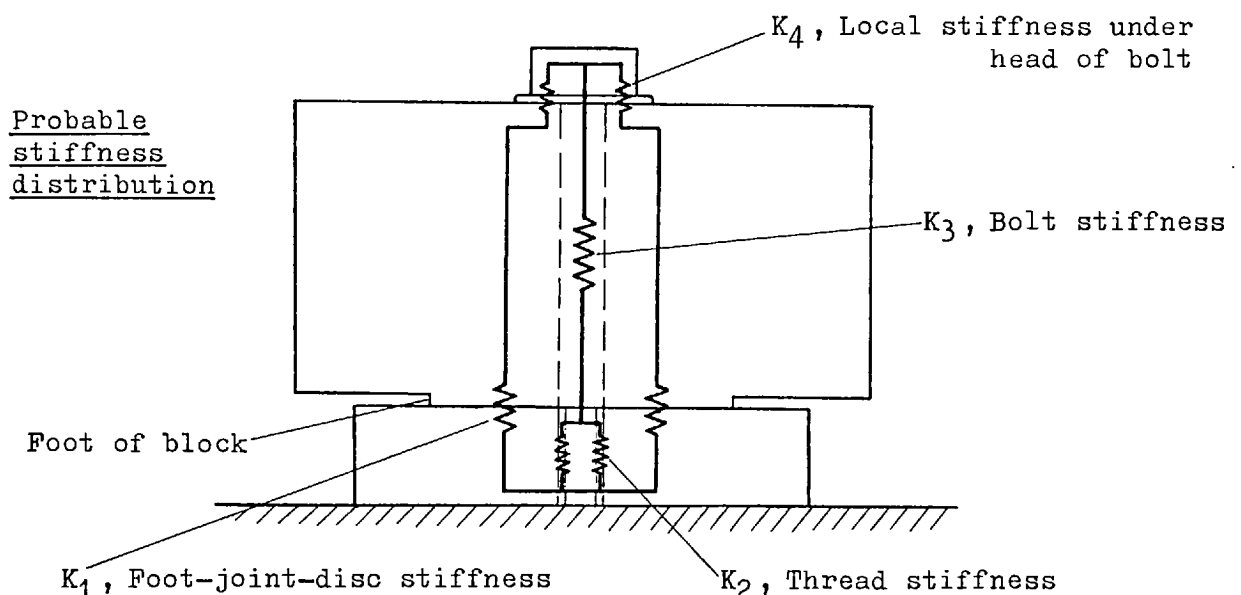
where the relevant data have been obtained from the direct inertiance curves for $\frac{\ddot{z}}{F_z}$, $\frac{\ddot{\alpha}}{M_\alpha}$ and $\frac{\ddot{\theta}}{M_\theta}$, given in Figs. IV.10, IV.12 and IV.13 respectively. In the case of $\frac{\ddot{x}}{F_x}$, $\frac{\ddot{\alpha}}{M_\alpha}$ and $\frac{\ddot{\theta}}{M_\theta}$, the measured "low frequency" response is very close to the theoretical, so the theoretical figures have been used for the effective mass or moment of inertia. However, in the case of $\frac{\ddot{z}}{F_z}$ the

measured data correspond to a Z axis passing through the centre of the exciting block*, whilst the theoretical data correspond to an axis along the surface of the steel block. This has caused a 3dB difference at the "low frequencies", and consequently the measured effective mass has been used in calculating the stiffness K_z .

Although these stiffnesses have been attributed to the exciting block, they probably arise from the combined effects of exciting block stiffness, joint stiffness, and the local stiffness of the steel mass. However, due to load spreading by the 100 mm steel disc, the first two of these are probably the more important in the present case.

One might imagine that the stiffnesses were associated solely with the foot on the exciting block, but a simple calculation yields a compressive stiffness of 3.5×10^{11} N/m for the 1 mm slice. This is 70 times greater than the measured value of K_x .

In the present case it is unlikely that the stiffness is affected to any large extent by the fixing bolt. From the diagram below it is seen that the bolt acts as a spring in parallel with the local stiffness K_1 around the foot, so the bolt can only have an effect if the combination



* To be strictly correct, the force is applied through the block centre, whilst the measured acceleration corresponds to an axis 3 mm above.

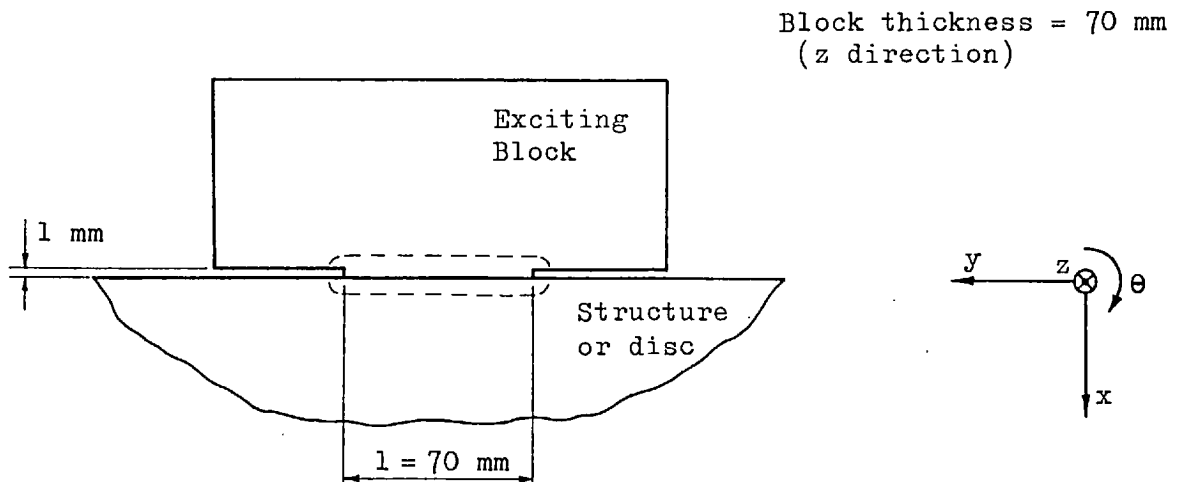
of K_2 , K_3 and K_4 is comparable with or greater than K_1 . Since the bottom of the foot and the surface of the disc were machined surfaces, and the thin film of adhesive ensured a solid connection over a large area, it seems highly probable that K_1 would be greater than the combined effects of the thread stiffness (K_2) and the local stiffness under the head of the bolt (K_4).

Hence, the exact mode of deformation is unknown at present. However, it seems probable that it is associated with the region around the foot of the block.

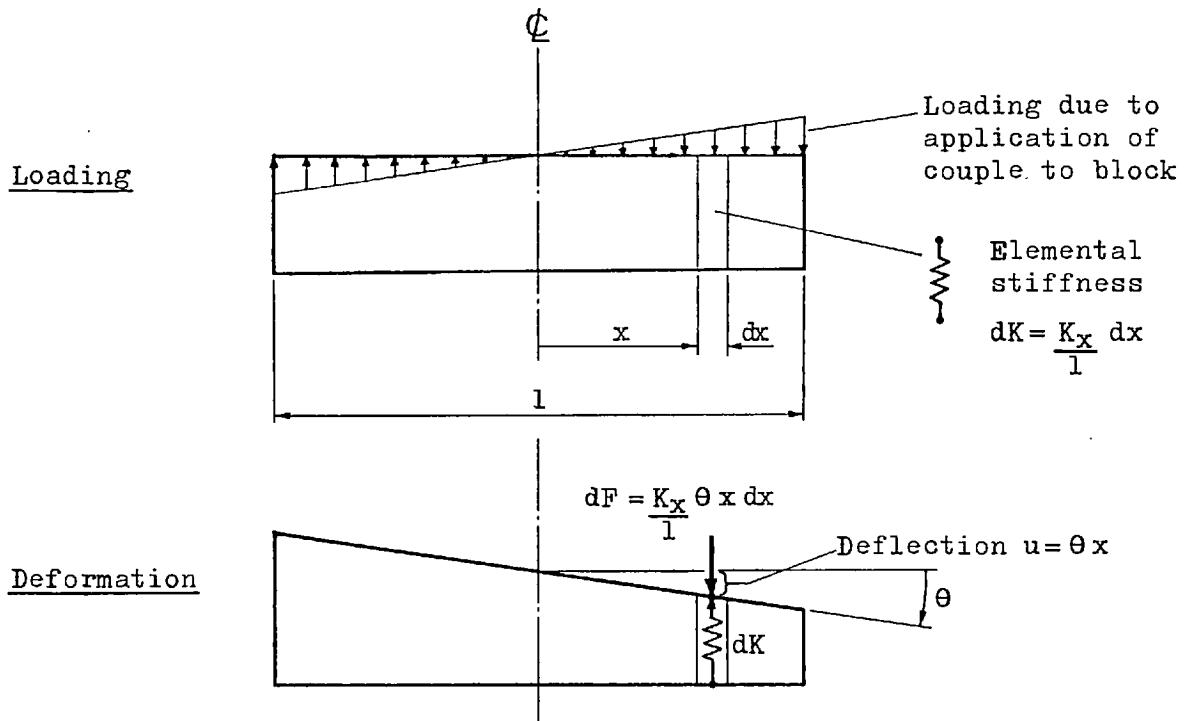
The relationship between linear and rotational effective stiffnesses

Whilst it does not appear to be possible to calculate the effective stiffnesses in the linear directions, it does seem that a simple relationship exists between the linear and rotational stiffnesses. This will be demonstrated with reference to the x and θ stiffnesses.

Considering the exciting block shown below, we shall postulate that the linear stiffness K_x is associated with the region enclosed within the dashed line, and that the cross section of this region in the y - z plane is exactly the same as that of the foot.



This seems reasonable, if the total stiffness is due to the combined effects of foot, adhesive and disc stiffnesses. If we now isolate this region we have a piece of material of length l and width equal to that of the block:



Since the total effective stiffness is $K_X = 5.08 \times 10^9$ N/m, the stiffness per unit length is obviously $\frac{K_X}{l}$. The application of a couple to the exciting block causes a force $dF = \frac{K_X}{l} \theta x dx$ to act on an element at distance x from the centre. The total applied couple is therefore

$$M_\theta = \int_{x=-\frac{l}{2}}^{x=+\frac{l}{2}} x dF = \frac{K_X \theta}{l} \int_{x=-\frac{l}{2}}^{x=+\frac{l}{2}} x^2 dx = \frac{K_X l^2}{12} \theta$$

whence the rotational stiffness

$$K_\theta = \frac{M_\theta}{\theta} = \frac{K_X l^2}{12} \quad (\text{IV.3})$$

and for $K_X = 5.08 \times 10^9$ N/m and $l = 0.070$ m, we obtain

$$\underline{\underline{K_\theta = 2.08 \times 10^6 \text{ N-m/rad}}}$$

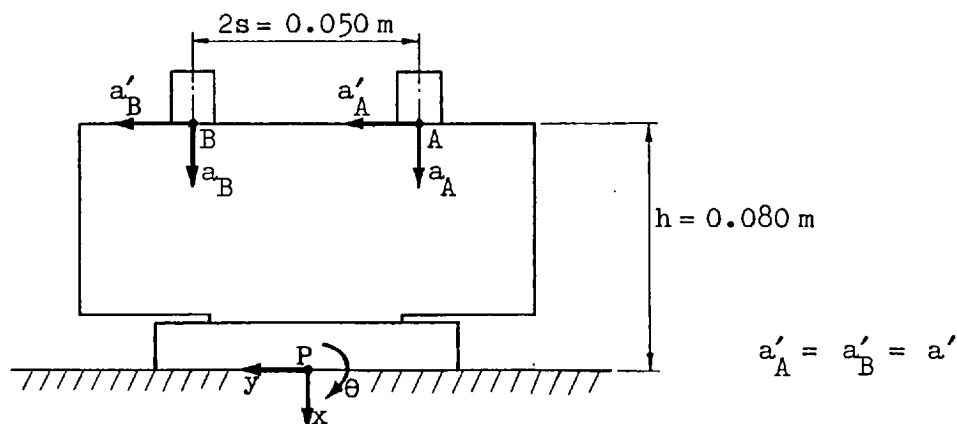
This may be compared with the measured figure of 3.49×10^6 N-m/rad. The remarkably good agreement seems to substantiate the assumption that the stiffness is a local effect associated with the foot, adhesive, etc.

Accelerometer cross-sensitivity

An important source of inaccuracy in multi-directional measurements is the effect of accelerometer cross-sensitivity. This is well illustrated by the lower graphs in Figs. IV.8 and IV.10: These show that the measured x response to a force F_z was only about 32 dB less than the corresponding Z response, whilst theoretically it should have been zero (-∞ dB). The measured signal was almost certainly the result of transverse or cross-axis motion, and the 32 dB difference in fact corresponds to a cross-sensitivity of $2\frac{1}{2}\%$, which is of the right sort of order for the pair of accelerometers used in these tests.

In the case of the other response curves the cross-sensitivity effect is less obvious, since the component due to transverse motion forms only a relatively small part of the total measured signal. However, under the right conditions it is not difficult to obtain errors as large as 30%, particularly on rotation measurements. This will be illustrated with reference to the $\frac{\ddot{\theta}}{M_\theta}$ response:

Since the output from an accelerometer comprises components due to the axial and transverse accelerations a and a' , the amplified voltage signal $e = \frac{1}{\bar{S}_{AC}}(a + \epsilon a')$, where \bar{S}_{AC} and ϵ are the acceleration scale factor and the cross-sensitivity respectively. Let us now consider the exciting block and accelerometer arrangement:



The rotation signal emerging from the difference unit may be written in terms of the true accelerations at A and B:

$$e_A - e_B = \frac{1}{S_{AC}} (a_A + \epsilon_A a'_A) - \frac{1}{S_{AC}} (a_B + \epsilon_B a'_B) = \frac{1}{S_{AC}} [(a_A - a_B) + a'(\epsilon_A - \epsilon_B)] \tag{IV.4}$$

Using the theoretical data given in Fig. IV.7, we have

$$\frac{\ddot{\theta}}{M_\theta} = 0.794 \frac{\text{rad/s}^2}{\text{N-m}} \quad \text{and} \quad \frac{\ddot{y}}{M_\theta} = -0.097 \frac{\text{m/s}^2}{\text{N-m}}$$

Then, assuming a couple $M_\theta = 1 \text{ N-m}$, we obtain the acceleration difference

$$(a_A - a_B) = 2s\ddot{\theta} = 0.050 \times 0.794 = 0.040 \text{ m/s}^2$$

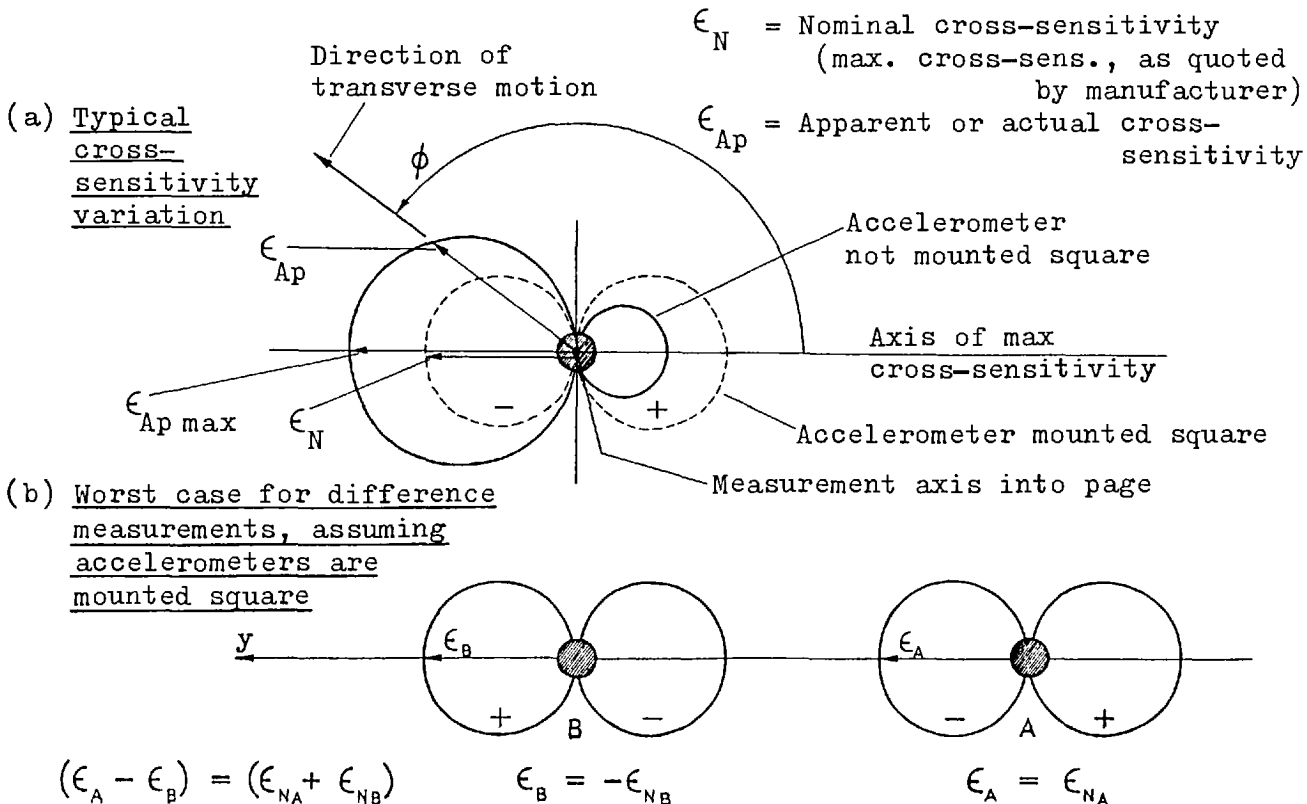
and the transverse acceleration

$$a' = \ddot{y} - h\ddot{\theta} = -0.097 - 0.080(0.794) = -0.160 \text{ m/s}^2$$

Substituting these figures in (IV.4), we obtain the difference signal

$$e_A - e_B = \frac{1}{S_{AC}} [0.040 - 0.160(\epsilon_A - \epsilon_B)] = \frac{0.040}{S_{AC}} [1 - 4.0(\epsilon_A - \epsilon_B)] \tag{IV.5}$$

Before examining the possible magnitude of the error term, we must consider the nature of the cross sensitivity, since it is a variable quantity which depends upon the orientation of the accelerometer relative to the direction of transverse motion, and also upon the squareness of the attachment surface to the required axis of measurement. This is discussed in some detail in reference (21), where it is shown that the cross-sensitivity may vary in the manner shown below.



To obtain an estimate of the possible error in the difference signal (IV.5), let us assume that the accelerometers are mounted squarely, with their axis of maximum cross-sensitivity parallel to the y direction, as shown in (b) above. Accelerometer B is also rotated through 180° relative to accelerometer A. Using the manufacturer's cross-sensitivity figures of 3 and 5% respectively for the two accelerometers used in the tests, the cross-sensitivity difference ($\epsilon_A - \epsilon_B$) is -8%. and we obtain

$$e_A - e_B = \frac{0.040}{S_{AC}} [1 - 0.320] \quad \text{Error} = 32\% = 2.4 \text{ dB}$$

Thus an error of the order of 30% is quite possible, and this could well be the reason for the slightly low $\frac{\ddot{\theta}}{M_\theta}$ measurements before the anti-resonance. The same approach leads to a similar conclusion in the case of the $\frac{\ddot{\theta}}{F_x}$ response. Although the error might in fact be less, it could equally well be greater if the accelerometers were not mounted squarely.

In the case of translational response measurements the signals are generally much larger, and cross-sensitivity is not so much of a problem. However, in assessing its importance one should bear in mind that the measurement is obtained as the sum of two signals, and in consequence the error is proportional to the cross-sensitivity sum ($\epsilon_A + \epsilon_B$).

If the axis of maximum cross sensitivity is known, one may be able to orientate the accelerometer to minimise the effect. However, in the case of general three dimensional motion the best orientation will not be known in advance. The easiest way of reducing the problem is to use very low cross-sensitivity accelerometers, carefully aligned relative to the required axis of measurement.

Conclusions

Despite the quite large errors at the higher frequencies, the various response curves testify to the adequacy of the direct measurement technique for obtaining acceptably accurate multi-directional data for

many applications. It should be remembered that the mass used in these tests had a very low mobility at high frequencies, and therefore provided a more severe test than most typical engineering structures. On the other hand, the low mobility also made exciting block inertia effects insignificant.

The most significant limitation of the measurement technique is certainly the combined stiffness of the exciting block and of the interface with the structure, and this appears to be most serious in the case of a couple excitation, due to the relatively low rotational effective stiffness. Expression (IV.3) shows that this stiffness is dependent upon the linear effective stiffness and the foot size, and a significant improvement can only be obtained by increasing them both. An improvement in block stiffness may be effected by using beryllium instead of aluminium. Due to its high stiffness/weight ratio, the extra stiffness can be obtained without a corresponding increase in mass.

At the lower frequencies, before the block deformation became significant, the errors were due to two causes. In the case of measurements in the y and z directions the primary source of error was the non-coincidence of the measurement axes with the surface of the mass. The error in $\frac{\ddot{z}}{M_\alpha}$ was as large as 5 dB, but the other responses were a little better, with errors of only 3 dB or less. The other source of error was accelerometer cross-sensitivity, and it has been shown that this may easily affect rotational results by several dB. In the case of linear measurements its main effect is to prevent the measurement of very small motions in the plane at right angles to the direction of the principal motion. If the true motion in the plane is more than about 30 dB below the principal motion, an accelerometer with its axis in the plane will produce a signal which is predominantly due to its cross-axis motion, so the true motion cannot be measured.

APPENDICES FOR PART 3

	<u>Page</u>
V THE CONVERGENCE RATE OF ENERGY INTEGRALS IN THE FINITE ELEMENT METHOD	502
VI "STANDARD" MATRICES ARISING IN THE FINITE ELEMENT ANALYSIS OF SANDWICH BEAMS	505
VII EXTENSIONAL AND BENDING STRAIN ENERGIES IN A THIN PLATE	507
VIII THE FORMATION OF A TIP DYNAMIC STIFFNESS MATRIX FOR A MULTI-ELEMENT BEAM	510

Note that all references quoted in these appendices are given in the reference list for Part 3, on Page 283

APPENDIX VTHE CONVERGENCE RATE OF ENERGY INTEGRALS IN THE FINITE ELEMENT METHOD

The assumed displacement functions are finite series, which can rarely describe the exact displacement distribution over the length of the element. In consequence, the strain and kinetic energy expressions formulated in terms of these series are only approximate. The procedure outlined here gives an estimate of the order of the error when using polynomial displacement functions.

The total energy in a beam finite element of length L may be expressed in terms of a number of integrals of the form $\int_0^L \delta_1 \cdot \delta_2 \, dx$ where δ_1 and δ_2 are polynomials in x , and may be either the displacement functions or their derivatives. If a displacement is represented by a polynomial of degree n , then its k 'th derivative is represented by a polynomial of degree $n-k$, so those energy integrals which involve only displacements are inherently more accurate than those involving their derivatives. The non-uniformity of accuracy is unavoidable, but it is possible to match together the different displacement functions so as to set a uniform minimum level of accuracy, and thereby fix the overall accuracy of the finite element representation.

The effect of the degree of the polynomials on the accuracy of any energy integral may be examined in a fairly general manner by considering a pair of quartic polynomials:

$$\begin{aligned} \delta_1 &= r_0 + r_1 x + r_2 x^2 + r_3 x^3 + r_4 x^4 \\ \delta_2 &= s_0 + s_1 x + s_2 x^2 + s_3 x^3 + s_4 x^4 \end{aligned} \quad (V.1)$$

These are capable of representing anything up to a cubic polynomial displacement function or derivative, together with an error term.

The integral of their product is

$$\begin{aligned}
\int_0^L \delta_1 \cdot \delta_2 dx &= (r_0 s_0)L + \frac{1}{2}(r_1 s_0 + r_0 s_1)L^2 + \frac{1}{3}(r_2 s_0 + r_1 s_1 + r_0 s_2)L^3 \\
&+ \frac{1}{4}(r_3 s_0 + r_2 s_1 + r_1 s_2 + r_0 s_3)L^4 + \frac{1}{5}(r_4 s_0 + r_3 s_1 + r_2 s_2 + r_1 s_3 + r_0 s_4)L^5 \\
&+ \frac{1}{6}(r_4 s_1 + r_3 s_2 + r_2 s_3 + r_1 s_4)L^6 + \frac{1}{7}(r_4 s_2 + r_3 s_3 + r_2 s_4)L^7 \\
&+ \frac{1}{8}(r_4 s_3 + r_3 s_4)L^8 + \frac{1}{9}(r_4 s_4)L^9
\end{aligned} \tag{V.2}$$

The expression (V.2) may now be used to examine specific integrals, as is demonstrated by the following example:

Example from the symmetrical 5-layer beam.

$$\begin{aligned}
\int_0^L \alpha' w'' dx & \quad \alpha = b_0 + b_1 x + b_2 x^2 \\
& \quad w = a_0 + a_1 x + a_2 x^2 + a_3 x^3
\end{aligned}$$

$$\begin{aligned}
\text{The derivatives are } \alpha' &= b_1 + 2b_2 x (+ \epsilon_{\alpha'} x^2) = \delta_1 \\
w'' &= 2a_2 + 6a_3 x (+ \epsilon_{w''} x^2) = \delta_2
\end{aligned}$$

where $\epsilon_{\alpha'} x^2$ and $\epsilon_{w''} x^2$ represent the higher order terms which are ignored when one uses only a few terms for α and w . The constants in the "standard polynomials" (V.1) are therefore

$$r_0 = b_1, \quad r_1 = 2b_2, \quad r_2 = \epsilon_{\alpha'}, \quad r_3 = r_4 = 0, \quad s_0 = 2a_2, \quad s_1 = 6a_3, \quad s_2 = \epsilon_{w''}, \quad s_3 = s_4 = 0$$

and expression (V.2) gives

$$\begin{aligned}
\int_0^L \alpha' w'' dx &= (2a_2 b_1)L + \frac{1}{2}(4a_2 b_2 + 6a_3 b_1)L^2 \\
&+ \frac{1}{3}(2a_2 \epsilon_{\alpha'} + 12a_3 b_2 + b_1 \epsilon_{w''})L^3 + \frac{1}{4}(6a_3 \epsilon_{\alpha'} + 2b_2 \epsilon_{w''})L^4
\end{aligned}$$

It is seen that the term in L^4 is the first to contain only the error coefficients $\epsilon_{\alpha'}$, and $\epsilon_{w''}$. Therefore, provided that $12a_3 b_2 \gg 2a_2 \epsilon_{\alpha'} + b_1 \epsilon_{w''}$ in the L^3 term, the energy integral will have a convergence rate proportional to L^4 or $1/N^{4*}$, where N is the number of elements along the length of the beam.

* Note that Element length, $L = \text{Beam length}/N$.

It may similarly be shown that the above displacement functions gives $\int_0^L \alpha'^2 dx$ and $\int_0^L w''^2 dx$ to the same accuracy, thereby fixing the convergence rate of the total strain energy at a uniform minimum level proportional to $1/N^4$.

APPENDIX VI"STANDARD" MATRICES ARISING IN THE FINITE ELEMENT ANALYSIS OF SANDWICH BEAMS

$$[T_1] = \begin{bmatrix} 1 & 0 & 0 & 0 \\ 0 & 1 & 0 & 0 \\ -3 & -2 & 3 & -1 \\ 2 & 1 & -2 & 1 \end{bmatrix}$$

$$[T_2] = \begin{bmatrix} 1 & 0 & 0 \\ -3 & -1 & 4 \\ 2 & 2 & -4 \end{bmatrix}$$

$$[A_1] = \begin{bmatrix} 8 & -2 & 4 \\ -2 & 8 & 4 \\ 4 & 4 & 32 \end{bmatrix}$$

$$[A_2] = \begin{bmatrix} 36 & 3 & -36 & 3 \\ 3 & 4 & -3 & -1 \\ -36 & -3 & 36 & -3 \\ 3 & -1 & -3 & 4 \end{bmatrix}$$

$$[A_3] = \begin{bmatrix} -6 & 7 & 6 & -3 \\ -6 & -3 & 6 & 7 \\ -48 & -4 & 48 & -4 \end{bmatrix}$$

APPENDIX VI contd."STANDARD" MATRICES ARISING IN THE FINITE ELEMENT ANALYSIS OF SANDWICH BEAMS

$$[A_4] = \begin{bmatrix} 7 & 1 & -8 \\ 1 & 7 & -8 \\ -8 & -8 & 16 \end{bmatrix}$$

$$[A_5] = \begin{bmatrix} 12 & 6 & -12 & 6 \\ 6 & 4 & -6 & 2 \\ -12 & -6 & 12 & -6 \\ 6 & 2 & -6 & 4 \end{bmatrix}$$

$$[A_6] = \begin{bmatrix} 4 & 3 & -4 & 1 \\ 4 & 1 & -4 & 3 \\ -8 & -4 & 8 & -4 \end{bmatrix}$$

$$[A_7] = \begin{bmatrix} 156 & 22 & 54 & -13 \\ 22 & 4 & 13 & -3 \\ 54 & 13 & 156 & 22 \\ -13 & -3 & -22 & 4 \end{bmatrix}$$

APPENDIX VIIEXTENSIONAL AND BENDING STRAIN ENERGIES IN A THIN PLATEIn-plane stretching energy in an element of thickness dz

Referring to Fig. VII.1a, the plane stress system σ_x, σ_y gives rise to the strains

$$\begin{aligned}\frac{\partial u}{\partial x} &= \frac{1}{E} (\sigma_x - \nu \sigma_y) \\ \frac{\partial v}{\partial y} &= \frac{1}{E} (\sigma_y - \nu \sigma_x)\end{aligned}\quad (\text{VII.1})$$

Solving for the stresses we obtain

$$\begin{aligned}\sigma_x &= \frac{E}{(1-\nu^2)} \left[\frac{\partial u}{\partial x} + \nu \frac{\partial v}{\partial y} \right] \\ \sigma_y &= \frac{E}{(1-\nu^2)} \left[\frac{\partial v}{\partial y} + \nu \frac{\partial u}{\partial x} \right]\end{aligned}\quad (\text{VII.2})$$

The stretching energy in the element is given by

$$\begin{aligned}dV_{\text{Stretch}} &= \frac{1}{2} \left[\sigma_x \frac{\partial u}{\partial x} + \sigma_y \frac{\partial v}{\partial y} \right] dx dy dz \\ &= \frac{1}{2} \frac{E}{(1-\nu^2)} \left[\left(\frac{\partial u}{\partial x} \right)^2 + \left(\frac{\partial v}{\partial y} \right)^2 + 2\nu \frac{\partial u}{\partial x} \frac{\partial v}{\partial y} \right] dx dy dz\end{aligned}\quad (\text{VII.3})$$

In-plane shearing energy in an element of thickness dz

Referring to Fig. VII.1b, the shear stress τ_{xy} gives rise to a shear strain

$$\gamma_{xy} = \frac{\partial u}{\partial y} + \frac{\partial v}{\partial x} = \frac{1}{G} \tau_{xy}\quad (\text{VII.4})$$

The shearing energy in the element is then given by

$$\begin{aligned}dV_{\text{Shear}} &= \frac{1}{2} \tau_{xy} \gamma_{xy} dx dy dz \\ &= \frac{1}{2} G \left(\frac{\partial u}{\partial y} + \frac{\partial v}{\partial x} \right)^2 = \frac{1}{2} \frac{E}{2(1+\nu)} \left(\frac{\partial u}{\partial y} + \frac{\partial v}{\partial x} \right)^2 dx dy dz\end{aligned}\quad (\text{VII.5})$$

* Note that $G = \frac{E}{2(1+\nu)}$

Total in-plane energy in an element of thickness dz

The total in-plane strain energy in the element is given by the sum of (VII.3) and (VII.5):

$$dV_{\text{in-plane}} = \frac{1}{2} \cdot \frac{E}{(1-\nu^2)} \left[\left(\frac{\partial u}{\partial x} \right)^2 + \left(\frac{\partial v}{\partial y} \right)^2 + 2\nu \frac{\partial u}{\partial x} \frac{\partial v}{\partial y} + \frac{(1-\nu)}{2} \left(\frac{\partial u}{\partial y} + \frac{\partial v}{\partial x} \right)^2 \right] dx dy dz \quad (\text{VII.6})$$

Total in-plane or "extensional" energy in a uniform plate of thickness t

For in-plane stretching and shearing, the displacements u and v are constant through the thickness of the plate. If its dimensions in the x and y directions are a and b respectively, expression (VII.6) yields the energy integral

$$V_{\text{ext}} = \frac{1}{2} \cdot \frac{Et}{(1-\nu^2)} \int_0^b \int_0^a \left[\left(\frac{\partial u}{\partial x} \right)^2 + \left(\frac{\partial v}{\partial y} \right)^2 + 2\nu \frac{\partial u}{\partial x} \frac{\partial v}{\partial y} + \frac{(1-\nu)}{2} \left(\frac{\partial u}{\partial y} + \frac{\partial v}{\partial x} \right)^2 \right] dx dy \quad (\text{VII.7})$$

Total bending energy in a uniform plate of thickness t

When the plate bends, the displacements u and v vary linearly through the thickness, and are both zero on the neutral surface. From Fig. VII.2 it is seen that $u = -z \frac{\partial w}{\partial x}$ and $v = -z \frac{\partial w}{\partial y}$, and when we substitute these displacements in expression (VII.6), we obtain the energy integral

$$\begin{aligned} V_{\text{bend}} &= \frac{1}{2} \cdot \frac{E}{(1-\nu^2)} \int_0^{t/2} \int_0^b \int_0^a z^2 \left[\left(\frac{\partial^2 w}{\partial x^2} \right)^2 + \left(\frac{\partial^2 w}{\partial y^2} \right)^2 + 2\nu \frac{\partial^2 w}{\partial x^2} \frac{\partial^2 w}{\partial y^2} + \frac{(1-\nu)}{2} \left(\frac{\partial^2 w}{\partial y \partial x} + \frac{\partial^2 w}{\partial x \partial y} \right)^2 \right] dx dy dz \\ &= \frac{1}{2} \cdot \frac{Et^3}{12(1-\nu^2)} \int_0^b \int_0^a \left[\left(\frac{\partial^2 w}{\partial x^2} \right)^2 + \left(\frac{\partial^2 w}{\partial y^2} \right)^2 + 2\nu \frac{\partial^2 w}{\partial x^2} \frac{\partial^2 w}{\partial y^2} + 2(1-\nu) \left(\frac{\partial^2 w}{\partial x \partial y} \right)^2 \right] dx dy \end{aligned} \quad (\text{VII.8})$$

The coefficient $\frac{Et^3}{12(1-\nu^2)}$ is known as the "Plate Flexural Rigidity", and is generally represented by the letter D .

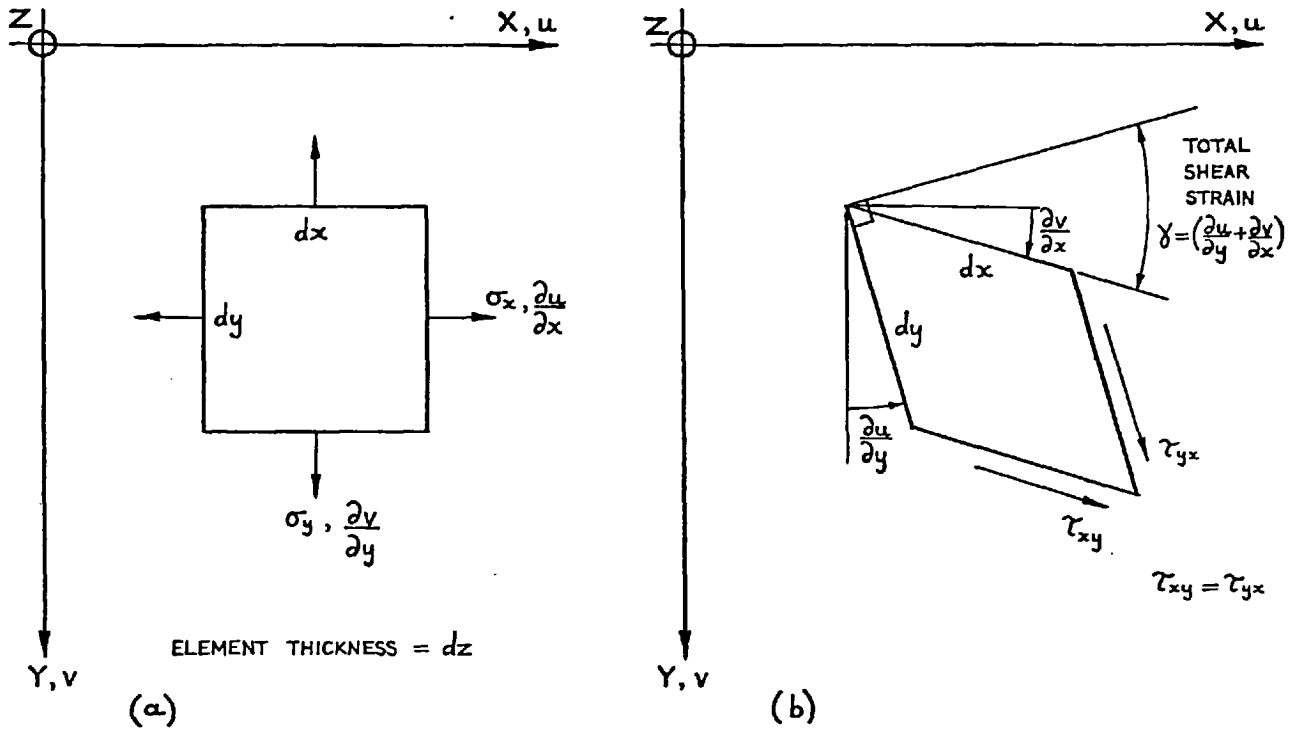


FIG. VII.1 PLATE ELEMENT SUBJECTED TO PLANE STRESSES

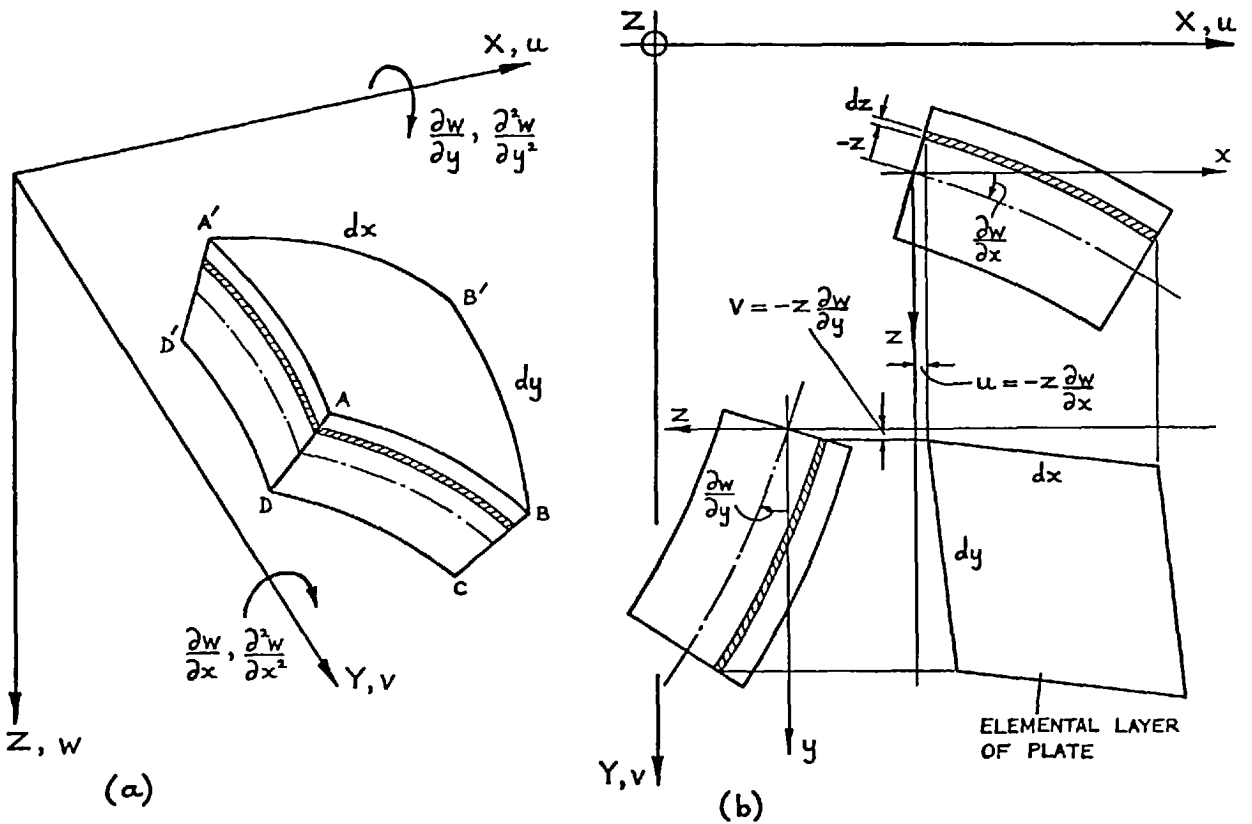
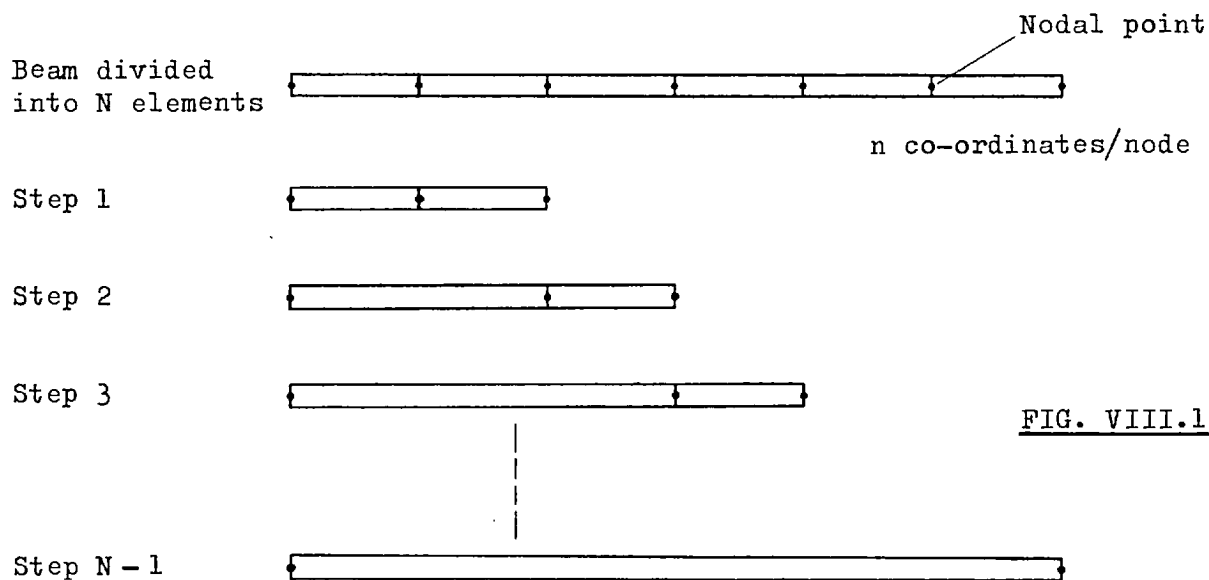


FIG. VII.2 PLATE ELEMENT SUBJECTED TO FLEXURE

APPENDIX VIII

THE FORMATION OF A TIP DYNAMIC STIFFNESS MATRIX FOR A MULTI-ELEMENT BEAM

The beam shown in Fig.VIII.1 has been divided into N finite elements. In the case of a uniform beam all the elements may be identical, but in the general case this will not be so. However, it will be assumed that all elements are of the same basic type, with n co-ordinates per node. If the elements are joined together using the straightforward stiffness coupling procedure, the laws of force equilibrium and displacement compatibility are applied at each node and a banded stiffness matrix is formed, which relates to the $n(N + 1)$ nodal co-ordinates.



Unfortunately, in vibration analysis it is often necessary to use a large number of elements in order to adequately describe the higher modes, and the beam model may have as many as 70 degrees of Freedom* — just for bending in one plane! If this beam is to be joined to other components which are also represented by a large number of finite elements, the stiffness matrix for the coupled system may become enormous. Unless it is necessary to know the mode shapes in detail, it is better to simplify the

* e.g. For the 10'th. mode of a free-free unsymmetrical 4 or 5 layer beam (5d.f./node), one must use at least 13 elements, giving 70 d.f.

whole procedure by eliminating all unnecessary co-ordinates at the component building stage. In the case of the beam in Fig.VIII.1, it is relatively easy to eliminate all the nodal co-ordinates other than those at the two ends, thereby forming a tip dynamic stiffness matrix for the whole beam which is only of the same size as the individual element matrices. As is illustrated, the procedure is quite systematic and the complete elimination is carried out in $N - 1$ steps. Two elimination techniques are available and these will be discussed below.

The Transfer Matrix Method

This well known dynamic analysis technique had its origins in the tabular methods developed by Holzer^{(43)*} and Myklestad⁽⁴⁴⁾, for the torsion of shafts and the bending of beams respectively, and it developed rapidly during the fifties with the advent of the high-speed digital computer. A fairly comprehensive survey of the method has been made by Uhrig⁽⁴⁵⁾, who compares it with other analysis techniques and points out its limitations.

Instead of working with element stiffness matrices, one works with hybrid "transfer matrices", which transform the "state vector" for one end of an element into the state vector for the other end. The state vector in this case contains the displacements and forces at a nodal point.

Consider the two adjacent elements of a uniform beam:

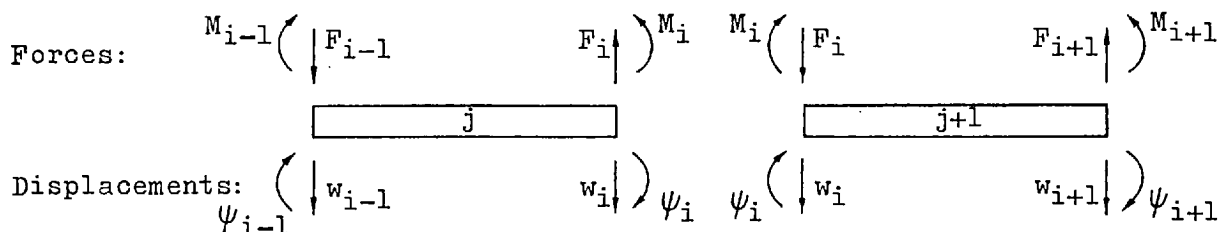


FIG. VIII.2 TRANSFER MATRIX SIGN CONVENTION

* References for Appendices V to VIII are given on Page 283.

For these elements we may write the transfer relations

$$\begin{Bmatrix} \delta \\ \bar{F} \end{Bmatrix}_{i+1} = \begin{bmatrix} T_{j+1} \end{bmatrix} \begin{Bmatrix} \delta \\ \bar{F} \end{Bmatrix}_i \quad \text{and} \quad \begin{Bmatrix} \delta \\ \bar{F} \end{Bmatrix}_i = \begin{bmatrix} T_j \end{bmatrix} \begin{Bmatrix} \delta \\ \bar{F} \end{Bmatrix}_{i-1} \quad (\text{VIII.1})$$

where the state vector $\begin{Bmatrix} \delta \\ \bar{F} \end{Bmatrix} = \begin{Bmatrix} W \\ \psi \\ F \\ M \end{Bmatrix}$

Combining the two transfer relations of (VIII.1), we obtain

$$\begin{Bmatrix} \delta \\ \bar{F} \end{Bmatrix}_{i+1} = \begin{bmatrix} T_{j+1} \end{bmatrix} \begin{bmatrix} T_j \end{bmatrix} \begin{Bmatrix} \delta \\ \bar{F} \end{Bmatrix}_{i-1} \quad (\text{VIII.2})$$

From this it is obvious that any number of elements may be coupled end-to-end by simply multiplying together the element transfer matrices. However, one must first obtain the transfer matrices from the stiffness and inertia matrices normally derived for a finite element.

Fig. VIII.3 on page 514 shows the sign convention generally used in the finite element analysis of beams. Using this convention we obtain the dynamic stiffness relation

$$\begin{Bmatrix} F_{i-1} \\ F_i \end{Bmatrix} = \left(\begin{bmatrix} K \end{bmatrix} - \omega^2 \begin{bmatrix} M \end{bmatrix} \right) \begin{Bmatrix} \delta_{i-1} \\ \delta_i \end{Bmatrix} = \begin{bmatrix} Z_{11} & Z_{12} \\ Z_{12}^T & Z_{22} \end{bmatrix} \begin{Bmatrix} \delta_{i-1} \\ \delta_i \end{Bmatrix} \quad (\text{VIII.3})$$

As the sign of the forces at the right hand end differs from that used in the transfer matrix method, we must introduce a negative sign into the dynamic stiffness matrix in order to convert to the transfer matrix convention:

* \bar{F} is a force sub-vector consistent with the sign convention in Fig. VIII.2 (Transfer matrix convention).

+ F is a force sub-vector consistent with the sign convention in Fig. VIII.3 (Finite element convention).

$$\begin{bmatrix} \bar{F}_{i-1} \\ \bar{F}_i \end{bmatrix} = \begin{bmatrix} Z_{11} & Z_{12} \\ -Z_{12}^T & -Z_{22} \end{bmatrix} \begin{bmatrix} \delta_{i-1} \\ \delta_i \end{bmatrix} \quad (\text{VIII.4})$$

Now, the forces and displacements correspond exactly to those in (VIII.1)

Re-arranging these equations we obtain the transfer relation

$$\begin{bmatrix} \delta_i \\ \bar{F}_i \end{bmatrix} = \begin{bmatrix} T_{11} & T_{12} \\ T_{21} & T_{22} \end{bmatrix} \begin{bmatrix} \delta_{i-1} \\ \bar{F}_{i-1} \end{bmatrix} = \begin{bmatrix} -Z_{12}^{-1}Z_{11} & Z_{12}^{-1} \\ -Z_{12}^T + Z_{22}Z_{12}^{-1}Z_{11} & -Z_{22}Z_{12}^{-1} \end{bmatrix} \begin{bmatrix} \delta_{i-1} \\ \bar{F}_{i-1} \end{bmatrix} \quad (\text{VIII.5})$$

To return to the dynamic stiffness relation, with the sign convention of Fig. VIII.3, we use the inverse transformation

$$\begin{bmatrix} F_{i-1} \\ F_i \end{bmatrix} = \begin{bmatrix} Z_{11} & Z_{12} \\ Z_{21} & Z_{22} \end{bmatrix} \begin{bmatrix} \delta_{i-1} \\ \delta_i \end{bmatrix} = \begin{bmatrix} -T_{12}^{-1}T_{11} & T_{12}^{-1} \\ -T_{21} + T_{22}T_{12}^{-1}T_{11} & -T_{22}T_{12}^{-1} \end{bmatrix} \begin{bmatrix} \delta_{i-1} \\ \delta_i \end{bmatrix} \quad (\text{VIII.6})$$

The coupling procedure therefore involves finding the element dynamic stiffness using (VIII.3), converting these to transfer matrices using (VIII.5), forming the product of the transfer matrices in the manner of (VIII.2), and converting the overall transfer matrix to a dynamic stiffness matrix using (VIII.6). For the common case where all elements are identical, the element transfer matrix (VIII.5) need only be computed once, and the whole procedure then only requires two matrix inversions.

Dokainish⁽⁴⁶⁾ has recently applied this same basic procedure to the analysis of plate vibrations. He divides the plate into several strips, with a number of nodes on the left and right hand sections of each strip. Each strip is then subdivided into triangular plate elements, and the stiffness and inertia matrices are obtained for the individual strips. Strip transfer matrices are then formed in the same way as those for the beam considered above, and the transfer matrix for the whole plate is obtained by multiplying together the individual transfer matrices. As his interest lies in determining natural frequencies, he then follows the standard procedure of applying the boundary conditions to the overall

transfer matrix, and searching for zeros of the determinant of a submatrix of this transfer matrix.

It should be noted that numerical difficulties may be encountered with the transfer method when applied to the search for natural frequencies. This is discussed in references (45) and (47), where various procedures are given for avoiding the difficulties.

The Method of Substructures

This method is commonly used in finite element analysis in order to group together a number of simple elements into one large "refined" element or substructure, and unlike the transfer method, it is equally well suited to two- and three-dimensional problems as to the present one-dimensional beam problem. It also utilises stiffness matrices directly, so it is a more convenient procedure in some ways if the element dynamic properties are obtained by the finite element displacement method. The same basic technique, under the name "detachment of constants", was proposed by Falk⁽⁴⁸⁾ as a means for overcoming the numerical difficulties inherent in the transfer method.

Let us consider the two beam elements shown in Fig. VIII.3

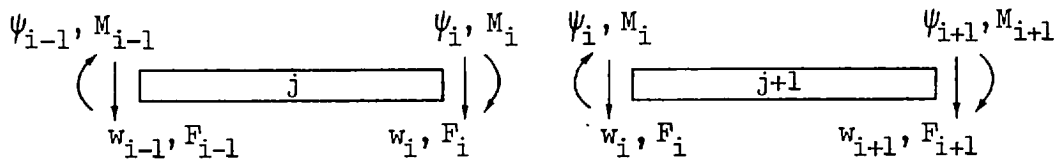


FIG. VIII.3 FINITE ELEMENT SIGN CONVENTION

For these elements we may write the dynamic stiffness relations

$$\begin{bmatrix} F_{i-1}^{(j)} \\ F_i^{(j)} \end{bmatrix} = \begin{bmatrix} Z_{11}^{(j)} & Z_{12}^{(j)} \\ Z_{21}^{(j)} & Z_{22}^{(j)} \end{bmatrix} \begin{bmatrix} \delta_{i-1} \\ \delta_i \end{bmatrix}$$

(VIII.7)

$$\begin{bmatrix} F_i^{(j+1)} \\ F_{i+1}^{(j+1)} \end{bmatrix} = \begin{bmatrix} Z_{11}^{(j+1)} & Z_{12}^{(j+1)} \\ Z_{21}^{(j+1)} & Z_{22}^{(j+1)} \end{bmatrix} \begin{bmatrix} \delta_i \\ \delta_{i+1} \end{bmatrix}$$

(VIII.8)

If no external force acts at node i , then $F_i^{(j+1)} = -F_i^{(j)}$. Combining equations (VIII.7) and (VIII.8), we obtain

$$\begin{Bmatrix} F_{i-1} \\ 0 \\ F_{i+1} \end{Bmatrix} = \begin{bmatrix} Z_{11}^{(j)} & Z_{12}^{(j)} & 0 \\ Z_{21}^{(j)} & Z_{22}^{(j)} + Z_{11}^{(j+1)} & Z_{12}^{(j+1)} \\ 0 & Z_{21}^{(j+1)} & Z_{22}^{(j+1)} \end{bmatrix} \begin{Bmatrix} \delta_{i-1} \\ \delta_i \\ \delta_{i+1} \end{Bmatrix}$$

which may be rearranged to form

$$\begin{Bmatrix} F_{i-1} \\ F_{i+1} \\ 0 \end{Bmatrix} = \begin{bmatrix} Z_{11}^{(j)} & 0 & Z_{12}^{(j)} \\ 0 & Z_{22}^{(j+1)} & Z_{21}^{(j+1)} \\ Z_{21}^{(j)} & Z_{12}^{(j+1)} & Z_{22}^{(j)} + Z_{11}^{(j+1)} \end{bmatrix} \begin{Bmatrix} \delta_{i-1} \\ \delta_{i+1} \\ \delta_i \end{Bmatrix}$$

In the manner illustrated on page 217, the equations pertaining to the co-ordinate δ_i may now be eliminated:

$$\begin{Bmatrix} F_{i-1} \\ F_{i+1} \end{Bmatrix} = \left(\begin{bmatrix} Z_{11}^{(j)} & 0 \\ 0 & Z_{22}^{(j+1)} \end{bmatrix} - \begin{bmatrix} Z_{12}^{(j)} \\ Z_{21}^{(j+1)} \end{bmatrix} \left[Z_{22}^{(j)} + Z_{11}^{(j+1)} \right]^{-1} \begin{bmatrix} Z_{21}^{(j)} & Z_{12}^{(j+1)} \end{bmatrix} \right) \begin{Bmatrix} \delta_{i-1} \\ \delta_{i+1} \end{Bmatrix} \quad (\text{VIII.9})$$

The resulting stiffness matrix for the two elements is therefore of the same size as the original element matrices. To build up a complete beam, one just repeats the procedure, joining the two-element section to a single element to form a three-element section, and so on. Since each node elimination requires one matrix inversion, a total of $N - 1$ inversions are carried out in building a beam of N elements. Therefore, for more than three elements this method takes longer than the transfer method.* However, it does have the advantages of being more direct and of avoiding certain numerical difficulties. This procedure is simply the Gaussian elimination process by which one would solve the large banded set of stiffness equations obtained by coupling all the elements

* Note that the building procedure may be significantly speeded up in the case of uniform beams, since all elements are then the same. Thus, one may join together 2 elements to form a 2-element section, then take 2 of these sections to form a 4-element section, and so on in the sequence 8, 16, 32, ... elements. For this case the method of substructures only takes longer than the transfer method if there are more than 4 elements.

together directly.

Although ordinary uniform beam elements have been considered above, the procedure is equally well applicable to sandwich beams, in which case the sub-vectors $\{\delta\}$ and $\{F\}$ just contain extra displacements and forces.

APPENDICES FOR PART 4

		<u>Page</u>
IX	DERIVATION OF DYNAMIC STIFFNESS MATRICES FOR SPRING-MASS MODEL OF RUBBER V-BLOCK (RB)	
	IX.1 Point Dynamic Stiffness on Upper Faces of Block	518
	IX.2 Transfer Dynamic Stiffness across the Block	521
X	DERIVATION OF DYNAMIC STIFFNESS MATRIX FOR MALE V-PIECE (VB)	530
XI	DERIVATION OF DYNAMIC STIFFNESS MATRIX FOR FEMALE V-SUPPORT (VS)	537

Note that all references quoted in these appendices are given in the reference list for Part 4, on Page 430

APPENDIX IX

DERIVATION OF DYNAMIC STIFFNESS MATRICES FOR SPRING-MASS MODEL OF RUBBER

V-BLOCK (RB)

IX.1 POINT DYNAMIC STIFFNESS ON UPPER FACES OF BLOCK

A matrix will be derived which gives the relationship between the applied forces and the displacements on the two upper faces of the block, it being assumed that the two faces are uncoupled. In order to avoid difficulties due to the indeterminate nature of the spring-mass model, we shall divide it into mathematically determinate sub-assemblies and then join these together.

$\frac{1}{4}$ V-Block

We commence with the simple spring system shown in Fig.IX.1. This represents one quarter of the total V-block and is mathematically determinate.

By considering force equilibrium at the two free nodes A and B we obtain a relationship between the externally applied forces F_1 to F_6 and the compressive forces C in the members:

$$\begin{Bmatrix} F \\ F_{AB} \end{Bmatrix}_{6 \times 1} = \begin{bmatrix} T \\ T_{FC} \end{bmatrix}_{6 \times 6} \begin{Bmatrix} C \end{Bmatrix}_{6 \times 1} \quad (\text{IX.1})$$

The transformation matrix is given in Fig.IX.5.

The member AB is necessarily a pure spring*, since it is assumed that the same compressive force acts on its two ends. The remaining five members are two degree-of-freedom spring-mass systems, and their stiffnesses are consequently frequency-dependent. The axial dynamic stiffness of such a member at its free end is given in Fig. IX.2. Grouping together the dynamic load-compression relations for the six members, we may form a

* This member is only introduced in order to form a non-collapsible $\frac{1}{4}$ V-block. It will subsequently be "shorted out" by a rigid massless plate which joins A and B.

diagonal transformation matrix which relates the loads C to the member compressions Δ :

$$\begin{Bmatrix} C \end{Bmatrix}_{6 \times 1} = \begin{bmatrix} Z_{MEM} \end{bmatrix}_{6 \times 6} \begin{Bmatrix} \Delta \end{Bmatrix}_{6 \times 1} \quad (IX.2)$$

The relation between the compressions Δ and the nodal displacements δ_i to δ_6 is given by the transposed force transformation:

$$\begin{Bmatrix} \Delta \end{Bmatrix}_{6 \times 1} = \begin{bmatrix} T_{\Delta\delta} \end{bmatrix} \begin{Bmatrix} \delta_{AB} \end{Bmatrix}_{6 \times 1} = \begin{bmatrix} T_{FC} \end{bmatrix}^T \begin{Bmatrix} \delta_{AB} \end{Bmatrix}_{6 \times 1} \quad (IX.3)$$

This may be proved by considering the work done by the internal and external forces.

Combining (IX.1), (IX.2) and (IX.3), we obtain the 6 x 6 stiffness matrix relating the forces on the nodes A and B to the corresponding displacements:

$$\begin{Bmatrix} F_{AB} \end{Bmatrix}_{6 \times 1} = \left(\begin{bmatrix} T_{FC} \end{bmatrix}_{6 \times 6} \begin{bmatrix} Z_{MEM} \end{bmatrix}_{6 \times 6} \begin{bmatrix} T_{FC} \end{bmatrix}^T_{6 \times 6} \right) \begin{Bmatrix} \delta_{AB} \end{Bmatrix}_{6 \times 1} = \begin{bmatrix} Z_{AB} \end{bmatrix}_{6 \times 6} \begin{Bmatrix} \delta_{AB} \end{Bmatrix}_{6 \times 1} \quad (IX.4)$$

$\frac{1}{2}$ V-Block

The half V-block is shown in Fig. IX.3. It is formed by introducing a second quarter V-block, which is a mirror image of the first, and joining the two by a rigid massless plate which is attached to the four nodes A, B, A' and B'. The dynamic stiffness matrix $\begin{bmatrix} Z_{A'B'} \end{bmatrix}$ for the second quarter V block differs from $\begin{bmatrix} Z_{AB} \end{bmatrix}$ only in the signs of those elements* which are a function of either d or e. For the two uncoupled quarters we have the 12 x 12 matrix

$$\begin{Bmatrix} F_{AB} \\ F_{A'B'} \end{Bmatrix}_{12 \times 1} = \begin{bmatrix} Z_{AB} & 0 \\ 0 & Z_{A'B'} \end{bmatrix}_{12 \times 12} \begin{Bmatrix} \delta_{AB} \\ \delta_{A'B'} \end{Bmatrix}_{12 \times 1} \quad (IX.5)$$

* Elements (1,2), (2,3), (4,5), (5,6) and their transposes.

which relates the 12 nodal forces to the corresponding displacements.

The attachment of a rigid plate to the four nodes prevents their independent movement, and six equations of constraint are introduced. Considering forces, rather than displacements, we obtain the constraint equations relating the 6 forces applied at the centre of the plate to the 12 forces transmitted to the nodes:

$$\begin{Bmatrix} F_P \end{Bmatrix}_{6 \times 1} = \begin{bmatrix} T_F \end{bmatrix}_{6 \times 12} \begin{Bmatrix} F_{AB} \\ F_{A'B'} \end{Bmatrix}_{12 \times 1} \quad (\text{IX.6})$$

The transformation matrix is given in Fig. IX.6. As before, the displacement transformation is given by the transpose of the force transformation.

Combining (IX.5) and (IX.6), we obtain the 6 x 6 stiffness matrix relating the forces at the plate centre P to the corresponding displacements:

$$\begin{Bmatrix} F_P^1 \end{Bmatrix}_{6 \times 1} = \left(\begin{bmatrix} T_F \end{bmatrix}_{6 \times 12} \begin{bmatrix} Z_{AB} & 0 \\ 0 & Z_{A'B'} \end{bmatrix}_{12 \times 12} \begin{bmatrix} T_F^T \end{bmatrix}_{12 \times 6} \right) \begin{Bmatrix} \delta_P^1 \end{Bmatrix}_{6 \times 1} = \begin{bmatrix} Z_P^1 \end{bmatrix}_{6 \times 6} \begin{Bmatrix} \delta_P^1 \end{Bmatrix}_{6 \times 1} \quad (\text{IX.7})$$

where the superscript 1 refers to the first half V-block. We thus have a stiffness matrix for one face of the rubber block.

Full V-Block

The full V-block is made up of two uncoupled half blocks, as shown in Fig. IX.4. The stiffness matrix $[Z_P^2]$ for the second half block differs from that for the first half block only in the signs of the coupling terms between the x, α and the y, z, β, θ co-ordinates.* This is due to the different choice of positive directions for the local y, z, β and θ co-ordinates. The dynamic stiffness relation for the attachment points on the two upper faces of the V-block is therefore

* Elements (1,2), (1,3), (1,5), (1,6), (2,4), (3,4), (4,5), (4,6) and their transposes.

$$\begin{matrix} \begin{bmatrix} F_P^1 \\ F_P^2 \end{bmatrix} \\ 12 \times 1 \end{matrix} = \begin{matrix} \begin{bmatrix} Z_P^1 & | & 0 \\ \hline 0 & | & Z_P^2 \end{bmatrix} \\ 12 \times 12 \end{matrix} \begin{matrix} \begin{bmatrix} \delta_P^1 \\ \delta_P^2 \end{bmatrix} \\ 12 \times 1 \end{matrix} \quad \begin{matrix} \text{(IX.8)} \\ \text{Point Stiffness} \end{matrix}$$

IX.2 TRANSFER DYNAMIC STIFFNESS ACROSS THE BLOCK

A matrix will be derived which gives the relationship between the forces transmitted to the supporting structure and the displacements on the two upper faces of the block.

The displacements at the nodes A, B, A' and B' of the half V-block are related to those at point P by the transpose of the force transformation matrix in expression (IX.6):

$$\begin{matrix} \begin{bmatrix} \delta_{AB} \\ \delta_{A'B'} \end{bmatrix} \\ 12 \times 1 \end{matrix} = \begin{matrix} \begin{bmatrix} T_F^T \end{bmatrix} \\ 12 \times 6 \end{matrix} \begin{matrix} \left\{ \delta_P \right\} \\ 6 \times 1 \end{matrix} \quad \text{(IX.9)}$$

For the quarter V-blocks with free node pairs A, B and A', B' respectively, the member compressions are given by the vectors $\{\Delta_{AB}\}$ and $\{\Delta_{A'B'}\}$. The vector $\{\Delta_{AB}\}$ is related to the nodal displacements $\{\delta_{AB}\}$ by the transposed force transformation $[T_{FC}^{AB}]$ given in expression (IX.3), and the matrix relating $\{\Delta_{A'B'}\}$ to $\{\delta_{A'B'}\}$ is obtained from this transformation by changing the signs of those elements which are a function of either d or e. Thus, the 12 member compressions may be expressed in terms of the 12 nodal displacements:

$$\begin{matrix} \begin{bmatrix} \Delta_{AB} \\ \Delta_{A'B'} \end{bmatrix} \\ 12 \times 1 \end{matrix} = \begin{matrix} \begin{bmatrix} (T_{FC}^{AB})^T & | & 0 \\ \hline 0 & | & (T_{FC}^{A'B'})^T \end{bmatrix} \\ 12 \times 12 \end{matrix} \begin{matrix} \begin{bmatrix} \delta_{AB} \\ \delta_{A'B'} \end{bmatrix} \\ 12 \times 1 \end{matrix} \quad \text{(IX.10)}$$

Except for member 1, the transfer dynamic stiffness of a member relates the axially transmitted force \bar{C} at the fixed end to the compression Δ of the member. This force is identical to the axial reaction force applied to the member by the supporting structure, and due to the effect of the mass within the member, it differs from the compressive force C applied at the free end of that member. Member 1 may be treated as a pure spring with transfer stiffness K_1 , and the calculated force is simply the force in the member. However, it is not used in the ensuing calculation. The general transfer stiffness expression is given in Fig. IX.2.

Since the second quarter V-block is a mirror image of the first, the two quarters have identical members. Hence we may write

$$\begin{Bmatrix} \bar{C}_{AB} \\ \bar{C}_{A'B'} \end{Bmatrix}_{12 \times 1} = \begin{bmatrix} T_{MEM} & 0 \\ 0 & T_{MEM} \end{bmatrix}_{12 \times 12} \begin{Bmatrix} \Delta_{AB} \\ \Delta_{A'B'} \end{Bmatrix}_{12 \times 1} \quad (\text{IX.11})$$

where the vectors $\{\bar{C}_{AB}\}$ and $\{\bar{C}_{A'B'}\}$ contain the axial reaction forces acting on the two quarter V-blocks, and the 6×6 diagonal matrix $[T_{MEM}]$ contains the six member transfer stiffnesses.

The axial reaction forces \bar{C} may be transformed into reaction forces \bar{F} acting in the global X, Y and Z directions at the grounded nodes O, C, D and E:

$$\begin{Bmatrix} \bar{F} \end{Bmatrix}_{12 \times 1} = \begin{bmatrix} T_{\bar{F}\bar{C}} \end{bmatrix}_{12 \times 12} \begin{Bmatrix} \bar{C}_{AB} \\ \bar{C}_{A'B'} \end{Bmatrix}_{12 \times 1} \quad (\text{IX.12})$$

The transformation matrix is given in Fig. IX.7.

The product of the transformations (IX.9) to (IX.12) yields the relationship between the reaction forces \bar{F} and the displacements δ_p on the upper face of the half V-block:

$$\begin{aligned}
 \left\{ \bar{F}^1 \right\}_{12 \times 1} &= \left(\left[\begin{array}{c|c} T_{\bar{F}\bar{C}} & \\ \hline & \begin{bmatrix} T_{MEM} & 0 \\ 0 & T_{MEM} \end{bmatrix} \\ & \begin{bmatrix} (T_{FC}^{AB})^T & 0 \\ 0 & (T_{FC}^{A'B'})^T \end{bmatrix} \\ & T_F^T \end{array} \right] \left\{ \delta_P^1 \right\}_{6 \times 1} \right) \\
 &= \left[Z_T^1 \right]_{12 \times 6} \left\{ \delta_P^1 \right\}_{6 \times 1} \quad (IX.13)
 \end{aligned}$$

where the superscript 1 refers to the first half V-block.

A similar transfer stiffness matrix may be formed for the second half V-block. This only differs from $[Z_T^1]$ in the signs of columns 2, 3, 5 and 6, the change being due to the different choice of positive directions for the local y , z , β and θ co-ordinates. For the separate halves we may write

$$\left\{ \begin{array}{c} \bar{F}^1 \\ \bar{F}^2 \end{array} \right\}_{24 \times 1} = \left[\begin{array}{c|c} Z_T^1 & 0 \\ \hline 0 & Z_T^2 \end{array} \right]_{24 \times 12} \left\{ \begin{array}{c} \delta_P^1 \\ \delta_P^2 \end{array} \right\}_{12 \times 1} \quad (IX.14)$$

By joining together the two half blocks at the nodes O and E, and grouping together all the reaction forces \bar{F} , we may form a complete transfer stiffness matrix relating the 14 transmitted forces P to the displacements on the two upper faces of the V-block:

$$\left\{ P \right\}_{14 \times 1} = \left[T_{P\bar{F}} \right]_{14 \times 24} \left[\begin{array}{c|c} Z_T^1 & 0 \\ \hline 0 & Z_T^2 \end{array} \right]_{24 \times 12} \left\{ \begin{array}{c} \delta_P^1 \\ \delta_P^2 \end{array} \right\}_{12 \times 1} = \left[Z_T \right]_{14 \times 12} \left\{ \begin{array}{c} \delta_P^1 \\ \delta_P^2 \end{array} \right\}_{12 \times 1} \quad (IX.15)$$

Transfer Stiffness

The directions of the transmitted forces are given in Fig. IX.4, and these have been chosen to yield the force transmission normal to and in the plane of the lower beams of the seating. The transformation matrix $[T_{P\bar{F}}]$ therefore not only groups together the various reaction forces but also effects a rotation of co-ordinates (see Fig. IX.8).

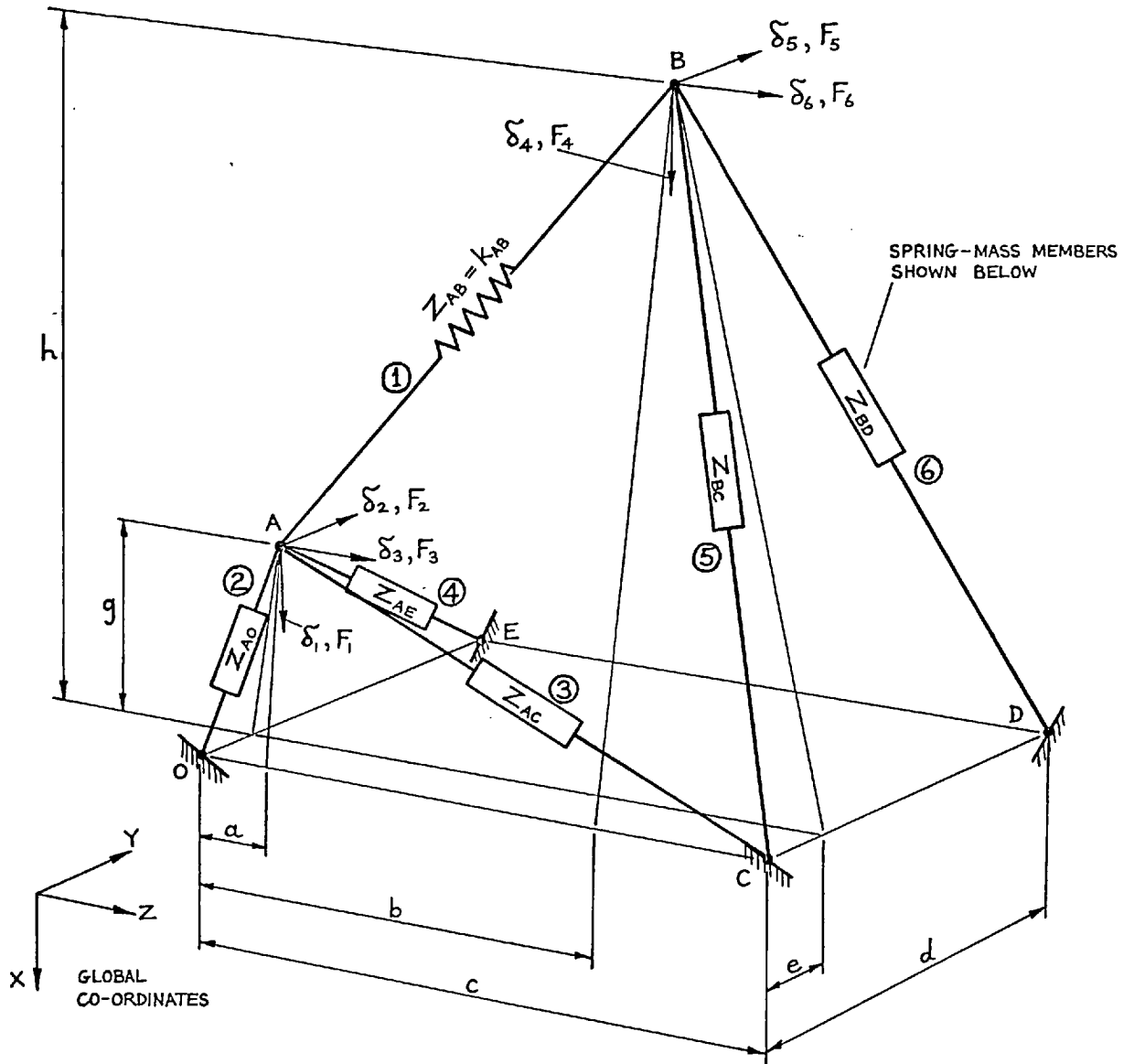
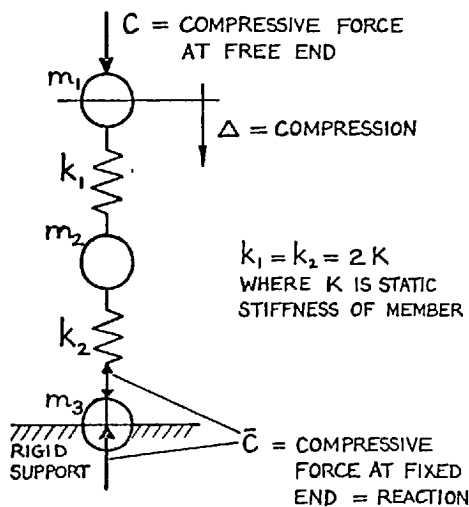


FIG. IX.1 SPRING-MASS MODEL FOR QUARTER V-BLOCK (ABOVE)

FIG. IX.2 DYNAMIC STIFFNESS RELATIONS FOR A MEMBER (BELOW)

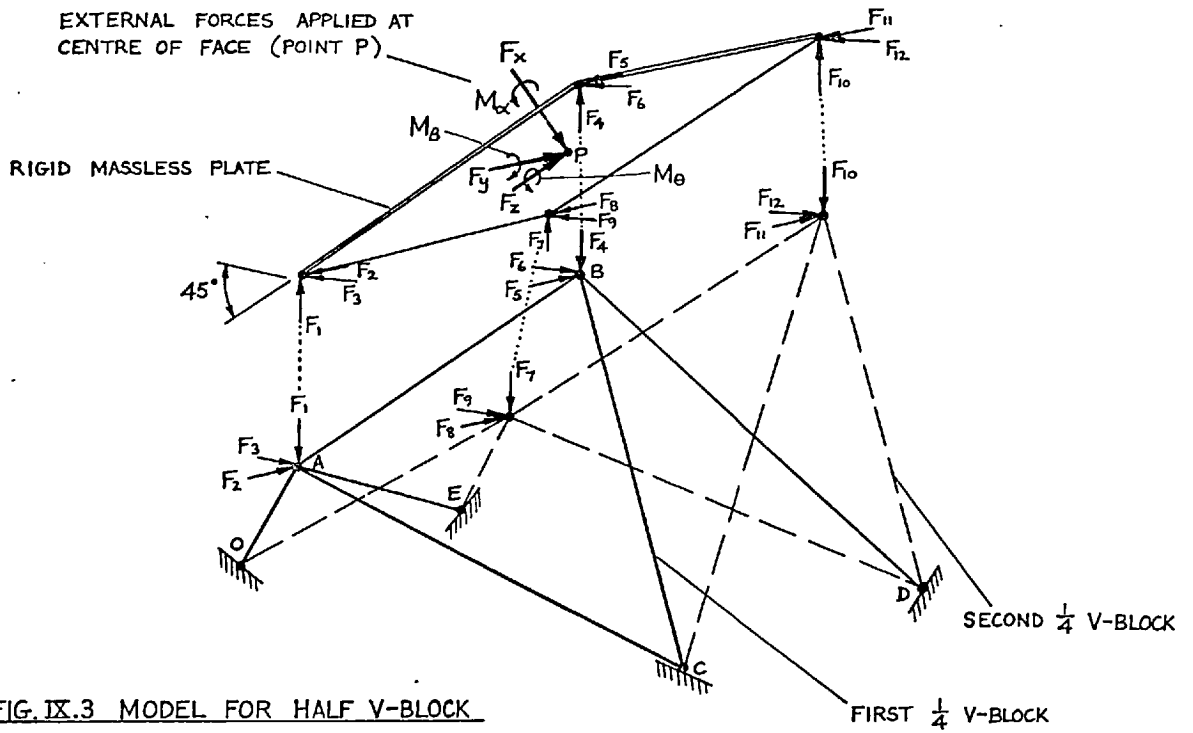


POINT DYNAMIC STIFFNESS AT FREE END

$$Z = \frac{C}{\Delta} = \frac{(k_1 - \omega^2 m_1)(k_1 + k_2 - \omega^2 m_2) - k_1^2}{(k_1 + k_2 - \omega^2 m_2)}$$

TRANSFER DYNAMIC STIFFNESS

$$\bar{C} = \frac{k_1 k_2}{k_1 + k_2 - \omega^2 m_2}$$



$\frac{1}{2}$ BLOCK 2 IS A COPY OF $\frac{1}{2}$ BLOCK 1, WITH POSITIVE DIRECTIONS OF CO-ORDINATES $y_p, z_p, \beta_p, \theta_p$ CHANGED

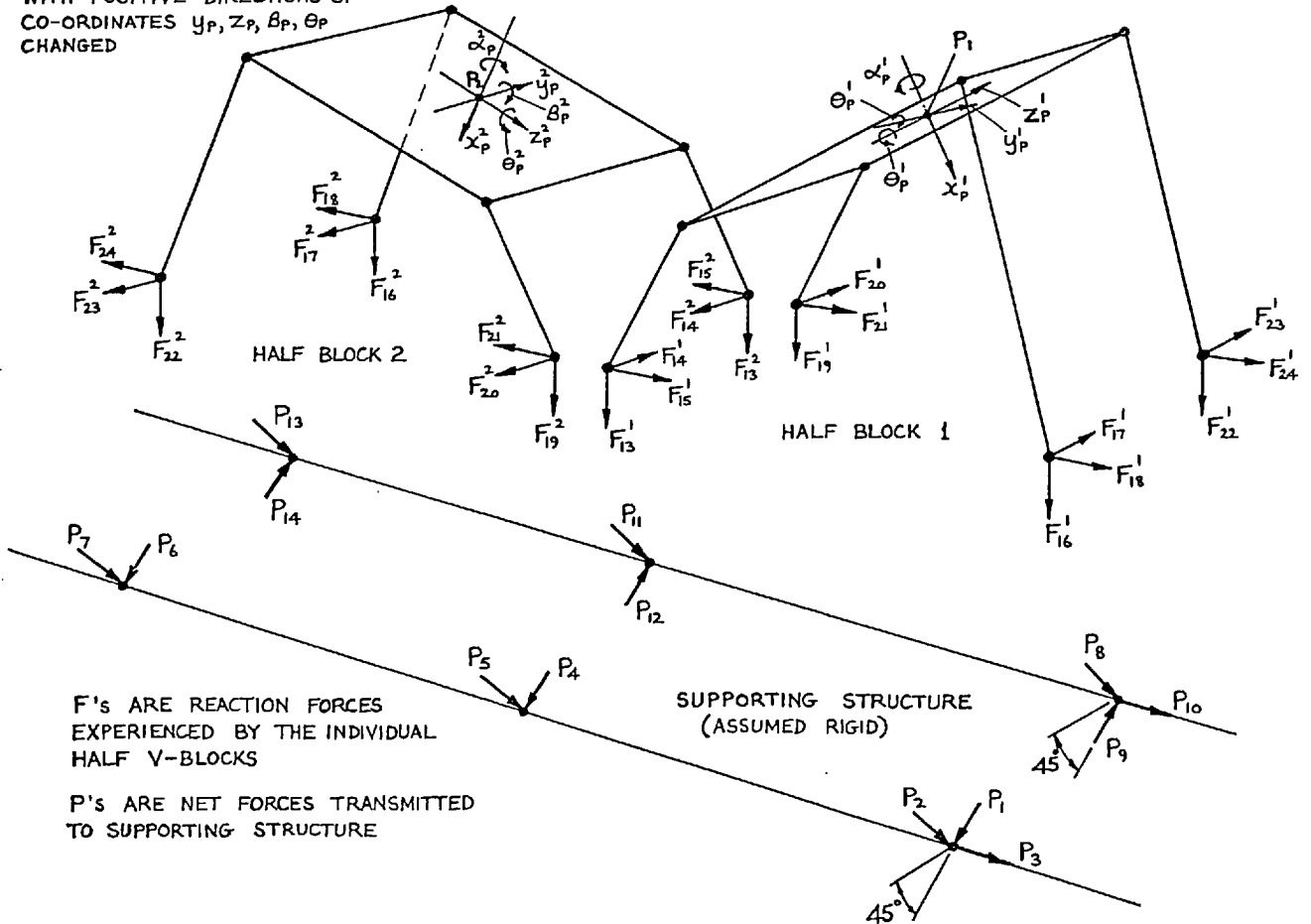


FIG. IX.4 COMPLETE V-BLOCK AND TRANSMITTED FORCES

$$\begin{Bmatrix} F_1 \\ F_2 \\ F_3 \\ F_4 \\ F_5 \\ F_6 \end{Bmatrix} = \begin{bmatrix} 1 & 2 & 3 & 4 & 5 & 6 \\ \frac{-(h-g)}{AB} & \frac{g}{AO} & \frac{g}{AC} & \frac{g}{AE} & 0 & 0 \\ 0 & \frac{-e}{AO} & \frac{-e}{AC} & \frac{(d-e)}{AE} & 0 & 0 \\ \frac{(b-a)}{AB} & \frac{-a}{AO} & \frac{(c-a)}{AC} & \frac{-a}{AE} & 0 & 0 \\ \frac{(h-g)}{AB} & 0 & 0 & 0 & \frac{h}{BC} & \frac{h}{BD} \\ 0 & 0 & 0 & 0 & \frac{-e}{BC} & \frac{(d-e)}{BD} \\ \frac{-(b-a)}{AB} & 0 & 0 & 0 & \frac{(c-b)}{BC} & \frac{(c-b)}{BD} \end{bmatrix} \begin{Bmatrix} C_{AB} \\ C_{AO} \\ C_{AC} \\ C_{AE} \\ C_{BC} \\ C_{BD} \end{Bmatrix}$$

FIG. IX.5 NODAL FORCE / MEMBER COMPRESSIVE FORCE RELATION FOR QUARTER V-BLOCK $\{F_{AB}\} = [T_{FC}]\{C\}$

F_x	1	2	3	4	5	6	7	8	9	10	11	12	F_1	1
	$+\frac{1}{\sqrt{2}}$	0	$+\frac{1}{\sqrt{2}}$	$+\frac{1}{\sqrt{2}}$	0	$+\frac{1}{\sqrt{2}}$	$+\frac{1}{\sqrt{2}}$	0	$+\frac{1}{\sqrt{2}}$	$+\frac{1}{\sqrt{2}}$	0	$+\frac{1}{\sqrt{2}}$	F_2	2
F_y	0	+1	0	0	+1	0	0	+1	0	0	+1	0	F_3	3
F_z	$-\frac{1}{\sqrt{2}}$	0	$+\frac{1}{\sqrt{2}}$	$-\frac{1}{\sqrt{2}}$	0	$+\frac{1}{\sqrt{2}}$	$-\frac{1}{\sqrt{2}}$	0	$+\frac{1}{\sqrt{2}}$	$-\frac{1}{\sqrt{2}}$	0	$+\frac{1}{\sqrt{2}}$	F_4	4
M_α	$\frac{(d-2e)}{2\sqrt{2}}$	$+\frac{AB}{2}$	$-\frac{(d-2e)}{2\sqrt{2}}$	$\frac{(d-2e)}{2\sqrt{2}}$	$-\frac{AB}{2}$	$-\frac{(d-2e)}{2\sqrt{2}}$	$-\frac{(d-2e)}{2\sqrt{2}}$	$+\frac{AB}{2}$	$\frac{(d-2e)}{2\sqrt{2}}$	$-\frac{(d-2e)}{2\sqrt{2}}$	$-\frac{AB}{2}$	$\frac{(d-2e)}{2\sqrt{2}}$	F_5	5
M_B	$-\frac{AB}{2\sqrt{2}}$	0	$-\frac{AB}{2\sqrt{2}}$	$+\frac{AB}{2\sqrt{2}}$	0	$+\frac{AB}{2\sqrt{2}}$	$-\frac{AB}{2\sqrt{2}}$	0	$-\frac{AB}{2\sqrt{2}}$	$+\frac{AB}{2\sqrt{2}}$	0	$+\frac{AB}{2\sqrt{2}}$	F_6	6
M_e	$\frac{(d-2e)}{2\sqrt{2}}$	0	$\frac{(d-2e)}{2\sqrt{2}}$	$\frac{(d-2e)}{2\sqrt{2}}$	0	$\frac{(d-2e)}{2\sqrt{2}}$	$-\frac{(d-2e)}{2\sqrt{2}}$	0	$-\frac{(d-2e)}{2\sqrt{2}}$	$-\frac{(d-2e)}{2\sqrt{2}}$	0	$-\frac{(d-2e)}{2\sqrt{2}}$	F_7	7
													F_8	8
													F_9	9
													F_{10}	10
													F_{11}	11
													F_{12}	12

FIG. IX.6 POINT FORCE / NODAL FORCE RELATION FOR HALF V-BLOCK

$$\{F_P\} = [T_F] \begin{Bmatrix} F_{AB} \\ F_{A'B'} \end{Bmatrix}$$

F_{13}	=	1	2	3	4	5	6	7	8	9	10	11	12	1
F_{14}		0	$-\frac{g}{AO}$	0	0	0	0	0	0	0	$-\frac{g}{AE}$	0	0	\bar{C}_{AB}
F_{15}		0	$\frac{e}{AO}$	0	0	0	0	0	0	0	$\frac{(d-e)}{AE}$	0	0	\bar{C}_{Ao}
F_{16}		0	$\frac{a}{AO}$	0	0	0	0	0	0	0	$\frac{a}{AE}$	0	0	\bar{C}_{AC}
F_{17}		0	0	$-\frac{g}{AC}$	0	$-\frac{h}{BC}$	0	0	0	0	0	0	$-\frac{h}{BD}$	\bar{C}_{AE}
F_{18}		0	0	$\frac{e}{AC}$	0	$\frac{e}{BC}$	0	0	0	0	0	0	$\frac{(d-e)}{BD}$	\bar{C}_{BC}
F_{19}		0	0	$-\frac{(c-a)}{AC}$	0	$-\frac{(c-b)}{BC}$	0	0	0	0	0	0	$-\frac{(c-b)}{BD}$	\bar{C}_{BD}
F_{20}		0	0	0	$-\frac{g}{AE}$	0	0	0	$-\frac{g}{AO}$	0	0	0	0	\bar{C}'_{AB}
F_{21}		0	0	0	$-\frac{(d-e)}{AE}$	0	0	0	$-\frac{e}{AO}$	0	0	0	0	\bar{C}'_{AE}
F_{22}		0	0	0	$\frac{a}{AE}$	0	0	0	$\frac{a}{AO}$	0	0	0	0	\bar{C}'_{AD}
F_{23}		0	0	0	0	$-\frac{h}{BD}$	0	0	$-\frac{g}{AC}$	0	$-\frac{h}{BC}$	0	0	\bar{C}'_{Ao}
F_{24}		0	0	0	0	$-\frac{(d-e)}{BD}$	0	0	$-\frac{e}{AC}$	0	$-\frac{e}{BC}$	0	0	\bar{C}'_{BD}
		0	0	0	0	$-\frac{(c-b)}{BD}$	0	0	$-\frac{(c-a)}{AC}$	0	$-\frac{(c-b)}{BC}$	0	0	\bar{C}'_{BC}

FIG. IX.7 X-Y-Z REACTION FORCE / AXIAL REACTION FORCE RELATION FOR HALF V-BLOCK $\{\bar{F}\} = [T_{F\bar{C}}] \begin{Bmatrix} \bar{C}_{AB} \\ \bar{C}'_{AB} \end{Bmatrix}$

	1	2	3	4	5	6	7	8	9	10	11	12	13	14	15	16	17	18	19	20	21	22	23	24			
P_1	0	0	0	$-\frac{1}{\sqrt{2}}$	$\frac{1}{\sqrt{2}}$	0	0	0	0	0	0	0	0	0	0	0	0	0	0	0	0	0	0	0	0	1	F_{13}^1
P_2	0	0	0	$-\frac{1}{\sqrt{2}}$	$-\frac{1}{\sqrt{2}}$	0	0	0	0	0	0	0	0	0	0	0	0	0	0	0	0	0	0	0	0	2	F_{14}^1
P_3	0	0	-1	0	0	-1	0	0	0	0	0	0	0	0	0	0	0	0	0	0	0	1	0	0	1	3	F_{15}^1
P_4	$-\frac{1}{\sqrt{2}}$	$\frac{1}{\sqrt{2}}$	0	0	0	0	0	0	0	0	0	0	0	0	0	0	0	0	$-\frac{1}{\sqrt{2}}$	$-\frac{1}{\sqrt{2}}$	0	0	0	0	0	4	F_{16}^1
P_5	$-\frac{1}{\sqrt{2}}$	$-\frac{1}{\sqrt{2}}$	0	0	0	0	0	0	0	0	0	0	0	0	0	0	0	0	$-\frac{1}{\sqrt{2}}$	$\frac{1}{\sqrt{2}}$	0	0	0	0	0	5	F_{17}^1
P_6	0	0	0	0	0	0	0	0	0	0	0	0	0	0	0	0	0	0	0	0	0	$-\frac{1}{\sqrt{2}}$	$-\frac{1}{\sqrt{2}}$	0	6	F_{18}^1	
P_7	0	0	0	0	0	0	0	0	0	0	0	0	0	0	0	0	0	0	0	0	$-\frac{1}{\sqrt{2}}$	$\frac{1}{\sqrt{2}}$	0	0	7	F_{19}^1	
P_8	0	0	0	0	0	0	0	0	0	$-\frac{1}{\sqrt{2}}$	$-\frac{1}{\sqrt{2}}$	0	0	0	0	0	0	0	0	0	0	0	0	0	0	8	F_{20}^1
P_9	0	0	0	0	0	0	0	0	0	$\frac{1}{\sqrt{2}}$	$-\frac{1}{\sqrt{2}}$	0	0	0	0	0	0	0	0	0	0	0	0	0	0	9	F_{21}^1
P_{10}	0	0	0	0	0	0	0	0	0	0	0	-1	0	0	1	0	0	1	0	0	0	0	0	0	0	10	F_{22}^1
P_{11}	0	0	0	0	0	0	$-\frac{1}{\sqrt{2}}$	$-\frac{1}{\sqrt{2}}$	0	0	0	0	$-\frac{1}{\sqrt{2}}$	$\frac{1}{\sqrt{2}}$	0	0	0	0	0	0	0	0	0	0	0	11	F_{23}^1
P_{12}	0	0	0	0	0	0	$\frac{1}{\sqrt{2}}$	$-\frac{1}{\sqrt{2}}$	0	0	0	0	$\frac{1}{\sqrt{2}}$	$\frac{1}{\sqrt{2}}$	0	0	0	0	0	0	0	0	0	0	0	12	F_{24}^1
P_{13}	0	0	0	0	0	0	0	0	0	0	0	0	0	0	0	$-\frac{1}{\sqrt{2}}$	$\frac{1}{\sqrt{2}}$	0	0	0	0	0	0	0	0	13	F_{13}^2
P_{14}	0	0	0	0	0	0	0	0	0	0	0	0	0	0	0	$\frac{1}{\sqrt{2}}$	$\frac{1}{\sqrt{2}}$	0	0	0	0	0	0	0	0	14	F_{14}^2

FIG. IX.8 TRANSMITTED FORCE / REACTION FORCE RELATION FOR TWO HALF BLOCKS COMBINED

$$\{P\} = [T_{PF}] \begin{Bmatrix} \bar{F}^1 \\ \bar{F}^2 \end{Bmatrix}$$

APPENDIX X

DERIVATION OF DYNAMIC STIFFNESS MATRIX FOR MALE V-PIECE (VB)

An exploded view of the V-piece is given in Fig. X.1, and from this it is seen that there are three components, which are welded together to form a very stiff assembly. To the inclined faces of the triangular plates 2 and 3 are affixed PVC pads. It will therefore be assumed that the support may be adequately represented by a rigid inertia with damped springs attached to its inclined faces.

Before obtaining the inertial properties of the assembly, we must firstly determine the position of the centre of gravity G in the manner indicated in Fig. X.2. The next step is to obtain the inertial properties of each of the three components, referred to the X, Y and Z axes passing through G (i.e. the principal axes of the assembly). The moments of inertia of the top plate (Component 1) and of the triangular plates (Components 2 and 3) are given in Figs. X.3 and X.4 respectively. The inertial properties of the three components may be combined, as shown in Fig X.5, in order to form a 6 x 6 diagonal inertia matrix for the complete assembly:

$$\begin{Bmatrix} F_G \\ 6 \times 1 \end{Bmatrix} = \begin{bmatrix} M \\ 6 \times 6 \end{bmatrix} \begin{Bmatrix} \ddot{\delta}_G \\ 6 \times 1 \end{Bmatrix} \quad (X.1)$$

where the vectors $\{F_G\}$ and $\{\ddot{\delta}_G\}$ contain the forces and accelerations in the X, Y and Z directions at point G. In order to couple the damped springs to the assembly, it is necessary to work in terms of receptances, and the corresponding receptance relation is

$$\begin{Bmatrix} \delta_G \\ 6 \times 1 \end{Bmatrix} = -\frac{1}{\omega^2} \begin{bmatrix} M \\ 6 \times 6 \end{bmatrix}^{-1} \begin{Bmatrix} F_G \\ 6 \times 1 \end{Bmatrix} \quad (X.2)$$

where the inversion of the diagonal matrix is accomplished simply by inverting its diagonal elements.

However, we require the receptance properties not at the centre of

gravity G , but at the three points P , A and B . These points and the corresponding co-ordinates of interest are shown in Fig. X.6. It should be noted that the assumed coupling points A and B lie in the planes of the inclined faces of the V-piece, midway between the two triangular plates. Considering force inputs in all 16 directions, the net force system acting at G is given by the relation

$$\begin{Bmatrix} F_G \\ \vdots \\ \vdots \\ \vdots \end{Bmatrix}_{6 \times 1} = \begin{bmatrix} T_F \\ \vdots \\ \vdots \\ \vdots \end{bmatrix}_{6 \times 16} \begin{Bmatrix} F_P \\ F_A \\ F_B \end{Bmatrix}_{16 \times 1} \quad (X.3)$$

which is shown in Fig. X.8. Since the displacements at P , A and B are related to those at G by the transpose of the above transformation, we may write

$$\begin{Bmatrix} \delta_P \\ \delta_A \\ \delta_B \end{Bmatrix}_{16 \times 1} = -\frac{1}{\omega^2} \left(\begin{bmatrix} T_F^T \\ \vdots \\ \vdots \\ \vdots \end{bmatrix} \begin{bmatrix} M \\ \vdots \\ \vdots \\ \vdots \end{bmatrix}^{-1} \begin{bmatrix} T_F \\ \vdots \\ \vdots \\ \vdots \end{bmatrix} \right) \begin{Bmatrix} F_P \\ F_A \\ F_B \end{Bmatrix}_{16 \times 1} \quad (X.4)$$

which relates the displacements at P , A and B to the corresponding forces.

We must now obtain the stiffness properties of the PVC pads attached to the inclined surfaces of the V-piece. The rectilinear and rotational stiffnesses of the pair of pads on each "face" may be expressed in terms of the three rectilinear stiffnesses of a single pad, as is shown in Fig. X.7. The two in-plane stiffnesses of a rubber pad are associated with pure shear, and are given by simple theory. However, the compressive stiffness K_{xx} is not only associated with pure elastic compression, but also with the lateral bulging restraint imposed by the metal surfaces between which the pad is sandwiched. Although the pads were not stuck in place, the V-piece was bolted up tightly to the transverse beams, so it is unlikely that the pad surfaces were able to slip over the metal surfaces. Thus, the compressive stiffness is given by an elastic compression term, yielded by simple theory, plus a bulging restraint term which is a function of the

Shape Factor, $S_F = (\text{loaded area of pad})/(\text{force free area of pad})$. The reader is referred to references(12) and (25)* for a fuller discussion of this topic.

If the 6 x 6 diagonal matrix of stiffnesses is $[K]$, the corresponding receptance matrix is $[K]^{-1}$, and this is obtained by inverting the diagonal elements of the stiffness matrix. By adding the pad receptance matrices to the receptance matrix (X.4), we obtain the overall receptance of the steel V-piece plus the PVC pads. Upon inverting this relation, we finally obtain the required dynamic stiffness matrix:

$$\begin{Bmatrix} F_P \\ F_A \\ F_B \end{Bmatrix}_{16 \times 1} = \left(\begin{bmatrix} 0 & 0 & 0 \\ 0 & K^{-1} & 0 \\ 0 & 0 & K^{-1} \end{bmatrix} - \frac{1}{\omega^2} \begin{bmatrix} T_F^T \\ \\ \end{bmatrix} \begin{bmatrix} M \\ \\ \end{bmatrix}^{-1} \begin{bmatrix} T_F \\ \\ \end{bmatrix} \right)^{-1} \begin{Bmatrix} \delta_P \\ \delta_A \\ \delta_B \end{Bmatrix}_{16 \times 1} \quad \delta_P = \bar{\delta}_P \quad (X.5)$$

which relates the applied forces at the three points to the displacements at those points. The displacement vectors $\{\delta_A\}$ and $\{\delta_B\}$ refer to the two assumed coupling points in the planes of the free faces of the pads, whereas the vectors $\{\bar{\delta}_A\}$ and $\{\bar{\delta}_B\}$ in (X.4) referred to the corresponding points in the planes of the inclined faces of the rigid steel assembly.

* References for Appendices IX to XI are given on Page 430.

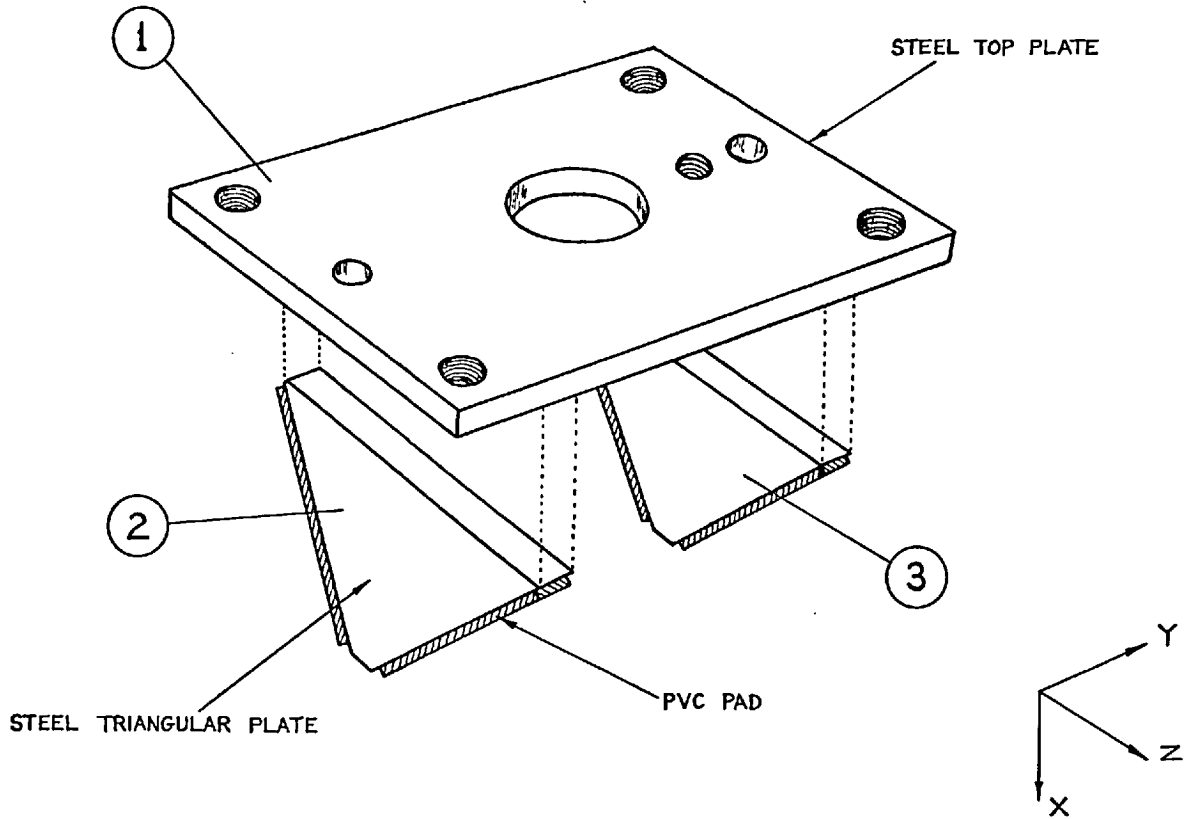
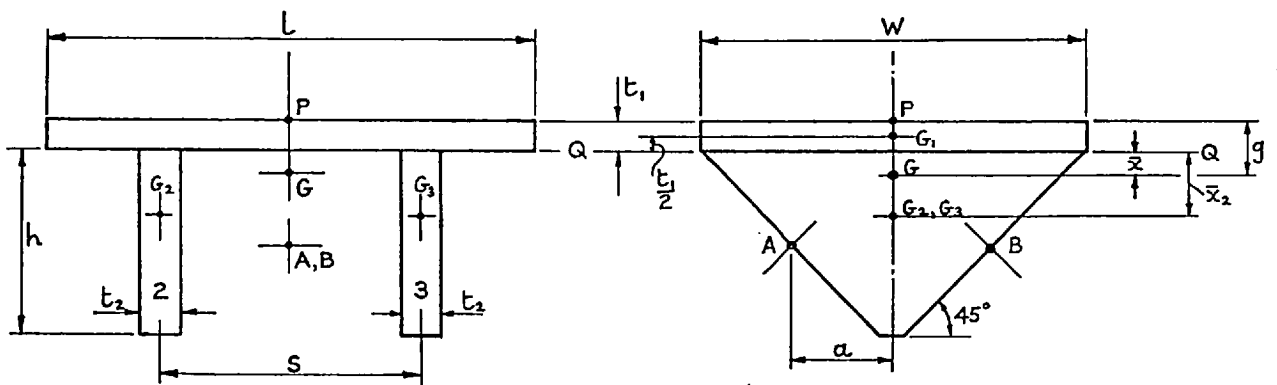


FIG. X.1 EXPLODED VIEW OF MALE V-PIECE



G_1, G_2 AND G_3 ARE C.G.'S OF TOP PLATE AND OF THE TWO TRIANGULAR PLATES, AND G IS C.G. OF COMPLETE ASS'Y.

THE DENSITY ρ AND THE DIMENSIONS w, l, d, h, t_1, t_2 AND s ARE GIVEN QUANTITIES.

MASSES OF COMPONENT PARTS

$$m_1 = \rho t_1 [wl - \frac{\pi d^2}{4}]$$

$$m_2 = m_3 = \rho t_2 h [w - h]$$

\therefore TOTAL MASS, $m = m_1 + 2m_2$

CALCULATED DIMENSIONS

$$\bar{x}_2 = \frac{h}{2} \left[\frac{w - 4h}{w - h} \right]$$

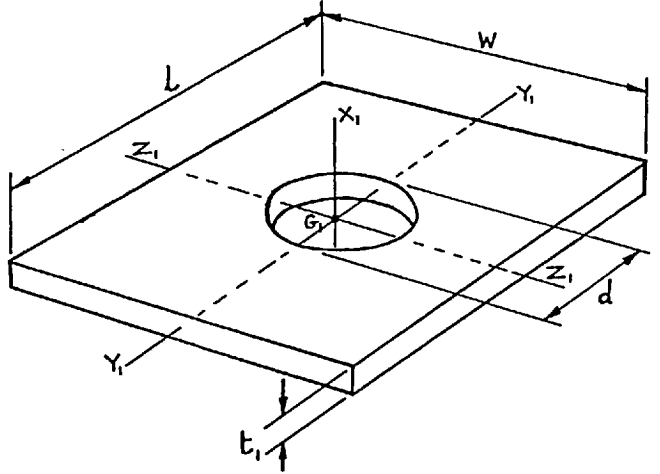
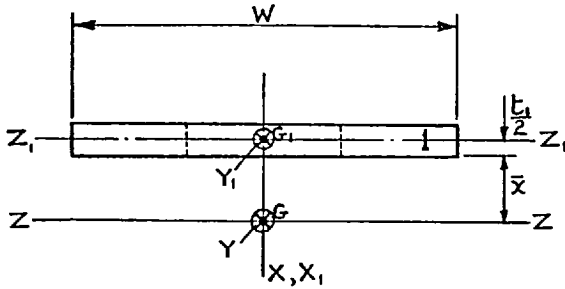
$$\bar{x} = \frac{-m_1 \frac{t_1}{2} + 2m_2 \bar{x}_2}{m}$$

DISTANCE OF C.G. FROM TOP FACE,

$$g = \bar{x} + t$$

FIG. X.2 MASS AND CENTRE OF GRAVITY OF MALE V-PIECE

G_1 IS C.G. OF TOP PLATE
 G IS C.G. OF ASSEMBLY



$$\text{MASS, } m_1 = \rho t_1 \left[wl - \frac{\pi d^2}{4} \right]$$

MOMENTS OF INERTIA REFERRED TO PRINCIPAL AXES OF THE TOP PLATE

$$I_{Y_1 Y_1}^{(1)} = \rho t_1 \left[\frac{L W^3}{12} - \frac{\pi d^4}{64} \right]$$

$$I_{Z_1 Z_1}^{(1)} = \rho t_1 \left[\frac{W L^3}{12} - \frac{\pi d^4}{64} \right]$$

$$I_{X_1 X_1}^{(1)} = I_{Y_1 Y_1}^{(1)} + I_{Z_1 Z_1}^{(1)}$$

MOMENTS OF INERTIA REFERRED TO PRINCIPAL AXES X, Y, Z OF THE ASSEMBLY

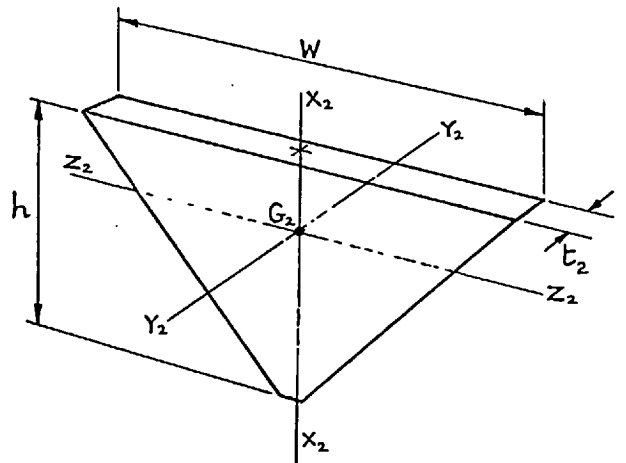
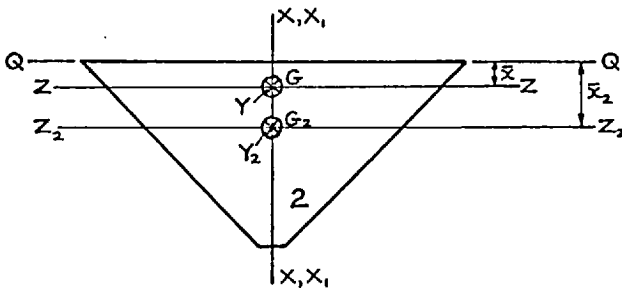
$$I_{xx}^{(1)} = I_{X_1 X_1}^{(1)}$$

$$I_{yy}^{(1)} = I_{Y_1 Y_1}^{(1)} + m_1 \left(\bar{x} + \frac{t_1}{2} \right)^2$$

$$I_{zz}^{(1)} = I_{Z_1 Z_1}^{(1)} + m_1 \left(\bar{x} + \frac{t_1}{2} \right)^2$$

FIG. X.3 INERTIAL PROPERTIES OF TOP PLATE OF MALE V-PIECE

G_2 IS C.G. OF TRIANGULAR PLATE



$$\text{MASS, } m_2 = m_3 = \rho t_2 h (w-h)$$

MOMENTS OF INERTIA REFERRED TO PRINCIPAL AXES OF THE TRIANGULAR PLATE

$$I_{X_2 X_2}^{(2)} = \frac{\rho t_2}{96} \left[W^4 - (W-2h)^4 \right]$$

$$I_{Z_2 Z_2}^{(2)} = \frac{\rho t_2 h^3}{3} \left[W - \frac{3}{2} h \right] - m_2 \bar{x}_2^2$$

$$I_{Y_2 Y_2}^{(2)} = I_{X_2 X_2}^{(2)} + I_{Z_2 Z_2}^{(2)}$$

MOMENTS OF INERTIA REFERRED TO PRINCIPAL AXES X, Y, Z OF THE ASSEMBLY

$$I_{xx}^{(2)} = I_{X_2 X_2}^{(2)} = I_{X_2 X_2}^{(2)} + \frac{m_2 S^2}{4}$$

$$I_{yy}^{(2)} = I_{Y_2 Y_2}^{(2)} = I_{Y_2 Y_2}^{(2)} + m_2 (\bar{x}_2 - \bar{x})^2$$

$$I_{zz}^{(2)} = I_{Z_2 Z_2}^{(2)} = I_{Z_2 Z_2}^{(2)} + m_2 \left[(\bar{x}_2 - \bar{x})^2 + \frac{S^2}{4} \right]$$

FIG. X.4 INERTIAL PROPERTIES OF TRIANGULAR PLATES OF MALE V-PIECE

$$\begin{bmatrix} F_x \\ F_y \\ F_z \\ M_\alpha \\ M_\beta \\ M_\theta \end{bmatrix}_G = \begin{bmatrix} m & 0 & 0 & 0 & 0 & 0 \\ 0 & m & 0 & 0 & 0 & 0 \\ 0 & 0 & m & 0 & 0 & 0 \\ 0 & 0 & 0 & I_{xx}^{(1)} + 2I_{xx}^{(2)} & 0 & 0 \\ 0 & 0 & 0 & 0 & I_{yy}^{(1)} + 2I_{yy}^{(2)} & 0 \\ 0 & 0 & 0 & 0 & 0 & I_{zz}^{(1)} + 2I_{zz}^{(2)} \end{bmatrix} \begin{bmatrix} \ddot{x} \\ \ddot{y} \\ \ddot{z} \\ \ddot{\alpha} \\ \ddot{\beta} \\ \ddot{\theta} \end{bmatrix}_G$$

FIG. X.5 6 x 6 INERTIA MATRIX FOR MALE V-PIECE (REFERRED TO C.G.)

$$\{F_G\} = [M_G]\{\ddot{\delta}_G\}$$

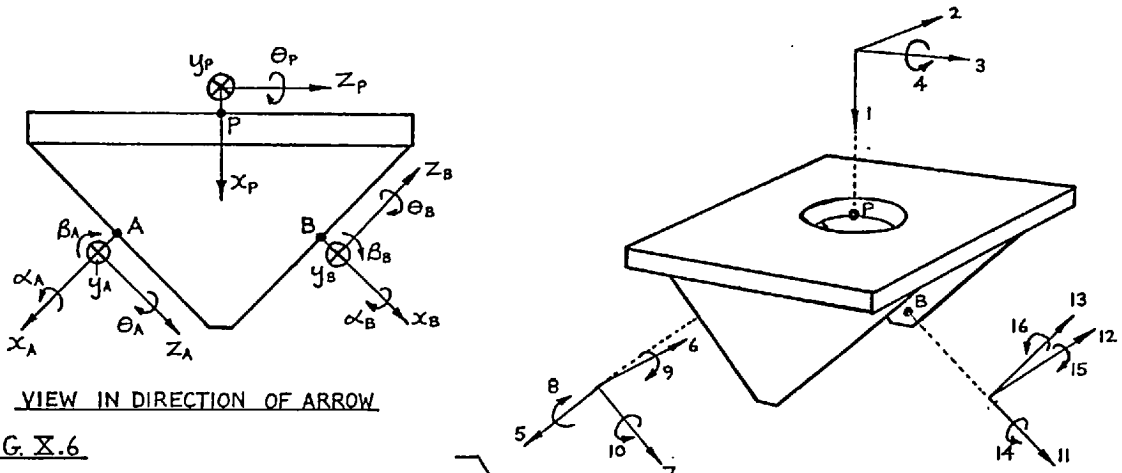


FIG. X.6 THE 16 CO-ORDINATES IN TERMS OF WHICH THE DYN. STIFF. IS TO BE EXPRESSED

NUMBERS INDICATE ORDER IN DISPLACEMENT VECTOR

X, Y AND Z STIFFNESSES OF A SINGLE PAD

$$\bar{k}_{xx} = \frac{\bar{E} W_p L_p}{t_p} \quad \text{WHERE } \bar{E} = \frac{E}{1-\nu^2} (1 + k S_F^2) = 4G (1 + k S_F^2)$$

$$\bar{k}_{yy} = \bar{k}_{zz} = \frac{G W_p L_p}{t_p}$$

IF $\nu = 0.5$ AND $E = 3G$.
 $k = 0.64$ FOR 55 IRHD RUBBER.
 SHAPE FACTOR, $S_F = \frac{W_p}{2 t_p}$
 (SEE REF. 12)

STIFFNESSES OF PAIR OF PADS

$$\begin{aligned}
 k_{xx} &= 2 \bar{k}_{xx} \\
 k_{yy} &= 2 \bar{k}_{yy} \\
 k_{zz} &= 2 \bar{k}_{zz} \\
 k_{\alpha\alpha} &= \frac{s^2 \bar{k}_{zz}}{2} \\
 k_{\beta\beta} &= \frac{L_p^2 \bar{k}_{xx}}{6} \\
 k_{\theta\theta} &= \frac{s^2 \bar{k}_{xx}}{2}
 \end{aligned}$$

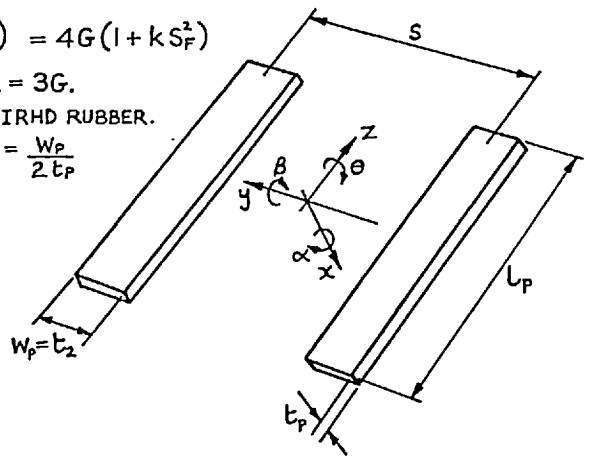


FIG. X.7 COMPOSITE STIFFNESSES OF PAIR OF PVC PADS FOR LOWER FACES OF MALE V-PIECE

$$\begin{Bmatrix} F_{xG} \\ F_{yG} \\ F_{zG} \\ M_{\alpha G} \\ M_{\beta G} \\ M_{\theta G} \end{Bmatrix} = \begin{bmatrix} 1 & 0 & 0 & 0 & \frac{1}{\sqrt{2}} & 0 & \frac{1}{\sqrt{2}} & 0 & 0 & 0 & \frac{1}{\sqrt{2}} & 0 & \frac{1}{\sqrt{2}} & 0 & 0 & 0 \\ 0 & 1 & 0 & 0 & 0 & 1 & 0 & 0 & 0 & 0 & 0 & 1 & 0 & 0 & 0 & 0 \\ 0 & 0 & 1 & 0 & -\frac{1}{\sqrt{2}} & 0 & \frac{1}{\sqrt{2}} & 0 & 0 & 0 & \frac{1}{\sqrt{2}} & 0 & \frac{1}{\sqrt{2}} & 0 & 0 & 0 \\ 0 & 0 & 0 & 0 & 0 & a & 0 & \frac{1}{\sqrt{2}} & 0 & \frac{1}{\sqrt{2}} & 0 & -a & 0 & \frac{1}{\sqrt{2}} & 0 & -\frac{1}{\sqrt{2}} \\ 0 & 0 & g & 0 & \frac{a-(h-g)}{\sqrt{2}} & 0 & \frac{-a-(h-g)}{\sqrt{2}} & 0 & 1 & 0 & \frac{a-(h-g)}{\sqrt{2}} & 0 & \frac{-a-(h-g)}{\sqrt{2}} & 0 & 1 & 0 \\ 0 & -g & 0 & 1 & 0 & (h-g) & 0 & -\frac{1}{\sqrt{2}} & 0 & \frac{1}{\sqrt{2}} & 0 & (h-g) & 0 & \frac{1}{\sqrt{2}} & 0 & \frac{1}{\sqrt{2}} \end{bmatrix} \begin{Bmatrix} F_{xP} \\ F_{yP} \\ F_{zP} \\ M_{\theta P} \\ F_{xA} \\ F_{yA} \\ F_{zA} \\ M_{\alpha A} \\ M_{\beta A} \\ M_{\theta A} \\ F_{xB} \\ F_{yB} \\ F_{zB} \\ M_{\alpha B} \\ M_{\beta B} \\ M_{\theta B} \end{Bmatrix}$$

$$\{F_G\} = [T_F] \begin{Bmatrix} F_P \\ F_A \\ F_B \end{Bmatrix}$$

FIG. X.8 EQUIVALENT FORCE SYSTEM AT C.G. OF MALE V-PIECE IN TERMS OF FORCES APPLIED AT POINTS P, A AND B.

APPENDIX XIDERIVATION OF DYNAMIC STIFFNESS MATRIX FOR FEMALE V-SUPPORT (VS)

An exploded view of the V-support is given in Fig. IX.1 and from this it is seen that there are five components, which are welded together to form a relatively stiff assembly. To the face plates 2 and 4 of this assembly are affixed PVC pads. It will therefore be assumed that the support may be adequately represented by a rigid inertia with damped springs attached to its upper faces. The only immediately apparent flexibility in the steel assembly is in torsion of the face plates about their respective gusset plates, but this may be calculated approximately using plate finite elements, and the relevant stiffness may be combined with the corresponding stiffness of the PVC pad.

Before proceeding to obtain the inertial properties of the assembly, we must first determine the position of the centre of gravity G in the manner indicated in Fig. XI.2. We may next obtain the inertial properties of the five components, referred to axes passing through G. In the case of the base plate (Component 1), the moments of inertia may be obtained about the X, Y and Z axes through G, as shown in Fig. XI.3. However, the moments of inertia of the face plates (Components 2 and 4) and of the triangular gusset plates (Components 3 and 5) are more readily obtained about the U, V and Z axes, as shown in Figs. XI.4 and XI.5. The inertial properties of the five components may be combined to give a 6 x 6 diagonal inertia matrix for the complete assembly:

$$\begin{Bmatrix} F_G \\ 6 \times 1 \end{Bmatrix} = \begin{bmatrix} M \\ 6 \times 6 \end{bmatrix} \begin{Bmatrix} \ddot{\delta}_G \\ 6 \times 1 \end{Bmatrix} \quad (\text{XI.1})$$

where the vectors $\{F_G\}$ and $\{\ddot{\delta}_G\}$ contain the forces and accelerations in the X, Y and Z directions at point G. The combining together of the component data is shown in Fig. XI.6

In order to couple the damped springs to the assembly, it is necessary

to work in terms of receptances, and the corresponding receptance relation is

$$\begin{Bmatrix} \delta_G \\ \delta_G \\ \delta_G \end{Bmatrix}_{6 \times 1} = -\frac{1}{\omega^2} \begin{bmatrix} M \\ M \\ M \end{bmatrix}_{6 \times 6}^{-1} \begin{Bmatrix} F_G \\ F_G \\ F_G \end{Bmatrix}_{6 \times 1} \quad (\text{XI.2})$$

where the inversion of the diagonal matrix is accomplished simply by inverting its diagonal elements.

However, we require the receptance properties not at the centre of gravity G, but at the three coupling points A, B and C shown in Fig. XI.2. Considering the six possible force inputs at each point, the net force system acting at G is given by the relation

$$\begin{Bmatrix} F_G \\ F_G \\ F_G \end{Bmatrix}_{6 \times 1} = \begin{bmatrix} T_F \\ T_F \\ T_F \end{bmatrix}_{6 \times 18} \begin{Bmatrix} F_A \\ F_B \\ F_C \end{Bmatrix}_{18 \times 1} \quad (\text{XI.3})$$

This relation and the corresponding 18 co-ordinates are given in Fig. XI.7. Since the displacements at A, B and C are related to those at G by the transpose of the above transformation, we may write

$$\begin{Bmatrix} \delta_A \\ \delta_B \\ \delta_C \end{Bmatrix}_{18 \times 1} = -\frac{1}{\omega^2} \left(\begin{bmatrix} T_F^T \\ T_F^T \\ T_F^T \end{bmatrix} \begin{bmatrix} M \\ M \\ M \end{bmatrix}^{-1} \begin{bmatrix} T_F \\ T_F \\ T_F \end{bmatrix} \right) \begin{Bmatrix} F_A \\ F_B \\ F_C \end{Bmatrix}_{18 \times 1} \quad (\text{XI.4})$$

which relates the displacements at A, B and C to the corresponding forces.

We must now obtain the stiffness properties of the PVC facing pads, and the torsional stiffness of the face plate itself. The pad stiffnesses have been derived using simple elasticity theory, and they are listed in Fig. XI.8. The internal damping in the pads is introduced by making the compressive and shear moduli complex. Due to uncertainty as to the exact area of contact between the pad and the metal surfaces of the face plate and of the attached beam, one cannot possibly calculate the stiffnesses exactly. The compressive stiffness could have been expressed more correctly in terms

of the shape factor $(12)^*$, but by using $\nu = 0.495$ in the stiffness expressions derived, a more realistic stiffness is probably obtained, since it is about half the value obtained by considering the shape factor.

The torsional stiffness of the face plates of the assembled support has been calculated using a plate finite element programme. The division into triangular elements and the assumed loading are shown in Fig. XI.9. The assumption that the gusset plate provides a simple support ensures a lower bound on the stiffness. However, since there is not a true point connection on the face, the actual effective torsional stiffness can only be obtained approximately.

As the face plate stiffness K_{BB} and the rotational stiffness of the pad are in series, their total effective stiffness is given by

$$k'_{BB} = \frac{k_{BB} \cdot k_{BB \text{ FACE}}}{k_{BB} + k_{BB \text{ FACE}}} \quad (\text{XI.5})$$

If the 6 x 6 diagonal matrix of stiffnesses is $[K]$, the corresponding receptance matrix is $[K]^{-1}$, and this is obtained by inverting the diagonal elements of the stiffness matrix. By adding the pad/face plate receptance matrices to the receptance matrix (XI.4) for the rigid assembly, we obtain the overall receptance of the complete support. Upon inverting this relation, we finally obtain the dynamic stiffness matrix for the V-support with the pads:

$$\begin{Bmatrix} F_A \\ F_B \\ F_C \end{Bmatrix}_{18 \times 1} = \left(\begin{bmatrix} K^{-1} & 0 & 0 \\ 0 & K^{-1} & 0 \\ 0 & 0 & 0 \end{bmatrix} - \frac{1}{\omega^2} \begin{bmatrix} T_F^T \\ \\ \end{bmatrix} \begin{bmatrix} M^{-1} \\ \phantom{M^{-1}} \\ \phantom{M^{-1}} \end{bmatrix} \begin{bmatrix} T_F \\ \\ \end{bmatrix} \right)^{-1} \begin{Bmatrix} \tilde{\delta}_A \\ \tilde{\delta}_B \\ \tilde{\delta}_C \end{Bmatrix}_{18 \times 1} \quad (\text{XI.6})$$

$\tilde{\delta}_c = \tilde{\delta}_c$

which relates the input forces at the three points to the displacements at those points. The displacement vectors $\{\tilde{\delta}_A\}$ and $\{\tilde{\delta}_B\}$ refer to the

* References for Appendices IX to XI are given on Page 430.

coupling points on the free faces of the two pads, whereas the vectors $\{\bar{\delta}_A\}$ and $\{\bar{\delta}_B\}$ in (XI.4) referred to the points on the upper faces of the rigid V-assembly.

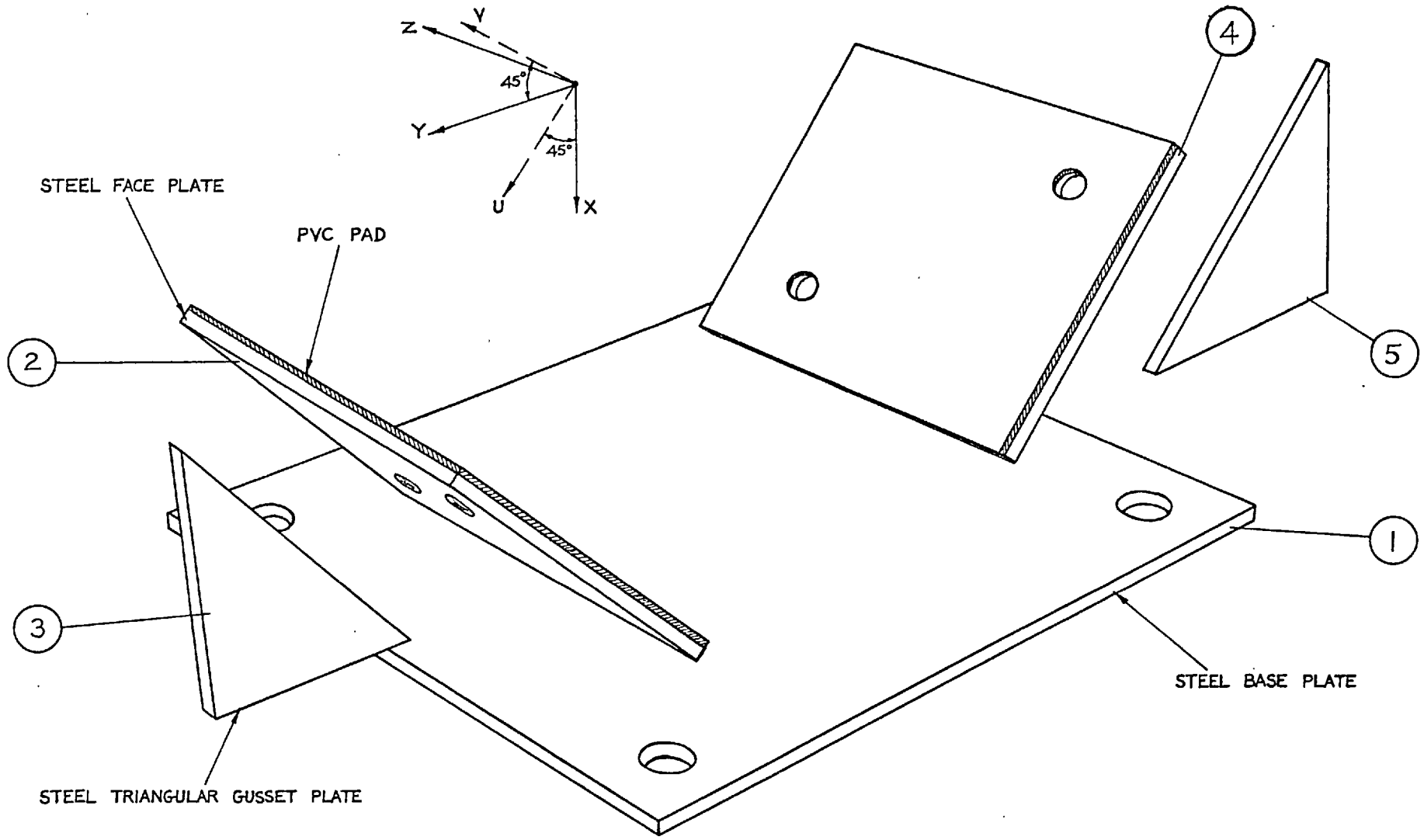
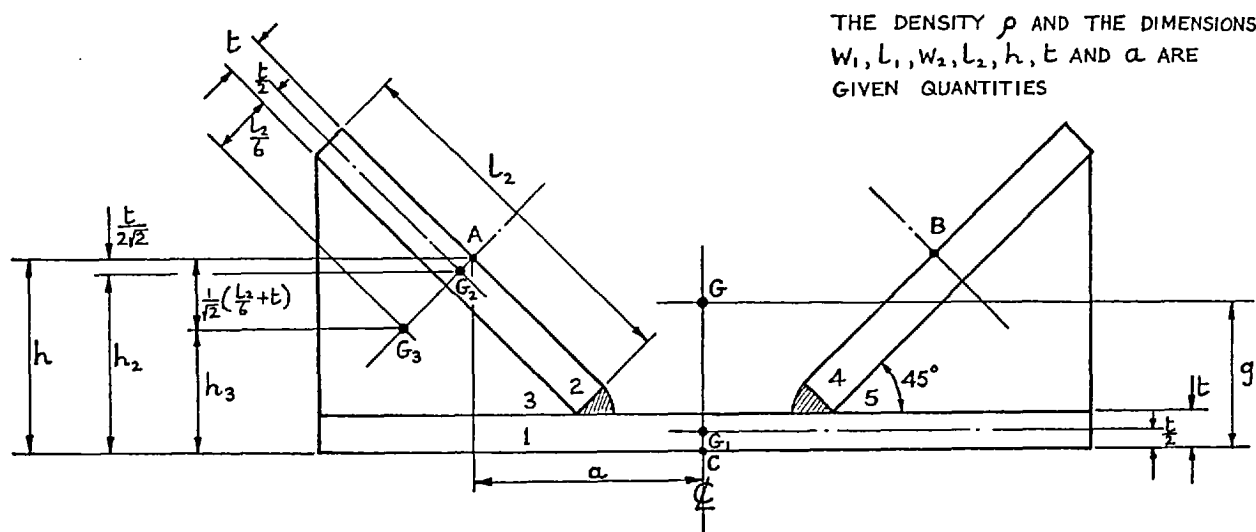


FIG. XI.1 EXPLODED VIEW OF V-SUPPORT



MASSES OF COMPONENT PARTS

$$m_1 = \rho t w_1 l_1 \quad m_2 = m_4 = \rho t w_2 l_2$$

$$m_3 = m_5 = \frac{\rho t l_2^2}{4}$$

$$\therefore \text{TOTAL MASS, } m = m_1 + 2(m_2 + m_3)$$

CALCULATED DIMENSIONS

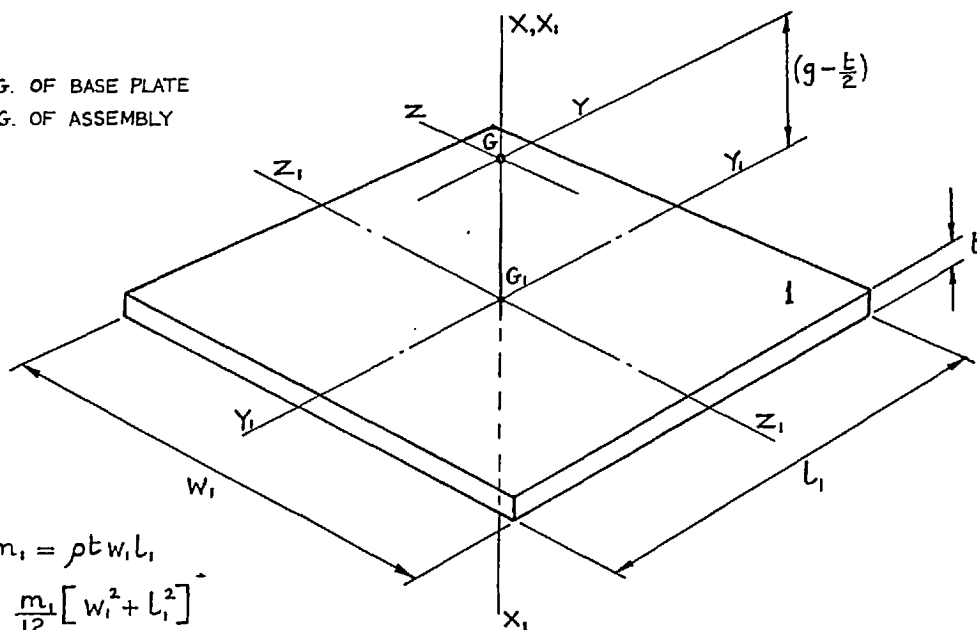
$$h_2 = h - \frac{t}{2\sqrt{2}}$$

$$h_3 = h - \frac{1}{\sqrt{2}} \left(\frac{l_2}{6} + t \right)$$

$$\text{HEIGHT OF C.G., } g = \frac{m_1 \frac{t}{2} + 2m_2 h_2 + 2m_3 h_3}{m}$$

FIG. XI.2 MASS AND CENTRE OF GRAVITY OF V-SUPPORT

G_1 IS C.G. OF BASE PLATE
 G IS C.G. OF ASSEMBLY



$$\text{MASS, } m_1 = \rho t w_1 l_1$$

$$I_{xx}^{(1)} = \frac{m_1}{12} [w_1^2 + l_1^2]$$

$$I_{yy}^{(1)} = m_1 \left[\frac{w_1^2}{12} + \left(g - \frac{t}{2} \right)^2 \right]$$

$$I_{zz}^{(1)} = m_1 \left[\frac{l_1^2}{12} + \left(g - \frac{t}{2} \right)^2 \right]$$

FIG. XI.3 INERTIAL PROPERTIES OF BASE PLATE OF V-SUPPORT (REFERRED TO X-Y-Z AXES)

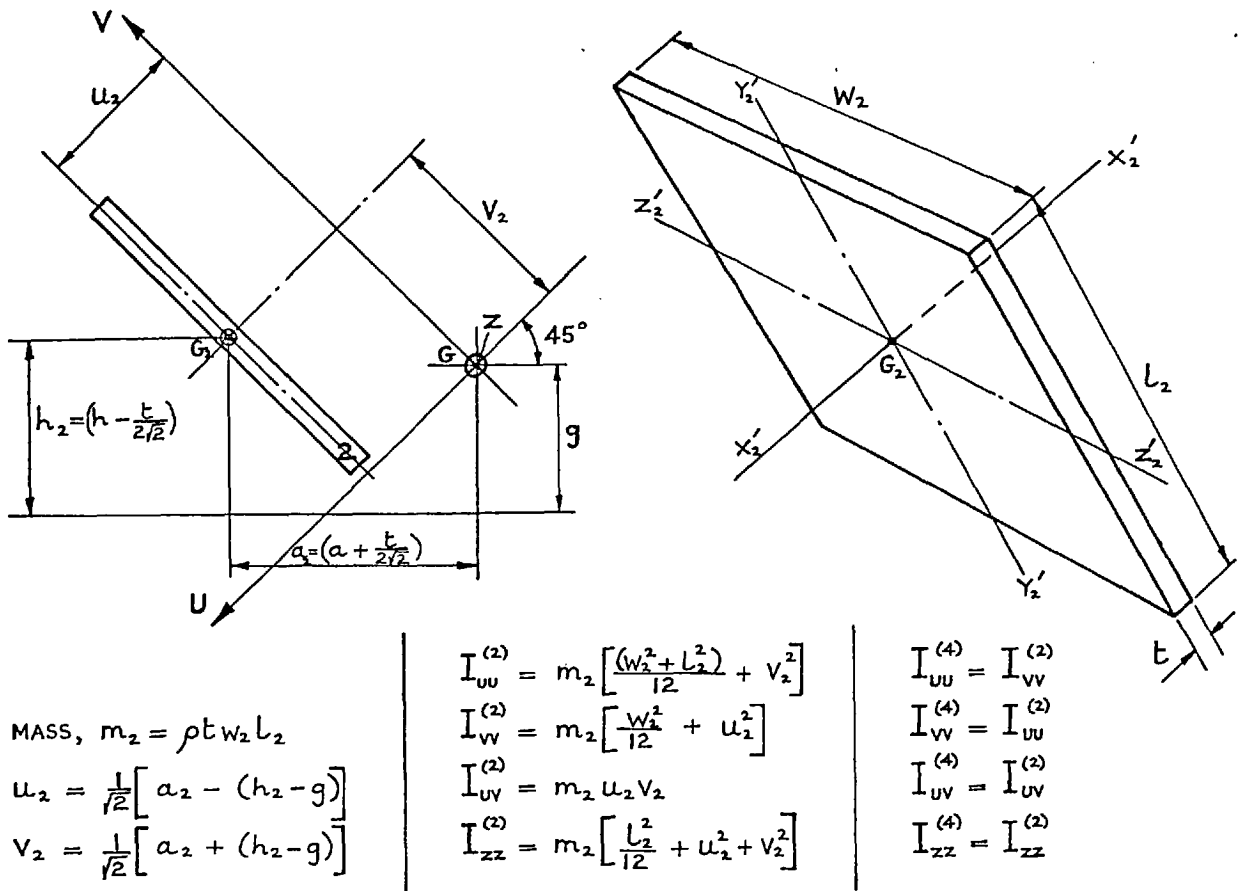


FIG. XI.4 INERTIAL PROPERTIES OF FACE PLATES OF V-SUPPORT (REFERRED TO U-V-Z AXES)

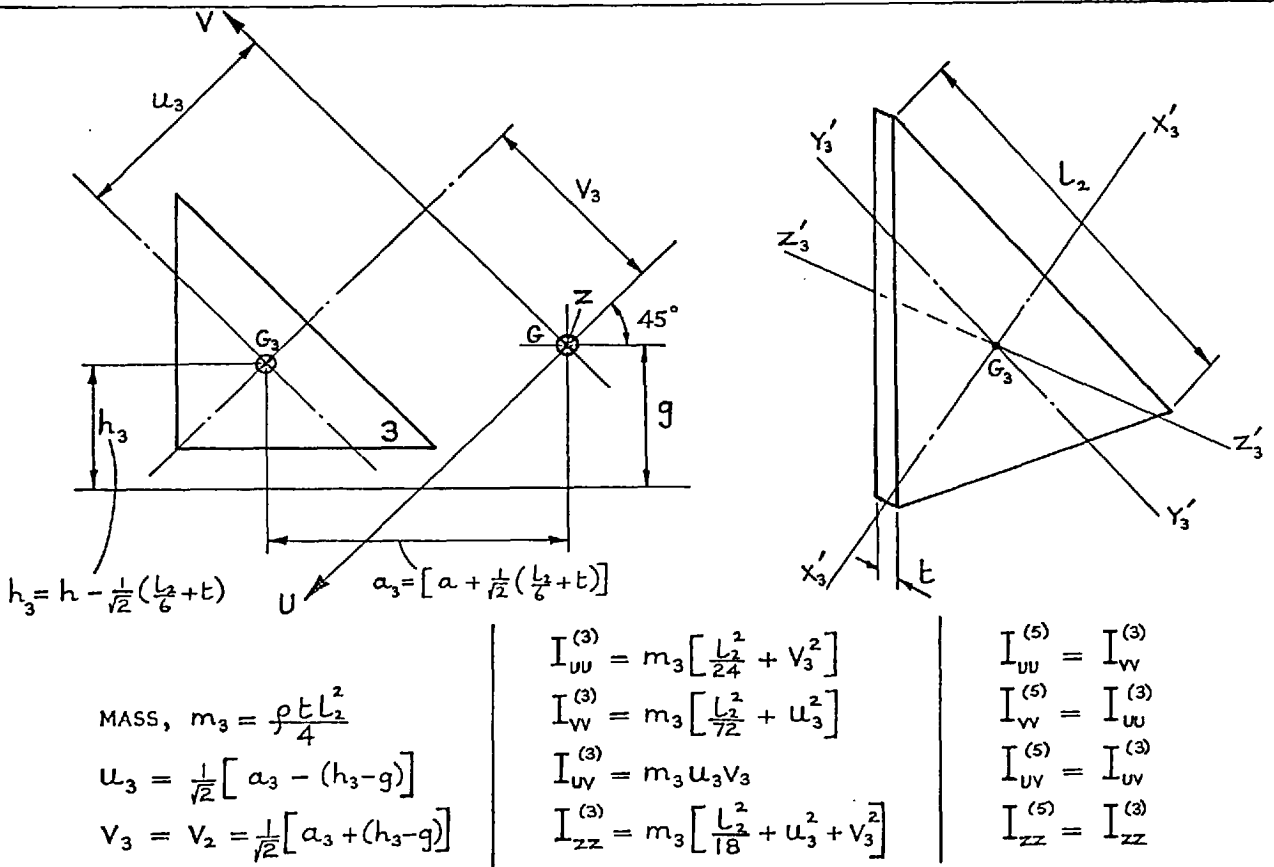


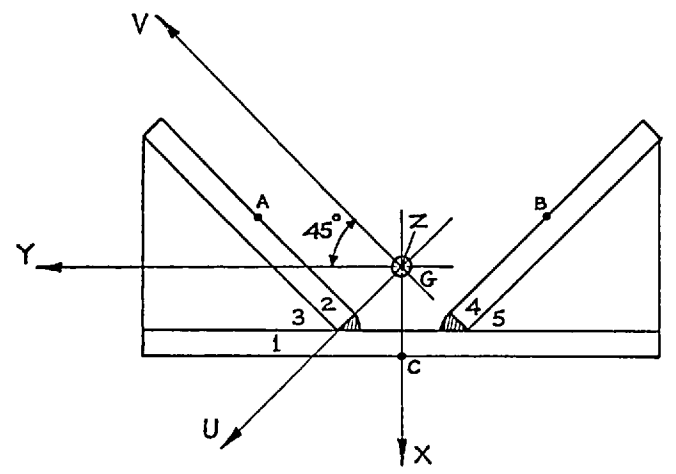
FIG. XI.5 INERTIAL PROPERTIES OF TRIANGULAR GUSSET PLATES (REFERRED TO U-V-Z AXES)

$$\begin{Bmatrix} F_x \\ F_y \\ F_z \\ M_\alpha \\ M_\beta \\ M_\theta \end{Bmatrix}_G = \begin{bmatrix} m & 0 & 0 & 0 & 0 & 0 \\ 0 & m & 0 & 0 & 0 & 0 \\ 0 & 0 & m & 0 & 0 & 0 \\ 0 & 0 & 0 & I_{xx}^{(1)} & 0 & 0 \\ 0 & 0 & 0 & 0 & I_{yy}^{(1)} & 0 \\ 0 & 0 & 0 & 0 & 0 & I_{zz}^{(1)} \end{bmatrix} + \begin{bmatrix} 0 & 0 & 0 & 0 & 0 & 0 \\ 0 & 0 & 0 & 0 & 0 & 0 \\ 0 & 0 & 0 & 0 & 0 & 0 \\ 0 & 0 & 0 & \frac{1}{\sqrt{2}} & -\frac{1}{\sqrt{2}} & 0 \\ 0 & 0 & 0 & \frac{1}{\sqrt{2}} & \frac{1}{\sqrt{2}} & 0 \\ 0 & 0 & 0 & 0 & 0 & 1 \end{bmatrix} \begin{bmatrix} 0 & 0 & 0 & 0 & 0 & 0 \\ 0 & 0 & 0 & 0 & 0 & 0 \\ 0 & 0 & 0 & 0 & 0 & 0 \\ 0 & 0 & 0 & I_{uu}^{(2,3,4,5)} & I_{uv}^{(2,3,4,5)} & 0 \\ 0 & 0 & 0 & I_{uv}^{(2,3,4,5)} & I_{vv}^{(2,3,4,5)} & 0 \\ 0 & 0 & 0 & 0 & 0 & I_{zz}^{(2,3,4,5)} \end{bmatrix} \begin{Bmatrix} \ddot{x} \\ \ddot{y} \\ \ddot{z} \\ \ddot{\alpha} \\ \ddot{\beta} \\ \ddot{\theta} \end{Bmatrix}_G$$

COMPOSITE MOMENTS OF INERTIA

$$\begin{aligned}
 I_{uu}^{(2,3,4,5)} &= I_{vv}^{(2,3,4,5)} = I_{uu}^{(2)} + I_{uu}^{(3)} + I_{vv}^{(2)} + I_{vv}^{(3)} \\
 I_{uv}^{(2,3,4,5)} &= 2(I_{uv}^{(2)} + I_{uv}^{(3)}), \quad I_{zz}^{(2,3,4,5)} = 2(I_{zz}^{(2)} + I_{zz}^{(3)})
 \end{aligned}$$

WHERE SUPERSCRIPTS ARE COMPONENT NUMBERS



THIS REDUCES TO THE DIAGONAL FORM GIVEN BELOW

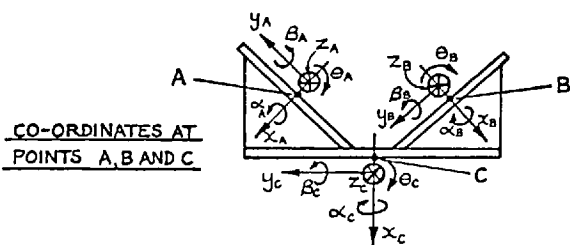
$$\begin{aligned}
 I_{xx} &= I_{xx}^{(1)} + (I_{uu}^{(2,3,4,5)} - I_{uv}^{(2,3,4,5)}) \\
 I_{yy} &= I_{yy}^{(1)} + (I_{uu}^{(2,3,4,5)} + I_{uv}^{(2,3,4,5)}) \\
 I_{zz} &= I_{zz}^{(1)} + I_{zz}^{(2,3,4,5)}
 \end{aligned}$$

$$\begin{Bmatrix} F_x \\ F_y \\ F_z \\ M_\alpha \\ M_\beta \\ M_\theta \end{Bmatrix}_G = \begin{bmatrix} m & & & & & \\ & m & & & & \\ & & & \text{ZERO} & & \\ & & & & m & \\ & & & & & I_{xx} \\ \text{ZERO} & & & & & & I_{yy} \\ & & & & & & & I_{zz} \end{bmatrix} \begin{Bmatrix} \ddot{x} \\ \ddot{y} \\ \ddot{z} \\ \ddot{\alpha} \\ \ddot{\beta} \\ \ddot{\theta} \end{Bmatrix}_G$$

$$\{F_G\} = [M_G] \{\ddot{\delta}_G\}$$

FIG. XI.6 6 x 6 INERTIA MATRIX FOR V-SUPPORT (REFERRED TO C.G.)

$\begin{Bmatrix} F_{xG} \\ F_{yG} \\ F_{zG} \\ M_{\alpha G} \\ M_{\beta G} \\ M_{\theta G} \end{Bmatrix} =$	1	2	3	4	5	6	7	8	9	10	11	12	13	14	15	16	17	18	$\begin{Bmatrix} F_{xA} \\ F_{yA} \\ F_{zA} \\ M_{\alpha A} \\ M_{\beta A} \\ M_{\theta A} \\ F_{xB} \\ F_{yB} \\ F_{zB} \\ M_{\alpha B} \\ M_{\beta B} \\ M_{\theta B} \\ F_{xC} \\ F_{yC} \\ F_{zC} \\ M_{\alpha C} \\ M_{\beta C} \\ M_{\theta C} \end{Bmatrix}$			
	$\frac{1}{\sqrt{2}}$	$-\frac{1}{\sqrt{2}}$	0	0	0	0	$\frac{1}{\sqrt{2}}$	$\frac{1}{\sqrt{2}}$	0	0	0	0	0	1	0	0	0	0		0	1	
	$\frac{1}{\sqrt{2}}$	$\frac{1}{\sqrt{2}}$	0	0	0	0	$-\frac{1}{\sqrt{2}}$	$\frac{1}{\sqrt{2}}$	0	0	0	0	0	0	1	0	0	0		0	0	2
	0	0	1	0	0	0	0	0	0	1	0	0	0	0	0	1	0	0		0	0	3
	0	0	a	$\frac{1}{\sqrt{2}}$	$-\frac{1}{\sqrt{2}}$	0	0	0	0	-a	$\frac{1}{\sqrt{2}}$	$\frac{1}{\sqrt{2}}$	0	0	0	0	1	0		0	0	4
	0	0	(h-g)	$\frac{1}{\sqrt{2}}$	$\frac{1}{\sqrt{2}}$	0	0	0	0	(h-g)	$-\frac{1}{\sqrt{2}}$	$\frac{1}{\sqrt{2}}$	0	0	0	-g	0	1		0	0	5
	$\frac{-a-(h-g)}{\sqrt{2}}$	$\frac{a-(h-g)}{\sqrt{2}}$	0	0	0	1	$\frac{a+(h-g)}{\sqrt{2}}$	$\frac{a-(h-g)}{\sqrt{2}}$	0	0	0	0	1	0	g	0	0	0		0	1	6



$$\{F_G\} = [T_F] \begin{Bmatrix} F_A \\ F_B \\ F_C \end{Bmatrix}$$

FIG. XI.7 EQUIVALENT FORCE SYSTEM AT C.G. OF V-SUPPORT IN TERMS OF FORCES APPLIED AT POINTS A, B AND C

PAD STIFFNESSES

$$k_{xx} = \frac{\bar{E} W_2 L_2}{t_p}$$

$$k_{yy} = \frac{G W_2 L_2}{t_p}$$

$$k_{zz} = k_{yy}$$

$$k_{\alpha\alpha} = \frac{G I_{xx}}{t_p}$$

$\frac{W_2 L_2 (W_2^2 + L_2^2)}{12}$

$$k_{\beta\beta} = \frac{\bar{E} L_2 W_2^3}{12 t_p}$$

$$k_{\theta\theta} = \frac{\bar{E} W_2 L_2^3}{12 t_p}$$

WHERE $\bar{E} = \frac{E(1-\nu)}{(1+\nu)(1-2\nu)}$

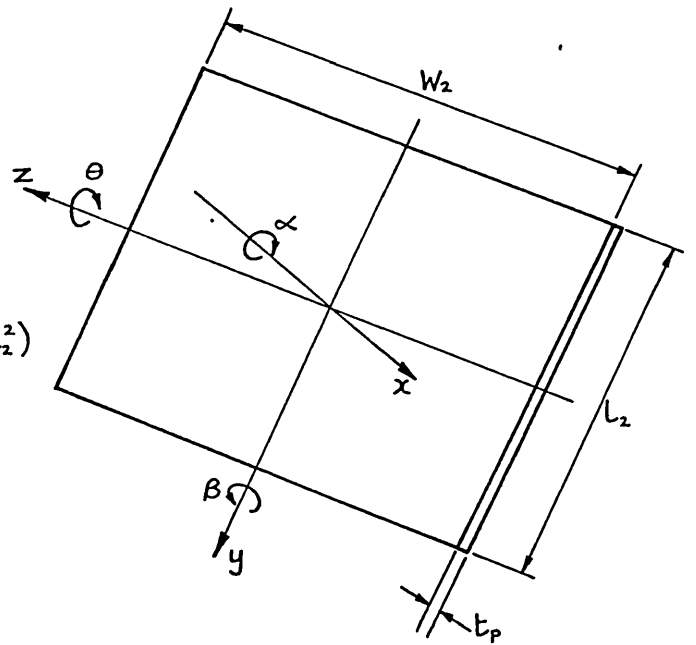


FIG. XI.8 STIFFNESSES OF PVC PAD FOR FACE PLATES

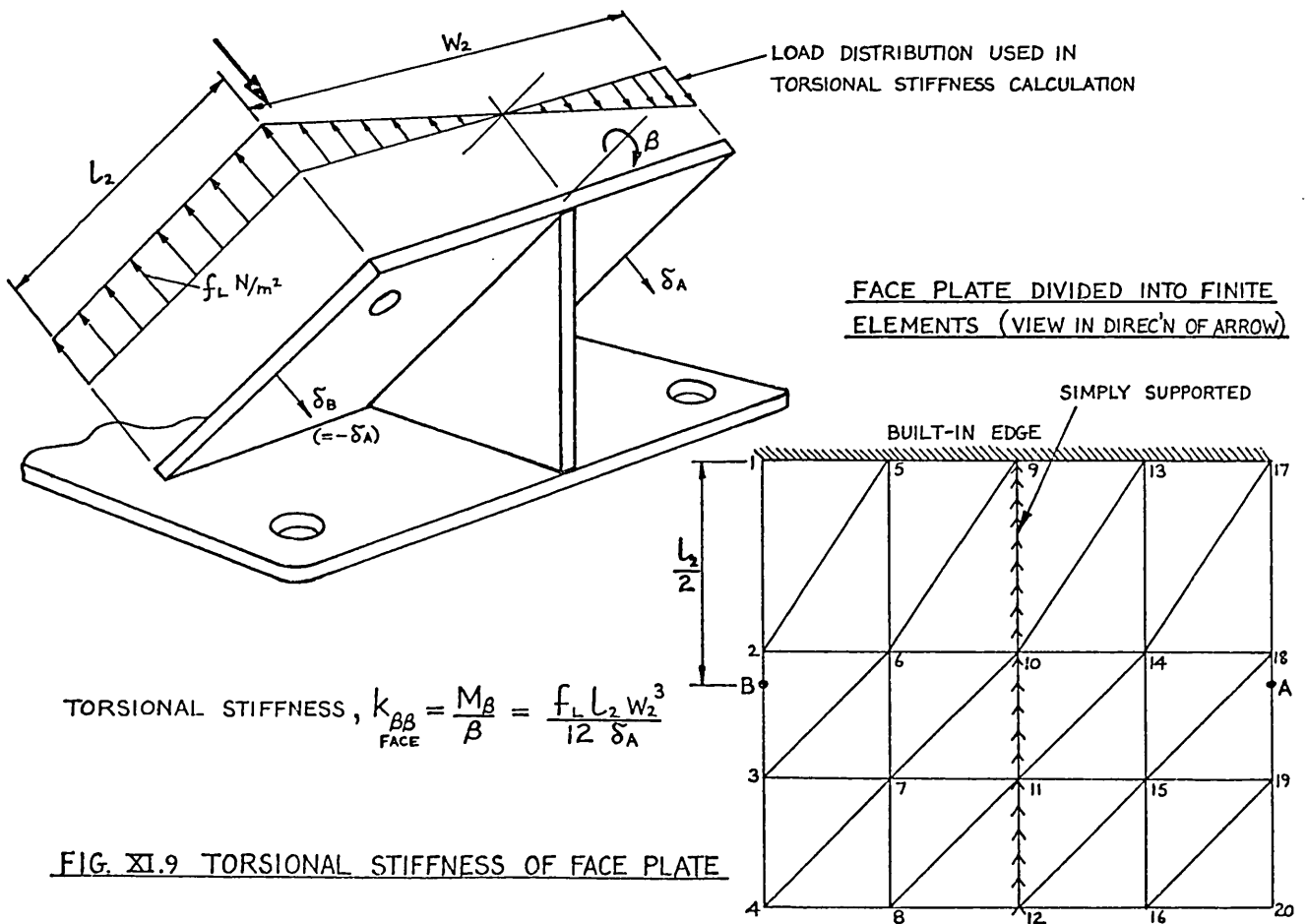


FIG. XI.9 TORSIONAL STIFFNESS OF FACE PLATE

PUBLICATIONS

- 1 MOBILITY MEASUREMENTS FOR THE VIBRATION
 ANALYSIS OF CONNECTED STRUCTURES

 by D.J. Ewins and M.G. Sainsbury

 Shock and Vibration Bulletin, Vol. 42,
 No. 1, 1972

- 2 VIBRATION ANALYSIS OF A DAMPED MACHINERY
 FOUNDATION STRUCTURE USING THE DYNAMIC
 STIFFNESS COUPLING TECHNIQUE

 by M.G. Sainsbury and D.J. Ewins

 Transactions of the American Society of
 Mechanical Engineers, Journal of Engineer-
 ing for Industry, August 1974, Page 1000

 Presented at the ASME Design Engineering
 Technical Conference, Cincinnati, Ohio,
 September 1973. Paper No. 73-DET-136

Bulletin 42
(Part 1 of 5 Parts)

REPRINTED FROM

THE
SHOCK AND VIBRATION
BULLETIN

JANUARY 1972

A Publication of
THE SHOCK AND VIBRATION
INFORMATION CENTER
Naval Research Laboratory, Washington, D.C.



Office of
The Director of Defense
Research and Engineering

MOBILITY MEASUREMENTS FOR THE VIBRATION ANALYSIS
OF CONNECTED STRUCTURES

D.J. Ewins and M.G. Sainsbury
Imperial College of Science and Technology,
London, England

The mobility or impedance coupling technique is widely used for the vibration analysis of structures which comprise an assembly of connected components. Its application is straightforward when the components are amenable to theoretical analysis, but if certain components are too complex to be analysed their mobilities must be obtained experimentally. Standard 'impedance' testing methods are generally inadequate for measuring the required multidirectional mobility data, and the work described in this paper is an attempt to develop techniques for obtaining such data. Measurements have been made on a freely supported beam and on a resiliently mounted block, and these data have been used to predict the response of the system formed by bolting the beam and the block together. The results illustrate the importance of obtaining sufficiently complete and accurate data if mobility measurements are to be used for the vibration analysis of connected structures.

INTRODUCTION

Vibration analysis of complex structures which comprise an assembly of connected components is often made using the mobility or impedance coupling technique. This approach permits analysis of each component individually and then couples them together by matching forces and velocities at each connection point, which is considerably more convenient than attempting to analyse the complete structure at once. It is in fact a standard technique in dynamic analysis. However, it often happens that one (or more) of the components is itself too complex to be analysed directly and for such a case, recourse may be made to an experimental approach in order to obtain the mobility data which is required for the analysis of the complete assembly. This paper is concerned with the development of experimental techniques suitable for measuring this data.

When the mobility coupling technique is applied analytically, it is customary to consider as many co-

ordinates at each connection point as are necessary to realistically describe the conditions at that junction. The motion of a point on a structure is completely defined by six co-ordinates, three translational and three rotational, but in the analysis of specific cases it is often possible to ignore some of these by virtue of the symmetry of the structure. In the simplest case where motion is known to occur in a single direction, such as a mass moving in a straight line, then only one co-ordinate is required. In practice, this degree of symmetry is seldom encountered, especially with the complex engineering structures that we are considering, so vibration analysis using a single co-ordinate is usually unrealistic. However, in many practical cases, motion is confined to a single plane involving vibration in three directions - two translation and one rotation - and for these it is necessary and sufficient to include three of the six co-ordinates in the analysis of vibration.

Such considerations are made regularly in theoretical vibration analysis

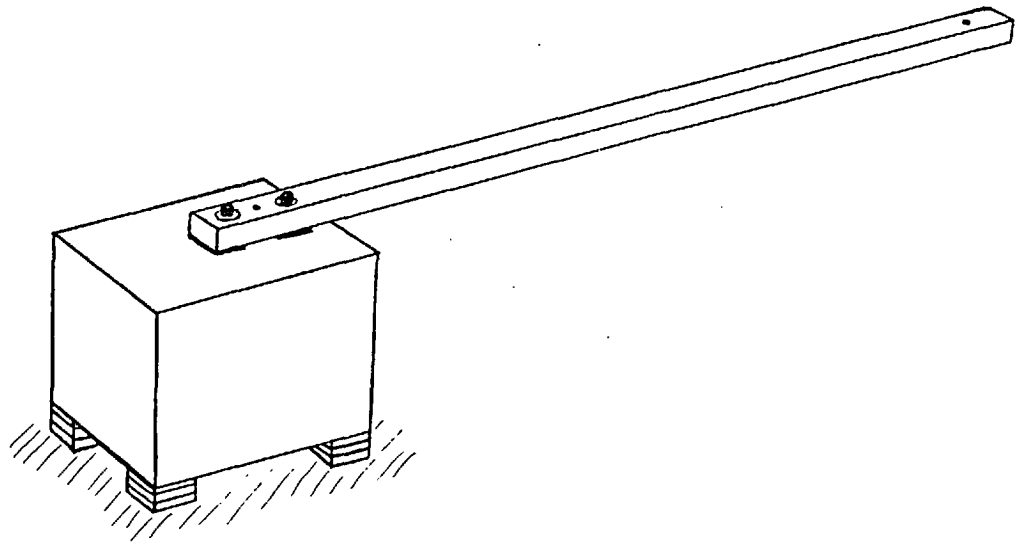


Fig. 1 BLOCK AND BEAM ASSEMBLY

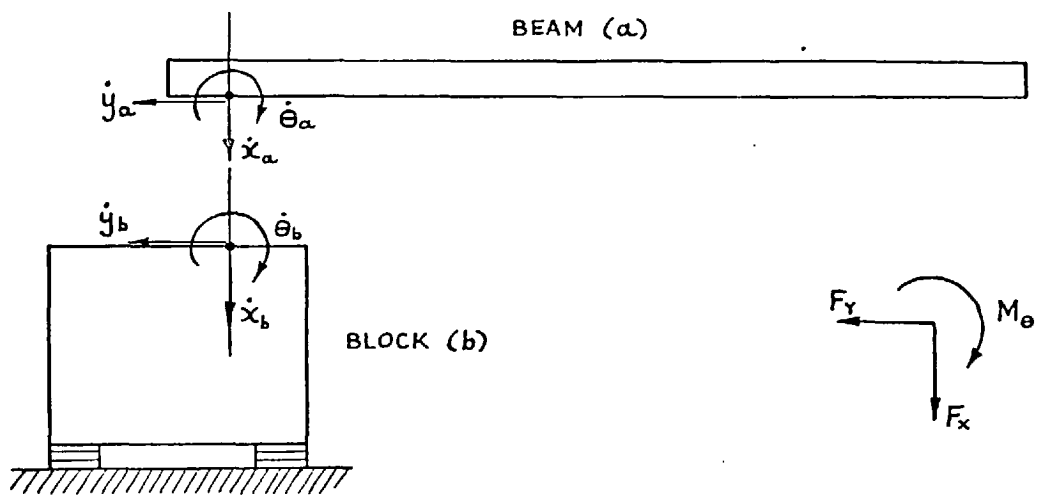


Fig. 2 CO-ORDINATES FOR COUPLING BEAM AND BLOCK

but are seldom included in those exercises which make use of experimental data for one of the components. Standard 'impedance' testing techniques are confined to measuring mobility in a single direction and are generally inadequate for the acquisition of such complete data as are required for a realistic analysis of a complex structure. This limitation has been identified already [1], [2] and previous work has demonstrated the difficulty and extent of the task of measuring the complete 6 x 6 mobility matrix for a structure [2]. However, as mentioned above, many practical structures do have a certain degree of symmetry and this permits us to confine our attention to motion in one plane and to consider only three co-ordinates at a time. The mobility data required in this case constitutes a 3 x 3 matrix which is considerably easier to handle than the complete 6 x 6 matrix.

This paper describes a case study made to assess the feasibility of using experimental data to analyse connected components and employs a particular structure composed of two components as an example. The first stage was to specify those mobility data which are required in order to analyse the vibrations of the assembled structure. Next, an experimental technique was developed for obtaining these data to the required accuracy. Finally, predictions of the dynamic characteristics of the assembled structure based on measurements of the individual components were compared with measurements made on the structure itself.

CASE STUDY

The structure treated in this study comprised two simple components. The first was a solid steel block 9" x 9" x 12" resting on four identical rubber pads, one under each corner, while the second was a uniform rectangular steel beam 1½" x 2" x 72". The assembled structure was formed by attaching the beam to the block in such a way as to obtain symmetry in one vertical plane but not in the other, as shown in Figure 1. Interest was confined to vibrations in the vertical plane containing the longitudinal axis of the beam, although a similar analysis could be made for motion in the other planes.

THEORETICAL APPROACH

In order to predict theoretically the vibration properties of the assem-

bly formed by these two components, use is made of the mobility coupling technique. By considering each of the components individually, we may derive mobility expressions for each of these which relate the velocities at the point of connection to forces and couples applied at that point. This data may be presented generally by the matrix equation:

$$\{\dot{X}\} = [Y]\{F\} \text{ or } \{F\} = [Z]\{\dot{X}\} \quad (1)$$

where $[Y]$ is the mobility matrix and $[Z] = [Y]^{-1}$ is the impedance matrix for that point on the structure, $\{\dot{X}\}$ is a vector of velocities in the co-ordinate directions included and $\{F\}$ is the vector of forces (or couples) in those directions. These matrices and vectors, and all those which follow, have complex elements in order to describe both the amplitude and the phase of the various quantities represented.

Equations for two components (a and b) connected together may be related by virtue of the fact that at the connection point their respective velocities must be identical, so that

$$\{\dot{X}_a\} = \{\dot{X}_b\} = \{\dot{X}\} \quad (2)$$

Furthermore, by considering equilibrium at the point of connection,

$$\{F_a\} + \{F_b\} = \{P\} \quad (3)$$

where $\{P\}$ is an externally applied force.

Combination of equations (2) and (3) leads to an expression for the mobility of the combined structure at the connection point $[Y_c]$:

$$[Y_c] = ([Y_a]^{-1} + [Y_b]^{-1})^{-1} \quad (4)$$

As mentioned earlier, as many as six co-ordinates may be necessary to define the motion of a point on a structure (in which case the order of these matrices and vectors would be 6), but in this case, as in many others, we may limit our interests to a limited number of these. Figure 2 shows the connection point for each component and indicates those co-ordinates and forces which should be included. Because of the symmetry of the structure, the other three co-ordinates (which include

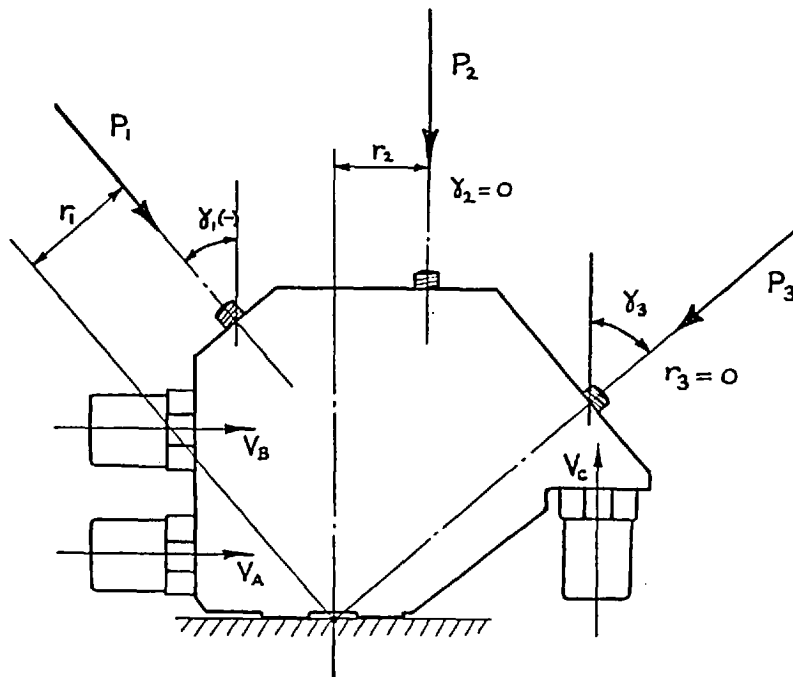


FIG. 3(a) EXCITING BLOCK MK 1 (Not to Scale)

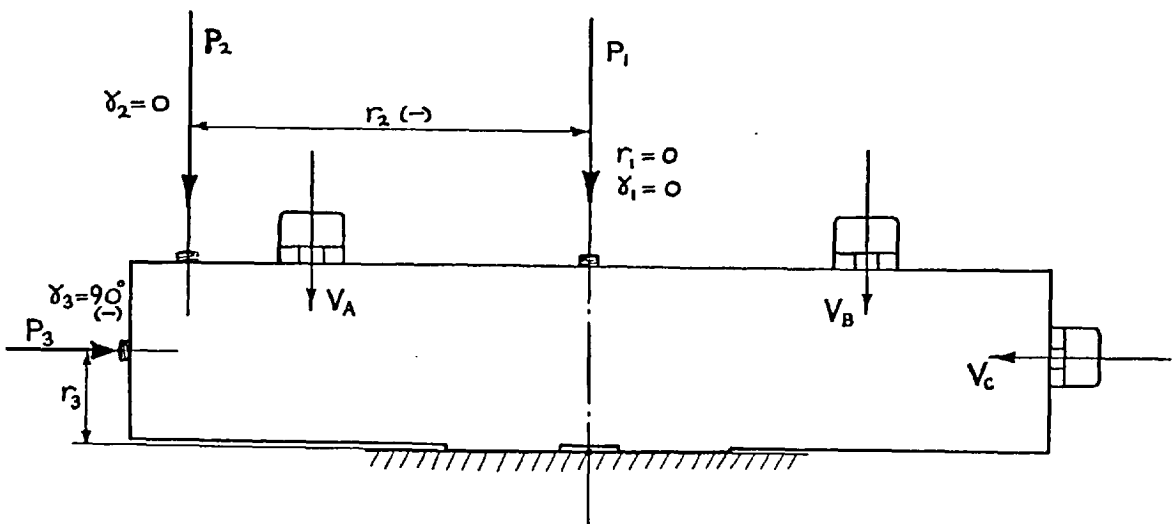


FIG. 3(b) EXCITING BLOCK MK 2 (Not to Scale)

motion out of the plane of the paper) may be ignored in this analysis or, if required, treated separately. Thus the equations defining the mobility matrix above (1) are in this case:

$$\begin{Bmatrix} \dot{x} \\ \dot{y} \\ \dot{\theta} \end{Bmatrix} = \begin{bmatrix} Y_{xx} & Y_{xy} & Y_{x\theta} \\ Y_{yx} & Y_{yy} & Y_{y\theta} \\ Y_{\theta x} & Y_{\theta y} & Y_{\theta\theta} \end{bmatrix} \begin{Bmatrix} F_x \\ F_y \\ M_\theta \end{Bmatrix} \quad (5)$$

The object of this analysis is to predict the vibration characteristics of the complete assembly formed by the two components, and this information is contained in the assembly mobility, $[Y_c]$. It will be seen from equation (4) that this technique involves a number of matrix inversions and these can be the source of some difficulty in numerical applications. In the first instance, the component mobility matrices $[Y_a]$ and $[Y_b]$ become ill-conditioned and are difficult to invert at frequencies close to one of their respective natural frequencies. A similar limitation applies to the combined expression $([Y_a]^{-1} + [Y_b]^{-1})$ which also has to be inverted. Secondly, it is known that operations involving the mobility matrices can be sensitive to small errors in the individual mobility expressions, and this feature must be taken into account when experimental data is to be incorporated.

Theoretical expressions for the component mobility matrices were derived by standard methods [3], although it was necessary to use experimentally derived data for the dynamic stiffness and damping capacity of the rubber pads which support the steel block. Calculations were made using these expressions and the results are presented later in the paper. A further series of calculations were made to predict the mobility of the assembled structure, again using the mobility coupling technique, and these will also be presented and discussed later, together with corresponding results from the experimental approach.

EXPERIMENTAL APPROACH

We shall now consider a situation in which mobility data for the individual components are to be determined solely from experimental measurements, as opposed to theoretical analysis. This is a matter of necessity when dealing with particularly complex structures.

In exactly the same way that it was considered necessary to include

three co-ordinates in the theoretical approach, so it is necessary to include all three in an approach using experimental data. The requirement for such comprehensive data may not be met using conventional methods of measuring mobility (collectively referred to as 'impedance tests') as these are insufficiently developed to provide either the completeness or the accuracy demanded for this application. In all but very exceptional cases, mobility measurements are confined to those expressions which relate response to a translational force in a direction normal to the surface of the structure under test. The response to applied couples or in-plane forces is not generally measured so that the mobility matrices required here may not be obtained directly from current experimental methods.

One previous worker has attempted to measure the complete mobility matrix and has developed a twin shaker unit to apply either a direct force (with the two shakers in phase) or a couple (with them in antiphase) to the structure [2]. An alternative solution to the problem of rotational excitation is being explored in the design of a torsional electromagnetic shaker, but this is at an early stage of development. A third approach is provided by the technique described in this paper which is based upon the use of a single shaker and other standard impedance testing equipment with the minimum of specially designed attachments. The aim of this measurement technique is to determine the 3×3 structural mobility matrix described above in relation to the case study which is used here as an example, and is achieved in the following way.

There are nine elements of the mobility matrix to be determined and these are obtained by measuring the three responses (\dot{x} , \dot{y} and $\dot{\theta}$) to each of three different excitation conditions. Thus three tests over the chosen frequency range are required and in each of these the shaker is attached so that a different combination of the three reference forces (F_x , F_y and M_θ) is applied to the structure. Knowing these specific combinations, it is then possible to extract the responses to each of these forces individually and thus derive the required mobility matrix. Details of the specific shaker attachment arrangements used are discussed in the next section.

It is clear that whatever technique is employed to measure this mobility data, there is a vast quantity of

information to be handled. Essentially, all that is required from the exercise is a prediction of the vibration properties of the assembled structure and all the mobility measurements made on the separate components are of no inherent interest beyond that of enabling the calculation of the assembly properties. The mobility coupling process (i.e. application of equation (4)) is applied at each of a number of discrete frequencies using the component data measured at those frequencies. Thus it is convenient if such data are in a digital format rather than analogue (i.e. in the form of graphs). Since there is considerably more of this intermediate data than is eventually required to describe the assembly properties, it is most conveniently acquired and stored in digital form, either on punched tape or in the memory of a digital computer which is subsequently employed to carry out the matrix manipulations for extracting the required information. This requirement indicates the suitability of the digital transfer function analysers currently available which may be readily interfaced with a small digital computer to provide an automatic testing facility.

MEASUREMENT TECHNIQUE

Based upon the concept of a single shaker technique for measuring multidirectional mobility data, a number of specific configurations for attaching the shaker were investigated. It was necessary in all of these to attach an 'exciting block' to the point of interest on the structure and to connect the shaker to this block in different ways so as to exert the chosen excitation conditions to the structure. The first design for this block is illustrated in Figure 3(a). The shaker was attached to the block in each of the directions indicated by P_1 , P_2 and P_3 in turn, and the corresponding components of the excitations in the three directions (F_x , F_y and M_θ) are given by the matrix equation:

$$\begin{Bmatrix} F_x \\ F_y \\ M_\theta \end{Bmatrix}_i = \begin{Bmatrix} \cos \delta_i \\ \sin \delta_i \\ r_i \end{Bmatrix} P_i \quad \text{or} \quad \{F\}_i = \{\Gamma\}_i P_i \quad (6) \\ i=1,2,3$$

For each shaker position, measurements were made at specific frequencies of the input force and the three responses, and from the collected results of all three runs the required mobility expressions could be derived as follows. The response was measured at three convenient stations on the block and by

assuming the block to be rigid, these could be related to the response of the structure itself in the three reference directions by means of a simple geometric transformation:

$$\begin{Bmatrix} \dot{x} \\ \dot{y} \\ \dot{e} \end{Bmatrix} = [T] \begin{Bmatrix} V_A \\ V_B \\ V_C \end{Bmatrix} \quad \text{or} \quad \{\dot{x}\} = [T]\{V\} \quad (7)$$

For each excitation position, we may write

$$\{\dot{x}\}_i = [T]\{V\}_i = [Y]\{F\}_i \quad (8)$$

$$\therefore \{\dot{x}\}_i = [Y]\{\Gamma\}_i P_i$$

or

$$[T] \frac{1}{P_i} \{V\}_i = [Y]\{\Gamma\}_i \quad (9)$$

$$\therefore [T]\{Y_{app}\}_i = [Y]\{\Gamma\}_i$$

where $\{Y_{app}\}_i$ is a vector of apparent mobilities and $\{\Gamma\}_i$ is the force transformation vector for the i th excitation position. Combining the three equations for $i = 1, 2, 3$ gives

$$[T][Y_{app}] = [Y][\Gamma]$$

or

$$[Y] = [T][Y_{app}][\Gamma]^{-1} \quad (10)$$

relating the measured quantities with the required properties.

The first stage in assessing the suitability of the proposed exciting block design was a check on the sensitivity of the numerical manipulation described by equation (10) to realistic errors in the measured data. This was performed numerically by taking a specific mobility matrix for the structure, computing the apparent mobilities that would be observed in the three runs with the exciting block, polluting this data with random or systematic errors typical of those which might be expected from the experimental equipment used and then recomputing the structure mobility with this polluted data. It was soon found from this exercise that the exciting block shown in Figure 3(a) would not be suitable for obtaining the required mobility data because errors in measured quantities of the order to 0.01% in amplitude and 0.01° in phase were sufficient to generate large errors in the computed mobilities (in excess of 5 dB). Accordingly, alternative designs for the exciting block were investigated and the one finally adopted for all the tests reported here is shown in Figure 3(b). This has a

simpler transformation to the reference co-ordinates and the checks on error sensitivity described above indicated that a measurement accuracy of 1% in amplitude and 1° in phase was usually sufficient to maintain an accuracy of better than 1 dB in the mobility of the structure computed from equation (10).

In addition to the basic force transformation from the shaker positions to the reference co-ordinates, it was also considered necessary to allow for the presence of the exciting block and the transducers mounted on it between the force measuring transducer and the structure. By assuming the block to behave as a rigid mass, it is possible to incorporate this correction in the transformations described above and the complete equation relating measured and required data then becomes:

$$[Y] = [T][Y_{app}]([F] - j\omega[M][T][Y_{app}])^{-1} \quad (11)$$

where $[M]$ is an inertia matrix for the specific exciting block.

Consideration of mobilities in more than one direction leads to an appreciation of some of the limitations of conventional impedance testing. In particular, it is noted that if a structure is not symmetrical, or is not excited through its mass centre, there will often be a significant response in directions other than that in which the forcing is being applied. If this effect is not properly allowed for, erroneous results can easily be obtained. For example, in measuring the mobility at the end of a simple cantilever beam it is found that there is a significant rotational response to an applied transverse force. In most cases, the shaker and its connection are not completely free to accommodate this rotation and as a result, they impose a restraint on it. This is equivalent to applying a couple to the end of the beam in addition to the intended force. This couple is not measured, but the response which is measured is the sum of that generated by the force and the couple and is not the information which is sought. In order to overcome this difficulty, it is generally sufficient to incorporate a 'decoupling rod' between the shaker and the structure which has a low stiffness in all directions other than that in which it is desired to apply excitation [4] and accordingly, this has been adopted as standard practice in all tests of the current study. A series of measurements were made to indicate the importance of using such a device. The results are given in Figure 4 which shows measurements of the response of

the steel block using a range of decoupling rods and clearly demonstrates the limitations of a direct connection between the shaker and the structure.

In order to measure and process the data required in this exercise, a digital transfer function analyser (DTFA) was used in conjunction with a small digital computer to form an integrated system, described in reference [5]. Measurements were made at discrete frequencies in a chosen range (as opposed to a continuous sweep through that range) and the computer was programmed to select these frequencies, control the DTFA while it measured each of the transducer outputs in turn, and then store or output these results for subsequent processing. The amount of information which has to be acquired in order to derive the required mobility is considerably in excess of the actual data to be determined for the assembled structure. In order to compute the amplitude and phase of one mobility expression for the complete assembly, it is necessary to measure a total of 24 quantities on the components. Thus, while the information sought may be handled or presented in the form of a graph, the same is not true of the intermediate data and because of this it was decided that the automatic data handling facility was an essential feature of this measuring technique.

RESULTS

The measurements which were made on the individual components - the steel block on rubber pads and the freely supported beam - were carefully checked against theoretical predictions of their mobilities. Care was taken to ensure a high degree of accuracy throughout the experiment. The volume of the complete set of results (a total of 18 graphs for the two components) prohibits their inclusion here. However, two of the nine mobility expressions for each component are illustrated in Figures 5 and 6, for the block and beam respectively. In each case, the two examples shown represent the best and the worst correlation between theory and experiment, and apart from some difficulties encountered with signal noise at the low frequencies (below 50 Hz), the results are considered to be satisfactory.

The complete mobility data for the two components were then used in conjunction with equation (4) to predict the mobility of the assembled structure formed by connecting them together as shown in Figure 1. This process

derives the 3×3 mobility matrix for the assembled structure and from these data the specific information that is required may be extracted. In many cases the properties of greatest interest are the natural frequencies of the structure, and these may be conveniently described by a single mobility expression.

For the case being studied here, the direct mobility of the assembly in the x direction was computed from the component measurements and is shown in Figure 7 alongside the corresponding data obtained by measurements made direct on the assembled structure. There is an unexplained discrepancy between the two results in the magnitude of the third natural frequency (near 90 Hz) but otherwise the agreement is quite close. Perhaps the most significant result, however, is that illustrated in Figure 8 which again shows the mobility of the assembled structure predicted from the measured component mobilities, but in this case we have used the limited data which might be obtained from a conventional impedance test. This result is obtained by application of the mobility coupling technique but with only a single co-ordinate included in the analysis (in this case, the x co-ordinate). The errors in the natural frequencies predicted by this over simplified approach are quite striking, and they clearly indicate the need for the more complete data which has been measured by the method described above.

A final result given in Figure 9 shows the measured mobility of the assembled structure compared with that predicted entirely from theoretical analysis. Such an approach was only possible in this case because of the simplicity of the two components. The result illustrates the important point that even for such simple structures as were used in this study, agreement between theoretically predicted and experimentally measured characteristics is not remarkable. In fact, the data predicted from the component mobility measurements shows better agreement than that predicted from theory.

DISCUSSION

We have shown that it is both possible and practical to predict the vibration characteristics of an assembly of connected components using experimentally measured mobility data. However, it must be emphasised that such an approach is only reliable when the measured data is sufficiently com-

plete and accurate and this requirement is not usually satisfied by conventional impedance testing techniques.

At the outset of a theoretical vibration analysis it is necessary to consider which co-ordinates must be included in order to satisfactorily define the motion of the components concerned. Only exceptional cases demand all six co-ordinates at each point of connection between components, but on the other hand, very few may be treated with only a single co-ordinate. Exactly the same considerations must be made for an analysis which employs experimentally obtained data. There are many applications in which one or more components may not be analysed directly because of their complexity and for which experimental measurement of mobility data is undertaken. The majority of mobility measurements are made with standard 'impedance testing' techniques and these are often totally inadequate for the application of such data to a mobility coupling exercise. Standard testing is usually confined to a single direction - that normal to the structure in most cases - while mobility data in other directions can be of equal or even greater importance. This fact is illustrated by the case studied here where exclusion of the rotation co-ordinate, Θ , results in a marked deterioration in the quality of the predictions (cf. Figures 7 and 8).

While it is essential to include as many co-ordinates as are necessary, it is also important to ensure that the unimportant ones are omitted. The reason for this is that as the order of the matrices increases (by the inclusion of more co-ordinates in the analysis), so does the sensitivity of the numerical operations to small errors. Thus it is possible to gain no benefit from the inclusion of an extra co-ordinate (providing this is a relatively unimportant one) without simultaneously improving the accuracy of the measured quantities.

In the majority of cases, it will be necessary to measure mobility data in more than one direction. The two main problems encountered in making these measurements are (i) the application of a couple, and (ii) the application of in-plane forces, to the structure under test. The first of these may be overcome by using a torsional shaker or by using a twin shaker system but the second is very difficult to overcome. In some cases, it is possible to excite with a force parallel to the surface but raised above it by an amount sufficient to accommodate the

shaker. This gives rise to an applied couple in addition to the desired force and although this may be small, the response due to it could be of the same order of magnitude (even greater) as that due to the force. Thus unless the response to a couple (i.e. the rotational mobility data) is known, this technique must be used with a degree of caution.

One general solution to these difficulties is the experimental technique described in this paper, where it is accepted that the required mobility data may not be measured directly but must be extracted from a series of carefully controlled and designed experiments. By this approach, it is possible to determine the mobility matrix for a component using a single shaker in conjunction with an 'exciting block' which is attached to the test structure, and other standard equipment. However experience has shown that care must be exercised in the design of the exciting block in order to maintain an acceptable degree of accuracy in the final results. It is also an accepted feature of the technique that a large amount of data has to be measured, acquired and processed in order to obtain relatively little desired information. Since it is likely that this data is itself required for detailed analysis (as for the mobility coupling in this example), then it is convenient to present it in a digital format, readily stored on punched tape and available for further computation. Thus it was decided that an automatic instrumentation system based on a digital computer and digital transfer function analyser was necessary for efficient application of the technique.

CONCLUSIONS

It has been shown that vibration analysis of an assembly of connected structures may be made using experimentally measured mobility data for the components. However, this approach is only practicable when the measured data is sufficiently accurate and complete for the structure in question. This requirement demands the measurement of mobility data in more than one direction for most practical structures.

An experimental technique using a single shaker has been described for measuring mobility in up to three directions and this has been tested in a case study of two connected components. The results of the exercise confirm that the experimental method is

satisfactory and that the additional complexity involved in multi-directional measurement is essential to a realistic analysis of typical engineering structures.

ACKNOWLEDGEMENT

The authors wish to thank the Ministry of Defence (Admiralty Engineering Laboratory) for the sponsorship of the contract under which this work was conducted.

Thanks are also due to Solartron Ltd. who supplied the computer-controlled transfer function analyser for making the measurements.

REFERENCES

1. D.U. Noiseux and E.B. Meyer, "Applicability of mechanical admittance techniques," Shock and Vibration Bulletin, 38, 1968.
2. J.E. Smith, "Measurement of the total structural mobility matrix," Shock and Vibration Bulletin, 40, 1970.
3. R.E.D. Bishop and D.C. Johnson, The Mechanics of Vibration, Cambridge University Press, 1960.
4. Kerlin and Snowdon, "Driving Point Impedance of Cantilever Beams," JASA, Vol.47 No.1(Pt 2) 1970.
5. A. Martin and C. Ashley, "A computer controlled digital transfer function analyser and its application in automobile testing," Society of Environmental Engineers Symposium on Dynamic Testing, 1971.

THE EFFECT OF THE VIBRATOR - IMPEDANCE HEAD CONNECTION ON THE MEASURED DATA

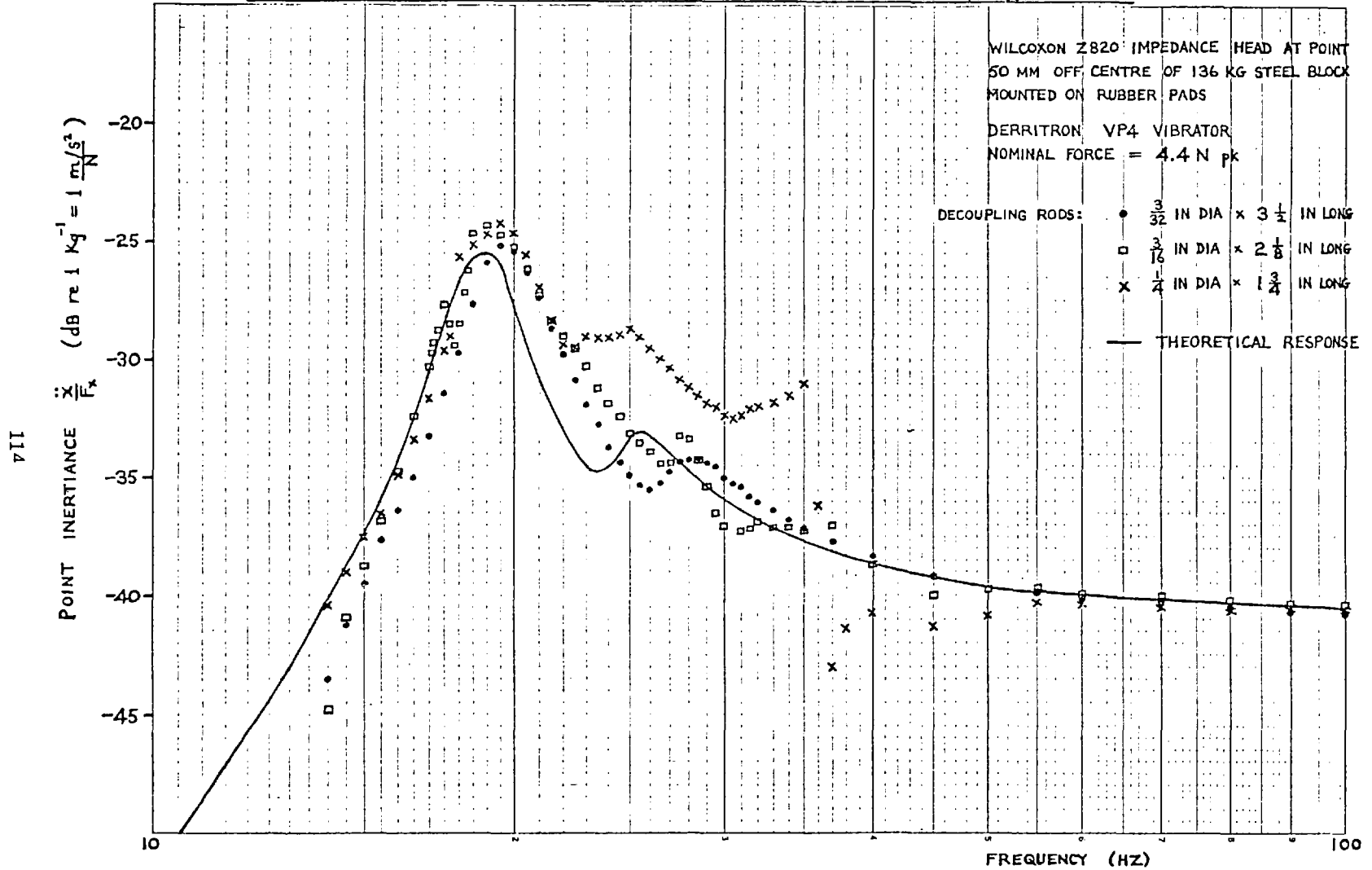


FIG 4

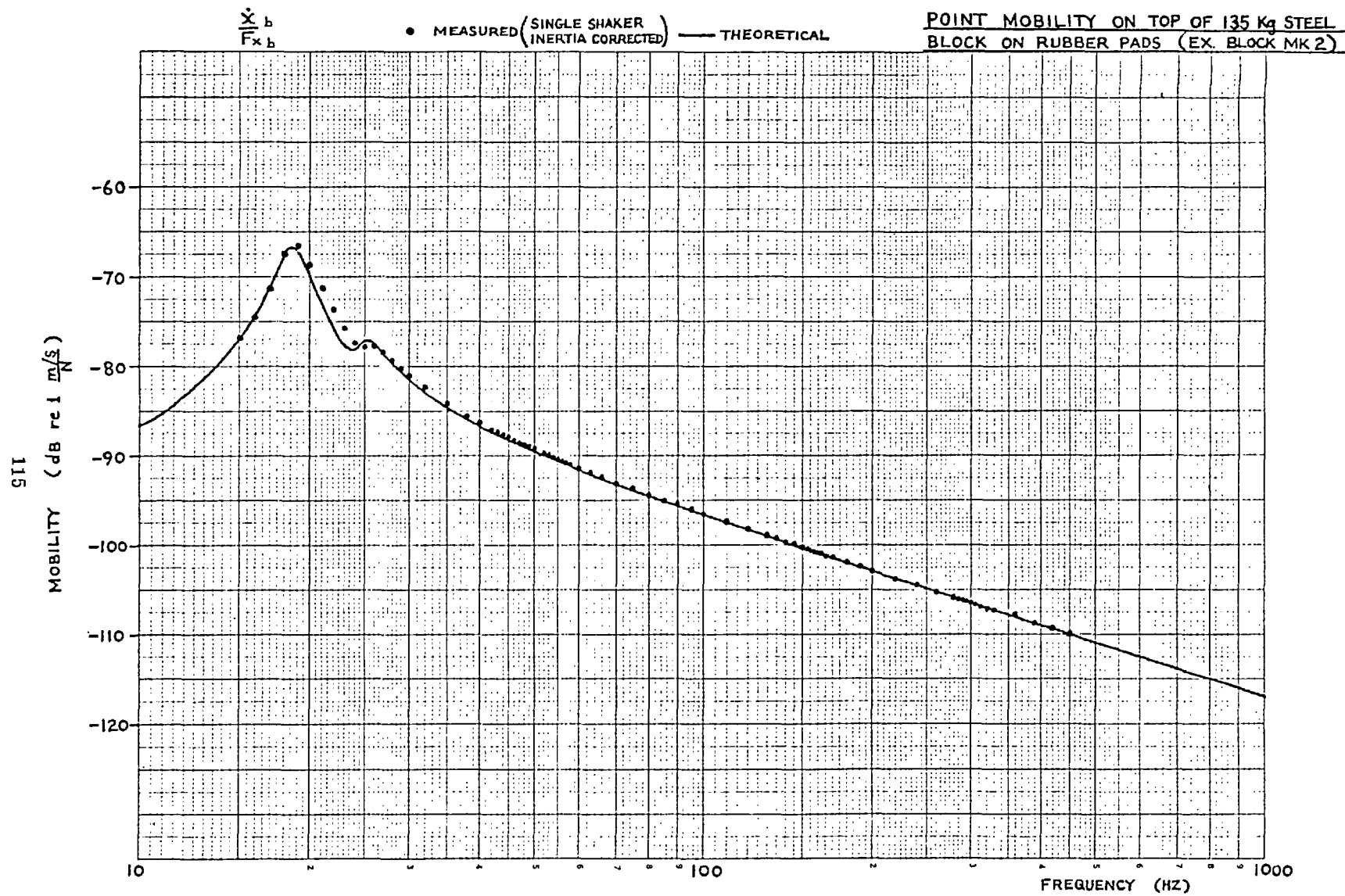


FIG. 5(-)

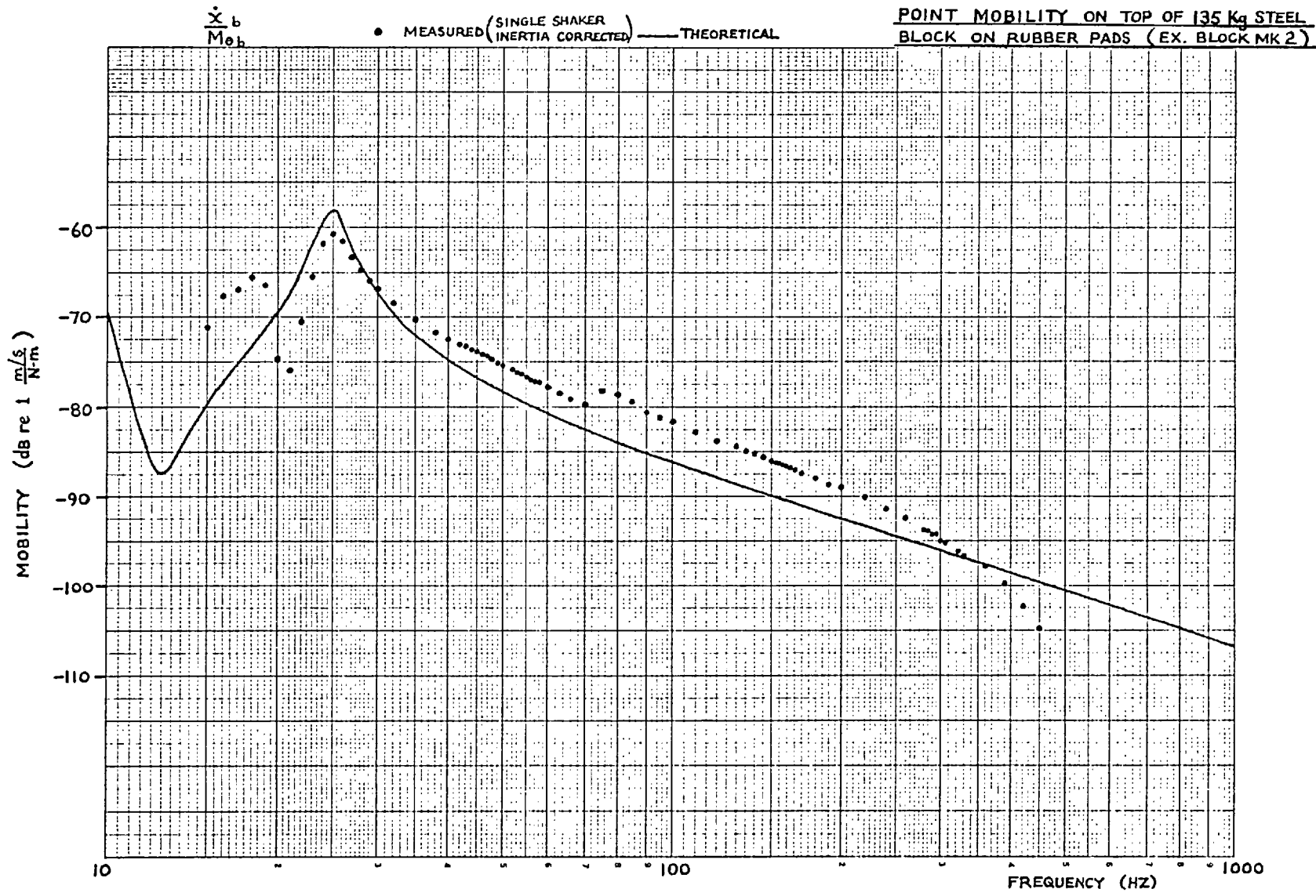


FIG. 5(b)

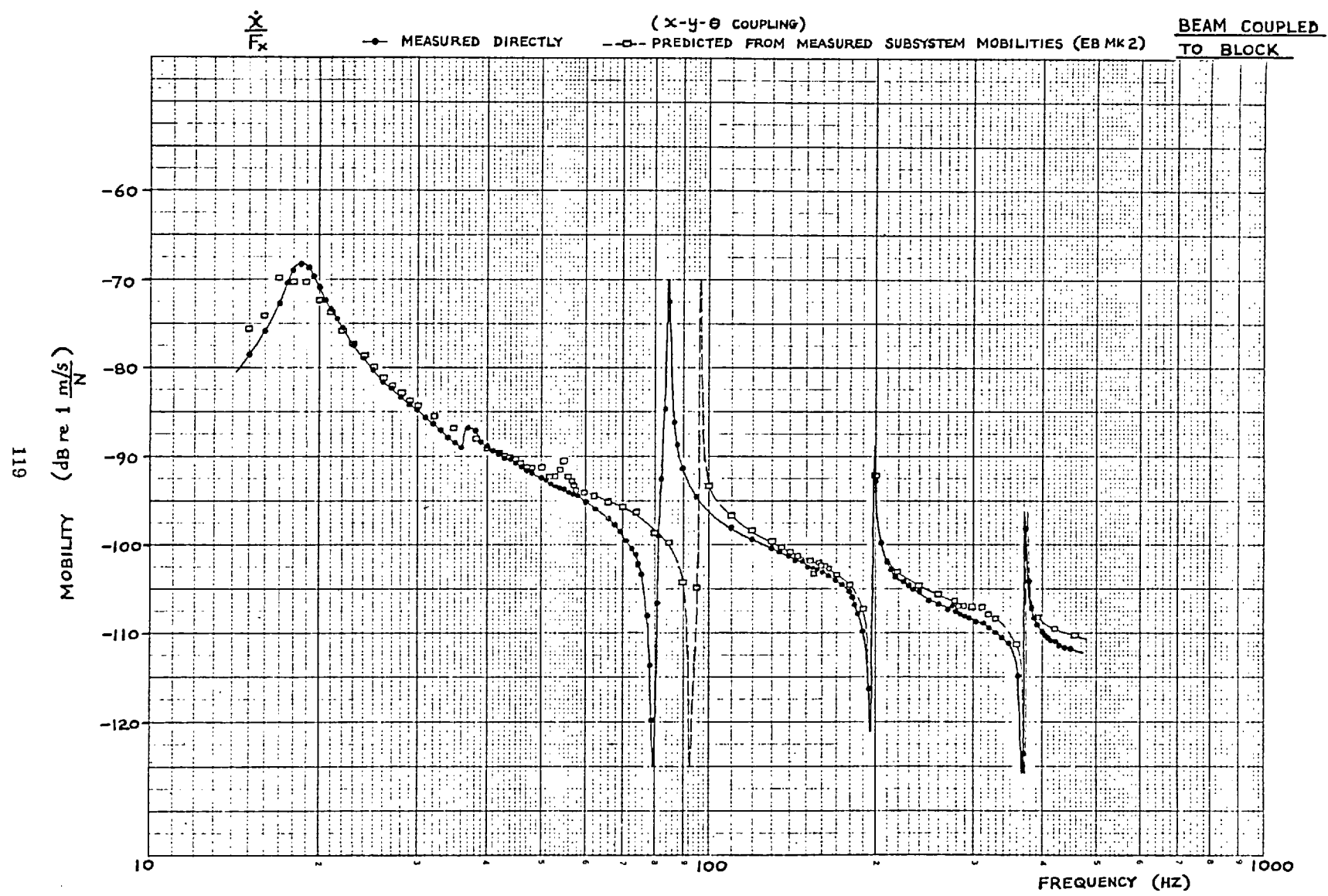


FIG. 7

120

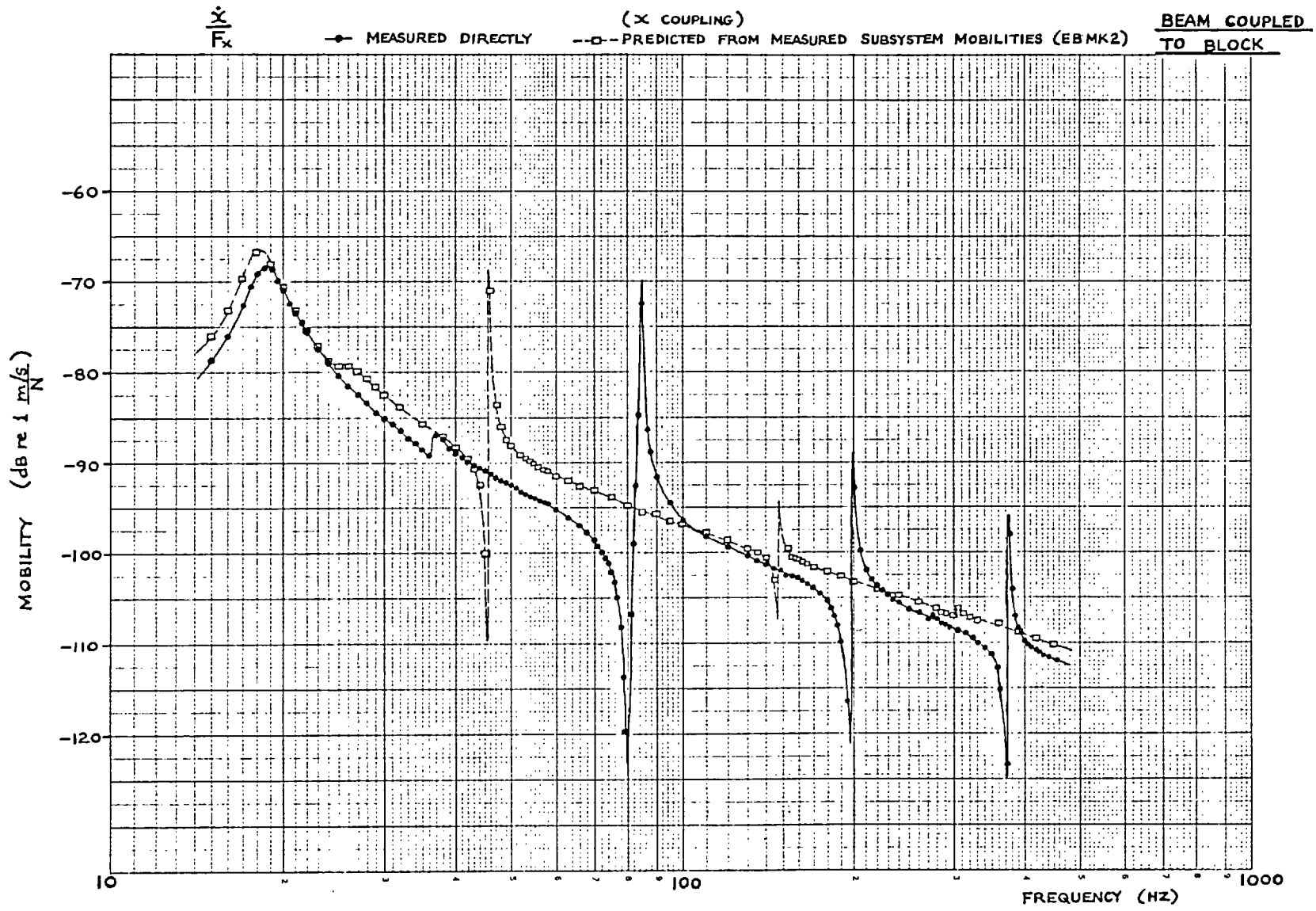


FIG. 8

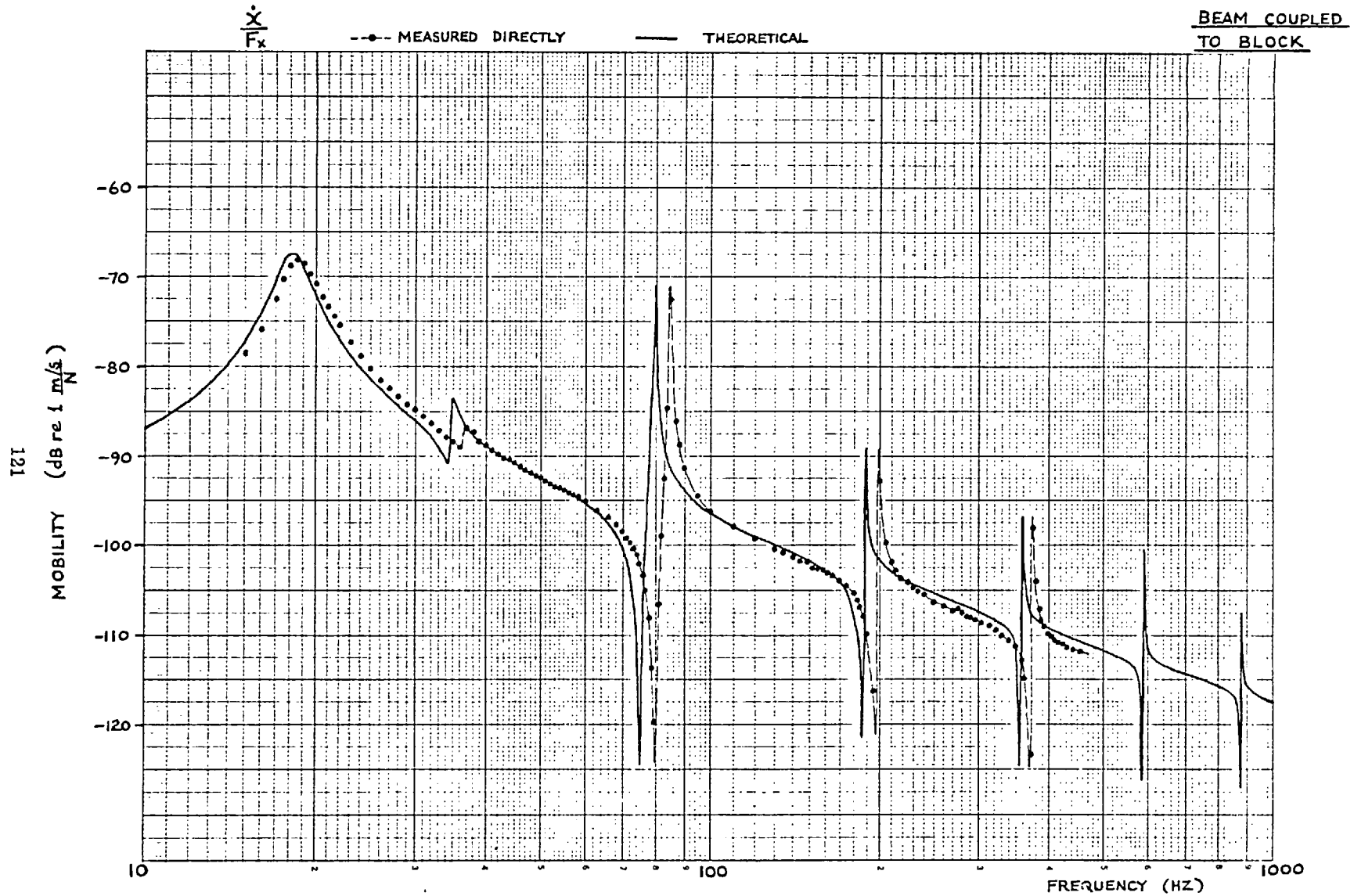


FIG. 9

DISCUSSION

Voice: Could you say something about the time required to compute the measurements from the raw data?

Mr. Ewins: On the full 3 x 3 matrix, we have not used the PDP-8 for that calculation. The system that you saw in the photograph was the preproduction prototype. There is only one in existence, and the store that is attached to it is not sufficient to do the matrix calculation. We have been using that for running the test, for storing the data and putting the data onto paper tape which we feed into our CDC computer. The actual computation time in a CDC is a matter of seconds - less than a minute. If we were to use the PDP-8, it is not sufficient to store all the data. We need an extra magnetic tape or extra disc storage. It would presumably take somewhat longer, but, using the PDP-8 to interface with a larger computer, it is a very short time -- on the order of a minute.

Mr. Bouche (Endevco): Is there some practical solution to your noise problems at low frequencies such as using accelerometers with higher sensitivity or narrow band filtering?

Mr. Ewins: The accelerometers that we used had a sensitivity of 300 picacoulombs per g. I do not think we could use more sensitive ones. The digital transfer function analyzer does the filtering in a quasi-digital manner. It handles a very high noise level very well. The problem was that the mobility levels we were measuring were so low at these low frequencies that they just could not be handled. The main difficulty on the beam example, where we had rather poor agreement between the theoretical curve and the measured one was that it was in the region of the first antiresonance where you have effectively zero mobility. It was in getting this antiresonance through that we ran into the noise problems at about 15 Hz. I think it was probably an extreme condition for the equipment to be tried on.



The Society shall not be responsible for statements or opinions advanced in papers or in discussion at meetings of the Society or of its Divisions or Sections, or printed in its publications.

\$3.00 PER COPY \$1.00 TO ASME MEMBERS

M. G. SAINSBURY

Research Assistant.

D. J. EWINS

Lecturer.

Department of Mechanical Engineering,
Imperial College,
London, England

Vibration Analysis of a Damped Machinery Foundation Structure Using the Dynamic Stiffness Coupling Technique

A detailed dynamic analysis is made of a heavily damped foundation structure designed for the multidirectional isolation of machinery vibrations. The principal components of the structure are damped sandwich beams and complex-shaped rubber blocks. In order to study the complete structure, each component was analyzed for its mechanical impedance data. Where possible, these were obtained theoretically, but in some cases it was necessary to resort to experimental measurement. The individual components were then connected together using the dynamic stiffness coupling technique in order to predict the vibration characteristics of the complete structure. The accuracy of the final results testifies to the feasibility of combining measured and theoretical data in this way in order to analyze a complex mechanical structure.

Introduction

It is now widely accepted that the practical problems of vibration isolation of machinery are not adequately described by the traditional one-degree-of-freedom concepts. A number of workers have considered the problem of vibration isolation of a nonrigid machine which has to be mounted on a nonrigid floor [1, 2, 3].¹ For this situation, a considerably more detailed form of analysis is required in order to predict the isolation afforded by the mounting. In this paper we describe one such analysis which has been made of an antivibration mounting for a diesel engine.

The engine (referred to as the source) had to be mounted on a relatively flexible and lightly damped receiver structure. Because the receiver was susceptible to vibration, it was important that the machinery foundation (interposed between the source and the receiver) should prevent vibrations generated within the engine from being transmitted to the receiver. It was also important that this isolation should be effective in *all* directions and not just the vertical. A foundation structure was designed which had the properties of flexibility in all directions while at the same time possessing no internal resonances which would seriously impair its isolation performance. The structure, which is described in detail below, was formed of heavily damped sandwich beams and rubber blocks.

In order to design this structure to have an optimum isolation performance, it was necessary to formulate a detailed mathematical model of it. With this, and data describing the dynamic properties of both the engine and the base structure, it would be possible to predict the transmission of vibrations from the engine through to the base. This paper describes the development of a vibration analysis for the foundation structure.

Method of Analysis

The philosophy underlying the vibration analysis used for this problem is sometimes referred to as the "building block" approach [4]. Its basis is to consider the structure as an assembly of connected components and to perform a detailed analysis of each component individually. The specific information sought from these analyses is the mechanical impedance² data for each component at all points where it is connected to other components in the assembled structure. The analysis of the complete structure is then achieved by suitable combination of the component impedance data.

The main advantage of this approach is that it enables each part of the system to be analyzed by whichever method is most convenient; some components inevitably being more amenable to theoretical analysis than others. In fact, it may well be that certain data is not readily determined by direct analysis, and in such cases, it may be expedient to resort to experimental measurement of impedance.

We have found it convenient to classify typical engineering components into three groups:

- 1 Components suitable for direct analysis, whose impedance

¹ Numbers in brackets designate References at end of paper.
Contributed by the Vibration and Sound Committee of the Design Engineering Division of the American Society of Mechanical Engineers for presentation at the Design Engineering Technical Conference, Cincinnati, Ohio, September 9-12, 1973. Manuscript received at ASME Headquarters June 11, 1973. Paper No. 73-DET-136.

² "Mechanical impedance data" is used here to indicate any of the various forms of structural frequency response such as mobility, dynamic stiffness, mechanical impedance, etc.

Copies will be available until June, 1974.

properties may be confidently predicted from theory.

2 Components for which predictions of impedance data need to be checked experimentally, or for which only part of the necessary data can be predicted from theory. This class requires some limited experimental measurement.

3 Components for which theoretical analysis is extremely difficult and for which experimental measurement of impedance data is essential.

In order to obtain a comprehensive analysis of the complete assembly, full use has been made of both theoretical and experimental techniques.

The method chosen to combine the various components was that of "dynamic stiffness coupling". In general terms, this is based on the principle that at any frequency the dynamic stiffness (or mechanical impedance) of a structure composed of two components connected together may be obtained by adding the dynamic stiffness (or impedance) of each component at the connection point. Thus impedance properties of the assembled structure may be expressed in terms of the corresponding properties of the individual components. A more detailed explanation of the coupling process is given below.

Application of this process to a specific case involves the acquisition and storage of the dynamic stiffness or impedance properties of each component at the various connection points and at a number of frequencies. Then, frequency by frequency, the stiffness coupling is applied at each junction and response properties of the assembled structure are derived. This method was chosen in favor of other more sophisticated modelling methods for a number of reasons. First, component properties were to be obtained from a number of sources—direct analysis, finite element modelling and experimental measurement—all of which could be readily adapted to provide the data as dynamic stiffness. Second, it was considered likely that it would be necessary to allow for material property variations in the frequency range of interest (10 to 1000 Hz), especially for the viscoelastic layers in the sandwich beams. This could not be so easily achieved with a mathematical procedure which required the component data as separate inertia and stiffness matrices, and which solved for the forced response by summing modal responses.

The Structure

We shall now describe the foundation structure in more detail

and the method used to obtain the required dynamic stiffness data for each component.

The structure is a highly damped machinery foundation, to be interposed between the vibration source and a receiver structure, and having multidirectional vibration isolation properties. It consists of two identical subsystems mounted on a fairly stiff base with the two subsystems each supporting one end of the engine. This study is confined to an analysis of one subsystem, an illustration of which is given in Fig. 1. It comprises six components: a pair of sandwich beams, a pair of rubber blocks and a pair of male V-pieces. There are thus three basic items which are designated UT, RB, and VB, respectively. The rubber blocks (RB) are attached to the base of the structure which is in turn connected to the receiver, and since they are considerably more flexible than the base, it is assumed in the analysis that they are effectively attached to rigid supports. The cross beams (UT) are bolted onto the rubber blocks, and the V-pieces (VB) sit in the "V" formed by the two beams. There is however no metal-to-metal contact between the V-pieces and the beams since there are 3.5 mm (0.138 in.) rubber pads separating them. The top faces of the V-pieces take the low-frequency engine mounts and are thus the input points of the foundation structure.

Cross Beams. The cross beams are of sandwich construction in order to ensure a high damping capacity and eliminate sharp resonances of the foundation structure. The sandwich is of the symmetrical 5-layer type, comprising 3 layers of aluminum and 2 of PVC, the latter material being chosen because of its high loss factor ($\eta = \frac{1}{Q} \approx 0.6$).

It may be readily appreciated that the configuration of the system is such that these beams are subjected to bending and torsion, and if accurate response predictions are to be made for the assembled structure up to relatively high frequencies, it is necessary to consider all 6 motions at each connection point on the beams. Although this is not uncommon in analyses using uniform beams, the authors are not aware of any such analysis having been carried out with highly damped sandwich beams. Practically all the standard references on sandwich beam vibration deal with the 3-layer type, with the usual textbook boundary conditions such as simply supported, etc., and certainly no mention is ever made of bending in the plane of the layers or of torsion about the beam axis. Only in references [5 and 6] are 5-layer beams considered, but the resulting equations have either been

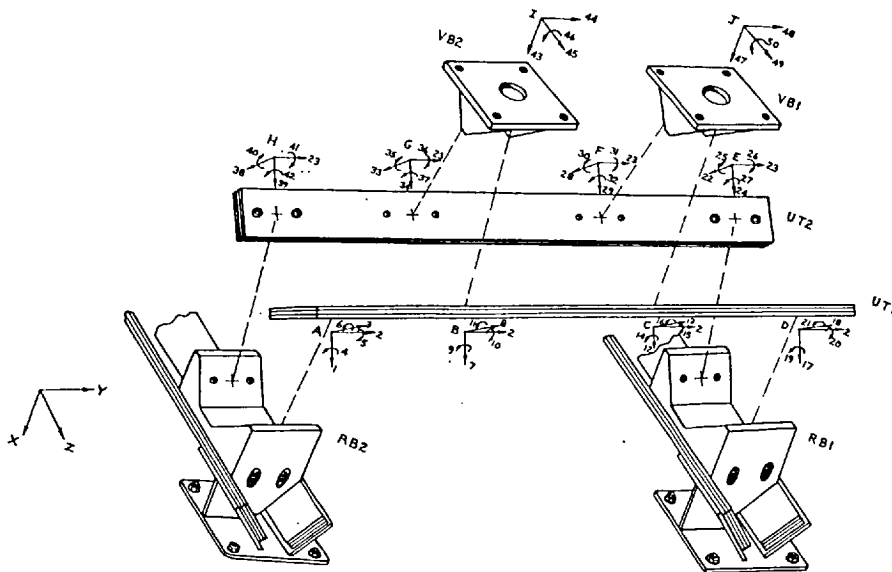


Fig. 1 Foundation structure

solved by the finite difference method or by Rayleigh-Ritz, again assuming the usual simple boundary conditions. In view of the lack of any suitable solution for the bending and torsional characteristics of the beams it was therefore necessary to examine sandwich beams in some depth, and to derive a solution in a form suitable for inclusion in the dynamic stiffness coupling procedure. The obvious choice was to use the finite element displacement method, since this approach yields stiffness matrices which may be utilized directly in the coupling process. Hence elements have been derived for flexure and for torsion of the symmetrical 5-layer beam, these having 7 and 8 deg of freedom, respectively. The derivation of the stiffness and inertia matrices for the flexural element is outlined briefly in Appendix 1, but it is hoped to give full details of this and of the torsional element at some future stage.

It was considered necessary to check the dynamic stiffness data predicted by this new finite element analysis against experimental measurement. In fact, it was only at a late stage that it was found possible to analyze the beam for torsional motion about its longitudinal axis and it was originally planned to obtain the relevant stiffness data from experiment. Thus, the beams fall into our category 2, above, where recourse was made to experimental data to check the validity of the analysis.

Fig. 2 shows theoretical and experimental values for four of the six direct mobility responses for point A on beam UT1 with the beam in a free-free condition. The $\frac{\dot{x}}{F_x}$, $\frac{\dot{\theta}}{M_\theta}$ and $\frac{\dot{z}}{F_z}$ theoretical curves were obtained using the flexural finite element, but in the

case of the last of these, the beam was assumed solid and undamped, and only layers 2 and 4 were used, thereby permitting the inclusion of shear distortion. The $\frac{\dot{\beta}}{M_\beta}$ theoretical curve was

obtained using the torsional finite element. The measured $\frac{\dot{z}}{F_z}$ data were obtained with an impedance head, while the other data were obtained by the multidirectional measurement technique outlined in Appendix 2. The good agreement between experiment and theory testifies to the adequacy of the finite element solution and of the measurement technique, and was obtained notwithstanding the use of measured data for the shear modulus of the PVC, which is frequency-temperature and strain-dependent.

Rubber Blocks. The rubber V blocks are solid and were molded from an almost natural rubber. Owing to their rather complex shape and to uncertainty about the exact dynamic properties of the rubber, it was necessary to resort to measurement in order to obtain their multidirectional dynamic stiffness characteristics (category 3 in the foregoing). However, in order to avoid having to measure the complete six-directional stiffness matrix for each face of the block it was decided to measure only selected linear and rotational mobilities and to use these data to model the block with an equivalent set of springs. Not only did such a procedure reduce the number of measurements required, but it also provided a means for examining the transmission of force into the

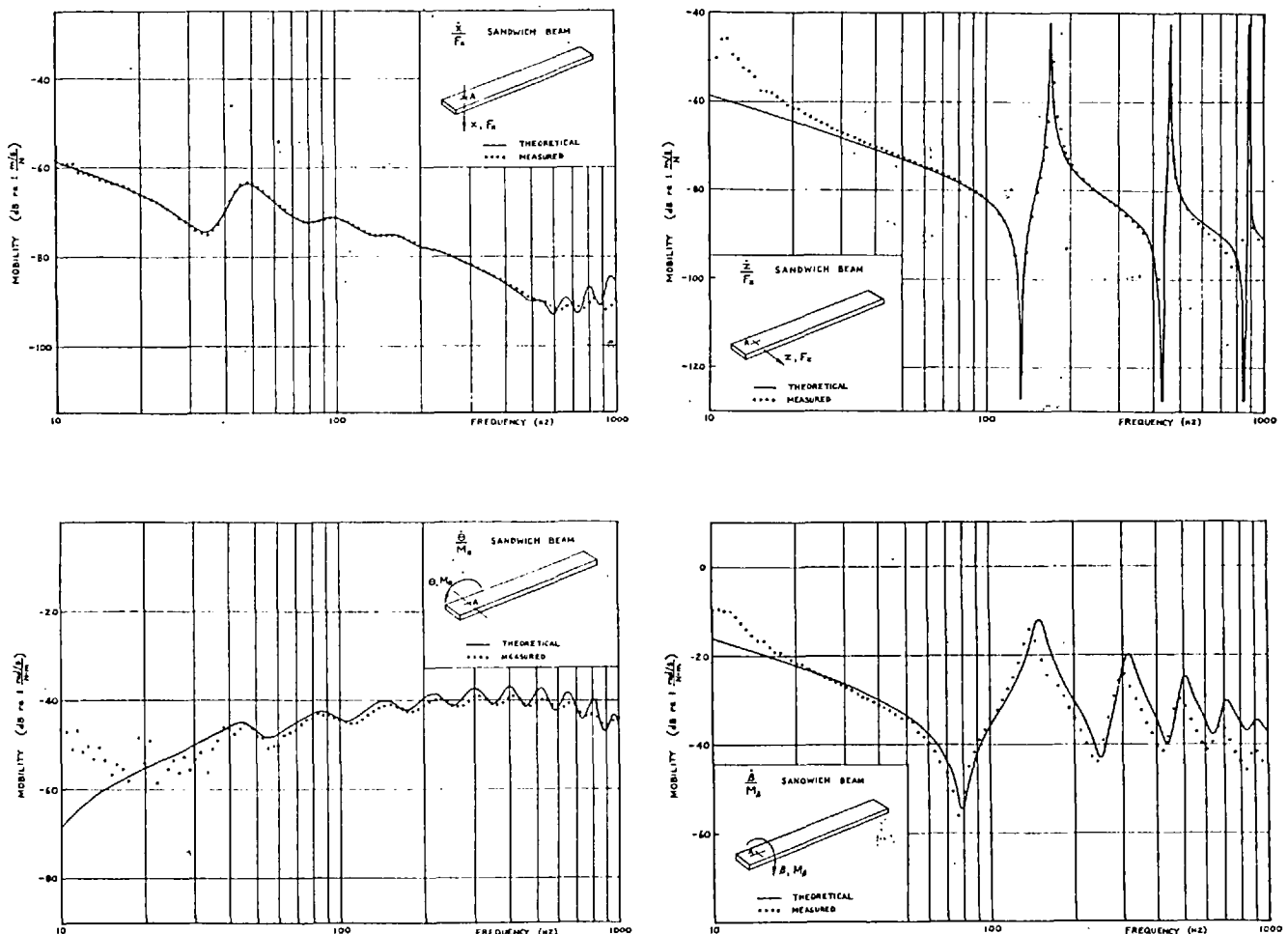


Fig. 2 Response curves for sandwich beam

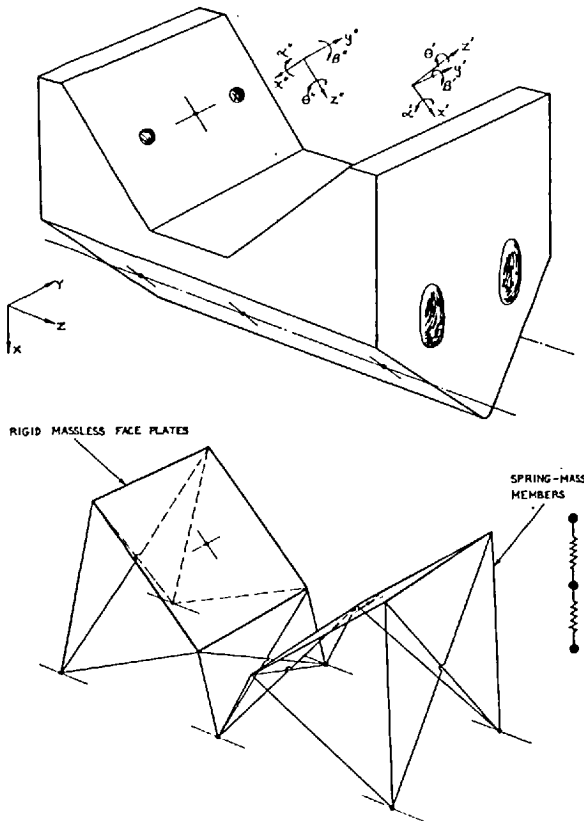


Fig. 3 Rubber block and its spring model

base structure. The block and the associated spring model are shown in Fig. 3. The dimensions of the model were chosen from a physical consideration of the likely directions of force flow through to the base, and the spring stiffnesses were chosen by a process of trial and error until reasonable agreement was obtained between the data measured on the faces of the block and that predicted by the model. An allowance was made for internal resonances of the block by lumping mass at the ends and midpoint of each spring.

V-Pieces. Each V piece is made of 25 mm (1 in.) steel plate, and consists of a top plate and two triangular plates which are welded to it. On the faces of the V are the 3.5 mm (0.138 in.) PVC pads which separate it from the cross beams. In the analysis, the steel V piece plus the pads have been considered as a single item. In view of its fairly stiff construction, and the way in which forces are applied to its top face, the steel piece was considered as a rigid body with six-directional inertial properties, and thus its response could be calculated relatively easily. The PVC pads were represented as hysteretically damped springs (linear and rotational), concentrated at a single point on each of the faces of the V. The spring stiffnesses were calculated using simple theory and the same measured data for the PVC properties as was used in the beam analysis.

Analysis and Results for the Assembled Structure

Having thus obtained the component data in a suitable form, the six components were then coupled together using a general-purpose computer program for dynamic stiffness coupling. The coupling procedure is outlined in Fig. 4, where the submatrices and vectors relate to the various connection points, and are of order 6 or less. At each frequency, dynamic stiffness data were derived for each of the six components; then, using force equilibrium and displacement compatibility relations, these component stiffnesses were combined to form the overall system dynamic stiffness matrix. This matrix relates the externally applied forces at each of the connection points to the corresponding

displacements, and for the present system was 50×50 and complex. The required displacement responses were obtained by inverting the matrix and multiplying by various force vectors. Using the response data for the top faces of the rubber block, the forces transmitted to the supporting structure could then be computed with a subsidiary program.

Frequency response information has been obtained over the relatively wide frequency range of 10 to 1000 Hz, and four selected response curves are shown in Fig. 5. Each of the computed curves is accompanied by the corresponding measured data, obtained from experiments on the assembled structure.

Figs. 5(a) and 5(b) show the velocity responses in directions normal to and up the face of block RB2 (coordinates 1 and 3) due to a vertical force applied slightly off the center of VB2. This input was represented theoretically by a force and a couple acting on coordinates 43 and 46, respectively. Fig. 5(c) and 5(d) show the responses in the same directions on RB2 when a horizontal force is applied on coordinate 45.

The four curves show quite good agreement between the measurements and the theoretical predictions, especially bearing in mind the complexity of the system. As one might expect, the results in the frequency range 10 to 100 Hz show better agreement than those at the higher frequencies, where the beam and V-piece assembly ceases to behave as a solid mass. The principal sources of error are thought to be inaccuracy in the measurement and modelling of the stiffness of the rubber blocks and the assumption of point coupling between the components.

Conclusions

In order to make a detailed vibration analysis of a complex mechanical structure, it has been found necessary to obtain de-

(a) DYNAMIC STIFFNESS MATRICES FOR COMPONENTS

$$\begin{aligned}
 & \text{UT1} & & \text{2 - UT2} \\
 \begin{Bmatrix} F_A^1 \\ F_B^1 \\ F_C^1 \\ F_D^1 \end{Bmatrix} &= \begin{bmatrix} Z_{AA}^1 & Z_{AB}^1 & Z_{AC}^1 & Z_{AD}^1 \\ Z_{BA}^1 & Z_{BB}^1 & Z_{BC}^1 & Z_{BD}^1 \\ Z_{CA}^1 & Z_{CB}^1 & Z_{CC}^1 & Z_{CD}^1 \\ Z_{DA}^1 & Z_{DB}^1 & Z_{DC}^1 & Z_{DD}^1 \end{bmatrix} \begin{Bmatrix} \delta_A \\ \delta_B \\ \delta_C \\ \delta_D \end{Bmatrix} & & \begin{Bmatrix} F_E^2 \\ F_F^2 \\ F_G^2 \\ F_H^2 \end{Bmatrix} = \begin{bmatrix} Z_{EE}^2 & Z_{EF}^2 & Z_{EG}^2 & Z_{EH}^2 \\ Z_{FE}^2 & Z_{FF}^2 & Z_{FG}^2 & Z_{FH}^2 \\ Z_{GE}^2 & Z_{GF}^2 & Z_{GG}^2 & Z_{GH}^2 \\ Z_{HE}^2 & Z_{HF}^2 & Z_{HG}^2 & Z_{HH}^2 \end{bmatrix} \begin{Bmatrix} \delta_E \\ \delta_F \\ \delta_G \\ \delta_H \end{Bmatrix} \\
 & \text{3 - RBI} & & \text{4 - RB2} \\
 \begin{Bmatrix} F_I^3 \\ F_J^3 \end{Bmatrix} &= \begin{bmatrix} Z_{II}^3 & Z_{IJ}^3 \\ Z_{JI}^3 & Z_{JJ}^3 \end{bmatrix} \begin{Bmatrix} \delta_I \\ \delta_J \end{Bmatrix} & & \begin{Bmatrix} F_K^4 \\ F_L^4 \end{Bmatrix} = \begin{bmatrix} Z_{KK}^4 & Z_{KL}^4 \\ Z_{LK}^4 & Z_{LL}^4 \end{bmatrix} \begin{Bmatrix} \delta_K \\ \delta_L \end{Bmatrix} \\
 & \text{5 - VBI} & & \text{6 - VB2} \\
 \begin{Bmatrix} F_M^5 \\ F_N^5 \\ F_O^5 \end{Bmatrix} &= \begin{bmatrix} Z_{MM}^5 & Z_{MN}^5 & Z_{MO}^5 \\ Z_{NM}^5 & Z_{NN}^5 & Z_{NO}^5 \\ Z_{OM}^5 & Z_{ON}^5 & Z_{OO}^5 \end{bmatrix} \begin{Bmatrix} \delta_M \\ \delta_N \\ \delta_O \end{Bmatrix} & & \begin{Bmatrix} F_P^6 \\ F_Q^6 \\ F_R^6 \end{Bmatrix} = \begin{bmatrix} Z_{PP}^6 & Z_{PQ}^6 & Z_{PR}^6 \\ Z_{QP}^6 & Z_{QQ}^6 & Z_{QR}^6 \\ Z_{RP}^6 & Z_{RQ}^6 & Z_{RR}^6 \end{bmatrix} \begin{Bmatrix} \delta_P \\ \delta_Q \\ \delta_R \end{Bmatrix}
 \end{aligned}$$

(b) DYNAMIC STIFFNESS MATRIX FOR SYSTEM

$$\begin{Bmatrix} F_A \\ F_B \\ F_C \\ F_D \\ F_E \\ F_F \\ F_G \\ F_H \\ F_I \\ F_J \\ F_K \\ F_L \\ F_M \\ F_N \\ F_O \\ F_P \\ F_Q \\ F_R \end{Bmatrix} = \begin{bmatrix} Z_{AA}^1 & Z_{AB}^1 & Z_{AC}^1 & Z_{AD}^1 & - & - & - & Z_{AH}^1 & - & - \\ Z_{BA}^1 & Z_{BB}^1 & Z_{BC}^1 & Z_{BD}^1 & Z_{BB}^1 & - & - & Z_{BB}^1 & - & Z_{BT}^1 & - \\ Z_{CA}^1 & Z_{CB}^1 & Z_{CC}^1 + Z_{CC}^3 & Z_{CD}^1 & - & - & - & - & - & Z_{CT}^1 & - \\ Z_{DA}^1 & Z_{DB}^1 & Z_{DC}^1 & Z_{DD}^1 + Z_{DD}^3 & Z_{DE}^1 & - & - & - & - & - & - \\ - & - & - & Z_{EE}^2 & Z_{EF}^2 & Z_{EG}^2 & Z_{EH}^2 & Z_{EE}^2 & Z_{EF}^2 & - & - \\ - & - & - & - & Z_{FF}^2 & Z_{FG}^2 & Z_{FH}^2 & Z_{FF}^2 & Z_{FG}^2 & - & - \\ - & Z_{GG}^2 & - & - & Z_{GG}^2 & Z_{GH}^2 & Z_{GH}^2 & Z_{GG}^2 & Z_{GH}^2 & - & - \\ Z_{HH}^2 & - & - & - & Z_{HH}^2 & Z_{HI}^2 & Z_{HI}^2 & Z_{HH}^2 & Z_{HI}^2 & - & - \\ - & Z_{II}^3 & - & - & - & Z_{II}^3 & - & - & Z_{II}^3 & - & - \\ - & - & Z_{JJ}^3 & - & - & - & - & - & - & Z_{JJ}^3 & - \\ - & - & - & Z_{KK}^4 & - & - & - & - & - & - & Z_{KK}^4 \\ - & - & - & - & - & Z_{LL}^4 & - & - & - & - & - \\ - & - & - & - & - & - & Z_{MM}^5 & - & - & - & - \\ - & - & - & - & - & - & - & Z_{NN}^5 & - & - & - \\ - & - & - & - & - & - & - & - & Z_{OO}^5 & - & - \\ - & - & - & - & - & - & - & - & - & Z_{PP}^6 & - \\ - & - & - & - & - & - & - & - & - & - & Z_{QQ}^6 \\ - & - & - & - & - & - & - & - & - & - & - & Z_{RR}^6 \end{bmatrix} \begin{Bmatrix} \delta_A \\ \delta_B \\ \delta_C \\ \delta_D \\ \delta_E \\ \delta_F \\ \delta_G \\ \delta_H \\ \delta_I \\ \delta_J \\ \delta_K \\ \delta_L \\ \delta_M \\ \delta_N \\ \delta_O \\ \delta_P \\ \delta_Q \\ \delta_R \end{Bmatrix}$$

Fig. 4 Dynamic stiffness coupling of the six components

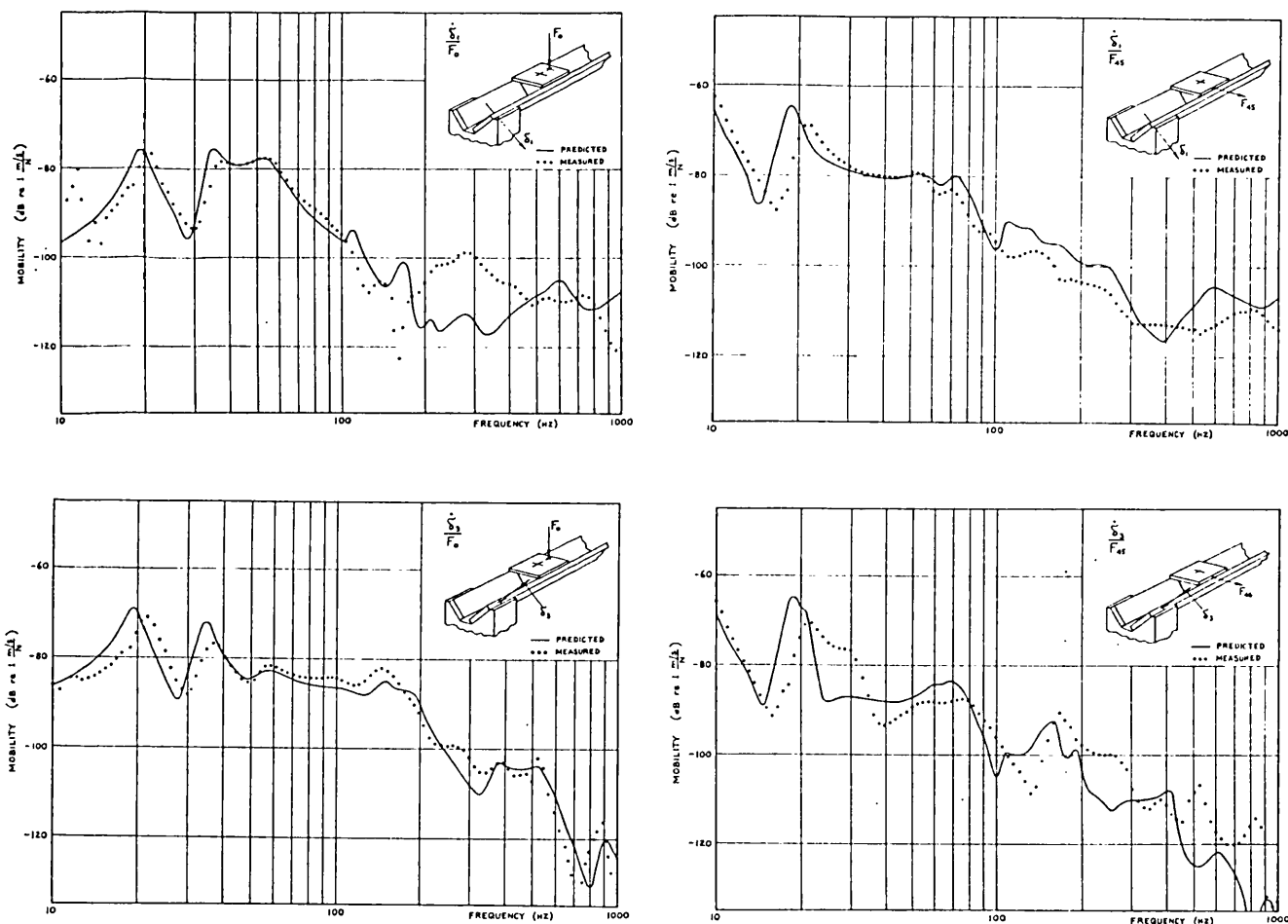


Fig. 5 Response curves for assembled structure

tailed impedance data on each of that structure's component parts. Where possible, such data has been derived from theoretical analysis but in certain cases it has been necessary to resort to experimental measurement. Using a combination of theoretical and measured impedance data is has been possible to predict accurately the dynamic behavior of an assembly of several components.

The machinery foundation structure studied in this way has been found to possess good multidirectional isolation properties over a wide frequency range.

APPENDIX 1

Finite Element for Symmetrical 5 Layer Beam in Flexure. Referring to Fig. 6, when the beam is loaded any plane section AB distorts to the shape $A'B'$. The displacement of any point on the section is expressible in terms of the transverse displacement W and the rotations $\frac{\partial W}{\partial x}$ and α . The total significant strain energy in a

finite element of beam of length L is then given by

$$\begin{aligned}
 V = & 2(1/2bk_2G_2t_2) \int_0^L \left(\alpha - \frac{\partial W}{\partial x} \right)^2 dx + 2(1/2bE_1t_1) \\
 & \times \int_0^L \left[t_2 \frac{\partial \alpha}{\partial x} + \left(\frac{t_1 + t_3}{2} \right) \frac{\partial^2 W}{\partial x^2} \right]^2 + \frac{t_1^2}{12} \left(\frac{\partial^2 W}{\partial x^2} \right)^2 dx \\
 & + 2(1/2bE_2t_2) \int_0^L \frac{1}{4} \left[t_2 \frac{\partial \alpha}{\partial x} + t_3 \frac{\partial^2 W}{\partial x^2} \right]^2 + \frac{t_2^2}{12} \left(\frac{\partial \alpha}{\partial x} \right)^2 dx \\
 & + (1/2bE_3t_3) \int_0^L \left(\frac{\partial^2 W}{\partial x^2} \right)^2 dx
 \end{aligned}$$

where b is the beam width and $k, G, E,$ and t are, respectively, the shear factor, shear modulus, elastic modulus and thickness of a layer. This expression takes into account the symmetry about the neutral axis, and it includes direct and bending effects in all the layers, and shear in the visco-elastic layers.

The total kinetic energy comprises contributions from the transverse motion and from rotary inertia, but it has not so far been found necessary to include the latter. Hence

$$T = 1/2b(2\rho_1t_1 + 2\rho_2t_2 + \rho_3t_3) \int_0^L \left(\frac{\partial W}{\partial t} \right)^2 dx$$

where ρ is the density of a layer.

The following "shape functions" have been assumed for W and α :

$$\begin{aligned}
 W &= a_0 + a_1x + a_2x^2 + a_3x^3 \\
 \alpha &= b_0 + b_1x + b_2x^2
 \end{aligned}$$

and the 7 constants have been related to the 7 nodal displacements indicated in Fig. 6. The strain and kinetic energy expressions have been written in terms of these nodal displacements, and the element stiffness and inertia matrices have been obtained from the energy expressions using Lagrange's equation.

Provided that the element is only used for harmonic vibration, the damping within the visco-elastic layers is introduced by making the moduli G_2 and E_2 complex. Thus the element stiffness matrix is a complex matrix.

Readers unfamiliar with the finite element analysis of beam vibration should consult the papers of Archer [7] or of Leckie and Lindberg [8] for the basic uniform beam element. The only sandwich beam element to appear in the literature has been

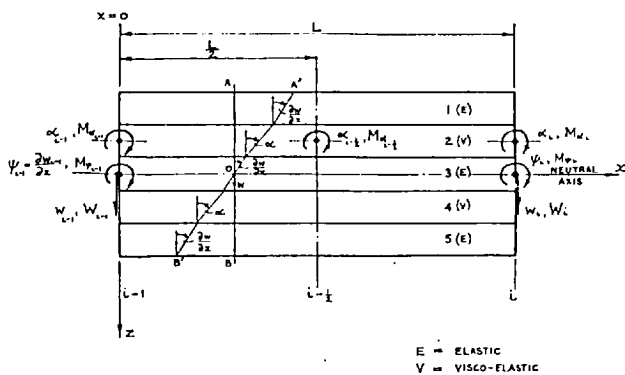


Fig. 6 Finite element of symmetrical 5-layer beam

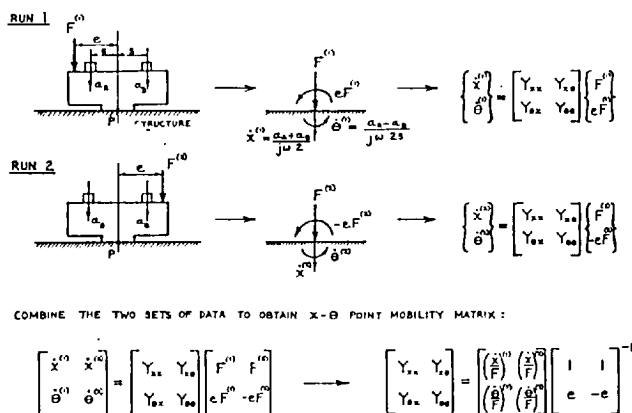


Fig. 7 Outline of multidirectional mobility measurement technique

that derived by Ahmed [9] for a curved symmetrical 3-layer beam.

APPENDIX 2

Multidirectional Point Mobility Measurement. Owing to the lack of suitable shakers, force gauges and accelerometers, the measurement of rotational mobility presents some difficulty. In consequence, a measurement technique has been developed which only requires the use of a single conventional shaker and conventional transducers [10]. The technique is illustrated in Fig. 7. A metal "exciting block," upon which is mounted a pair of accelerometers, is attached to the structure at the point where the mobility properties are required. A sinusoidal excitation is applied at one end of the block, and the force and accelerations are measured at a number of discrete frequencies, as the frequency is swept incrementally through the required range. A second test is then performed, through the same set of frequencies, but with the excitation being applied at the other end of the block. From the two sets of measurements the 2×2

point mobility matrix may be derived for each frequency, and if necessary, the inertia effect of the exciting block may be cancelled. The diagonal terms of this matrix are the "direct" mobilities in the linear and rotational directions, and the off-diagonal terms are the "cross" mobilities relating forces and motions in the two directions.

Using a digital transfer function analyzer under the control of a small computer [11] such measurements have been automated, and the processing of the data is carried out within the computer during the second run. Although only one element of the 2×2 complex matrix may be plotted during the test, the information may be punched onto paper tape for subsequent plotting or other use.

The greatest inaccuracy is always apparent in the rotational mobility, and is a function of the relative magnitudes of the two direct mobilities, of accelerometer cross-sensitivity, etc. Nevertheless, the measurements on the sandwich beam show that the technique is capable of producing quite good results.

It should be mentioned that Smith [12] has developed a similar technique for multidirectional measurements but he uses a pair of shakers and also he avoids the use of force gauges.

Acknowledgment

The authors gratefully acknowledge the support provided for this work by Ministry of Defence Contract No. DC 20(1)/55384/69.

References

- Skudrzyk, E., "Simple and Complex Vibratory Systems," Pennsylvania State University Press, 1968.
- Ungar, E. E., and Dietrich, C. W., "High Frequency Vibration Isolation," *Journal of Sound and Vibration*, Vol. 4, No. 2, 1966, pp. 224-241.
- Snowdon, J. C., *Vibration and Shock in Damped Mechanical Systems*, Wiley, New York, 1968.
- Klosterman, A. L., and Lemon, J. R., "Building Block Approach to Structural Dynamics," American Society of Mechanical Engineers Annual Vibrations Conference Paper, 69-VIBR-30.
- Aghasiere, J. A., and Grootenhuys, P., "Flexural Vibration of Symmetrical Multilayer Beams With Viscoelastic Damping," *Journal of Mechanical Engineering Science*, Vol. 10, No. 3, 1968, p. 269.
- Nakra, B. C., "Vibration of Unsymmetrically Damped Laminated Structures," University of London PhD thesis, 1966.
- Archer, J. S., "Consistent Mass Matrix for Distributed Systems," *Proceedings of American Society of Civil Engineers*, Vol. 89, No. ST4, 1963, p. 161.
- Leckie, F. A., and Lindberg, G. M., "The Effect of Lumped Parameters on Beam Frequencies," *Aeronautical Quarterly*, Vol. 14, 1963, pp. 224-240.
- Ahmed, K. M., "Free Vibration of Curved Sandwich Beams by the Method of Finite Elements," *Journal of Sound and Vibration*, Vol. 18, 1971, pp. 61-74.
- Ewins, D. J., and Sainsbury, M. G., "Mobility Measurements for the Vibration Analysis of Connected Structures," *Shock and Vibration Bulletin*, Vol. 42, Part 1, 1972.
- Martin, A., and Ashley, C., "A Computer Controlled Digital Transfer Function Analyser and Its Application in Automobile Testing," Society of Environmental Engineers Symposium on Dynamic Testing, London, 1971.
- Smith, J. E., "Measurement of the Total Structural Mobility Matrix," *Shock and Vibration Bulletin*, Vol. 40, 1970.